Faculty of Mathematical, Physical and Natural Sciences
Department of Environmental Biology

PhD in Environmental and Evolutionary Biology

Curriculum: Ecological Sciences

XXXII Cycle

New Insights for Health and Environmental Impact Assessment of PM Released by Specific Emission Sources

PhD Candidate

Dr. Lorenzo Massimi [a,b]

Supervisor

Prof. Silvia Canepari [a]

PhD Coordinator

Prof. Gabriella Pasqua [b]

[a] Department of Chemistry, Sapienza University of Rome, Rome 00185, Italy

[b] Department of Environmental Biology, Sapienza University of Rome, Rome 00185, Italy

Academic Year

2019-2020

Table of Contents

Abstract **4**

Description and Objectives of the PhD Thesis **8**

1. Introduction **11**

1.1. PM Definition and Classifications **11**

1.1.1. Modal Classification 12

1.1.2. Dimensional Cut-Off Classification 12

1.1.3. Dosimetric Classification 13

1.2. PM Chemical Composition **14**

1.2.1. Inorganic Macro-Components 14

1.2.2. Inorganic Micro-Components 14

1.2.3. Carbon-Containing Compounds 15

1.3. PM Sampling, Analysis and Chemical Characterization **16**

1.3.1. Sampling and Measurement Methods of PM_{10} and $PM_{2.5}$ 16

1.3.2. Cascade Impactor 17

1.3.3. Chemical Characterization of the Carbon Fraction 18

1.3.4. Chemical Characterization of the Inorganic Ionic Fraction 18

1.3.5. Elemental Analyses 19

1.4. PM Health and Environmental Impact **21**

1.4.1. Effects on Human Health and the Environment 21

1.4.2. Regulation Concerning Air Quality Levels 22

1.4.3. Oxidative Stress Induction 23

1.4.5. Oxidative Potential Assays 24

2. Health and Environmental Impact Assessment of PM Released by Specific Emission Sources **33**

2.1. (A) Evaluation of the Potential of PM-Selected Components to Induce Oxidative Stress in Biological Organisms **33**

2.1.1. (A1) Oxidative Potential of Particulate Matter Components Generated by Specific Emission Sources 34

2.1.2. (A2) Assessment of the Adverse Effects of Atmospheric Pollutants using the Animal Model *Caenorhabditis elegans* 62

2.1.3. (A3) Potential of PM-Selected Components to Induce Oxidative Stress and Root System Alteration in a Plant Model Organism 96

2.1.4. (A4) Nitric Oxide Alleviates the Damages Induced by Cadmium but not Those Induced by Arsenic in Rice Roots 131

2.2. (B) Size and Chemical Fractionation of PM Released by Outdoor and Indoor Emission Sources 162

2.2.1. (B1) A Combined Chemical/Size Fractionation Approach to Study Winter/Summer Variations, Ageing and Source Strength of Atmospheric Particles 163

2.2.2. (B2) Ultrafine, Fine and Coarse Airborne Particle Mass Concentration in Workplaces 190

2.2.3. (B3) Evidences of Copper Nanoparticle Exposure in Indoor Environments: Long-Term Assessment, High-Resolution Field Emission Scanning Electron Microscopy Evaluation, in Silico Respiratory Dosimetry Study and Possible Health Implications 206

2.3. (C) Spatially-Resolved Analyses of PM for Localization and Impact Assessment of Emission Sources 238

2.3.1. (C1) Monitoring and Evaluation of Terni (Central Italy) Air Quality through Spatially-Resolved Analyses 240

2.3.2. (C2) Spatial and Dimensional Distribution of Levoglucosan and Alternative Biomass Burning Tracers in Atmospheric Aerosols, in an Urban and Industrial Hot-spot of Central Italy 264

2.3.3. (C3) Spatial Mapping of Element Concentrations in PM_{10}: a Powerful Tool for Localization and Impact Assessment of Emission Sources 306

2.3.4. (C4) Lichen Transplants as Indicators of Atmospheric Element Concentrations: a High Spatial Resolution Comparison with PM_{10} Samples in a Polluted Area (Central Italy) 358

2.3.5. (C5) Evaluation of the Efficiency of *Arundo donax* L. Leaves as Biomonitors for Atmospheric Element Concentrations in an Urban and Industrial Area of Central Italy 400

2.4. (D) Evaluation of Rapid Analytical Methods for Human Exposure Assessment to Toxic Elements 431

2.4.1. (D1) Simple and Rapid Method for the Determination of Mercury in Human Hair by Cold Vapour Generation Atomic Fluorescence Spectrometry 433

2.4.2. (D2) A New Rapid Treatment of Human Hair for Elemental Determination by Inductively Coupled Mass Spectrometry 468

2.4.3. (D3) A Prophylactic Multi-Strain Probiotic Treatment to Reduce the Absorption of Toxic Elements: In-Vitro Study and Biomonitoring of Breast Milk and Infant Stools 509

3. Conclusions and Perspectives 556

4. Appendix 559

4.1. (E) Efficiency Evaluation of Food Waste Materials for the Removal of Pollutants from Wastewater 559

4.1.1. (E1) Efficiency Evaluation of Food Waste Materials for the Removal of Metals and Metalloids from Complex Multi-Element Solutions 560

4.1.2. (E2) Food Waste Materials Appear Efficient and Low-Cost Adsorbents for the Removal of Organic and Inorganic Pollutants from Wastewater 584

4.1.3. (E3) Food Waste Materials as Low-Cost Adsorbents for the Removal of Volatile Organic Compounds from Wastewater 591

4.2. Conclusions and Perspectives 616

Abstract

This study is aimed to improve the knowledge about the association between health and environmental effects of particulate matter (PM) and its chemical composition and sources and it is focused on the integration of different observation systems and monitoring techniques. PM samples originated from different sources were collected and analyzed by traditional and innovative analytical methods, thus reaching a very detailed knowledge of their inorganic and organic chemical composition.

(A) Acellular assays: 1,4-dithiothreitol (DTT), ascorbic acid (AA) and 2',7'-dichlorodihydrofluorescein (DCFH), able to give information about PM capacity to generate oxidative stress, were applied to PM-selected components to estimate the oxidative potential (OP) of PM released by different emission sources **(A1)**. Plant and animal model organisms were exposed *in vivo* under controlled conditions to the PM-selected components. Oxidative stress and other biological responses were evaluated and correlated to the OP and chemical composition of PM and the reliability of the OP methods as proxies of the production of reactive oxygen (ROS) and nitrogen (RNS) species was assessed **(A2, A3)**. Furthermore, the potential of NO to restore the cellular balance between the ROS and the RNS in the root system of a plant species exposed to As and Cd was evaluated **(A4)**.

(B) To obtain valuable information for PM source apportionment and thus for the assessment of health and climate impact, a chemical/size fractionation method was applied to sampling campaigns carried out for seven consecutive years in the Po Valley (Northern Italy) **(B1)**. PM_{10} and size-segregated PM samples collected in workplaces **(B2)** and in indoor environments of private dwellings **(B3)** were analyzed to investigate the health impact of particles emitted in different size fractions by specific indoor sources.

(C) Innovative and very-low volume samplers were used for high spatial resolution analyses of PM chemical components in the Terni basin (Central Italy), which can be considered as an open air laboratory for studying the spatial distribution of PM, since it is characterized by atmospheric stability and by the presence of several anthropic PM sources **(C1, C2, C3)**. The impact of local emission sources was assessed and the spatial variability of PM element concentrations was mapped **(C3)** and compared with the results achieved by biomonitoring through lichen transplants **(C4)** and leaf deposition on riparian species **(C5)**, to verify the reliability of biomonitoring techniques for the assessment of atmospheric element concentrations. The experimental approach, based on the

mapping of spatially-resolved PM chemical data, is a powerful tool for a reliable assessment of population exposure to PM air pollutants and also promises to be effective for optimization and validation of dispersion models. This approach, combined with on-site human biomonitoring will allow further investigations on the relationships between health effects and PM chemical composition and sources.

(D) To investigate relationships between health effects and PM chemical composition and sources, the suitability of different biological matrixes for on-site human biomonitoring exposure to environmental pollution was evaluated. Rapid analytical methods for routine elemental analysis of a significant number of human hair samples were developed and validated **(D1, D2)**. Moreover, Hg As, Pb and Cd levels in breast milk were assessed to provide valuable information on the maternal toxic load and to be used as an indicator for prenatal and post-natal exposure of infants to these chemicals. In addition, we assessed the capacity of a multi-strain probiotic to protect the infants from their exposure **(D3)**.

(E) Finally, during the PhD research, environmental remediation techniques for inorganic and organic pollutants were investigated. The potential of food waste materials as low-cost adsorbents for the removal of toxic elements, heavy metals **(E1)** and volatile organic compounds **(E2, E3)** from wastewater was evaluated. The adsorption capacity of food waste materials was assessed by comparing the removal efficiency of elements and VOCs from complex solutions, maintaining homogeneous experimental conditions, which allowed us comparing the adsorption capacity of the individual sorbents.

(A1) Oxidative Potential of Particulate Matter Components Generated by Specific Emission Sources
Journal of Aerosol Science (2018), *126*, 99-109

(A2) Assessment of the Adverse Effects of Atmospheric Pollutants using the Animal Model *Caenorhabditis elegans*
Ecotoxicology and Environmental Safety (2019), *Reviewed*

(A3) Potential of PM-Selected Components to Induce Oxidative Stress and Root System Alteration in a Plant Model Organism
Environment international (2019), *132*, 105094

(A4) Nitric Oxide Alleviates the Damages Induced by Cadmium but not Those Induced by Arsenic in Rice Roots

Plant Physiology and Biochemistry (2019), *Reviewed*

(B1) A Combined Chemical/Size Fractionation Approach to Study Winter/Summer Variations, Ageing and Source Strength of Atmospheric Particles

Environmental Pollution (2019), *253*, 19-28

(B2) Ultrafine, Fine and Coarse Airborne Particle Mass Concentration in Workplaces

Atmospheric Pollution Research (2019), *10*(5), 1685-1690

(B3) Evidences of Copper Nanoparticle Exposure in Indoor Environments: Long-Term Assessment, High-Resolution Field Emission Scanning Electron Microscopy Evaluation, in Silico Respiratory Dosimetry Study and Possible Health Implications

Science of the Total Environment (2019), *653*, 1192-1203

(C1) Monitoring and Evaluation of Terni (Central Italy) Air Quality through Spatially-Resolved Analyses

Atmosphere (2017), *8*(10), 200

(C2) Spatial Distribution of Levoglucosan and Alternative Biomass Burning Tracers in an Urban and Industrial Hot-Spot of Central Italy

Atmospheric Research (2019), *Reviewed*

(C3) Spatial Mapping of Element Concentrations in PM_{10}: a Powerful Tool for Localization and Impact Assessment of Emission Sources

Atmospheric Research (2019), *With Editor*

(C4) Lichen Transplants as Indicators of Atmospheric Element Concentrations: a High Spatial Resolution Comparison with PM_{10} Samples in a Polluted Area (Central Italy)

Ecological indicators (2019), *101*, 759-769

(C5) Evaluation of the Efficiency of Arundo donax L. Leaves as Biomonitors for Atmospheric Element Concentrations in an Urban and Industrial Area of Central Italy

Atmosphere (2019), *Reviewed*

(D1) Simple and Rapid Method for the Determination of Mercury in Human Hair by Cold Vapour Generation Atomic Fluorescence Spectrometry

Microchemical Journal (2019), *150*, 104186

(D2) A New Rapid Treatment of Human Hair for Elemental Determination by Inductively Coupled Mass Spectrometry

Analytical Methods (2019), *Reviewed*

(D3) A Prophylactic Multi-Strain Probiotic Treatment to Reduce the Absorption of Toxic Elements: In-Vitro Study and Biomonitoring of Breast Milk and Infant Stools

Environment international (2019), *130*, 104818

(E1) Efficiency Evaluation of Food Waste Materials for the Removal of Metals and Metalloids from Complex Multi-Element Solutions

Materials (2018), *11*(3), 334

(E2) Food Waste Materials Appear Efficient and Low-Cost Adsorbents for the Removal of Organic and Inorganic Pollutants from Wastewater

Research & Development in Material Science (2018), *5*(2), 1-3

(E3) Food Waste Materials as Low-Cost Adsorbents for the Removal of Volatile Organic Compounds from Wastewater

Materials (2019), *12*(24), 4242

Description and Objectives of the PhD Thesis

Atmospheric particulate matter is considered as one of the air pollutants that exerts the most severe effects on health and the environment. The negative effects of PM have been extensively investigated and many studies revealed that several PM properties (chemical composition, particle dimension etc.) influence its health and environmental effects. Nevertheless, no sufficient evidence that associates each property to specific outcomes has been yet identified (WHO, 2013). Therefore, PM mass concentration is typically used to estimate population exposure to PM. However, this indicator misestimate the overall impact of PM, since it does not take into account the multiple toxicological effects of the different pollutants that make up the particulate matter. This limitation can be exceeded by identifying possible relationships between specific PM physic-chemical properties and their toxicity on biological organisms.

Recent studies identified the generation of oxidative stress as one of the major mechanisms by which PM exerts its adverse biological effects (Li et al., 2015). The ability of PM to induce oxidative stress is frequently estimated by acellular oxidative potential measurements. Different methods have been proposed in the literature, but their ability to correctly represent the *in vivo* mechanisms has not been yet demonstrated (Fang et al. 2015). Furthermore, the *in vivo* exposure has been poorly applied to study the biological effects of PM (Marcoccia et al., 2017), but it is crucial to understand the toxicological pathways of PM interaction with living organisms and to identify relationships among OP and PM toxicological effects.

The aim of this PhD thesis is to improve the knowledge about the existing relationships between the chemical composition and sources of PM and its adverse effects on health and environment, useful to plan the mitigation measures that are necessary to protect citizens health in the area of study. To this aim, we carried out a multidisciplinary study based on the synergic application to PM of traditional and innovative approaches. In this study, we evaluate the reliability of the OP methods as proxies of the production of ROS and RNS in biological organisms by assessing the capacity of PM-selected components to induce oxidative stress in living organisms, and we describe an integrated method, transferable to other monitoring campaigns, for the spatial mapping of PM chemical components, which is a powerful tool for a reliable geo-referenced assessment of population exposure to PM air pollutants. This approach, combined with on-site human biomonitoring will allow further investigations on the relationships between specific physic-chemical properties of PM and its adverse outcomes for human health.

The study considers field PM samples, collected at sites differently impacted by anthropic activities, and PM-selected components (road dust, brake dust, soil dust, Saharan dust, pellet ash, coke and certified material NIST1648a – urban dust) that are directly attributable to defined emission sources. The collection of PM samples was performed by cascade impactors, biomonitoring methods and very-low volume samplers recently developed with the purpose of allowing spatially-resolved determination of PM chemical components. Most of the sampling sites were located in the Terni basin (Central Italy). Terni can be considered as an open air laboratory for studying the spatial distribution of PM, as it includes several spatially disaggregated sources (vehicular traffic, rail network, domestic heating, power plant for waste treatment, steel industry pole) and is characterized by peculiar meteorological conditions that reduce air mixing and air pollutants transport, favoring their accumulation. These factors have been associated with an increase of morbidity and mortality due to the onset of cardiopulmonary environment-related diseases, which made this area of national interest for environmental remediation (SENTIERI-ReNaM, 2016). The very-low volume samplers were located at various sites of Terni to map the spatial distribution of PM and of its elemental components. Biomonitors (lichen transplants *Evernia prunastri* (L.) Ach. and leaf deposition on the riparian species *Arundo donax* (L.)) were employed along with the samplers, to verify the reliability of biomonitoring techniques for the assessment of atmospheric element concentrations. Other sampling sites were located in the Po Valley (Northern Italy), to obtain valuable information for PM source apportionment through a chemical/size fractionation procedure, and in indoor environments of private dwellings and workplaces, to assess the health impact of particles emitted in different size fractions by specific indoor sources.

In these studies, a detailed chemical composition of the PM samples was obtained by applying the most advanced and consolidated methods (Perrino et al., 2014) for the determination of inorganic ions, elements, water-soluble organic carbon (WSOC) and levoglucosan (LVG). Soluble and insoluble PM fractions were studied separately to increase the selectivity of elements as source tracers and to estimate the environmental mobility and bio-accessibility of toxic elements. Oxidative potential of the PM-selected components was measured by different acellular methods (DTT, AA and DCFH) and correlated to PM ability of inducing oxidative stress in living organism, in order to verify the predictive ability of the considered assays. Health and environmental effects of PM were studied by using plant and animal model organisms. *Arabidopsis thaliana* (L.) Heynh was used as plant model organism because of its ease of growing in laboratory conditions and because the morphology and development of its roots may be severely damaged by heavy metals and toxic elements in a dose dependent manner (Feigl et al., 2014; Fattorini et al., 2017; Ronzan et al., 2018).

The nematode *Caenorhabditis elegans* provided an ideal invertebrate model for monitoring the toxicogenomic effects of PM exposure since it is easily cultured in the laboratory, its genetic variability is decreased and its genome has been sequenced. To investigate relationships between health effects and PM chemical composition and sources, the suitability of different biological matrixes for on-site human biomonitoring exposure to environmental pollution was evaluated. Rapid analytical methods for routine elemental analysis of a significant number of biological samples were developed and validated.

1. Introduction

1.1. PM Definition and Classifications

Airborne particulate matter is a mixture of solid and liquid particles suspended in the atmosphere, with an aerodynamic diameter ranging between 0.01 and 100 µm and with a heterogeneous composition (e.g. soot, dust, differently originated salts, fly ashes, trace metals, viruses, bacteria, fungi, spores and pollen; Manahan 2000; EPA 1997; Fig. 1.1).

Firstly, PM can be classified depending on the type of emission source that originated it:

• *Natural sources*: volcanic eruptions, forest fires, erosion and disintegration of rocks, pollen, plant residues, spores, sea spray;

• *Anthropogenic sources*: combustion engines, domestic heating, mechanical abrasion of brakes and tires, construction works, industries, agricultural processes, incinerators and power plants, tobacco smoke. The anthropogenic sources are able to introduce into the atmosphere a greater amount of particles toxicologically harmful to human health and the environment.

Secondly, airborne particles can be classified depending on their mechanisms of formation:

• *Primary particles*: particles directly released into the atmosphere by natural and/or anthropogenic emission sources;

• *Secondary particles*: organic aerosols formed by the photochemically induced oxidation of volatile organic compounds and particles formed in the air, generally by chemical reactions of gaseous precursors, such as sulphur dioxide (SO_2), nitrogen oxides (NOx) and ammonia (NH_3), to form particulate sulphates and nitrates.

Finally, the atmospheric particles can be classified referring to the *aerodynamic diameter* (a.d.), defined as the diameter of a unit-density spherical particle (1 g/cm^3) having the same aerodynamic properties (sedimentation rate) of a given particle (John 2001).

The airborne particles can be thus divided into three different sub-classifications related to dimensional characteristics.

• *Modal*: based on the mechanisms of formation of the particles and consequently on their number, surface area and mass distribution;

• *Dimensional (size) cut-off*: based on the efficiency of the sampling head device during the PM collection;

• *Dosimetric*: based on the particles' ability to enter and penetrate into the respiratory system.

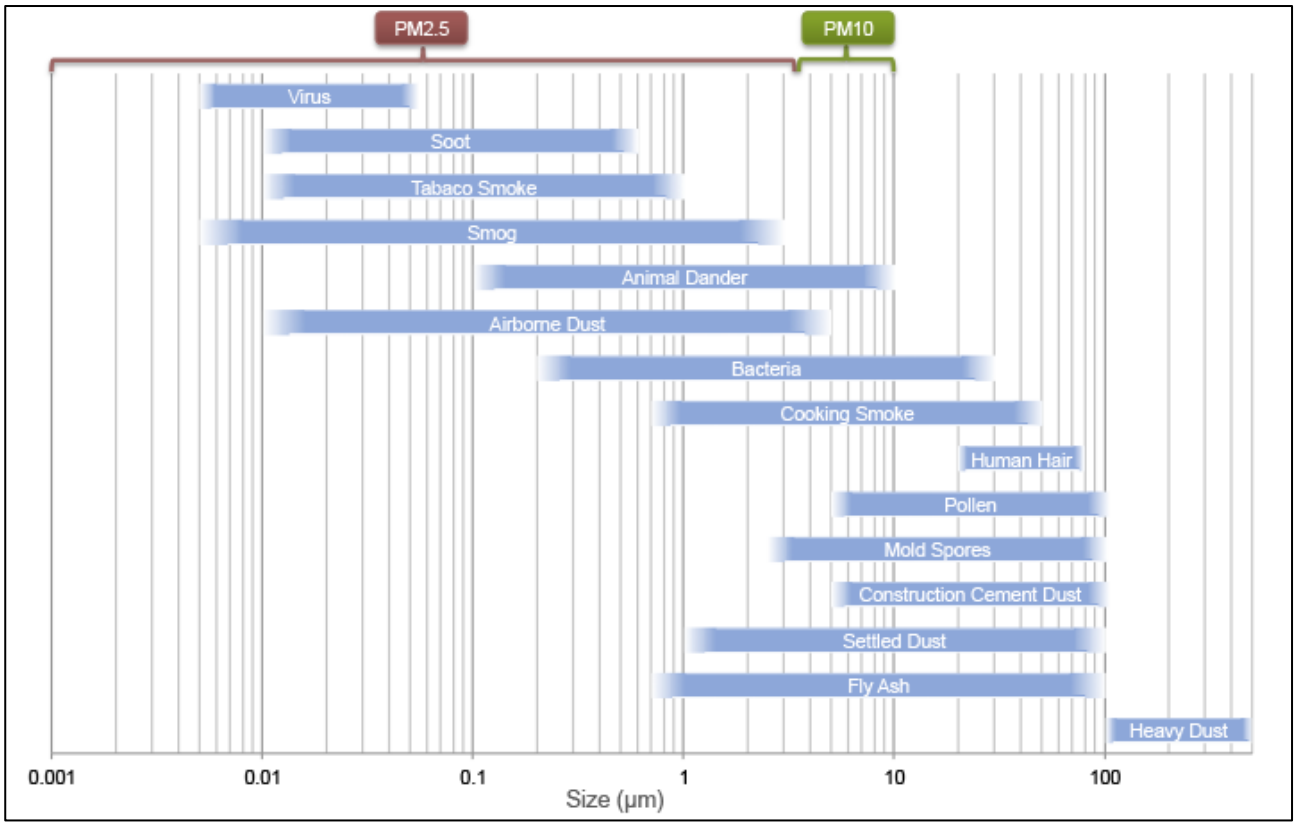

Fig. 1.1. Size distribution in micrometers (µm) of various types of airborne particles (https://www.teilch.com/the-air-you-breathe/).

1.1.1. Modal Classification

Particles with aerodynamic diameter less than 0.1 µm (ultrafine fraction), which are generally released by combustion processes, are found in the nucleation mode.

The accumulation mode considers those particles having an aerodynamic diameter between 0.1 and 1-2 µm (fine fraction), generated by coagulation and condensation of ultrafine particles.

Finally, the coarse mode includes particles with an aerodynamic diameter between 1-2 and 100 µm, which are usually generated by mechanical processes, such as erosion, abrasion, re-suspension of dust and fragments of organic materials, air masses transported from marine or desertic areas (John 2001; Puxbaum 1991).

1.1.2. Dimensional Cut-Off Classification

PM_X is the fraction of particulate matter that has been collected by a selective inlet impactor with a 50% efficiency cut-off at X µm aerodynamic diameter (EC 1997). Indeed, the instruments usually used in the air sampling collect particles that fall within a size range rather than one single size.

The most commonly available sampling heads for commercial samplers collect mainly PM_{10} and $PM_{2.5}$ fractions, being the most interesting for both health effects and investigations on the life cycle of airborne particles. Therefore, the *fine* fraction will be intended for $PM_{2.5}$, while the *coarse* one for particles with aerodynamic diameter between 2,5 and 10 µm (EPA 1999). Conventional PM_{10} and $PM_{2.5}$ samplers show a 50% efficiency in collecting particles with 10 ± 0.5 µm or 2.5±0.5 µm aerodynamic diameter.

1.1.3. Dosimetric Classification

The dosimetric classification is based on the capability of airborne particles to enter, infiltrate, deposit and react with the different zones of the respiratory system, as showed in Fig. 1.2.

Particles greater than 10 µm a.d. are mainly deposited in the upper system, particles between 5 and 10 µm are deposited in the trachea and pharynx, and particles of less than 2 µm penetrate significantly into the bronchi and alveoli. Therefore, under this classification, particles are identified by four fractions.

Inhalable: particles that pass through the nose and mouth;

Thoracic: particles that are deposited in the lower respiratory tract, including those particles that reach lungs;

Respirable: particles penetrating significantly up to the gas-exchange region of alveoli; *Respirable "high risk"*: particles of the respirable fraction with harmful effects on children and people suffering from cardio-pulmonary diseases (Mark, 1999).

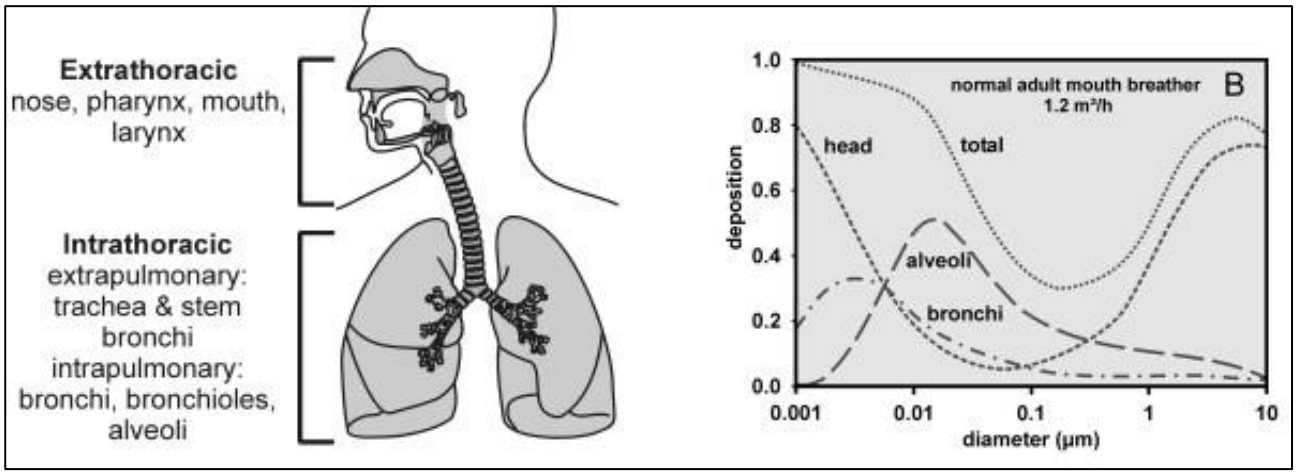

Fig. 1.2 Potential deposition of particles with different sizes into the respiratory system (Geiser and Kreyling, 2010).

1.2. PM Chemical Composition

Particulate matter includes a large number of chemical species that can be divided into two major classes.

• *Macro-components*: inorganic ions, elements and carbon-containing compounds that exceed more than 1% of the PM mass;

• *Micro-components*: elements and organic compounds present in trace amount (< 1% of PM mass).

Typically, the *fine* fraction of PM is mostly constituted by chemical components such as elemental carbon (EC), sulphates (normally present as ammonium salts) and various organic compounds of primary and secondary origin. On the contrary, the *coarse* fraction is mainly formed by elements coming from the earth's crust (Ca, Al, Si, Mg, Fe) and some bio-organic materials such as pollen, spores, plants and animal wastes.

1.2.1. Inorganic Macro-Components

Among the macro-components can be found anions (e.g. Cl^-, NO^{3-}, SO_4^{2-}, CO_3^{2-}, SiO_4^{4-}), cations (e.g. Na^+, NH_4^+, K^+, Mg^{2+}, Ca^{2+}) and some elements (e.g. Al, Si, Fe). In addition, elemental carbon (EC) and organic matter constitute a relevant fraction of the macro-components. It is possible to subdivide the ions depending on their primary or secondary nature.

The primary ions are: *chlorides*, coming from marine aerosol or from waste incineration; *sodium* and *magnesium*, coming from marine aerosol and partly from soil resuspension; *calcium*, coming from soil, wildfires and industrial activities; *potassium*, coming from soil, biomass combustion and agricultural fertilization; *sulphates*, coming from marine aerosol even if mainly present as secondary species; *silicates* and *carbonates*, coming from soil since they are mainly present in the earth's crust. The secondary inorganic compound formation has different gaseous precursors such as *suplhur oxides* and *nitrogen oxides*, mainly coming from coal and fuel combustion processes (e.g. power plants, heating plants, vehicular traffic), and *ammonia*, coming from the microbiological activity of the soil and sea and originated by stock farms and vehicular exhausts.

1.2.2. Inorganic Micro-Components

PM includes also a great number of trace elements coming from natural and anthropogenic sources. Trace metals coming from natural sources are related to the geological composition of the earth's crust and their suspension in the air is due to physic-chemical and biological processes, such as resuspension of soil particles, volcanic emissions (which emit Cd, Hg, As, Cr, Cu, Ni, Pb and Sb),

sea spray (which leads to an enrichment in Cd, Cu, Ni, Pb and Zn) and forest fires (which may originate metals such as Cu, Pb and Zn: Pacyna, 1999).

The release of trace elements into the atmosphere by anthropogenic activities is much more significant and is attributable to various industrial processes (e.g. production of electricity, combustion of fossil fuels) and to vehicular traffic. These sources are responsible for more than 50% of the total emissions of Cr, Mn and V and for 20-30% of the annual release into the atmosphere of metals such as Cu, Mo, Ni, Pb, Sb, as, Se, Hg, Sn and Zn (Moore,1994). Other sources of trace elements can be identified with the waste incineration, emitting elements mainly included in the *fine* fraction (e.g. Cu, Zn, Cd, Sb, Pb, Ca, Cr, Mn and Ni; Abbas et al., 2001; Phongphiphat et al., 2011), and with soil resuspension from paved roads, releasing elements mainly contained in the *coarse* fraction (e.g. Al, Si, K, Ca, Ti and Fe).

By studying the spatial distributions and the seasonal variations of the trace elements, it would be possible to identify their emission sources and to obtain more information about the environmental pollution phenomena.

1.2.3. Carbon-Containing Compounds

The total carbon fraction of PM (20-60% of the total mass) can be divided into organic carbon (OC) and elemental carbon (EC). EC is directly emitted into the atmosphere by combustion processes as either single particles or clusters with variable shape and size (Barone et al., 2006), while OC is constituted by a complex mix of numerous compounds, present at very different concentrations (macro and micro), of which only a few are known. Some of these are very harmful to human health such as alkanes, benzoic acids, benzaldehydes, phenols, furans, carboxylic acids, polycarboxylic aromatic acids, aliphatic acids, polycyclic aromatic hydrocarbons (PAHs), polycyclic aromatic ketones, sterols and pesticides.

1.3. PM Sampling, Analysis and Chemical Characterization

In the literature, many studies are focused on the chemical analysis of PM, eventually combined to source-apportionment applications (EPA 1999; Kleeman et al. 1998; Querol et al. 2003). A complete chemical characterization of airborne particulate matter includes the determinations of the volatile, hydro-soluble and insoluble fractions of inorganic ions, organics and elements.

1.3.1. Sampling and Measurement Methods of PM_{10} and $PM_{2.5}$

The measure of airborne particulate matter is effectively defined for European regulatory purposes by the European Committee for Standardization (CEN). For PM_{10}, the European Reference Method is described in the CEN standard EN 12341, adopted by CEN in November 1998 (CEN 1998) while for $PM_{2.5}$ the standard are set in the EN 14907 adopted in 2005 (CEN 2005). They define a PM sampling inlet coupled with a filter substrate and a regulated flow device. These systems allow sampling PM according to the particle aerodynamic size. Also by increasing the sampling time, a sufficient quantity of powder can be collected to obtain both an accurate determination of the mass and the subsequent chemical analysis.

Table 1.1. Characteristics of the membranes used to collect PM.

Filter material	Advantage	Disadvantage
Glass fiber	High retention capacity.	Release of material due to the fibrous structure.
Quartz	Resistance to high temperatures; available to analyze carbonaceous compounds by means of thermal methods.	Tendency to adsorb volatile organic compounds.
Teflon	No release of material due to the continue structure; low blank value, suitable to analyze trace elements.	Fast clogging with high PM concentrations.

The conventional samplers are constituted by a sampling head that draw the airflow and select the particles of a certain size. The air thus is conveyed through a filtration membrane able to retain the selected particles. Downstream of sampling line, a pump generates the pressure gradient necessary to the airflow. Collected samples are then constituted by all the particles contained in the *fine* mode and most of the particles belonging to the *coarse* mode. The choice of setting the cut to 10 and 2.5 µm was determined by toxicological considerations, since the particles with a.d < 10 µm can penetrate into the respiratory system, while the particles with a.d < 2.5 µm are considered particularly harmful. Samplers can be divided in two main group: the high volume samplers (HVS) that allow to collect high amounts of dust on large filters (diameter 150 mm) and the low volume samplers (LVS) that allow to collect small amounts of dust (Few mg) on membranes of 47 or 37 mm diameter. The flow rate is critical to maintain the PM cut point and, when using the standard impactor dimension following the criteria for the CEN standard (CEN 1998), a constant flow rate of 68 m^3/h (1133 l/min) is required for a high volume sampler and 2.3 m^3/h (38 l/min) for a low volume sampler. Different membranes can be used to collect PM depending on the chemical analysis to perform after the sampling phase. In table 1.1 the advantages and disadvantages of the most used materials are reported. The mass collected on the filter is gravimetrically measured by means of a micro-balance under ambient air conditions. The handling of filters should be made in clean air and all equipment should be stored in plastic bags in a dust free environment. It is required by EN 12341 (CEN 1998) that the filters are equilibrated before the weighing, at 20° C (±1) and 50% R.H. (±5), for 48 hours. This is helpful to make the determination of mass independent from any external condition.

1.3.2. Cascade Impactor

Cascade impactor allows to fractionate the particles in restricted ranges of different aerodynamic diameters. The size-segregated PM sampled in multiple stages can be analyzed to determine the chemical composition as a function of the particle size.

Airborne particles enter in the device by means of a nozzle, are accelerated to a uniform velocity by a pump and are blocked on a solid plate oriented perpendicularly to the nozzle axis; particles pass through every plate and are exhausted through a back-up filter. Each impactor stage consists of a specific aerodynamic diameter range and successive stages are aimed to collect smaller particles (Hering et al., 1978).

1.3.3. Chemical Characterization of the Carbon Fraction

Typically, the carbon fraction constitutes more than 30% of the PM mass and contains elemental carbon (EC) and a huge number of different organic compounds (OC). Measurements of EC and OC are usually carried out for health and source apportionment studies. Indeed, the ratio between EC and OC (EC/OC) is often used as a valuable tool to understand the origin of the air masses. A variety of methods is available for the measurement of the carbon content of the aerosols (Heintzenberg and Winkler 1991). The recommended method to determine EC is based on the volatilization and oxidation of the sample, followed by the determination of the evolved CO_2, either directly or after conversion to CH_4 by a flame ionization detector (FID).

1.3.4. Chemical Characterization of the Inorganic Ionic Fraction

The major inorganic ions to be determined in the particulate matter are reported in Table 1.2.

Table 1.2. Recommended and alternatives methods for chemical analysis of inorganic ions.

Methods for Chemical Analysis of Inorganic Ions		
Component or parameter	**Recommended methods**	**Alternative**
Conductivity	Conductivity cell and resistance bridge	
Hydrogen ion (H^+)	Potentiometry (glass electrode) pH<5.0	Titration
Ammonium ion (NH_4^+)	Ion chromatography	Spectrophotometry (indophenol blue color reaction)
Sodium ion (Na^+)	Atomic absorption spectrophotometry (AAS)	Ion chromatography
Potassium ion (K^+)	AAS	Ion chromatography
Magnesium ion (Mg^{2+})	AAS	Ion chromatography
Calcium (Ca^{2+})	AAS	Ion chromatography
Sulphate ion (SO_4^{2-})	Ion chromatography	
Nitrate ion (NO_3^-)	Ion chromatography	Reduction to nitrite and diazotation
Chloride ion (Cl^-)	Ion chromatography	Displacement of SCN^- in Hg $(SCN)_4^{2-}$, determination of colored Fe(SCN) complex.

The more used analytical method for ionic determination is the ion chromatography after water extraction of the Teflon membrane filter.

1.3.5. Elemental Analyses

Generally, macro-elements Al, Fe, K, Mg, Ca, Ti, S and Si are analyzed by energy-dispersive X-Ray fluorescence (EPD-XRF, X-Lab 2000, SPECTRO), before performing following chemical analyses on PM filters. Subsequently, the filters are acid-digested and analyzed for micro and trace elements by inductively coupled plasma with optical (ICP-OES) and mass spectrometer detection (ICP-MS).

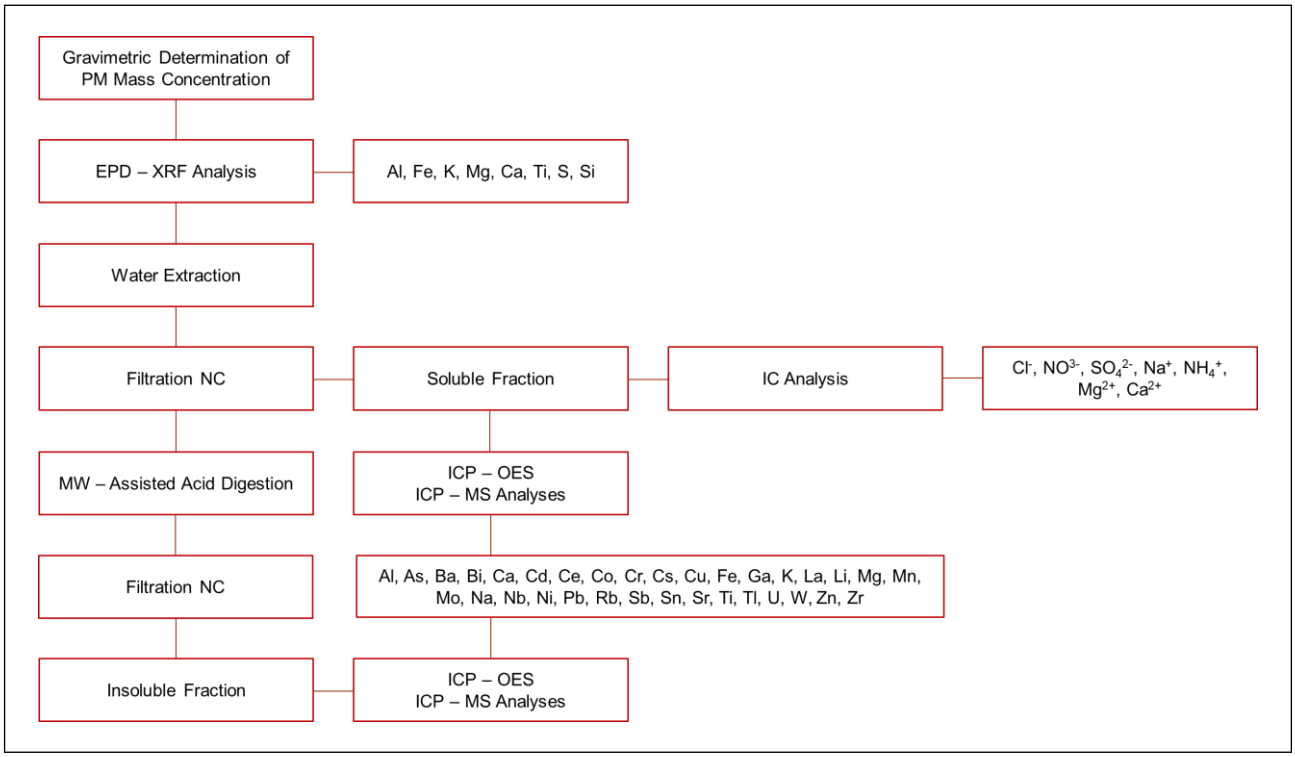

Fig. 1.3 Determination of PM_{10} mass and element concentrations by using the chemical fractioning procedure followed by ICP-MS analyses.

In our laboratory, we apply to Teflon membrane filters a chemical fractioning procedure, previously optimized and validated (Canepari et al., 2010), for the determination of the water-soluble and insoluble fraction of the elements. Each membrane filter is extracted in water by using an ultrasonic bath for 30 min. Then, the solution is divided into two aliquots, one analyzed for anions (Cl^-, NO_3^-, SO_4^{2-}) and cations (Na^+, NH_4^+, Mg^{2+}, Ca^{2+}) by Ion Chromatography (DX 100, DIONEX Co., CA-USA), and the other analyzed for the extractable fraction of the elements (Al, As, Cd, Cu, Fe, Mg, Mn, Ni, Pb, Sb, S, Si, Ti, V, Zn), by ICP-OES and/or ICP-MS (Bruker 820, equipped with a reaction

cell, CRI, and a 400 µl/min MicroMist nebulizer). The choice of the extracting solution was driven by the intention to increase the selectivity of elements as PM source tracers but also to estimate the environmental mobility and bio-accessible fraction of toxic elements (Canepari et al. 2010). The residual Teflon filter is digested in a mix of HNO_3 and H_2O_2 (2:1) using a microwave oven (Milestone Ethos Touch Control with HPR 1000/6S rotor) and the mineralized fraction is then analyzed by ICP-OES and/or ICP-MS for its insoluble elemental content. The use of both ICP-OES and ICP-MS enables the analysis of a larger number of elements. Matrix-matched standard solutions are used for calibration; Y is used as internal standard; the collision reaction interface (CRI) is activated for As, Se, Fe and V determination.

Overall, this procedure allows the determination of macro-elements (including Al and Si, which show a low recovery after the acid digestion), soluble inorganic ions and the extracted and residual fractions of micro and trace elements on individual filters; furthermore the determination of the same element with different analytical techniques (e.g. Fe, Mg, S) makes it possible to check the quality control of the determinations by means of an inter-techniques comparison (Canepari et al. 2009b).

1.4. PM Health and Environmental Impact

Air pollution is one of the major risk factors for human health and the environment worldwide. Indeed, over the years, it has been associated to a great number of adverse outcomes for human health, following both acute and chronic exposure. In particular, airborne particulate matter is considered one of the main causes of concern for the air quality status since several epidemiological studies have spotlighted strong correlations between PM exposure and the onset of respiratory (asthma, chronic obstructive pulmonary disease) and cardiovascular diseases (myocardial infarction, heart failure, cerebrovascular accidents).

During the last decades, PM effects on human health and the environment have led to numerous studies focused on its complex and variable composition and toxicology, and on the individuation of its emission sources. In fact, information about concentrations, forms and toxic effects of the chemical species of PM released by specific sources, may be useful to study and explain the possible cause-effect relationships between harmful pollutants and human health (Hlavay et al., 2001, Ricci and Cirillo, 1985). The World Health Organization (WHO) considers outdoor air pollution as one of the key determinants of health and estimates that PM air pollution contributes to approximately 800,000 premature deaths each year. In 2013 the International Agency for Research on Cancer (IARC) classified outdoor air pollution and particulate matter as carcinogenic of Group 1 to humans. Therefore, there is nowadays the necessity of identification, quantification and apportionment of PM pollutants to facilitate their reduction through proper management plans.

The individuation of the PM chemical compounds released by different emission sources and the study of their toxicity on biological organisms is essential for the assessment of the different biological responses to specific PM physic-chemical properties.

1.4.1. Effects on Human Health and the Environment

Most epidemiological studies on the health effects of air pollution use PM_{10} and $PM_{2.5}$ as exposure indicators. However, these indicators misestimate the overall impact of PM, since they do not take into account the multiple toxicological effects of the different pollutants that make up the particulate matter. Indeed, the only determination of the total concentration do not provide any information about the bioavailability of the species and their interaction with biological organisms. An element can be beneficial or toxic depending on its oxidation and this represents a great limitation. For example, Cr(III) can be an essential element for the metabolism of glucose, while Cr(VI) is carcinogenic. The oxidation state can also affect the absorption and elimination time of an element. The ion Fe(II) is soluble in physiological conditions, it diffuses freely through the membranes, while the Fe(III) does

not easily enter into the cells, and is more subject to hydrolysis in biological systems. Moreover, the mobility of an element depends on many other factors, such as solubility, pH and ionic strength. For instance, Cr(III) is not soluble in neutral water solutions, but may become soluble at a more basic pH values (Goodarzi and Huggins, 2001). However, these substances undergo transformation, interconversion and degradation processes, affected by the environmental conditions; giving rise to products with physic-chemical properties and toxicity different from those of the originating compounds.

As regards PM effects on the environment, PM absorbs and/or reflects the sunlight radiations as a function of the particle size and chemical composition: on one hand, particles reflect sunlight, leading to a cooling of the earth surface; on the other hand, they have a role in the absorption of terrestrial infrared radiations, contributing positively to the global warming. The light absorption is directly related to the chemical composition of the particles; carbonaceous substances absorb strongly the solar radiation (Barry and Chorley, 1992). PM also acts on the environment through acid rains: gaseous components (SO_2, SO_3, NO_x and CO_2) coming from combustion and industrial activities can be transformed in acid (H_2SO_4, HNO_3, HNO_2) by means of reactions with H_2O or OH radical, giving rise to acid precipitations. The fallout on the ground of acid pollutants occurs through wet or dry deposition. The first one is the most known and occurs in the form of rain, snow, acid fog. The dry deposition consists of the fallout on the soil of acidic substances in the form of gas or microscopic particles (Morselli, 1991). These phenomena can cause an alteration of the chemical composition of the vegetation, rocks, groundwater, lakes, rivers and seawaters.

1.4.2. Regulation Concerning Air Quality Levels

The standards concerning air quality are constantly evolving because of the increasing need to protect the human health and the environment and to assure a sustainable development for the next generations. A key role is played by the European Union (EU), which has established new regulations to ensure a significant reduction of the ambient concentrations of pollutants. The Italian Dlgs 60/2002 (transposition of the European Directive 1999/30/CE), sets the daily limit value for PM_{10} to 50 $\mu g/m^3$ not to be exceeded more than 35 times a year, while 40 $\mu g/m^3$ is the yearly average value. In 2008 the EU adopted a new directive 2008/50/CE, transposed in Italy as Dlgs 155/2010, promoting further studies in the air quality field and recognizing, for the first time, the limits of the only PM mass concentration determination. In particular, it introduced the measurement of the $PM_{2.5}$ mass concentration, considered potentially more dangerous to human health, while the limit values for PM_{10} have remained unaltered. Furthermore, it establishes the obligation to measure the concentration

of some specific components, useful to allow the differentiation among the background, local and regional contributions. Unlike the previous one, this legislation requires the chemical characterization of PM samples, necessary to understand the mechanisms of formation of secondary particles. To date, only few chemical species present in the atmosphere are normed:

• The Italian Dlgs 60/2002 contains the limit values and alert thresholds for NO_2, NO_x, SO_2, CO, O^3, PM_{10}, Benzene and Pb (Dlgs 60/2002).

• The Dlgs 155/2010 establishes target values for As, Cd, Ni, Hg and Benzo (a) pyrene (Dlgs 155/2010).

1.4.3. Oxidative Stress Induction

Numerous epidemiological studies have shown a correlation between exposure to airborne particulate matter and cardiorespiratory disease outbreaks, which can be related to the generation of oxidative stress (Brook et al., 2010). Oxidative stress arises when there is an imbalance between the levels of reactive oxygen, nitrogen species or free radicals, and the biological system's natural antioxidant defense. ROS and RNS can be generated directly on PM surface or indirectly when cells interact with PM and can damage membrane lipids, proteins, and DNA, which can result in cell death via either necrotic or apoptotic processes. Elevated levels of oxidative stress lead to inflammatory response via activation of various transcription factors and stimulation of cytokine production. The right balance between oxidizing and antioxidant substances is essential to maintain unaltered physiological functions.

Oxidative phosphorylation processes and mitochondrial electron transport are the basis of ROS formation in cells by generating superoxide ion (O_2^-), hydroxyl radical hydroxide and hydrogen peroxide (H_2O_2). These molecules are able to interact with DNA, lipids and proteins creating physiological alterations. In particular, the superoxide ion, produced at the mitochondrial level, reacts with the sulfhydric centers of some enzymes and is converted into hydrogen peroxide by the superoxide dismutase enzyme. Hydrogen peroxide can also react with metals by reacting Fenton producing the hydroxyl radical (Schwarze et al., 2006; Vidrio et al., 2008).

$$Fe^{2+} + H_2O_2 \rightarrow Fe^{3+} + OH\cdot + OH^-$$

$$Fe^{3+} + H_2O_2 \rightarrow Fe^{2+} + OOH\cdot + H^+$$

Some enzymes such as superoxide dismutase, catalase and glutathione peroxidase (GPX; Brook et al., 2010), and antioxidant molecules such as vitamins, flavonoids, carotenoids, uric acid and glutathione provide antioxidant defenses in the body. If these are not enough to avoid oxidative action, the cell may suffer damage to the membrane phospholipids, causing the loss of selective transport

function. In addition, alterations in genetic expression can be caused by damage to nucleic acids and proteins by oxidation of cysteine groups with loss of protein structure.

Several studies indicates that the chemical composition, surface area and other characteristics of PM are potentially more closely linked to the induction of toxic responses (Kelly et al., 2012; Borm et al., 2007; Nel et al., 2005). As it is known, transition metals such as iron (Fe), copper (Cu), vanadium (V), and nickel (Ni) have been implicated as potential mediators of PM-related respiratory inflammation and associated with mortality and increased hospital admissions (Kelly et al., 2012; Cassee et al., 2013). Especially Fe and Cu are considered important in PM induced formation of ROS through the Fenton reaction (Schwarze, et al 2006; Vidrio et al., 2008). Furthermore, EC (also called black carbon or soot) and OC constitute a large part of particle mass and have been associated with mortality and hospital admissions in epidemiological studies. (Kelly et al., 2012; Janssen, et al., 2011; World Health Organization. REVIHAAP project: final technical report, 2013). The organic fraction of PM includes compounds such as PAHs and quinones, which have the ability to catalyze production of ROS (i.e. hydrogen peroxide) by undergoing redox recycling and reducing oxygen to produce superoxide radicals. Finally, the role of secondary organic aerosols (SOA), which are formed after photochemical oxidation of volatile organic precursors, is still unclear as presently it is difficult to distinguish between their toxicity and that of primary organic aerosols (Cassee, et al., 2013).

Thanks to the study of the chemical composition of the particles and the measurement of the PM oxidative potential, it would be possible to obtain important information about toxicological effects of the different chemical species that make up the PM.

1.4.5. Oxidative Potential Assays

Over the last years, several acellular assays (Table 1.3) have been developed to assess the PM oxidative potential. These assays reflect the chemical properties of PM, which are responsible for the oxidative stress induction in biological organisms. In the literature, the most used methods for this purpose are: 1,4-dithiothreitol (DTT), ascorbic acid (AA) and 2',7'-dichlorodihydrofluorescein (DCFH).

The 1,4-dithiothreitol ($HSCH_2CH(OH)CH(OH)CH_2SH$) is a strong reducing agent, commonly used as an acellular method for measuring the oxidative potential induced by airborne particulate matter (Verma et al., 2011; Cho et al., 2005). The assay is based on the measurement of the DTT depletion due to PM components able to transfer electrons to DTT, producing radical superoxide and other ROSs, such as hydrogen peroxide and radical hydroxide. Although it is a widely used method, in the literature there is little information about the specific substances that can oxidize DTT. Despite

several works have shown that the major substances responsible for oxidation of DTT are carbon species, such as elemental carbon, water-soluble organic carbon and polycyclic aromatic hydrocarbons (Verma et al., 2011; Cho et al., 2005), recent studies have shown its affinity for some metals, especially for Cu and Mn (Ntziachristos et al., 2007).

The AA assay consists of a simplified reproduction of the respiratory tract fluid (RTFL). RTFL is a fluid thin layer able to minimize respiratory tract diseases thanks to a high antioxidant power, it is rich in enzymes, proteins and small molecules such as vitamin E and C. In vitro and *in vivo* studies have shown that ascorbic acid, uric acid and glucose peroxide present in RTFL are consumed following the exposure of ozone, nitrogen dioxide and PM (Zielinski et al., 1999), making ineffective the natural antioxidant defenses, and generating oxidative stress. Ascorbic acid is a physiological antioxidant that prevents oxidation of lipids and proteins and its variation in RTLF may be determinant in the generation of adverse effects on human health.

The assay consists in the measurement of the AA depletion by UV-VIS detection. The decrease in concentration of the ascorbic acid corresponds to the capacity of the PM reactive species to catalyze the transfer of electrons from AA to oxygen, generating oxidative potential. Numerous studies have shown that ascorbic acid is mainly related to the redox activity of transition metals, but recent applications show further affinity for organic compounds, especially for quinones.

The 2',7'-dichlorodihydrofluorescein assay is widely used to measure the oxidative potential of atmospheric PM. It is based on the oxidation of DCFH, a non-fluorescent reagent, to DCF, a fluorescent compound, in the presence of ROS and horseradish peroxidase (HRP), a redox enzyme that primarily reacts with hydrogen peroxide and organic hydroperoxides. In general, the reaction mechanism involves two stages: in the first step, PM reacts with the enzyme, in the second step, the DCFH is oxidized to DCF, whose concentration, detected by fluorescence, is proportional to the ROS concentration. The measured fluorescence intensity is converted into hydrogen peroxide equivalents, which is used as an indicator of the ROS reactivity, by calibration of the instrument performed with H_2O_2 standard (Wang et al., 2012). For a proper evaluation of the final fluorescence measurement, it has to be considered that H_2O_2 is constantly present in deionized water, in equilibrium with the dissolved oxygen; as a consequence, there is a background signal not due to the presence of ROS.

Table 1.3. Overview of available acellular assays to assess the oxidative potential of PM.

Assay	Methodology/Principle
Depletion of antioxidants	Depletion of antioxidants in a synthetic respiratory tract lining fluid (RTFL) consisting of single or composite solutions of ascorbate acid, reduced glutathione, uric acid, measured by reverse phase high pressure liquid chromatography (HPLC) or spectrophotometer (Stoeger et al., 2009).
Consumption of dithiothreitol (DTT)	Based on the ability of PM to transfer electrons from DTT to oxygen, generating superoxide (Cho et al., 2005).
Fluorescent probes	Based on the principle that a fluorescent product is generated when a nonfluorescent probe molecule reacts with ROS: • p-hydroxyphenyl acetic acid (POHPAA) with horseradish peroxidase enzyme to detect hydroperoxides (Hasson et al., 2003). • DCFH probe which gets oxidized in the presence of ROS and horseradish peroxidase (Hung et al., 2001). • BPEAnit: probe based on trapping of ROS by profluorescent nitroxides (Miljevic et al., 2010). • CRAT: chemiluminogenic compounds, where certain acridinium esters are sensitive to superoxide (Zomer et al., 2011).
Formation of hydroxyl radical	• Based on the reaction of salicylic acid with hydroxyl radical to form dihydroxybenzoate (DHBA), measured by HPLC (DiStefano et al., 2009). • Measures OH-radical production by adding dimethyl sulfoxide (DMSO), quantified fluorometrically (Alaghmand et al., 2007). • Electron paramagnetic/spin resonance (EPR/ESR): Measures the formation of the hydroxyl (•OH) radical in PM suspensions in the presence of hydrogen peroxide and 5,5-dimethyl-1-pyrroline-N-oxide (DMPO) as a specific spin-trap (Shi et al., 2003).
Glyceraldehyde-3- Phosphate dehydrogenase (GAPDH) in activation	Based on the reaction between an electrophile and a reactive thiolate in GAPDH (Shinyashiki et al., 2008).

In addition, dissolved oxygen can interact with HRP to oxidize DCFH to DCF. Both these background signals are eliminated by subtracting the blank value to the value measured in the presence of PM. Furthermore, to reduce the background signal of H_2O_2 and to prevent photo-oxidation of DCFH, the procedure is performed in the dark. Today, DCFH is one of the most common methods used for ROS measurement in PM (Venkatachari et al., 2005).

References

Abbas, Z., Steenari, B. M., Lindqvist, O. 2001. A study of Cr (VI) in ashes from fluidized bed combustion of municipal solid waste: leaching, secondary reactions and the applicability of some speciation methods. Waste Management, 21(8), 725-739.

Alaghmand, M., Blough, N. V. 2007. Source-dependent variation in hydroxyl radical production by airborne particulate matter. Environmental Science and Technology, 41(7), 2364-2370.

Barone, T. L., Lall, A. A., Zhu, Y., Yu, R. C., Friedlander, S. K. 2006. Inertial deposition of nanoparticle chain aggregates: theory and comparison with impactor data for ultrafine atmospheric aerosols. Journal of Nanoparticle Research, 8(5), 669-680.

Barry, R. G., Chorley, R. J. 1992. Atmosphere, weather and climate. 6th ed. Routledge, London.

Borm, P. J., Kelly, F., Künzli, N., Schins, R. P., Donaldson, K. 2007. Oxidant generation by particulate matter: from biologically effective dose to a promising, novel metric. Occupational and environmental medicine, 64(2), 73-74.

Brook, R. D., Rajagopalan, S., Pope, C. A., Brook, J. R., Bhatnagar, A., Diez-Roux, A. V., ... Kaufman, J. D. 2010. Particulate matter air pollution and cardiovascular disease an update to the scientific statement from the American Heart Association. Circulation, 121, 2331–2378. https://doi.org/10.1161/CIR.0b013e3181dbece1.

Canepari, S., Perrino, C., Astolfi, M. L., Catrambone, M., Perret, D. 2009. Determination of soluble ions and elements in ambient air suspended particulate matter: Inter-technique comparison of XRF, IC and ICP for sample-by-sample quality control. Talanta, 7, 1821–1829.

Canepari, S., Marconi, E., Astolfi, M. L., Perrino, C. 2010. Relevance of Sb (III), Sb (V), and Sb-containing nano-particles in urban atmospheric particulate matter. Analytical and Bioanalytical Chemistry, 397, 2533–2542.

Cassee, F. R., Héroux, M. E., Gerlofs-Nijland, M. E., Kelly, F. J. 2013. Particulate matter beyond mass: recent health evidence on the role of fractions, chemical constituents and sources of emission. Inhalation Toxicology, 2514, 802-812.

CEN 1998. Air Quality. Determination of the PM_{10} fraction of suspended particulate matter – Reference method and field test procedure to demonstrate reference equivalence of measurement methods. Brussel (EN12341).

CEN 2005. Ambient air quality. Standard gravimetric measurement method for the determination of the PM2.5 mass fraction of suspended particulate matter (EN 14907).

Cho, A. K., Sioutas, C., Miguel, A. H., Kumagai, Y., Schmitz, D. A., Singh, M., Fernandez, F.A., Froines, J. R. 2005. Redox activity of airborne particulate matter at different sites in the Los Angeles Basin. Environmental Research, 99(1), 40-47.

DiStefano, E., Eiguren-Fernandez, A., Delfino, R. J., Sioutas, C., Froines, J. R., Cho, A. K. 2009. Determination of metal-based hydroxyl radical generating capacity of ambient and diesel exhaust particles. Inhalation toxicology, 21(9), 731-738.

EC 1997. Working Group on Particles. Position Paper on Ambient Air Pollution by Particulate Matter. http://europa.eu.int/comm.

EPA 1997. Reference Method for the Determination of Particulate Matter as PM_{10} in the Atmosphere. Federal Registrer, 62, No 138, Appendix M to part 50.

EPA 1999. Particulate Matter (PM2.5) Speciation Guidance (available at: http://www.epa.gov/ttn/amtic/files/ambient/pm25/).

Fang, T., Verma, V., Bates, J. T., Abrams, J., Klein, M., Strickland, M. J., Sarnat, S. E., Chang, H. H., Mulholland, J. A., Tolbert, P. E., Russell, A. G. 2015. Oxidative potential of ambient water-soluble PM 2.5 measured by Dithiothreitol (DTT) and Ascorbic Acid (AA) assays in the southeastern United States: contrasts in sources and health associations. Atmospheric Chemistry & Physics Discussions, 15(21) 30609-30644.

Fattorini, L., Ronzan, M., Piacentini, D., Della Rovere, F., De Virgilio, C., Sofo, A., Altamura, M.M., Falasca, G. 2017. Cadmium and arsenic affect quiescent centre formation and maintenance in Arabidopsis thaliana post-embryonic roots disrupting auxin biosynthesis and transport. Environ. Exp. Bot. 144, 37-48.

Feigl, G., Lehotai, N., Molnár, Á., Ördög, A., Rodríguez-Ruiz, M., Palma, J.M., Corpas, F.J., Erdei L., Kolbert, Z. 2014. Zinc induces distinct changes in the metabolism of reactive oxygen and nitrogen species (ROS and RNS) in the roots of two Brassica species with different sensitivity to zinc stress. Ann. Bot. 116(4), 613-625.

Goodarzi, F., Huggins, F. E. 2001. Monitoring the species of arsenic, chromium and nickel in milled coal, bottom ash and fly ash from a pulverized coal-fired power plant in western Canada. Presented at the Whistler 2000 Speciation Symposium, Whistler Resort, BC, Canada, June 25 - July 1, 2000. Geological Survey of Canada (GSC) Contribution No. 2000113. Journal of Environmental Monitoring, 3(1), 1-6.

Hasson, A. S., Paulson, S. E. 2003. An investigation of the relationship between gas-phase and aerosol-borne hydroperoxides in urban air. Journal of Aerosol Science, 34(4), 459-468.

Heintzenberg, J., Winkler, P. 1991. Elemental carbon in the atmosphere: challenges for the trace analyst. Fresenius' journal of analytical chemistry, 340(9), 540-543.

Hering, S. V., Flagan, R. C., Friedlander, S. K. 1978. Design and evaluation of new low-pressure impactor. I. Environmental Science and Technology, 12(6), 667-673.

Hlavay, J., Polyak, K., Weisz, M. 2001. Monitoring of the natural environment by chemical speciation of elements in aerosol and sediment samples. Presented at the Whistler 2000 Speciation Symposium, Whistler Resort, BC, Canada, June 25–July 1, 2000. Journal of Environmental Monitoring, 3(1), 74-80.

Hung, H. F., Wang, C. S. 2001. Experimental determination of reactive oxygen species in Taipei aerosols. Journal of Aerosol Science, 32, 1201–1211.

Kelly, F. J., Fuller, G. W., Walton, H. A., Fussell, J. C. 2012. Monitoring air pollution: Use of early warning systems for public health. Respirology, 17(1), 7-19.

Kleeman, M. J., Cass, G. R. 1998. Source contributions to the size and composition distribution of urban particulate air pollution. Atmospheric Environment, 32(16), 2803-2816.

Janssen, N. A., Hoek, G., Simic-Lawson, M., Fischer, P., Van Bree, L., Ten Brink, H., Keuken, M., Atkinson, R.W., Anderson, H.R., Brunekreef, B., Cassee, F. R. 2011. Black carbon as an additional indicator of the adverse health effects of airborne particles compared with PM10 and PM2. 5. Environmental health perspectives, 119(12), 1691.

John, W. 2001. Size Distribution Characteristics of Aerosols in: Baron, P. A., Willeke, K. Aerosol Measurement – Wiley InterScience New York.

Li, R., Kou, X., Geng, H., Xie, J., Yang, Z., Zhang, Y., Cai, Z., Dong, C. 2015. Effect of ambient PM 2.5 on lung mitochondrial damage and fusion/fission gene expression in rats. Chem. Res. Toxicol. 28, 408-418.

Manahan 2000. Chimica dell'ambiente, Editor: L Zoccolillo, Chapter 10, PICCIN.

Marcoccia, M., Ronci, L., De Matthaeis, E., Setini, A., Perrino, C., Canepari, S. 2017. In-vivo assesment of the genotoxic and oxidative stress effects of particulate matter on Echinogammarus Veneris. Chemosphere, 173, 124–134. https://doi.org/10.1016/j.chemosphere.2017.01.019.

Mark, D. 1999. Atmospheric Aerosol Sampling in: Harrison R M and. Van Grieken R E, Atmospheric Particles Vol 5.

Miljevic, B., Fairfull-Smith, K. E., Bottle, S. E., Ristovski, Z. D. 2010. The application of profluorescent nitroxides to detect reactive oxygen species derived from combustion-generated particulate matter: Cigarette smoke–A case study. Atmospheric Environment, 44(18), 2224-2230.

Moore, J. W., Ramamoorthy S. 1994. Heavy Metals in Natural Waters, Springer-Verlag, New York.

Morselli, L. (Ed.). 1991. Deposizioni acide: i precursori, l'interazione con l'ambiente ei materiali. Maggioli.

Mudway, I. S., Stenfors, N., Duggan, S. T., Roxborough, H., Zielinski, H., Marklund, S. L., Blomberg, A., Frew, A.J, Sandström, T., Kelly, F. J. 2004. An in vitro and in vivo investigation of the effects of diesel exhaust on human airway lining fluid antioxidants. Archives of Biochemistry and Biophysics, 423(1), 200-212.

Nel, A. 2005. Air pollution-related illness: effects of particles. Science 308(5723), 804-806.

Ntziachristos, L., Froines, J. R., Cho, A. K., & Sioutas, C. 2007. Relationship between redox activity and chemical speciation of size-fractionated particulate matter. Particle and fibre toxicology, 4(1), 5.

Pacyna, J. M. 1999. Source Inventories for Atmospheric Trace Metals in: Harrison R M and Van Grieken R E, Atmospheric Particles, Vol 5.

Perrino, C., Catrambone, M., Dalla Torre, S., Rantica, E., Sargolini, T., Canepari, S. 2014. Seasonal variations in the chemical composition of particulate matter: a case study in the Po Valley. Part I: macro-components and mass closure. Environmental Science and Pollution Research, 216, 3999-4009.

Phongphiphat, A., Ryu, C., Finney, K. N., Sharifi, V. N., Swithenbank, J. 2011. Ash deposit characterisation in a large-scale municipal waste-to-energy incineration plant. Journal of hazardous materials, 186(1), 218-226.

Puxbaum, H. 1991. Metal Compounds In The Atmosphere in: Merian E (Edr), Metals And Their Compounds In The Environment, pp 257-286.

Querol, X., Salvador, P., Sanchez de la Campa, A. 2003. D.G. Environmental Quality and Evaluation, pp 424. (In Spanish with English summary).

Ricci, P. F., Cirillo, M. C. 1985. Uncertainty in health risk analysis. Journal of hazardous materials, 10(2-3), 433-447.

Ronzan, M., Piacentini, D., Fattorini, L., Della Rovere, F., Eiche, E., Riemann, M., Altamura, M.M., Falasca, G. 2018. Cadmium and arsenic affect root development in Oryza sativa L. negatively interacting with auxin. Environ. Exp. Bot.151, 64-75.

Schwarze, P. E., Øvrevik, J., Låg, M., Refsnes, M., Nafstad, P., Hetland, R. B., Dybing, E. 2006. Particulate matter properties and health effects: consistency of epidemiological and toxicological studies. Human & experimental toxicology, 25(10), 559-579.

SENTIERI-ReNaM, GdL, Binazzi, A., Mangone, L. 2016. SENTIERI - Epidemiological study of residents in national priority contaminated sites: incidence of mesothelioma. Epidemiologia e prevenzione, 40(5Suppl1), 1-116.

Shi, T., Schins, R. P., Knaapen, A. M., Kuhlbusch, T., Pitz, M., Heinrich, J., Borm, P. J. 2003. Hydroxyl radical generation by electron paramagnetic resonance as a new method to monitor ambient particulate matter composition. Journal of Environmental Monitoring, 5(4), 550-556.

Shinyashiki, M., Rodriguez, C. E., Di Stefano, E. W., Sioutas, C., Delfino, R. J., Kumagai, Y., Froines, J.R., Cho, A. K. 2008. On the interaction between glyceraldehyde-3-phosphate dehydrogenase and airborne particles: evidence for electrophilic species. Atmospheric Environment, 42(3), 517-529.

Stoeger, T., Takenaka, S., Frankenberger, B., Ritter, B., Karg, E., Maier, K., Schulz, H., Schmid, O. 2009. Deducing in vivo toxicity of combustion-derived nanoparticles from a cell-free oxidative potency assay and metabolic activation of organic compounds. Environmental Health Perspectives, 117(1), 54.

Venkatachari, P., Hopke, P. K., Grover, B. D., Eatough, D. J. 2005. Measurement of particle-bound reactive oxygen species in rubidoux aerosols. Journal of Atmospheric Chemistry, 50, 49–58.

Vidrio, E., Jung, H., & Anastasio, C. 2008. Generation of hydroxyl radicals from dissolved transition metals in surrogate lung fluid solutions. Atmospheric Environment, 42(18), 4369-4379.

Wang, M., Beelen, R., Eeftens, M., Meliefste, K., Hoek, G., Brunekreef, B. 2012. Systematic evaluation of land use regression models for NO_2. Environmental science & technology, 46(8), 4481-4489.

WHO 2013. Review of evidence on health aspects of air pollution – REVIHAAP. First Results. WHO's Regional Office for Europe, Copenhaguen, 28 pp., http://www.euro.who.int/ data/ assets/pdf file/0020/182432/e96762-final.pdf, 2013.

Zielinski, H., Mudway, I. S., Berube, K. A., Murphy, S., Richards, R., Kelly, F. J. 1999. Modeling the interactions of particulates with epithelial lining fluid antioxidants. American Journal of Physiology, 277, L719–L726.

Zomer, B., Collé, L., Jedyńska, A., Pasterkamp, G., Kooter, I., Bloemen, H. 2011. Chemiluminescent reductive acridinium triggering (CRAT) - mechanism and applications. Analytical and bioanalytical chemistry, 401(9), 2945.

2. Health and Environmental Impact Assessment of PM Released by Specific Emission Sources

2.1. (A) Evaluation of the Potential of PM-Selected Components to Induce Oxidative Stress in Biological Organisms

Nowadays there is a growing scientific consensus in affirming that one of the mechanisms by which PM causes negative effects on biological organisms is the generation of oxidative stress. In fact, PM ability to generate ROS and RNS in biological systems contributes to genotoxicity and cytotoxic mechanisms responsible for cell damages.

As described above, various acellular assays, such as DTT, AA and DCFH, able to give information about PM capacity to generate oxidative stress, have been developed to estimate the toxicity of particulate matter released by different emission sources. However, each of these methods responds diversely to different PM components and simulates one of the many possible mechanisms of oxidative stress induction. Therefore, none of the OP assays can be *a-priori* considered as representative of ROS and RNS generation pathways in biological organisms. Furthermore, few studies have been addressed to the *in vivo* evaluation of PM effects on plants or animals so far, hence, relationships among OP and PM toxicological effects on living organisms are still largely unknown.

For these reasons, to evaluate the reliability of the OP methods as proxies of the production of ROS and RNS and to investigate relations among the oxidative potential of PM and its capacity to induce oxidative stress in biological organisms, we assessed the OPs of PM-selected components through the AA, DTT, and DCFH assays (OP^{AA}, OP^{DTT} and OP^{DCFH}) and then we studied their effects on the animal model *Caenorhabditis elegans* and on the root system of the plant model *Arabidopsis thaliana* (L.) Heynh. Finally, we deepened the knowledge on NO involvement in the root system development of *Oryza sativa* L. after exposure to As and Cd, to evaluate the potential of NO to restore the cellular balance between the ROS and the RNS.

2.1.1. (A1) Oxidative Potential of Particulate Matter Components Generated by Specific Emission Sources

Journal of Aerosol Science (2018), *126*, 99-109

Giulia Simonetti [a,*], Elena Conte [a], Lorenzo Massimi [a], Daniele Frasca [a,b], Cinzia Perrino [c], Silvia Canepari [a]

[a] Chemistry Department, Sapienza University of Rome, P. le Aldo Moro, 5, Rome 00185, Italy;
[b] CREA - Experimental Laboratory Renewable Energies – Biomass, Via della Pascolare, 16, Monterotondo, Rome 00015, Italy;
[c] C.N.R. Institute of Atmospheric Pollution Research, Via Salaria, Km 29,300, Monterotondo St., Rome 00015, Italy.

Abstract: Different acellular assays are currently used for the determination of the oxidative potential (OP) of particular matter (PM). In order to better understand the existing correlations between OP and the PM generated by specific emission sources, dusts generated from seven different sources (urban dust, soil, road dust, brake dust, pellet ash, coke, and desert dust) were chemically characterized and analyzed using three OP assays: dithiothreitol (DTT), acid ascorbic (AA) and 2′,7′-dichlorofluorescin (DCFH). In agreement with some previous literature studies, these assays provided very different results for each selected dust: their reliability as a proxy of ROS generation in biological system need then to be further investigated. When applied to the soluble fraction of these dusts, the DTT and AA assays were particularly sensitive toward pellet ash, while the highest OPDCFH values were measured for road dust. Multivariate analysis was used to confirm the correlations between the OP assay results and the chemical characteristics of the dust soluble fractions. DTT and AA assays appeared mostly influenced by organic and inorganic components, respectively. In the case of the DCFH assay, no clear correlations were highlighted, but, differently from the other assays, relevant OP values were measured also for dust of crustal origin. The insoluble fraction of the dusts, which is often not considered in this kind of study, generated, for all the considered assays, OP values even higher than those related to the soluble fraction.

Keywords: chemical characterization; soluble and insoluble fractions; 2′,7′-dichlorofluorescein (DCFH) assay; dithiothreitol (DTT) assay; acid ascorbic (AA) assay.

1. Introduction

Several epidemiological studies have established a consistent association between particulate matter (PM) concentrations and increased morbidity and mortality due to respiratory and cardiovascular diseases (Brook et al., 2010, Brunekreef et al., 2002, Hoek et al., 2013). Furthermore, various experimental studies have provided a plausible correlation between the PM oxidative capacity and its toxicity (Brook et al., 2010, Donaldson et al., 2001; Nel, 2005; Shi, Knaapen et al., 2003; Shi, Schins et al., 2003; Zielinski et al., 1999; Kelly & Fussell, 2012). Toxicological studies documented the ability of the inhaled PM to interfere in the oxidative stress processes and to induce pro-inflammatory effects in the nose, lungs, and cardiovascular system (Donaldson et al., 2001, Ning et al., 2003, Sheesley et al., 2003). Oxidative stress occurs when there is an imbalance between the level of reactive oxygen species (ROS) and the natural antioxidant defense of the biological system. The ROS class includes families of free radicals, ions, and other oxygenated molecules (such as organic and inorganic peroxides). Their formation in cells occurs through the reduction of oxygen by biological reducing agents such as nicotinamide adenine dinucleotide (NADH) and nicotinamide adenine dinucleotide phosphate (NADPH). Electron transfer enzymes and redox active chemical species, of both organic and inorganic nature, facilitate these processes (Donaldson et al., 2001, Ning et al., 2003). It is now commonly thought that oxidative damage occurs at high levels when the anti-oxidant defense is overwhelmed. These types of oxidative damages are detrimental for cells and can lead to cell death. However, the relationships between the toxicological mechanisms and the physico-chemical properties of PM are still largely unknown and need further research.

Literature studies describe several methods to measure the so-called aerosol oxidative potential (OP). The objective of these acellular assays is to provide a proxy of the oxidative capacity of PM samples. Dithiothreitol (DTT), ascorbic acid (AA) and 2′,7′-dichlorofluorescin (DCFH) are among the most commonly used methods. DTT is considered a chemical surrogate of the cellular reductants (such as NADH or NADPH) which reduce O_2 to superoxide anion (O_2^-) (Ayres et al., 2008, Kumagai et al., 2002). AA is a physiological antioxidant that prevents the oxidation of lipids and proteins (Valko, Morris, & Cronin, 2005). The DTT and AA assays involve the controlled incubation of the anti-oxidant (DTT or AA) in aqueous extracts of PM under controlled conditions (T = 37 °C and pH 7.4) and the measurement of its depletion over time (by following the decrease of absorbance at the wavelengths of 412 and 265 nm, respectively) (Cho et al., 2005, Fang et al., 2016). The antioxidant

loss rate represents the ability of the aerosol redox-active species to transfer electrons from DTT or AA to oxygen.

The DCFH assay was formerly developed for the in-vitro determination of ROS in biological cells (Keston & Brandt, 1965; Lebel, Ischiropoulos, & Bondy, 1992; Wang & Joseph, 1999; Halliwell & Whiteman, 2004), but in recent years it has been adapted and applied as an acellular method. In this assay, the non-fluorescent DCFH is oxidized to the fluorescent dichlorofluorescein (DCF) by ROS in the presence of horseradish peroxidase (HRP). The fluorescence of the DCF formed can easily be measured at the excitation and emission wavelengths of 485 and 530 nm, respectively (Hung & Wang, 2001; Venkatachari, Hopke, Grover, & Eatough, 2005; Venkatachari et al., 2007).

Although these methods are frequently applied to predict PM biological effects, there is still a gap of knowledge about the associations between the oxidative potential results obtained using these assays and health endpoints (Fang et al., 2016). Also, the role of the individual chemical species in OP measured by each one of these assays (OPDTT, OPAA and OPDCFH) still needs further investigation (Chirizzi et al., 2017, Perrone et al., 2016). Concentration of some transition metals (such as Cu and Mn) has been demonstrated to be very influent on the measured OPDTT and OPAA values, but its relationship with the ROS activity and with the subsequent toxicity of the dust is far to be ascertained (Charrier & Anastasio, 2012; Xiong, Yu, Wang, Wei, & Verma, 2017). Redox-active secondary organic species, such as quinones and their derivatives, have been shown to be relevant for OPDTT generation (Xiong et al., 2017) but their relevance for OPAA and OPDCFH is still to be assessed. According to DTT assay biomass burning showed high OP values, but its activity in OPAA is questionable, mechanisms and chemical species responsible for ROS production could be different for the two assays (Calas et al., 2018, Crobeddu et al., 2017, Fang et al., 2016). In the literature, the DCFH assays have received attention as the mechanisms involved in this enzymatic assay could be more representative of ROS generation pathways in cells and its behaviour as a proxy of oxidative stress in living organisms merits to be deepened (Fuller Wragg, Nutter, & Kalberer, 2014; Wang, Hopke, Sun, Chalupa, & Utell, 2011; Venkatachari & Hopke, 2008).

The knowledge of the relative relevance of the single source contributes in building up OP values could be of great help for properly addressing PM mitigation measures. Source apportionment of OP results from field campaigns have been attempted in some studies, but contradictory results were found (Calas et al., 2018, Chirizzi et al., 2017, Fang et al., 2016, Perrone et al., 2016).

In this work, we used AA, DTT, and DCFH assays for the determination of the OP of seven types of dust obtained from various emission sources and characterized by very different chemical composition. The aim was to investigate the roles of the single PM sources in OP measuring. Besides

the certified material NIST1648 (urban dust, UD), we considered some of the major PM sources. Soil (S) is the major natural component of PM while road dust (RD) is a complex mixture of natural soil with particles formed by mechanical abrasion of vehicle components (brakes, tires) and by deposition of road surfaces (asphalt). The contribution of road dust to PM is mainly due to resuspension caused by vehicular traffic, which is particularly relevant in urban areas (Canepari et al., 2008; Pant & Harrison, 2013). Brake dust (BD), produced by brake pad linings, is the part of RD containing the highest concentration of heavy metals and other toxic elements (Thorpe & Harrison, 2008; Canepari, Marconi, Astolfi, & Perrino, 2010). Saharan dust (SD) constitutes a major contribution to PM in the Mediterranean area after events of long-range transport from North Africa, these events are usually responsible for high PM_{10} concentrations and have been recently recognized as potentially harmful to human health (Pant & Harrison, 2013; Canepari et al., 2010; Goudie, 2014). Pellet ash (PA) is one of the few components of PM increased in concentration during recent years. This is because of the growing proliferation of pellet stoves for domestic heating. Several studies have recognized the damage caused by this emission source, which contains harmful species such as polycyclic aromatic hydrocarbons and toxic elements (De Oliveira Alves et al., 2011). Coke (C) was chosen because it contains very high concentrations of organic toxic species, which have been considered responsible for genotoxic and oxidative stress effects (Taioli et al., 2007, Vernile et al., 2013).

In most literature studies, the OP assays are applied only to the soluble fraction of PM samples collected on membrane filters (Fang et al., 2016, Fushimi et al., 2017, Simonetti et al., 2018; Charrier & Anastasio, 2012). In a few recent studies, however, there is evidence that the role of the insoluble fraction of PM in generating oxidative stress is not negligible at all (Knaapen et al., 2002, Marcoccia et al., 2017, Yi et al., 2014). Only in a few studies OP assays were applied to a water suspension of the whole dust collected by specific samplers (Cho et al., 2005, Daher et al., 2011, Huang et al., 2016). In this work, we applied the three assays to both the soluble and insoluble fractions of the dusts, in order to deepen understanding of the relationship between the solubility of the chemical species and the OP.

2. Experiments

2.1. Dust Collection

The dust samples were collected in different and very specific areas. The soil dust (S) was sampled in rural areas around the city of Rome, within a radius of 20 km. Road dust (RD) was obtained by freshly collecting the dust deposited on the road surface at several traffic sites in the centre of Rome (Central Italy). Brake dust (BD) was freshly collected from the brake linings of three different cars.

Saharan dust (SD) was collected in 2012 in Algeria, in the north of the Sahara Desert. The ash produced by pellet burning (PA) was freshly collected inside the hood of a domestic pellet stove and coke (C) was collected near a refinery plant, on the ground near a coal park (April 2016). More details about the collection procedure of these dust samples are given in Marcoccia et al. (2017) and in Pietrodangelo, Salzano, Rantica, and Perrino (2013). All the dust samples were homogenized and sieved (50 μm, Giuliani, Torino, Italy) before use with the exception of SD, which was sieved at 100 μm. All samples were stored at − 18 °C until the analysis in order to reduce the possible degradation of the samples. The stability of the freshly collected dusts was evaluated by analyzing the sample several times at regular intervals (after 1 and 2 weeks and after a month). The results did not show significant variation over time. In addition to the above dust samples, the certified material NIST1648a was used as the urban dust (UD) sample. Although not being representative of a freshly sampled urban dust, this dust is very stable and the measured parameters add further information on this certificate material. We could estimate the dimensional distribution of UD, S, BD and C by optical microscopy (Zeiss Imager M1m; Carl Zeiss Inc., Thornwood, NJ—USA). Images were converted into black/white and automatically enumerated by the freely available NIH ImageJ software v.1.46r (National Institute of Health, Bethesda, MD—USA, Perrino & Marcovecchio, 2016). Although the system did not allow to measure particles smaller than about 1 μm, for all the dusts more than 50% of particles had diameters lower than 10 μm (Supplementary Materials S1). This estimation was not possible for SD, PA and RD because of the low contrast of the images; a visive observation showed however similar results.

2.2. Dust Chemical Characterization

Macro-elements, soluble and insoluble fractions of micro-elements, elemental carbon (EC), water soluble and total organic content (WSOC and OC, respectively) and inorganic ions were determined in all the examined dusts. Major elements (Al, Si, Fe, Ca, Cr, and Ti) were determined using x-ray fluorescence (XRF, X-Lab2000, Spectro Analytical Instruments, Kleve-D), 3 g of sample and 4 g of extra-pure wax were pressed to obtain a tablet. The quantification of soluble inorganic ions (Ca^{2+}, Cl^-, NO_2^-, NO_3^- and SO_4^{2-}) was performed by ion chromatography (ICS1000, Dionex Co., Sunnyvale, CA, USA) after extraction in deionized water. Inductively coupled plasma mass spectroscopy (ICP-MS, Bruker 820, Bremen, Germany) was used for the determination of As, B, Cd, Ce, Co, Cs, Cu, La, Mn, Mo, Ni, Pb, Rb, Sb, Se, Sn, Sr, Tl, V, Zn, and Zr in their soluble (after water extraction of samples) and insoluble (after microwave assisted digestion of the residual by 2:1 HNO_3/H_2O_2 mixture) fractions. ICP-MS analysis of Al, Si, Ti, Fe and Cr was performed only on the

soluble fraction, due to the low efficiency of the acid digestion for these elements. A collisional reaction interface (CRI), alimented by 30 mL min^{-1} helium and 35 mL min^{-1} hydrogen (SOL Spa, Monza, Italy), was used to reduce the polyatomic interference of ^{75}As, ^{51}V, ^{52}Cr, and ^{55}Mn. A thermo-optical analyser (ECOC analyser, Sunset Laboratory, OR, USA, NIOSH-QUARTZ temperature protocol) was used for the determination of the total organic and elemental carbon, to this aim, known amounts (about 2 mg) of dust were deposited on a portion of quartz filter (Tissuquartz 2500QAT, 47 mm, PALL Life Sciences). Further details about the experimental procedures of these analyses are reported elsewhere (Canepari et al., 2009, Perrino et al., 2009). Water-soluble organic carbon (WSOC) was analysed by TOC-VCSH (Shimadzu) using the NPOC (non-purgeable organic carbon) procedure (Saarikoski et al., 2007). Before the instrumental analysis of WSOC, samples were extracted in 20 mL of Milli–Q water and subjected to mechanical agitation for 20 min. The solutions were then filtered through nitrocellulose (Millipore, pore size 0.45 µm) and 100 µL of chloride acid (10 M) were added.

2.3. Oxidative Potential Assays

Next, exactly 50 mg of each dust was weighed (Analytical Balance Gibertini Elettronica E505, sensitivity of 0.01 mg) and then extracted by mechanical agitation (20 min) in 50 mL of Milli-Q water. Subsequently the solutions were centrifuged (30 min at 13,145g and 25 °C, ALC Multispeed refrigerated centrifuge PK131R) in order to separate the soluble and the insoluble fractions. The soluble part was further filtered through a nitrocellulose filter (MF-Merck membrane, pore size 0.45 µm) before the application of the three OP assays. The insoluble part was re-suspended in 50 mL of water and again analysed for OP by the same procedures used for the soluble fraction. The suspensions were filtered (NC 0.45 µm) just prior to each instrumental analysis. For each sample, six replicates were performed. Lower dust amounts (25 mg) were also tested and OP values normalized by mass were equivalent to those measured at 50 mg.

2.3.1. DTT Procedure

According to the method reported by Fang et al. (2016), five aliquots (0.7 mL) of the soluble or residual fractions were mixed with 0.2 mL of phosphate buffer (1 M) and with 0.1 mL of DTT 1 mM, then incubated at 37 °C in a thermostatic bath (HAAKE DC3, Fisons). At regular intervals (0, 5, 10, 15 and 20 min), 1 mL of trichloroacetic acid 10% was added to one of the aliquots to stop the reaction. Then, 1 mL of each solution was mixed with 2 mL of Tris-buffer (0.08 M, containing EDTA 4 mM) and with 50 µL of 5,50-dithiobis-2-nitrobenzoic acid (DTNB) 0.2 mM. After 5 min, the absorbance

of the solutions was measured at 412 nm by UV–Vis spectrophotometry (UV–Vis, Varian Cary 50 UV–VIS Spectrometer). An operative blank was always measured in parallel. OPDTT was calculated as DTT consumption rate per unit of PM mass as follows:

$$\sigma DTT = -\sigma Abs \times \frac{N_0}{Abs_0};\ OP^{DTT} = \frac{\sigma DTT_s - \sigma DTT_b}{\frac{V_a}{V_e} \times m_{dust}}$$

where σAbs is the slope of absorbance at 412 nm vs. time (min^{-1}), Abs_0 is the initial absorbance calculated from the intercept of the linear regression of absorbance vs. time, N_0 is the initial number of moles of DTT added in the reaction (100 nmol), σDTT_s and σDTT_b are the rate of DTT consumption for the sample and for the operative blank (nmol min^{-1}), Ve and Va are the extraction volume (50 mL) and the actual sample volume added to the reaction vial (0.7 mL), respectively, m_{dust} is the weighted amount of dust (µg) and OP^{DTT} represents the mass normalized DTT activity (nmol min^{-1} μg^{-1}).

2.3.2. DCFH Procedure

The DCFH procedure was adapted from Huang, Zhang, Zhang, and Zeng (2016). Operating in the dark, a weighed amount (about 5 mg) of 2′,7′-Dichlorofluorescin diacetate was dissolved in 5 mL of ethanol and mixed with 20 mL of 0.01 M NaOH in order to favour de-acetalisation. The 5 µM DCFH solution was then kept in the dark at room temperature for 30 min before use. The HRP solution (0.5 units mL^{-1}) was prepared by dissolving the proper weight of commercial product (Type VI, essentially salt-free, lyophilized powder, ≥250 units/mg solid) in 1 L of phosphate buffer 25 mM at pH 7.4. It was incubated at 37 °C for 15 min before use. Aliquots of 5 mL of the HRP solution were mixed with 1.5 mL of the sample (soluble or residual fraction) and with 125 µL of the DCFH solution. The mixture was then kept at 37 °C for 15 min and transferred by a peristaltic pump (1 mL min^{-1}) to a fluorescence detector (Jasco FP-920) for the measurement of the emitted radiation at 530 nm (excitation wavelength 427 nm). A calibration curve was obtained daily using standard H_2O_2 solutions (5×10^{-8}, 1×10^{-7}, 2×10^{-7}, 5×10^{-7} and 1×10^{-6} M) instead of the sample. The OP values (OP^{DCFH}, nmol H_2O_2 μg^{-1}) were obtained using the calibration curve to convert the obtained fluorescence intensity into H_2O_2 equivalents.

2.3.3. AA Procedure

According to the method reported by Fang et al. (2016), 2.4 mL of sample (soluble or residual fraction) were mixed with 0.3 mL of 0.5 mM phosphate buffer at pH 7.4 with 100 µL of 2 mM ascorbic acid and the mixture was kept at 37 °C. The absorbance variation at 265 nm was then

followed for 20 min by UV–Vis spectroscopy. OP^{AA} was calculated as the AA consumption rate per mass unit (nmol min^{-1} μg^{-1}) according to the following equations:

$$\sigma AA = -\sigma Abs \times \frac{N_0}{Abs_0};\ OP^{AA} = \frac{\sigma AA_s - \sigma AA_b}{\frac{V_a}{V_e} \times m_{dust}}$$

where σAbs is the slope of the absorbance of blanks vs. time (min^{-1}), Abs_0 is the initial absorbance calculated from the intercept of the linear regression of absorbance vs. time, N_0 is the number of AA moles added in the reaction vial (200 nmol), σAA_s and σAA_b are the rate of AA consumption for the sample and for the blank, respectively (nmol min^{-1}), V_e and V_a are the extraction volume (50 mL) and sample volume added to the reaction vial (2.4 mL), respectively, and m_{dust} is the weighted amount of dust (μg).

2.4. Statistical Elaboration

Multivariate statistical computations were performed using the statistical software R (R-project for statistical computing, Ver. 3.0, 32-bit). A principal component analysis (PCA) was calculated on the OP assay results (DTT, DCFH and AA) and on the data obtained by the chemical characterization of the dusts (EC, WSOC, OC, Al, Si, Fe, Ca, Cr, Ti, As, B, Cd, Ce, Co, Cs, Cu, La, Mn, Mo, Ni, Pb, Rb, Sb, Se, Sn, Sr, Tl, V, Zn, Zr Ca^{2+}, Cl^-, NO^{2-}, NO^{3-} and SO_4^{2-}). The PCA was performed in order to confirm possible correlations between the OP assay results and the chemical characteristics of the dusts. Soluble and insoluble fractions of the dusts were examined separately. The matrix of the data (seven dusts, six replicates) was transformed by performing row and column autoscaling. Autoscaling operations enable to correct variations of the data due to different scaling and units of the examined variables. These operations allowed to correct multiplicative variations of the data caused by variations in sample physical properties or in sample preparation and presentation.

3. Results and Discussion

3.1. Chemical Composition of the Dusts

Tables 1 and 2 report the concentrations of the analysed chemical species in the soluble and insoluble (respectively) fractions of the selected dusts. Because of analytical hindrances, the concentration of some species in the insoluble fraction could not be directly measured. In particular, Al, Si, Fe, Ti and Cr concentration in the residual fraction were calculated by subtracting the value obtained by ICP-MS (soluble fraction) from the value obtained by XRF. Similarly, the concentration of the insoluble fraction of Ca was obtained as the difference between their total concentration measured by XRF and the concentration of Ca^{2+} ion measured by IC, while the insoluble organic content (WIOC) was

obtained by subtracting WSOC from OC. As expected, the chemical composition of the two fractions differed significantly among the dusts. For all the samples, the insoluble fraction contained more than 50% of the total determined concentration. In the coke sample only 2% of the measured components were present as soluble species, while in the NIST, soil and pellet ash samples the overall percentage of soluble species was of about 40%. Soluble species represented about 10–15% of the total measured concentration in brake dust, road dust and Saharan dust. More specifically, most of the elements that are typically associated with the geo-crustal component (Al, Si, Ti and Cr) are almost completely contained in the insoluble fraction, independent from the dust considered. Among the crustal elements, only Ca had a solubility percentage of about 50%.

Fe, Mn and Cu are often indicated as redox-active elements (Mates, Perez Gomez, & Nunez De Castro, 1999). Fe is a major component of brake dust (about 20% of the total mass), as a consequence, its concentration is relatively high also in the other dusts influenced by vehicular traffic (NIST and Road dust, about 40 and 60 g/kg, respectively). Its solubility is low and the soluble fraction of Fe is of about 6 g/kg in brake dust and NIST, and 0.5 g/kg in road dust. Cu was present in significant concentrations in brake dust, its total concentration was split into 4.2 g/kg of insoluble species and 0.7 g/kg of soluble species. Mn was present in the selected dusts mainly as insoluble species (solubility percentages lower than 25% for all the dusts, with the exception of NIST in which the soluble fraction was about 45%). Mn concentration was very high in the pellet ash: about 2 g/kg in the soluble fraction and almost 18 g/kg in the insoluble fraction. In all the other dusts, the total Mn concentration was lower than 1.5 g/kg.

The distribution of the remaining elements, including toxic elements such as Ni, Cd, Pb and As, between the soluble and insoluble fraction was variable. Their overall concentration as soluble species was higher than 2 g/kg in NIST, brake dust and pellet ash (3.9, 2.3 and 2.0 g/kg, respectively) and lower than 1 g/kg in the other dusts (0.1, 0.9, 0.4 and 0.2 g/kg in coke, road dust, Saharan dust and soil, respectively). Their total concentration as insoluble species was about 6 g/kg in NIST and brake dust, about 2 g/kg in road dust and pellet ash, 1.2 g/kg in coke and less than 1 g/kg in soil and Saharan dust (0.6 and 0.1, respectively). It is worth noting that Pb was present at very high concentration (6.5 g/kg, with a solubility percentage of 37%) in NIST, a urban dust collected before unleaded fuels were adopted.

Inorganic oxygenated ions (SO_4^{2-}, NO_3^- and NO_2^-) were present in PM almost exclusively as soluble salts. They were the predominant species in the soluble fraction of NIST (sulphate: 154 g/kg, nitrate: 47 g/kg) and were also present in significant concentrations in pellet ash and Saharan dust (overall concentrations: 46 and 28 g/kg, respectively).

Elemental carbon is an insoluble component that may play a key role in the redox equilibria, due to its adsorption and catalytic properties. It accounts for more than 30% of the coke sample and its concentrations are significant also in pellet ash and NIST, as combustion residue, and in brake dust, where it is probably present as a filling component.

Organic carbon is a major component in both the soluble and insoluble fractions of all the samples, with the only exception of Saharan dust. WSOC in PM is generally composed of a mixture of high-molecular-weight carboxylic, keto/carbonyl, amino/imino and nitro multifunctional organic compounds, as well as of smaller organic molecules such as anhydrides, sugars and keto- and α,ω-dicarboxylic acids (Cappiello et al., 2003, Ding et al., 2008, Duarte et al., 2007, Fuzzi et al., 2006, Graham et al., 2002). Most of these compounds could be involved in redox equilibria. Pellet ash and NIST contained a significant mass fraction of WSOC (about 2%). Although a determination of the speciation of OC was not attempted in this work, it can be reasonably hypothesized that the WSOC was mainly constituted by oxygenated species secondary organic aerosol (SOA) formation in NIST (Simoneit et al., 1999) and by degradation products of cellulose (such as levoglucosan) in pellet ash (Miyazaki et al., 2009).

3.2. Oxidative Potential of the Soluble Fraction

Fig. 1 shows the results obtained by the application of the three OP assays to the soluble fraction of dusts (s-OP). All the assays gave very different results among the selected dusts. As largely expected and as already evidenced in other studies, the chemical composition is a key factor in determining the redox behaviour of the samples (Chirizzi et al., 2017, Perrone et al., 2016). However, very significant differences were also observed in the relative sensitivity of the three assays toward the same dust. The DCFH assay was the least selective method and led to appreciable s-OP values for all the considered dusts. Road dust, particularly rich in inorganic and organic soluble species, provided the highest s-OP^{DCFH} values. Similarly, high s-OP^{DCFH} values were measured for coke and Saharan dust, which contained the lowest overall concentration of soluble species.

The DTT assay yielded completely different results: the highest s-OP^{DTT} values were obtained for pellet ash and NIST, which contained the highest concentration of overall soluble species. In particular, with respect to the other considered samples, pellet ash and NIST were characterized by very high WSOC concentrations. Brake dust and coke, which also contained relevant WSOC concentrations, provided significant values of s-OP^{DTT}, while very low s-OP^{DTT} values were measured in the other samples. These results are in agreement with those of previous studies (Calas et al., 2018, Cho et al., 2005, Fang et al., 2016), which indicate that soluble organic compounds

contain species able to catalyse ROS generation by various reactions. These reactions lead to the formation of superoxide radicals that are probably responsible for oxidative potential values.

The AA assay was particularly sensitive toward pellet ash, but significant s-OP^{AA} values were measured also in brake dust, NIST and coke. It is worth noting that the OP values obtained in this study are smaller than observed in other studies; this is probably due to the different size distribution of the particles. Dusts that were considered in this study contain particles of dimensions up to 50 µm (100 µm for Saharan dust) that have smaller surface to mass ratio respect to PM_{10} or $PM_{2.5}$ samples, usually considered in literature studies. Larger particles are generally characterized by lower solubility (Canepari et al., 2008), but their contribution to the mass (by which OP data are normalized) is high.

The principal component analysis (PCA) performed on the obtained data confirmed correlations between the OP assay results and the chemical characteristics of the dusts. The high variability of the data provided statistically significant results. From Fig. 2 we observe that the 69.7% of the total explored variance was explained by the first two principal components (PC1 and PC2). Variables were grouped in three main clusters, each one characterized by the presence of one OP assay.

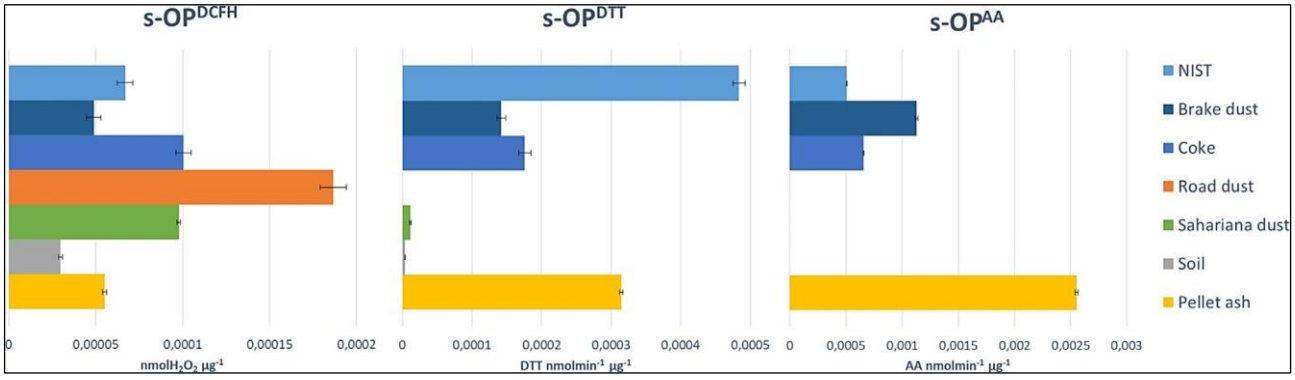

Fig. 1. Oxidative potentials measured in the soluble fraction of dusts.

The s-OP^{AA} is in the lower part of the loading plot as well as Mn, Sr, Rb, Se, P and Ca, which are in high concentrations in pellet ash (lower part of the score plot). Hence, we can confirm that acid ascorbic assay is sensitive towards pellet ash because it responds to high concentrations of water soluble fractions of Mn, Sr, Rb, Se, P and Ca. The same goes for DCFH and DTT. The position occupied by s-OP^{DCFH}, which is near Si, Zr, Ce, Al, La and Ti confirms that DCFH assay is sensitive towards soil, coke, brake dust, road dust and saharan dust because it responds to water soluble fractions of the crustal components of PM (typically characterized by elements such as Ti, Al and Si). Finally, Fig. 2 shows that DTT assay is influenced by several parameters including Mo, Ni, Cl^-, SO_4^{2-}

, Cd and WSOC, which are in the same part of the loading plot of s-OP^{DTT}. These variables allow for hypothesizing the sensitivity of DTT assay towards the combustive and secondary compounds of PM. Although the involved mechanisms have not been fully understood, Cu is assumed to be one of the most active PM component in generating s-OP^{AA} and s-OP^{DTT} (Keston & Brandt, 1965; Vernile et al., 2013; Miyazaki et al., 2009; Zou, Jin, Su, Li, & Zhu, 2016). By the principal component analysis performed on the data obtained in this study, Cu (near the loading plot centre of Fig. 2) appeared active in generating both s-OP^{AA} and s-OP^{DTT}. In fact, even though DCFH assay resulted sensitive towards soil, coke, brake dust, road dust and saharan dust, in the score plot of Fig. 2, brake dust appeared separated on the PC1 (41,3% of variance) from the other dusts characterized by high content of PM crustal components. The position of the brake dust, which is the examined powder with the highest concentration of Cu, can be explained by the higher sensitivity of AA and DTT assays towards Cu than DCFH assay.

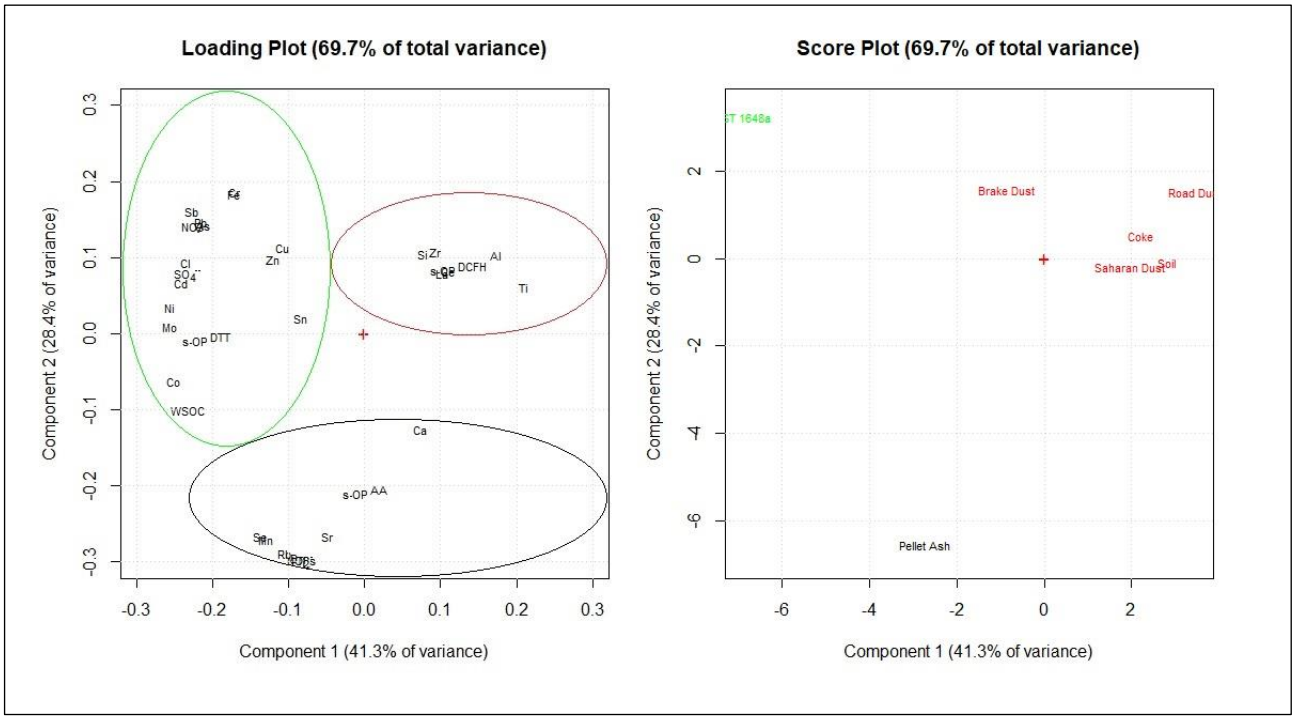

Fig. 3. Principal component analysis of OP assays' results and chemical characteristics of dusts' soluble fraction.

Overall, the obtained results confirm that the three OP assays have a different sensitivity towards the PM components, as already evidenced in other studies (Fang et al., 2016, Fang et al., 2017, Hedayat et al., 2015, Vernile et al., 2013). In terms of response to the single PM sources, AA and DTT assays

showed some similarities (significant OP values for pellet ash, NIST, brake dust and coke, very low OP values for soil, road dust and Saharan dust) that could account for the positive correlations that have been found between OP^{AA} and OP^{DTT} (Vernile et al., 2013) in some field studies. However, the two assays, both based on the depletion of a reductant, confirmed to have different affinities towards the chemical species that are contained in the dusts, probably also because of different synergistic and antagonistic effects, which merit to be further investigated (Zou et al., 2016). Dusts of crustal origin, as well as other PM components, have been demonstrated to induce oxidative stress in living organisms (Marcoccia et al., 2017, Taioli et al., 2007). Among the considered OP assays, only DCFH produced significant OP values for RD, S and SD, therefore, its association with oxidative stress and health endpoints merits to be further investigated.

3.3. Oxidative Potential of the Insoluble Fraction

Some recent studies have evidenced the role of water-insoluble species in inducing OP (Fang et al., 2017, Verma et al., 2012, Zou et al., 2016). Generally, in these studies organic solvent are used to solubilize organic species of low or medium polarity, such as quinons and their derivatives, that have been demonstrated to be particularly active in generating ROS (Charrier & Anastasio, 2012; Verma et al., 2012; Yang et al., 2014). In this work, the OP values related to the insoluble fraction (i-OP) of dusts, as specified in the experimental section, were obtained by applying the assays to suspensions of the insoluble part of the dusts that remained after water extraction. To our knowledge, this procedure has never been used in previous studies and, undoubtedly, the obtained results are hardly indicative of the ability of dusts to generate ROS in living organisms. However, this approach could highlight new aspects that could influence the redox activity of dusts, such as surface morphology and composition, particle dimension etc. Furthermore, it has to be considered that the contact of solid particles with cells will occur in the respiratory tract, furthermore, in the case of combustion sources, nanoparticles able to enter blood stream may be present (Canepari et al., 2014, Sauvain et al., 2012).

The obtained i-OP results are reported in Fig. 3. As can be noted, the i-OP values are generally much higher than the s-OP ones (in most cases, one order of magnitude or more). This result confirms the role of the insoluble PM components in the generation of oxidative stress, already evidenced in a few studies (Fang et al., 2017, Verma et al., 2012, Zou et al., 2016).

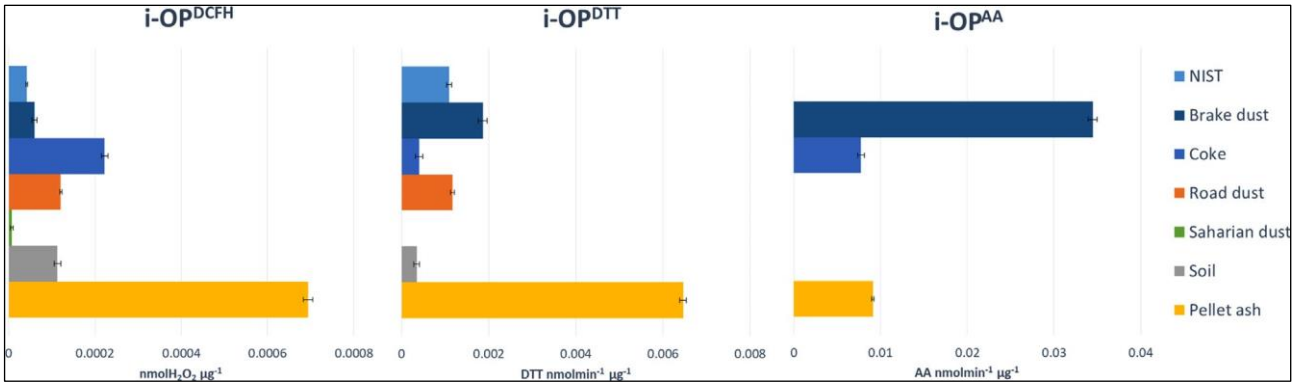

Fig. 2. Oxidative potentials measured in the insoluble fraction of dusts.

Pellet ash provided the highest i-OP^{DCFH} and i-OP^{DTT} values. It is noteworthy that for this dust, i-OP^{DTT} was more than 20-fold s-OP^{DTT}, and i-OP^{DCFH} more than 10-fold s-OP^{DCFH}. This result suggests that emissions due to domestic biomass burning, increased during the last years (Reche et al., 2012), may be particularly harmful for human health and environment. It is also interesting to note that, in the insoluble fraction, by using the DCFH and DTT assays, the only dust that exhibited low i-OP was the soil, and that the relative sensitivities of these two assays towards the considered dusts were quite similar. The AA assay, also regarding the insoluble fraction, showed instead very different behaviour: the i-OP^{AA} values were in fact particularly high (more than 30-fold the s-OP^{AA}) for the brake dust and significant for pellet ash and coke only.

A completely different behaviour was observed when the dataset relative to the insoluble fraction of dusts was elaborated using multivariate statistical analyses. From the principal component analysis of the OP assay results and the chemical characteristics of the dust insoluble fractions, no specific clusters were individuated in the loading plot or in the score plot (Supplementary Material S2). Therefore, for these data it was not possible to reliably correlate the three methods with the different specific chemical species of each dust. In this case, the correlations were much lower and difficult to interpret, probably also because in these samples there were many hydrophobic species that in this work were cumulatively identified as WIOC. The presence of a great number of components that affect the total variability makes the study of the residual parts very interesting. It is worth noting that the dusts considered in this study were not subjected to ageing processes and that the contribution from secondary organic species, which are considered to be among the main responsible of OP in the water insoluble fraction (Tuet et al., 2017, Verma et al., 2012, Xiong et al., 2017), should be low. Pursuing this study by identifying the insoluble organic chemical species that could be responsible

for the measured OP values and by considering morphological and surface characteristic of particles may provide more information about the mechanisms involved in these three methods.

4. Conclusions

The oxidative potential of the selected dusts obtained by the three assays indicated that most of the PM components are potentially able to induce oxidative stress in living organisms.

The soluble and insoluble fractions of each dust were separately analysed. In the soluble fraction, the DTT assay showed high sensitivity towards pellet ash and road dust, and seemed to be influenced mainly by the organic compounds of PM, including water-soluble organic carbon (WSOC). The ascorbic acid assay was more sensitive to dusts rich in metals and metalloids, such as brake dusts and pellet ash. The DCFH assay showed a certain affinity to organic species, but seemed to be less selective then the other assays. DCFH is the only assay that showed a relevant activity toward crustal components, whose ability in inducing in-vivo oxidative stress was shown in previous studies (Marcoccia et al., 2017). The suitability of this acellular assay to act as a proxy of ROS generation merits further investigations. Thanks to multivariate statistical computations of the data obtained it was possible to confirm the correlations between the OP assay results and the chemical characteristics of the soluble fraction of the dust.

The insoluble fraction of all the dusts provided noteworthy contributions to the oxidative potential. Although the three OP assays showed different sensitivity to the selected dusts, all of them yielded OP values higher in the insoluble fraction than in the soluble one. Knowledge of the chemical species and morphological characteristic responsible for this contribution, and of the mechanisms involved in the redox activities of the solid components, needs to be deepened.

Our results does not provide a univocal information about the most potent source contribution in terms of OP; due to the different mechanisms of oxidative stress generation in biological systems, it is probable that each assay only represent a partial indication about the capability of dusts to interfere in the oxidative stress processes. The effective ability of each OP assay as a proxy of oxidative stress processes need still to be fully verified. Future studies should be then focused toward achieving a deeper understanding of the relationships between acellular OP assay results and in-vivo biological effects of the dusts produced by individual sources.

Table 1. Chemical composition of the soluble fraction (mean and standard deviation; six replicates)

			NIST1648a	Brake dust	Coke	Road dust	Saharan dust	Soil	Ash pellet
Technique	**UoM**		**Mean** ± *SD*	**Mean** ± *SD*	**Mean** ± *SD*	**Mean** ± *SD*	**Mean** ± *SD*	**Mean** ± *SD*	**Mean** ± *SD*
ICP-MS	g/Kg	**Al**	**0.28** ± *0.04*	**0.162** ± *0.003*	**0.9** ± *0.1*	**1.76** ± *0.03*	**0.4** ± *0.1*	**0.69** ± *0.01*	**0.097** ± *0.002*
ICP-MS	mg/Kg	**As**	**81** ± *3*	**1.13** ± *0.05*	**0.60** ± *0.03*	**2.1** ± *0.1*	**1.1** ± *0.1*	**7.9** ± *0.6*	**2.9** ± *0.3*
ICP-MS	mg/Kg	**B**	**19.0** ± *0.4*	**8.5** ± *0.2*	**2.8** ± *0.8*	**1.7** ± *0.0*	**11.0** ± *0.6*	**0.4** ± *0.1*	**590** ± *30*
IC	g/Kg	**Ca**	**9.6** ± *0.2*	**27.9** ± *0.4*	**1.29** ± *0.02*	**48** ± *1*	**17.1** ± *0.3*	**139** ± *2*	**74** ± *1*
ICP-MS	mg/Kg	**Cd**	**48** ± *4*	**0.30** ± *0.02*	**0.02** ± *0.01*	**0.07** ± *0.01*	**0.12** ± *0.01*	**0.019** ± *0.001*	**13** ± *1*
ICP-MS	mg/Kg	**Ce**	**0.180** ± *0.001*	**0.106** ± *0.005*	**0.022** ± *0.005*	**2.2** ± *0.1*	**0.16** ± *0.01*	**0.30** ± *0.03*	**0.041** ± *0.002*
IC	mg/Kg	**Cl**	**4540** ± *80*	**660** ± *8*	**19** ± *4*	**190** ± *20*	**1220** ± *30*	**41** ± *7*	**1090** ± *60*
ICP-MS	mg/Kg	**Co**	**5.40** ± *0.01*	**1.06** ± *0.00*	**0.05** ± *0.00*	**0.62** ± *0.01*	**0.18** ± *0.01*	**0.24** ± *0.01*	**4.3** ± *0.3*
ICP-MS	mg/Kg	**Cr**	**28.0** ± *0.4*	**24.7** ± *0.4*	**0.83** ± *0.01*	**13.7** ± *0.2*	**4.0** ± *0.1*	**3.8** ± *0.1*	**4.6** ± *0.1*
ICP-MS	mg/Kg	**Cs**	**0.003** ± *0.001*	**0.210** ± *0.001*	**0.010** ± *0.003*	**0.212** ± *0.003*	**0.020** ± *0.002*	**0.28** ± *0.02*	**2.7** ± *0.2*
ICP-MS	mg/Kg	**Cu**	**275** ± *1*	**765** ± *2*	**13** ± *2*	**9** ± *1*	**3** ± *4*	**1.2** ± *0.1*	**37** ± *6*
ICP-MS	g/Kg	**Fe**	**5.9** ± *0.1*	**6.4** ± *0.1*	**1.0** ± *0.3*	**0.46** ± *0.01*	**0.24** ± *0.01*	**0.43** ± *0.01*	**0.02** ± *0.02*
ICP-MS	mg/Kg	**La**	**0.160** ± *0.002*	**0.067** ± *0.001*	**0.011** ± *0.006*	**1.585** ± *0.004*	**0.111** ± *0.002*	**0.17** ± *0.02*	**0.062** ± *0.004*
ICP-MS	mg/Kg	**Mn**	**340** ± *1*	**119.7** ± *0.3*	**6.4** ± *0.1*	**29.7** ± *0.1*	**6.2** ± *0.1*	**25** ± *1*	**1751** ± *24*
ICP-MS	mg/Kg	**Mo**	**5.70** ± *0.01*	**3.80** ± *0.01*	**0.827** ± *0.003*	**0.038** ± *0.002*	**0.009** ± *0.001*	**0.053** ± *0.005*	**3.6** ± *0.2*
ICP-MS	mg/Kg	**Ni**	**20.0** ± *0.4*	**3.97** ± *0.01*	**1.88** ± *0.04*	**1.15** ± *0.03*	**0.8** ± *0.1*	**1.6** ± *0.1*	**9** ± *1*
ICP-MS	mg/Kg	**Pb**	**2424** ± *9*	**5.94** ± *0.02*	**9.85** ± *0.1*	**5.36** ± *0.04*	**2.5** ± *0.2*	**0.54** ± *0.05*	**0.42** ± *0.02*
ICP-MS	mg/Kg	**Rb**	**26.4** ± *0.5*	**5.6** ± *0.1*	**0.6** ± *0.1*	**0.68** ± *0.05*	**6.4** ± *0.5*	**0.8** ± *0.1*	**310** ± *26*
ICP-MS	mg/Kg	**Sb**	**26.0** ± *0.1*	**13.9** ± *0.4*	**0.16** ± *0.03*	**0.047** ± *0.003*	**0.415** ± *0.001*	**0.002** ± *0.001*	**1.6** ± *0.2*
ICP-MS	mg/Kg	**Se**	**5.7** ± *0.2*	**0.27** ± *0.01*	**0.37** ± *0.01*	**0.44** ± *0.01*	**1.2** ± *0.1*	**0.15** ± *0.01*	**23** ± *8*
ICP-MS	g/kg	**Si**	**1.41** ± *0.03*	**0.52** ± *0.02*	**0.4** ± *0.1*	**5.2** ± *0.1*	**1.48** ± *0.01*	**0.32** ± *0.02*	**0.39** ± *0.01*
ICP-MS	mg/Kg	**Sn**	**0.310** ± *0.005*	**1.62** ± *0.03*	**0.130** ± *0.002*	**0.056** ± *0.002*	**0.002** ± *0.001*	**0.09** ± *0.01*	**0.46** ± *0.04*
ICP-MS	mg/Kg	**Sr**	**125** ± *4*	**98** ± *3*	**4** ± *3*	**164** ± *2*	**350** ± *10*	**150** ± *10*	**542** ± *29*
ICP-MS	mg/Kg	**Ti**	**1.20** ± *0.02*	**0.98** ± *0.02*	**13** ± *1*	**7.6** ± *0.1*	**8.6** ± *0.1*	**13.1** ± *0.2*	**0.061** ± *0.001*
ICP-MS	mg/Kg	**Tl**	**0.008** ± *0.002*	**0.04** ± *0.01*	**0.002** ± *0.001*	**0.026** ± *0.001*	**0.03** ± *0.01*	**0.014** ± *0.002*	**1.05** ± *0.05*
ICP-MS	mg/Kg	**V**	**89** ± *3*	**1.29** ± *0.04*	**1.08** ± *0.01*	**2.14** ± *0.01*	**0.84** ± *0.03*	**1.2** ± *0.1*	**3.7** ± *0.4*
ICP-MS	mg/Kg	**Zn**	**1023** ± *56*	**2120** ± *8*	**100** ± *5*	**673** ± *18*	**7** ± *2*	**18** ± *3*	**525** ± *27*
ICP-MS	mg/Kg	**Zr**	**0.270** ± *0.002*	**2.31** ± *0.01*	**0.018** ± *0.001*	**4.83** ± *0.03*	**0.007** ± *0.001*	**0.58** ± *0.02*	**0.07** ± *0.01*
IC	g/Kg	**NO_2^-**	**<0.1**	**<0.1**	**<0.1**	**<0.1**	**<0.1**	**<0.1**	**6.5** ± *0.3*
IC	g/Kg	**NO_3^-**	**47** ± *2*	**4.0** ± *0.4*	**<0.1**	**<0.1**	**<0.1**	**<0.1**	**2.2** ± *0.3*
IC	g/Kg	**SO_4^{--}**	**154** ± *4*	**5.9** ± *0.2*	**<0.1**	**<0.1**	**28.0** ± *1.0*	**0.9** ± *0.2*	**37** ± *1*
TOC	g/Kg	**WSOC**	**22** ± *1*	**5.7** ± *0.1*	**9.5** ± *0.2*	**2.1** ± *0.1*	**0.53** ± *0.02*	**0.3** ± *0.1*	**22** ± *1*

Table 2. Chemical composition of the insoluble fraction (mean and standard deviation; six replicates)

			NIST1648a	Brake dust	Coke	Road dust	Saharan dust	Soil	Ash pellet
Technique	**UoM**		**Mean** ± *SD*	**Mean** ± *SD*	**Mean** ± *SD*	**Mean** ± *SD*	**Mean** ± *SD*	**Mean** ± *SD*	**Mean** ± *SD*
XRF/ICP-MS	g/Kg	**Al**	**34*** ± *1*	**14.7** ± *0.4*	**12** ± *2*	**70** ± *2*	**69** ± *2*	**9.7** ± *0.2*	**6.1** ± *0.1*
ICP-MS	mg/Kg	**As**	**35.0** ± *0.2*	**18.0** ± *0.1*	**0.52** ± *0.04*	**1.6** ± *0.2*	**0.3** ± *0.1*	**87** ± *10*	**2.3** ± *0.3*
ICP-MS	mg/Kg	**B**	**44** ± *2*	**23.1** ± *0.8*	**0.7** ± *0.3*	**48.2** ± *0.8*	**2.2** ± *0.2*	**1.2** ± *0.3*	**235** ± *18*
XRF/IC	g/Kg	**Ca**	**53*** ± *1*	**12.9** ± *0.3*	**1.38** ± *0.03*	**29** ± *1*	**15** ± *1*	**131** ± *3*	**74** ± *2*
ICP-MS	mg/Kg	**Cd**	**26** ± *3*	**0.73** ± *0.08*	**0.05** ± *0.04*	**0.28** ± *0.03*	**0.76** ± *0.07*	**0.072** ± *0.002*	**20** ± *3*
ICP-MS	mg/Kg	**Ce**	**546** ± *4*	**26.2** ± *0.2*	**0.3** ± *0.1*	**109** ± *5*	**1.0** ± *0.1*	**10** ± *1*	**9** ± *1*
XRF/IC	mg/Kg	**Cl**	**-**	**-**	**1.0** ± *0.3*	**-**	**100** ± *4*	**-**	**-**
ICP-MS	mg/Kg	**Co**	**13.0** ± *0.4*	**13.9** ± *0.5*	**1.02** ± *0.04*	**10.8** ± *0.3*	**0.55** ± *0.02*	**1.6** ± *0.1*	**9** ± *1*
XRF/ICP-MS	mg/Kg	**Cr**	**374*** ± *9*	**3083** ± *74*	**9.6** ± *0.2*	**57** ± *1*	**48** ± *1*	**36** ± *1*	**20.4** ± *0.5*
ICP-MS	mg/Kg	**Cs**	**1.70** ± *0.02*	**2.99** ± *0.03*	**0.04** ± *0.01*	**20.90** ± *0.04*	**0.005** ± *0.001*	**2.5** ± *0.3*	**0.43** ± *0.05*
ICP-MS	mg/Kg	**Cu**	**336** ± *1*	**4286** ± *17*	**43** ± *11*	**71** ± *14*	**10** ± *18*	**13** ± *1*	**204** ± *53*
XRF/ICP-MS	g/Kg	**Fe**	**33*** ± *1*	**198** ± *5*	**16** ± *4*	**59** ± *1*	**40.7** ± *0.3*	**3.5** ± *0.1*	**3.7** ± *0.1*
ICP-MS	mg/Kg	**La**	**32** ± *1*	**12.7** ± *0.2*	**0.3** ± *0.2*	**54.4** ± *0.2*	**26.5** ± *0.1*	**5** ± *1*	**5.5** ± *0.6*
ICP-MS	mg/Kg	**Mn**	**450** ± *2*	**1093** ± *4*	**40** ± *1*	**475** ± *2*	**22.5** ± *0.4*	**96** ± *4*	**17869** ± *364*
ICP-MS	mg/Kg	**Mo**	**8.30** ± *0.03*	**171** ± *1*	**75.5** ± *0.1*	**0.83** ± *0.05*	**0.15** ± *0.02*	**0.65** ± *0.09*	**1.2** ± *0.1*
ICP-MS	mg/Kg	**Ni**	**61.0** ± *0.2*	**108** ± *3*	**355** ± *1*	**14.2** ± *0.1*	**5.1** ± *1.0*	**9** ± *1*	**28** ± *4*
ICP-MS	mg/Kg	**Pb**	**4127** ± *22*	**677** ± *4*	**8.9** ± *0.1*	**67.0** ± *0.7*	**0.010** ± *0.002*	**11** ± *2*	**55** ± *5*
ICP-MS	mg/Kg	**Rb**	**26** ± *1*	**27** ± *1*	**0.5** ± *0.1*	**240** ± *3*	**1.1** ± *0.1*	**10** ± *2*	**31** ± *4*
ICP-MS	mg/Kg	**Sb**	**23.4** ± *0.1*	**292** ± *1*	**4.07** ± *0.01*	**0.204** ± *0.002*	**2.08** ± *0.01*	**0.4** ± *0.1*	**1.7** ± *0.3*
ICP-MS	mg/Kg	**Se**	**20** ± *1*	**9.0** ± *0.4*	**9.0** ± *0.2*	**3.1** ± *0.1*	**0.37** ± *0.03*	**11** ± *2*	**0.02** ± *0.01*
XRF/ICP-MS	g/Kg	**Si**	**128*** ± *4*	**26** ± *1*	**21** ± *1*	**173** ± *5*	**228** ± *2*	**16** ± *1*	**6.5** ± *0.3*
ICP-MS	mg/Kg	**Sn**	**55.0** ± *0.1*	**1419** ± *3*	**14.7** ± *0.3*	**1.97** ± *0.01*	**0.02** ± *0.01*	**2.7** ± *0.5*	**21** ± *3*
ICP-MS	mg/Kg	**Sr**	**90** ± *4*	**159** ± *7*	**6** ± *7*	**674** ± *11*	**2.7** ± *0.1*	**375** ± *36*	**717** ± *57*
XRF/ICP-MS	mg/Kg	**Ti**	**3900*** ± *94*	**526** ± *13*	**894** ± *21*	**3835** ± *92*	**4532** ± *109*	**241** ± *6*	**18.9** ± *0.5*
ICP-MS	mg/Kg	**Tl**	**1.9** ± *0.5*	**0.3** ± *0.1*	**0.03** ± *0.01*	**1.30** ± *0.01*	**0.004** ± *0.002*	**0.11** ± *0.03*	**0.9** ± *0.1*
ICP-MS	mg/Kg	**V**	**38** ± *2*	**7.6** ± *0.4*	**557** ± *1*	**118** ± *4*	**4.9** ± *0.3*	**10** ± *1*	**8** ± *1*
ICP-MS	mg/Kg	**Zn**	**1200** ± *7*	**3197** ± *18*	**160** ± *12*	**318** ± *12*	**40** ± *18*	**86** ± *21*	**1157** ± *91*
ICP-MS	mg/Kg	**Zr**	**28.0** ± *0.3*	**87** ± *1*	**11.1** ± *0.1*	**89** ± *1*	**9.4** ± *0.1*	**12** ± *1*	**10** ± *2*
ECOC	g/Kg	**EC**	**23.0** ± *2.0*	**17** ± *1*	**310** ± *15*	**0.07** ± *0.01*	**<0.001**	**<0.001**	**44** ± *4*
ECOC/TOC	g/Kg	**WIOC**	**83** ± *4*	**30** ± *3*	**146** ± *5*	**12** ± *1*	**0.10** ± *0.02*	**41** ± *3*	**4** ± *1*

* certificate values of the reference material were used instead of XRF values, due to the low available amount of dust.

Acknowledgements

The work was partially funded by Sapienza Univerity of Rome, Italy (prot. n. RG11715C7C8801CF). A special thank is due to Francesca Marcovecchio (CNR-IIA) for analysis and interpretation of the dust images obtained by optical microscopy.

Conflicts of Interest

The authors declare no conflict of interest.

References

Ayres, J. G., Borm, P., Cassee, F. R., Castranova, V., Donaldson, K., Ghio, A., ... Marano, F. (2008). Evaluating the toxicity of airborne particulate matter and nanoparticles by measuring oxidative stress potential - A workshop report and consensus statement. Inhalation Toxicology, 20(1), 75–99.

Brook, R. D., Rajagopalan, S., Pope, C. A., Brook, J. R., Bhatnagar, A., Diez-Roux, A. V., ... Kaufman, J. D. (2010). Particulate matter air pollution and cardiovascular disease an update to the scientific statement from the American Heart Association. Circulation, 121, 2331–2378. https://doi.org/10.1161/CIR.0b013e3181dbece1.

Brunekreef, B., Stephen, T., & Holgate, S. T. H. (2002). Air pollution and health. The Lancet, 360(9341), 1233–1242. https://doi.org/10.1016/S0140-6736(02) 11274-8.

Calas, A., Uzu, G., Kelly, F. J., Houdier, S., Martins, J. M., Thomas, F., ... Jaffrezo, J. L. (2018). Comparison between five acellular oxidative potential measurement assays performed with detailed chemistry on PM 10 samples from the city of Chamonix (France). Atmospheric Chemistry and Physics, 18(11), 7863–7875. https:// doi.org/10.5194/acp-18-7863-2018.

Canepari, S., Perrino, C., Olivieri, F., & Astolfi, M. L. (2008). Characterisation of the traffic sources of PM through size-segregated sampling, sequential leaching and ICP analysis. Atmospheric Environment, 42(35), 8161–8175.

Canepari, S., Perrino, C., Astolfi, M. L., Catrambone, M., & Perret, D. (2009). Determination of soluble ions and elements in ambient air suspended particulate matter: Inter-technique comparison of XRF, IC and ICP for sample-by-sample quality control. Talanta, 7, 1821–1829.

Canepari, S., Marconi, E., Astolfi, M. L., & Perrino, C. (2010). Relevance of Sb (III), Sb (V), and Sb-containing nano-particles in urban atmospheric particulate matter. Analytical and Bioanalytical Chemistry, 397, 2533–2542.

Canepari, S., Astolfi, M. L., Farao, C., Maretto, M., Frasca, D., Marcoccia, M., & Perrino, C. (2014). Seasonal variations in the chemical composition of particulate matter: A case study in the Po Valley. Part II: Concentration and solubility of micro- and trace-elements. Environmental Science and Pollution Research, 21, 4010–4402.

Cappiello, A., De Simoni, E., Fiorucci, C., Mangani, F., Palma, P., Trufelli, H., ... Fuzzi, S. (2003). Molecular characterization of the water-soluble organic compounds in fogwater by ESIMS/MS. Environmental Science & Technology, 37, 1229–1240.

Charrier, J. G., & Anastasio, C. (2012). On dithiothreitol (DTT) as a measure of oxidative potential for ambient particles: Evidence for the importance of soluble transition metals. Atmospheric Chemistry, 201212, 9321–9333.

Chirizzi, D., Cesari, D., Guascito, M. R., Dinoi, A., Giotta, L., Donateo, A., & Contini, D. (2017). Influence of Saharan dust outbreaks and carbon content on oxidative potential of water-soluble fractions of PM2.5 and PM10. Atmospheric Environment, 163, 1–8.

Cho, A. K., Sioutas, C., Miguel, A. H., Kumagai, Y., Schmitz, D. A., Singh, M., ... Froines, J. R. (2005). Redox activity of airborne particulate matter at different sites in the Los Angeles Basin. Environmental Research, 99, 40–47.

Crobeddu, B., Aragao-Santiago, L., Bui, L. C., Boland, S., & Squiban, A. B. (2017). Oxidative potential of particulate matter 2.5 as predictive indicator of cellular stress. Environmental Pollution, 230, 125–133.

Daher, N., Ning, Z., Cho, A. K., Shafer, M., Schauer, J. J., & Sioutas, C. (2011). Comparison of the chemical and oxidative characteristics of particulate matter (PM) collected by different methods: Filters, impactors, and biosamplers. Aerosol Science and Technology, 45(11), 1294–1304.

De Oliveira Alves, N., Matos Loureiro, A. L., Cavalcante dos Santos, F., Halter Nascimento, K., Dallacort, R., De Castro Vasconcellos, P., ... Batistuzzo de Medeiros, S. R. (2011). Genotoxicity and

composition of particulate matter from biomass burning in the eastern Brazilian Amazon region. Ecotoxicology and Environmental Safety, 74, 1427–1433.

Ding, X., Zheng, M., Yu, L. P., Zhang, X. L., Weber, R. J., Yan, B., ... Wang, X. M. (2008). Spatial and seasonal trends in biogenic secondary organic aerosol tracers and water-soluble organic carbon in the southeastern United States. Environmental Science & Technology, 42, 5171–5176.

Donaldson, K., Stone, V., Seaton, A., & MacNee, W. (2001). Ambient Particle Inhalation and the Cardiovascular System: Potential Mechanisms. Environmental Health Perspectives, 109, 523–527.

Duarte, R. M. B. O., Santos, E. B. H., Pio, C. A., & Duarte, A. C. (2007). Comparison of structural features of water-soluble organic matter from atmospheric aerosols with those of aquatic humic substances. Atmospheric Environment, 41, 8100–8113.

Fang, T., Verma, V., Bates, J. T., Abrams, J., Klein, M., Strickland, M. J., ... Weber, R. J. (2016). Oxidative Potential of Ambient Water-Soluble PM2.5 in the Southeastern United States: Contrasts in Sources and Health Associations between Ascorbic Acid (AA) and Dithiothreitol (DTT) Assays. Atmospheric Chemistry, 16, 3865–3879. https://doi.org/10.5194/acp-16-3865-2016.

Fang, T., Zeng, L., Gao, D., Verma, V., Stefaniak, A. B., & Weber, R. J. (2017). Ambient size distributions and lung deposition of aerosol dithiothreitol-measured oxidative potential: Contrast between soluble and insoluble particles. Environmental Science & Technology, 51(12), 6802–6811.

Fuller, S. J., Wragg, F. P. H., Nutter, J., & Kalberer, M. (2014). Comparison of on-line and off-line methods to quantify reactive oxygen species (ROS) in atmospheric aerosols. Atmospheric Environment, 92, 97–103.

Fushimi, A., Saitoh, K., Hayashi, K., Ono, K., Fujitani, Y., Villalobos, A. M., ... Schauer, J. J. (2017). Chemical characterization and oxidative potential of particles emitted from open burning of cereal straws and rice husk under flaming and smoldering conditions. Atmospheric Environment, 163, 118–127.

Fuzzi, S., Andreae, M. O., Huebert, B. J., Kulmala, M., Bond, T. C., Boy, M., ... Poeschl, U. (2006). Critical assessment of the current state of scientific knowledge,

terminology, and research needs concerning the role of organic aerosols in the atmosphere, climate, and global change. Atmospheric Chemistry, 6, 2017–2038.

Goudie, A. (2014). Desert dust and human health disorders. Environment International, 63, 101–113.

Graham, B., Mayol-Bracero, O. L., Guyon, P., Roberts, G. C., Decesari, S. M., Facchini, M. C., ... Andreae, M. O. (2002). Water-soluble organic compounds in biomass burning aerosols over Amazonia − 1. characterization by NMR and GC-MS. Journal of Geophysical Research: Atmospheres, 107–8047.

Halliwell, B., & Whiteman, M. (2004). Measuring reactive species and oxidative damage *in vivo* and in cell culture: How should you do it and what do the results mean? British Journal of Pharmacology, 142, 231–255. https://doi.org/10.1038/sj.bjp.0705776.

Hedayat, F., Stevanovic, S., Miljevic, B., Bottle, S., & Ristovski, Z. D. (2015). Evaluating the molecular assays for measuring the oxidative potential of particulate matter. Chemical Industry & Chemical Engineering Quarterly, 21(1–2), 201–210.

Hoek, G., Ranjini, M. K., Beelen, R., Peters, A., Ostro, B., Brunekreef, B., & Kaufman, J. (2013). Long-term air pollution exposure and cardio- respiratory mortality: A review. Environmental Health, 12, 43. https://doi.org/10.1186/1476-069X-12-43.

Huang, W., Zhang, Y., Zhang, Y., Fang, D., & Schauer, J. J. (2016). Optimization of the measurement of particle-bound reactive oxygen species with 2',7'-di- chlorofluorescin (DCFH). Water, Air, & Soil Pollution, 227, 164. https://doi.org/10.1007/s11270-016-2860-9.

Huang, W., Zhang, Y., Zhang, Y., Zeng, L., Dong, H., Huo, P., & Schauer, J. J. (2016). Development of an automated sampling-analysis system for simultaneous measurement of reactive oxygen species (ROS) in gas and particle phases: GAC-ROS. Atmospheric Environment, 134, 18–26.

Hung, H. F., & Wang, C. S. (2001). Experimental determination of reactive oxygen species in Taipei aerosols. Journal of Aerosol Science, 32, 1201–1211. Kelly, F. J., & Fussell, J. C. (2012). Size, source and chemical composition as determinants of toxicity attributable to ambient particulate matter. Atmospheric Environment, 60, 504–526. https://doi.org/10.1016/j.atmosenv.2012.06.039.

Keston, A. S., & Brandt, R. (1965). The fluorometric analysis of ultramicro quantities of hydrogen peroxide. Analytical Biochemistry, 11, 1–5.

Knaapen, A. M., Shi, T., Borm, P. J., & Schins, R. P. (2002). Soluble metals as well as the insoluble particle fraction are involved in cellular DNA damage induced by particulate matter. Molecular and Cellular Biochemistry, 1, 317–326.

Kumagai, Y., Koide, S., Taguchi, K., Endo, A., Nakai, Y., Yoshikawa, T., & Shimojo, N. (2002). Oxidation of proximal protein sulfhydrics by phenanthraquinone, a component of diesel exhaust particles. Chemical Research in Toxicology, 15, 483–489. https://doi.org/10.1021/tx0100993.

Lebel, C. P., Ischiropoulos, H., & Bondy, S. C. (1992). Evaluation of the probe 2',7'-dichlorofluorescin as an indicator of reactive oxygen species formation and oxidative stress. Chemical Research in Toxicology, 5, 227–231.

Marcoccia, M., Ronci, L., De Matthaeis, E., Setini, A., Perrino, C., & Canepari, S. (2017). In-vivo assesment of the genotoxic and oxidative stress effects of particulate matter on Echinogammarus Veneris. Chemosphere, 173, 124–134. https://doi.org/10.1016/j.chemosphere.2017.01.019.

Mates, J. M., Perez Gomez, C., & Nunez De Castro, I. (1999). Antioxidant enzymes and human diseases. Clinical Biochemistry, 8, 595–603.

Miyazaki, Y., Kondo, Y., Shiraiwa, M., Takegawa, N., Miyakawa, T., Han, S., ... Weber, R. J. (2009). Chemical characterization of water-soluble organic carbon aerosols at a rural site in the Pearl River Delta, China, in the summer of 2006. Journal of Geophysical Research, 114, D14208. https://doi.org/10.1029/2009JD011736.

Nel, A. (2005). Air pollution-related illness: Effects of particles. Science, 308, 804–806. https://doi.org/10.1126/science.1108752.

Ning, L., Sioutas, C., Cho, A., Schmitz, D., Misra, C., Meiying Wang, J. S., ... Nel, A. (2003). Ultrafine particulate pollutants induce oxidative stress and mitochondrial damage. Environmental Health Perspectives, 111, 455–460.

Pant, P., & Harrison, R. M. (2013). Estimation of the contribution of road traffic emissions to particulate matter concentrations from field measurements: A review. Atmospheric Environment, 77, 78–97.

Perrino, C., Canepari, S., Catrambone, M., Dalla, Torre, S., Rantica, E., & Sargolini, T. (2009). Influence of natural events on the concentration and composition of atmospheric particulate matter. Atmospheric Environment, 43, 4766–4779.

Perrino, C., & Marcovecchio, F. (2016). A new method for assessing the contribution of primary biological atmospheric particles to the mass concentration of the atmospheric aerosol. Environment International, 87, 108–115.

Perrone, M. G., Zhou, J., Malandrino, M., Sangiorgi, G., Rizzi, C., Ferrero, L., ... Bolzacchini, E. (2016). PM chemical composition and oxidative potential of the soluble fraction of particles at two sites in the urban area of Milan, Northern Italy. Atmospheric Environment, 128, 104–113.

Pietrodangelo, A., Salzano, R., Rantica, E., & Perrino, C. (2013). Characterisation of the local topsoil contribution to airborne particulate matter in the area of Rome (Italy). Source profiles. Atmospheric Environment, 69, 1–14.

Reche, C., Viana, M., Amato, F., Alastuey, A., Moreno, T., Hillamo, R., ... Querol, X. (2012). Biomass burning contributions to urban aerosols in a coastal Mediterranean city. Science of the Total Environment, 427–428, 175–190. https://doi.org/10.1016/j.scitotenv.2012.04.012.

Saarikoski, S., Sillanpa, M., Sofiev, M., Timonen, H., Saarnio, K., Teinila, K., ... Hillamo, R. (2007). Chemical composition of aerosols during a major biomass-burning

episode over northern Europe in spring 2006: Experimental and modelling assessments. Atmospheric Environment, 41, 3577–3589.

Sauvain, J.-J., Rossi, M. J., & Riediker, M. (2012). Comparison of three acellular tests for assessing the oxidation potential of nanomaterials. Aerosol Science and Technology, 47, 218–227.

Sheesley, R. J., Schauer, J. J., Chowdhury, Z., Cass, G. R., & Simoneit, B. R. T. (2003). Characterization of organic aerosols emitted from the combustion of biomass indigenous to South

Asia. Journal of Geophysical Research: Atmospheres, 108, 4285. https://doi.org/10.1029/2002JD002981.

Shi, T., Knaapen, A. M., Begerow, J., Birmili, W., Borm, P. J., & Schins, R. P. (2003a). Temporal variation of hydroxyl radical generation and 8-hydroxy-2'-deox- yguanosine formation by coarse and fine particulate matter. Occupational and Environmental Medicine, 60, 315–321.

Shi, T., Schins, R. P., Knaapen, A. M., Kuhlbusch, T., Pitz, M., Heinrich, J., & Borm, P. J. (2003b). Hydroxyl radical generation by electron paramagnetic resonance as a new method to monitor ambient particulate matter composition. Journal of Environmental Monitoring, 5, 550–556.

Simoneit, B. R., Schauer, J. J., Nolte, C. G., Oros, D. R., Elias, V. O., Fraser, M. P., ... Cass, G. R. (1999). Levoglucosan, a tracer for cellulose in biomass burning and atmospheric particles. Atmospheric Environment, 33, 173–182.

Simonetti, G., Conte, E., Perrino, C., & Canepari, S. (2018). Oxidative potential of size-segregated PM in a urban and an industrial area of Italy. Atmospheric Environment, 187, 292–300.

Taioli, E., Šrám, R. J., Garte, S., Kalina, I., Popov, T. A., & Farmer, P. B. (2007). Effects of polycyclic aromatic hydrocarbons (PAHs) in environmental pollution on

exogenous and oxidative DNA damage (EXPAH Project): description of the population under study. Mutation Research, 620, 1–6.

Thorpe, A., & Harrison, R. M. (2008). Sources and properties of non-exhaust particulate matter from road traffic: A review. Science of the Total Environment, 400, 270–282.

Tuet, W. Y., Chen, Y., Xu, L., Fok, S., Gao, D., Weber, R. J., & Ng, N. L. (2017). Chemical oxidative potential of secondary organic aerosol (SOA) generated from the photooxidation of biogenic and anthropogenic volatile organic compounds. Atmospheric Chemistry, 17(2), 839–853.

Valko, M., Morris, H., & Cronin, M. T. (2005). Metals, toxicity and oxidative stress. Current Medicinal Chemistry, 12, 1161–1208. https://doi.org/10.2174/ 0929867053764635.

Venkatachari, P., Hopke, P. K., Grover, B. D., & Eatough, D. J. (2005). Measurement of particle-bound reactive oxygen species in rubidoux aerosols. Journal of Atmospheric Chemistry, 50, 49–58.

Venkatachari, P., Hopke, P. K., Brune, W. H., Ren, X., Lesher, R., Mao, J., & Mitchell, M. (2007). Characterization of wintertime reactive oxygen species concentrations in Flushing, New York. Aerosol Science and Technology, 41, 97–111. https://doi.org/10.1080/02786820601116004.

Venkatachari, P., & Hopke, P. K. (2008). Development and laboratory testing of an automated monitor for the measurement of atmospheric particle-bound reactive oxygen species (ROS). Aerosol Science and Technology, 42(8), 629–635.

Verma, V., Rico-Martinez, R., Kotra, N., King, L., Liu, J., Snell, T. W., & Weber, R. J. (2012). Contribution of water-soluble and insoluble components and their hydrophobic/hydrophilic subfractions to the reactive oxygen species-generating potential of fine ambient aerosols. Environmental Science & Technology, 46(20), 11384–11392.

Vernile, P., Tutino, M., Bari, G., Amodio, M., Spagnuolo, M., De Gennaro, G., & De Lillo, E. (2013). Particulate matter toxicity evaluation using bioindicators and comet assay. Aerosol and Air Quality Research, 13, 172–178.

Wang, H., & Joseph, J. A. (1999). Quantifying cellular oxidative stress by dichlorofluorescein assay using microplate reader. Free Radical Biology & Medicine, 27, 612–616.

Wang, Y., Hopke, P. K., Sun, L., Chalupa, D. C., & Utell, M. J. (2011). Laboratory and field testing of an automated atmospheric particle-bound reactive oxygen species sampling-analysis system. Journal of Toxicology (Article ID 419476).

Xiong, Q., Yu, H., Wang, R., Wei, J., & Verma, V. (2017). Rethinking dithiothreitol-based particulate matter oxidative potential: measuring dithiothreitol consumption versus reactive oxygen species generation. Environmental Science & Technology, 51, 6507–6514. https://doi.org/10.1021/acs.est.7b01272.

Yang, A., Jedynska, A., Hellack, B., Kooter, I., Hoek, G., Brunekreef, B., ... Janssen, N. A. (2014). Measurement of the oxidative potential of PM2.5 and its constituents: The effect of extraction solvent and filter type. Atmospheric Environment, 83, 35–42.

Yi, S., Zhang, F., Qu, F., & Ding, W. (2014). Water-insoluble fraction of airborne particulate matter (PM10) induces oxidative stress in human lung epithelial A549 cells. Environmental Toxicology, 2, 226–233. https://doi.org/10.1002/tox.21750.

Zielinski, H., Mudway, I. S., Berube, K. A., Murphy, S., Richards, R., & Kelly, F. J. (1999). Modeling the interactions of particulates with epithelial lining fluid antioxidants. American Journal of Physiology, 277, L719–L726.

Zou, Y., Jin, C., Su, Y., Li, J., & Zhu, B. (2016). Water soluble and insoluble components of urban PM 2.5 and their cytotoxic effects on epithelial cells (A549) in vitro. Environmental Pollution, 212, 627–635.

Supplementary Material S1.

Dimensional distribution of UD, S, BD and C obtained by optical microscopy. Particle dimensions were estimated as the average between major and minor axis evaluated by the NIH ImageJ software v.1.46r (National Institute of Health, Bethesda, MD—USA).

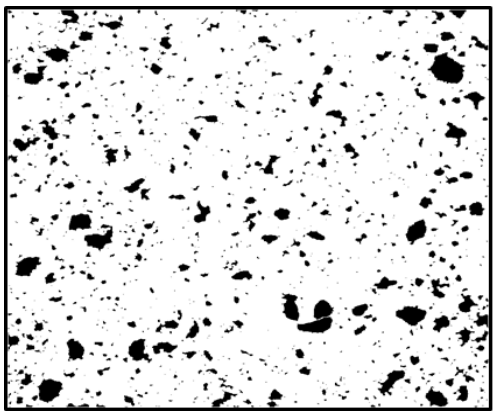

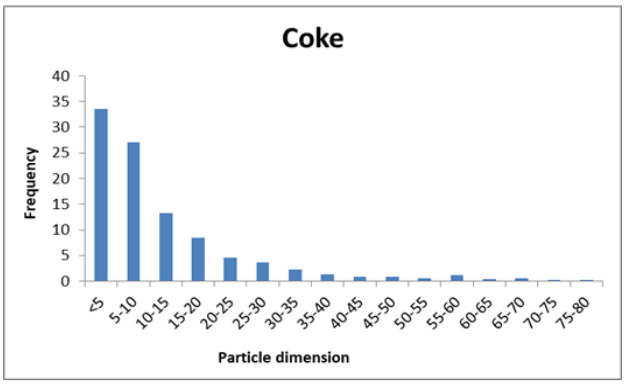

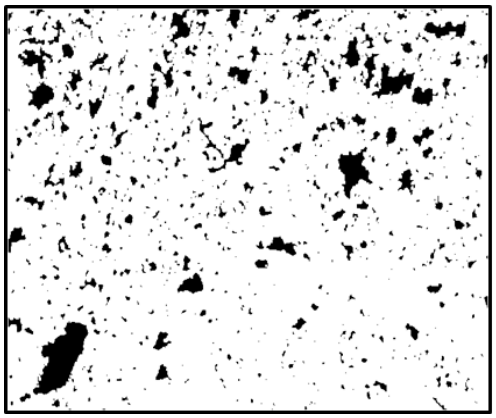

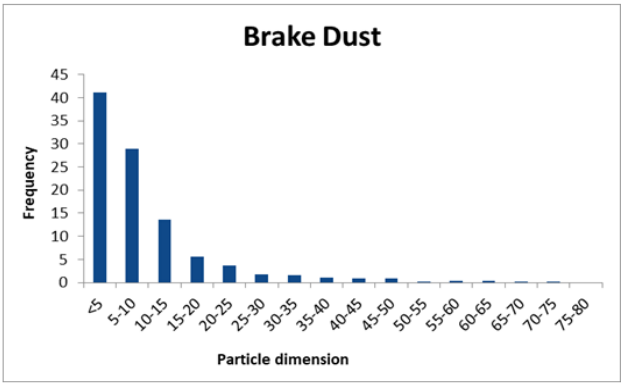

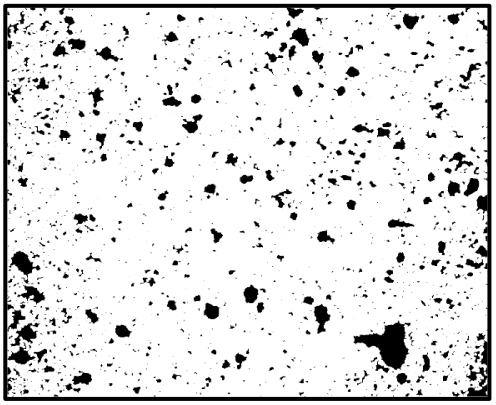

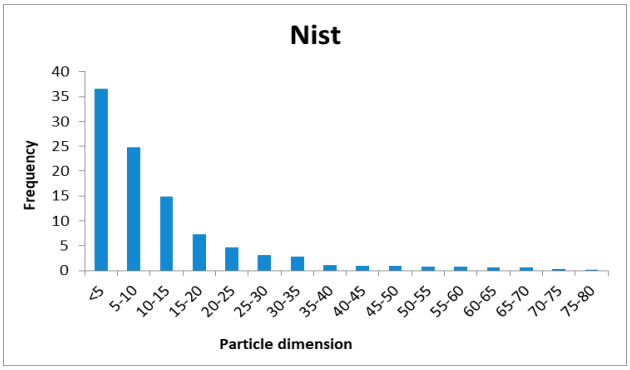

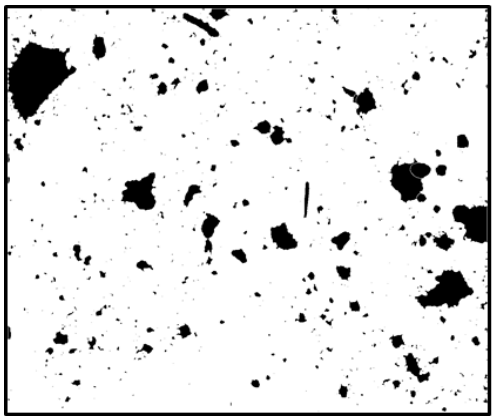

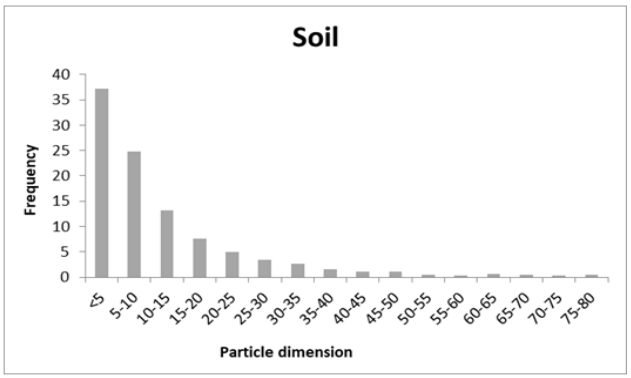

Supplementary Material S2.

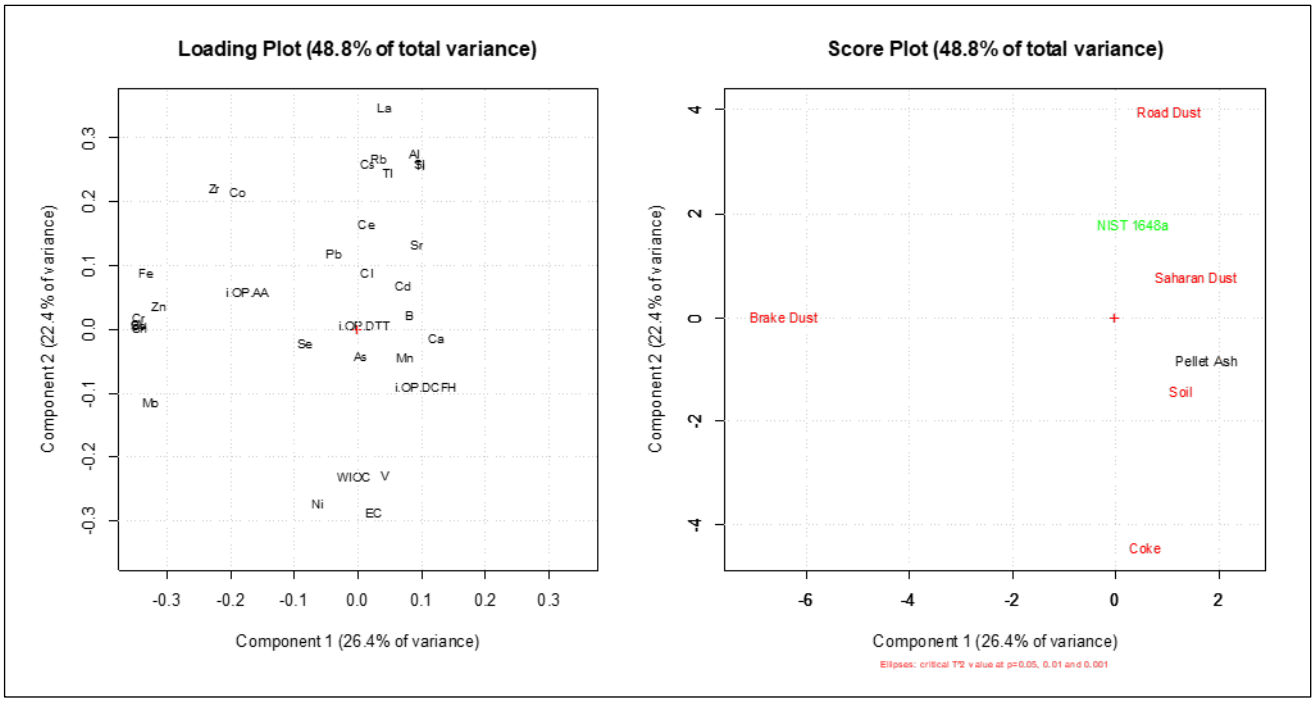

Fig. S2. Principal component analysis of OP assays' results and chemical characteristics of dusts' insoluble fraction.

2.1.2. (A2) Assessment of the Adverse Effects of Atmospheric Pollutants using the Animal Model *Caenorhabditis elegans*

Ecotoxicology and Environmental Safety (2019), *Reviewed*

Graziella Ficociello [a], Agnese Inverni [a,b], Lorenzo Massimi [b], Giulio Buccini [a], Silvia Canepari [b], Daniela Uccelletti [a,*]

[a] Department of Biology and Biotechnology "Charles Darwin", Sapienza University of Rome, P.le Aldo Moro, 5, 00185 Rome, Italy;
[b] Chemistry Department, Sapienza University of Rome, P.le Aldo Moro, 5, 00185 Rome, Italy;
[c] C.N.R. Institute of Atmospheric Pollution Research, Via Salaria, Km 29,300, Monterotondo St., 00015 Rome, Italy.

Abstract: Air pollution is recognized as the world's largest environmental health risk. In this work we evaluated *in vivo* the adverse effects of three relevant components of atmospheric dusts (brake dust, pellet ash and Saharian dust) employing the animal model *Caenorhabditis elegans*. Main endpoints of *C. elegans* such as life span, brood size and oxidative stress were addressed by exposing the nematodes to different dust concentrations. Brake dust and pellet ash affected the life span and increased significantly the oxidative stress of exposed nematodes, while Saharan dust showed no effects. Water soluble and insoluble fractions of these dusts were used to investigate the impact of the single fraction on *C. elegans*. The two factions of brake dust and pellet ash exerted different effects on *C. elegans* endpoints in terms of life span and oxidative stress response. These fractions influenced in different ways also the worm susceptibility to infection of two human pathogens (*Staphylococcus aureus* and *Pseudomonas aeruginosa)* altering besides the mRNA levels of innate immunity genes. In conclusion, our study showed that *C. elegans* is a valuable tool to investigate *in vivo* possible effects of atmospheric dusts.

Keywords: *Caenorhabditis elegans*, particulate matter, oxidative stress, immunity, *Pseudomonas aeruginosa*, *Staphylococcus aureus*.

1. Introduction

The term Particulate Matter (PM) indicates a mixture of solid and liquid particles suspended in the air. These particles are defined by the aerodynamic diameter (AD) that describe its transport ability in the atmosphere and/or inhaling ability through a respiratory organism (Esworthy, 2013).

Indeed, PM_{10} represents the sum of particles with AD up to 10 μm, $PM_{2.5}$ contains particles with AD up to 2.5 μm, and $PM_{0.1}$ or "ultrafine PM" particles with AD < 0.1 μm.

The chemical constituents of PM are very diversified and include inorganic ions (like sulphates, nitrates, ammonium, sodium, potassium, calcium, magnesium, and chloride); organic and elemental carbon, crustal material, metals (including cadmium, copper, nickel, vanadium, and zinc), and polycyclic aromatic hydrocarbons (PAH) (Cheung et al., 2011). In addition, biological elements such as allergens and microbial compounds had also been found as constituents of PM (Perrino and Marcovecchio, 2016; WHO, 2013).

The formation of airborne PM is associated to both anthropogenic and natural activities (Atkinson et al., 2010). Anthropogenic sources include solid-fuel combustion, industrial and agricultural activities as well as emissions from vehicles and from waste and biomass burning for household and commercial needs (Kim et al., 2015). A substantial contribute to PM in urban areas is also due to the erosion of the pavement by road traffic, and abrasion of brakes and tires (Srimuruganandam and Nagendra, 2012). The natural activities that induce PM formation are for example forest fires, volcanoes, dust storms and living vegetation (Misra et al., 2001).

In addition to the outdoor PM, the levels of indoor PM play also an important role on the human health. Various activities can generate particulates in indoor environment like cooking, pets, home stoves, liquid aerosols generate by household products and office or electronic equipment (Madureira et al., 2012, Manigrasso et al., 2019).

Many epidemiological studies have demonstrated that the exposure to PM is linked to severe adverse effects for human health (Kelly and Fussell, 2012; Khan et al., 2010; Merbitz et al., 2012; Pope et al., 2011; Raaschou-Nielsen et al., 2013; Turner et al., 2011). Indeed, exposure to airborne pollution has been associated with a range of cardiovascular and respiratory disease like acute coronary problems (Cesaroni et al., 2014) and stroke (Stafoggia et al., 2014), lung function alterations in adults (Adam et al., 2015) and children (Gehring et al., 2013), asthma (Cai et al., 2017) and cystic fibrosis (Goeminne et al., 2013). Moreover, in 2015 the Global Burden of Diseases Study has estimated that particulate matter is associated with 7.6% of global deaths and 4.2% of world disability-adjusted life years (Cohen et al., 2017).

Moreover, epidemiological studies demonstrated that PM exposure increases the susceptibility to respiratory infections (Neupane et al., 2010; Nuorti et al., 2000; Medina-Ramon et al., 2006). Data from *in vivo* and *in vitro* experiments supported the evidence of the capacity of PM to weaken the function of alveolar macrophages and airway epithelium cells, increasing the risk of infection, such as pneumoniae (Migliaccio et al., 2013; Mushtaq et al., 2011). Furthermore, exposure to fine PM is associated with accelerated bacterial colonization and aggravated respiratory infection (Brugha and Grigg, 2014; Chang et al., 2015; MacIntyre et al., 2014).

Jedrychowski and colleagues (Jedrychowski et al., 2013) show that exposure to air pollution may increase vulnerability of infants to respiratory infections. Indeed their cohort study show that children born to mothers exposed to high levels of outdoor $PM_{2.5}$ present more episodes of recurrent bronchitis and pneumonia.

Increasingly studies provide good evidence that PM adverse effects on pathogen infections are mediated by impairing immune responses in the respiratory tract. For instance, mice pre-exposed to diesel exhaust particles (DEPs), and subsequently infected with *P. aeruginosa*, show impaired bacterial clearance and increased airway cell death compared to controls (Harrod et al., 2005). Again, human monocyte-derived macrophages exposed to diesel exhaust show impaired cytokine release in response to bacterial products *in vitro* (Chaudhuri et al., 2012). Moreover, exposure to PM alters the immune responses against *Mycobacterium tuberculosis* in human respiratory epithelium, deregulating the expression of antimicrobial peptides (Rivas-Santiago et al, 2015).

Many *in vitro* studies on PM toxicity identified the generation of oxidative stress as one of the major players through which atmospheric particulate exerts its adverse biological effects (Li et al., 2008, 2015; Evans et al., 2013; Cachon et al., 2014). Oxidative stress can be defined as the imbalance between the generation of reactive oxygen species (ROS) and their neutralization by antioxidant mechanisms within an organism (Davies et al., 1999). ROS, because of their strong oxidative potential and indiscriminate reactivity, may damage cellular components like lipids in biological membranes, enzymatic proteins and DNA (Stadman and Levine, 2000; Jackson and Loeb, 2001).

It is worth noting that most of the epidemiological studies only considered the total PM mass concentration. Indeed, PM collected in a specific site is not a single entity, being composed by various urban and background dusts. Its chemical composition may substantially change in cities, from street to street, day to day and from season to season, depending on the strength of local and/or regional sources (Putaud et al., 2010); this variability is expected to have an influence on PM health effects, which still requires further investigations (Weinmayr et al., 2018). The availability of information on

the biological effects of the single compounds or PM sources may then furnish a relevant support in this field.

The nematode *Caenorhabditis elegans* is a widely used model organism, with 40% of the genome homologue to the human genome. Furthermore, many stress responses pathways, diseases, and physiological processes are conserved between higher organisms and *C. elegans* (Titus and Hengartner, 2006).

C. elegans is also widely applicable to investigate *in vivo* the adverse effects of toxicants at the organism level (Leung et al., 2008; Zhao et al., 2013). A series of sublethal endpoints such as life span, reproduction, development, locomotion, and oxidative stress have been employed to evaluate the effects of different environmental toxicants on nematodes (Donkin and Dusenbery, 1993; Leelaja and Rajini, 2013; Liu et al., 2012; McElwee et al., 2013; Tseng et al., 2013).

This model organism was used to investigate the pollution from different types of environmental sources (Clavijo et al., 2016; Rai et al., 2019; Zuo et al., 2017). However, only few studies explored the sensitivity of *C. elegans* to air pollutants (Chung et al., 2019; Sun et al., 2016; Wang et al., 2019; Zhao et al., 2014).

Herein, the toxicological impact of three samples of dust, which are representative of three important PM source contributions (brake dust, pellet ash and desert dust), on the nematode *C. elegans* was investigated analysing main endpoints like life span, reproduction (brood size) as well as oxidative stress. Additionally, the soluble and insoluble fractions of these dusts were employed to address the effects of the single fraction on the *C. elegans* endpoints.

C. elegans is also widely used as a model organism to dissect host innate immune responses in the host- pathogen interaction. Although *C. elegans* has no cell-mediated immunity, it presents a complex innate immune system that acts in infection resistance comprising avoidance behaviors, physical barriers, secretion and action of antimicrobial molecules, including lectins, lysozymes, and antibacterial factors (references in Marsh and May, 2012).

Thus, we further evaluated if the pre-treatment of *C. elegans* with our PM samples can affect the susceptibility to pathogen infection using the human pathogenic bacteria *Staphylococcus aureus* and *Pseudomonas aeruginosa*.

2. Materials and Methods

2.1. Sample Collection and Preparation

The dusts utilized in this work were collected as described in Pietrodangelo et al., 2013. Briefly, brake dust (BD) derived from the brake linings of three different cars; the pellet ash (PA), produced by pellet burning, was collected inside the hood of a domestic stove , while the Saharan dust (SD) originated in Algeria, in the North of the Sahara desert. All dusts were homogenized and sieved at 50 micron (Giuliani, Torino, Italy) before use.

Both the morphological and chemical analysis was previously described by Marcoccia et al., 2017. The dust preparations used for the *C. elegans* treatments were made in K –medium (0.3% w/v NaCl and 0.24% w/v KCl) with a stock solution of 10 mg/mL maintained at -20°C until use. To obtain the soluble and insoluble fractions a 10 mg/mL dust suspension was centrifugated to allow the separation of the two fractions. Then, the insoluble part was resuspendend in new K-medium at the concentration of 10 mg/mL. Elemental concentrations in the two K-medium solubility fractions (solution and suspension of insoluble compounds) used for the *C. elegans* exposure experiments are reported in Supplementary Table 1.

2.2. Worm and Bacterial Strains and Maintenance

The *C. elegans* strains used in the present study were provided by the *Caenorhabditis elegans* Genetics Center (CGC, University of Minnesota, USA). We used the wild type strain Bristol N2 and the transgenic stain CL2166 (dvIs19 [(pAF15)gst-4p::GFP::NLS] III.

The nematodes were maintained at 16 °C on nematode growth medium (NGM), and *Escherichia coli* (OP50; uracil-deficient strain) as food, according to standard procedure described by Brenner (Brenner, 1974). Before each experiment, the worms were incubated at 16°C until the plates had a high density of eggs and gravid nematodes. These were then washed off the plates, placed into centrifuge tubes, and the gravid nematodes were lysed with a bleaching mixture leaving only the eggs to obtain age synchronized populations.

Staphylococcus aureus ATCC 25923 and *P. aeruginosa* ATCC 15692 were the bacterial strains used in this work. Both bacteria were grown in LB broth at 37 °C for 16 hours. Bacterial lawns used for *C. elegans* infection assays were prepared by spreading 10µL of *S. aureus* or 200 µL of *P. aueruginosa* overnight culture on tryptic soy agar (TSA, BD, Sparks, MD) or modified NGM (50 mM NaCl and 0.35% peptone) agar plates, respectively. The plates were incubated at 37°C for an overnight.

2.3. C. elegans Life Span

Synchronized young adult N2 hermaphrodites were placed on 3.5 cm K-agar (2.36 g KCl, 3 g NaCl, 2.5 g Bacto-peptone, 17 g Bacto-agar, 1 mL cholesterol 5 mg/mL, 1 mL 1 M $CaCl_2$, 1 mL 1 M $MgSO_4$ in 1 L dH_2O) plate containing 120 µL of 5 or 10 mg/mL dust samples. The worms were maintained without food for all the time and 40 animals were utilized for each treatment. The plates were incubated at 16°C. Alive, censored (lost), and dead nematodes were recorded every 12 hours using the worm picker to assess viability.

2.4. Brood Size Assay

The brood size assay was conducted exposing, from the hatching until the L4 stage, the synchronized hermaphrodites to 5 mg/mL of total, soluble or insoluble fraction of dusts and fed with heat killed *E. coli* OP50. Then, randomly picked worms were transferred to a new 3.5 cm K-agar plate seeded with heat killed OP50 but without dusts. The adult worms were transferred to new K-agar plate every day until the parent worms stopped laying eggs (approximately 5 d), and the newly hatched larvae were counted.

2.5. Measurement of Intracellular ROS

The total levels of ROS were measured by using the fluorescent probe 2′, 7′-dichlorofluorescein diacetate (H_2DCFDA). Age-synchronized young adult N2 nematodes were exposed to 5 or 10 mg/mL dust samples at 16°C on K- agar, where no food source was provided. After 24 hours, they were washed three times to remove all dust traces and transferred into a 96-well microtiter plate containing 0.1 mL of 50 µM H_2DCFDA. The fluorescent intensity was measured immediately and after 180 min with an excitation wavelength of 485 nm and a 520 nm emission filter. Initial values were subtracted to the final values and results were expressed relative to untreated control.

2.6. Fluorescence Analysis of C. elegans GST-4::GFP Protein

Synchronized young adult worms expressing *gst-4::gfp* gene were treated for 24 hours with dust samples on K-agar plates without food. The hermaphrodites were then anesthetized with 20 mM sodium azide on 3% agarose pad on a glass slide and the fluorescence was viewed under a Zeiss Axiovert 25 microscope. The experiments were repeated three times with 10 worms per condition used each time. Images were processed using ImageJ (NIH, Bethesda, MD, USA) software.

2.7. Bacteria Colonization Assay

N2 worms at young adult stage were pre-treated for 24 hours with 5 mg/mL of dusts on K-agar plates, in the absence of food. Subsequently, nematodes were shifted for 48 hours at 25°C on TSA and modified NGM agar plates to be infected with *S. aureus* or *P. aeruginosa*, respectively. After infection, 10 animals per condition were washed and lysed according to Uccelletti et al., 2010. The worm lysates were plated onto LB-agar plates and the number of colony forming units (CFU) was counted after 48 hours of incubation at 37 ◦C.

2.8. Survival Assays of Infected C. elegans Animals

Synchronized young adult worms were pre-treated for 24 hours with the indicated dust fractions at 16°C on K-agar plates, without feeding. After this time, they were shifted at 25°C on TSA or modified NGM plates overspread with *S. aureus* or *P. aeruginosa*, respectively. 40 infected animals were transferred each day to new 3.5-cm-diameter plates containing the pathogen. Worm death was scored by the absence of movement provoked by the touch of a platinum wire.

2.9. Total RNA Extraction and Quantitative Real-time PCR Analysis

After 24 hours of exposure to dust samples on K-agar without food at 16°C, N2 worms were washed three times and total RNA was isolated using the miRNeasy Micro Kit (Qiagen, Cat. No. 217084) according to manufacturer's instructions. All samples were DNase treated (Ambion, Life Technologies, USA, Cat. No. AM1906) and cDNA was synthesized from 1 µg RNA using a SensiFast cDNA Synthesis Kit (Bioline, Cat. No. BIO-65053). Quantitative real-time PCR (qRT-PCR) analysis was performed on a RotorGene Q HRM real time PCR machine (QIAGEN, Hannover, Germany) in triplicate with the SensiFAST™ SYBR® Green Kit (Bioline, Cat. No BIO-98005, USA), according to data sheet instructions. Descriptions of primers for RT-PCR analysis are presented in Supplementary Table 2. Gene expression was normalized to reference gene (*cdc-42*) using the ΔΔCt method (Livak and Schmittgen, 2001).

2.10. Statistical Analysis

All experiments were performed at least in triplicate and data were plotted and analysed using GraphPad Prism 6 (San Diego, California, USA) software. The Kaplan-Meier graphs were used to evaluate the effects of the dust samples on the life span of the nematodes. The other data in this article were expressed as means ± standard deviation from the mean (S.D.). Differences between groups

were determined using analysis of variance (ANOVA) coupled with a Bonferroni post-test. Differences with *p* values <0.05 were considered significant and were indicated as follows: *$p<0.05$, ** $p<0.01$, ***$p<0.001$.

3. Results and Discussion

3.1. Impact of PM Constituents on C. elegans Life Span and Reproduction

We first analyzed if the exposure to collected samples could affect the life span of nematodes. For this reason, age-synchronized young adult worms were exposed in continuous to 5 or 10 mg/mL total material of the brake dust, pellet ash or Saharan dust.

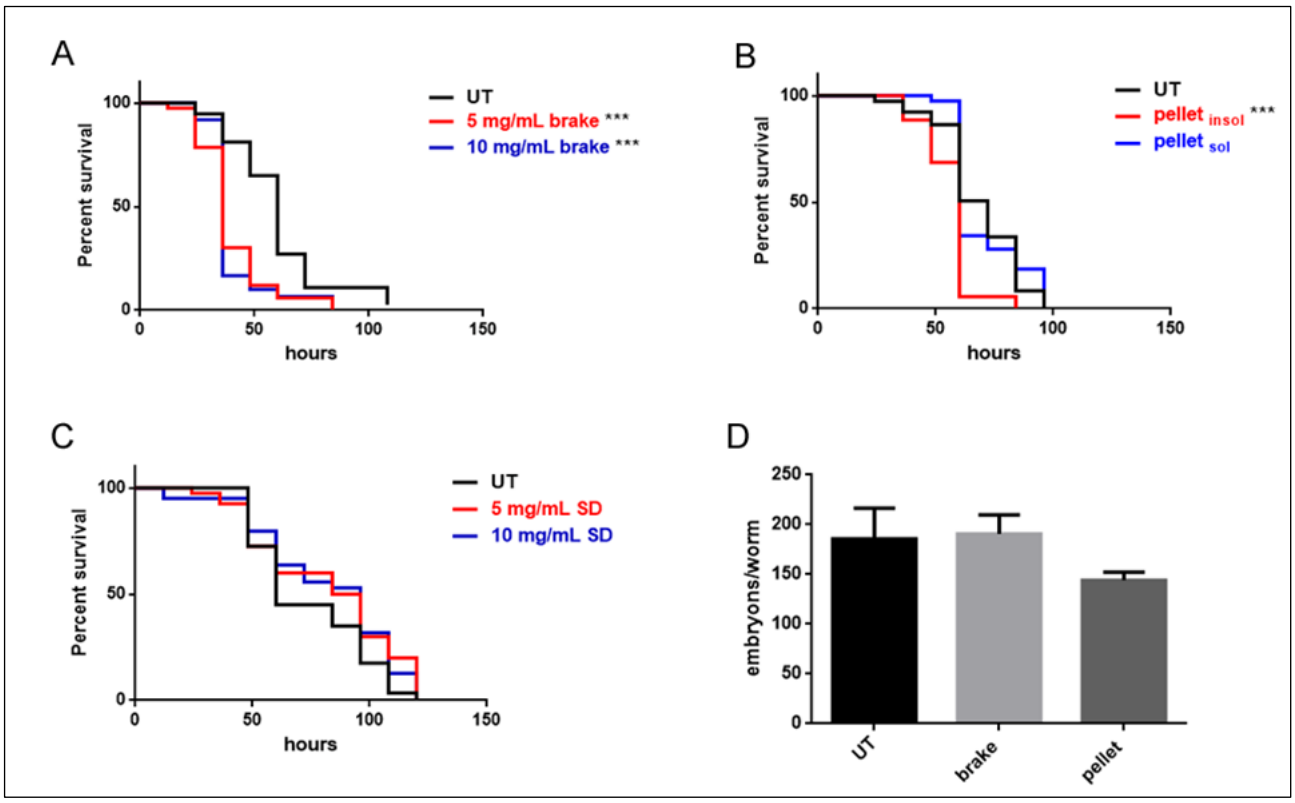

Fig. 1. Effects of collected urban dusts on life span and brood size of *C. elegans.* Survival curve of young adult N2 worms untreated (UT) or treated, in continuous, with the indicated concentrations of (A) brake dust, (B) pellet ash and (C) Saharan dust; ***p<0,001.(D)The ability of C. elegans to produce offspring after exposition to field dusts. Error bars represent standard errors.

Brake dust resulted significantly toxic both at 5 mg/mL and 10 mg/mL concentrations, meanwhile the ash, derived from the burned pellet, seemed to be toxic only at low concentration (Fig. 1A-B). This could be due to the aggregation of the ash in the aqueous solution at highest concentrations that makes the dust chemical components less bioavailable for the animals. The Saharan dust instead resulted to exert no adverse effect on nematode survival (Fig. 1C). We also examined the ability of our PM components to affect the embryo production in *C. elegans*. Brood size is indeed an important parameter for evaluating the influence of environmental stresses on reproduction of nematodes (Jiang et al., 2016). Thus, we exposed the wild type hermaphrodites to the total suspensions of our samples from embryos to L4 stages and later we analyzed the brood size of each worms. As shown in Fig. 1D, no significantly differences in the number of eggs laid per worm were observed for both concentrations of all types of dust. Thus, our results indicated as both brake dust and pellet ash affected the nematodes survival, meanwhile Saharan dust resulted ineffective. This reflects the different chemical composition of the dusts. Indeed, brake dust and pellet ash are enriched in toxic known elements as heavy metals and polyaromatic compounds, respectively, meanwhile Saharan dusts contained mainly crustal elements like Al, Si, Ca (Marcoccia et al., 2017).

3.2. Oxidative Stress Analysis of Worms Exposed to the Field Dusts

Several studies have shown as particulate matter can exert its toxic effects inducing oxidative stress (Jin et al., 2018; Li et al., 2008; Rao et al., 2018). For example Danielsen and colleagues showed as PM samples collected from a rural ambient with many operating wood stoves and the wood smoke PM (WSPM) are able to increase the production of ROS in both human lung epithelial cells A549 and monocytic THP-1 cell line (Danielsen et al., 2011). Moreover, rats exposed to fine (FP) and ultrafine (UFP) atmospheric particles present an increase of lung protein oxidation and the activation of the oxidative stress related genes both in the lung and aorta (Aztatzi-Aguilar et al., 2018). Based on this, we analyzed if our PM materials were able to induce oxidative stress in *C. elegans*. Employing H_2DCFDA assay we checked ROS levels in untreated and treated worms. We observed a 10-fold increase of ROS levels in nematodes exposed to both 5 mg/mL and 10 mg/mL of brake suspension. On the other hand, in animals treated with pellet ash, ROS content was about 60-fold more abundant than untreated animals. This result was in line with the data obtained by Marcoccia and colleagues that showed as pellet ash was more effective to generate oxidative damage, evaluated as DNA breaks using the comet assay on the amphipod *Echinogammarus veneris* (Marcoccia et al., 2017). Brake dust and pellet ash were also identified in a recent study (Piacentini et al., 2019) as the PM components

with the highest potential of inducing oxidative stress and root development alteration in *Arabidopsis thaliana*, a plant model organism. The obtained data also agree with the results obtained by applying to the same dusts three oxidative potential (OP) assays, which constitute acellular metrics for estimating the PM capability of inducing oxidative stress in living organisms largely used in the recent literature (Bates et al., 2019;).

Pellet ash at 10 mg/mL instead, did not alter the ROS level probably because, as for life span experiments, at the highest concentration it was less bioavailable. Moreover, Saharan dust resulted ineffective also in the induction of ROS production, (Fig. 2A), so that this dust could be considered as a negative control.

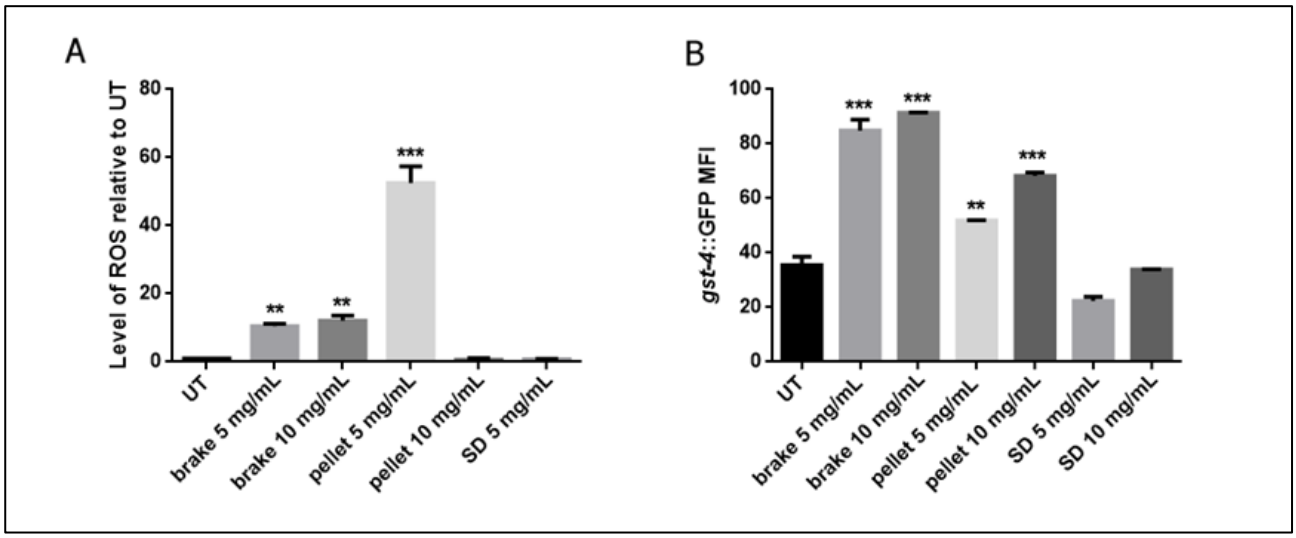

Fig. 2. Oxidative stress induction after exposure to PM samples. (A) ROS production levels estimated by H2DCFDA assay in treated and untreated (UT) N2 worms. (B) Graphical representation, using ImageJ software, of mean fluorescence intensity for *gst-4*::GFP strain after 24h of treatment with the indicated concentrations of dusts. Data, expressed as GST-4::GFP intensity (mean±SD), was obtained using at least 10 worms in each experimental group. **p<0.01, ***p<0.001.

Next, we examined whether the elevated levels of ROS observed in nematodes treated with brake and pellet dusts were correlated with variations in the detoxifying system. To test this, we used a reporter strain *dvls19* (GST-4::GFP) in which the GFP is fused to the promoter of the *gst-4* (glutathione *S*-transferase 4) gene that encodes one of the major antioxidant enzyme implicated in the oxidative

stress response and in regulation of ROS levels (Back et al., 2012; Link and Johnson, 2002; Tawe et al. 1998).

We treated the young adult transgenic animals for 24 hours with the PM samples at the indicated concentrations and then the GFP fluorescence was quantified in the whole body of the worms. As reported in Fig. 2B both brake dust and pellet ash induced a remarkably increase of GST-4::GFP signal. However, the level of fluorescence was higher in brake dust treated animals (about 50-fold higher than UT) than pellet ash treated ones (about 25 to 30- fold higher than UT). Saharan dust did not affect the GST-4 expression and the fluorescence was similar to that of the control animals. Since GST-4 is involved in the detoxification not only of reactive oxygen species but also of xenobiotics, this could explain why we found an higher GST-4::GFP fluorescence in worms treated with brake dusts but a lower ROS content than animals exposed to pellet. Indeed the brake dust shows, respect to pellet ash, a more elevated content of metals that is usually associated to the toxicity of PM (Chen and Lipmann, 2009; Fortoul et al., 2015; Marcoccia et al., 2017). Furthermore, we found that pellet ash at 10 mg/mL was more effective to induce GST-4::GFP expression than at 5 mg/mL. This probably accounts for the presence of a reduced amount of chemical elements available to the nematodes that activates signaling pathways protecting the cells against injury.

3.3. Evaluation of C. elegans Survival With the Insoluble and Soluble Fraction of PM Materials

Our next goal was to investigate the contribution of the water soluble and insoluble fractions of each dust on *C. elegans* endpoints. Since the 5 mg/mL concentration of PM resulted the best concentration in previous experiments, we decided to continue only with this concentration in the next tests. First, we assessed the survival exposing the young adult animals to the insoluble or soluble fractions of brake dust, pellet ash and Saharan dust. As showed in Fig. 3, the separate fractions of brake dust did not influence the life span of nematodes (fig. 3A), indicating that is necessary the combination of the two fractions to exert effects on *C. elegans* life span. Furthermore, we observed that the insoluble part of pellet ash, but not the soluble one, reduced significantly the *C. elegans* survival (fig. 3B). These data are in agreement with the chemical analysis of the two fractions of the collected dusts showing that most of the chemical elements are present mainly as insoluble species (Supplemental Table 1). Moreover, the results obtained exposing the amphipod *Echinogammarus veneris* to the dust fractions suggest that bioaccumulation in the gammarids occurs preferably through the interaction with suspended solids. (Marcoccia et al., 2017). Besides, Zou and colleagues showed as, on A549 cells, the insoluble water fraction of $PM_{2.5}$ induces with respect to soluble part, an higher cytotoxic

effect assessed with a lactic dehydrogenase (LDH) assay to check the loss of cell membrane integrity (Zou et al., 2016). On the contrary, we found that the sand dust fractions exerted a beneficial effect on worm survival inducing an extension of nematode life span (fig. 3C).

Like for the total suspensions, we also examined the brood size of N2 worms exposed to the dust fractions from the embryonic stage to L4; in this case also we did not observe changes in the nematode ability to produce offspring (data not shown).

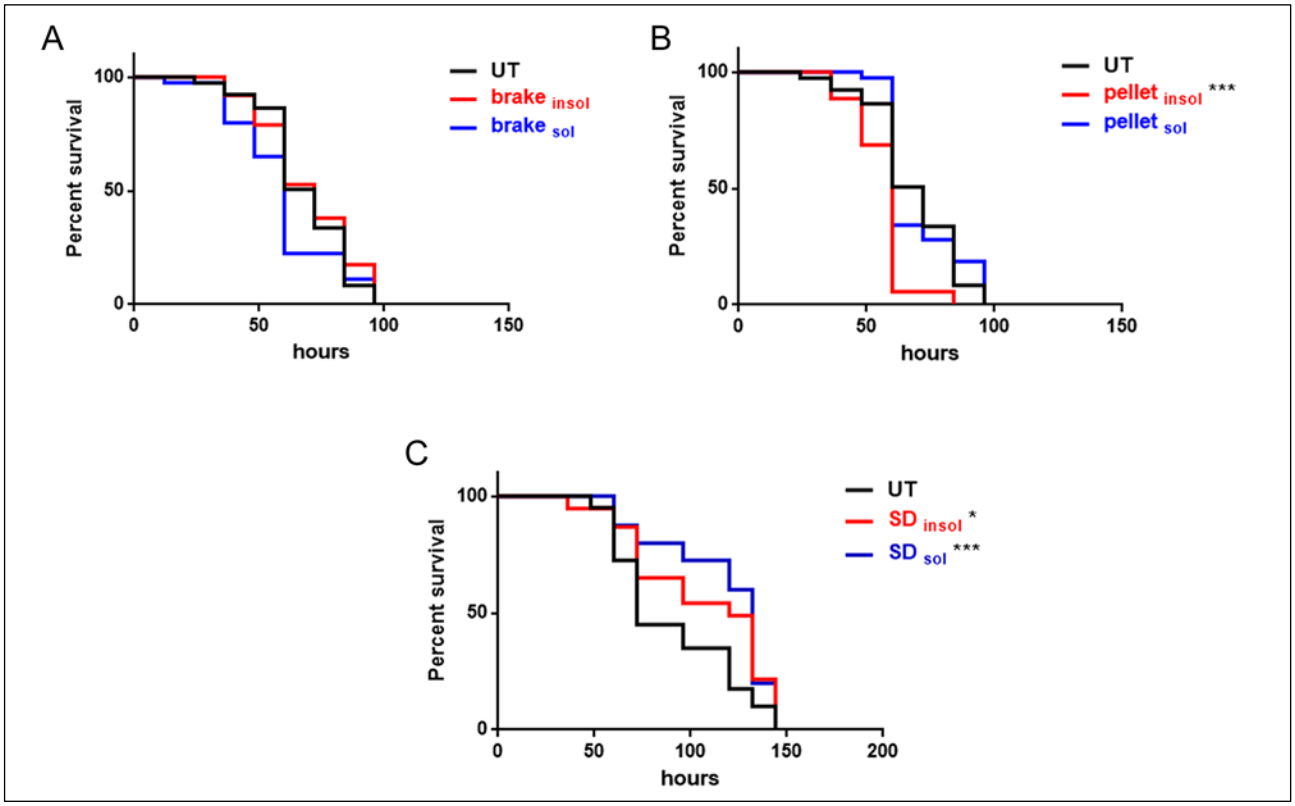

Fig. 3. Effects of fractionated dusts on nematode survival. Kaplan–Meier survival plot of N2 worms untreated (UT) or exposed to 5 mg/mL of the insoluble or soluble fraction of (A) brake dust, (B) pellet ash and (C) Saharan sand dust. Forty worms were used per single data point, and each experiment was repeated at least twice *p<0.05,***p<0.001.

3.4. Oxidative Stress Induction After Worm Exposure to Dust Fractions

Since the induction of oxidative stress in our model organism by total PM samples, we investigated how the insoluble and soluble fractions contributed to oxidative alterations in wild type worms. We first measured the ROS levels in young adult nematodes exposed for 24 hours to dust fractions (Fig.

4A). We observed for both brake dust and pellet ash that only the insoluble part was able to induce ROS production with a 5- and 6-fold increase, respectively, compared to untreated animals. These results are in agreement with that observed in the case of the amphipod and the A549 cells that, after 24 and 48 hours of exposure to $PM_{2.5}$, showed a higher content of ROS in the presence of insoluble materials (Marcoccia et al., 2017; Zou et al., 2016). Furthermore, it is reported that the total and the water insoluble fraction of $PM_{2.5}$ are the mainly possible inducers of oxidative stress in neonatal rat cardiomyocytes. Indeed, in cells exposed for 48 hours, the total and insoluble components of $PM_{2.5}$ are able to induce ROS production at higher concentrations than water soluble part (Qi et al., 2019). It is worth noting that the insoluble fraction of brake dust and pellet ash had been previously identified also as the dust components responsible for the highest values of OP measured by the ascorbic acid (OP^{AA}) and dithiothreitol (OP^{DTT}) assays, respectively (Simonetti et al., 2018). The relevance of these acellular tests as predictors of the PM capacity of inducing oxidative stress in biological systems is one cutting-edge issue in the recent literature (Øvrevik, 2019). The results obtained by *C. elegans* suggest that both the OP assays have the potential of predicting the oxidative stress generation in living organisms, but their different sensitivity still need to be properly evaluated. The approach used in this work could constitute a helpful tool to deepen this relevant aspect. However, in our experiments, the insoluble fraction lead to a lower ROS induction than their total counterparts. The Saharan dust fractions did not induce ROS production in *C. elegans*, as for the experiments with the total part of this dust.

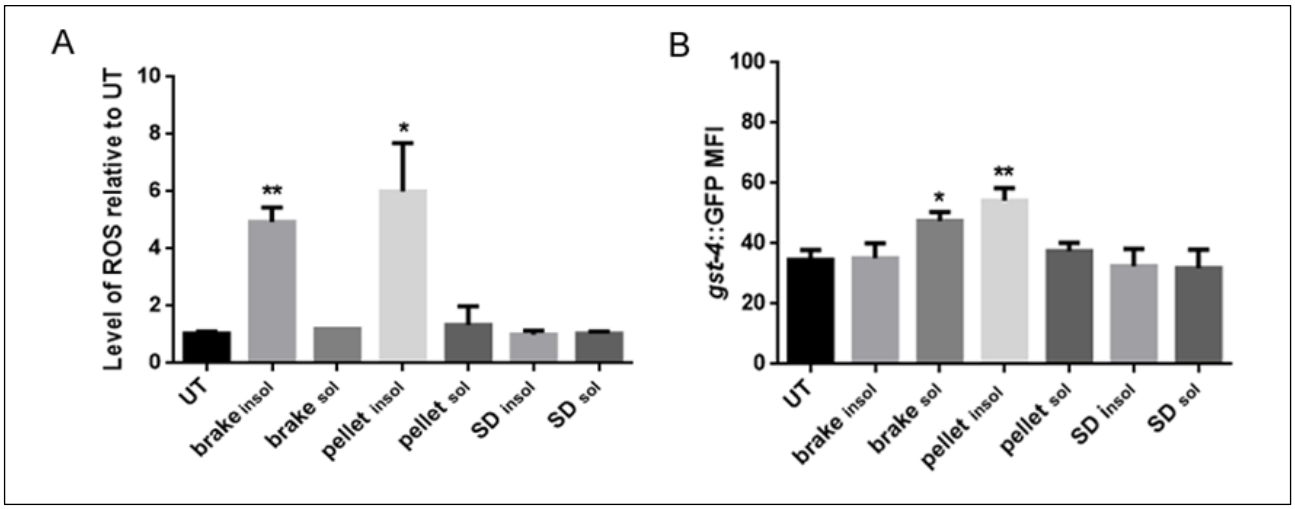

Fig. 4. ROS evaluation and GST-4::GFP pattern expression after exposure to dust fractions. (A) Measurement of ROS levels in N2 worms untreated (UT) or treated for 24 hours with 5 mg/mL of

indicated dust fractions. (B) Quantification of fluorescence intensity of treated or untreated (UT) *C. elegans* strain expressing *gst-4*::GFP. Data are expressed as mean ± standard deviation.*p<0.05, **p<0,01.

Next, we assessed the GST-4::GFP fluorescence intensity in the dvls19 transgenic worms exposed to the different dust fractions. As showed in Fig. 4B, in the brake dust, the water soluble part was able to increase the fluorescent signal (~10-fold higher than UT), meanwhile for the pellet ash the insoluble materials increased significantly the GST-4::GFP expression. The comparison with the data obtained with the total dusts indicated that the soluble part of the brake dust was mainly responsible for the induction of GST-4 expression but not enough to raise the fluorescent signal as in the animal treated with the total part. Instead, for pellet ash, the GFP signal observed in animals exposed to insoluble fraction was similar to the value obtained with total suspension, indicating that the induction of GST-4 for the pellet was mainly ascribed to the action of water insoluble material.

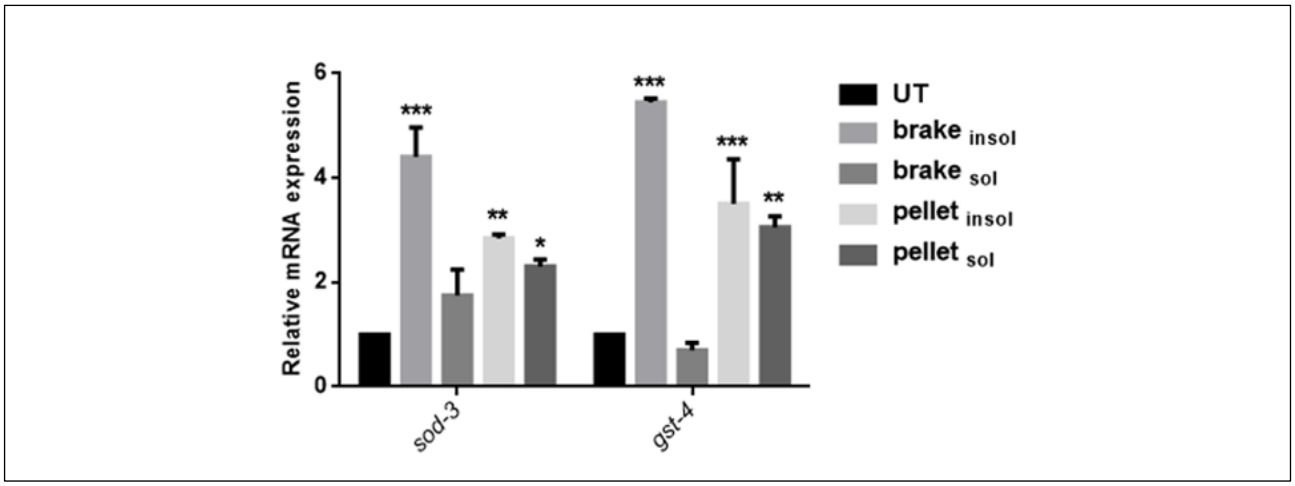

Fig. 5. Quantitative real-time PCR of oxidative stress related genes. The mRNA levels of detoxifying genes sod-3 and gst-4 in young adult N2 nematodes exposed for 24 hours to the insoluble and soluble fraction of the investigated dusts. Untreated worms were used as control. cdc-42 was used as the housekeeping gene * $p < 0.05$, ** $p < 0.01$, *** $p < 0.001$.

Since the different ability to induce oxidative stress in *C. elegans* exerted by the water soluble and insoluble fractions of these PM components, we decided to analyze the mRNA levels of genes involved in the detoxification of radicals, like *sod-3* and *gst-4*. We performed a quantitative RT-PCR

using young adult N2 nematodes exposed for 24 hours to the fractions of brake and pellet dust. As showed in Fig. 5 only the insoluble part of brake dust was able to induce an up-regulation of oxidative stress related genes. Meanwhile, both the insoluble and soluble fractions of pellet ash significantly increase the expression of *sod-3* and *gst-4* genes. However, the two pellet fractions and the water insoluble part of brake dust induced higher levels of *gst-4* mRNA than *sod-3*, according to the fact that GST-4 is specifically involved in the xenobiotic detoxification (Lindblom and Dodd, 2006). The highest transcription of both *sod-3* and *gst-4* was reached when worms were exposed to water insoluble part of the dusts. This result is in agreement with the elevated ROS levels observed in the *C. elegans* treated with the insoluble materials of brake dust and pellet ash (Fig. 4A).

These data are in line with that obtained for mammalian models; indeed rats exposed to $PM_{2.5}$ for two weeks showed in pulmonary arteries a significant vascular oxidative stress and enhanced protein expression of Cu/Zn- and Mn-superoxide dismutase (SOD) (Davel et al., 2012). Furthermore, long-term exposure to ambient fine particulate pollution lead, in exposed mice, an increase in the expression of NF-E2-related factor 2 (Nrf2) as well as the induction of phase II antioxidant response genes, which are transcriptionally regulated by this transcription factor (Xu et al., 2011). However, to the best of our knowledge, this is the first time to report about the differential impact of water-insoluble and soluble fractions of these selected components of airborne PM on the transcription profile of the oxidative stress related genes.

3.5. Susceptibility to Pathogen Infection of Nematodes Exposed to Dust Fractions

Different epidemiological studies indicated a strong association between $PM_{2.5}$ exposure and increased susceptibility to respiratory pathogen infection (Neupane et al., 2010; Strickland et al., 2016).

To investigate whether dust pre-treatment sensitize *C. elegans* to pathogen infections we monitored the survival of wild type worms exposed for 24 hours to the total, insoluble and soluble parts of brake dust and pellet ash and then infected with the Gram positive bacterium *Staphylococcus aureus*. *S. aureus* is a human respiratory tract commensal but also globally important human pathogen causing significant respiratory, skin and tissue disease (Edwards et al., 2012; Hall et al., 2017; Shak et al., 2013).

The Fig. 6A-B indicates as, for both brake dust and pellet ash, only the water soluble part increased the susceptibility of *C. elegans* to this microbe, with a decrease of nematode survival.

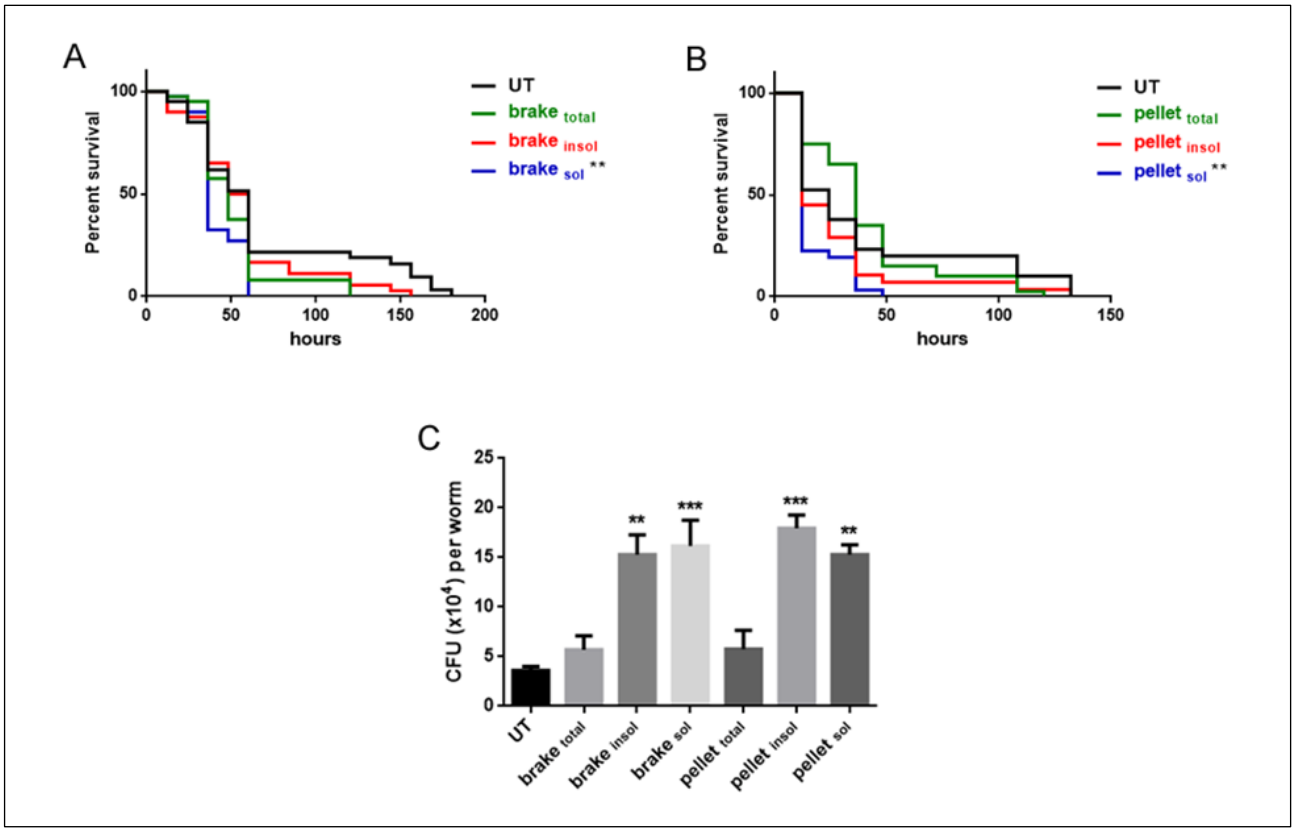

Fig. 6. Susceptibility to *S. aureus* infection after exposure to PM constituents. Survival of synchronized N2 worms pre-treated for 24 hours with total, insoluble and soluble part of (A) brake dust or (B) pellet ash and then fed with *S. aureus.* (C) Colony forming Units (CFU) assays in wild type nematodes pre-treated with the indicated urban sample fractions and infected with *S. aureus* for 48 hours. Data represents 3 independent experiments. ** $p < 0.01$, ***$p < 0.001$).

Furthermore, we analyzed the ability of *S. aureus* to colonize the *C. elegans* intestine in worm previously exposed for 24 hours to the dusts fractions. In this case, we found that both the insoluble and soluble part of brake dust and pellet ash induced a higher susceptibility to intestine colonization compared to the control and the nematode exposed to the total dust part (Fig. 6C).

Thus, although the insoluble fraction correlates with increased gut colonization of the pathogen, it did not affect the *C. elegans* survival. This probably account for the induction of a stress response, with a highest production of ROS (Fig. 4A) and a *sod-3* and *gst-4* up-regulation (Fig.5) that may protect worms from the infection. Indeed, it has been reported as the production of ROS and the activation of an oxidative stress response is part of *C. elegans* innate immunity to protect nematode from different pathogens including *S. aureus* (Chávez et al., 2007, 2009; Hoeven et al 2011).

Zhao and colleagues showed that rats exposed to a single dose of $PM_{2.5}$ and then infected with *S. aureus* significantly increased inflammatory cells and the levels of inflammatory cytokines in bronchoalveolar lavage fluids. Furthermore, pre-exposition to $PM_{2.5}$ significantly decreased the natural killer (NK) cells recruited into the airways following *S. aureus* infection (Zhao et al., 2014). Additionally, in mice exposed to the combination of PM and *S. aureus* occurs a significant increase of oxidative alterations and immune response compared to animals exposed to the individual matter (Wang et al., 2019).

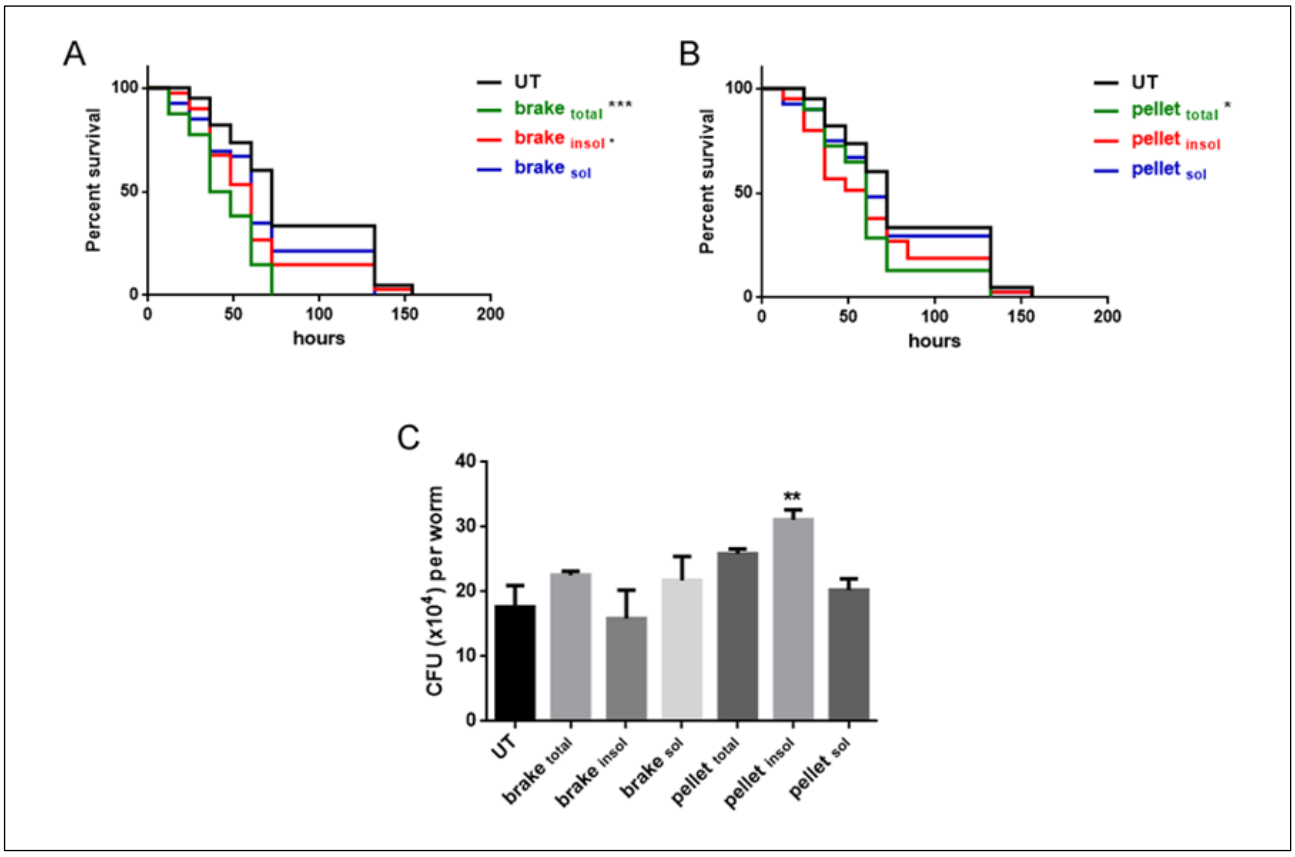

Fig. 7. *P. aeruginosa* infection of N2 *C. elegans* treated with PM fractions. N2 worms pre-treated for 24 hours with the fractionated (A) brake or (B) pellet dust and then infected with *P. aeruginosa*, to assess the survival . (C) Effects of dust pre-treatment on *P. aeruginosa* CFU count in the *C. elegans* gut. *p<0.05, ** p<0.01, ***p<0.001).

Next, we assessed whether our PM samples altered the *C. elegans* susceptibility to infection of another opportunistic pathogen, *Pseudomonas aeuruginosa*. This Gram negative bacterium is one of

the most common pathogens responsible for respiratory infections in hospitalized patients (Gellatly and Hancock, 2013; Lyczak et al., 2000).

We first analyzed the survival of young adult nematodes pre-treated for 24 hours with the dust fractions and then exposed to *P. aeruginosa*. While the insoluble and the total part of brake dust reduced significantly the survival of nematodes infected with the pathogen, only the total pellet ash exerted a negative effect on *C. elegans* life span (Fig. 7A-B). On the other hand, CFU assay showed that only the water insoluble component of pellet was able to increase the *P. aeruginosa* colonization of *C. elegans* intestine (Fig. 7C).

The effects of PM on *P. aeruginosa* infection was investigated in human bronchial epithelial cells by Chen and colleagues in 2018. These authors showed, using CFU assay, that cells exposed to increasing concentrations of PM prior to *P. aeruginosa* infection show a higher bacteria intracellular invasion than unexposed cells (Chen et al., 2018). Moreover they observed that the highest predisposition to *P. aeruginosa* invasion is linked to oxidative stress generate by PM. This could explain why the main effects on the infection susceptibility of *C. elegans* were exerted by the insoluble and total fractions of brake dust and pellet ash; indeed these PM components increased significantly the ROS levels in exposed nematodes.

3.6. Quantitative RT-PCR of Genes Involved in C. Elegans Innate Immune Response

In the last part of our work we analyzed whether the water soluble and insoluble fractions of brake and pellet dusts could differently affect the immunity response in *C. elegans*. To this aim, a quantitative RT-PCR was performed to analyze the expression of two important genes of innate immune pathway in *C. elegans*: *sek-1* and *pmk-1*. Indeed SEK-1 and PMK-1 are two components of the mitogen-activated protein kinase (p38 MAPK) pathway that plays a key role in *C. elegans* innate immunity (Kim et al., 2002; Shivers et al., 2010; Troemel et al., 2006). As showed in Fig. 8 the exposure for 12 hours to the PM fractions affects predominantly the *sek-1* expression with a significant decrease of this transcript, especially in animals treated with insoluble and soluble part of brake dust and with the soluble component of pellet ash. *pmk-1* mRNA level resulted instead unaffected except for the condition in which nematodes were treated with the insoluble material of pellet ash. Indeed, in this case we observed an increase of *pmk-1* transcription compared to untreated worms. Thus, these findings revealed that PM materials down-modulated *C. elegans* immune pathway mainly affecting *sek-1* transcription.

The ability of PM to down-modulate the immune response has been previously reported; human bronchial epithelial cells infected with *P. aeruginosa* after pre-treatment with PM show a lower mRNA levels of the antimicrobial peptide β-defensin-2 (hBD-2) compared to cells only infected with *P. aeruginosa* (Chen et al., 2018). Furthermore, early-life exposure to combustion-derived particulate matter (CDPM) affects the allergic asthma development in infants (Saravia et al., 2014). In fact, in an infant asthma mouse model, CDPM brings to a failed development of a typical asthma phenotype with an attenuated adaptive immune response and a decreased expression of *Muc5ac* gene, encoding a mucin forming gel that contributes to the viscoelastic properties of mucus, essential for clearance and protection of the lung epithelium from pathogen infections (Sidhaye and Koval, 2017).

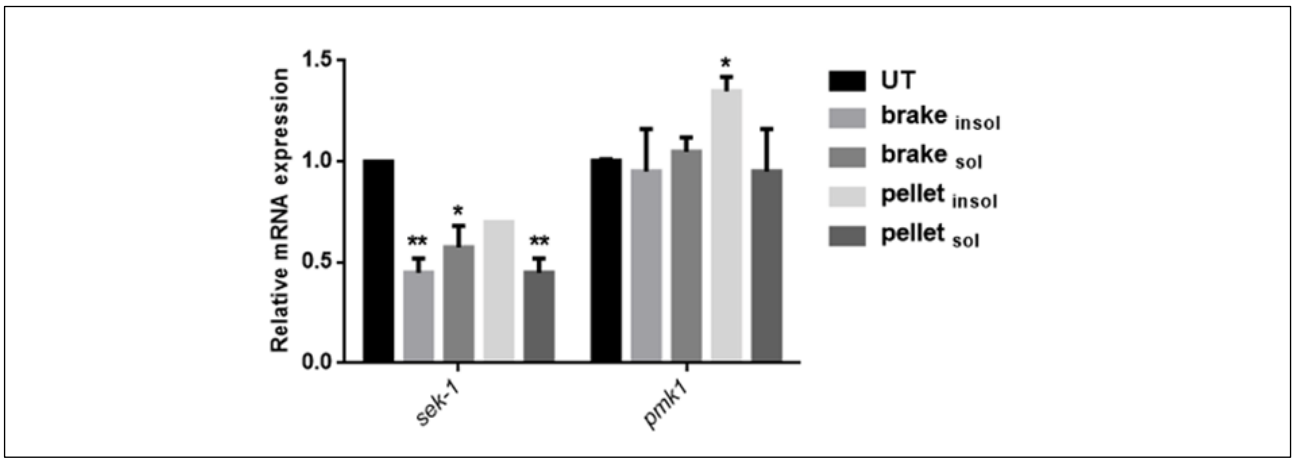

Fig. 8. Expression of immune response genes. Quantitative real-time PCR for genes involved in the nematode innate immunity using synchronized N2 worms pre-exposed for 12 hours to the insoluble or soluble part of indicated PM constituents. The untreated worms were used as control. *cdc-42* was used as the housekeeping gene. p * < 0.05, p ** < 0.01.

The soluble and insoluble fraction of the considered dusts were able to change in a different way the *C. elegans* susceptibility to both *S. aureus* and *P. aeruginosa*, probably altering the innate immunity response. The differences observed in the impact of PM fractions on the animals infected with the two bacteria are most probably related to the different pathogenesis exerted by the two pathogens during the *C. elegans* infection. In fact, *P. aeruginosa* induces an intestinal distension and intracellular invasion of C. elegans with an active pathogen-induced damage in nematodes. On the contrary, *S. aureus* causes an intestinal epithelium destruction and complete degradation of internal

organs and the host response to the infection seems to be mediated by the recognition of some *S. aureus* structures by worm receptor(s) (Irazoqui et al., 2010).

4. Conclusions

In summary, we evaluated the toxicity of atmospheric particulate matter by exposing *in vivo* the nematode *C. elegans* to different atmospheric dust components: brake dust, pellet ash and Saharan dust. We investigated multiple toxic endpoints like life span, reproduction and oxidative stress induction. Our data suggest that brake dust and pellet ash severely impact on the survival of the nematodes and induce a significant oxidative stress response. On the contrary, both dusts does not affect the reproductive ability of the nematode. Saharan dust, instead, exerted no toxic effect on *C. elegans*. Although additional studies will be required to further establish a link, our results show as soluble part of atmospheric PM behaves differently from insoluble suspended one, with strong toxic effects induced by the water insoluble fraction on the life span and the oxidative stress response of the animals. Moreover, our findings highlight as the total, insoluble and soluble part of brake dust and pellet ash affect in a different way the *C. elegans* susceptibility to the infection of human pathogens. To conclude, our data confirm that not only the size and dosage of atmospheric PM but also its solubility should be taken into consideration when evaluating the toxicity of airborne PM.

Acknowledgements

This work was partially supported by the project 2017 RG11715C7C8801CF, financed by Sapienza University of Rome.

Author Contributions

G. Ficociello, L. Massimi, D. Uccelletti and S. Canepari planned the experiments; L. Massimi performed the chemical analyses; G. Ficociello, A. Inverni and G. Buccini performed the experiments with *C. elegans*; G. Ficociello and D. Uccelletti elaborated the data and wrote the manuscript; S. Canepari reviewed the manuscript; D. Uccelletti and S. Canepari coordinated the group and supervised the manuscript.

Conflicts of Interest

The authors declare no conflict of interest.

References

Adam, M., Schikowski, T., Carsin, A. E., Cai, Y., Jacquemin, B., Sanchez, M., Vierkotter, A., Marcon, A., Keidel, D., Sugiri, D., et al., 2015. Adult lung function and long-term air pollution. ESCAPE: A multicentre cohort study and meta-analysis. Eur. Respir. J. 45, 38–50.

Atkinson, R. W., Fuller, G. W., Anderson, H. R., Harrison, R. M., Armstrong, B., 2010. Urban ambient particle metrics and health: a time-series analysis. Epidemiology 21, 501–511.

Aztatzi-Aguilar, O. G., Valdés-Arzate, A., Debray-García, Y., Calderón-Aranda, E. S., Uribe-Ramirez, M., Acosta-Saavedra, L., Gonsebatt, M. E., Maciel-Ruiz, J. A., Petrosyan, P., Mugica-Alvarez, V. et al., 2018. Exposure to ambient particulate matter induces oxidative stress in lung and aorta in a size- and time-dependent manner in rats. Toxicology Research and Application 2, 1–15.

Back, P., Braeckman, B. P., Matthijssens, F., 2012. ROS in aging *Caenorhabditis elegans*: damage or signaling? Oxid. Med. Cell Longev. 2012, 608478.

Bates, J. T., Fang, T., Verma, V., Zeng, L., Weber, R. J., Tolbert, P. E., Abrams, J. Y., Sarnat, S. E., Klein, M., Mulholland, J. A., et al., 2019. Review of acellular assays of ambient particulate matter oxidative potential: methods and relationships with composition, sources, and health effects. Environ. Sci. Technol. 53, 4003-4019.

Brenner, S., 1974. The genetics of *Caenorhabditis elegans*. Genetics 77, 71–94.

Brugha, R., Grigg, J., 2014. Urban air pollution and respiratory infections. Paediatr. Respir. Rev. 15, 194-199.

Cachon, B.F., Firmin, S., Verdin, A., Ayi-Fanou, L., Billet, S., Cazier, F., Martin, P.J., Aissi, F., Courcot, D., Sanni, A., Shirali, P., 2014. Proinflammatory effects and oxidative stress within human bronchial epithelial cells exposed to atmospheric particulate matter (PM 2.5 and PM > 2.5) collected from Cotonou. Benin. Environ. Pollut. 185, 340-351.

Cai, Y., Zijlema, W. L., Doiron, D., Blangiardo, M., Burton, P. R., Fortier, I., Gaye, A., Gulliver, J., de Hoogh, K., Hveem, K., et al., 2017. Ambient air pollution, traffic noise and adult asthma prevalence: A BioSHaRE approach. Eur. Respir. J. 49, 1502127.

Cesaroni, G., Forastiere, F., Stafoggia, M., Andersen, Z. J., Badaloni, C., Beelen, R., Caracciolo, B., de Faire, U., Erbel, R., Eriksen, K. T., et al., 2014. Long term exposure to ambient air pollution and incidence of acute coronary events: Prospective cohort study and meta-analysis in 11 European cohorts from the ESCAPE Project. BMJ 348, f7412.

Chang, X., Zhou, L., Tang, M., Wang, B., 2015. Association of fine particles with respiratory disease mortality: a meta-analysis. Arch. Environ. Occup. Health 70, 98-101.

Chaudhuri, N., Jary, H., Lea, S., Khan, N., Piddock, K. C., Dockrell, D. H., Donaldson, K., Duffin, R., Singh, D., Parker, L. C., Sabroe, I., 2012. Diesel exhaust particle exposure *in vitro* alters monocyte differentiation and function. PLoS One 7, e51107.

Chávez, V., Mohri-Shiomi, A., Garsin, D. A., 2009. Ce-Duox1/BLI-3 generates reactive oxygen species as a protective innate immune mechanism in *Caenorhabditis elegans.* Infect Immun. 77, 4983–4989.

Chávez, V., Mohri-Shiomi, A., Maadani, A., Vega, L. A., Garsin, D. A., 2007. Oxidative stress enzymes are required for DAF-16-mediated immunity due to generation of reactive oxygen species by *Caenorhabditis elegans*.

Chen, L. C., Lippmann, M., 2009. Effects of metals within ambient air particulate matter (PM) on human health. Inhal Toxicol. 21, 1-31.

Chen, X., Liu, J., Zhou, J., Wang, J., Chen, C., Song, Y., Pan, J., 2018. Urban particulate matter (PM) suppresses airway antibacterial defence. Respir Res. 19, 5.

Cheung, K., Daher, N., Kam, W., Shafer, M. M., Ning, Z., Schauer, J.J., et al., 2011. Spatial and temporal variation of chemical composition and mass closure of ambient coarse particulate matter ($PM_{10–2.5}$) in the Los Angeles area. Atmos. Environ. 45, 2651–2662.

Chung, M. C., Tsai, M. H., Que, D. E., Bongo, S. J., Hsu, W. L., Tayo, L. L., Lin, Y. H., Lin, S. L., Gou, Y. Y., Hsu, Y. C., et al., 2019. Fine particulate matter-induced toxic effects in an animal model of *Caenorhabditis elegans*. Aerosol Air Qual. Res. 19, 1068–1078.

Clavijo, A., Kronberg, M. F., Rossen, A., Moya, A., Calvo, D., Salatino, S. E., Pagano, E. A., Morábito, J. A., Munarriz, E. R., 2016. The nematode *Caenorhabditis elegans* as an integrated toxicological tool to assess water quality and pollution. Sci. Total Environ. 569– 570, 252–261.

Cohen, A. J., Brauer, M., Burnett, R., Anderson, H. R., Frostad, J., Estep, K., Balakrishnan, K., Brunekreef, B., Dandona, L., Dandona, R., et al., 2017. Estimates and 25-year trends of the global burden of disease attributable to ambient air pollution: an analysis of data from the Global Burden of Diseases Study 2015. Lancet 389, 1907-1918.

Danielsen,P. H., Møller, P., Jensen, K. A., Sharma, A. K., Wallin, H., Bossi, R., Autrup, H., Mølhave, L., Ravanat, J. L., Briedé, J. J., et al., 2011. Oxidative stress, DNA damage, and inflammation induced by ambient air and wood smoke particulate matter in human A549 and THP-1 cell Lines. Chem. Res. Toxicol. 24, 168–184.

Davel, A. P., Lemos, M., Pastro, L. M., Pedro, S. C., de André, P. A., Hebeda, C., Farsky, S. H., Saldiva, P. H., Rossoni, L. V., 2012. Endothelial dysfunction in the pulmonary artery induced by concentrated fine particulate matter exposure is associated with local but not systemic inflammation. Toxicology 295, 39-46.

Davies, K. J., 1999. The broad spectrum of responses to oxidants in proliferating cells: a new paradigm for oxidative stress. IUBMB Life 48, 41-47.

Donkin, S. G., Dusenbery, D. B., 1993. A soil toxicity test using the nematode *Caenorhabditis elegans* and an effective method recovery. Arch. Environ. Contam. Toxicol. 25, 145–151.

Edwards, A. M., Bowden, M. G., Brown, E. L., Laabei, M., Massey R. C., 2012. *Staphylococcus aureus* extracellular adherence protein triggers TNFα release, promoting attachment to endothelial cells via protein A. PLoS One 7, e43046.

Esworthy, R., 2013. Air quality: EPA's 2013 changes to the particulate matter (PM) standard. Congressional Research Service 7-5700, n. R42934; p. 6.

Evans, J., Donkelaar, A., Martin, R.V., Burnett, R., Rainham, D.G., Birkett, N.J., Krewski, D., 2013. Estimates of global mortality attributable to particulate air pollution using satellite imagery. Environ. Res. 120, 33-42.

Fortoul, T. I., Rodriguez-Lara, V., Gonzalez-Villalva, A., Rojas-Lemus, M., Colin-Barenque, L., Bizarro-Nevares, P., García-Peláez, I., Ustarroz-Cano, M., López-Zepeda, S., Cervantes-Yépez, S., et al., 2015. Health effects of metals in particulate matter. In Current Air Quality Issues, (Nejadkoorki, F., Eds.), 571–608. InTech, Rijeka, Croatia.

Gehring, U., Gruzieva, O., Agius, R. M., Beelen, R., Custovic, A., Cyrys, J., Eeftens, M., Flexeder, C., Fuertes, E., Heinrich, J., et al., 2013. Air pollution exposure and lung function in children: The ESCAPE Project. Environ. Health Perspect. 121, 1357–1364.

Gellatly, S. L., Hancock, R. E., 2013. *Pseudomonas aeruginosa*: new insights into pathogenesis and host defenses. Pathog Dis. 67, 159-173.

Goeminne, P. C., Kiciński, M., Vermeulen, F., Fierens, F., De Boeck, K., Nemery, B., Nawrot, T. S., Dupont, L. J., 2013. Impact of air pollution on cystic fibrosis pulmonary exacerbations: a case-crossover analysis. Chest 143, 946-954.

Hall, J. W., Yang, J., Guo, H., Ji, Y., 2017. The *Staphylococcus aureus* AirSR two-component system mediates reactive oxygen species resistance via transcriptional regulation of staphyloxanthin production. Infect Immun. 85, e00838-16.

Harrod, K. S., Jaramillo, R. J., Berger, J. A., Gigliotti, A. P., Seilkop, S. K., Reed, M. D., 2005. Inhaled diesel engine emissions reduce bacterial clearance and exacerbate lung disease to *Pseudomonas aeruginosa* infection *in vivo*. Toxicol. Sci. 83, 155-165.

Hoeven, R., McCallum, K. C., Cruz, M. R., Garsin, D. A., 2011. Ce-Duox1/BLI-3 generated reactive oxygen species trigger protective SKN-1 activity via p38 MAPK signaling during infection in *C. elegans*. PLoS Pathog. 7, e1002453.

Irazoqui, J. E., Troemel, E. R., Feinbaum, R. L., Luhachack, L. G., Cezairliyan, B. O., Ausubel, F. M., 2010. Distinct pathogenesis and host responses during infection of *C. elegans* by *P. aeruginosa* and *S. aureus*. PLoS Pathog. 6, e1000982.

Jackson, A.L., Loeb, L.A., 2001. The contribution of endogenous sources of DNA damage to the multiple mutations in cancer. Mutat. Res.-Fund. Mol. M. 477, 7-21.

Jedrychowski, W. A., Perera, F. P., Spengler, J. D., Mroz, E., Stigter, L., Flak, E., Majewska, R., Klimaszewska-Rembiasz, M., Jacek, R., 2013. Intrauterine exposure to fine particulate matter as a risk factor for increased susceptibility to acute broncho- pulmonary infections in early childhood. Int. J. Hyg. Environ. Health 216, 395–401.

Jiang, Y., Chen, J., Wu, Y., Wang, Q., Li, H., 2016. Sublethal toxicity endpoints of heavy metals to the nematode *Caenorhabditis elegans*. PLoS One 11, e0148014.

Jin, S. P., Li, Z., Choi, E. K., Lee, S., Kim, Y. K., Seo, E. Y., Chung, J. H., Cho, S., 2018. Urban particulate matter in air pollution penetrates into the barrier-disrupted skin and produces ROS-dependent cutaneous inflammatory response *in vivo*. J. Dermatol. Sci. 91, 175–183.

Kelly, F.J., Fussell, J. C., 2012. Size, source and chemical composition as determinants of toxicity attributable to ambient particulate matter. Atmos. Environ. 60, 504–526.

Khan, M. F., Hirano, K., Masunaga S., 2010. Quantifying the sources of hazardous elements of suspended particulate matter aerosol collected in Yokohama, Japan. Atmos. Environ. 44, 2646-2657.

Kim, D. H., Feinbaum, R., Alloing, G., Emerson, F. E., Garsin, D. A., Inoue, H., Tanaka-Hino, M., Hisamoto, N., Matsumoto, K., Tan, M. W., Ausubel, F. M., 2002. A conserved p38 MAP kinase pathway in Caenorhabditis elegans innate immunity. Science 297, 623-626.

Kim, K. H., Kabir, E., Kabir, S., 2015. A review on the human health impact of airborne particulate matter. Environ. Int. 74, 136-143.

Leelaja, B. C., Rajini, P. S., 2013. Biochemical and physiological responses in *Caenorhabditis elegans* exposed to sublethal concentrations of the organophosphorus insecticide, monocrotophos. Ecotoxicol. Environ. Saf. 94, 8-13.

Leung, M. C., Williams, P. L., Benedetto, A., Au, C., Helmcke, K. J., Aschner, M., Meyer, J. N., 2008. *Caenorhabditis elegans*: an emerging model in biomedical and environmental toxicology. Toxicol. Sci. 106, 5-28

Li, N., Xia, T., Nel, A. E., 2008. The role of oxidative stress in ambient particulate matter-induced lung diseases and its implications in the toxicity of engineered nanoparticles. Free Radic. Biol Med. 44, 1689-1699.

Li, R., Kou, X., Geng, H., Xie, J., Yang, Z., Zhang, Y., Cai, Z., Dong, C., 2015. Effect of ambient PM 2.5 on lung mitochondrial damage and fusion/fission gene expression in rats. Chem. Res. Toxicol. 28, 408-418.

Lindblom, T. H., Dodd, A. K., 2006. Xenobiotic detoxification in the nematode *Caenorhabditis elegans*. J. Exp. Zool. A Comp. Exp. Biol. 305, 720-730.

Link, C. D., Johnson, C. J., 2002. Reporter transgenes for study of oxidant stress in *Caenorhabditis elegans*. Methods Enzymol. 353, 497-505.

Liu, P. D., He, K. W., Li, Y. X., Wu, Q. L., Yang, P., Wang, D. Y., 2012. Exposure to mercury causes formation of male-specific structural deficits by inducing oxidative damage in nematodes. Ecotoxicol. Environ. Saf. 79, 90–100.

Livak, K. J., Schmittgen, T. D., 2001. Analysis of relative gene expression data using real-time quantitative PCR and the 2(-Delta Delta C(T)) Method. Methods 25, 402-408.

Lyczak, J. B., Cannon, C. L., Pier, G. B., 2000. Establishment of *Pseudomonas aeruginosa* infection: lessons from a versatile opportunist. Microbes Infect. 2, 1051-1060.

MacIntyre, E. A., Gehring, U., Mölter, A., Fuertes, E., Klümper, C., Krämer, U., Quass, U., Hoffmann, B., Gascon, M., Brunekreef, B., et al., 2014. Air Pollution and Respiratory Infections during Early Childhood: An Analysis of 10 European Birth Cohorts within the ESCAPE Project. Environ. Health Perspect. 122, 107–113.

Madureira, J., Paciência, I., Fernandes, E. O., 2012. Levels and indoor–outdoor relationships of size specific particulate matter in naturally ventilated Portuguese schools. J. Toxicol. Environ. Health A 75, 1423–1436.

Manigrasso, M., Protano, C., Martellucci, S., Mattei, V., Vitali, M., Avino, P., 2019. Evaluation of the submicron particles distribution between mountain and urban site: contribution of the

transportation for defining environmental and human health issues. Int. J. Environ. Res. Public Health 16, 1339.

Marcoccia, M., Ronci, L., De Matthaeis, E., Setini, A., Perrino, C., Canepari, S., 2017. In-vivo assesment of the genotoxic and oxidative stress effects of particulate matter on *Echinogammarus veneris*. Chemosphere 173, 124-134.

Marsh, E. K., May, R. C., 2012. *Caenorhabditis elegans*, a model organism for investigating immunity. Appl. Environ. Microbiol. 78, 2075-2081.

McElwee, M. K., Ho, L. A., Chou, J. W., Smith, M. V., Freedman, J. H., 2013. Comparative toxicogenomic responses of mercuric and methyl-mercury. BMC Genomics 14, 698.

Medina-Ramón, M., Zanobetti, A., Schwartz, J., 2006. The effect of ozone and PM10 on hospital admissions for pneumonia and chronic obstructive pulmonary disease: a national multicity study. Am. J. Epidemiol. 163, 579-588.

Merbitz, H., Fritz, S., Schneider, C., 2012. Mobile measurements and regression modeling of the spatial particulate matter variability in an urban area. Sci. Total Environ. 438, 389-403.

Migliaccio, C. T., Kobos, E., King, Q. O., Porter, V., Jessop, F., Ward, T., 2013. Adverse effects of wood smoke $PM_{2.5}$ exposure on macrophage functions. Inhal. Toxicol. 25, 67–76.

Misra, C., Geller, M. D., Shah, P., Sioutas, C., Solomon, P. A., 2001. Development and evaluation of a continuous coarse ($PM_{10–PM2.5}$) particle monitor. J. Air Waste Manage. Assoc. 51, 1309–1317.

Mushtaq, N., Ezzati, M., Hall, L., Dickson, I., Kirwan, M., Png, K. M., Mudway, I. S., Grigg, J., 2011. Adhesion of Streptococcus pneumoniae to human airway epithelial cells exposed to urban particulate matter. J. Allergy Clin. Immunol. 127, 1236-1242.e2.

Neupane, B., Jerrett, M., Burnett, R. T., Marrie, T., Arain, A., Loeb, M., 2010. Long-term exposure to ambient air pollution and risk of hospitalization with community-acquired pneumonia in older adults. Am. J. Respir. Crit. Care Med. 181, 47–53.

Nuorti, J.P., Butler, J. C., Farley, M. M., Harrison, L. H., McGeer, A., Kolczak, M. S., Breiman, R. F., 2000. Cigarette smoking and invasive pneumococcal disease. Active Bacterial Core Surveillance Team. N. Engl. J. Med. 342, 681-689.

Øvrevik, J., 2019. Oxidative potential versus biological effects: a review on the relevance of cell-free/abiotic assays as predictors of toxicity from airborne particulate matter. Int. J. Mol. Sci. 20, 4772.

Perrino, C., Marcovecchio, F., 2016. A new method for assessing the contribution of primary biological atmospheric particles to the mass concentration of the atmospheric aerosol. Environ. Int. 87, 108-115.

Piacentini, A., Falasca, G., Canepari, S., Massimi, L., 2019. Potential of PM-selected components to induce oxidative stress and root system alteration in a plant model organism. Environ. Int. 132, 105094.

Pietrodangelo, A., Salzano, R., Rantica, E., Perrino, C., 2013. Characterisation of the local topsoil contribution to airborne particulate matter in the area of Rome (Italy). Source profiles. Atmos. Environ. 69, 1-14.

Pope III, C. A, Brook, R. D., Burnett, R. T., Dockery, D. W., 2011. How is cardiovascular disease mortality risk affected by duration and intensity of fine particulate matter exposure? An integration of the epidemiologic evidence. Air Qual. Atmos. Health 4, 5-14.

Putaud, J. P., Van Dingenen, R., Alastuey, A., Bauer, H., Birmili, W., Cyrys, J., Flentje, H., Fuzzi, S., Gehrig, R., Hanssoni, H. C., et al., 2010. A European aerosol phenomenology–3: physical and chemical characteristics of particulate matter from 60 rural, urban, and kerbside sites across Europe. Atmos. Environ. 44, 1308-1320.

Qi, Z., Song, Y., Ding, Q., Liao, X., Li, R., Liu, G., Tsang, S., Cai, Z., 2019. Water soluble and insoluble components of $PM_{2.5}$ and their functional cardiotoxicities on neonatal rat cardiomyocytes *in vitro*. Ecotoxicol. Environ. Saf. 168, 378-387.

Raaschou-Nielsen, O., Andersen, Z. J., Beelen, R., Samoli, E., Stafoggia, M., Weinmayr, G., Hoffmann, B., Fischer, P., Nieuwenhuijsen, M. J., Brunekreef, B., et al., 2013. Air pollution and lung

cancer incidence in 17 European cohorts: prospective analyses from the European Study of Cohorts for Air Pollution Effects (ESCAPE). Lancet Oncol. 14, 813–822.

Rai, N., Sjöberg, V., Forsberg, G., Karlsson, S., Olsson, P. E., Jass, J., 2019. Metal contaminated soil leachates from an art glass factory elicit stress response, alter fatty acid metabolism and reduce life span in *Caenorhabditis elegans*. Sci. Total Environ. 651, 2218–2227.

Rao, X., Zhong, J., Brook, R. D., Rajagopalan, S., 2018. Effect of particulate matter air pollution on cardiovascular oxidative stress pathways. Antioxid. Redox Signal. 28, 797-818.

Rivas-Santiago, C. E., Sarkar, S., Cantarella, P. IV, Osornio-Vargas, Á., Quintana-Belmares, R., Meng, Q., Kirn, T. J., Ohman Strickland, P., Chow, J. C., Watson, J. G., et al., 2015. Air pollution particulate matter alters antimycobacterial respiratory epithelium innate immunity. Infect. Immun. 83, 2507-2517.

Saravia, J., You, D., Thevenot, P., Lee, G. I., Shrestha, B., Lomnicki, S., Cormier, S. A., 2014. Early-life exposure to combustion-derived particulate matter causes pulmonary immunosuppression. Mucosal Immunol. 7, 694–704.

Shak, J. R., Vidal, J. E., Klugman, K. P., 2013. Influence of bacterial interactions on pneumococcal colonization of the nasopharynx. Trends Microbiol. 21, 129–135.

Shivers, R. P., Pagano, D. J., Kooistra, T., Richardson, C. E., Reddy, K. C., Whitney, J. K., Kamanzi, O., Matsumoto, K., Hisamoto, N., Kim, DH., 2010. Phosphorylation of the conserved transcription factor ATF-7 by PMK-1 p38 MAPK regulates innate immunity in *Caenorhabditis elegans*. PLoS Genet. 6, e1000892.

Sidhaye, V. K., Koval, M. 2017. Lung Epithelial Biology in the Pathogenesis of Pulmonary Disease. Academic Press.

Simonetti, G., Conte, E., Massimi, L., Frasca, D., Perrino, C., Canepari, S., 2018. Oxidative potential of particulate matter components generated by specific emission sources. J. Aerosol Sci. 126, 99-109.

Srimuruganandam, B., Nagendra, S., 2012. Source characterization of PM_{10} and $PM_{2.5}$ mass using a chemical mass balance model at urban roadside. Sci. Total Environ. 433, 8–19.

Stadman, E.R., Levine, R.L., 2000. Protein oxidation. Ann. NY. Acad. Sci. 899, 191-208.

Stafoggia, M., Cesaroni, G., Peters, A., Andersen, Z. J., Badaloni, C., Beelen, R., Caracciolo, B., Cyrys, J., de Faire, U., de Hoogh, K., et al., 2014. Long-term exposure to ambient air pollution and incidence of cerebrovascular events: Results from 11 European cohorts within the ESCAPE Project. Environ. Health Perspect. 122, 919–925.

Strickland, M. J., Hao, H., Hu, X., Chang, H. H., Darrow, L. A., Liu, Y., 2016. Pediatric emergency visits and short-term changes in PM2.5 concentrations in the U.S. state of Georgia. Environ. Health Perspect. 124, 690-696.

Sun, L., Wu, Q., Liao, K., Yu, P., Cui, Q., Rui, Q., Wang, D., 2016. Contribution of heavy metals to toxicity of coal combustion related fine particulate matter ($PM_{2.5}$) in *Caenorhabditis elegans* with wild-type or susceptible genetic background. Chemosphere 144, 2392–2400.

Tawe, W. N., Eschbach, M. L., Walter, R. D., Henkle-Dührsen K., 1998. Identification of stress-responsive genes in *Caenorhabditis elegans* using RT-PCR differential display. Nucleic Acids Res. 26, 1621-1627.

Titus, K., Hengartner, M.O., 2006. Finding function in novel targets: *C. elegans* as a model organism. Nat. Rev. Drug Discov. 5, 387–398.

Troemel, E. R., Chu, S. W., Reinke, V., Lee, S. S., Ausubel, F. M., Kim, D. H., 2006. p38 MAPK regulates expression of immune response genes and contributes to longevity in *C. elegans*. PLoS Genet. 2, e183.

Tseng, I. L., Yang, Y. F., Yu, C. W., Li, W. H., Liao, V. H. C., 2013. Phthalates induce neurotoxicity affecting locomotor and thermotactic behaviors and AFD neurons through oxidative stress in *Caenorhabditis elegans*. PLoS One 8, e82657.

Turner, M. C., Krewski, D., Pope III, C. A., Chen, Y., Gapstur, S. M., Thun, M. J., 2011. Long-term ambient fine particulate matter air pollution and lung cancer in a large cohort of never-smokers. Am. J. Respir. Crit. Care Med. 184, 1374-1381.

Uccelletti, D., Zanni, E., Marcellini, L., Palleschi, C., Barra, D., Mangoni, M. L., 2010. Anti-Pseudomonas activity of frog skin antimicrobial peptides in a *Caenorhabditis elegans* infection model: a plausible mode of action *in vitro* and *in vivo*.

Wang, F., Wang, R., Liu, H., 2019. The acute pulmonary toxicity in mice induced by *Staphylococcus aureus*, particulate matter, and their combination. Exp Anim. 68, 159–168.

Wang, M., Nie, Y., Liu, Y., Dai, H., Wang, J., Si, B., Yang, Z., Cheng, L., Liu, Y., Chen, S., Xu, A., 2019. Transgenerational effects of diesel particulate matter on *Caenorhabditis elegans* through maternal and multigenerational exposure. Ecotoxicol. Environ. Saf. 170, 635-643.

Weinmayr, G., Pedersen, M., Stafoggia, M., Andersen, Z. J., Galassi, C., Munkenast, J., Jaensch, A., Oftedal, B., Krog, N. H., Aamodt, G., et al., 2018. Particulate matter air pollution components and incidence of cancers of the stomach and the upper aerodigestive tract in the European Study of Cohorts of Air Pollution Effects (ESCAPE). Environ. Int. 120, 163-171.

World Health Organization (WHO); Regional Office for Europe, 2013. Health Risks of Air Pollution in Europe—HRAPIE Project: Recommendations for Concentration-Response Functions for Cost-Benefit Analysis of Particulate Matter, Ozone and Nitrogen Dioxide; WHO Regional Office for Europe: Copenhagen, Denmark.

Xu, X., Liu, C., Xu, Z., Tzan, K., Zhong, M., Wang, A., Lippmann, M., Chen, L. C., Rajagopalan, S., Sun, Q., 2011. Long-term exposure to ambient fine particulate pollution induces insulin resistance and mitochondrial alteration in adipose tissue. Toxicol. Sci. 124, 88-98.

Zhao, H., Li, W., Gao, Y., Li, J., Wang, H., 2014. Exposure to particular matter increases susceptibility to respiratory *Staphylococcus aureus* infection in rats via reducing pulmonary natural killer cells.

Zhao, Y., Lin, Z., Jia, R., Li, G., Xi, Z., Wang, D., 2014. Transgenerational effects of traffic-related fine particulate matter (PM2.5) on nematode *Caenorhabditis elegans*. J. Hazard. Mater. 274, 106–114.

Zhao, Y. L., Wu, Q. L., Li, Y. P., Wang, D. Y., 2013. Translocation transfer and *in vivo* safety evaluation of engineered nanomaterials in the non-mammalian alternative toxicity assay model of nematode *Caenorhabditis elegans*. RSC Adv. 3, 5741–5757.

Zuo, Y. T., Hu, Y., Lu, W. W., Cao, J. J., Wang, F., Han, X., Lu, W. Q., Liu, A. L., 2017. Toxicity of 2,6- dichloro-1,4-benzoquinone and five regulated drinking water disinfection by-products for the *Caenorhabditis elegans* nematode. J. Hazard. Mater. 321, 456–463.

Zou, Y., Jin, C., Su, Y., Li, J., Zhu, B., 2016. Water soluble and insoluble components of urban $PM_{2.5}$ and their cytotoxic effects on epithelial cells (A549) in vitro. Environ. Pollut. 212, 627-635.

Supplementary Material S1.

S1. Sample Preparation and Analysis

500 mg (exactly weighted) of dusts were suspended in 50 mL of K-medium solution (three replicates) to obtain a final total concentration of 10 mg/mL; the suspension was placed in an ultrasonic bath for 30 min. The extracted solutions were then filtered on a cellulose nitrate filter (Merck Millipore Ltd., Billerica, MA, USA, 0.45 μm pore size). After the extraction step, the residual solid on collected on cellulose nitrate filter was acid-digested in a microwave oven (Ethos Touch Control with Q20 rotor, Milestone, Italy) by using 4 mL of HNO_3 (67% Promochem) and 2 mL of H_2O_2 (30% Suprapur, Merck Millipore Ltd.). The digested solutions were diluted in 50 mL of K-medium and filtered with syringe filters (GVS Filter Technology, 25 mm diameter, 0.45 μm pore size, Manufacturer in Morecambe, UK). The elemental concentrations determined in both extract (soluble fraction) and mineralized residue (insoluble fraction) solutions by using inductively coupled plasma mass spectrometry (ICP-MS, Bruker 820-MS, Bruker Daltonics s.r.l. Macerata, Italy). Further details on the analytical procedure are given in Canepari et al., 2009.

Limits of detection (LODs) were calculated as the mean plus three time the standard deviation of operative blanks (6 replicates).

Table S1. Limit of detection (LOD) and elemental composition of the soluble and insoluble fraction of BD, PA and SD - average mean (AM) and standard deviation (SD).

	UoM	LOD		Brake Dust (BD)				Pellet Ash (PA)				Saharan Dust (SD)			
		Soluble	Insoluble	Soluble		Insoluble		Soluble		Insoluble		Soluble		Insoluble	
				AM	*SD*	AM	*SD*	AM	*SD*	AM	*SD*	AM	*SD*	AM	*SD*
Al	mg/mL	1.4	7	2.9	*0.1*	923	*69*	12	*0.1*	460	*29*	6.2	*0.8*	49	*4*
As	mg/mL	0.5	1	< LOD		2.0	*0.1*	< LOD		< LOD		< LOD		< LOD	
Ba	mg/mL	2	20	26	*2*	774	*46*	11	*1*	193	*6.9*	3.3	*0.5*	23	*3*
Bi	mg/mL	0.2	0.1	< LOD		5.6	*0.2*	< LOD		0.114	*0.002*	< LOD		< LOD	
Cd	mg/mL	0.04	0.05	< LOD		< LOD		< LOD		2	*0.066*	< LOD		< LOD	
Ce	mg/mL	0.2	0.2	< LOD		2.9	*0.3*	< LOD		0.62	*0.16*	< LOD		< LOD	
Co	mg/mL	0.2	0.2	< LOD		2.1	*0.1*	< LOD		0.76	*0.05*	< LOD		< LOD	
Cr	mg/mL	0.1	1	< LOD		80	*3*	0.27	*0.04*	2.7	*0.3*	< LOD		< LOD	
Cs	mg/mL	0.008	0.009	0.017	*0.0014*	0.50	*0.04*	0.21	*0.0011*	0.047	*0.002*	0.0058	*0.0009*	0.015	*0.002*
Cu	mg/mL	0.1	3	5.8	*0.2*	1027	*85*	0.60	*0.06*	17	*0.8*	0.26	*0.009*	< LOD	
Fe	mg/mL	7	40	< LOD		25455	*918*	11	*3.6*	745	*9*	17	*0.75*	18	*1*
Ga	mg/mL	0.05	0.05	< LOD		0.6	*0.052*	< LOD		0.11	*0.0074*	< LOD		< LOD	
La	mg/mL	0.05	0.05	< LOD		1.6	*0.1*	< LOD		0.40	*0.08*	< LOD		0.037	*0.01*
Li	mg/mL	0.02	0.02	0.033	*0.002*	0.82	*0.06*	0.23	*0.01*	1.0	*0.1*	0.050	*0.004*	0.053	*0.006*
Mn	mg/mL	0.06	6	1.71	*0.04*	223	*13*	0.58	*0.03*	743	*39*	0.23	*0.07*	< LOD	
Mo	mg/mL	0.5	0.4	< LOD		15	*1*	< LOD		0.66	*0.02*	< LOD		< LOD	
Nb	mg/mL	0.06	0.05	< LOD		0.94	*0.01*	< LOD		< LOD		< LOD		< LOD	
Ni	mg/mL	0.09	0.6	0.17	*0.02*	15	*1*	0.14	*0.06*	3.0	*0.1*	0.14	*0.03*	0.70	*0.03*
P	mg/mL	15	400	< LOD		1608	*212*	< LOD		10071	*477*	18	*1*	< LOD	
Pb	mg/mL	0.05	0.3	0.057	*0.04*	5.7	*0.1*	0.11	*0.02*	3.8	*0.1*	0.12	*0.02*	0.14	*0.01*
Rb	mg/mL	0.07	0.3	2.0	*0.1*	4.9	*0.3*	22.6	*0.3*	3.7	*0.7*	1.0	*0.1*	0.92	*0.11*
Sb	mg/mL	0.03	0.04	1.55	*0.02*	208	*7*	0.026	*0.014*	0.71	*0.05*	< LOD		< LOD	
Se	mg/mL	0.3	0.4	0.72	*0.02*	< LOD		0.89	*0.16*	< LOD		1.08	*0.01*	< LOD	
Si	mg/mL	20	100	< LOD		2738	*147*	< LOD		1392	*312*	103	*13*	440	*106*
Sn	mg/mL	0.08	0.07	< LOD		126	*2*	< LOD		1.60	*0.04*	< LOD		< LOD	
Sr	mg/mL	0.1	1	3.11	*0.02*	30	*2*	7.9	*0.1*	78	*3*	14	*1*	4.2	*1.0*
Ti	mg/mL	0.1	0.6	0.32	*0.04*	61	*6*	0.34	*0.02*	31	*5*	0.45	*0.04*	1.9	*0.2*
Tl	mg/mL	0.006	0.006	0.010	*0.001*	0.069	*0.001*	0.017	*0.002*	0.149	*0.001*	0.017	*0.002*	0.016	*0.002*
U	mg/mL	0.06	0.05	< LOD		0.13	*0.012*	< LOD		< LOD		< LOD		< LOD	
V	mg/mL	0.06	0.2	< LOD		5.9	*0.3*	< LOD		0.49	*0.02*	< LOD		< LOD	
W	mg/mL	0.2	0.1	< LOD		0.40	*0.02*	0.64	*0.0078*	1.6	*0.1*	< LOD		< LOD	
Zn	mg/mL	0.8	6	2.95	*0.05*	267	*28*	1.7	*0.4*	119	*2*	7.6	*0.9*	13	*1*
Zr	mg/mL	0.02	0.3	0.040	*0.024*	30	*2*	0.026	*0.003*	2.3	*0.2*	< LOD		1.1	*0.1*

2.1.3. (A3) Potential of PM-Selected Components to Induce Oxidative Stress and Root System Alteration in a Plant Model Organism

Environment international (2019), *132*, 105094

Diego Piacentini [a], Giuseppina Falasca [a], Silvia Canepari [b], Lorenzo Massimi [b,*]

[a] Department of Environmental Biology, Sapienza University of Rome, P. le Aldo Moro, 5, Rome 00185, Italy;
[b] Department of Chemistry, Sapienza University of Rome, P. le Aldo Moro, 5, Rome 00185, Italy.

Abstract: Over the last years, various acellular assays have been used for the evaluation of the oxidative potential (OP) of particular matter (PM) to predict PM capacity to generate reactive oxygen (ROS) and nitrogen (RNS) species in biological systems. However, relationships among OP and PM toxicological effects on living organisms are still largely unknown. This study aims to assess the effects of atmospheric PM-selected components (brake dust - BD, pellet ash - PA, road dust - RD, certified urban dust NIST1648a - NIST, soil dust - S, coke dust - C and Saharan dust - SD) on the model plant *A. thaliana* development, with emphasis on their capacity to induce oxidative stress and root morphology alteration. Before growing *A. thaliana* in the presence of the PM-selected components, each atmospheric dust has been chemically characterized and tested for the OP through dithiothreitol (DTT), ascorbic acid (AA) and 2′,7′-dichlorofluorescin (DCFH) assays. After the exposure, element bioaccumulation in the *A. thaliana* seedlings, i.e., in roots and shoots, was determined and both morphological and oxidative stress analyses were performed in roots. The results indicated that, except for SD and S, all the tested dusts affected *A. thaliana* root system morphology, with the strongest effects in the presence of the highest OPs dusts (BD, PA and NIST). Principal component analysis (PCA) revealed correlations among OPs of the dusts, element bioaccumulation and root morphology alteration, identifying the most responsible dust-associated elements affecting the plant. Lastly, histochemical analyses of NO and $O_2^{\bullet-}$ content and distribution confirmed that BD, PA and NIST induce oxidative stress in *A. thaliana*, reflecting the high OPs of these dusts and ultimately leading to cell membrane lipid peroxidation.

Keywords: *Arabidopsis thaliana*; atmospheric dust; element bioaccumulation; oxidative potential; oxidative stress; root morphology.

1. Introduction

Over the last few decades, particulate matter (PM) toxicity on living systems has been extensively evaluated by *in vitro* human cells culture and the generation of oxidative stress has been identified as one of the major mechanisms by which atmospheric particulate exerts its adverse biological effects (Evans et al., 2013; Cachon et al., 2014; Li et al., 2015). Oxidative stress is a general response of living organisms to many harmful environmental factors and it occurs when there is an imbalance between the level of reactive oxygen (ROS) and nitrogen (RNS) species and the natural antioxidant defence. High levels of ROS and RNS can cause lipid and protein oxidation, damages to nucleic acids, enzyme inhibition and activation of programmed cell death pathway (PCD), ultimately leading to cell death (Sharma et al., 2012).

During the last years, various experimental studies have provided a plausible correlation among PM toxicity and PM potential to generate ROS and RNS in biological systems (Shi et al., 2003a, 2003b; Nel, 2005; Brook et al., 2010; Kelly and Fussell, 2012). Acellular assays, such as dithiothreitol (DTT), ascorbic acid (AA) and 2′,7′-dichlorofluorescin (DCFH) assays, have been widely used to measure the oxidative potential (OP) of atmospheric particulate in order to provide a predictive index of the oxidative capacity of PM samples (Simonetti et al., 2018a).

In a recent study, Simonetti and co-authors (2018a) applied the DTT, AA and DCFH assays to the soluble and insoluble fractions of NIST1648a (urban dust certified for its elemental content; NIST) and other six types of widespread atmospheric dusts (brake dust, pellet ash, road dust, soil dust, coke dust and Saharan dust) characterized by very different chemical compositions, which can be associated with different adverse health effects (Marcoccia et al., 2017 and references therein). Brake dust (BD), produced by brake pads lining, contains high concentrations of heavy metals and toxic elements (Thorpe and Harrison, 2008; Canepari et al., 2010a). Pellet ash (PA) is a PM component, whose contribution increased during the last decades due to the diffusion of wood and pellet stoves for domestic heating (Reche et al., 2012). Road dust (RD) is a complex mixture of particles produced by mechanical abrasion of vehicle components (brakes, tires) and natural soil particles resuspended by vehicular traffic (Canepari et al., 2008; Pant and Harrison, 2013). Soil dust (S) is the major natural component of PM; Saharan dust (SD) constitutes a major contribute to PM during long-range transport (Perrino et al., 2016). Coke dust (C), produced by refinery plants, contains high

concentrations of organic toxic species, which have been considered responsible for genotoxic and oxidative stress effects in animals and a risk for human health (Taioli et al., 2007; Vernile et al., 2013).

The three oxidative potential assays have provided very different results for each dust, confirming that none of the examined methods can be *a-priori* considered as representative of ROS and RNS generation pathways in biological organisms. Until now, few studies have been addressed to the *in vivo* evaluation of PM effects on plants or animals (Trifuoggi et al., 2019). Daresta and co-authors (2015) shown a toxic effect of PM_{10}, collected on quartz filters, on the root and shoot growth of tomato (*Solanum lycopersicum L.*) plants, while Popek and co-authors (2018) demonstrated a deleterious effect of PM on the efficiency of the photosynthetic apparatus of seven different deciduous plant species. Finally, Verma and Singh (2006) observed changes in the photosynthetic pigments, protein contents, leaf area and foliar surface architecture of two selected plant species grown in a highly auto-exhaust polluted area.

However, relationships among OP and PM toxicological effects on living organisms are still largely unknown (Costabile et al., 2019).

In this study, we assessed the OPs of the seven PM-selected components (BD, PA, RD, NIST, S, C and SD) through the AA, DTT, and DCFH assays (OP^{AA}, OP^{DTT} and OP^{DCFH}) and studied their effects on *Arabidopsis thaliana* (L.) Heynh seedlings. The bioaccumulation of PM elements in exposed plants and the capacity of each dust to induce oxidative stress in the roots were evaluated. This plant was chosen as model organism because of its ease of growing in *in vitro* conditions.

The roots are common and primary target organs of soil pollution (Zanella et al., 2016; Ronzan et al., 2018). *Arabidopsis thaliana* root system consists of primary root (PR) established during embryogenesis and post-embryonic lateral roots (LRs), whose morphology and development may be severely damaged by the presence of heavy metals and toxic elements (Feigl et al., 2014; Fattorini et al., 2017) in a dose-dependent manner and with the strongest effects in case of multiple contaminations (Sofo et al., 2013; Vitti et al., 2014; Fattorini et al., 2017). These pollutants may induce the production of high levels of ROS and RNS, such as superoxide anion ($O_2^{\bullet -}$) and nitric oxide (NO), which can cause oxidative damages and lead to root-elongation and meristem growth inhibition, as well as root biomass reduction, possibly resulting in plant death (Singh et al., 2007; Achary et al., 2008; Yuan and Huang, 2016). Unsaturated lipid peroxidation of biological membranes is one of the most evident symptoms of oxidative stress, leading to plasma membrane integrity

alteration, perturbing the bilayer structure and modifying membrane properties (Wong-Ekkabut et al., 2007).

This work aims to find correlations among the OP of the seven types of dust and their different capacity to alter primary root length (PRL) and lateral root density (LRD) and to generate ROS and RNS (high levels of $O_2^{\bullet-}$ and NO) in the root system of *A thaliana*. In addition, the element concentrations of each dust accumulated in the plant tissues were determined with the aim to identify the role of the single PM components in the alteration of the root system. Moreover, the correlations among OPs of the dusts, element bioaccumulation and root morphology alteration were individuated by performing principal component analysis (PCA). Lastly, NO, $O_2^{\bullet-}$ and lipid peroxidation content and cell/tissue distribution were performed to verify the induction of oxidative stress in the *A. thaliana* root apparatus by the selected atmospheric dusts.

2. Materials and Methods

2.1. Collection and Chemical Analyses of the Atmospheric Dusts

Brake dust was collected from the brake linings of three different cars. Ash produced by pellet burning was collected from the hood of a domestic pellet stove. Road dust was obtained by collecting the dust deposited on the road surface at several traffic sites in the city centre of Rome (Central Italy). Certified material NIST1648a (Urban particulate matter, NIST1648A, Sigma-Aldrich) was used as urban dust. Soil dust was collected from rural areas around the city of Rome, within a perimeter of 50 km. Coke dust was collected from the ground in proximity of a coal park, near a refinery plant. Finally, Saharan dust was collected in Algeria, in the North of Sahara Desert. More details about the collection of the dusts are reported by Canepari and co-authors (2010b) and by Marcoccia and co-authors (2017).

Each dust is a quite complex mixture of particles having different size and morphology; therefore, they were homogenized, sieved at 50 microns (Giuliani, Torino, Italy) and stored at -20° C until use. Chemical analyses of the dusts were performed by adapting to bulk dust an analytical procedure allowing the determination of both macro-components and trace elements on PM filters, previously optimized and validated by Canepari and co-authors (2006a, 2006b). The method used for the chemical analyses of the seven dusts is in accordance with Marcoccia and co-authors (2017).

2.2. Oxidative Potential Assays on the PM-selected Components

50 mg of each dust were weighed (Analytical Balance Gibertini Elettronica E505, sensitivity of 0.01 mg) and then suspended in 50 mL of Milli-Q water (produced by Arioso UP 900 Integrate Water Purification System); the obtained suspensions were then stirred for 20 min by mechanical agitation. Subsequently, the three OP assays (AA, DTT, and DCFH) were applied to the suspension of the seven dusts and the samples were filtered through a nitrocellulose filter (0.45 μm pore size, Merck Millipore Ltd., Billerica, MA, USA) just prior to each instrumental analysis. The followed DTT, AA and DCFH procedures are detailed in Simonetti et al (2018a). For each sample, three replicates were performed.

2.3. A. thaliana Exposure to the PM-selected Components

Seeds of *Arabidopsis thaliana* (L.) Heynh ecotype Columbia (Col, wild type, WT), were stratified and sterilized according to Della Rovere et al. (2013). The seeds were sown on a medium containing half-strength basal salt mixture (Duchefa Biochemie B.V, Haarlem, The Netherlands), 1% sucrose and 0.7% agar, at pH 5.8 (Murashige and Skoog, 1962) (Control). The medium was supplemented with 1000 mg L^{-1} of BD (BD), 125 μg L^{-1}, 250 μg L^{-1}, 500 μg L^{-1} or 1000 μg L^{-1} of PA (PA), 1000 mg L^{-1} of RD (RD), 1000 mg L^{-1} of NIST (NIST), 1000 mg L^{-1} of S, 1000 mg L^{-1} of C (C) and with 1000 mg L^{-1} of SD (SD), separately. The concentrations of the dusts were selected on the base of our preliminary unpublished data.

The seeds were grown in phytatrays (Phytatray^{tm} II, P5929 Sigma-Aldrich; n=8 seeds each phytatray and n=5 phytatrays each treatment) for 11 days at 22 ± 2 °C, 70% humidity, 16 h light/8 h dark conditions and at white light (intensity 100 μEm^{-2} s^{-1}). Milli-Q water (produced by Arioso UP 900 Integrate Water Purification System) was used for all culture media. In this work, we proposed *A. thaliana* as a model organism to study root system organization, development and oxidative stress in relation to PM pollutants, due to its small size, easy growth requirements and simple root structure. In addition, to date *A. thaliana* represents the most widely studied species for research in plant responses to environmental stresses. (Van Norman and Benfey, 2009).

2.4. Morphological Analyses of A. thaliana Root Apparatus

Primary root length (PRL) and lateral root density (LRD) were evaluated in 30 seedlings per treatment. PRL was measured under a LEICA MZ8 stereomicroscope (Leica Microsystems, Wetzlar, Germany) using the AxioVision software (Carl Zeiss, Release 4.7.2) from digital images captured by Zeiss AxioCam camera (Zeiss, Oberkochen, Germany). Lateral roots (LRs) and lateral root primordia

(LRPs) were observed and counted under light microscope, the corresponding LRD was calculated by dividing the total number of LRs and LRPs by the PR length where they were formed and expressed as mean number cm^{-1} (±SE).

2.5. Elemental Chemical Analysis of A. thaliana Tissues

Element bioaccumulation was evaluated in 4 groups of 5 seedlings per treatment. For each dust exposure, 20 seedlings were sampled in order to obtain 4 replicates per treatment, each one containing 5 seedlings exposed to the same dust. The 5 seedlings of each replicate were washed for three times with Milli-Q water and then oven (Inter Continental Equipment) dried at 55 °C for 48 hours. Subsequently, the seedlings were weighed and transferred into graduated 2.5 mL polyethylene tubes (Artiglass s.r.l., Due Carrare, PD, Italy) with the addition of 200 µL of ultrapure concentrated HNO_3 (67%; Promochem, LGC Standards GmbH, Wesel, Germany) and 100 µL of H_2O_2 (30%; Promochem, LGC Standards GmbH, Wesel, Germany). Each sample was then subjected to acid digestion for 30 min at 100 °C in an open vessel heated in a water bath, according to previous studies (Di Dato et al., 2017; Astolfi et al., 2018). After the acid digestion, the solutions were diluted into a final volume of 5 mL with Milli-Q water and then filtered through a pre-cleaned syringe filter (cellulose nitrate membranes, 0.45 µm pore size; GVS Filter Technology, Indianapolis, IN, USA). Fifteen of the 30 seedlings per treatment, previously analysed for root morphology, were also individually mineralised by using 100 µL of HNO_3 and 50 µL of H_2O_2 and then diluted into a final volume of 2.5 mL with Milli-Q water and filtered through a pre-cleaned syringe filter. Three blank solutions, consisting of Milli-Q water and reagents, were treated together with each digested sample set to trace possible contributions of sample contaminants.

Concentration of 32 elements (Al, As, Bi, Ca, Cd, Ce, Co, Cr, Cs, Cu, Fe, K, La, Li, Mg, Mn, Mo, Na, Nb, Ni, Pb, Rb, Sb, Sn, Sr, Ti, Tl, U, V, W, Zn, Zr) in the *A. thaliana* tissues of each sample was determined by using a quadrupole inductively coupled plasma mass spectrometer (ICP-MS, model 820-MS; Bruker, Bremen, Germany) equipped with a glass nebulizer (0.4 mL min^{-1}; Analytik Jena AG, Jena, Germany). For each element, external standard calibration curve was performed in the 1-500 µg L^{-1} range by serially diluting standard stock solutions (1000 ± 2 mg L^{-1} ; Exaxol Italia Chemical Manufacturers Srl, Genoa, Italy; Ultra Scientific, North Kingstown, RI, USA; Merck Millipore Ltd, Billerica, MA, USA). Rhodium (1000 ± 2 mg L^{-1}; Panreac Química, Barcelona, Spain) was set at 5 µg L^{-1} as internal standard for all the measurements to control the nebulizer efficiency.

Further details about the performance of the method and the used instrumental conditions are reported in Canepari et al. (2009) and in Astolfi et al. (2018), respectively.

Finally, the element concentrations were divided by the dry weight of each sample to obtain the element bioaccumulation expressed in μg g^{-1}.

Standard deviations of the four replicates per treatment were all below 20%.

2.6. Multivariate Statistical Analyses

Principal component analysis (Conti et al., 2007; Massimi et al., 2017, 2018), was performed to individuate correlations among the OPs of the dusts, element bioaccumulation and root morphology alteration in the plant model organism.

Multivariate statistical computations were operated on the data of the 15 seedlings per treatment morphologically and chemically analysed. The matrix of the data, composed of 119 samples (15 seedlings for each of the 7 treatments and 2 seedlings for each of the 7 controls) and 37 variables (3 dust OPs: OP^{AA}, OP^{DTT} and OP^{DCFH}; 32 element concentrations: Al, As, Bi, Ca, Cd, Ce, Co, Cr, Cs, Cu, Fe, K, La, Li, Mg, Mn, Mo, Na, Nb, Ni, Pb, Rb, Sb, Sn, Sr, Ti, Tl, U, V, W, Zn, Zr; 2 morphological measurements: PRL and LRD), was transformed by performing column mean centring and row and column autoscaling (to correct variations of the data due to the different scaling and units of the examined variables) and analysed by using the PCA. Multivariate statistical analyses were performed using the statistical software R (R-project for statistical computing, Ver. 3.0, 32-bit).

2.7. Detection of NO and $O_2^{\bullet-}$ Accumulation in the A. thaliana Root Apparatus

Intracellular NO content in roots was quantified using the cell-permeable diacetate derivative diamino-fluorescein-FM (DAF-FM DA solution, D2321 Sigma-Aldrich). Five roots per treatment were incubated in 20 mM HEPES/NaOH buffer (pH 7.4) ($C_8H_{18}N_2O_4S$ ≥99.5%; H4034 Sigma-Aldrich; NaOH ≥98%; 30620 Honeywell Fluka™) supplemented with 10 μM DAF-FM DA for 30 min at 25°C (Liu et al., 2017). After washing three times with the buffer to remove the excess of the fluorescent probe, roots were observed using a LEICA DMRB microscope (Leica Microsystems, Wetzlar, Germany) equipped with the specific set of filters (EX 450–490, DM 510, LP 515). No significant epifluorescence signal was detectable with the buffer alone. The images were acquired with a LEICA DC500 digital camera and analysed with the IM1000 image-analysis software (Leica Microsystems).

Nitro blue tetrazolium (NBT) is a chemical compound that is reduced by superoxide anion ($O_2^{\bullet-}$) forming a purple/blue precipitate called formazan, thus representing a useful assay to study the intracellular production of the superoxide anion. Five *A. thaliana* roots per treatment were stained for 30 min in a solution of 0.5 mg mL^{-1} nitro blue tetrazolium (NBT; Roche Diagnostics Corp., Gmbh, Germany) in 10 mM Tris-HCl (pH 7.40 ± 0.05; T-2663 Sigma-Aldrich). After having transferred the roots in distilled water to stop the reaction, they were kept in the chloral hydrate solution ($Cl_3CCH(OH)_2$ crystallized, ≥98.0%; 23100 Sigma-Aldrich) and instantly observed with LEICA DMRB light microscope equipped with Nomarski optics.

2.8. Visualization of Lipid Peroxidation in the A. thaliana Root Apparatus

Aldehydes that originated from lipid hydroperoxides (LOOHs) in the roots were visualized with Schiff's reagent (109033 Merk Millipore) as described by Yamamoto and co-authors (2003). Five root tips per treatment were excised and stained with Schiff's reagent for 20 min, rinsed with a freshly prepared sulphite solution (0.5% [w/v] $K_2S_2O_5$ in 0.05 m HCl; $K_2S_2O_5$ ≥ 98%; P2522 Sigma-Aldrich; HCl 32 wt. % in H_2O; W530574 Sigma-Aldrich), and then kept in the chloral hydrate solution (Weigel and Glazebrook, 2002). After, they were mounted on microscope slides and observed with Nomarski optics applied to a LEICA DMRB microscope, equipped with a LEICA DC 500 camera. The image analysis was performed using LEICA IM1000 Image Manager Software (LEICA).

Fig. 1 shows a block diagram of the conducted research in the work.

3. Results and Discussion

3.1. Oxidative Potentials of the PM-selected Components

Fig. 2 shows that the application of the three OP assays (AA, DTT, and DCFH) to the seven atmospheric dusts gave different results. The AA assay was particularly sensitive toward BD and NIST, while DTT and DCFH assays were less selective and the highest OP^{DTT} and OP^{DCFH} values were obtained for PA (Fig. 2 A-C). In fact, chemical composition of dusts is a key factor in determining the redox behaviour of the samples (Perrone et al., 2016; Chirizzi et al., 2017).

The three OP assays have demonstrated to be responsive to different chemical compounds, thus showing a dissimilar response to atmospheric dusts coming from different sources (Bates et al., 2019). For example, AA has been usually found to be sensitive to metals like copper and iron, mainly released in coarse particles by mechanical abrasion of vehicle brakes (Simonetti et al., 2018b). On the other hand, DTT has been found to be responsive to copper as well as to several quinones (Charrier

and Anastasio, 2012; Xiong et al., 2017) while both DTT and DCFH have demonstrated to be sensitive toward fine particles containing high amounts of organic compounds and mainly released by combustion processes such as biomass burning (Perrone et al., 2016).

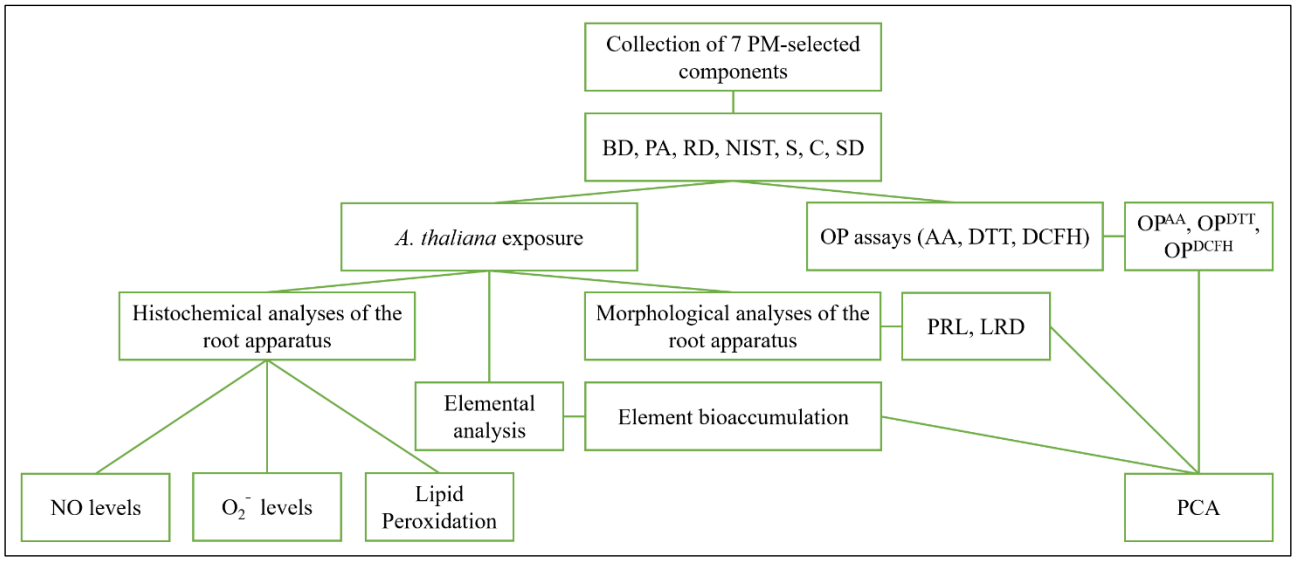

Fig. 1. Block diagram of the conducted research in the work.

Our results confirmed relevant differences in the relative sensitivity of the three assays toward the same dust. These results are in good agreement with those obtained by Simonetti et al. (2018a) for the insoluble fraction of the seven examined dusts. Overall, BD, PA and NIST were found to be the dusts with the highest oxidative potentials.

These dusts are characterized by high concentrations of several dangerous compounds, such as heavy metals and toxic organic species (Marcoccia et al., 2017), which may be identified as the main responsible for the capacity of the dusts to generate oxidative stress. AA was confirmed to be particularly sensitive toward dusts released by resuspension of particles formed through the abrasion of vehicle brakes and tires, such as BD and NIST. The high OP^{DCFH} and OP^{DTT} of PA suggest that emission of particles containing high concentrations of secondary organics (such as oxygenated polycyclic aromatic hydrocarbons) from biomass pellet burning, may drives oxidative responses in biological organisms, thus being particularly harmful for human health (Gilardoni et al., 2016). It is worth noting that the role on the adverse health effects of biomass burning, whose contribution to PM is increasing in the last years, is a very interesting issue that still requires further explorations.

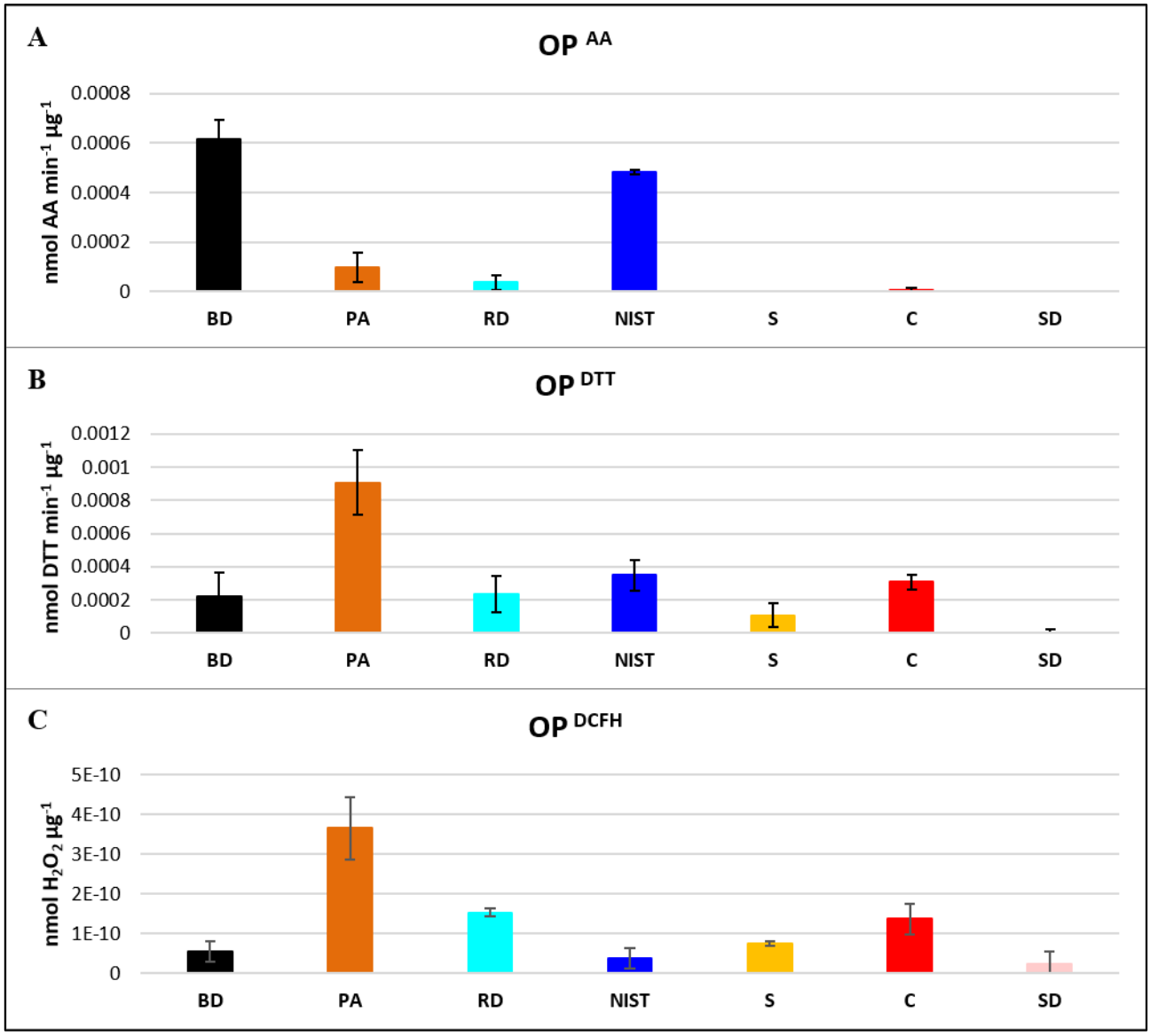

Fig. 2. Oxidative potentials of the seven PM-selected components, obtained through ascorbic acid (AA, A), dithiothreitol (DTT, B) and 2′,7′-dichlorofluorescin (DCFH, C) assays. Means (±SE) of three technical replicates.

To our knowledge, previous studies have been mostly focused on the oxidative potential evaluation of the soluble fraction of PM samples, which is thought to be more indicative of the ability of the dusts to generate ROS and RNS in living organisms. However, since the *A. thaliana* seedlings were exposed to both the soluble and insoluble PM-selected components, it must be considered that also the insoluble particles contained in the atmospheric dusts may have direct contact with the cells of the *A. thaliana* root and so may establish *in vivo* redox equilibria. In fact, although the interactions of

the insoluble particles with living organisms are still largely unknown, it is well known that PM released by combustion processes contains insoluble nanoparticles that are deemed to be able to enter organisms (Canepari et al., 2010a). This behaviour allows us to hypothesize a possible role of both the soluble and insoluble PM components in the generation of the oxidative stress (Knaapen et al., 2004; Zou et al., 2016).

3.2. Effects of the PM-selected Components on the A. thaliana Root Growth and Morphology

Morphology and development of PR and LR of *A. thaliana* seedlings grown in the presence of the dusts were differently altered. Fig. 3 shows that BD heavily and significantly ($P<0.001$) inhibited PR growth (i.e., 91,2%) and reduced lateral root density of 25% compared to Control. This behavior may be due to the high heavy metal and toxic element content in BD, as recently reported (Dodd et al., 2014; Maiorana et al., 2019).

Pellet ash treatment markedly affected PRL ($P<0.01$), while no statistically significant effects were detected for LRD (Fig. 3). It is worth noting that in the case of PA, we tested several concentrations, but the dramatic effects of PA at concentrations higher than 125 μg L^{-1} on plant germination and development, did not allow us to measure PRL and LRD. Therefore, we reported the results obtained by using 125 μg L^{-1} (Fig. 3). PA-treated root growth inhibition may be related to the high concentrations of Mn, toxic elements and organic toxic substances such as polycyclic aromatic hydrocarbons, which are released from wood pellet stove for domestic heating (Toscano et al., 2014; Abdoli et al., 2018). Road dust treatment altered root development by reducing LRD of 30.8% in comparison with Control ($P<0.01$, Fig. 3 B). This behavior may be related to the high As content in RD; in fact, it has been demonstrated that high As concentration can lead to alteration of *A. thaliana* root formation and development (Fattorini et al., 2017).

Urban dust exposure did not significantly alter PRL, while negatively affected LRD, which was reduced by 59.3% in comparison with Control ($P<0.001$, Fig. 3 B). Soil dust treatment increased PRL of 28.5% compared to Control ($P<0.01$), while no significant effects were detected for LRD (Fig. 3). In the coke dust treatment, we observed an increase of PR growth ($P<0.05$) and a reduction of LRD of 46.2% ($P<0.01$). The high organic content in C (Marcoccia et al., 2017) may explain the negative effects of this treatment on *A. thaliana* root system.

Lastly, no strong effects on *A. thaliana* root morphology and development were detected for SD treatment. Saharan dust had slight and no significant effects on *A. thaliana* roots probably because of its low metallic content (Marcoccia et al., 2017) (Fig. 3).

In addition, the different responses between PRL and LRD to the same dust might be explained by considering the different origins of PRs and LRs; embryonically pre-formed the first, post-embryonically formed the latter.

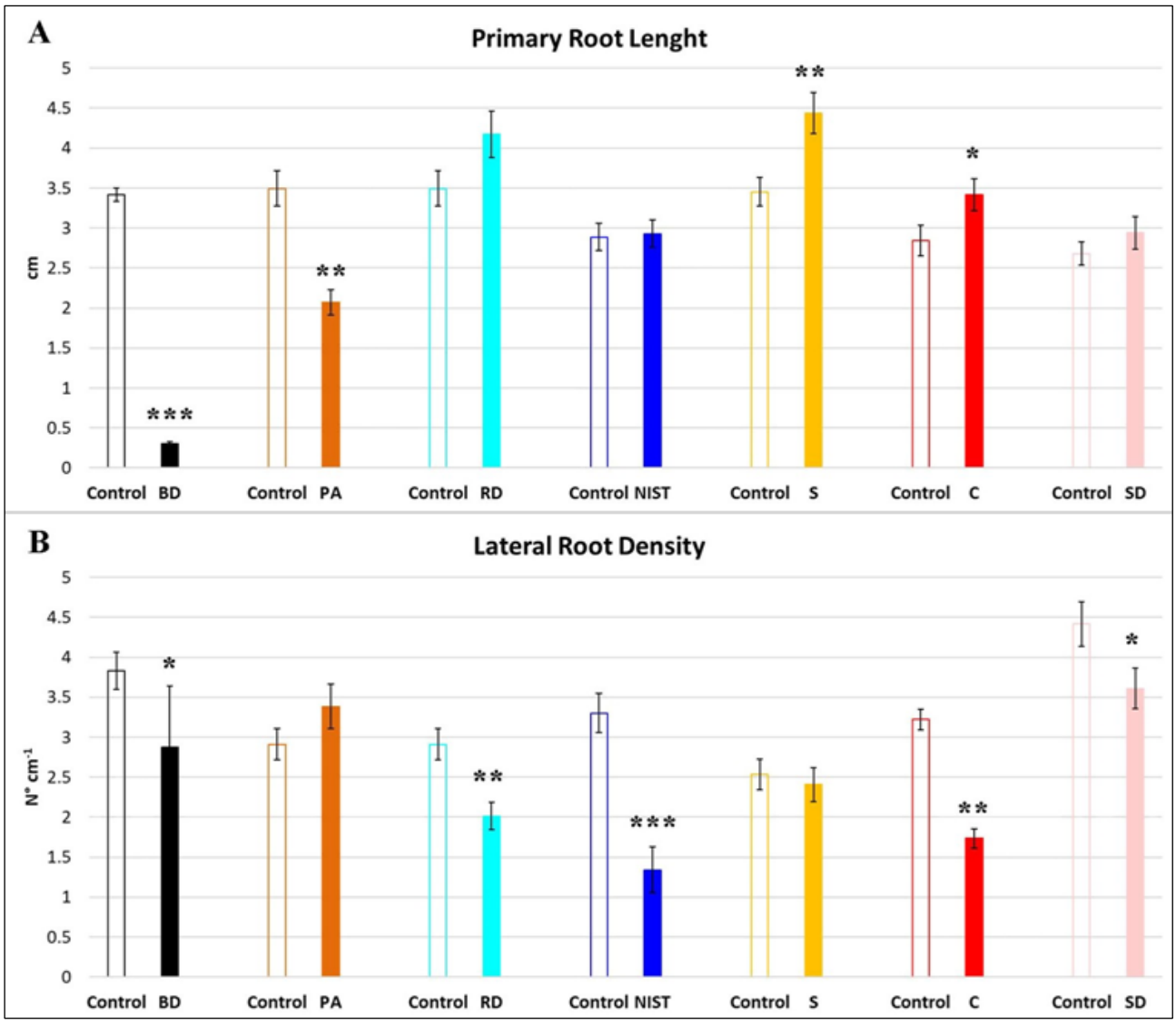

Fig. 3. Means (±SE) of primary root length and lateral root density of *A. thaliana* seedlings, exposed to the seven dusts. Asterisks represent statistical significance with respect to control at *P<0.05, **P<0.01 and ***P<0.001 (Student's t-test).

3.3. Accumulation of the Elements of the PM-selected Components in the A. thaliana Seedlings

Accumulation of the elements of the atmospheric dusts in the *A. thaliana* tissues after 11 days exposure to 1000 mg L^{-1} of BD, RD, NIST, S, C, SD and to 125 mg L^{-1} of PA, is reported in Table 1.

Table 1. Accumulation of the elements of the seven dusts in the *A. thaliana* seedlings (µg g^{-1}).

Elements	Mean of all controls		BD		PA		RD		NIST		S		C		SD	
			1000 mg L^{-1}		125 mg L^{-1}		1000 mg L^{-1}		1000 mg L^{-1}		1000 mg L^{-1}		1000 mg L^{-1}		1000 mg L^{-1}	
	Mean	*SD*	**Mean**	*SD*	**Mean**	*SD*	**Mean**	*SD*	**Mean**	*SD*	**Mean**	*SD*	**Mean**	*SD*	**Mean**	*SD*
Al	**100**	*7*	**452**	*72*	**68**	*13*	**68**	*14*	**828**	*3*	**180**	*22*	**99**	*13*	**37**	*4*
As	**0.28**	*0.06*	**0.97**	*0.19*	**0.065**	*0.14*	**1.2**	*0.2*	**0.0011**	*0.0003*	**0.33**	*0.06*	**1.0**	*0.2*	**0.055**	*0.007*
Bi	**0.22**	*0.01*	**0.79**	*0.12*	**0.099**	*0.019*	**0.043**	*0.011*	**0.58**	*0.06*	**0.036**	*0.005*	**0.030**	*0.007*	**0.031**	*0.009*
Ca	**9226**	*798*	**28176**	*1827*	**8731**	*1477*	**7621**	*1298*	**22204**	*397*	**10402**	*1748*	**10035**	*1868*	**2449**	*378*
Cd	**1.0**	*0.2*	**0.72**	*0.03*	**0.29**	*0.04*	**0.11**	*0.03*	**7.5**	*0.5*	**0.31**	*0.04*	**0.81**	*0.09*	**0.68**	*0.05*
Ce	**1.1**	*0.2*	**2.1**	*0.2*	**0.20**	*0.05*	**0.24**	*0.06*	**2.5**	*0.6*	**0.72**	*0.18*	**0.38**	*0.06*	**1.3**	*0.2*
Co	**0.68**	*0.01*	**2.0**	*0.2*	**0.21**	*0.06*	**0.14**	*0.04*	**1.9**	*0.3*	**0.31**	*0.02*	**0.34**	*0.03*	**0.40**	*0.08*
Cr	**16**	*1*	**28**	*5*	**2.8**	*0.6*	**2.3**	*0.5*	**75**	*19*	**4.2**	*0.9*	**13**	*1*	**26**	*6*
Cs	**0.071**	*0.006*	**0.68**	*0.05*	**0.017**	*0.002*	**0.019**	*0.004*	**0.37**	*0.01*	**0.057**	*0.009*	**0.024**	*0.002*	**0.026**	*0.004*
Cu	**36**	*2*	**194**	*8*	**15**	*2*	**14**	*2*	**64**	*1*	**27**	*3*	**28**	*5*	**14**	*1*
Fe	**521**	*36*	**2389**	*53*	**262**	*34*	**259**	*31*	**2102**	*115*	**359**	*37*	**346**	*22*	**526**	*67*
K	**18668**	*3004*	**19529**	*1017*	**43621**	*8114*	**27226**	*4528*	**40736**	*3067*	**4363**	*356*	**23318**	*4530*	**12106**	*916*
La	**0.54**	*0.06*	**0.20**	*0.03*	**0.092**	*0.012*	**0.12**	*0.02*	**1.4**	*0.2*	**0.49**	*0.02*	**0.26**	*0.03*	**0.80**	*0.20*
Li	**0.57**	*0.03*	**3.5**	*0.1*	**0.14**	*0.03*	**0.12**	*0.02*	**1.5**	*0.1*	**0.41**	*0.14*	**0.18**	*0.04*	**0.10**	*0.02*
Mg	**1690**	*49*	**2043**	*47*	**1661**	*244*	**1311**	*56*	**2946**	*265*	**1188**	*99*	**1463**	*284*	**1594**	*385*
Mn	**200**	*26*	**214**	*9*	**1388**	*361*	**180**	*31*	**332**	*31*	**168**	*31*	**320**	*30*	**216**	*45*
Mo	**7.3**	*0.8*	**6.0**	*0.1*	**11**	*2*	**11**	*2*	**10**	*1*	**4.7**	*1.5*	**11**	*1*	**4.4**	*0.6*
Na	**2671**	*342*	**10352**	*732*	**2930**	*1570*	**2783**	*2154*	**6832**	*1166*	**2579**	*815*	**2496**	*672*	**2371**	*1695*
Nb	**0.079**	*0.004*	**0.56**	*0.12*	**0.0070**	*0.0020*	**0.0074**	*0.0034*	**0.23**	*0.05*	**0.017**	*0.004*	**0.018**	*0.003*	**0.016**	*0.002*
Ni	**20**	*1*	**40**	*1*	**4.4**	*0.8*	**4.7**	*1.0*	**102**	*16*	**6.3**	*0.6*	**10**	*1*	**31**	*9*
Pb	**4.0**	*0.2*	**29**	*2*	**0.8**	*0.1*	**1.0**	*0.2*	**37**	*1*	**6.6**	*0.5*	**6.1**	*1.0*	**2.79**	*0.82*
Rb	**6.3**	*1.2*	**11**	*1*	**7.8**	*1.3*	**5.0**	*1.1*	**16**	*2*	**2.6**	*0.6*	**5.0**	*1.1*	**6.2**	*1.2*
Sb	**0.38**	*0.03*	**9.7**	*0.4*	**0.18**	*0.03*	**0.11**	*0.02*	**1.7**	*0.1*	**0.20**	*0.05*	**0.15**	*0.04*	**0.086**	*0.019*
Sn	**0.49**	*0.09*	**3.6**	*0.2*	**0.21**	*0.05*	**3.8**	*0.8*	**3.2**	*0.4*	**0.31**	*0.04*	**0.26**	*0.06*	**0.22**	*0.04*
Sr	**21**	*1*	**19**	*3*	**20**	*4*	**31**	*5*	**40**	*5*	**68**	*11*	**57**	*5*	**31**	*5*
Ti	**4.6**	*0.1*	**11**	*1*	**2.5**	*0.4*	**2.3**	*0.3*	**28**	*1*	**5.4**	*1.0*	**4.6**	*0.8*	**3.3**	*0.3*
Tl	**0.058**	*0.002*	**0.69**	*0.13*	**0.035**	*0.007*	**0.010**	*0.002*	**0.12**	*0.02*	**0.059**	*0.011*	**0.031**	*0.003*	**0.013**	*0.002*
U	**0.076**	*0.002*	**0.25**	*0.07*	**0.0074**	*0.0014*	**0.012**	*0.003*	**0.13**	*0.01*	**0.061**	*0.007*	**0.027**	*0.001*	**0.026**	*0.003*
V	**0.34**	*0.02*	**3.9**	*0.2*	**0.24**	*0.08*	**0.23**	*0.06*	**3.7**	*0.1*	**1.5**	*0.3*	**5.5**	*0.4*	**0.32**	*0.05*
W	**0.035**	*0.007*	**0.98**	*0.04*	**0.28**	*0.05*	**0.017**	*0.003*	**0.25**	*0.01*	**0.077**	*0.011*	**0.074**	*0.018*	**0.040**	*0.007*
Zn	**409**	*36*	**1561**	*123*	**171**	*32*	**171**	*33*	**825**	*40*	**358**	*52*	**916**	*80*	**296**	*39*
Zr	**0.34**	*0.02*	**5.8**	*1.1*	**0.11**	*0.04*	**0.11**	*0.04*	**2.6**	*0.1*	**0.35**	*0.06*	**0.068**	*0.013*	**0.16**	*0.01*

Results of the elemental analyses showed that the most bioaccumulated elements were Cd, Ce, Co, Cu, Fe, Mn, Pb, Sb, Sn, Ti, V, Zn and Zr. As expected, element concentrations in the exposed individuals were extremely variable depending on the dust type, and, in most cases, considerably higher than the control. The enrichment factors (ratio between the concentration in exposed and in control individuals) were particularly high (up to about five times) for Cs, Li, Nb, Pb, Sb, Sn, Tl, V, W and Zr after exposure to BD; Mn and W after exposure to PA; Sn after exposure to RD; Al, Cd, Pb, Sn, Ti, V, W, Zr after exposure to NIST; and V after exposure to C. In general, the enrichment factors tended to increase together with the increase of the element concentration in the different dusts. In fact, Mn and Pb are the most concentrated elements in PA and NIST, respectively, while Cu, Sb and Sn are the main constituents of BD. On the other hand, high amounts of Sn are in RD, V is one of the most abundant elements in C, and heavy metals and toxic elements are less concentrated in S and SD (Marcoccia et al., 2017).

Pearson correlation coefficients among the element concentration in the dusts and in the *A. thaliana* tissues were calculated to verify the element bioaccumulation capacity of *A. thaliana*. Low bioaccumulation capacity was found for As, Bi, Ca, Cr, Cs, K, La, Li, Mg, Mo, Na, Nb, Ni, Rb, Sr, Tl, U and W (Person coefficients < 0.5), while Cd, Ce, Co, Cu, Fe, Mn, Pb, Sb, Sn, Ti, V, Zn and Zr were efficiently bioaccumulated (Person coefficients > 0.5). Among these elements, Cd, Co, Cu, Mn and Sb were found to be the most bioaccumulated (Person coefficients > 0.8).

Overall, *A. thaliana* turned out to be able to accumulate high amounts of elements released through the abrasion of vehicle brakes, such as Cu, Fe, Mn, Sb, Sn (Massimi et al., 2019), and tires, such as Zn (Councell et al., 2004), whose concentrations are particularly high in BD, RD and NIST. Besides, it was able to accumulate high amounts of Mn and Pb released in particles produced by biomass pellet burning (Simonetti et al., 2018b), whose concentrations are particularly high in PA.

3.4. Principal Component Analysis

Principal component analysis was performed to individuate correlations among OPs of the dusts, element bioaccumulation and root morphology alteration, in order to identify the most responsible dust-associated elements affecting the model plant growth. Five significant components accounting for 83.94% were obtained (the scores and loadings are shown in supplementary material S1); the variance explained by each component is: 47.58%, 18.32%, 10.12%, 4.48% and 3.44%.

First component (PC1), which explains the 47.58% of the total variance, well separates the samples whereby the highest concentrations of elements for which AA is particularly sensitive were

bioaccumulated (*A. thaliana* seedlings exposed to BD and NIST) from the others. However, PC1, along with the second component (PC2), is unable to separate the samples exposed to PA, RD, C, SD and S from the controls (score plot and loading plot of PC1 and PC2 are shown in supplementary material S1). PC2 well explains the element bioaccumulation variability between the samples exposed to BD and the samples exposed to NIST while the third component (PC3) well separates the samples exposed to PA from the others depending on the Mo, Mn and K bioaccumulation and the OP^{DTT} and OP^{DCFH} variability in the PM-selected components. Therefore, PC2 and PC3, which explain the 28.42% of the total variance, were represented, since they better reflect the element bioaccumulation and OPs variability in all the examined samples. PCA results are summarized in the score plot and in the loading plot of Fig. 4.

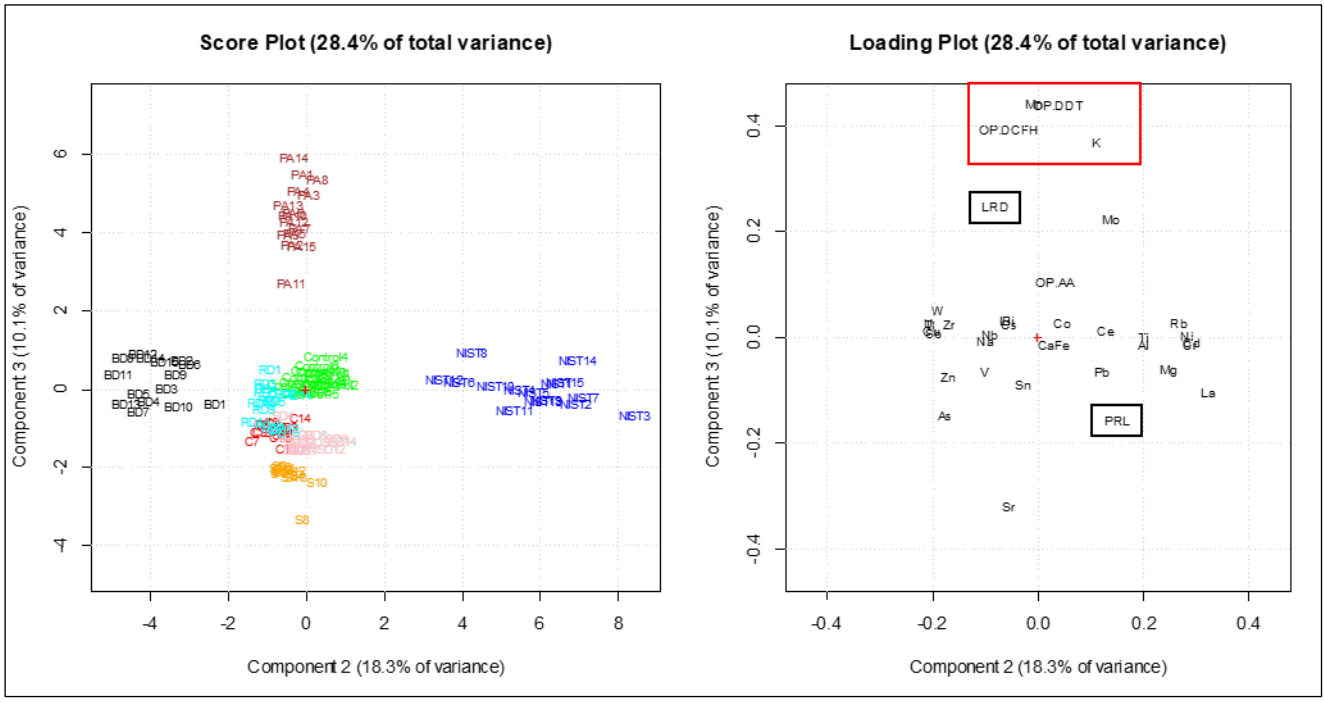

Fig. 4. Score plot and loading plot of PC2 and PC3 of the PCA performed on the OPs of the dusts, element bioaccumulation and PRL and LRD alteration in the *A. thaliana* seedlings.

From Fig. 4, we can observe that the samples are separated along PC2 and PC3 depending on the OP^{AA}, OP^{DTT} and OP^{DCFH} of the dusts, the element concentrations accumulated in the *A. thaliana* tissues, and the PRL and LRD of the examined seedlings after each dust exposure. The controls are plotted on the central part of the score plot, thus showing PRL and LRD mean values and no element

bioaccumulation, since they were not grown in the presence of PM-selected components. BD samples are in the left part of the score plot, in the opposite direction along PC2 respect to PRL of the loading plot, since the seedlings exposed to brake dust showed the highest PRL reduction. From the loading plot, we can observe that in BD samples, the high bioaccumulation of As, Bi, Cs, Cu, Li, Na, Nb, Sb, Sn, Tl, U, V, W, Zn and Zr may be responsible for the strong inhibition of the primary root growth. On the other hand, NIST samples are plotted on the right part of the score plot, since the seedlings exposed to urban dust showed a slight increase of PRL and the highest decrease of LRD.

From the loading plot, we can observe that the inhibition of the lateral root production may be due to the high bioaccumulation of Al, Cd, Ce, Cr, La, Mg, Ni, Pb, Rb and Ti. In fact, as previously mentioned, it is well known that the root cell division and differentiation pattern may be severely damaged by the presence of heavy metals such as Cd, Cr, Ni and Pb, in a dose-dependent manner and with the strongest effects in case of multiple contamination (Vitti et al., 2014; Zanella et al., 2016; Fattorini et al., 2017). On the contrary, PA samples are in the upper part of the score plot, since the seedlings exposed to pellet ash showed a strong reduction of PRL ($P<0.01$) and a slight and not statistically significance increase of LRD. From the loading plot, in PA samples the highest concentrations of K and Mn were bioaccumulated; these elements could be then responsible for the inhibition of the primary root length growth as reported by Zhao and co-authors (2017). Finally, RD, C, S and SD samples are plotted on the central lower part of the score plot, since the *A. thaliana* seedlings exposed to road dust, coke dust, soil dust and Saharan dust, showed a slight PRL increase and LRD reduction, which may be attributed to the high bioaccumulation of As, Sn, Sr, V and Zn. Arsenic and tin were mostly bioaccumulated in RD samples, strontium in S samples, and vanadium and zinc in C samples.

OPs of the dusts are all plotted on the upper part of the loading plot, in the same direction of PA samples. OP^{DTT} and OP^{DCFH} were found to be well correlated with the K and Mn concentrations accumulated in the *A. thaliana* seedlings exposed to PA, while OP^{AA} appeared to be related with Mo and other elements bioaccumulated in BD, RD and NIST samples (Bi, Ce, Co, Cs, Cu, Li, Mo, Nb, Ni, Rb, Sb, Ti, Tl, U, W and Zr). These results agree with those obtained in Simonetti et al. (2018a), where Mn concentration has been found to be highly correlated with the OP^{DTT} and the OP^{DCFH} of the insoluble fraction of PA and Co, Ce, Cu, Mo, Ni, Ti and Zr have been identified as responsible for the generation of the OPs of BD and NIST. Lastly, OP^{AA}, OP^{DTT} and OP^{DCFH} are plotted on the opposite direction respect to PRL; this indicates that OPs of the dusts are positively correlated with PRL reduction. Therefore, since primary root is established during the *A. thaliana* embryogenesis and

the inhibition of the primary root length was observed only in BD, PA and NIST samples, we can suppose that brake dust, pellet ash and urban dust induced oxidative stress during the early stages of post-embryogenic development of the exposed seedlings. This led to a slight increase of the post-embryonic lateral root production only in the case of PA exposure. Overall, pellet ash, which contains toxic elements and toxic organic compounds was found to be the dust with the highest potential to induce oxidative stress in the test living organism (de Oliveira Alves et al., 2011).

3.5. Detection of NO and $O_2^{\bullet-}$ *Levels and Lipid Peroxidation in A. thaliana roots*

The roots of 11-days old *A. thaliana* seedlings grown in the presence of BD, PA, RD and NIST were collected and treated for NO, $O_2^{\bullet-}$ and lipid peroxidation visualization, respectively, to verify if the PM-selected components may trigger to oxidative stress in the tested biological system. The endogenous level and distribution of NO in roots greatly changed with respect to the control depending on the type of atmospheric dust tested (Fig. 5).

In the roots grown in control conditions, NO expression was weak and mainly localized in the epidermis of LRPs and both in the vascular tissues and cortical parenchyma of LRs and PRs, while low NO expression was detected in the root apical meristem (Fig. 5, A-C).

Brake dust and PA deeply increased and delocalized endogenous NO in *A. thaliana* roots respect to the control (Fig. 5 D-I and A-C in comparison). Pellet ash increased NO production in all the tissues of both LRs and PRs and in the epidermis of LRPs as well, while BD strongly increased NO level and distribution in the stele, cortex and epidermis of the LRs. Road dust weak increased NO signal in the cortex and epidermis of LRs tip and mature zone (Fig. 5, J-L). Interestingly, NIST treated roots showed reduced level of NO both in LRs and PRs respect to the control (Fig. 5, M-O).

This result indicates that the endogenous level and distribution of NO in *A. thaliana* roots are differently modulated by all the seven dusts, probably because of the peculiar mechanisms of action of the different chemical compounds of each dust.

The alteration of the root cell redox homeostasis, due to dust exposure, causing a variation of NO concentration and localization, was also related to different $O_2^{\bullet-}$ levels, as shown by NBT assay (Fig. 6).

In the roots not exposed to dusts, NBT staining was very weak in the basal portion of the LRPs, while in the LRs and PRs was strictly localized in the vasculature of the elongation and differentiation zones and absent in the apical meristem (Fig. 6, A-C).

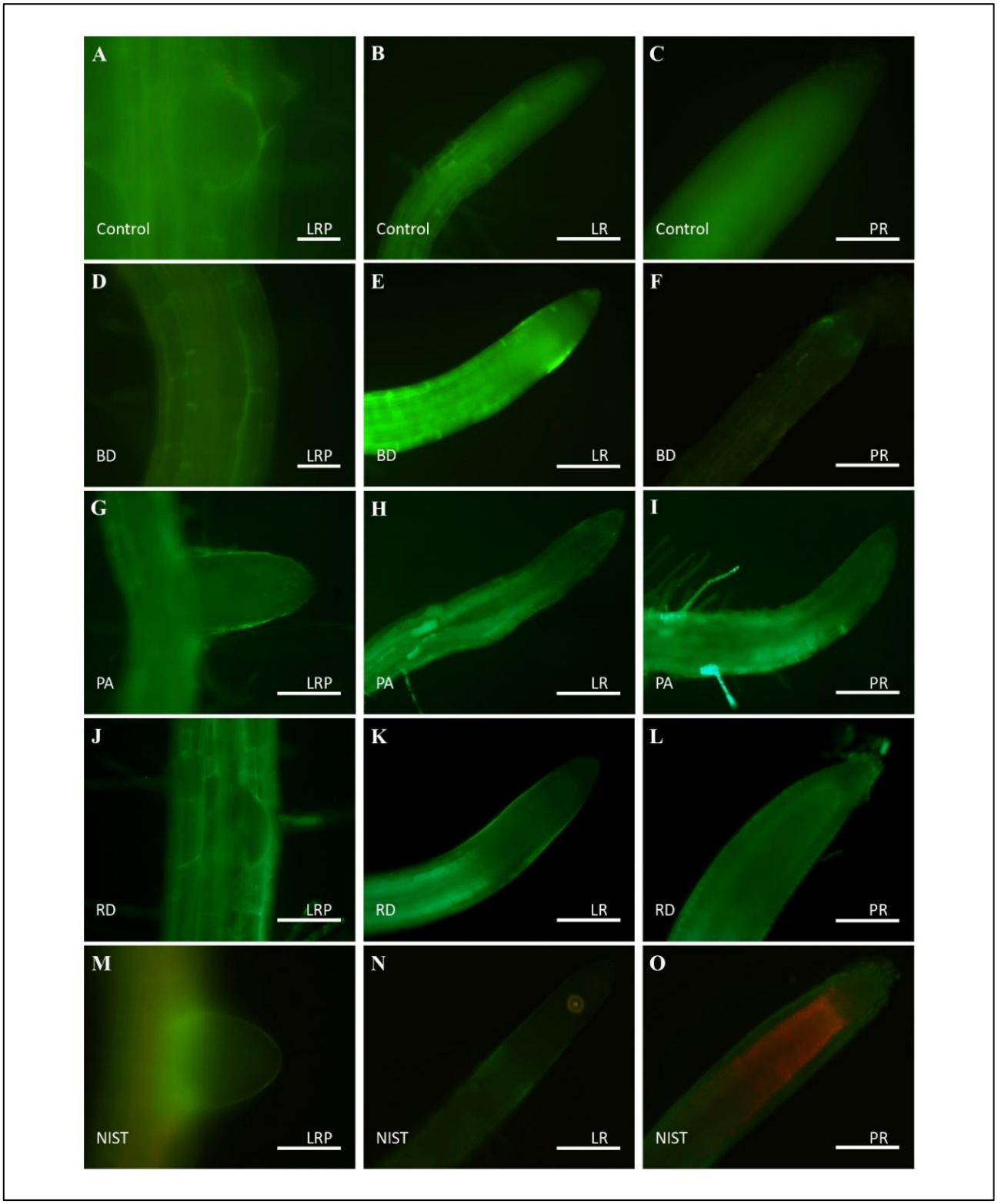

Fig. 5. NO signal (bright green color) in *A. thaliana* LRPs, LRs and PRs not exposed (control, A-C) or exposed to BD (D-F), PA (G-I), RD (J-L) and NIST (M-O). Bars = 30µm (A, M) and 100µm (B-L, N-O).

Brake dust treatment (Fig. 6, D-F) significantly increased the NBT staining and pattern both in the LRs and PRs and in the LRPs. Indeed, in this treatment the signal was expressed in the entire LRPs, including the surrounding tissues, while was heavily located in the tip and in the vasculature of the LRs and PRs.

Pellet ash treatment (Fig. 6, G-I) greatly delocalized and increased the staining, especially in the meristematic zone of LRs and PRs, while low effects were detected in the LRPs compared to the NIST and BD treatments.

In the LRPs treated with RD, the $O_2^{\bullet-}$ signal was comparable to the control, while the LRs and PRs showed an increase of the signal in the differentiation and elongation zones, and it was quite extended to the meristematic zone of the root (Fig. 6, J-L). Finally, NIST (Fig. 6, M-O) treated LRPs showed a strong increase of the staining, which deeply covered the entire LRPs, while in the LRs and PRs spread in a similar manner to BD treatment. These analyses demonstrated that all the examined dusts were able to induce an increase of $O_2^{\bullet-}$ production in *A. thaliana* roots. In addition, dust-related $O_2^{\bullet-}$ production involved root tissues where $O_2^{\bullet-}$ is normally present at very low concentration, such as in the root apical meristem.

The damaging effects of the oxidative stress of the selected dusts, which are related to a variation in both NO and $O_2^{\bullet-}$ accumulation and localization were also highlighted by the Schiff test in the *A. thaliana* roots. Schiff's reagent reacts with aldehydes that originate from lipid peroxides downstream of reactive oxygen species to produce an imine, also called a Schiff base, which is magenta or purple in color, thus representing a useful tool for the indirect detection of lipid peroxidation (Gilbert and Martin, 2016).

All the examined dusts increased the lipid peroxidation of *A. thaliana* seedling roots, with the strongest effects induced by PA and RD (Fig. 7). Control of LRs and PRs did not show notable dye formation, except for a faint staining in the tissues of PRs next to the forming LRPs and in the epidermis of the same LRPs (Fig. 7 A-C). This fact is probably due to the histochemical reaction between the reagent and the byproducts of enzymes, whose activity is related to cortical cell separation during the lateral root primordium emergence (Seo et al., 1998).

In all the treatments, histochemical staining in the LRPs significantly increased compared to the control LRPs (Fig. 7 D, G, J, M). Moreover, the stele, cortex and epidermis tissues of the PRs mature zone of the roots exposed to PA were positive to Schiff reaction (Fig. 7 I). The BD treatment induced a localized staining in the LRPs and in the vascular tissues and pericycle of the PRs close to the LRPs (Fig. 7 D). NIST and BD-treated LR tips showed a slight increase of the staining (Fig. 7, N and E).

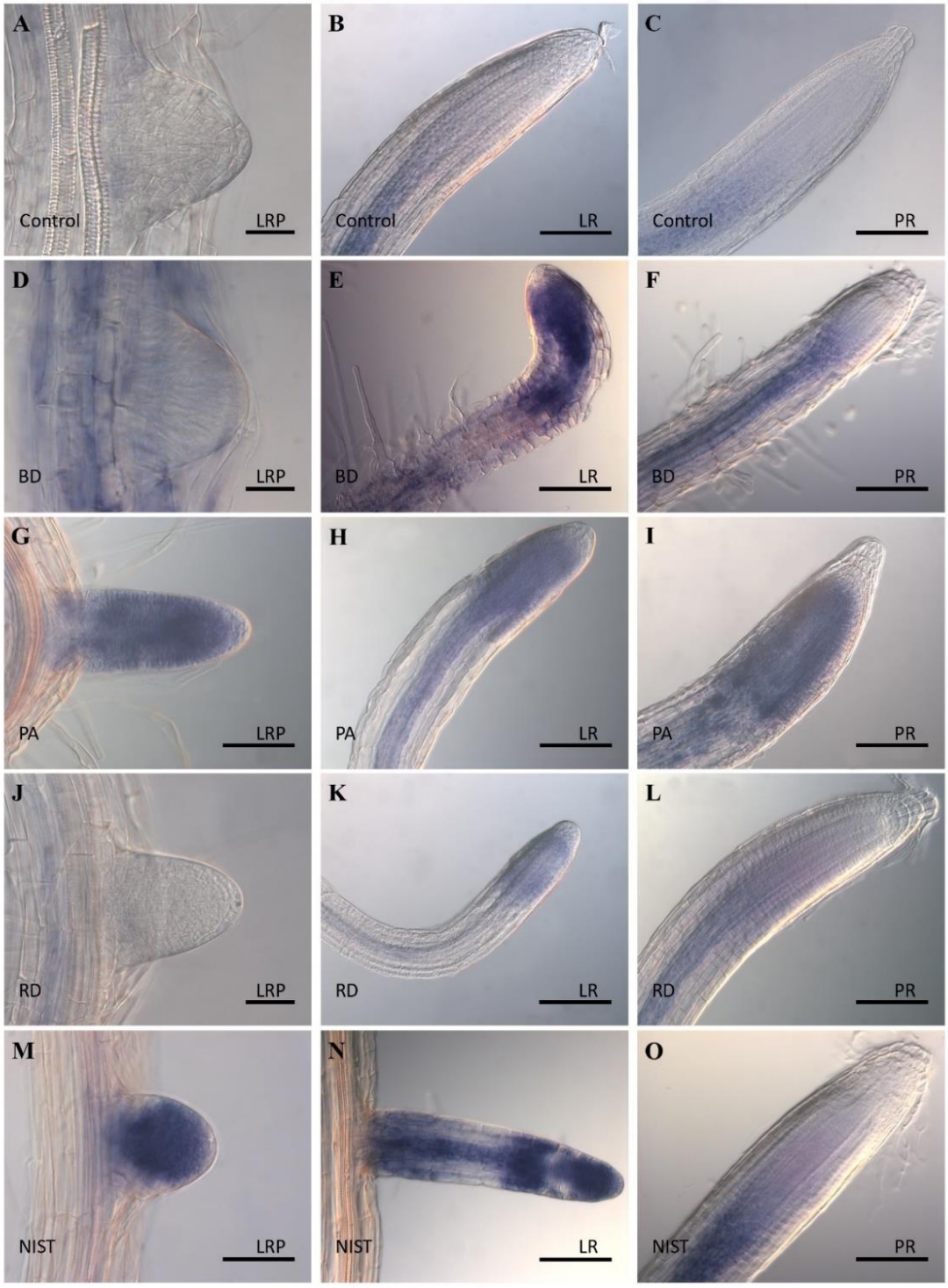

Fig. 6. Superoxide radical (purple/blue color) detected by NBT staining in *A. thaliana* LRPs, LRs and PRs not exposed (control, A-C) or exposed to BD (D-F), PA (G-I), RD (J-L) and NIST (M-O). Bars = 30µm (A, D, M) and 100µm (B-C; E-L; N-O).

Road dust and PA-treated LRs showed a more evident peroxidation process activity with respect to the control (Fig. 7, K and H). Pellet ash was the treatment that most affected the *A. thaliana* cell membrane roots integrity. In fact, in this treatment both the LRs and the PRs showed a very strong and widespread histochemical staining, reflecting a deep degradation of the cell membrane lipids. (Fig. 7 G-I) The toxicity of PA also affected the definition of the root tissues, causing a precocious differentiation of the primary tissues in LRs (Fig. 7 H). Lastly, *A. thaliana* RD, NIST and BD-treated PR tips did not, or only weakly showed, an increase of the histochemical staining, compared to the control (Fig. 7).

Overall, results showed that BD, PA, RD and NIST can deeply alter the cellular redox homeostasis of *A. thaliana* roots, acting on the biosynthesis and distribution of NO and $O_2^{\bullet-}$ and thus leading to oxidative damages and root cell membrane degradation. In addition, the generation of superoxide anion and nitric oxide in plant cells may lead to the formation of more reactive oxygen and nitrogen species such as hydroxyl radical (•OH), singlet oxygen ($^1O_2$) and peroxynitrite ($ONOO^-$), each of which may cause membrane lipid peroxidation and cellular damages, as previously reported for *A. thaliana* (Triantaphylidès et al., 2008; Corpas et al., 2014).

The observed increase and distribution alteration of NO and $O_2^{\bullet-}$ in *A. thaliana* roots may be explained by the high bioaccumulation of toxic elements and heavy metals in the seedlings grown in the presence of the PM-selected components.

In addition, this has been confirmed by several reports, which highlighted the role of both NO and $O_2^{\bullet-}$ as key mediators of metal toxicity in plants (Singh et al., 2017; Yuan and Huang, 2016). It is worth nothing that also the less bioaccumulated elements such as As, Cr and Ni, which can be toxic at very low concentrations, may have contributed to the oxidative damages observed in the *A. thaliana* roots. Pellet ash was the treatment that mostly affected the oxidative balance in the *A. thaliana* roots and the high bioaccumulation of Mn and K in the PA-treated seedlings was probably the main cause of the strong increase of NO and $O_2^{\bullet-}$ observed in the LRs and PRs.

Finally, Schiff's reagent analyses confirmed the role of the dusts as strong oxidizing agents, which ultimately led to lipid peroxidation and membrane injury in *A. thaliana* roots, by acting on the NO and $O_2^{\bullet-}$ content and distribution. Here too, PA treated roots were the most stained, revealing a close correspondence between aldehydes accumulation, NO and $O_2^{\bullet-}$ content in roots, thus indicating PA as the most toxic PM-selected component tested.

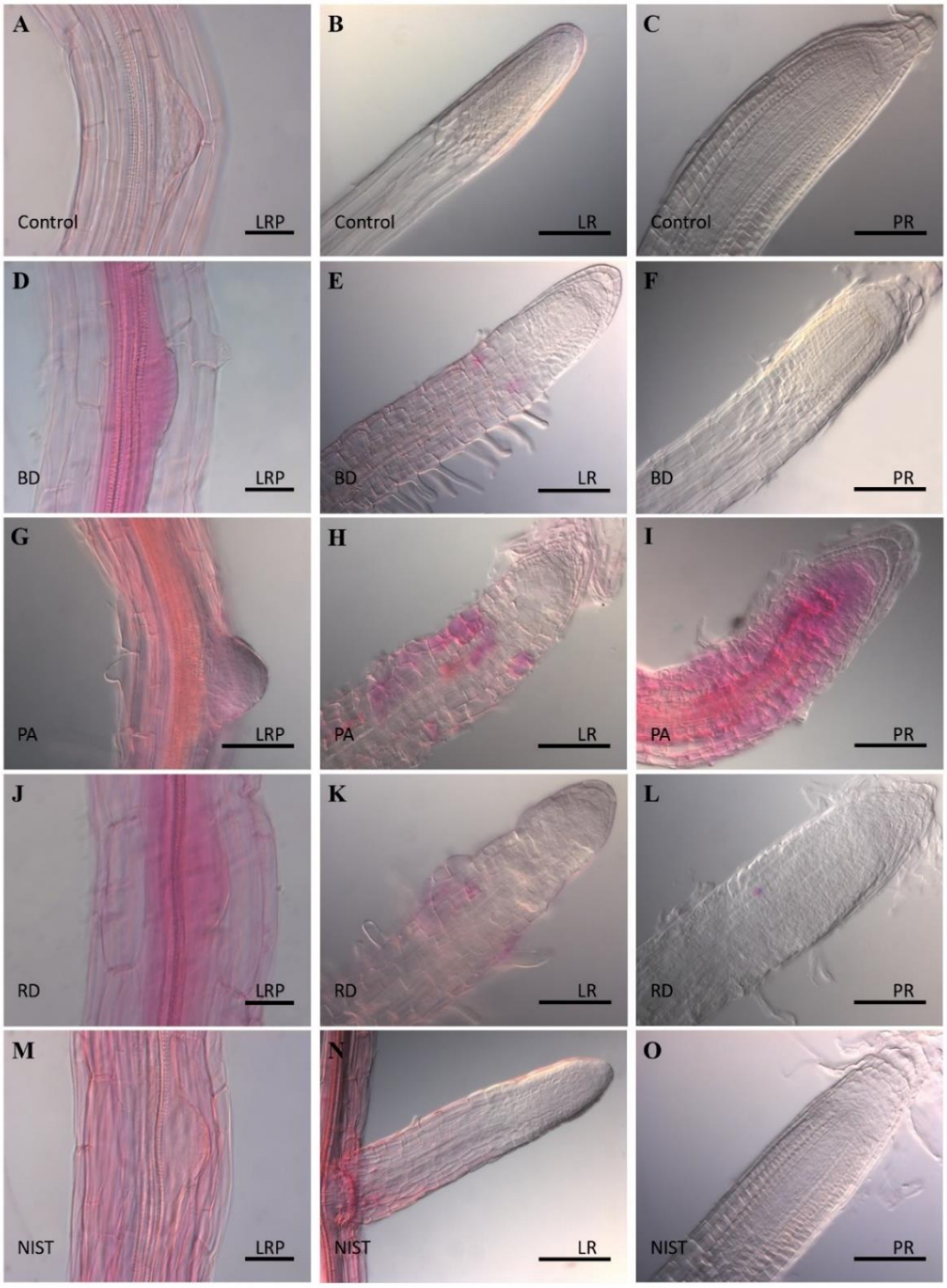

Fig. 7. Lipid peroxidation highlighted by Schiff's reagent in *A. thaliana* LRPs, LRs and PRs not exposed (control, A-C) or exposed to BD (D-F), PA (G-I), RD (J-L) and NIST (M-O). Bars: = 30µm (A, D, J, M) and 100µm (B-C; E-I; K-L; N-O).

The different alteration of the cellular redox homeostasis in the roots of the *A. thaliana* seedlings exposed to the atmospheric dusts confirmed that the divergent relative sensitivity of the AA (more sensitive for BD and NIST), DTT and DCFH (more sensitive for PA) assays toward the PM-selected components is mainly due to the peculiar oxidative mechanisms of actions of their different chemical compounds.

4. Conclusions

We evaluated the oxidative potentials and the effects of seven PM-selected components, previously chemically analysed, on the model plant *A. thaliana*. Bioaccumulation of the elements of the atmospheric dusts in the *A. thaliana* seedlings was determined and both root morphological and oxidative stress analyses were performed.

Brake dust, PA and NIST showed the highest oxidative potentials. In fact, BD and NIST were the most responsive dusts to the OP^{AA} assay, while PA was the dust with the highest values for OP^{DTT} and OP^{DCFH} assays. Except for S and SD, all the examined dusts altered *A. thaliana* root morphology, with the strongest effects for the dusts that showed the highest OPs (BD, PA and NIST). Indeed, brake dust and pellet ash were the only PM-selected components that inhibited primary root growth, while urban dust heavily inhibited lateral root density. High concentrations of Cs, Li, Nb, Pb, Sb, Sn, Tl, V, W and Zr were found to be accumulated in the tissues of the seedlings exposed to BD; Mn and W in the seedlings grown in the presence of PA and Al, Cd, Pb, Sn, Ti, V, W, Zr in the seedlings exposed to NIST. PCA revealed correlations among OPs of the dusts, element bioaccumulation and root morphology alteration, identifying the most responsible dust-associated elements affecting the plant model organism. OP^{DTT} and OP^{DCFH} were found to be well correlated with the K and Mn concentrations accumulated in the *A. thaliana* seedlings exposed to PA, while OP^{AA} appeared to be related with Mo and other elements bioaccumulated in BD, RD and NIST samples. Moreover, OPs of the dusts were found to be positively correlated with PRL and LRD inhibition. Therefore, BD, PA and NIST were identified as the PM-selected components with the highest potential inducing oxidative stress and root development alteration.

The analysis of $O_2^{\bullet-}$ and NO production and cell membrane oxidation in *A. thaliana* roots confirmed the capacity of the dusts to induce oxidative stress, leading to plant redox homeostasis alteration and root cellular damages, and verified the reliability of the OP assays for the prediction of the ROS and RNS generation pathways in biological organisms. Indeed, the highest levels of NO and O^{-2} and lipid

peroxidation in *A. thaliana* roots were observed after the treatment with PA, BD and NIST which, as previously mentioned, were the dusts with the highest OPs.
Finally, our study validated *A. thaliana* as a suitable model for bio-indicator studies and encourage its employment for further investigations about the detection of PM toxicity on living organisms.

Acknowledgements

This work was partially funded by the project 2017 RG11715C7C8801CF (Principal Investigator Dr. S. Canepari), financed by Sapienza University of Rome.
The authors gratefully thank Valeria Vicarietti for her help in the morphological and chemical analyses of the samples and Martina Ristorini and Maria Agostina Frezzini for their support in the application of the oxidative potential assays on the examined atmospheric dusts.

Author Contributions

L. Massimi, D. Piacentini, S. Canepari and G. Falasca conceived and planned the experiments; L. Massimi performed the oxidative potential, chemical and multivariate statistical analyses; D. Piacentini performed the morphological and oxidative stress analyses; L. Massimi and D. Piacentini elaborated the data and wrote the manuscript; S. Canepari and G. Falasca coordinated the group and supervised the manuscript.

Conflicts of Interest

The authors declare no conflicts of interest.

References

Abdoli, M.A., Golzary, A., Hosseini, A., Sadeghi, P., 2018. Wood pellet emissions, in: Wood Pellet as a Renewable Source of Energy, Springer International Publishing, Cham, pp. 161-184. https://doi.org/10.1007/978-3-319-74482-7.

Achary, V.M.M., Jena, S., Panda, K.K., Panda, B.B., 2008. Aluminium induced oxidative stress and DNA damage in root cells of Allium cepa L. Ecotoxicol. Environ. Saf. 70(2), 300-310.

Astolfi, M.L., Marconi, E., Protano, C., Vitali, M., Schiavi, E., Mastromarino, P., Canepari, S., 2018. Optimization and validation of a fast digestion method for the determination of major and trace elements in breast milk by ICP-MS. Anal. Chim. Acta. 1040, 49-62.

Bates, J.T., Fang, T., Verma, V., Zeng, L., Weber, R.J., Tolbert, P.E., Abrams, J.Y., Sarnat, S.E., Klein, M., Mulholland, J.A., Russell, A.G., 2019. Review of acellular assays of ambient particulate matter oxidative potential: methods and relationships with composition, sources, and health effects. J. Environ. Sci. Technol. 53(8), 4003-4019.

Brook, R.D., Rajagopalan, S., Pope, C.A. 3rd, Brook, J.R., Bhatnagar, A., Diez-Roux, A.V., Holguin, F., Hong, Y, Luepker, R.V., Mittleman, M.A, Peters, A., Siscovick, D., Smith, S.C. Jr, Whitsel, L., Kaufman, J.D., 2010. Particulate matter air pollution and cardiovascular disease: an update to the scientific statement from the American Heart Association. Circulation 121(21), 2331-2378.

Cachon, B.F., Firmin, S., Verdin, A., Ayi-Fanou, L., Billet, S., Cazier, F., Martin, P.J., Aissi, F., Courcot, D., Sanni, A., Shirali, P., 2014. Proinflammatory effects and oxidative stress within human bronchial epithelial cells exposed to atmospheric particulate matter (PM2. 5 and PM> 2.5) collected from Cotonou, Benin. Environ. Pollut. 185, 340-351.

Canepari, S., Cardarelli, E., Giuliano, A., Pietrodangelo, A., 2006a. Determination of metals, metalloids and non-volatile ions in airborne particulate matter by a new two-step sequential leaching procedure Part A: Experimental design and optimization. Talanta 69(3), 581-587.

Canepari, S., Cardarelli, E., Pietrodangelo, A., Strincone, M., 2006b. Determination of metals, metalloids and non-volatile ions in airborne particulate matter by a new two-step sequential leaching procedure: Part B: Validation on equivalent real samples. Talanta 69(3), 588-595.

Canepari, S., Perrino, C., Olivieri, F., Astolfi, M.L., 2008. Characterisation of the traffic sources of PM through size-segregated sampling, sequential leaching and ICP analysis. Atmos. Environ. 42(35), 8161-8175.

Canepari, S., Pietrodangelo, A., Perrino, C., Astolfi, M.L., Marzo, M.L., 2009. Enhancement of source traceability of atmospheric PM by elemental chemical fractionation. Atmos. Environ. 43(31), 4754-4765.

Canepari, S., Marconi, E., Astolfi, M.L., Perrino, C., 2010a. Relevance of Sb (III), Sb (V), and Sb-containing nano-particles in urban atmospheric particulate matter. Anal. Bioanal. Chem. 397(6), 2533-2542.

Canepari, S., Astolfi, M.L., Moretti, S., Curini, R., 2010b. Comparison of extracting solutions for elemental fractionation in airborne particulate matter. Talanta 82(2), 834-844.

Charrier, J.G., Anastasio, C., 2012. On dithiothreitol (DTT) as a measure of oxidative potential for ambient particles: evidence for the importance of soluble transition metals. Atmos. Chem. Phys. 12(5), 11317.

Chirizzi, D., Cesari, D., Guascito, M.R., Dinoi, A., Giotta, L., Donateo, A., Contini, D., 2017. Influence of Saharan dust outbreaks and carbon content on oxidative potential of water-soluble fractions of PM2. 5 and PM10. Atmos. Environ. 163, 1-8.

Conti, M.E., Iacobucci, M., Cucina, D., Mecozzi, M., 2007. Multivariate statistical methods applied to biomonitoring studies. Int. J. Environ. Pollut. 29(1-3), 333-343.

Corpas, F.J., Barroso, J.B., 2014. Peroxynitrite ($ONOO^-$) is endogenously produced in Arabidopsis peroxisomes and is overproduced under cadmium stress. Ann. Bot. 113(1), 87-96.

Costabile, F., Gualtieri, M., Canepari, S., Tranfo, G., Consales, C., Grollino, M.G., Paci, E., Petralia, E., Pigini, D., Simonetti, G., 2019. Evidence of association between aerosol properties and in-vitro cellular oxidative response to PM1, oxidative potential of PM2.5, a biomarker of RNA oxidation, and its dependency on the combustion aerosol. Atmos. Environ. (in press).

Councell, T.B., Duckenfield, K.U., Landa, E.R., Callender, E., 2004. Tire-wear particles as a source of zinc to the environment. J. Environ. Sci. Technol. 38(15), 4206-4214.

Daresta, B.E., Italiano, F., de Gennaro, G., Trotta, M., Tutino, M., Veronico, P., 2015. Atmospheric particulate matter (PM) effect on the growth of Solanum lycopersicum cv. Roma plants. Chemosphere 119, 37-42.

de Oliveira Alves, N., Loureiro, A.L.M., Dos Santos, F.C., Nascimento, K.H., Dallacort, R., de Castro Vasconcellos, P., de Souza Hacon, S., Artaxo, P., De Medeiros, S.R.B., 2011. Genotoxicity and

composition of particulate matter from biomass burning in the eastern Brazilian Amazon region. Ecotoxicol. Environ. Saf. 74(5), 1427-1433.

Della Rovere, F., Fattorini, L., D'Angeli, S., Veloccia, A., Falasca, G., Altamura, M.M., 2013. Auxin and cytokinin control formation of the quiescent centre in the adventitious root apex of Arabidopsis. Ann. Bot. 112(7), 1395-1407.

Di Dato, C., Gianfrilli, D., Greco, E., Astolfi, M., Canepari, S., Lenzi, A., Isidori, A.M., Giannetta, E., 2017. Profiling of selenium absorption and accumulation in healthy subjects after prolonged L-selenomethionine supplementation. J. Endocrinol. Invest. 40(11), 1183-1190.

Dodd, M.D., Ebbs, S.D., Gibson, D.J., Filip, P., 2014. Alteration of root growth by lettuce, wheat, and soybean in response to wear debris from automotive brake pads. Arch. Environ. Contam. Toxicol. 67(4), 557-564.

Evans, J., van Donkelaar, A., Martin, R.V., Burnett, R., Rainham, D.G., Birkett, N.J., Krewski, D., 2013. Estimates of global mortality attributable to particulate air pollution using satellite imagery. Environ. Res. 120, 33-42.

Fattorini, L., Ronzan, M., Piacentini, D., Della Rovere, F., De Virgilio, C., Sofo, A., Altamura, M.M., Falasca, G., 2017. Cadmium and arsenic affect quiescent centre formation and maintenance in Arabidopsis thaliana post-embryonic roots disrupting auxin biosynthesis and transport. Environ. Exp. Bot. 144, 37-48.

Feigl, G., Lehotai, N., Molnár, Á., Ördög, A., Rodríguez-Ruiz, M., Palma, J.M., Corpas, F.J., Erdei L., Kolbert, Z., 2014. Zinc induces distinct changes in the metabolism of reactive oxygen and nitrogen species (ROS and RNS) in the roots of two Brassica species with different sensitivity to zinc stress. Ann. Bot. 116(4), 613-625.

Gilardoni, S., Massoli, P., Paglione, M., Giulianelli, L., Carbone, C., Rinaldi, M., Decesari, S., Sandrini, S., Costabile, F., Gobbi, G.P., Pietrogrande, M.C., Visentin, M., Scotto, F., Fuzzi, S., Facchini, M.C., 2016. Direct observation of aqueous secondary organic aerosol from biomass-burning emissions. Proc. Natl. Acad. Sci. 113(36), 10013-10018.

Gilbert, J.C., Martin, S.F., 2016. Experimental organic chemistry: a miniscale & microscale approach, sixth ed. Cengage Learning, CA.

Kelly, F.J., Fussell, J.C., 2012. Size, source and chemical composition as determinants of toxicity attributable to ambient particulate matter. Atmos. Environ. 60, 504-526.

Knaapen, A.M., Borm, P.J., Albrecht, C., Schins, R.P., 2004. Inhaled particles and lung cancer. Part A: Mechanisms. Int. J. Cancer. 109(6), 799-809.

Li, R., Kou, X., Geng, H., Xie, J., Yang, Z., Zhang, Y., Cai, Z., Dong, C., 2015. Effect of ambient PM 2.5 on lung mitochondrial damage and fusion/fission gene expression in rats. Chem. Res. Toxicol. 28, 408-418.

Liu, M., Liu, X.X., He, X.L., Liu, L.J., Wu, H., Tang, C.X., Zhang, Y.S., Jin, C.W., 2017. Ethylene and nitric oxide interact to regulate the magnesium deficiency-induced root hair development in Arabidopsis. New Phytol. 213(3), 1242-1256.

Maiorana, S., Teoldi, F., Silvani, S., Mancini, A., Sanguineti, A., Mariani, F., Cella, C., Lopez, A., Potenza, M.A.C., Lodi, M., Dupin, D., Sanvito, T., Bonfanti, A., Benfenati, E., Baderna, D., 2019. Phytotoxicity of wear debris from traditional and innovative brake pads. Environ. Int. 123, 156-163.

Marcoccia, M., Ronci, L., De Matthaeis, E., Setini, A., Perrino, C., Canepari, S., 2017. In-vivo assesment of the genotoxic and oxidative stress effects of particulate matter on Echinogammarus veneris. Chemosphere 173, 124-134.

Massimi, L., Ristorini, M., Eusebio, M., Florendo, D., Adeyemo, A., Brugnoli, D., Canepari, S., 2017. Monitoring and evaluation of Terni (Central Italy) air quality through spatially resolved analyses. Atmosphere 8(10), 200.

Massimi, L., Giuliano, A., Astolfi, M.L., Congedo, R., Masotti, A., Canepari, S., 2018. Efficiency evaluation of food waste materials for the removal of metals and metalloids from complex multi-element solutions. Materials 11(3), 334.

Massimi, L., Conti, M.E., Mele, G., Ristorini, M., Astolfi, M.L., Canepari, S., 2019. Lichen transplants as indicators of atmospheric element concentrations: a high spatial resolution comparison with PM10 samples in a polluted area (Central Italy). Ecol. Indic. 101, 759-769.

Murashige, T., Skoog, F., 1962. A revised medium for rapid growth and bio assays with tobacco tissue cultures. Physiol. Plant. 15(3), 473-497.

Nel, A., 2005. Air pollution-related illness: effects of particles. Science 308(5723), 804-806.

Pant, P., Harrison, R.M., 2013. Estimation of the contribution of road traffic emissions to particulate matter concentrations from field measurements: a review. Atmos. Environ. 77, 78-97.

Perrino, C., Catrambone, M., Farao, C., Canepari, S., 2016. Assessing the contribution of water to the mass closure of PM10. Atmos. Environ. 140, 555-564.

Perrone, M.G., Zhou, J., Malandrino, M., Sangiorgi, G., Rizzi, C., Ferrero, L., Dommen, J., Bolzacchini, E., 2016. PM chemical composition and oxidative potential of the soluble fraction of particles at two sites in the urban area of Milan, Northern Italy. Atmos. Environ. 128, 104-113.

Popek, R., Przybysz, A., Gawrońska, H., Klamkowski, K., Gawroński, S.W., 2018. Impact of particulate matter accumulation on the photosynthetic apparatus of roadside woody plants growing in the urban conditions. Ecotoxicol. Environ. Saf. 163, 56-62.

Reche, C., Viana, M., Amato, F., Alastuey, A., Moreno, T., Hillamo, R., Teinilä, K., Saarnio, K., Seco, R., Peñuelas, J., Mohr, C., Prévôt, A.S., Querol, X., 2012. Biomass burning contributions to urban aerosols in a coastal Mediterranean City. Sci. Total Environ. 427, 175-190.

Ronzan, M., Piacentini, D., Fattorini, L., Della Rovere, F., Eiche, E., Riemann, M., Altamura, M.M., Falasca, G., 2018. Cadmium and arsenic affect root development in Oryza sativa L. negatively interacting with auxin. Environ. Exp. Bot.151, 64-75.

Seo, M., Akaba, S., Oritani, T., Delarue, M., Bellini, C., Caboche, M., Koshiba, T., 1998. Higher activity of an aldehyde oxidase in the auxin-overproducing superroot1 mutant of Arabidopsis thaliana. Plant Physiol. 116(2), 687-693.

Sharma, P., Jha, A.B., Dubey, R.S., Pessarakli, M., 2012. Reactive oxygen species, oxidative damage, and antioxidative defense mechanism in plants under stressful conditions. J. Bot. 2012, 1-26. http://dx.doi.org/10.1155/2012/217037.

Shi, T., Knaapen, A.M., Begerow, J., Birmili, W., Borm, P.J.A., Schins, R.P.F., 2003a. Temporal variation of hydroxyl radical generation and 8-hydroxy-2′-deoxyguanosine formation by coarse and fine particulate matter. Occup. Environ. Med. 60(5), 315-321.

Shi, T., Schins, R.P., Knaapen, A.M., Kuhlbusch, T., Pitz, M., Heinrich, J., Borm, P.J., 2003b. Hydroxyl radical generation by electron paramagnetic resonance as a new method to monitor ambient particulate matter composition. J. Environ. Monit. 5(4), 550-556.

Simonetti, G., Conte, E., Massimi, L., Frasca, D., Perrino, C., Canepari, S., 2018a. Oxidative potential of particulate matter components generated by specific emission sources. J. Aeros. Scien. 126, 99-109.

Simonetti, G., Conte, E., Perrino, C., Canepari, S., 2018b. Oxidative potential of size-segregated PM in an urban and an industrial area of Italy. Atmos. Environ. 187, 292-300.

Singh, H.P., Batish, D.R., Kohli, R.K., Arora, K., 2007. Arsenic-induced root growth inhibition in mung bean (Phaseolus aureus Roxb.) is due to oxidative stress resulting from enhanced lipid peroxidation. Plant Growth Regul. 53(1), 65-73.

Singh, P.K., Indoliya, Y., Chauhan, A.S., Singh, S.P., Singh, A.P., Dwivedi, S., Tripathi, R.D., Chakrabarty, D., 2017. Nitric oxide mediated transcriptional modulation enhances plant adaptive responses to arsenic stress. Sci. Rep. 7(1), 3592.

Sofo, A., Vitti, A., Nuzzaci, M., Tataranni, G., Scopa, A., Vangronsveld, J., Remans, T., Falasca, G., Altamura, M.M., Degola, F., Sanità di Toppi, L., 2013. Correlation between hormonal homeostasis and morphogenic responses in Arabidopsis thaliana seedlings growing in a Cd/Cu/Zn multi-pollution context. Physiol. Plant. 149(4), 487-498.

Taioli, E., Sram, R.J., Garte, S., Kalina, I., Popov, T.A., Farmer, P.B., 2007. Effects of polycyclic aromatic hydrocarbons (PAHs) in environmental pollution on exogenous and oxidative DNA damage (EXPAH project): description of the population under study. Mutat. Res. 620(1), 1-6.

Thorpe, A., Harrison, R.M., 2008. Sources and properties of non-exhaust particulate matter from road traffic: a review. Sci. Total. Environ. 400(1-3), 270-282.

Toscano, G., Duca, D., Amato, A., Pizzi, A., 2014. Emission from realistic utilization of wood pellet stove. Energy 68, 644-650.

Trifuoggi, M., Pagano, G., Oral, R., Gravina, M., Toscanesi, M., Mozzillo, M., Siciliano, A., Burić, P., Lyons, D.M., Palumbo, A., Thomas, P.J., D'Ambra, L., Crisci, A., Guida, M., Tommasi, F., 2019. Topsoil and urban dust pollution and toxicity in Taranto (southern Italy) industrial area and in a residential district. Environ. Monit. Assess. 191(1), 43. https://doi.org/10.1007/s10661-018-7164-7.

Triantaphylidès, C., Krischke, M., Hoeberichts, F.A., Ksas, B., Gresser, G., Havaux, M., Van Breusegem, F., Mueller, M.J., 2008. Singlet oxygen is the major reactive oxygen species involved in photooxidative damage to plants. Plant Physiol. 148(2), 960-968.

Van Norman, J.M., Benfey, P.N., 2009. Arabidopsis thaliana as a model organism in systems biology. Wiley Interdiscip. Rev. Syst. Biol. Med. 1(3), 372-379.

Verma, A., Singh, S.N., 2006. Biochemical and ultrastructural changes in plant foliage exposed to auto-pollution. Environ. Monit. Assess. 120(1-3), 585-602.

Vernile, P., Tutino, M., Bari, G., Amodio, M., Spagnuolo, M., de Gennaro, G., de Lillo, E., 2013. Particulate matter toxicity evaluation using bioindicators and comet assay. Aerosol Air. Qual. Res. 13, 172-178.

Vitti, A., Nuzzaci, M., Scopa, A., Tataranni, G., Tamburrino, I., Sofo, A., 2014. Hormonal response and root architecture in Arabidopsis thaliana subjected to heavy metals. Int. J. Plant Biol. 5(1), 16-21.

Weigel, D., Glazebrook, J., 2002. Arabidopsis: a laboratory manual, first ed. CSHL Press, New York.

Wong-Ekkabut, J., Xu, Z., Triampo, W., Tang, I.M., Tieleman, D.P., Monticelli, L., 2007. Effect of lipid peroxidation on the properties of lipid bilayers: a molecular dynamics study. Biophys. J. 93(12), 4225-4236.

Xiong, Q., Yu, H., Wang, R., Wei, J., Verma, V., 2017. Rethinking dithiothreitol-based particulate matter oxidative potential: measuring dithiothreitol consumption versus reactive oxygen species generation. Environ. Sci. Technol. 51(11), 6507-6514.

Yamamoto, Y., Kobayashi, Y., Devi, S.R., Rikiishi, S., Matsumoto, H., 2003. Oxidative stress triggered by aluminum in plant roots. Plant Soil 255(1), 239-243.

Yuan, H.M., Huang, X., 2016. Inhibition of root meristem growth by cadmium involves nitric oxide-mediated repression of auxin accumulation and signalling in Arabidopsis. Plant Cell Environ. 39(1), 120-135.

Zanella, L., Fattorini, L., Brunetti, P., Roccotiello, E., Cornara, L., D'Angeli, S., Della Rovere, F., Cardarelli, M., Barbieri, M., Sanità di Toppi, L., Degola, F., Lindberg, S., Altamura, M.M., Falasca, G., 2016. Overexpression of AtPCS1 in tobacco increases arsenic and arsenic plus cadmium accumulation and detoxification. Planta 243(3), 605-622.

Zhao, J., Wang, W., Zhou, H., Wang, R., Zhang, P., Wang, H., Pan, X., Xu, J., 2017. Manganese toxicity inhibited root growth by disrupting auxin biosynthesis and transport in Arabidopsis. Front. Plant Sci. 8, 272. https://doi.org/10.3389/fpls.2017.00272.

Zou, Y., Jin, C., Su, Y., Li, J., Zhu, B., 2016. Water soluble and insoluble components of urban PM2. 5 and their cytotoxic effects on epithelial cells (A549) in vitro. Environ. Pollut. 212, 627-635.

Supplementary Material S1.

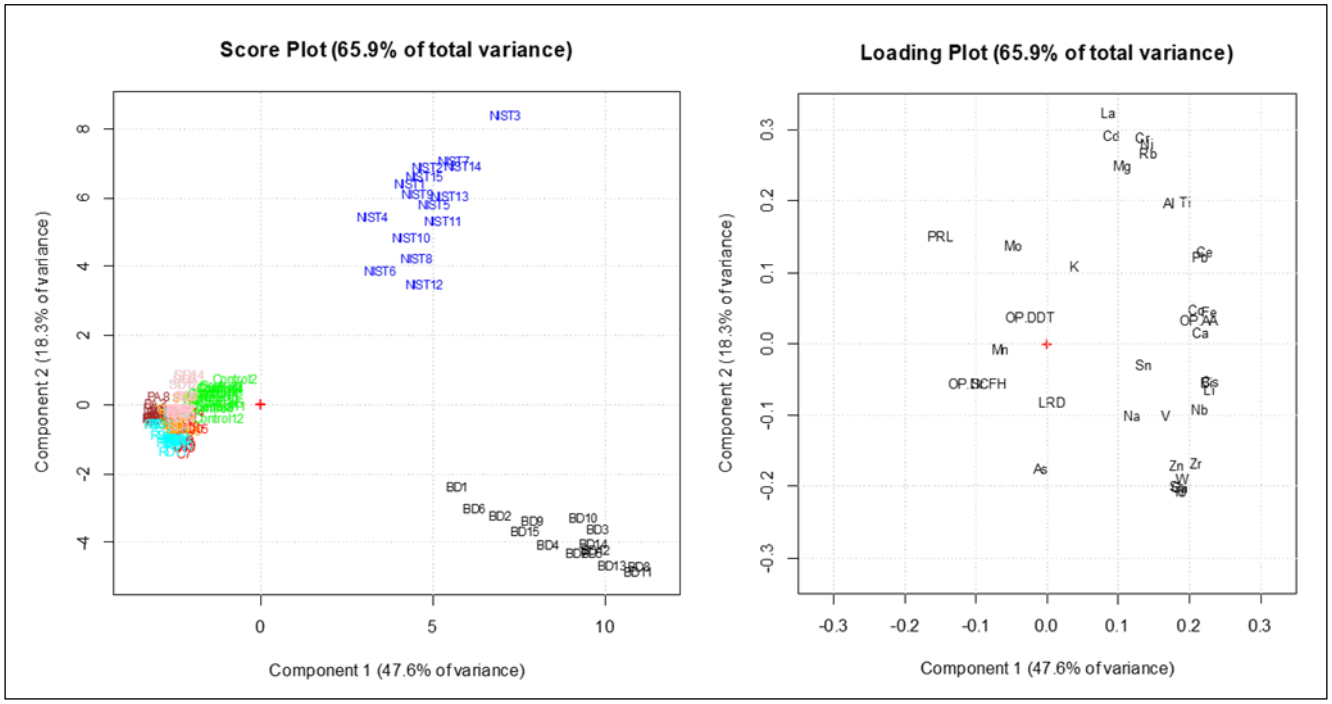

Fig. S1. Score plot and loading plot of PC1 and PC2 of the PCA performed on the OPs of the dusts, element bioaccumulation and PRL and LRD alteration in the *A. thaliana* seedlings.

Table S1.1. Scores of the five significant components (accounting for 83.54%) obtained by the PCA performed on the OPs of the dusts, element bioaccumulation and PRL and LRD alteration in the *A. thaliana* seedlings.

	Scores										
	PC1	**PC2**	**PC3**	**PC4**	**PC5**		**PC1**	**PC2**	**PC3**	**PC4**	**PC5**
Control1	-1.157	0.575	0.438	-0.269	-0.634	**BD1**	5.717	-2.357	-0.353	-1.023	1.493
Control2	-0.756	0.767	0.137	-0.900	-0.894	**BD2**	6.945	-3.202	0.764	-0.649	-0.333
Control3	-1.247	0.454	0.176	-0.662	-0.825	**BD3**	9.795	-3.595	0.033	-0.201	-1.440
Control4	-1.163	0.492	0.835	0.285	-0.873	**BD4**	8.358	-4.030	-0.321	1.412	7.950
Control5	-1.157	0.078	-0.035	-0.867	-0.737	**BD5**	9.635	-4.288	-0.119	-0.194	0.721
Control6	-1.574	0.260	0.616	0.099	-0.962	**BD6**	6.205	-2.999	0.662	-0.227	-0.116
Control7	-1.375	-0.072	-0.045	-1.443	-0.704	**BD7**	9.176	-4.291	-0.568	-0.509	-0.236
Control8	-1.465	-0.047	0.304	-0.750	-0.729	**BD8**	11.010	-4.682	0.823	-0.448	-1.885
Control9	-1.210	0.524	0.252	-0.627	-0.641	**BD9**	7.899	-3.326	0.388	-0.200	-0.027
Control10	-1.388	0.245	0.477	-0.330	-0.995	**BD10**	9.378	-3.280	-0.410	0.867	1.826
Control11	-1.182	-0.018	0.211	-0.551	-0.893	**BD11**	10.964	-4.832	0.383	-0.363	-3.169
Control12	-1.245	-0.357	0.105	-0.821	-1.184	**BD12**	9.720	-4.204	0.897	-0.458	-1.520
Control13	-1.289	0.406	0.452	-0.167	-0.923	**BD13**	10.210	-4.639	-0.378	0.360	0.619
Control14	-1.394	0.376	0.173	-0.708	-0.619	**BD14**	9.670	-4.010	0.817	-0.359	-0.807
Control15	-1.526	0.187	-0.107	-1.281	-0.516	**BD15**	7.677	-3.645	0.713	-0.149	-0.665
NIST1	4.319	6.424	0.158	-0.471	1.250	**SD1**	-2.456	-0.138	-1.518	-1.898	-0.128
NIST2	4.853	6.894	-0.360	0.446	1.354	**SD2**	-2.226	-0.083	-1.343	-2.220	-0.240
NIST3	7.112	8.402	-0.642	0.280	-0.483	**SD3**	-2.385	-0.101	-1.161	-1.974	-0.345
NIST4	3.257	5.459	0.005	0.480	0.719	**SD4**	-2.370	-0.591	-0.643	-2.269	-0.847
NIST5	5.034	5.815	-0.059	0.408	0.362	**SD5**	-2.460	-0.194	-1.537	-1.971	-0.032
NIST6	3.482	3.897	0.190	-0.169	0.138	**SD6**	-2.191	0.792	-1.244	-1.741	-0.084
NIST7	5.610	7.082	-0.194	0.992	-1.178	**SD7**	-2.416	-0.279	-1.526	-2.080	-0.323
NIST8	4.524	4.241	0.935	0.664	-1.610	**SD8**	-2.184	0.267	-1.171	-1.921	-0.246
NIST9	4.554	6.137	-0.258	0.122	0.400	**SD9**	-2.150	0.308	-1.343	-2.007	-0.124
NIST10	4.381	4.870	0.089	-0.083	0.824	**SD10**	-2.291	-0.347	-1.311	-2.053	-0.175
NIST11	5.283	5.343	-0.534	0.128	-1.437	**SD11**	-2.320	-0.119	-1.511	-2.179	-0.131
NIST12	4.743	3.519	0.254	0.610	0.197	**SD12**	-2.235	0.628	-1.498	-2.095	-0.218
NIST13	5.481	6.080	-0.318	0.313	0.162	**SD13**	-2.412	-0.103	-1.468	-1.988	-0.152
NIST14	5.870	6.945	0.747	0.477	-0.023	**SD14**	-2.074	0.897	-1.337	-1.977	-0.085
NIST15	4.763	6.649	0.187	0.655	0.309	**SD15**	-2.355	-0.195	-1.242	-2.075	-0.274
PA1	-3.093	-0.087	5.476	-0.319	0.913	**S1**	-2.107	-0.447	-2.236	-0.786	0.908
PA2	-3.064	-0.358	3.704	-0.507	0.746	**S2**	-2.561	-0.669	-1.949	-0.666	0.094
PA3	-3.061	0.058	4.971	-0.005	0.795	**S3**	-2.461	-0.639	-2.091	-0.490	0.304
PA4	-3.011	-0.207	5.086	-0.335	0.914	**S4**	-2.742	-0.229	-2.215	-0.299	0.353
PA5	-2.874	-0.306	3.989	-0.374	0.324	**S5**	-1.941	-0.726	-2.071	-0.606	1.491
PA6	-2.837	-0.349	4.536	-0.439	0.651	**S6**	-2.602	-0.573	-1.969	-0.529	0.105
PA7	-2.994	-0.175	4.116	-0.157	-0.313	**S7**	-2.459	-0.233	-2.164	-0.638	0.287
PA8	-2.954	0.277	5.357	0.719	0.366	**S8**	-2.819	-0.122	-3.293	0.680	0.556
PA9	-2.999	-0.459	3.951	-0.672	0.193	**S9**	-2.284	-0.528	-2.051	-0.668	0.182
PA10	-2.824	-0.372	4.430	-0.475	0.625	**S10**	-2.251	0.245	-2.381	-0.348	0.509
PA11	-3.032	-0.383	2.703	-0.638	0.375	**S11**	-2.628	-0.565	-1.999	-0.471	0.095
PA12	-2.961	-0.346	4.304	-0.186	0.178	**S12**	-2.339	-0.302	-2.071	-0.655	0.274
PA13	-2.978	-0.484	4.716	-0.786	0.477	**S13**	-2.413	-0.274	-2.225	-0.235	0.675
PA14	-2.984	-0.332	5.929	-0.273	0.287	**S14**	-2.358	-0.669	-2.018	-0.492	0.403
PA15	-2.818	-0.153	3.680	-0.166	0.439	**S15**	-2.451	-0.663	-2.108	-0.407	0.347
RD1	-2.535	-0.921	0.510	0.563	-0.750	**C1**	-2.405	-0.697	-1.036	0.665	0.723
RD2	-2.606	-0.965	-0.251	1.299	-0.955	**C2**	-2.166	-0.837	-0.834	-0.023	0.847
RD3	-2.481	-1.049	0.176	2.072	-1.072	**C3**	-2.073	-0.405	-0.964	1.250	1.107
RD4	-2.474	-1.018	0.024	1.751	-0.805	**C4**	-2.134	-1.069	-0.870	0.741	1.151
RD5	-2.412	-0.828	-0.303	1.868	-1.038	**C5**	-2.236	-0.660	-0.956	1.014	1.032
RD6	-2.408	-1.034	-0.053	1.853	-1.110	**C6**	-2.328	-1.164	-0.887	0.801	0.903
RD7	-2.858	-0.850	-1.029	2.786	-1.084	**C7**	-2.247	-1.393	-1.312	-0.251	0.360
RD8	-2.947	-0.537	-0.118	3.343	-1.122	**C8**	-2.174	-0.865	-0.810	0.727	0.903
RD9	-2.664	-1.066	-0.515	2.412	-1.339	**C9**	-2.095	-1.178	-1.078	0.684	0.721

RD10	-2.355	-1.172	-0.337	2.672	-1.287	**C10**	-1.968	-0.641	-1.023	1.705	0.952
RD11	-2.550	-1.313	-0.806	2.746	-1.585	**C11**	-2.309	-0.496	-1.508	1.371	0.616
RD12	-2.980	-0.563	-0.979	3.156	-0.850	**C12**	-2.105	-0.632	-1.144	0.923	1.313
RD13	-2.417	-0.961	-0.906	3.228	-0.302	**C13**	-2.242	-1.199	-1.079	1.120	0.337
RD14	-2.431	-0.213	-0.148	2.258	-0.434	**C14**	-1.947	-0.179	-0.744	1.131	1.166
RD15	-2.667	-0.562	-1.061	3.364	-0.791	**C15**	-1.856	-0.672	-1.219	1.247	1.167

Table S1.2. Loadings of the five significant components (accounting for 83.54%) obtained by the PCA performed on the OPs of the dusts, element bioaccumulation and PRL and LRD alteration in the *A. thaliana* seedlings.

	Loadings				
	PC1	**PC2**	**PC3**	**PC4**	**PC5**
OP^{AA}	0.212	0.033	0.106	0.061	0.021
OP^{DTT}	-0.024	0.038	0.442	0.116	0.112
OP^{DCFH}	-0.099	-0.055	0.396	0.144	0.062
PRL	-0.149	0.151	-0.155	0.217	0.035
LRD	0.007	-0.081	0.249	-0.075	-0.295
Al	0.171	0.198	-0.013	0.113	-0.007
As	-0.010	-0.174	-0.144	0.593	-0.092
Bi	0.225	-0.054	0.035	-0.024	-0.207
Ca	0.215	0.017	-0.012	0.057	0.153
Cd	0.091	0.292	-0.007	0.069	0.020
Ce	0.222	0.130	0.014	0.014	0.024
Co	0.210	0.048	0.029	0.002	-0.225
Cr	0.134	0.291	-0.013	-0.038	-0.027
Cs	0.230	-0.052	0.026	-0.015	-0.146
Cu	0.186	-0.201	0.014	0.002	0.140
Fe	0.228	0.046	-0.011	-0.027	0.090
K	0.039	0.111	0.371	0.226	0.146
La	0.085	0.324	-0.101	-0.102	-0.030
Li	0.228	-0.063	0.034	0.058	-0.027
Mg	0.106	0.249	-0.060	-0.015	0.168
Mn	-0.066	-0.006	0.443	-0.005	0.111
Mo	-0.047	0.139	0.225	0.352	-0.199
Na	0.119	-0.100	-0.004	0.082	0.512
Nb	0.214	-0.090	0.009	-0.035	-0.210
Ni	0.141	0.282	0.004	0.019	-0.010
Pb	0.216	0.122	-0.062	-0.001	-0.003
Rb	0.141	0.268	0.030	-0.017	0.026
Sb	0.183	-0.199	0.010	-0.016	0.137
Sn	0.137	-0.028	-0.088	0.466	-0.241
Sr	-0.098	-0.055	-0.316	0.302	0.077
Ti	0.195	0.200	0.002	0.037	0.017
Tl	0.186	-0.205	0.027	-0.055	-0.182
U	0.191	-0.206	0.030	-0.060	-0.130
V	0.167	-0.100	-0.063	0.137	0.398
W	0.190	-0.188	0.053	-0.017	0.001
Zn	0.182	-0.170	-0.071	-0.017	0.124
Zr	0.210	-0.167	0.026	-0.029	0.046

2.1.4. (A4) Nitric Oxide Alleviates the Damages Induced by Cadmium but not Those Induced by Arsenic in Rice Roots

Plant Physiology and Biochemistry (2019), *Reviewed*

Diego Piacentini [a], Marilena Ronzan [a], Laura Fattorini [a], Federica Della Rovere [a], Lorenzo Massimi [b], Maria Maddalena Altamura [a], Giuseppina Falasca [a,*]

[a] Department of Environmental Biology, Sapienza University of Rome, P. le Aldo Moro, 5, Rome 00185, Italy;
[b] Department of Chemistry, Sapienza University of Rome, P. le Aldo Moro, 5, Rome 00185, Italy.

A**bstract:** Nitric oxide (NO) is a gaseous molecule, belonging to reactive nitrogen species (RNS), with important signalling roles in plant physiology and abiotic stress response. Cadmium (Cd) and arsenic (As) soil pollution induces alterations in organ development, mainly in roots. Cadmium and As induced-stress increases NO cellular content and triggers reactive oxygen species (ROS) production. Interactions of NO with ROS are essential for plant tolerance to heavy metals/metalloids, but the mechanism underlying this process remains unclear. However, NO and superoxide anion are known to react quickly to form peroxynitrite, a RNS involved in the regulation of cell signalling during Cd/As responses**.** Our goal was to deepen the knowledge on NO involvement in the rice root system development after exposure to Cd or As, mainly focusing on possible differences in NO behaviour in the presence of the heavy metal/metalloid. To the aim, morphological, histological, chemical and epifluorescence analyses were carried out on rice roots exposed to Cd or As alone or combined with a NO donor. The results highlight that an increased intracellular NO level alleviates morphological/histological damages induced by Cd but not those induced by As. NO decreases the uptake of both Cd and As and exogenous NO recovers ROS/RNS cell balance under Cd exposure but not As exposure. Altogether, results show that NO has different effects in rice response to these pollutants depending on their type and level.

Keywords: arsenic; cadmium; nitric oxide; *Oryza sativa*; peroxynitrite; root development; superoxide anion.

1. Introduction

Nitrogen monoxide (nitric oxide – NO) is a ubiquitous gaseous molecule involved in numerous animal and plant physiological processes, and it is also a mediator of plant development and abiotic/biotic stresses response. Different environmental stresses rapidly induce NO production, which, in turn, participates to the regulation of the plant responses. Several researches have highlighted the involvement of NO in the regulation of plant response to toxic elements, including cadmium (Cd) and arsenic (As) (Kopyra and Gwoźdź, 2003; Kopyra et al., 2006; Singh et al., 2017). The NO involvement in different plant physiological/metabolic processes is due to its capabilities to modify numerous proteins, either directly through post-translational mechanisms, such as S-nitrosylation, nitration and nitrosylation, or indirectly by controlling the transcription of genes that encode proteins involved in stress responses (Fancy et al., 2017).

Various reports highlight that NO has an important role in reducing the damages in plant organs due to abiotic stresses by enhancing the activity of antioxidant enzymes. However, its role in the physiological processes depends on its cellular level. Indeed, at very low concentrations it functions as a signal molecule, on the contrary at higher levels becomes a stress-inducing molecule (Fancy et al., 2017).

Nitric oxide is a reactive nitrogen species (RNS) easily reacting in the cell with a wide range of proteins, as transcription factors, messengers or receptors, but mainly with the reactive oxygen species (ROS). These last are also induced by almost all abiotic stresses including metal/metalloid stresses. One of the fastest reactions taking place in biological systems occurs between NO and superoxide anion ($O_2^{\cdot -}$) to form peroxynitrite ($ONOO^-$) (Arasimowicz-Jelonek and Floryszak-Wieczorek, 2011; Corpas and Barroso 2015). Peroxynitrite, an unstable anion belonging to the RNS family, was identified as a mediator of cell death in animal cells at the end of the last century. Only later it was demonstrated to have a positive role in the regulation of cell signalling transduction pathways, principally by post-translational modification of proteins through tyrosine nitration (Vandelle and Delle donne, 2011). Moreover, the $ONOO^-$synthesis can be also used by the biological systems to reduce cellular NO levels (Wulff et al., 2009). Now, it is well known that $ONOO^-$, at low levels, is not toxic for plant cells, but an increase in its cellular levels is associated with various stress

responses. In particular, it was reported that peroxynitrite levels increase in Arabidopsis roots exposed to Cd (Corpas and Barroso, 2014). Similarly, it is also possible that $ONOO^-$ levels enhance in plants exposed to As considering that this metalloid triggers NO and ROS levels in numerous plant species, including Arabidopsis and rice (Leterrier et al., 2012; Singh et al., 2017).

Cadmium and As soil pollution is of great concern because it prevents plant development by altering primary metabolic functions, by decreasing water and mineral nutrient uptake, and by inducing a general alteration in organ development, mainly in the roots. Besides, the presence of Cd and/or As in soil compromises the commercial value of the edible crops, and represents a potential risk to human health. Cadmium is present in the soil mainly as Cd^{2+}. It easily enters in the root cells using the transporters of the essential nutrients, thus competing with them, or through aquaporins. Arsenic is present in the environment in two inorganic forms: arsenite [As(III)], and arsenate [As(V)] (Zhao et al. 2009). Arsenate, being an analogue of phosphate, enters the plant cells by the inorganic phosphate transport system (Meharg and MacNair 1992), whereas arsenite uses the aquaporins of NIP subfamily. In the root cells As(V) is easily reduced to As(III) (Meharg and Hartley-Whitaker 2002), with this reaction contributing to increase the cytosolic levels of ROS (Abbas et al., 2018).

The most serious plant damages caused by the toxic elements occur in the root system. Examples are the reduction of primary root (PR) elongation, and the alterations in the root stem cell niche definition and root differentiation pathways. Modifications of the lateral (LR) and adventitious (AR) root formation were also reported (Fattorini et al. 2017; Ronzan et al., 2018). Thus in this organ the first strategies to defend the entire plant from the pollutants are implemented (Fattorini et al. 2017; Ronzan et al., 2018; Piacentini et al., 2019).

Plants may active defence strategies at molecular, cellular and physiological levels to cope with toxic elements. In any case, these mechanisms involve a complex signalling network that must guarantee the perception and transmission of the stress signals, for subsequently start a plethora of defence responses. Plants defend themselves from metal/metalloid toxicity either by keeping under control the cellular levels of free ions through exclusion, immobilization, chelation with binding thiol-peptides and vacuolar compartmentalization (Cobbet 2000; Clemens et al., 2002; Tuli et al., 2010), or by reprogramming the entire plant metabolism to ensure to the cells to re-establish redox homeostasis (Farnese et al., 2016, and references therein).

In the last few decades, numerous studies have indicated that the interaction between RNS, in particular NO, and ROS is essential for plant tolerance to heavy metals/metalloids, however the mechanism on the base of this process remains unclear.

In fact, based on their levels in cells, ROS and NO may cause an oxidative/nitrosative stress in the cells or may act as signalling molecules (Farnese et al., 2016 and references therein).

Plants exposed to Cd toxicity can modify NO metabolism; however contradictory results have been reported regarding the impact of Cd^{2+} on NO endogenous production (Besson-Bard et al., 2009, and references therein). In fact, Cd can either increase NO levels, as reported in various plant species (Bartha et al., 2005; Corpas and Barroso, 2014), or inhibit them (Rodríguez-Serrano et al., 2006). Moreover, exogenous treatments with an NO donor showed to protect plant organs against the oxidative damage triggered by Cd^{2+} by promoting ROS scavenging (Kopyra et al., 2006; Noriega et al., 2007).

It is known that As, either as As (V) or As (III), also provokes alterations in the NO metabolism in various plants, with a significant increase in NO content determining nitro-oxidative stress (Leterrier et al., 2012; Singh et al., 2017; Rodríguez-Ruiz et al., 2019). Moreover, exogenous NO supplementation seems to limit As-induced damages in rice exposed to As(III) (Singh et al., 2017).

It is thus evident that NO has a crucial role in the regulation of biological processes activated by plants in response to metal toxicity, however the exact mechanism of NO signalling is still unclear.

One of the most widely used methods to supply NO to plants, whether grown in soils or in synthetic media or in hydroponic systems, is the treatment with the NO donor compound sodium nitroprusside (SNP). It has been reported that rice plants exposed to Cd show an increased tolerance to heavy metal when supplied with SNP (Xiong, et al., 2009). Similarly, the exogenous application of NO, through SNP treatment, alleviated As-induced toxicity in germinating seeds of mung bean (Ismail, 2012).

In light of literature information, it is important to investigate the role of NO in the plant responses to Cd and As, two of the most dangerous and common soil pollutants, in an agronomically important species like *Oryza sativa* L.. Thus, the aim of this research was to deepen the knowledge on the involvement of NO in the organization of the root rice system after exposure to Cd and As, investigating whether the behaviours of NO and of the NO-derived peroxynitrite and of the superoxide anion, were in the presence of the heavy metal or the metalloid was different.

The results highlight that the exogenous treatments with the NO donor SNP are able to increase intracellular NO levels in rice roots not exposed or exposed to Cd or As. The enhanced cellular NO content alleviates morphological and histological damages induced in the root by Cd, but not those due to As. NO decreases the uptake of both Cd and As. Finally, exogenous NO differently affects ROS and RNS cell balance in rice roots exposed to Cd or As.

2. Materials and Methods

2.1. Plant Material and Growth Conditions

Seeds of *Oryza sativa* ssp. Japonica (cv. Nihonmasari) were surface sterilized with ethanol 70% (v/v) for 1.30 min, rinsed three times with Milli-Q water, soaked in a solution of 40% (v/v) sodium hypochlorite (5-9% active chlorine, Carlo Erba Reagents S.R.L., Milano, Italy) for 25 min, and again rinsed in sterile ultra-pure water for three times. Then, the seeds were sown in 11.4 cm × 8.6 cm × 10.2 cm phytatrays vessels (Phytatray™, Sigma-Aldrich, Saint Louis, MO, USA) containing a half-strength Murashige and Skoog (MS, 1962), 0.1% sucrose and 0.8% agar, at pH 5.6–5.8 (Control medium). To the Control medium, 25 µM $NaAsO_2$ (25 µM As(III)), or 100 µM $Na_2HAsO_4 \cdot 7H_2O$ (100 µM As(V)) or 100 µM $CdSO_4$ (100 µM Cd) were added, combined or not with 50 µM $Na_2[Fe(CN)_5NO] \cdot 2H_2O$ (sodium nitroprusside dehydrate, Sigma –Aldrich) (50 µM SNP). Ultra-pure water (Milli-Q) was used for all culture media.

The As(V) and Cd concentrations were selected based on our previous data (Ronzan et al., 2018; Ronzan et al., 2019), while the As(III) and SNP concentrations were chosen based on preliminary experiments showing that As(III) or SNP concentrations higher than 25 µM and 50 µM respectively, induced strong damages to the entire plant, while lower concentrations of SNP combined with Cd and As did not induce evident morphological modifications with respect to the treatments with the pollutants only (Supplementary Material 1 and 2).

Thirty seeds per each treatment were sown on the media and kept in long-day conditions (14 h light/10 h dark) for 10 days at 210 µmol/$m^{-2}s^{-1}$ intensity of white light and 70% of relative humidity.

2.2. Elemental Analysis

Ten-day old rice seedlings were harvested, desorbed in 20 mM Na_2-EDTA for 15 min to remove apoplastic Cd and As, and washed thoroughly three times with Milli-Q water. Then, they were separated into roots and shoots and oven dried at 70 °C for 72 h, weighed and subjected to a microwave assisted acid digestion for 30 min at 180°C by using a HNO_3/H_2O_2 mixture (2:1, v/v). The digested solutions were then diluted to 50 mL with Milli-Q water and filtered with syringe filters (25 mm diameter, 0.45 µm pore size). Cadmium and As concentrations were determined by a quadrupole inductively coupled plasma mass spectrometer (ICP-MS, model 820-MS; Bruker, Bremen, Germany) equipped with a glass nebulizer (0.4 mL min^{-1}; Analytik Jena AG, Jena, Germany). External standard calibration curve was performed for Cd and As by serially diluting

standard stock solution (1000 ± 2 mg L^{-1}; Exaxol Italia Chemical Manufacturers Srl, Genoa, Italy). To control the nebulizer efficiency, rhodium was set at 5 µg L^{-1} as internal standard for all the measurements and was prepared from standard stock solution (1000 ± 2 mg L^{-1}; Panreac Química, Barcelona, Spain). The values of blanks, subjected to similar sample preparation and analytical procedures, were deducted from all measurements and the limits of detection (LODs; 0.018 µg L^{-1} for Cd and 0.022 µg L^{-1} for As) were set at 3 times the standard deviation (SD) of 10 replicate blank determinations. Standard deviations of the replicates were all below 20%. The used instrumental conditions and the performance of the method are detailed in Astolfi et al. (2018).

The obtained Cd and As concentrations (mg/Kg) were divided by the dry weight of each sample.

The bioaccumulation factor (BF) and the translocation factor (TF) were also calculated as the ratio of the total heavy metal/metalloid concentration in the shoot to that in the culture medium or in the root system respectively (Rezvani and Zaefarian 2011).

2.3. Morphological Analyses

After the growing period, the root system of 30 seedlings per treatment was collected and analyzed by measuring the mean fresh weight, the mean number and length of the embryonic crown roots, i.e., embryonic adventitious roots (ARs), the mean lateral root (LR) density and the mean PRL/RL percentage as well (± SE).

The length and the number of the ARs were measured under a LEICA MZ8 stereomicroscope using Zeiss Zen 2.3 software from digital images captured with Zeiss AxioCam camera. The LRs were counted with a Leica DMRB optical microscope equipped with a Leica DC 500 camera, and the corresponding mean density expressed as mean number cm^{-1} (± SE).

2.4. Detection of NO, $O_2^{\bullet-}$ *and* $ONOO^-$ *in Rice Roots*

Nitric oxide content was evaluated in *Oryza sativa* roots (LRPs and elongated LRs), by using the specific NO fluorescent probe 4-amino-5-aminomethyl-2′,7′-difluorofluorescein diacetate (DAF-FM DA, Sigma-Aldrich, Saint Louis, MO, USA), as previously described (Chen et al., 2015). Briefly, rice roots non-exposed (Control) or exposed to100 µM As(V), 25 µM As(III) or 100 µM Cd, combined or not with 50 µM SNP, were incubated with 10 µM DAF-FM DA in 20 mM HEPES-NaOH buffer (pH 7.5) for 30 min at 25°C in the dark. After incubation, the roots were washed three times with fresh 20 mM HEPES/NaOH buffer to remove excess probe and immediately observed

under a Leica DMRB optical microscope equipped with a Leica DC 500 camera (excitation 490 nm; emission 515 nm), and the relative fluorescence quantified using ImageJ 1.52a software (https://imagej.nih.gov/ij).

For $O_2^{\bullet-}$ detection, rice roots exposed or not to 100 μM As(V), 25 μM As(III) or 100 μM Cd, alone or combined with 50 μM SNP, were stained for 30 min in a solution of 0.5 mg mL^{-1} nitroblue tetrazolium (NBT; Roche Diagnostics Corp., Gmbh, Germany) in 10 mM Tris-HCl (pH 7.4). After having transferred the roots into distilled water to stop the reaction, they were kept in the chloral hydrate solution ($Cl_3CCH(OH)_2$, Sigma-Aldrich, Saint Louis, MO, USA) and directly observed with LEICA DMRB light microscope equipped with Nomarski optics. For peroxynitrite ($ONOO^-$) detection, the rice roots exposed or not to 100 μM As(V), 25 μM As(III) or 100 μM Cd, alone or combined with 50 μM SNP were incubated in a solution of 10 μM 3'-(p-aminophenyl) fluorescein (APF) (Invitrogen - Italy) dissolved in 10 mM Tris-HCl (pH 7.4) at 25°C for 1h in the dark. After incubation, the roots were washed with the buffer for 15 min, then mounted on a slide and instantly observed under an optical microscope (excitation 490 nm; emission 515 nm) and the relative fluorescence quantified as described above for NO.

2.5. Histological and Autofluorescence Analyses

The apical region of five ARs (~ 2.0 cm from the root tip) non-exposed (Control) or exposed to 100 μM As(V) or 100 μM Cd, alone or combined with 50 μM SNP, were fixed in 70% (v/v) ethanol, dehydrated by an ethanol series, embedded in Technovit 7100 (Heraeus Kulzer, Germany), longitudinally and radially sectioned at 8 μm with a Microm HM 350 SV microtome (Microm, Germany), stained with 0.05% toluidine blue, and observed under a light microscope. To detect cell wall autofluorescence, root tip regions were transversally sectioned and observed under UV light, and the relative fluorescence quantified by measuring the average pixel intensity using ImageJ 1.52a software (https://imagej.nih.gov/ij).

2.6. Statistical Analysis

Statistical analysis was performed using one-way ANOVA test followed by Tukey's post-test through GraphPad Prism 8 software. All experiments were performed in three replicates.

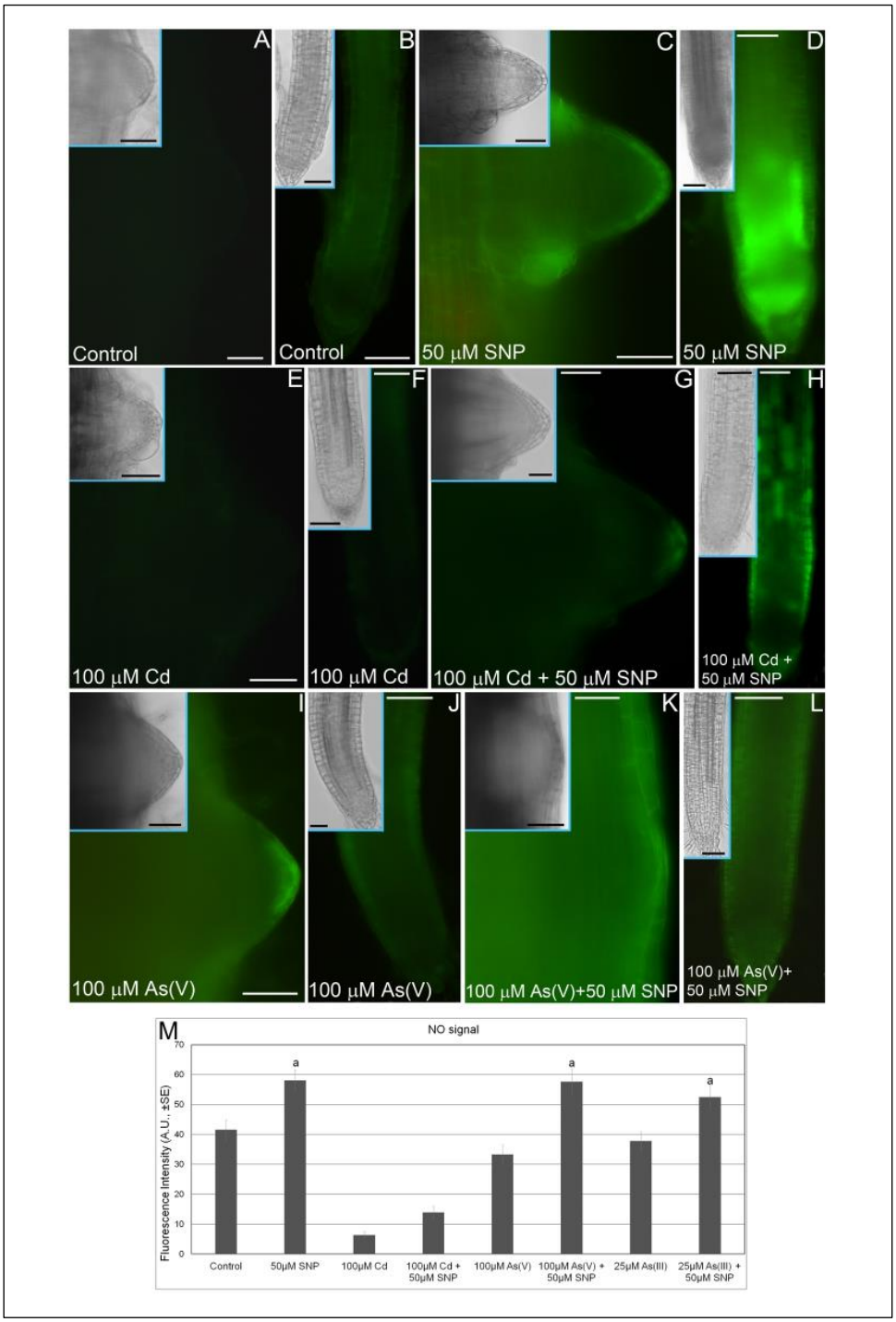

Fig. 1. Nitric oxide (NO) epifluorescence signal (**A**-**L**) in rice lateral roots and its quantification (**M**). **A**-**L**, NO signal in bright green colour in lateral root primordia (LRPs; **A**,**C**,**E**,**G**,**I** and **K**) and elongated lateral roots (LRs; **B**,**D**,**F**,**H**,**J** and **L**) treated or not treated (Control) with 100 μM $CdSO_4$ (100μM Cd), 100 μM $Na_2HAsO_4 \cdot 7H_2O$ (100μM As(V)) or 25μM $NaAsO_2$ (25μM As(III)) alone or combined with 50 μM $Na_2[Fe(CN)_5NO] \cdot 2H_2O$ (50μM SNP). LRPs and LRs (**A**-**L**) taken from 10-

days-old seedlings were loaded with 4-amino-5-aminomethyl-2′,7′-difluorofluorescein diacetate (DAF-FM DA). Insets in Figs **A**-**L** show LRPs and LRs in white light. Bars = 30 µm (A, F-G) and 50 µm (B-E, H-L and Insets). **M**, Mean values of NO fluorescence intensity (±SE) in LRPs/LRs measured using ImageJ 1.52a software and expressed in arbitrary units (AUs). Letters show statistical differences, at least at $P<0.05$ level, within the same treatment with/ without SNP. N =30.

3. Results

3.1. Sodium Nitroprusside (SNP) Treatment Increases Intracellular NO Levels in Rice Roots

To verify whether exogenous sodium nitroprusside (SNP), a NO donor, induced an increase of intracellular NO levels in rice roots, an epifluorescence analysis was carried out on roots exposed or not to 50 µM SNP, after incubating them with the NO fluorescent probe 4-amino-5-aminomethyl-2′,7′-difluorofluorescein diacetate (DAF-FM DA). The fluorescent signal was also quantified. Lateral root primordia (LRPs) formed on adventitious roots (ARs) of Control seedlings, i.e., those not treated with Cd or As or SNP, showed a very weak NO signal (Fig. 1A). On the contrary, the signal was stronger in elongated lateral roots (LRs), especially in their apex and in the elongation region (Fig. 1A-B). The treatment with SNP significantly ($P<0.01$) reinforced the NO signal either in the LRPs or in the LRs (Fig. 1C-D, M). This highlights that the NO donor added to the culture medium is able to increase the NO intracellular levels in the roots.

Moreover, to check whether Cd and As caused a change in the NO levels, the roots exposed to the heavy metal or the metalloid, (both the chemical forms of As(III) and As(V)), were treated with the NO fluorescent probe. Surprisingly, Cd alone strongly ($P<0.001$) reduced the NO signal in both LRPs and LRs in comparison with Control. The treatment with Cd plus SNP weakly increased it (Fig. 1E-H, M). Arsenic, either as arsenite or arsenate, slightly decreased the NO signal in LRPs and LRs in comparison with the Control (Fig. 1M). The combined treatments of As and SNP significantly ($P<0.01$) increased the NO levels, in comparison with As alone, up to levels comparable to those observed in the SNP alone treatment (Fig. 1I-L, M). All together these results show that the SNP treatment is able to restore the reduction of NO levels induced by Cd or As alone.

3.2. Nitric Oxide Alleviates Cd Induced Morphological Damages in Rice Root Architecture but not Those Due to As

A morphological analysis was carried out on the root system of rice seedlings, treated or not with Cd or As, and with or without 50 µM SNP. The results show that SNP, at this concentration, did not affect the morphological parameters analysed, i.e., the root fresh weight, the mean length of the embryonic ARs, the mean density of the LRs, including LRPs and LRs, and the percentage ratio between the de novo formed LRPs and the LRs in comparison to the Control (Fig. 2).

The root fresh weight significantly ($P<0.01$) decreased in the Cd, As(V) and As(III) treatments in comparison with the Control (Fig. 2A). The highest levels of NO, due to treatment with SNP, were able to significantly ($P<0.05$) increase the root fresh weight when SNP was combined with Cd, but they further reduced it when SNP was combined with As(V), mainly, or As(III) (Fig. 2A).

Cadmium and As(III), alone or combined with SNP, did not affect the mean number of embryonic ARs in comparison with Control. Arsenate alone also did not change the mean number of ARs whereas the combination of SNP with As(V) significantly ($P<0.01$) reduced it (Fig. Supplementary Material 3).

The mean length of the ARs was significantly ($P<0.01$) reduced by Cd alone, on the contrary As(V) alone did not changed it, whereas As(III) alone strongly ($P<0.01$) enhanced it in comparison with the Control (Fig. 2B). The NO donor induced a significant ($P<0.01$) recovery of the length of the ARs exposed to Cd, but it was not able to restore the AR length when combined with the arsenate, further significantly ($P<0.01$) reducing it (Fig. 2B). The combined treatment of As(III) and SNP also reduced the AR length in comparison with As(III) alone, i.e., the treatment causing the highest AR elongation (Fig. 2B)

The mean density of de novo formed LRs, including LRPs, was strongly and significantly reduced by As(V), As(III), and mainly by Cd, in comparison with the Control. When SNP was combined with the heavy metal, a significant ($P<0.001$) recovery of the LRP/LR density, in comparison with Cd alone, was observed (Fig. 2C). On the contrary, the NO donor added to As(V) or As(III) did not change LRP/LR density (Fig. 2C).

Finally, the mean number of LRPs with respect to the LRs was evaluated to verify whether NO had a role in supporting the development of the LRPs into LRs under the pollution stress. The results show that NO was able to increase the mean number of LRs when combined with Cd in comparison with Cd alone (Fig. 2D). It should be emphasized that Cd applied alone strongly reduced the mean density of LRPs/LRs (Fig. 2C) and that about 90% of them remained at the LRP stage (Fig. 2D). The

ratio of LRPs vs LRs was in favour of LRPs also in the presence of As(V) or As(III), and the combined treatments with SNP did not improve this ratio (Fig. 2D).

Altogether the morphological data point up that NO alleviates damages on rice root architecture induced by Cd, but it is not able to restore alteration due to As.

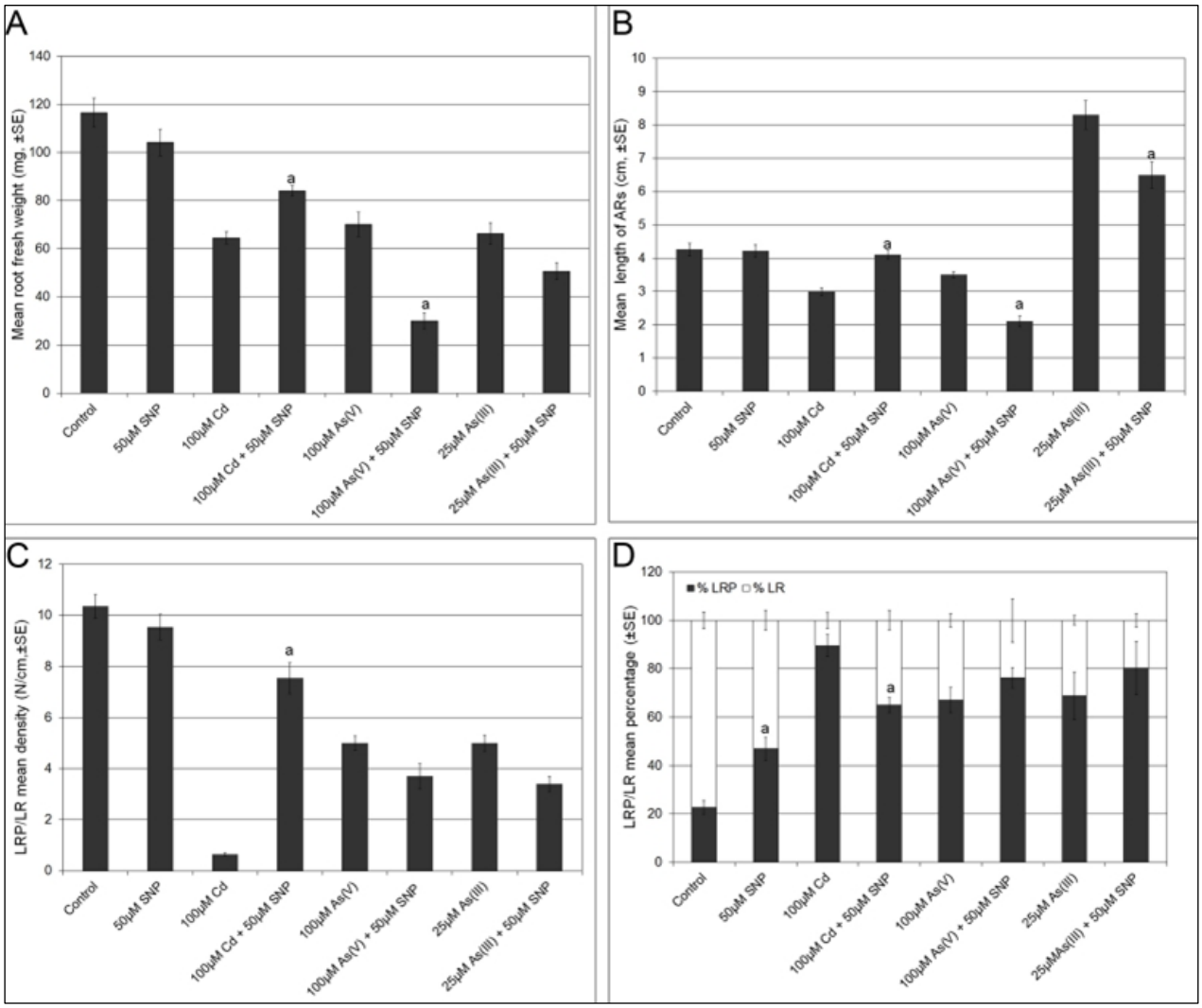

Fig. 2. Mean values (±SE) of rice root fresh weight (**A**), adventitious root (AR) length (**B**), density of lateral root primordia (LRPs) and elongated lateral roots (LRs) (*C*) and percentage of LRPs and LRs (**D**) in seedlings exposed or not for 10 days to 100 µM $CdSO_4$ (100µM Cd), 100 µM $Na_2HAsO_4 \cdot 7H_2O$ (100µM As(V)) or 25µM $NaAsO_2$ (25µM As(III)) alone or combined with 50 µM $Na_2[Fe(CN)_5NO] \cdot 2H_2O$ (50µM SNP). Letters show statistical differences, at least at $P<0.05$ level, within the same treatment with/ without SNP. N =30.

3.3. Nitric Oxide Decreases Cd and As Uptake in Rice Seedlings

In order to investigate the effects of exogenous NO on Cd or As uptake and translocation, the accumulation of the heavy metal and of the metalloid was evaluated in the roots and shoots of the seedlings. Thirty seeds per treatments were sown in the absence or presence of SNP and in the absence or presence of Cd, As(III) or As(V), alone or combined with SNP, and the roots and shoots were separately analysed by ICP-MS.

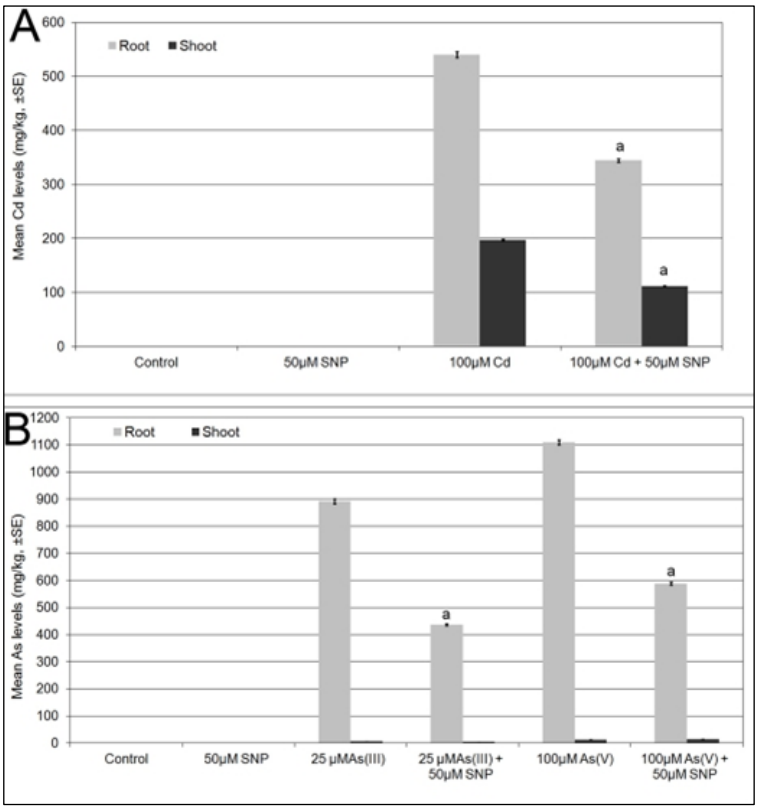

Fig. 3. Cadmium (**A**) and Arsenic (**B**) accumulation in roots and shoots of rice seedlings treated or not for 10 days with 100 µM $CdSO_4$ (100µM Cd), 100 µM $Na_2HAsO_4 \cdot 7H_2O$ (100µM As(V)) or 25µM $NaAsO_2$ (25µM As(III)) alone or combined with 50 µM $Na_2[Fe(CN)_5NO] \cdot 2H_2O$ (50µM SNP). Letters show statistical differences, at least at $P<0.05$ level, within the same treatment with/without SNP. Mean of tree biological replicates.

Arsenic and Cd were mainly accumulated in the roots, and As, added to culture media either as As(III) or As(V), was taken up more than Cd (Fig. 3A-B). The treatment with SNP significantly ($P<0.01$) reduced the accumulation in the roots of both Cd and As (Fig. 3). The transport of Cd to the

aerial organs was low and the presence of SNP furtherly and significantly ($P<0.01$) reduced it (Fig. 3A). Even the As was transported to the shoot at very low amounts, independently from the SNP presence (i.e., 6,41, 4,96, 12,06 and 9,11 mg/kg for As(III), As(III) plus SNP, As(V) and as(V) plus SNP respectively) (Fig. 3B). The evaluation of the translocation factor (FT) and bioaccumulation factor (BF) of both the elements, taken alone or combined with SNP, showed that the NO donor did not affect the rice translocation capability of the heavy metal and the metalloid from the root to the shoot. Overall the results highlight a significant role of NO in the reduction of the uptake of these elements in rice.

3.4. Exogenous NO Differently Changes ROS and RNS Cell Balance in Roots Exposed to Cd or As

To verify whether the root morphological alterations were due to an unbalance of ROS/RNS levels induced by the heavy metal and metalloid treatments, and whether exogenous NO was able to restore the ROS/RNS balance, the superoxide anion ($O_2^{\cdot -}$) and peroxynitrite ($ONOO^-$) contents were evaluated in LRPs and LRs.

The cellular content of $O_2^{\cdot -}$ was evaluated by nitro blue tetrazolium (NBT) staining in LRPs and LRs 10 days from sowing in the presence or absence of the heavy metal or the metalloid, alone or combined with SNP. Nitro blue tetrazolium is a chemical compound that is reduced by $O_2^{\cdot -}$ forming a purple/blue precipitate called formazan, thus representing a useful tool to study the intracellular production of the superoxide anion.

The LRPs and LRs of the Control seedlings showed a weak NBT staining in the apex (Fig. 4A-B). The staining increased in these roots after SNP treatment (Fig. 4C-D). Cadmium alone induced an increase in $O_2^{\cdot -}$ levels in both LRPs and LRs (Fig. 4E-F), but mainly in the elongated LRs (Fig. 4F). The presence of SNP combined with Cd reduced superoxide anion level only in the elongated roots (Fig. 4G-H).

Arsenate alone determined a localization of the $O_2^{\cdot -}$ mainly in the apical region of the LRP (Fig. 4I). However, in the elongated LRs the $O_2^{\cdot -}$ signal remained localized mainly in the stele (Fig. 4J). Surprisingly, when As was combined with SNP the level of superoxide anion strongly increased either in LRPs and in LRs (Fig. 4K-L). The levels of peroxynitrite ($ONOO^-$) were also detected, using 3′-(p-aminophenyl) fluorescein (APF), in LRPs and LRs after exposure, or not, to Cd or As, alone or combined with SNP. The LRPs and LRs of the Control showed a weak fluorescent signal (Fig. 5A-B, M).

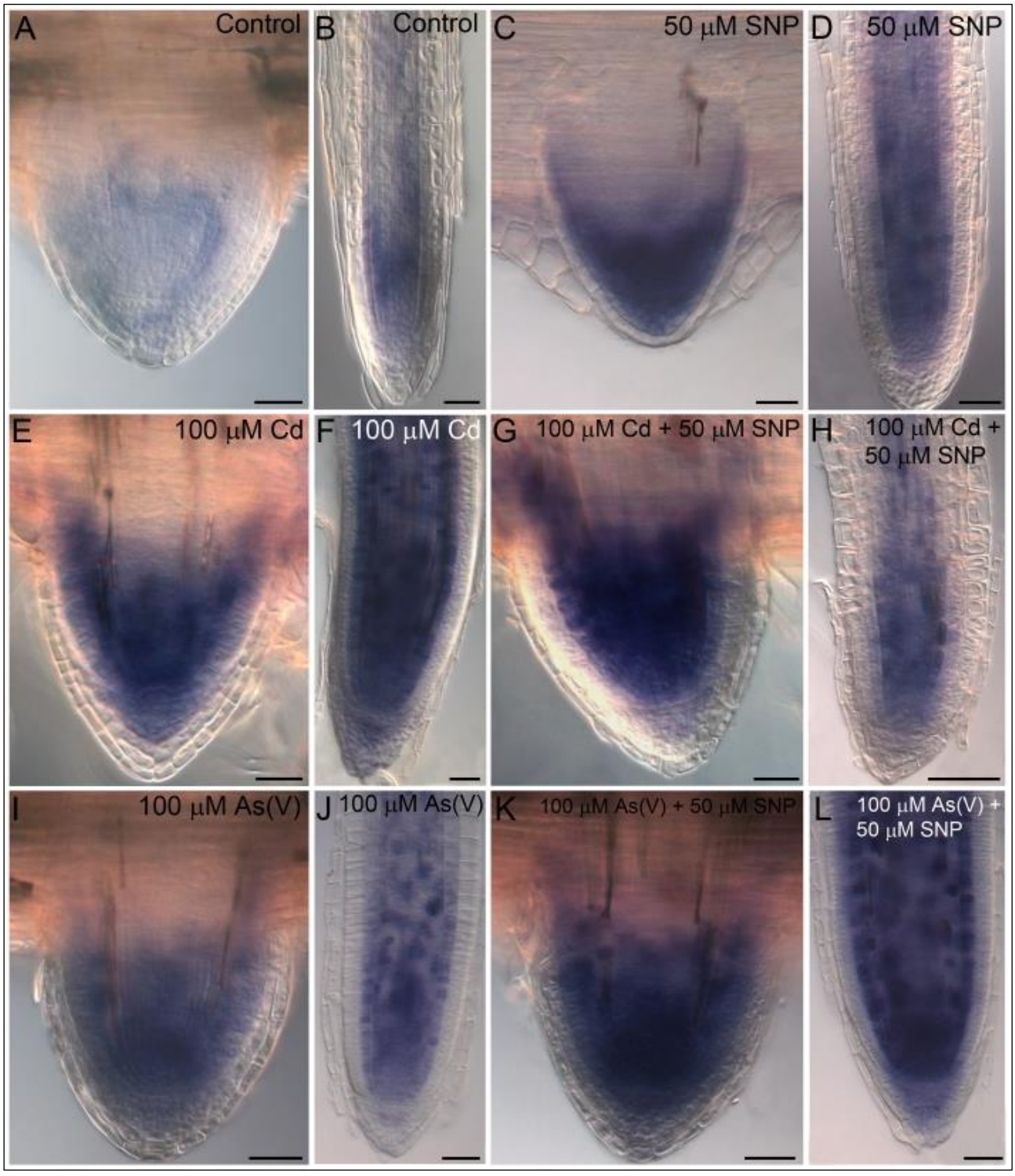

Fig. 4. Superoxide anion (blue colour) detected by NBT staining in lateral root primordia (LRPs; **A**,**C**,**E**,**G**,**I** and **K**) and elongated lateral roots (LRs; **B**,**D**,**F**,**H**,**J** and **L**) of rice seedlings treated or not for 10 days with 100 μM $CdSO_4$ (100μM Cd), 100 μM $Na_2HAsO_4 \cdot 7H_2O$ (100μM As(V)) or 25μM

$NaAsO_2$ (25µM As(III)) alone or combined with 50 µM $Na_2[Fe(CN)_5NO]\cdot 2H_2O$ (50µM SNP). Bars = 30 µm.

The fluorescence was significantly ($P<0.01$) reinforced in the LRPs and LRs cultured in the presence of SNP (Fig. 5C-D, M). The exposure to Cd alone significantly ($P<0.01$) increased the $ONOO^-$ signal both in LRPs and LRs, in comparison with the Control (Fig. 5E-F, M). When Cd was combined with SNP the peroxynitrite signal furtherly, but not significantly, increased respect to Cd alone (Fig. 5G-H, M).

The treatment with both arsenic species alone reduced the peroxynitrite signal in LRPs and LRs in comparison with the Control, and As(V), in particular (Fig. 5M). The presence of SNP combined with As did not change or only weakly increased the fluorescent signal (Fig. 5I-M).

The evaluation of the $O_2^{\cdot -}$ and $ONOO^-$ levels in roots exposed to Cd or As combined with SNP demonstrate that NO reduces ROS levels due to Cd treatment by triggering peroxynitrite production (Figs 4E-H and 5E-H,M in comparison). On the contrary, NO does not reduce $O_2^{\cdot -}$ levels induced by the As treatments (Figs 4 I-L and 5I-M, in comparison), this led to very high levels of $O_2^{\cdot -}$ and to low levels of $ONOO^{\cdot -}$ in LRP and LR cells.

3.5. Nitric Oxide Reduces the Histological Damages Induced by Cd but it Does not Recover Those Induced by As

It is known that Cd and As induce extensive damages in rice roots either in ARs and, in particular, in the formation of LRPs and during their development into LRs (Ronzan et al., 2018). To verify if increased intracellular NO levels were able to reduce Cd- and As-induced damages, seeds of rice were sown in the presence or absence of Cd or As(V), combined or not with SNP, and after 10 days, a histological analysis was carried out at the beginning of the AR primary structure. The autofluorescence of lignin in sclerenchyma and endodermis cell walls, under UV radiation, was detected and quantified (Fig. 6).

The histological analysis showed that the Control roots and the SNP-treated roots, as expected, were characterized by epidermis, exoderms, sclerenchyma layer, cortical parenchyma, endodermis and regularly differentiated vascular bundles (Fig. 6 A-B, D-E). The autofluorescence analysis showed that the sclerenchyma cells were mildly lignified (Fig. 6C, F, small arrows, and S) while the differentiated endodermic cells did not show lignin deposition in the cell wall (Fig. 6C, F, arrowheads, and S).

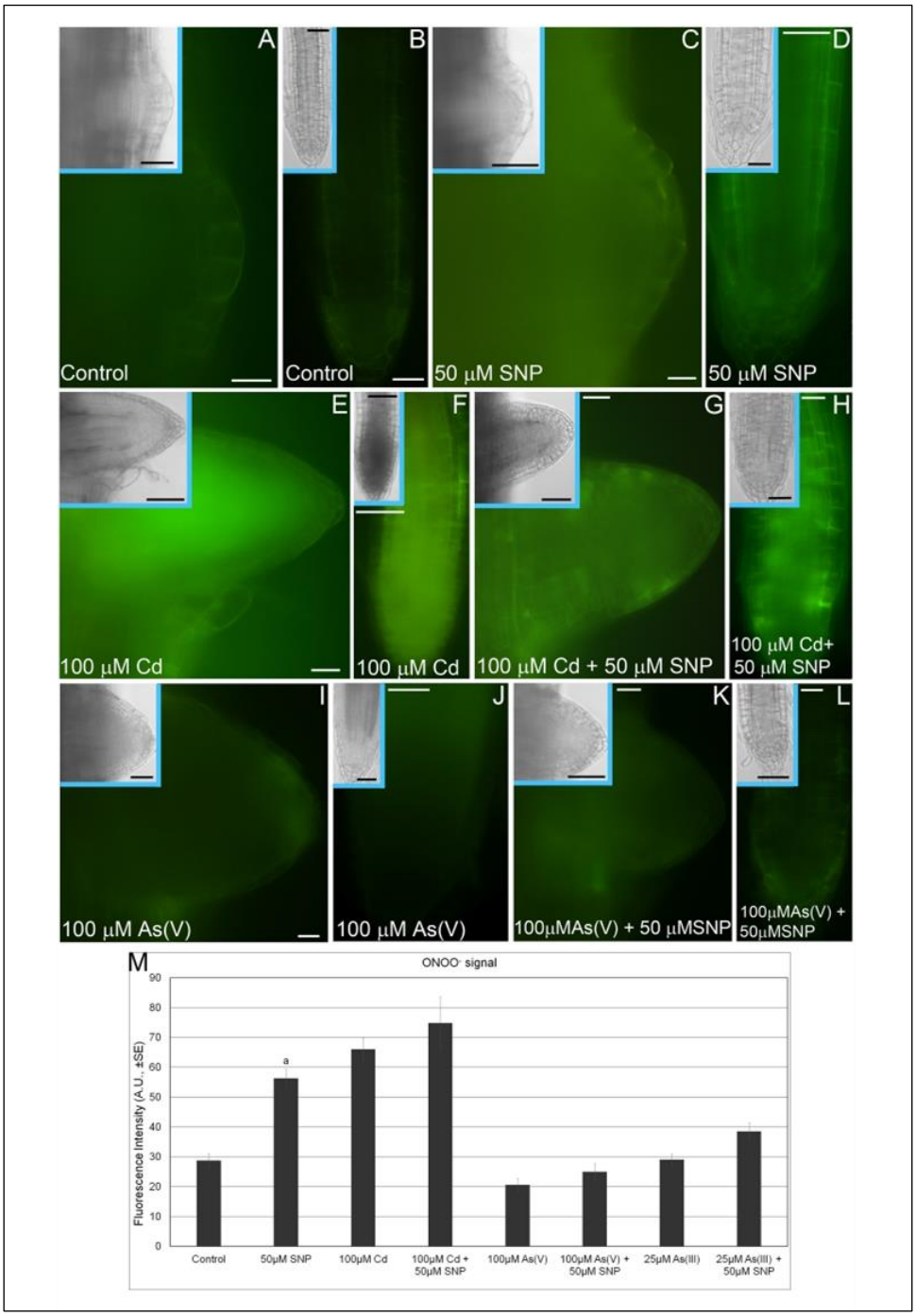

Fig. 5. Peroxynitrite levels (bright green colour) in rice lateral root primordia (LRPs; **A**,**C**,**E**,**G**,**I** and **K**) and elongated lateral roots (LRs; **B**,**D**,**F**,**H**,**J** and **L**) treated or not with 100 µM $CdSO_4$ (100µM Cd), 100 µM $Na_2HAsO_4 \cdot 7H_2O$ (100µM As(V)) or 25µM $NaAsO_2$ (25µM As(III)) alone or combined with 50 µM $Na_2[Fe(CN)_5NO] \cdot 2H_2O$ (50µM SNP). LRPs and LRs taken from 10-days-old seedlings were loaded with 3'-(p-aminophenyl) fluorescein (APF). Bars =20 µm (A-E, G-I, K-L, Inset in D) and 50 µm (F, J, Insets in A-C, E-L). **M**, Mean of $ONOO^-$ fluorescence intensity (±SE) in LRPs/LRs

measured using ImageJ 1.52a software and expressed in arbitrary units (AUs). Letters show statistical differences, at least at $P<0.05$ level, within the same treatment with/without SNP. N =30.

The Cd alone treatment induced a precocious aerenchyma formation and a strong thickening of the sclerenchyma cell walls due to higher lignin deposition (Fig. 6G-I). The increase of the cell wall thickening of the sclerenchyma cells determined the crush of the exoderms (Fig. 6G-H). The endodermic cells were also characterized by lignin deposition (Fig. 6I, arrowheads). The significant increase of lignin in the cell walls of the sclerenchyma and the endodermis was also detected by the raise of the lignin auto-florescence signal in both tissues (Fig. 6S). Moreover, a moderate cell wall lignification was observed in the inner cortical cells and in the pericycle cells and fibres inside the stele (Fig. 6G-I).

The combined treatment of Cd and SNP significantly reduced cell wall lignification in the sclerenchyma and endodermis cells (Fig. 6J-L). The lignin autofluorescence decreased up to values similar to those of the Control roots, especially in the sclerenchyma layer (Fig. 6S). The less thickened of the sclerenchyma layer was associated with a less damaged exoderms (Fig. 6J-K).

Considering that As(V) and As(III) induced similar alterations in root morphology (Fig. 1), the histological analysis was performed on arsenate-exposed roots only. The As alone determined an increase in the sclerenchyma and endodermis cell wall thickening, similarly to Cd, and a related enhancement of the lignin autofluorescence (Fig. 6M-O, S). Moreover, As also induced precocious aerenchyma formation, in addition to an anomalous proliferation of the sclerenchyma cells (Fig. 6M-N, arrows) and an alteration of exoderms (Fig. 4M). Conspicuous cell wall lignification were observed in the inner cortical cells and in the fibres inside the stele (Fig. 6N-O). The NO donor combined with As reduced lignin deposition in the endodermal cells, and the related autofluorescence (Fig. 6P-R, S). However, the reduction of the lignin deposition was less evident in the sclerenchyma layer. An anomalous cell proliferation, frequently associated to plasmolysis, was observed in the cortical cells after the treatment with As plus SNP (Fig. 6P-Q, arrows).

These results demonstrate that NO is able to counteract the increase in the cell wall thickness of the sclerenchyma and endodermis, the tissues committed to protect the root from the toxicity of the heavy metal and metalloid. However, in the presence of As, NO reduces lignification in these tissues, and in the endodermis in particular, but induces anomalous divisions in the parenchyma cells.

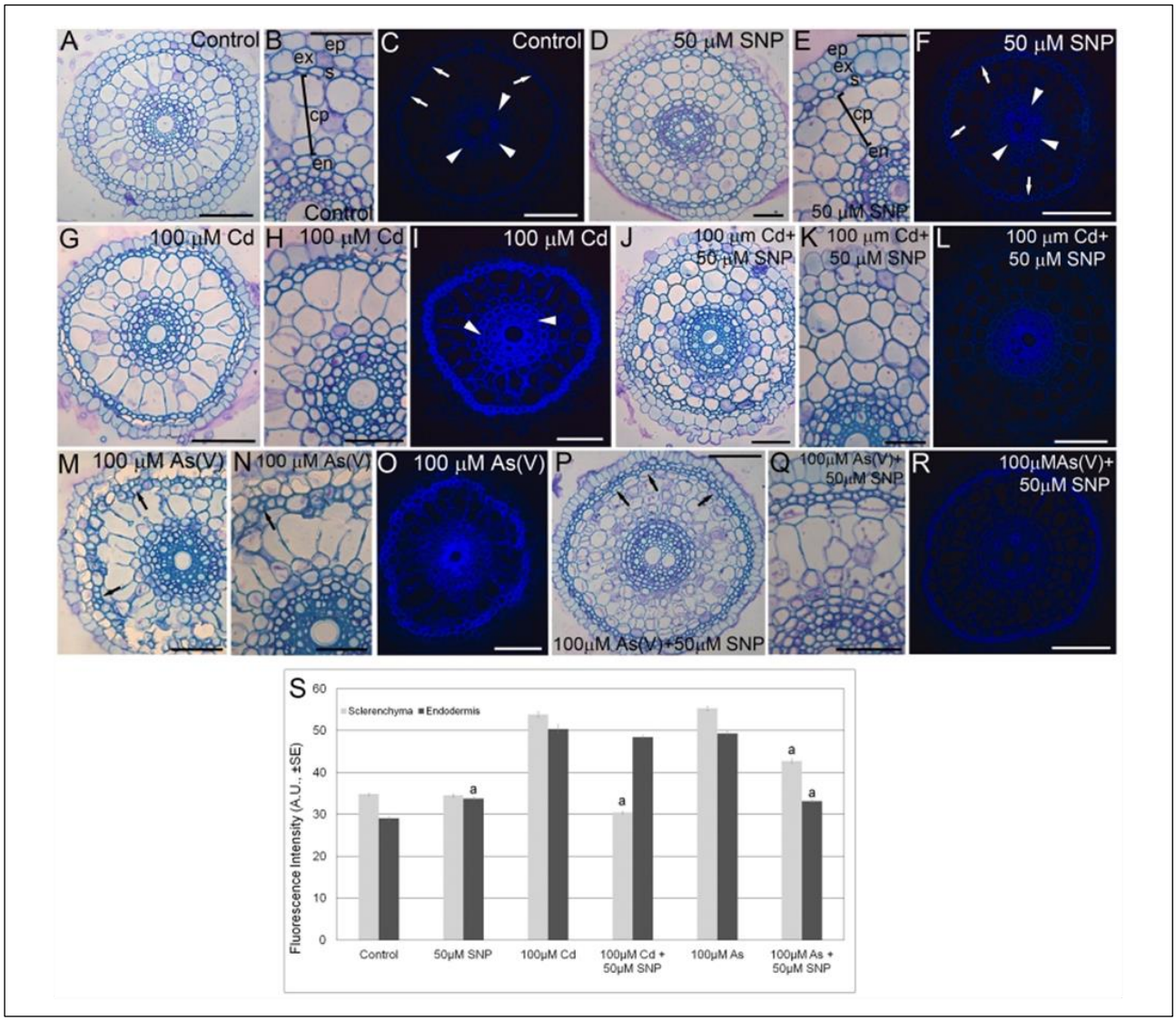

Fig. 6. Transverse sections of ARs at 2.0 cm from the root tip taken from rice seedlings treated or not for 10 days with 100 μM $CdSO_4$ (100μM Cd) , 100 μM $Na_2HAsO_4 \cdot 7H_2O$ (100μM As(V)) or 25μM $NaAsO_2$ (25μM As(III)) alone or combined with 50 μM $Na_2[Fe(CN)_5NO] \cdot 2H_2O$ (50μM SNP). **A**-**B**, **D**-**E**, **G**-**H**, **J**-**K**, **M**-**N** and **P**-**Q** light microscope images of sections stained with toluidine blue. **C**,**F**,**I**, **L**,**O** and **R** images showing lignin autofluorescence (bright blue colour) in sclerenchyma and endodermis cell walls. Bar = 50 μm (B, E, H, K, N, Q) and 100 μm (A, C-D, F-G, I-J, L-M, O-P, R). cp, cortical parenchyma; ep, epidermis; ex, exoderms; s, sclerenchyma layer; en, endodermis. **S**, mean values (±SE) of lignin autofluorescence intensity measured using ImageJ 1.52a software and expressed in arbitrary units (AUs). Letters show statistical differences, at least at $P<0.05$ level, for the same tissue and treatment, with/without SNP. N=30.

4. Discussion

The present results highlight a different behaviour of NO in modulating the rice responses to the toxicity of the heavy metal Cd and the metalloid As. In fact, an increased intracellular NO level in root cells, as a consequence of the application of the exogenous NO donor SNP, alleviates morphological and histological damages and restores ROS/RNS cell balance induced by Cd, but it is not able to restore the damages and the oxidative system imbalance caused by As.

In the last decade, numerous researches have demonstrated the involvement of NO in the defence responses against toxic elements (Besson-Bard et al., 2009; Manai et al., 2014; Silveira et al., 2015; Kharbech et al., 2017, just to name a few). In particular, it is emerging that a correct cellular balance between NO and ROS is of fundamental importance to allow plants to counteract the toxicity induced by the most dangerous and common soil pollutants, such as Cd or As (Farnese et al., 2016, and references therein). Most research attributes a positive role to NO in alleviating the toxicity of heavy metals/metalloids, however some researches also report that an increase in endogenous levels of NO can intensify the dangerous effects of the toxic metals (Besson-Bard et al., 2009; Yuan and Huang 2016).

Our results show that Cd alone significantly decreased the NO levels in rice roots (Fig. 1), and this is in accordance with previously results obtained in *Medicago truncatula*, *Pisum sativum* and *Oryza sativa* after exposition to heavy metals (Xiong et al., 2009; Xu et al., 2010 and Rodríguez-Serrano et al., 2006). In particular, Rodriguez-Serrano and co-workers (2009) attribute the reduction of NO level to a prolonged exposure to high Cd concentrations that could inactive the enzymes involved in NO synthesis (NOS-like enzymes). The same mechanism may be activated in rice seedlings, because we exposed them to high Cd (100 μM $CdSO_4$) levels for a long period (10 days). Thus, it is possible that the near absence of NO in rice root cells exposed to Cd alone could not allow the activation of the appropriate strategies to withstand the heavy metal toxicity. On the contrary, the exposure to As, and mainly to As(III) did not significantly reduce root NO levels compared to the Control and this could be positively correlated with a root morphology alteration less than that caused by Cd (Fig. 1). On the one hand, these observations support the already known role of NO in metal toxicity responses; on the other, they show different effects of Cd and As on NO metabolism.

We show that an exogenous application of SNP, a common NO donor, increases the intracellular NO content in the roots, either when combined with Cd or with both arsenite or arsenate (Fig.1). The increase in NO levels in the roots exposed to Cd and SNP, even if slight, seems sufficient to alleviate

the damages caused by the heavy metal, according to what has been reported for *M. truncatula* and tomato (Cui et al., 2010; Xu et al., 2010). In fact, when Cd was combined with SNP, all the morphological parameters showed an improvement compared to Cd alone (Fig. 2).

Sodium nitroprusside combined with both the inorganic As forms induced very high levels of NO in rice root already starting from the early stages of LRP formation (Fig. 1). This effect probably does not allow the plant to improve the development of the root system, differently from what reported for the same rice plant by Praveen and Gupta (2018). In fact, it is known that NO must be present in the cells at low levels to act as a positive mediator of plant responses to abiotic stresses, including those induced by metals (Terron-Camero et al., 2019). At the same time, too high levels of NO accentuate the cell suffering by inducing nitrosative stress because they can trigger the nitrosylation of key proteins of the cellular metabolism (Molassiotis and Fotopoulos 2011).

Cadmium or As stresses induce ROS formation as shown by present results (Fig. 4) in accordance with many other Authors. Increased ROS production determines oxidative stress in plant cells and damages to the plant as a whole. Thus, the cellular levels of ROS must be kept under control by enzymatic and non-enzymatic antioxidant systems in order to protect the plant against the oxidative damages (Gill et al., 2010). As above reported, the heavy metal and the metalloid also directly interfere with NO metabolism either increasing or decreasing its levels (Arasimowicz-Jelonek et al., 2011). Nitric oxide, at specific concentrations, in turn, activates enzymatic and non-enzymatic antioxidant systems to scavenge ROS, thus protecting cells against the oxidative damage. In our conditions, it is possible that the strong reduction of NO induced by Cd reduces the ROS scavenging activity mediated by the signal molecule. By contrast, NO levels useful for activating antioxidant system can be restored after adding SNP to the heavy metal. Arsenic per se increases NO levels and, after adding SNP to the metalloid, the levels of NO become too high to counteract its toxicity.

An active interplay between ROS and RNS modulates plant responses to environmental stresses. It is crucial to keep the ROS/RNS levels below the values that trigger the oxidation/nitrosylation reactions in the cells. This interaction is based on different mechanisms, but the most recurrent and immediate one is the reaction between the ROS $O_2^{\cdot -}$ and NO to form the $ONOO^-$, a RNS , to which an important role in the signalling processes has been given in recent years (Molassiotis and Fotopoulos 2011). The peroxinitrite, at very high levels, however, induces nitro-oxidative stress (Corpas and Barroso 2014 and references therein). The present results show that Cd alone or, mainly combined with SNP, increased peroxinitrite formation, and this is consistent with the low NO levels and the reduction of the superoxide anion simultaneously observed in rice roots (Figs. 1, 4 and 5). It

is possible that in our conditions, in particular when Cd was combined with SNP, a favourable balance between ROS and RNS levels is achieved and this allows rice plant to counteract the heavy metal toxicity.

In the presence of As(V) or As(III), alone, and above all combined with SNP, $ONOO^-$ levels remained rather low. On the contrary, the levels of NO and $O_2^{\cdot -}$ were high (Figs. 1, 4 and 5). As reported, in the root cells a reaction converts As(V) to As(III) and this contributes to increase the cytosolic levels of ROS (Meharg and Hartley-Whitaker 2002; Abbas et al., 2018). It is therefore possible that the higher ROS levels induced by As in comparison with Cd alter the ROS/RNS ratio so much that the NO donor becomes unable to rebalance it, and to mitigate the damages due to As.

It is therefore clear that, for NO to have a positive role in alleviating metal-induced toxicity, a perfect cellular balance must be achieved between ROS and RNS, with $ONOO^-$ acting as an effector of NO-mediated signalling, as previously reported by Vandelle and Delle donne (2011). However, the cellular ROS/RNS balance depends on the culture conditions, but above all on the concentrations and on the exposure times to the toxic elements.

The present results show that Cd alone induces a strong increase in lignin deposition in the cell walls of the sclerenchyma and endodermis of the ARs (Fig. 6). This can be considered as a strategy to limit the entry of the heavy metal into the cortical and vascular cells, similarly to what is observed in the fronds of *Pteris vittata* exposed to Cd (Ronzan et al., 2017). Moreover, the SNP treatment combined to Cd was able to reduce lignin deposition, mainly in the sclerenchyma cells. This seems positively linked with the effects of exogenous NO on the heavy metal uptake (Fig. 3). In fact, increased NO levels significantly reduced Cd levels in the roots. Thus, a lower Cd content and a rebalance of ROS/RNS ratio, which is obtained when SNP is combined with Cd, can be responsible of the positive actions on the histological organization of the developing LRs. The As treatments also increase lignin deposition in the walls of the sclerenchyma and endodermis cells. Moreover, the metalloid triggers anomalous cell divisions in the sclerenchyma layer and in the cortex. The SNP treatment, combined with both the As forms, reduces the lignification of the endodermis, but less than that of the sclerenchyma cells, and is not able to reduce anomalous cell proliferation. Sodium nitroprusside treatment also reduces uptake of As (Fig.3) but not enough to limit its toxicity, collectively showing a different behaviour of a NO with As.

5. Conclusions

In conclusion, the results highlight that NO differently affects the responses of rice plants to the toxicity of Cd and As. In fact, increased cellular levels of NO are able to alleviate root damages induced by Cd by improving the entire root system, but they are not able to improve the root system when exposed to As. The explanation of this different behaviour probably is to be attributable to the ability to restore the ROS/RNS cellular balance, which is differently altered by the two toxic pollutants.

Therefore, our data help to understand NO action, but further researches are needed to shed light on the mechanisms that govern this action.

Authors Contributions

D.P. designed, carried out the research, analysed the data and performed the statistical analysis. M.R., L.F. and F.D.R. contributed to perform the morphological, histological and fluorescence analyses. L.M. carried out the elemental analysis. M.M.A. and G.F. analysed and interpreted the data, wrote, revised and edited the manuscript. All authors read and approved the manuscript.

Acknowledgements

This work was supported by Progetti Ateneo Sapienza University of Rome – Italy (2018) – Prot. Number RM 118164286B32D4 to F.L. and AR118163F8C319B7 to P.D.

The Authors gratefully thank Dr. S. Belcastro for her help in the morphological and histological analyses.

Conflicts of Interest

The authors declare no conflict of interest.

References

Abbas, G., Murtaza, B., Bibi, I., Shahid, M., Niazi, N.K., Khan, M.I., Amjad, M., Hussain, M., Natasha, 2018. Arsenic uptake, toxicity, detoxification, and speciation in plants: physiological, biochemical, and molecular aspects. Int. J. Environ. Res. Public Health 15, 59. https://doi.org/10.3390/ijerph15010059.

Arasimowicz-Jelonek, M., Floryszak-Wieczorek, J., 2011. Understanding the fate of peroxynitrite in plant cells–from physiology to pathophysiology. Phytochemistry 72, 681-688. https://doi.org/10.1016/j.phytochem.2011.02.025.

Arasimowicz-Jelonek, M., Floryszak-Wieczorek, J., Gwóźdź, E.A., 2011. The message of nitric oxide in cadmium challenged plants. Plant Sci. 181, 612-620. https://doi.org/10.1016/j.plantsci.2011.03.019.

Astolfi, M. L., Marconi, E., Protano, C., Vitali, M., Schiavi, E., Mastromarino, P., Canepari, S. 2018. Optimization and validation of a fast digestion method for the determination of major and trace elements in breast milk by ICP-MS. Analytical Chimica Acta, 1040, 49-62. https://doi.org/10.1016/j.aca.2018.07.037.

Bartha, B., Kolbert, Z., Erdei, L., 2005. Nitric oxide production induced by heavy metals in *Brassica juncea* L. Czern. and *Pisum sativum* L. Acta Biol. Szeged. 49, 9-12.

Besson-Bard, A., Gravot, A., Richaud, P., Auroy, P., Duc, C., Gaymard, F., Taconnat, L., Renou, J.P., Pugin, A., Wendehenne, D., 2009. Nitric oxide contributes to cadmium toxicity in Arabidopsis by promoting cadmium accumulation in roots and by up-regulating genes related to iron uptake. Plant Physiol. 149, 1302-1315. https://doi.org/10.1104/pp.108.133348.

Chen, J., Liu, X., Wang, C., Yin, S.S., Li, X.L., Hu, W.J., Simon, M., Shen, Z.J., Xiao, Q., Chu, C.C., Peng, X.X., Zheng, H.L., 2015. Nitric oxide ameliorates zinc oxide nanoparticles-induced phytotoxicity in rice seedlings. J Hazard. Mater. 297, 173-182. https://doi.org/10.1016/j.jhazmat.2015.04.077.

Clemens, S., Palmgren, M.G., Krämer, U., 2002. A long way ahead: understanding and engineering plant metal accumulation. Trends Plant Sci. 7, 309-315. https://doi.org/10.1016/S1360-1385(02)02295-1.

Cobbett, C.S., 2000. Phytochelatins and their roles in heavy metal detoxification. Plant Physiol. 123, 825-832. https://doi.org/10.1104/pp.123.3.825.

Corpas, F.J., Barroso, J.B., 2014. Peroxynitrite (ONOO−) is endogenously produced in Arabidopsis peroxisomes and is overproduced under cadmium stress. Ann. Bot. 113, 87-96. https://doi.org/10.1093/aob/mct260.

Corpas, F.J., Barroso, J.B., 2015. Functions of Nitric Oxide (NO) in Roots during Development and under Adverse Stress Conditions. Plants 4, 240-252. doi:10.3390/plants4020240

Cui, X.M., Zhang, Y.K., Wu, X.B., Liu, C.S., 2010. The investigation of the alleviated effect of copper toxicity by exogenous nitric oxide in tomato plants. Plant Soil Environ. 56, 274–281. https://doi.org/10.17221/98/2009-PSE.

Fancy, N.N., Bahlmann, A.K., Loake, G.J., 2017. Nitric oxide function in plant abiotic stress. Plant Cell Environ. 40, 462-472. https://doi.org/10.1111/pce.12707.

Farnese, F.S., Menezes-Silva, P.E., Gusman, G.S., Oliveira, J.A., 2016. When bad guys become good ones: the key role of reactive oxygen species and nitric oxide in the plant responses to abiotic stress. Front. Plant Sci. 7, 471. https://doi.org/10.3389/fpls.2016.00471.

Fattorini, L., Ronzan, M., Piacentini, D., Della Rovere, F., De Virgilio, C., Sofo, A., Altamura, M.M., Falasca, G., 2017. Cadmium and arsenic affect quiescent centre formation and maintenance in *Arabidopsis thaliana* post-embryonic roots disrupting auxin biosynthesis and transport. Environ. Exp. Bot. 144, 37-48. https://doi.org/10.1016/j.envexpbot.2017.10.005.

Gill, S.S., Tuteja, N., 2010. Reactive oxygen species and antioxidant machinery in abiotic stress tolerance in crop plants. Plant Physiol. Biochem. 48, 909-930. https://doi.org/10.1016/j.plaphy.2010.08.016.

Ismail, G.S.M., 2012. Protective role of nitric oxide against arsenic-induced damages in germinating mung bean seeds. Acta Physiol. Plant. 34, 1303-1311. https://doi.org/10.1007/s11738-012-0927-9.

Kharbech, O., Houmani, H., Chaoui, A., Corpas, F.J., 2017. Alleviation of Cr(VI)-induced oxidative stress in maize (*Zea mays* L.) seedlings by NO and H_2S donors through differential organ-dependent regulation of ROS and NADPH-recycling metabolisms. J. Plant. Physiol. 219, 71-80. https://doi.org/10.1016/j.jplph.2017.09.010.

Kopyra, M., Gwóźdź, E.A., 2003. Nitric oxide stimulates seed germination and counteracts the inhibitory effect of heavy metals and salinity on root growth of *Lupinus luteus.* Plant Physiol. Biochem. 41, 1011-1017. https://doi.org/10.1016/j.plaphy.2003.09.003.

Kopyra, M., Stachoń-Wilk, M., Gwóźdź, E.A., 2006. Effects of exogenous nitric oxide on the antioxidant capacity of cadmium-treated soybean cell suspension. Acta Physiol. Plant 28, 525-536. https://doi.org/10.1007/s11738-006-0048-4.

Leterrier, M., Airaki, M., Palma, J.M., Chaki, M., Barroso, J.B., Corpas, F.J., 2012. Arsenic triggers the nitric oxide (NO) and S-nitrosoglutathione (GSNO) metabolism in *Arabidopsis*. Environ. Pollut. 166, 136-143. https://doi.org/10.1016/j.envpol.2012.03.012.

Manai, J., Kalai, T., Gouia, H., Corpas, F.J., 2014. Exogenous nitric oxide (NO) ameliorates salinity-induced oxidative stress in tomato (*Solanum lycopersicum*) plants. J. Soil Sci. Plant Nutr. 14, 433-446. http://dx.doi.org/10.4067/S0718-95162014005000034.

Meharg, A.A., Hartley-Whitaker, J., 2002. Arsenic uptake and metabolism in arsenic resistant and nonresistant plant species. New Phytol. 154, 29-43. https://doi.org/10.1046/j.1469-8137.2002.00363.x.

Meharg, A.A., MacNair, M.R., 1992. Genetic correlation between arsenate tolerance and the rate of influx of arsenate and phosphate in *Holcus lanatus* L. Heredity 69, 336-341. https://doi.org/10.1038/hdy.1992.133.

Molassiotis, A., Fotopoulos, V., 2011. Oxidative and nitrosative signaling in plants: two branches in the same tree? Plant Signal. Behav. 6, 210-214. https://doi.org/10.4161/psb.6.2.14878.

Murashige, T., Skoog, F., 1962. A revised medium for rapid growth and bio assays with tobacco tissue cultures. Physiol. Plant. 15, 473–497. https://doi.org/10.1111/j.13993054.1962.tb08052.x.

Noriega, G.O., Yannarelli, G.G., Balestrasse, K.B., Batlle, A., Tomaro, M.L., 2007. The effect of nitric oxide on heme oxygenase gene expression in soybean leaves. Planta 226, 1155-1163. https://doi.org/10.1007/s00425-007-0561-8.

Piacentini, D., Falasca, G., Canepari, S., Massimi, L., 2019. Potential of PM-selected components to induce oxidative stress and root system alteration in a plant model organism. Environment International, 132, 1-13. https://doi.org/10.1016/j.envint.2019.105094.

Praveen, A., Gupta, M., 2018. Nitric oxide confronts arsenic stimulated oxidative stress and root architecture through distinct gene expression of auxin transporters, nutrient related genes and modulates biochemical responses in *Oryza sativa* L. Environ. Pollut. 240, 950-962. https://doi.org/10.1016/j.envpol.2018.04.096.

Rezvani, M., Zaefarian, F., 2011. Bioaccumulation and translocation factors of cadmium and lead in *Aeluropus littoralis*. Aust. J. Agric. Eng. 2, 114-119.

Rodríguez-Ruiz, M., Aparicio-Chacón, M.V., Palma, J.M., Corpas, F.J., 2019. Arsenate disrupts ion balance, sulfur and nitric oxide metabolisms in roots and leaves of pea (*Pisum sativum* L.) plants. Environ. Exp. Bot. 161, 143–156. https://doi.org/10.1016/j.envexpbot.2018.06.028.

Rodríguez-Serrano, M., Romero-Puertas, M.C., Zabalza, A., Corpas, F.J., Gómez, M., Del Río, L.A., Sandalio, L.M., 2006. Cadmium effect on oxidative metabolism of pea (*Pisum sativum* L.) roots. Imaging of reactive oxygen species and nitric oxide accumulation *in vivo*. Plant Cell Environ. 29, 1532-1544. https://doi.org/10.1111/j.1365-3040.2006.01531.x.

Ronzan, M., Piacentini, D., Fattorini, L., Della Rovere, F., Caboni, E., Eiche, E., Zeigler, J., Hause, B., Riemann, M., Betti, C., Altamura, M.M., Falasca, G., 2019. Auxin-jasmonate crosstalk in *Oryza sativa* L. root system formation after cadmium and/or arsenic exposure. Environ. Exp. Bot. 165, 59-69. https://doi.org/10.1016/j.envexpbot.2019.05.013.

Ronzan, M., Piacentini, D., Fattorini, L., Della Rovere, F., Eiche, E., Riemann, M., Altamura, M.M., Falasca, G., 2018. Cadmium and arsenic affect root development in *Oryza sativa* L. negatively interacting with auxin. Environ. Exp. Bot. 151, 64-75. https://doi.org/10.1016/j.envexpbot.2018.04.008.

Ronzan, M., Zanella, L., Fattorini, L., Della Rovere, F., Urgast, D., Cantamessa, S., Nigro, A., Barbieri, M., Sanità di Toppi, L., Berta, G., Feldmann, J., Altamura, M.M., Falasca, G., 2017. The morphogenic responses and phytochelatin complexes induced by arsenic in *Pteris vittata* change in

the presence of cadmium. Environ. Exp. Bot. 133, 176-187. https://doi.org/10.1016/j.envexpbot.2016.10.011.

Silveira, N.M., de Oliveira, J.A., Ribeiro, C., Canatto, R.A., Siman, L., Cambraia, J., Farnese, F., 2015. Nitric oxide attenuates oxidative stress induced by arsenic in lettuce (*Lactuca sativa*) leaves. Water Air Soil Pollut. 226, 379. https://doi.org/10.1007/s11270-015-2630-0.

Singh, A.P., Dixit, G., Kumar, A., Mishra, S., Kumar, N., Dixit, S., Singh, P.K., Dwivedi, S., Trivedi, P.K., Pandey, V., Dhankher, O.P., Norton, G.J., Chakrabarty, D., Tripathi, R.D., 2017. A protective role for nitric oxide and salicylic acid for arsenite phytotoxicity in rice (*Oryza sativa* L.). Plant Physiol. Biochem.115, 163-173. https://doi.org/10.1016/j.plaphy.2017.02.019.

Terrón-Camero, L.C., Peláez-Vico, M.Á., Del-Val, C., Sandalio, L.M., Romero-Puertas, M.C., 2019. Role of nitric oxide in plant responses to heavy metal stress: exogenous application versus endogenous production. J. Exp. Bot. 70, 4477-4488. https://doi.org/10.1093/jxb/erz184.

Tuli, R., Chakrabarty, D., Trivedi, P.K., Tripathi, R.D., 2010. Recent advances in arsenic accumulation and metabolism in rice. Mol. Breeding 26, 307-323. https://doi.org/10.1007/s11032-010-9412-6.

Vandelle, E., Delledonne, M., 2011. Peroxynitrite formation and function in plants. Plant Sci. 181, 534-539. https://doi.org/10.1016/j.plantsci.2011.05.002.

Wulff, A., Oliveira, H.C., Saviani, E.E., Salgado, I., 2009. Nitrite reduction and superoxide-dependent nitric oxide degradation by Arabidopsis mitochondria: influence of external NAD(P)H dehydrogenases and alternative oxidase in the control of nitric oxide levels. Nitric Oxide 21, 132-139. https://doi.org/10.1016/j.niox.2009.06.003.

Xiong, J., An, L., Lu, H., Zhu, C., 2009. Exogenous nitric oxide enhances cadmium tolerance of rice by increasing pectin and hemicellulose contents in root cell wall. Planta 230, 755-765. https://doi.org/10.1007/s00425-009-0984-5.

Xu, J., Wang, W., Yin, H., Liu, X., Sun, H., Mi, Q., 2010. Exogenous nitric oxide improves antioxidative capacity and reduces auxin degradation in roots of *Medicago truncatula* seedlings under cadmium stress. Plant Soil 326, 321–330. https://doi.org/10.1007/s11104-009-0011-4.

Yuan, H.M., Huang, X., 2016. Inhibition of root meristem growth by cadmium involves nitric oxide-mediated repression of auxin accumulation and signalling in Arabidopsis. Plant Cell Environ. 39, 120-135. https://doi.org/10.1111/pce.12597.

Zhao, F.J., Ma, J.F., Meharg, A.A., McGrath, S.P., 2009. Arsenic uptake and metabolism in plants. New Phytol. 181, 777-794. https://doi.org/10.1111/j.1469-8137.2008.02716.x.

Supplementary Material S1.

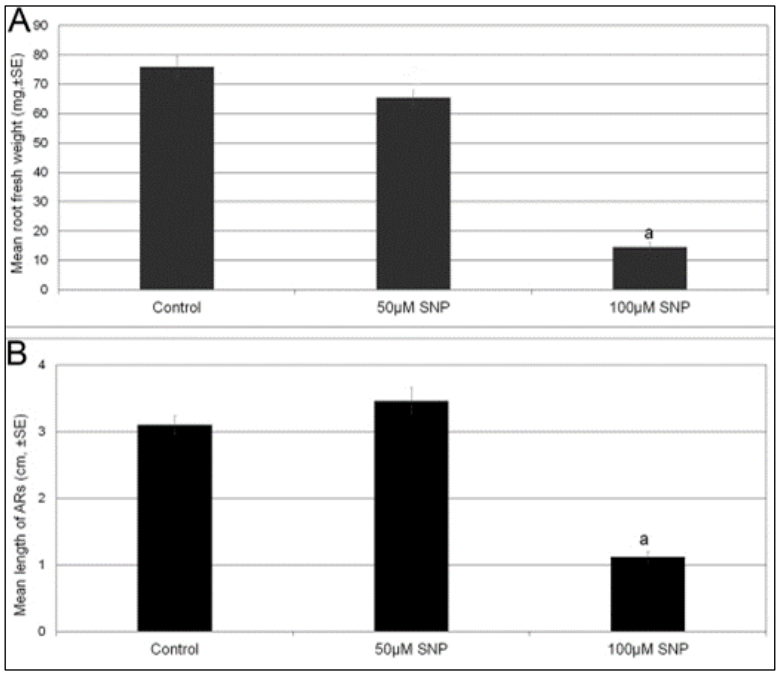

Fig. S1. Mean values (±SE) of rice root fresh weight (**A**) and adventitious root (AR) length (**B**) in seedlings exposed or not for 10 days to 50 and 100 μM $Na_2[Fe(CN)_5NO]\cdot 2H_2O$ (50μM and 100μM SNP). Letters show statistical differences, at least at $P<0.05$ level. N =30.

Supplementary Material S2.

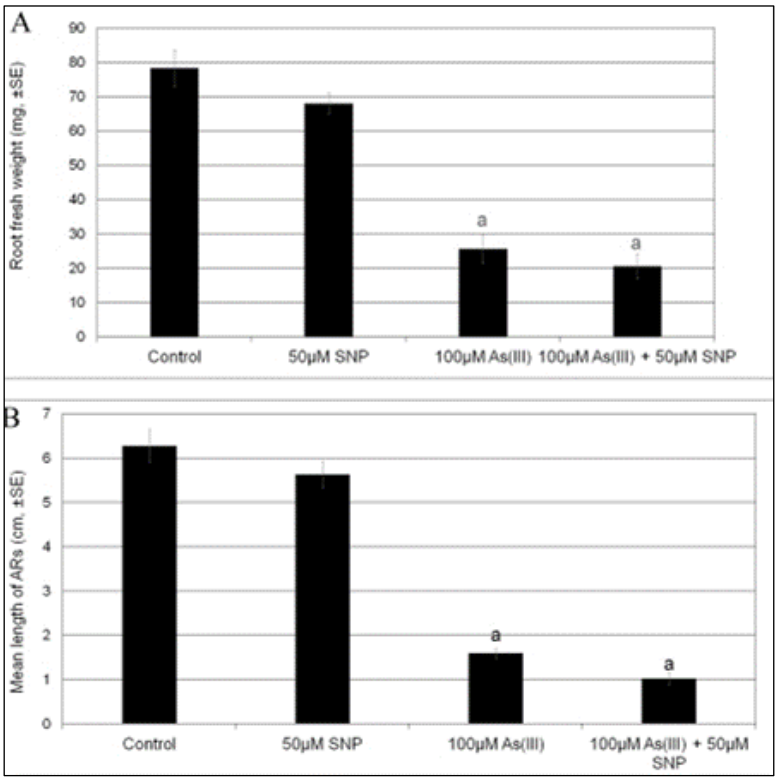

Fig. S2. Mean values (±SE) of rice root fresh weight (**A**) and adventitious root (AR) length (**B**) in seedlings exposed or not for 10 days to days to 100 µM $NaAsO_2$ (100µM As(III)) alone or combined with 50 µM $Na_2[Fe(CN)_5NO]\cdot 2H_2O$ (50µM SNP). N =30.

Supplementary Material S3.

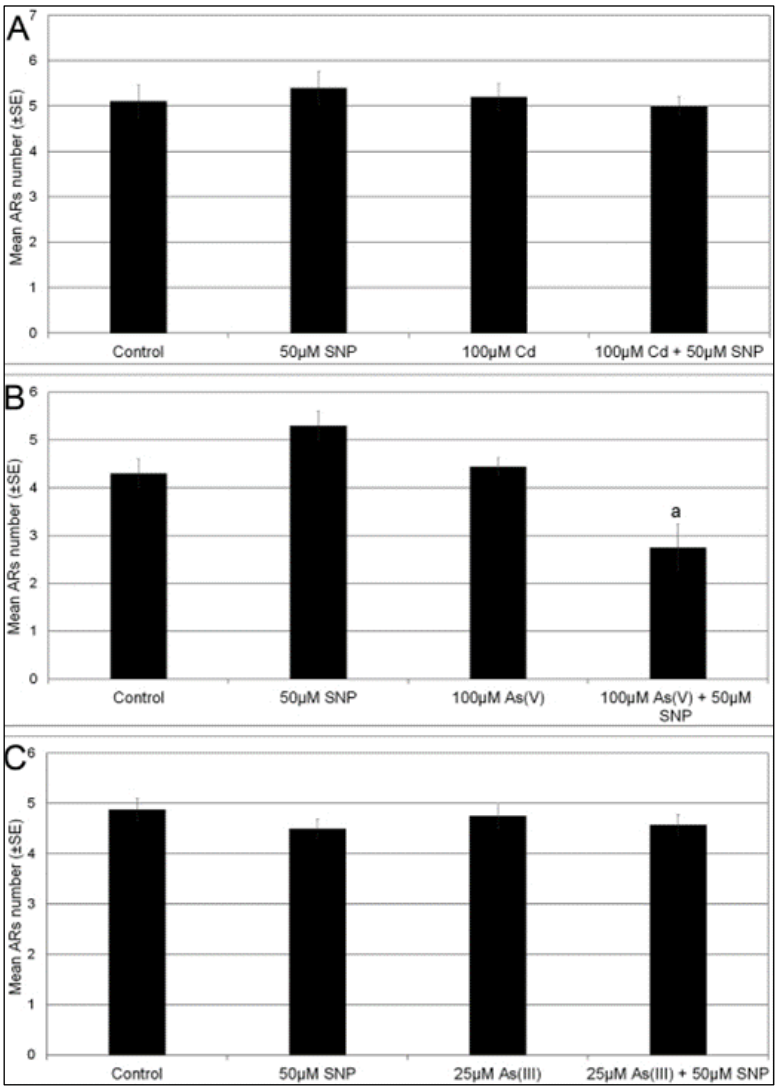

Fig. S3. Mean number of embryonic adventitious roots (ARs; ±SE) in rice seedlings exposed or not for 10 days to 100 µM $CdSO_4$ (100µM Cd) (**A**), 100 µM $Na_2HAsO_4 \cdot 7H_2O$ (100µM As(V)) (**B**) or 25µM $NaAsO_2$ (25µM As(III)) (**C**) alone or combined with 50 µM $Na_2[Fe(CN)_5NO] \cdot 2H_2O$ (50µM SNP). Letter show statistical differences, at least at $P<0.05$ level, within the same treatment with/ without SNP. N =30.

2.2. (B) Size and Chemical Fractionation of PM Released by Outdoor and Indoor Emission Sources

Epidemiological studies have shown a significant correlation between PM exposure and the onset of cardiopulmonary diseases and have indicated fine ($PM_{2.5}$; particles with aerodynamic diameter (Dp) ≤ 2.5 μm) and even further ultrafine PM ($PM_{0.1}$; nanoparticles; Dp ≤ 100 nm) as major contributors of respiratory illness and mortality. In fact, $PM_{2.5}$ as well as $PM_{0.1}$, generally released by combustion processes, can penetrate deeper into the airways of the respiratory tract, reaching the alveoli and thus causing an inflammatory response. Moreover, the small size of the nanoparticles (NPs) allows them to persist for longer times, to easily contaminate indoor environments and/or to be transported over long ranges. On the other hand, coarse particles (2.5 ≤ Dp ≤ 10 μm), mainly resulting from mechanical processes, in spite of having a shorter residence time in the atmosphere, also present health risks in the respiratory tract and can cause asthma. Therefore, size distribution of atmospheric PM also defines the effects it produces on human health and the environment.

Size variability of atmospheric PM strictly depends on PM sources and the atmospheric processes that particles undergo during their lifetime. Hence, the study of the dimensional distribution of PM chemical components can be of great help in providing valuable information for PM source apportionment and thus for the assessment of health and climate impact. For this reason, we applied a chemical/size fractionation method to 14 sampling campaigns carried out in the Po Valley, in the proximity of Ferrara (Northern Italy), during the winter and summer of seven consecutive years.

PM impact on humans is even greater in indoor environments and in workplaces, because of the longer time spent inside and because air pollution levels can be greater than the environmental background values. For this reason, we analyzed PM_{10} and size-segregated PM samples collected inside private dwellings (located in an industrial area of the Terni basin, Central Italy) and workplaces (an analytical chemistry laboratory, a wastewater treatment plant, a livestock farming activity, a municipal solid waste composting plant and a waste electrical and electronic equipment treatment facility), respectively, to investigate the health impact of particles emitted in different size fractions by specific indoor sources, such as nanoparticles containing insoluble Cu, released by brush electric motors, which are deemed to be able to enter organisms.

2.2.1. (B1) A Combined Chemical/Size Fractionation Approach to Study Winter/Summer Variations, Ageing and Source Strength of Atmospheric Particles

Environmental Pollution (2019), *253*, 19-28

Silvia Canepari [a,*], Maria Luisa Astolfi [a], Maria Catrambone [b], Daniele Frasca [a,b], Melissa Marcoccia [a], Francesca Marcovecchio [b], Lorenzo Massimi [a], Elena Rantica [b], Cinzia Perrino [b]

[a] Department of Chemistry, Sapienza University of Rome, P.le Aldo Moro, 5, Rome, 00185, Italy; [b] C.N.R. Institute of Atmospheric Pollution Research, Via Salaria, Km 29,300, Monterotondo St. (Rome), 00015, Italy.

Abstract: We studied the size distribution of ions (Cl^-, NO_3^-, $SO_4^=$, Na^+, NH_4^+, K^+, Mg^{++}, Ca^{++}) and elements (As, Ba, Cd, Co, Cs, Cu, Fe, Li, Mn, Ni, Pb, Rb, Sb, Se, Sn, Sr, Ti, Tl, V, Zn) during the winter and summer seasons of seven consecutive years (2008 – 2014) in an area of the Po Valley (Northern Italy) characterised by industrial, agricultural and urban settings. The study included the collection and analysis of 41 series of size-segregated samples (MOUDI sampler, 10 stages, cut sizes from 0.18 to 18 ∝m). Ions were analysed by ion chromatography; elemental analysis was carried out by ICP-MS, by applying a chemical fractionation method able to increase the selectivity of PM source tracers. Our results indicate that important winter/summer variations occurred in both the concentration and size distribution of most PM components. These variations were explained in terms of variations in the strength of the prevailing sources of each component. The contribution of biomass burning for domestic heating was highlighted by the well-known tracer K^+ but also by the soluble fraction of Rb, Cs and Li. Biomass burning contribution to atmospheric PM was mostly contained in the fine fraction, with a broad size-distribution from 0.18 to 1.8 ∝m. This source also appreciably increased the concentration of other elements in fine PM (As, Cd, Co, Mn, Pb, Sb, Sn). A few PM components (tracers of sea-spray, brake lining and some industries) did not show marked seasonal variations in concentration and size distribution. However, during winter, for brake lining and

industry tracers we observed an upward shift in the dimension of fine particles and a downward shift in the dimension of coarse particles, due to the ageing of the air masses.

Keywords: Size distribution; MOUDI impactor; elemental composition; source tracers; biomass burning.

1. Introduction

It is well known that the size distribution of atmospheric particles strictly depends on their sources and on the atmospheric processes they undergo during their lifetime. The size distribution of atmospheric particulate matter (PM) also defines the effects it produces on human health and on the ecosystem (EPA, 2004). Consequently, the study of the size distribution of the chemical components of PM can be of great help in providing valuable information for the source apportionment, the study of particle ageing processes and the identification of health and climate effects (Canepari et al., 2008; Cassee et al., 2013; Liu et al., 2015; Gao et al., 2016; Bernardoni et al., 2017).

In the case of elements, their chemical fractionation constitutes a further, precious source of information for evaluating the strength of PM sources. The independent measurement of elemental fractions characterised by different solubility, in fact, ensures a better accuracy in the use of tracers for the identification of PM sources (Canepari et al., 2009, 2014; Wang et al., 2015; Arhami et al., 2017).

Even more powerful is the combination of chemical and size fractionation. Previous scientific works (Canepari et al., 2008, 2010; Wang et al., 2016; Barbaro et al., 2019) showed the potential of this approach, particularly suitable for geographical areas characterized by frequent and long-lasting atmospheric stabilities, where co-variation of pollutants is frequently observed. This combination of chemical and size fractionation is also of great help in tricky situations where it is necessary to identify and evaluate the impact of different emission sources that share many chemical PM components.

Many literature studies concern the size distribution of PM (Salma et al., 2005; Maudlin et al., 2015; Nirmalkar et al., 2016; Castro et al., 2018; Ma et al., 2019) and the seasonal variations of PM_{10} and/or $PM_{2.5}$ concentration (Perrino et al., 2014; Hwang et al., 2018). However, very few papers examine the seasonal variations in concentration and composition of size-segregated PM samples (Chrysikou and Samara, 2009; Taiwo et al., 2014; Zhang et al., 2018).

In this work we applied the chemical/size fractionation method to 14 sampling campaigns carried out in the Po Valley during winter and summer of seven consecutive years (2008 – 2014). PM collection

was carried out by using 10-stage MOUDI impactors. Size-segregated samples were analysed for PM mass, ions, extracted and residual fractions of elements.

The Po Valley is a geographical area sited in Northern Italy, characterised by a relevant impact due to urban areas, industrial facilities, agricultural activity and breeding farms. This area may be regarded as a challenging open-air laboratory, due to frequent, long-lasting and intense atmospheric stability periods that cause fast worsening of air quality, formation of secondary species and relevant ageing of the air masses (Marcazzan et al., 2002; Pernigotti et al., 2012; Bigi and Ghermandi, 2014; Perrino et al., 2014, 2016). This area is thus an ideal training ground to check the performance of the chemical/dimensional fractionation approach.

2. Experimental

Sampling was carried out in the vicinity of Ferrara, a city of about 130.000 inhabitants located in the eastern Po Valley, in Northern Italy. In the study area there are several PM sources: a highway, running at about 0.4 Km from the main sampling site, a major industrial site including a power plant, a urban incinerator and many small and medium size enterprises, located at about 2.5 Km, the city, at about 5 Km.

The study was carried out in one, two or three sites, according to the period. The main site, where all the 14 sampling campaigns were carried out, was a residential area located in the hamlet of Cassana (site C; Google co-ordinates: 44°50'54.95"N, 11°33'40.36"E). A site located inside the industrial area was added during the period 2011 – 2014 (site A; Google co-ordinates: 44°51'26.26"N, 11°33'36.90"E). A rural site, located as far as feasible from the main emission sources, was added during the period 2011 – 2012 (site B; Google co-ordinates: 44°49'31.53"N, 11°32'55.01"E). The location of three sampling sites in the study area is shown in Supplementary Material S1. Concentration and chemical composition of PM_{10} and $PM_{2.5}$, elemental solubility and strength of the main PM sources at the three sampling sites were widely described in previous papers (Canepari et al., 2014; Farao et al., 2014; Perrino et al., 2014). As shown in these papers, the three sites, which are a few kilometers away from each other, can be considered as equivalent in terms of PM concentration and composition. This spatial homogeneity of the air masses is a peculiar feature of the Po Valley, due to the frequent very low mixing of the atmosphere. An interesting consequence of this feature is that the results obtained in individual monitoring sites may be considered as representative of a wide area.

The study was carried out during the winter (January-February) and the summer (June) of each year from 2008 to 2014, for a total of 14 periods. Each sampling campaign lasted for 3 or 4 weeks and was carried out simultaneously in one, two or three of the above sites. The inclusion of the additional sites strengthened the reliability of the dataset. The duration of each sampling was 2 or 3 weeks. In some cases, two sequential samplings per period were carried out. A total of 41 series of samples were collected during the whole study. Details about the sampling periods and sites are reported in Table 1.

Size-segregated sampling was carried out by using three Micro-Orifice Uniform-Deposit Impactors (MOUDI mod. 110-R and 120-R, MSP Co., U.S.A.) operating at the flow rate of 30 L min^{-1} and having ten collection stages (cut-sizes of 0.18, 0.32, 0.56, 1.0, 1.8, 3.2, 5.6, 10 and 18 μm in aerodynamic diameter). Sampling flow rate was daily adjusted to keep its variations within 5%. The impactors were equipped with Teflon membrane filters (TEFLO, 47 mm, 2.0 micron pore size, PALL Life Sciences). The performance of the three impactors had been previously compared during a preliminary campaign, in which they were run simultaneously for 3 weeks and analysed for ions. The sampling was carried out during the autumn of 2007 in a periurban site close to Rome. The relative standard deviation of the three replicates for each stage, which includes also the uncertainty of the analytical procedure, was always lower than 25%. The results are reported in Supplementary Material S2.

It is worth noting that long-duration samplings carried out by using cascade impactors might undergo sampling artefacts. Among these, loss by evaporation of ammonium nitrate and chloride may lead to depletion of these ions. However, to our knowledge, there are no solid and recognized methods to correct the data for this artefact. Furthermore, particle bouncing-off phenomena may be responsible for a modification of the original size distribution of atmospheric particles (EPA, 2004). However, Teflon filters are generally considered as a suitable sampling material from this point of view, able to minimize the bouncing-off (Giorio et al., 2013). Moreover, none of these phenomena change the chemical composition of the individual particles and the co-variation of source tracers is nevertheless maintained.

Mass concentration on the MOUDI stages was determined gravimetrically by using an automated microbalance (1 ∝g sensitivity, mod. ME5, Sartorius AG, Goettingen, Germany): Filters were equilibrated for two days at 20°C and 50% RH before and after the sampling..

Table 1. Schedule and location of the samplings carried out during the study.

Year	Season	Monitoring Period	Site	Number and Duration of Samplings	Total Number of Samples
2008	Winter	15/01 – 12/02	C	2 X 2 Weeks	2
2008	Summer	29/05 – 12/06	C	1 X 2 Weeks	1
2009	Winter	08/01 – 05/02	C	2 X 2 Weeks	2
2009	Summer	27/05 – 10/06	C	1 X 2 Weeks	1
2010	Winter	12/01 – 09/02	C	2 X 2 Weeks	2
2010	Summer	02/06 – 16/06	C	1 X 2 Weeks	1
2011	Winter	11/01 – 07/02	A, B, C	2 X 2 Weeks	6
2011	Summer	31/05 – 28/06	A, B, C	2 X 2 Weeks	6
2012	Winter	12/01 – 09/02	A, B, C	2 X 2 Weeks	6
2012	Summer	30/05 – 27/05	A, B, C	2 X 2 Weeks	6
2013	Winter	10/01 – 31/01	A, C	1 X 3 Weeks	2
2013	Summer	30/05 – 20/06	A, C	1 X 3 Weeks	2
2014	Winter	09/01 – 30/01	A, C	1 X 3 Weeks	2
2014	Summer	05/06 – 26/06	A, C	1 X 3 Weeks	2

For the analysis of ions and element on the same Teflon filter, the extraction was carried out in deionized water and the solution was first analyzed for ions (Cl^-, NO_3^-, $SO_4^=$, Na^+, NH_4^+, K^+, Mg^{++}, Ca^{++}) by ion chromatography (ICS1000, Dionex Co., CA, U.S.A.); then acetate buffer (CH_3COOH/CH_3COOK 0.01M; ph4.3) was added and the solution was filtered and analyzed for the extracted fraction of elements (As, Ba, Cd, Co, Cs, Cu, Fe, Li, Mn, Ni, Pb, Rb, Sb, Se, Sn, Sr, Ti, Tl, V, Zn) by inductively coupled plasma mass spectroscopy (ICP-MS, Bruker 820MS). Solid residual on both the sampling filter and the filtration filter was subjected to microwave-assisted acid digestion and analyzed by ICP-MS for the same elements (residual fraction). The procedure was previously optimized and fully validated and the relative repeatability for all the considered variables was found to below 10%; more details about the analytical performances are reported in Canepari et al. (2009b). Limits of Detection (LODs) were calculated as mean value of filter blanks (6 replicates) plus three times its standard deviation.

To obtain an easy comparison among the results and to reduce the effect of the variability in the environmental concentrations occurring during different sampling periods, the analytical results were treated as follows. For each PM component and for each MOUDI sample, the results obtained from the analysis of the ten stages were added up and each individual result was expressed as a per cent with respect to the sum. The per cent values obtained for each stage in all winter or summer samples were averaged to obtain a winter/summer mean percentage (and standard deviation). These mean per cent values (winter/summer average per cent distribution) were recalculated considering as reference value the highest one between the two sum values obtained for winter and for summer. This latter choice was aimed at visualizing the seasonal differences in each graph.

3. Results and Discussion

In general, the mass concentration and chemical composition of atmospheric PM in the area of the Po Valley are spatially homogeneous, particularly during the winter season (Marcazzan et al., 2002; Canepari et al., 2014; Perrino et al., 2014). This characteristic was confirmed during the years 2011-2012 of our study, when the samplings were simultaneously carried out at sites A, B and C. As an example, in Fig. 1 we report the size-segregated mass concentration measured at the three sites during the winter (upper panel) and the summer (lower panel) of 2012. The distance between the two furthest sites, A and C, is about 3.5 Km. The results obtained at the three sites were very similar, not only in terms of concentration but also as far as the size distribution is concerned. The results obtained from the whole study can be thus considered as representative of a wider area.

The data reported in Fig. 1 also show that there are noteworthy seasonal differences in the concentration and size distribution of PM: during winter, concentration values were much higher (about three times) than summer values and the size distribution showed a clear prevalence of the fine fraction, with maximum concentrations in the size range 1.0 – 1.8 ∝m. During summer, instead, the size distribution showed a bi-modal pattern, with a first maximum in the coarse fraction (size range 3.2 – 5.6 ∝m) and a second maximum in the fine fraction (0.32 – 0.56 ∝m).

These results are in agreement with the winter increase in the concentration of fine particles due to both the formation of secondary species in conditions of strong and long-lasting atmospheric stability (Marcazzan et al., 2002; Bigi and Ghermandi, 2014) and the switch-on of domestic heating, especially by biomass burning. Both mechanisms are responsible for the production of particles in the fine dimensional range. During the summer period, instead, the more efficient atmospheric mixing and

the absence of domestic heating causes a decrease in the concentration of fine particles, while the aridity favours the re-suspension of soil particles, increasing the concentration of the coarse fraction of PM (Kulshrestha et al., 2009). It is worth noting that the summer concentration of PM in the coarse fraction widely exceeded the winter values.

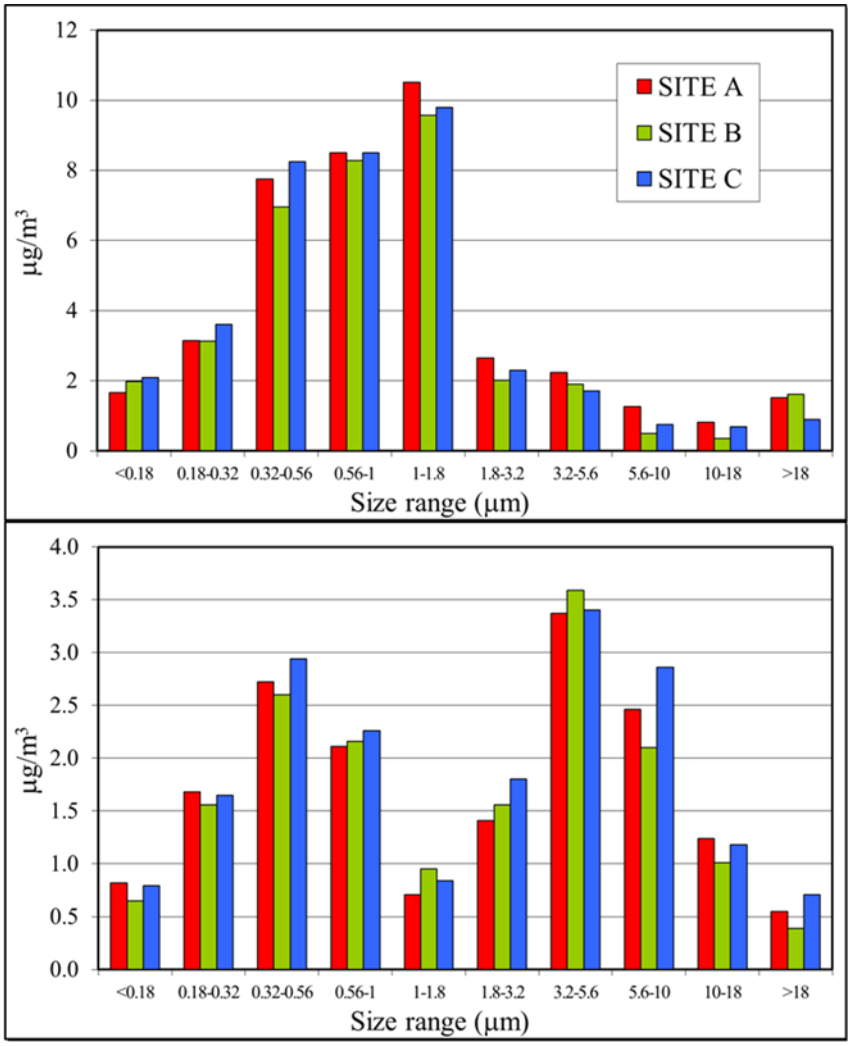

Fig. 1. Size distribution of PM at the three sampling sites during the winter (upper panel) and the summer (lower panel) of 2012.

The concentration of the considered PM components (ions, elements expressed as sum of the extracted and residual fractions) during all the sampling periods of the winter and summer campaigns are reported in Table 2 as mean and standard deviation of the sum of the ten MOUDI stages.

Table 2. Detection Limit (LOD) on individual stages and total concentration (sum of the 10 stages) during the two seasons: mean value of all the results and standard deviation. Units are $\propto g/m^3$, for ions and ng/m^3 for elements.

	Analytical Technique	LOD	WINTER (N=22)		SUMMER (N=19)	
			MEAN	ST. DEV.	MEAN	ST.DEV.
Cl^-	IC	0.0001	0.39	0.05	0.11	0.01
NO_3^-	IC	0.0003	9.1	0.6	1.1	0.1
$SO_4^=$	IC	0.0005	3.1	0.1	2.0	0.1
Na^+	IC	0.0002	0.32	0.03	0.25	0.02
NH_4^+	IC	0.0002	2.7	0.2	0.70	0.03
K^+	IC	0.0003	0.32	0.02	0.094	0.005
Mg^{++}	IC	0.0003	0.049	0.003	0.053	0.003
Ca^{++}	IC	0.0008	0.52	0.03	0.38	0.02
As	ICP-MS	0.003	0.78	0.04	0.59	0.02
Ba	ICP-MS	0.005	3.5	0.2	3.2	0.1
Cd	ICP-MS	0.01	0.33	0.02	0.10	0.01
Co	ICP-MS	0.0005	0.11	0.01	0.080	0.009
Cs	ICP-MS	0.00005	0.037	0.003	0.026	0.002
Cu	ICP-MS	0.01	8.7	0.6	6.5	0.3
Fe	ICP-MS	0.3	170	8	159	10
Li	ICP-MS	0.0005	0.14	0.01	0.24	0.01
Mn	ICP-MS	0.015	7.9	0.4	6.3	0.3
Ni	ICP-MS	0.005	2.5	0.2	3.0	0.5
Pb	ICP-MS	0.005	8.6	0.4	2.7	0.1
Rb	ICP-MS	0.005	1.4	0.1	1.6	0.1
Sb	ICP-MS	0.001	1.5	0.1	0.83	0.04
Se	ICP-MS	0.001	0.98	0.10	1.0	0.1
Sn	ICP-MS	0.001	2.1	0.1	1.0	0.1
Sr	ICP-MS	0.03	1.4	0.1	1.4	0.1
Ti	ICP-MS	0.005	1.8	0.1	3.5	0.2
Tl	ICP-MS	0.00005	0.028	0.002	0.024	0.001
V	ICP-MS	0.01	1.2	0.1	1.8	0.1
Zn	ICP-MS	0.5	57	4	39	4

The reported LODs refer to a sampling volume of 600 m^3 (2 weeks). In the case of elements, they were obtained as sum of the extracted and residual fractions.

An overview of the data shows that for some PM components the winter and summer concentrations were very different. Among ions, nitrate concentration exhibited a very high winter to summer ratio (W/S > 8) as during winter it was mainly in the form of ammonium nitrate, a secondary species deeply affected by the frequent conditions of strong atmospheric stability occurring in the area during the cold season. In the Po valley, ammonium nitrate may constitute up to 30% of the PM mass, often constituting the most abundant individual PM component. In other geographical areas, instead, secondary inorganic species are dominated by ammonium sulphate (Ma et al., 2019).

Significant seasonal differences (W/S > 3) were also shown by K^+, which is affected by biomass burning emission. For sulphate ion, the seasonal difference were smaller (W/S = 1.6), as during winter this species is affected by the influence of atmospheric stability and by the transport from Eastern Europe (Squizzato et al., 2012; Canepari et al., 2014), while the contribution due to photochemical formation of ammonium sulphate prevails during summer. Winter concentration of chloride exceeded summer values (W/S > 3) due to the contribution of ammonium chloride, which during winter adds to the contribution due to sea-salt. PM release from sea did not show clear seasonal differences in this area, as demonstrated also by Na^+ and Mg^{++} values. For Ca^{++}, mainly contained in soil dust, winter concentration was generally lower than summer values (W/S = 0.7).

Among elements, considerable differences between winter and summer were recorded for Cd, Pb (W/S > 3) and, at a less extent, Sb and Sn (W/S > 2). For those elements, winter increase could be due to the switch on of a typical seasonal source (domestic heating). W/S values below one were recorded for Li and Ti (W/S ≈ 0.5), elements that are typically contained in soil dust, more efficiently re-suspended during the warm, dry months.

Table 3 reports the solubility percentage of the elements, expressed as mean and standard deviation and referred to the sum of the ten MOUDI stages. In general, each element showed a typical solubility value. For example, Fe and Ti were found almost exclusively as insoluble species, while Cd, Rb, Tl and V were mostly in the extracted fraction. The other elements were distributed between the two solubility fractions. It is interesting to note that in some cases (e.g.: Cs and Li) there were significant seasonal variations in the solubility percentage, pointing at significant seasonal changes in the strength of the main sources of these elements.

The size distribution of the eight considered ions during the winter and the summer periods are reported in Fig. 2 as seasonal mean and standard deviation. All the values were normalized as explained in the Experimental Section.

Table 3. Solubility percentage of the elements during the two seasons: mean value and standard deviation of all the results.

	WINTER (N=22)		**SUMMER (N=19)**	
	MEAN	**ST.DEV.**	**MEAN**	**ST.DEV.**
As	77	6	62	15
Ba	51	9	33	11
Cd	81	4	77	11
Co	35	9	36	15
Cs	72	8	33	15
Cu	47	10	33	8
Fe	12	3	9	3
Li	63	12	23	13
Mn	58	9	53	9
Ni	31	9	30	13
Pb	35	6	43	8
Rb	93	2	77	12
Sb	62	8	52	5
Se	74	21	52	14
Sn	23	7	21	5
Sr	55	7	66	10
Ti	6	2	3	2
Tl	89	5	91	11
V	70	12	72	12
Zn	55	17	50	12

The size distributions of Na^{+} and Mg^{++} were very similar and unimodal, with maximum values in the range 3.2 – 5.6 ∝m, during both winter and summer. The prevalence of the coarse fraction is in agreement with the main source of these ions, from the sea.

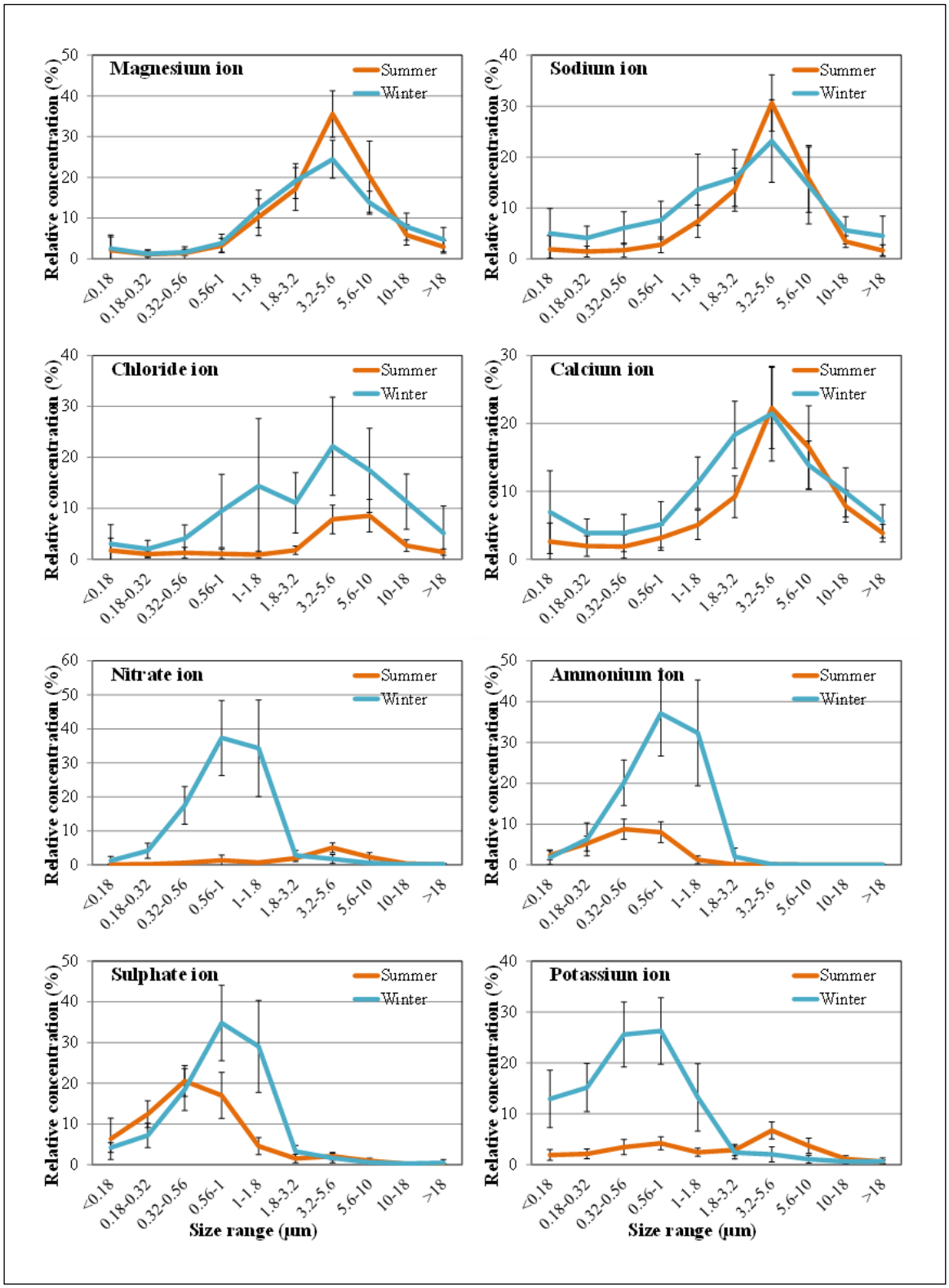

Fig. 2. Size distribution of ions during summer (orange line) and winter (blue line); mean values and standard deviation of all the values recorded during the study.

During winter, the same distribution in the coarse fraction was found for chloride; this ion, however, showed a bimodal distribution with a second maximum in the range 1-1.8 ∝m, due to ammonium chloride. During summer, instead, the concentration of coarse chloride was lower, probably as a result of the reaction between acidic species (mainly HNO_3) and NaCl, which produces sodium salts (mainly $NaNO_3$) and releases gas-phase HCl (EPA, 2004; Braun et al., 2017). As during the warm months the concentration of ammonium chloride is generally negligible, the summer distribution of chloride was unimodal.

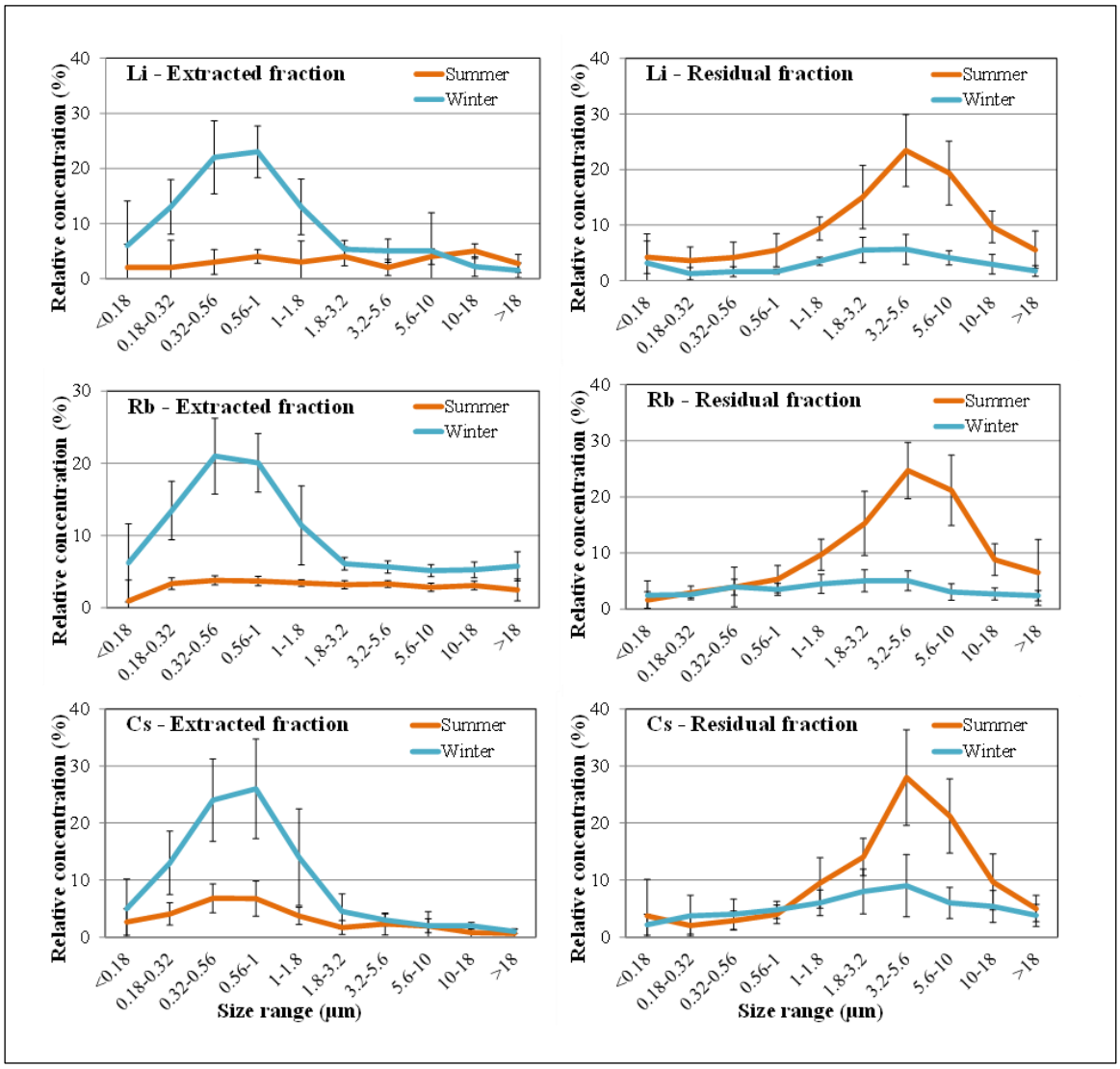

Fig. 3. Size distribution of the extracted and residual fractions of Rb, Li and Cs; mean values and standard deviation of all the values recorded during the study.

A unimodal distribution almost completely confined in the coarse fraction, with maximum in the range 3.2 – 5.6 ∝m, was found for Ca^{++}, in agreement with the main source of this ion, originating from soil dust.

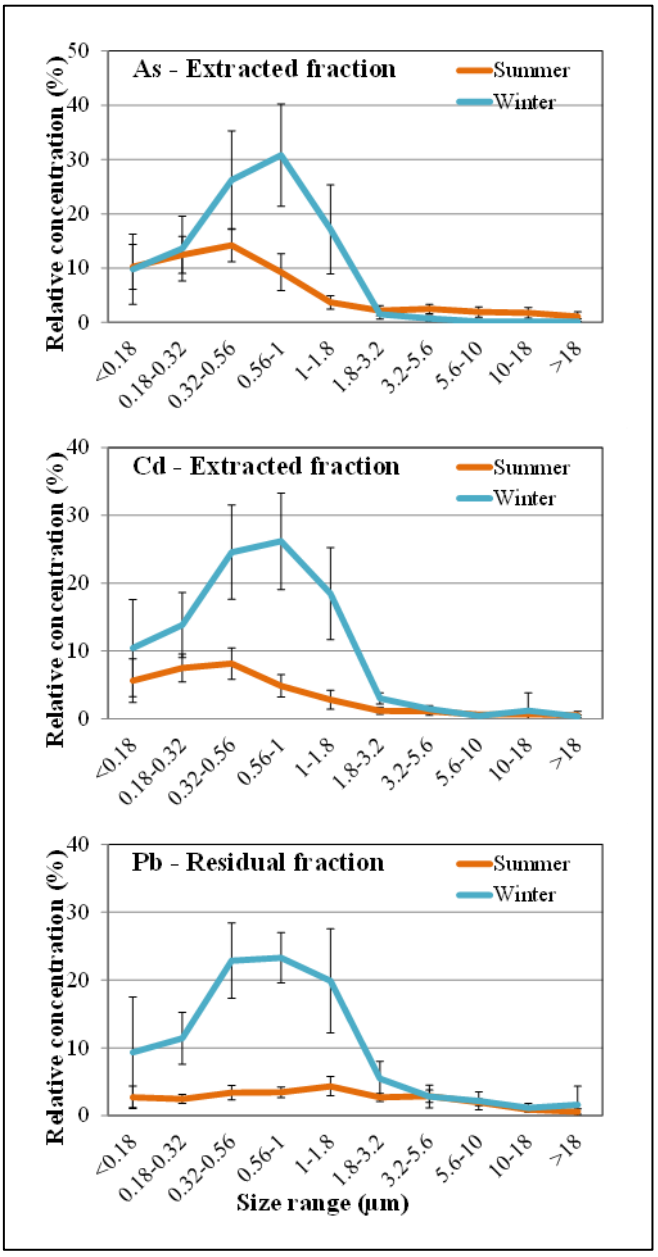

Fig. 4. Size distribution of As_{ext}, Cd_{ext}, Pb_{res}; mean values and standard deviation of all the values recorded during the study.

During winter, ammonium, nitrate and sulphate ions showed overlapping size distributions, almost exclusively in the fine fraction (maxima in the range 0.56 – 1.0 ∝m), in agreement with the secondary formation of ammonium nitrate and ammonium sulphate. During the summer period, instead, the concentration of ammonium nitrate severely decreased, as observed in the case of ammonium chloride, and the size distribution of nitrate became bimodal, with a prevailing contribution in the coarse fraction and maximum in the range 3.2 – 5.6 ∝m. This latter contribution was probably due to soil dust and to the products of the above cited reaction between HNO_3 and NaCl. NH_4^+ and $SO_4^=$ showed the same size distribution also during summer, in agreement with the photochemical formation of ammonium sulphate. It is worth noting that during summer the peak in the size distribution of sulphate was in the range 0.32 – 0.56 ∝m, while it was in the range 0.56 – 1.0 ∝m during winter. This constitutes a first indication of the effect due to the ageing of the air masses, which is of longer duration during the cold months.

In the case of K^+, remarkable winter-summer differences were observed, due to the prevalence of different sources: during summer this species is mainly released from the soil and showed a maximum in the coarse range 3.2 – 5.6 ∝m, as in the case of Ca^{++}; during winter, instead, the release from biomass burning largely prevails and the size distribution of K^+ was almost completely in the fine fraction, with a broad maximum in the size range 0.32 – 1.0 ∝m. A similar size distribution was attributed to a relevant contribution of wood burning also in other studies (Ma et al., 2019).

Fig. 3 reports the size distribution of the extracted ($_{ext}$) and residual ($_{res}$) fractions of Rb, Li e Cs. All three elements showed noticeable differences in the size distribution of the two solubility fractions. The soluble fraction populated almost exclusively the fine fraction of PM, while the residual fraction was found mostly in coarse particles. A similar behaviour was observed for the majority of the considered elements. These substantial differences in the size distribution of the two solubility fractions support the ability of the chemical fractionation method to differentiate PM sources (Canepari et al., 2008, 2009, 2014).

The results in Fig. 3 show that the concentration of Rb_{ext}, Li_{ext} and Cs_{ext} was much higher during winter than during summer, while the opposite pattern was observed in the case of Rb_{res}, Li_{res} and Cs_{res}. The overlap of the size distributions and seasonal profiles supports the hypothesis of common sources, at least two, for these three elements. These sources could be identified in biomass burning for domestic heating during the winter period and in re-suspension of soil dust during the summer

period. Biomass burning therefore affects mainly the soluble fraction of Rb, Li and Cs, while soil re-suspension impacts on their residual fraction.

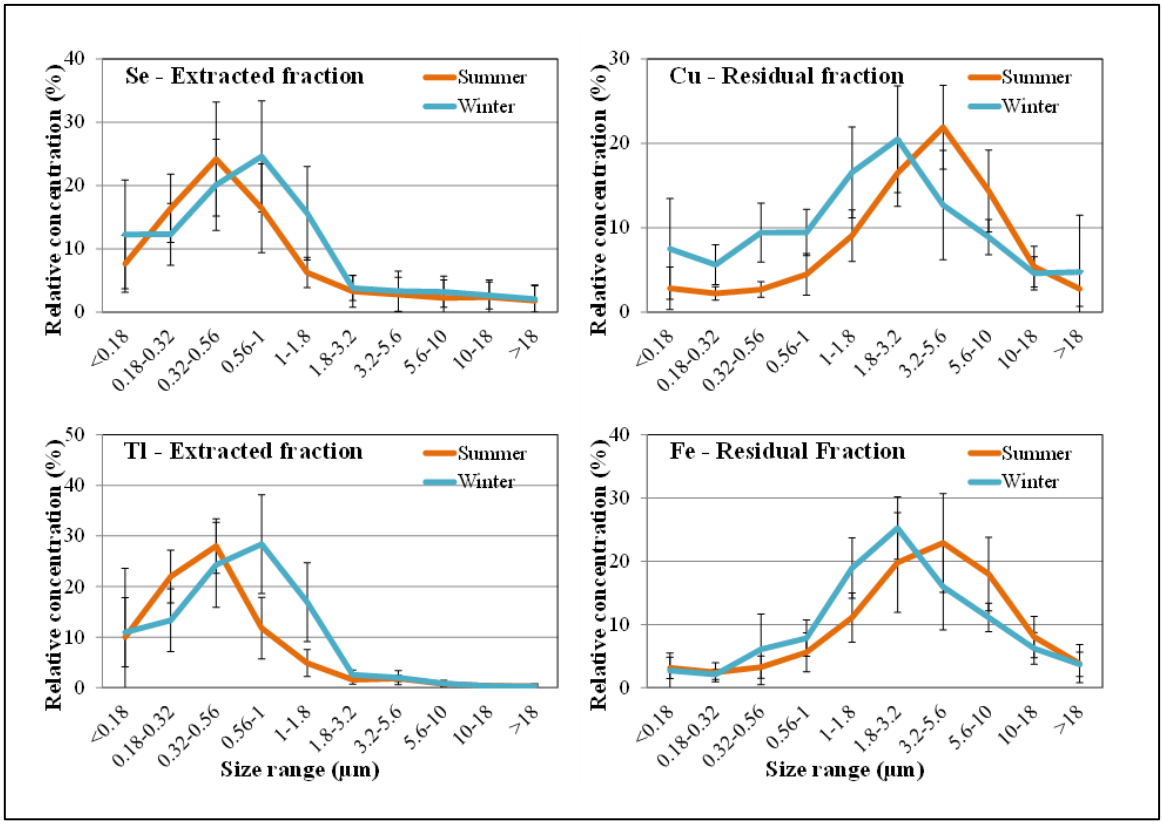

Fig. 5. Size distribution of Se_{ext}, Tl_{ext}, Fe_{res} and Cu_{res}; mean values and standard deviation of all the values recorded during the study.

It is interesting to note that the size distributions of Rb_{ext}, Li_{ext} and Cs_{ext} and their seasonal differences overlapped the results obtained for K^+, further confirming the existence of a common source. It should be noted that in the scientific literature K^+ is widely used as a tracer of biomass burning, while Rb, Li and Cs are not considered as reliable tracers of this source because the measurement of the total concentration, carried out in most studies, does not allow any distinction between the contributions of biomass burning and of soil (Vicente and Alves, 2018; Perrino et al., 2019).

Fig. 4 reports the size distribution of As_{ext}, Cd_{ext}, Pb_{res}, all elements regulated by the European legislation. Also in this case the fine fraction dominated the size distribution and the winter concentration exceeded summer values. Furthermore, their size distribution resembles those of K^+ and of the elements reported in the left column of Fig. 3. This suggests that, during winter, biomass

burning significantly contributed to the air concentration of these elements. The production of particles containing Pb in biomass combustion had been already reported in the literature (Vicente and Alves, 2018; Ma et al., 2019), while for As and Cd this link was less well-known. Also for these elements, adopting a chemical fractionation scheme and using the fraction that is more sensitive to the considered source resulted in a considerable improvement of the selectivity of the element as a tracer.

A similar behavior, although less clear, is shown by some other elements: Co_{ext}, Mn_{ext}, Sb_{ext}, Sn_{res} (Supplementary Material S3) and also in these cases it is reasonable to presume a non-negligible contribution of biomass burning. It is worth noting that most of these elements (Co, Sb, Sn) are generally considered as tracers of industrial sources (Farao et al., 2014; Ma et al., 2019). Nevertheless, the combined chemical/size fractionation approach allowed a reliable identification of the biomass burning contribution even in a heavily industrialized area.

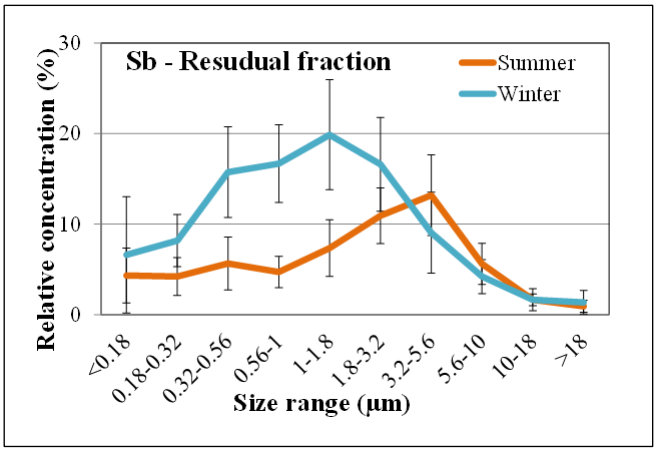

Fig. 6. Size distribution of Se_{res}; mean values and standard deviation of all the values recorded during the study.

Se_{ext}, Tl_{ext}, Fe_{res} and Cu_{res}, instead, showed a size distribution characterised by small seasonal variations (Fig. 5). This indicates that the strength of the PM sources containing these elements was quite constant during the year. These sources may be identified in the industrial plants for Se_{ext} and Tl_{ext}, which were mostly found in the fine fraction of PM, and in the braking systems of vehicles, releasing particles in the coarse range, for Fe_{res} and Cu_{res} (Canepari et al., 2008; 2014).

However, we can notice a winter-summer difference in the size distribution of these elemental fractions. Se_{ext} and Tl_{ext}, which were mainly in the fine fraction, show a shift in the size distribution

towards higher values of the aerodynamic diameters during the winter, while in the case of Fe_{res} and Cu_{res}, mainly in the coarse fraction, the winter shift is towards lower values of the aerodynamic diameters. These variations can be explained considering that in winter atmospheric particles remain in the atmosphere for a much longer time than in summer.

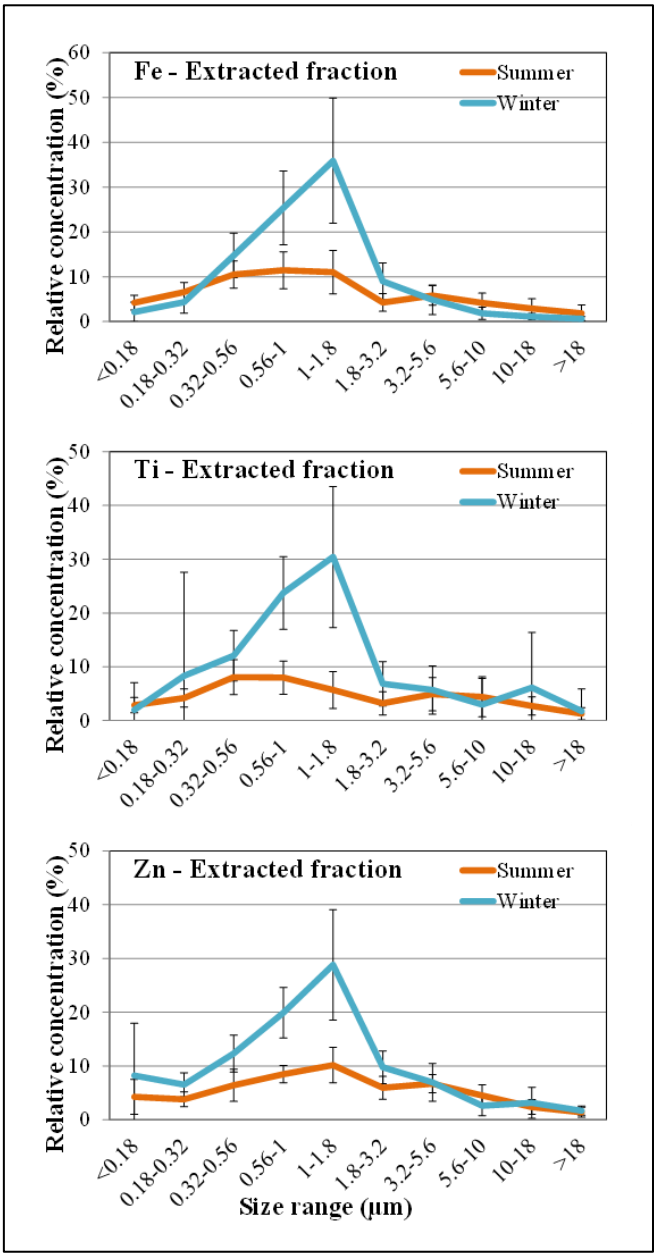

Fig. 7. Size distribution of Fe_{ext}, Ti_{ext} and Zn_{res}; mean values and standard deviation of all the values recorded during the study.

During ageing of the air masses, particles in the accumulation mode tend to increase their dimensions due to condensation/coagulation processes and water uptake, while particles in the coarse mode tend to decrease their dimensions because of the fall-off of the larger particles (EPA, 2004).

Very interesting is the case of Sb, which is often used as a tracer of brake wear, together with Cu and Fe (Grigoratos and Martini, 2015). Previous studies carried out by applying the same chemical fractionation procedure used in this work, showed that the residual fraction is the solubility fraction that is most sensitive to this source (Canepari et al., 2008). During the warm period the size distribution of Sb_{res}, reported in Fig. 6, overlapped the pattern of Cu_{res} and Fe_{res} (Fig. 5), confirming the existence of a main common source. During winter, instead, the size distribution profile of Sb_{res} differed from Cu_{res} and Fe_{res}, suggesting the existence of two superimposed patterns due to different sources: one ascribable to brake wear, which contributed to the size fractions larger than 1.0 -1.8 ∝m, the other one responsible for a sharp increase in the size fractions below 1.8 ∝m and probably nameable as biomass burning.

The extracted fractions of Fe, Ti and Zn, shown in Fig. 7, exhibited a still different behaviour. While the residual fractions of these elements, which were quantitatively prevailing, were distributed mainly the coarse fraction, Fe_{ext},, Ti_{ext}, and Zn_{ext} were almost completely found in the fine fraction of PM and shared the same winter distribution, with maxima in the size range 1.0-1.8 ∝m. Even if the contribution of the source of these elements increased during winter, the size distribution was different from that described for biomass burning. We may think that these tracers were released from an industrial source that released fine particles and that was very far from the receptor. Therefore, in winter the particles produced by this source were long-range transported and, because of the atmospheric stability typical of the studied area, underwent ageing and dimensional increase. During the warm period PM was more easily diluted by convective mixing of the atmosphere and these particles might have not reached, or reached at a less extent, the receptor site.

4. Conclusions

The study of a high number (41) of size-segregated samples collected during 7 years in a complex area such as the Po Valley allowed an in-depth study of the size distribution of ions and elements in atmospheric PM during the winter and the summer seasons.

The results of this study confirmed the typical size distribution of ions (mainly coarse for Na+, Cl^-, Mg^{++} and Ca^{++}, mainly fine for NO_3^-, $SO_4^=$, NH_4^+ and K^+) and the very high concentrations of ammonium nitrate during the winter season.

The combination of the size fractionation with the elemental fractionation allowed us to draw interesting information about the reliability of some elements as source tracers. We identified the extracted fraction of Rb, Cs and Li as good and selective tracers of biomass burning, and observed that some other elements show a partial contribution from the same source (As_{ext}, Cd, Pb_{res}, Sb_{res}, Mn, Co_{ext}, Sn). This group includes some toxic elements, highlighting, once more, the potential danger to human health due to the emission from biomass burning for domestic heating.

For some elements released in the atmosphere from non-seasonal PM sources (Cu_{res}, Fe_{res}, Se_{ext}, Tl_{ext}) it was possible to observe an increase in the dimensions of fine particles during winter and a decrease in the dimension of coarse particles during summer, both ascribed to air mass ageing.

Acknowledgements

The authors are indebted to S. Dalla Torre, T. Sargolini and S. Pareti for technical assistance during the sampling and the analytical phases of this work.

References

Arhami, M., Hosseini, V., Shahne, M. Z., Bigdeli, M., Lai, A., Schauer, J. J. 2017. Seasonal trends, chemical speciation and source apportionment of fine PM in Tehran. Atmospheric Environment, 153, 70-82.

Barbaro, E., Feltracco, M., Cesari, D., Padoan, S., Zangrando, R., Contini, D., Barbante, C., Gambaro, A. 2019. Characterization of the water soluble fraction in ultrafine, fine, and coarse atmospheric aerosol. Science of The Total Environment, 658, 1423-1439.

Bernardoni, V., Elser, M., Valli, G., Valentini, S., Bigi, A., Fermo, P., Piazzalunga, A., Vecchi, R. 2017. Size-segregated aerosol in a hot-spot pollution urban area: Chemical composition and three-way source apportionment. Environmental Pollution, 231, 601-611.

Bigi, A., Ghermandi, G. 2014. Long-term trend and variability of atmospheric PM 10 concentration in the Po Valley. Atmospheric Chemistry and Physics, 1410, 4895-4907.

Braun, R. A., Dadashazar, H., MacDonald, A. B., Aldhaif, A. M., Maudlin, L. C., Crosbie, E., Aghdam, M.A., Mardi, A.H., Sorooshian, A. 2017. Impact of wildfire emissions on chloride and bromide depletion in marine aerosol particles. Environmental science & technology, 5116, 9013-9021.

Canepari, S., Perrino, C., Olivieri, F., Astolfi, M.L. 2008. Characterisation of the traffic sources of PM through size-segregated sampling, sequential leaching and ICP analysis. Atmospheric Environment, 42, 8161-8175.

Canepari, S., Pietrodangelo, A., Perrino, C., Astolfi, M. L., Marzo, M. L. 2009. Enhancement of source traceability of atmospheric PM by elemental chemical fractionation. Atmospheric Environment, 4331, 4754-4765.

Canepari, S., Perrino, C., Astolfi, M. L., Catrambone, M., Perret, D. 2009b. Determination of soluble ions and elements in ambient air suspended particulate matter: inter-technique comparison of XRF, IC and ICP for sample-by-sample quality control. Talanta, 775, 1821-1829.

Canepari, S., Astolfi, M. L., Moretti, S., Curini, R. 2010. Comparison of extracting solutions for elemental fractionation in airborne particulate matter. Talanta, 822, 834-844.

Canepari, S., Astolfi, M. L., Farao, C., Maretto, M., Frasca, D., Marcoccia, M., Perrino, C. 2014. Seasonal variations in the chemical composition of particulate matter: a case study in the Po Valley. Part II: concentration and solubility of micro-and trace-elements. Environmental Science and Pollution Research, 216, 4010-4022.

Cassee, F. R., Héroux, M. E., Gerlofs-Nijland, M. E., Kelly, F. J. 2013. Particulate matter beyond mass: recent health evidence on the role of fractions, chemical constituents and sources of emission. Inhalation Toxicology, 2514, 802-812.

Castro, T., Peralta, O., Salcedo, D., Santos, J., Saavedra, M. I., Espinoza, M. L., Salcido, a., Celada-Murillo, A.T., Carreon-Sierra, S., Alvarez-Ospina, H., Carabali, G., Barrera, V, Madronich, S. 2018. Water-soluble inorganic ions of size-differentiated atmospheric particles from a suburban site of Mexico City. Journal of Atmospheric Chemistry, 752, 155-169.

Chrysikou, L. P., Samara, C. A. 2009. Seasonal variation of the size distribution of urban particulate matter and associated organic pollutants in the ambient air. Atmospheric Environment, 4330, 4557-4569.

EPA. Air Quality Criteria for Particulate Matter Final Report, 2004. U.S. Environmental Protection Agency, Washington, DC, EPA 600/P-99/002aF-bF, 2004.

Farao, C., Canepari, S., Perrino, C., Harrison, R. M. 2014. Sources of PM in an industrial area: comparison between receptor model results and semiempirical calculations of source contributions. Aerosol and Air Quality Research, 146, 1558-1572.

Gao, Y., Lee, S. C., Huang, Y., Chow, J. C., Watson, J. G. 2016. Chemical characterization and source apportionment of size-resolved particles in Hong Kong sub-urban area. Atmospheric Research, 170, 112-122.

Giorio, C., Tapparo, A., Scapellato, M. L., Carrieri, M., Apostoli, P., Bartolucci, G. B. 2013. Field comparison of a personal cascade impactor sampler, an optical particle counter and CEN-EU standard methods for PM10, PM2. 5 and PM1 measurement in urban environment. Journal of Aerosol Science, 65, 111-120.

Grigoratos, T., Martini, G. 2015. Brake wear particle emissions: a review. Environmental Science and Pollution Research, 224, 2491-2504.

Hwang, S. L., Chi, M. C., Guo, S. E., Lin, Y. C., Chou, C. T., Lin, C. M. 2018. Seasonal variation and source apportionment of PM 2.5-bound trace elements at a coastal area in southwestern Taiwan. Environmental Science and Pollution Research, 259, 9101-9113.

Kulshrestha, A., Satsangi, P. G., Masih, J., Taneja, A. 2009. Metal concentration of PM2. 5 and PM10 particles and seasonal variations in urban and rural environment of Agra, India. Science of the Total Environment, 40724, 6196-6204.

Liu, X., Zhai, Y., Zhu, Y., Liu, Y., Chen, H., Li, P., Peng, C., Xu, B:, Li, C., Zeng, G. 2015. Mass concentration and health risk assessment of heavy metals in size-segregated airborne particulate matter in Changsha. Science of the Total Environment, 517, 215-221.

Ma, L., Dadashazar, H., Braun, R. A., MacDonald, A. B., Aghdam, M. A., Maudlin, L. C., Sorooshian, A. 2019. Size-resolved Characteristics of Water-Soluble Particulate Elements in a Coastal Area: Source Identification, Influence of Wildfires, and Diurnal Variability. Atmospheric Environment, 206, 72-84.

Marcazzan, G. M., Valli, G., Vecchi, R. 2002. Factors influencing mass concentration and chemical composition of fine aerosols during a PM high pollution episode. Science of the Total Environment, 2981-3, 65-79.

Maudlin, L. C., Wang, Z., Jonsson, H. H., Sorooshian, A. 2015. Impact of wildfires on size-resolved aerosol composition at a coastal California site. Atmospheric Environment, 119, 59-68.

Nirmalkar, J., Deshmukh, D. K., Deb, M. K., Chandrawanshi, S., & Tiwari, S. 2016. Seasonal size distribution and possible health implications of atmospheric aerosols collected from a rural site of eastern central India. Atmospheric Pollution Research, 72, 278-287.

Pernigotti, D., Georgieva, E., Thunis, P., Bessagnet, B. 2012. Impact of meteorology on air quality modeling over the Po valley in northern Italy. Atmospheric Environment, 51, 303-310.

Perrino, C., Catrambone, M., Dalla Torre, S., Rantica, E., Sargolini, T., Canepari, S. 2014. Seasonal variations in the chemical composition of particulate matter: a case study in the Po Valley. Part I: macro-components and mass closure. Environmental Science and Pollution Research, 216, 3999-4009.

Perrino, C., Catrambone, M., Farao, C., Canepari, S. 2016. Assessing the contribution of water to the mass closure of PM10. Atmospheric Environment, 140, 555-564.

Perrino, C., Tofful, L., Dalla Torre, S., Sargolini, T., Canepari, S. 2019. Biomass burning contribution to PM10 concentration in Rome Italy: Seasonal, daily and two-hourly variations. Chemosphere, 222, 839-848.

Salma I., Ocskay R., Raes N., Maenhaut W. 2005 Fine structure of mass size distributions in an urban environment. Atmospheric Environment, 39,5363–5374.

Squizzato, S., Masiol, M., Innocente, E., Pecorari, E., Rampazzo, G., Pavoni, B. 2012. A procedure to assess local and long-range transport contributions to PM2. 5 and secondary inorganic aerosol. Journal of Aerosol Science, 46, 64-76.

Taiwo, A.M., Beddows, D.C.S., Shi, Z., Harrison, R.M. 2014. Mass and number size distribution of particulate matter components: Comparison of an industrial site and an urban background site. Science of the Total Environment, 475, 29-38.

Vicente, E. D., Alves, C. A. 2018. An overview of particulate emissions from residential biomass combustion. Atmospheric Research, 199, 159-185.

Wang, Q., Ma, Y., Tan, J., Zheng, N., Duan, J., Sun, Y., He, K., Zhang, Y. 2015. Characteristics of size-fractionated atmospheric metals and water-soluble metals in two typical episodes in Beijing. Atmospheric Environment, 119, 294-303.

Wang, J., Zhou, M., Liu, B. S., Wu, J. H., Peng, X., Zhang, Y. F., Han S.Q., Zhu, T. 2016. Characterization and source apportionment of size-segregated atmospheric particulate matter collected at ground level and from the urban canopy in Tianjin. Environmental Pollution, 219, 982-992.

Zhang, J., Tong, L., Huang, Z., Zhang, H., He, M., Dai, X., Zheng, J., Xiao, H. 2018. Seasonal variation and size distributions of water-soluble inorganic ions and carbonaceous aerosols at a coastal site in Ningbo, China. Science of The Total Environment, 639, 793-803.

Supplementary Material S1.

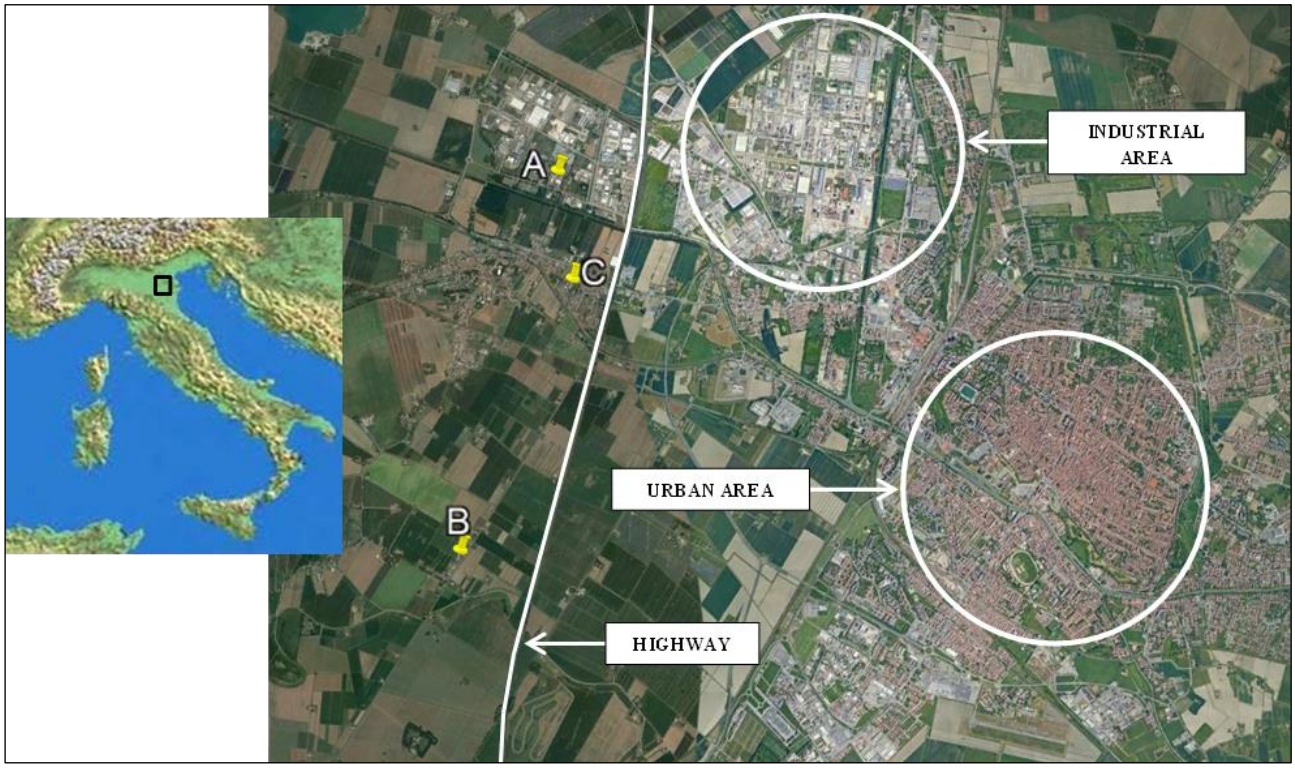

Fig. S1. Area of the study.

Supplementary Material S2.

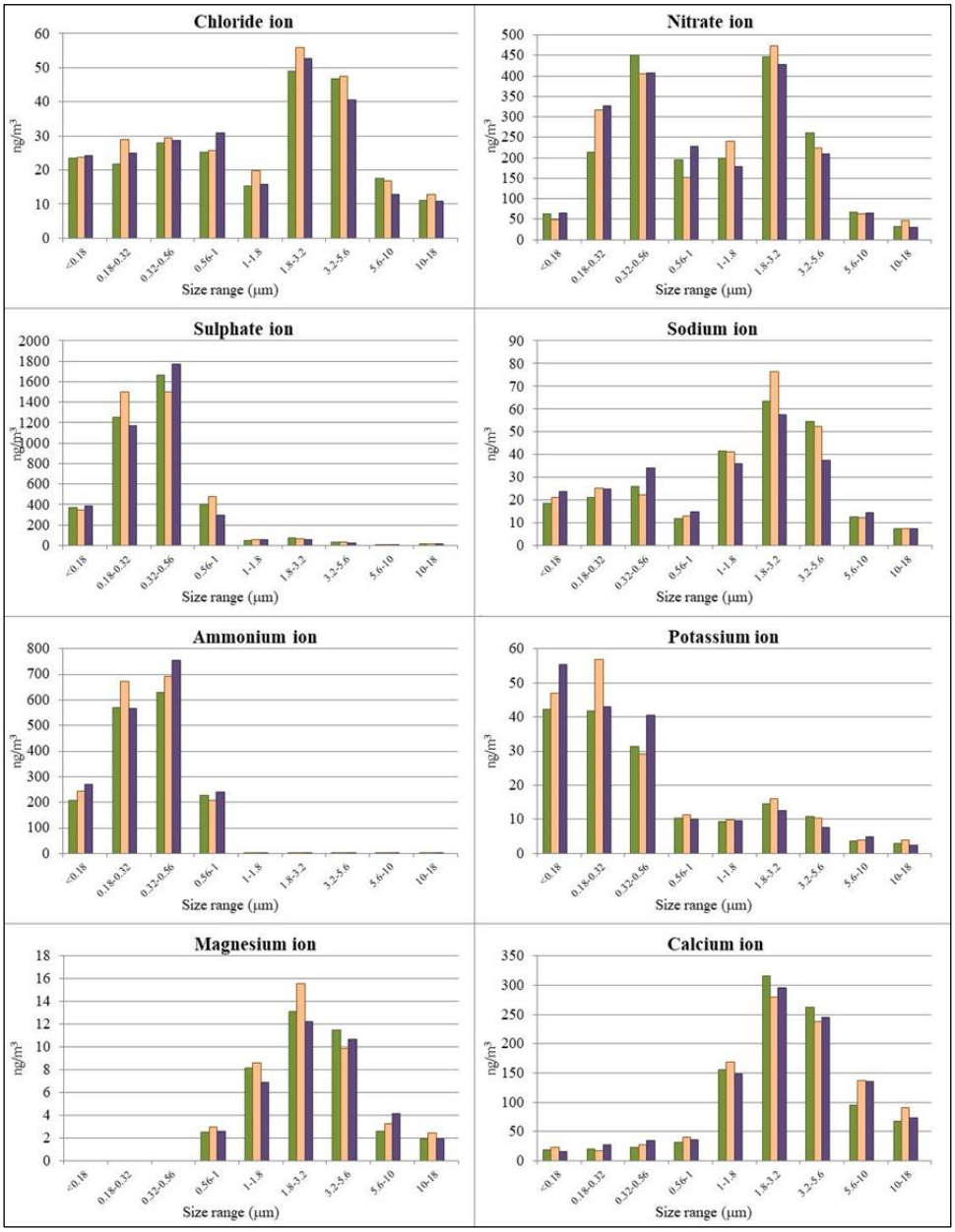

Fig. S2. Size distribution of ions during the preliminary campaign. Sampling was carried out during the autumn 2007 in a peri-urban location close to Rome (Italy) by using 3 MOUDI samplers (two mod. 110-R and one mod. 120-R) identified in the graphs by different bar colors.

Supplementary Material S3.

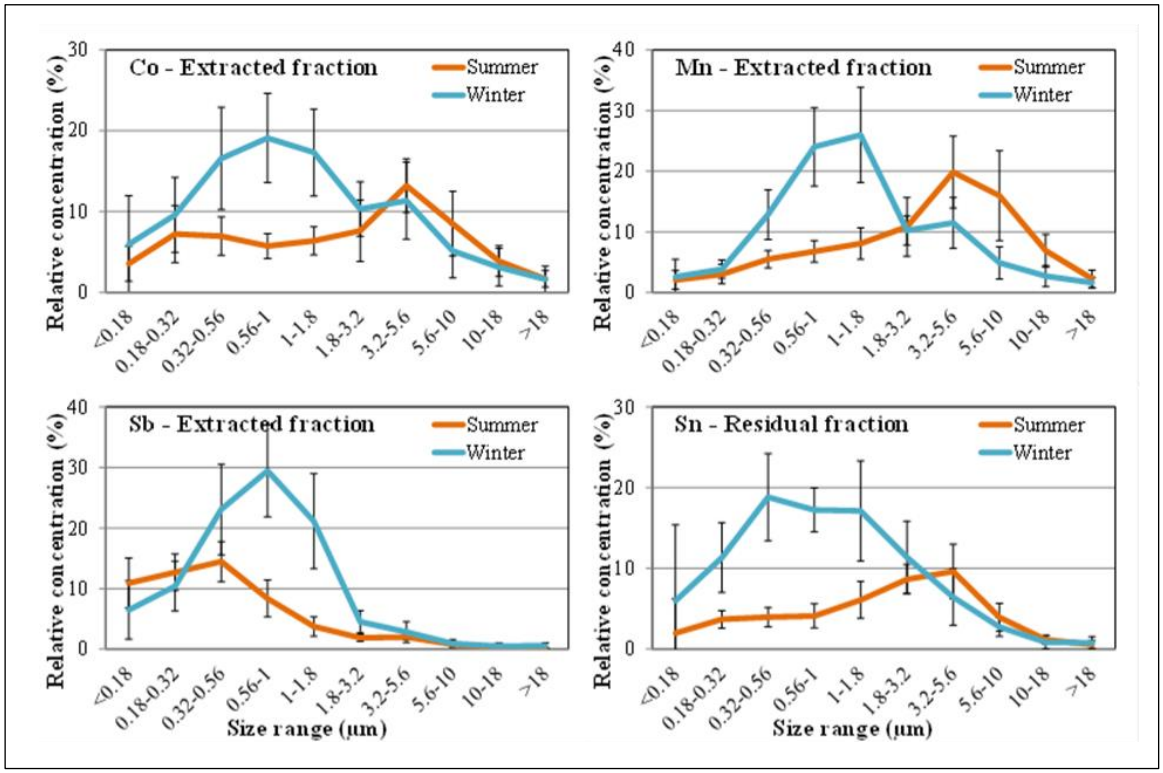

Fig. S3. Size distribution of Co_{ext}, Mn_{ext}, Sb_{ext}, Sn_{res}; mean values and standard deviation of all the values recorded during the study.

2.2.2. (B2) Ultrafine, Fine and Coarse Airborne Particle Mass Concentration in Workplaces

Atmospheric Pollution Research (2019), *10*(5), 1685-1690

Francesca Buiarelli [a], Patrizia Di Filippo [a,b,*], Lorenzo Massimi [a], Donatella Pomata [a,b], Carmela Riccardi [a,b], Giulia Simonetti [a], Elena Sonego [a]

[a] Department of Chemistry, Sapienza University of Rome, P. le Aldo Moro, 5, Rome 00185, Italy;
[b] INAIL Research, Certification and Control Division, DIPIA, Via di Fontana Candida 1, 00040 Monteporzio Catone, Rome, Italy.

Abstract: As epidemiological studies have shown a significant association between exposure to particles and mortality and morbidity, depending on their different deposition efficiency in the pulmonary region, size-segregated particulate matter (PM) samples were collected in workplaces where high PM concentrations were expected and compared with the results from urban and background atmospheres. We investigated the following workplaces: an analytical chemistry laboratory, a wastewater treatment plant, a livestock farming activity, a municipal solid waste composting plant, and a waste electrical and electronic equipment (WEEE) Treatment Facility. The highest PM concentrations were found in the last three sites. Ultrafine PM ($PM_{0.1}$: aerodynamic diameter less than 0.1 µm) mass concentrations also proved to be especially high in the livestock farming activity, in the municipal solid waste composting plant, and in the WEEE treatment facility, ranging between 4.7 and 19.8 µg m^{-3} as mean values, suggesting that this particulate fraction should be monitored and controlled. On the other hand, in both natural and urban environments, ultrafine particles occurred at concentrations 0.1 – 0.3 times the workplace values. It would have been interesting to determine the increase in cancer risk due to ultrafine particles, but cohort studies on $PM_{0.1}$ are lacking. Therefore, effects on the workers were investigated starting from the lifetime average daily $PM_{2.5}$ dose. Even with this limitation, the results show that people working in municipal solid waste composting plant and in a WEEE Treatment Facility are exposed to a not negligible additional lifetime risk on respect citizens.

Keywords: ultrafine particles; fine particles; workplaces; risk assessment.

1. Introduction

Epidemiologic studies have observed airborne particulate matter (PM) causes an inflammatory response deep in the lungs, with associations between PM mass concentration and the adverse human health effects, the latter being the more significant, the smaller the particles are (Valavanidis et al. 2008).

Studies indicate that fine ($PM_{2.5}$; particles with aerodynamic diameter (Dp) ≤2.5 μm), and even more ultrafine PM ($PM_{0.1}$; Dp≤100 nm), ubiquitous in air and mainly resulting from combustion processes, are major contributors of respiratory illness and mortality. They can penetrate deeper into the airways of the respiratory tract and can reach the alveoli, causing an inflammatory response which occurs in the presence of genotoxins (Kumar et al. 2014). With regard specifically to the ultrafine fraction, its direct transfer into the vascular system causes negative cardiovascular effects (Utell et al. 2002).

Coarse particles (2.5≤Dp≤10 μm) are also an important part of the atmospheric aerosol. $PM_{>2.5}$ are mechanically generated particles from agriculture, road traffic, and related sources. Because of their large size, coarse particles have a short residence time in the atmosphere, and when removed from the air, they soil buildings, contaminate water bodies, and may change the chemistry of precipitation. $PM_{>2.5}$ particles also play an important role in cloud formation, acting as condensation nuclei in the precipitation process. Their surfaces may adsorb gaseous pollutants and small particles (Noll et al. 1990). However, the inhalable fraction (PM_{100}, Dp≤10 μm), by involving particulates that can enter the respiratory organ, also presents health risks independent of deposition site in the respiratory tract, and is commonly measured in workplaces because it can cause asthma.

Not only airborne particles are major contributors of adverse effects on the quality of urban air, but the impact on humans, due to indoor- and work-places air quality, is even greater because of longer time periods spent inside and because, in the case of workplaces, levels can be greater than the environmental background values.

Among nonindustrial indoor workplaces, laboratories, where chemical instrumentations are placed together with personal computers and printers, can be characterized by significant concentrations of atmospheric particulate matter (Destaillats et al. 2008). Higher concentrations are however observed in industrial environments, where particles are emitted by different kinds of processes e.g. crushing, grinding, milling, using diesel-powered motors, and welding, etc. (Brouwer et al. 2004).

Although exposure to air particulate pollution is a specific risk factor causing ill health to people without any link to socioeconomic status, occupational health studies have shown that manual workers have higher respiratory diseases than white collar employees.

In wastewater treatment plants (WWTP), aerosol is generated during the different phases of the processes. Strong aerosolization causes the production of liquid droplets or solid particles in surrounding atmosphere, and, due to the outdoor location, PM concentrations depend on transport through the wind, gravitational settling, dilution effects, adsorption on surfaces, and atmospheric mixed layer events (Karra and Katsivela 2007).

In intensive livestock farming activities, concentrated animal feeding operations and the presence of dry fecal waste lead to raised PM levels (Cambra-López et al. 2010; Donham et al. 2007).

By now, composting facilities operate in a closed environment, where organic matter undergoes a controlled breakdown by microbial populations converting organic material into a biologically stable product. Buildings are maintained under a slight negative pressure, and air from the plant is scrubbed, filtered before dispersal to atmosphere. High concentrations of PM inside the plants depend on the process phase being carried out.

In WEEE (waste electrical and electronic equipment) Treatment Facility, manual removal of components, disassembly and trituration processes produce large amounts of dust.

This study has concentrated on both indoor and outdoor size-segregated airborne particles, and the objective was to compare PM mass concentrations observed at a background, an urban, a chemistry laboratory and four industrial sites.

In particular, as the ultrafine fraction ($PM_{0.1}$) has the highest oxidative and mutagenic potential, the paper focuses on $PM_{0.1}$ in the different life and work environments. This fraction is rarely measured, although it is believed to be important for improving assessments of the level of human exposure and a necessary step in determining the health risk from working environments

Since cohort studies on $PM_{0.1}$ are lacking, a brief comparison of potential carcinogenic risk due to fine particle exposure, among the different workers, is presented.

2. Materials and Methods

Two DLPI (Dekati Low Pressure Impactor, Dekati, Kangasala, Finland) consisting of thirteen stages (from 10000 to 30 nm of aerodynamic diameter, Dp) samplers operating at a flow rate of 10 L min^{-1}, were used to trap particles on polytetrafluoroethylene (PTFE) membrane filters, 0.45 μm pore size, 25 mm diameter (Merck Millipore, Merck S.p.a., Vimodrone, Milan, Italy). Total particulate matter

particles were also collected with personal sampling pumps (DeLux, SKC Ltd, Dorset, UK) on PTFE Membrane Disc Filters with PMP (polymethyl-pentene) support ring, 2 µm pore size, 37 mm diameter (Pall Italia Srl, Buccinasco, Milan, Italy), at a flow rate of 4 L min^{-1}. Filters were weighed to within ±0.001 mg, before and after sampling on a microbalance MC5 Sartorius, (Sartorius Lab Holding GmbH, Goettingen, Germany), located in a climate-controlled chamber. All weighings were done in triplicate.

Measurements were conducted between March 2016 and March 2018 for a total of 834 days of sampling.

Particle collection was performed from 30 January to 4 September 2017, in an indoor workplace (named WP1): a chemistry laboratory, equipped with three analytical instrumentations, personal computers and printers, in a building downtown Rome. The lab was provided with two windows and one door usually closed.

Table 1. Sampling sites description, abbreviations, number of samplings, duration of each sampling.

		N° Samplings	**Days/Sampling**
Urban atmosphere (outdoor)	OP1	28	14
Background site (outdoor)	OP2	4	14
Analytical chemistry laboratory (indoor)	WP1	7	14
Wastewater treatment plant (outdoor)	WP2	9	14
livestock farming activities (outdoor)	WP3	20	7
municipal solid waste composting plant (indoor)	WP4	18	1
WEEE Treatment Facility (indoor)	WP5	4	<1

One of the samplers for the outdoor urban atmosphere (named OP1) was located 300 m outside the lab, from March 2016 to November 2017. The background site (named OP2) was a semi-rural outdoor station about 25 km from the center of Rome. The samplings were performed in December, February, June and September, in parallel with the ones in OP1.

WP2 was an outdoor workplace: a wastewater treatment plant, where the biological treatment process in oxidation pond efficiently removes bacteria, biodegradable organics, phosphorous and nitrogen, after suspended solid filtration and sedimentation of water. Samplings were carried out from March 2016 to March 2017.

WP3 was a sampling site, about 35 km from the center of Rome, where open barns house dairy and slaughter cows and beef calves. Airborne PM was sampled from October 2017 to March 2018, in two different sites within the farm, some of them in parallel, nearby a shed used as stables and next to a shed for the grinding, mixing, and storing of feeds.

WP4 was a municipal solid waste composting plant, an indoor workplace, where a natural biological process biodegrades organic waste such as food waste, paper, manure, and crop residues and converts waste into valuable soil amendments. In WP4 high concentrations of PM are due to the grinding and mixing of the lignocellulose fraction with decomposable organic fraction and the maturing in biocells. Samplings were performed in February and March 2018.

A particularly polluted indoor workplace (named WP5) was a WEEE Treatment Facility, 95 km from the center of Rome. It was an open space with two doors open during working hours. Samplings were performed in March 2016, with both the multistage impactor and personal sampling pumps.

Table 1 summarizes the sampling sites examined in the present study, and the sampling protocol.

Sampling protocol in the sites OP1, OP2, WP1, WP2 consisted of collection of particles with the multistage impactor operating for fourteen consecutive days, in WP3 for seven consecutive days. In WP4 and WP5, a sampling of only twenty hours or less was performed to avoid filter overloads.

The number of samplings (n) in the sites was quite different: in OP1 n=28, in OP2 n=4, in WP1 n=7, in WP2 n=9, in WP3 n=20, in WP4 n=18, in WP5 n=4. The difference was due to many reasons. OP sites, as outdoor atmospheres, give results depending on meteorological conditions, and, at least 4 seasonal samplings are needed. Attention has been paid to the urban site, which may undergo significant changes in concentration over time. In WP3, the operating procedures are on a routine basis, and the samplings were carried out to cover all the operations.

WP5 PM concentrations depend on the variable amount of waste delivered and therefore treated, and the samplings were carried out in days characterized by different volume of waste received by the facility but with the sampler always positioned nearby the shredders.

3. Results and Discussion

Fig. 1 reports the results of size segregated particle concentrations (μg m^{-3}) in all sampling sites, averaged over all samplings. The variability among the samplings in the same station (data not shown) is acceptable and representative of the site; higher data dispersion was obtained where the productive process causes a major amount of dust.

First, WP5 results were reported in the secondary axis, being the PM concentrations about two orders of magnitude higher than the other sites. Second, WP5, the municipal solid waste composting WP4 plant, and the livestock farm (WP3) have a significantly higher mass concentration of PM on respect the other fractions. PM similar abundance and trend in OP1, OP2, and WP2 show both downtown and countryside outdoor atmospheres suffer from the same common sources of particulate matter. Differently, the indoor lab, without any coarse PM source, shows low concentrations of $PM_{>2.5}$, according to literature (Hoek et al., 2008). Regarding the finer fractions of PM, all the sites show a maximum corresponding to the particles with Dp=0.4 μm, except for WP4 and WP5, where the size segregated PM mass concentrations increase with increasing aerodynamic diameter.

Table 2. $PM_{0.1}$, $PM_{0.1\text{-}2.5}$, C, $PM_{>10}$, $PM_{2.5}$, PM_{10}, TSP concentrations (μg m^{-3}), in seven sites, averaged over n samplings, with n (shown in brackets in the first line, for each sampling site) variable depending on the site. Percentages with respect to TSP.

	OP1 (n=28)	**OP2 (n=4)**	**WP1 (n=7)**	**WP2 (n=9)**	**WP3 (n=20)**	**WP4 (n=18)**	**WP5 (n=4)**
$PM_{0.1}$ (μg m^{-3})	1.7 (0.6-3.3)*	0.5 (0.2-1.2)*	1.9 (1.3-2.6)*	1.8 (1.5-2.1)*	4.7 (1.0-36.1)*	19.8 (6.3-56.8)*	17.6 (6.6-25.9)*
$PM_{0.1\text{-}2.5}$ (μg m^{-3})	16.6 (9.6-23.9)*	9.1 (6.9-11.8)*	15.8 (10.2-27.9)*	18.3 (12.9-25.0)*	37.1 (8.3-209.1)*	131.8 (39.2-523.9)*	477.7 (147.1-704.6)*
Coarse (μg m^{-3})	8.3 (4.0-16.1)*	7.7 (5.0-12.3)*	2.7 (1.5-4.1)*	9.5 (5.5-14.1)*	26.8 (3.7-150.8)*	78.2 (17.9-259.5)*	1179.2 (445.9-2347.4)*
$PM_{>10}$ (μg m^{-3})	5.1 (1.5-8.2)*	2.7 (2.2-2.9)*	0.5 (0.0-0.7)*	5.0 (2.1-9.4)*	37.6 (3.6-362.1)*	65.4 (7.5-703.0)*	3392.3 (1710.1-6604.0)*
$PM_{2.5}$ (μg m^{-3})	18.3 (10.7-26.2)*	9.6 (7.1-13.0)*	17.7 (11.5-30.0)*	20.1 (15.0-26.5)*	41.8 (9.4-210.4)*	151.6 (46.1-569.6)*	495.2 (153.7-730.5)*
PM_{10} (μg m^{-3})	26.6 (15.8-35.9)*	17.3 (12.1-25.3)*	20.4 (13.0-33.0)*	29.6 (20.5-40.6)*	68.6 (13.1-316.0)*	229.8 (64.0-703.2)*	1674.4 (599.6-3077.9)*
TSP (μg m^{-3})	31.8 (18.1-41.3)*	20.0 (14.3-28.2)*	20.8 (13.6-33.5)*	34.5 (23.0-48.2)*	106.2 (17.6-400.0)*	295.2 (72.7-1406.2)*	5066.8 (2309.7-9682.0)*
% $PM_{2.5}$/TSP	58%	48%	85%	58%	39%	51%	10%
% $PM_{>10}$/TSP	16%	13%	2%	14%	35%	22%	67%
% $PM_{0.1}$/TSP	5%	3%	9%	5%	4%	7%	0.3%

**in brackets: range*

OP1: urban atmosphere (outdoor)

OP2: background site (outdoor)

WP1: analytical chemistry laboratory (indoor)

WP2: wastewater treatment plant (outdoor)

WP3: livestock farming activities (outdoor)

WP4: municipal solid waste composting plant (indoor)

WP5: WEEE Treatment Facility (indoor)

The concentrations in μg m^{-3} of the thirteen PM fractions collected in the seven sampling sites, joined in seven outcomes are reported in table 2: $PM_{0.1}$, $PM_{0.1-2.5}$, (particles with 0.1<Dp<2.5μm) and coarse fractions, respirable and thoracic PM fractions ($PM_{2.5}$, PM_{10}), $PM_{>10}$ and total suspended particulate matter (TSP).

Commonly, in outdoor atmospheres, the percentage of fine particle mass on the total PM is about 50% (Di Filippo et al., 2010). In the present study, this percentage ranges between 39 and 58%, with the lower value in the livestock farming area (WP3), due to the high coarse particle mass concentration, caused by the feed mechanical pre-treatment and the particle resuspension during manure and slurry applications or washing operations.

About the indoor atmospheres, WP1 shows a very high percentage ($PM_{2.5}$/TSP = 85%) due to an exiguous concentration of coarse particles, being only $PM_{2.5}$ highly correlated with outdoor concentrations. No previous papers have been published on airborne particles in chemistry laboratories. Only relationships of indoor/outdoor PM mass have been reported in literature, always confirming a high correlation for fine PM and a low one for coarse particles, as in the present study (Götschi et al., 2002; Nazaroff, 2004; Hoek et al., 2008).

On the contrary, in WP5 the trituration processes product large amount of the coarse fraction, yielding a $PM_{2.5}$/TSP percentage equal to 10%. WP3, WP4 and WP5 are also characterized by higher percentage of $PM_{>10}$/TSP, due to the dust-producing processes nearby the sampling points, thus collecting the particles before they have time to settle.

Regarding fine and coarse particles, it is known that the agricultural industry typically generates several milligrams per hour of PM with much larger mass median diameters than urban dusts (Sweeten et al. 1998; Hinz et al., 2002; Wanjura et al. 2005; Winkel et al., 2014). PM concentrations averaging between 0.8 and 2.4 mg m^{-3} of dust can be find in indoor cow stables (Basinas et al., 2014, and references therein). In the present study, the open barns, with ceiling fans installed, were characterized by lower PM concentrations, with the maximum concentration found of 0.4 mg m^{-3}.

As in a WWTP in Phoenix area (Upadhyay et al. 2012), mass concentrations of both $PM_{2.5}$ and PM_{10} measured in the present work, in the wastewater treatment plant WP2, were approximately comparable to those of the urban area OP1 where the plant is located.

It's also well known that large concentrations of inhalable particles (PM_{100}) in ambient air generated by waste handling and mechanical agitation, shredding, piles breakdown, and unloading activities affect municipal solid waste composting plant atmosphere (mainly organic dust) (Schlosser et al.

2009). Shlosser reported concentrations of PM_{100} up to 5.5 mg m^{-3}. In the present study, the concentration of TSP equal to 1.4 mg m^{-3} was never exceeded.

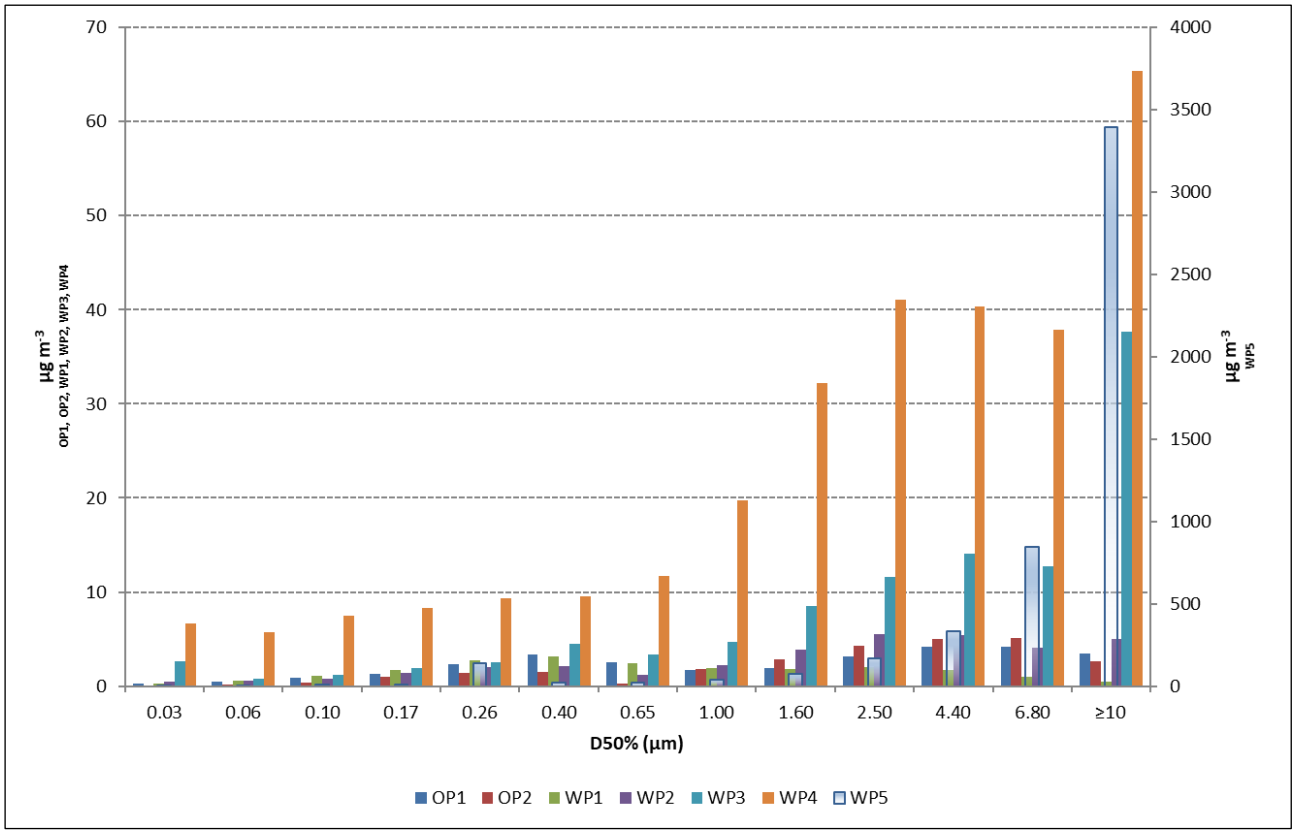

Fig. 1. Size-segregated particle concentrations obtained in each sampling site as an average over the samplings described in table1. WP5 concentrations are plotted on the secondary y-axis.

E-waste dismantling activities release dust particles (coarse and fine particles) in the surrounding atmosphere (Sepúlveda at al. 2010). Sjödin found TSP concentrations ranging from 0.4 to 3.3 mg m^{-3}, similarly to An, reporting a range from 0.36 to 2.21 mg m^{-3}, in samples collected in WEEE Treatment Facility in Sweden and China, respectively (Sjödin et al. 2001; An et al. 2011). In the present study, the monitored WEEE Treatment Facility exhibited a maximum concentration of TSP equal to 9.7 mg m^{-3}, three times higher than in the other studies, probably due to the unsuitable technologies the facility adopts to minimize the release of particulate emissions to the atmosphere. Parallel samplings, carried out with personal samplers, confirmed the TSP concentrations. Table 3 shows TSP concentrations measured with the SKC pumps and as sum of the thirteen fractions of the DLPI, for each of the four samplings in WP4.

Table 3. Total suspended particulate concentration measured with low volume samplers in the site WP5.

	LVS	**DLPI**
May 15 _ PM (mg m^{-3})	1.99	2.31
June 5 _ PM (mg m^{-3})	4.09	4.54
June 8 _ PM (mg m^{-3})	8.04	9.68
June 12 _ PM (mg m^{-3})	2.03	3.74

As regard ultrafine particles, the mass concentration was the lowest in the background site, and increasingly higher as the working environment became more complex. $PM_{0.1}$ average mass concentrations measured in the livestock farm, in the municipal solid waste composting plant and in the WEEE Treatment Facility with maxima at 36, 57 and 26 µg m^{-3}, respectively, were 3, 11 and 10 times more concentrated compared to the average obtained in the other sites. In urban atmosphere, an average of 1.7 with a maximum at 3.3 µg m^{-3} is comparable with other published studies.

$PM_{0.1}$ concentrations in urban areas (Hu et al., 2014 and references therein) are around 3 µg m^{-3} even in polluted atmospheres, mainly due to fresh vehicular emissions. A higher concentration (4.34 µg m^{-3}) was found in California (Sardar et al. 2005a). In areas downwind busy streets and power plants and oil refineries, values of a few µg m^{-3} and a percentage of about 5% on respect total PM are found, demonstrating vehicular emissions and secondary aerosol formation are the primary sources of ultrafine particles (Sardar et al. 2005b; Cyrys et al. 2003; Shi et al. 1999; Di Filippo et al. 2010; Di Filippo et al. 2015).

Unlike OP1, OP2, WP1, and WP2 showing mean $PM_{0.1}$ values lower than 2 µg m^{-3}, $PM_{0.1}$ concentrations in WP3 WP4 and WP5 are unusually high.

As regard ultrafine particulate matter, mass concentrations in workplaces are hardly measured, requiring large and cumbersome devices not suitable on a routine basis. Number and surface area size distribution are instead usually determined, using electrical mobility separation techniques (Wake et al. 2002; Brouwer et al. 2004). Elihn and Berg, in 2009, in some job activities, found that more than 95% of the particles was ultrafine but, due to their small size, the total mass of ultrafine particles is negligible compared to the mass of larger particles, even though the ultrafine particles are often very numerous (Elihn and Berg 2009).

In the present study, ultrafine particles ~~a~~ ranged from 3-7% of the total sampled PM in all the sites except for WP1 and WP5.

WP5 showed lower percentages (0.3%), for the huge mass of larger particles. On respect the other sampling sites, where the size distribution follows a classical trend, in WP5 the high release of coarse PM affects the anomalous percentage.

On the contrary, a higher percentage was found in WP1 (9%), due to the low concentration of the coarse particles, being an indoor environment, therefore protected by dust resuspension, without any coarse PM source.

PM_{10} concentrations exceeded the annual mean limit in ambient air of 40 µg m^{-3} (current WHO guideline value and Council Directive 1999/30/EC of 22 April 1999) in the livestock farm, the municipal solid waste composting plant and the WEEE Treatment Facility. There is no specific occupational exposure standards for these workplaces, where the threshold limit of 5 mg m^{-3} for respirable dusts (particulates not otherwise regulated, PNOR) was never exceeded (current OSHA Permissible Exposure Limits in workplaces).

WP3 is the outdoor environment with the highest PM concentrations. Although agricultural activity is a major contributor to particulate matter emissions and most agricultural emissions originate from livestock production, no specific legislation regarding Threshold Limit Values for PM mass concentration is adopted. Only recommendations or guidelines are available in individual countries. In Denmark and Belgium, in the United Kingdom and in Germany, legally binding workplace exposure limits recommend a threshold of 3 or 4 and 10 mg m^{-3} for $PM_{2.5}$ end PM_{10} respectively (Cambra-López et al., 2010, Winkel et al., 2014).

3.1. Carcinogenic Risk

In order to compare the health problems associated with the different categories of workers, the health risk at the five workplaces, posed by $PM_{2.5}$ inhaled by the workers, was assessed.

Doses, inhalation rate, exposure duration, average body weight, number of days of the exposure were used to calculate the individual risk (EPA/600/P-95/002Fa August 1997; EPA/600/8-89/043 - May 1989). The potential average daily dose in terms of lifetime probabilities ($LADDs_{pot}$) was multiplied to the inhalation slope factor (SFI; i.e., human cancer risk per unit dose) (EPA 540-R-02-002 OSWER 9285.7-45 PB2002 963302, December 2001).

The parameters used to calculate LADD were: inhalation rate: 15.2 m^3/day, body weight: 71.8 kg, exposure duration 253 days, averaging time 25550 days. No correction of parameters based on job

activity was applied. For the inhalation slope factor a $PM_{2.5}$ risk factor of 0.008 $(\mu g\ m^{-3})^{-1}$ was adopted (Greene and Morris 2006, Pope et al., 2002). Table 4 reports the so calculated carcinogenic risk for each workplace.

Table 4. Carcinogenic risk due to $PM_{2.5}$ calculated as product of lifetime average daily doses and the inhalation slope factor.

	OP1	**OP2**	**WP1**	**WP2**	**WP3**	**WP4**	**WP5**
Risk ($LADDs_{pot}$*SFI)	0.00145	0.00076	0.00140	0.00159	0.00331	0.01201	0.03923

OP1: outdoor urban atmosphere

OP2: background site

WP1: analytical chemistry laboratory

WP2: wastewater treatment plant

WP3: livestock farming activities

WP4: municipal solid waste composting plant

WP5: WEEE Treatment Facility

Although the value calculated disregards each additional contribution due to carcinogenic substances characterizing the workplaces (for example halogenated flame retardants in WEEE Treatment Facility), an increase in cancer risk is found mainly in municipal solid waste composting plant and the WEEE Treatment Facility. In these two sites, workers are exposed to a risk higher than 15 and 50 times, respectively, compared to the inhabitants of rural areas. Moreover, two-fold increase of potential risk with respect to the background site can be noticed in the city, in the laboratory and in the wastewater treatment plant, whilst in the livestock farming plant a quadruple risk is detected. Therefore, people working in a lab, in a wastewater treatment plant and in a livestock farming activity are not exposed to additional risk due to $PM_{2.5}$ on respect citizens; instead, risks can result from specific pollutants as VOC, bioaerosol, etc.

On the contrary, people working in a municipal solid waste composting plant or in WEEE Treatment Facility are subjected to an estimated increase in probability of developing lung cancer within 70 years of 1.2 and 3.9%, respectively.

Few samplings are deemed insufficient to evaluate the individual lifetime lung cancer risk and this risk assessment is not measured for additive factors, nevertheless we do believe the measured concentrations are representative of those particular workplaces. This study therefore suggests the

need for more in-depth investigations in workplaces and above all careful attention should be placed on OSHA 5 mg m^{-3} 8-hour TWA PEL (measured as the respirable fraction) rule.

4. Conclusions

Because airborne particles are responsible for increased incidence of respiratory and cardiovascular symptoms and mortality, PM samplings in different work and life environments were performed and the resulting concentrations were compared. In the present work, particularly high PM concentrations were found in the livestock farming activity, in the municipal solid waste composting plant, and above all in WEEE Treatment Facility. Although there is no specific legislation in order to ensure the enhanced quality of air in these workplaces, pertaining to PM mass concentration, the average and maximum values of $PM_{2.5}$ at the three sites found in this study are of concern.

The results also show very high concentrations of coarse particles in workplaces where such amounts are expected. The contemporary collection of ultrafine fraction, hardly carried out in complex work sites, demonstrated surprisingly high $PM_{0.1}$ particle amounts. It is not known whether adverse health effects originate from the particles themselves, from their content in genotoxins, or from a combination of the two, but concerning specifically ultrafine particles, they appear to cause oxidative stress related to the large particle surface area.

To date, $PM_{0.1}$ particle exposure data are insufficient for epidemiological studies, especially in work places where high particulate concentration is expected; monitoring and control of this particulate fraction should be broadly supported, and cohort studies promoted. In the absence of them, in the present work, the risk assessment was calculated based on $PM_{2.5}$ concentrations, showing an increased cancer risk mainly in municipal solid waste composting plant and the WEEE Treatment Facility in comparison to the other sites.

Despite limitation due to the few samplings in some sites and although the possible contribution of carcinogenic substances was disregarded, this study suggests the need for more in-depth investigations in the workplaces investigated.

Acknowledgements

Supported by INAIL, BRIC 2016 ID23. We thank Dr, Giuseppe Castellet Ballarà and Dr. Annalisa Guercio (INAIL-Contarp) for their help in field sampling.

References

An, T., Zhang, D., Li, G., Mai, B., Fu, J., 2011. On-site and off-site atmospheric PBDEs in an electronic dismantling workshop in south China: Gas-particle partitioning and human exposure assessment. Environ. Pollut. 159, 3529-3535, https://doi.org/10.1016/j.envpol.2011.08.014.

Basinas, I., Sigsgaard, T., Erlandsen, M., Andersen, N.T., Takai, H., Heederik, D., Omland, Ø., Kromhout, H., Schlünssen, V., 2014. Exposure-Affecting Factors of Dairy Farmers' Exposure to Inhalable Dust and Endotoxin. Ann. Occup. Hyg. 58, 6, 707–723. https://doi:10.1093/annhyg/meu024.

Brouwer, D. H., Gijsbers, J. H., Lurvink, M. W., 2004 . Personal exposure to ultrafine particles in the workplace: exploring sampling techniques and strategies. Ann. Occup. Hyg. 48, 439-453, https://doi.org/10.1093/annhyg/meh040.

Cambra-López, M., Aarnink, A. J., Zhao, Y., Calvet, S., Torres, A. G., 2010. Airborne particulate matter from livestock production systems: A review of an air pollution problem. Environ. Pollut. 158, 1-17, https://doi.org/10.1016/j.envpol.2009.07.011.

Cyrys, J., Stölzel, M., Heinrich, J., Kreyling, W. G., Menzel, N., Wittmaack, K., Tuch, T., Wichmann, H. E., 2003. Elemental composition and sources of fine and ultrafine ambient particles in Erfurt, Germany. Sci. Total Environ. 305, 143-156, https://doi.org/10.1016/S0048-9697(02)00494-1.

Destaillats, H., Maddalena, R. L., Singer, B. C., Hodgson, A. T., McKone, T. E., 2008. Indoor pollutants emitted by office equipment: A review of reported data and information needs. Atmos. Environ. 42(7), 1371-1388, https://doi.org/10.1016/j.atmosenv.2007.10.080.

Di Filippo, P., Pomata, D., Riccardi, C., Buiarelli, F., Gallo, V., 2015. Oxygenated polycyclic aromatic hydrocarbons in size-segregated urban aerosol. J. Aerosol Sci. 87, 126-134, https://doi.org/10.1016/j.jaerosci.2015.05.008.

Di Filippo, P., Riccardi, C., Pomata, D., Buiarelli, F., 2010. Concentrations of PAHs, and nitro-and methyl-derivatives associated with a size-segregated urban aerosol. Atmos. Environ. 44, 2742-2749, https://doi.org/10.1016/j.atmosenv.2010.04.035.

Donham, K.J., Wing, S., Osterberg, D., Flora, J. L., Hodne, C., Thu. K. M., Thorne, P. S., 2007. Community health and socioeconomic issues surrounding concentrated animal feeding operations. Environ. Health Perspect. 115, 317, https://doi.org /10.1289/ehp.8836.

Elihn, K., & Berg, P., 2009. Ultrafine particle characteristics in seven industrial plants. Ann. Occup. Hyg. 53, 475-484, https://doi.org/10.1093/annhyg/mep033.

Götschi T., Oglesby L., Mathys P., Monn C., Manalis N., Koistinen K., Jantunen M., Hänninen O., Polanska L., Künzli N., 2002. Comparison of Black Smoke and PM2.5 Levels in Indoor and Outdoor Environments of Four European Cities. Environ. Sci. Technol., 36, 6, 1191-1197.

Greene, N. A., Morris, V. R., 2006. Assessment of Public Health Risks Associated with Atmospheric Exposure to PM2.5 in Washington, DC, USA. Int. J. Environ. Res. Public Health, 3, 86-97.

Hoek, G., Kos, G., Harrison, R., De Hartog, J., Meliefste, K., Ten Brink, H., Katsouyanni, K., Karakatsani, A., Lianou, M., Kotronarou ,A., Kavouras, I., Pekkanen, J., Vallius, M., Kulmala, M., Puustinen, A., Thomas, S., Meddings, C., Ayres, J., Van Wijnen, J., Hameri, K., 2008. Indoor–outdoor relationships of particle number and mass in four European cities. Atmos. Environ. 42, 1, 156-169.

Karra, S., Katsivela, E., 2007. Microorganisms in bioaerosol emissions from wastewater treatment plants during summer at a Mediterranean site. Water Res. 41, 1355-1365, https://doi.org/10.1016/j.watres.2006.12.014.

Kumar, P., Morawska, L., Birmili, W., Paasonen, P., Hu, M., Kulmala, M., Harrison, R. M., Norford, L., Britter, R., 2014. Ultrafine particles in cities. Environ Int. 66, 1-10, https://doi.org/10.1016/j.envint.2014.01.013.

Pope, C. A. III, Burnett, R. T., Thun, M. J., Calle, E. E., Krewski, D., Ito, K., Thurston, G. D., 2002. Lung cancer, cardiopulmonary mortality, and long-term exposure to fine particulate air pollution. JAMA 287, 1132-1141, https://doi.org/10.1001/jama.287.9.1132.

Sardar, S.B., Fine, P.M., Sioutas, C., 2005a. Seasonal and spatial variability of the size-resolved chemical composition of particulate matter (PM_{10}) in the Los Angeles Basin. J. Geophys Res. 110, D07S08, https://doi:10.1029/2004JD004627.

Sardar, S. B., Fine, P. M., Mayo, P. R., Sioutas, C., 2005b. Size-fractionated measurements of ambient ultrafine particle chemical composition in Los Angeles using the NanoMOUDI. Environ. Sci. Technol. 39, 932-944, https://doi.org/10.1021/es049478j.

Schlosser, O., Huyard, A., Cartnick, K., Yañez, A., Catalán, V., Do Quang, Z., 2009. Bioaerosol in composting facilities: occupational health risk assessment. Water Environ. Res. 81, 866-877, https://doi.org/10.2175/106143009X407258.

Sepúlveda, A., Schluep, M., Renaud, F. G., Streicher, M., Kuehr, R., Hagelüken, C., Gerecke, A. C., 2010. A review of the environmental fate and effects of hazardous substances released from electrical and electronic equipments during recycling: Examples from China and India. Environ. Impact Asses. 30, 28-41, https://doi.org/10.1016/j.eiar.2009.04.001.

Shi, J. P., Khan, A. A., Harrison, R. M., 1999. Measurements of ultrafine particle concentration and size distribution in the urban atmosphere. Sci. Total Environ. 235, 51-64, https://doi.org/10.1016/S0048-9697(99)00189-8.

Sjödin, A., Carlsson, H., Thuresson, K. A. J., Sjölin, S., Bergman, Å., Östman, C., 2001. Flame retardants in indoor air at an electronics recycling plant and at other work environments. Environ. Sci. Technol. 35, 448-454, https://doi.org 10.1021/es000077n.

Upadhyay, N., Sun, Q., Allen, J.O., Westerhoff, P., Herckes, P., 2013. Characterization of aerosol emissions from wastewater aeration basins. J. Air Waste Manag. Assoc. 63, 20–26, https://doi.org/10.1080/10962247.2012.726693.

U.S. Environmental Protection Agency. EPA/600/8-89/043 - May 1989.

U.S. Environmental Protection Agency. EPA/600/P-95/002Fa August 1997.

U.S. Environmental Protection Agency. EPA 540-R-02-002 OSWER 9285.7-45 PB2002 963302 www.epa.gov/superfund/RAGS3A/index.htm December 2001.

Utell, M. J., Frampton, M. W., Zareba, W., Devlin, R. B., Cascio, W. E., 2002. Cardiovascular effects associated with air pollution: potential mechanisms and methods of testing. Inhal. Toxico. 14, 1231-1247, https://doi.org/10.1080/08958370290084881.

Valavanidis, A., Fiotakis, K., Vlachogianni, T., 2008. Airborne particulate matter and human health: toxicological assessment and importance of size and composition of particles for oxidative damage and carcinogenic mechanisms. J Environ. Sci. Health Part C, 26, 339-362, https://doi.org/10.1080/10590500802494538.

Wake, D., Mark, D., Northage, C., 2002. Ultrafine aerosols in the workplace. Ann. Occup. Hyg. 46 (suppl_1), 235-238, https://doi.org/10.1093/annhyg/46.suppl_1.235.

Wanjura, J. D., Parnell, C. B., Shaw, B. W., Lacey, R. E., 2005. Design and evaluation of a low-volume total suspended particulate sampler. Trans .ASAE, 48, 1547-1552.

Winkel, A., Demeyer, P., Feilberg, A., Jørgensen, M., Puterflam, J., Engel, P., 2014. Measurement of particulate matter: recommendations for the VERA test protocol on air cleaning technologies. A working group report from the project "ICT-AGRI: Development of harmonized methods for sampling and measurement of odour, ammonia and dust emission" developed on the initiative of the international VERA organization, https://library.wur.nl/WebQuery/wurpubs/fulltext/320606.

Particulate Matter in and from Agriculture. Edited by Torsten Hinz, Birgit Rönnpagel and Stefan Linke. Proceedings of the Conference organized by the Institut für Technologie und Biosystemtechnik, Bundesforschungsanstalt für Landwirtschaft (FAL) held at Braunschweig, 3rd and 4th June, 2002.

2.2.3. (B3) Evidences of Copper Nanoparticle Exposure in Indoor Environments: Long-Term Assessment, High-Resolution Field Emission Scanning Electron Microscopy Evaluation, in Silico Respiratory Dosimetry Study and Possible Health Implications

Science of the Total Environment (2019), *653*, 1192-1203

Maurizio Manigrasso [a,*], Carmela Protano [b], Maria Luisa Astolfi [c], Lorenzo Massimi [c], Pasquale Avino [d], Matteo Vitali [b], Silvia Canepari [c]

[a] Department of Technological Innovations, INAIL, Via IV Novembre 144, 00187 Rome, Italy;
[b] Department of Public Health and Infectious Diseases, Sapienza University of Rome, P.le Aldo Moro, 5, 00185 Rome, Italy;
[c] Department of Chemistry, Sapienza University, P.le Aldo Moro 5, 00185 Rome, Italy;
[d] Department of Agricultural, Environmental and Food Sciences (DiAAA), University of Molise, via De Sanctis, 86100 Campobasso, Italy.

Abstract: A variety of appliances operated by brush electric motors, widely used in indoor environments, emit nanoparticles (NPs). Due to electric arc discharge during the operation of such motors, some NPs contain Copper (Cu). Their dimensions are the same of those found in brain tissue samples by other authors who speculated their possible translocation to brain through olfactory bulb. Cu have been reported to play an important role in the etiopathogenesis of Alzheimer's disease. Thus, the present study was performed to: 1. estimate by means of Multiple-Path Particle Dosimetry model the doses of NPs released by electric appliances that can potentially deposit on the olfactory bulb; 2. investigate the morphology and the composition of particles emitted by some electric appliances daily used in indoor environments; 3. monitor for a long time period the Cu contamination of indoor environments due to this kind of appliances. About 10^6-10^7 NPs deposit on the olfactory bulb during the operation (1.5-6 min) of such appliances, with a major contribution due to 10-20 nm NPs. HR-FESEM characterization confirmed the presence of such NPs, that were observed both as individual particles (20-40 nm) and aggregated to form particles in the μm sizes range. XEDS microanalysis

revealed the presence of Cu together with other elements. Relevant daily contamination of indoor environments due to these appliances has been confirmed by monitoring throughout a year the Cu content of PM_{10} samples collected both indoor and outdoor private dwellings. Cu was present in great part as an insoluble form. This means that, following protracted exposure, Cu NPs of such origin may undergo tissue accumulation. This is cause of concern because general population is chronically exposed to such Cu nanoparticles in indoor environments and in view of the role assigned to Cu in the development of neurological disorders.

Keywords: indoor copper nanoparticles; brush electric motors; chronic exposure; olfactory bulb; multiple-path particle dosimetry model; high-resolution field emission scanning electron microscopy.

1. Introduction

Air pollution remains an issue of great concern for public health, and it is one of the major risk factor for environmental and human health worldwide. The update 2018 of the World Health Organization Global Ambient Air Quality Database reported that, globally, seven million deaths were attributable to the joint effects of ambient and household air pollution (WHO, 2018). Indeed, over the years, air pollution was associated to a great number of adverse outcomes for human health, following both acute and chronic exposure. In particular, several evidences linked air pollution exposure to adverse health effects, such as respiratory (asthma, chronic obstructive pulmonary disease) and cardiovascular diseases (myocardial infarction, heart failure, cerebrovascular accidents) (Mannucci et al., 2015), endocrine disorders (Darbre, 2018), neuroinfiammation and neurodegenerative diseases (Levesque et al., 2011). Outdoor air pollution was recently recognized as IARC Group 1, carcinogenic to humans (IARC, 2013). Besides, air pollution has been related to several adverse outcomes during intrauterine development (Buuris and Baccarelli, 2017; Westergaard et al., 2017; Veleminsky et al., 2016).

Despite the increasing growth of scientific evidence on negative outcomes related to air pollution exposure, many gaps in this field still wait to be filled. First of all, it is well-known that air pollution is a complex mixture; thus, it is important to understand which are the components most dangerous for human health. Over the years, many researchers focalized the attention on Particular Matter (PM), especially on fine particles (< 2500 nm diameter), and nanoparticles (NPs; < 100 nm diameter). Indeed, independently from its chemical composition, PM has been linked to numerous human health adverse effects affecting respiratory, cardiovascular, endocrine and neurological systems (Anderson et al., 2012; Noh et al., 2016; Wang et al., 2017). In particular, NPs seem to play an important role

on the health threats related to PM exposure (Hoek et al., 2010) because the small size of these particles allows them to persist for longer times, to easily contaminate indoor environments (Brauer et al., 1989) and/or to be transported over long ranges. Their high surface area, confer them an increased ability to adsorb organic molecules. Moreover, their size is smaller than those of cellular structures, so that they can penetrate into cellular targets in the lung and systemic circulation (Li et al., 2003; Pagano et al., 1996). Another important issue on air pollution is related to the contribution of outdoor and indoor air quality on human health. Traditionally, the attention of the scientific community was focused on outdoor air pollution, but in the last decades, indoor air quality has become increasingly important for two main reasons: 1. people spends a great part of their time in enclosed environments (more than 90%) (Hubal et al., 2000; CalEPA, 2004); 2. the quality of indoor air may be worse than outdoor, because indoor air contaminants not only derive from the outdoor pollutants, but are also produced directly indoor (Morawska et al., 2017; Śmiełowska et al., 2017). As regards to the indoor sources of air pollutants, several combustion activities (tobacco smoking, cooking activities, burning mosquito coils, burning incense and candles, traditional and alternative heating systems such as biomass-burning heating, etc) represent well-known particles sources in indoor environments (Sarwar et al., 2004; Hsu et al., 2012; Huang et al., 2012; Liu et al., 2014; Protano et al., 2016; Protano et al., 2017; Stabile et al., 2018, Frasca et al., 2018; Drago et al., 2018). More recently, some studies demonstrated that the use of several non-combustion sources (drills, flat irons, hair dryers, laser printer, electronic smoking devices, etc) contribute to the PM indoor pollution, increasing significantly the levels of indoor ultrafine- and NPs (Castellano et al., 2012; Manigrasso et al., 2017; Scungio et al., 2017).

Within this context, in previous studies (Manigrasso et al., 2017; Manigrasso et al. 2018) we addressed that potential sources present in domestic environments determine very intense exposure patterns to NPs. In particular, we observed that a fraction of NPs with mode of about 10 nm is present in the aerosol emitted by appliances operated by brush electric motors. This fraction is of great concern for human health for its size range. Indeed, anthropogenic particles of similar size were recovered in brain samples by other researchers, that hypothesized that such particles may bypass the typical way of uptake (circulatory system, blood-brain barrier) and reach the brain directly through the olfactory bulb (Maher et al., 2016). This fraction is cause of concern also due to its chemical composition. It contains copper NPs and copper ions have been reported to play an important role in the etiopathogenesis of Alzheimer's disease (AD) (Huang et al., 1999a, 1999b; Tabner et al., 2011).

Following our previous findings, the aims of this study are:

1. to estimate the doses of NPs that can potentially deposit on the olfactory bulb, because they are candidate to possibly translocate to the brain;
2. to investigate the morphology and the composition of particles emitted by some electric appliances daily (or even several time a day) used in indoor environments, because their possible health effects derive from the association of their size and their chemical composition (Cu content);
3. to monitor for a long time period the Cu contamination of indoor environments due to this kind of appliances, in order to assess the time-exposure pattern of the general population.

2. Materials and Methods

Aerosol measurements were performed both in a test-room and in real scenario indoor environments. Aerosol number size distributions were measured in the test-room and were used to estimate the dose of particle deposited on the olfactory bulb. In the same room aerosol samples were collected for High-Resolution Field Emission Scanning Electron Microscopy (HR-FESEM) characterization.

In the real scenario environments PM_{10} samples were collected throughout a year to determine airborne concentrations of Cu and Antimony (Sb, as a tracer of vehicular traffic).

2.1 Test-room Aerosol Measurements and Sampling

Aerosol was released during the operation (about 5 min) of a brush electric motor vacuum cleaner, an electric drill and a hairdryer in a test room. A detailed aerosol characterization is reported in a previous study (Manigrasso et al., 2017). Briefly, aerosol measurements were carried out in a 52.7 m^3 room where the door and window were both closed. During the aerosol measurements, the room temperature and relative humidity ranged between 24 °C and 26 °C and 25 % and 32 %, respectively. The air exchange rate (λ), calculated using the tracer gas technique (Laussmann and Helm, 2011), was equal to 0.67 h^{-1}.

Due to the fast evolution of the aerosol studied (Manigrasso and Avino, 2012; Manigrasso et al., 2013), aerosol number size distributions were measured by means of a Fast Mobility Particle Sizer (FMPS, model 3091, TSI, Shoreview, MN, USA). The instrument counts and classifies particles according to their electrical mobility in 32 size channels ranging from 5.6 to 560 nm with a 1 s time resolution. FMPS operates at a high flow rate (10 L min^{-1}) to minimize diffusion losses. It operates at ambient pressure to prevent the evaporation of volatile and semivolatile particles (TSI, 2015).

In the same test-room, for each appliance studied, aerosol samples for HR-FESEM characterization were collected on polycarbonate filters (0.8 µm, 47 mm, Sterlitech Corporation, WA, USA) at a sampling flow rate of 20 L min^{-1}. Before each sampling, air was completely changed and a blank sample was collected.

2.1.1 Aerosol Dosimetry

The fractions of particles deposited on the olfactory bulb upon inhalation ($F^{Olf}(d_i)$) have been estimated using the Multiple-Path Particle Dosimetry model (MPPD v3.01, ARA 2015, ARA, Arlington, VA, USA) (Asgharian et al., 2001). For this estimate, MPPD relies on the study of Garcia et al. (2015). To estimate the dose of particles deposited in the head region, the 60^{th} percentile human stochastic lung was considered along with the following settings: (i) a uniformly expanding flow, (ii) an upright body orientation, and (iii) nasal breathing with a 0.5 inspiratory fraction and no pause fraction. Moreover, the following parameters were used for a Caucasian adult male under light work physical activity, based on the ICRP report (ICRP, 1994): (i) a functional residual capacity (FRC) of 3300 mL, (ii) an upper respiratory tract (URT) volume equal to 50 mL, (iii) a 20 min^{-1} breathing frequency, and (iv) an air volume inhaled during a single breath (tidal volume, V_t) of 1.25 L.

Since FMPS measures aerosol size number distribution as a function of the electrical mobility diameter (d), d values have been transformed to aerodynamic diameter (d_a) according to equation (1) (Li et al., 2016).

$$d_a = d\sqrt{\chi \times \frac{\rho \times C_c(d_m)}{C_c(d_a)}} \quad (1)$$

Where C_c is the Cunningham slip factor for a given diameter, χ is the particle dynamic shape factor, (χ = 1, i.e. spherical particles have been assumed) and ρ is the particle density. Particles with electrical mobility diameters from 6.4 to 14.3 have been considered as due to the emissions from the copper windings in the rotor whereas particles from 16.5 to 25.5 have been considered to arise from graphite electrodes (Bau et al., 2010) in the stator of the electric motor. The relevant particle densities as functions of particle mobility diameters have been calculated using the equations derived by Charvet et al. (2014).

For each respiratory act, the doses below described were calculated:

Size number dose distributions of particles deposited on the olfactory bulb upon inhalation as function of time (t):

$$D^{Olf}(d_i, t) = F^{Olf}(d_i) \times C(d_i, t) \times V_t \quad (2)$$

where d_i is the diameter of particles classified in the i^{th} FMPS size channel, $F^{Olf}(d_i)$ is the relevant olfactory bulb deposition fraction, $C(d_i,t)$ is the concentration of particles in the i^{th} FMPS size channel as a function of time, V_t is the tidal volume.

Cumulative size number dose distribution and cumulative number doses were calculated over the time interval of source operation (from t_0 to t_s) according to equations (3) and (4), respectively.

$$D_c^{Olf}(d_i, t_s) = \sum_{t=t_0}^{t_s} D^{Olf}(d_i, t) \quad (3)$$

$$D_c^{Olf}(t_s) = \sum_{1=1}^{32} D_c^{Olf}(d_i, t_s) \quad (4)$$

where 32 is the number of FMPS size classes.

The surface area doses $S^{Olf}(d_i,t)$, $S_C{}^{Olf}(d_i,t_s)$, $S_C{}^{Olf}(t_s)$, were calculated from $D^{Olf}(d_i,t)$, $D_C{}^{Olf}(d_i,t_s)$, $D_C{}^{Olf}(t_s)$ under the hypothesis of spherical particles.

Background respiratory doses $D_C{}^{Olf}(d_i,t_s)$ and $S_C{}^{Olf}(d_i,t_s)$ have been calculated using the particle size number distributions averaged over 5 min time interval, before the operation of each indoor source considered.

2.1.2 Scanning Electron Microscopy Characterization

A HR-FESEM (model AURIGA; Carl Zeiss Microscopy GmbH, Jena, Germany) equipped with an energy dispersive spectrometer for x-ray microanalysis (XEDS, model QUANTAX; Bruker Italia S.r.l., MI, Italy) was used for individual particle characterization of Cu.

A small portion of sample (about a quarter of total filter area) was cut in the center of polycarbonate membranes and coated with an ultra-thin gold layer (5 nm) by sputtering machine (Q150T Turbo-Pumped Sputter Coater/Carbon Coater; Quorum Technologies Ltd, East Sussex, United Kingdom).

HR-FESEM XEDS acquisitions were performed under high vacuum (10^{-6} hPa) at 20 keV accelerating voltage. Micrographs were acquired by Secondary Electron Detector (SED) at magnification, Working Distance (WD), tilt angle, and spot size conditions properly adjusted on a case-sensitive scale to optimize image resolution.

The microanalysis was performed at WD and magnification ranging from 9.6 mm to 12.4 mm and from 25 k x to 600 k x, respectively.

2.2 Real Scenario Indoor Aerosol Sampling

Samplings were performed in two dwellings located in the Terni basin (Central Italy), an area characterized by quite intensive urban and industrial PM emissions (Massimi et al., 2017; Fig. 1).

The dwellings were both located at the first floor and at short distance from the industrial area (steel plant): the first one (DW1) was in close proximity (about 20 m) to a trafficked urban road; the second one (DW2) was at about 150 m from a secondary road. Samplings were performed by low cost samplers (High Spatial Resolution Samplers; HSRS, recently made available from Fai Instrument s.r.l., Fonte Nuova, Rome, Italy), equipped with a PM_{10} sampling head. These samplers are very silent and work at a very low flow rate (0.5 L min^{-1}). Thus they enable to accumulate PM on membrane filters for long times (one month or more), ensuring a high representativeness of the measured concentrations without excessive costs.

Fig. 1. Geographical location of sampling sites (QGis 2.18 Las Palmas). Legend - violet: industrial areas; red: urban areas; grey: agricultural areas; yellow: semi-natural areas; green: forests (Corine Land Cover 2012).

At each dwelling two samplers were placed: one indoor (in the dining room, at about 2 meters from the window) and one in the outdoor environment at about 8 meters from the dining room window. Both dining rooms were naturally ventilated, South-exposed and both kitchens were separated from

the dining room and equipped with a methane stove and with an exhaust system. At each site, PM_{10} was sampled on a Teflon® membrane (37 mm diameter, 2 μm pore size, PALL Corporation, Port Washington, New York, NY, USA) at the same time. The monitoring activities lasted for about one year and the sampling periods are reported in Table 1.

Table 1. Sampling periods at dwelling 1 and 2.

Start	**Stop**	**Name of Period**
January, 21st, 2017	February, 20th, 2017	Feb
February, 25th, 2017	March, 27th, 2017	Mar
April, 1st, 2017	May, 1st, 2017	Apr
May, 6th, 2017	June 5th, 2017	May
June, 10th, 2017	July, 17th, 2017	Jul
July, 22nd, 2017	August, 28th, 2017	Aug
September, 2nd, 2017	October, 2nd 2017	Sep
October 21st, 2017	November, 20th, 2017	Nov
November, 25th, 2017	January, 15th, 2018	Dec

In the first dwelling (DW1) a vacuum cleaner equipped with a bag filter and a 1300 W brush electric motor (the same used for aerosol measurements in the test-room) was used; no other appliance operated by this kind of electric motors was ever used. In the second dwelling (DW2) the floor cleaning was carried out by means of a vacuum cleaner equipped with a HEPA filter (class H11) and a 900 W brushless electric motor. This kind of motors is more efficient than brush electric ones, does not generate sparks, and consequently does not emit aerosol, as brush motors do. This is confirmed by Fig 2 were the aerosol emissions measured in the test room of the two vacuum cleaners is compared. In particular, the temporal trends of particle number concentrations in the range 5.6-560 nm measured close to the breathing zone of the user are shown.

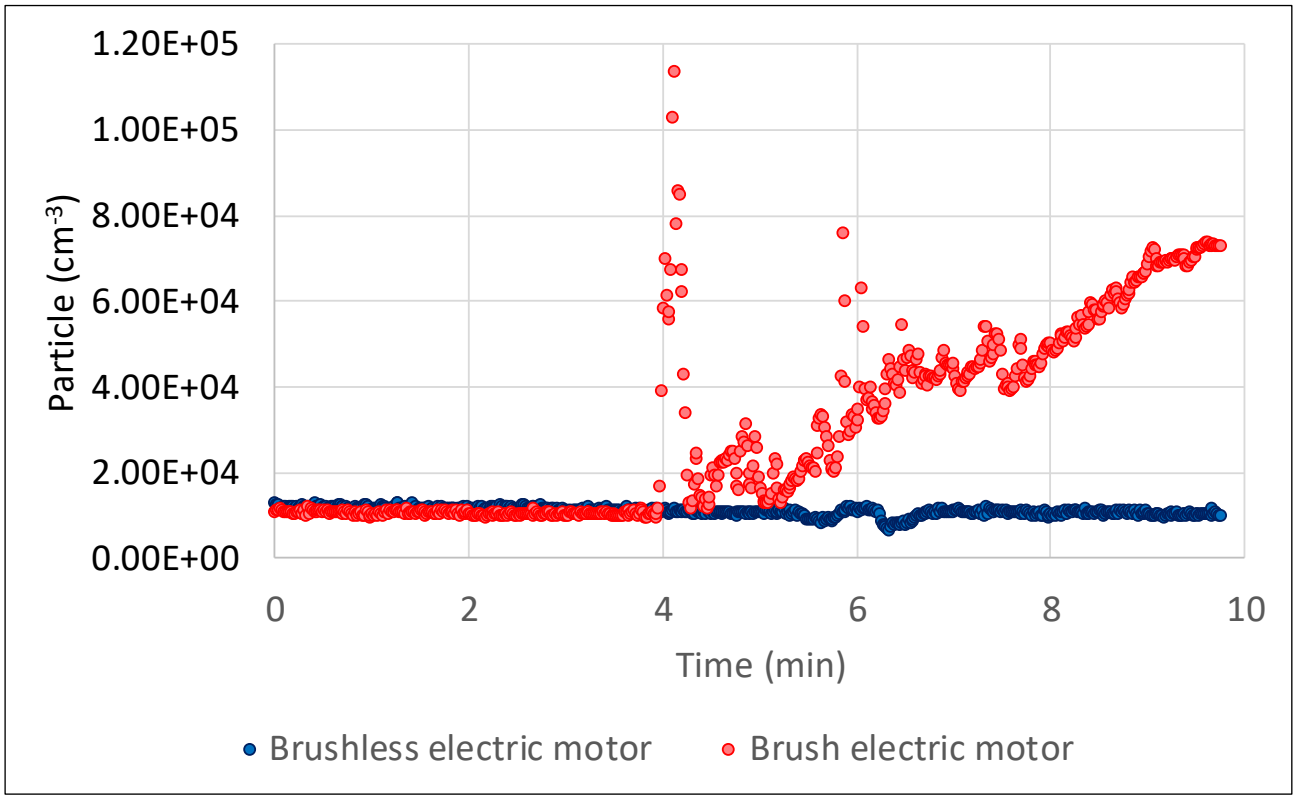

Fig. 2. Temporal trends of particle number concentrations in the range 5.6-560 nm measured for two vacuum cleaner equipped respectively with a brush and a brushless electric motor (respectively used at DW1 and DW2). The two vacuum cleaners were turned-off for the first 4 minutes.

2.2.1 Chemical Analysis

PM_{10} mass concentration was gravimetrically determined by weighting Teflon® filters before and after sampling (Sartorius AG mod. ME5, Goettingen, Germany; 1 µg sensitivity). All the filters were conditioned at 50% R.H. and 20 °C for 48 hours before each weighing step. After sampling, filters were sealed in plastic Petri dishes and stored at 5 °C until the chemical analysis.

A detailed description of the analytical procedure is reported in Canepari et al. (2006a, 2006b, 2010a). Briefly, sampled Teflon® membrane was deprived of the supporting polymethylpentene ring and subjected to ultrasound-assisted extraction (30 min; 40 KHz, 240 W; Ulsonic Proclean 10.0; Zielona Gora, Poland) in 20 mL of ultra-pure deionized water (Elga LabWater Purelab Plus, Wycombe, United Kingdom). The solution was then filtered on nitrate cellulose (NC) filters (porosity 0.45 µm, Millipore, Billerica, Massachusetts, USA) to obtain the soluble fraction. The insoluble particles on the NC and Teflon® filters were digested in microwave oven (quartz vessels; Ethos 1 Touch Control,

Milestone, USA) by 3 mL of 2:1 concentrated HNO_3/H_2O_2 mixture (Promochem, LGC Standards GmbH, Wesel, Germany). The obtained solution was diluted to 50 mL with ultrapure water and again filtered, by using disposable syringe (Einmalspritzen Luer 20 mL, Sandtler) equipped with NC fiber filter (0.45 um porosity, GVS Filter Techonoly – Indianapolis, USA), to obtain the residual fraction. Both the soluble and insoluble fractions were analyzed by Inductively Coupled Plasma Mass Spectrometry (ICP-MS; Bruker 820 MS, Bremen, Germany, equipped with a glass nebulizer working at 0.4 mL min^{-1}- MicroMistTM; Analytik Jena AG, Jena, Germany). Five-point matrix-matched calibration was used for the quantification of ^{65}Cu and ^{121}Sb; ^{89}Y was used as internal standard. An exhaustive description of ICP-MS operative conditions is reported in Astolfi et al (2018).

2.3 Quality Assurance

Before the measuring campaign, the performances of FMPS were checked by comparison with a Scanning Mobility Particle Sizer (SMPS, model 3936, TSI) equipped with an Electrostatic Classifier (model 3080, TSI), a Differential Mobility Analyser (DMA, model 3081, TSI) and a Condensation Particle Counter (model 3775, TSI). The FMPS number concentrations were approximately 15% lower than the diffusion loss corrected SMPS number concentrations, in agreement with the findings of Jeong and Evans (2009).

The performances of HSR Samplers were evaluated in terms of efficiency and repeatability (Perrino et al., paper in preparation). The repeatability of PM_{10} mass concentration measurements performed by HSRS (nine samplings, three replicates each) was acceptable, with relative standard deviation (RSD%) ranging from 2% to 25%. These values are probably mostly affected by the alteration of solid-vapor equilibria of volatile species, such as NH_4NO_3, during the prolonged HSRS sampling period. Very good repeatability (RSD% ranging from 6 to 15%, which includes contributes from chemical analysis) was obtained for stable elements, such as Cu and Sb.

The analytical procedure applied to the PM_{10} samples for the determination of elemental concentrations was previously fully validated (Canepari et al., 2006b, 2009). Cu and Sb were recovered from certificate material NIST1648 (urban dust) with recovery percentages higher than 90% and repeatability on field PM_{10} paired samples was very good, with RSD% lower than 10%.

2.4 Statistical Elaboration

Statistical analyses were performed using IBM-SPSS version 25.0 software (IBM Corp. Released 2017. IBM SPSS Statistics for Windows, Version 25.0. Armonk, NY: IBM Corp.). Firstly, the

Kolmogorov–Smirnov test was used to assess the normality of the distribution both for particles number concentrations and for Cu, Sb and PM_{10} levels. Particles number concentrations exhibited a not normal distribution; thus non-parametric tests were used for statistical evaluations. In particular, Mann-Whitney U test was used for assessing differences in median levels of the $D^{Olf}(d_i,t)$ for each particle diameter measured respectively before and during the period of each appliance operation. We considered particle diameters from 5.6 to 93 nm because above such size range, the particle deposition fraction $F^{Olf}(d_i)$ were negligible. Cu, Sb and PM_{10} levels were normally distributed; therefore, statistical elaborations were performed via parametric techniques. In particular, t-Student test for paired data was used to compare differences in mean levels of Cu, Sb and PM_{10} found indoor and outdoor, independently considering DW1 and DW2 sites. Besides, simple regression analyses were run to assess the relationship between Cu and Sb levels, separately for DW1 indoor, DW1 outdoor, DW2 indoor and DW2 outdoor concentrations. Finally, ANOVA test with Bonferroni post-hoc tests were used to assess the differences in the percentages of indoor and outdoor Cu soluble fractions for DW1 and DW2 sites.

3. Results and Discussion

3.1 Dosimetry

Fig. 3 a, b, c describe the particle number dose size distributions $D^{Olf}(d,t)$ of the particles deposited on the olfactory bulb, for each respiratory act, upon inhalation, during and after the operation of a brush electric motor vacuum cleaner, a hairdryer and an electric drill.

For these appliances, a major mode was present at about 10 nm, due to the Cu NPs emitted by the electric arc discharge between the Cu windings and the graphite electrodes of the brush electric motor (Manigrasso et al., 2015, Manigrasso et al., 2017; Szymczak et al., 2007). A minor mode at about 16 nm and, for the hairdryer and the vacuum cleaner, a shoulder at about 29 nm were probably due to particle coagulation and/or to the contribution from the graphite brushes (Roth et al., 2004). Following a single respiratory act, due to aerosol spike emissions, up to 7.6×10^4, 1.7×10^5 and 3.3×10^5 particles were respectively deposited on the olfactory bulb, with a major contribution, respectively of 1.3×10^4, 2.7×10^4 and 6.2×10^4 particles, from 9-10 nm particles. Throughout the time interval of appliance operation (6 min, 5 min, 1.5 min, respectively for the vacuum cleaner, the hairdryer and the electric drill), overall 3.8×10^6, 9.0×10^6 and 2.6×10^6 particles ($D_c{}^{Olf}(t_s)$) were deposited. Median levels of $D^{Olf}(d_i,t)$ for each particle diameter were significantly greater over the period of appliance operation than those estimated before starting the operation (p-value < 0.05) in all cases, with the

exception of the highest size fractions that were not appreciably affected by the appliance aerosol emissions.

In terms of particle surface area (Fig. 3d, e, f), such doses correspond to 61.3, 1.5×10^2, 1.4×10^2 μm^2 after a single respiratory act and to 3.2×10^3, 7.4×10^3, 1.2×10^3 μm^2, throughout the time interval of appliance operation ($(S_c^{Olf}(t_s)$).

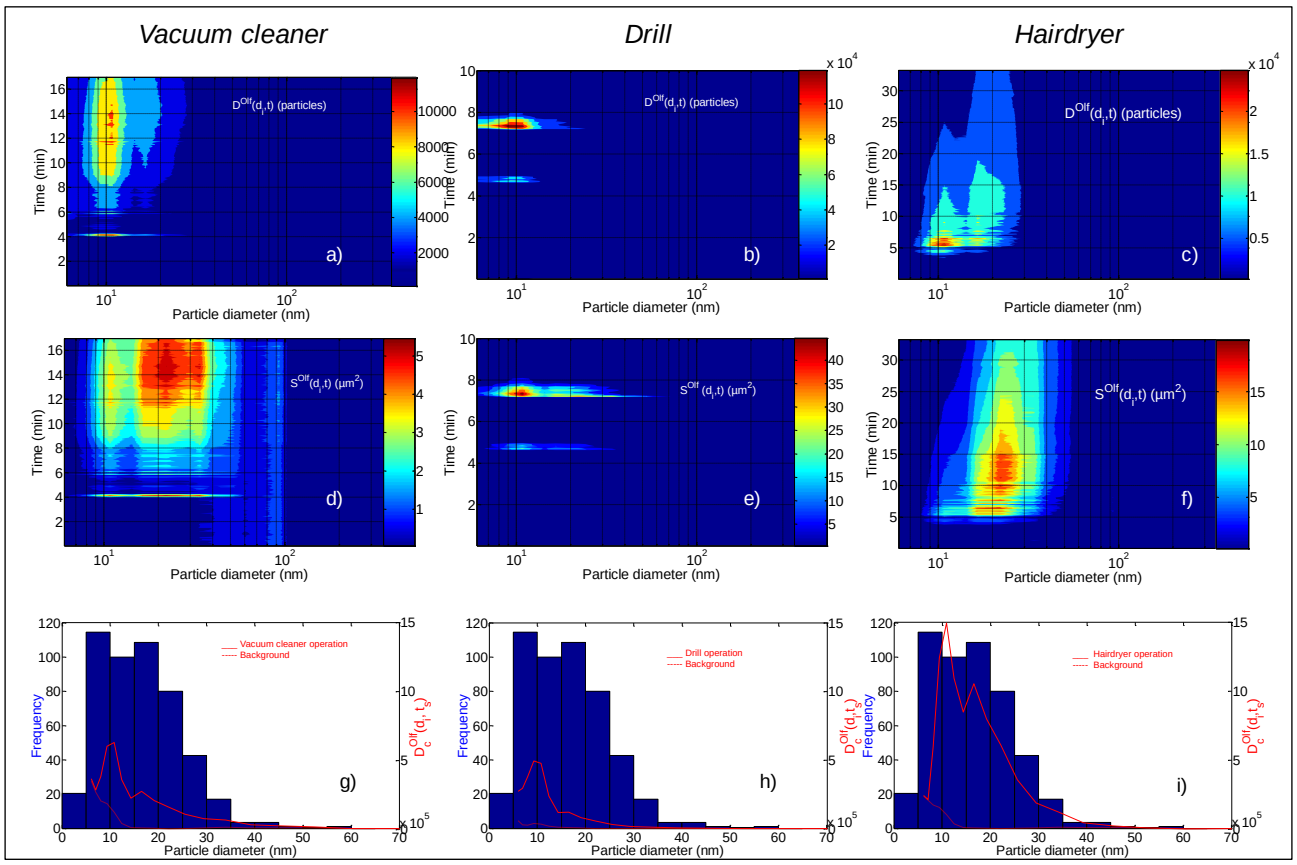

Fig. 3. Size number dose distributions $D^{Olf}(d_i,t)$. d, e, f: size surface area dose distributions $S^{Olf}(d_i,t)$, g, h, i: cumulative size number dose distribution $D_c^{Olf}(d_i,t_s)$ of particles deposited on the olfactory bulb upon inhalation following the operation for t_s min of a brush electric motor vacuum cleaner (t_s = 6 min) an electric drill (t_s = 1.5 min) and a hairdryer (t_s = 5 min) compared with the average value of the frequencies of the magnetite NPs retrieved by Maher et al. (2016) in brain tissue samples, as a function of the longest and of the shortest particle diameters.

Particle surface area doses represent an important piece of information because NPs, compared with larger-sized particles of the same chemical composition, can generate higher level of Reactive

Oxygen Species (ROS), due to their higher surface area per unit mass and to their surface reactivity (Oberdörster et al., 2005). ROS generation has been addressed as the main feature explaining toxic effects of inhaled NPs (Nel et al., 2006), such as DNA damage, unregulated cell signaling, changes in cell motility, citotoxicity, apoptosis and cancer initiation and promotion (Nel et al., 2006; Xia et al., 2008; Zhu et al., 2013).

The doses reported here represent a small fraction, respectively 0.51%, 0.50% and 0.57%, in terms of particle number metric ($D_c^{Olf}(t_s)$), and 0.15%, 0.27% and 0.43%, in terms of particle surface area metric ($S_c^{Olf}(t_s)$), of the doses deposited in the head region after the same operation time (respectively 7.5×10^8, 1.8×10^9, 4.6×10^8 particles and 2.1×10^6, 2.7×10^6, 2.7×10^5 μm^2, respectively) (Manigrasso et al., 2018). Nonetheless, they are toxicologically relevant, due to their possible translocation to brain (Oberdörster et al., 2005). On this point, Fig. 3 g, h, i compare the number size distribution of the total amount of particle deposited on the olfactory bulb after the appliance operation, $D_c^{Olf}(d_i,t_s)$, (continuous line) with the relevant doses due to the inhalation of background indoor aerosol concentration for the same time interval (dotted line). Bimodal size distributions with modes in between 9 and 11 nm and at 16.5 nm were observed well above the relevant background ones. The histogram in the same Fig. represents the average value of the frequencies of the magnetite NPs retrieved by Maher et al. (2016) in brain tissue samples, as a function of the longest and of the shortest particle diameters. The authors hypothesized that such NPs may have reached the brain directly through the olfactory bulb. The dimensions of these particles are almost the same of those deposited on the olfactory bulb, as estimated in this work. Their elimination, once they have reached the brain, has been reported to possibly proceed by means of the cerebrospinal fluid (CSF) through its connections to the nasal lymphatic system and to the blood circulation (Czerniawska, 1970; Oberdörster et al., 2009; Segal, 2000). More recently, Louveau et al. (2015) have discovered the existence of a meningeal lymphatic system that may represent a further route for CSF to leave the central nervous system.

Health concerns arise due to the role recognized to redox-active metals, such as manganese (Michalke and Fernsebner, 2014; Flynn and Susi, 2009; Santos et al., 2012), iron (Khan et al., 2006; Everett et al., 2018) and Cu (Huang et al., 1999a, 1999b; Fahmy and Cormier, 2009; Tabner et al., 2011) in neurodegenerative diseases, due to their ability to produce ROS. In particular, hot spot Cu and zinc, at higher concentrations than calcium and iron, have been observed, with high spatial correlation, in the amyloid β plaques present in Alzheimer's disease brain tissue samples (Miller et al. 2006). As to the persistence of metal NPs in brain, no much data are available. However, low elimination rates are

expected for insoluble NPs, considering also that their metabolic degradation is not envisaged (Geraets et al., 2014). For instance, Geraets et al. (2014) reported half-lives of titanium dioxide NPs in the range 28-650 days, depending on the TiO_2 particles and on the organ investigated. Specifically, as regards Cu NPs solubility, Wongrakpanich et al. (2016) reported that 50% dissolution of 4 nm Cu oxide NPs in RPMI-1640 media at 37 °C occurred over 1 h period, whereas 24 nm NPs took longer (over 24 h). The same authors showed that 24 nm CuO NPs elicit higher cytotoxicity and higher intracellular and mitochondrial ROS production than 4 nm CuO NPs. The authors argued that the 4 nm NP cytotoxicity proceeds through a pathway initiated by the extracellular release of Cu^{2+}, whereas for 24 nm CuO NPs, it seems to be due to the greater intracellular and mitochondria ROS production resulting for the more efficient intracellular access. Therefore, in terms of health effects, both the solubility and the size of Cu NPs are relevant. Moreover, the insoluble form is expected to be biopersistent and to undergo tissue accumulation following repeated exposures.

On this basis, it is relevant both to assess the size together with the metal composition of the NPs released by these appliances and to ascertain the copper indoor contamination, making distinction between its soluble and insoluble fractions, as discussed in the next sessions.

3.2 HR-FESEM Characterization

HR-FESEM observation and XEDS microanalyses were performed on filters after sampling of the aerosol emitted from appliances operated by brush electric motors, in order to obtain a qualitative description of individual particle morphology and elemental composition. Fig. 4 and Fig. 5 refer to aerosol sampled from the brush electric motor vacuum cleaner used at DW1. They are representative of what has been observed also for the other electric appliances as well (data not shown). Different morphologies of particles were observed. In particular, they were present both as single NPs (20-40 nm) (Fig. 4 A) and aggregated in clusters (Fig. 5 A). The NP diameters were assumed as the same of the equivalent spherical cross sectional area (Reid et al., 2003; Kandler et al., 2007; Choël et al., 2007) measured by means of HR-FESEM. It is worth observing that also particles of lower sizes (about 10 nm) have been observed, but due to their small dimensions HR-FESEM images were blurred and XEDS microanalysis was not possible to perform (Fig. 6).

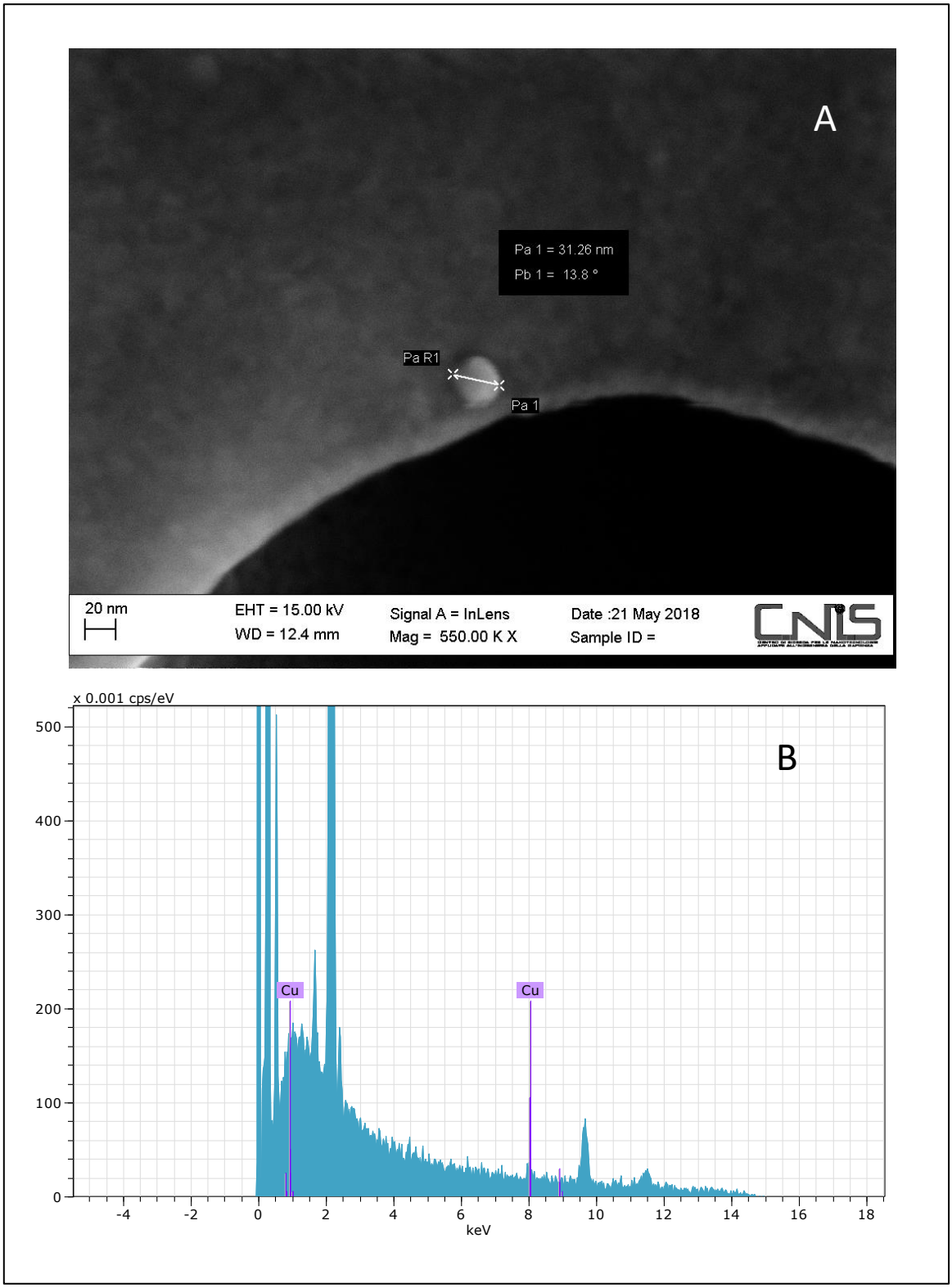

Fig. 4. HR-FESEM micrograph (A) and XEDS microanalysis (B) of nanoparticle emitted by the vacuum cleaner used in DW1.

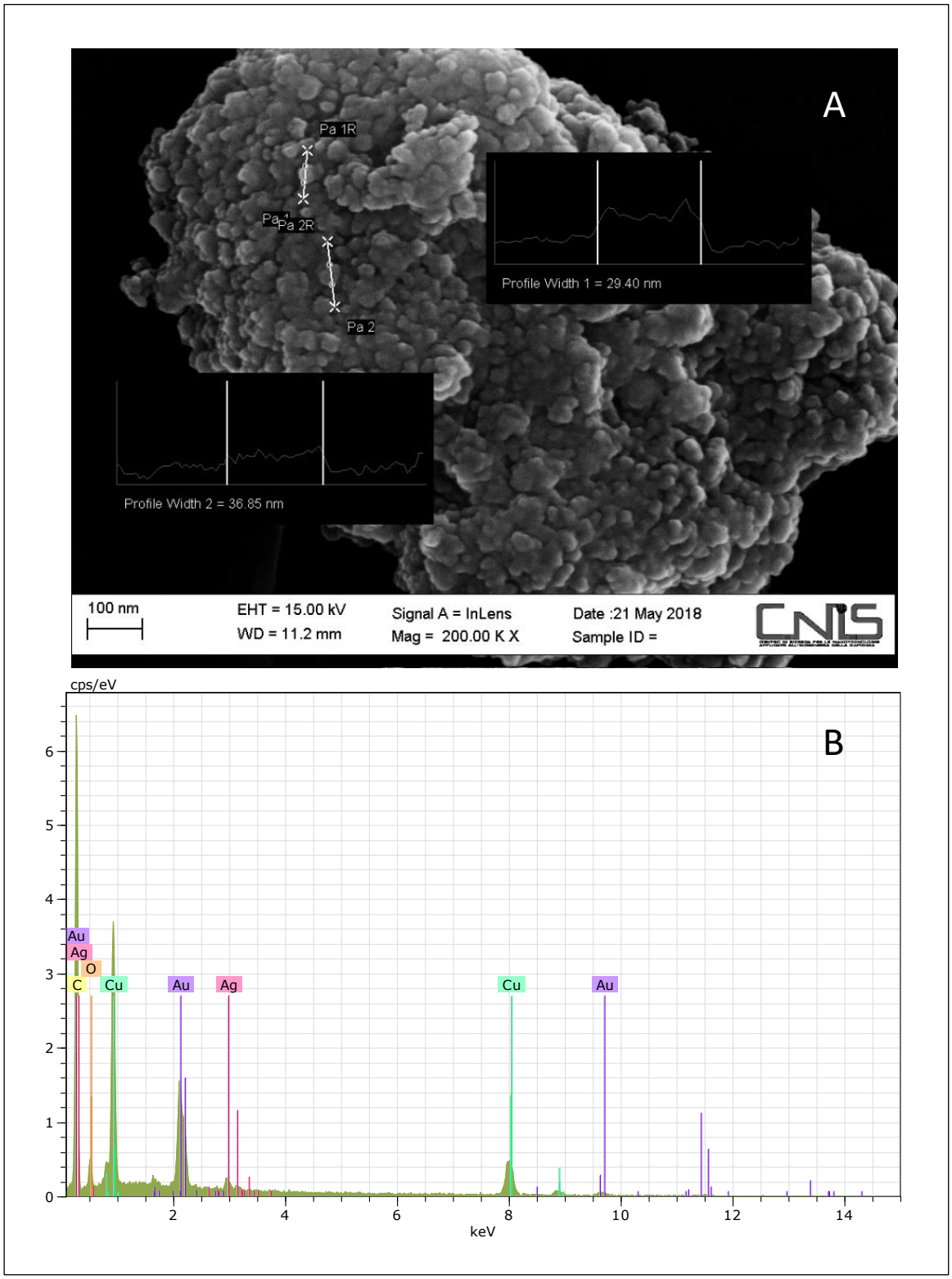

Fig. 5. HR-FESEM micrograph (A) and XEDS microanalysis (B) of a cluster of nanoparticles emitted by the vacuum cleaner used in DW1

In Fig. 4 B and Fig. 5 B spectra from XEDS microanalysis were reported and the presence of copper particles was confirmed for all the NPs found. In particular, Fig. 5 B shows the presence of oxygen, suggesting the possibility that Cu is present in the form of an oxide (CuO NPs). As reported in literature (Jeong et al., 2008), Cu NPs easily get oxidized and form particle-particle junctions when heat-treated at high temperature. It should be considered that also the polycarbonate filter may contribute to the oxygen signal, even if such eventuality seems unlike because the XEDS spectrum has been acquired on a particle of large size (1-2 μm). Moreover, the presence of Ag NPs (Fig. 5 B) may favor the formation of Cu NPs as aggregates or agglomerates (Fig. 5 A), even of large size, through some weak bonds between adjacent particles (Li et al., 2017). Generally, silver-coated copper powders are used wherever high conductivity (electrical and thermal) is required. In fact, the electrical conductivity of pure Cu is typically deteriorated at elevated temperatures due to oxidation and formation of non-conductive oxides on the surface (Li et al., 2016). Instead, the use of Cu together with Ag shows a considerably high electrical conductivity and a high oxidation resistance (Li et al., 2016; Li et al., 2017). From the spectrum shown in Fig. 5 B, it was possible to highlight the presence of other elements such as Au and C. The presence of Au is due to the treatment of gilding of the filter, necessary for the HR-FESEM XEDS analysis, while C may arise from graphite electrodes of the brush electric motors as well as from grease or lubricant from the motor, or else may also come from the polycarbonate membranes.

Our observations on Cu particles emitted by brush electric motors are in agreement with the findings of Szymczak et al. (2007), who studied the aerosol emissions of a professional vacuum cleaner. Using a MOUDI impactor, they measured broad Cu mass size distributions with modes of about 1-2 μm. Observing that the mass size distribution displayed a higher value for the backup filter than for the lower impactor stage, the authors inferred that a remarkable contribution of Cu NPs was also present. The abundant emission of Cu NPs in the emissions of such appliances is confirmed by the HR-FESEM reported in the present study, and by the highly time resolved aerosol number size distributions reported in a previous study (Manigrasso et al., 2017). Moreover, for the first time, this study shows the relevance of such NPs in terms of the related doses deposited on the olfactory bulb. The data reported in this paragraph refer to observation of aerosol emitted throughout a few minute operation time interval. A further step forward is to assess in real indoor environments how protracted in time the general population exposure to such NPs is (Section 3.3).

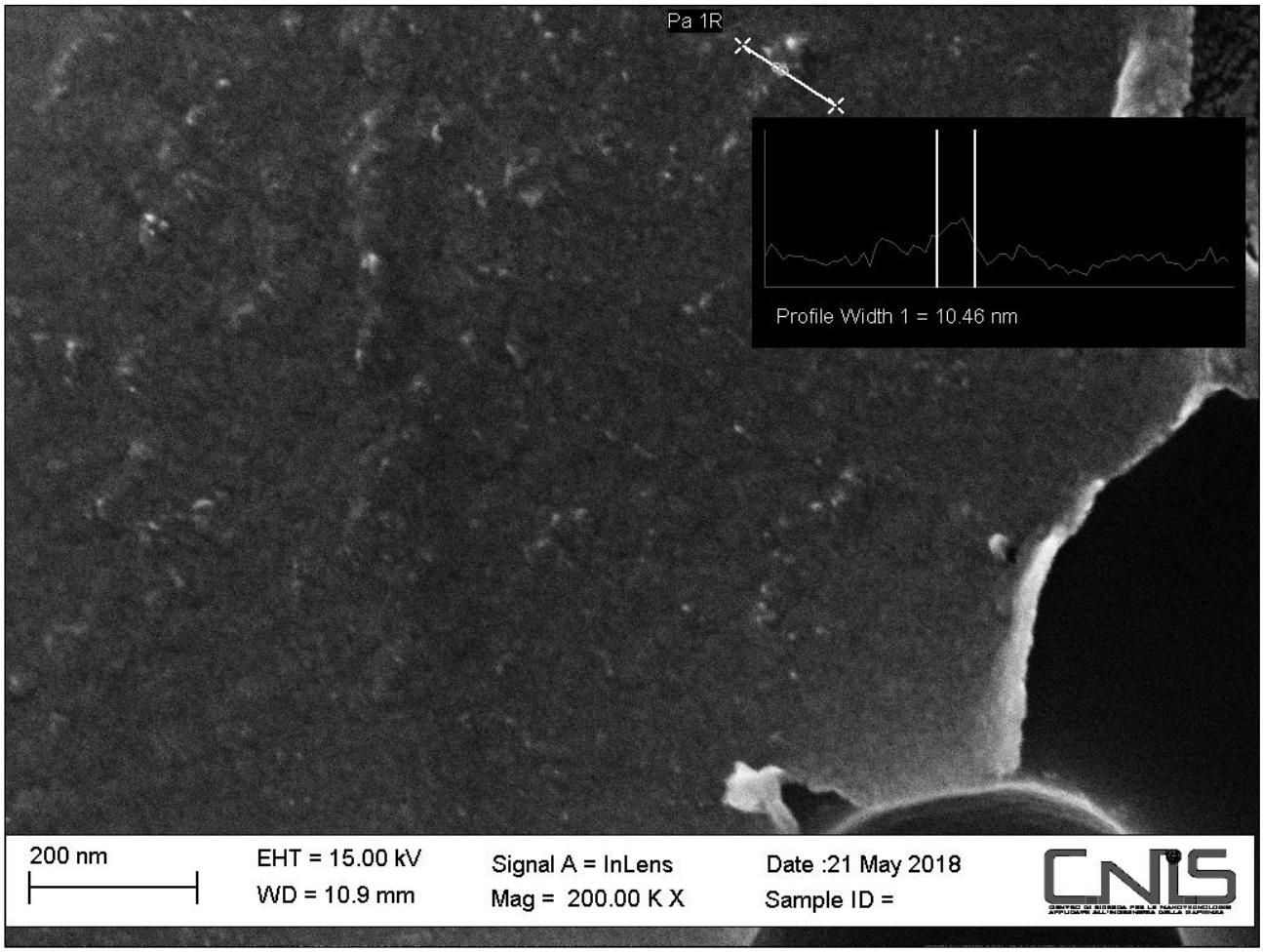

Fig. 6. HR-FESEM micrograph evidencing the presence of NPs of about 10 nm

3.3 Cu Levels in Real Scenarios Indoor Environments

In outdoor environments, Cu is considered as a reliable tracer of the non-combustive contribution to PM due to vehicular traffic. Its concentration in PM_{10} at urban sites is generally very highly correlated to that of Sb, as they share a common prevalent source: antimony trisuplhur and Cu are in fact present at high concentration in most brake pad formulations (Pakkanen et al., 2001, Canepari et al., 2010b; Grigoratos and Martini, 2015).

Fig. 7 shows the total Cu and Sb concentrations together with the PM_{10} levels measured throughout one year period in the indoor and outdoor environments at DW1 and DW2 dwellings, where a vacuum cleaner operated by brush and a vacuum cleaner brushless electric motors were respectively used. At both the considered sites, outdoor PM_{10} concentrations (Fig. 7 C and F) were higher during the winter season. Terni city is located in an intra-mountain depression and its peculiar geomorphological

characteristics cause, especially during the winter, severe episodes of atmospheric stability, which favour the accumulation of air pollutants (Ferrero et al., 2012; Massimi et al., 2017). Seasonal trend of the outdoor Cu and Sb concentrations (Fig. 7 A, B, D and E) was less pronounced because during summer the low humidity favours the resuspension of road dust. Furthermore, outdoor PM_{10} concentrations were slightly higher at the DW1 site (brush), more influenced by vehicular traffic than DW2 site (brushless). For the same reason, outdoor concentrations of Cu and Sb were generally higher at DW1 that at DW2. As shown in Fig. 8, outdoor concentrations of Cu and Sb are well correlated at both sites, further confirming the relevance of traffic as the main shared source of both elements. It is worth noting that the ratio Cu/Sb was of about 10, much higher than the value (about 4.5) reported in literature as diagnostic of brake pads contribution to PM (Grigoratos and Martini, 2015). This was probably due to the progressive diffusion in recent years of antimony-free brake pads (Martinez and Echeberria, 2016).

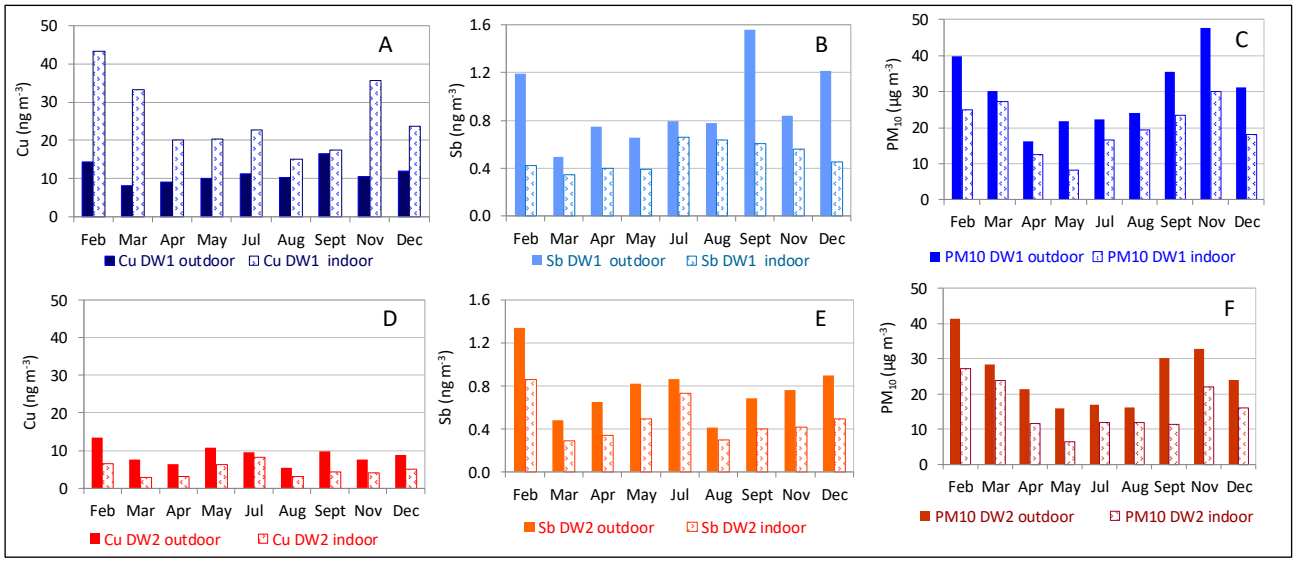

Fig. 7. PM_{10}, Cu and Sb concentration measured indoor and outdoor for DW1 (brush vacuum cleaner - A, B, C) and DW2 (brushless vacuum cleaner - D, E, F) dwellings throughout one-year period (9 aerosol samples).

Indoor concentrations of PM_{10} and of Sb were always significantly lower than indoor concentrations, both at DW1 and DW2 sites. The same happened for Cu concentrations measured at DW2 site (Fig. 7 D), whereas the reverse situation was observed at DW1 (Fig. 7 A) site. Linear regression analysis of Sb vs Cu indoor concentration at DW2 (brushless vacuum cleaner used) still maintains a good

correlation (Fig. 8), denoting that infiltration from outside of traffic-related particles was the main source of these two elements. At DW1 site (brush electric motor vacuum cleaner used), Sb and Cu were instead well correlated only outdoor, whereas they were totally uncorrelated indoor. These results clearly indicate the presence of a relevant Cu source in the DW1 indoor environment (indoor Cu levels higher than outdoor), very likely associated to the use of brush electric motor.

Descriptive statistic for indoor and outdoor Cu, Sb and PM_{10} concentration in the two dwellings are reported in Table 2. It is important to note that mean indoor Cu concentration resulted more than two-fold higher than outdoor at DW1 (p-value <0.001). These findings demonstrate that the contribute from the vacuum cleaner operated by brush motor to the indoor Cu concentration at DW1 was very relevant and significantly increased the exposure to Cu of inhabitants during all the year.

Table 2. Mean levels of PM_{10}, Cu and Sb found indoor and outdoor for DW1 and DW2 dwellings throughout one-year period (9 aerosol samples).

Electric Motor	Pollutant	in/out	Mean	SD	p-value
Brush (DW1)	PM_{10}	out	29.87	9.93	0.0044
		in	20.86	7.41	
	Cu	out	11.33	2.62	<0.001
		in	25.77	9.47	
	Sb	out	0.92	0.33	0.002
		in	0.50	0.12	
Brushless (DW2)	PM_{10}	out	25.19	8.72	0.023
		in	15.81	6.99	
	Cu	out	8.80	2.42	0.001
		in	4.85	1.84	
	Sb	out	0.77	0.27	0.020
		in	0.48	0.20	

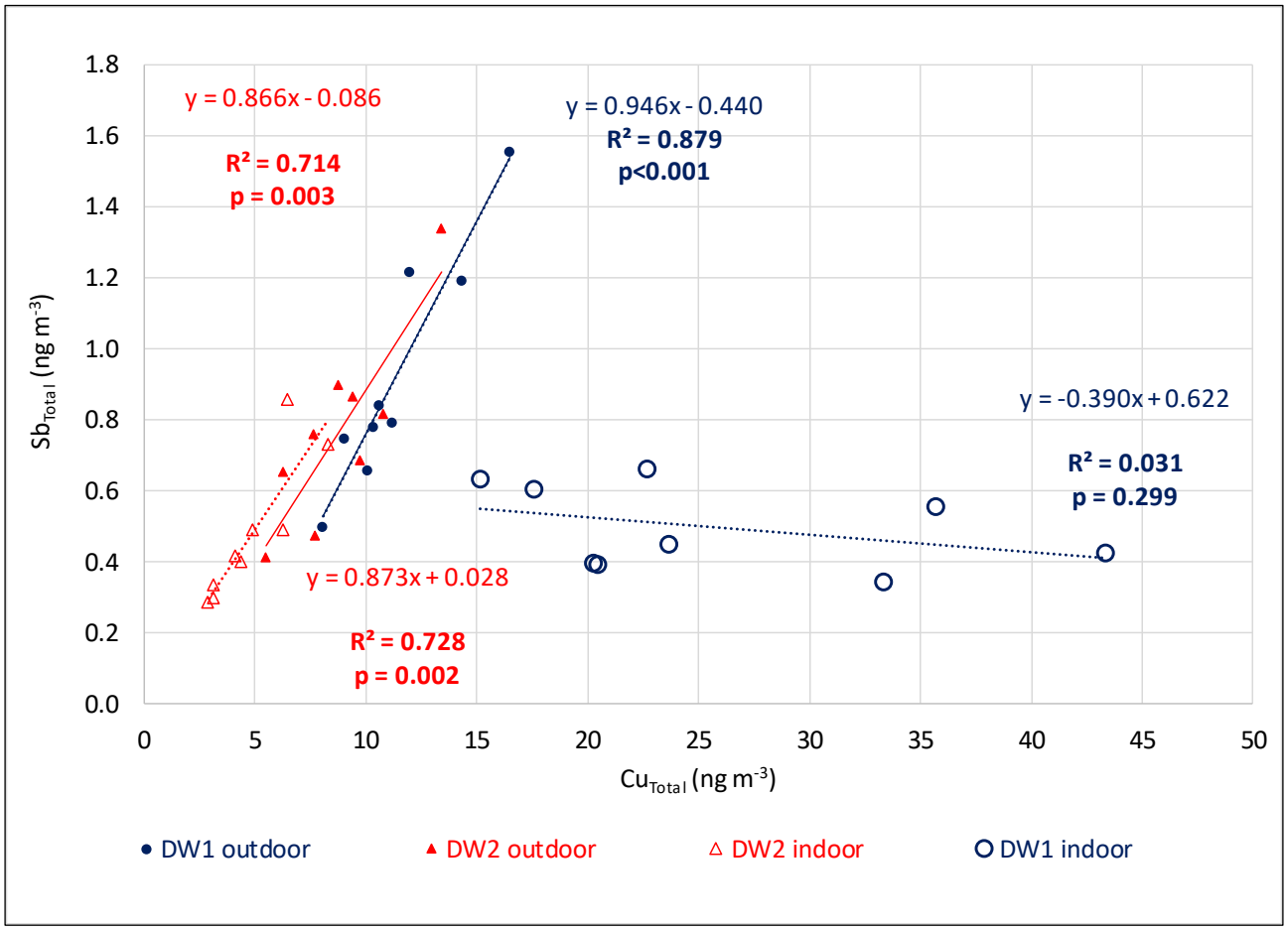

Fig. 8. Relationship between Cu and Sb concentrations measured indoor and outdoor for DW1 (brush vacuum cleaner) and DW2 (brushless vacuum cleaner) dwellings throughout one-year period (9 aerosol samples).

Fig. 9 shows the % contribution of the Cu soluble fraction to the total concentration. Similar percentages are observed both indoor and outdoor at DW2 site and outdoor at DW1 site. On the contrary, significantly lower values were measured indoor at DW1 site, suggesting that the indoor Cu emission throughout the whole year monitored brought about an important contribution of insoluble Cu particles. It is worth observing that insoluble NPs are more biopersistent and thus susceptible to undergo tissue accumulation. ANOVA test with Bonferroni post-hoc tests confirm that the percentages of the Cu soluble fraction recovered indoor at DW1 site were significantly different from all the other sets of measurements (p-values < 0.001 in all cases).

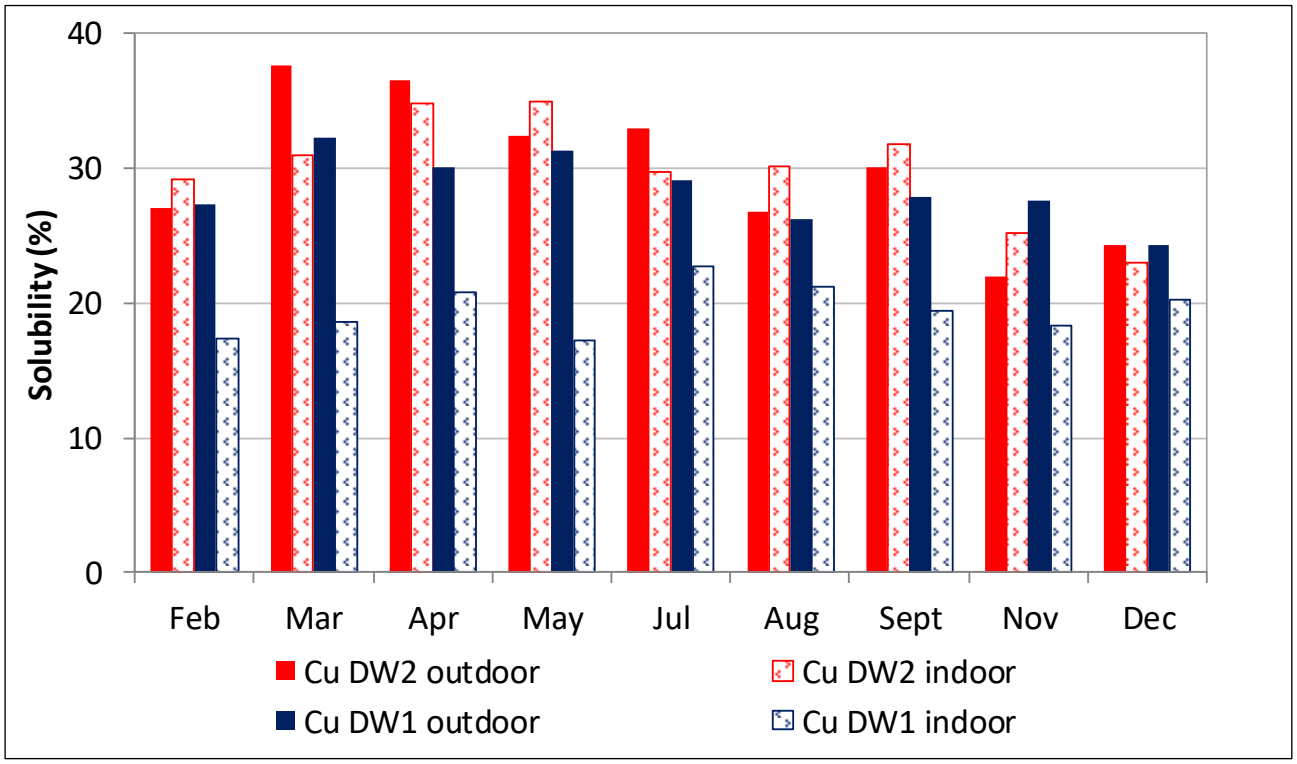

Fig. 9. Percentage of Cu solubility for indoor and outdoor aerosol samples collected in DW1 (brush vacuum cleaner) and DW2 (brushless vacuum cleaner) dwellings throughout one-year period (9 aerosol samples).

4. Conclusions

The data discussed show that 10^6-10^7 NPs deposit on the olfactory bulb throughout the use of appliance operated by brush electric motors (operation time 1.5-6 min). The main contribution arises form NPs of the same dimensions of those found by other authors in brain tissue samples. The health relevance of such NPs is not only due to their possible translocation to brain, but also to their chemical composition. As confirmed by HR-FESEM observations, they almost invariably contained Cu, an element addressed by many studies to play an important role on the onset of neurodegenerative diseases. To ascertain to what extent the general population is exposed, about 1-month averaged PM_{10} samples were collected in private dwellings throughout a year, and the relevant Cu content was determined. It was demonstrated that the operation of this kind of appliances caused indoor Cu concentrations more than two–fold higher than in outdoor, with a predominant contribution of the Cu insoluble fraction. Moreover, the exposure pattern is chronic. Cu NPs, for the amount they provide to the insoluble fraction, has the potential of undergoing harmful tissue accumulation.

The electric appliances considered in this study are widely diffused and are currently used in indoor environments with daily, and in some case more than daily, frequency. Every individual is directly exposed while utilizing them and indirectly, by simply residing in the environments where they have been used.

Acknowledgements

This research did not receive any specific grant from funding agencies in the public, commercial, or not-for-profit sectors.

The authors gratefully thank Mr. R. Palomba for his helpful support in carrying out the measurements and to Dr. M. Ristorini for her essential help in PM_{10} samplings. Thanks are also due to Dr. F. Mura for his kind assistance in HR-FESEM micrograph and XEDS microanalysis acquisition, and to ARA for MPPD version 3.01. This study was carried out as a part of the research program 2016-2018 of the National Institute for Insurance against Accidents at Work (INAIL) and of the framework agreement between INAIL and La Sapienza University of Rome.

References

Anderson, J.O., Thundiyil, J.G., Stolbach, A., 2012. Clearing the air: a review of the effects of particulate matter air pollution on human health. J. Med. Toxicol. 8, 166-175. DOI: 10.1007/s13181-011-0203-1.

Asgharian, B., Hofmann, W., Bergmann, R., 2001. Particle deposition in a multiple-path model of the human lung. Aerosol Sci. Technol. 34, 332-339. DOI: 10.1080/02786820119122.

Astolfi, M.L., Marconi, E., Protano, C., Vitali, M., Schiavi, E., Mastromarino, P., Canepari, S., 2018. Optimization and validation of a fast digestion method for the determination of major and trace elements in breast milk by ICP-MS. Analytica Chimica Acta, in press, DOI: 10.1016/j.aca.2018.07.037.

Bau, S., Witschger, O., Gensdarmes, F., Thomas, D., Borra, J.-P., 2010. Electrical properties of airborne nanoparticles produced by a commercial spark-discharge generator. J. Nanopart. Res. 12, 1989-1995. DOI : 10.1007/s11051-010-9856-y.

Brauer, M., Koutrakis, P., Spengler, J.D., 1989. Personal exposures to acidic aerosols and gases.

Environ. Sci. Technol. 23, 1408-1412. DOI: 10.1021/es00069a013.

Burris, H.H., Baccarelli, A.A., 2017. Air pollution and in utero programming of poor fetal growth. Epigenomics. 9, 213-216. DOI: 10.2217/epi-2017-0008.

CalEPA, 2004. Indoor Air Pollution in California. Air Resources Board, California Environmental Protection Agency, Sacramento, CA.

Canepari S., Cardarelli, E., Giuliano, A., Pietrodangelo, A., 2006a. Determination of metals, metalloids and non-volatile ions in airborne particulate matter by a new two-step sequential leaching procedure. Part A: Experimental design and optimisation. Talanta. 69, 581-587. doi: 10.1016/j.talanta.2005.10.024.

Canepari, S., Cardarelli, E., Pietrodangelo, A., Strincone, M., 2006b. Determination of metals, metalloids and non-volatile ions in airborne particulate matter by a new two-step sequential leaching procedure. Part B: Validation on equivalent real samples. Talanta. 69, 588-595. DOI: 10.1016/j.talanta.2005.10.023.

Canepari, S., Perrino, C., Astolfi, M. L., Catrambone, M., Perret, D., 2009. Determination of soluble ions and elements in ambient air suspended particulate matter: inter-technique comparison of XRF, IC and ICP for sample-by-sample quality control. Talanta. 77, 1821-1829. DOI: 10.1016/j.talanta.2008.10.029.

Canepari, S., Marconi, E., Astolfi, M. L., Perrino, C. 2010a. Relevance of Sb (III), Sb (V), and Sb-containing nano-particles in urban atmospheric particulate matter. Anal. Bioanal. Chem. 397, 2533-2542. DOI 10.1007/s00216-010-3818-1.

Canepari, S., Astolfi, M. L., Moretti, S., Curini, R., 2010b. Comparison of extracting solutions for elemental fractionation in airborne particulate matter. Talanta. 82, 834-844. DOI: 10.1016/j.talanta.2010.05.068.

Castellano, P., Canepari, S., Ferrante, R., L'Episcopo, N., 2012. Multiparametric approach for an exemplary study of laser printer emissions. J. Environ. Monit., 14, 446-454. DOI: 10.1039/c2em10696e.

Charvet, A., Bau, S., Paez Coy, N.E., Bemer, D., Thomas, D., 2014. Characterizing the effective density and primary particle diameter of airborne nanoparticles produced by spark discharge using mobility and mass measurements (tandem DMA/APM). J. Nanopart. Res. 16, 2418. DOI 10.1007/s11051-014-2418-y.

Choël, M., Deboudt, K., and Flament, P., 2007. Evaluation of quantitative procedures for x-ray microanalysis of environmental particles. Microsc. Res. Techniq. 70, 996–1002. DOI:10.1002/jemt.20510, 2007.

Czerniawska, A., 1970. Experimental investigations on the penetration of 198Au from nasal mucous membrane into cerebrospinal fluid. Acta Otolaryngol. 70, 58-61.

Darbre, P.D., 2018. Overview of air pollution and endocrine disorders. Int. J. Gen. Med. 11, 191-207. DOI: 10.2147/IJGM.S102230.

Drago, G., Perrino, C., Canepari, S., Ruggieri, S., L'Abbate, L., Longo, V., Colombo, P., Frasca, D., Balzan, M., Cuttitta, G., Scaccianoce, G., Piva, G., Buccheri, S., Melis, M., Viegi, G., Cibella, F., 2018. Relationship between domestic smoking and metals and rare earth elements concentration in indoor PM 2.5. Environ. Res. 165, 71-80. DOI: 10.1016/j.envres.2018.03.026.

Everett, J., Collingwood, J.F., Tjendana-Tjhin, V., Brooks, J., Lermyte, F., Plascencia-Villa, G., Hands-Portman, I., Dobson, J., Perry, G., Telling, N.D., 2018. Nanoscale synchrotron X-ray speciation of iron and calcium compounds in amyloid plaque cores from Alzheimer's disease subjects. Nanoscale. DOI: 10.1039/c7nr06794a.

Fahmy, B., Cormier, S.A., 2009. Copper oxide nanoparticles induce oxidative stress and cytotoxicity in airway epithelial cells. Toxicol In Vitro. 23, 1365-1371. DOI: 10.1016/j.tiv.2009.08.005.

Flynn, M.R., Susi, P., 2009. Neurological risks associated with manganese exposure from welding operations--a literature review. Int J Hyg Environ Health. 212, 459-469. doi: 10.1016/j.ijheh.2008.12.003.

Frasca, D., Marcoccia, M., Tofful, L., Simonetti, G., Perrino, C., Canepari, S., 2018. Influence of advanced wood-fired appliances for residential heating on indoor air quality. Chemosphere. 211, 62-71. DOI: 10.1016/j.chemosphere.2018.07.102.

Ferrero, L., Cappelletti, D., Moroni, B., Sangiorgi, G., Perrone, M. G., Crocchianti, S., Bolzacchini, E. (2012). Wintertime aerosol dynamics and chemical composition across the mixing layer over basin valleys. Atmospheric environment, 56, 143-153. DOI: 10.1016/j.atmosenv.2012.03.071.

Garcia, G.J., Schroeter, J.D., Kimbell, J.S., 2015. Olfactory deposition of inhaled nanoparticles in humans. Inhal. Toxicol. 27, 394-403. DOI: 10.3109/08958378.2015.1066904.

Geraets, L., Oomen, A.G., Krystek, P., Jacobsen, N.R., Wallin, H., Laurentie, M., Verharen, H.W., Brandon, E.F., de Jong, W.H., 2014. Tissue distribution and elimination after oral and intravenous administration of different titanium dioxide nanoparticles in rats. Part Fibre Toxicol. 11, 30. DOI: 10.1186/1743-8977-11-30.

Grigoratos, T., Martini, G., 2015. Brake wear particle emissions: a review. Environ. Sci. Pollut. Res. 22, 2491-2504. DOI: 10.1007/s11356-014-3696-8.

Hoek, G., Boogaard, H., Knol, A., de Hartog, J., Slottje, P., Ayres, J.G., Borm, P., Brunekreef, B., Donaldson, K., Forastiere, F., Holgate, S., Kreyling, W.G., Nemery, B., Pekkanen, J., Stone, V., Wichmann, H.E., van der Sluijs, J., 2010. Concentration response functions for ultrafine particles and all-cause mortality and hospital admissions: results of a European expert panel elicitation. Environ. Sci. Technol. 44, 476-482. DOI: 10.1021/es9021393.

Hsu, D.J., Huang, H.L., Sheu, S.C., 2012. Characteristics of air pollutants and assessment of potential exposure in spa centers during aromatherapy. Environ. Eng. Sci. 29, 79-85. DOI: 10.1089/ees.2011.0004.

Huang, H.L., Tsai, T.J., Hsu, N.Y., Lee, C.C., Wu, P.C., Su, H.J., 2012. Effects of essential oils on the formation of formaldehyde and secondary organic aerosols in an aromatherapy environment. Build. Environ. 57, 120-125. DOI: 10.1016/j.buildenv.2012.04.020.

Huang, X., Atwood, C. S., Hartshorn, M. A., Multhaup, G., Goldstein, L.E., Scarpa, R.C., Cuajungco, M.P., Gray, D.N., Lim, J., Moir, R.D., Tanzi, R.E., Bush, A.I., 1999a. The Aβ peptide of Alzheimer's disease directly produces hydrogen peroxide through metal ion reduction. Biochem. 38, 7609-7616. DOI: 10.1021/bi990438f.

Huang, X., Cuajungco, M.P., Atwood, C.S., Hartshorn, M.A., Tyndall, J.D.A., Hanson, G.R., Stokes,

K.C., Leopold, M., Multhaup, G., Goldstein, L.E., Scarpa, R.C., Saunders, A.J., Lim, J., Moir, R.D., Glabe, C., Bowden, E.F., Masters, C.L., Fairlie, D.P., Tanzi, R.E., Busha, A.I., 1999b. Cu(II) potentiation of Alzheimer Aβ neurotoxicity. Correlation with cell-free hydrogen peroxide production and metal reduction. J. Biol. Chem. 274, 37111-37116.

Hubal, E.A.C., Sheldon, L.S., Burke, J.M., McCurdy, T.R., Berry, M.R., Rigas, M.L., Zartarian, V.G., Freeman, N.C., 2000. Children's exposure assessment: a review of factors influencing children's exposure, and the data available to characterize and assess that exposure. Environ. Health Perspect. 108, 475-486.

IARC, 2013. IARC: Outdoor air pollution a leading environmental cause of cancer deaths. Available at: https://www.iarc.fr/en/media-centre/iarcnews/pdf/pr221_E.pdf. (last accessed 06 June 2018).

ICRP, 1994. Human respiratory tract model for radiological protection. A report of a task group of the International Commission on Radiological Protection. Ann. ICRP 24, 1-482.

Jeong, C.-H., Evans, G.J., 2009. Inter-comparison of a fastmobility particle sizer and a scanning mobility particle sizer incorporating an ultrafine water based condensation particle counter. Aerosol Sci. Technol. 43, 364-373. DOI: 10.1080/02786820802662939

Jeong, S., Woo, K., Kim, D., Lim, S., Kim, J.S., Shin, H., Xia, Y., Moon, J., 2008. Controlling the thickness of the surface oxide layer on Cu nanoparticles for the fabrication of conductive structures by Ink-Jet printing, Adv. Funct. Mater. 18, 679–686. DOI: 10.1002/adfm.200700902.

Kandler, K., Benker, N., Bundke, U., Cuevas, E., Ebert, M., Knippertz, P., Rodríguez, S., Schütz, L., and Weinbruch, S., 2007. Chemical composition and complex refractive index of Saharan Mineral Dust at Izaˇna, Tenerife (Spain) derived by electron microscopy. Atmos. Environ. 41, 8058–8074.

Khan, A., Dobson, J.P., Exley, C., 2006. Redox cycling of iron by Abeta42. Free Radic Biol Med. 40, 557-569. DOI: 10.1016/j.freeradbiomed.2005.09.013.

Laussmann, D., Helm, D., 2011. Air change measurements using tracer gases: methods and results. Significance of air change for indoor air quality. In: Mazzeo, M. (Ed.), Chemistry, Emission Control, Radioactive Pollution and Indoor Air Quality. InTech, Rijeka, Croatia, pp. 365-406.

Levesque, S., Surace, M.J., McDonald, J., Block, M.L., 2011. Air pollution & the brain: Subchronic diesel exhaust exposure causes neuroinflammation and elevates early markers of neurodegenerative disease. J. Neuroinflammation. 8, 105. DOI: 10.1186/1742-2094-8-105.

Li, J., Li, Y., Wang, Z., Bian, H., Hou, Y., Wang, F., Xu, G., Liu, B., Liu, Y., 2016. Ultrahigh oxidation resistance and high electrical conductivity in Copper-Silver powder. Sci. Rep. 6, 39650. DOI: 10.1038/srep39650.

Li, N., Sioutas, C., Cho, A., Schmitz, D., Misra, C., Sempf, J., Wang, M., Oberley, T., Froines, J., Nel, A., 2003. Ultrafine particulate pollutants induce oxidative stress and mitochondrial damage. Environ. Health Perspect. 11, 455-460.

Li, W., Hu, D., Li, L., Li, C.-F., Jiu, J., Chen, C., Ishina, T., Sugahara, T., Suganuma, K., 2017. Printable and flexible Copper−Silver alloy electrodes with high conductivity and ultrahigh oxidation resistance. ACS Appl. Mater. Interfaces. 9, 24711−24721. DOI: 10.1021/acsami.7b05308.

Li, X., Yan, C., Patterson, R.F., Zhu, Y., Yao, X., Zhu, Y., Ma, S., Qiu, X., Zhu, T., Mei Zheng, M., 2016. Modeled deposition of fine particles in human airway in Beijing, China. Atmos. Environ. 124, 387-395. doi: 10.13227/j.hjkx.201610040.

Liu, J., Fung, D., Jiang, J., Zhu, Y., 2014. Ultrafine particle emissions from essential-oil-based mosquito repellent products. Indoor Air 24, 327-335. DOI: 10.1111/ina.12080.

Louveau, A., Smirnov, I., Keyes, T.J., Eccles, J.D., Rouhani, S.J., Peske, J.D., Derecki, N.C., Castle, D., Mandell, J.W., Lee, K.S., Harris, T.H., Kipnis, J., 2015. Structural and functional features of central nervous system lymphatic vessels. Nature. 523, 337-341. DOI: 10.1038/nature14432.

Maher, B.A., Ahmed, I.A.M., Karloukovski, V., MacLaren, D.A., Foulds, P.G., Allsop, D., Mann, D.M.A., Torres-Jardón, R., Calderon-Garciduenas, L., 2016. Magnetite pollution nanoparticles in the human brain. P. Natl. Acad. Sci. USA 113, 10797-10801. doi: 10.1073/pnas.1605941113.

Manigrasso, M., Avino, P., 2012. Fast evolution of urban ultrafine particles: implications for deposition doses in the human respiratory system. Atmos. Environ. 51, 116-123. DOI: 10.1016/j.atmosenv.2012.01.039.

Manigrasso, M., Stabile, L., Avino, P., Buonanno, G., 2013. Influence of measurement frequency on the evaluation of short-term dose of sub-micrometric particles during indoor and outdoor generation events. Atmos. Environ. 67, 130-142. DOI: 10.1016/j.atmosenv.2012.10.059.

Manigrasso, M., Guerriero, E., Avino, P., 2015. Ultrafine particles in residential indoors and doses deposited in the human respiratory system. Atmosphere. 6, 1444-1461. DOI: 10.3390/atmos6101444.

Manigrasso, M., Vitali, M., Protano, C., Avino, P., 2017. Temporal evolution of ultrafine particles and of alveolar deposited surface area from main indoor combustion and non-combustion sources in a model room. Sci. Total Environ. 15, 1015-1026. DOI: 10.1016/j.scitotenv.2017.02.048.

Manigrasso, M., Vitali, M., Protano, C., Avino, P., 2018. Ultrafine particles in domestic environments: Regional doses deposited in the human respiratory system. Environ Int. 118, 134-145. DOI: 10.1016/j.envint.2018.05.049.

Mannucci, P.M., Harari, S., Martinelli, I., Franchini, M., 2015. Effects on health of air pollution: a narrative review. Intern. Emerg. Med. 10, 657-662. DOI: 10.1007/s11739-015-1276-7.

Martinez, A. M., Echeberria, J. (2016). Towards a better understanding of the reaction between metal powders and the solid lubricant Sb2S3 in a low-metallic brake pad at high temperature. Wear, 348, 27-42. DOI:10.1016/j.wear.2015.11.014.

Massimi, L., Ristorini, M., Eusebio, M., Florendo, D., Adeyemo, A., Brugnoli, D., Canepari, S., 2017. Monitoring and evaluation of Terni (Central Italy) air quality through spatially resolved analyses. Atmosphere. 8, 200. DOI: 10.3390/ecas2017-04129.

Michalke, B., Fernsebner, K., 2014. New insights into manganese toxicity and speciation. J Trace Elem Med Biol. 28, 106-116. doi: 10.1016/j.jtemb.2013.08.005.

Miller, L.M., Wang, Q., Telivala, T.P., Smith, R.J., Lanzirotti, A., Miklossy, J., 2006. Synchrotron-based infrared and X-ray imaging shows focalized accumulation of Cu and Zn co-localized with beta-amyloid deposits in Alzheimer's disease. J Struct Biol. 155, 30-37. DOI: 10.1016/j.jsb.2005.09.004

Morawska, L., Ayoko, G.A., Bae, G.N., Buonanno, G., Chao, C.Y.H., Clifford, S., Fu, S.C., Hänninen, O., He, C., Isaxon, C., Mazaheri, M., Salthammer, T., Waring, M.S., Wierzbicka, A., 2017.

Airborne particles in indoor environment of homes, schools, offices and aged care facilities: The main routes of exposure. Environ. Int. 108, 75-83. DOI: 10.1016/j.envint.2017.07.025.

Nel, A., Xia, T., Mädler, L., Li, N., 2006. Toxic potential of materials at the nanolevel. Science. 311, 622-627. DOI: 10.1126/science.1114397.

Noh, J., Sohn, J., Cho, J., Kim, C., Shin, D.C., 2016. YIA 02-02 long-term effects of fine particulate matter exposures on major adverse cardiovascular events. J. Hypertens. 34, e202. DOI: 10.1097/01.hjh.0000500437.46224.7e.

Oberdörster, G., Elder, A., Rinderknecht, A., 2009. Nanoparticles and the brain: cause for concern?. J Nanosci Nanotechnol. 9, 4996-5007. DOI: 10.1166/jnn.2009.GR02.

Oberdörster, G., Oberdörster, E., Oberdörster, J., 2005. Nanotoxicology: an emerging discipline evolving from studies of ultrafine particles. Environ Health Perspect. 113, 823-839. DOI: 10.1289/ehp.7339.

Pagano, P., De Zaiacomo, T., Scarcella, E., Bruni, S., Calamosca, M., 1996. Mutagenic activity of total and particle-sized fractions of urban particulate matter. Environ. Sci. Technol. 30, 3512-3516. DOI: 10.1021/es960182q.

Pakkanen, T.A., Loukkola, K., Korhonen, C.H., Aurela, M., Mäkelä, T., Hillamo, R.E., Aarnio, P., Koskentalo, T., Kousa, A., Maenhaut, W., 2001. Sources and chemical composition of atmospheric fine and coarse particles in the Helsinki area. Atmospheric Environ. 35, 5381-5391. DOI: 10.1016/S1352-2310(01)00307-7.

Protano, C., Manigrasso, M., Avino, P., Sernia, S., Vitali, M., 2016. Second-hand smoke exposure generated by new electronic devices (IQOS® and e-cigs) and traditional cigarettes: submicron particle behaviour in human respiratory system. Ann. Ig. 28, 109-112. DOI: 10.7416/ai.2016.2089.

Protano, C., Manigrasso, M., Avino, P., Vitali, M., 2017. Second-hand smoke generated by combustion and electronic smoking devices used in real scenarios: Ultrafine particle pollution and age-related dose assessment. Environ. Int. 107, 190-195. DOI: 10.1016/j.envint.2017.07.014.

Reid, J.S., Jonsson, H.H., Maring, H.B., Smirnov, A., Savoie, D.L., Cliff, S.S., Reid, E.A.,

Livingston, J.M., Meier, M.M., Dubovik, O., and Tsay, S.C., 2003. Comparison of size and morphological measurements of coarse mode dust particles from Africa. J. Geophys. Res., 108, 8593, DOI: 10.1029/2002JD002485.

Roth, C., Ferron, G.A., Karg, E., Lentner, B., Schumann, G., Takenaka, S., Heyder, J., 2004. Generation of ultrafine particles by spark discharging. Aerosol Sci. Technol. 38, 228–235. DOI: 10.1080/02786820490247632.

Santos, D., Milatovic, D., Andrade, V., Batoreu, M.C., Aschner, M., Marreilha dos Santos, A.P., 2012. The inhibitory effect of manganese on acetylcholinesterase activity enhances oxidative stress and neuroinflammation in the rat brain. Toxicology. 292, 90-98. DOI: 10.1016/j.tox.2011.11.017.

Sarwar, G., Olson, D.A., Corsi, R.L., Weschler, C.J., 2004. Indoor fine particles: the role of terpene emissions from consumer products. J. Air Waste Manage. Assoc. 54, 367-377. DOI: 10.1080/10473289.2004.10470910.

Scungio M., Vitanza T., Stabile L., Buonanno G., Morawska L., 2017. Characterization of particle emission from laser printers. Sci Total Environ. 586, 623-630. DOI: 10.1016/j.scitotenv.2017.02.030.

Segal, M.B., 2000 The choroid plexuses and the barriers between the blood and the cerebrospinal Fluid. Cell. and Mol. Neurobiol. 20, 183–196.

Śmiełowska, M., Marć, M., Zabiegała, B., 2017. Indoor air quality in public utility environments-a review. Environ. Sci. Pollut. Res. 24, 11166-11176. DOI: 10.1007/s11356-017-8567-7.

Stabile, L., Buonanno, G., Avino, P., Frattolillo, A., Guerriero E., 2018. Indoor exposure to particles emitted by biomass-burning heating systems and evaluation of dose and lung cancer risk received by population. Environ Pollut. 235, 65-73. DOI: 10.1016/j.envpol.2017.12.055.

Szymczak, W., Menzel, N., Keck, L., 2007. Emission of ultrafine copper particles by universal motors controlled by phase angle modulation. Aerosol Sci. 38, 520–531. DOI: 10.1016/j.jaerosci.2007.03.002.

Tabner, B.J., Mayes, J., Allsop, D., 2011. Hypothesis: soluble Aβ oligomers in association with redox-activemetal ions are the optimal generators of reactive oxygen species in Alzheimer's disease.

Int. J. Alzheimers Dis. 546380. DOI: 10.4061/2011/546380.

TSI Particle Technology, 2015. Available online. http://www.tsi.com/Fast-Mobility-Particle-Sizer-Spectrometer-3091/# (last accessed on 13 June 2018).

Veleminsky. M- Jr., Hanzl. M-, Sram. R.J., 2016. The impact of air pollution in the Southern Bohemia Region on fetuses and newborns. Neuro Endocrinol. Lett. 37(suppl 2), 52-57.

Wang, Y., Xiong. L., Tang, M., 2017. Toxicity of inhaled particulate matter on the central nervous system: neuroinflammation, neuropsychological effects and neurodegenerative disease. J. Appl. Toxicol. 37, 644-667. DOI: 10.1002/jat.3451.

Westergaard, N., Gehring, U., Slama, R., Pedersen, M., 2017. Ambient air pollution and low birth weight - are some women more vulnerable than others? Environ. Int. 104, 146-154. DOI: 10.1016/j.envint.2017.03.026.

WHO, 2018. Air Pollution. WHO Global Ambient Air Quality Database (update 2018). Available at: http://www.who.int/airpollution/data/cities/en/ (last accessed 06 June 2018).

Wongrakpanich, A., Mudunkotuwa, I.A., Geary, S.M., Morris, A.S., Mapuskar, K.A., Spitz, D.R., Grassian, V.H., Salem A.K., 2016. Size-dependent cytotoxicity of copper oxide nanoparticles in lung epithelial cells. Environ Sci Nano. 3, 365-374. DOI: 10.1039/C5EN00271K.

Xia T., Kovochich M., Liong M., Mädler L., Gilbert B., Shi H., Yeh J.I., Zink J.I., Nel A.E., 2008. Comparison of the mechanism of toxicity of zinc oxide and cerium oxide nanoparticles based on dissolution and oxidative stress properties. ACS Nano. 2, 2121-2134. DOI: 10.1021/nn800511k.

Zhu, X., Hondroulis, E., Liu, W., Li, C.Z., 2013. Biosensing approaches for rapid genotoxicity and cytotoxicity assays upon nanomaterial exposure. Small. 9, 1821-1830. DOI: 10.1002/smll.201201593.

2.3. (C) Spatially-Resolved Analyses of PM for Localization and Impact Assessment of Emission Sources

The study of the spatial distribution of PM chemical compounds is essential for a reliable identification of emission sources, the evaluation of particle dispersion over the territory and the assessment of personal exposure. However, due to the very high cost of a network based on traditional PM samplers, ambient air quality assessment and epidemiological studies are usually based on measurements taken at a few sampling points. Consequently, to obtain a reliable assessment of population exposure, the information collected at these few points needs to be extended to wider areas by evaluating the dispersion properties of pollutants.

Typically, PM dispersion is estimated through mathematical models, which are usually used for the definition of targeted strategies to control atmospheric pollution. The modeling approach offers a series of advantages, such as the reduction of time and costs and the possibility of covering very large areas. However, it simplifies the reality and may not be able to properly describe the complexity of PM transport and transformation processes. Hence, the evaluation of particle dispersion through mathematical models is a quite complex issue in particularly polluted areas, where PM sources are various and variable. Moreover, the reliability of dispersion models needs to be in any case verified through the acquisition of experimental data. Therefore, there is an increasing demand for low-cost air quality monitoring techniques that can be easily applied to evaluate the spatial distribution of PM chemical compounds.

Over the last few decades, the use of cosmopolite organisms to assess air pollution has developed notably and low-cost biomonitoring methods have been widely used to evaluate pollutant concentrations in the environment for integrated measurements over time. Leaf deposition and accumulative species, if properly calibrated, can give valuable information about deposition of atmospheric elements. However, the reliability of the biological monitoring for high spatial resolution measurements of PM elemental components still has to be investigated. Indeed, there are no many studies that have examined simultaneously at several sites the possible correlation between biomonitoring and traditional analyses of PM. This can be ascribed to the very high costs associated with a monitoring network based on traditional PM samplers. For this reason, in the last few years, a self-powered, automatic and very-low volume device for PM sampling on membrane filters (suitable for subsequent chemical analyses) has been developed with the purpose of allowing spatially-resolved determination of PM chemical components. Since the innovative sampler assures long-term

(1-2 months) collection of PM, it can work autonomously for long periods of time, thus allowing a good representativeness of data and a substantial reduction of maintenance costs of the monitoring network. The sampler was employed in a wide and dense network across Terni, an urban and industrial hot-spot of Central Italy (23 sampling sites, about 1 km between each other), for 15 consecutive months, during which the spatial distribution of PM_{10} mass and elements was evaluated and mapped. To verify the reliability of the biomonitoring techniques, lichen transplants (*Evernia prunastri* (L.) Ach.) and leaf deposition on riparian species (*Arundo donax* (L.)) were used, along with the very-low volume sampler, for the assessment of atmospheric element concentrations and for the evaluation of the impact of PM anthropogenic emission sources.

The new experimental approach, based on the mapping of spatially-resolved PM chemical data, allows to obtain high spatial resolution information about PM concentration and chemical composition and is a powerful tool for a reliable assessment of population exposure to PM air pollutants. This approach also promises to be effective for optimization and validation of dispersion models and will allow further investigations on relationships between adverse outcomes for human health and PM chemical composition and sources, useful to plan the mitigation measures that are necessary to protect citizens health in the area of study.

2.3.1. (C1) Monitoring and Evaluation of Terni (Central Italy) Air Quality through Spatially-Resolved Analyses

Atmosphere (2017), *8*(10), 200

Lorenzo Massimi [a,*], Martina Ristorini [a], Marta Eusebio [a], Darla Florendo [b], Adeola Adeyemo [b], Davide Brugnoli [a], Silvia Canepari [a]

[a] Department of Chemistry, Sapienza University of Rome, Piazzale Aldo Moro, 5, 00185 Roma;
[b] School of Chemistry & Pharmaceutical Sciences, DIT—Dublin Institute of Technology, Kevin Street, Dublin 2, Ireland.

Abstract: A study of spatial variability of PM_{10} elemental components was conducted in Terni city (Central Italy), situated in an intramountain depression characterized by the presence of several particulate matter emission sources. The meteorological conditions of the Terni basin limit the dispersion and enhance the accumulation of atmospheric pollutants. Thanks to the utilization of new smart samplers, used for the first time and working in parallel at 23 sampling sites, spatially resolved data were obtained. Localizations of the samplers were chosen in order to evaluate the impact of different local PM_{10} sources. Chemical composition of the samples was determined in combination with a chemical fractioning procedure that allowed us to discriminate water-soluble and residual fractions of analyzed elements in which proved to be a valuable approach for increasing selectivity of elements as source tracers. Spatial variability of elements underlined the contribution of local emission sources and the different dispersion capacity of each element. The city of Terni resulted to be an ideal area to test and validate a new experimental method for the acquisition of spatially resolved data providing the possibility to properly evaluate the spatial variability of PM_{10} and its chemical components.

Keywords: Terni air quality; particulate matter; PM_{10}; spatially resolved data; spatial variability; dispersion capacity; smart samplers; chemical fractionation; emission sources; source tracers; chemical source profiles.

1. Introduction

Particulate matter air pollution is an air-suspended mixture of solid and liquid particles that vary in size, shape, chemical composition, solubility and origin [1]. Its direct and indirect effects on human health and on the environment have led to numerous studies focusing upon its complex composition and toxicology [2]. One of the most efficient tools for the formulation of better control strategies for the atmospheric pollutant is the PM source apportionment, relevant to identify the role of different particulate matter emission sources. Typically, in air pollution control, the dispersion of air pollutants released from different emission sources are estimated through atmospheric dispersion mathematical models, without using wide and expensive monitoring networks [3,4]. However, it is important to consider the limitations of mathematical models [5–8]. Reducible error results from inadequate air quality data inputs and from difficulties of models to describe such a complex issue like PM dispersion, due the large number of different sources and the complexity of PM transport and transformation processes [9,10]. The spatial distribution of particulate matter, in fact, strictly depends on factors such as the location and emission rate of its sources and the dispersion capacity of each single contribute, which varies as a function of the particle dimension, shape, chemical composition and density [11].

The purpose of this study is to elaborate a new experimental procedure for source apportionment studies, exceeding the limits of modeling approach and the high costs associated to the realization of an extended monitoring network. The site of the study is the city of Terni, one of the most polluted urban and industrial area in Central Italy [12]. Terni is situated in an intramountain depression, delimited by the Apennine mountain range. This area is characterized by the presence of typical urban PM emission sources such as vehicular traffic, domestic heating and industrial emission sources such as a power plant for waste treatment and a steel plant [13]. Peculiar geomorphological and meteorological conditions of the Terni basin limit the dispersion and enhance the accumulation of the atmospheric pollutants. For these reasons, Terni city is an ideal area to test and validate a new experimental method for the evaluation of the spatial variability of PM_{10} and its chemical components through the acquisition of spatially resolved data. Thanks to the utilization of smart, innovative, low cost, automatic and self-powered samplers, a wide and extensive monitoring network was designed across Terni in order to represent the contributions to the total PM_{10} of each local emission source. The present study represents the first application in the field of these smart samplers and is also proposed to contribute to their validation and optimization through a real monitoring campaign. The aim of the study was the evaluation of the spatial variability of the chemical components of PM_{10},

some of which can be used as efficient source tracers. For increasing selectivity of the elements as source tracers, a chemical fractionation procedure, previously optimized and validated [14–16], was applied to the collected samples. Chemical fractioning based on elemental solubility allows us to get information on the chemical form in which the element is released and this may be typical of its emission source [17]. Moreover the use of the chemical fractioning yields useful information for an estimate of the environmental mobility of the elements. Biogeochemical distribution and bioaccessibility, health and environmental effects are in fact strongly related to the chemical form of the elements [18–20]. The use of the smart samplers, in combination with the chemical characterization and fractioning procedure applied on the samples, allowed to analyze the spatial variability of the elemental components of PM_{10} in Terni. Through the acquisition of data with high spatial resolution, we could identify the source profiles of the different local emission sources present in the area and experimentally evaluate the dispersion capacities of each analyzed elemental component.

2. Experiments

2.1. Sampling Sites and Sampling Equipment

The first phase of this study required great commitment and large amount of time for the identification and the choice of the best locations for the installation of 23 samplers. At first, in the selection of locations, a particulate matter dispersion grid, already developed by the regional agency for environmental protection (ARPA Umbria*)*, was used as a reference system (Fig. 1). It was also very important to guarantee that each sampler (SMART SAMPLER Fai Instruments, Fonte Nuova, Roma, Italy) was positioned at the same height (within 4 m) and with the same exposition (southern exposition) to ensure homogeneous sampling conditions. Particular attention was also paid to the representativeness of sites with respect to each local emission source of PM, as follows:

- power plant for waste treatment located in the West of the city;
- railway;
- vehicular traffic due to the presence of streets with heavy traffic;
- domestic biomass heating;
- very extensive steel plant in the East of the city.

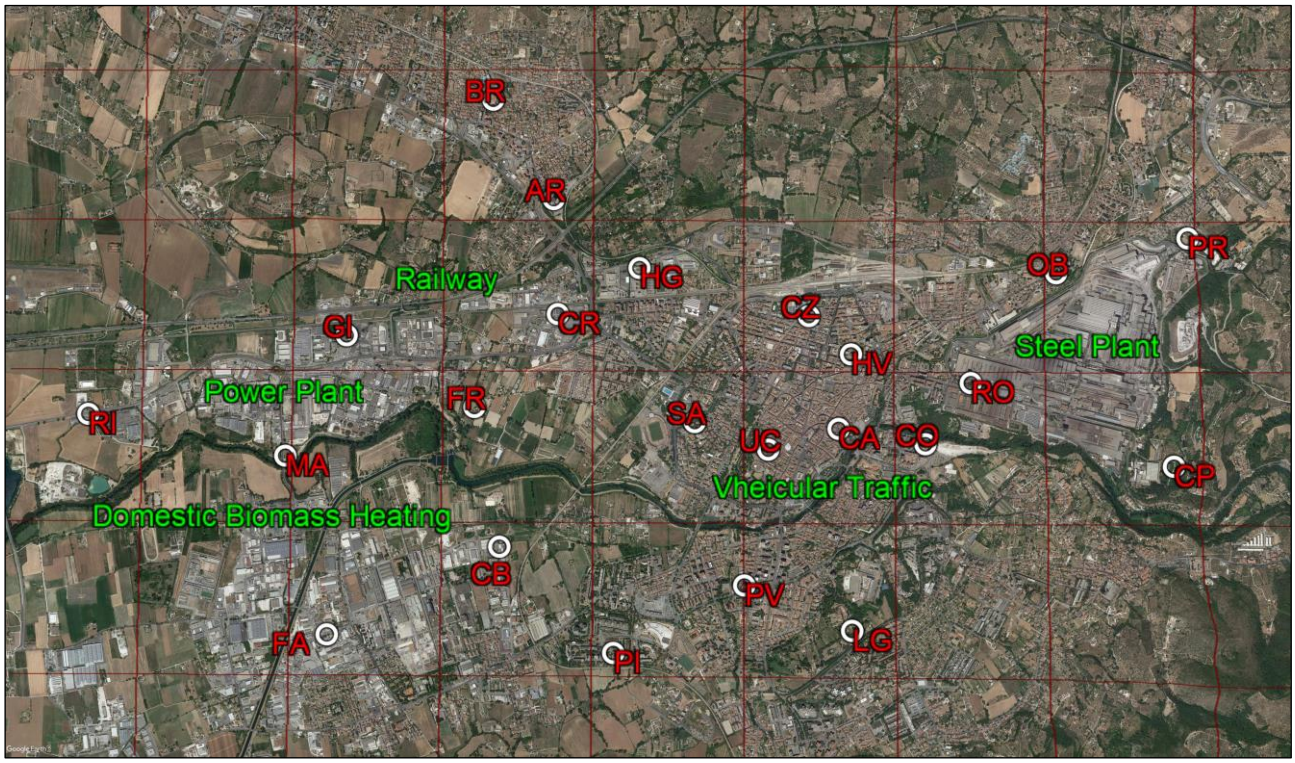

Fig. 1. Map of monitoring sites of Terni (Google Earth Pro) with the particulate matter dispersion grid and the main local emission sources represented.

Table 1 reports the geographical coordinates of the 23 selected sites. BR, AR (North of the city), PI and LG (South of the city) are sites located just outside the high density urban areas (urban background sites); MA, RI, GI, FR, CR, HG, FA and CB are situated in the West of the city, in an industrial area near the power plant for waste treatment (Terni En.A.) where domestic biomass heating systems are used; RO, PR, OB and CP are industrial sites close to (RO and PR) and in proximity (OB and CP) of the steel plant, in the East of the city (Terni AST); CO is a site located between the steel plant and the city center; CZ, HV, SA, UC, CA and PV are sites situated in high density urban areas and/or near heavy traffic streets (urban sites). In these 23 selected sites, innovative smart samplers (Fig. 2) that have never been used on field before were installed.

Fig. 2. Smart samplers (SMART SAMPLER Fai Instruments, Fonte Nuova, Roma, Italy) installed in 4 of the 23 monitoring sites of Terni.

Smart samplers are low cost, small, light, automatic, self-powered (with a power supply system constituted by a rechargeable battery and a small solar panel) and characterized by a flow of 0.5 L/min (with a consumption of 0.2 W for the intake system). The use of these samplers, which can be installed on balconies, railings, or light poles, improved access to a larger number of sampling locations, consenting to design an inexpensive, extended and extensive network across Terni. Hence, thanks to the utilization of the smart samplers, it was possible to obtain analytical data of the PM elemental components with a monthly time resolution (good representativeness) and at the same time with a huge spatial resolution (approximately 1 km of distance between the samplers) that could not be obtained by using the conventional 24 h samplers. Furthermore, due to the capacity of such samplers to work autonomously for long periods of time, the monitoring campaign had substantial reduction of associated costs. Smart samplers that possess a size selection inlet (PM_{10} or $PM_{2.5}$) protected from the sun and rain by a small shield were equipped with PM_{10} sampling head filter system (filter holder diameter 37 mm). Samples of PM_{10} were collected by using Teflon membrane filters (PTFE membranes, 37 mm diameter, 2 μm pore size, PALL Corporation, Port Washington, New York, NY, USA). All the membrane filters were weighed before and after the sampling, in order to gravimetrically determine the PM_{10} mass concentration. Smart samplers are equipped with a SD card from which it was possible to download the volumes of sampled air (m^3), used for the calculation of the mass concentration of PM_{10} and its elemental components.

Table 1. Geographical coordinates of the monitoring sites of Terni.

Type of Site & Major Local PM Emission Sources		Geographical Coordinates	
		Latitude	**Longitude**
RI	Industrial Site-Power Plant & Biomass Domestic Heating	42°33′52.02″ N	12°35′21.94″ E
MA	Industrial Site-Power Plant	42°33′41.42″ N	12°36′19.05″ E
FA	Industrial Site-Power Plant	42°33′03.19″ N	12°36′29.76″ E
GI	Industrial Site-Power Plant & Railway	42°34′06.28″ N	12°36′48.27″ E
FR	Industrial Site-Power Plant & Biomass Domestic Heating	42°33′53.22″ N	12°37′11.44″ E
CB	Industrial Site-Power Plant	42°33′20.30″ N	12°37′20.45″ E
PI	Urban Background Site (South of the City)	42°32′56.96″ N	12°37′52.26″ E
BR	Urban Background Site (North of the City)	42°34′56.19″ N	12°37′23.30″ E
AR	Urban Background Site (North of the City)	42°34′34.23″ N	12°37′39.88″ E
CR	Industrial Site-Power Plant & Railway	42°34′09.49″ N	12°37′39.81″ E
HG	Urban Site-Vehicular Traffic & Railway	42°34′19.32″ N	12°37′56.02″ E
SA	Urban Site-Heavy Vehicular Traffic	42°33′45.16″ N	12°38′18.45″ E
PV	Urban Site-Vehicular Traffic	42°33′06.96″ N	12°38′35.20″ E
LG	Urban Background Site (South of the City)	42°32′59.75″ N	12°39′01.16″ E
CZ	Urban Site-Vehicular Traffic	42°34′06.90″ N	12°38′52.97″ E
HV	Urban Site-Vehicular Traffic	42°33′58.33″ N	12°39′04.74″ E
UC	Urban Site-Vehicular Traffic	42°33′38.09″″ N	12°38′47.62″ E
CA	Urban Site-Heavy Vehicular Traffic	42°33′39.01″ N	12°39′03.11″ E
CO	Industrial Site-Steel Plant & Heavy Vehicular Traffic	42°33′34.23″ N	12°39′22.62″ E
RO	Industrial Site-Steel Plant	42°33′51.16″ N	12°39′39.15″ E
OB	Industrial Site-Steel Plant	42°34′18.64″ N	12°40′05.57″ E
PR	Industrial Site-Steel Plant	42°34′20.30″ N	12°40′44.23″ E
CP	Industrial Site-Steel Plant	42°33′31.65″ N	12°40′36.04″ E

The monitoring campaign was carried out from December 2016 to April 2017. The lack of PM_{10} mass concentration values and elemental concentration values for some collection sites is due to the progressive extension of the monitoring network during the monitoring campaign and sometimes to the malfunction of some samplers. Therefore, it was not possible to acquire sampling data with monthly time resolution at each of the 23 collection sites.

2.2. Analytical Procedure

The analytical procedure for the elemental chemical fractionation, previously optimized and validated [14–16], was carried on each PTFE membrane collected during the campaign. This procedure allows to discriminate water-soluble from insoluble fraction of each analyzed element and resulted to be useful in increasing the selectivity of each element as source tracer [14]. First, the supporting polymethylpentene rings were removed from each sampled PTFE membrane. During the first phase of the chemical fractionation procedure, the sampled PTFE membranes were extracted in an ultrasonic bath in 10 mL of deionized water (produced by Arioso UP 900 Integrate Water Purification System) for 30 min. The extracted solutions were then filtered on a cellulose nitrate filter (0.45 μm pore size, Merck Millipore Ltd., Billerica, MA, USA). After the extraction step, both the cellulose nitrate filter and the original PTFE filter were acid-digested in a microwave oven (Ethos Touch Control with Q20 rotor, Milestone, Italy) by using 2 mL of HNO_3 (67% Promochem) and 1 mL of H_2O_2 (30% Suprapur, Merck Millipore Ltd., Billerica, MA, USA). In the beginning of the digestion program, the temperature was linearly increased to 100 °C in 5 min. In the second step, the temperature was linearly increased to 180 °C in 12 min. In the third step, the temperature was kept at 180 °C for 15 min. After 30 min of ventilation and cooling down, the digested solutions were diluted in 50 mL of deionized water. These solutions were filtered with syringe filters (25 mm diameter, 0.45 μm pore size, GVS Filter Technology, Morecambe, UK). The concentrations of 34 elements (Al, As, B, Ba, Bi, Ca, Cd, Ce, Co, Cr, Cs, Cu, Fe, Ga, La, Li, Mg, Mn, Mo, Na, Nb, Ni, Pb, Rb, Sb, Sn, Sr, Ti, Tl, U, V, W, Zn and Zr) were determined in both extract and mineralized residue fractions obtained from each sample by using inductively coupled plasma mass spectrometry (ICP-MS, Bruker 820-MS, Billerica, MA, USA).

2.3. Statistical Analysis

Multivariate statistical computations were performed by the statistical software: R-3.0Gui (32-bit) for Windows (R-project for statistical computing). Multivariate analyses were operated on the data yielded by the analytical determinations on the elemental components of PM_{10} at each collection site. Two principal component analyses (PCA) were performed. The first one was performed for the 23 monitoring sites by including the averages of the 34 monthly total elemental concentration data (sum of the extracted and residual fractions) recorded at each collection site. The second one was performed for the 23 monitoring sites by including the 34 total elemental concentration data (sum of the extracted and residual fractions) recorded each month at each collection site. The first PCA was performed to

separate or group the monitoring sites depending on the type and on the concentration of the source tracers recorded at each site in order to identify the main emission source tracers and their action at each site. The second PCA was performed in order to assess the monthly action of the source tracers at each site and to evaluate the monthly variations of the elemental components of PM_{10} in the monitored area. The 23 monitoring sites benefit from the choice of the best locations for the 23 smart samplers, hence collection sites are well differentiated for type and location, allowing a detailed discussion about differences in source nature and monthly contributions. In the data set used, some outliers (six outliers in Cr, Fe and Ni water-soluble fraction concentrations of two samples collected in December 2016 at FA and at CA, reasonably attributed to the contamination of these samples during the sample preparation for the extraction procedure) were excluded after having assessed that their presence increased unstable results of PCA.

2.4. Element Solubility Percentages

Solubility percentages of PM_{10} elemental components were calculated by dividing the soluble fraction of each element analyzed to its total fraction (sum of the extracted and residual fractions) and multiplying by 100. The monthly solubility percentage for each element analyzed in the entire monitored area was obtained making each month an average of the solubility percentages calculated for each element at all the 23 monitoring sites. Standard deviations were calculated to evaluate the contribution of local emission sources to the variability of the elements solubility in the entire monitored area.

3. Results and Discussion

3.1. PM_{10} Mass Concentration

Fig. 3 reports the mass concentrations of PM_{10} recorded in the 23 collection sites during the five-month monitoring campaign. The left and the right sector of the graphs in Fig. 3 and 4 represent, respectively, the data obtained by the collection sites located in the West (industrial sites near the power plant) and in the East (industrial sites in proximity or close to the steel plant) of the city. The central part of the graphs represents the urban sites PV, CZ, HV, SA, UC and CA.

The average of PM_{10} mass concentrations recorded at all the collection sites of Terni during the monitoring campaign resulted of 42.3 $\mu g/m^3$ (56.5 $\mu g/m^3$ in December, 66.9 $\mu g/m^3$ in January, 39 $\mu g/m^3$ in February, 30.7 $\mu g/m^3$ in March and 18.3 $\mu g/m^3$ in April). The data above demonstrate that a clear increase in PM concentration occurred in all the sites during the winter. The highest PM_{10}

mass concentration (96 μg/m^3) was recorded in January, during the colder period, at CO located between the heavily trafficked streets of the city and the steel plant. The lowest PM_{10} mass concentration (6.2 μg/m^3) was recorded in April, during the warmer period, at the monitoring station FR located in the West of the city in an industrial area near the power plant, far from the city center.

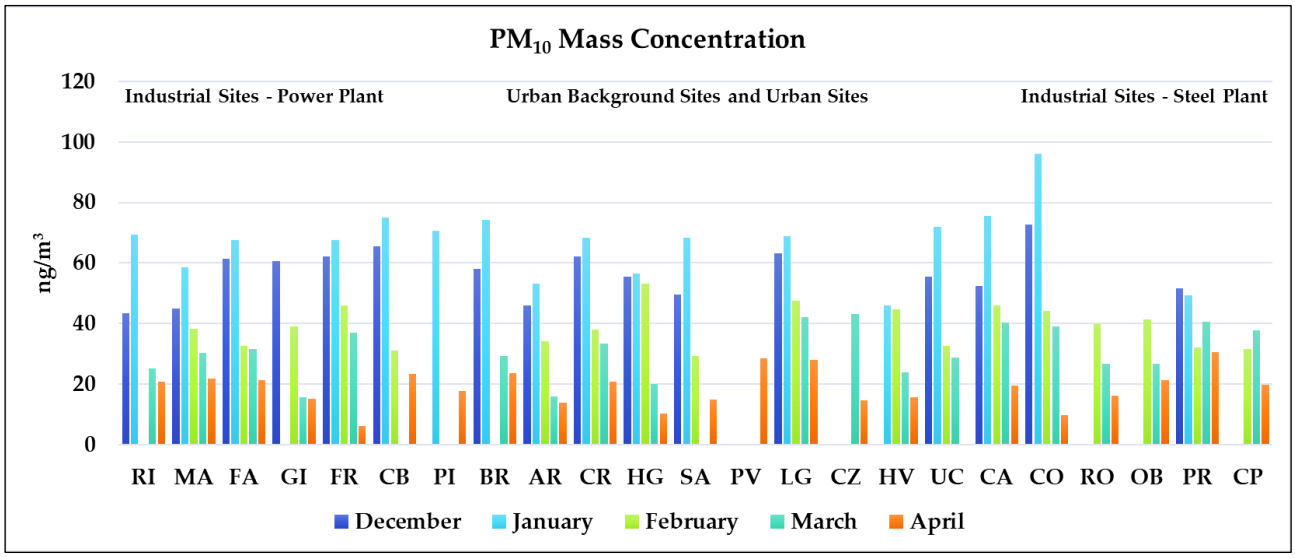

Fig. 3. PM_{10} mass concentrations (μg/m^3) recorded at the 23 collection sites during the five-month monitoring campaign.

The data in Fig. 3 show that the concentration of PM_{10} was driven by the contribution of different PM local emission sources as well as by the meteorological conditions. In general, the PM_{10} mass concentration reflects the strength of the contribution from traffic-related sources at these sites [14]. In fact the highest values of PM_{10} were recorded during the winter at urban sites CO, CA and UC. The increase of PM_{10} mass concentrations during the colder months (December and January) can be explained by a combination of two factors: the less efficient mixing of the lower atmosphere during the winter and the strength of some seasonal PM sources, which include domestic heating [18,19,21]. The meteorological conditions of Terni basin limit the dispersion and enhance the accumulation of the atmospheric pollutants. Therefore the local circulation is often weak and this leads to a more stable atmosphere which is generally responsible for a concentration increase in all PM chemical species. Particularly during the winter, the meteorological conditions favor the development of temperature inversions, leading to extended periods of high atmospheric stability.

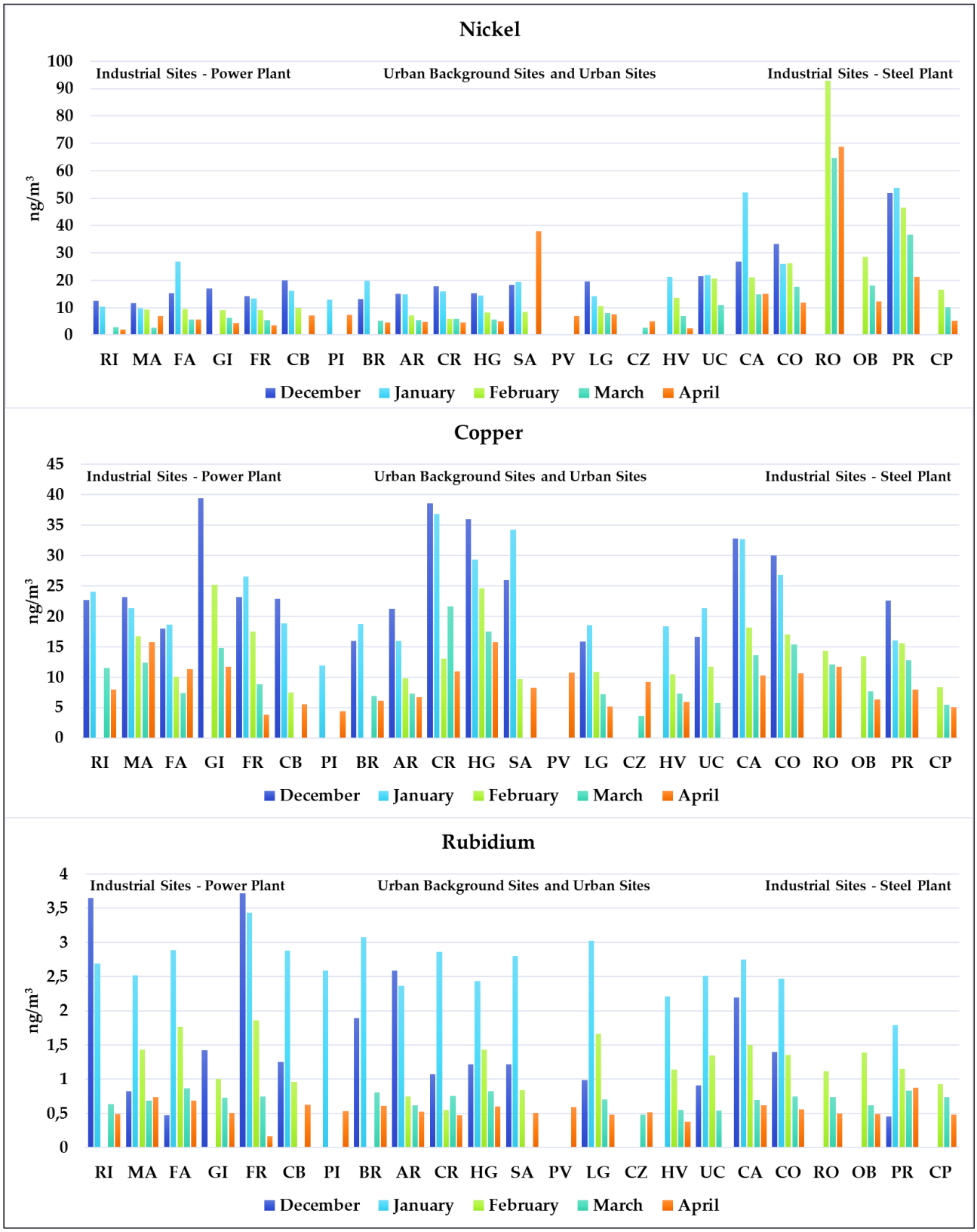

Fig. 4. Variations of Ni, Cu and Rb monthly concentrations (ng/m^3) recorded during the five-month monitoring campaign at the 23 collection sites.

3.2. Elemental Concentration

Spatially resolved data obtained by sampling in parallel at 23 collection sites consented to properly evaluate the spatial variability of PM_{10} as well as of some PM_{10} chemical components and in particular of tracers of the principal local sources. For example Fig. 4 reports the monthly values of the total concentrations (sum of the extracted and residual fractions) of Ni, Cu and Rb in PM_{10} collected from the 23 collection sites during the five-month monitoring campaign. Fig. 4 shows how, also for the elements, the highest elemental concentrations, at all the 23 monitoring sites, were recorded during the colder months, due to the presence of additional PM sources and/or to the lower mixing of the atmosphere [18]. The concentration of most elements increased with the level of urbanization at the collection site and with the proximity of the site to one of the main emission sources of the city: the steel plant.

3.2.1. Ni, Cr, Mn, Mo, Pb and Fe Concentration

Cr, Mn and Mo showed the same behavior as Ni (upper panel of Fig. 4) with a relevant increase of concentrations at the sites in proximity of the steel plant: RO, PR, OB, CP and CO. The highest concentrations of Ni were individuated in February at RO: 93 ng/m^3. It is worth noting that this value is almost five times higher than the European Union (EU) target value (20 ng/m^3), calculated on yearly averages (EU 2008/50/CE). Ni, Cr, Mo and Mn were identified as the main source tracers of the steel plant emission source. Cr and Ni are the basic composition of stainless steel which allows them to be the known tracers of the industry. Cr enables the steel to become resistant to chemical oxidation. Ni functions to create properties such as strength, ductility and toughness. Mn and Mo are secondary components of the stainless steel. Mo increases the corrosion resistance of the steel. Mn is used to increase toughness and tensile strength [22]. Even though the general behavior of the four tracers was similar, the results showed that Ni and Mo resulted less dispersed than Cr and Mn. The limited dispersion of these elements in the monitored area suggests that particles containing Ni and Mo had a lower diffusion capacity than those containing Cr and Mn. The low spatial dispersion of this steel plant related contribute suggest that, at least in part, mechanical and abrasive processes are more relevant than combustion ones. In fact, it is well known that fine particles, mainly produced by combustive processes, are easily carried by the wind, while coarse ones, mainly produced by mechanical and abrasive processes, tend to remain within the local emission area [23]. Each emission source is responsible for the release of particles having different dimensional ranges and containing chemical species having different solubility.

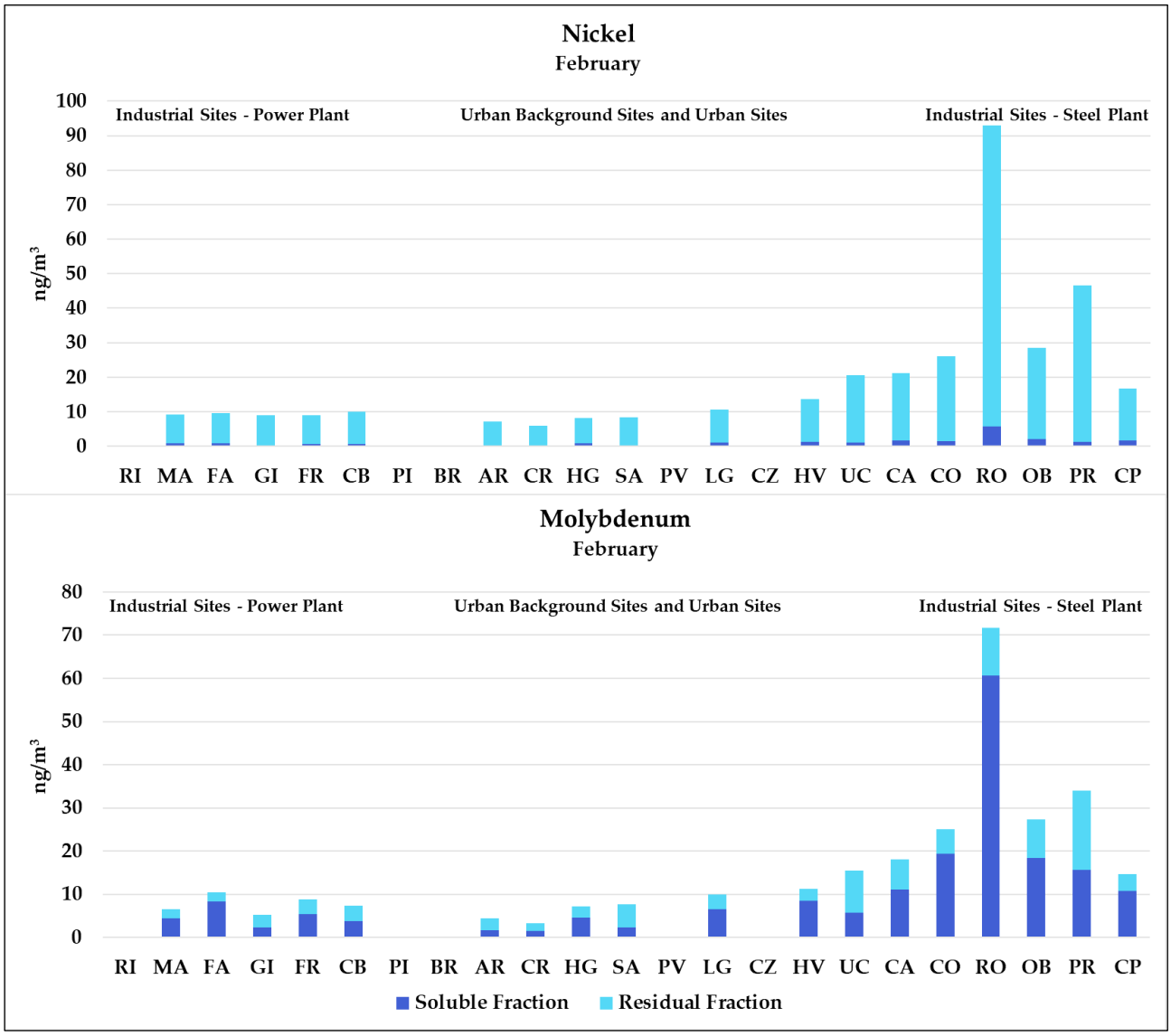

Fig. 5. Soluble and residual fractions of Ni and Mo concentrations (ng/m^3) recorded in February at the 23 collection sites.

Fig. 5 reports the concentration of Ni and Mo measured in their soluble and residual fractions during the month of February. It is possible to observe that the two elements showed quite the same dispersion profiles, but they had a very different solubility distribution: Mo was emitted mainly as soluble species, while Ni was almost entirely contained in the residual fraction. Hence, it is possible to suppose that the steel plant released course particles containing mainly water-soluble species of Mo and insoluble species of Ni.

The concentration of Pb demonstrated a consistent distribution throughout the city. At site PR, close to the steel industry, the Pb concentrations were especially high. This suggests that Pb must be emitted by the steel plant, possibly when it is added to carbon-steels in order to improve their machinability. Fe concentration (mainly present in the insoluble fraction) is also affected by the contribution from the steel plant, but it showed a different spatial profile respect to Ni, Cr, Mo and Mn, which are to be considered as more selective steel plant source tracers [24]. Fe in fact is also influenced by vehicular traffic and railway emission sources. Concentration peaks of Fe (>1000 ng/m^3) in PM_{10} were individuated during the winter at CA which is in proximity of heavy traffic streets, at sites close to the steel plant (RO and PR) and at CO, which is located between the steel plant and the high density urban area and at sites in proximity of the railway (GI, CR and HG).

3.2.2. Cu and Sb Concentration

As it is possible to see from the second panel of Fig. 4, Cu resulted to be a more representative traffic-related source tracer. It showed concentration peaks in December only at sites located in proximity of heavy traffic streets (CA, SA and CO) and at sites in proximity of the railway (GI, CR and HG). Cu, Fe and Sb showed a similar distribution pattern at sites HG, CA and CO, in which their concentrations are relatively high because they are in proximity of the most trafficked roads of the city. Differently to what was previously described for the steel plant tracers, for Cu and Sb, the differences in terms of concentration between the monitoring sites resulted less marked, highlighting the role of vehicular traffic as the most common and distributed emission source of the city.

3.2.3. Rb, Bi, Sr, Mg and V Concentration

Finally, as it is possible to note from the third panel of Fig. 4, Rb was emitted in higher concentrations during the winter months of December and January at sites in the West of the city (left part of the graph). Rb (main in the water-soluble fraction) was emitted in highest concentrations in December at sites RI and FR which are located in an industrial area in proximity of the power plant where domestic biomass heating systems are used. Therefore, Rb (water-soluble fraction) was identified as the most representative source tracer of biomass burning. It is worth noting that Rb concentration during the month of December also reflected the contribution of New Year's fireworks, together with Bi, Sr and Mg. The analyses of the spatial variability in concentrations of other elements such as V did not reveal significant differences between the sites, without defining clear source profiles. The spatial homogeneity of V in the PM_{10} within the city is due to the lack of influence of local sources responsible for its emission.

3.3. Source Tracers Identification by Principal Component Analysis

Results from the two principal component analyses performed in this study were evaluated and reported in Fig. 6; all the total concentrations of the elemental components of PM_{10} recorded were considered to identify the source tracers. The monitoring sites were represented in the left panels of Fig. 6 with different colors depending on the type and location of each site, as follows:

- the urban background sites, located in the South and in the North of the city, outside the high density urban areas, (BR, AR, PI and LG) are represented with the green color;
- the sites situated in the West of the city, in the industrial area near the power plant for waste treatment where domestic biomass heating systems are used (MA, RI, GI, FR, CR, HG, FA and CB) are represented with the blue color;
- the sites located in the East of the city, in proximity of the steel plant (OB and CP) or between the steel plant and the city center (CO) are represented with the black color;
- the sites located in the East of the city, close to the steel plant (RO and PR) are represented with the red color;
- the urban sites, situated in high density urban areas and/or near heavy traffic streets (CZ, HV, SA, UC, CA and PV) are represented with the brown color.

An overview of all sources affecting the 23 monitoring sites used for the multivariate statistical analysis was obtained by performing a first preliminary PCA (upper panels of Fig. 6) including the averages of all the 34 monthly total elemental concentration data (sum of the extracted and residual fractions) recorded at each collection site. Thanks to the first PCA, it was possible to separate or group the monitoring sites (scores) in the score plot depending on the type and on the concentration of the source tracers (loading) recorded at each site (upper panels of Fig. 6). Hence, it was possible to properly identify the main source tracers (loadings) of the monitored area and their action at each site. The 63.1% of the total variance was explained by the first two principal components (PC1 and PC2). The urban background sites (green color) were positioned in the center of the score plot (left upper panel of Fig. 6) because at these monitoring sites, lower concentrations of all the elemental components of PM_{10} were recorded. The sites in the industrial area near the power plant (blue color), were separated from these on the PC2 by Zr, Sb, Bi, Tl, Sn, Ba and Rb, which were classified as biomass burning source tracers. The urban sites (brown color) resulted well distributed on the two principal components confirming the role of vehicular traffic as most common and distributed emission source of the city.

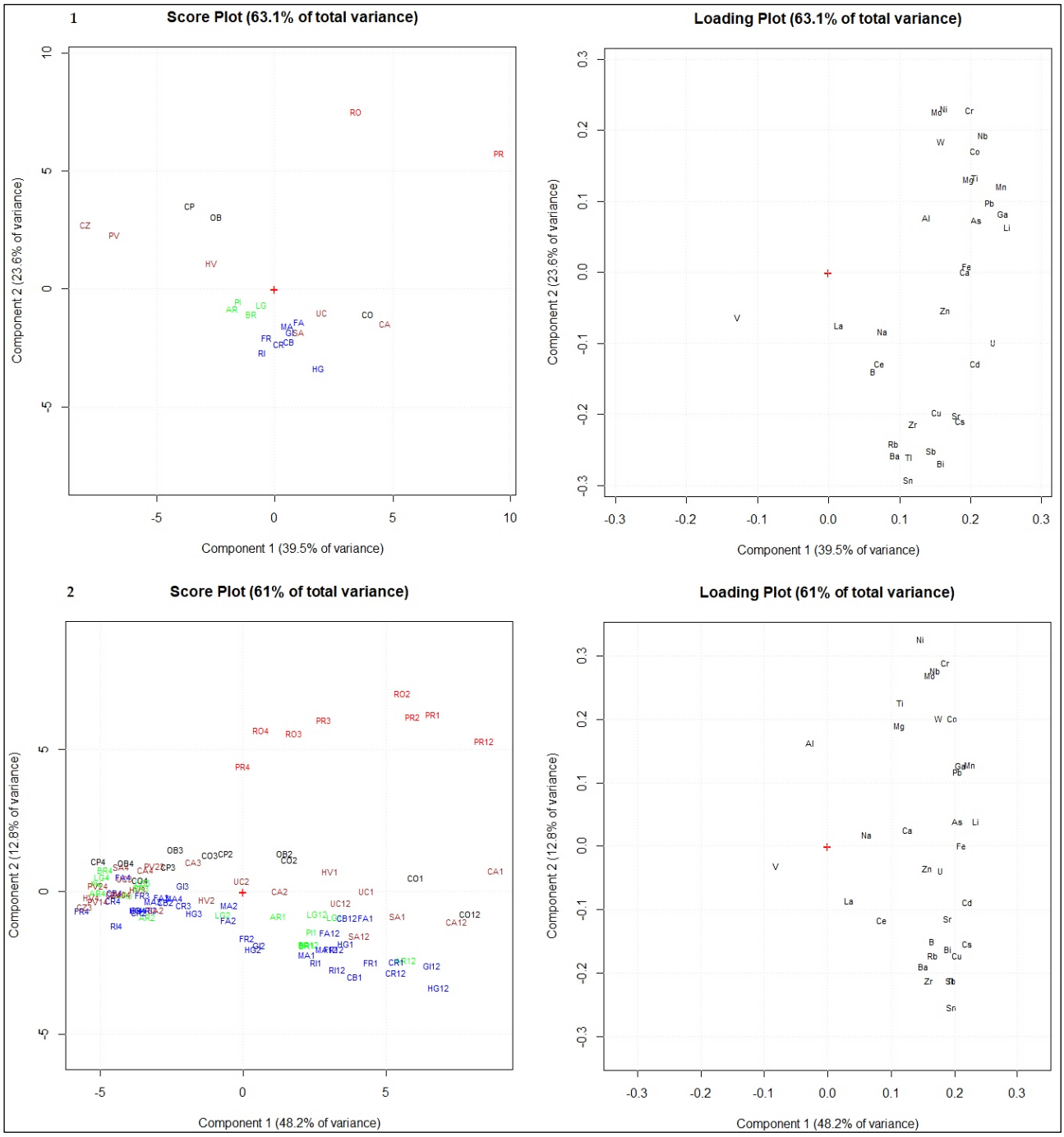

Fig. 6. Panel 1 - Score and loading plots of the PCA performed by using the averages of the 34 monthly total elemental concentration data recorded at each collection site. Panel 2 - Score and loading plot of the PCA performed by using the 34 total elemental concentration data recorded each month at each collection site.

The sites CZ, PV and HV, which are located in the city center but quite distant from the heavy traffic streets, were separated from UC, SA and CA by Sb, Cd, Fe, Cu, Ba and Zn, which are typical source tracers of vehicular traffic, by Rb, tracer of domestic heating and by Bi and Sr, which are fireworks burning source tracers. The sites at the East of the city, closer to the steel plant, were separated from all the other monitoring sites on the PC2 by Ni, Cr, Mo and Mn, which were already identified as steel plant source tracers, and by Ti, Nb, W, Co, Mg and Pb. It is interesting to note that PR was separated from RO on the PC1 by Pb, Mg, Mn and Ti. This suggests the presence of different steel plant local emission sources. The sites in proximity of the steel plant or between the steel plant and the city center (black color) were positioned exactly between the urban sites and the sites closer to the steel plant, confirming the action of both vehicular traffic and steel plant emission source at site CO. V did not reveal significant differences between the sites confirming the spatial homogeneity of V in the PM_{10} within the city. From the second PCA performed, it was possible to assess the monthly action of the source tracers at each monitoring site and to evaluate the monthly variations of the elemental components of PM_{10} at each collection site. As can be seen from the lower panels of Fig. 6, the first two components explained the 60.6% of the total variance. The number associated to the name of the monitoring sites in the left lower panel of Fig. 6 correspond to the month of sampling at each site: December: 12, January: 1, February: 2, March: 3 and April: 4. The second PCA confirmed the progressively decrease of PM_{10} elemental components' concentrations at each site from December to April, due to the presence of additional PM sources and/or to the lower mixing of the atmosphere during the colder months. The months of sampling at each collection site were separated on the PC1 from the right part to the left part of the score plot, following the monthly sequence of sampling, from December to April. The different types of monitoring sites were maintained separated on the PC2 confirming the efficiency of the source tracers identified from the first PCA performed.

3.4. Seasonal Variability of Element Solubility Percentages in PM_{10}

The monthly solubility percentages obtained for each element analyzed in the entire monitored area (Table 2) allowed to evaluate the seasonal variability of the element soluble fractions in PM_{10} and to estimate the environmental mobility and the bio-accessibility of each element [18].

Table 2. Means (AM) and standard deviations (SD) of the elements solubility percentages (%) calculated monthly for each element at all the 23 monitoring sites.

Month	December			January			February			March			April		
	AM	±	SD	AM	±	SD	AM	±	SD	AM	±	SD	AM	±	SD
Li	65	±	6	68	±	5	57	±	13	34	±	9	68	±	16
B	51	±	14	79	±	9	67	±	19	53	±	29	70	±	22
Na	39	±	17	44	±	27	53	±	10	55	±	15	49	±	11
Mg	51	±	6	57	±	10	47	±	9	37	±	6	54	±	9
Al	9	±	3	9	±	3	5	±	2	1	±	1	3	±	1
Ca	47	±	17	64	±	13	50	±	15	26	±	11	57	±	15
Ti	1	±	0	3	±	2	4	±	2	1	±	0	4	±	2
V	32	±	14	51	±	27	51	±	25	45	±	18	75	±	11
Cr	6	±	2	6	±	3	4	±	2	3	±	2	9	±	4
Mn	45	±	5	47	±	5	38	±	9	26	±	9	45	±	8
Fe	3	±	2	3	±	2	3	±	2	1	±	0	4	±	1
Co	15	±	4	20	±	15	14	±	6	10	±	6	23	±	13
Ni	10	±	5	9	±	3	7	±	3	5	±	3	15	±	8
Cu	22	±	5	22	±	4	23	±	7	12	±	7	32	±	7
Zn	47	±	14	54	±	12	43	±	11	13	±	7	37	±	12
Ga	11	±	3	14	±	3	13	±	6	5	±	3	32	±	20
As	59	±	12	65	±	8	51	±	21	15	±	9	87	±	8
Rb	67	±	21	90	±	1	86	±	8	52	±	7	70	±	14
Sr	48	±	12	74	±	10	65	±	16	45	±	11	75	±	10
Zr	1	±	1	1	±	1	5	±	3	1	±	1	6	±	7
Nb	1	±	1	1	±	1	4	±	2	1	±	1	39	±	21
Mo	43	±	7	60	±	10	60	±	16	63	±	9	82	±	7
Cd	89	±	9	70	±	13	71	±	18	38	±	20	93	±	5
Sn	1	±	0	2	±	1	7	±	4	4	±	2	15	±	6
Sb	26	±	5	35	±	9	27	±	12	29	±	10	53	±	12
Cs	77	±	4	81	±	2	66	±	9	31	±	7	95	±	5
Ba	29	±	9	42	±	10	28	±	0	28	±	0	47	±	15
La	7	±	4	8	±	6	12	±	8	3	±	2	6	±	4
Ce	4	±	2	4	±	3	11	±	8	3	±	1	3	±	5
W	37	±	6	47	±	6	42	±	13	43	±	15	70	±	20
Tl	81	±	5	77	±	5	69	±	13	49	±	10	95	±	20
Pb	19	±	4	12	±	3	15	±	5	6	±	4	20	±	6
Bi	3	±	1	6	±	1	8	±	4	5	±	3	28	±	29
U	11	±	2	7	±	4	15	±	7	9	±	6	88	±	0

From the standard deviations calculated, it was also possible to evaluate the contribution of local sources to the variability of the elements solubility in the entire monitored area. Cd, B, Rb, Sr, Mo, Cs and Tl showed the highest solubility percentages and bio-accessibility during the five-month monitoring campaign while Al, Ti, Cr, Fe, Ni, Zr, Nb, Sn, La, Ce, Pb and Bi resulted released mostly in the residual fraction. Zn, Ni, Fe, Cr and Pb are considered as some of the most potential dangerous elements for human health. However, the bio-accessibility of these elements in the monitored area appeared quite limited because they resulted predominantly present in the residual fraction at all the 23 locations. The solubility percentages of the elements in PM_{10} did not show a clear seasonal variability. From December to March, the elements solubility percentages resulted constant, while a slight, and in some cases considerable, increase was recorded for the majority of the elements in the month of April. This increase might be due to the variation of some local emission sources that released particles containing mostly insoluble chemical species.

4. Conclusions

The results obtained proved the efficiency of the new experimental procedure elaborated for the evaluation of the spatial variability of PM_{10} and its chemical components through the acquisition of spatially resolved data. In particular, the innovative smart samplers, used for the first time in this campaign, allowed to build an extended and extensive monitoring network, with low associated costs, which was able to represent the different emission source contributes to total PM_{10} in the monitored area. From the acquisition of spatially resolved data, it was possible to properly evaluate the dispersion capacity of PM_{10} and its elemental components. The elemental analyses associated with the chemical fractionation procedure and the statistical treatment of the data allowed to identify the source tracers of each PM_{10} local emission source which will be used for future source apportionment studies. Chemical fractionation, by providing information on the chemical form, improved the selectivity of different source tracers. Spatial variability of Ni, Cr, Mn (insoluble fraction) and Mo (water-soluble fraction) concentrations showed the steel plant role in the emission of PM_{10}. Spatial variability of Fe (insoluble fraction) resulted to be correlated not only to the steel plant emission but also to the influence of vehicular traffic sources. The role of this emission source was also confirmed by the spatial variability of element such as Sb and Cu, which showed high concentrations at the sites near high-traffic streets and the railway. Rb (soluble fraction) was confirmed to be a good tracer of biomass combustion processes. This experimental approach, based on the acquisition of spatially resolved data for analyzing spatial variability of PM_{10} and its chemical components, will be effective

for the validation of dispersion models without the high costs associated to an air quality monitoring network.

Acknowledgements

The work was partially founded by Sapienza University of Rome. The authors gratefully thank FAI Instruments (Fonte Nuova, Roma, Italy), the citizens of Terni and the Terni district of ARPA Umbria (regional agency for environmental protection) with special regard to Caterina Austeri, Giancarlo Caiello and Marco Pompei for the support in the installation and in the management of the sampling equipment as well as for the help in the choice of the sampling sites.

Author Contributions

L. Massimi is the principal investigator and wrote the paper; L. Massimi, M. Ristorini, M. Eusebio and S. Canepari conceived and planned the monitoring; L. Massimi and M. Eusebio performed the samplings; L. Massimi, M. Ristorini, D. Florendo [b], A. Adeyemo and D. Brugnoli performed the chemical analysis; L. Massimi and M. Ristorini analyzed the data; S. Canepari coordinated the group.

Conflicts of Interest

The authors declare no conflicts of interest.

References

1. Pope, C.A.; Burnett, R.T.; Thun, M.J.; Calle, E.E.; Krewski, D.; Ito, K.; Thurston, G.D. Lung Cancer Cardiopulmonary Mortality, and Long-term Exposure to Fine Particulate Air Pollution. *J. Am. Med. Assoc.* 2002, *287*, 1132–1141, doi:10.1001/jama.287.9.1132.
2. Hwang, I.; Hopke, P.K. Estimation of Source Apportionment and Potential Source Locations of $PM_{2.5}$ at a West Coastal IMPROVE Site. *Atmos. Environ.* 2007, *4*, 506–518, doi:10.1016/j.atmosenv.2006.08.043.
3. Conti, G.O.; Heibati, B.; Kloog, I.; Fiore, M.; Ferrante, M. A review of AirQ Models and their applications for forecasting the air pollution health outcomes. *Environ. Sci. Pollut. R.* 2017, *24*, 6426–6445, doi:10.1007/s11356-016-8180-1.

4. Vitali, L.; Morabito, A.; Adani, M.; Assennato, G.; Ciancarella, L.; Cremona, G.; Giua, R.; Pastore, T.; Piersanti, A.; Righini, G.; et al. A Lagrangian modelling approach to assess the representativeness area of an industrial air quality monitoring station. *Atmos. Pollut. Res.* 2016, *7*, 990–1003, doi:10.1016/j.apr.2016.06.002.

5. Weil, J.C.; Sykes, R.I.; Venkatram, A. Evaluating air quality models: Review and Outlook. *J. Appl. Meteorol.* 1992, *31*, 1121–1145, doi:10.1175/1520-0450(1992)031<1121:EAQMRA>2.0.CO;2.

6. Irwin, J.C. A suggested method for dispersion model evaluation. *J. Air Waste Manag. Assoc.* 2014, *4*, 255–264, doi:10.1080/10962247.2013.83314.

7. Padoan, E.; Malandrino, M.; Giacomino, A.; Grosa, M.M.; Lollobrigida, F.; Martini, S.; Abollino, O. Spatial distribution and potential sources of trace elements in PM_{10} monitored in urban and rural sites of Piedmont Region. *Chemosphere* 2016, *145*, 495–507, doi:10.1016/j.chemosphere.2015.11.094.

8. Kim, B.U.; Bae, C.; Kim, H.C.; Kim, E.; Kim, S. Spatially and chemically resolved source apportionment analysis: Case study of high particulate matter event. *Atmos. Environ.* 2017, *162*, 55–70, doi:10.1016/j.atmosenv.2017.05.006.

9. Fox, D.G. Uncertainty in Air Quality Modeling. *Bull. Am. Meteorol. Soc.* 1984, *65*, 27–36, doi:10.1175/1520-0477(1984)065<0027:UIAQM>2.0.CO;2.

10. Almeida, S.M.; Pio, C.A.; Freitas, M.C.; Reis, M.A.; Trancoso, M.A. Source apportionment of atmospheric urban aerosol based on weekdays/weekend variability: Evaluation of road re-suspended dust contribution, *Atmos. Environ.* 2006, *40*, 2058–2067, doi:10.1016/j.atmosenv.2005.11.046.

11. Perrino, C.; Canepari, S.; Pappalardo, S.; Marconi, E. Time-resolved measurements of water-soluble ions and elements in atmospheric particulate matter for the characterization of local and long-range transport events. *Chemosphere* 2010, *80*, 1291–1300, doi:10.1016/j.chemosphere.2010.06.050.

12. Moroni, B.; Ferrero, L.; Crocchianti, S.; Cappelletti, D. Aerosol dynamics upon Terni basin (Central Italy): Results of integrated vertical profile measurements and electron microscopy analysis. *Rendiconti Lincei* 2013, *24(4)*, 319–328, doi:10.1007/s12210-013-0230-8.

13. Guerrini, R. Qualità dell'aria nella provincia di Terni tra il 2002 e il 2011. *Quad. ARPA Umbria* 2012, *XXXIII*, 81–87, doi:10.1007/s13398-014-0173-7.2.

14. Canepari, S.; Pietrodangelo, A.; Perrino, C.; Astolfi, M.L.; Marzo, M.L. Enhancement of source traceability of atmospheric PM by elemental chemical fractionation. *Atmos. Environ.* 2009, *43*, 4754–4765, doi:10.1007/s00216-010-3818.

15. Canepari, S.; Cardarelli, E.; Giuliano, A.; Pietrodangelo, A. Determination of metals, metalloids and non-volatile ions in airborne particulate matter by a new two-step sequential leaching procedure Part A: Experimental design and optimization. *Talanta* 2006, *69*, 581–587, doi:10.1016/j.talanta.2005.10.023.

16. Canepari, S.; Cardarelli, E.; Giuliano, A.; Strincone, M. Determination of metals, metalloids and non-volatile ions in airborne particulate matter by a new two-step sequential leaching procedure Part B: Validation on equivalent real samples. *Talanta* 2006, *69*, 588–595, doi:10.1016/j.talanta.2005.10.024.

17. Templeton, D.M.; Ariese, F.; Cornelis, R.; Danielsson, L.G.; Muntau, H.; Van Leeuwen H.P.; Lobinski, R. Guidelines for terms related to chemical speciation and fractionation of elements. Definitions, structural aspects,and methodological approaches (IUPAC Recommendations 2000). *Pure Appl. Chem.* 2000, *72*, 1453–1470, doi:10.1351/pac200072081453.

18. Canepari, S.; Astolfi, M.L.; Farao, C.; Maretto, M.; Frasca, D.; Marcoccia, M.; Perrino, C. Seasonal variations in the chemical composition of particulate matter: A case study in the Po Valley. Part II: Concentration and solubility of micro- and trace-elements. *Environ. Sci. Pollut. R.* 2014, *21*, 4010–4022, doi:10.1007/s11356-013-2298-1.

19. Perrino, C.; Catrambone, M.; Dalla Torre, S.; Rantica, E.; Sargolini, T; Canepari, S. Seasonal variations in the chemical composition of particulate matter: A case study in the Po Valley. Part I: Macro-components and mass closure. *Environ. Sci. Pollut. R.* 2014, *21*, 3999–4009, doi:10.1007/s11356-013-2067-1.

20. Harrison, R.M.; Yin, J. Particulate matter in the atmosphere: Which particle properties are important for its effects on health? *Sci. Total Environ.* 2000, *249*, 85–101, doi:10.1016/S0048-9697(99)00513-6.

21. Perrino, C.; Tofful, L.; Canepari, S. Chemical characterization of indoor and outdoor fine particulate matter in an occupied apartment in Rome, Italy. *Indoor Air* 2016, *26*, 558–570, doi:10.1111/ina.12235.

22. Blair, M.; Stevens, T.L. *Steel Castings Handbook*, 6th ed.; Steel Founders' Society and ASM International: Novelty, OH, USA, 1995; pp. 2–34.

23. Li, R.; Wiedinmyer, C.; Hannigan, M.P. Contrast and correlations between coarse and fine particulate matter in the United States. *Sci. Total Environ.* 2013, *456–457*, 346–358, doi:10.1016/j.scitotenv.2013.03.041.

24. Taiwo, A.M.; Harrison, R.M.; Shi, Z. A review of receptor modelling of industrially emitted particulate matter. *Atmos. Environ.* 2014, *97*, 109–120, doi:10.1016/j.atmosenv.2014.07.051.

Supplementary Material S1.

Table S1.1. Monitoring periods at each of the 23 collection sites.

	December	January	February	March	April
RI	19/11 - 12/12	17/12 - 16/01		25/02 - 27/03	01/04 - 01/05
MA	19/11 - 12/12	17/12 - 16/01	21/01 - 20/02	25/02 - 27/03	01/04 - 01/05
FA	19/11 - 12/12	17/12 - 16/01	21/01 - 20/02	25/02 - 27/03	01/04 - 01/05
GI	19/11 - 12/12		21/01 - 20/02	25/02 - 27/03	01/04 - 01/05
FR	19/11 - 12/12	17/12 - 16/01	21/01 - 20/02	25/02 - 27/03	01/04 - 01/05
CB	19/11 - 12/12	17/12 - 16/01	21/01 - 20/02		01/04 - 01/05
PI					01/04 - 01/05
BR	19/11 - 12/12	17/12 - 16/01		25/02 - 27/03	01/04 - 01/05
AR	19/11 - 12/12	17/12 - 16/01	21/01 - 20/02	25/02 - 27/03	01/04 - 01/05
CR	19/11 - 12/12	17/12 - 16/01	21/01 - 20/02	25/02 - 27/03	01/04 - 01/05
HG	19/11 - 12/12	17/12 - 16/01	21/01 - 20/02	25/02 - 27/03	01/04 - 01/05
SA	19/11 - 12/12	17/12 - 16/01	21/01 - 20/02		01/04 - 01/05
PV					01/04 - 01/05
LG	19/11 - 12/12	17/12 - 16/01	21/01 - 20/02	25/02 - 27/03	01/04 - 01/05
CZ				25/02 - 27/03	01/04 - 01/05
HV			21/01 - 20/02	25/02 - 27/03	01/04 - 01/05
UC	19/11 - 12/12	17/12 - 16/01	21/01 - 20/02	25/02 - 27/03	
CA	19/11 - 12/12	17/12 - 16/01	21/01 - 20/02	25/02 - 27/03	01/04 - 01/05
CO	19/11 - 12/12	17/12 - 16/01	21/01 - 20/02	25/02 - 27/03	01/04 - 01/05
RO			21/01 - 20/02	25/02 - 27/03	01/04 - 01/05
OB			21/01 - 20/02	25/02 - 27/03	01/04 - 01/05
PR	19/11 - 12/12	17/12 - 16/01	21/01 - 20/02	25/02 - 27/03	01/04 - 01/05
CP			21/01 - 20/02	25/02 - 27/03	01/04 - 01/05

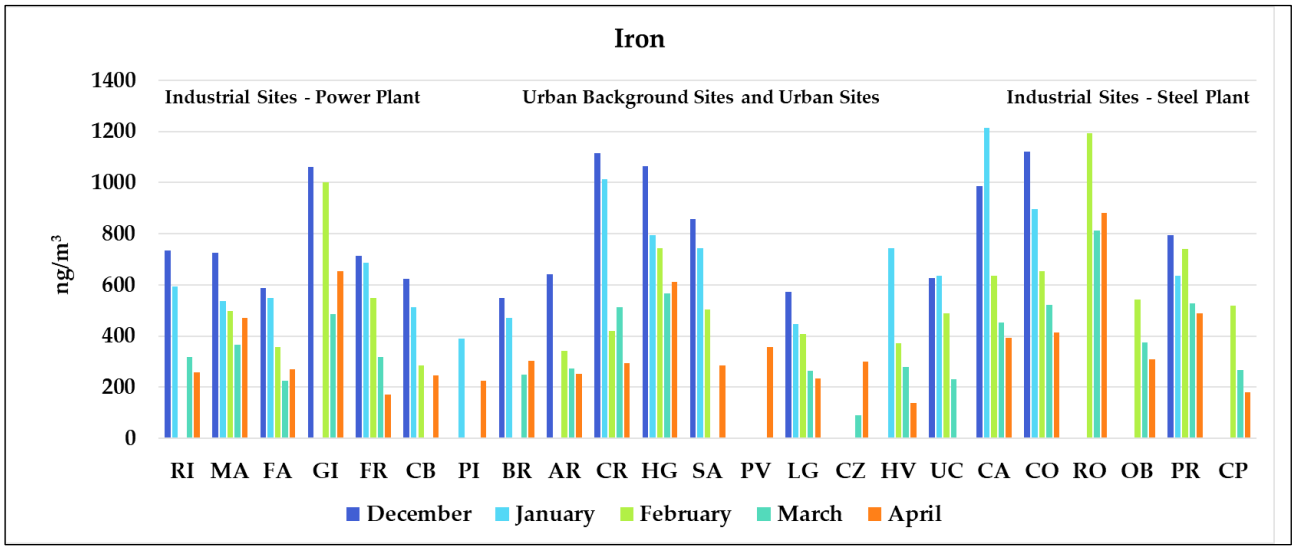

Fig. S1. Variations of Fe monthly concentrations (ng/m^3) recorded during the five-month monitoring campaign at the 23 collection sites.

2.3.2. (C2) Spatial and Dimensional Distribution of Levoglucosan and Alternative Biomass Burning Tracers in Atmospheric Aerosols, in an Urban and Industrial Hot-spot of Central Italy

Atmospheric Research (2019), *Reviewed*

Lorenzo Massimi [a,*], Giulia Simonetti [a], Francesca Buiarelli [a], Patrizia Di Filippo [a,b], Donatella Pomata [a,b], Carmela Riccardi [a,b], Martina Ristorini [a], Maria Luisa Astolfi [b], Silvia Canepari [a]

[a] Department of Chemistry, Sapienza University of Rome, P. le Aldo Moro, 5, Rome 00185, Italy; [b] INAIL Research, Certification and Control Division, DIPIA, Via di Fontana Candida 1, 00040 Monteporzio Catone, Rome, Italy.

Abstract: Domestic biomass heating and wildfires strongly affect particulate matter (PM) concentration in the atmosphere. The individuation of alternative chemical tracers may provide a valuable tool to apportion different possible contributions to biomass burning. In this study, we used a new experimental procedure, based on high spatial resolution analyses of PM10, to assess the spatial distribution of levoglucosan (LVG) and evaluate the possible use of alternative biomass burning tracers in the Terni basin, a wide urban and industrial hot-spot of Central Italy, which includes several spatially disaggregated sources. Spatially-resolved chemical characterization of PM10 was obtained through the use of innovative samplers working in parallel in a dense monitoring network (20 sampling sites, about 1 km between each other), during wintertime. PM10 samples were analyzed for LVG, water-soluble organic carbon (WSOC) and water-soluble and insoluble fraction of 33 elements. Principal component analysis (PCA) on the obtained spatially-resolved data allowed us to identify biomass burning tracers across the polluted study area. Analyses of size-segregated PM samples showed the presence of LVG, WSOC, and water-soluble Cd, Cs, K, Rb and Tl in particles with size fraction smaller than 1 µm, confirming them as tracers of combustion processes (mainly related to biomass burning). Pearson correlation coefficients demonstrated that concentrations of WSOC and water-soluble Cd, Cs, K, Rb and Tl were well correlated with the spatial variability of LVG concentration. The combined use of spatially and dimensionally resolved data was found to be

particularly advantageous for the identification of alternative source tracers, which were used to reliably trace the main local biomass burning sources in the study area.

Keywords: wood burning; levoglucosan; water-soluble element; spatial variability; PCA; size distribution.

1. Introduction

Over the last few decades, a series of studies on the apportionment of specific anthropogenic and natural particulate matter (PM) sources have spotlighted biomass burning as one of the most significant air pollution sources. Biomass burning has been pointed out as one of the largest sources of fine particles in the troposphere, with global, regional and local impacts on air quality, public health and climate (Chen et al., 2017; Vicente and Alves, 2018). Residential heating by wood combustion (especially during the coldest periods of the year, Szidat et al., 2007), the use of pellet stoves in urban areas (Puxbaum et al., 2007), wildfires (Phuleria et al., 2005; Yamasoe et al., 2010; Van Drooge et al., 2012), the burning of agricultural waste in rural areas (Frasca et al., 2018; Lee et al., 2008) and the energy production by biomass, contribute to the aerosol levels (Andreae and Merlet, 2001), resulting in a large impact on global climate and human health (Barregard et al., 2007; Seagrave et al., 2006; Naeher et al., 2007).

During the last years, levoglucosan (LVG; 1,6-anhydro- β-D-glucopyranose) has received increasing attention as a very selective tracer for biomass burning (Van Drooge et al., 2014). In fact, the formation of LVG is usually due to the combustion of wood and other materials composed of polysaccharides like cellulose (Elias et al., 2001).

Besides LVG, WSOC, potassium (K) and rubidium (Rb), have been deemed to be good biomass burning tracers. Urban et al. (2012) showed a significant linear correlation between LVG and WSOC in a rural area of São Paulo State, thus identifying biomass burning as a very important source of WSOC. On the other hand, K and Rb, in their water-soluble fraction, have been identified as biomass burning tracers, since their release during biomass combustion has been observed (Duan et al., 2004; Zhang et al., 2015; Simonetti et al., 2018b, 2018c)., while the insoluble fraction of K and Rb in PM is usually attributed to sea salt and soil dust resuspension (Aiken et al., 2010; Frasca et al., 2018; Simonetti et al., 2018b, 2018c; Canepari et al., 2019). Studies reporting parallel trend of water-soluble K and Rb in aerosol sampled at different sites and their similar particle size distribution in fine fraction seemed to confirm biomass burning as common main emission source of these elements (Canepari et

al., 2014; Frasca et al., 2018; Simonetti et al., 2018b; Canepari et al., 2019). Furthermore, Simonetti et al. (2018a), thanks to the optimization of a new system, used to obtain elemental profiles of some specific indoor and outdoor sources, showed that relatively high concentrations of Cs, Cd, K, Rb and Tl can be released by wood and pellet burning as well as by the cleaning of pellet stoves and thermo-fireplaces.

Overall, the impact of biomass burning on the environment and on human health have led to numerous studies focused on the chemical characterization of the particles released by this emission source in order to evaluate their dispersion over the territory and to assess the personal exposure. The quantitative assessment of biomass burning contribution to PM is usually obtained by applying to LVG concentration experimental emission factors, whose value may change depending on the wood type and combustion conditions (Piazzalunga et al., 2011, Vicente and Alves, 2018, Perrino et al., 2019). Therefore, the individuation of alternative chemical tracers, in relation to those usually reported in the literature (Achad et al., 2018; Thepnuan et al., 2018) is of major importance, as may provide a valuable tool to apportion different possible contributions to biomass burning (Duan et al., 2004). Furthermore, the use of soluble elements may be a convenient alternative to LVG, due to the faster and cheaper analytical procedure.

Spatial distribution of the particles depends on several factors such as their dispersion capacity (which varies as a function of their dimension, shape, chemical composition and density), the location and the emission rate of their sources and the complexity of PM transport and transformation processes (Fox, 1984; Almeida et al., 2006; Perrino et al., 2010). In this study, we used a new experimental procedure, based on high spatial resolution analyses of PM10 (Massimi et al., 2017, 2019) to identify organic and inorganic biomass burning tracers in the Terni basin, a wide urban and industrial hot-spot of Central Italy. Spatially-resolved chemical characterization of PM10 was obtained through the use of innovative devices for PM sampling on membrane filters (HSRS - High Spatial Resolution Sampler; Fai Instruments, Fonte Nuova, Rome, Italy; Fig. 1) working in parallel at twenty sites, during a two-month winter monitoring period. The study area was chosen for spatially representing the main anthropic PM emission sources (i.e. vehicular traffic, rail network, power plant, steel plant, domestic biomass heating) located in different sites of the town. To individuate alternative tracers able to recognize the contribution from different possible sources associated to the combustion of biomass, we characterized the thoracic fraction of airborne particulate matter (PM10) for LVG, WSOC and 33 elements (Al, As, Ba, Bi, Ca, Cd, Ce, Co, Cr, Cs, Cu, Fe, Ga, K, La, Li, Mg, Mn, Mo, Na, Nb, Ni, Pb, Rb, Sb, Sn, Sr, Ti, Tl, U, W, Zn, Zr) at the twenty monitoring sites. To increase the

selectivity of the elements as biomass burning tracers, a chemical fractioning procedure, previously optimized and validated (Canepari et al., 2006a, 2006b), was applied to the PM10 samples, in order to assess the chemical form in which each element was released (water-soluble and insoluble fraction), which may be typical of its emission source (Templeton et al., 2000). To identify and evaluate biomass burning tracers, the obtained spatially-resolved data were analyzed by performing principal component analysis (PCA) and by considering Pearson correlation coefficients. Furthermore, size distribution of the particles released by different local PM emission sources was evaluated to confirm the attribution of the identified chemical tracers to combustion processes (mainly related to biomass burning).

2. Materials and Methods

2.1. Sampling Sites

The city of Terni is located in a basin of Central Italy (Moroni et al., 2013), in southern Umbria region (42°34′N; 12°39′E). It is a town of 211.90 km^2, counting around 112,000 inhabitants (Sgrigna et al., 2015). The territory of Terni is a wide plain surrounded by mountains and hills, characterized by the presence of urban and industrial PM emission sources (Guerrini, 2012) and by meteorological conditions (very-low wind speed predominantly directed from East-North-East to West-South-West; Capelli et al., 2011) that favor accumulation of air pollutants (Ferrero et al., 2012). In addition, differently from the city center, in marginal neighborhoods in the South and in the North of the town, most of the dwellings are townhouses, frequently heated by biomass burning appliances.

PM_{10} samples were collected at twenty monitoring sites from the 25th of November 2017 to the 15th of January 2018. The sampling sites were chosen in order to cover the whole basin with around 1 km spatial resolution, allowing us to identify areas characterized by the presence of different local PM emission sources. In particular:

- power plant for waste treatment in the West of the city (industrial area): MA, FR;
- carpentry in the South-West of the city (industrial area): FA;
- craftsmanship lab in the South-West of the city (industrial area): CB;
- rail network in the North-West of the city (urban area): GI, CR, HG;
- trafficked and heavily trafficked streets in the city center (urban area): HV, SA, UC, CA, CO;

- domestic biomass heating in the South and in the North of the city (urban areas): BR, AR, CR PI, PV, LG;
- very extensive steel plant in the East of the city (industrial area): RO, OB, PR.

Geographical coordinates of the twenty selected sites (MA, FA, GI, FR, CB, PI, BR, AR, CR, HG, SA, PV, LG, HV, UC, CA, CO, RO, OB, PR) are reported in supplementary material S1 and more details about the characteristics of the monitoring sites are reported in Massimi et al. (2017 and 2019). Three low-pressure impactors, able to fractionate particles in 10 size fractions, were deployed in the East (PR), center (CA) and West (MA) of the city.

2.2. Sampling Equipment

High spatial resolution sampler (HSRS; Fig. 1), used in this study to collect PM_{10} samples, is a low-cost and self-powered device recently developed for long term (1-2 months; flow rate of 0.5 L min^{-1}) samplings of PM on membrane filters (diameter of 37 mm), suitable for successive chemical analyses. The low volume device has been evaluated in terms of efficiency and repeatability (Catrambone et al., 2019). For the validation step, three PM_{10} samplers have been operated side-by-side for 1 year (30- or 45-day samplings) and PM_{10} samples have been analyzed for PM mass, levoglucosan and elements. The results have been evaluated in terms of relative standard deviation of the replicates and compared with the average values obtained from daily samplings carried out by a reference sampler operating at the flow rate of 2.3 m^3 h^{-1}. The comparison with the reference sampler was very good for stable, fine components (e.g.: sulphate, potassium, LVG, elements) and satisfactory for stable coarse components (e.g.: sodium, magnesium, calcium). Moreover, the HSRS showed high repeatability, especially for metals and metalloids (5.6–16%).

In addition, the efficiency of the HSRS has been also evaluated in the field. In fact, the sampler has been already employed in the area of Terni for different monitoring campaigns (Massimi et al., 2017, 2019) and has been found to be effective for the construction of monitoring networks for atmospheric PM, for the evaluation of the spatial variability of PM_{10} chemical components and for the representation of the different emission source contributions in the monitored area. The HSRS can be easily installed on various supports, thus improving the access to a large number of sampling locations. To ensure homogeneous sampling conditions, all the devices, equipped with PM_{10} sampling head filter system, have been deployed within 4 m above ground level and with southern exposition.

The low-pressure impactors (Micro-Orifice Uniform Deposition Impactors; MOUDI) working in parallel during the two-month winter monitoring period at three sites in the East (PR), center (CA) and West (MA) of the city, operate at the flow rate of 30 L min^{-1} and have 10-stage cut-sizes of 0.18, 0.32, 0.56, 1.0, 1.8, 3.2, 5.6, 10 and 18 μm in aerodynamic diameter (AD; mod. 110.R, MSP Corporation, U.S.A.).

The PM_{10} samplers and the 10-stage impactors were equipped with Teflon membrane filters with a diameter of 37 and 47 mm, respectively (PTFE membranes, 2 μm pore size, PALL Corporation, Port Washington, New York, NY, USA).

Fig.1. Samplers (HSRS - High Spatial Resolution Sampler; Fai Instruments, Fonte Nuova, Rome, Italy) deployed in Terni.

2.3. Analytical Procedures

2.3.1. Water-soluble and Insoluble Element Fraction

Chemical analysis of the elemental content in the sampled PM_{10} was performed by using a procedure that separates water-soluble fraction of the analyzed elements (Canepari et al., 2006a, 2006b). Since each element is released as specific chemical species by each emission source, this method allowed

for increasing the selectivity of elements as tracers of sources that mainly release water-soluble particles (Canepari et al., 2009, 2014; Perrino et al., 2010).

Briefly, after removing the supporting polymethylpentene ring, each PTFE membrane filter was subjected to an ultrasound assisted extraction for 30 min in 10 mL of deionized water (Arioso UP 900 Integrate Water Purification System). The extracted solution was filtered on a cellulose nitrate filter (0.45 µm pore size, Merck Millipore Ltd., Billerica, MA, USA) to obtain the water-soluble fraction. The insoluble dust on the two membrane filters (sampling and filtration) was subjected to a microwave assisted acid digestion (Ethos Touch Control with Q20 rotor, Milestone, Bergamo, Italy) by using 2 mL of ultrapure concentrated HNO_3 (67%; Promochem, LGC Standards GmbH, Wesel, Germany) and 1 mL of H_2O_2 (30%; Promochem, LGC Standards GmbH, Wesel, Germany). The digested solution was diluted to 50 mL with deionized water and filtered with syringe filters (25 mm diameter, 0.45 µm pore size, GVS Filter Technology, Morecambe, UK) to obtain the insoluble fraction.

After the two-step sequential leaching, the concentrations of 33 elements (Al, As, Ba, Bi, Ca, Cd, Ce, Co, Cr, Cs, Cu, Fe, Ga, K, La, Li, Mg, Mn, Mo, Na, Nb, Ni, Pb, Rb, Sb, Sn, Sr, Ti, Tl, U, W, Zn, Zr) in both the fractions was determined by using a quadrupole inductively coupled plasma mass spectrometer (ICP-MS; model 820-MS; Bruker, Bremen, Germany) equipped with a glass nebulizer (0.4 mL min-1; Analytik Jena AG, Jena, Germany). For each element, external standard calibration curve was performed in the 1-500 µg L^{-1} range by serially diluting standard stock solutions (1000 ± 2 mg L^{-1}; Exaxol Italia Chemical Manufacturers Srl, Genoa, Italy; Ultra Scientific, North Kingstown, RI, USA; Merck Millipore Ltd., Billerica, MA, USA). To control the nebulizer efficiency, yttrium (1000 ± 2 mg L^{-1}; Panreac Química, Barcelona, Spain) was set at 5 µg L^{-1} as internal standard for all the measurements (Astolfi et al., 2018; Conti et al., 2018). The values of blanks, subjected to similar sample preparation and analytical procedures, were deducted from all measurements and the limits of detection (LODs) were set at 3 times the standard deviation (SD) of 10 replicate blank determinations (Table 1, supplementary material S2, supplementary material S3).

Further details about the used instrumental conditions and the analytical performance of the method are reported in Astolfi et al. (2018) and in Canepari et al. (2009), respectively.

2.3.2. Water-soluble Organic Carbon

Water-soluble organic carbon (WSOC) was analyzed in the water-soluble fraction by TOC-VCSH (Shimadzu Corporation, Kyoto, Japan), using the NPOC (non-purgeable organic carbon) procedure

(Saarikoski et al., 2007). Before WSOC instrumental analysis, each sample was diluted 1:10 with deionized water and 100 µL of HCl 10 M (Promochem, LGC Standards GmbH, Wesel, Germany).

2.3.3. Levoglucosan

LVG analysis was performed in the water-soluble fraction according to Buiarelli et al. (2018). Each sample was analyzed by HPLC (1260 Infinity II system Agilent Technologies Italia S.p.A., Cernusco sul Naviglio, MI, Italy), coupled to a triple quadrupole mass spectrometer (API 2000 AB SCIEX S.r.l. Forster City, CA) provided with an electrospray ionization (ESI) source.

The mobile phase (200 µL min^{-1}) consisted in water (H_2O) and acetonitrile (CH_3CN) and a step elution was used, changing the mobile phase composition from H_2O-CH_3CN=5:95 to H_2O-CH_3CN=65:35. Chromatographic analysis was performed on SeQuant® ZIC®-HILIC column (5 µm polymer 150 x 2.1 mm), equipped with the same protective guard column (Merk S.p.a Vimodrone, Milano, Italy).

Data were collected in negative ion mode by multiple reactions monitoring (MRM). Mass spectrometric parameters were optimized by infusion at 10 µL min^{-1} of LVG standard solution (Sigma Aldrich Fine Chemicals St. Louis, MO). The ion transitions for the HPLC analysis in MRM mode: 160.8 $[M-H]^-$→100.9 (quantifier ion), 160.8→85.1, 160.8→113.1 (qualifier ions), were used for the LVG detection. LVG retention time was 7.5 min.

The limits of detection (LODs) were set at 3 times the standard deviation (SD) of 10 replicate blank determinations (Table 1, supplementary material S2).

2.4. Statistical Analyses

Principal component analysis (PCA; Massimi et al., 2017, 2018, 2019), was performed by using the statistical software R (R-project for statistical computing, Ver. 3.0, 32-bit). Concentrations of LVG, WSOC and water-soluble and insoluble fraction of the 33 elements, determined in the PM_{10} sampled in Terni, were examined together. The matrix of the data was transformed by performing row and column autoscaling to correct variations of the data due to the different scaling and units of the variables.

The reliability of the identified chemical tracers was evaluated through the individuation of Pearson correlation coefficients (Sedgwick, 2012). Pearson coefficients between LVG concentration and the concentrations of WSOC and water-soluble and insoluble fraction of the 33 elements in PM_{10} and size-segregated samples, were calculated to assess and compare the spatial and dimensional

variability of the biomass burning tracers across the polluted study area. In order to make the two sets of values (spatial and dimensional) comparable, we normalized the concentrations of each set by dividing the values of each variable by the maximum value of each set: all variables were thus included in the range 0-1.

3. Results and Discussion

3.1 Identification of Biomass Burning Tracers through Principal Component Analysis

PCA on the whole dataset was performed with the aim to identify and cluster biomass burning tracers according to the concentrations of LVG, WSOC and water-soluble (_s) and insoluble fraction (_i) of the 33 elements, determined at the twenty collection sites, during the two-month winter monitoring period. Concentration data are reported in supplementary Material S2.

Five significant components accounting for 88.78% were obtained (the scores and loadings are shown in supplementary material S3); the variance explained by each component is: 52.26%, 18.04%, 8.71%, 5.42% and 4.35%. First component (PC1), which explains the 52.31% of the total variance, well separates the samples (scores) collected at the monitoring sites where the impact of the main local PM emission sources was higher (FA for biomass burning, RO and PR for the steel plant) from the others. In fact, at these sites the highest concentrations of the analyzed chemical components (loadings) were found. However, PC1 does not explain the spatial variability of the chemical compounds released at lower concentrations at all the other sites. On the contrary, the second, the third and the fourth PCs (PC2, PC3 and PC4) well separates the samples depending on the concentration variability of the chemical components among all the sites (biplots of PC1 and PC2 and of PC2 and PC3 are shown in supplementary material S3). PC2 well separates the samples collected at the sites where the impact of biomass burning and rail network emissions was higher from the samples collected in the vicinity of the steel plant (RO, OB and PR). PC3 explains the concentration variability of the chemical compounds released by the steel plant at RO from those released at PR and OB. PC4 well separates the samples collected at the sites where the impact of biomass burning (FA, CB, BR, AR, CR, PI, PV and LG) was higher from the samples collected in proximity of the rail network (GI, CR and HG). Therefore, PC2 and PC4, which explain the 23.46% of the total variance, were represented in the biplot of Fig. 2 and in the score plot of Fig.3, since they better reflect the spatial distribution of the chemical compounds across the study area and well cluster the chemical components released by biomass burning.

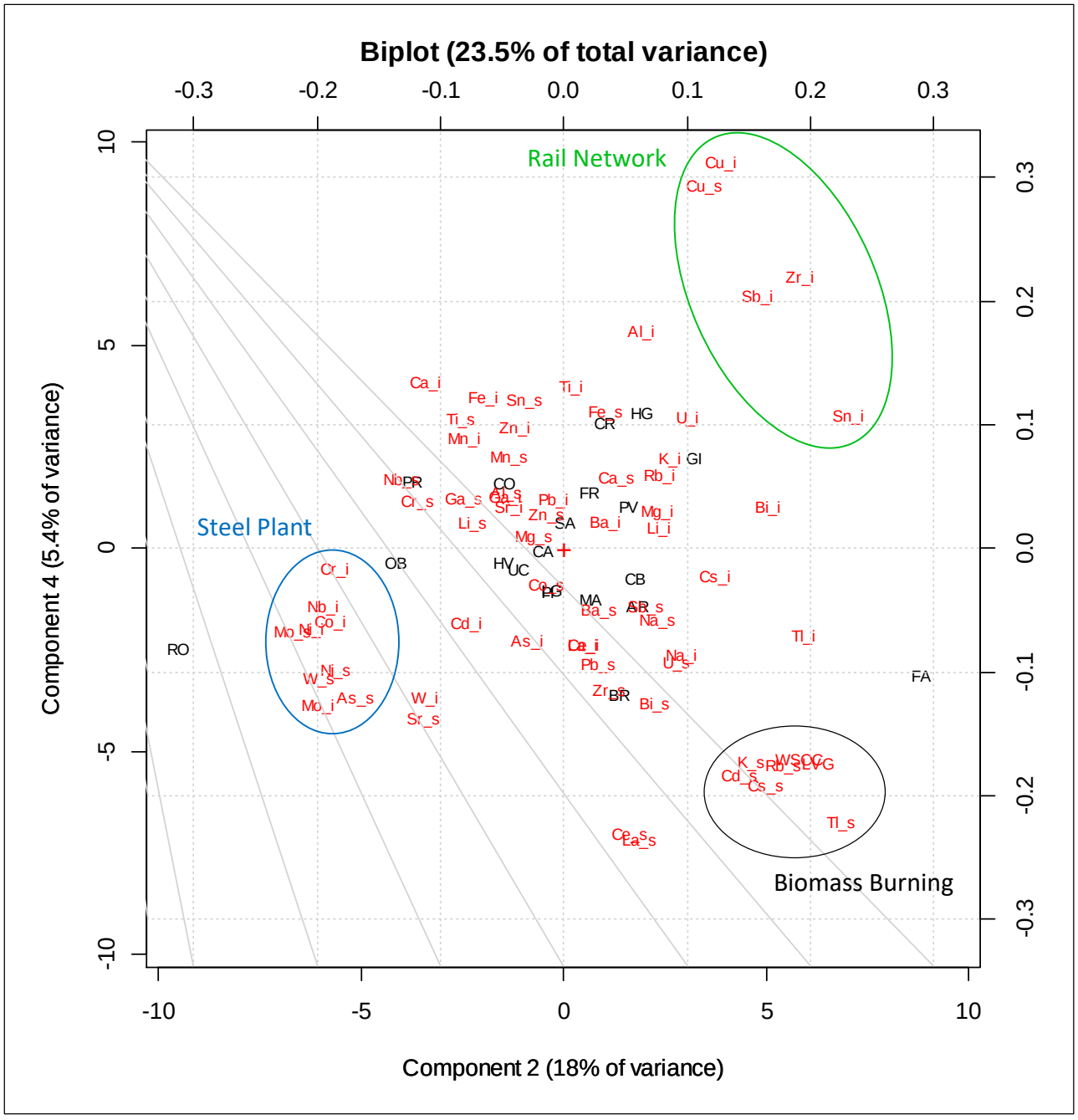

Fig. 2. Biplot of the PCA (PC2 and PC4) performed on the concentration data of LVG, WSOC and water-soluble (_s) and insoluble (_i) fraction of the 33 elements, determined at the twenty collection sites. The biomass burning tracers are circled in black, the steel plant tracers in blue and the rail network tracers in green.

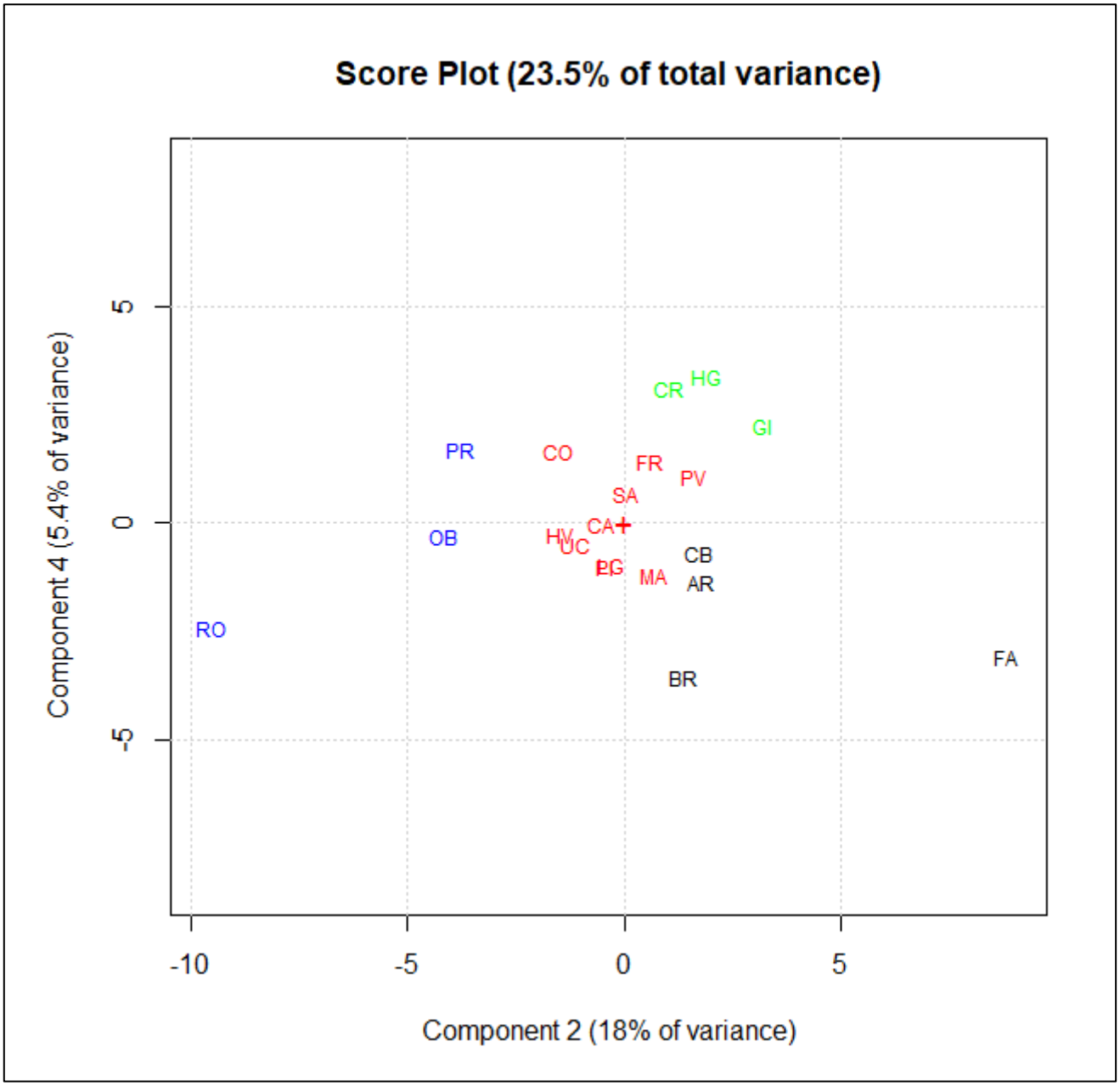

Fig. 3. Score plot of the PCA (PC2 and PC4) performed on the concentration data of LVG, WSOC and water-soluble and insoluble fraction of the 33 elements, determined at the twenty collection sites. The steel plant sites are marked blue, the rail network sites in green, the biomass burning sites in black and the other sites in red.

From Fig. 2, we can observe that the chemical compounds are separated along PC2 and PC4 depending on the spatial variability of their concentrations among all the sampling sites. In the central part of the biplot are all the PM_{10} chemical components that did not show high spatial variability; the

other chemical compounds are clustered in three main groups (circled in three different colors), each one characterized by the impact of an intense local PM emission source.

The first group (circled in blue), on the left lower part of the biplot, is composed of elements released at high concentrations by the steel plant: As_s, Co_i, Cr_i, Mo_i, Mo_s, Nb_i, Ni_i, Ni_s and W_s. All these elements are present in the stainless steel since they are used to increase its toughness, ductility, tensile strength and resistance to chemical oxidation (Massimi et al., 2017). The closest site to the steel plant: RO (marked in blue), is plotted on the left lower part of the biplot because at this site the highest concentrations of As_s, Co_i, Cr_i, Mo_i, Mo_s, Nb_i, Ni_i, Ni_s and W_s were found. PR and OB (also marked in blue), which are other monitoring sites in proximity of the steel plant, are also plotted on the direction of these elements.

The second group of Fig. 2 (circled in green), on the right upper part of the biplot, is composed of elements considered to be reliable tracers of rail network emissions: Cu_i, Cu_s, Sb_i, Sn_i and Zr_i. In fact, these elements are mainly released by mechanical abrasion of train brakes (Weckwerth, 2001; Abbasi et al., 2012; Querol et al., 2012; Kam et al., 2013; Namgung et al., 2016). GI, HG and CR (marked in green), which are the closest sites to the railway, where the highest concentrations of Cu_i, Cu_s, Sb_i, Sn_i and Zr_i were found, are plotted on the left upper part of the biplot, on the direction of these elements.

The third group (circled in black), on the right lower part of the biplot, is characterized by the presence of LVG and includes WSOC, Cd_s, Cs_s, K_s, Rb_s and Tl_s. This cluster reasonably represents the contributions from biomass burning related sources. In fact, monosaccharide anhydride LVG is well known to be produced from thermal alteration of cellulose and released during the pyrolysis of cellulose at temperatures above 300 °C. As LVG is a dominant organic component emitted in fine smoke particulate matter by wood burning, it has been often proposed as a highly selective biomass burning tracer (Simoneit et al., 1999; Schauer et al., 2001; Simoneit et al., 2002, 2004; Engling et al., 2006; Sullivan et al., 2008). Although LVG is stable to degradation, when exposed to ambient conditions and sunlight (Fraser and Lakshmanan, 2000; Jordan et al., 2006), it may not be fully conserved during transport due to atmospheric oxidative processes (Hoffmann et al., 2009; Kessler et al., 2010; Slade and Knopf, 2013, 2014). Since our study occurred during wintertime and the main sources of LVG were local biomass burning emissions with little transport time or distance, LVG was likely stable enough to be quantified by membrane filter collection and to be used as a robust tracer for biomass burning. Water-soluble organic carbon was used as biomass burning tracer too (Graham et al., 2002), even though it is generally much less selective than LVG, because it includes

soluble species generated by wood burning (such as LVG and other anhydro-sugars), but soluble organic species are also released/formed by biogenic materials, chemical oxidation of VOCs in the atmosphere, soil resuspension and fuel combustion (Urban et al., 2012). The presence of WSOC in the same cluster of LVG indicates that in our study biomass burning was the strongest WSOC source. Water-soluble elemental potassium is also well known to be produced from the combustion of biomass and it is commonly used as wood smoke tracer (Chow et al., 2007). Potassium can be also released in the atmosphere by resuspension of crustal components, but this source mainly releases K as insoluble species (Canepari et al., 2014; Simonetti et al., 2018b, 2018c). Other known sources of potassium are sea salt and cooking aerosol, but, in outdoor environments far from the coasts, they are usually responsible for a small fraction of K (Li et al., 2003). Water-soluble rubidium, although less studied than LVG, WSOC and K, has also been proposed as a reliable tracer of biomass burning; the fine fraction of Rb is usually released by wood burning, while the coarse fraction, less soluble, originates from soil and can be related to resuspension of settled dust or to the release of wood ash during residential biomass heating cleaning (Frasca et al., 2018; Simonetti et al., 2018b, 2018c; Canepari et al., 2019). Typically, the source due to soil erosion (coarse particles containing insoluble species) predominates during the summer, while the contribution from combustion sources (fine particles containing soluble species) prevails during the winter, when domestic biomass heating is switched on (Canepari et al., 2014; Frasca et al., 2018). Water-soluble thallium, cesium and cadmium are less documented in the literature as biomass burning tracers (Canepari et al., 2019; Perrino et al., 2019). However, Tl is usually contained in plants at detectable concentrations (approximately 0.05 mg kg^{-1}; Krasnodębska-Ostręga and Golimowski, 2008) and thus it may be released during their combustion. In addition, water-soluble Tl, Cs and Cd can be released by biomass burning as a relevant increase of their concentrations has been detected in wood and pellet ashes originated from domestic biomass heating systems (Simonetti et al., 2018b, 2018c; Piacentini et al., 2019). It is worth noting that Cd_s, Cs_s, Rb_s and Tl_s are not among the main components of wood and pellet combustion ashes (Simonetti et al., 2018a). However, in the Terni basin, they are more sensitive as environmental source tracers respect to the main components, because of their very low levels at all the sites less affected by biomass burning contributions, which make their relative concentrations considerably higher at the biomass burning sites.

Site FA (marked in black), which is in close proximity of a carpentry, where the highest concentrations of LVG, WSOC, Cd_s, Cs_s, K_s, Rb_s and Tl_s were found, is plotted on the right lower part of the biplot, on the direction of these chemical components. At BR (also marked in black),

which is a monitoring site located in an area where most of the dwellings were heated by biomass burning appliances, high concentrations of these chemical compounds were recorded. Hence, also BR is plotted on the direction of these chemical components.

Overall, thanks to the principal component analysis, LVG, WSOC and water-soluble Cd, Cs, K, Rb and Tl were identified as biomass burning tracers in the Terni basin. These chemical compounds were reasonably released at the highest concentrations by the burning of carpentry waste products (FA) and domestic biomass heating (BR).

It is worth noting that the insoluble fraction of the same elements is not clustered with LVG; this confirms that the insoluble species are mainly released by other sources than biomass burning. Chemical fractioning procedure allowed us to purge contributions from these interfering sources and to increase the selectivity of Cd, Cs, K, Rb and Tl as source tracers.

3.2. Size Distribution of Levoglucosan and the Other Identified Biomass Burning Tracers

Analyses of size-segregated PM samples collected at sites PR, CA and MA, where low-pressure 10-stage impactors were deployed, allowed us to evaluate the size distribution of LVG, WSOC and water-soluble Cd, Cs, K, Rb and Tl, in the East (PR), center (CA) and West (MA) of the city. Table 1 reports the size distribution of water-soluble fraction of the 33 elements determined at PR, CA and MA; element concentrations in the insoluble fraction are reported in supplementary Material S4. From Table 1, we can observe that at all three monitoring sites, LVG, WSOC and water-soluble Cd, Cs, K, Rb and Tl were found only in fine particles with size fraction smaller than 1 µm, confirming that combustion processes were much more relevant than mechanical and abrasive ones (mainly producing coarse particles; Weckwerth, 2001; Li et al., 2013; Namgung et al., 2016).

At PR, concentrations of LVG, WSOC and water-soluble Cd, Cs, K, Rb and Tl strongly increased as size fraction declined and the highest concentrations were found in the size fraction smaller than 0.18 µm. The similar size distribution of the examined chemical compounds suggests that at PR they were all released by the same PM emission source.

At MA, LVG, WSOC and water-soluble Cd, Cs, K, Rb and Tl were found at high concentrations in all the particles with size fraction smaller than 1 µm, confirming them as tracers of combustion processes (mainly related to biomass burning). Anyway, the highest concentrations of LVG, WSOC and water-soluble Cd, Cs, K, Rb were found in the size fraction 0.32-0.56 µm, while water-soluble Tl concentration increased as size fraction declined, showing the highest value in the size fraction smaller than 0.18 µm. Since Tl may be also released in the slag and ash produced by coal combustion

(Finkelman, 1999; Cvjetko et al., 2010) in areas near industrially relevant objects, such as the power plant (Karbowska, 2016), its different size distribution at MA may be due to the slight contribution from the power plant for waste treatment.

At CA, the concentrations of all the identified biomass burning tracers showed a broad peak in the 0.18-1 μm size range, with the highest values in the size fraction 0.32-0.56 μm. Since the monitoring site CA is far from the main biomass burning emissions of the city (FA, BR), we can reasonably hypothesize that particles containing LVG, WSOC and water-soluble Cd, Cs, K, Rb and Tl were transported to this site. This also explains the very low concentrations of the examined chemical components found in particles with size smaller than 0.18 μm, typically attributed to fresh emissions, with respect to those found at PR and MA. In fact, although it is well known that fine particles, mainly produced by combustive processes, are more persistent in the atmosphere and more easily propagate in large areas than coarse ones (mainly produced by mechanical and abrasive processes; Weckwerth, 2001; Li et al., 2013; Namgung et al., 2016), it is also known that the smallest particles have a very low residence time in the atmosphere, as they tend to aggregate with other particles growing toward the fine fraction (they are quickly removed by coagulation mechanisms).

Overall, size distribution analyses of LVG, WSOC and water-soluble Cd, Cs, K, Rb and Tl proved their attribution to combustion processes (mainly related to biomass burning).

Table 1a. Limits of detection (LODs; μg L^{-1}), mean of blank values (μg L^{-1}) and size distribution of the fine fraction (ng m^{-3}) of LVG, WSOC and water-soluble fraction of the 33 elements determined at PR, CA and MA. The LODs were set at 3 times the standard deviation (SD) of 10 replicate blank determinations**.**

Water-soluble Species	LOD (μg L^{-1})	Mean Blank Values (μg L^{-1})	<0.18 μm			0.18-0.32 μm			0.32-0.56 μm			0.56-1 μm		
			PR	CA	MA	PR	CA	MA	PR	CA	MA	PR	CA	MA
Al	3.4	1.4	0.22	0.11	0.22	0.49	0.20	0.30	0.48	0.24	1.0	0.53	1.7	3.7
As	0.086	0.050	0.16	0.042	0.028	0.085	0.070	0.059	0.066	0.083	0.069	0.029	0.080	0.077
Ba	3.7	0.069	0.052	0.049	0.066	0.054	0.053	0.057	0.16	0.059	0.085	0.059	0.19	0.12
Bi	0.0011	0.00023	0.0054	0.00025	0.0019	0.0058	0.0025	0.0027	0.0057	0.0051	0.0069	0.0031	0.0082	0.011
Ca	370	56	9.1	3.4	8.7	5.1	5.7	6.5	9.2	7.7	5.6	15	21	17
Cd	0.0038	0.00080	0.042	0.0048	0.025	0.033	0.027	0.026	0.022	0.044	0.034	0.012	0.034	0.028
Ce	0.0096	0.0041	0.0011	0.00084	0.041	0.0011	0.0020	0.061	0.00083	0.0024	0.0028	0.0016	0.0023	0.0019
Co	0.0073	0.0025	0.0059	0.0017	0.0020	0.0044	0.0028	0.0024	0.0038	0.0036	0.0040	0.0026	0.0049	0.0046
Cr	0.081	0.13	0.97	0.11	0.23	0.82	0.36	0.22	0.53	0.53	0.37	0.27	0.52	0.36
Cs	0.0033	0.00090	0.021	0.0023	0.010	0.015	0.012	0.010	0.0080	0.014	0.011	0.0032	0.010	0.011
Cu	0.20	0.13	0.21	0.14	0.088	0.16	0.094	0.083	0.18	0.16	0.089	0.086	0.28	0.29
Fe	3.0	0.55	1.6	0.31	0.92	2.5	1.4	1.9	2.5	2.6	3.7	2.6	5.3	6.6
Ga	0.0018	0.00057	0.0055	0.00014	0.0011	0.0093	0.0032	0.0026	0.0079	0.0090	0.0041	0.0041	0.0098	0.012
K	64	40	98	9.5	58	91	83	82	56	106	98	20	71	81
La	0.0033	0.0014	0.00052	0.00021	0.031	0.00063	0.00058	0.035	0.00056	0.00095	0.0010	0.0010	0.0012	0.0010
Li	0.0063	0.0031	0.10	0.0093	0.023	0.054	0.040	0.026	0.020	0.039	0.026	0.0082	0.024	0.020
Mg	3.9	2.1	0.79	0.19	0.63	1.1	0.43	0.46	1.6	0.79	0.51	2.2	2.5	2.2
Mn	0.17	0.033	1.1	0.018	0.22	1.7	0.37	0.35	2.1	0.96	0.94	1.6	2.1	1.9
Mo	0.049	0.041	2.4	0.50	0.62	1.7	0.65	0.36	1.5	0.79	0.36	0.43	0.67	0.34
Na	19	10	13	1.9	6.6	12	7.8	6.9	10	12	8.0	12	17	16
Nb	0.00082	0.00030	0.00020	0.0000083	0.000072	0.00024	0.00012	0.00016	0.00042	0.00022	0.00029	0.00050	0.00085	0.00056
Ni	0.35	0.050	0.15	0.13	0.038	0.19	0.078	0.054	0.27	0.14	0.063	0.12	0.51	0.11
Pb	0.10	0.044	0.90	0.021	0.15	0.83	0.33	0.24	0.55	0.61	0.39	0.41	0.69	0.77
Rb	0.031	0.020	0.28	0.027	0.19	0.24	0.22	0.22	0.15	0.28	0.24	0.055	0.20	0.20
Sb	0.0094	0.0026	0.054	0.0058	0.046	0.049	0.032	0.053	0.054	0.053	0.058	0.023	0.061	0.059
Sn	0.013	0.0048	0.019	0.0079	0.026	0.011	0.012	0.027	0.015	0.021	0.031	0.0035	0.032	0.029
Sr	0.20	0.037	0.020	0.0081	0.018	0.016	0.014	0.015	0.025	0.020	0.016	0.035	0.048	0.042
Ti	0.15	0.064	0.0044	0.0016	0.0046	0.0067	0.0055	0.0035	0.0071	0.010	0.0035	0.0083	0.014	0.018
Tl	0.00010	0.00010	0.052	0.0092	0.063	0.037	0.041	0.053	0.017	0.043	0.039	0.0056	0.026	0.029
U	0.00092	0.00047	0.00020	0.000041	0.000074	0.00013	0.000069	0.000087	0.000073	0.00013	0.00012	0.000057	0.00016	0.00021
W	0.0015	0.0041	0.034	0.0071	0.022	0.022	0.011	0.043	0.014	0.012	0.045	0.0047	0.0092	0.049
Zn	15	3	5.4	0.37	1.6	4.9	2.0	1.9	5.2	3.5	3.1	4.4	8.1	6.8
Zr	0.00052	0.0061	0.00028	0.000072	0.00026	0.00037	0.00023	0.00046	0.00073	0.00098	0.0010	0.012	0.0040	0.0069
WSOC	190	43	600	50	380	530	390	420	400	590	490	180	480	490
LVG	8.0	1.8	360	<LOD	140	200	140	150	170	130	160	14	130	160

Table 1b. Size distribution of the coarse fraction (ng m^{-3}) of LVG, WSOC and water-soluble fraction of the 33 elements determined at PR, CA and MA. The LODs were set at 3 times the standard deviation (SD) of 10 replicate blank determinations**.**

Water-Soluble Species	1-1.8 µm			1.8-3.2 µm			3.2-5.6 µm			5.6-10 µm			10-18 µm			>18 µm		
	PR	CA	MA	PR	CA	MA	PR	CA	MA	PR	CA	MA	PR	CA	MA	PR	CA	MA
Al	0.30	0.72	1.10	0.29	0.32	0.19	0.83	0.39	0.24	0.66	0.40	0.25	0.31	0.36	0.12	0.35	0.18	0.091
As	0.0038	0.022	0.036	0.0083	0.011	<LOD	0.0069	0.0032	0.0042	<LOD	0.0041	0.0065	0.0040	0.0057	<LOD	<LOD	0.0062	<LOD
Ba	0.073	0.22	0.14	0.12	0.41	0.15	0.59	0.58	0.43	0.13	0.42	0.25	0.051	0.15	0.055	0.047	0.090	0.070
Bi	0.00050	0.0030	0.0062	0.00045	0.00036	0.00030	0.00069	0.00043	0.00045	0.00025	0.00011	0.00013	0.000079	0.0014	0.000056	0.00020	0.000033	0.000050
Ca	13	44	56	59	57	65	80	115	80	83	80	74	23	37	22	25	24	15
Cd	0.0022	0.0094	0.018	0.00052	0.0022	0.0012	0.0014	0.0014	0.0015	0.00077	0.00046	0.0012	0.00023	0.0012	0.00022	0.00047	0.00012	0.00041
Ce	0.00044	0.0013	0.0018	0.00059	0.00088	0.00057	0.0018	0.00083	0.00088	0.00064	0.00069	0.00073	0.00082	0.00072	0.00039	0.00024	0.00013	0.00020
Co	0.0010	0.0034	0.0047	0.0012	0.0019	0.0039	0.0012	0.0023	0.0032	0.00079	0.00095	0.0016	0.00023	0.00069	0.00063	0.00032	0.00044	0.00039
Cr	0.036	0.14	0.15	0.028	0.024	0.0071	0.021	0.024	0.020	0.018	0.0070	0.013	0.0023	0.0058	0.0025	0.0031	0.0015	<LOD
Cs	0.00040	0.0021	0.0033	0.00013	0.00019	0.000093	0.00017	0.00012	0.00012	0.000067	0.000039	0.00012	0.000057	0.000083	0.000044	0.000048	0.000033	0.000034
Cu	0.05	0.32	0.33	0.10	0.26	0.40	0.082	0.30	0.45	0.032	0.12	0.19	0.010	0.058	0.040	0.011	0.038	0.019
Fe	0.40	2.3	6.5	0.62	0.86	0.53	0.87	1.3	1.1	0.66	0.75	0.84	0.26	0.66	0.33	0.23	0.27	0.23
Ga	0.00037	0.0021	0.0034	0.000044	0.00016	0.000072	0.000033	0.00013	0.000081	0.000048	0.000074	0.000040	0.000010	0.000086	0.000037	0.000035	0.000074	0.000040
K	7.1	15	22	11	7.6	7.9	11	7.9	13	5.3	7.0	12	2.0	3.3	6.0	2.3	3.1	3.8
La	0.00025	0.00075	0.0010	0.00035	0.00052	0.00035	0.00092	0.00055	0.00061	0.00048	0.00058	0.00052	0.00051	0.00056	0.00030	0.00018	0.00014	0.00013
Li	0.0021	0.0068	0.0093	0.0029	0.0023	0.0019	0.0027	0.0036	0.0052	0.0015	0.0015	0.0031	0.00046	0.00065	0.00095	0.00037	0.00060	0.00043
Mg	3.2	6.7	9.6	6.5	6.4	5.1	4.2	11	16	2.7	3.9	8.5	0.72	1.3	2.1	0.8	1.4	1.1
Mn	0.34	0.88	1.2	0.15	0.25	0.16	0.15	0.34	0.35	0.26	0.19	0.19	0.061	0.079	0.053	0.057	0.055	0.036
Mo	0.12	0.24	0.19	0.15	0.10	0.11	0.12	0.13	0.073	0.061	0.048	0.050	0.018	0.019	0.030	0.015	0.016	0.027
Na	17	40	67	48	42	39	37	83	130	16	25	71	4.2	8.0	17	3.3	11	12
Nb	0.00038	0.00060	0.00055	0.00054	0.00025	0.00044	0.00054	0.00038	0.00025	0.00048	0.00019	0.00020	0.00011	0.00070	0.000037	0.000083	0.000080	0.000012
Ni	0.033	0.19	0.13	0.037	0.058	0.016	0.098	0.033	0.027	0.013	0.012	0.013	0.0041	0.011	0.0058	0.016	0.0040	0.0052
Pb	0.040	0.21	0.40	0.014	0.011	0.013	0.012	0.0054	0.012	0.0047	0.0031	0.0045	0.0030	0.0092	0.0047	0.0029	0.0011	0.0034
Rb	0.0093	0.040	0.050	0.0074	0.0060	0.0042	0.0084	0.0091	0.014	0.0031	0.0023	0.0060	0.00079	0.00020	0.0012	<LOD	0.00066	<LOD
Sb	0.0036	0.021	0.056	0.0041	0.0080	0.047	0.0041	0.010	0.016	0.0017	0.0049	0.0086	0.00035	0.0017	0.0017	0.00050	0.00086	0.0011
Sn	0.00085	0.010	0.021	0.0013	0.0037	0.0030	0.0012	0.0035	0.0045	0.00035	0.0012	0.0018	<LOD	0.0018	0.00034	<LOD	0.00046	0.00019
Sr	0.039	0.10	0.14	0.11	0.12	0.20	0.14	0.23	0.22	0.10	0.13	0.15	0.033	0.054	0.046	0.027	0.041	0.029
Ti	0.0082	0.011	0.017	0.012	0.0052	0.015	0.017	0.0079	0.013	0.0061	0.0067	0.0087	0.0023	0.0093	0.0047	0.0030	0.0023	0.0022
Tl	0.00046	0.0037	0.0059	0.00017	0.00044	0.00025	0.00010	0.00030	0.00038	0.000024	0.000061	0.00026	<LOD	0.000025	0.000053	<LOD	0.000041	0.000037
U	0.000025	0.00010	0.00020	0.00014	0.000055	0.00019	0.00016	0.00016	0.00018	0.00011	0.00010	0.00017	0.000067	0.000066	0.000056	0.000038	0.000061	0.000019
W	0.0012	0.0031	0.030	0.00093	0.0010	0.0012	0.00061	0.0011	0.0032	0.00050	0.00033	0.0028	0.00023	0.00023	0.00059	0.00032	0.00019	<LOD
Zn	1.4	5.4	7.2	0.28	1.4	0.83	0.36	0.69	0.88	0.19	0.34	0.41	0.060	0.21	0.14	0.14	0.068	0.13
Zr	0.00035	0.0022	0.0087	0.00060	0.00060	0.0046	0.00055	0.0012	0.0018	0.00042	0.00030	0.0013	0.000032	0.00033	0.00014	0.0027	0.000028	0.00022
WSOC	50	140	280	46	31	150	28	42	110	10	25	43	<LOD	40	12	7.7	1.7	7.6
LVG	1.2	41	54	1.3	5.4	2.2	0.90	2.9	7.3	0.52	1.0	1.1	0.44	0.011	<LOD	0.11	<LOD	<LOD

3.3. Correlations Between Levoglucosan and the Other Identified Biomass Burning Tracers

Biomass burning includes wood burning for home heating during wintertime and smoke transported from wildfires or prescribed burns (Lee et al., 2010; Yamasoe et al., 2010; Liu et al., 2015; Brown et al., 2016). During wintertime, when the samplings were performed, wildfires in Terni were minimal, so the main biomass burning influence was from residential biomass heating and prescribed burns.

From levoglucosan concentration map of Fig. 4, (upper panel) we can observe that the highest concentration of LVG was found at FA (5000 ng m^{-3}), located in close proximity of a carpentry. Then, high concentrations of LVG were found at CB (2900 ng m^{-3}), sited near a craftsmanship lab and at the monitoring sites located in urban areas far from heavily trafficked streets, in the North and in the South of the city: BR, AR, CR, PV and LG (3500 ng m^{-3}; 2500 ng m^{-3}; 2900 ng m^{-3}; 2300 ng m^{-3} and 2300 ng m^{-3}, respectively), where domestic biomass heating systems were largely used during the two-month winter monitoring period. Therefore, the main contributions to the total LVG concentration in Terni were found to be related to the burning of carpentry waste products and domestic biomass heating, as expected.

The reliability of WSOC and water-soluble Cd, Cs, K, Rb and Tl as biomass burning tracers was evaluated through the individuation of Pearson correlation coefficients (ρ; showed in the titles of the lower panels of Fig. 4), calculated between LVG concentration and the concentrations of WSOC and the water-soluble elements, determined at the twenty collection sites, during the two-month winter monitoring period. Water-soluble Tl and WSOC showed the highest correlations with LVG spatial distribution (ρ= 0.82). Moreover, water-soluble Rb and Cs were found to be well correlated with the spatial variability of LVG concentration (ρ= 0.77 and ρ= 0.73, respectively), while water-soluble K and Cd appeared to be less correlated (ρ= 0.69 and ρ= 0.62, respectively). At sites BR and CR, which are located in areas where most of the dwellings were heated by biomass burning appliances, the relative concentrations of the target analytes were found to be a little lower than LVG. Instead, at PR we found a bit higher relative concentrations of these chemical compounds (except for thallium). This behavior may be due to the presence of a local steel plant exhaust emission that slightly increased the concentrations of the examined PM_{10} chemical components at PR and at the sites in its vicinity (OB, RO, CO and CA).

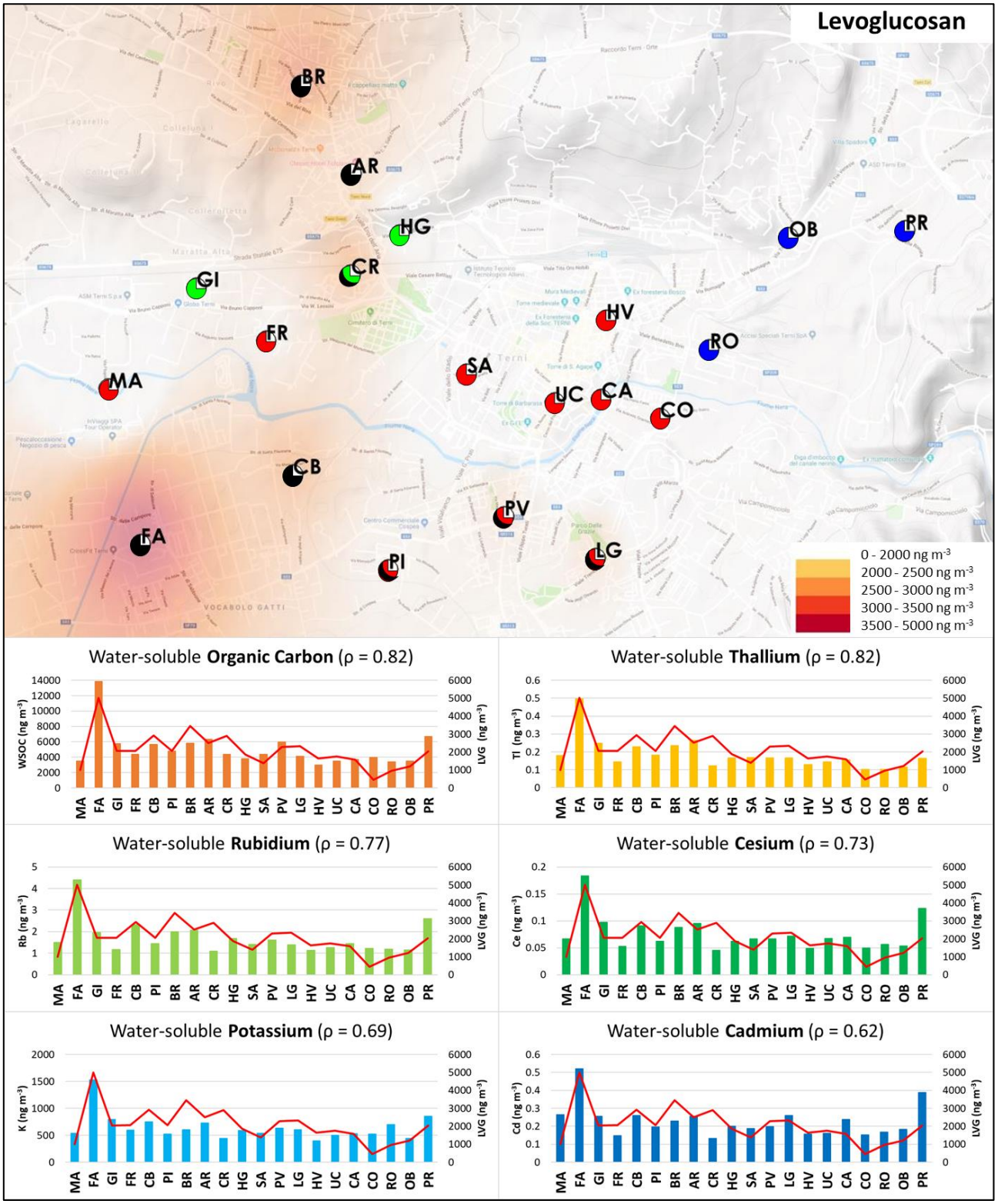

Fig. 4. Map of LVG concentrations obtained using inverse distance weighting spatial interpolation (QGis 2.18 Las Palmas; upper panel) and comparison between the spatial variability of LVG concentration and the concentrations of the other identified biomass burning tracers in Terni (WSOC

and water-soluble Cd, Cs, K, Rb and Tl; lower panel). Blue color: steel plant sites; green color: rail network sites, black color: biomass burning sites; red color: other sites.

Lower Pearson coefficients for K and Cd are mainly due, respectively, to the higher relative concentration of K at RO, and to the higher relative concentration of Cd at MA, where Cd, which is usually contained in wasted plastics (thermoplastics may contain high percentages of cadmium based color pigments; Ernst et al., 2000; Schlummer et al., 2007) may be marginally released by combustion processes from the close power plant for waste treatment.

Table 2. Correlation matrix of biomass burning tracer concentrations in PM_{10} and size-segregated samples.

Water-soluble	**Cd**	**Cs**	**K**	**Rb**	**Tl**	**WSOC**	**LVG**
Cd	1.00						
Cs	0.96	1.00					
K	0.96	0.93	1.00				
Rb	0.97	0.95	0.99	1.00			
Tl	0.89	0.92	0.91	0.93	1.00		
WSOC	0.93	0.88	0.95	0.96	0.86	1.00	
LVG	0.83	0.92	0.82	0.83	0.84	0.78	1.00

In order to confirm the relevance of wood burning emissions on the selected tracer concentrations, we evaluated their inter-correlation on the whole data-set, which included both spatially and dimensionally resolved samples; in fact, tracers that share their spatial and dimensional distributions will be very reasonably associated to the same emission source. The two sets of values (spatial and dimensional) were made comparable by normalizing the concentrations of each variable for the maximum value of each set, as detailed in paragraph 2.4. Pearson correlations of LVG with all the analyzed elements in the soluble and insoluble fraction are reported in Supplementary Materials S5. The obtained results confirmed and strengthened the above considerations: LVG showed the highest correlation coefficients with the soluble fraction of Cd, Cs, K, Rb, Tl and WSOC, while very poor correlations were found between LVG and the insoluble fraction of the same elements (Fig. S5); this confirms the robustness of the selected tracers (same spatial and dimensional distribution of LVG)

and the increased selectivity of chemically fractionated elements towards specific emission sources (the soluble and insoluble fraction of the same element is emitted by different sources).

In order to make the discussion easier, Table 2 reports the correlation matrix of the identified biomass burning tracers only. The very high correlation among all the elemental tracers confirms that they share the same predominant source. Correlations of elements with WSOC and LVG are still very good, but generally somewhat weaker, in agreement with the presence of low contributions to elements coming from sources that do not release LVG and WSOC. The weakest correlation was found between LVG and WSOC; in this study, WSOC concentration was dominated by biomass burning emission, but small contributions from other sources are expected (Urban et al., 2012).

4. Conclusions

The use of the new experimental procedure, based on high spatial resolution analyses of PM_{10} (Massimi et al., 2017, 2019) allowed us to identify and evaluate alternative organic and inorganic biomass burning tracers, in relation to those usually reported in the literature. The achieved results were supported by results obtained in size-segregated samples collected in parallel in the same area. The combined use of spatially and dimensionally resolved data was found to be particularly advantageous for the identification of reliable source tracers. The covariance of the analyzed parameters in this kind of samples is in fact not influenced by the variability of meteorological conditions, which similarly modulates all the air pollutant concentrations.

Thanks to the principal component analysis performed on the obtained spatially-resolved data, LVG, WSOC and water-soluble Cd, Cs, K, Rb and Tl were individuated as possible biomass burning tracers in the Terni basin. These chemical compounds were reasonably released at the highest concentrations by the burning of carpentry waste products, (FA) and domestic biomass heating.

Chemical fractioning procedure allowed us to increase the selectivity of Cd, Cs, K, Rb and Tl as source tracers, since only their water-soluble fraction was found to be related to biomass burning emissions.

Pearson correlation coefficients demonstrated that concentrations of WSOC and water-soluble Cd, Cs, K, Rb and Tl were well correlated with the spatial and dimensional distribution of LVG. The combined use of spatially and dimensionally resolved data was found to be a powerful tool for the identification of alternative source tracers, which were used to reliably trace the main local biomass burning sources in the study area.

The use of water-soluble Cd, Cs, K, Rb and Tl may be a convenient alternative to LVG, due to the faster and cheaper analytical procedure.

Acknowledgements

This work was funded by the project 2017 RG11715C7C8801CF (Principal Investigator Dr. S. Canepari), financed by Sapienza University of Rome, and was partially financed by INAIL Research, Certification and Control Division, DIPIA.

The authors gratefully thank FAI Instruments (Fonte Nuova, Rome, Italy), the citizens of Terni and the Terni district of ARPA Umbria (regional agency for environmental protection) with special regard to Giancarlo Caiello, Caterina Austeri and Marco Pompei for the support in the installation and in the management of the sampling equipment as well as for the help in the choice of the sampling sites.

Author Contributions

L. Massimi, G. Simonetti, F. Buiarelli and S. Canepari conceived and planned the monitoring and the experiments; L. Massimi and M. Ristorini performed the samplings; L. Massimi, G. Simonetti, D. Pomata and M. L. Astolfi performed the chemical analysis; L. Massimi and G. Simonetti elaborated the data and wrote the manuscript; F. Buiarelli, P. Di Filippo, C. Riccardi and S. Canepari coordinated the group and supervised the manuscript.

Conflicts of Interest

The authors declare no conflicts of interest.

References

Abbasi, S., Olander, L., Larsson, C., Olofsson, U., Jansson, A., Sellgren, U. 2012. A field test study of airborne wear particles from a running regional train. Proceedings of the Institution of Mechanical Engineers, Part F: J. Rail Rapid Transit., 226(1), 95-109. https://doi.org/10.1177%2F0954409711408774.

Achad, M., Caumo, S., de Castro Vasconcellos, P., Bajano, H., Gómez, D., Smichowski, P. 2018. Chemical markers of biomass burning: Determination of levoglucosan, and potassium in size-

classified atmospheric aerosols collected in Buenos Aires, Argentina by different analytical techniques. Microchem. J., 139, 181-187. https://doi.org/10.1016/j.microc.2018.02.016.

Aiken, A. C., Foy, B. D., Wiedinmyer, C., DeCarlo, P. F., Ulbrich, I. M., Wehrli, M. N., Szidat, S., Prevot, A. S. H., Noda, J., Wacker, L., Fortner, E.,Wang, J., Laskin, A., Shutthanandan, V., Zheng, J., Zhang, R., Paredes-Miranda, G., Arnott, W. P., Molina, L. T., Sosa, G., Querol, X., Jimenez, J. L., Volkamer, R. 2010. Mexico city aerosol analysis during MILAGRO using high resolution aerosol mass spectrometry at the urban supersite (T0)–Part 2: Analysis of the biomass burning contribution and the non-fossil carbon fraction. Atmos. Chem. Phys., 10(12), 5315-5341. https://doi:10.5194/acp-10-5315-2010.

Almeida, S. M., Pio, C. A., Freitas, M. C., Reis, M. A., Trancoso, M. A. 2006. Source apportionment of atmospheric urban aerosol based on weekdays/weekend variability: evaluation of road re-suspended dust contribution. Atmos. Environ., 40(11), 2058-2067. http://dx.doi.org/10.1016/j.atmosenv.2005.11.046.

Andreae, M. O., Merlet, P. 2001. Emission of trace gases and aerosols from biomass burning. Global Biogeochem. Cycles, 15 (4), 955-966. https://doi.org/10.1029/2000GB001382.

Astolfi, M. L., Marconi, E., Protano, C., Vitali, M., Schiavi, E., Mastromarino, P., Canepari, S. 2018. Optimization and validation of a fast digestion method for the determination of major and trace elements in breast milk by ICP-MS. Anal. Chim. Acta, 1040, 49-62. https://doi.org/10.1016/j.aca.2018.07.037.

Barregard, L., Sallsten, G., Andersson, L., Almstrand, A. C., Gustafson, P., Andersson, M., Olin, A. C. 2007. Experimental exposure to wood smoke: effects on airway inflammation and oxidative stress. J. Occup. Environ. Med., 65(5), 319-324. https://doi.org/10.1136/oem.2006.032458.

Brown, S. G., Lee, T., Roberts, P. T., Collett, J. L. 2016. Wintertime residential biomass burning in Las Vegas, Nevada; marker components and apportionment methods. Atmosphere, 7(4), 58. https://doi.org/10.3390/atmos7040058.

Buiarelli, F., Di Filippo, P., Pomata, D., Riccardi, C., Simonetti, G. 2018. A rapid method for the determination of levoglucosan in NIST standard reference material 1649a by HPLC-MS/MS. Atmos. Environ., 195, 24-29. https://doi.org/10.1016/j.atmosenv.2018.09.051.

Canepari, S., Cardarelli, Giuliano, A., E., Pietrodangelo, A. 2006a. Determination of metals, metalloids and non-volatile ions in airborne particulate matter by a new two-step sequential leaching procedure Part A: Experimental design and optimization. Talanta, 69(3), 581-587. https://doi.org/10.1016/j.talanta.2005.10.023.

Canepari, S., Cardarelli, E., Pietrodangelo, A., Strincone, M. 2006b. Determination of metals, metalloids and non-volatile ions in airborne particulate matter by a new two-step sequential leaching procedure: Part B: Validation on equivalent real samples. Talanta, 69(3), 588-595. https://doi.org/10.1016/j.talanta.2005.10.024.

Canepari, S., Pietrodangelo, A., Perrino, C., Astolfi, M. L., Marzo, M. L. 2009. Enhancement of source traceability of atmospheric PM by elemental chemical fractionation. Atmos. Environ., 43(31), 4754-4765. https://doi.org/10.1016/j.atmosenv.2008.09.059.

Canepari, S., Astolfi, M. L., Farao, C., Maretto, M., Frasca, D., Marcoccia, M., Perrino, C. 2014. Seasonal variations in the chemical composition of particulate matter: a case study in the Po Valley. Part II: concentration and solubility of micro-and trace-elements. Environ. Sci. Pollut. Res., 21(6), 4010-4022. https://doi.org/10.1007/s11356-013-2298-1.

Canepari, S., Astolfi, M. L., Catrambone, M., Frasca, D., Marcoccia, M., Marcovecchio, F., Massimi, L., Rantica, E., Perrino, C. (2019). A combined chemical/size fractionation approach to study winter/summer variations, ageing and source strength of atmospheric particles. Environ. Poll., 253, 19-28. https://doi.org/10.1016/j.envpol.2019.06.116

Capelli, L., Sironi, S., Del Rosso, R., Céntola, P., Rossi, A., Austeri, C. 2011. Olfactometric approach for the evaluation of citizens' exposure to industrial emissions in the city of Terni, Italy. Sci. Total Environ., 409(3), 595-603. https://doi.org/10.1016/j.scitotenv.2010.10.054.

Catrambone, M., Canepari, S., Cerasa, M., Sargolini, T., Perrino, C. 2019. Performance evaluation of a very-low-volume sampler for atmospheric particulate matter. Aerosol Air Qual. Res. https://doi.org/10.4209/aaqr.2019.04.0195.

Chen, J., Li, C., Ristovski, Z., Milic, A., Gu, Y., Islam, M. S., Guo, H. 2017. A review of biomass burning: Emissions and impacts on air quality, health and climate in China. Sci. Total. Environ., 579, 1000-1034.

Chow, J. C., Watson, J. G., Lowenthal, D. H., Chen, L. W. A., Zielinska, B., Mazzoleni, L. R., Magliano, K. L. 2007. Evaluation of organic markers for chemical mass balance source apportionment at the Fresno Supersite. Atmos. Chem. Phys., 7(7), 1741-1754. https://doi.org/10.5194/acp-7-1741-2007.

Cvjetko, P., Cvjetko, I., Pavlica, M. 2010. Thallium toxicity in humans. Arh. Hig. Rada. Toksikol., (1), 111-119. https://doi.org/10.2478/10004-1254-61-2010-1976.

Duan, F., Liu, X., Yu, T., Cachier, H. 2004. Identification and estimate of biomass burning contribution to the urban aerosol organic carbon concentrations in Beijing. Atmos. Environ., 38(9), 1275-1282. http://dx.doi.org/10.1016/j.atmosenv.2003.11.037.

Elias, V. O., Simoneit, B. R., Cordeiro, R. C., Turcq, B. 2001. Evaluating levoglucosan as an indicator of biomass burning in Carajás, amazônia: a comparison to the charcoal record. Geochim. Cosmochim. Acta, 65(2), 267-272. http://dx.doi.org/10.1016/S0016-7037(00)00522-6.

Engling, G., Herckes, P., Kreidenweis, S. M., Malm, W. C., Collett Jr, J. L. 2006. Composition of the fine organic aerosol in Yosemite National Park during the 2002 Yosemite Aerosol Characterization Study. Atmos. Environ., 40(16), 2959-2972. http://dx.doi.org/10.1016/j.atmosenv.2005.12.041.

Ernst, T., Popp, R. van Eldik, R., 2000. Quantification of heavy metals for the recycling of waste plastics from electrotechnical applications. Talanta, 52, 347-357. http://dx.doi.org/10.1016/S0039-9140(00)00491-4.

Ferrero, L., Cappelletti, D., Moroni, B., Sangiorgi, G., Perrone, M. G., Crocchianti, S., Bolzacchini, E. 2012. Wintertime aerosol dynamics and chemical composition across the mixing layer over basin valleys. Atmos. Environ., 56, 143-153. http://dx.doi.org/10.1016/j.atmosenv.2012.03.071.

Finkelman, R. B. 1999. Trace elements in coal. Biol. Trace Elem. Res., 67(3), 197-204. https://doi.org/10.1007/BF02784420.

Fox, D.G. Uncertainty in Air Quality Modeling. Bull. Am. Meteorol. Soc., 1984, 65, 27–36.

Frasca, D., Marcoccia, M., Tofful, L., Simonetti, G., Perrino, C., Canepari, S. 2018. Influence of advanced wood-fired appliances for residential heating on indoor air quality. Chemosphere, 211, 62-71. https://doi.org/10.1016/j.chemosphere.2018.07.102.

Fraser, M. P., Lakshmanan, K. 2000. Using levoglucosan as a molecular marker for the long-range transport of biomass combustion aerosols. Environ. Sci. Technol., 34(21), 4560-4564. https://doi.org/10.1021/es991229l.

Graham, B., Mayol-Bracero, O. L., Guyon, P., Roberts, G. C., Decesari, S., Facchini, M. C., Fuzzi, S., Andreae, M. O. 2002. Water-soluble organic compounds in biomass burning aerosols over Amazonia 1. Characterization by NMR and GC-MS. J. Geophys. Res. Atmos., 107(D20), LBA-14. https://doi.org/10.1029/2001JD000336.

Guerrini, R. 2012. Qualità dell'aria nella provincia di Terni tra il 2002 e il 2011. Quad ARPA Umbria, 81-87.

Hoffmann, D., Tilgner, A., Iinuma, Y., Herrmann, H. 2009. Atmospheric stability of levoglucosan: a detailed laboratory and modeling study. Environ. Sci. Technol., 44(2), 694-699. https://doi.org/10.1021/es902476f.

Jordan, T. B., Seen, A. J., Jacobsen, G. E. 2006. Levoglucosan as an atmospheric tracer for woodsmoke. Atmos. Environ., 40(27), 5316-5321. https://doi.org/ 10.1016/j.atmosenv.2006.03.023.

Kam, W., Delfino, R. J., Schauer, J. J., Sioutas, C. 2013. A comparative assessment of PM 2.5 exposures in light-rail, subway, freeway, and surface street environments in Los Angeles and estimated lung cancer risk. Environ. Sci. Process Impacts, 15(1), 234-243. http://dx.doi.org/10.1039/C2EM30495C.

Karbowska, B. 2016. Presence of thallium in the environment: sources of contaminations, distribution and monitoring methods. Environ. Monit. Assess., 188(11), 640. https://doi.org/10.1007/s10661-016-5647-y.

Kessler, S. H., Smith, J. D., Che, D. L., Worsnop, D. R., Wilson, K. R., Kroll, J. H. 2010. Chemical sinks of organic aerosol: Kinetics and products of the heterogeneous oxidation of erythritol and levoglucosan. Environ. Sci. Technol., 44(18), 7005-7010. https://doi.org/10.1021/es101465m.

Krasnodębska-Ostręga, B., Golimowski, J. 2008. Zielona gałązka, która truje: Thallus. Analityka: nauka i praktyka, 46-50.

Lee, S., Kim, H. K., Yan, B., Cobb, C. E., Hennigan, C., Nichols, S., Chamber, M., Edgerton, E. S., Jansen, J. J., Hu, Y. Weber, R. J., Russell, A. G., Zheng, M. 2008. Diagnosis of aged prescribed burning plumes impacting an urban area. Environ. Sci. Technol., 42(5), 1438-1444. https://doi.org/10.1021/es7023059.

Lee, T., Sullivan, A. P., Mack, L., Jimenez, J. L., Kreidenweis, S. M., Onasch, T. B., Collett Jr, J. L. 2010. Chemical smoke marker emissions during flaming and smoldering phases of laboratory open burning of wildland fuels. Aerosol Sci. Technol., 44(9), i-v. https://doi.org/10.1080/02786826.2010.499884.

Li, Jia, Mihály Pósfai, Peter V. Hobbs, Peter R. Buseck. 2003. Individual aerosol particles from biomass burning in southern Africa: 2, Compositions and aging of inorganic particles." J. Geophys. Res. Atmos., 108, no. D13. https://doi.org/10.1029/2002JD002291.

Li, R., Wiedinmyer, C., Hannigan, M. P. 2013. Contrast and correlations between coarse and fine particulate matter in the United States. Sci. Total. Environ., 456, 346-358. https://doi.org/10.1016/j.scitotenv.2013.03.041.

Liu, W., Wang, Y., Russell, A., Edgerton, E. S. 2005. Atmospheric aerosol over two urban–rural pairs in the southeastern United States: Chemical composition and possible sources. Atmos. Environ., 39(25), 4453-4470. http://dx.doi.org/10.1016/j.atmosenv.2005.03.048.

Massimi, L., Ristorini, M., Eusebio, M., Florendo, D., Adeyemo, A., Brugnoli, D., Canepari, S. 2017. Monitoring and evaluation of Terni (Central Italy) air quality through spatially resolved analyses. Atmosphere, 8(10), 200. https://doi.org/10.3390/ecas2017-04129.

Massimi, L., Giuliano, A., Astolfi, M.L., Congedo, R., Masotti, A., Canepari, S., 2018. Efficiency evaluation of food waste materials for the removal of metals and metalloids from complex multi-element solutions. Materials, 11(3), 334. https://doi.org/10.3390/ma11030334.

Massimi, L., Conti, M. E., Mele, G., Ristorini, M., Astolfi, M. L., Canepari, S. 2019. Lichen transplants as indicators of atmospheric element concentrations: a high spatial resolution comparison with PM10 samples in a polluted area (Central Italy). Ecol. Indic., 101, 759-769. http://dx.doi.org/10.1016/j.ecolind.2018.12.051.

Moroni, B., Ferrero, L., Crocchianti, S., Perrone, M. G., Sangiorgi, G., Bolzacchini, E., Cappelletti, D. 2013. Aerosol dynamics upon Terni basin (Central Italy): results of integrated vertical profile measurements and electron microscopy analyses. Rendiconti Lincei, 24(4), 319-328. https://doi.org/10.1007/s12210-013-0230-8.

Naeher, L. P., Brauer, M., Lipsett, M., Zelikoff, J. T., Simpson, C. D., Koenig, J. Q., Smith, K. R. 2007. Wood smoke health effects: a review. Inhal. Toxicol., 19(1), 67-106. https://doi.org/10.1080/08958370600985875.

Namgung, H. G., Kim, J. B., Woo, S. H., Park, S., Kim, M., Kim, M. S., Bae, G. N., Park, D., Kwon, S. B. 2016. Generation of nanoparticles from friction between railway brake disks and pads. Environ. Sci. Technol., 50(7), 3453-3461. https://doi.org/10.1021/acs.est.5b06252.

Perrino, C., Canepari, S., Pappalardo, S., Marconi, E. 2010. Time-resolved measurements of water-soluble ions and elements in atmospheric particulate matter for the characterization of local and long-range transport events. Chemosphere, 80(11), 1291-1300. https://doi.org/10.1016/j.chemosphere.2010.06.050.

Perrino, C., Tofful, L., Dalla Torre, S., Sargolini, T., Canepari, S. 2019. Biomass burning contribution to PM10 concentration in Rome (Italy): Seasonal, daily and two-hourly variations. Chemosphere, 222, 839-848. https://doi.org/10.1016/j.chemosphere.2019.02.019.

Phuleria, H. C., Fine, P. M., Zhu, Y., Sioutas, C. 2005. Air quality impacts of the October 2003 Southern California wildfires. J. Geophys. Res. Atmos., 110(D7). https://doi.org/10.1029/2004JD004626.

Piacentini, D., Falasca, G., Canepari, S., Massimi, L. 2019. Potential of PM-selected components to induce oxidative stress and root system alteration in a plant model organism. Environ. Int., 132, 105094.

Piazzalunga, A., Belis, C., Bernardoni, V., Cazzuli, O., Fermo, P., Valli, G., Vecchi, R. 2011. Estimates of wood burning contribution to PM by the macro-tracer method using tailored emission factors. Atmos. Environ., 45(37), 6642-6649. http://dx.doi.org/10.1016/j.atmosenv.2011.09.008.

Puxbaum, H., Caseiro, A., Sánchez-Ochoa, A., Kasper-Giebl, A., Claeys, M., Gelencsér, A., Legrand, M., Preunkert, S., Pio, C. 2007. Levoglucosan levels at background sites in Europe for assessing the impact of biomass combustion on the European aerosol background. ." J. Geophys. Res. Atmos., 112(D23). https://doi.org/10.1029/2006JD008114.

Querol, X., Moreno, T., Karanasiou, A., Reche, C., Alastuey, A., Viana, M., Font, O., Gil, J., de Miguel, E., Capdevila, M. 2012. Variability of levels and composition of PM 10 and PM 2.5 in the Barcelona metro system. Atmos. Chem. Phys., 12(11), 5055-5076. https://doi.org/10.5194/acp-12-5055-2012.

Saarikoski, S., Sillanpää, M., Sofiev, M., Timonen, H., Saarnio, K., Teinilä, K., Karppinen, A., Kukkonen, J., Hillamo, R. 2007. Chemical composition of aerosols during a major biomass burning episode over northern Europe in spring 2006: Experimental and modelling assessments. Atmos. Environ., 41(17), 3577-3589. https://doi.org/10.1016/j.atmosenv.2006.12.053.

Schauer, J. J., Kleeman, M. J., Cass, G. R., Simoneit, B. R. 2001. Measurement of emissions from air pollution sources. 3. C1− C29 organic compounds from fireplace combustion of wood. Environ. Sci. Technol., 35(9), 1716-1728. https://doi.org/10.1021/es001331e.

Seagrave, J., McDonald, J. D., Bedrick, E., Edgerton, E. S., Gigliotti, A. P., Jansen, J. J., Ke, L., Naeher, L.P., Seilkop, S.K., Zheng, M., Mauderly, J. L. 2006. Lung toxicity of ambient particulate matter from southeastern US sites with different contributing sources: relationships between

composition and effects. Environ. Health Perspect., 114(9), 1387. https://dx.doi.org/10.1289%2Fehp.9234.

Sedgwick, P. 2012. Pearson's correlation coefficient. Br. Med. J., 345. https://doi.org/10.1136/bmj.e4483.

Schlummer, M., Gruber, L., Mäurer, A., Wolz, G. Van Eldik, R. 2007. Characterisation of polymer fractions from waste electrical and electronic equipment (WEEE) and implications for waste management. Chemosphere, 67, 1866–1876. https://doi.org/10.1016/j.chemosphere.2006.05.077.

Sgrigna, G., Sæbø, A., Gawronski, S., Popek, R., Calfapietra, C. (2015). Particulate Matter deposition on Quercus ilex leaves in an industrial city of central Italy. Environ. Pollut., 197, 187-194. https://doi.org/10.1016/j.envpol.2014.11.030.

Simoneit, B. R., Schauer, J. J., Nolte, C. G., Oros, D. R., Elias, V. O., Fraser, M. P., Rogge, W.F., Cass, G. R. 1999. Levoglucosan, a tracer for cellulose in biomass burning and atmospheric particles. Atmos. Environ., 33(2), 173-182. https://doi.org/10.1016/S1352-2310(98)00145-9.

Simoneit, B. R. 2002. Biomass burning - a review of organic tracers for smoke from incomplete combustion. Appl. Geochem., 17(3), 129-162. https://doi.org/10.1016/S0883-2927(01)00061-0.

Simoneit, B. R., Elias, V. O., Kobayashi, M., Kawamura, K., Rushdi, A. I., Medeiros, P. M., Rogge, W. F., Didyk, B. M. 2004. Sugars dominant water-soluble organic compounds in soils and characterization as tracers in atmospheric particulate matter. Environ. Sci. Technol., 38(22), 5939-5949. https://doi.org/10.1021/es0403099.

Simonetti, G., Frasca, D., Marcoccia, M., Farao, C., Canepari, S. 2018a. Multi-elemental analysis of particulate matter samples collected by a particle-into-liquid sampler. Atmos. Pollut. Res., 9(4) 747-754. https://doi.org/10.1016/j.apr.2018.01.006.

Simonetti, G., Conte, E., Perrino, C., Canepari, S. 2018b. Oxidative potential of size-segregated PM in an urban and an industrial area of Italy. Atmos. Environ., 187, 292-300. http://dx.doi.org/10.1016/j.atmosenv.2018.05.051.

Simonetti, G., Conte, E., Massimi, L., Frasca, D., Perrino, C., Canepari, S. 2018c. Oxidative potential of particulate matter components generated by specific emission sources. J. Aerosol Sci., 126, 99-109. http://dx.doi.org/10.1016/j.jaerosci.2018.08.011.

Slade, J. H., Knopf, D. A. 2013. Heterogeneous OH oxidation of biomass burning organic aerosol surrogate compounds: assessment of volatilization products and the role of OH concentration on the reactive uptake kinetics. Phys. Chem. Chem. Phys., 15(16), 5898-5915. http://dx.doi.org/10.1039/C3CP44695F.

Slade, J. H., Knopf, D. A. 2014. Multiphase OH oxidation kinetics of organic aerosol: The role of particle phase state and relative humidity. Geophys. Res. Lett., 41(14), 5297-5306. https://doi.org/10.1002/2014GL060582.

Sullivan, A. P., Holden, A. S., Patterson, L. A., McMeeking, G. R., Kreidenweis, S. M., Malm, W. C., Hao, W. M., Wold, C. E., Collett Jr, J. L. 2008. A method for smoke marker measurements and its potential application for determining the contribution of biomass burning from wildfires and prescribed fires to ambient PM2.5 organic carbon. J. Geophys. Res. Atmos., 113(D22). https://doi.org/10.1029/2008JD010216.

Szidat, S., Prévôt, A. S., Sandradewi, J., Alfarra, M. R., Synal, H. A., Wacker, L., Baltensperger, U. 2007. Dominant impact of residential wood burning on particulate matter in Alpine valleys during winter. Geophys. Res. Lett., 34(5). https://doi.org/10.1029/2006GL028325.

Templeton, D. M., Ariese, F., Cornelis, R., Danielsson, L. G., Muntau, H., van Leeuwen, H. P., Lobinski, R. 2000. Guidelines for terms related to chemical speciation and fractionation of elements. Definitions, structural aspects, and methodological approaches (IUPAC Recommendations 2000). Pure Appl. Chem., 72(8), 1453-1470. https://doi.org/10.1351/pac200072081453.

Thepnuan, D., Chantara, S., Lee, C. T., Lin, N. H., Tsai, Y. I. 2018. Molecular markers for biomass burning associated with the characterization of PM2. 5 and component sources during dry season haze episodes in Upper South East Asia. Sci. Total Environ. https://doi.org/10.1016/j.scitotenv.2018.12.201.

Urban, R. C., Lima-Souza, M., Caetano-Silva, L., Queiroz, M. E. C., Nogueira, R. F., Allen, A. G., Cardoso, A.A, Held, G., Campos, M. L. A. 2012. Use of levoglucosan, potassium, and water-soluble organic carbon to characterize the origins of biomass-burning aerosols. Atmos. Environ., 61, 562-569. http://dx.doi.org/10.1016/j.atmosenv.2012.07.082.

Van Drooge, B. L., Crusack, M., Reche, C., Mohr, C., Alastuey, A., Querol, X., Prevot, A., Day, A. D. Jimenez, J. L., Grimalt, J. O. 2012. Molecular marker characterization of the organic composition of submicron aerosols from Mediterranean urban and rural environments under contrasting meteorological conditions. Atmos. Environ., 61, 482-489. http://dx.doi.org/10.1016/j.atmosenv.2012.07.039.

Van Drooge, B. L., Fontal, M., Bravo, N., Fernández, P., Fernández, M. A., Muñoz-Arnanz, J., Jiménez, B., Grimalt, J. O. 2014. Seasonal and spatial variation of organic tracers for biomass burning in PM 1 aerosols from highly insolated urban areas. Environ. Sci. Pollut. R., 21(20), 11661-11670. https://doi.org/10.1007/s11356-014-2545-0.

Vicente, E. D., Alves, C. A. 2018. An overview of particulate emissions from residential biomass combustion. Atmos. Res., 199, 159-185.

Weckwerth, G. 2001. Verification of traffic emitted aerosol components in the ambient air of Cologne (Germany). Atmos. Environ., 35(32), 5525-5536. https://doi.org/10.1016/S1352-2310(01)00234-5.

Yamasoe, M. A., Artaxo, P., Miguel, A. H., Allen, A. G. 2000. Chemical composition of aerosol particles from direct emissions of vegetation fires in the Amazon Basin: water-soluble species and trace elements. Atmos. Environ., 34(10), 1641-1653. https://doi.org/10.1016/S1352-2310(99)00329-5.

Zhang, Z., Gao, J., Engling, G., Tao, J., Chai, F., Zhang, L., Zhang, R., Sang, X., Chan, C., Lin, Z., Cao, J. 2015. Characteristics and applications of size-segregated biomass burning tracers in China's Pearl River Delta region. Atmos. Environ., 102, 290-301. http://dx.doi.org/10.1016/j.atmosenv.2014.12.009.

Supplementary Material S1.

Table S1. Type of site, main local PM emission sources and geographical coordinates of the twenty monitoring sites in Terni.

Type of Site & Main Local PM Emission Sources		Latitude	Longitude
MA	Industrial Site - Power Plant (West of the City)	42°33′41.42″ N	12°36′19.05″ E
FA	Industrial Site - Power Plant & Industrial Biomass Heating (West of the City)	42°33′03.19″ N	12°36′29.76″ E
GI	Industrial Site - Power Plant & Rail Network (North-West of the City)	42°34′06.28″ N	12°36′48.27″ E
FR	Industrial Site - Power Plant & Domestic Biomass Heating (West of the City)	42°33′53.22″ N	12°37′11.44″ E
CB	Industrial Site - Power Plant & Industrial Biomass Heating (West of the City)	42°33′20.30″ N	12°37′20.45″ E
PI	Urban Background Site - Domestic Biomass Heating (South of the City)	42°32′56.96″ N	12°37′52.26″ E
BR	Urban Background Site - Domestic Biomass Heating (North of the City)	42°34′56.19″ N	12°37′23.30″ E
AR	Urban Background Site - Domestic Biomass Heating (North of the City)	42°34′34.23″ N	12°37′39.88″ E
CR	Industrial Site - Domestic Biomass Heating & Rail Network (North-West of the City)	42°34′09.49″ N	12°37′39.81″ E
HG	Urban Site - Trafficked Streets & Rail Network (North-West of the City)	42°34′19.32″ N	12°37′56.02″ E
SA	Urban Site - Trafficked Streets (City Centre)	42°33′45.16″ N	12°38′18.45″ E
PV	Urban Background Site - Domestic Biomass Heating (South of the City)	42°33′06.96″ N	12°38′35.20″ E
LG	Urban Background Site - Domestic Biomass Heating (South of the City)	42°32′59.75″ N	12°39′01.16″ E
HV	Urban Site - Trafficked Streets (City Centre)	42°33′58.33″ N	12°39′04.74″ E
UC	Urban Site - Trafficked Streets & Domestic Biomass Heating (City Centre)	42°33′38.09″ N	12°38′47.62″ E
CA	Urban Site - Heavily Trafficked Streets (City Centre)	42°33′39.01″ N	12°39′03.11″ E
CO	Urban-industrial Site - Heavily Trafficked Streets & Steel Plant (City Centre)	42°33′34.23″ N	12°39′22.62″ E
RO	Industrial Site - Steel Plant (East of the City)	42°33′51.16″ N	12°39′39.15″ E
OB	Industrial Site - Steel Plant (East of the City)	42°34′18.64″ N	12°40′05.57″ E
PR	Industrial Site - Steel Plant (East of the City)	42°34′20.30″ N	12°40′44.23″ E

Supplementary Material S2.

Table S2.1. Limits of detection (LODs; µg L^{-1}), mean of blank values (µg L^{-1}) and concentrations (ng m^{-3}) of LVG, WSOC and water-soluble fraction of the 33 elements, determined at the twenty collection sites. The LODs were set at 3 times the standard deviation (SD) of 10 replicate blank determinations.

Water-soluble Fraction	LOD (µg L^{-1})	Mean Blank Values (µg L^{-1})	Mean (ng m^{-3})	MA	FA	GI	FR	CB	PI	BR	AR	CR	HG	SA	PV	LG	HV	UC	CA	CO	RO	OB	PR
Al	1.1	0.44	16	18	25	12	14	12	11	11	17	7.5	14	11	18	10	12	8.2	11	16	18	14	67
As	0.10	0.058	0.40	0.27	0.59	0.42	0.16	0.25	0.27	0.24	0.30	0.18	0.35	0.34	0.15	0.23	0.28	0.26	0.40	0.41	1.4	0.58	0.83
Ba	2.9	0.054	7.8	5.3	14	8.8	5.5	6.8	4.7	5.4	7.0	7.4	8.6	8.5	12	7.1	5.9	6.7	7.8	6.0	13	6.3	8.9
Bi	0.0080	0.0017	0.036	0.041	0.071	0.038	0.027	0.036	0.039	0.022	0.036	0.017	0.029	0.037	0.035	0.034	0.039	0.025	0.040	0.018	0.033	0.028	0.068
Ca	87	13	1000	823	2287	882	648	993	524	633	716	862	1188	765	1228	741	633	626	730	1182	901	742	2976
Cd	0.0092	0.0019	0.23	0.26	0.52	0.26	0.15	0.26	0.20	0.23	0.26	0.13	0.20	0.19	0.20	0.26	0.16	0.16	0.24	0.15	0.17	0.18	0.39
Ce	0.0018	0.00077	0.025	0.025	0.040	0.016	0.014	0.016	0.016	0.138	0.020	0.014	0.025	0.015	0.020	0.015	0.015	0.011	0.017	0.019	0.014	0.017	0.040
Co	0.013	0.0045	0.040	0.036	0.077	0.052	0.043	0.039	0.034	0.029	0.048	0.028	0.039	0.028	0.034	0.028	0.033	0.026	0.033	0.034	0.060	0.047	0.10
Cr	0.032	0.050	2.4	1.3	2.5	1.5	1.0	1.6	1.6	1.2	2.2	1.0	1.5	1.5	1.3	1.2	1.7	1.6	1.9	1.9	4.9	3.2	14
Cs	0.003	0.00082	0.1	0.1	0.2	0.1	0.1	0.1	0.1	0.1	0.1	0.0	0.1	0.1	0.1	0.1	0.0	0.1	0.1	0.0	0.1	0	0.12306
Cu	0.074	0.047	3.7	3.3	4.5	9.5	3.8	2.6	1.8	2.0	4.4	4.3	6.8	3.7	4.2	2.0	2.3	2.1	3.3	3.0	2.6	2.9	4.2
Fe	2.0	0.36	18	14	25	32	14	16	19	14	26	16	21	17	16	10	13	11	13	14	18	16	40
Ga	0.0045	0.0014	0.014	0.008	0.017	0.010	0.007	0.013	0.014	0.009	0.017	0.007	0.011	0.010	0.009	0.008	0.012	0.007	0.013	0.011	0.017	0.017	0.065
K	17	11	641	536	1531	793	599	748	523	602	731	444	588	535	637	605	401	503	534	523	700	445	852
La	0.0080	0.0034	0.013	0.014	0.022	0.0075	0.0079	0.0092	0.0077	0.063	0.009	0.007	0.012	0.0082	0.010	0.007	0.0073	0.0056	0.0082	0.011	0.0063	0.010	0.019
Li	0.011	0.0054	0.22	0.14	0.33	0.17	0.11	0.21	0.15	0.13	0.21	0.10	0.16	0.15	0.16	0.15	0.14	0.15	0.18	0.19	0.29	0.28	0.91
Mg	3.2	1.7	111	67	186	102	58	123	86	85	128	69	104	94	98	79	90	93	72	102	120	106	351
Mn	0.12	0.023	11	8.7	17	11	11	10	6.8	6.5	11	6.9	9.8	8.1	7.5	6.8	7.7	7.3	8.2	8.8	11	12	46
Mo	0.064	0.053	12	2.9	6.0	5.0	3.2	4.7	4.3	3.4	6.6	4.4	5.9	5.0	5.0	4.6	6.3	7.0	8.6	14	70	25	45
Na	19	10	676	441	1289	717	459	856	596	606	955	455	701	542	568	488	574	630	415	649	552	612	1414
Nb	0.0046	0.0017	0.0068	0.0012	0.0031	0.0015	0.0012	0.0020	0.0029	0.0012	0.0042	0.0012	0.0030	0.0025	0.0012	0.0012	0.0037	0.0014	0.0012	0.0037	0.021	0.011	0.067
Ni	0.098	0.014	1.1	0.60	1.1	0.92	0.47	0.78	0.76	0.84	1.4	0.59	0.77	0.71	0.51	0.54	0.95	0.75	0.75	0.83	3.5	1.7	3.1
Pb	0.061	0.027	1.7	1.3	4.0	1.3	1.1	1.6	1.7	1.5	3.4	0.62	0.99	1.3	0.87	1.3	1.5	1.1	1.4	0.69	1.2	1.3	6.3
Rb	0.022	0.014	1.7	1.5	4.4	2.0	1.2	2.3	1.4	2.0	2.1	1.1	1.7	1.4	1.6	1.4	1.1	1.3	1.4	1.2	1.2	1.2	2.6
Sb	0.0097	0.0027	0.38	0.41	0.89	0.47	0.31	0.49	0.24	0.26	0.43	0.27	0.38	0.32	0.30	0.20	0.26	0.24	0.27	0.28	0.45	0.25	0.93
Sn	0.017	0.0063	0.11	0.076	0.19	0.11	0.089	0.088	0.063	0.071	0.13	0.15	0.14	0.094	0.11	0.036	0.077	0.061	0.063	0.12	0.16	0.094	0.38
Sr	0.31	0.058	3.5	2.2	6.3	3.0	1.8	3.2	2.3	1.9	2.6	2.1	3.0	4.1	4.2	3.0	2.4	2.8	2.8	3.2	11	2.4	5.9
Tl	0.0038	0.0016	0.18	0.18	0.50	0.25	0.15	0.23	0.18	0.23	0.26	0.12	0.17	0.17	0.17	0.17	0.13	0.14	0.16	0.10	0.10	0.12	0.16
Ti	0.028	0.028	0.18	0.060	0.18	0.061	0.084	0.092	0.072	0.082	0.10	0.084	0.19	0.10	0.14	0.049	0.10	0.065	0.081	0.17	0.22	0.20	1.5
U	0.0044	0.0022	0.0015	0.0012	0.0030	0.0015	0.0012	0.0019	0.0012	0.0012	0.0024	0.0012	0.0012	0.0012	0.0012	0.0012	0.0012	0.0014	0.0012	0.0012	0.0012	0.0012	0.0031
W	0.0071	0.020	0.13	0.054	0.15	0.073	0.12	0.080	0.057	0.042	0.077	0.049	0.064	0.061	0.061	0.095	0.065	0.076	0.10	0.13	0.64	0.20	0.35
Zn	3.9	0.78	28	35	92	43	28	42	31	31	42	25	39	34	32	29	32	29	36	31	41	39	198
Zr	0.0072	0.084	0.10	0.64	0.045	0.022	0.013	0.047	0.0090	0.024	0.78	0.013	0.056	0.050	0.031	0.0061	0.0067	0.011	0.0088	0.0080	0.012	0.10	0.051
WSOC	220	50	2300	3500	14000	5800	4400	5700	4800	5800	6300	4400	3800	4400	6000	4100	3000	3500	3700	3900	3400	3500	6700
LVG	8.0	1.8	2100	1000	5000	2100	2100	2900	2100	3500	2500	2900	1900	1400	2300	2300	1600	1700	1600	450	950	1200	2000

Table S2.2. Limits of detection (LODs; μg L^{-1}), mean of blank values (μg L^{-1}) and concentrations (ng m^{-3}) of insoluble fraction of the 33 elements, determined at the twenty collection sites. The LODs were set at 3 times the standard deviation (SD) of 10 replicate blank determinations.

Insoluble Fraction	LOD (μg L^{-1})	Mean Blank Values (μg L^{-1})	Mean (ng m^{-3})	MA	FA	GI	FR	CB	PI	BR	AR	CR	HG	SA	PV	LG	HV	UC	CA	CO	RO	OB	PR
Al	3.9	3.9	159	91	278	173	167	163	106	93	122	141	178	135	197	122	100	95	189	272	100	90	363
As	0.023	0.1	0.59	0.51	1.36	0.75	0.49	0.78	0.38	0.31	0.25	0.37	0.37	0.30	0.44	0.39	0.40	0.26	0.57	0.63	1.1	0.80	1.4
Ba	0.37	0.40	21	12	33	16	11	24	24	28	13	27	19	15	30	12	17	27	14	15	13	19	52
Bi	0.00074	0.0015	0.43	0.38	1.0	0.49	0.53	0.46	0.29	0.21	0.31	0.41	0.49	0.39	0.57	0.41	0.35	0.33	0.45	0.40	0.36	0.25	0.56
Ca	145	162	272	97	245	121	243	402	96	97	99	456	337	96	97	225	96	112	98	250	441	614	1208
Cd	0.0038	0.0052	0.13	0.066	0.21	0.038	0.082	0.13	0.081	0.022	0.059	0.051	0.060	0.10	0.10	0.30	0.18	0.12	0.089	0.13	0.12	0.34	0.30
Ce	0.19	0.0078	0.97	16	0.32	0.16	0.13	0.21	0.13	0.13	0.13	0.13	0.13	0.13	0.13	0.13	0.13	0.15	0.13	0.13	0.13	0.13	0.34
Co	0.022	0.003555556	0.26	0.10	0.32	0.21	0.15	0.20	0.11	0.092	0.12	0.18	0.21	0.14	0.16	0.15	0.15	0.16	0.19	0.35	1.1	0.41	0.65
Cr	1.0	0.62	31	13	37	26	18	21	11	10	11	24	27	14	12	14	18	19	23	47	130	47	104
Cs	0.00048	0.0010	0.035	0.027	0.10	0.033	0.026	0.037	0.021	0.026	0.028	0.034	0.037	0.024	0.041	0.032	0.019	0.020	0.027	0.045	0.027	0.024	0.075
Cu	0.24	0.16	11	8.3	19	21	17	9.5	4.7	5.3	9.1	17	25	9.5	12.8	7.0	5.9	6.6	10	11	9.3	7.4	13
Fe	10	7.4	513	332	770	680	385	440	240	247	392	659	789	439	542	302	283	296	431	579	1110	518	817
Ga	0.0019	0.0017	0.088	0.11	0.16	0.073	0.059	0.088	0.047	0.037	0.046	0.072	0.072	0.059	0.072	0.071	0.057	0.047	0.078	0.10	0.12	0.086	0.31
K	60	225	613	387	1328	693	758	732	397	361	536	644	657	493	498	427	410	405	506	593	491	644	1302
La	0.14	0.0050	0.55	8.9	0.23	0.12	0.09	0.15	0.091	0.092	0.094	0.092	0.091	0.091	0.092	0.092	0.091	0.11	0.093	0.10	0.091	0.10	0.24
Li	0.0013	0.00010	0.10	0.068	0.24	0.083	0.080	0.11	0.065	0.064	0.071	0.093	0.12	0.072	0.11	0.081	0.068	0.064	0.077	0.13	0.10	0.082	0.21
Mg	2.5	4.6	38	25	90	41	31	40	26	23	32	38	41	27	36	28	27	26	28	40	35	34	88
Mn	0.063	0.27	12	8.1	19	13	9.3	12.9	5.4	4.7	7.8	12.0	11.9	8.2	8.4	6.1	7.0	6.8	8.7	13	22	13	48
Mo	0.0071	0.017	8.3	3.8	9.6	6.5	4.3	6.8	5.2	4.0	6.8	4.6	5.5	5.0	4.7	7.2	5.5	7.2	9.9	9.4	30	15	15
Na	59	61	154	133	364	170	176	215	178	131	166	119	132	39	109	91	122	111	120	120	129	127	335
Nb	0.0017	0.013	0.23	0.075	0.25	0.14	0.10	0.14	0.10	0.064	0.10	0.12	0.15	0.11	0.12	0.11	0.12	0.12	0.15	0.31	1.08	0.39	0.84
Ni	1.2	0.32	14	5.0	14	9.6	6.6	9.8	6.1	4.8	5.8	8.6	9.9	7.2	5.7	7.2	8.6	9.1	11	17	63	26	39
Pb	0.025	0.093	7.1	4.1	16	5.5	4.7	7.1	4.1	3.4	5.3	5.1	5.1	11	5.1	4.6	4.4	4.0	5.0	5.8	7.0	5.4	30
Rb	0.027	0.045	0.35	0.21	0.78	0.34	0.19	0.44	0.26	0.32	0.17	0.20	0.59	0.31	0.27	0.26	0.32	0.25	0.34	0.31	0.13	0.31	0.97
Sb	0.0036	0.011	1.2	1.1	2.1	3.6	1.0	1.4	0.50	0.62	1.1	1.5	1.8	1.1	1.3	0.63	0.61	0.66	1.0	1.1	0.76	0.56	1.1
Sn	0.10	0.036	4.8	5.1	9.7	8.5	5.0	5.3	3.1	4.3	6.4	6.6	7.8	5.0	4.9	3.1	2.8	2.9	4.0	3.8	2.6	2.4	3.5
Sr	0.043	0.16	1.5	0.84	2.6	1.2	1.1	1.8	1.1	1.1	1.0	1.5	1.5	1.1	1.5	1.1	1.0	1.3	1.1	1.5	2.1	1.7	4.2
Ti	0.027	0.24	4.5	2.3	10.0	3.8	3.0	3.6	2.1	1.9	2.6	6.8	5.2	3.0	4.8	2.7	2.7	2.4	3.1	5.9	4.7	3.2	16
Tl	0.00014	0.00010	0.069	0.074	0.19	0.093	0.058	0.086	0.043	0.061	0.064	0.074	0.071	0.049	0.067	0.058	0.037	0.050	0.055	0.077	0.049	0.045	0.085
U	0.00025	0.00030	0.0023	0.0017	0.0081	0.0020	0.0022	0.0020	0.00016	0.00017	0.00055	0.0036	0.0046	0.00093	0.0041	0.0011	0.00016	0.00019	0.00054	0.0046	0.0028	0.0018	0.0038
W	0.0066	0.0064	0.13	0.10	0.22	0.19	0.11	0.13	0.08	0.08	0.09	0.06	0.11	0.084	0.070	0.090	0.080	0.093	0.11	0.12	0.37	0.15	0.22
Zn	7.1	7.7	28	10	55	19	23	28	10	11	19	32	31	16	18	17	14	17	22	27	31	40	119
Zr	0.081	0.39	0.75	0.63	1.5	1.1	0.73	0.80	0.44	0.47	0.76	1.3	1.3	0.90	0.92	0.55	0.34	0.37	0.59	0.69	0.41	0.40	0.84

Supplementary Material S3.

Table S3.1. Scores of the five significant components (accounting for 88.78%) obtained by the PCA performed on the concentration data of LVG, WSOC and water-soluble and insoluble fraction of the 33 elements, determined at the twenty collection sites.

	Scores				
	PC1	**PC2**	**PC3**	**PC4**	**PC5**
MA	-3.605	0.690	1.416	-1.196	-6.104
FA	12.250	8.825	-3.167	-3.088	0.866
GI	0.650	3.201	-3.041	2.270	-1.571
FR	-2.930	0.607	-0.151	1.432	0.313
CB	0.461	1.758	0.334	-0.698	0.650
PI	-3.844	-0.412	1.964	-1.003	0.568
BR	-3.806	1.375	2.588	-3.557	2.073
AR	-0.883	1.793	1.099	-1.367	-2.241
CR	-2.298	1.013	-0.846	3.127	0.930
HG	0.000	1.902	-1.789	3.404	-0.047
SA	-2.962	0.043	0.084	0.692	0.060
PV	-1.257	1.617	-0.771	1.086	1.008
LG	-3.506	-0.310	0.801	-0.979	1.102
HV	-3.978	-1.486	1.712	-0.276	0.574
UC	-4.114	-1.122	1.180	-0.489	0.932
CA	-2.569	-0.522	-0.032	-0.003	0.259
CO	-0.854	-1.503	-0.616	1.671	0.785
RO	4.159	-9.534	-6.498	-2.414	-0.413
OB	-0.593	-4.169	0.541	-0.305	0.560
PR	19.678	-3.765	5.193	1.692	-0.302

Table S3.2. Loadings of the five significant components (accounting for 88.78%) obtained by the PCA performed on the concentration data of LVG, WSOC and water-soluble (_s) and insoluble (_i) fraction of the 33 elements, determined at the twenty collection sites.

	Loadings										
	PC1	**PC2**	**PC3**	**PC4**	**PC5**		**PC1**	**PC2**	**PC3**	**PC4**	**PC5**
Al_i	0.131	0.062	0.030	0.176	0.078	**Al_s**	0.149	-0.046	0.143	0.046	-0.081
As_i	0.149	-0.030	-0.095	-0.073	-0.013	**As_s**	0.102	-0.169	-0.180	-0.120	-0.044
Ba_i	0.118	0.033	0.162	0.023	0.179	**Ba_s**	0.096	0.028	-0.264	-0.048	0.062
Bi_i	0.103	0.165	-0.132	0.034	0.034	**Bi_s**	0.129	0.074	0.048	-0.125	-0.116
Ca_i	0.127	-0.113	0.087	0.135	0.049	**Ca_s**	0.159	0.042	0.042	0.058	0.014
Cd_i	0.077	-0.079	0.094	-0.060	0.128	**Cd_s**	0.124	0.142	0.025	-0.183	-0.074
Ce_i	-0.021	0.015	0.057	-0.077	-0.486	**Ce_s**	0.015	0.053	0.118	-0.230	0.129
Co_i	0.099	-0.190	-0.176	-0.058	0.010	**Co_s**	0.161	-0.015	-0.012	-0.029	-0.080
Cr_i	0.115	-0.186	-0.123	-0.015	-0.003	**Cr_s**	0.141	-0.118	0.128	0.039	-0.029
Cs_i	0.142	0.121	-0.034	-0.022	0.059	**Cs_s**	0.117	0.164	-0.004	-0.191	-0.020
Cu_i	0.058	0.127	-0.189	0.313	-0.030	**Cu_s**	0.041	0.113	-0.150	0.294	-0.165
Fe_i	0.112	-0.066	-0.259	0.123	-0.014	**Fe_s**	0.132	0.034	0.024	0.111	-0.130
Ga_i	0.156	-0.048	0.070	0.043	-0.081	**Ga_s**	0.143	-0.081	0.165	0.041	-0.026
K_i	0.150	0.085	-0.011	0.073	0.048	**K_s**	0.119	0.151	-0.121	-0.172	0.005
La_i	-0.020	0.015	0.058	-0.078	-0.486	**La_s**	0.019	0.062	0.116	-0.235	0.123
Li_i	0.151	0.077	-0.044	0.018	0.081	**Li_s**	0.152	-0.074	0.126	0.021	-0.019
Mg_i	0.159	0.076	-0.014	0.031	0.044	**Mg_s**	0.158	-0.024	0.114	0.011	0.006
Mn_i	0.156	-0.081	0.036	0.090	-0.026	**Mn_s**	0.151	-0.044	0.141	0.074	-0.048
Mo_i	0.080	-0.200	-0.182	-0.125	0.015	**Mo_s**	0.092	-0.220	-0.114	-0.067	-0.013
Na_i	0.140	0.095	0.038	-0.086	-0.008	**Na_s**	0.146	0.076	0.071	-0.057	0.014
Nb_i	0.112	-0.196	-0.110	-0.046	-0.003	**Nb_s**	0.136	-0.132	0.130	0.057	-0.027
Ni_i	0.096	-0.206	-0.147	-0.064	0.004	**Ni_s**	0.113	-0.185	-0.061	-0.097	-0.047
Pb_i	0.155	-0.009	0.105	0.040	0.007	**Pb_s**	0.143	0.029	0.156	-0.092	-0.061
Rb_i	0.140	0.077	0.096	0.060	0.081	**Rb_s**	0.116	0.178	-0.024	-0.175	0.008
Sb_i	0.046	0.156	-0.183	0.205	-0.128	**Sb_s**	0.157	0.067	-0.013	-0.046	-0.110
Sn_i	0.039	0.230	-0.156	0.108	-0.111	**Sn_s**	0.155	-0.033	0.039	0.120	-0.030
Sr_i	0.160	-0.046	0.036	0.035	0.084	**Sr_s**	0.101	-0.114	-0.228	-0.136	0.010
Ti_i	0.156	0.006	0.038	0.131	0.051	**Ti_s**	0.139	-0.084	0.168	0.105	-0.007
Tl_i	0.102	0.194	-0.115	-0.071	-0.017	**Tl_s**	0.065	0.225	-0.063	-0.220	-0.019
U_i	0.105	0.100	-0.177	0.107	0.052	**U_s**	0.141	0.090	0.074	-0.091	-0.045
W_i	0.109	-0.113	-0.227	-0.119	-0.059	**W_s**	0.092	-0.198	-0.162	-0.105	-0.011
Zn_i	0.156	-0.040	0.089	0.099	0.043	**Zn_s**	0.157	-0.015	0.135	0.029	-0.030
Zr_i	0.067	0.191	-0.139	0.220	-0.012	**Zr_s**	-0.013	0.037	0.075	-0.115	-0.457
LVG	0.051	0.206	-0.003	-0.172	0.192	**WSOC**	0.103	0.191	-0.053	-0.169	0.071

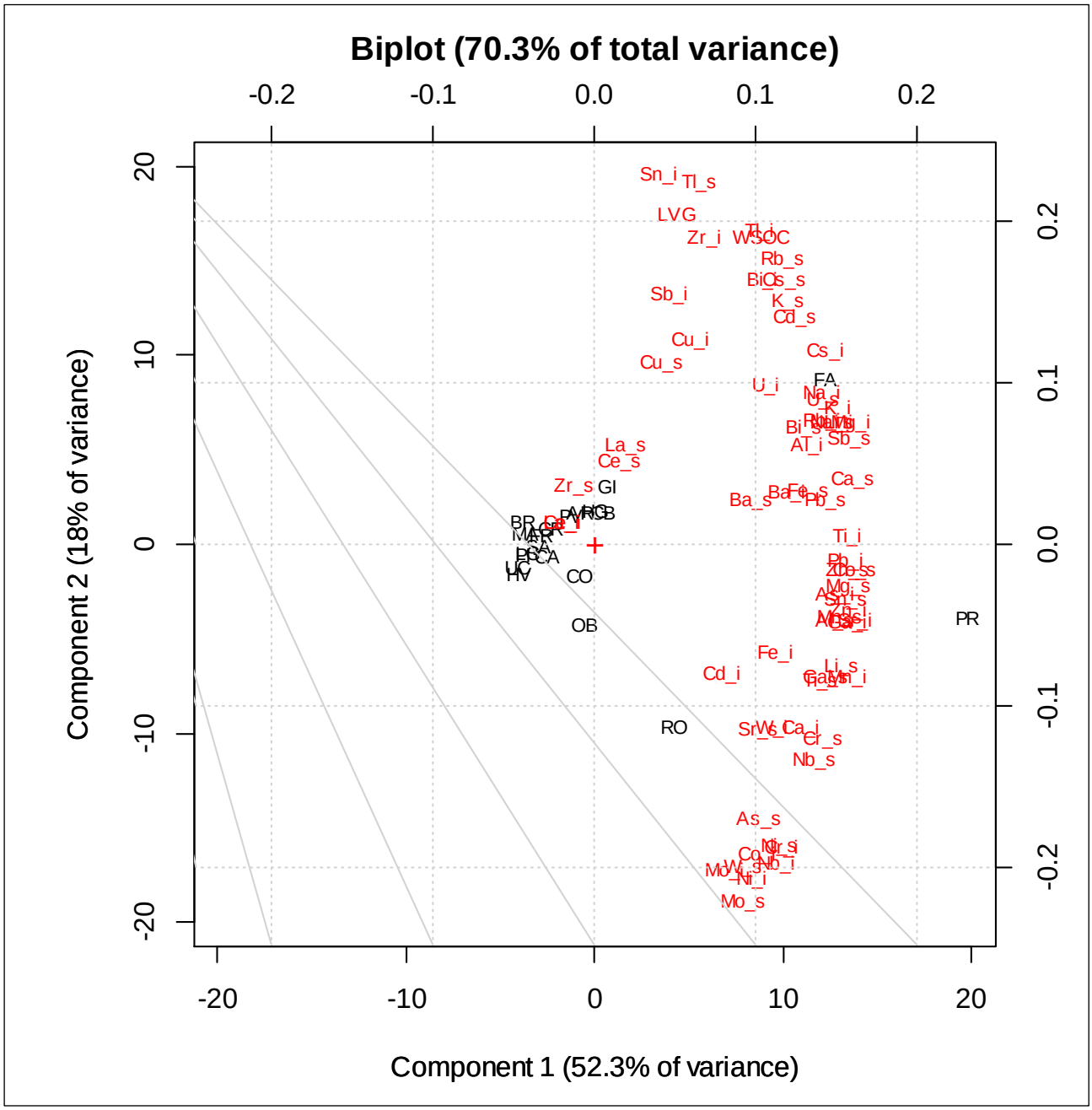

Fig. S3.1. Biplot of the PCA (PC1 and PC2) performed on the concentration data of LVG, WSOC and water-soluble and insoluble fraction of the 33 elements, determined at the twenty collection sites.

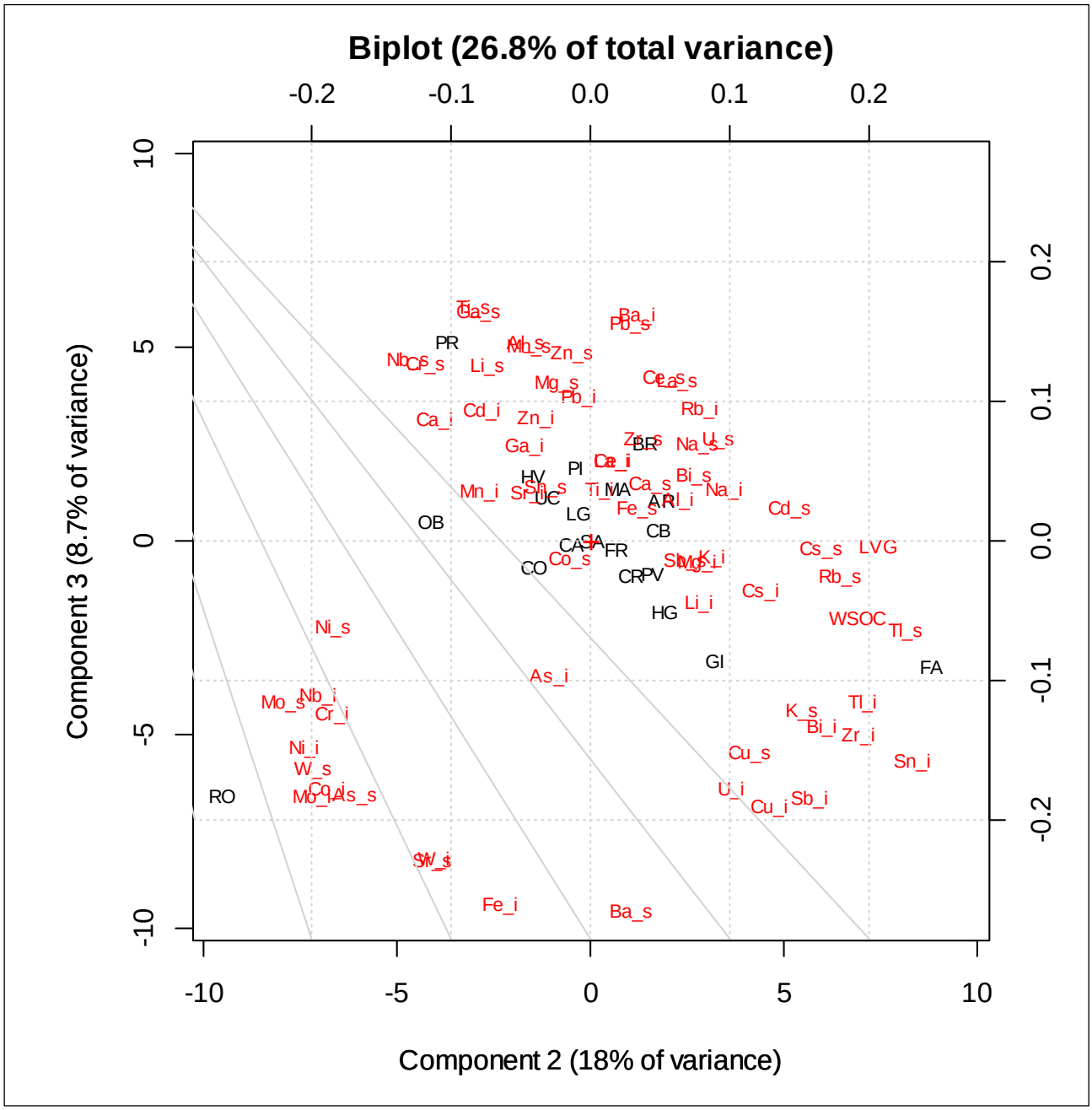

Fig. S3.2. Biplot of the PCA (PC2 and PC3) performed on the concentration data of LVG, WSOC and water-soluble and insoluble fraction of the 33 elements, determined at the twenty collection sites.

Supplementary Material S4.

Table S4.1a. Limits of detection (LODs; µg L^{-1}) mean of blank values (µg L^{-1}) and size distribution of the fine fraction (ng m^{-3}) of insoluble fraction of the 33 elements determined at PR, CA and MA. The LODs were set at 3 times the standard deviation (SD) of 10 replicate blank determinations**.**

Insoluble Fraction	LOD (µg L^{-1})	Mean Blank Values (µg L^{-1})	<0.18 µm			0.18-0.32 µm			0.32-0.56 µm			0.56-1 µm		
			PR	CA	MA	PR	CA	MA	PR	CA	MA	PR	CA	MA
Al	8.8	5	1.7	0.84	1.4	1.3	1.1	1.7	2.2	1.7	1.8	2.9	2.5	1.9
As	3.8	0.064	0.085	0.039	0.028	0.079	0.068	0.027	0.051	0.052	0.026	0.055	0.064	0.023
Ba	0.18	0.19	1.2	0.34	0.61	0.50	0.23	0.65	0.77	0.85	0.65	0.36	0.91	0.78
Bi	0.44	0.0019	0.030	0.0036	0.0046	0.020	0.011	0.0077	0.013	0.016	0.0092	0.016	0.024	0.014
Ca	0.0017	588	17	21	34	6.4	13	16	14	48	14	12	29	17
Cd	932	0.0040	0.0047	0.0058	0.0047	0.0032	0.011	0.0055	0.0034	0.0093	0.0054	0.0082	0.0069	0.0048
Ce	0.0031	0.018	<LOD	<LOD	1.1	<LOD	<LOD	1.2	<LOD	<LOD	<LOD	<LOD	0.0044	<LOD
Co	0.033	0.0053	0.027	0.0011	0.0022	0.023	0.0091	0.0021	0.019	0.019	0.0045	0.034	0.029	0.0067
Cr	0.0022	2.9	3.1	0.31	0.45	2.3	1.1	0.33	2.2	1.7	0.75	4.7	3.5	0.86
Cs	0.86	0.0016	0.0013	0.0013	0.00088	0.00095	0.0019	0.0010	0.00064	0.0011	0.0011	0.0021	0.0031	0.0011
Cu	0.0017	0.20	0.52	0.084	0.18	0.46	0.25	0.14	0.36	0.42	0.41	0.43	0.56	0.32
Fe	0.24	11	13	1.7	5.5	12	5.8	3.5	14	10	9	22	25	12
Ga	9.6	0.0020	0.0099	0.00059	0.0036	0.0078	0.0037	0.0043	0.0071	0.0070	0.0047	0.011	0.011	0.0047
K	0.0021	78	40	45	35	41	59	47	29	42	36	68	90	29
La	827	0.010	<LOD	<LOD	0.56	<LOD	<LOD	0.61	<LOD	<LOD	<LOD	<LOD	<LOD	<LOD
Li	0.016	0.0014	0.0051	0.0055	0.0022	0.0037	0.0066	0.0029	0.0023	0.0032	0.0035	0.0071	0.0091	0.0031
Mg	0.0040	7.9	0.92	0.76	1.1	0.77	0.76	0.94	1.0	1.2	1.3	2.3	1.8	1.0
Mn	8.8	0.33	0.83	0.043	0.18	1.1	0.32	0.20	1.2	0.70	0.73	2.2	1.7	0.84
Mo	0.17	0.021	2.8	0.96	0.54	2.6	1.5	0.41	1.1	1.2	0.29	0.88	0.87	0.18
Na	0.012	67	5.5	7.7	8.2	6.2	8.9	8.8	6.4	6.3	15	9.1	11	7.3
Nb	23	0.0087	0.0018	0.00047	0.0011	0.0018	0.0010	0.00051	0.0037	0.0017	0.0013	0.0091	0.0084	0.0017
Ni	0.012	0.39	1.6	0.050	0.10	2.0	0.64	0.13	1.7	1.2	0.27	2.4	2.0	0.41
Pb	0.17	0.14	1.3	0.14	0.31	1.1	0.43	0.30	0.87	0.59	0.42	0.89	1.1	0.62
Rb	0.15	0.052	0.012	0.018	0.017	0.018	0.041	0.019	0.0021	0.018	0.025	0.035	0.050	0.015
Sb	0.023	0.010	0.069	0.011	0.033	0.073	0.061	0.034	0.060	0.043	0.040	0.041	0.12	0.045
Sn	0.0094	0.041	0.77	0.31	0.26	0.44	0.54	0.27	0.28	0.36	0.26	0.15	0.63	0.25
Sr	0.027	0.38	0.064	0.051	0.077	0.042	0.074	0.060	0.055	0.10	0.057	0.055	0.089	0.065
Ti	0.57	0.37	0.025	0.014	0.043	0.023	0.031	0.018	0.053	0.036	0.050	0.14	0.11	0.069
Tl	0.40	0.00027	0.0092	0.0091	0.011	0.0060	0.012	0.0083	0.0018	0.0063	0.0048	0.0037	0.0082	0.0025
U	0.00034	0.00047	<LOD	<LOD	<LOD	<LOD	<LOD	<LOD	<LOD	<LOD	<LOD	<LOD	<LOD	<LOD
W	0.00062	0.0057	0.026	0.0088	0.0042	0.015	0.013	0.0032	0.0063	0.0051	0.0026	0.0055	0.011	0.0015
Zn	0.0037	2	1.8	1.1	1.5	2.4	1.7	1.1	2.2	4.1	1.8	4.2	4.8	2.2
Zr	47	0.49	0.0033	0.0061	0.010	0.0052	0.0051	0.0071	0.010	0.0084	0.0084	0.028	0.017	0.017

Table S4.1b. Size distribution of the fine fraction (ng m^{-3}) of insoluble fraction of the 33 elements determined at PR, CA and MA. The LODs were set at 3 times the standard deviation (SD) of 10 replicate blank determinations**.**

Insoluble Fraction	1-1.8 µm			1.8-3.2 µm			3.2-5.6 µm			5.6-10 µm			10-18 µm			>18 µm		
	PR	CA	MA	PR	CA	MA	PR	CA	MA	PR	CA	MA	PR	CA	MA	PR	CA	MA
Al	9.1	5.3	4.3	7.7	12	15	14	16	23	10	15	14	4.8	7.4	5.9	4.7	6.1	5.4
As	0.036	0.035	0.019	0.014	0.031	0.035	0.033	0.050	0.036	0.030	0.024	0.034	0.011	0.027	0.031	0.022	0.012	0.028
Ba	0.84	1.4	0.59	0.65	2.1	2.8	0.92	2.6	2.6	1.2	2.3	1.5	1.8	1.1	1.5	0.72	1.2	1.3
Bi	0.014	0.018	0.0254	0.0072	0.025	0.032	0.0081	0.034	0.035	0.0036	0.024	0.014	0.0037	0.0089	0.0052	0.00086	0.0054	0.0033
Ca	36	19	34	33	49	79	81	99	118	60	86	71	67	48	45	35	45	35
Cd	0.0092	0.0054	0.0036	0.0033	0.0025	0.0036	0.0025	0.0027	0.0031	0.0022	<LOD	0.0022	0.0025	0.0020	0.0027	0.0020	0.0072	0.0030
Ce	<LOD	0.0018	<LOD	<LOD	0.012	0.012	0.0046	0.024	0.032	<LOD	0.022	0.013	<LOD	0.0045	<LOD	<LOD	0.017	<LOD
Co	0.044	0.033	0.011	0.024	0.043	0.029	0.032	0.046	0.031	0.019	0.032	0.017	0.0076	0.013	0.0070	0.0066	0.011	0.0082
Cr	5.9	4.1	1.5	3.6	6.0	3.0	6.4	5.7	2.9	3.6	3.4	2.0	1.4	1.6	0.92	1.0	0.97	0.71
Cs	0.0023	0.0018	0.0010	0.0010	0.0030	0.0033	0.0019	0.0038	0.0052	0.0010	0.0034	0.0028	0.00064	0.0017	0.0015	0.00044	0.0013	0.0010
Cu	0.60	0.71	0.36	0.39	1.5	1.9	0.51	2.0	1.9	0.28	1.5	0.84	0.11	0.49	0.27	0.085	0.38	0.20
Fe	47	51	25	31	84	86	42	105	96	24	78	47	11	30	17	9.9	28	16
Ga	0.0075	0.0063	0.0028	0.0027	0.0064	0.0052	0.0041	0.0062	0.0070	0.0017	0.0045	0.0033	0.00072	0.0016	0.0013	0.00055	0.0014	0.0011
K	56	46	32	27	56	54	29	57	55	26	55	39	30	39	30	28	63	29
La	<LOD	0.00058	<LOD	<LOD	0.0050	0.0044	0.0011	0.010	0.012	<LOD	0.0096	0.0035	<LOD	0.0016	<LOD	<LOD	0.0095	<LOD
Li	0.011	0.0078	0.0048	0.0065	0.013	0.016	0.010	0.015	0.020	0.0061	0.013	0.011	0.0034	0.0062	0.0050	0.0032	0.0054	0.0045
Mg	9.6	3.2	1.8	5.8	8.6	10	14	9.4	7.8	11	9.3	5.2	6.0	5.0	2.9	6.3	4.9	4.0
Mn	2.6	1.4	0.57	1.3	1.6	1.5	2.4	1.8	1.6	1.4	1.4	0.91	0.63	0.58	0.37	0.58	0.51	0.36
Mo	0.59	0.34	0.081	0.17	0.36	0.21	0.21	0.33	0.19	0.11	0.24	0.10	0.050	0.088	0.047	0.049	0.063	0.066
Na	25	17	7.9	7.7	31	36	6.2	22	9.2	8.4	20	8.4	7.6	15	7.7	8.7	18	12
Nb	0.033	0.014	0.0034	0.039	0.020	0.0077	0.090	0.021	0.020	0.046	0.022	0.010	0.012	0.0080	0.0059	0.011	0.0082	0.0047
Ni	2.8	2.0	0.55	1.4	2.5	1.2	1.8	2.5	1.1	1.1	1.7	0.68	0.35	0.70	0.28	0.35	0.54	0.29
Pb	0.66	0.54	0.50	0.13	0.25	0.33	0.15	0.17	0.29	0.082	0.10	0.13	0.038	0.043	0.054	0.031	0.043	0.041
Rb	0.033	0.017	0.015	0.013	0.031	0.037	0.020	0.052	0.054	0.020	0.048	0.034	0.012	0.023	0.022	0.00093	0.025	0.015
Sb	0.036	0.054	0.051	0.032	0.095	0.092	0.037	0.10	0.21	0.013	0.090	0.080	0.0035	0.020	0.027	0.0020	0.015	0.014
Sn	0.13	0.26	0.29	0.086	0.37	0.34	0.092	0.46	0.50	0.036	0.34	0.18	0.015	0.097	0.058	0.025	0.073	0.034
Sr	0.18	0.11	0.092	0.13	0.25	0.34	0.25	0.36	0.41	0.17	0.34	0.26	0.17	0.19	0.16	0.10	0.17	0.13
Ti	0.59	0.23	0.21	0.68	0.59	0.55	1.7	0.79	0.86	1.2	0.84	0.54	0.55	0.46	0.30	0.60	0.42	0.26
Tl	0.0017	0.0019	0.00032	0.00022	0.0011	0.0012	0.00026	0.00061	0.0010	<LOD	0.00033	0.00033	<LOD	0.00015	0.00011	0.00016	0.00014	0.00019
U	0.00025	0.00015	0.00012	0.00020	0.00072	0.00096	0.00093	0.0012	0.0013	0.00052	0.00113	0.00076	0.00017	0.00048	0.00020	<LOD	0.00039	0.00017
W	0.0075	0.0057	0.0023	0.0053	0.0062	0.0037	0.0064	0.0054	0.0071	0.0029	0.0049	0.0044	0.0018	0.0018	0.0019	0.0017	0.0015	0.0012
Zn	5.1	2.7	1.8	1.4	2.6	3.4	1.6	3.3	3.3	1.0	2.1	1.8	1.7	1.1	1.3	0.73	2.5	1.0
Zr	0.046	0.060	0.050	0.047	0.11	0.15	0.069	0.15	0.15	0.044	0.10	0.064	0.019	0.036	0.034	0.022	0.032	0.017

Supplementary Material S5.

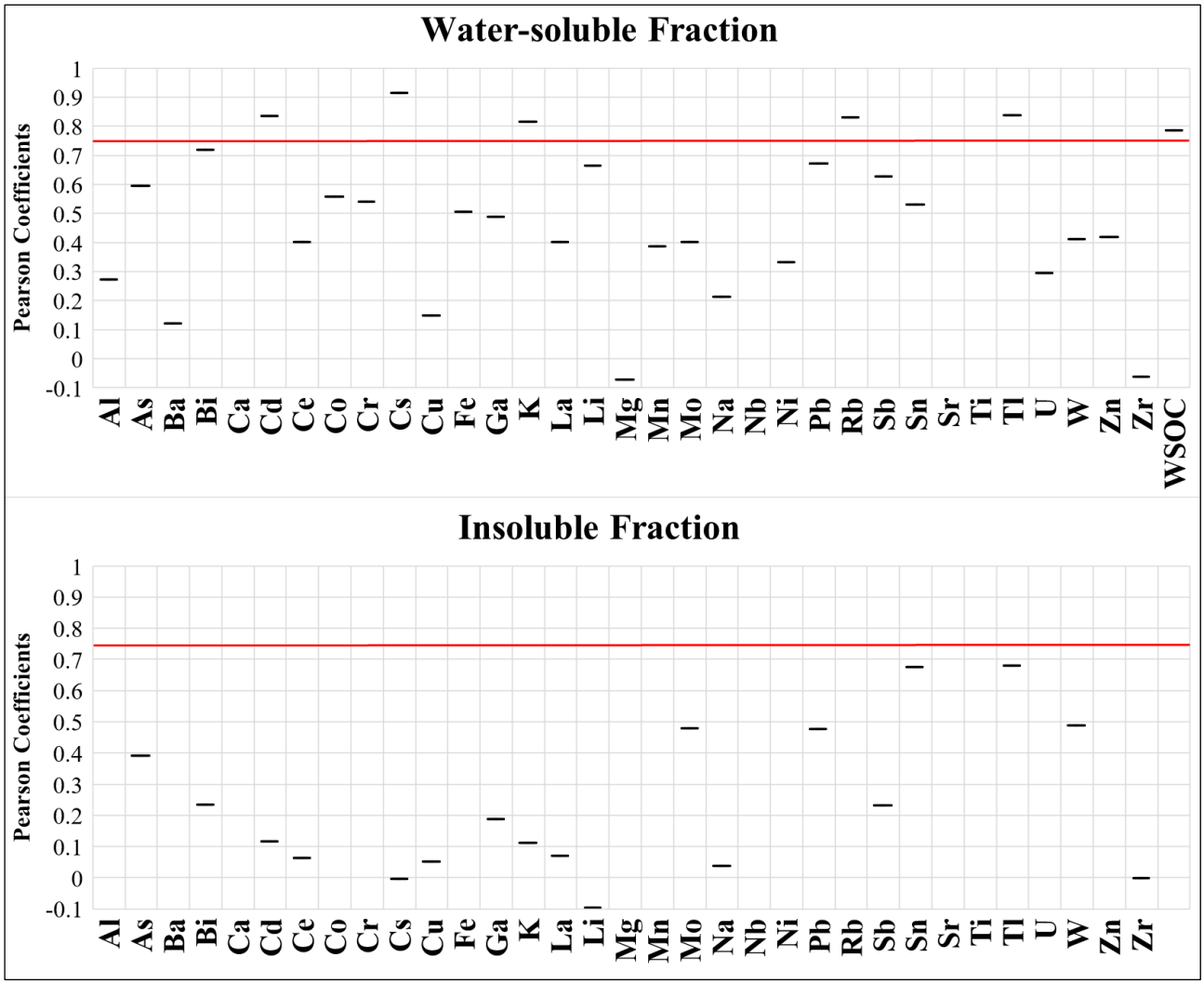

Fig. S5. Pearson correlation coefficients calculated between LVG concentration and the concentrations of WSOC and water-soluble and insoluble fraction of the 33 elements in PM_{10} and size-segregated samples. Coefficients higher than 0.75 (good correlation; red lines) indicate high reliability of the chemical components as biomass burning tracers.

2.3.3. (C3) Spatial Mapping of Element Concentrations in PM_{10}: a Powerful Tool for Localization and Impact Assessment of Emission Sources

Atmospheric Research (2019), *With Editor*

Lorenzo Massimi [a,*], Martina Ristorini [b], Maria Luisa Astolfi [a], Cinzia Perrino [c], Silvia Canepari [a]

[a] Department of Chemistry, Sapienza University of Rome, P. le Aldo Moro, 5, Rome 00185, Italy;
[b] Department of Bioscience and Territory, University of Molise, Pesche (IS), 86090, Italy;
[c] C.N.R. Institute of Atmospheric Pollution Research, Via Salaria, Km 29,300, Monterotondo St. (Rome), 00015, Italy.

Abstract: A very-low volume sampler of particulate matter (PM) on membrane filters, recently developed with the purpose of allowing spatially-resolved determination of PM and of its chemical components, was employed from December 2016 to February 2018 in a wide and dense monitoring network across Terni, an urban and industrial hot-spot of Central Italy (23 sampling sites, about 1 km between each other). Terni basin can be considered as an open air laboratory for studying the spatial distribution of PM, as it includes several spatially disaggregated sources. PM_{10} samples were chemically characterized for the water-soluble and insoluble fraction of 33 elements (Al, As, Ba, Bi, Ca, Cd, Ce, Co, Cr, Cs, Cu, Fe, Ga, K, La, Li, Mg, Mn, Mo, Na, Nb, Ni, Pb, Rb, Sb, Sn, Sr, Ti, Tl, U, W, Zn, Zr). Spatial variability of the element concentrations across Terni was then mapped by using the ordinary kriging interpolation method. The spatial distribution of the analyzed elements successfully traced the various PM_{10} sources. In particular, the spatial mapping of Ba (water-soluble fraction), Bi, Cu, Sb, Sn and Zr (insoluble fraction) traced PM_{10} emission from the rail network and vehicular traffic, Ce, Cs, La, Li, Rb, Sr and U (insoluble fraction) traced soil resuspension, Cd, Cs, K, Rb and Tl (water-soluble fraction) biomass burning and Co, Cr, Mn, Nb, Ni, Pb (insoluble fraction), As, Cr, Ga, Li, Mo, Mn, W and Zn (water-soluble fraction) the steel industry pole. Principal component analysis was performed on the spatially-resolved chemical data to cluster the elements tracing the main PM_{10} sources. The winter and summer size distribution of the water-soluble and insoluble elements was analyzed to verify their link with the emission sources. The proposed

experimental approach promises to be very effective for the assessment of population exposure to different PM_{10} sources.

Keywords: PM_{10} element; chemical fractionation; source tracer; spatial variability; seasonal variation; size distribution.

1. Introduction

Particulate matter air pollution is a serious threat to human health (Lubczyńska et al., 2017). The World Health Organization estimates that PM air pollution contributes to approximately 800,000 premature deaths each year (Anderson et al., 2012). Various epidemiological studies have spotlighted strong correlations between exposure to PM and the onset of cardiovascular and respiratory diseases (Pope and Dockery, 2006). Urban and industrial PM is known to increase morbidity and mortality due to cardiopulmonary diseases related to inflammatory processes and genotoxic effects (Perez et al., 2009, Zanobetti and Schwartz, 2009). Therefore, the identification, quantification and apportionment of PM sources is necessary to facilitate their reduction through proper management plans (Taiwo et al., 2014).

The study of the spatial distribution of PM chemical compounds is essential for a reliable identification of emission sources, the evaluation of particle dispersion over the territory and the assessment of personal exposure. However, due to the very high cost of a network based on traditional PM samplers, ambient air quality assessment and epidemiological studies are usually based on measurements taken at a few sampling points (Hoek et al., 2002; Minguillón et al., 2012; Mangia et al., 2013). Consequently, to obtain a reliable assessment of population exposure, the information collected at these few points needs to be extended to wider areas by evaluating the dispersion properties of pollutants (Setton et al., 2010; Kloog et al., 2013; Minguillón et al., 2014). Typically, PM dispersion is estimated through mathematical models (Irwin, 2014; Vitali et al., 2016; Kim et al., 2017), which may not be able to properly describe the complexity of PM transport and transformation processes. Indeed, since PM dispersion varies as a function of the particle dimension, shape, chemical composition and density (Yu et al., 2018; Meng et al., 2019), its evaluation through mathematical models is a quite complex issue in particularly polluted areas, where PM sources are various and variable. Moreover, the reliability of dispersion models needs to be in any case verified through the acquisition of experimental data.

For these reasons, in the last few years, a self-powered, automatic and very-low volume device (High spatial resolution sampler, HSRS; FAI Instruments, Fonte Nuova, Rome, Italy) for PM sampling on membrane filters (suitable for subsequent chemical analyses) has been developed with the purpose of allowing spatially-resolved determination of PM and of its chemical components. The sampler can be employed for the construction of wide and dense air quality monitoring networks across urban and industrial areas. In addition, it can work autonomously for long periods of time (1-2 months), thus allowing a good data representativeness and a substantial reduction of maintenance costs of the monitoring network.

In this study, the HSRS was employed to evaluate the winter and summer spatial variability of PM_{10} mass and element concentrations at 23 sampling sites (approximately 1 km of distance between each other) in Terni (Central Italy), during a 15-month monitoring period. Terni is located in an intra-mountain depression characterized by quite intensive urban PM emissions (vehicular traffic, rail network, domestic heating) and a high density of industrial activities (power plant for waste treatment, steel industry pole), which makes it the most industrialized city of Central Italy (Capelli et al., 2011; Guerrini, 2012). The peculiar meteorological conditions of the Terni basin reduce air mixing and air pollutants transport, favoring their accumulation (Ferrero et al., 2012). These factors have been associated with an increase of morbidity and mortality due to the onset of cardiopulmonary environment-related diseases, which made this area of national interest for environmental remediation (SENTIERI-ReNaM, 2016). Therefore, the Terni basin was found to be particularly suitable for the application of the high spatial resolution sampling technique.

This work is aimed to identify reliable tracers for the main PM_{10} sources in Terni and to map their winter and summer spatial distribution through the experimental approach here described.

2. Materials and Methods

2.1. Study Area

Terni is a medium-sized city of around 112,000 inhabitants (Sgrigna et al., 2015), located in a basin in the southwest of the Umbria region (42°34′N; 12°39′E), Central Italy. The territory of Terni is a wide plain of 211.90 km^2 surrounded by the Apennine mountains, which limit the dispersion of air pollutants (Ferrero et al., 2012), reducing air mixing, especially during the severe winter episodes of atmospheric stability (Moroni et al., 2013; Curci et al., 2015). The weather is characterized by very-low winds, whose predominantly direction is from North-East (Capelli et al., 2011).

According to the Köppen climate classification (Peel et al., 2007), the area of Terni belongs to the temperate climate of the middle latitudes. The winter is cold and rainy, spring and autumn are mild and humid, while summer is hot, humid, muggy and not rainy (Morini et al., 2016).

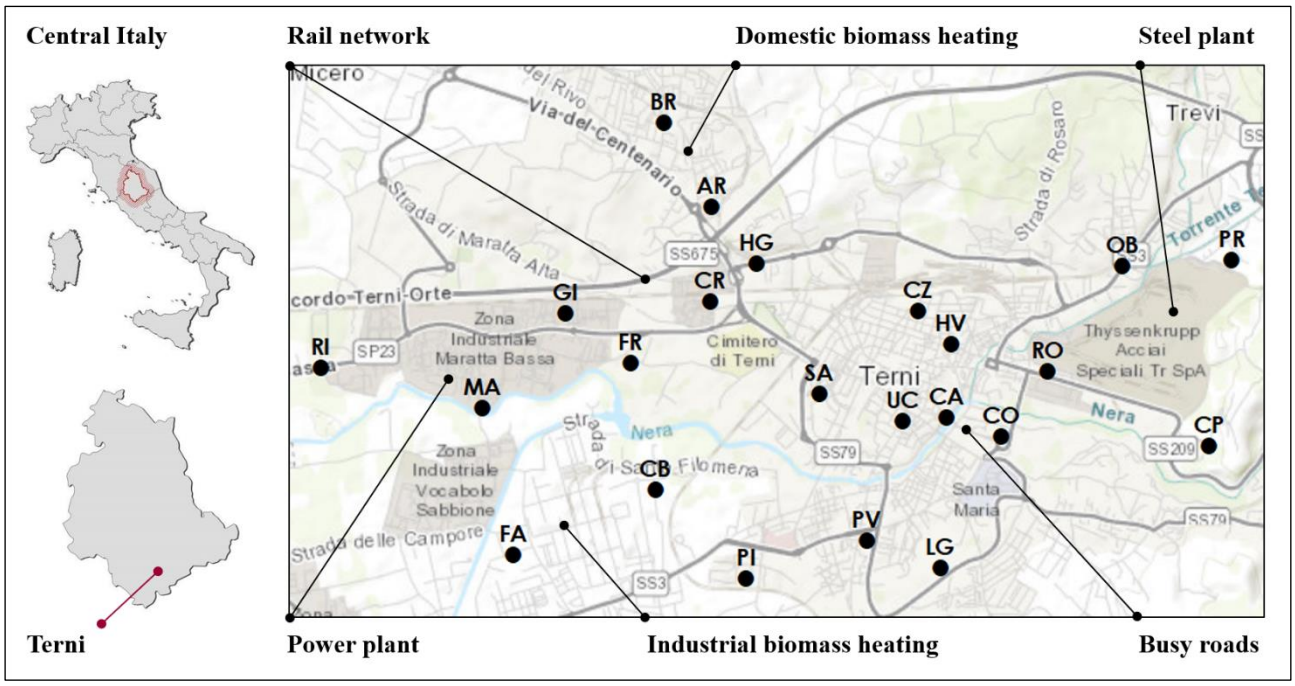

Fig. 1. Map of the 23 sampling sites in the study area (Terni, Central Italy) with the location of the main local PM_{10} emission sources (ArcMap 10.3.1, ArcGis Desktop; ESRI, Redlands, CA, USA).

2.2. Sampling Sites

The first phase of the study required great commitment and large amount of time for selecting appropriate sites for the deployment of the 23 HSRS. The sampling sites were chosen, with the support and help of the regional environmental protection agency ARPA Umbria, in order to cover the whole basin with a spatial resolution of about 1 km, allowing us to represent the contribution of the main local PM_{10} emission sources (Fig. 1). In particular:

- power plant for waste treatment in the West of the city: RI, MA;
- railway in the North-West of the city: GI, CR, HG;
- trafficked streets in the city center: CZ, HV, SA, UC, CA, CO;
- industrial biomass heating (carpentry and craftsmanship lab) in the South-West of the city: FA, CB;

- domestic biomass heating (townhouses frequently heated by biomass burning appliances) in the North and in the South of the city: FR, BR, AR, PI, PV, LG;
- very extensive steel plant in the East of the city: RO, OB, PR, CP.

To ensure homogeneous sampling conditions, all the HSRS were deployed within 4 m above ground level and with southern exposition. The geographical coordinates of the 23 sites (RI, MA, FA, GI, FR, CB, PI, BR, AR, CR, HG, SA, PV, LG, CZ, HV, UC, CA, CO, RO, OB, PR, CP) are reported in supplementary material S1 and additional characteristics about the sampling sites are detailed in Massimi et al. (2017, 2019a, 2019b).

The 15-month monitoring campaign was carried out from November 19th 2016 to February 19th 2018.

2.3. Sampling Equipment

2.3.1. High Spatial Resolution Sampler

The High spatial resolution sampler (HSRS; FAI Instruments, Fonte Nuova, Rome, Italy) operates with a flow rate of 0.5 L min^{-1}. It was powered by a rechargeable battery and a small solar panel and was equipped with PM_{10} sampling head filter system. The sampler assures long-term (1-2 months) collection of PM_{10} and it is small and light enough to be easily installed on existing structures such as light poles, railings and balconies, thus improving access to a larger number of sampling locations. The HSRS was evaluated by Catrambone et al. (2019) in terms of efficiency and repeatability and it showed very good sampling efficiency for stable and fine PM_{10} chemical compounds (such as the elements) and high repeatability, especially for metals and metalloids (5.6–16%). In addition, the HSRS was already employed in the area of Terni and was found to be effective for the construction of wide and dense monitoring networks and for the evaluation of the spatial variability of PM_{10} chemical components (Massimi et al., 2017, 2019a, 2019b).

The very-low volume samplers were deployed at the 23 sites. They worked in parallel for 12 sampling periods: seven samplings during the winter (November 2016 - March 2017 and October 2017 - February 2018) and five samplings during the summer (April - October 2017). The start and stop dates of each period are reported in supplementary material S2. The HSRS were equipped with 37 mm Teflon membrane filters (2 μm pore size, PALL Corporation, Port Washington, NY, USA).

2.3.2. Micro-Orifice Uniform Deposition Impactor

The Micro-orifice uniform deposition impactor (MOUDI; model 110-NR; MSP Corporation, Shoreview, MN, USA) is a low-pressure cascade impactor for the collection of size-segregated PM

samples. It operates at the flow rate of 30 L min^{-1} and it has 10 impaction stages, low internal-loss characteristics and sharp cut-size aerodynamic diameters of 0.18, 0.32, 0.56, 1.0, 1.8, 3.2, 5.6, 10 and 18 µm. MOUDI samples used for PM mass and elemental concentration measurements were collected on 47 mm Teflon membranes (2 µm pore size, PALL Corporation, Port Washington, NY, USA). The MOUDI worked in parallel at three sites in the East (PR), center (CA) and West (MA) of the city for 20 days during the winter (February 15th - March 6th, 2018) and 16 days during the warm season (September 15th - 30th, 2017), allowing us to obtain information on the winter and summer size distribution of the PM mass and of the water-soluble and insoluble fraction of the elements. Size-segregated PM was also collected on aluminum foils (47 mm, MSP Corporation, Shoreview, MN, USA) during a 3-day period (February 12nd - 14th 2018) at PR (East of the city).

2.4. Analytical Procedure

Teflon membrane filters were weighed before and after sampling, in order to determine PM mass concentrations.

PM_{10} samples and size-segregated PM samples were chemically characterized for the water-soluble and insoluble fraction of the elements by using a chemical fractionation procedure, previously optimized and validated (Canepari et al., 2006a, 2006b). Chemical fractionation consists in the water extraction of PM membrane filters followed by digestion of the residue, combined with the determination of the element concentrations in the two obtained fractions. This procedure allowed us to assess the chemical form in which each element was released, which may be typical of its emission source (Templeton et al., 2000), thus increasing the selectivity of the elements as source tracers (Canepari et al., 2009; Perrino et al. 2010).

Briefly, the supporting polymethylpentene ring was removed from each membrane filter, which was subjected to an ultrasound assisted extraction for 30 min in 10 mL of deionized water (Arioso UP 900 Integrate Water Purification System, Cole-Parmer Co Ltd., Saint Neots, England, UK). The extracted solution was then filtered on a cellulose nitrate filter (0.45 µm pore size, Merck Millipore Ltd., Billerica, MA, USA). Subsequently, both the membrane filter and the cellulose nitrate filter were subjected to a microwave assisted acid digestion (Ethos Touch Control with Q20 rotor, Milestone, Bergamo, Italy) by using 2 mL of ultrapure concentrated HNO_3 (67%; Promochem, LGC Standards GmbH, Wesel, Germany) and 1 mL of H_2O_2 (30%; Promochem, LGC Standards GmbH, Wesel, Germany). The digested solution was then diluted to 50 mL with deionized water and filtered with syringe filters (25 mm diameter, 0.45 µm pore size, GVS Filter Technology, Morecambe,

England, UK). After the two-step sequential leaching, the concentrations of 33 elements (Al, As, Ba, Bi, Ca, Cd, Ce, Co, Cr, Cs, Cu, Fe, Ga, K, La, Li, Mg, Mn, Mo, Na, Nb, Ni, Pb, Rb, Sb, Sn, Sr, Ti, Tl, U, W, Zn, Zr) in the water-soluble and insoluble fraction of each sample was determined by a quadrupole inductively coupled plasma mass spectrometer (ICP-MS; model 820-MS; Bruker, Bremen, Germany) equipped with a glass nebulizer (0.4 mL min^{-1}; Analytik Jena AG, Jena, Germany). For each element, external standard calibration curve was performed in the 1-500 µg L^{-1} range by serially diluting standard stock solutions (1000 ± 2 mg L^{-1}; Exaxol Italia Chemical Manufacturers Srl, Genoa, Italy; Ultra Scientific, North Kingstown, RI, USA; Merck Millipore Ltd., Billerica, MA, USA). To control the nebulizer efficiency, yttrium (1000 ± 2 mg L^{-1}; Panreac Química, Barcelona, Spain) was set at 5 µg L^{-1} as internal standard for all the measurements (Astolfi et al., 2018; Conti et al., 2018). The limits of detection (LODs; supplementary material S3) were set at 3 times the standard deviation (SD) of 10 replicate blank determinations.

The instrumental conditions and the performance of the method are detailed in Astolfi et al. (2018) and in Canepari et al. (2009), respectively.

2.5. Spatial Mapping

The winter and summer spatial distribution of the water-soluble and insoluble elements was mapped by the software ArcMap 10.3.1 (ArcGis Desktop; ESRI, Redlands, CA, USA).

To create a continuous surface from the 23 measured sample points and predict the values at unmeasured locations (Kumar et al., 2007), the element concentrations determined at the 23 sampling sites were interpolated by using the ordinary kriging (OK) method (Johnston et al., 2001). Kriging is based on the assumption that the parameter being interpolated can be treated as a regionalized variable and its estimator is given by a linear combination of the observed values with weights, which are derived from the kriging equations using a semivariogram function (Xie et al., 2011). In the OK the data are assumed to be generated from a stochastic process which is split into a constant but unknown trend component and an error component (Beelen et al., 2009).

As the skewed dataset showed clear trends of the element concentrations, log transformation was applied. The variogram was computed on the transformed data, and the experimental semivariances were fitted by a spherical function (spherical semivariogram model), by weighted least-squares approximation (Jian et al., 1996). This function was then used for the kriging.

2.6. Multivariate Statistical Analyses

To cluster the tracers of the main PM_{10} emission sources in Terni, principal component analysis (PCA) was performed on the spatially-resolved data of PM_{10} mass concentration and water-soluble and insoluble fraction of elements.

The matrix of the data (9660 data) used for the PCA is composed of 276 samples (23 samples for each of the 12 sampling periods) and of 34 selected variables: PM_{10} mass concentration and 33 water-soluble (_s) and/or insoluble (_i) element concentrations (As_s, Ba_s, Bi_i, Cd_s, Ce_i, Co_i, Cr_i, Cr_s, Cs_i, Cs_s, Cu_i, Fe_i, Ga_s, K_s, La_i, Li_i, Li_s, Mn_i, Mn_s, Mo_s, Nb_i, Ni_i, Pb_i, Rb_i, Rb_s, Sb_i, Sn_i, Sr_i, Tl_s, U_i, W_s, Zn_s, Zr_i). The variables were selected depending on the ability of the elements to trace PM_{10} emission sources. Before performing the PCA, the matrix of the data was transformed by column mean centering and row and column autoscaling in order to correct for variations of the data due to the different scaling of the examined variables (Conti et al., 2007; Massimi et al., 2017, 2018). Multivariate statistical analyses were performed using the statistical software R (R-project for statistical computing, Ver. 3.0, 32-bit).

2.7. Scanning Electron Microscopy Characterization

A small portion of the samples collected by MOUDI (about 0.8 cm^2) on aluminum foils was cut in the center, fixed to aluminum stubs by self-adhesive carbon discs (TAAB, 12 mm diameter) and coated with an ultra-thin carbon layer (5 nm) by a vacuum evaporator (108 Carbon A; Scientific Instruments Ltd., Cressington, England, UK). Subsequently, PM samples in the range 3.2-5.6 μm and 0.32-0.56 μm were morphologically characterized by a High resolution field emission scanning electron microscopy (HR-FESEM; model AURIGA; Carl Zeiss Microscopy GmbH, Jena, Germany), equipped with an energy dispersive spectrometer for X-ray microanalysis (XEDS; model QUANTAX; Bruker Italia S.r.l., MI, Italy), to qualitative describe the morphology and elemental composition of particles released by the steel plant in the fine and coarse fraction. HR-FESEM XEDS acquisitions were performed under high vacuum (10^{-6} hPa) at 20 keV accelerating voltage. Micrographs were acquired by secondary electron detector (SED) at magnification, working distance (WD), tilt angle, and spot size conditions properly adjusted on a case-sensitive scale to optimize image resolution. The microanalysis was performed at WD ranging from 9.6 mm to 12.4 mm and at magnification ranging from 25,000x to 600,000x.

3. Results and Discussion

3.1. PM_{10} and elemental concentration

Spatially-resolved data, obtained by sampling in parallel at the 23 sites, were used to evaluate the spatial variability of PM_{10} mass concentration in Terni. The seasonal mean (AM) concentrations of the PM_{10} mass determined in the winter and summer were considered.

From Fig. 2, we can observe that a clear increase in PM_{10} mass concentration occurred at all the sampling sites during the winter. This can be explained by a combination of two factors: the increase in the strength of some typical winter sources, such as domestic biomass burning, and the frequent temperature inversion occurring during the cold season, which leads to a less efficient mixing of the lower atmosphere and to severe episodes of atmospheric stability (Moroni et al., 2013; Curci et al., 2015).

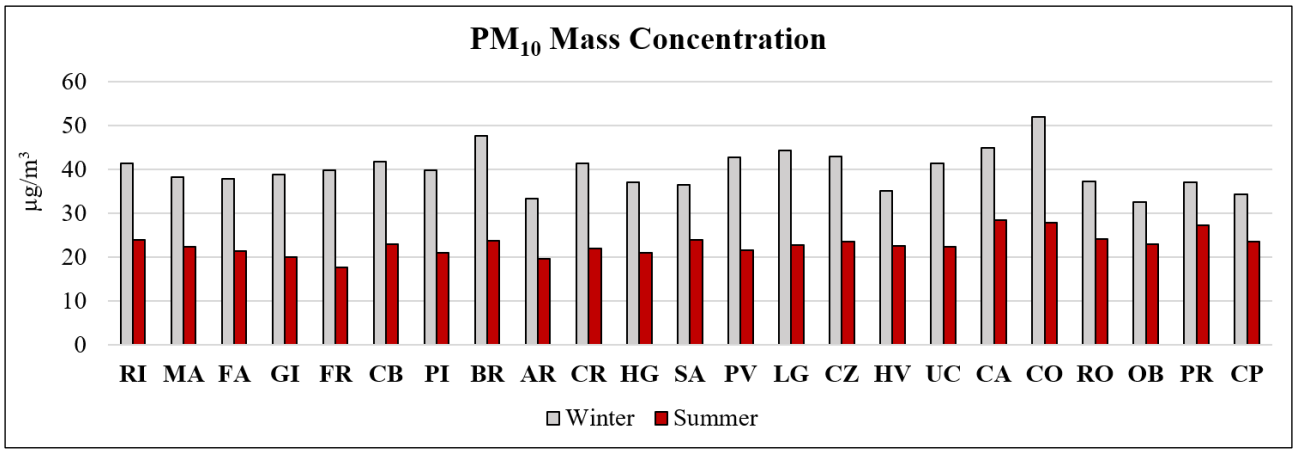

Fig. 2. AM of the PM_{10} mass concentrations ($\mu g/m^3$) recorded at the 23 sampling sites in Terni during the winter and summer monitoring periods.

Mean PM_{10} mass concentration at all the sites during the winter was 40 $\mu g/m^3$, while during the summer it was 23 $\mu g/m^3$. The highest PM_{10} mass concentration (52 $\mu g/m^3$) was found during the winter at CO, which is located between high-speed roads and the steel plant. High winter PM_{10} mass concentration was recorded also at CA (close to CO; 45 $\mu g/m^3$) and at BR (48 $\mu g/m^3$), where domestic biomass heating systems were largely used during the cold season. During the summer, the lowest PM_{10} mass concentration was recorded at FR (urban background site; 18 $\mu g/m^3$), while higher concentrations were found at sites close to busy roads (CO, CA) and to the steel industry pole (RO,

OB, PR, CP), sources whose strength increased probably because of the more easily resuspension of vehicle components and steel particles in the warm and dry season.

Winter and summer mean concentrations of all the measured elements in their water-soluble and insoluble fraction are reported in Supplementary Materials S3. As already observed for PM_{10}, the average concentration of most elements was higher during the winter. A different behaviour was observed only for elements that are generally considered as released by the soil (Ce_i, Cs_i, La_i, Li_s, Rb_i, Sr_i), whose resuspension is favoured during the dry season.

The data in S3 also show that at all the 23 sites the solubility percentages of the elements were fairly constant. For example, Cd, Mo, Rb and Tl were found, at all sites, mainly in their soluble fraction, while Al, Bi, Ce, Co, Cr, Fe, Ga, La, Nb, Ni, Pb, Sn, Ti, U and Zr were found in the residual fraction. This indicates that the relative strength of the sources of each element did not change in the whole area of the Terni basin. For some elements (Cd, Cs, Rb, Tl), however, we observed great seasonal differences in the solubility percentage, which indicate the activity of seasonal sources.

It is worth noting that at all the sampling sites the yearly average concentration of As, Cd and Pb in PM_{10} was well below the values set by the European Union (EU 2008/50/CE) as target value (As, Cd) or limit value (Pb). The yearly average concentration of Ni, instead, was above the EU target value (20 ng/m^3) in all the East area of the city, where the steel industry pole is located. The maximum Ni concentration was found at RO, where it was almost five times the target value (98 ng/m^3). The identification and characterization of the source/s responsible for these high values constitutes a valuable tool for planning the mitigation measures that are necessary to protect citizens health in the area of study.

3.2. Spatial Mapping of the Water-soluble and Insoluble Element Concentrations

The winter and summer spatial distribution of the water-soluble and/or insoluble fraction of the 33 selected elements are reported in supplementary material S4. The maps allow an easy identification of the location and strength of the local sources of each element. They also give reliable indications about the horizontal diffusion of the particles in which the elements are contained.

For some elements (Cr, Cs, Li, Mn, Rb), the spatial maps of the soluble and of the residual fraction were different. As an example, in Fig. 3 (panels a-d) we report the spatial distribution of Cs_s and Cs_i. The concentration of Cs_s was clearly higher during the winter period in all the residential area. The highest values were recorded at FA, which is close to the carpentry, and at sites close to townhouses frequently heated by biomass burning appliances, such as BR. The spatial distribution of

Cs_s (panels a,b) was practically identical to those of K_s, which is widely recognized as a robust tracer of biomass burning, and of Cd_s, Rb_s and Tl_s, which also have been identified as possible biomass burning tracers (Frasca et al., 2018; Simonetti et al., 2018a; Massimi et al., 2019b).
The insoluble fraction of Cs (panels c,d), instead, showed a completely different spatial distribution and seasonal variability. In fact, its concentration was higher during the summer and its maximum values were recorded at the sites most affected by traffic, particularly those close to high-speed roads. A similar spatial pattern was observed also for elements that are typically contained in soil (Ce_i, Cs_i, La_i, Li_i, Rb_i, Sr_i, U_i), as the traffic favours their resuspension, particularly during warm and dry periods (Amato et al., 2009; Simonetti et al., 2018a; Bencharif-Madani et al., 2019; Soleimanian et al., 2019). It is thus clear that insoluble and soluble species of Cs were released into the environment by different sources. This confirms the effectiveness of the chemical fractionation based on solubility in increasing the selectivity of the elements as source tracers (Canepari et al., 2009; Perrino et al., 2010; Massimi et al., 2017).

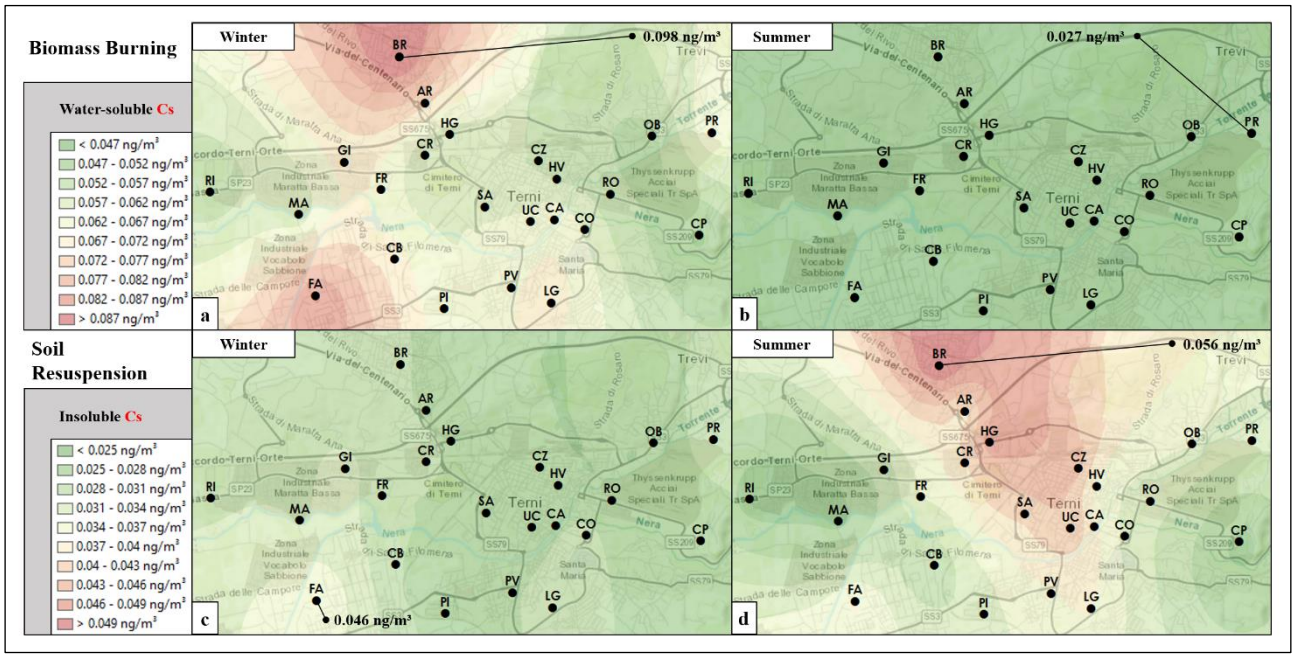

Fig. 3. Map of the winter and summer spatial distribution of water-soluble (panels a,b) and insoluble Cs (panels c,d).

The concentration of some elements (Co, Cr, Fe, Mn, Mo, Nb, Ni, Pb, W) was, as expected, higher in the Eastern area of the basin, where the steel plant is located. All these elements are used in steel

production: Cr, Fe and Ni are basic components of steel, while Co, Mn, Mo, Nb, Ni and W are used to increase its toughness, ductility, tensile strength and corrosion resistance (Querol et al., 2007; Owoade et al., 2015; Massimi et al., 2017; Marcias et al., 2018).

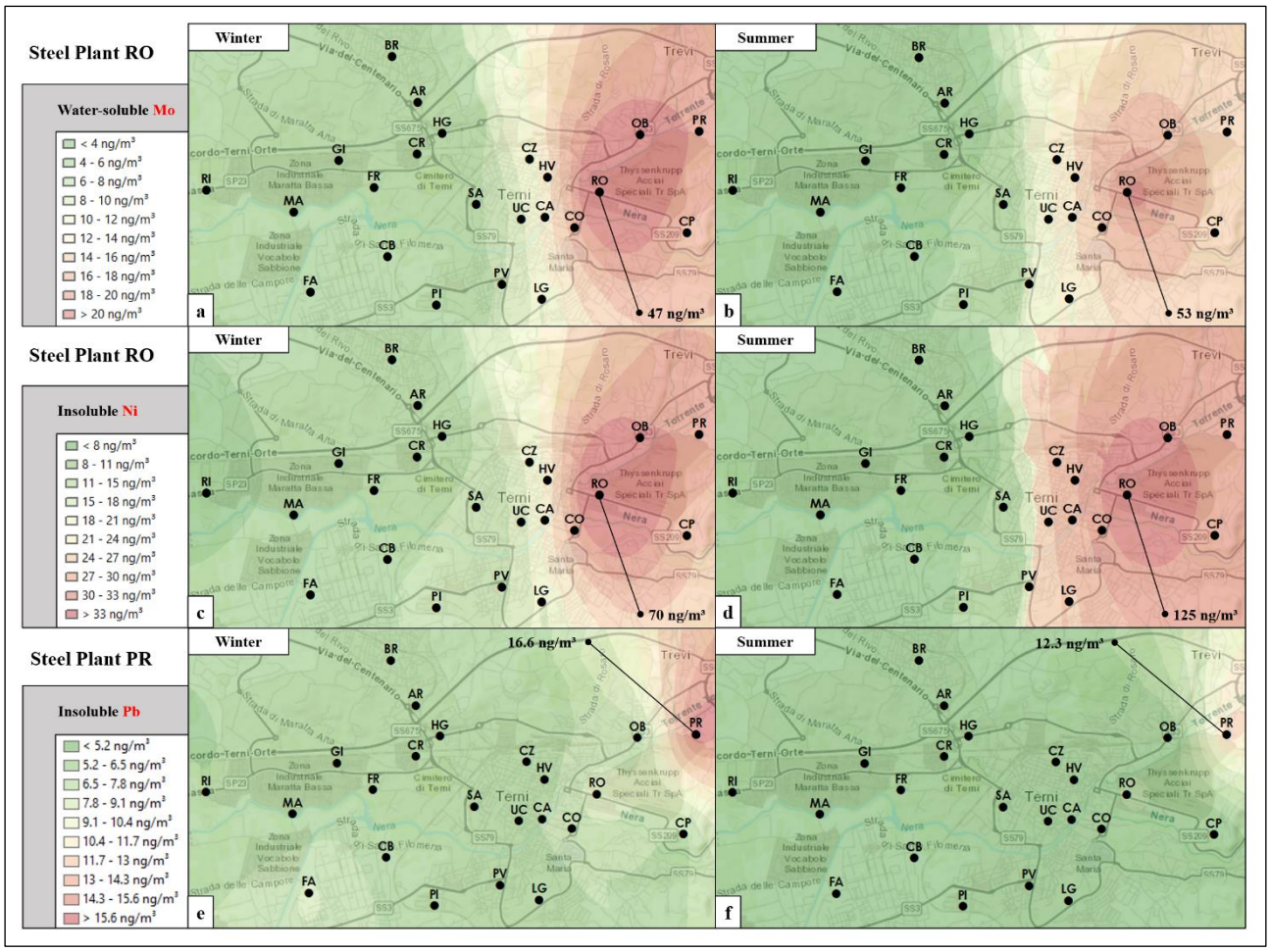

Fig. 4. Map of the winter and summer spatial distribution of water-soluble Mo (panels a,b), insoluble Ni (panels c,d) and Pb (panels e,f).

In Fig. 4 we report the spatial maps of Mo_s, Ni_i and Pb_i, obtained during the winter and summer periods. These examples show that during the winter months the spatial distribution of Mo_s and Ni_i were practically identical, suggesting the existence of a common main source (Fig. 4, panels a,c). For both these elements, the maximum concentration was measured at RO, very close to the steel rolling plants; this activity seems therefore to be the main cause of the measured values. Also during the summer period, the maximum concentrations of Mo_s and Ni_i were measured at RO, but their

seasonal variability showed some differences (Fig. 4, panels b,d). In both cases, during the summer the strength of the local sources at the hot spot site (RO) was higher with respect to the winter period, but the summer increase was definitely more remarkable in the case of Ni_i (average concentrations were 70 ng/m^3 during the winter and 125 ng/m^3 during the summer) than in the case of Mo_s (average concentrations were 47 ng/m^3 and 53 ng/m^3, respectively). Furthermore, the spatial diffusion of Mo_s was lower during the summer than during the winter, while the opposite was observed for Ni_i. These observations suggest the possible coexistence of two different types of emission in the same area, which are differently affected by seasonal variations of the meteorological conditions.

High concentrations of Pb_i (Fig. 4, panels e,f) were recorded at PR, which is the closest site to the furnaces for the annealing of the cold rolled product of the steel industry pole (Capelli et al., 2011) and to the steel waste storage site. A similar behavior was observed also for Cr_s, Li_s, Ga_s, Mn_s and Zn_s (supplementary material S4). Also these elements were then probably emitted by steel plant related sources, but the involved processes should be different from those releasing Ni and Mo. In fact, for these elements, the mean concentrations at PR and in the whole basin were higher during the winter. This indicates a contribution to PM that is not seasonal and that is then susceptible to the conditions of stronger atmospheric stability which are typical of the cold period.

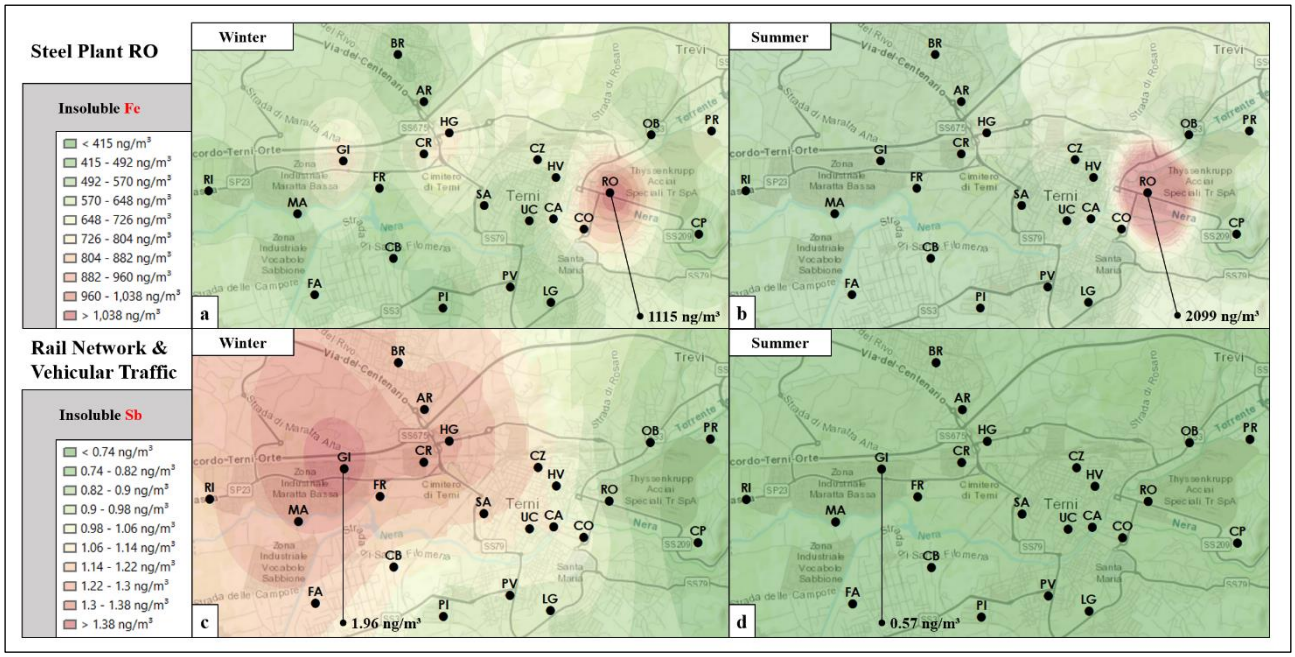

Fig. 5. Map of the winter and summer spatial distribution of insoluble Fe (panels a,b) and Sb (panels c,d).

Similarly to Ni_i, also Fe_i showed the maximum concentrations at RO (Fig. 5, panels a,b), where summer concentration was much higher than winter values (2099 ng/m^3 and 1115 ng/m^3, respectively). Ni and Fe are among the main components of stainless steel; it is thus possible that they were both released by mechanical processes such as brushing and polishing operations on rolled steel (Noe et al., 1996). This release could be more important during the dry summer period (Canepari et al., 2008; Pant and Harrison, 2013; Simonetti et al., 2018a). Mainly during the winter months, the spatial distribution of Fe_i showed the existence of additional sources of moderate strength, mostly sited along the railway (GI, CR, HG) and probably due to abrasion of rolling stock.

The contribution of the railway is very clear also for Sb_i, as well as for Bi_i, Sn_i and Zr_i, summer and winter maps for this element are shown in Fig. 5 (panels c,d; maps for Bi_i, Sn_i, and Zr_i are reported in supplementary material S4). It is worth noting that these elements are generally considered as robust tracers of non-exhaust emission from vehicular traffic, as they are contained in high concentration in brake pads. Our spatial maps show that the rail network, which employs brake systems similar to those used by vehicles, can be considered a much more important source of these elements with respect to vehicular traffic. In particular, the highest release of dust by abrasion of rolling stock was found at GI, located at approximately 3 km of distance to the station, where the trains start breaking for the entrance to the residential area of the city.

3.3. Principal Component Analysis

To cluster the tracers of the main PM_{10} emission sources in Terni, principal component analysis was performed on the spatially-resolved chemical data recorded at the 23 sampling sites.

Four significant components accounting for 80.6% were obtained (the scores and loadings are shown in supplementary material S5); the variance explained by each component is: 40.1%, 19.2%, 15.2% and 6.1%. First component (PC1), which explains the 40.1% of the total variance, well separates the samples (scores) whereby the highest element concentrations (loadings) were found from the others. However, PC1 does not cluster the elements released by the different emission sources. On the contrary, PC2, PC3 and PC4 well separate the elements depending on their concentration variability among the sampling sites (the loading plots of PC1/PC2 and of PC2/PC3 are shown in supplementary material S5). Along the PC3 are clustered the insoluble elements released by soil resuspension. PC2 well separates the elements at high concentrations in the samples of the sites where the impact of the rail network, vehicular traffic and biomass burning was higher (GI, CR, HG, CZ, HV, SA, UC, CA, CO, FA, CB, FR, BR, AR, PI, PV, LG) from the elements released by the steel plant (RO, PR).

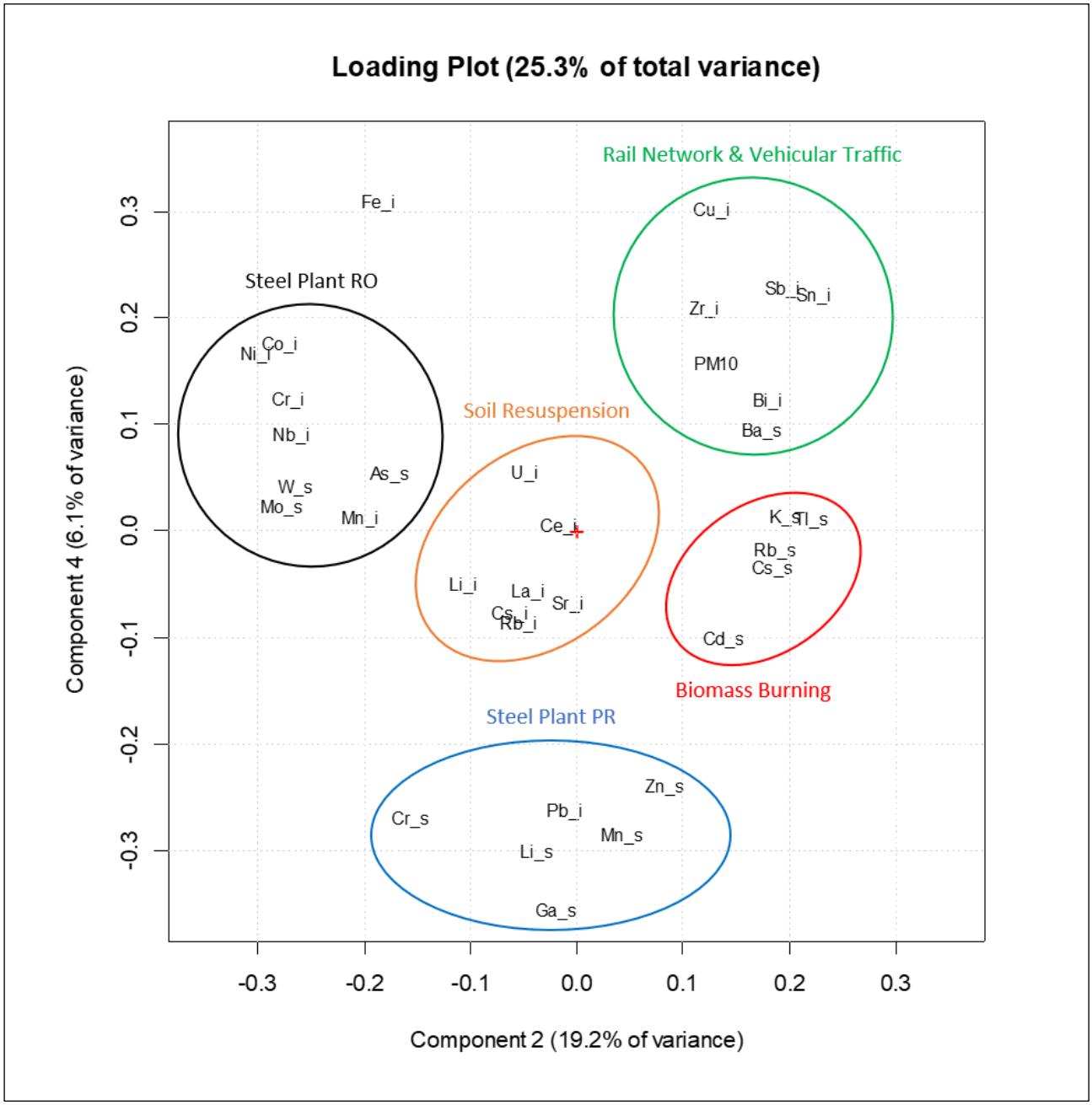

Fig. 6. Loading plot of the PCA (PC2/PC4) performed on the concentration data of the PM_{10} mass and of the 33 selected water-soluble and/or insoluble elements, determined at the 23 collection sites.

However, PC2 does not separate the elements released by the railway and vehicular traffic from the water-soluble elements released by biomass burning, which are well clustered along the PC4. Therefore, PC2 and PC4, which explain the 25.3% of the total variance, were represented in the

loading plot of Fig. 6, since they better reflect the spatial variability of the PM_{10} mass and element concentrations in the study area.From Fig. 6, we can observe that the water-soluble and/or insoluble elements are clustered in five main groups, each one containing tracers of a specific emission source. The first group, on the left upper part of the loading plot, is composed of elements found at high concentrations at RO (As_s, Co_i, Cr_i, Mn_i, Mo_s, Nb_i, Ni_i, W_s). RO is the closest site to the rolling plants of the steel industry pole and it is in the close proximity to the plant for the treatment of the effluents from casting and hot rolling section. All these elements, which are present in stainless steel as basic components (Cr, Fe, Ni) or to increase its toughness, ductility, tensile strength and corrosion resistance (Co, Mn, Mo, Nb, Ni, W; Querol et al., 2007; Owoade et al., 2015; Massimi et al., 2017; Marcias et al., 2018), can be reasonably used as tracers for the steel rolling emission from the steel plant (Taiwo et al., 2014).

The second group, on the lower part of the loading plot, is composed of elements released at PR (Cr_s. Ga_s, Li_s, Mn_s, Pb_i, Zn_s), probably by primary emission from the close furnaces for the annealing of the cold rolled product (Capelli et al., 2011). These elements appeared to be efficient tracers for the combustion emission from the steel industry.

The third group, on the central part of the loading plot, is composed of elements (Ce_i, Cs_i, La_i, Li_i, Rb_i, Sr_i, U_i) originated from resuspension of soil dust from dry surfaces by vehicular traffic (Canepari et al., 2008; Pant and Harrison, 2013).

The fourth group, on the central right part of the loading plot, is composed of water-soluble elements (Cd_s, Cs_s, K_s, Rb_s, Tl_s) reasonably released by biomass burning related sources (Cvjetko et al., 2010; Canepari et al., 2014; Karbowska, 2016; Simonetti et al., 2018a; Frasca et al., 2018) such as industrial biomass heating (carpentry at FA and craftsmanship lab at CB) and domestic biomass burning (townhouses frequently heated by biomass burning appliances are present at FR, BR, AR, PI, PV, LG).

The fifth group, on the right upper part of the loading plot, is composed of elements (Ba_s, Bi_i, Cu_i, Sb_i, Sn_i, Zr_i) generally considered as tracers of railway and vehicular traffic emissions, as they are usually released by mechanical abrasion and resuspension of vehicle/train components (brake disks and pads lining, tires; Weckwerth, 2001; Abbasi et al., 2012; Querol et al., 2012; Kam et al., 2013; Namgung et al., 2016). Insoluble Fe (Fe_i) is between this group and the group of tracers for the steel rolling emission from the steel plant as it is affected by both contributions. Finally, PM_{10} mass concentration (PM10) is in this last group of vehicular traffic tracers and it is in the same direction of the biomass burning tracers along PC2; this because PM mass is constituted for a relevant

fraction (20-60%) by carbon-containing compounds, which are generally released in large amount by vehicular traffic and biomass burning (Perrino et al., 2007, 2009; Canepari et al., 2009; Massimi et al., 2019b).

3.4. Size Distribution of Water-soluble and Insoluble Element Concentrations

Given the well-known relationship between size distribution of PM and its emission processes, we carried out elemental analysis of size-segregated PM samples to verify their link with the emission sources in the Terni basin. The behavior of some elements representative of the PCA clusters are shown in Fig. 7 (size distribution of the other elements is reported in supplementary material S6). We can observe that the concentration of Cs_i (panel a), as well as of the other elements originated from resuspension of soil dust by vehicular traffic (Ce_i, La_i, Li_i, Rb_i, Sr_i, U_i), was particularly high in the coarse mode, with a maximum in the size fraction 3.2-5.6 µm, in agreement with PM production by mechanical abrasion. Moreover, the concentration of these elements was higher in the summer, when the higher temperature and the lower rainfall led to a major dryness of the road surfaces and to an easier resuspension of soil dust. The same considerations (size distribution and seasonal pattern) are to be maintained for Sb_i (panel b) and the other elements that trace PM production by abrasion from railway and non-exhaust vehicular traffic emissions (Ba_s, Bi_i, Cu_i, Sn_i, Zr_i).

On the other hand, K_s (panel c), as well as the other identified biomass burning tracers (Cd_s, Cs_s, Rb_s, Tl_s), was found mostly in particles below 1 µm, at much higher concentration during the winter. This is consistent with an emission by combustion sources whose strength increases during the cold period (biomass burning).

Insoluble Pb (Pb_i; panel d) and the other elements reasonably released by primary emission from the furnaces for the annealing of the cold rolled product at PR (Cr_s, Ga_s, Li_s, Mn_s, Zn_s), were likewise all found in fine particles in the winter as well as in the summer. Consequently, their size distribution is in agreement with the combustion emission from the steel industry.

Finally, the different size distribution of the elements identified as tracers for the steel rolling emission (cluster “Steel Plant RO” in Fig. 6) revealed the presence of two different types of emission acting in this area. Water-soluble Mo (Mo_s; panel e), as well as As_s and W_s (supplementary material S6), were found in particles smaller than 1 µm, indicating that they were released by hot works, such as casting and hot rolling. Instead, Ni_i (panel f) together with Co_i, Cr_i, Mn_i and Nb_i, showed also a relevant coarse fraction, indicating a main role of cold processes (abrasion, brushing and polishing of rolled steel).

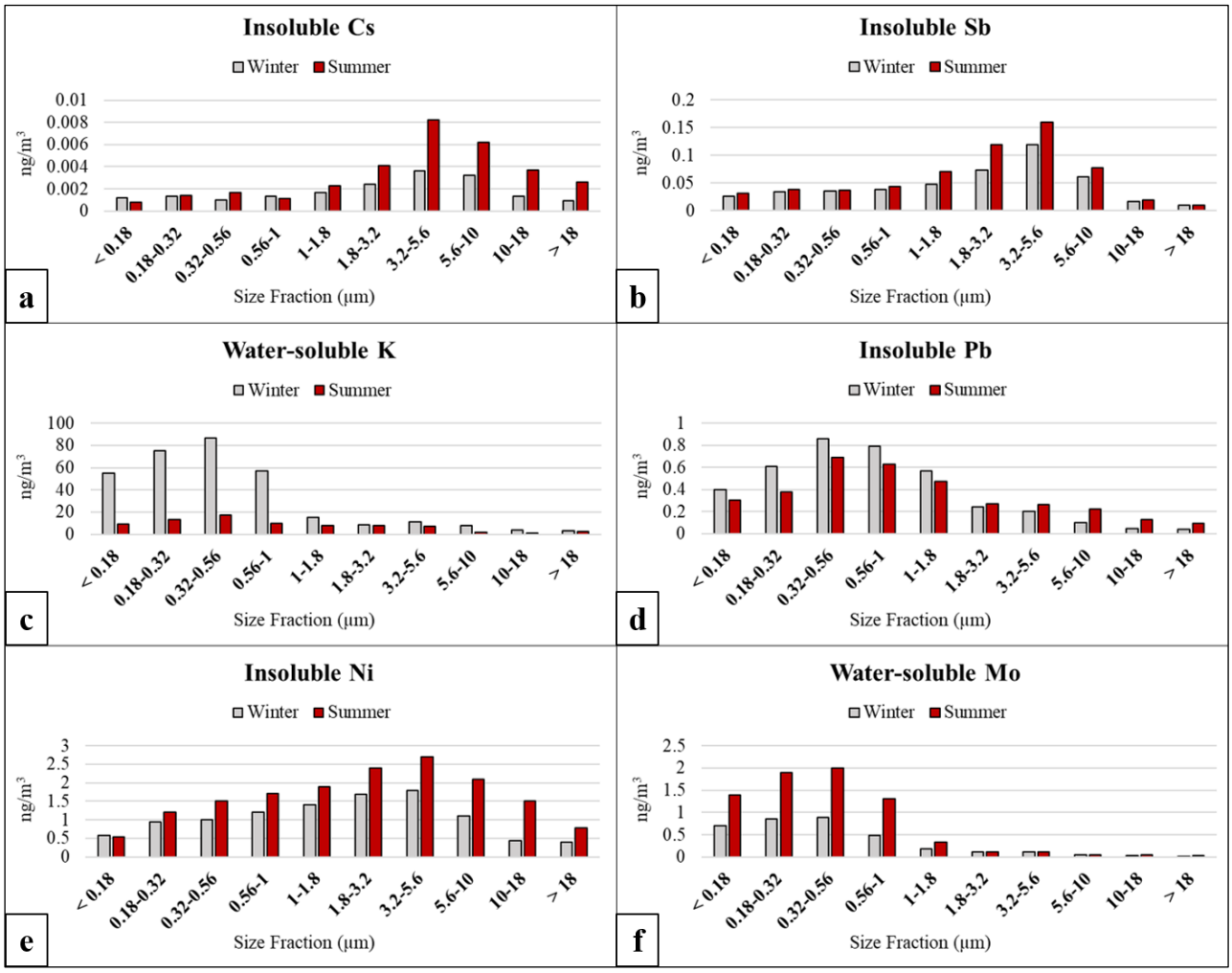

Fig. 7. Size distribution of the winter and summer insoluble Cs, Sb, Pb, Ni (panels a,b,d,e) and water-soluble K and Mo (panels c,f).

3.5. HR-FESEM characterization

HR-FESEM observation and XEDS microanalyses were performed on the 3.2-5.6 µm and 0.32-0.56 µm size-segregated PM samples collected at PR, which is in the close proximity of the steel industry pole, to qualitative describe the morphology and elemental composition of the coarse and fine particles released by the steel plant.

Fig. 8 shows two particles that contain elements typically released by the steel industry and that are representative of two types of emission. The first particle, belonging to the size fraction 3.2-5.6 µm (panel a), was about 5 µm of diameter, irregular in shape and its microanalysis (panel b) showed the basic components of stainless steel: Cr, Fe and Ni. This particle seems to have been originated from mechanical abrasion of steel. The second one (size fraction 0.32-0.56 µm, about 0.4 µm in diameter,

panel c) showed a regular and spherical shape and was composed of Cr, Fe and different elements used in steel processing-related activities, including Pb (panel d). It may be attributed to condensation of supersaturated vapors (Džiugys and Peters, 2001). Panel d shows the presence of Pb, O and S, suggesting the possibility that Pb was released in the form of lead oxide (PbO) or as lead sulphate ($PbSO_4$).

The morphological characterization of the size-segregated PM samples confirmed that the coarse particles originated from the steel industry pole may have been emitted by abrasive machining of steel from the rolling plants, while the fine ones, containing Pb_i and Cr_s, Ga_s, Li_s, Mn_s, Zn_s, may have been released by combustive processes from the furnaces for the annealing of the cold rolled product.

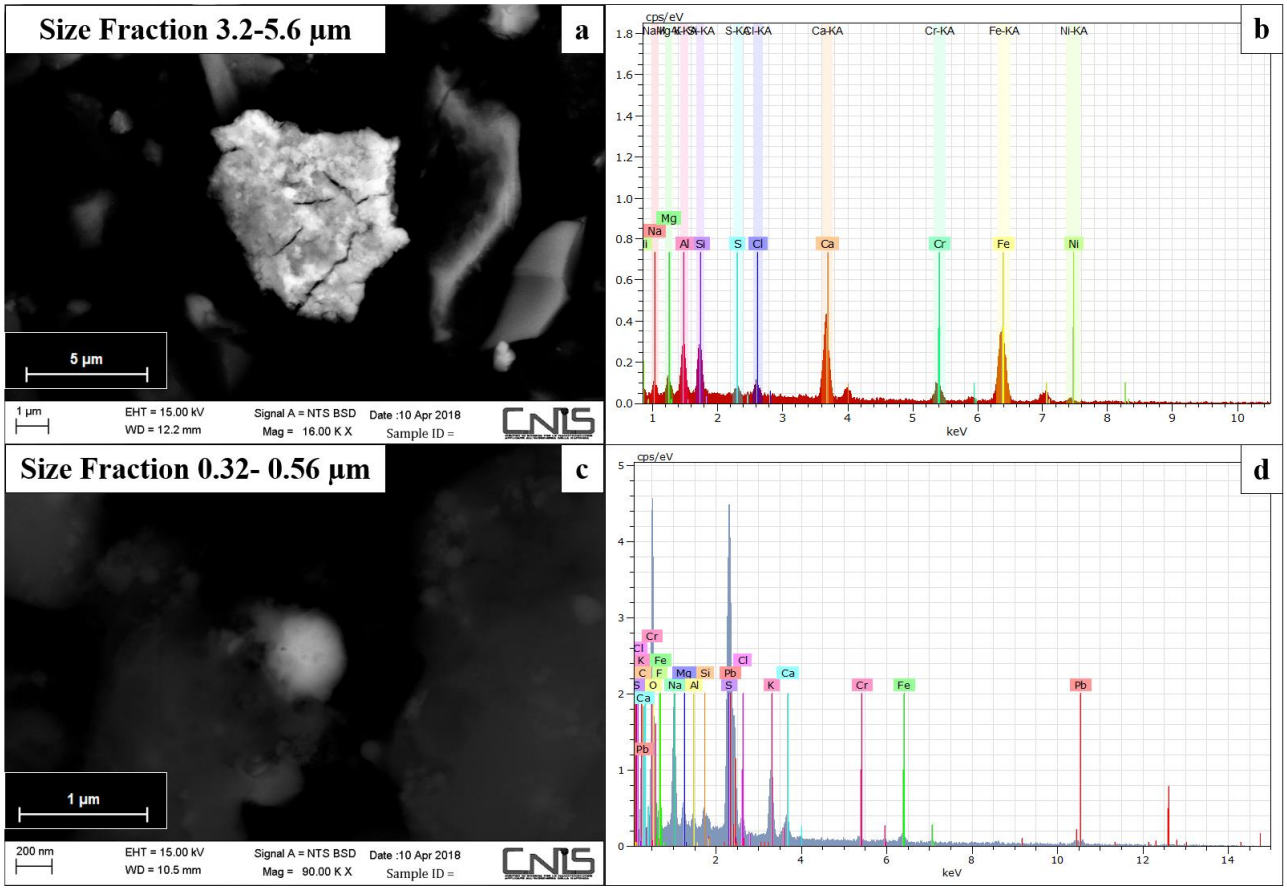

Fig. 8. HR-FESEM micrographs (panels a,c) and XEDS microanalyses (panels b,d) of particles emitted by the steel plant at PR in the size fractions 3.2-5.6 µm (panels a,b) and 0.32-0.56 µm (panels c,d).

4. Conclusions

The winter and summer spatial and size distribution of the water-soluble and insoluble elements allowed a reliable identification and characterization of the main local PM_{10} sources in the Terni basin. It was also possible to evaluate the diffusion capacity of the emitted particles. A clear increase in PM_{10} mass concentration occurred at all the sites during the winter, due to the strength of winter PM sources (such as domestic biomass heating) and the temperature inversion during the cold season. By clustering the analyzed elements and by observing their spatial distribution, we identified reliable and selective source tracers for rail network and vehicular traffic (Ba_s, Bi_i, Cu_i, Sb_i, Sn_i, Zr_i), soil resuspension (Ce_i, Cs_i, La_i, Li_i, Rb_i, Sr_i, U_i), biomass burning (Cd_s, Cs_s, K_s, Rb_s, Tl_s) and steel plant (As_s, Co_i, Cr_i, Cr_s, Ga_s, Li_s, Mo_s, Mn_i, Mn_s, Nb_i, Ni_i, Pb_i, W_s, Zn_s).

Furthermore, size distribution of source tracers and HR-FESEM characterization allowed us to distinguish between contributes originated by mechanical abrasion processes (resuspension of soil, abrasion of vehicle/train components and steel particles), characterized by particles belonging to the coarse mode, and contributes associated to combustion processes or hot works (biomass burning, combustion emission and annealing of the cold rolled product from the steel industry), which typically produce fine particles.

Each identified source showed characteristic winter and summer spatial distributions, depending on the different persistence in atmosphere of coarse and fine particles and on the seasonal variation of meteorological conditions and sources strength.

The described experimental approach enabled us to overcome the limits connected to the study of PM dispersion through the use of mathematical models and the limits associated to the high cost of a monitoring network based on traditional PM samplers. This kind of high spatial resolution chemical data also promises to be effective for the optimization and validation of dispersion models and is a powerful tool for a reliable geo-referenced assessment of population exposure to PM. This last aspect could also constitute an appealing starting point in studies aimed to deepen the relationship between health effects and PM chemical composition and sources.

Acknowledgements

This work was funded by the project 2017 RG11715C7C8801CF (Principal Investigator Dr. S. Canepari) and the project 2018 AR1181641E22B570 (Principal Investigator Dr. L. Massimi) financed by Sapienza University of Rome.

The authors gratefully thank FAI Instruments (Fonte Nuova, Rome, Italy), the citizens of Terni and the Terni district of ARPA Umbria (regional agency for environmental protection), with special regard to Giancarlo Caiello, Caterina Austeri and Marco Pompei, for the support in the installation and management of the sampling equipment as well as for the help in the choice of the sampling sites.

Author Contributions

L. Massimi and S. Canepari conceived and planned the monitoring and the experiments; L. Massimi and M. Ristorini performed the samplings; L. Massimi, M. Ristorini and M. L. Astolfi performed the chemical analyses; L. Massimi elaborated the data and wrote the manuscript; C. Perrino and S. Canepari coordinated the group and supervised the manuscript.

Conflicts of Interest

The authors declare no conflicts of interest.

References

Abbasi, S., Olander, L., Larsson, C., Olofsson, U., Jansson, A., Sellgren, U. 2012. A field test study of airborne wear particles from a running regional train. Proceedings of the Institution of Mechanical Engineers, Part F: Journal of Rail and Rapid Transit, 226(1), 95-109.

Almeida, S. M., Pio, C. A., Freitas, M. C., Reis, M. A., Trancoso, M. A. 2005. Source apportionment of fine and coarse particulate matter in a sub-urban area at the Western European Coast. Atmospheric Environment, 39(17), 3127-3138.

Amato, F., Pandolfi, M., Viana, M., Querol, X., Alastuey, A., Moreno, T. 2009. Spatial and chemical patterns of PM10 in road dust deposited in urban environment. Atmospheric Environment, 43(9), 1650-1659.

Anderson, J. O., Thundiyil, J. G., & Stolbach, A. 2012. Clearing the air: a review of the effects of particulate matter air pollution on human health. Journal of Medical Toxicology, 8(2), 166-175.

Astolfi, M. L., Marconi, E., Protano, C., Vitali, M., Schiavi, E., Mastromarino, P., Canepari, S. 2018. Optimization and validation of a fast digestion method for the determination of major and trace elements in breast milk by ICP-MS. Analytical Chimica Acta, 1040, 49-62.

Beelen, R., Hoek, G., Pebesma, E., Vienneau, D., de Hoogh, K., Briggs, D. J. 2009. Mapping of background air pollution at a fine spatial scale across the European Union. Science of the Total Environment, 407(6), 1852-1867.

Bencharif-Madani, F., Ali-Khodja, H., Kemmouche, A., Terrouche, A., Lokorai, K., Naidja, L., Bouziane, M. 2019. Mass concentrations, seasonal variations, chemical compositions and element sources of PM10 at an urban site in Constantine, northeast Algeria. Journal of Geochemical Exploration, 206, 106356.

Canepari, S., Cardarelli, Giuliano, A., E., Pietrodangelo, A. 2006a. Determination of metals, metalloids and non-volatile ions in airborne particulate matter by a new two-step sequential leaching procedure Part A: Experimental design and optimization. Talanta, 69(3), 581-587.

Canepari, S., Cardarelli, E., Pietrodangelo, A., Strincone, M. 2006b. Determination of metals, metalloids and non-volatile ions in airborne particulate matter by a new two-step sequential leaching procedure: Part B: Validation on equivalent real samples. Talanta, 69(3), 588-595.

Canepari, S., Perrino, C., Olivieri, F., Astolfi, M.L. 2008. Characterisation of the traffic sources of PM through size-segregated sampling, sequential leaching and ICP analysis. Atmospheric Environment, 42(35), 8161-8175.

Canepari, S., Pietrodangelo, A., Perrino, C., Astolfi, M. L., Marzo, M. L. 2009. Enhancement of source traceability of atmospheric PM by elemental chemical fractionation. Atmospheric Environment, 43(31), 4754-4765.

Canepari, S., Astolfi, M. L., Farao, C., Maretto, M., Frasca, D., Marcoccia, M., Perrino, C. 2014. Seasonal variations in the chemical composition of particulate matter: a case study in the Po Valley. Part II: concentration and solubility of micro-and trace-elements. Environmental Science and Pollution Research, 21(6), 4010-4022.

Canepari, S., Astolfi, M. L., Catrambone, M., Frasca, D., Marcoccia, M., Marcovecchio, F., Massimi, L., Rantica, E., Perrino, C. 2019. A combined chemical/size fractionation approach to study winter/summer variations, ageing and source strength of atmospheric particles. Environmental Pollution.

Capelli, L., Sironi, S., Del Rosso, R., Céntola, P., Rossi, A., Austeri, C. 2011. Olfactometric approach for the evaluation of citizens' exposure to industrial emissions in the city of Terni, Italy. Science of the Total Environment, 409(3), 595-603.

Catrambone, M., Canepari, S., Cerasa, M., Sargolini, T., Perrino, C. 2019. Performance evaluation of a very-low-volume sampler for atmospheric particulate matter. Aerosol Air Quality Research.

Conti, M. E., Canepari, S., Finoia, M. G., Mele, G., Astolfi, M. L. 2018. Characterization of Italian multifloral honeys on the basis of their mineral content and some typical quality parameters. Journal of Food Composition and Analysis, 74, 102-113.

Curci, G., Ferrero, L., Tuccella, P., Barnaba, F., Angelini, F., Bolzacchini, E., Carbone, C., Denier van der Gon, H. A. C., Facchini, M. C., Gobbi, G. P., Kuenen, J. P. P., Landi, T. C., Perrino, C., Perrone, M. G., Sangiorgi, G., Stocchi, P. 2015. How much is particulate matter near the ground influenced by upper-level processes within and above the PBL? A summertime case study in Milan (Italy) evidences the distinctive role of nitrate. Atmospheric Chemistry and Physics, 15(5), 2629-2649.

Cvjetko, P., Cvjetko, I., Pavlica, M. 2010. Thallium toxicity in humans. Archives of Industrial Hygiene and Toxicology, 61(1), 111-119.

Džiugys, A., and Peters, B. 2001. An approach to simulate the motion of spherical and non-spherical fuel particles in combustion chambers. Granular matter, 3(4), 231-266.

Ferrero, L., Cappelletti, D., Moroni, B., Sangiorgi, G., Perrone, M. G., Crocchianti, S., Bolzacchini, E. 2012. Wintertime aerosol dynamics and chemical composition across the mixing layer over basin valleys. Atmospheric Environment, 56, 143-153.

Frasca, D., Marcoccia, M., Tofful, L., Simonetti, G., Perrino, C., Canepari, S. 2018. Influence of advanced wood-fired appliances for residential heating on indoor air quality. Chemosphere, 211, 62-71.

Guerrini, R. 2012. Qualità dell'aria nella provincia di Terni tra il 2002 e il 2011. Quad ARPA Umbria, 81-87.

Hoek, G., Meliefste, K., Cyrys, J., Lewné, M., Bellander, T., Brauer, M., Fischer, P., Gehring, U., Heinrich, J., Van Vliet, P., Brunekreef, B. 2002. Spatial variability of fine particle concentrations in three European areas. Atmospheric Environment 36, 4077-4088.

Irwin, J. S. 2014. A suggested method for dispersion model evaluation. Journal of the Air & Waste Management Association, 64(3), 255-264.

Jacobson, M. Z., Seinfeld, J. H. 2004. Evolution of nanoparticle size and mixing state near the point of emission. Atmospheric Environment, 38(13), 1839-1850.

Janhäll, S., Olofson, K. F. G., Andersson, P. U., Pettersson, J. B., Hallquist, M. 2006. Evolution of the urban aerosol during winter temperature inversion episodes. Atmospheric Environment, 40(28), 5355-5366.

Jian, X., Olea, R. A., & Yu, Y. S. 1996. Semivariogram modeling by weighted least squares. Computers & Geosciences, 22(4), 387-397.

Johnston, K., Ver Hoef, J. M., Krivoruchko, K., Lucas, N. 2001. Using ArcGIS geostatistical analyst (Vol. 380). Redlands: Esri.

Kam, W., Delfino, R. J., Schauer, J. J., Sioutas, C. 2013. A comparative assessment of $PM_{2.5}$ exposures in light-rail, subway, freeway, and surface street environments in Los Angeles and estimated lung cancer risk. Environmental Science: Processes & Impacts, 15(1), 234-243.

Karbowska, B. 2016. Presence of thallium in the environment: sources of contaminations, distribution and monitoring methods. Environmental monitoring and assessment, 188(11), 640.

Kim, B. U., Bae, C., Kim, H. C., Kim, E., Kim, S. 2017. Spatially and chemically resolved source apportionment analysis: Case study of high particulate matter event. Atmospheric Environment, 162, 55-70.

Kloog, I., Ridgway, B., Koutrakis, P., Coull, B.A., Schwartz, J.D. 2013. Long- and short term exposure to $PM_{2.5}$ and mortality using novel exposure models. Epidemiology 24, 555-561.

Kumar, A., Maroju, S., Bhat, A. 2007. Application of ArcGIS geostatistical analyst for interpolating environmental data from observations. Environmental Progress, 26(3), 220-225.

Li, R., Wiedinmyer, C., & Hannigan, M. P. 2013. Contrast and correlations between coarse and fine particulate matter in the United States. Science of the Total Environment, 456, 346-358.

Lubczyńska, M. J., Sunyer, J., Tiemeier, H., Porta, D., Kasper-Sonnenberg, M., Jaddoe, V. W., Xavier Basagaña, X., Dalmau-Bueno, A., Forastiere, F., Wittsiepe, J., Hoffmann, B., Nieuwenhuijsen, M., Hoek, G., de Hoogh, K., Brunekreef, B., Guxens, M. 2017. Exposure to elemental composition of outdoor PM2. 5 at birth and cognitive and psychomotor function in childhood in four European birth cohorts. Environment international, 109, 170-180.

Mangia, C., Gianicolo, E. A., Bruni, A., Vigotti, M. A., Cervino, M. 2013. Spatial variability of air pollutants in the city of Taranto, Italy and its potential impact on exposure assessment. Environmental monitoring and assessment, 185(2), 1719-1735.

Massimi, L., Ristorini, M., Eusebio, M., Florendo, D., Adeyemo, A., Brugnoli, D., Canepari, S. 2017. Monitoring and evaluation of Terni (Central Italy) air quality through spatially resolved analyses. Atmosphere, 8(10), 200.

Massimi, L., Giuliano, A., Astolfi, M.L., Congedo, R., Masotti, A., Canepari, S. 2018. Efficiency evaluation of food waste materials for the removal of metals and metalloids from complex multi-element solutions. Materials, 11(3), 334.

Massimi, L., Conti, M. E., Mele, G., Ristorini, M., Astolfi, M. L., Canepari, S. 2019a. Lichen transplants as indicators of atmospheric element concentrations: a high spatial resolution comparison with PM_{10} samples in a polluted area (Central Italy). Ecological Indicators, 101, 759-769.

Massimi, L., Simonetti, G., Buiarelli, F., Di Filippo, P., Pomata, D., Riccardi, C., Ristorini, M., Astolfi, M. L., Canepari, S. 2019b. Spatial distribution of levoglucosan and alternative biomass burning tracers in an urban and industrial hot-spot of Central Italy. Atmospheric Research, *under review*.

Meng, X., Wu, Y., Pan, Z., Wang, H., Yin, G., Zhao, H. 2019. Seasonal characteristics and particle-size distributions of particulate air pollutants in Urumqi. International Journal of Environmental Research and Public Health, 16(3), 396.

Minguillón, M.C., Rivas, I., Aguilera, I., Alastuey, A., Moreno, T., Amato, F., Sunyer, J., Querol, X. 2012. Within-city contrasts in PM composition and sources and their relationship with nitrogen oxides. Journal of Environmental Monitoring 14, 2718-2728.

Minguillón, M. C., Cirach, M., Hoek, G., Brunekreef, B., Tsai, M., de Hoogh, K., Jedynskag, A., Kooterg, I. M., Nieuwenhuijsen, M., Querol, X. 2014. Spatial variability of trace elements and sources for improved exposure assessment in Barcelona. Atmospheric Environment, 89, 268-281.

Morini, E., Touchaei, A., Castellani, B., Rossi, F., Cotana, F. 2016. The impact of albedo increase to mitigate the urban heat island in Terni (Italy) using the WRF model. Sustainability, 8(10), 999.

Moroni, B., Ferrero, L., Crocchianti, S., Perrone, M. G., Sangiorgi, G., Bolzacchini, E., & Cappelletti, D. 2013. Aerosol dynamics upon Terni basin (Central Italy): Results of integrated vertical profile measurements and electron microscopy analyses. Rendiconti Lincei, 24(4), 319-328.

Namgung, H. G., Kim, J. B., Woo, S. H., Park, S., Kim, M., Kim, M. S., Bae, G. N., Park, D., Kwon, S. B. 2016. Generation of nanoparticles from friction between railway brake disks and pads. Environmental Science and Technology, 50(7), 3453-3461.

Noe, R., Noe, A., & Baukloh, D. 1996. U.S. Patent No. 5,554,235. Washington, DC: U.S. Patent and Trademark Office.

Owoade, K. O., Hopke, P. K., Olise, F. S., Ogundele, L. T., Fawole, O. G., Olaniyi, B. H., Jegede, O. O., Ayoola, M. A., & Bashiru, M. I. 2015. Chemical compositions and source identification of particulate matter (PM2.5 and PM2.5–10) from a scrap iron and steel smelting industry along the Ife–Ibadan highway, Nigeria. Atmospheric Pollution Research, 6(1), 107-119.

Pant, P., Harrison, R.M. 2013. Estimation of the contribution of road traffic emissions to particulate matter concentrations from field measurements: a review. Atmospheric Environment 77, 78-97.

Peel, M. C., Finlayson, B. L., McMahon, T. A. 2007. Updated world map of the Köppen-Geiger climate classification. Hydrology and earth system sciences discussions, 4(2), 439-473.

Perez, L., Medina-Ramón, M., Künzli, N., Alastuey, A., Pey, J., Pérez, N., Garcia, R., Tobias, A., Querol, X., Sunyer, J. 2009. Size fractionate particulate matter, vehicle traffic, and case-specific daily mortality in Barcelona, Spain. Environmental Science and Technology 43, 4707-4714.

Perrino, C., Canepari, S., Cardarelli, E., Catrambone, M., Sargolini, T. 2007. Inorganic constituents of urban air pollution in the Lazio region (Central Italy), Environmental Monitoring and Assessment, 128, 133-151.

Perrino, C., Canepari S., Catrambone, M., Dalla Torre, S., Rantica, E., Sargolini, T. 2009. Influence of natural events on the concentration and composition of atmospheric particulate matter. Atmospheric Environment 43, 4766–4779.

Perrino, C., Canepari, S., Pappalardo, S., Marconi, E. 2010. Time-resolved measurements of water-soluble ions and elements in atmospheric particulate matter for the characterization of local and long-range transport events. Chemosphere, 80(11), 1291-1300.

Pope III, C. A., Dockery, D. W. 2006. Health effects of fine particulate air pollution: lines that connect. Journal of the air and waste management association, 56(6), 709-742.

SENTIERI-ReNaM, GdL, Binazzi, A., Mangone, L. 2016. SENTIERI - Epidemiological study of residents in national priority contaminated sites: incidence of mesothelioma. Epidemiologia e prevenzione, 40(5Suppl1), 1-116.

Querol, X., Viana, M., Alastuey, A., Amato, F., Moreno, T., Castillo, S., Pey, J., de la Rosa, J., Sánchez de la Campa, A., Artíñano, B., Salvador, P., García Dos Santos, S., Fernández-Patier, R., Moreno-Grau, S., Negral, L., Minguillón, M. C., Monfort, E., Gil, J. I., Inza, A., Ortega, L. A., Santamaría, J. M., & Zabalza, J. 2007. Source origin of trace elements in PM from regional background, urban and industrial sites of Spain. Atmospheric Environment, 41(34), 7219-7231

Querol, X., Moreno, T., Karanasiou, A., Reche, C., Alastuey, A., Viana, M., Font, O., Gil, J., de Miguel, E., Capdevila, M. 2012. Variability of levels and composition of PM_{10} and $PM_{2.5}$ in the Barcelona metro system. Atmospheric Chemistry and Physics, 12(11), 5055-5076.

Setton, E., Marshall, J.D., Brauer, M., Lundquist, K.R., Hystad, P., Keller, P., Cloutier Fisher, D. 2010. The impact of daily mobility on exposure to traffic-related air pollution and health effect estimates. Journal of Exposure Science and Environmental Epidemiology 21, 42-48.

Simonetti, G., Frasca, D., Marcoccia, M., Farao, C., Canepari, S. 2018a. Multi-elemental analysis of particulate matter samples collected by a particle-into-liquid sampler. Atmospheric Pollution Research, 9(4) 747-754.

Simonetti, G., Conte, E., Perrino, C., Canepari, S. 2018b. Oxidative potential of size-segregated PM in an urban and an industrial area of Italy. Atmospheric Environment, 187, 292-300.

Sgrigna, G., Sæbø, A., Gawronski, S., Popek, R., Calfapietra, C. 2015. Particulate Matter deposition on Quercus ilex leaves in an industrial city of central Italy. Environmental Pollution, 197, 187-194.

Soleimanian, E., Taghvaee, S., Mousavi, A., Sowlat, M. H., Hassanvand, M. S., Yunesian, M., Naddafi, K., Sioutas, C. 2019. Sources and Temporal Variations of Coarse Particulate Matter (PM) in Central Tehran, Iran. Atmosphere, 10(5), 291.

Taiwo, A. M., Harrison, R. M., Shi, Z. 2014. A review of receptor modelling of industrially emitted particulate matter. Atmospheric environment, 97, 109-120.

Templeton, D. M., Ariese, F., Cornelis, R., Danielsson, L. G., Muntau, H., van Leeuwen, H. P., Lobinski, R. 2000. Guidelines for terms related to chemical speciation and fractionation of elements. Definitions, structural aspects, and methodological approaches (IUPAC Recommendations 2000). Pure and applied chemistry, 72(8), 1453-1470.

Vitali, L., Morabito, A., Adani, M., Assennato, G., Ciancarella, L., Cremona, G., Giua, R., Pastore, T., Piersanti, A., Righini, G., Russo, F., Spagnolo, S., Tanzarella, A., Tinarelli, G., Zanini, G. 2016. A Lagrangian modelling approach to assess the representativeness area of an industrial air quality monitoring station. Atmospheric Pollution Research, 7(6), 990-1003.

Weckwerth, G. 2001. Verification of traffic emitted aerosol components in the ambient air of Cologne (Germany). Atmospheric Environment, 35(32), 5525-5536.

Xie, Y., Chen, T. B., Lei, M., Yang, J., Guo, Q. J., Song, B., & Zhou, X. Y. 2011. Spatial distribution of soil heavy metal pollution estimated by different interpolation methods: Accuracy and uncertainty analysis. Chemosphere, 82(3), 468-476.

Yu, F., Wang, Q., Yan, Q., Jiang, N., Wei, J., Wei, Z., Yin, S. 2018. Particle size distribution, chemical composition and meteorological factor analysis: A case study during wintertime snow cover in Zhengzhou, China. Atmospheric research, 202, 140-147.

Zanobetti, A., Schwartz, J. 2009. The effect of fine and coarse particulate air pollution on mortality: a national analysis. Environmental health perspectives, 117(6), 898-90.

Zhang, K. M., Wexler, A. S. 2002. Modeling the number distributions of urban and regional aerosols: theoretical foundations. Atmospheric Environment, 36(11), 1863-1874.

Supplementary Material S1.

Table S1.1. Type of site, main local PM emission sources and geographical coordinates of the 23 sampling sites in Terni.

	Type of Site & Main Local PM Emission Sources	Latitude	Longitude
RI	Industrial Site - Power Plant (West of the City)	42°33′52.02″ N	12°35′21.94″ E
MA	Industrial Site - Power Plant (West of the City)	42°33′41.42″ N	12°36′19.05″ E
FA	Industrial Site - Industrial Biomass Heating (West of the City)	42°33′03.19″ N	12°36′29.76″ E
GI	Urban Site - Rail Network (North-West of the City)	42°34′06.28″ N	12°36′48.27″ E
FR	Urban Site - Domestic Biomass Heating (West of the City)	42°33′53.22″ N	12°37′11.44″ E
CB	Industrial Site - Industrial Biomass Heating (West of the City)	42°33′20.30″ N	12°37′20.45″ E
PI	Urban Site - Domestic Biomass Heating (South of the City)	42°32′56.96″ N	12°37′52.26″ E
BR	Urban Site - Domestic Biomass Heating (North of the City)	42°34′56.19″ N	12°37′23.30″ E
AR	Urban Site - Domestic Biomass Heating (North of the City)	42°34′34.23″ N	12°37′39.88″ E
CR	Urban Site - Rail Network (North-West of the City)	42°34′09.49″ N	12°37′39.81″ E
HG	Urban Site - Rail Network (North-West of the City)	42°34′19.32″ N	12°37′56.02″ E
SA	Urban Site - Trafficked Streets (City Centre)	42°33′45.16″ N	12°38′18.45″ E
PV	Urban Site - Domestic Biomass Heating (South of the City)	42°33′06.96″ N	12°38′35.20″ E
LG	Urban Site - Domestic Biomass Heating (South of the City)	42°32′59.75″ N	12°39′01.16″ E
CZ	Urban Site - Trafficked Streets (City Centre)	42°34′06.90″ N	12°38′52.97″ E
HV	Urban Site - Trafficked Streets (City Centre)	42°33′58.33″ N	12°39′04.74″ E
UC	Urban Site - Trafficked Streets (City Centre)	42°33′38.09″ N	12°38′47.62″ E
CA	Urban Site - Trafficked Streets (City Centre)	42°33′39.01″ N	12°39′03.11″ E
CO	Urban Site - Trafficked Streets (City Centre)	42°33′34.23″ N	12°39′22.62″ E
RO	Industrial Site - Steel Plant (East of the City)	42°33′51.16″ N	12°39′39.15″ E
OB	Industrial Site - Steel Plant (East of the City)	42°34′18.64″ N	12°40′05.57″ E
PR	Industrial Site - Steel Plant (East of the City)	42°34′20.30″ N	12°40′44.23″ E
CP	Industrial Site - Steel Plant (East of the City)	42°33′31.65″ N	12°40′36.04″ E

Supplementary Material S2.

Table S2.1. Start and stop dates of the 12 HSRS samplings during the 15-month monitoring campaign in Terni.

Start and Stop Dates of the Twelve Samplings			
Season	**Sampling**	**Start Date**	**Stop Date**
Winter	**1°**	19/11/2016	12/12/2016
	2°	17/12/2016	12/01/2017
	3°	21/01/2017	20/02/2017
	4°	25/02/2017	27/03/2017
Summer	**5°**	01/04/2017	01/05/2017
	6°	06/05/2017	05/06/2017
	7°	10/06/2017	17/07/2017
	8°	22/07/2017	28/08/2017
	9°	02/09/2017	02/10/2017
Winter	**10°**	21/10/2017	20/11/2017
	11°	25/11/2017	15/01/2018
	12°	20/01/2018	19/02/2018

Supplementary Material S3.

Table S3.1. Limits of detection (LODs) of the concentrations (µg/L) of the water-soluble and insoluble fraction of the analyzed elements set at 3 times the standard deviation (SD) of 10 replicate blank determinations.

	UoM	LODs Water-soluble Fraction	LODs Insoluble Fraction
Al	µg/L	3.4	3.8
As	µg/L	0.086	0.18
Ba	µg/L	3.7	0.44
Bi	µg/L	0.0011	0.0017
Ca	µg/L	370	932
Cd	µg/L	0.0038	0.0031
Ce	µg/L	0.0096	0.033
Co	µg/L	0.0073	0.0022
Cr	µg/L	0.081	0.86
Cs	µg/L	0.0033	0.0017
Cu	µg/L	0.2	0.24
Fe	µg/L	3	9.6
Ga	µg/L	0.0018	0.0021
K	µg/L	64	827
La	µg/L	0.0033	0.016
Li	µg/L	0.0063	0.004
Mg	µg/L	3.9	8.8
Mn	µg/L	0.17	0.17
Mo	µg/L	0.049	0.012
Na	µg/L	19	23
Nb	µg/L	0.00082	0.012
Ni	µg/L	0.35	0.17
Pb	µg/L	0.1	0.15
Rb	µg/L	0.031	0.023
Sb	µg/L	0.0094	0.0094
Sn	µg/L	0.013	0.027
Sr	µg/L	0.2	0.57
Ti	µg/L	0.15	0.4
Tl	µg/L	0.00012	0.00062
U	µg/L	0.00092	0.00062
W	µg/L	0.0015	0.0037
Zn	µg/L	15	47
Zr	µg/L	0.00052	0.28

Table S3.2. Average (AM) PM_{10} mass and insoluble element concentrations determined at the 23 sampling sites for the winter monitoring period.

Winter - PM_{10} Mass and Insoluble Element Concentrations (AM)																								
	UoM	**RI**	**MA**	**FA**	**GI**	**FR**	**CB**	**PI**	**BR**	**AR**	**CR**	**HG**	**SA**	**PV**	**LG**	**CZ**	**HV**	**UC**	**CA**	**CO**	**RO**	**OB**	**PR**	**CP**
PM_{10}	µg/m³	41	38	38	39	40	42	40	48	33	41	37	37	43	44	43	35	41	45	52	37	33	37	34
Al	ng/m³	130	204	166	184	144	136	268	130	233	154	144	190	164	209	119	238	156	191	199	151	146	290	193
As	ng/m³	0.33	0.43	0.64	0.47	0.41	0.67	0.47	0.55	0.41	0.36	0.45	0.44	0.48	0.42	0.65	0.48	0.46	0.47	0.51	0.67	0.49	0.67	0.58
Ba	ng/m³	16	15	19	17	13	16	16	17	15	26	19	18	18	14	21	16	17	16	23	12	11	18	12
Bi	ng/m³	0.35	0.29	0.42	0.39	0.36	0.27	0.23	0.31	0.27	0.43	0.41	0.3	0.31	0.28	0.32	0.27	0.3	0.37	0.34	0.23	0.18	0.29	0.17
Ca	ng/m³	1057	980	1241	1090	764	1032	1064	854	726	654	1721	563	912	574	1136	902	1108	991	799	945	821	1641	1009
Cd	ng/m³	0.067	0.035	0.115	0.058	0.08	0.08	0.054	0.048	0.028	0.054	0.069	0.065	0.066	0.11	0.042	0.076	0.085	0.074	0.13	0.1	0.1	0.15	0.08
Ce	ng/m³	0.27	0.27	0.34	0.31	0.24	0.28	0.24	0.25	0.21	0.29	0.38	0.26	0.29	0.27	0.37	0.28	0.27	0.31	0.31	0.22	0.23	0.27	0.26
Co	ng/m³	0.18	0.18	0.25	0.26	0.2	0.24	0.21	0.2	0.22	0.23	0.24	0.25	0.26	0.23	0.24	0.29	0.33	0.39	0.48	1.23	0.45	0.67	0.28
Cr	ng/m³	19	21	25	32	23	25	22	25	24	29	28	27	29	24	28	34	38	42	52	124	57	88	38
Cs	ng/m³	0.029	0.026	0.046	0.034	0.03	0.026	0.021	0.028	0.025	0.031	0.029	0.024	0.029	0.031	0.027	0.023	0.025	0.028	0.035	0.024	0.022	0.036	0.022
Cu	ng/m³	12	11	11	21	14	9	7.6	10	10	19	20	12	11	9.2	14	9.4	9.3	15	16	11	8.2	12	6.7
Fe	ng/m³	449	458	473	816	466	399	335	416	449	717	766	547	490	393	590	570	454	633	801	1115	491	612	377
Ga	ng/m³	0.066	0.083	0.091	0.09	0.072	0.072	0.081	0.07	0.082	0.077	0.077	0.078	0.082	0.09	0.072	0.096	0.084	0.1	0.11	0.14	0.11	0.21	0.096
K	ng/m³	1161	1352	1297	1335	940	1018	1495	1747	1838	1335	1815	1293	1356	1258	1876	1270	1187	1702	1141	1198	972	1338	1338
La	ng/m³	0.15	0.13	0.18	0.15	0.11	0.18	0.13	0.1	0.11	0.13	0.17	0.12	0.14	0.13	0.2	0.15	0.14	0.15	0.15	0.1	0.12	0.13	0.15
Li	ng/m³	0.09	0.08	0.13	0.11	0.09	0.09	0.08	0.09	0.10	0.1	0.1	0.08	0.09	0.1	0.09	0.08	0.09	0.1	0.11	0.1	0.09	0.13	0.08
Mg	ng/m³	43	38	67	53	41	48	41	44	42	46	51	44	45	48	55	47	50	57	53	46	41	85	48
Mn	ng/m³	8.3	9.7	11	15	11	9.8	7.4	7.6	9.8	12	12	10	8.7	7.6	10	9.9	9.5	11	13	24	12	27	9.4
Mo	ng/m³	2.7	2.9	4.4	4.4	4.1	4.4	4.7	5.3	4.5	3.7	3.8	5.0	5.3	5.5	4	4.3	6.1	7.1	7.1	14.9	7.7	9.6	5
Na	ng/m³	199	273	352	305	241	286	240	319	171	188	231	250	291	254	326	280	270	407	251	322	229	309	234
Nb	ng/m³	0.089	0.085	0.12	0.13	0.1	0.1	0.1	0.11	0.12	0.13	0.13	0.13	0.12	0.11	0.14	0.16	0.16	0.2	0.26	0.66	0.25	0.57	0.14
Ni	ng/m³	6.2	6.7	11	9.7	8.2	12	12	10	11	9.3	9.6	11	11	10	10	13	15	18	28	70	24	37	14
Pb	ng/m³	5.2	5.4	8.1	6.2	5.8	6.0	5.3	5.7	5.6	5.5	5.5	5.8	5.8	5.7	5.5	5.8	5.8	6.7	6.9	8.6	6.8	16.6	6.2
Rb	ng/m³	0.28	0.24	0.41	0.31	0.26	0.3	0.22	0.27	0.25	0.26	0.35	0.25	0.27	0.28	0.25	0.22	0.21	0.3	0.28	0.19	0.19	0.37	0.2
Sb	ng/m³	1.1	1.3	1.2	2	1.1	0.93	0.73	1	1	1.5	1.7	1.2	1	0.77	1.2	0.80	0.88	1.3	1.4	0.75	0.65	0.80	0.48
Sn	ng/m³	6.2	6.2	5.9	8.6	6.1	4.6	4.1	6.7	6.5	7.5	8.5	5.8	5	4.2	6.2	4.5	4.3	5.7	5.5	3.2	3.1	3.2	2.6
Sr	ng/m³	1.6	1.3	2.1	2.2	1.3	1.7	1.5	1.2	1.6	1.7	2.2	1.4	1.7	1.5	2.5	1.5	1.9	1.8	1.9	1.5	1.2	2.4	1.5
Ti	ng/m³	3.7	4.4	6.2	5.3	3.9	4.1	3.5	4.1	4.6	5.9	5.4	4.3	5.3	4.9	4.4	4.3	4.1	4.7	5.9	5.9	5.2	11	3.8
Tl	ng/m³	0.046	0.044	0.082	0.065	0.056	0.051	0.039	0.062	0.044	0.056	0.048	0.051	0.052	0.045	0.04	0.038	0.05	0.054	0.063	0.041	0.035	0.045	0.028
U	ng/m³	0.0082	0.0072	0.01	0.0096	0.0073	0.0067	0.0066	0.0069	0.0068	0.0084	0.0098	0.0069	0.008	0.0075	0.0081	0.007	0.0075	0.0081	0.01	0.0084	0.0072	0.01	0.0058
W	ng/m³	0.074	0.08	0.11	0.2	0.09	0.1	0.084	0.1	0.091	0.089	0.090	0.1	0.081	0.089	0.091	0.088	0.091	0.12	0.15	0.28	0.12	0.16	0.095
Zn	ng/m³	30	32	78	43	34	38	53	30	32	34	67	28	43	30	50	43	44	49	39	41	41	82	42
Zr	ng/m³	0.77	0.76	0.8	1.2	0.77	0.52	0.46	0.62	0.73	1.2	1.2	0.76	0.67	0.57	0.88	0.51	0.49	0.76	0.87	0.52	0.43	0.57	0.38

Table S3.3. Average (AM) water-soluble element concentrations determined at the 23 sampling sites for the winter monitoring period.

	Winter - Water-soluble Element Concentrations (AM)																							
	UoM	**RI**	**MA**	**FA**	**GI**	**FR**	**CB**	**PI**	**BR**	**AR**	**CR**	**HG**	**SA**	**PV**	**LG**	**CZ**	**HV**	**UC**	**CA**	**CO**	**RO**	**OB**	**PR**	**CP**
Al	ng/m³	7.9	9.1	11	8.7	12	8.0	8.7	9.2	12	7.3	9.5	9.6	9.3	9.1	8.7	8.7	8.2	12	9.3	13	9.5	27	7.8
As	ng/m³	0.33	0.33	0.42	0.29	0.32	0.32	0.37	0.29	0.37	0.28	0.38	0.34	0.37	0.35	0.39	0.37	0.34	0.47	0.52	1.08	0.47	0.61	0.36
Ba	ng/m³	6.6	6.5	6.4	9.1	5.3	4.4	4.9	7.6	9.5	9.4	9.2	8.3	7.6	6.9	9.2	6.6	6.4	7.5	7.4	5.8	4.4	5.5	4.9
Bi	ng/m³	0.023	0.02	0.028	0.018	0.016	0.018	0.017	0.017	0.022	0.015	0.02	0.016	0.017	0.02	0.017	0.019	0.017	0.021	0.017	0.022	0.018	0.029	0.016
Ca	ng/m³	924	864	1270	825	809	843	599	752	715	820	910	720	974	852	925	711	670	898	1163	921	725	1295	564
Cd	ng/m³	0.14	0.17	0.25	0.18	0.16	0.18	0.19	0.24	0.23	0.13	0.16	0.17	0.18	0.2	0.17	0.20	0.16	0.24	0.14	0.2	0.19	0.26	0.16
Ce	ng/m³	0.013	0.023	0.019	0.015	0.012	0.011	0.019	0.035	0.021	0.014	0.029	0.017	0.024	0.021	0.019	0.015	0.015	0.017	0.016	0.013	0.016	0.018	0.063
Co	ng/m³	0.043	0.038	0.045	0.048	0.039	0.039	0.045	0.035	0.043	0.036	0.046	0.042	0.044	0.039	0.049	0.048	0.053	0.067	0.054	0.065	0.049	0.046	0.036
Cr	ng/m³	1.4	1.4	1.4	1.4	1.4	1.6	2.2	1.6	2.0	1.3	1.6	1.8	1.9	1.7	1.8	1.9	1.9	1.8	2.4	4.6	2.8	5.8	2.1
Cs	ng/m³	0.052	0.055	0.092	0.07	0.066	0.07	0.062	0.098	0.073	0.054	0.059	0.061	0.066	0.07	0.055	0.055	0.062	0.07	0.061	0.053	0.049	0.069	0.044
Cu	ng/m³	3.4	4	3.2	7.4	3.3	2.3	2	2.8	4.2	5.1	6.6	3.7	2.9	2.4	5	3	2.4	4.2	3.6	2.7	2.6	2.6	2
Fe	ng/m³	10	13	14	24	12	14	18	13	22	18	22	12	13	12	18	12	10	13	13	17	12	14	11
Ga	ng/m³	0.0082	0.0094	0.012	0.010	0.0078	0.01	0.011	0.0096	0.014	0.0097	0.012	0.0094	0.0096	0.01	0.013	0.011	0.01	0.015	0.013	0.018	0.017	0.030	0.017
K	ng/m³	488	468	722	554	630	534	518	722	572	495	545	532	531	556	451	463	502	681	496	419	391	462	351
La	ng/m³	0.0081	0.012	0.0098	0.0073	0.0074	0.0071	0.0076	0.018	0.01	0.0077	0.014	0.0086	0.015	0.012	0.011	0.0081	0.0066	0.0089	0.0089	0.0070	0.0098	0.0094	0.035
Li	ng/m³	0.11	0.12	0.17	0.13	0.13	0.15	0.14	0.16	0.16	0.12	0.14	0.14	0.15	0.16	0.15	0.15	0.15	0.19	0.19	0.25	0.2	0.36	0.16
Mg	ng/m³	53	48	81	58	53	63	57	66	73	56	65	59	61	61	72	62	62	57	69	76	65	117	57
Mn	ng/m³	6	7.8	8.9	9.5	9	7.6	6.7	8.1	9.2	8	9.1	7.9	7.2	7.2	8.8	7.8	7.2	9.1	8.6	10	10	19	8.2
Mo	ng/m³	4	4.1	4.9	4.3	4.4	4.7	4.2	4	5.3	4.5	5.3	5.3	5.3	5.4	5.9	6.2	7.2	9.5	15	47	16	21	8.4
Na	ng/m³	361	295	531	374	365	397	358	450	489	336	409	335	331	369	450	372	379	342	410	369	373	450	340
Nb	ng/m³	0.0019	0.0031	0.0024	0.0029	0.0019	0.0023	0.0019	0.0021	0.003	0.0022	0.0026	0.0026	0.0019	0.002	0.0029	0.003	0.0024	0.0037	0.0047	0.018	0.0084	0.025	0.0051
Ni	ng/m³	0.96	0.7	0.78	1.1	0.91	0.86	1.1	0.98	1.3	0.99	0.89	0.99	0.95	0.82	1	1.1	1.2	1.5	1.2	3.8	1.6	1.7	1.1
Pb	ng/m³	0.72	1	1.6	0.94	0.93	1.1	1.2	1.5	1.8	0.7	0.89	0.98	1	1.3	0.99	1.1	1	1.2	0.75	1.3	1.3	2.7	1.5
Rb	ng/m³	1.4	1.1	1.8	1.3	1.7	1.4	1.2	1.9	1.5	1	1.2	1.1	1.2	1.3	1	1	1.1	1.3	1.1	0.9	0.86	1	0.77
Sb	ng/m³	0.43	0.63	0.68	0.47	0.43	0.43	0.33	0.34	0.43	0.39	0.46	0.4	0.36	0.32	0.47	0.39	0.33	0.49	0.4	0.4	0.34	0.53	0.28
Sn	ng/m³	0.17	0.23	0.2	0.2	0.15	0.12	0.085	0.084	0.15	0.19	0.26	0.11	0.11	0.11	0.19	0.15	0.087	0.16	0.21	0.31	0.2	0.22	0.14
Sr	ng/m³	2.4	2.1	3.1	2.3	2.3	2.2	2	2.2	2.0	2.4	2.6	2.4	2.6	2.6	2.4	2.1	2.3	2.5	3.0	3.3	1.7	2.6	1.5
Ti	ng/m³	0.1	0.11	0.11	0.079	0.083	0.094	0.056	0.087	0.092	0.079	0.13	0.084	0.097	0.086	0.11	0.087	0.086	0.1	0.16	0.25	0.18	0.48	0.11
Tl	ng/m³	0.11	0.14	0.22	0.17	0.15	0.15	0.15	0.24	0.18	0.12	0.14	0.14	0.14	0.15	0.12	0.12	0.13	0.14	0.11	0.09	0.098	0.092	0.09
U	ng/m³	0.0012	0.0014	0.0017	0.0012	0.0011	0.0013	0.0011	0.0012	0.0018	0.001	0.0014	0.0011	0.0011	0.0012	0.002	0.0015	0.0011	0.0012	0.0011	0.0015	0.0018	0.0017	0.0015
W	ng/m³	0.054	0.058	0.077	0.061	0.076	0.064	0.054	0.058	0.071	0.058	0.067	0.067	0.065	0.075	0.072	0.068	0.082	0.10	0.13	0.46	0.14	0.18	0.085
Zn	ng/m³	31	33	45	34	32	40	34	36	39	29	36	32	34	35	35	33	31	40	33	39	38	77	36
Zr	ng/m³	0.076	0.026	0.02	0.23	0.012	0.016	0.012	0.017	0.031	0.012	0.029	0.014	0.012	0.014	0.016	0.01	0.0079	0.014	0.011	0.034	0.03	0.021	0.024

Table S3.4. Average (AM) PM_{10} mass and insoluble element concentrations determined at the 23 sampling sites for the summer monitoring period.

Summer - PM_{10} Mass and Insoluble Element Concentrations (AM)																								
	UoM	**RI**	**MA**	**FA**	**GI**	**FR**	**CB**	**PI**	**BR**	**AR**	**CR**	**HG**	**SA**	**PV**	**LG**	**CZ**	**HV**	**UC**	**CA**	**CO**	**RO**	**OB**	**PR**	**CP**
PM_{10}	µg/m³	24	22	21	20	18	23	21	24	20	22	21	24	22	23	24	23	22	28	28	24	23	27	24
Al	ng/m³	154	192	269	189	192	176	244	309	311	237	271	288	185	263	250	271	190	266	253	204	189	249	271
As	ng/m³	0.23	0.33	0.39	0.36	0.4	0.26	0.30	0.42	0.44	0.29	0.27	0.32	0.24	0.33	0.52	0.44	0.33	0.33	0.35	0.67	0.33	0.2	0.31
Ba	ng/m³	6.8	4	5.2	6.3	4.5	2.7	2.1	2.7	3.4	8.3	7.2	4.9	4	4.7	7.2	5.9	4.1	3.4	3.2	2.6	1.9	1.2	1
Bi	ng/m³	0.077	0.11	0.09	0.12	0.073	0.038	0.048	0.085	0.095	0.21	0.22	0.11	0.11	0.083	0.15	0.075	0.099	0.13	0.12	0.095	0.075	0.11	0.062
Ca	ng/m³	1489	1593	1232	1507	1359	1156	911	1368	1259	986	1387	1664	1297	1258	1087	884	975	783	1296	1026	976	1433	1012
Cd	ng/m³	0.022	0.018	0.029	0.023	0.032	0.015	0.02	0.024	0.025	0.02	0.033	0.024	0.017	0.02	0.022	0.024	0.039	0.024	0.014	0.036	0.023	0.045	0.021
Ce	ng/m³	0.22	0.25	0.31	0.24	0.39	0.31	0.32	0.39	0.32	0.3	0.35	0.39	0.31	0.34	0.35	0.29	0.31	0.34	0.46	0.3	0.32	0.29	0.27
Co	ng/m³	0.075	0.1	0.13	0.11	0.13	0.13	0.13	0.13	0.12	0.13	0.16	0.17	0.13	0.13	0.14	0.14	0.26	0.24	0.29	1.98	0.2	0.28	0.1
Cr	ng/m³	9.3	16	16	15	14	19	17	18	16	18	19	19	16	15	15	15	22	46	41	206	23	42	16
Cs	ng/m³	0.023	0.023	0.039	0.029	0.035	0.027	0.033	0.056	0.036	0.04	0.05	0.04	0.036	0.038	0.046	0.033	0.044	0.038	0.033	0.032	0.035	0.032	0.023
Cu	ng/m³	5.3	7.4	6.3	8.4	4.8	4	4.5	5.2	5.8	8.1	13	6	7.2	5.2	8.7	5.3	5.6	7.5	8.1	11.1	5.7	5.9	3.5
Fe	ng/m³	254	349	312	426	269	290	283	329	321	410	591	371	383	306	447	394	396	531	537	2080	343	424	213
Ga	ng/m³	0.026	0.045	0.071	0.04	0.044	0.041	0.054	0.072	0.056	0.057	0.078	0.066	0.041	0.063	0.058	0.057	0.064	0.083	0.076	0.145	0.055	0.12	0.061
K	ng/m³	331	651	611	430	505	276	390	761	443	377	894	709	387	508	830	636	937	1079	376	314	417	264	517
La	ng/m³	0.14	0.16	0.2	0.15	0.25	0.18	0.16	0.24	0.21	0.2	0.23	0.22	0.18	0.18	0.22	0.17	0.16	0.21	0.25	0.17	0.17	0.15	0.17
Li	ng/m³	0.1	0.13	0.15	0.1	0.13	0.12	0.13	0.19	0.15	0.16	0.19	0.14	0.11	0.14	0.16	0.1	0.13	0.17	0.15	0.16	0.11	0.14	0.1
Mg	ng/m³	54	65	72	59	63	56	70	95	84	72	96	82	57	68	82	64	62	72	76	61	58	99	61
Mn	ng/m³	4.9	6.6	7	8.4	6.8	6.4	6.1	6.9	7.2	8.5	10	7.6	6.4	6.1	8.5	6.8	7.9	9.8	9.9	32.3	7.2	19.2	6.3
Mo	ng/m³	0.88	1.7	1.4	1.3	1.2	1.5	1.9	0.99	0.96	1.2	1.6	1.4	1.3	1.4	1.3	1.2	3.1	3	4	15	1.9	2.3	1
Na	ng/m³	207	292	256	226	269	274	259	467	375	354	375	256	285	389	353	357	253	334	339	278	255	226	334
Nb	ng/m³	0.025	0.037	0.061	0.043	0.049	0.063	0.071	0.059	0.046	0.056	0.087	0.087	0.059	0.054	0.068	0.058	0.12	0.13	0.18	1.3	0.16	0.59	0.075
Ni	ng/m³	3.2	6.2	6.4	5.1	5.3	7.4	7.7	4.9	6	5.9	5.9	7.5	6.9	7.9	6.6	5.9	14	18	22	125	13	17	5.6
Pb	ng/m³	2.1	2.8	2.9	2.6	2.8	2.6	2.6	2.8	2.7	2.8	3.1	3.0	2.9	2.9	3.8	3.2	3.6	4.1	3.2	5.7	3.5	12	3.2
Rb	ng/m³	0.28	0.47	0.47	0.34	0.41	0.39	0.44	0.62	0.42	0.48	0.57	0.54	0.41	0.48	0.53	0.22	0.36	0.45	0.5	0.31	0.32	0.35	0.27
Sb	ng/m³	0.41	0.61	0.5	0.57	0.43	0.35	0.27	0.42	0.44	0.63	0.96	0.56	0.41	0.3	0.67	0.3	0.38	0.48	0.54	0.5	0.24	0.32	0.15
Sn	ng/m³	1.5	1.8	1.5	2.1	1.3	0.93	1	1.5	1.6	2.1	3.5	1.5	1.5	0.93	2.3	1.2	1.3	1.6	1.8	1.4	0.84	1.1	0.61
Sr	ng/m³	1.9	1.8	2	1.8	1.8	1.5	1.8	2.6	2	1.8	2.4	2	1.9	1.8	2.3	1.8	1.5	2.3	2.2	1.4	1.3	1.7	1.8
Ti	ng/m³	3.5	5	7.9	4.1	5.3	4.7	4.6	7.1	4.8	7.8	7.7	6.3	4.4	4.6	6.5	4.1	5	6.3	6.1	8.9	5.4	17	4
Tl	ng/m³	0.011	0.0098	0.018	0.017	0.02	0.0095	0.0097	0.012	0.014	0.015	0.017	0.014	0.008	0.009	0.016	0.012	0.017	0.0095	0.0057	0.0076	0.008	0.0087	0.0055
U	ng/m³	0.0053	0.0054	0.0078	0.0064	0.0066	0.006	0.0074	0.011	0.0079	0.0087	0.012	0.011	0.0075	0.0078	0.0094	0.0066	0.0098	0.0083	0.0073	0.0081	0.0081	0.0092	0.0052
W	ng/m³	0.021	0.028	0.036	0.181	0.035	0.031	0.031	0.04	0.036	0.037	0.047	0.042	0.033	0.029	0.041	0.027	0.061	0.04	0.05	0.368	0.05	0.074	0.02
Zn	ng/m³	30	34	35	42	34	36	31	41	39	28	34	48	36	34	32	26	31	52	37	34	29	53	30
Zr	ng/m³	0.66	0.56	0.51	0.65	0.48	0.32	0.31	0.52	0.49	0.70	1.03	0.58	0.58	0.43	0.76	0.56	0.49	0.66	0.59	0.49	0.39	0.6	0.24

Table S3.5. Average (AM) water-soluble element concentrations determined at the 23 sampling sites for the summer monitoring period.

Summer - Water-soluble Element Concentrations (AM)																							
	UoM	**RI**	**MA**	**FA**	**GI**	**FR**	**CB**	**PI**	**BR**	**AR**	**CR**	**HG**	**SA**	**PV**	**LG**	**CZ**	**HV**	**UC**	**CA**	**CO**	**RO**	**OB**	**PR**	**CP**
Al	ng/m³	5.2	6.8	12.9	7.1	7.5	4.5	6	5.7	13.2	6.6	4.7	4.8	5.7	5.7	5.9	5.3	4.7	5.9	4.4	8	6.6	12.9	5.6
As	ng/m³	0.17	0.18	0.21	0.21	0.15	0.19	0.15	0.2	0.21	0.23	0.2	0.22	0.19	0.19	0.26	0.26	0.26	0.29	0.29	0.8	0.23	0.3	0.17
Ba	ng/m³	4.8	5.0	3.1	4.8	3.7	3.7	4	3.6	4.1	5.7	5.9	3.7	3.8	4.3	5.2	4	2.9	3.7	3.9	4	3.5	3.9	3
Bi	ng/m³	0.0054	0.0063	0.0071	0.0065	0.0044	0.006	0.0078	0.011	0.01	0.0091	0.0072	0.0058	0.0059	0.0076	0.0096	0.0067	0.0070	0.011	0.0048	0.0082	0.0094	0.0099	0.0072
Ca	ng/m³	787	754	931	768	820	759	607	769	781	864	648	702	886	718	834	673	653	741	764	949	939	1573	548
Cd	ng/m³	0.026	0.032	0.034	0.049	0.042	0.04	0.037	0.036	0.055	0.044	0.039	0.041	0.039	0.04	0.045	0.044	0.045	0.055	0.036	0.085	0.051	0.031	0.037
Ce	ng/m³	0.021	0.014	0.013	0.026	0.013	0.0085	0.017	0.019	0.036	0.029	0.02	0.018	0.013	0.014	0.015	0.022	0.017	0.014	0.011	0.013	0.016	0.0087	0.011
Co	ng/m³	0.025	0.024	0.028	0.028	0.032	0.022	0.034	0.033	0.033	0.03	0.032	0.035	0.028	0.031	0.033	0.036	0.037	0.045	0.028	0.08	0.039	0.027	0.025
Cr	ng/m³	0.7	0.97	0.89	0.99	0.95	1	1.2	0.86	1.1	1.1	0.98	1.2	1.3	1.4	1.4	1.4	1.6	2.4	1.7	5.2	2.1	3.9	1.3
Cs	ng/m³	0.0089	0.012	0.013	0.014	0.011	0.01	0.013	0.013	0.02	0.015	0.012	0.013	0.014	0.012	0.016	0.017	0.016	0.017	0.012	0.021	0.016	0.027	0.011
Cu	ng/m³	1.8	2.3	1.5	2.9	1.6	1.3	1.8	1.9	2.5	2.8	3.5	1.9	2.8	2	3.1	2	1.7	2.8	2.2	2.5	1.9	1.2	1.2
Fe	ng/m³	9.8	9.4	9.4	14	9.2	9.1	8.5	9	11	11	11	8.1	10	9.1	11	8.7	8	11	8.8	19	12	15	7.2
Ga	ng/m³	0.0032	0.007	0.0061	0.0043	0.0075	0.0048	0.0081	0.0075	0.008	0.0066	0.0054	0.005	0.0069	0.0067	0.0079	0.0088	0.0074	0.0076	0.0052	0.0079	0.0084	0.0155	0.01
K	ng/m³	89	111	130	136	129	119	118	122	165	153	125	119	133	132	144	122	146	130	111	150	149	162	108
La	ng/m³	0.013	0.012	0.0085	0.014	0.0093	0.0095	0.012	0.012	0.027	0.019	0.009	0.013	0.0076	0.0096	0.0093	0.011	0.0078	0.0063	0.0067	0.0079	0.0081	0.0079	0.0058
Li	ng/m³	0.047	0.065	0.073	0.067	0.070	0.067	0.072	0.06	0.073	0.075	0.064	0.076	0.09	0.085	0.099	0.097	0.092	0.13	0.091	0.21	0.13	0.23	0.085
Mg	ng/m³	44	48	53	48	48	52	60	60	74	63	56	59	68	60	75	62	60	66	58	87	73	113	61
Mn	ng/m³	3	4	4.1	5.9	4.9	3.8	3.8	4.3	5.1	5.7	4.7	4.4	4.4	4.3	5.5	4.7	4.4	5.6	4.2	7.2	6	8.5	4.7
Mo	ng/m³	1.7	3.2	3.3	2.5	3	4.1	3.9	2.3	2.6	2.9	2.4	4.1	5.3	5.7	3.7	4	7.1	11	12	53	11	9	3.5
Na	ng/m³	275	294	321	259	271	309	380	385	481	382	336	337	390	350	458	369	356	345	320	375	370	382	340
Nb	ng/m³	0.0021	0.003	0.0029	0.0028	0.003	0.003	0.0041	0.0035	0.0033	0.003	0.0033	0.0031	0.0043	0.0039	0.0038	0.0041	0.005	0.0074	0.006	0.0329	0.0076	0.0196	0.0063
Ni	ng/m³	0.83	0.93	0.62	0.73	1.2	0.76	0.98	0.68	0.86	0.8	0.71	0.92	0.92	0.93	0.85	0.86	1.1	1.6	1.1	5.9	1.8	1.1	0.76
Pb	ng/m³	0.28	0.35	0.32	0.36	0.28	0.44	0.48	0.37	0.55	0.36	0.3	0.41	0.38	0.38	0.43	0.42	0.36	0.54	0.29	0.61	0.64	1.3	0.47
Rb	ng/m³	0.27	0.31	0.35	0.38	0.36	0.3	0.33	0.39	0.48	0.4	0.33	0.33	0.38	0.35	0.39	0.38	0.41	0.4	0.29	0.42	0.38	0.52	0.25
Sb	ng/m³	0.29	0.43	0.54	0.35	0.44	0.42	0.29	0.38	0.43	0.45	0.37	0.36	0.35	0.31	0.41	0.32	0.34	0.54	0.27	0.41	0.3	0.33	0.28
Sn	ng/m³	0.22	0.24	0.2	0.21	0.2	0.18	0.18	0.25	0.25	0.23	0.21	0.16	0.17	0.17	0.22	0.17	0.15	0.21	0.15	0.2	0.19	0.21	0.13
Sr	ng/m³	1.7	1.8	2	1.8	1.8	1.7	1.7	1.9	2.1	2.1	1.7	1.9	2.3	2	2.3	1.7	1.6	1.8	1.8	2.2	2.1	3	1.5
Ti	ng/m³	0.071	0.084	0.097	0.119	0.089	0.082	0.089	0.11	0.144	0.21	0.079	0.079	0.095	0.12	0.12	0.11	0.094	0.13	0.1	0.15	0.13	0.24	0.12
Tl	ng/m³	0.024	0.029	0.035	0.041	0.024	0.027	0.028	0.033	0.044	0.033	0.029	0.026	0.027	0.022	0.035	0.035	0.031	0.026	0.016	0.021	0.024	0.017	0.017
U	ng/m³	0.0018	0.0022	0.0023	0.0018	0.0021	0.0015	0.0022	0.0030	0.0028	0.0025	0.0027	0.0019	0.0021	0.0022	0.0028	0.0023	0.0021	0.0024	0.0020	0.0023	0.0021	0.0024	0.0021
W	ng/m³	0.024	0.036	0.042	0.036	0.035	0.042	0.043	0.025	0.029	0.035	0.031	0.042	0.055	0.057	0.044	0.046	0.074	0.11	0.1	0.51	0.099	0.093	0.03
Zn	ng/m³	10	16	15	21	14	16	15	14	17	16	13	16	18	17	17	16	15	24	16	26	23	27	20
Zr	ng/m³	0.078	0.057	0.04	0.037	0.02	0.031	0.028	0.028	0.031	0.023	0.023	0.014	0.021	0.022	0.019	0.042	0.02	0.042	0.024	0.026	0.026	0.022	0.015

Supplementary Material S4.

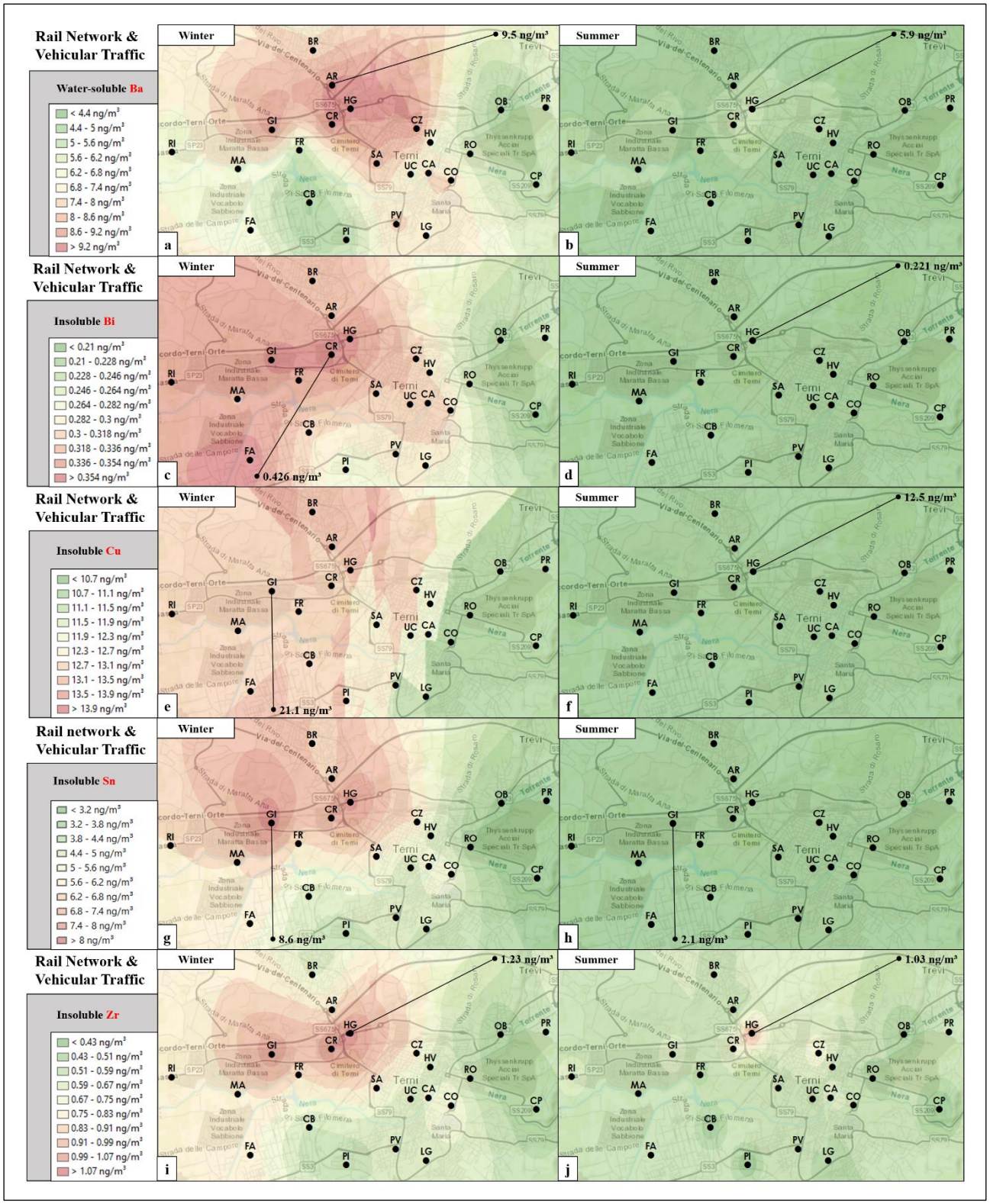

Fig. S4.1. Map of the winter and summer spatial distribution of water-soluble Ba (panels a,b), insoluble Bi (panels c,d), Cu (panels e,f), Sn (panels g,h) and Zr (panels i,j).

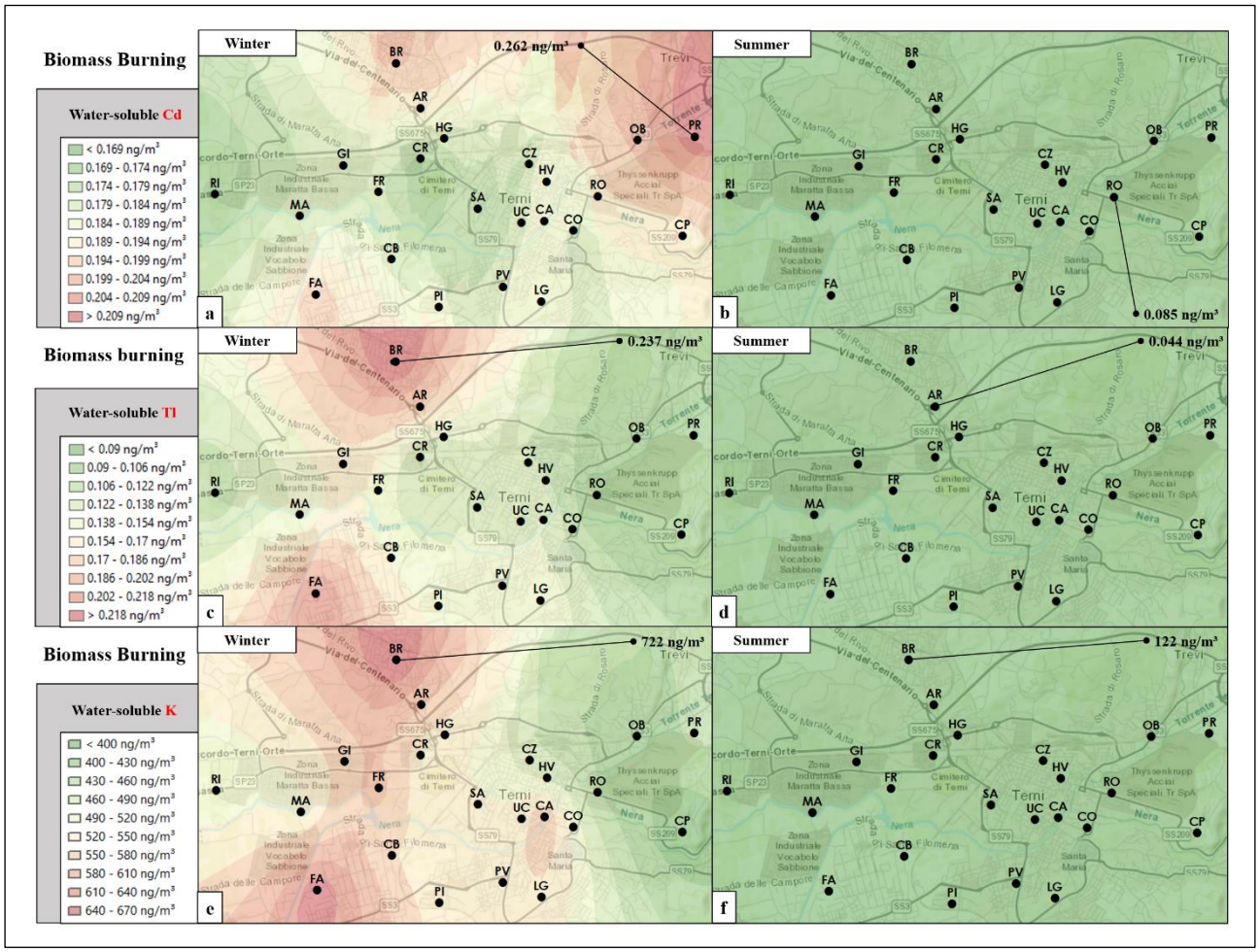

Fig. S4.2 Map of the winter and summer spatial distribution of water-soluble Cd (panels a,b), Tl (panels c,d) and K (panels e,f).

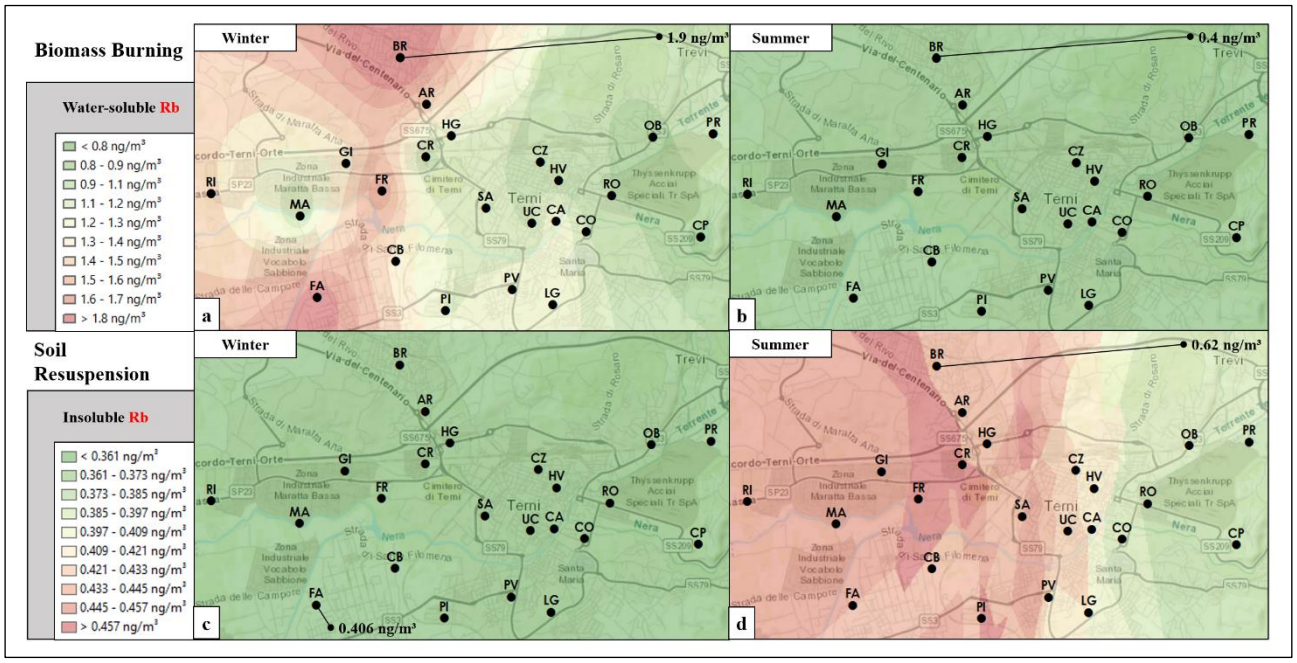

Fig. S4.3. Map of the winter and summer spatial distribution of water-soluble (panels a,b) and insoluble Rb (panels c,d).

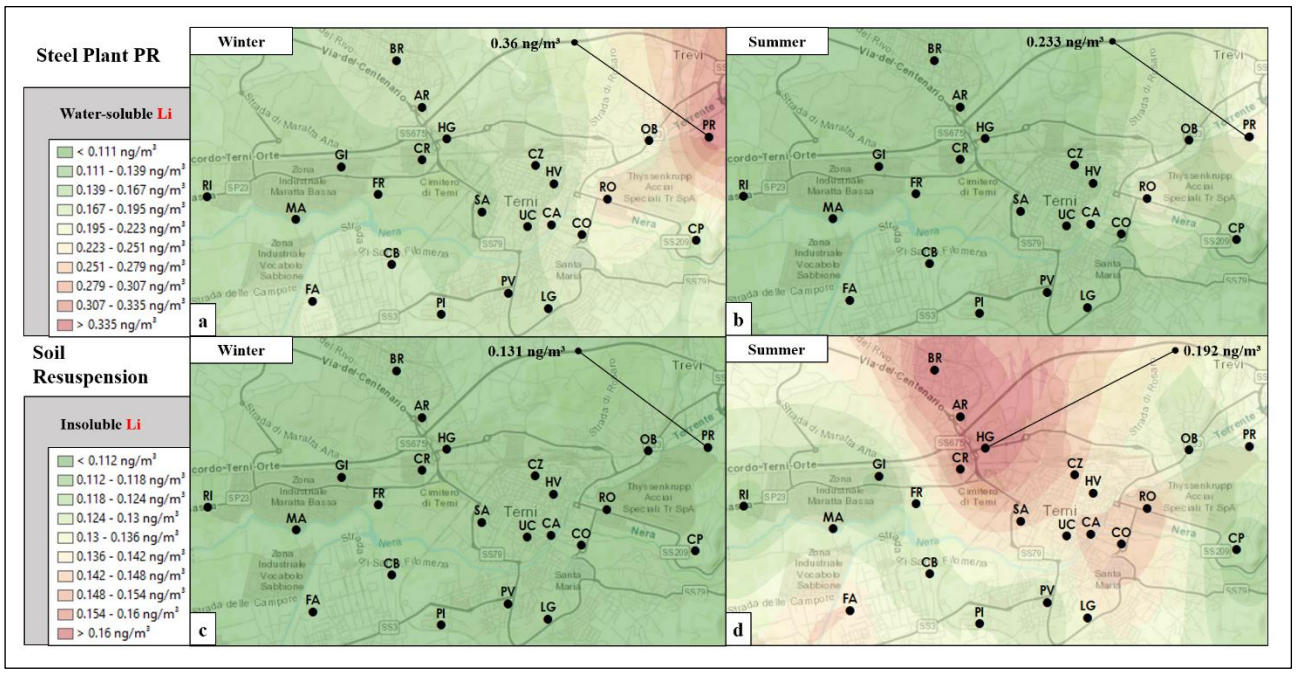

Fig. S4.4. Map of the winter and summer spatial distribution of water-soluble (panels a,b) and insoluble Li (panels c,d).

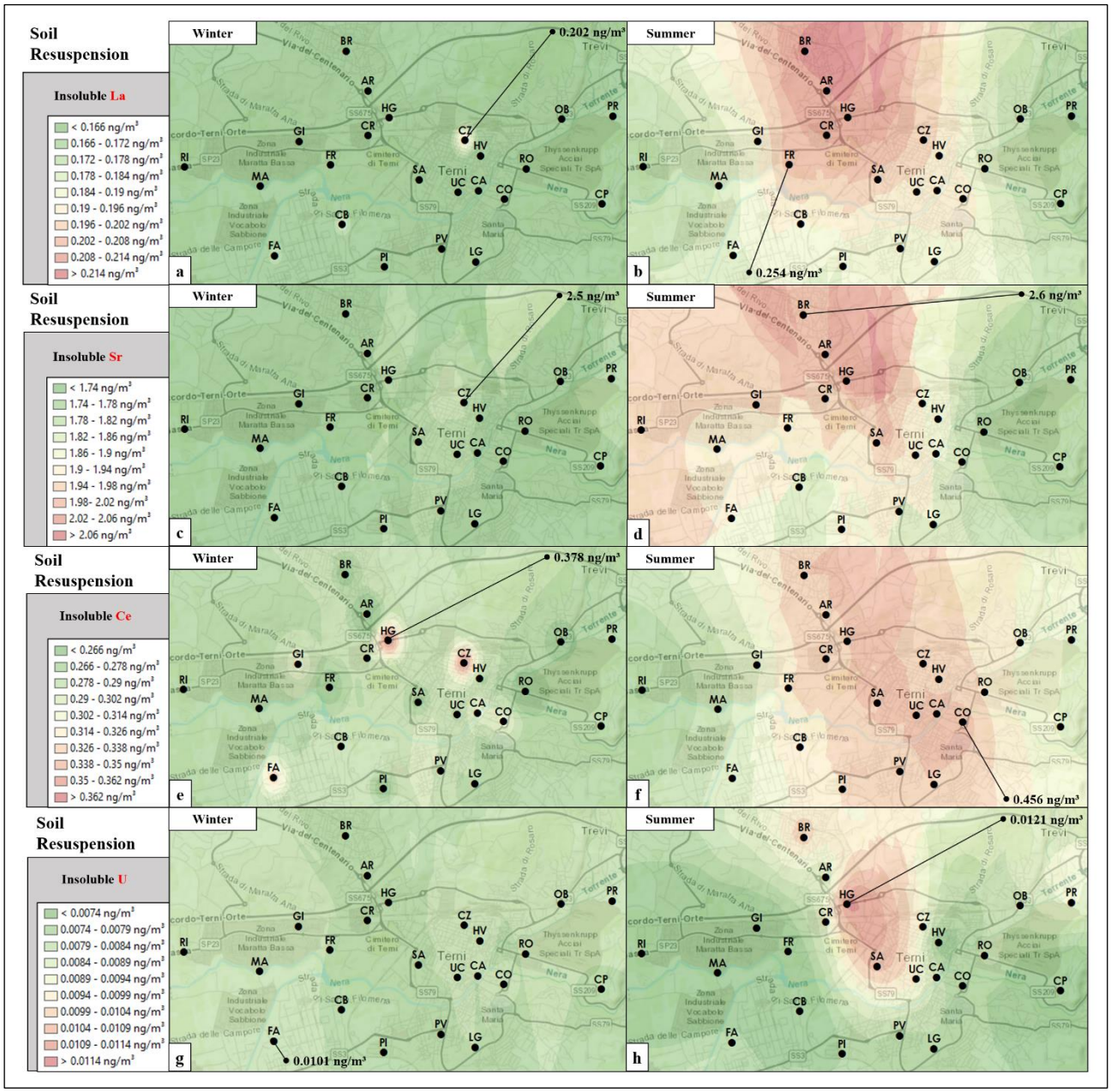

Fig. S4.5. Map of the winter and summer spatial distribution of insoluble La (panels a,b), Sr (panels c,d), Ce (panels e,f) and U (panels g,h).

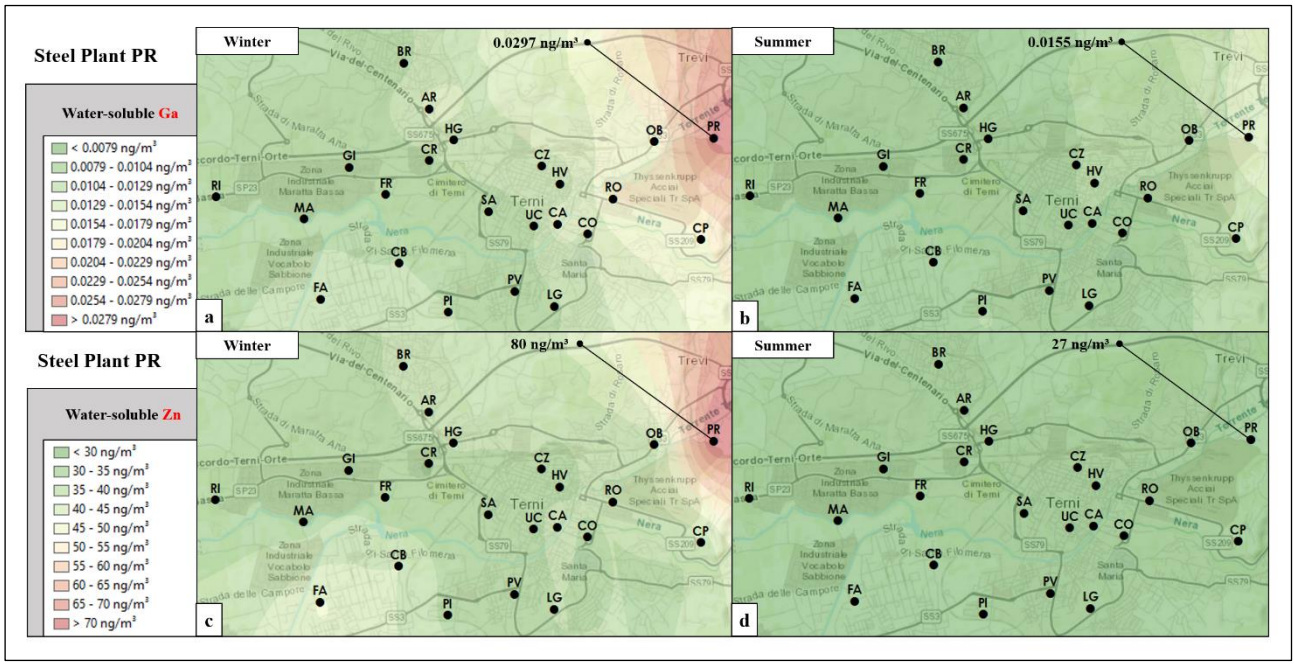

Fig. S4.6. Map of the winter and summer spatial distribution of water-soluble Ga (panels a,b) and Zn (panels c,d).

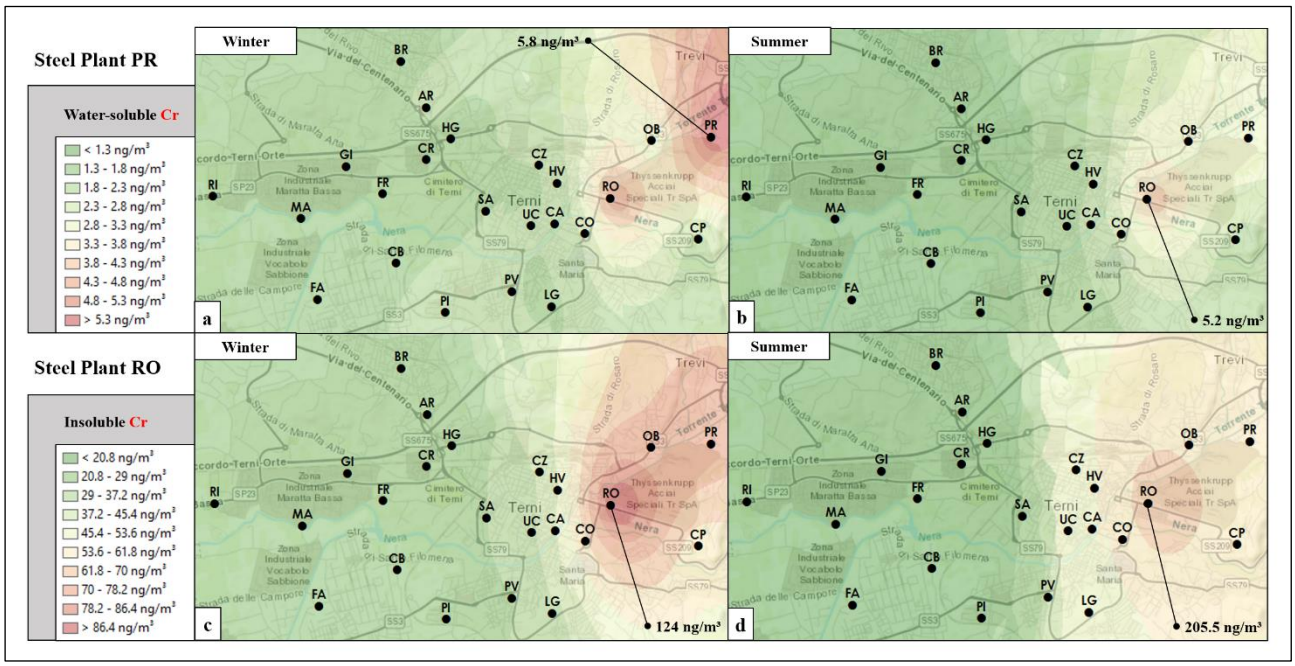

Fig. S4.7. Map of the winter and summer spatial distribution of water-soluble (panels a,b) and insoluble Cr (panels c,d).

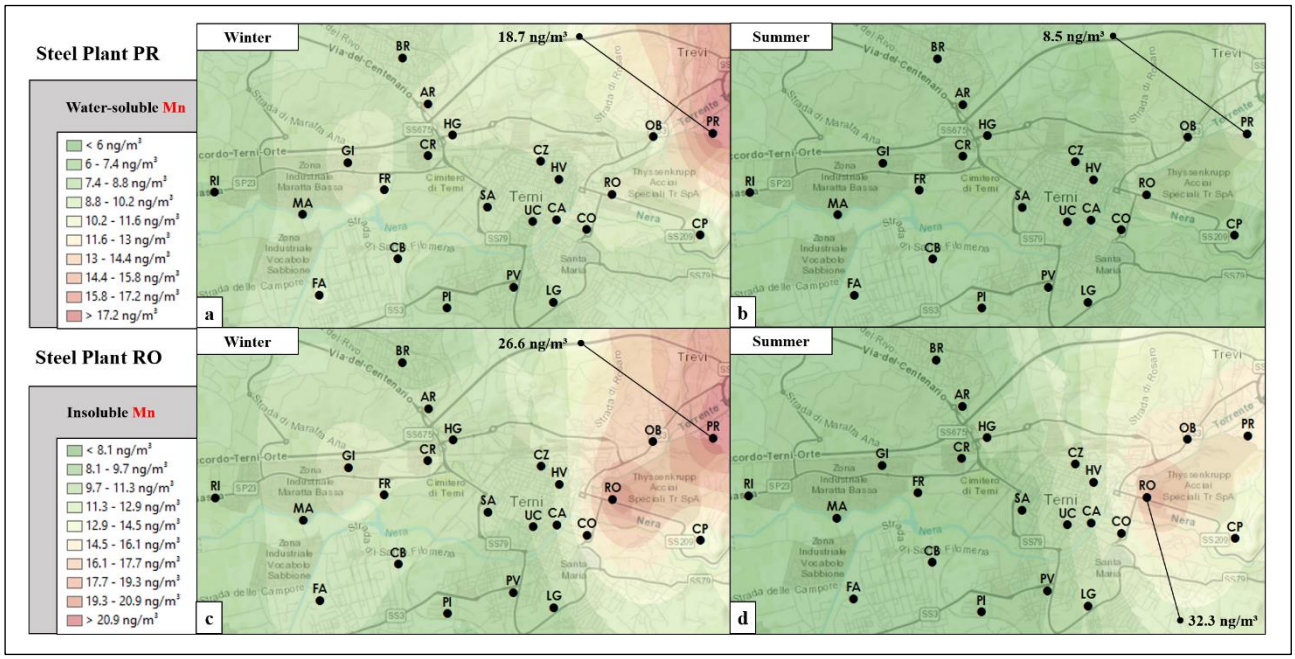

Fig. S4.8. Map of the winter and summer spatial distribution of water-soluble (panels a,b) and insoluble Mn (panels c,d).

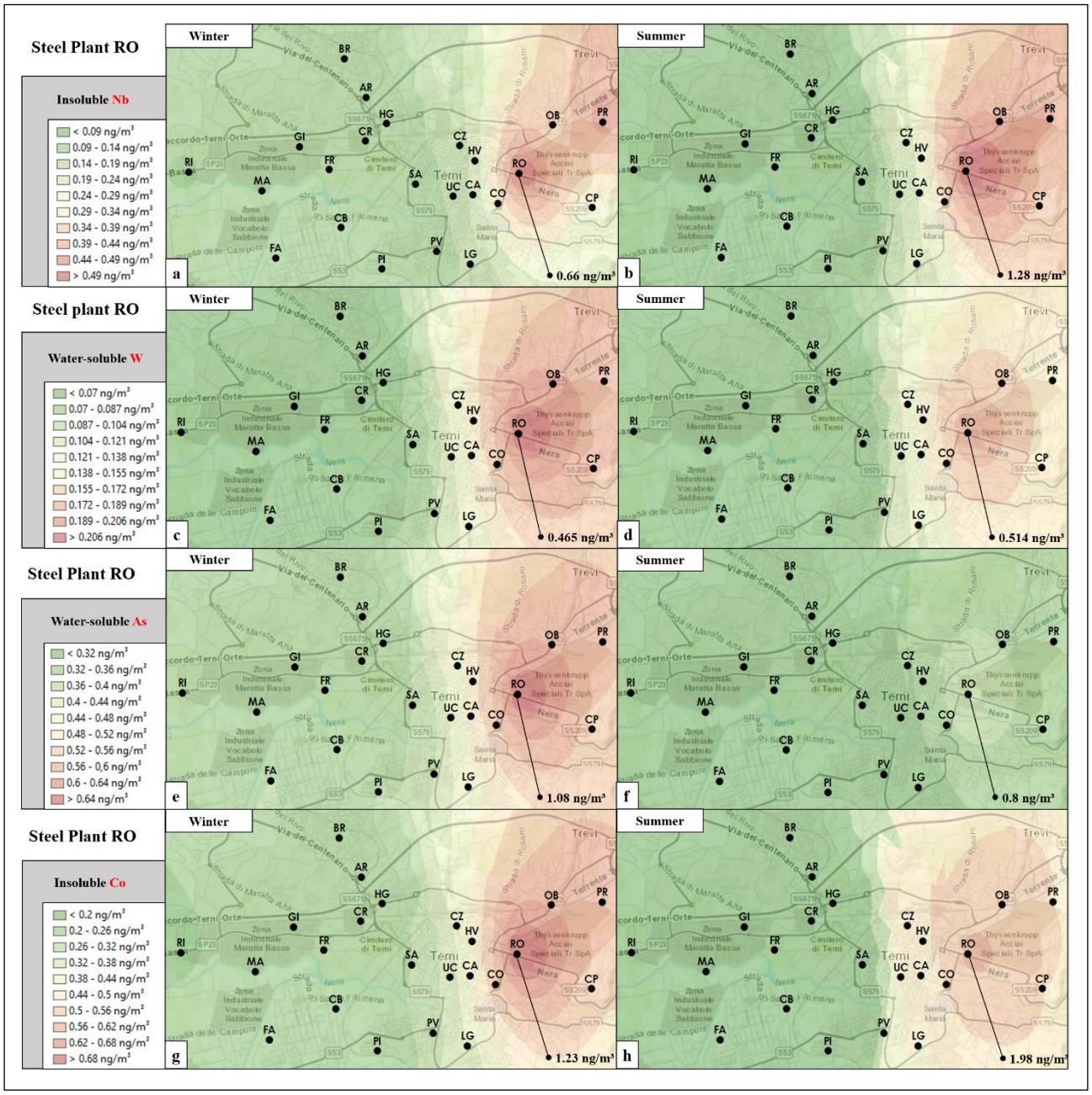

Fig. S4.9. Map of the winter and summer spatial distribution of insoluble Nb (panels a,b), Co (panels g,h), water-soluble W (panels c,d) and As (panels e,f).

Supplementary Material S5.

Table S5.1. Scores of the four significant components (accounting for 80.6%) obtained by performing the PCA on the matrix of the data composed of 276 samples (23 samples for each of the 12 samplings) and 34 selected variables: PM_{10} mass concentration and 33 water-soluble (_s) and insoluble (_i) element concentrations.

Scores 1° Sampling Month				
Site	**PC1**	**PC2**	**PC3**	**PC4**
RI_1	4.661	3.213	-1.530	0.916
MA_1	3.792	2.576	-0.506	1.094
FA_1	2.592	1.399	-3.333	0.176
GI_1	6.863	3.588	-3.354	2.572
FR_1	4.627	3.130	0.449	1.406
CB_1	4.037	1.811	0.802	-0.834
PI_1	2.601	1.779	0.847	0.026
BR_1	4.115	3.345	1.675	-0.282
AR_1	7.132	3.206	-0.890	-1.368
CR_1	6.946	3.735	-1.714	2.496
HG_1	7.329	3.244	-5.274	1.581
SA_1	5.407	2.531	-0.668	0.953
PV_1	3.302	1.641	0.169	-0.172
LG_1	3.620	1.805	0.474	-0.303
CZ_1	6.217	2.664	-3.612	1.180
HV_1	5.106	2.083	-1.950	0.778
UC_1	3.756	1.384	-0.840	-0.129
CA_1	7.935	2.246	-1.487	1.160
CO_1	7.317	1.194	-2.902	1.889
RO_1	6.234	-4.616	2.931	-0.952
OB_1	3.050	-1.223	1.936	-1.870
PR_1	9.111	-2.297	1.131	-3.862
CP_1	2.123	-0.362	1.609	-1.796

Scores 2° Sampling Month				
Site	**PC1**	**PC2**	**PC3**	**PC4**
RI_2	4.392	3.601	1.428	1.259
MA_2	3.699	3.182	1.168	0.655
FA_2	4.888	3.262	0.752	-0.474
GI_2	4.806	3.313	-0.347	2.756
FR_2	6.369	4.154	1.184	1.206
CB_2	4.478	2.345	-2.998	-0.236
PI_2	3.229	2.191	0.070	-1.054
BR_2	4.421	4.109	2.198	0.979
AR_2	3.025	2.270	2.842	0.034
CR_2	6.999	3.490	-0.724	2.812
HG_2	5.176	3.056	0.402	1.997
SA_2	6.453	2.812	0.441	1.180
PV_2	4.089	2.197	0.296	-0.218
LG_2	4.634	2.896	0.681	-0.453
CZ_2	5.031	2.136	-0.134	1.040
HV_2	3.842	0.780	2.758	0.161
UC_2	5.191	2.059	0.266	0.805
CA_2	9.080	3.310	-0.440	0.616
CO_2	6.895	0.982	-0.465	1.474
RO_2	6.792	-3.794	2.566	-0.216
OB_2	3.258	-1.647	2.415	-1.790
PR_2	7.741	-3.453	3.100	-3.253
CP_2	2.469	0.556	1.267	-1.571

Scores 3° Sampling Month				
Site	**PC1**	**PC2**	**PC3**	**PC4**
RI_3	1.252	2.293	0.382	1.336
MA_3	0.190	1.772	1.510	0.743
FA_3	0.048	1.571	1.531	-0.221
GI_3	0.330	1.715	-1.316	3.505
FR_3	0.975	2.136	0.694	1.102
CB_3	-2.501	0.794	1.834	0.342
PI_3	-1.173	1.221	1.587	-0.294
BR_3	-0.055	2.073	1.012	0.996
AR_3	-2.713	1.369	1.661	1.368
CR_3	-3.169	1.076	1.533	1.779
HG_3	1.493	2.527	0.802	1.791
SA_3	-2.726	0.726	1.674	1.143
PV_3	0.790	1.304	0.701	-0.031
LG_3	0.293	1.596	1.129	-0.284
CZ_3	0.326	1.475	1.122	0.613
HV_3	-0.196	0.707	1.368	-0.513
UC_3	-0.050	0.201	-0.210	0.672
CA_3	1.815	0.645	0.689	0.639
CO_3	1.941	-0.431	1.651	0.407
RO_3	5.677	-7.516	4.301	1.691
OB_3	2.128	-0.759	1.765	-0.742
PR_3	3.549	-3.354	-0.999	-0.018
CP_3	0.650	-0.866	1.510	-2.464

Table S5.2. Scores of the four significant components (accounting for 80.6%) obtained by performing the PCA on the matrix of the data composed of 276 samples (23 samples for each of the 12 samplings) and 34 selected variables: PM_{10} mass concentration and 33 water-soluble (_s) and insoluble (_i) element concentrations.

Scores 4° Sampling Month				
Site	**PC1**	**PC2**	**PC3**	**PC4**
RI_4	-3.428	0.569	-0.026	1.144
MA_4	-3.272	0.370	-0.742	1.205
FA_4	-3.879	-0.044	-0.792	0.279
GI_4	-2.598	0.135	-1.424	1.552
FR_4	-3.472	0.060	-0.003	0.728
CB_4	-3.360	0.306	1.081	0.023
PI_4	-3.892	0.281	1.807	-0.156
BR_4	-3.828	0.175	-0.037	0.329
AR_4	-4.194	0.089	0.848	0.452
CR_4	-2.259	0.451	-1.702	2.098
HG_4	-2.429	0.581	-1.414	1.999
SA_4	-3.504	0.111	1.401	0.482
PV_4	-2.822	0.291	1.233	0.119
LG_4	-3.471	-0.085	-0.096	0.339
CZ_4	-5.025	0.531	2.453	0.135
HV_4	-3.850	-0.195	0.167	0.378
UC_4	-4.019	-0.337	1.832	0.437
CA_4	-2.016	-0.379	-0.876	1.314
CO_4	-1.776	-0.817	-1.287	1.702
RO_4	0.609	-5.334	0.524	1.992
OB_4	-3.055	-1.170	0.276	0.654
PR_4	0.687	-3.472	-1.603	0.513
CP_4	-3.347	-0.641	-0.537	-0.042

Scores 5° Sampling Month				
Site	**PC1**	**PC2**	**PC3**	**PC4**
RI_5	-3.776	0.981	1.689	0.488
MA_5	-2.892	0.317	0.134	0.488
FA_5	-3.724	0.305	1.525	-0.153
GI_5	-2.757	0.712	2.118	0.095
FR_5	-5.378	0.126	2.285	0.046
CB_5	-3.700	0.166	2.200	-0.553
PI_5	-4.229	-0.036	2.572	-0.705
BR_5	-4.489	0.091	1.321	-0.017
AR_5	-4.245	0.382	2.213	-0.275
CR_5	-3.555	0.569	2.240	-0.053
HG_5	-2.890	0.651	1.517	0.809
SA_5	-3.799	-0.006	2.099	-0.381
PV_5	-3.516	0.293	1.923	0.005
LG_5	-3.990	0.005	2.295	-0.490
CZ_5	-3.714	0.282	2.046	-0.260
HV_5	-4.167	0.251	2.650	-0.884
UC_5	-3.570	-0.287	1.528	0.033
CA_5	-2.706	-0.327	1.991	0.025
CO_5	-2.609	-0.364	2.323	0.022
RO_5	1.430	-5.567	4.082	0.657
OB_5	-3.029	-0.588	2.679	-0.884
PR_5	0.039	-1.978	1.768	-2.316
CP_5	-3.922	-0.099	2.391	-1.172

Scores 6° Sampling Month				
Site	**PC1**	**PC2**	**PC3**	**PC4**
RI_6	-3.509	0.495	0.223	0.500
MA_6	-3.881	0.366	1.130	0.225
FA_6	-4.120	-0.163	0.226	0.009
GI_6	-3.259	0.476	0.564	0.560
FR_6	-4.433	-0.107	0.918	-0.299
CB_6	-3.875	-0.395	0.842	-0.509
PI_6	-5.017	-0.383	0.410	-0.099
BR_6	-4.894	0.211	1.692	-0.382
AR_6	-4.136	0.010	1.173	-0.085
CR_6	-3.577	0.113	0.477	0.242
HG_6	-3.944	0.553	1.596	0.543
SA_6	-4.214	0.198	1.928	-0.588
PV_6	-4.022	0.097	1.584	-0.060
LG_6	-4.198	-0.304	0.982	-0.395
CZ_6	-3.873	-0.118	1.158	-0.058
HV_6	-4.042	-0.174	1.655	-0.423
UC_6	-3.809	-1.056	-0.206	0.081
CA_6	-1.933	-1.528	0.109	-0.137
CO_6	-2.066	-1.414	-0.129	0.632
RO_6	5.747	-12.439	4.574	3.146
OB_6	-4.243	-0.158	2.280	-0.483
PR_6	-1.411	-1.877	1.607	-1.295
CP_6	-4.384	-0.329	1.201	-0.897

Table S5.3. Scores of the four significant components (accounting for 80.6%) obtained by performing the PCA on the matrix of the data composed of 276 samples (23 samples for each of the 12 samplings) and 34 selected variables: PM_{10} mass concentration and 33 water-soluble (_s) and insoluble (_i) element concentrations.

Scores 7° Sampling Month				
Site	**PC1**	**PC2**	**PC3**	**PC4**
RI_7	-4.593	-0.139	-0.245	0.009
MA_7	-2.570	-0.178	-1.135	-0.774
FA_7	-2.069	-1.495	-4.910	-0.938
GI_7	-3.285	-0.504	-2.100	-0.186
FR_7	-1.413	-1.391	-5.866	-1.893
CB_7	-5.205	-0.116	1.086	-0.248
PI_7	-1.906	-1.331	-2.595	-1.753
BR_7	1.638	-2.111	-12.022	-2.004
AR_7	-2.009	-0.881	-4.244	-0.997
CR_7	-1.303	-0.311	-3.364	-0.508
HG_7	0.060	-0.128	-5.946	0.868
SA_7	-2.316	-0.918	-3.471	0.126
PV_7	-1.627	-1.260	-4.685	-0.707
LG_7	-2.304	-1.305	-3.163	-1.257
CZ_7	-1.309	-0.835	-5.023	-1.162
HV_7	-3.152	-0.788	-1.470	-1.229
UC_7	-0.889	-1.975	-2.028	-1.383
CA_7	1.044	-2.803	-5.595	-1.003
CO_7	2.095	-4.317	-7.484	-0.182
RO_7	6.253	-11.370	0.240	2.234
OB_7	0.410	-2.949	-4.439	-1.777
PR_7	2.202	-3.329	-1.977	-3.273
CP_7	-1.924	-1.300	-2.233	-2.319

Scores 8° Sampling Month				
Site	**PC1**	**PC2**	**PC3**	**PC4**
RI_8	-4.087	-0.377	-0.906	0.063
MA_8	-3.461	-0.547	-1.345	-0.189
FA_8	-3.130	-0.761	-2.016	-0.303
GI_8	-2.455	0.049	-1.298	0.307
FR_8	-2.943	-0.626	-2.268	-0.705
CB_8	-2.311	-1.736	-4.991	-0.923
PI_8	-3.010	-1.164	-3.860	-0.244
BR_8	-3.708	-1.570	-6.044	0.015
AR_8	-2.294	-0.935	-3.998	-0.939
CR_8	-2.084	-1.111	-5.002	-0.001
HG_8	-1.045	-1.342	-8.676	1.728
SA_8	-1.805	-2.014	-6.931	0.151
PV_8	-2.353	-1.158	-2.861	-0.330
LG_8	-2.556	-1.209	-3.295	-0.610
CZ_8	-0.882	-0.734	-4.786	0.165
HV_8	-2.032	-0.980	-1.598	-0.242
UC_8	-2.808	-1.672	-1.335	-0.270
CA_8	-1.189	-2.034	-2.443	-0.455
CO_8	-1.653	-2.343	-3.415	0.845
RO_8	6.584	-12.930	-1.722	4.372
OB_8	-3.147	-1.526	-0.826	-0.473
PR_8	-0.381	-2.677	-2.476	-1.531
CP_8	-3.797	-0.881	-0.266	-0.827

Scores 9° Sampling Month				
Site	**PC1**	**PC2**	**PC3**	**PC4**
RI_9	-3.662	-0.208	-0.228	0.219
MA_9	-2.753	-0.454	-0.884	0.269
FA_9	-2.632	-0.384	-0.842	-0.009
GI_9	-1.273	0.289	-0.303	0.602
FR_9	-2.574	-0.250	-0.902	-0.248
CB_9	-2.949	-1.153	0.103	0.054
PI_9	-3.241	-0.504	0.766	-0.591
BR_9	-3.560	0.197	1.307	-0.309
AR_9	-1.721	0.083	-0.743	-0.419
CR_9	-1.310	0.063	-1.754	0.760
HG_9	-0.875	-0.128	-3.641	1.299
SA_9	-1.794	-0.642	-2.567	-0.023
PV_9	-2.742	-0.281	0.515	-0.246
LG_9	-2.649	-0.745	-1.390	-0.428
CZ_9	-0.192	-0.154	-3.671	0.630
HV_9	-1.170	-0.621	-1.356	0.251
UC_9	-1.699	-0.867	-0.935	-0.096
CA_9	-1.801	-1.625	-0.400	-0.092
CO_9	-4.986	-0.626	1.398	0.521
RO_9	9.406	-15.877	3.021	6.499
OB_9	-1.797	-1.423	0.614	-1.054
PR_9	1.097	-2.535	0.653	-2.546
CP_9	-4.132	-0.369	1.133	-0.588

Table S5.4. Scores of the four significant components (accounting for 80.6%) obtained by performing the PCA on the matrix of the data composed of 276 samples (23 samples for each of the 12 samplings) and 34 selected variables: PM_{10} mass concentration and 33 water-soluble (_s) and insoluble (_i) element concentrations.

Scores 10° Sampling Month				
Site	**PC1**	**PC2**	**PC3**	**PC4**
RI_10	-3.077	0.146	-0.130	0.433
MA_10	-2.002	0.690	1.336	0.187
FA_10	-2.013	0.063	0.373	0.007
GI_10	1.485	1.876	0.303	1.380
FR_10	-1.970	0.463	0.384	-0.548
CB_10	-2.056	-0.343	1.077	0.016
PI_10	-1.808	0.087	1.766	-0.176
BR_10	0.313	1.676	0.393	-0.261
AR_10	0.691	0.987	0.463	-0.008
CR_10	-0.372	1.197	0.008	1.808
HG_10	-0.270	0.895	-0.493	1.409
SA_10	-1.449	0.428	0.805	0.488
PV_10	-2.196	0.194	0.728	0.527
LG_10	-1.888	0.237	0.561	-0.458
CZ_10	1.180	0.399	-2.585	0.424
HV_10	-1.286	-0.727	1.200	0.365
UC_10	-1.025	-0.532	1.518	-0.342
CA_10	-0.870	-0.174	1.762	-0.072
CO_10	1.329	-1.929	1.043	2.467
RO_10	5.177	-8.827	3.368	1.931
OB_10	-1.007	-1.263	1.494	-0.609
PR_10	0.676	-1.532	1.670	-3.059
CP_10	-2.449	-0.350	1.033	-1.390

Scores 11° Sampling Month				
Site	**PC1**	**PC2**	**PC3**	**PC4**
RI_11	-1.419	1.214	0.259	0.077
MA_11	0.240	2.281	0.649	-0.280
FA_11	10.477	5.155	-2.603	-1.385
GI_11	4.103	4.082	0.767	2.128
FR_11	0.161	2.014	1.525	0.641
CB_11	2.308	2.492	0.889	-0.746
PI_11	-0.909	1.549	2.198	-1.318
BR_11	-0.621	2.409	2.110	-0.854
AR_11	1.795	2.833	2.254	-1.086
CR_11	0.546	1.943	0.434	1.817
HG_11	2.624	2.462	-0.273	1.628
SA_11	0.506	2.105	1.590	-0.061
PV_11	1.149	2.685	0.647	0.633
LG_11	-0.257	1.850	1.872	-0.541
CZ_11	0.944	1.275	-0.240	0.331
HV_11	-0.973	0.965	2.137	-1.059
UC_11	-0.633	1.333	2.189	-0.517
CA_11	0.808	1.405	1.864	-0.542
CO_11	1.252	-0.190	0.889	0.062
RO_11	6.973	-7.314	4.221	0.705
OB_11	1.828	-1.545	2.345	-1.675
PR_11	17.175	-4.320	-0.734	-12.843
CP_11	-0.293	-0.015	1.750	-1.202

Scores 12° Sampling Month				
Site	**PC1**	**PC2**	**PC3**	**PC4**
RI_12	-0.502	1.412	0.610	0.132
MA_12	0.414	1.610	0.960	0.188
FA_12	5.446	3.382	-0.822	-0.598
GI_12	5.324	3.259	-0.725	1.160
FR_12	0.335	1.577	1.203	-0.409
CB_12	0.828	1.416	0.961	-1.479
PI_12	1.417	1.035	0.765	-0.957
BR_12	6.660	4.943	1.196	-0.318
AR_12	4.228	2.518	-0.019	-1.182
CR_12	2.463	2.226	-0.194	0.985
HG_12	2.640	1.986	-0.907	1.287
SA_12	1.543	1.902	0.384	-0.196
PV_12	1.926	1.440	-0.476	0.523
LG_12	1.029	1.442	0.720	-0.325
CZ_12	1.495	1.453	-0.051	0.157
HV_12	0.900	1.098	0.994	-1.148
UC_12	0.716	0.641	1.197	-0.862
CA_12	1.172	0.639	1.133	-0.521
CO_12	2.179	0.466	0.973	-0.051
RO_12	8.523	-7.089	2.769	-0.451
OB_12	1.858	-0.599	2.064	-1.725
PR_12	3.763	-0.664	2.298	-3.802
CP_12	-0.754	0.220	1.988	-0.896

Table S5.5. Loadings of the four significant components (accounting for 80.6%) obtained by performing the PCA on the matrix of the data composed of 276 samples (23 samples for each of the 12 samplings) and 34 selected variables: PM_{10} mass concentration and 33 water-soluble (_s) and insoluble (_i) element concentrations.

Loadings									
Variable	**PC1**	**PC2**	**PC3**	**PC4**	**Variable**	**PC1**	**PC2**	**PC3**	**PC4**
PM_{10}	0.162	0.131	0.031	0.158	**Li_s**	0.235	-0.036	0.047	-0.299
As_s	0.189	-0.175	0.121	0.054	**Mn_i**	0.209	-0.204	-0.020	0.012
Ba_s	0.162	0.175	0.006	0.094	**Mn_s**	0.232	0.043	0.017	-0.285
Bi_i	0.193	0.180	-0.036	0.123	**Mo_s**	0.142	-0.277	0.118	0.024
Cd_s	0.202	0.139	0.084	-0.100	**Nb_i**	0.147	-0.268	0.035	0.090
Ce_i	0.068	-0.017	-0.349	0.006	**Ni_i**	0.140	-0.302	0.070	0.166
Co_i	0.165	-0.279	0.027	0.176	**Pb_i**	0.219	-0.011	0.008	-0.261
Cr_i	0.173	-0.271	0.069	0.124	**Rb_i**	0.008	-0.054	-0.370	-0.086
Cr_s	0.205	-0.157	0.055	-0.269	**Rb_s**	0.187	0.187	0.055	-0.017
Cs_i	0.040	-0.063	-0.372	-0.076	**Sb_i**	0.188	0.193	-0.052	0.228
Cs_s	0.225	0.185	0.052	-0.035	**Sn_i**	0.195	0.224	-0.014	0.221
Cu_i	0.198	0.127	-0.068	0.302	**Sr_i**	0.088	-0.008	-0.299	-0.066
Fe_i	0.181	-0.186	-0.028	0.308	**Tl_s**	0.193	0.222	0.068	0.012
Ga_s	0.198	-0.019	-0.046	-0.356	**U_i**	0.080	-0.049	-0.352	0.056
K_s	0.213	0.197	0.060	0.014	**W_s**	0.158	-0.264	0.093	0.042
La_i	0.003	-0.044	-0.318	-0.056	**Zn_s**	0.227	0.084	0.058	-0.239
Li_i	0.040	-0.107	-0.374	-0.049	**Zr_i**	0.146	0.121	-0.238	0.209

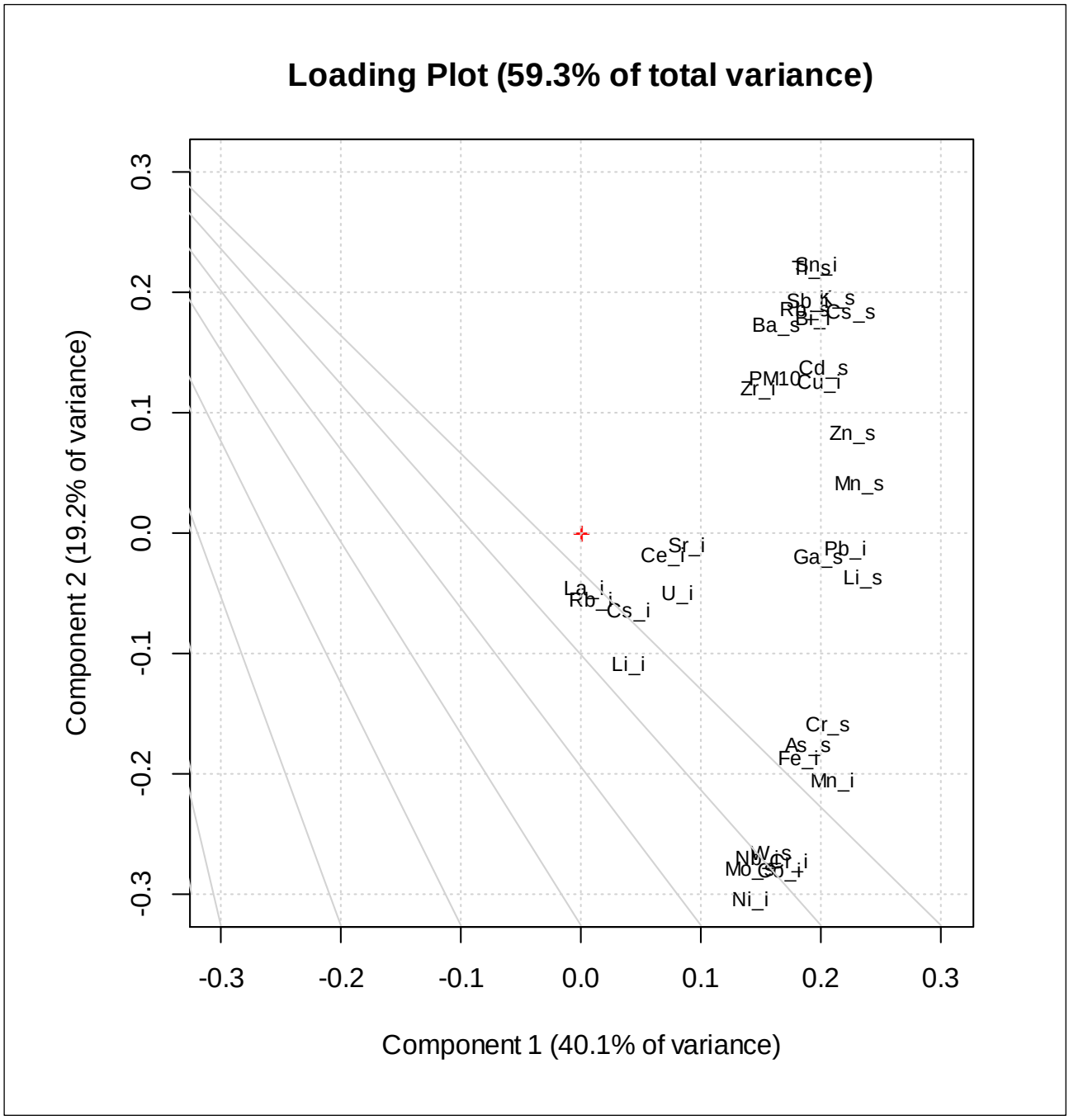

Fig. S5.1. Loading plot of PC1/PC2 performed on the matrix of the data composed of 276 samples (23 samples for each of the 12 samplings) and 34 selected variables: PM_{10} mass concentration and 33 water-soluble (_s) and insoluble (_i) element concentrations.

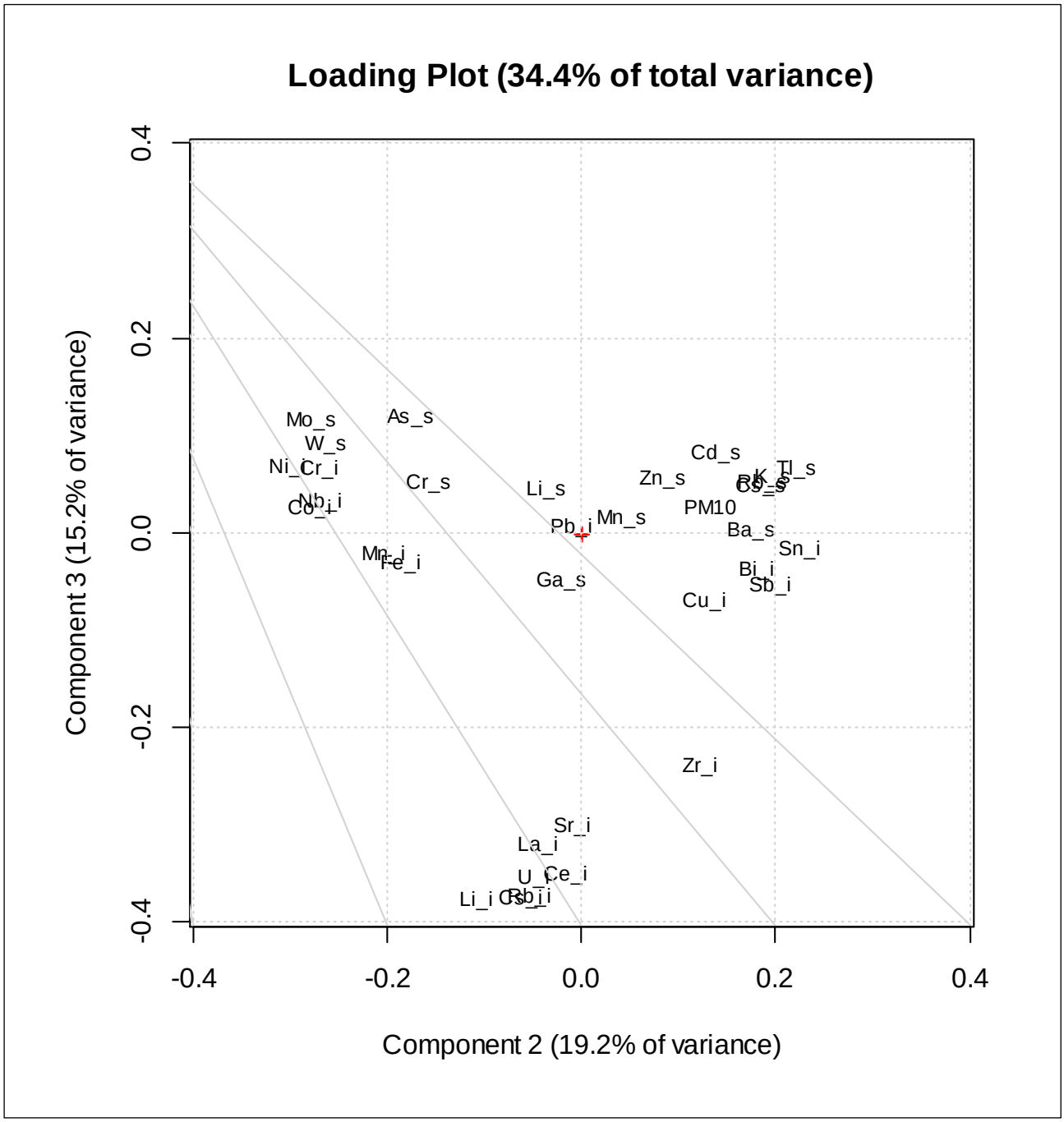

Fig. S5.2. Loading plot of PC2/PC3 performed on the matrix of the data composed of 276 samples (23 samples for each of the 12 samplings) and 34 selected variables: PM_{10} mass concentration and 33 water-soluble (_s) and insoluble (_i) element concentrations.

Supplementary Material S6.

Table S6.1. Average (AM) PM mass, insoluble and water-soluble element concentrations determined in size-segregated PM samples for the winter monitoring period.

		Winter - Size Distribution (µm) of PM Mass and Insoluble Element Concentrations (AM)										Winter - Size Distribution (µm) of Water-soluble Element Concentrations (AM)									
	UoM µm	<0.18	0.18 - 0.32	0.32 - 0.56	0.56 - 1	1 - 1.8	1.8 - 3.2	3.2 - 5.6	5.6 - 10	10 - 18	>18	<0.18	0.18 - 0.32	0.32 - 0.56	0.56 - 1	1 - 1.8	1.8 - 3.2	3.2 - 5.6	5.6 - 10	10 - 18	>18
PM	µg/m^3	2.8	3.3	3.9	4.4	2	3.1	3.8	1.8	1	1.0										
Al	ng/m^3	1.3	1.4	1.9	2	6.2	12	18	13	6	5.4	0.18	0.33	0.57	0.58	0.71	0.56	0.49	0.44	0.26	0.21
As	ng/m^3	0.041	0.042	0.043	0.043	0.04	0.040	0.04	0.029	0.023	0.021	0.077	0.071	0.073	0.062	0.021	0.0097	0.0048	0.0053	0.0049	0.0062
Ba	ng/m^3	0.71	0.46	0.76	0.68	0.95	1.8	2	1.7	1.5	1.1	0.056	0.055	0.1	0.12	0.14	0.23	0.53	0.27	0.085	0.069
Bi	ng/m^3	0.013	0.013	0.013	0.018	0.019	0.021	0.026	0.014	0.0059	0.0032	0.0025	0.0037	0.0059	0.0074	0.0032	0.00037	0.00052	0.00016	0.00051	0.000094
Ca	ng/m^3	24	12	25	19	29	54	99	72	53	38	7.1	5.8	7.5	18	38	60	92	79	27	21
Cd	ng/m^3	0.0051	0.0064	0.006	0.0066	0.0061	0.0032	0.0028	0.0009	0.0024	0.0041	0.024	0.029	0.033	0.025	0.0099	0.0013	0.0014	0.00081	0.00055	0.00033
Ce	ng/m^3	0.0016	0.002	0.002	0.001	0.002	0.0065	0.02	0.011	0.0025	0.00058	0.014	0.021	0.002	0.0019	0.0012	0.00068	0.0012	0.00069	0.00064	0.00019
Co	ng/m^3	0.01	0.011	0.014	0.023	0.029	0.032	0.036	0.023	0.0098	0.0088	0.0022	0.0032	0.0038	0.004	0.003	0.0023	0.0018	0.0011	0.00052	0.00038
Cr	ng/m^3	1.3	1.2	1.5	3	3.8	4.2	5	3	1.3	0.89	0.44	0.47	0.48	0.38	0.11	0.02	0.022	0.013	0.0035	0.0023
Cs	ng/m^3	0.0012	0.0013	0.001	0.0013	0.0017	0.0024	0.0036	0.0032	0.0013	0.00092	0.011	0.012	0.011	0.0081	0.0019	0.00014	0.00014	0.00011	0.00008	0.00004
Cu	ng/m^3	0.26	0.28	0.4	0.44	0.56	1.3	1.5	0.86	0.29	0.22	0.15	0.11	0.14	0.22	0.23	0.25	0.28	0.11	0.036	0.023
Fe	ng/m^3	6.7	7	11	20	41	67	81	49	19	18	0.94	1.9	2.9	4.8	3.1	0.67	1.1	0.75	0.42	0.24
Ga	ng/m^3	0.0047	0.0053	0.0063	0.0091	0.0066	0.0047	0.0038	0.0032	0.0022	0.001	0.0022	0.005	0.007	0.0086	0.002	0.000092	0.00006	0.00005	0.00004	0.00003
K	ng/m^3	40	49	50	62	45	45	47	40	33	40	55	75	87	57	15	8.8	11	8.1	3.8	3.1
La	ng/m^3	0.0018	0.002	0.0022	0.0025	0.0025	0.0041	0.0079	0.0037	0.0019	0.00028	0.011	0.012	0.00084	0.0011	0.00067	0.00041	0.00069	0.00053	0.00046	0.00015
Li	ng/m^3	0.0043	0.0044	0.003	0.0064	0.0079	0.012	0.015	0.01	0.0049	0.0044	0.044	0.04	0.028	0.017	0.0061	0.0024	0.0038	0.002	0.00069	0.00047
Mg	ng/m^3	0.94	0.82	1.2	1.7	4.8	8.3	11	9	4.7	5.1	0.54	0.66	0.97	2.3	4.5	6	10	5	1.4	1.1
Mn	ng/m^3	0.35	0.55	0.88	1.2	1.3	1.6	2	1.2	0.53	0.48	0.45	0.81	1.3	1.9	0.81	0.19	0.28	0.21	0.064	0.049
Mo	ng/m^3	1.1	0.9	0.86	0.64	0.34	0.25	0.24	0.15	0.062	0.059	0.7	0.85	0.88	0.48	0.18	0.12	0.11	0.053	0.022	0.019
Na	ng/m^3	7.2	7.9	9	9	17	25	32	34	10	13	7.2	8.9	10	15	31	43	83	37	9.7	8.8
Nb	ng/m^3	0.0011	0.0011	0.0022	0.0064	0.017	0.022	0.044	0.026	0.0087	0.008	0.00013	0.00017	0.00031	0.00064	0.00051	0.00041	0.00039	0.00029	0.00028	0.00026
Ni	ng/m^3	0.59	0.94	1	1.2	1.4	1.7	1.8	1.1	0.44	0.39	0.11	0.11	0.16	0.25	0.12	0.037	0.053	0.013	0.007	0.0084
Pb	ng/m^3	0.4	0.61	0.86	0.79	0.57	0.24	0.2	0.1	0.045	0.038	0.36	0.47	0.62	0.59	0.22	0.013	0.01	0.0041	0.0056	0.0025
Rb	ng/m^3	0.01	0.012	0.014	0.018	0.022	0.027	0.042	0.034	0.019	0.013	0.17	0.23	0.22	0.12	0.033	0.0059	0.011	0.0038	0.00073	0.00066
Sb	ng/m^3	0.026	0.034	0.036	0.038	0.047	0.073	0.12	0.061	0.017	0.01	0.035	0.045	0.055	0.048	0.027	0.02	0.01	0.0051	0.0013	0.00082
Sn	ng/m^3	0.22	0.22	0.2	0.24	0.24	0.27	0.35	0.19	0.057	0.044	0.018	0.017	0.022	0.022	0.011	0.0027	0.0031	0.0011	0.0011	0.00033
Sr	ng/m^3	0.064	0.059	0.069	0.069	0.13	0.24	0.34	0.26	0.17	0.13	0.015	0.015	0.02	0.042	0.093	0.14	0.2	0.13	0.044	0.032
Ti	ng/m^3	0.027	0.024	0.046	0.11	0.34	0.61	1.1	0.85	0.43	0.42	0.0035	0.0052	0.0069	0.013	0.012	0.011	0.013	0.0072	0.0054	0.0025
Tl	ng/m^3	0.001	0.0058	0.0059	0.0048	0.0013	0.00082	0.00064	0.00025	0.000087	0.00016	0.041	0.044	0.033	0.02	0.0034	0.00029	0.00026	0.00012	0.000039	0.000039
U	ng/m^3	0.0001	0.0001	0.000057	0.000042	0.00017	0.00063	0.0012	0.00081	0.00028	0.00021	0.00011	0.000095	0.00011	0.00014	0.00011	0.00013	0.00017	0.00013	0.000063	0.000039
W	ng/m^3	0.004	0.004	0.0047	0.0061	0.0052	0.0051	0.0063	0.0041	0.0018	0.0015	0.021	0.025	0.024	0.021	0.011	0.001	0.0016	0.0012	0.00035	0.00026
Zn	ng/m^3	1.5	1.7	2.7	3.7	3.2	2.9	2.7	1.6	1.4	1.4	2.5	2.9	3.9	6.4	4.7	0.84	0.64	0.31	0.14	0.11
Zr	ng/m^3	0.0065	0.0058	0.009	0.021	0.052	0.1	0.12	0.07	0.029	0.024	0.0002	0.00035	0.0009	0.0076	0.0038	0.0019	0.0012	0.00067	0.00017	0.001

Table S6.2. Average (AM) PM mass, insoluble and water-soluble element concentrations determined in size-segregated PM samples for the summer monitoring period.

		Summer - Size Distribution (µm) of PM_{10} Mass and Insoluble Element Concentrations (AM)										Summer - Size Distribution (µm) of Water-soluble Element Concentrations (AM)									
	UoM µm	**<0.18**	**0.18 - 0.32**	**0.32 - 0.56**	**0.56 - 1**	**1 - 1.8**	**1.8 - 3.2**	**3.2 - 5.6**	**5.6 - 10**	**10 - 18**	**>18**	**<0.18**	**0.18 - 0.32**	**0.32 - 0.56**	**0.56 - 1**	**1 - 1.8**	**1.8 - 3.2**	**3.2 - 5.6**	**5.6 - 10**	**10 - 18**	**>18**
PM_{10}	µg/m³	1.5	1.5	1.6	1.4	1.3	2	4.2	3.8	1.9	1.7										
Al	ng/m³	1.6	2.3	4	3	8.3	15	26	25	13	9.8	2.6	0.51	1.6	1	1.4	0.56	0.7	0.76	1.4	2.1
As	ng/m³	0.019	0.022	0.026	0.024	0.027	0.027	0.03	0.027	0.022	0.0068	0.07	0.058	0.041	0.029	0.018	0.0068	0.0034	0.0048	0.0018	0.0036
Ba	ng/m³	0.28	0.28	0.4	0.35	0.87	1.5	2	1.7	0.78	0.66	0.13	0.13	0.11	0.16	0.29	0.29	0.33	0.26	0.25	0.19
Bi	ng/m³	0.0063	0.0063	0.0065	0.0096	0.018	0.025	0.032	0.024	0.0093	0.004	0.0022	0.0024	0.0035	0.0035	0.0018	0.00025	0.00016	0.00013	0.00014	0.0004
Ca	ng/m³	24	42	32	24	42	89	210	259	154	125	40	32	29	34	49	87	122	109	105	91
Cd	ng/m³	0.00021	0.0049	0.0061	0.0025	0.0033	0.00068	0.0018	0.0014	0.0012	0.00081	0.011	0.014	0.028	0.013	0.0061	0.0037	0.003	0.003	0.004	0.0035
Ce	ng/m³	0.0073	0.009	0.011	0.0075	0.017	0.032	0.063	0.063	0.03	0.021	0.0016	0.0022	0.0026	0.003	0.002	0.0018	0.0019	0.0019	0.0017	0.0023
Co	ng/m³	0.01	0.018	0.022	0.023	0.038	0.053	0.072	0.076	0.042	0.027	0.0048	0.0061	0.0047	0.0051	0.0041	0.0036	0.0045	0.0029	0.0055	0.0026
Cr	ng/m³	1	2.2	2.4	2.6	4.6	7	7.9	8.4	4.8	2.7	0.58	0.59	0.41	0.41	0.23	0.12	0.17	0.11	0.44	0.15
Cs	ng/m³	0.0008	0.0014	0.0017	0.0011	0.0023	0.0041	0.0082	0.0062	0.0037	0.0026	0.0036	0.0034	0.0037	0.003	0.00067	0.00018	0.00021	0.00021	0.00022	0.00029
Cu	ng/m³	0.21	0.41	0.51	0.35	0.87	1.7	2.3	1.9	0.66	0.44	0.14	0.18	0.25	0.26	0.39	0.21	0.16	0.091	0.042	0.06
Fe	ng/m³	7.5	12	26	28	68	113	151	120	78	69	1.7	2.7	3.2	3.5	2.7	1.5	2.1	1.4	3.5	1.5
Ga	ng/m³	0.0022	0.0039	0.0038	0.0046	0.0066	0.0077	0.012	0.01	0.0044	0.0028	0.0016	0.0038	0.0042	0.0028	0.00085	0.00012	0.00011	0.0001	0.00018	0.00014
K	ng/m³	18	20	19	21	22	28	50	56	23	17	9	13	17	10	8	8	7	1.9	1.3	2.4
La	ng/m³	0.0022	0.0063	0.0064	0.0059	0.011	0.019	0.035	0.035	0.017	0.011	0.0012	0.0013	0.0011	0.0018	0.0011	0.0011	0.0012	0.0014	0.0011	0.0014
Li	ng/m³	0.0057	0.0066	0.0052	0.0031	0.0084	0.015	0.027	0.026	0.011	0.0076	0.018	0.024	0.023	0.019	0.0063	0.0053	0.0064	0.0074	0.0053	0.006
Mg	ng/m³	1.3	2	2.2	1.4	4.7	7.6	14	19	10	8.6	1.2	0.98	2	2.1	5.1	8.8	15	7	3.2	2.1
Mn	ng/m³	0.27	0.6	0.8	0.75	1.4	1.8	2.7	3	1.5	1	0.22	0.46	0.89	0.68	0.45	0.3	0.41	0.22	0.19	0.11
Mo	ng/m³	0.65	1	0.94	0.32	0.30	0.3	0.33	0.36	0.14	0.091	1.4	1.9	2	1.3	0.33	0.11	0.11	0.045	0.042	0.031
Na	ng/m³	11	14	13	10	16	17	18	30	12	11	6.2	6.7	11	10	27	49	84	36	11	7
Nb	ng/m³	0.0024	0.0021	0.0072	0.0048	0.017	0.024	0.054	0.064	0.036	0.029	0.0006	0.00044	0.00083	0.0008	0.00047	0.00053	0.00067	0.00034	0.00035	0.00025
Ni	ng/m³	0.53	1.2	1.5	1.71	1.9	2.4	2.7	2.1	1.5	0.79	0.16	0.27	0.32	0.49	0.28	0.098	0.14	0.081	0.26	0.11
Pb	ng/m³	0.3	0.38	0.69	0.63	0.47	0.27	0.26	0.22	0.13	0.091	0.22	0.29	0.4	0.38	0.074	0.0079	0.0056	0.007	0.0062	0.0088
Rb	ng/m³	0.0092	0.013	0.016	0.014	0.019	0.031	0.076	0.08	0.031	0.023	0.049	0.052	0.052	0.039	0.015	0.013	0.012	0.0082	0.011	0.0071
Sb	ng/m³	0.032	0.038	0.037	0.044	0.071	0.12	0.16	0.078	0.019	0.01	0.075	0.077	0.098	0.066	0.039	0.013	0.011	0.0047	0.0033	0.0029
Sn	ng/m³	0.1	0.12	0.13	0.13	0.18	0.28	0.4	0.27	0.064	0.032	0.083	0.057	0.051	0.037	0.012	0.0021	0.0019	0.00084	0.00074	0.0015
Sr	ng/m³	0.047	0.076	0.071	0.054	0.14	0.23	0.46	0.58	0.27	0.21	0.059	0.05	0.074	0.083	0.13	0.21	0.32	0.19	0.14	0.11
Ti	ng/m³	0.07	0.072	0.1	0.1	0.35	0.69	1.8	2.2	1.3	0.85	0.013	0.016	0.02	0.021	0.015	0.011	0.011	0.011	0.019	0.0088
Tl	ng/m³	0.0047	0.0058	0.0022	0.00086	0.0008	0.00086	0.0011	0.0015	0.00048	0.0004	0.029	0.014	0.0059	0.0044	0.00078	0.00031	0.0003	0.00016	0.00015	0.00014
U	ng/m³	0.0003	0.00024	0.00031	0.00026	0.0008	0.0015	0.003	0.0032	0.0016	0.0011	0.0002	0.00016	0.00015	0.0002	0.00016	0.00016	0.00019	0.00019	0.00016	0.0002
W	ng/m³	0.01	0.01	0.01	0.0098	0.0083	0.0088	0.017	0.012	0.0065	0.0035	0.025	0.02	0.014	0.01	0.0028	0.0021	0.0013	0.00081	0.0008	0.00056
Zn	ng/m³	1.1	3.2	3.6	3.5	3.7	4.1	4.4	3.7	2.8	2.1	2.2	2.6	4.4	4.7	3.5	2	1.6	1.2	1.1	1.6
Zr	ng/m³	0.016	0.013	0.015	0.02	0.069	0.13	0.18	0.15	0.063	0.046	0.0014	0.0014	0.0029	0.0035	0.0041	0.002	0.0033	0.0022	0.0021	0.0024

2.3.4. (C4) Lichen Transplants as Indicators of Atmospheric Element Concentrations: a High Spatial Resolution Comparison with PM_{10} Samples in a Polluted Area (Central Italy)

Ecological indicators (2019), *101*, 759-769

Lorenzo Massimi [a,*], Marcelo Enrique Conti [b], Giustino Mele [b], Martina Ristorini [a], Maria Luisa Astolfi [a], Silvia Canepari [a]

[a] Department of Chemistry, Sapienza University of Rome (Rome), 00185, Italy;
[b] Department of Management, Sapienza University of Rome (Rome), 00161, Italy.

Abstract: Lichen transplants *Evernia prunastri* (L.) Ach. and recently available low-cost PM_{10} samplers were placed side-by-side for one year at twenty-three sites located in an urban-industrial hot-spot of Central Italy, thus enabling the construction of an extensive and dense air quality monitoring network. Accumulation levels of the elements in lichens after five months and thirteen months of exposure were compared with the means of the element concentrations determined in the PM_{10} sampled during the same monitoring periods. Water-soluble and insoluble fractions of the elements in the PM_{10} were separately analysed. Correlations between lichen and PM_{10} element concentrations were examined by considering Pearson coefficients and by performing principal component analysis. The study allowed us to evaluate the reliability of lichen transplants as biomonitors for the assessment of the spatial variability of atmospheric element concentrations and for the individuation of the elements tracers of PM emission sources. Lichen transplants appeared to be reliable for high spatial resolution measurements of PM_{10} elemental components emitted at high concentrations by intense local PM emission sources such as the steel plant (Co, Cr, Fe, Mn, Mo, Nb, Ni, Ti and W) and the rail network (Cu, Sb and Sn), less reliable for spatially-resolved analyses of elements released by vehicular traffic (Cu, Sb and Sn) and not reliable for other elements emitted by the power plant, by industrial and domestic biomass heating and/or by other less intense emission sources (Ba, Bi, Cd, Cs, Mg, Pb, Rb and Tl). In general, bioaccumulation of the elements appeared to be more correlated with the total and insoluble fractions of the analysed elements than with the water-soluble one and reflected the solubility of the chemical species emitted by the main local PM emission sources.

Keywords: biomonitoring; lichen; *Evernia prunastri*; atmospheric element**;** spatial variability; PM_{10} sampler.

1. Introduction

Direct and indirect effects of atmospheric particulate matter on the environment and on human health have led to numerous studies focused on its complex composition and on the individuation of its main emission sources (Hwang and Hopke, 2007). The composition and the spatial distribution of particulate matter depend on several factors such as the location and the emission rate of its sources, the complexity of PM transport and transformation processes and the dispersion capacity of each single contribute (Fox, 1984; Almeida et al., 2006; Perrino et al., 2010).

The study of the spatial distribution of atmospheric PM and of its main chemical components is essential for the evaluation of particle dispersion over the territory and the assessment of personal exposure. However, the very high cost of a monitoring network based on traditional PM samplers generally prevents the achievement of these goals. Hence, PM dispersion over the territory is typically estimated through mathematical models (Irwin, 2014; Vitali et al., 2016; Kim et al., 2017), which often reveal limitations such as reducible errors resulted from inadequate air quality data inputs and from difficulties of models to describe such a complex issue. Therefore, there is an increasing demand for low-cost air quality monitoring techniques that can be easily applied with the aim to validate and optimize dispersion models.

Over the last decades, the use of cosmopolite organisms to assess the air pollution has developed notably and biomonitoring methods have been widely used. Accumulative species, if properly calibrated, can give valuable information about atmospheric deposition of the elements and may be used as biological monitors of pollutant concentrations in the environment for integrated measurements over time. This characteristic allows the comparison between pollution levels among different monitoring sites (Garty, 2001; Conti and Cecchetti, 2001; Jeran et al., 2002; Wolterbeek, 2002; Wolterbeek et al., 2003; Conti, 2008).

Lichens are considered to be the most efficient biomonitors of air pollution (Pignata et al., 2007; Conti and Tudino, 2016) because of their sensitivity to various environmental pollutants and their ability to accumulate airborne elements, since the concentrations found in their thalli can be directly correlated with those present in the environment. Lichens have been widely used as low-cost monitors of exposure in air pollution studies related to PM elemental components, by collecting native species (Folkeson, 1979; Sloof and Wolterbeek, 1993; State et al., 2011) or by deploying lichen transplants in different sites for given periods of time (Sloof, 1995; Cercasov et al., 2002; Conti et al., 2012,

2016; Pantelica et al., 2016). Other studies applied both methods simultaneously (native and lichen transplants) with the aim to determine the bioavailability of Ir, Pt and Rh levels at sites where vehicular traffic and anthropogenic activities were near to background levels (Pino et al., 2010).

The use of transplanted lichens as biomonitors for atmospheric element concentrations allows the construction of extended, dense and low-cost monitoring networks (Conti, 2002; Vannini et al., 2017). However, the reliability of the biological monitoring for high spatial resolution measurements of PM elemental components still has to be investigated. Are bioaccumulation data reliable for spatially-resolved analyses of PM elements? Are lichen transplants efficient biomonitors to assess the spatial variability of the concentrations of all the atmospheric elements?

Bari et al. (2001) demonstrated the significant correlation between metals accumulated in lichens and the metal air concentrations (measured with a continuous operating particulate sampler), showing their aptness to represent atmospheric contamination. However, there are no many studies that have examined simultaneously at several sites the possible/direct correlation between biomonitoring methods (i.e. lichen transplants) and traditional analyses of PM. This can be ascribed to the very high costs associated with a monitoring network based on traditional PM samplers. The new high spatial resolution sampler (HSRS) is a low-cost, automatic, self-powered and very low-volume device for PM sampling on membrane filters. The sampler constitutes promising possibility to build low-cost monitoring networks for atmospheric elements with the same spatial resolution of the biomonitors. The main advantage of this new device is to assure long-term collection of PM on membrane filters suitable for subsequent chemical analyses, thus enabling the spatially-resolved determination of PM chemical components.

The use of HSRS allowed us to enhance the information variety (Ashby, 1960). In fact, in several studies, the response of lichens to the environmental contamination is assessed by using a quite low number of parameters and sites (i.e. mainly toxic elements). The environment is a complex system, and according to the Ashby's Law (1960), the understanding of a complex system depends on the information variety (requisite variety) owned by the observer.

Hence, in this study, we tested the reliability of lichen transplants for the assessment of the spatial variability of PM elemental components in a wide polluted area of Central Italy, characterized by the presence of urban (such as vehicular traffic, rail network, domestic heating) and industrial PM emission sources (such as a power plant for waste treatment and a steel plant).

We have, in this regard, enhanced the information variety (i.e. 21 elements at 23 monitoring sites in polluted urban and industrial areas) in order to have more reliable results about the effective aptness of the lichen transplants to act as biomonitors of a complex system such as the environment.

2. Materials and Methods

2.1. Study Area

Samplers and lichen transplants were deployed in December 2016 at twenty-three monitoring sites in the Terni basin, a wide urban-industrial hot-spot of Central Italy (Moroni et al., 2013).

Terni is a city of 211,90 km^2 sited in an intramountain depression, where both urban (vehicular traffic, rail network, domestic heating) and industrial (power plant for waste treatment and a steel plant) PM emission sources are present (Guerrini, 2012).

The meteorological conditions of Terni basin, resulting from its peculiar geomorphological conformation, limit the dispersion and enhance the accumulation of atmospheric PM (Ferrero et al., 2012).

For these reasons Terni was chosen as a target area to assess the reliability of lichen transplants for high spatial resolution analyses of PM elemental components.

The monitoring campaign was carried out from December 2016 to January 2018.

2.2. Sampling Sites

The first phase of this study required great commitment and large amount of time for the individuation of the best sites (Fig. 1) for the deployment of twenty-three samplers (HSRS - High Spatial Resolution Sampler; Fai Instruments, Fonte Nuova, Rome, Italy; Fig. 2) and lichen transplants (*Evernia prunastri* (L.) Ach.; Fig. 2).

The twenty-three sampling sites were chosen in order to represent the contribution of each main local PM emission source:

- power plant for waste treatment in the West of the city (industrial area): RI, MA, FR;
- rail network in the North-West of the city (urban area): GI, CR, HG;
- trafficked streets and heavily trafficked streets in the city centre (urban area): CZ, HV, SA, UC, CA, CO;
- industrial and domestic biomass heating in the South-West and in the North of the city (urban and industrial areas): FA, CB, BR, AR, PI, PV, LG;
- very extensive steel plant in the East of the city (industrial area): RO, OB, PR, CP.

Geographical coordinates of the twenty-three selected sites (RI, MA, FA, GI, FR, CB, PI, BR, AR, CR, HG, SA, PV, LG, CZ, HV, UC, CA, CO, RO, OB, PR, CP) are reported in Table 1.

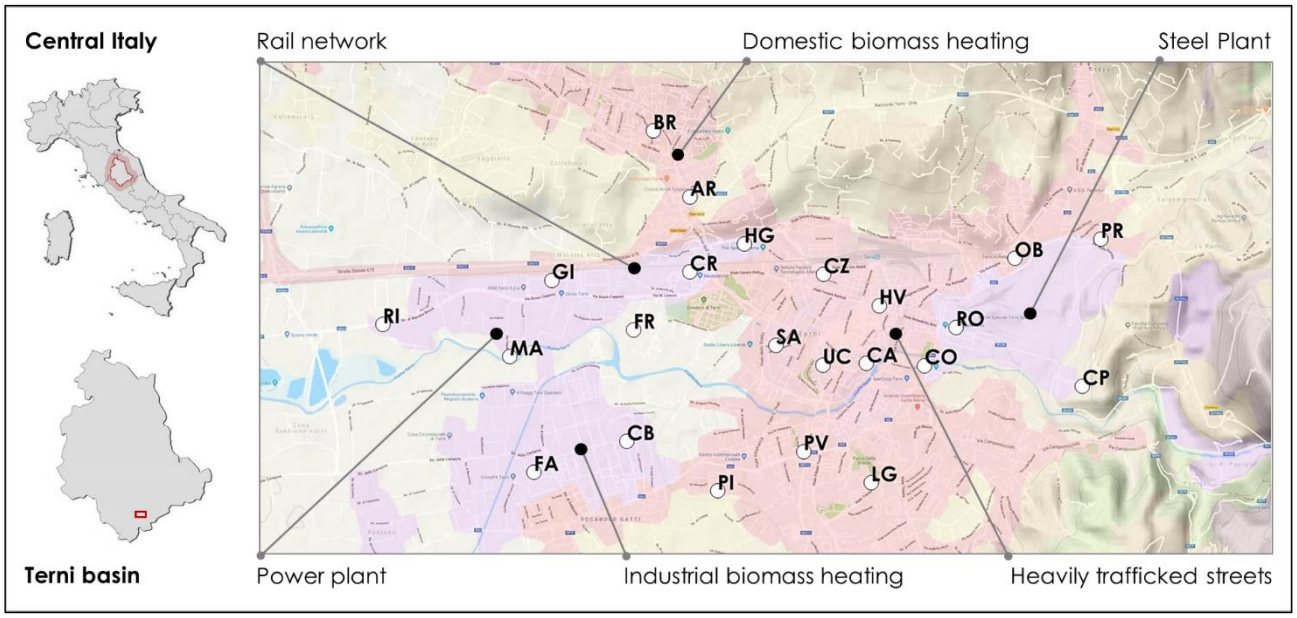

Fig. 1. Map of the twenty-three monitoring sites in Terni (Central Italy) with the locations of the main local PM emission sources in the study area (QGis 2.18 Las Palmas). Legend - violet: industrial area; red: urban area; grey: agricultural area; yellow: semi-natural area; green: forest (The legend refers to the colours available on the online version; Corine Land Cover 2012 by http://www.pcn.minambiente.it/mattm/servizio-wms/CLC2012, from Geoportale Nazionale).

2.3. Sampling Equipment and Analytical Procedures

2.3.1. Lichen Transplants

E. prunastri is a widely spread lichen with an extensive ecological amplitude and it is one of the most common epiphytic lichens. It has been used in various studies of element bioaccumulation (Cercasov et al., 2002; Conti et al., 2004; Balabanova et al., 2012; Sujetoviene and Sliumpaite, 2013), which showed its potential for the measurements of atmospheric element concentrations.

In November 2016, *E. prunastri* thalli were collected from the trunk of trees with inclination <10 %, at a height of 1-2 m above the ground level, in the National Park of Abruzzo (Central Italy), at a control site 1500 m a. s. l., located around 120 km away from the study area.

The lichen *E. prunastri* was transplanted to Terni, at the twenty-three urban and industrial monitoring sites (Fig. 2), and the bioaccumulation of the elements was assessed after five months (T1) and thirteen months (T2) of exposure.

Table 1. Type of site, main local PM emission sources and geographical coordinates of the twenty-three monitoring sites in Terni.

Type of Site & Main Local PM Emission Sources		Latitude	Longitude
RI	Industrial Site - Power Plant & Domestic Biomass Heating (West of the City)	42°33'52.02" N	12°35'21.94" E
MA	Industrial Site - Power Plant (West of the City)	42°33'41.42" N	12°36'19.05" E
FA	Industrial Site - Power Plant & Industrial Biomass Heating (West of the City)	42°33'03.19" N	12°36'29.76" E
GI	Industrial Site - Power Plant & Rail Network (North-West of the City)	42°34'06.28" N	12°36'48.27" E
FR	Industrial Site - Power Plant & Domestic Biomass Heating (West of the City)	42°33'53.22" N	12°37'11.44" E
CB	Industrial Site - Power Plant & Industrial Biomass Heating (West of the City)	42°33'20.30" N	12°37'20.45" E
PI	Urban Background Site - Domestic Biomass Heating (South of the City)	42°32'56.96" N	12°37'52.26" E
BR	Urban Background Site - Domestic Biomass Heating (North of the City)	42°34'56.19" N	12°37'23.30" E
AR	Urban Background Site - Domestic Biomass Heating (North of the City)	42°34'34.23" N	12°37'39.88" E
CR	Industrial Site - Domestic Biomass Heating & Rail Network (North-West of the City)	42°34'09.49" N	12°37'39.81" E
HG	Urban Site - Trafficked Streets & Rail Network (North-West of the City)	42°34'19.32" N	12°37'56.02" E
SA	Urban Site - Trafficked Streets (City Centre)	42°33'45.16" N	12°38'18.45" E
PV	Urban Background Site - Domestic Biomass Heating (South of the City)	42°33'06.96" N	12°38'35.20" E
LG	Urban Background Site - Domestic Biomass Heating (South of the City)	42°32'59.75" N	12°39'01.16" E
CZ	Urban Site - Trafficked Streets (City Centre)	42°34'06.90" N	12°38'52.97" E
HV	Urban Site - Trafficked Streets (City Centre)	42°33'58.33" N	12°39'04.74" E
UC	Urban Site - Trafficked Streets & Domestic Biomass Heating (City Centre)	42°33'38.09" N	12°38'47.62" E
CA	Urban Site - Heavily Trafficked Streets (City Centre)	42°33'39.01" N	12°39'03.11" E
CO	Urban-industrial Site - Heavily Trafficked Streets & Steel Plant (City Centre)	42°33'34.23" N	12°39'22.62" E
RO	Industrial Site - Steel Plant (East of the City)	42°33'51.16" N	12°39'39.15" E
OB	Industrial Site - Steel Plant (East of the City)	42°34'18.64" N	12°40'05.57" E
PR	Industrial Site - Steel Plant (East of the City)	42°34'20.30" N	12°40'44.23" E
CP	Urban Background Site - Steel Plant (East of the City)	42°33'31.65" N	12°40'36.04" E

The transplant method has the great advantage of being applicable in areas unsuited to lichen survival due to high pollution levels or where there are no suitable substrata (Conti and Cecchetti, 2001; Conti et al., 2002).

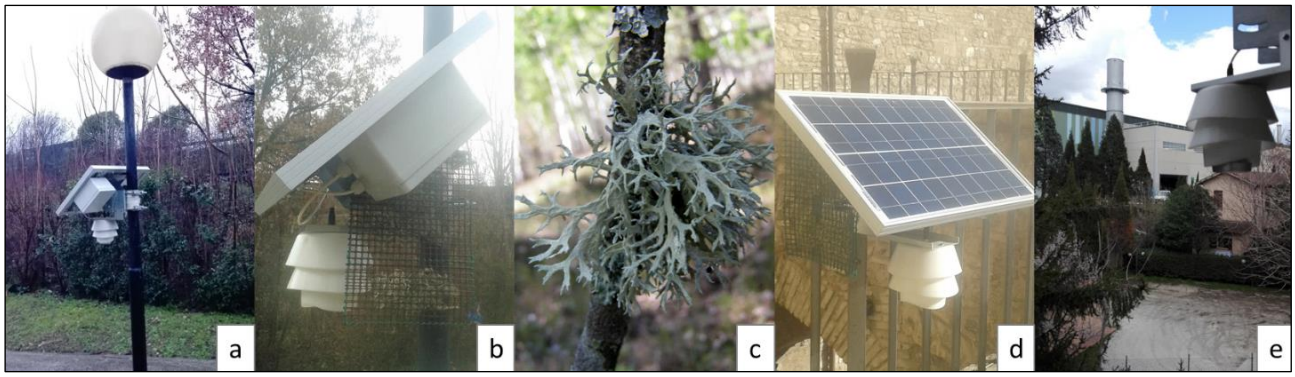

Fig. 2. PM_{10} samplers (HSRS - High Spatial Resolution Sampler; Fai Instruments, Fonte Nuova, Rome, Italy) and lichen transplants (*Evernia prunastri* (L.) Ach.) deployed in Terni: a) HSRS installed on a light pole at HG; b) lichen transplant fixed on a support composed of two plastic nets, sealed under the solar panel of the HSRS installed on a light pole, at CP; c) *E. prunastri* lichen on the trunk of a tree at a control site 1500 m a. s. l. (by Приходько Юрий; https://creativecommons.org/licenses/by-sa/4.0; from Wikimedia Commons, the free media repository); d) lichen transplant fixed on a support composed of two plastic nets, sealed under the solar panel of the HSRS installed on a balcony railing, at UC; e) PM_{10} sampling head of the HSRS installed on a balcony railing, at RO, in close proximity of the steel plant.

2.3.1.1. Lichen Transplants - Sampling and Analytical Procedures

Twenty-three lichen transplants with a mass of ca. 10 g were split into two parts: 5 g for the five-month exposure (T1) and 5 g for the thirteen-month exposure (T2). The two parts of each lichen were fixed on a support composed of two plastic nets. Then, each lichen was deployed in close proximity to the PM_{10} samplers (HSRS) installed in Terni (Fig. 2). Biomonitors were deployed at the same height (1-2 m above the ground level) and with the same exposition (southern exposition) of the samplers, to ensure homogeneous sampling conditions.

Lichens were transplanted to Terni in December 2016 and the samples were collected in May 2017 (5 g for the five-month exposure, T1) and in January 2018 (5 g for the thirteen-month exposure, T2). In the laboratory, lichen samples were sorted to remove as much extraneous material (Bargagli and Nimis, 2002; Conti et al., 2004) and then pulverized by grinding in a mill with Teflon balls.

The dry weight calculation (30 replicates) was carried out by oven drying 1 g of fresh material at 60 ± 2 °C until constant weight.

Subsequently, samples were mineralized in a microwave oven (Start D - Microwave Digestion System, Milestone, Bergamo, Italy) by using 5 mL of ultrapure concentrated HNO_3 (67%; Promochem, LGC Standards GmbH, Wesel, Germany) and 2 mL of H_2O_2 (30%; Promochem, LGC Standards GmbH, Wesel, Germany). After the acid-digestion, the obtained solutions were diluted in 90 mL of deionized water and then filtered with syringe filters (25 mm diameter, 0.45 μm pore size, GVS Filter Technology, Morecambe, UK). Lichen samples of the control site (CTR) were analysed to obtain the initial element concentrations (T0; before exposure).

The concentration of 21 elements (As, Ba, Bi, Cd, Co, Cr, Cs, Cu, Fe, Mg, Mn, Mo, Nb, Ni, Pb, Rb, Sb, Sn, Ti, Tl, W) in the mineralized lichens at T0, T1 and T2 was determined by using inductively coupled plasma mass spectrometry (ICP-MS, Bruker 820-MS, Billerica, MA, USA).

The element concentrations were divided by the dry weight of each lichen sample to obtain the element accumulation in lichens (μg g^{-1}).

Chemical determinations were conducted on two independent sub-samples taken from each lichen sample at T0, T1 and T2 (duplicate samples; standard deviations are shown in supplementary material S1).

The certified reference material BCR 482 lichen (IRMM, Geel, Belgium) was used to validate the entire analytical process and to test the accuracy of the measurements. Results (summarized in supplementary material S2) were in good agreement with certified values (95% confidence level) and their standard deviations showed that good precision was attained for all the measurements.

Further details about performances of the method are detailed elsewhere (Bocca et al., 2007; Pino et al. 2007).

2.3.2. High Spatial Resolution Samplers

The high spatial resolution sampler (HSRS; Fig. 2) is low-cost, small, light, automatic, self-powered (with a power supply system constituted by a rechargeable battery and a small solar panel) and characterized by a flow rate of 0.5 l min^{-1} (with a consumption of 0.2 W for the intake system and with a maximum adsorbed electric power of 1 W instead of 900-1200 W of traditional PM samplers). The device assures long-term (1-2 months) collection of PM on membrane filters, suitable for subsequent chemical analyses. The use of the very low-volume sampler (which can be installed on balconies, railings or light poles) improved access to a larger number of sampling locations, thus enabling the construction of a low-cost, dense and extensive monitoring network across Terni.

The employment of twenty-three HSRS in Terni (Fig. 2) allowed us to obtain PM data with a great spatial resolution (approximately 1 km of distance between the samplers) and with a monthly temporal resolution (good representativeness). Furthermore, due to the capacity of such samplers to work autonomously for long periods of time, the monitoring campaign had substantial reduction of maintenance costs of the samplers and associated costs.

2.3.2.1. High Spatial Resolution Samplers - Sampling and Analytical Procedures

The HSRS were equipped with PM_{10} sampling head filter system (filter holder diameter 37 mm) and with Teflon membrane filters (PTFE membranes, 37 mm diameter, 2 μm pore size, PALL Corporation, Port Washington, New York, NY, USA).

Chemical analysis of the PM samples was focused on the elemental content, using a chemical fractioning procedure that allowed us to discriminate water-soluble and insoluble fractions of the analysed elements (Canepari et al., 2006a; Canepari et al., 2006b).

Chemical fractioning is a two-step sequential leaching method consisting in the extraction in water of PM membrane filters and in the following digestion of the residue, combined with the multi-elemental determination of both the obtained water-soluble and insoluble fractions of PM. This approach, enables the assessment of the chemical form in which each element is released, which may be typical of its emission source (Templeton et al., 2000). The chemical fractioning procedure yields useful information about biogeochemical distribution, environmental mobility and bio-accessibility of the elements and proved to be valuable for increasing the selectivity of the elements as source tracers (Canepari et al., 2009; Perrino et al. 2010; Canepari et al., 2014). The procedure was applied to each PM membrane filter collected during the thirteen-month monitoring campaign.

Briefly, the supporting polymethylpentene ring was removed from each sampled Teflon membrane filter; then the PM membrane filters were extracted in 10 mL of deionized water (produced by Arioso UP 900 Integrate Water Purification System) by using an ultrasonic bath for 30 min. Subsequently, the extracted solutions were filtered on a cellulose nitrate filter (0.45 μm pore size, Merck Millipore Ltd., Billerica, MA, USA). After the extraction step, both the cellulose nitrate filter and the PM Teflon membrane filter were mineralized in a microwave oven (Ethos Touch Control with Q20 rotor, Milestone, Bergamo, Italy) by using 2 mL of ultrapure concentrated HNO_3 (67%; Promochem, LGC Standards GmbH, Wesel, Germany) and 1 mL of H_2O_2 (30%; Promochem, LGC Standards GmbH, Wesel, Germany). After the acid-digestion, the obtained solutions were diluted in 50 mL of deionized water and then filtered with syringe filters (25 mm diameter, 0.45 μm pore size, GVS Filter Technology, Morecambe, UK).

The concentration of 21 elements (As, Ba, Bi, Cd, Co, Cr, Cs, Cu, Fe, Mg, Mn, Mo, Nb, Ni, Pb, Rb, Sb, Sn, Ti, Tl, W) in the extracted and mineralized fractions of each sample was determined by using ICP-MS.

Details about the used instrumental conditions and the performances of the method are reported in Astolfi et al. (2018) and in Canepari et al. (2009), respectively.

2.4. Elaboration of the Data and Multivariate Statistical Analyses

Monthly accumulation of the elements in lichen samples was calculated by subtracting the initial element concentrations yielded at T0 in the samples of the control site (CTR), to the element concentrations determined in each lichen sample after five months (T1) and thirteen months (T2) of exposure and by normalizing the resulted values for the exposure months (T1-T0/5 and T2-T0/13).

The reliability of lichen transplants for high spatial resolution measurements of atmospheric element concentrations was evaluated through the comparison of the monthly bioaccumulation of the elements, with the mean values of the element concentrations founded in the PM_{10} sampled through HSRS, at T1 and at T2.

Pearson correlation coefficients between the spatial distribution of the element fractions (total, water-soluble and insoluble fractions) yielded through PM_{10} samplings and the spatial variability of the element concentrations accumulated in lichen samples were individuated at both T1 and T2.

Finally, multivariate statistical computations on the whole dataset were performed, using the statistical software R (R-project for statistical computing, Ver. 3.0, 32-bit), with the aim to identify the sites where the bioaccumulation of the elements was well correlated with the element concentrations obtained through PM_{10} samplings.

Concentration data yielded at each site after thirteen-month exposure (T2), through lichen transplant and HSRS (monthly mean values of the total element~~s~~ concentrations) samplings, were standardized and elaborated by using principal component analysis (PCA), which is considered a statistical tool able to discover structures in the experimental data (Brereton, 1990; Tabachnick and Fidell, 1996; Kannel et al., 2007; Conti et al., 2007; Zhou et al., 2007; Massimi et al., 2018).

3. Results and Discussion

3.1. Accumulation of the Elements in Lichen Transplants

Table 2 and Table 3 show the element concentrations determined in lichen samples of the control site (CTR) at T0 and in lichens exposed five months (T1) and thirteen months (T2) at the twenty-three sampling sites in Terni.

Results confirmed the data homogeneity for duplicate samples and the high repeatability of the chemical analyses. Standard deviations of the replicates (shown in supplementary material S1) were all below 20%; thus, we merged the data of duplicate samples. In Table 2 and in Table 3 are also reported the means (AM) and the standard deviations (SD) of the element concentrations determined at all the monitoring sites, at T1 and T2, respectively. Mean values (AM) represent the mean levels of the bioaccumulation of the elements in the Terni basin, while standard deviations (SD) represent the spatial variability of the elements bioaccumulated at the twenty-three sites.

Results show that the bioaccumulation levels of Cu in Terni are in good agreement with those determined in lichens of other urban environments of different geographical areas (Table 4; Ite et al., 2016; Liu et al., 2017; De La Cruz et al., 2018; comparisons are referred to d.w. basis). From Table 4, we can observe that Cu mean levels in Terni are slightly higher than in Cassino (Central Italy; Conti et al., 2004) while they are similar to those found at polluted traffic sites in Kaunas (Central Lithuania; Sujetoviene and Sliumpaite, 2013). Instead, lichens taken from the vicinity of the Bučim copper mine, located in the eastern region of the Republic of Macedonia, accumulated considerably higher Cu concentrations (highest value of 130 µg g^{-1}; Balabanova et al., 2012), as expected.

On the other hand, mean concentrations of cadmium and lead yielded in lichens in Terni are lower than those found in lichens of other urban and industrial areas (Table 4).

Lead values are very low if compared to *P. furfuracea* transplanted to Naples (Giordano et al., 2005). Besides, a remarkable decrease of Pb in lichens had been detected immediately after the ban of leaded gasoline (Loppi and Corsini, 2003; Loppi et al., 2004). A study conducted in Italy showed that Pb accumulation in lichens is not directly correlated to traffic (Paoli et al., 2013). These considerations agree with our results, which show that lichen transplants are not reliable for some elements emitted at low concentrations such as Pb.

Chromium concentrations bioaccumulated in Terni are higher than those measured in lichens of the Bučim copper mine (Balabanova, 2012) and of the industrial automobile factory of Piedimonte San Germano, where processes for reducing the use of metals in the production cycle had been implemented (Conti et al., 2004). The relevant Cr accumulation in Terni lichens (42 µg g^{-1} after thirteen months of exposure) well reflects the great amount of Cr (as well as of Co, Fe, Mn, Mo, Nb, Ni, Ti and W) that was released to the atmosphere by the steel plant (Massimi et al., 2017).

It is worth nothing that data comparison of Table 4 is of indicative value, due to different exposure time and the different species selected in the cited studies. However, it indicates (indirectly) that further research is needed in order to gain more information about exposure time and the species' selection.

The mean values (AM) reported in Table 2, show that after five months of exposure (T1), lichens transplanted to Terni did not accumulate Cd, Mg, Mn, Ni and Rb with respect to baseline data (T0; CTR). Instead, after thirteen months of exposure (Table 3; T2), lichens accumulated higher levels of all the analysed elements, with the exception of Cd. Cadmium was not bioaccumulated because it was not released at high concentrations by the main PM sources of the Terni basin, as reported in previous studies (Massimi et al., 2017).

Manganese and nickel, which were emitted at high concentrations by local emission sources (Massimi et al., 2017), were not bioaccumulated at T1 at most of the sites. High accumulation levels of Mn and Ni were measured only at monitoring sites in close proximity of the steel plant (RO, OB and PR).

A marked accumulation of Mg with respect to T0 was evidenced only at FA, CR, RO and PR, which are located in two different industrial areas in the West and in the East of the city (Fig. 1; Table 1).

Chromium, molybdenum, niobium and tungsten turned out to be the most bioaccumulated elements in Terni with respect to T0 baseline data, after five and after thirteen months of exposure. The high standard deviations of these elements (SD; Table 2 and Table 3) reveal high spatial variability of their concentrations, which is in agreement with the presence of an intense local PM emission source. In fact, Cr, Mo, Nb, and W were all emitted by the steel plant (Massimi et al., 2017), which is sited in the East of the city, between the monitoring sites RO, OB and PR. In lichens transplanted to these sites, Cr, Mo, Nb, and W were accumulated at the highest levels at both T1 and T2.

Cobalt, manganese, nickel and titanium are other elements released by steel plants (Querol et al., 2007; Taiwo et al., 2014; Owoade et al., 2015; Marcias et al., 2018). Also for these elements, the high standard deviations reveal high spatial variability, due to their high concentrations at RO, OB and PR.

Although Fe is another element emitted by the steel plant (Massimi et al., 2017), it was bioaccumulated at high levels at RO, OB and PR only after thirteen months of exposure. Iron concentration showed a different spatial profile with respect to Co, Cr, Mn, Mo, Nb, Ni, Ti and W, which are to be considered as the most selective steel plant tracers (Taiwo et al., 2014). In fact, Fe is also influenced by vehicular traffic and rail network emission sources; whereby, lichens accumulated high levels of Fe also at sampling sites close to the railway and to the heavily trafficked streets (GI, HV and CO).

The highest bioaccumulation levels of Co, Cr, Fe, Mn, Mo, Nb, Ni, Ti and W were found at RO, which is the closest site to the steel plant, while the highest concentrations of Nb and Ti were accumulated in lichens at PR, which is also in proximity of the industry. This behaviour may be due

to the presence of two or more different types of PM emission from the steel plant, which is related to different working processes, closer to RO or to PR.

Copper, antimony and tin, turned out to be other elements highly accumulated in lichens after five months and thirteen months of exposure. The lower SDs (Table 2 and Table 3) of Cu, Sb and Sn, respect to those of the elements emitted by the steel plant, reveal their lower spatial variability due to the presence of more distributed PM sources. In fact, high levels of Cu and Sb can be associated with rail network and vehicular traffic emissions. The railway is located between the monitoring sites GI, CR and HG, where Cu, Sb and Sn bioaccumulation levels were found higher with respect to T0, at both T1 and T2. Their concentrations increased, to a lesser extent, also at sites close to the heavily trafficked streets (SA, HV, UC, CA and CO). Therefore, differently to what was previously described for the steel plant tracers, for Cu, Sb and Sn, the differences in terms of bioaccumulation levels among the monitoring sites were found to be less marked, highlighting the role of vehicular traffic as the most distributed emission source of the city.

Results showed the highest bioaccumulation levels of Cu at GI, which is the closest site to the railway, and the highest bioaccumulation of Sb and Sn at CR, which is also in proximity of the rail network. The considerable accumulation increase of Cu, Sb and Sn, in lichens at sites closer to the railway than to heavily trafficked streets, reveals that these elements, through the biomonitoring, were found to be more efficient source tracers for the rail network than for vehicular traffic.

Finally, lichens transplanted to Terni were not able to accumulate high levels of elements emitted by the power plant, by industrial and domestic biomass heating and/or by other less intense emission sources (Ba, Bi, Cd, Cs, Mg, Pb, Rb and Tl). Therefore, through the biomonitoring technique, it was not possible to individuate elements tracers of these PM emission sources.

Overall, data underlined the outstanding bioaccumulation ability of *E. prunastri*, and, as a consequence, its aptitude to be used in biomonitoring studies.

Table 2. Elements concentrations (μg g^{-1} d.w.) yielded in lichen samples of the control site (CTR) at T0 and at the twenty-three monitoring sites in Terni after five months (T1) of exposure. AM and SD represent the mean values of the twenty-three monitoring sites and their standard deviations, respectively.

	As	Ba	Bi	Cd	Co	Cr	Cs	Cu	Fe	Mg	Mn	Mo	Nb	Ni	Pb	Rb	Sb	Sn	Ti	Tl	W
CTR	**0.11**	**8.7**	**0.013**	**0.13**	**0.27**	**1.4**	**0.085**	**3.1**	**619**	**609**	**22**	**0.12**	**0.065**	**6.3**	**1.5**	**3.2**	**0.060**	**0.18**	**24**	**0.011**	**0.0069**
RI	0.15	13	0.032	0.091	0.37	7.3	0.13	4.8	835	545	25	0.50	0.15	3.8	2.4	3.2	0.22	0.43	35	0.018	0.027
MA	0.073	11	0.031	0.052	0.23	11	0.087	3.8	664	413	18	0.39	0.10	2.9	1.1	2.5	0.12	0.36	26	0.014	0.015
FA	0.12	12	0.039	0.077	0.33	8.9	0.12	4.6	760	611	21	0.48	0.11	2.6	2.1	2.5	0.14	0.34	32	0.017	0.010
GI	0.12	14	0.048	0.10	0.42	40	0.12	8.0	795	565	28	0.80	0.16	3.9	2.3	3.4	0.24	0.65	27	0.016	0.21
FR	0.13	10	0.034	0.092	0.31	16	0.12	4.7	760	396	19	0.72	0.16	3.4	1.9	2.7	0.16	0.42	30	0.017	0.025
CB	0.050	6.8	0.016	0.051	0.17	4.3	0.063	3.9	423	332	11	0.32	0.074	2.1	1.7	1.7	0.11	0.23	19	0.010	0.0074
PI	0.091	11	0.018	0.061	0.25	3.4	0.091	3.8	593	467	15	0.24	0.08	1.8	2.6	2.2	0.090	0.25	23	0.015	0.010
BR	0.11	14	0.031	0.072	0.33	7.1	0.11	5.2	726	562	22	0.38	0.11	2.2	1.7	2.3	0.14	0.46	28	0.017	0.011
AR	0.10	7.0	0.015	0.030	0.15	3.1	0.062	4.5	525	460	12	0.27	0.09	1.9	1.0	2.1	0.089	0.28	19	0.010	0.0064
CR	0.082	17	0.051	0.082	0.36	11	0.11	6.0	735	660	31	0.61	0.13	3.4	2.3	3.4	0.21	0.86	25	0.015	0.030
HG	0.13	14	0.043	0.067	0.37	10	0.12	6.1	832	500	20	0.40	0.12	3.4	1.8	2.6	0.16	0.62	30	0.018	0.014
SA	0.14	10	0.022	0.061	0.29	3.5	0.090	3.6	763	544	18	0.34	0.093	1.9	1.2	2.6	0.09	0.29	23	0.011	0.010
PV	0.051	6.5	0.025	0.060	0.18	2.9	0.073	4.6	482	341	12	0.29	0.081	1.8	1.0	2.0	0.12	0.33	19	0.011	0.0085
LG	0.046	9.9	0.030	0.070	0.32	8.9	0.092	2.6	626	495	24	0.47	0.12	3.8	2.0	2.6	0.081	0.30	28	0.012	0.011
CZ	0.06	4.8	0.008	0.080	0.22	1.8	0.049	1.5	389	465	13	0.14	0.20	1.3	1.1	2.6	0.026	0.14	25	0.008	0.0072
HV	0.12	13	0.035	0.080	0.38	18	0.11	3.8	808	592	23	1.00	0.22	5.7	2.1	2.6	0.14	0.50	33	0.015	0.017
UC	0.12	11	0.028	0.046	0.32	18	0.094	4.0	795	565	20	0.80	0.16	3.9	1.3	2.0	0.14	0.35	27	0.016	0.031
CA	0.053	6.1	0.027	0.048	0.21	7.3	0.066	4.7	462	311	11	0.51	0.11	2.5	0.93	1.8	0.14	0.43	18	0.010	0.012
CO	0.076	9.7	0.025	0.039	0.25	7.0	0.082	4.8	592	434	15	0.57	0.11	3.1	1.3	2.2	0.12	0.38	25	0.013	0.012
RO	0.19	12	0.022	0.086	0.71	45	0.11	6.3	950	620	34	2.9	0.26	24	2.3	4.0	0.15	0.35	30	0.014	0.077
OB	0.17	11	0.033	0.082	0.55	42	0.12	5.0	898	596	30	1.9	0.36	13	2.4	3.3	0.18	0.34	33	0.017	0.039
PR	0.11	13	0.027	0.10	0.44	65	0.095	4.6	830	615	33	1.8	1.2	8.8	2.2	2.2	0.10	0.28	49	0.014	0.044
CP	0.078	10	0.020	0.057	0.19	11	0.077	3.8	625	522	19	0.85	0.22	3.3	1.2	2.3	0.12	0.27	26	0.013	0.013
AM	**0.12**	**11**	**0.031**	**0.084**	**0.32**	**15**	**0.10**	**4.5**	**688**	**498**	**21**	**0.71**	**0.18**	**4.5**	**3.0**	**2.7**	**0.14**	**0.42**	**27**	**0.015**	**0.030**
SD	**0.04**	**2.9**	**0.010**	**0.019**	**0.13**	**17**	**0.02**	**1.3**	**156**	**99**	**7**	**0.64**	**0.22**	**4.9**	**0.5**	**0.6**	**0.05**	**0.16**	**7**	**0.003**	**0.042**

Table 3. Elements concentrations (µg g^{-1} d.w.) yielded in lichen samples of the control site (CTR) at T0 and at the twenty-three monitoring sites in Terni after thirteen months (T2) of exposure. AM and SD represent the mean values of the twenty-three monitoring sites and their standard deviations, respectively.

	As	Ba	Bi	Cd	Co	Cr	Cs	Cu	Fe	Mg	Mn	Mo	Nb	Ni	Pb	Rb	Sb	Sn	Ti	Tl	W
CTR	**0.11**	**8.7**	**0.013**	**0.13**	**0.27**	**1.4**	**0.085**	**3.1**	**619**	**609**	**22**	**0.12**	**0.065**	**6.3**	**1.5**	**3.2**	**0.060**	**0.18**	**24**	**0.011**	**0.0069**
RI	0.32	20	0.058	0.10	0.54	17	0.17	6.3	1121	669	36	0.99	0.29	5.4	3.7	3.2	0.37	0.74	39	0.022	0.048
MA	0.16	13	0.183	0.078	0.33	19	0.12	5.8	774	531	21	0.80	0.19	4.2	2.0	2.7	0.28	0.60	31	0.022	0.041
FA	0.44	18	0.058	0.092	0.46	17	0.17	6.1	1093	705	30	0.80	0.19	4.9	3.2	3.2	0.25	0.57	39	0.024	0.036
GI	0.27	25	0.088	0.12	0.69	94	0.20	11	1375	879	47	1.9	0.28	7.6	3.8	4.5	0.35	1.1	45	0.029	0.33
FR	0.31	21	0.052	0.11	0.54	26	0.19	5.6	1228	909	35	1.0	0.24	5.4	3.4	3.4	0.21	0.59	45	0.026	0.043
CB	0.34	16	0.041	0.090	0.50	19	0.15	7.8	1061	1106	32	1.3	0.24	6.5	3.2	3.2	0.24	0.56	40	0.024	0.037
PI	0.27	26	0.032	0.083	0.38	9.8	0.16	4.9	919	677	21	0.78	0.17	3.9	4.7	2.7	0.24	0.61	32	0.022	0.031
BR	0.33	17	0.062	0.094	0.47	13	0.18	6.7	1179	736	29	0.79	0.20	3.9	2.8	3.4	0.24	0.79	43	0.026	0.028
AR	0.14	9.4	0.026	0.058	0.25	6.8	0.10	5.3	625	534	17	0.42	0.11	6.8	1.3	2.3	0.15	0.37	23	0.014	0.024
CR	0.16	39	0.141	0.11	0.50	32	0.16	8.5	1073	907	40	1.3	0.25	6.2	3.7	3.8	0.40	1.5	37	0.022	0.047
HG	0.26	21	0.089	0.087	0.42	28	0.14	8.5	1039	568	25	1.0	0.25	5.1	2.6	2.7	0.36	1.3	38	0.021	0.040
SA	0.26	15	0.036	0.075	0.36	8	0.11	4.6	840	833	24	0.70	0.15	3.4	1.9	2.7	0.14	0.47	28	0.017	0.024
PV	0.23	16	0.054	0.073	0.38	11	0.15	6.5	942	657	24	0.83	0.18	4.0	2.4	2.9	0.27	0.81	34	0.020	0.029
LG	0.31	16	0.056	0.088	0.55	22	0.18	4.5	1172	793	41	1.2	0.25	7.0	3.4	3.8	0.14	1.1	47	0.022	0.032
CZ	0.17	13	0.016	0.11	0.36	2.5	0.11	3.0	857	683	23	0.16	0.23	1.5	2.2	3.0	0.07	0.22	41	0.016	0.022
HV	0.22	21	0.051	0.11	0.53	39	0.14	5.1	1106	649	30	1.4	0.37	10	3.2	2.7	0.19	0.65	39	0.017	0.031
UC	0.20	14	0.054	0.068	0.47	26	0.13	5.4	963	686	27	1.6	0.35	9.6	2.5	2.1	0.20	0.59	33	0.018	0.050
CA	0.16	13	0.183	0.078	0.33	19	0.12	5.8	774	531	21	0.80	0.19	4.2	2.0	2.7	0.28	0.60	31	0.022	0.041
CO	0.33	15	0.069	0.068	0.46	29	0.12	8.5	955	681	26	1.8	0.32	11	2.0	2.2	0.35	1.1	29	0.016	0.051
RO	0.62	17	0.050	0.12	2.9	274	0.15	10	3415	885	81	14	1.91	133	3.6	4.3	0.25	0.91	45	0.021	0.34
OB	0.41	18	0.060	0.11	1.1	103	0.21	7.5	1800	813	54	3.8	0.94	35	4.2	5.1	0.48	0.65	55	0.022	0.13
PR	0.35	18	0.053	0.12	0.75	184	0.14	5.4	1281	1018	63	3.4	2.48	16	4.0	2.8	0.17	0.48	94	0.021	0.10
CP	0.25	12	0.029	0.079	0.30	16	0.10	4.6	745	564	23	1.2	0.32	4.0	1.9	2.4	0.14	0.32	30	0.017	0.028
AM	**0.31**	**18**	**0.069**	**0.11**	**0.58**	**42**	**0.15**	**6.4**	**1130**	**729**	**33**	**1.7**	**0.42**	**13**	**4.5**	**3.3**	**0.25**	**0.76**	**39**	**0.022**	**0.070**
SD	**0.11**	**6**	**0.044**	**0.02**	**0.53**	**65**	**0.03**	**1.9**	**553**	**158**	**15**	**2.7**	**0.58**	**27**	**0.9**	**0.8**	**0.10**	**0.31**	**14**	**0.004**	**0.088**

Table 4. Accumulation levels of Cu, Cd, Cr and Pb in lichens (µg g^{-1}) in Terni (mean levels at T1 and at T2) and in other urban and industrial environments of different geographical areas (comparisons are referred to d.w. basis).

Study Area	References	Lichen	Exposure Time	Cu	Cd	Cr	Pb
Pistoia (Italy)	Loppi and Corsini, 2003	*Parmelia caperata*	~ 1 year	8,4 - 15,3	0,24 - 0,95	2,1 - 2,2	16,2 - 24,8
Cassino (Italy)	Conti et al., 2004	*Evernia prunastri*	1 - 12 months	2 - 4,5	0,1 - 0,2	1,2 -2,5	3 - 6
Piedimonte San Germano (Italy)	Conti et al., 2004	*Evernia prunastri*	1 - 12 months	2 - 6	0,15 - 0,2	1,5 - 2	3 - 7
Montecatini Terme (Italy)	Loppi et al., 2004	*Flavoparmelia caperata*	~ 1 year	11,7 - 18,9	0,33 -0,52	2,2 - 3,2	35,3 - 66,7
Naples (Italy)	Giordano et al., 2005	*Pseudevernia furfuracea*	2 - 4 months	17,1 - 41,4	0,6 - 0,7	2,5 - 4,3	32 - 55
Bučim Mine (Macedonia)	Balabanova et al., 2012	*Evernia prunastri*	Not reported	1,5 - 130	0,05 - 0,38	1,0 - 6,9	0,61 - 120
Siena (Italy)	Paoli et al., 2013	*Punctelia borreri*	~ 1 year	6,0 - 7,6	0,19 - 0,20	1,1 - 1,4	5,8 - 6,0
Kaunas (Lithuania)	Sujetoviene and Sliumpaite, 2013	*Evernia prunastri*	5 weeks	4 - 7	0,18	-	5 - 7
Terni (Italy)	This work	*Evernia prunastri*	5 - 12 months	4,5 - 6,4	0,084 - 0,11	15 - 42	3 - 4,5

3.2. Reliability Evaluation of Lichen Transplants for High Spatial Resolution Measurements of PM_{10} Elemental Components

Accumulation of the elements in lichen samples after five months (T1) and thirteen months (T2) of exposure was compared with the mean values of the element concentrations founded in the PM_{10} sampled during the two monitoring periods.

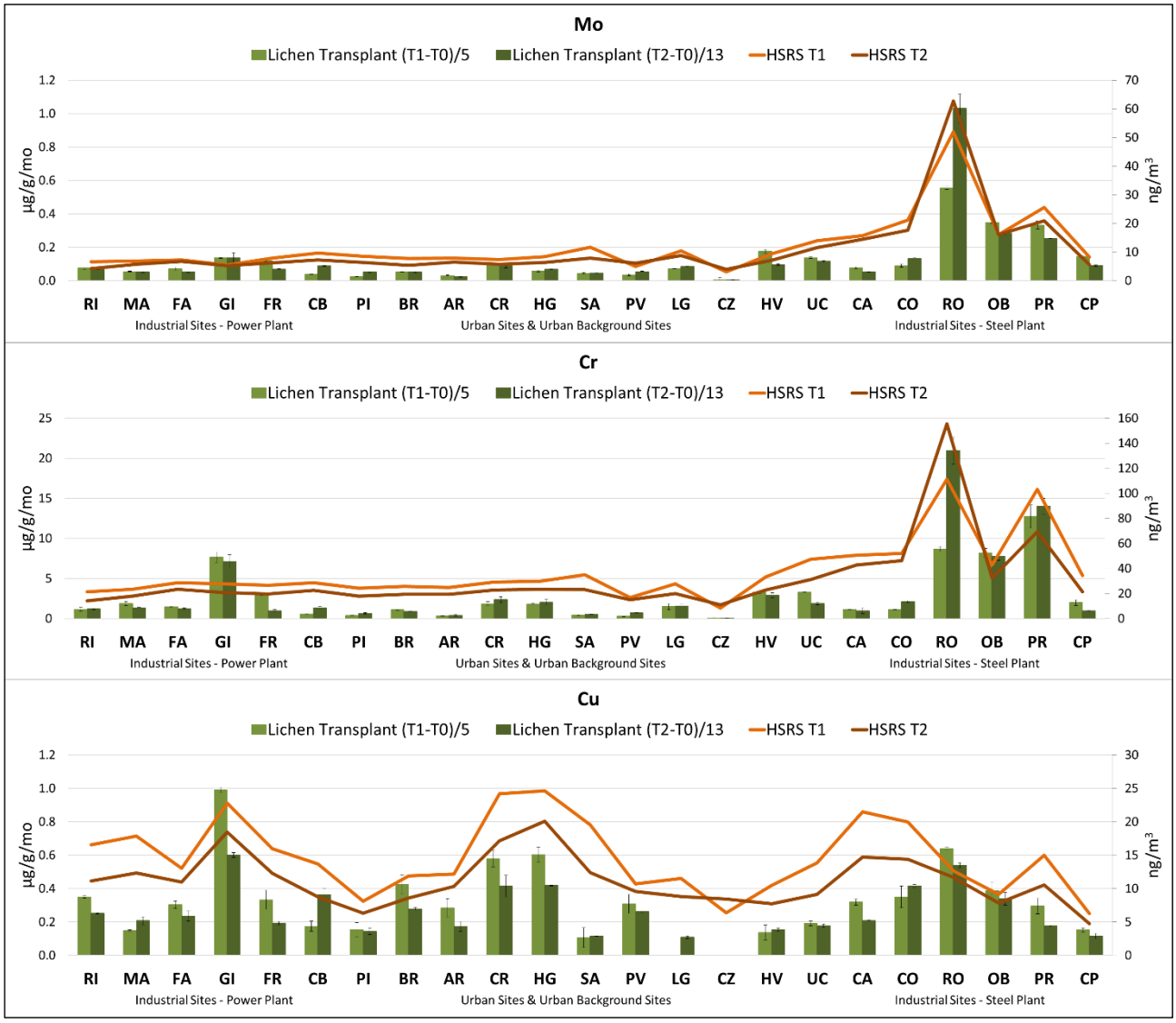

Fig. 3. Comparison of Mo, Cr and Cu accumulation in lichen samples after five months (T1) and thirteen months (T2) of exposure with their mean concentrations measured in PM_{10} during five (HSRS T1) and thirteen (HSRS T2) months.

In Fig. 3, we can observe the comparison between the monthly accumulation of Mo, Cr and Cu in lichen samples and the mean values of the total concentrations of Mo, Cr and Cu in the PM_{10} sampled

by HSRS during T1 and T2. Fig.s related to the other examined elements are reported in supplementary material S3.

Bioaccumulation data were found to be reliable for high spatial resolution measurements of some of the PM_{10} elemental components emitted at high concentrations by the steel plant: Cr, Mo (upper and middle panel of Fig. 3), Nb and Ni (middle panels of Fig. S3.3), and quite reliable for As, Co, Fe, Mn and W (Fig.s S3). For these elements, the spatial representativeness of the bioaccumulation data appeared to be quite good after five months (T1) as well as after thirteen months (T2) of exposure.

On the contrary, lichen transplants were found to be less reliable for spatially-resolved analyses of the elements released by vehicular traffic: Cu (lower panel of Fig. 3), Sb and Sn (middle panels of Fig. S3.4). Through the biomonitoring, spatial variability of these elements appeared to be more related with the rail network than with vehicular traffic PM_{10} source. In fact, lichen transplants accumulated high concentrations of Cu, Sb and Sn only at the sites closest to the railway (GI, CR and HG) and lower concentrations at sites in proximity of the trafficked and heavily trafficked streets (SA, HV, UC, CA and CO).

Data in Fig. 3 also show that Cr (as well as Co, Fe, Mn, Mo, Nb, Ni, Ti and W of Fig.s S3) was accumulated at high levels at GI, where its concentration in PM_{10}, determined through HSRS samplings, was low. The same happened to Cu (as well as to Sb and Sn of Fig. S3.4), which was accumulated at high levels at RO, even if the Cu concentration found in the PM_{10} at this site was low. Hence, lichens transplanted to RO and GI (the most affected sites by the contribution from the steel plant and the rail network, respectively), accumulated high concentrations of elements released by other farther emission sources.

This behaviour may be due to the stress conditions of the lichens exposed to high element concentrations. Stress conditions probably led lichens to be less selective in the accumulation of the elements. This behaviour, which merits further investigation, decreased the spatial representativeness of the obtain data and seems to reduce the potential of lichen transplants for the assessment of the spatial variability of atmospheric element concentrations, questioning their reliability for high spatial resolution measurements of PM elemental components.

3.2.1. Correlations Between the Spatial Variability of the Element Concentrations Determined through Lichen Transplant and HSRS Samplings

The reliability of lichen transplants for high spatial resolution measurements of atmospheric element concentrations was evaluated through the individuation of the Pearson correlation coefficients, calculated between the element concentrations (total, water-soluble and insoluble fractions) found in

the PM_{10} sampled by HSRS and the accumulation of the elements in lichen samples at T1 and T2 (Fig. 4). Coefficients higher than 0.7 (good correlation) indicate the reliability of transplanted lichens as biomonitors for the assessment of the spatial variability of the element total concentrations and of the element water-soluble and/or insoluble fractions.

From Fig. 4, we can observe that lichen transplants were found to be efficient biomonitors for the evaluation of the spatial variability of the total concentrations of Cr, Mo, Nb and Ni, after five months (T1) as well as after thirteen months (T2) of exposure.

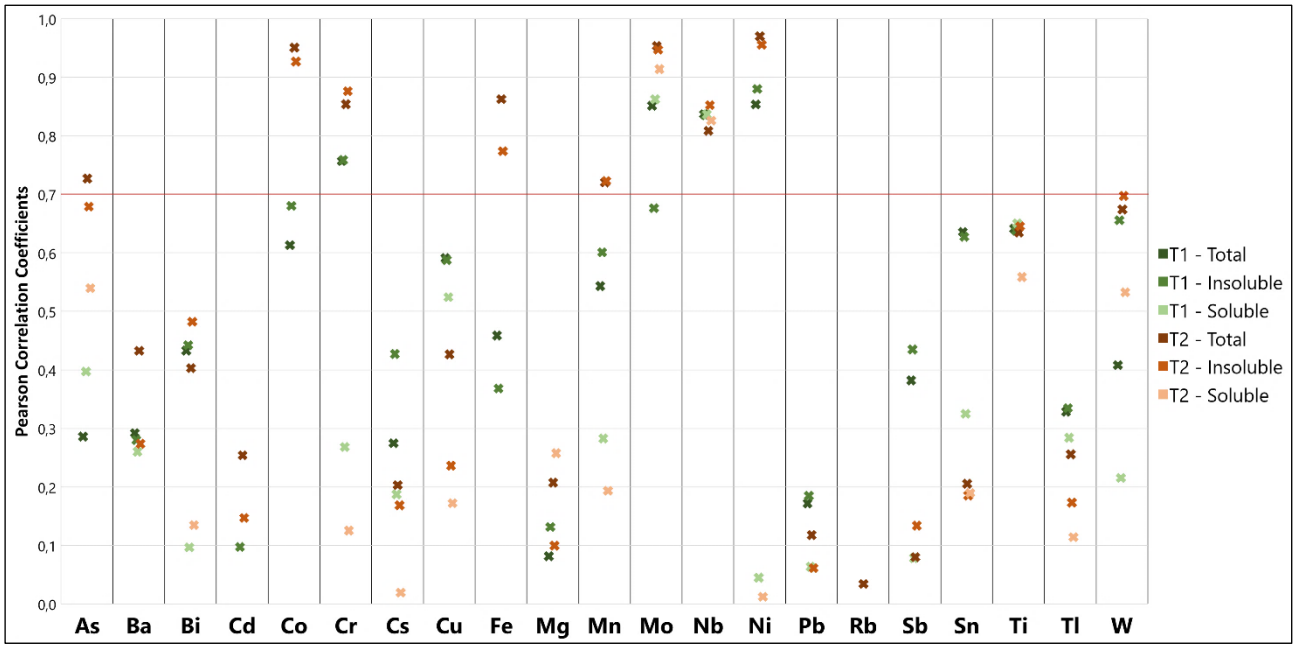

Fig. 4. Pearson correlation coefficients between the spatial variability of the element fractions yielded through HSRS samplings of PM_{10} and the accumulation of the elements in lichen samples after five months (T1) and thirteen months (T2) of exposure.

Chromium and nickel bioaccumulation is well correlated only with the total and residual fractions of these elements as they were emitted almost entirely as insoluble species by the steel plant (Massimi et al., 2017).

On the contrary, Mo and Nb bioaccumulation shows good correlations also with their water-soluble fractions.

Bioaccumulation of As, Co, Fe, Mn and W across the twenty-three monitoring sites shows good correlations with all the analysed fractions only at T2, because the increase of the steel plant activity during the last monitoring period led to a major bioaccumulation of these elements after thirteen months (T2) of exposure. At T2, As and W show quite good correlations with all the fractions while

Co, Fe, Mn show good correlations only with the total and residual fractions; also in this case, these correlations reflect the solubility of the species emitted by the steel plant (Massimi et al., 2017) and do not indicate a significant selectivity of the lichens toward water-soluble or insoluble fractions of the elements.

Copper and tin show quite good correlations and antimony weak correlations with the total and insoluble fractions only at T1; this is probably due to the higher contribution of the rail network and vehicular traffic emission sources during the first monitoring period. We can also observe that Cu, Sb and Sn bioaccumulation is less correlated with their water-soluble fractions, because these elements were released mostly as insoluble species by the mechanical abrasion of car and train brakes (Massimi et al., 2017).

Finally, Ba, Cd, Cs, Mg, Pb, Rb and Tl accumulation levels are poorly correlated with their concentrations in the PM_{10}, because lichen samples did not accumulate high levels of these elements.

3.2.2. Principal Component Analysis on the Element Concentrations Determined through Lichen Transplants and HSRS Samplings

Multivariate statistical computations on the two datasets were performed to classify the monitoring sites according to the element concentrations obtained through lichen transplant and HSRS samplings, considered simultaneously.

Concentration data yielded at each site through HSRS (monthly mean values of the total elements concentrations) and lichen samplings at T2 were standardized and analysed by principal component analysis (PCA).

The PCA was operated in order to identify correlations between the bioaccumulation of the elements and the element concentrations in the PM_{10} and to assess the lichen transplant reliability for the individuation of the elements tracers of PM emission sources.

Five significant components accounting for 89.92% were obtained; the variance explained by each component is 41.21%, 29.58%, 10.92%, 4.72% and 3.49%. The second and the third PCs (PC2 and PC3), which explain the 40.5% of the total variance, were considered. PCA results are summarized in the biplot and in the score plot of Fig. 5.

Loadings and scores of the five significant components obtained by the PCA are reported in Table 5.

The second group of Fig. 5, on the left upper part of the biplot, is composed of elements mainly released by the rail network and vehicular traffic: Cu, Sb, Sn and by Bi, Cd, Mn, Pb and Ti. Copper, antimony and tin are considered to be reliable tracers of these two emission sources; in fact, they are

generally released by mechanical abrasion of car and train brakes (Weckwerth, 2001; Abbasi et al., 2012; Querol et al., 2012; Kam et al., 2013; Namgung et al., 2016).

Finally, the third group, on the central left part of the biplot, is composed of elements which did not show high spatial variability across the twenty-three sampling sites: Ba, Cs, Mg, Rb and Tl.

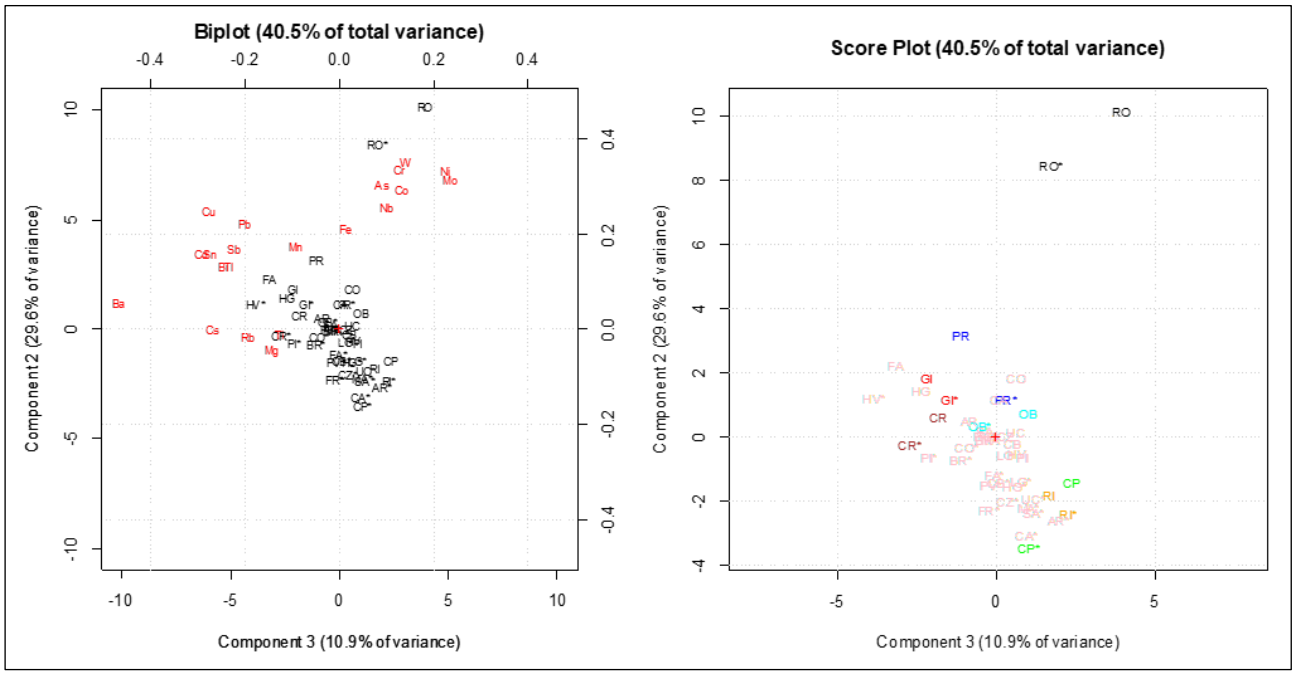

Fig. 5. Biplot and score plot of the PCA (PC2 and PC3) performed on the concentration data yielded at each site through lichen transplant and HSRS (monthly mean values of the total element concentrations) samplings at thirteen-month exposure (T2).

From Fig. 5, we can observe that RO, which is the closest site to the steel plant, is plotted on the right upper part of the biplot because at this site the highest concentrations of As, Co, Cr, Fe, Mo, Nb, Ni and W were found through both lichen transplant and HSRS samplings. PR, which is another site in proximity of the steel plant, is also plotted on the direction of these elements. Instead, GI and CR, which are the closest sites to the railway, where the highest concentrations of Cu, Sb and Sn where found, are plotted on the left upper part of the biplot, on the direction of these elements.

From the score plot of Fig. 5, we can observe, highlighted in different colours, the sampling sites where we found a similar variability of the element concentrations through the two monitoring techniques.

Table 5. Loadings and scores of the five significant components (accounting for 89.92%) obtained by the PCA performed on the concentration data yielded at each site through lichen transplant (marked with the asterisk; e.g. RO*, GI*, PR* etc.) and HSRS (without the asterisk; e.g. RO, GI, PR etc.) samplings at T2.

Loadings					
	PC1	PC2	PC3	PC4	PC5
As	0,168	0,304	0,092	0,219	0,125
Ba	-0,157	0,056	-0,469	-0,106	0,081
Bi	0,249	0,132	-0,245	-0,133	-0,134
Cd	-0,133	0,158	-0,296	0,498	0,077
Co	-0,197	0,296	0,133	-0,138	0,129
Cr	-0,130	0,337	0,128	-0,169	-0,273
Cs	-0,283	0,001	-0,270	0,045	0,189
Cu	0,158	0,250	-0,276	-0,338	0,154
Fe	-0,272	0,210	0,013	-0,170	0,148
Mg	-0,317	-0,043	-0,142	0,009	0,069
Mn	-0,291	0,176	-0,092	-0,070	-0,121
Mo	0,072	0,316	0,237	0,236	0,229
Nb	-0,168	0,257	0,099	-0,053	-0,636
Ni	-0,109	0,333	0,225	-0,102	0,157
Pb	0,069	0,223	-0,199	0,563	-0,217
Rb	-0,305	-0,015	-0,196	-0,017	0,266
Sb	0,275	0,169	-0,224	-0,154	-0,036
Sn	0,259	0,158	-0,275	-0,241	-0,034
Ti	-0,306	-0,010	-0,129	0,006	-0,320
Tl	0,257	0,134	-0,235	0,092	-0,071
W	0,045	0,352	0,139	0,024	0,228

Scores											
	PC1	PC2	PC3	PC4	PC5		PC1	PC2	PC3	PC4	PC5
RI	2,169	-1,803	1,639	-1,015	-0,277	RI*	0,576	-2,390	2,263	-1,429	-0,769
MA	3,129	-0,081	-0,186	-0,470	-0,262	MA*	-0,668	-2,219	1,036	-0,524	-0,157
FA	3,767	2,250	-3,164	1,292	-0,248	FA*	-2,068	-1,151	-0,055	0,016	0,464
GI	4,158	1,833	-2,176	-1,360	0,288	GI*	-3,397	1,159	-1,475	-0,707	0,951
FR	2,867	0,013	-0,284	-0,256	-0,151	FR*	-3,171	-2,269	-0,221	1,004	0,049
CB	2,397	-0,199	0,488	0,373	-0,195	CB*	-2,727	-1,437	0,065	-0,172	0,423
PI	2,023	-0,645	0,823	0,346	-0,121	PI*	-3,421	-0,623	-2,089	1,140	0,648
BR	2,552	-0,084	-0,386	0,092	-0,112	BR*	-3,134	-0,712	-1,093	0,221	0,644
AR	2,980	0,498	-0,837	0,057	-0,104	AR*	-0,970	-2,605	1,973	0,060	0,305
CR	3,592	0,648	-1,818	-1,910	-0,457	CR*	-2,655	-0,252	-2,676	-1,091	0,275
HG	3,682	1,440	-2,393	-1,822	0,073	HG*	-1,157	-1,504	0,589	-0,501	-0,131
SA	2,683	0,189	-0,397	0,071	-0,271	SA*	-1,969	-2,350	1,166	0,600	0,323
PV	2,785	0,039	-0,474	-0,604	-0,095	PV*	-2,005	-1,488	-0,177	-0,146	0,367
LG	1,937	-0,556	0,266	1,106	0,006	LG*	-2,097	-1,394	0,793	-0,025	-0,043
CZ	2,886	0,038	0,310	-0,864	-0,019	CZ*	-2,429	-2,019	0,352	0,746	0,376
HV	2,102	-0,504	0,641	0,493	-0,157	HV*	-5,562	1,190	-3,831	0,871	0,704
UC	2,145	0,147	0,595	0,523	-0,015	UC*	-1,735	-1,914	1,197	-0,109	0,058
CA	2,676	1,176	0,087	0,228	0,026	CA*	-0,906	-3,072	0,974	0,157	-0,443
CO	2,501	1,833	0,610	-0,463	0,340	CO*	-2,732	-0,293	-0,906	-0,072	0,528
RO	0,741	10,141	3,925	0,984	1,675	RO*	-7,817	8,456	1,747	-2,008	-0,293
OB	1,864	0,730	1,007	0,996	0,296	OB*	-3,627	0,362	-0,514	-0,562	-0,458
PR	1,544	3,163	-1,109	3,784	-1,434	PR*	-4,931	1,154	0,316	0,093	-4,274
CP	1,882	-1,427	2,358	0,398	-0,378	CP*	-0,462	-3,470	1,040	0,459	2,046

Lichen transplants were found to be reliable for high spatial resolution measurements of PM_{10} elemental components and for the individuation of the elements tracers of PM emission sources at RO, PR, OB, GI, CR, CP and RI.

At RO, PR and OB, the highest concentrations of As, Co, Cr, Fe, Mo, Nb, Ni and W were found in lichen samples as well in PM_{10} samples; at GI and CR, the highest concentrations of Cu, Sb and Sn were yielded through both the monitoring techniques and at CP and RI, the lowest concentrations of all these elements were found.

Correlations between the element concentrations obtained through lichen and HSRS samplings were not found at sites affected by vehicular traffic such as HV, UC, CA and CO.

Overall, multivariate statistical computations on the two datasets confirmed that lichen transplants are reliable for high spatial resolution measurements of PM_{10} elemental components emitted at high concentrations by local PM emission sources.

4. Conclusions

The employment of the high spatial resolution samplers (HSRS) along with lichen transplants, allowed us to evaluate the potential of the biomonitors for spatially-resolved analyses of atmospheric element concentrations and for the individuation of the elements tracers of PM emission sources.

In this study we enriched the requisite variety (21 elements in 23 monitoring sites) in order to confirm the reliability of lichens as biomonitors of a complex system such as the environment.

Overall, bioaccumulation of the elements was found to be well correlated with the element concentrations obtained through HSRS samplings of PM_{10} at sites closest to the main local PM emission sources of Terni.

Lichen transplants appeared to be reliable for high spatial resolution measurements of PM_{10} elemental components emitted at high concentrations by intense local PM emission sources such as the steel plant (Co, Cr, Fe, Mn, Mo, Nb, Ni, Ti and W) and the rail network (Cu, Sb and Sn), less reliable for spatially-resolved analyses of elements released by vehicular traffic (Cu, Sb and Sn) and not reliable for other elements emitted by the power plant, by industrial and domestic biomass heating and/or by other less intense emission sources (Ba, Bi, Cd, Cs, Mg, Pb, Rb and Tl).

In general, bioaccumulation of the elements appeared to be more correlated with the total and insoluble fractions of the analysed elements than with the water-soluble one. However, these correlations reflect the solubility of the chemical species emitted by the main local PM emission sources and do not indicate a significant selectivity of the lichens toward water-soluble or insoluble fractions of the elements.

Lichens transplanted to sites where PM_{10} element concentrations were particularly high, appeared to be in stress conditions which led them to be less selective in the accumulation of the elements. This behaviour, which merits further investigation, decreased the spatial representativeness of the obtained data and seems to reduce the potential of lichens for the assessment of the spatial variability of atmospheric element concentrations.

The two monitoring techniques, based on the acquisition of spatially resolved data for the evaluation of the spatial variability of PM_{10} and its elemental chemical components, may be integrated in the future to be even more effective and robust for the validation and optimization of dispersion models, without the high costs associated with an air quality monitoring network based on traditional PM samplers.

Acknowledgements

This work was funded by the project 2015 C26H15TY3S (Principal Investigator Prof. M.E. Conti) and by the project 2017 RG11715C7C8801CF (Principal Investigator Dr. S. Canepari), financed by Sapienza University of Rome. The authors gratefully thank FAI Instruments (Fonte Nuova, Rome, Italy), the citizens of Terni and the Terni district of ARPA Umbria (regional agency for environmental protection) with special regard to Giancarlo Caiello, Caterina Austeri and Marco Pompei for the support in the installation and in the management of the sampling equipment as well as for the help in the choice of the sampling sites.

Author Contributions

L. Massimi, M.E. Conti, M. Ristorini and S. Canepari conceived and planned the monitoring and the experiments; M.E. Conti and G. Mele collected the lichens and prepared the samples; L. Massimi, G. Mele, M. Ristorini and M.L. Astolfi performed the samplings and the chemical analyses; L. Massimi elaborated the data and wrote the manuscript; M.E. Conti and S. Canepari coordinated the group and supervised the manuscript.

Conflicts of Interest

The authors declare no conflicts of interest.

References

Abbasi, S., Olander, L., Larsson, C., Olofsson, U., Jansson, A., & Sellgren, U. (2012). A field test study of airborne wear particles from a running regional train. *Proceedings of the Institution of Mechanical Engineers, Part F: Journal of Rail and Rapid Transit*, *226*(1), 95-109.

Almeida, S. M., Pio, C. A., Freitas, M. C., Reis, M. A., & Trancoso, M. A. (2006). Source apportionment of atmospheric urban aerosol based on weekdays/weekend variability: evaluation of road re-suspended dust contribution. *Atmospheric Environment*, *40*(11), 2058-2067.

Ashby, W.R. (1960). *An Introduction to Cybernetics*, Chapman & Hall, London, UK.

Astolfi, M. L., Marconi, E., Protano, C., Vitali, M., Schiavi, E., Mastromarino, P., & Canepari, S. (2018). Optimization and validation of a fast digestion method for the determination of major and trace elements in breast milk by ICP-MS. *Analytica Chimica Acta*.

Balabanova, B., Stafilov, T., Sajn, R., & Baceva, K. (2012). Characterisation of heavy metals in lichen species *Hypogymnia physodes* and *Evernia prunastri* due to biomonitoring of air pollution in the vicinity of copper mine. *International Journal of Environmental Research*, *6*(3), 779-794.

Bari, A., Rosso, A., Minciardi, M. R., Troiani, F., & Piervittori, R. (2001). Analysis of heavy metals in atmospheric particulates in relation to their bioaccumulation in explanted *Pseudevernia furfuracea* thalli. *Environmental Monitoring and Assessment*, *69*(3), 205-220.

Bargagli, R., & Nimis, P. L. (2002). Guidelines for the use of epiphytic lichens as biomonitors of atmospheric deposition of trace elements. In *Monitoring with Lichens-Monitoring Lichens*(pp. 295-299). Springer, Dordrecht.

Bocca, B., Conti, M. E., Pino, A., Mattei, D., Forte, G., & Alimonti, A. (2007). Simple, fast, and low-contamination microwave-assisted digestion procedures for the determination of chemical elements in biological and environmental matrices by sector field ICP-MS. *International Journal of Environmental and Analytical Chemistry*, *87*(15), 1111-1123.

Brereton, R. G. (1990). *Chemometrics: applications of mathematics and statistics to laboratory systems*. Ellis Horwood Ltd, Chichester, UK.

Canepari, S., Cardarelli, Giuliano, A., E., Pietrodangelo, A. (2006). Determination of metals, metalloids and non-volatile ions in airborne particulate matter by a new two-step sequential leaching procedure Part A: Experimental design and optimization. *Talanta*, *69*(3), 581-587.

Canepari, S., Cardarelli, E., Pietrodangelo, A., & Strincone, M. (2006). Determination of metals, metalloids and non-volatile ions in airborne particulate matter by a new two-step sequential leaching procedure: Part B: Validation on equivalent real samples. *Talanta*, *69*(3), 588-595.

Canepari, S., Pietrodangelo, A., Perrino, C., Astolfi, M. L., & Marzo, M. L. (2009). Enhancement of source traceability of atmospheric PM by elemental chemical fractionation. *Atmospheric Environment*, *43*(31), 4754-4765.

Canepari, S., Astolfi, M. L., Farao, C., Maretto, M., Frasca, D., Marcoccia, M., & Perrino, C. (2014). Seasonal variations in the chemical composition of particulate matter: a case study in the Po Valley. Part II: concentration and solubility of micro-and trace-elements. *Environmental Science and Pollution Research*, *21*(6), 4010-4022.

Cercasov, V., Pantelică, A., Sălăgean, M., Caniglia, G., & Scarlat, A. (2002). Comparative study of the suitability of three lichen species to trace-element air monitoring. *Environmental Pollution*, *119*(1), 129-139.

Conti, M. E., & Cecchetti, G. (2001). Biological monitoring: lichens as bioindicators of air pollution assessment—a review. *Environmental pollution*, *114*(3), 471-492.

Conti, M. E. (2002). Il monitoraggio biologico della qualità ambientale. SEAM. Rome, 180 pp. ISBN: 888179411X

Conti, M. E., Tudino, M. B., Muse, J. O., & Cecchetti, G. (2002). Biomonitoring of heavy metals and their species in the marine environment: the contribution of atomic absorption spectroscopy and inductively coupled plasma spectroscopy. *Trends in Applied Spectroscopy*, *4*, 295-324.

Conti, M. E., Tudino, M., Stripeikis, J., & Cecchetti, G. (2004). Heavy metal accumulation in the lichen *Evernia prunastri* transplanted at urban, rural and industrial sites in Central Italy. *Journal of Atmospheric Chemistry*, *49*(1-3), 83-94.

Conti, M. E., Iacobucci, M., Cucina, D., & Mecozzi, M. (2007). Multivariate statistical methods applied to biomonitoring studies. *International journal of environment and pollution*, *29*(1-3), 333-343.

Conti, M. E. (2008). *Biological monitoring: theory & applications: bioindicators and biomarkers for environmental quality and human exposure assessment* (Vol. 17). WIT Press.

Conti, M. E., Finoia, M. G., Bocca, B., Mele, G., Alimonti, A., & Pino, A. (2012). Atmospheric background trace elements deposition in Tierra del Fuego region (Patagonia, Argentina), using transplanted *Usnea barbata* lichens. *Environmental monitoring and assessment*, *184*(1), 527-538.

Conti, M. E. & Tudino, M. (2016). Lichens as biomonitors of heavy-metal pollution (Chapter 6). *Comprehensive Analytical Chemistry: The Quality of Air*, *73*, 117-145.

Conti, M. E., Jasan, R., Finoia, M. G., Iavicoli, I., & Plá, R. (2016). Trace elements deposition in the Tierra del Fuego region (south Patagonia) by using lichen transplants after the Puyehue-Cordón Caulle (north Patagonia) volcanic eruption in 2011. *Environmental Science and Pollution Research*, *23*(7), 6574-6583.

De La Cruz, A. R. H., De La Cruz, J. K. H., Tolentino, D. A., & Gioda, A. (2018). Trace element biomonitoring in the Peruvian Andes metropolitan region using *Flavoparmelia caperata* lichen. *Chemosphere*, *210*, 849-858.

Ferrero, L., Cappelletti, D., Moroni, B., Sangiorgi, G., Perrone, M. G., Crocchianti, S., & Bolzacchini, E. (2012). Wintertime aerosol dynamics and chemical composition across the mixing layer over basin valleys. *Atmospheric environment*, *56*, 143-153.

Folkeson, L. (1979). Interspecies calibration of heavy-metal concentrations in nine mosses and lichens: Applicability to deposition measurements. *Water, Air, and Soil Pollution*, *11*(2), 253-260.

Fox, D. G. (1984). Uncertainty in air quality modelling. *Bulletin of the American Meteorological Society*, *65*(1), 27-36.

Garty, J. (2001). Biomonitoring atmospheric heavy metals with lichens: theory and application. *Critical reviews in plant sciences*, *20*(4), 309-371.

Giordano, S., Adamo, P., Sorbo, S., & Vingiani, S. (2005). Atmospheric trace metal pollution in the Naples urban area based on results from moss and lichen bags. *Environmental Pollution*, *136*(3), 431-442.

Guerrini, R. (2012). Qualità dell'aria nella provincia di Terni tra il 2002 e il 2011. *Quad ARPA Umbria*, 81-87.

Hwang, I., & Hopke, P. K. (2007). Estimation of source apportionment and potential source locations of PM2.5 at a west coastal IMPROVE site. *Atmospheric Environment*, *41*(3), 506-518.

Irwin, J. S. (2014). A suggested method for dispersion model evaluation. *Journal of the Air & Waste Management Association*, *64*(3), 255-264.

Ite, A. E., Ubong, U. U., Etesin, U. M., Nsi, E. W., Ukpong, E. J., Ekanem, A. N., Ufot, U. F., & Udo, A. I. (2016). Heavy metals in epiphytic lichens and mosses of Oil–Producing communities of Eket and Ibeno, Akwa Ibom State–Nigeria. *Am. J. Environ. Prot*, *4*, 38-47.

Jeran, Z., Jaćimović, R., Batič, F., & Mavsar, R. (2002). Lichens as integrating air pollution monitors. *Environmental Pollution*, *120*(1), 107-113.

Kam, W., Delfino, R. J., Schauer, J. J., & Sioutas, C. (2013). A comparative assessment of PM 2.5 exposures in light-rail, subway, freeway, and surface street environments in Los Angeles and estimated lung cancer risk. *Environmental Science: Processes & Impacts*, *15*(1), 234-243.

Kannel, P. R., Lee, S., Kanel, S. R., & Khan, S. P. (2007). Chemometric application in classification and assessment of monitoring locations of an urban river system. *Analytica Chimica Acta*, *582*(2), 390-399.

Kim, B. U., Bae, C., Kim, H. C., Kim, E., & Kim, S. (2017). Spatially and chemically resolved source apportionment analysis: Case study of high particulate matter event. *Atmospheric Environment*, *162*, 55-70.

Liu, H. J., Wang, J. G., Xia, Y., Yang, M. J., Liu, S. W., Zhao, L. C., Guo, X. P., Jiang, Y. J., Li, X., Wu, Q. F., & Fang, S. B. (2017). Elemental compositions of lichens from Duolun County, Inner Mongolia, China: Origin, road effect and species difference. *Scientific Reports*, *7*(1), 5598.

Loppi, S., & Corsini, A. (2003). Diversity of epiphytic lichens and metal contents of Parmelia caperata thalli as monitors of air pollution in the town of Pistoia (C Italy). *Environmental Monitoring and Assessment*, *86*(3), 289-301.

Loppi, S., Frati, L., Paoli, L., Bigagli, V., Rossetti, C., Bruscoli, C., & Corsini, A. (2004). Biodiversity of epiphytic lichens and heavy metal contents of Flavoparmelia caperata thalli as indicators of temporal variations of air pollution in the town of Montecatini Terme (central Italy). *Science of the Total Environment*, *326*(1-3), 113-122.

Marcias, G., Fostinelli, J., Catalani, S., Uras, M., Sanna, A. M., Avataneo, G., De Palma, D., Fabbri, G., Paganelli, M., Lecca, L. I., Buonanno, G., & Campagna, M. (2018). Composition of Metallic Elements and Size Distribution of Fine and Ultrafine Particles in a Steelmaking Factory. *International journal of environmental research and public health*, *15*(6).

Massimi, L., Ristorini, M., Eusebio, M., Florendo, D., Adeyemo, A., Brugnoli, D., & Canepari, S. (2017). Monitoring and evaluation of Terni (Central Italy) air quality through spatially resolved analyses. *Atmosphere*, *8*(10), 200.

Massimi, L., Giuliano, A., Astolfi, M. L., Congedo, R., Masotti, A., & Canepari, S. (2018). Efficiency evaluation of food waste materials for the removal of metals and metalloids from complex multi-element solutions. *Materials*, *11*(3), 334.

Moroni, B., Ferrero, L., Crocchianti, S., Perrone, M. G., Sangiorgi, G., Bolzacchini, E., & Cappelletti, D. (2013). Aerosol dynamics upon Terni basin (Central Italy): results of integrated vertical profile measurements and electron microscopy analyses. *Rendiconti Lincei*, *24*(4), 319-328.

Namgung, H. G., Kim, J. B., Woo, S. H., Park, S., Kim, M., Kim, M. S., Bae, G. N., Park, D., & Kwon, S. B. (2016). Generation of nanoparticles from friction between railway brake disks and pads. *Environmental science & technology*, *50*(7), 3453-3461.

Owoade, K. O., Hopke, P. K., Olise, F. S., Ogundele, L. T., Fawole, O. G., Olaniyi, B. H., Jegede, O. O., Ayoola, M. A., & Bashiru, M. I. (2015). Chemical compositions and source identification of particulate matter (PM2.5 and PM2.5–10) from a scrap iron and steel smelting industry along the Ife–Ibadan highway, Nigeria. *Atmospheric Pollution Research*, *6*(1), 107-119.

Paoli, L., Munzi, S., Fiorini, E., Gaggi, C., & Loppi, S. (2013). Influence of angular exposure and proximity to vehicular traffic on the diversity of epiphytic lichens and the bioaccumulation of traffic-related elements. *Environmental Science and Pollution Research*, *20*(1), 250-259.

Pantelica, A., Cercasov, V., Steinnes, E., Bode, P., & Wolterbeek, H. T. (2016). Determination of 54 elements in lichen transplants: Comparison of INAA, ICPMS, and EDXRF. *Rom. Journ. Phys*, *61*(7-8), 1380-1388.

Perrino, C., Canepari, S., Pappalardo, S., & Marconi, E. (2010). Time-resolved measurements of water-soluble ions and elements in atmospheric particulate matter for the characterization of local and long-range transport events. *Chemosphere*, *80*(11), 1291-1300.

Perrino, C., Catrambone, M., Dalla Torre, S., Rantica, E., Sargolini, T., & Canepari, S. (2014). Seasonal variations in the chemical composition of particulate matter: a case study in the Po Valley. Part I: macro-components and mass closure. *Environmental Science and Pollution Research*, *21*(6), 3999-4009.

Pignata, M. L., Plá, R. R., Jasan, R. C., Martinez, M. S., Rodriguez, J. H., Wannaz, E. D., Gudino, G. L., Carreras, H. A., & Gonzalez, C. M. (2007). Distribution of atmospheric trace elements and assessment of air quality in Argentina employing the lichen, *Ramalina celastri*, as a passive biomonitor: detection of air pollution emission sources. *International Journal of Environment and Health*, *1*(1), 29-46.

Pilegaard, K. (1979). Heavy metals in bulk precipitation and transplanted *Hypogymnia physodes* and *Dicranoweisia cirrata* in the vicinity of a Danish steelworks. *Water, Air, and Soil Pollution*, *11*(1), 77-91.

Pino, A., Alimonti, A., Botrè, F., Minoia, C., Bocca, B., & Conti, M. E. (2007). Determination of twenty-five elements in lichens by sector field inductively coupled plasma mass spectrometry and microwave-assisted acid digestion. *Rapid communications in mass spectrometry*, *21*(12), 1900-1906.

Pino, A., Alimonti, A., Conti, M. E., & Bocca, B. (2010). Iridium, platinum and rhodium baseline concentration in lichens from Tierra del Fuego (South Patagonia, Argentina). *Journal of Environmental Monitoring*, *12*(10), 1857-1863.

Querol, X., Viana, M., Alastuey, A., Amato, F., Moreno, T., Castillo, S., Pey, J., de la Rosa, J., Sánchez de la Campa, A., Artíñano, B., Salvador, P., García Dos Santos, S., Fernández-Patier, R., Moreno-Grau, S., Negral, L., Minguillón, M. C., Monfort, E., Gil, J. I., Inza, A., Ortega, L. A., Santamaría, J. M., & Zabalza, J. (2007). Source origin of trace elements in PM from regional background, urban and industrial sites of Spain. *Atmospheric Environment*, *41*(34), 7219-7231

Querol, X., Moreno, T., Karanasiou, A., Reche, C., Alastuey, A., Viana, M., Font, O., Gil, J., de Miguel, E., & Capdevila, M. (2012). Variability of levels and composition of PM 10 and PM 2.5 in the Barcelona metro system. *Atmospheric Chemistry and Physics*, *12*(11), 5055-5076.

Sloof, J. E., & Wolterbeek, B. T. (1993). Interspecies comparison of lichens as biomonitors of trace-element air pollution. *Environmental monitoring and assessment*, *25*(2), 149-157.

Sloof, J. E. (1995). Pattern recognition in lichens for source apportionment. *Atmospheric Environment*, *29*(3), 333-343.

State, G., Popescu, I., Gheboianu, A., Radulescu, C., Dulama, I., Bancuta, I., & Stirbescu, R. (2011). Identification of air pollution elements in lichens used as bioindicators, by the XRF and AAS methods. *Spectroscopy (ICP-AES)*, *7*, 13.

Sujetoviene, G., & Sliumpaite, I. (2013). Response of *Evernia prunastri* transplanted to an urban area in central Lithuania. *Atmospheric Pollution Research*, *4*(2), 222-228.

Taiwo, A. M., Harrison, R. M., & Shi, Z. (2014). A review of receptor modelling of industrially emitted particulate matter. *Atmospheric environment*, *97*, 109-120.

Tabachnick, B. G., & Fidell, L. S. (1996). Using Multivariate Statistics, 3rd ed. Harper Collins. *New York.*

Templeton, D. M., Ariese, F., Cornelis, R., Danielsson, L. G., Muntau, H., van Leeuwen, H. P., & Lobinski, R. (2000). Guidelines for terms related to chemical speciation and fractionation of elements. Definitions, structural aspects, and methodological approaches (IUPAC Recommendations 2000). *Pure and applied chemistry*, *72*(8), 1453-1470.

Vannini, A., Paoli, L., Nicolardi, V., Di Lella, L. A., & Loppi, S. (2017). Seasonal variations in intracellular trace element content and physiological parameters in the lichen *Evernia prunastri* transplanted to an urban environment. *Acta Botanica Croatica*, *76*(2), 171-176.

Vitali, L., Morabito, A., Adani, M., Assennato, G., Ciancarella, L., Cremona, G., Giua, R., Pastore, T., Piersanti, A., Righini, G., Russo, F., Spagnolo, S., Tanzarella, A., Tinarelli, G., & Zanini, G. (2016). A Lagrangian modelling approach to assess the representativeness area of an industrial air quality monitoring station. *Atmospheric Pollution Research, 7*(6), 990-1003.

Wadleigh, M. A., & Blake, D. M. (1999). Tracing sources of atmospheric sulphur using epiphytic lichens. *Environmental Pollution, 106*(3), 265-271.

Weckwerth, G. (2001). Verification of traffic emitted aerosol components in the ambient air of Cologne (Germany). *Atmospheric environment*, *35*(32), 5525-5536.

Wolterbeek, B. (2002). Biomonitoring of trace element air pollution: principles, possibilities and perspectives. *Environmental pollution*, *120*(1), 11-21.

Wolterbeek, H. T., Garty, J., Reis, M. A., & Freitas, M. C. (2003). Biomonitors in use: lichens and metal air pollution. In *Trace metals and other contaminants in the environment* (Vol. 6, pp. 377-419). Elsevier.

Zhou, F., Guo, H., & Hao, Z. (2007). Spatial distribution of heavy metals in Hong Kong's marine sediments and their human impacts: a GIS-based chemometric approach. *Marine Pollution Bulletin*, *54*(9), 1372-1384.

Supplementary material S1.

Chemical determinations were conducted on two independent sub-samples taken from each lichen sample at T0, T1 and T2 (duplicate samples). Results of Tables S1.1 and S1.2 confirmed the data homogeneity for duplicate samples; standard deviations of the replicates, which are all below 20%, shows that good precision was attained for all the measurements.

Table S1.1. Percent standard deviations of the element concentrations (%) yielded in duplicate lichen samples of the control site (CTR) at T0 and after five months (T1) of exposure. AM represents the mean of the percent standard deviations yielded at all the monitoring sites at T1.

	As	Ba	Bi	Cd	Co	Cr	Cs	Cu	Fe	Mg	Mn	Mo	Nb	Ni	Pb	Rb	Sb	Sn	Ti	Tl	W
	SD%	SD%	SD%	SD%	SD%	SD%	SD%	SD%	SD%	SD%	SD%	SD%	SD%	SD%	SD%	SD%	SD%	SD%	SD%	SD%	SD%
CTR	5,33	11,0	3,6	6,8	6,2	4,2	7,5	0,1	6,7	4,3	6,3	5,2	5,3	2,0	8,9	8,2	11,4	2,8	6,6	7,5	15,8
RI	1.3	10.1	6.1	13.6	9.0	17.3	8.7	0.7	6.0	8.5	9.2	8.0	14.1	17.9	8.4	10.2	19.5	10.0	14.5	11.3	16.3
MA	19.6	2.7	3.4	11.8	1.5	12.4	0.9	0.7	0.4	2.1	1.8	2.9	9.0	1.6	2.1	1.1	5.6	0.4	5.8	0.7	10.2
FA	5.1	11.2	13.2	2.5	9.3	1.1	8.0	7.8	6.9	8.4	7.7	8.0	2.9	5.2	8.1	0.9	13.6	9.4	2.6	8.0	14.4
GI	10.2	4.6	0.2	5.6	0.6	8.2	0.4	1.1	0.5	0.8	0.8	2.2	2.4	0.9	1.3	3.5	1.9	1.0	4.0	4.7	1.1
FR	9.0	16.1	13.1	15.3	5.0	2.2	5.7	6.9	5.4	4.3	5.6	4.4	4.2	8.3	6.2	1.6	13.9	6.7	2.8	7.8	4.2
CB	10.5	15.8	4.0	5.8	1.3	4.9	1.9	3.8	1.4	1.9	0.8	1.0	17.7	15.6	2.0	1.2	19.1	6.0	2.4	4.6	19.3
PI	6.5	10.9	8.6	3.6	4.8	1.0	6.5	5.5	5.2	6.5	6.4	0.9	8.5	10.1	2.9	12.9	3.5	2.0	4.7	8.2	1.4
BR	17.9	5.2	1.6	6.4	1.8	4.9	1.0	5.7	1.4	3.7	2.3	2.0	0.7	4.3	2.1	5.1	10.2	1.7	2.1	0.6	9.3
AR	13.5	8.6	4.9	14.9	6.1	2.8	9.6	6.1	8.2	5.9	7.6	4.7	3.5	8.3	6.3	3.8	10.4	4.2	2.1	3.6	19.0
CR	18.3	8.6	5.4	6.7	7.1	12.4	5.8	5.5	6.4	5.9	20.0	3.4	2.2	4.7	7.2	9.0	0.1	7.4	7.9	3.2	9.6
HG	7.3	7.2	11.2	6.0	12.0	5.5	7.4	4.9	7.7	5.8	6.0	4.0	5.7	12.3	12.2	7.7	11.1	12.9	6.2	12.1	5.0
SA	6.5	9.8	9.2	3.5	10.7	8.3	12.2	12.4	11.1	10.7	10.7	7.6	7.1	9.3	13.2	7.0	11.3	9.7	11.5	6.3	12.3
PV	16.9	19.8	18.4	9.4	9.3	0.0	8.4	10.1	10.2	9.8	10.0	10.6	5.4	13.9	7.6	10.2	17.5	9.1	4.8	8.3	11.5
LG	14.1	13.0	3.4	1.3	2.7	16.9	1.4	0.8	0.6	0.7	0.5	1.3	6.4	14.7	0.9	1.6	16.6	6.0	14.5	0.3	3.8
CZ	8.5	15.4	11.1	4.5	4.4	10.0	2.8	12.7	3.0	1.9	2.4	12.7	2.1	10.6	4.5	2.1	10.5	9.7	5.5	0.4	6.9
HV	2.9	10.7	6.6	14.9	7.1	5.5	3.3	17.1	4.8	4.8	4.3	5.7	3.3	14.3	7.4	5.8	5.6	6.0	2.6	0.5	8.0
UC	13.9	5.0	0.9	3.0	0.8	0.6	0.3	1.8	0.2	0.7	0.4	2.4	2.7	4.2	0.2	3.8	1.6	0.0	5.7	1.1	1.7
CA	15.8	9.8	0.6	2.3	3.8	2.3	2.0	2.0	3.9	1.9	3.4	4.7	1.7	2.6	4.7	2.6	8.3	6.2	5.7	0.2	7.0
CO	14.5	12.7	13.0	11.3	9.9	2.0	10.6	6.8	9.9	9.2	9.3	8.0	2.2	4.7	9.0	7.5	9.3	9.7	0.8	5.5	0.4
RO	9.5	8.5	5.8	0.3	1.1	3.7	2.9	0.7	2.5	3.8	1.6	1.5	1.5	6.1	0.5	3.4	9.7	0.7	1.1	8.6	4.7
OB	5.2	10.1	0.9	10.6	1.0	6.3	2.7	9.8	3.3	4.0	3.0	1.4	2.3	2.1	2.7	6.3	7.2	3.8	2.0	4.2	5.6
PR	16.0	12.5	11.4	9.8	8.6	11.2	8.7	7.8	8.4	7.0	0.3	6.6	6.3	10.4	7.1	12.1	7.3	8.7	7.3	10.6	18.3
CP	9.7	6.7	0.2	7.5	1.6	15.5	0.6	1.5	1.5	2.2	2.4	3.2	9.3	3.5	2.1	3.6	5.4	1.7	11.2	0.6	9.8
AM	**11.0**	**10.2**	**6.6**	**7.4**	**5.2**	**6.7**	**4.8**	**5.7**	**4.7**	**4.8**	**5.1**	**4.7**	**5.3**	**8.1**	**5.2**	**5.3**	**9.5**	**5.8**	**5.5**	**4.8**	**8.7**

Table S1.2. Percent standard deviations of the element concentrations (%) yielded in duplicate lichen samples of the control site (CTR) at T0 and after thirteen months (T2) of exposure. AM represents the mean of the percent standard deviations yielded at all the monitoring sites at T2.

	As	Ba	Bi	Cd	Co	Cr	Cs	Cu	Fe	Mg	Mn	Mo	Nb	Ni	Pb	Rb	Sb	Sn	Ti	Tl	W
	SD%	SD%	SD%	SD%	SD%	SD%	SD%	SD%	SD%	SD%	SD%	SD%	SD%	SD%	SD%	SD%	SD%	SD%	SD%	SD%	SD%
RI	17.2	2.2	0.5	15.3	1.4	5.8	2.8	0.4	1.6	1.0	0.1	2.5	14.6	0.5	1.9	3.4	4.9	3.9	10.1	4.6	9.9
MA	17.4	10.8	13.4	9.8	6.3	3.7	5.3	5.4	5.6	4.2	3.7	5.5	9.9	5.1	7.4	4.2	0.0	5.1	16.7	4.2	7.5
FA	11.5	6.2	11.4	3.8	6.2	9.0	8.7	6.2	5.4	6.4	6.2	5.0	5.5	8.3	5.8	11.2	1.9	8.8	8.0	4.3	1.7
GI	15.2	4.5	10.4	2.6	1.2	11.4	1.9	1.7	0.8	2.0	0.5	11.0	6.3	3.1	1.9	4.2	3.7	0.2	3.3	3.0	7.2
FR	7.3	3.2	0.8	6.2	2.3	5.7	2.7	2.4	2.3	3.9	1.9	3.0	4.4	2.8	2.0	4.2	0.4	3.3	2.6	1.2	12.1
CB	14.8	2.2	1.0	11.6	4.5	12.6	3.1	6.8	2.9	3.5	2.8	3.3	2.8	7.6	2.4	9.5	1.6	0.7	9.0	6.1	6.5
PI	13.0	7.0	6.2	16.6	5.3	11.9	9.1	5.1	6.9	7.0	6.3	5.5	3.1	3.6	7.2	3.5	5.5	7.0	1.1	14.3	13.0
BR	13.8	4.8	5.8	4.3	2.7	2.3	7.3	1.7	3.8	5.3	4.3	4.9	3.0	2.6	3.7	9.5	4.6	4.9	1.4	6.5	1.5
AR	13.4	1.9	5.8	11.4	7.4	13.9	4.8	7.0	6.1	6.7	6.8	6.8	8.7	5.6	9.2	5.6	5.8	8.7	8.6	12.4	0.8
CR	19.9	10.3	10.1	0.4	12.1	14.9	10.1	10.0	10.2	10.8	10.7	10.2	7.9	12.7	9.7	10.8	8.5	7.4	0.2	9.8	18.4
HG	16.5	1.9	2.2	2.1	1.2	17.8	2.3	0.4	0.1	0.7	0.1	2.2	4.7	3.2	8.2	1.0	2.0	0.0	10.5	3.6	5.3
SA	3.8	2.4	3.1	9.9	3.8	0.9	1.2	0.3	1.5	2.3	2.4	2.3	0.0	0.4	1.8	1.2	4.8	4.7	2.9	1.1	5.3
PV	0.2	1.6	0.4	6.5	0.4	2.4	2.5	1.7	1.2	0.9	1.2	5.0	5.5	3.4	2.8	0.7	3.3	4.4	5.9	9.6	3.1
LG	4.0	1.5	1.4	2.0	2.7	16.6	1.5	2.3	0.7	0.0	0.6	1.6	0.8	3.1	1.1	1.9	9.9	1.2	7.6	8.5	10.6
CZ	12.3	1.7	5.8	10.2	0.0	6.7	5.0	4.0	0.7	1.0	1.4	9.7	16.4	6.4	2.8	6.4	4.9	3.8	19.3	9.2	5.4
HV	5.8	5.8	8.9	0.3	2.7	9.2	3.7	2.9	4.5	4.2	5.4	4.7	0.0	1.6	5.4	4.6	13.9	4.7	0.7	4.8	17.2
UC	2.7	2.3	14.5	1.1	2.3	7.3	0.5	2.6	1.3	1.1	0.8	3.3	7.2	3.2	1.4	0.3	0.9	0.9	8.1	7.2	13.3
CA	14.1	2.5	2.7	14.2	2.0	15.1	1.5	0.9	1.9	1.8	1.5	0.9	9.2	6.4	1.4	3.8	6.7	2.5	0.7	2.5	15.2
CO	7.3	6.6	0.6	10.6	7.7	6.2	4.3	1.4	2.7	3.4	3.1	4.5	6.2	4.1	3.6	8.0	2.7	5.0	1.7	5.7	8.0
RO	4.1	9.3	2.5	11.9	5.6	16.2	0.4	1.9	2.7	2.1	2.5	8.4	5.8	5.1	2.3	0.2	1.4	1.5	2.7	9.7	6.2
OB	4.2	1.6	8.2	13.5	1.7	6.7	0.2	6.6	0.4	0.4	0.7	3.0	0.0	2.7	0.4	6.0	1.6	1.3	1.9	3.9	3.9
PR	13.9	2.5	6.9	4.0	4.0	6.9	2.0	0.9	0.8	0.6	0.5	0.6	0.4	3.0	0.2	0.3	3.4	0.7	0.9	3.8	13.6
CP	3.3	1.4	11.0	3.5	3.4	0.5	3.0	4.6	2.5	1.9	1.9	5.2	2.5	1.1	4.2	1.7	1.7	3.3	3.7	5.9	3.9
AM	**10.2**	**4.1**	**5.8**	**7.5**	**3.8**	**8.9**	**3.7**	**3.4**	**2.9**	**3.1**	**2.8**	**4.7**	**5.4**	**4.2**	**3.8**	**4.4**	**4.1**	**3.7**	**5.6**	**6.2**	**8.2**

Supplementary material S2.

The certified reference material BCR 482 lichen (IRMM, Geel, Belgium) was used to validate the entire analytical process and to test the accuracy of the measurements. All results were in good agreement with certified values. For non-certified elements, the standard deviations showed good results (T1 vs. T2 differences are lower tha SD of each data set).

Table S2.1. Mean values, standard deviations and recovery percentages (%) of the element concentrations obtained in duplicate lichen samples of the certified reference material BCR 482 lichen (IRMM, Geel, Belgium). Analyses of BCR were introduced in each set of field samples analyses (four replicates at T1 and four replicates at T2).

***Evernia prunastri* - BCR 482 (µg g^{-1}d.w.)**

		Certified Value		Obtained Value T1			Obtained Value T2		
	UoM	AM	± SD	AM	± SD	R (%)	AM	± SD	R (%)
As	µg g^{-1}	**0,85**	± 0,07	**0,78**	± 0,04	92 %	**0,82**	± 0,05	97 %
Ba	µg g^{-1}			**9,7**	± 1,0		**11,1**	± 0,8	
Bi	µg g^{-1}			**0,099**	± 0,002		**0,102**	± 0,004	
Cd	µg g^{-1}	**0,56**	± 0,02	**0,53**	± 0,02	95 %	**0,57**	± 0,02	102 %
Co	µg g^{-1}			**0,29**	± 0,01		**0,30**	± 0,02	
Cr	µg g^{-1}	**4,1**	± 0,2	**3,0**	± 0,1	72 %	**3,1**	± 0,2	80 %
Cs	µg g^{-1}			**0,20**	± 0,01		**0,21**	± 0,01	
Cu	µg g^{-1}	**7,0**	± 0,2	**6,8**	± 0,2	97 %	**6,7**	± 0,2	95 %
Fe	µg g^{-1}			**775**	± 26		**791**	± 7	
Mg	µg g^{-1}			**460**	± 13		**477**	± 25	
Mn	µg g^{-1}			**29**	± 1		**30**	± 0,3	
Mo	µg g^{-1}			**0,47**	± 0,02		**0,50**	± 0,03	
Nb	µg g^{-1}			**0,082**	± 0,002		**0,089**	± 0,002	
Ni	µg g^{-1}	**2,5**	± 0,1	**2,3**	± 0,1	92 %	**2,4**	± 0,1	97 %
Pb	µg g^{-1}	**41**	± 1	**38**	± 1	93 %	**41**	± 4	99 %
Rb	µg g^{-1}			**7,3**	± 0,5		**7,6**	± 0,1	
Sb	µg g^{-1}			**0,27**	± 0,01		**0,29**	± 0,01	
Sn	µg g^{-1}			**1,6**	± 0,1		**1,8**	± 1,0	
Ti	µg g^{-1}			**26**	± 1		**28**	± 1	
Tl	µg g^{-1}			**0,044**	± 0,003		**0,048**	± 0,003	
W	µg g^{-1}			**0,078**	± 0,005		**0,081**	± 0,001	

Supplementary Material S3.

From Fig.s S3 we can observe the comparison between the monthly accumulation of the elements in lichen samples and the mean values of the total element concentrations in the PM_{10} sampled by HSRS during the two exposure periods. Element concentrations yielded in lichens at T0 baseline data (CTR) were subtracted to those determined at T1 and T2, the obtained values were then normalized for the exposure months (T1-T0/5 and T2-T0/13).

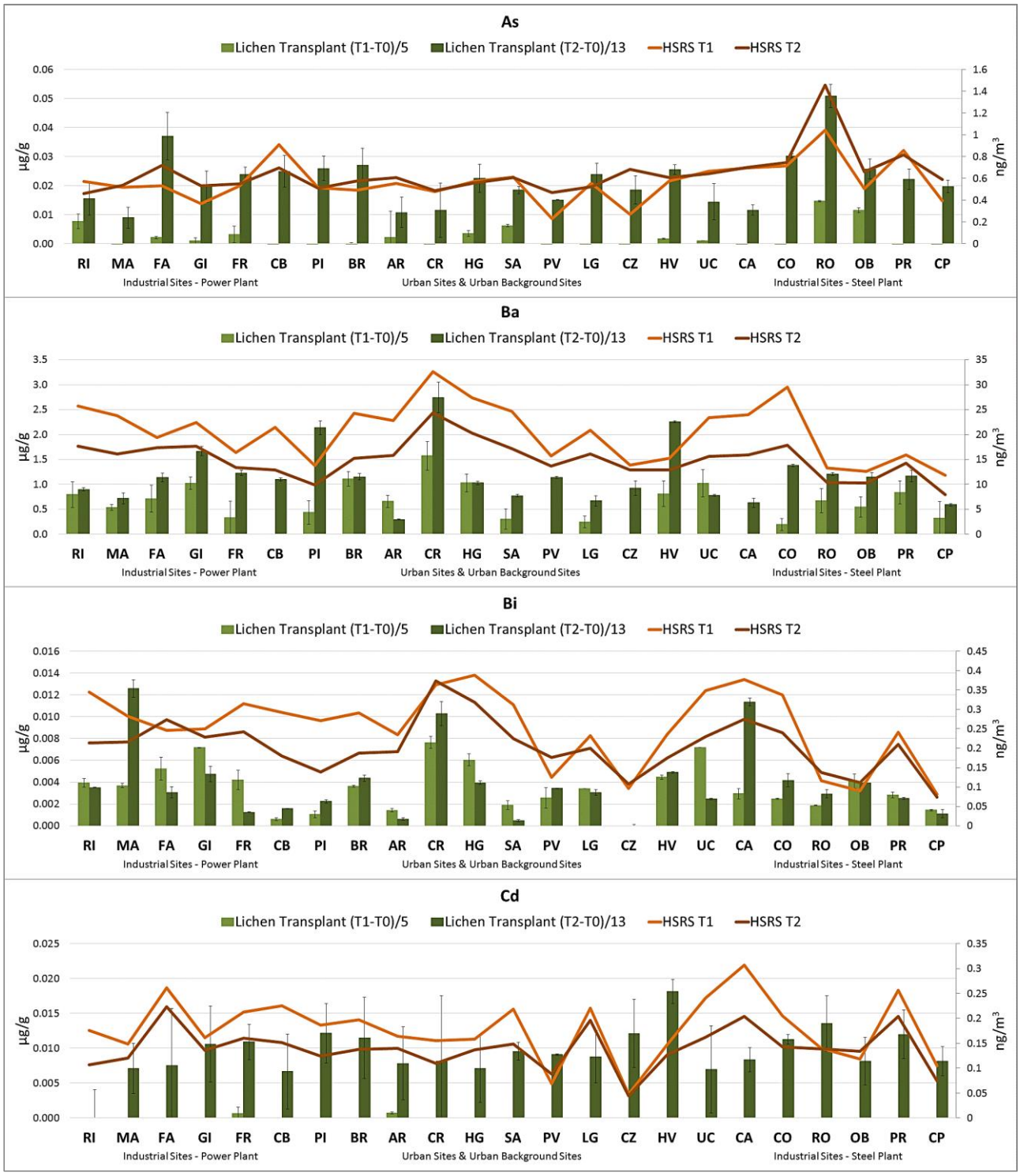

Fig. S3.1. Comparison of As, Ba, Bi and Cd accumulation in lichen samples after five months (T1) and thirteen months (T2) of exposure with their mean concentrations measured in PM_{10} during five (HSRS T1) and thirteen (HSRS T2) months.

Fig. S3.2. Comparison of Co, Cs, Fe and Mg accumulation in lichen samples after five months (T1) and thirteen months (T2) of exposure with their mean concentrations measured in PM_{10} during five (HSRS T1) and thirteen (HSRS T2) months.

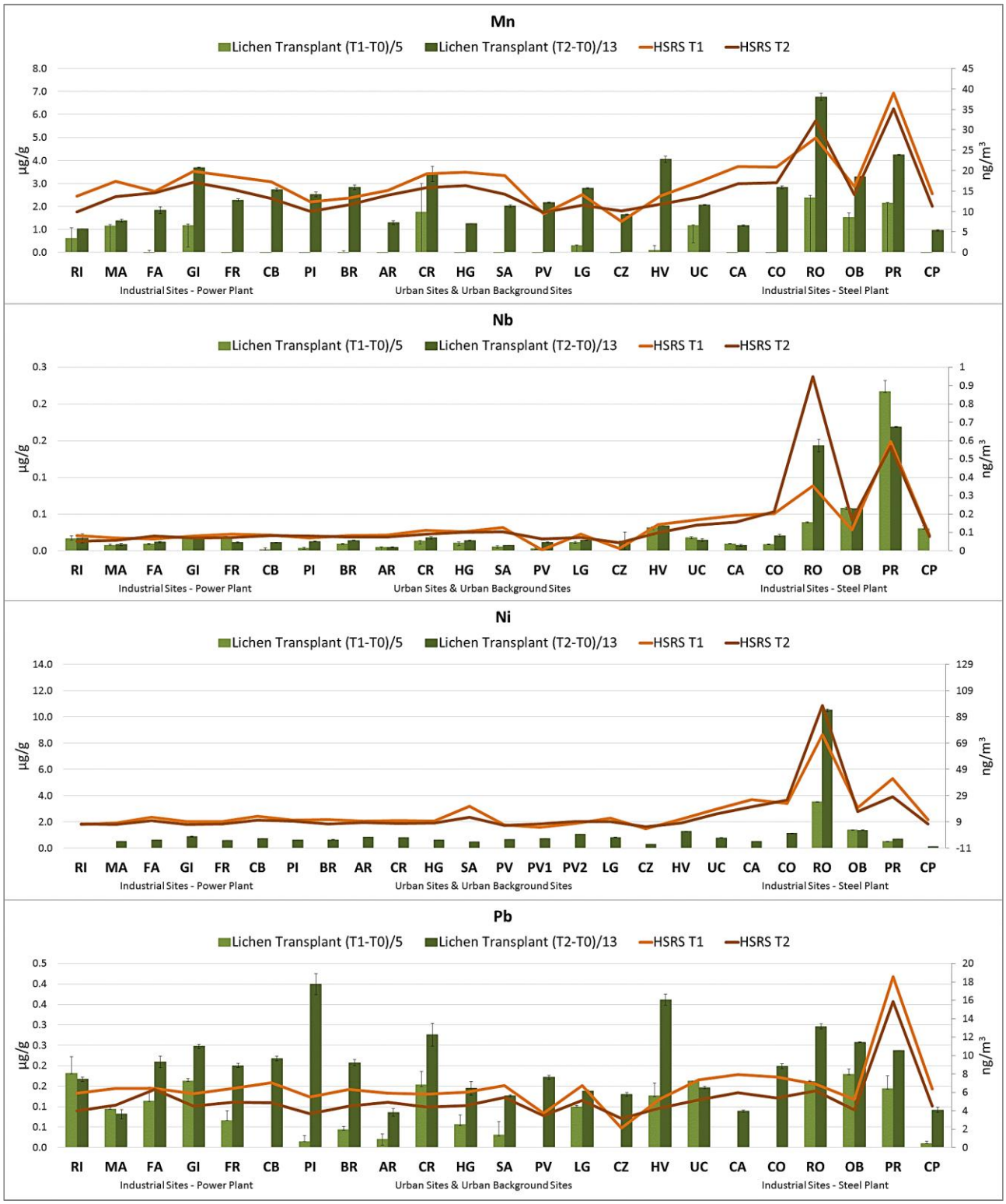

Fig. S3.3. Comparison of Mn, Nb, Ni and Pb accumulation in lichen samples after five months (T1) and thirteen months (T2) of exposure with their mean concentrations measured in PM_{10} during five (HSRS T1) and thirteen (HSRS T2) months.

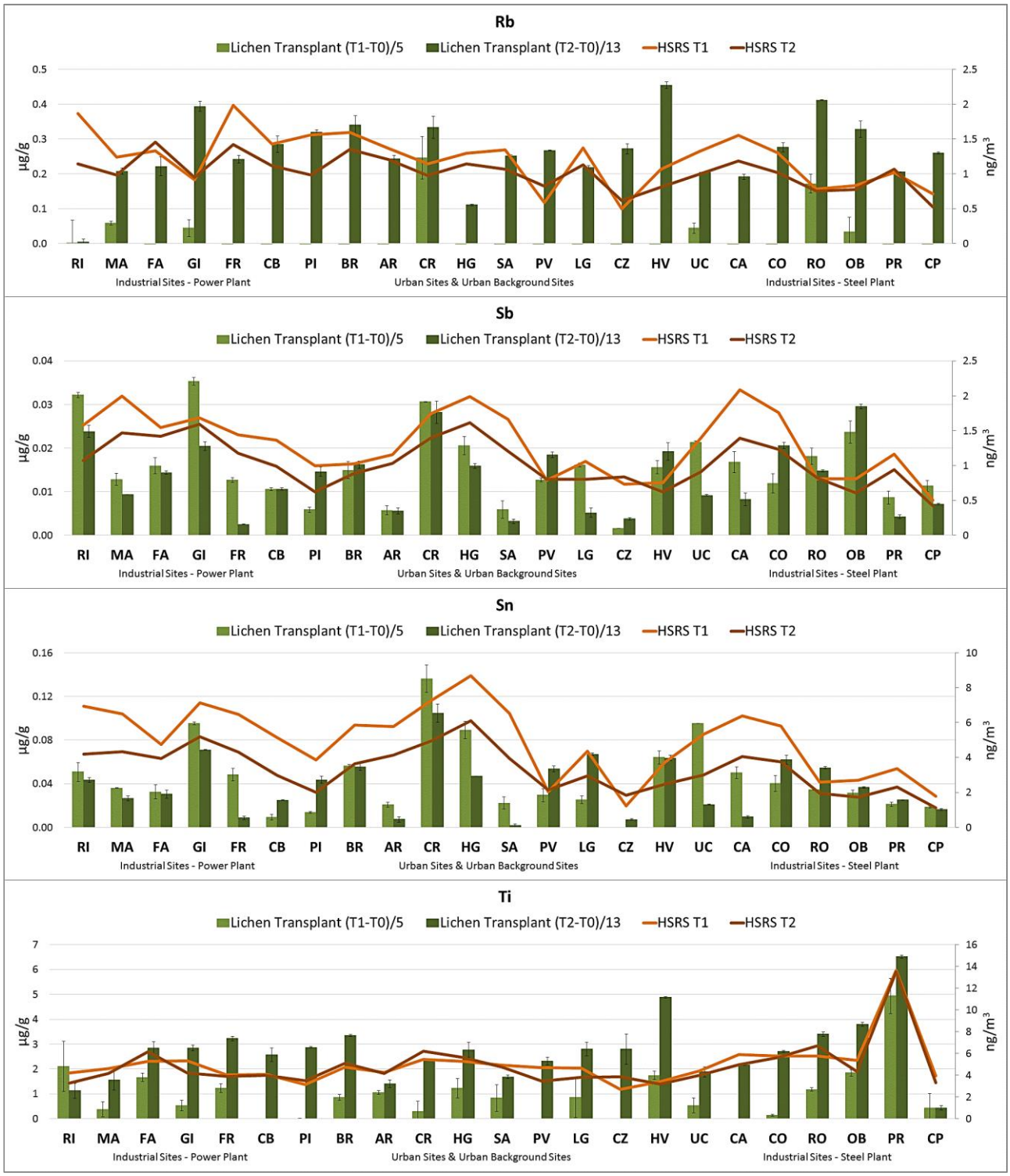

Fig. S3.4. Comparison of Rb, Sb, Sn and Ti accumulation in lichen samples after five months (T1) and thirteen months (T2) of exposure with their mean concentrations measured in PM_{10} during five (HSRS T1) and thirteen (HSRS T2) months.

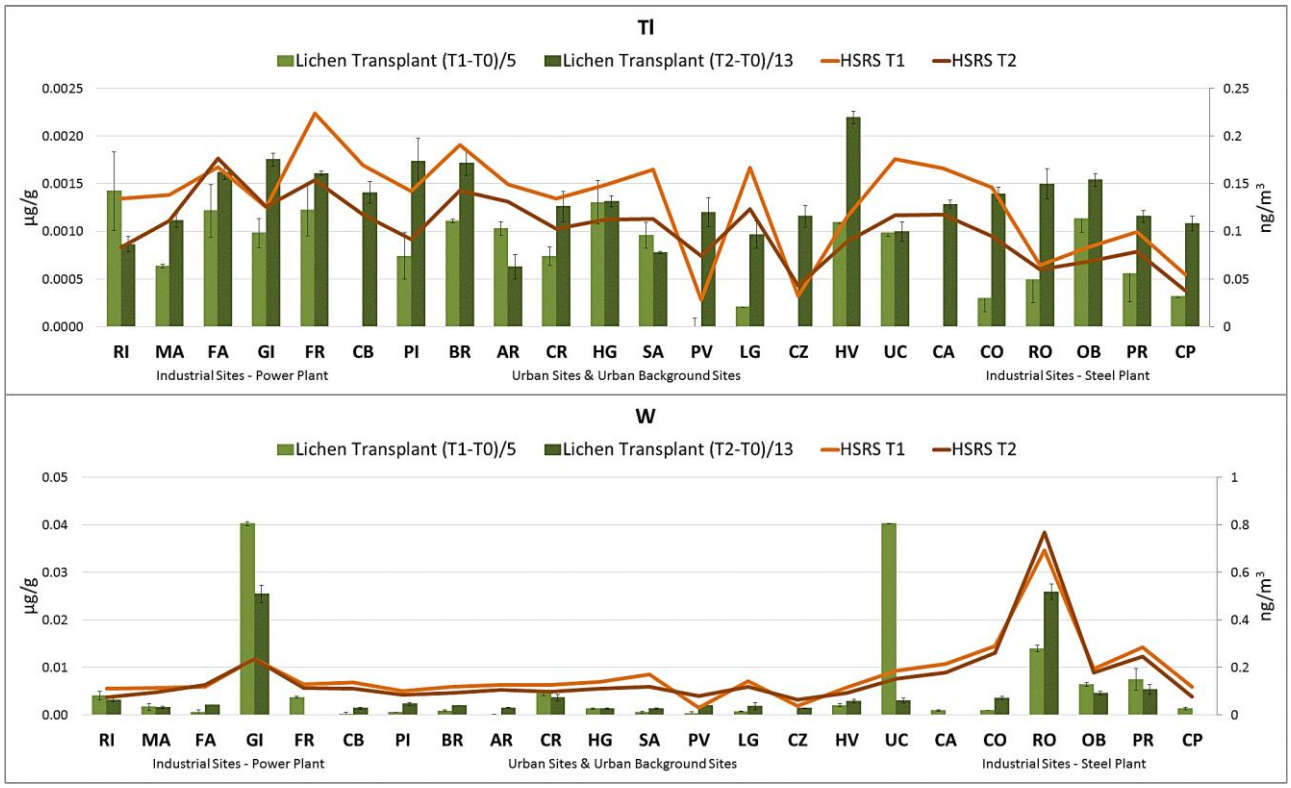

Fig. S3.5. Comparison of Tl and W accumulation in lichen samples after five months (T1) and thirteen months (T2) of exposure with their mean concentrations measured in PM_{10} during five (HSRS T1) and thirteen (HSRS T2) months.

2.3.5. (C5) Evaluation of the Efficiency of *Arundo donax* L. Leaves as Biomonitors for Atmospheric Element Concentrations in an Urban and Industrial Area of Central Italy

Atmosphere (2019), *Reviewed*

Martina Ristorini [a,b], Maria Luisa Astolfi [c], Silvia Canepari [c], Lorenzo Massimi [c,*]

[a] Department of Bioscience and Territory, University of Molise, Pesche (IS), 86090, Italy;
[b] Institute of Terrestrial Ecosystem research – Council of National research (IRET-CNR) Via G. Marconi 2, 05010 Porano (TR), Italy;
[c] Department of Chemistry, Sapienza University of Rome (Rome), 00185, Italy

Abstract: Washed and unwashed *A. donax* leaves were analyzed for elements and results were compared with element concentrations detected in river water and PM_{10}. Samples were collected along a river in an urban and industrial hot-spot of Central Italy, where element concentrations show relevant spatial gradients both in air and river water. The aim of this study is to identify the role of the two environmental matrices on leaves composition. Element concentrations of washed and unwashed leaves were compared to differentiate between the superficial deposition and the uptake into leaf tissues of elements. Water-soluble and insoluble element concentrations were measured in PM_{10} samples collected on membrane filters by using innovative high spatial resolution samplers. The comparison among leaf and atmospheric concentrations of PM_{10} elements showed a similar trend for Ni, Mo, Cr, Ti and Fe, which are reliable tracers of the PM_{10} contribution by steel plant and vehicular traffic. Soluble species appeared to be mainly bounded into leaf tissues, while insoluble species were deposited on their surface. On the other hand, element concentrations detected in washed *A. donax* leaves were poorly correlated with those measured in river water samples. The obtained results proved that *A. donax* leaves can be used as reliable biomonitors for the evaluation of the atmospheric concentrations of some PM_{10} elemental components.

Keywords*:* air quality; biomonitoring; particulate matter; leaf deposition; source tracers.

1. Introduction

Arundo donax L., commonly known as giant reed, is a tall perennial grass of the family *Poaceae*, typical of riparian areas and characterized by great productivity, growing up to 10 cm per day in optimal conditions [1-2]. Numerous studies had underlined the potential of this species for the phytoremediation of contaminated waters and soils, due to its tolerance to high concentrations of heavy metals, such as Cd, Cr, Ni [3] and its ability to absorb and bioaccumulate contaminants. In particular, *A. donax* turns out to be characterized by a root > leaf > stem translocation pattern [4], with the belowground biomass (roots and rhizomes) as the main bioaccumulation organs [5-7]. These characteristics make this species suitable to be used as bioindicator of heavy metal pollution of water and soil. Therefore, A. donax provides an alternative to the traditional sampling and analytical procedures applied to this task [8].

On the other hand, numerous studies underlined the potential of biomonitoring to assess airborne particulate matter (PM) pollution [9-11]. In this context, urban trees and shrubs leaves are often proposed as efficient and low-cost biomonitors for PM [12-14], since they are able to affect dispersion and deposition od airborne particles [15]. In particular, the evaluation of chemical and physical characteristics of particles deposited on leaves can be used to achieve information about the role and the impact of anthropogenic PM emission sources [16-17]. In fact, these characteristics can be directly influenced by the type of emission process and source [18-19]. PM is an extremely heterogenous mixture of airborne solid particles and liquid droplets, varying in size, shape, chemical composition, solubility, toxicity and origin [20]. It is considered one of the most relevant air pollutants in terms of human health effects [21-23]. In particular, PM_{10} (particles characterized by aerodynamic diameters ≤ 10 μm) includes particles that are able to interact at different levels with human respiratory system and induce negative health effects [24-25]. PM_{10} mass concentration is used as an air quality indicator, but to date, exceedances of guideline levels set for PM_{10} are still frequent in many urban and industrial areas (such as the daily limits of 50 ng m^{-3} for PM_{10} mass concentrations set by 2008/50/EC).

Dry deposition of PM on leaves is a complex and dynamic process, being influenced both by species-specific characteristics of vegetation and chemical-physical characteristics of airborne particles themselves [26-27]. To date, due to the high complexity of dry deposition processes and the heterogeneity of PM_{10}, the achievement of a complete characterization of leaf deposited particles is difficult to obtain. Numerous analytical procedures have been applied for the achievement of this task, but it is still uncertain which procedure is the most efficient. One of the main sources of uncertainty is connected to the leaf washing procedure, being still unsure whether this step should be carried out or not. In fact, the efficiency of leaf washing together with the chemical and physical

characteristics of the particles, can influence their encapsulation in leaf structures (waxes layer or stomata pores) [28-29]. These factors can affect the efficiency of any analytical procedure applied in the characterization of leaf deposited particles.

This study is aimed to evaluate the influence on element concentrations of *A. donax* leaves of two types of environmental contaminations to which plants are exposed: atmospheric PM_{10} and river water pollution. To this aim, *A. donax* leaves, PM_{10} sampled filters and river water samples were collected in parallel at sites impacted by different pollution sources. Element concentrations determined in the three matrices were compared. Washed and unwashed leaves were analyzed and compared to differentiate between superficial deposition and uptake into leaf tissues of PM_{10} elements. Furthermore, due to the hyper-accumulate ability of this riparian species, element concentrations detected in *A. donax* leaves were compared with those measured in river water samples. This was aimed to evaluate at what extent river water contamination can affect leaves elemental composition.

2. Materials and Methods

2.1. Study Area and Sampling Sites

The study was carried out in Terni city, an urban and industrial hot-spot of Central Italy. The choice of Terni was mainly driven by the presence of intense local emission sources. This study area is characterized by typical urban sources such as vehicular traffic and domestic heating, but also by a power plant for waste treatment and an extensive steel plant, occupying about 158 ha (Fig. 1). Due to its peculiar geomorphological and meteorological conditions, Terni basin is characterized by high PM_{10} mass and element concentrations, which make this area one of the most critical for human health in Central Italy [30-35]. In addition, these emission sources determines very relevant spatial variations of element concentrations in both PM_{10} and river water, making this area particularly suitable for studying correlations among biomonitors and environmental conditions. Six sampling sites (TE1, TE2, TE3, TE4, TE5, TE6) were individuated along the river Nera and chosen for the collection of *A. donax* leaves and river water samples. TE1 is located near the power plant, in the western part of the city, TE2 and TE3 near the main trafficked streets of the city center, and TE4, TE5 and TE6 are sited around the steel plant, in the eastern part of the city (Fig. 1, Table 1). In particular, TE6 is located upstream from the wastewater systems for the treatment of the steel plant effluents.

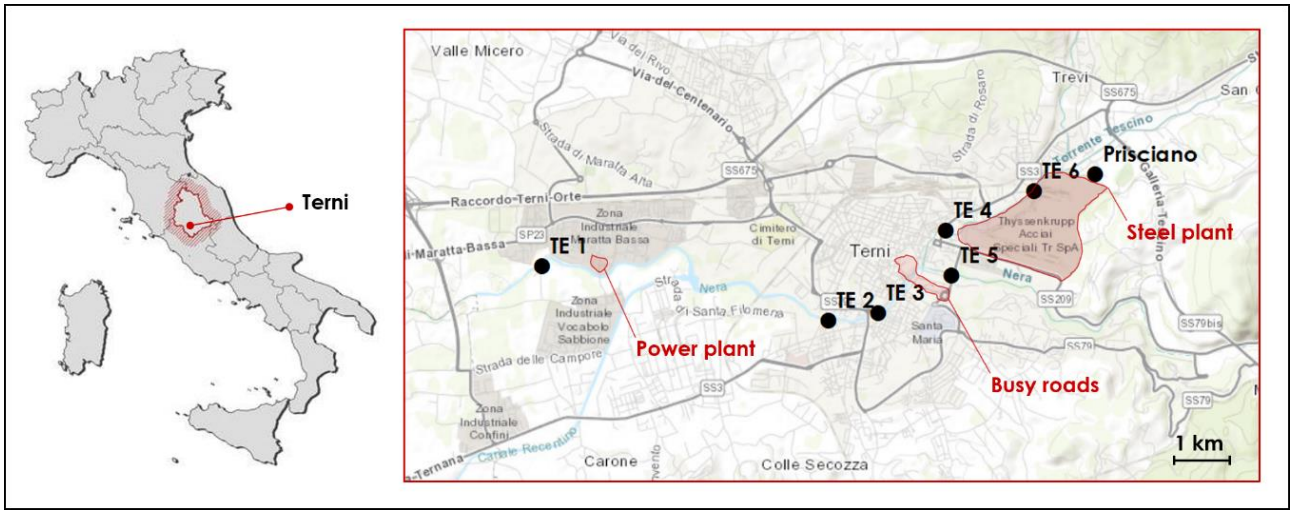

Fig. 1. Sampling sites of *A. donax* leaves and river water samples along the river Nera in Terni (Central Italy) and air quality station "Prisciano" controlled by ARPA Umbria (regional agency for environmental protection). Highlighted the main PM_{10} anthropogenic emission sources present in the study area.

Table 1. Latitude and longitude of the six sampling sites in Terni.

SAMPLING SITES	LATITUDE	LONGITUDE
TE1	42°33'43.84"N	12°35'47.18"E
TE2	42°33'22.27"N	12°38'21.02"E
TE3	42°33'25.29"N	12°38'47.81"E
TE4	42°33'58.02"N	12°39'24.08"E
TE5	42°33'40.12"N	12°39'27.33"E
TE6	42°34'13.53"N	12°40'11.41"E

2.2. Arundo donax Leaves and River Water Samples Collection and Preparation

A. donax leaves and river water samples were monthly collected at the six sampling sites (Fig. 1) from March to July 2017. For each site, 3 plants were selected and 6 leaves were collected from each plant for a total of 18 leaves collected each month. Leaves were detached, at least a week after the last rainfall event, from the same internode (second-last from the top of the stems), in order to avoid youngest leaves and ensure longer exposition time to both river water and PM_{10} atmospheric pollution. Furthermore, leaves were collected at a height comparable to that of PM_{10} active samplers (about 2 meters from the ground). Leaves samples were then stored at -18 °C in paper bags, to avoid external contamination. *A. donax* leaves collected at North-East of the Terni basin (42°38'25.95"N, 12°48'34.98"E), far from the direct impact of anthropogenic emission sources, were used as

background samples. Half of the collected leaves were washed thoroughly three times with 250 mL of deionized water (produced by Arioso UP 900 Integrate Water Purification System) for 5 minutes by using a rotating mixer (Rotator, Glas-Col, USA). The dry weight calculation (30 replicates) was carried out by oven drying 1 g of fresh leaves at 60 ± 2 °C until constant weight. Washed and unwashed leaves monthly collected at each site were then pulverized by grinding in a mill with Teflon balls and the obtained powders were homogenized and weighed (analytical balance Gibertini Europe 60; Gibertini Elettronica Srl, Milan, Italy). Subsequently, three replicates of about 30 mg of each sample (homogenized powders of washed or unwashed leaves monthly collected at each site) was subjected to a microwave assisted acid digestion (Ethos Touch Control with Q20 rotor, Milestone, Bergamo, Italy). The acid digestion was carried out for 30 min at 180°C by using a HNO_3/H_2O_2 mixture (2:1, v/v; 2 mL of ultrapure concentrated HNO_3 67%, Promochem, LGC Standards GmbH, Wesel, Germany; 1 mL of H_2O_2 30%, Promochem, LGC Standards GmbH, Wesel, Germany). The digested solutions were then diluted to 100 mL of deionized water. Since all the sampled plants were in close proximity to the river and the root system was often in direct contact with the river water (frequent overflowing of the river), each month, about 50 mL of river water was collected at each sampling site, for a total of 30 water samples. River water samples were taken from 10 to 15 cm below the water surface, according to APHA, 1998 [36].

2.3. PM_{10} Samples Collection and Preparation

PM_{10} was monthly sampled on Teflon membrane filters (PTFE membranes, 37 mm diameter, 2 μm pore size, PALL Corporation, Port Washington, New York, NY, USA) from March to July 2017 at 23 monitoring sites spread over the Terni basin by using innovative and very-low volume (0.5 l min^{-1}) PM_{10} active samplers (High spatial resolution sampler - HSRS, Fai Instruments, Fonte Nuova, Italy). The localization and the geographical coordinates of the 23 PM_{10} sampling sites as well as the characteristics of the used HSRS are deeply described in Massimi et al. 2017 and Massimi et al. 2019 [11, 31]. The monthly collected PM_{10} membrane filters were subjected to a chemical fractionation procedure, previously optimized and validated [37-38], useful to separate the water-soluble and insoluble fraction of each PM_{10} elemental component, thus increasing its selectivity as source tracer [11, 39-40]. Firstly, after removing the supporting polymethylpentene ring from each membrane filter, PM_{10} filters were extracted in 10 mL of deionized water for 30 min at 25 °C by using an ultrasonic bath (Proclean 10.0 ultrasonic cleaner, Ulsonix, Germany) and then filtered on cellulose nitrate filters (0.45 μm pore size, Merck Millipore Ltd., Billerica, MA, USA). Secondly, both the membrane and cellulose nitrate filters were acid-digested for 30 min at 180°C in the microwave oven

by using the HNO_3/H_2O_2 mixture (2:1, v/v) previously described. The digested solutions were then diluted to 50 mL with deionized water.

2.4. ICP-MS Analysis

The collected river water samples and all the acid-digested solutions were filtered with syringe filters (25 mm diameter, 0.45 µm pore size, GVS Filter Technology, Morecambe, England, UK) before instrumental analysis. The concentrations of 16 elements (Ba, Cd, Cr, Cs, Cu, Fe, Li, Mn, Mo, Ni, Pb, Rb, Sb, Sn, Sr, Ti) were determined in all the samples (river water samples, water-extracted and acid-digested PM_{10}, washed and unwashed *A. donax* leaves) by a quadrupole inductively coupled plasma mass spectrometer (ICP-MS, model 820-MS; Bruker, Bremen, Germany) equipped with a glass nebulizer (0.4 mL min^{-1} ; Analytik Jena AG, Jena, Germany). External matrix-matched standard calibration curves were performed for all the analyzed elements in the 1-500 µg L^{-1} range by serially diluting standard stock solutions (1000 ± 2 mg L^{-1}; Exaxol Italia Chemical Manufacturers Srl, Genoa, Italy). To control the nebulizer efficiency, yttrium and rhodium were set at 5 µg L^{-1} as internal standards for all measurements and were prepared from standard stock solutions (1000 ± 2 mg L^{-1}; Panreac Química, Barcelona, Spain; Ultra Scientific, North Kingstown, RI, USA; Merck Millipore Ltd., Billerica, MA, USA). The values of blanks, subjected to similar sample preparation and analytical procedures, were deducted from all measurements and the limits of detection (LODs; supplementary material S1; Table S1.1, S1.2, S1.3) were set at 3 times the standard deviation (Std Dev) of 10 replicate blank determinations. Standard deviations of the replicates were all below 20%. The used instrumental conditions and the performance of the method are detailed in Astolfi et al. 2018 [41].

2.5. Data Elaboration

Concentrations of the 16 elements derived from the three replicates analyses of washed and unwashed leaves, monthly collected at each site, were averaged in order to obtain a single monthly value. This was aimed to properly compare leaves element concentrations with results from the chemical analysis of PM_{10} samples (one filter monthly sampled for each site). The concentrations determined in the washed and unwashed *A. donax* leaves were divided by the dry weight of each sample (ng mg^{-1}). Then, monthly element concentrations were averaged for each monitoring site (supplementary material S2; Table S2.1, Table S2.2). The averaged element concentrations detected in washed leaves were subtracted to the unwashed ones to evaluate the elemental amount superficially deposed on leaves (SD in ng mg^{-1}). Element concentrations (µg l^{-1}) were determined in river water

samples collected at each site for each of the 5 collection months (three replicates of 10 mL). Also for river water samples, results obtained from the three replicates analyses were averaged to obtain one monthly result relative to each site. Then, monthly element concentrations were averaged for each monitoring site and these are reported in supplementary material S2 (Table S2.3). The element concentrations of the water-soluble and insoluble PM_{10} were divided by the air volume sampled on each PM_{10} membrane filter (ng m^{-3}). Total concentrations were calculated as the sum of the two solubility fractions. Since the *A. donax* leaves were collected at different sites with respect to the PM_{10} samples, ordinary kriging (OK, spherical semivariogram model) interpolation [42-43] was applied to the PM_{10} soluble, insoluble and total element concentrations monthly determined at the 23 PM_{10} sampling sites. Then, these concentrations were averaged over the 5 months collection period, in order to estimate their concentrations (supplementary material S2; Table S2.4, S2.5) at the leaves collection sites (TE1, TE2, TE3, TE4, TE5, TE6).

2.6. Statistical Analysis

Normal distribution of data was tested by using the Kolmogorov-Smirnov test. Then, paired t-tests were used to assess the statistical significance of the differences between mean values of each element detected in unwashed and washed leaves. Pearson correlation was used to assess the correlations between: SD results and element concentrations in the water-soluble and insoluble fraction of PM_{10}; washed leaves element concentrations and the element concentrations in the two fractions of $PM_{10;}$ washed leaves and river water element concentrations. Statistical analyses were carried out using IBM SPSS Statistics 25 software (IBM Corp., Armonk, NY, USA).

2.7. SEM Analysis of PM_{10} Samples

PM_{10} sampling on polycarbonate membranes (PCTE membranes, 37 mm diameter, 0.8 μm pore size, Sterlitech Corporation, Kent, Washington, USA) was carried out for three days, from the 2nd to the 4th of March, by using two HSRS working in parallel at the air quality station "Prisciano".The station is located in the East of the city (42°34'20.30"N 12°40'44.23"E), in the proximity of the steel plant and it is controlled by the regional agency for environmental protection (ARPA Umbria) (Fig. 1). Small portions of each polycarbonate membrane were cut, fixed to aluminum stubs by self-adhesive carbon disks (TAAB, 12mm diam.) and coated with an ultra-thin carbon layer in a vacuum evaporator (108 Carbon A; Scientific Instruments Ltd., Cressington, England, UK). Micrographs of each sample were acquired by a high-resolution field emission scanning electron microscopy (HR-FESEM; model AURIGA; Carl Zeiss Microscopy GmbH, Jena, Germany) equipped with an energy dispersive

spectrometer for X-ray microanalysis (XEDS; model QUANTAX; Bruker Italia S.r.l., MI, Italy). Micrographs were acquired through the use of backscatter electron detector (BSD) at magnification ranging from 25,000x to 600,000x and at working distance (WD) ranging from 9.6 mm to 12.4 mm.

3. Results and Discussion

3.1. Element Concentrations in Arundo donax Leaves

Fig. 2 reports the concentrations of elements associated to the steel plant emission (Cr, Fe, Mo, Ni and Ti) in unwashed and washed leaves. All these elements showed a marked concentration gradient in both washed and unwashed leaves, indicating that the measured concentrations are sensitive to environmental concentrations. A similar trend was found for all the considered elements, with higher concentrations at sites surrounding the steel plant.

Cr, Ni and Ti showed higher concentrations (ng mg^{-1}) in leaves collected at TE5 and TE6 (Fig. 2a, d and e), which are the sites closest to the steel plant. Furthermore, for these elements, concentrations in unwashed leaves were significantly higher than those in washed leaves. This means that a major part of the measured concentrations in unwashed leaves is probably due to superficial deposition of atmospheric particles. PM_{10} particles containing these elements are known to be emitted at high concentrations by the steel plant [31]. Chromium is usually used to increase the steel resistance to chemical oxidation and nickel is used to increase the steel strength, ductility and toughness. Titanium is used in steelmaking for deoxidation, grain-size control, carbon and nitrogen control, and stabilization [44]. The variation among the selected sites, observed for the leaf deposition of these elements, underlined the impact of the steel plant and proved the reliability of *A. donax* leaf deposition results for the individuation of the steel plant tracers.

In panel b of Fig. 2, we can observe that Fe concentrations (ng mg^{-1}) detected in unwashed leaves were higher at the sampling sites TE3, TE5 and TE6. Also in this case, concentrations were significantly higher in unwashed leaves. Iron is the principal component of stainless steel and higher deposition values in *A. donax* leaves collected at TE5 and TE6, which are the closest sites to the steel plant, confirmed its attribution to emissions from the steel plant. However, Fe is also a well-known tracer for vehicular traffic, being related to the mechanical abrasion of brakes and vehicle components [30, 45-46]. The increase of Fe concentration at TE3, located near the city center, is mainly related to its emission from the close busy roads. Therefore, the trend of Fe leaf deposition underlined the impact of two different emission sources: steel plant (at TE5 and TE6) and vehicular traffic (at TE3).

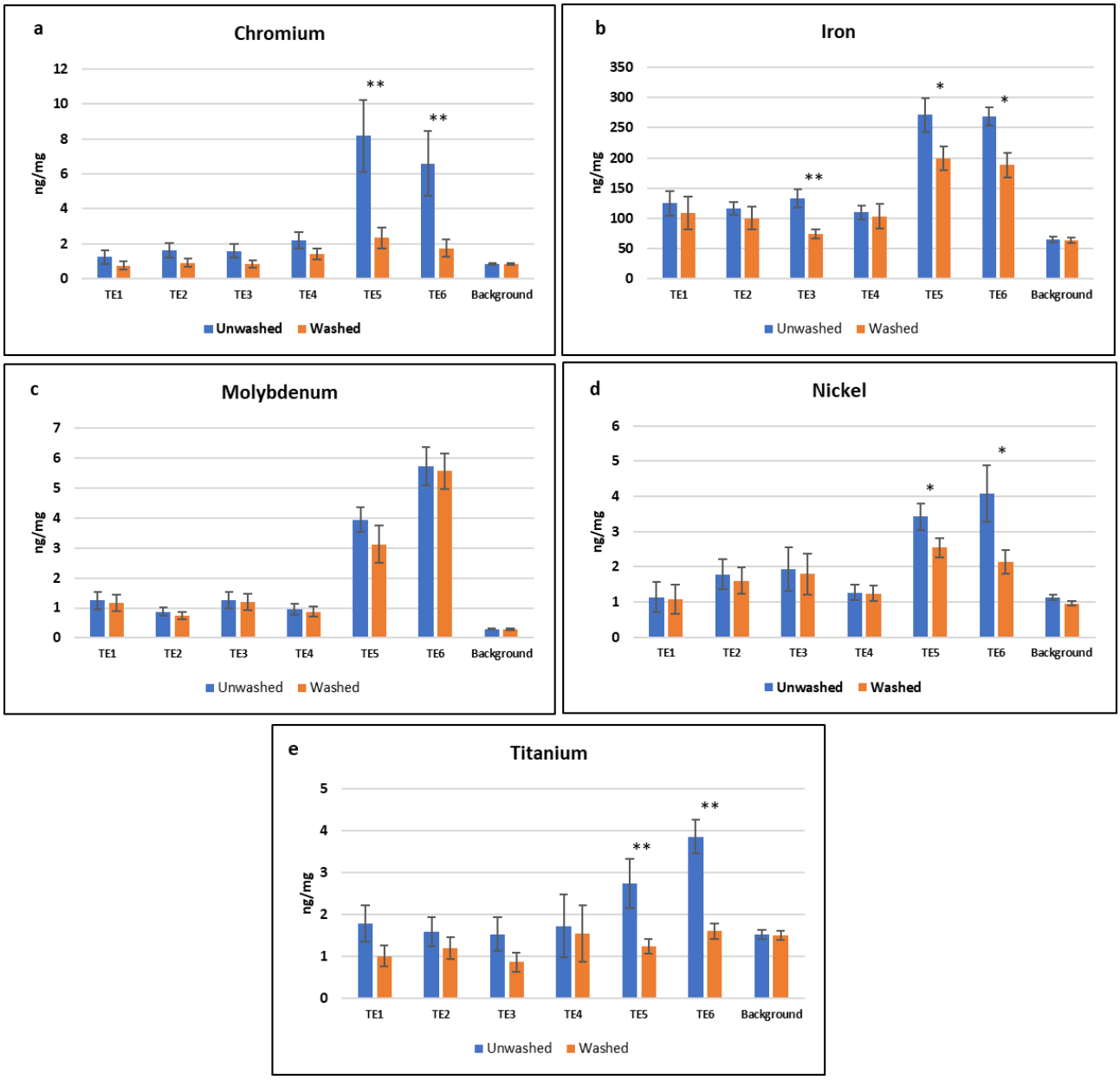

Fig. 2. Comparison between averaged concentrations (ng mg^{-1}) of Cr, Fe, Mo, Ni and Ti, detected in unwashed and washed leaves at the six sites (panel a, b, c, d and e). P values obtained by applying paired sample t-test (* $p<0.05$; ** $p<0.001$) and standard deviations calculated between monthly concentrations are reported.

In the specific case of molybdenum, higher concentrations were found at the same collection sites (TE5 and TE6) whereby were found high concentrations of Cr, Ni and Ti, highlighting the impact of the steel plant. In fact, Mo is typically used as secondary component to improve the resistance of stainless steel [44]. However, Mo concentrations in washed and unwashed leaves were very similar, indicating that this element is deeply bound to the leaves (Fig. 2c). This difference may be due to a

different uptake process (i.e. root absorption from water or soil) or to the different chemical and/or physical characteristics of atmospheric particles deposited on leaves. Further details on these issues can be obtained by comparing the element concentrations in leaves with those found in atmospheric PM_{10} and river water samples.

3.2. Comparison Between Leaf Deposition and PM_{10} Element Concentrations

To evaluate the potential of this biological approach, based on the evaluation of PM_{10} deposition on *A. donax* leaves for the assessment of the impact of the PM_{10} emission sources, we compared the element superficial deposition on leaves (SD) with the spatially-resolved atmospheric element concentrations detected in the PM_{10}.

From Fig. 3, we can observe that, for most of the identified steel plant tracers (Cr, Fe, Ni and Ti), the SD showed a similar trend to total concentrations in PM_{10} (Fig. 3a, b, e and f). For these elements, the difference between unwashed and washed concentrations in *A. donax* leaves seems then to be reliably representative of their atmospheric concentrations. In the case of Mo, much poorer correlations between SD and PM_{10} concentrations were found (Fig. 3c). For this element, we also reported the comparison between PM_{10} and washed leaves concentrations (Fig. 3d), which showed a much higher correlation. In order to investigate the different behavior of Mo with respect to the other steel plant tracers, we considered the solubility and the morphological characteristics of particles emitted by the steel plant.

Indeed, dimensions and morphological characteristics of airborne particles have proven to be able to influence the deposition of PM on leaves and its interaction with leaf tissues [26, 47-48]. For this reason, we carried out SEM analyses on PM_{10} sampled on polycarbonate membranes through HSRS working near the steel plant (Fig. 4).

From Fig. 4, we can observe the micrograph (panel a) with the respective EDX spectrum (panel b) of a particle containing the basic stainless steel components: Cr, Ni and Fe. This steel particle is coarse (up to 5 μm of diameter) and is characterized by an irregular, angular and sharp morphology. The peculiar dimension and morphology of this and other analyzed coarse particles with the same chemical composition, seems to be related to mechanical-abrasive emission processes. On the other hand, in the panel c, we can observe a fine particle (with diameter smaller than 1 μm) containing Mo and spherical in shape, which is the typical morphology of airborne particles formed by high temperature processes [49-50]. Even though these two types of particles are emitted by the same emission source (steel plant), they appeared to be characterized by different dimension and

morphology, revealing the presence of two different emission processes (high temperature and mechanical-abrasive processes).

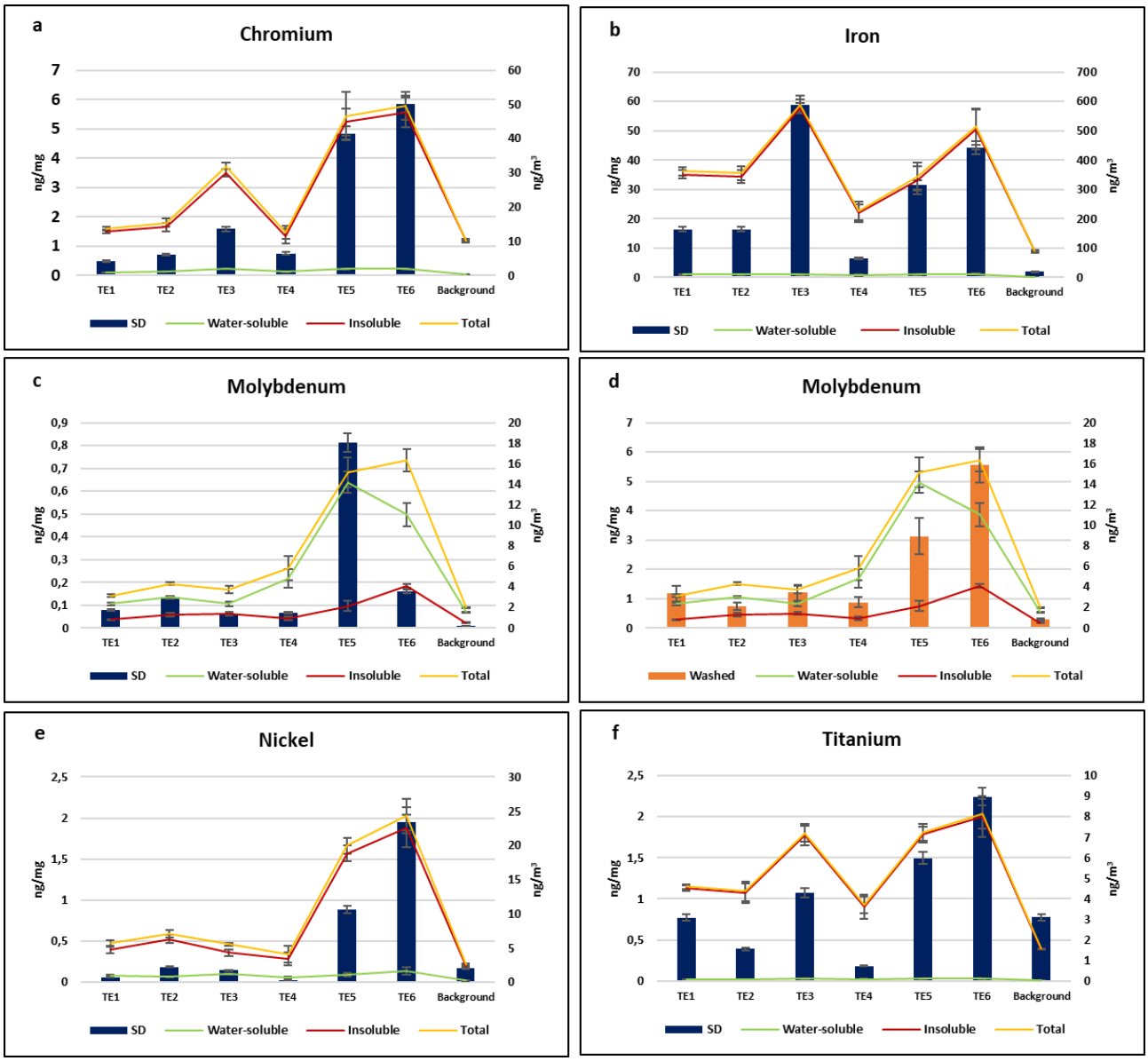

Fig. 3. Comparison between averaged SD results (ng mg^{-1}) and concentrations in the water-soluble, insoluble and total fraction of PM_{10} (ng m^{-3}) of Cr, Fe, Mo, Ni and Ti (panels a, b, c, e and f). Comparison between averaged Mo concentrations in washed leaves (ng mg^{-1}) and in the water-soluble, insoluble and total fraction of PM_{10} (ng m^{-3}) (panel d). Standard deviations calculated between monthly SD values, washed leaves and PM_{10} interpolated concentrations are reported.

The different physical characteristics of these particles may be considered responsible for the different behavior observed in Fig. 2 and 3. In particular, coarse particles containing Cr, Fe, and Ni

seem to have been deposited on the leaf surfaces, making it easy to wash them off and to detect significant differences between washed and unwashed leaves. On the other hand, fine particles containing Mo could be more likely to get encapsulated into the waxes layer or stomata pores situated on the leaf surface, making more difficult to wash them out from the leaves [28-29]. This can results in the lowest difference between unwashed and washed leaves, detected for molybdenum concentrations. In Fig. 3 we also reported water-soluble and insoluble fractions of each element in PM_{10}. As it can be noted, Cr, Fe, Ni and Ti are almost exclusively present as insoluble species, while Mo is mainly present in the water soluble fraction. Besides the small dimensions of particles containing Mo, the different behavior observed for this element may be due to the higher solubility of species containing Mo that might be then directly absorbed by the leaf surface.

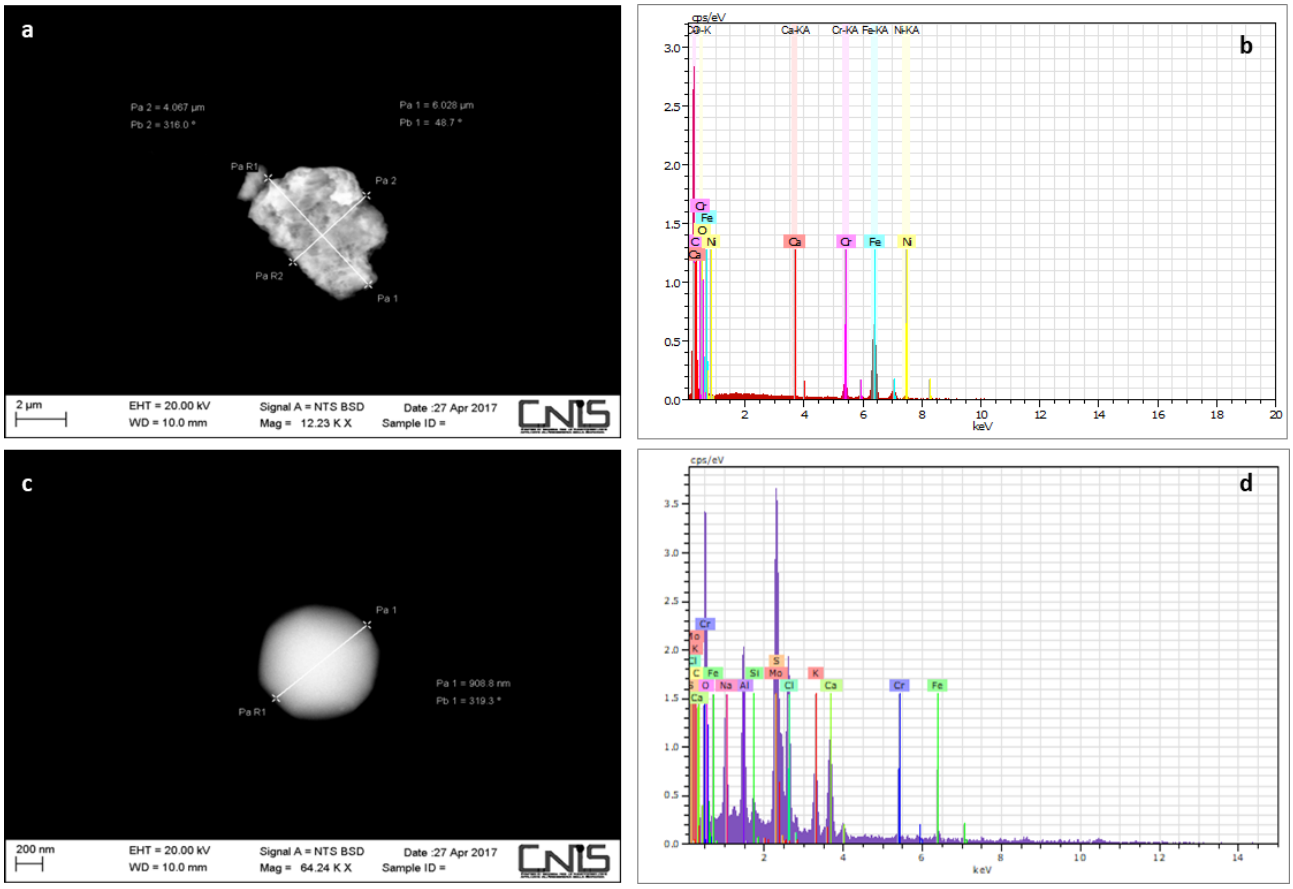

Fig. 3. SEM micrograph (a) and respective EDX spectrum (b) of a steel particle (Cr, Fe and Ni) sampled near the steel plant. SEM micrograph (c) and respective EDX spectrum (d) of a Mo particle sampled near the steel plant.

Table 2 reports Pearson's correlation coefficients (ρ) calculated between elements superficially deposited on leaves or bounded to leaf tissues (washed leaves) and their concentrations in the water-

soluble and insoluble fractions of PM_{10}. In general, the highest positive correlations were found between concentrations in insoluble fraction of PM_{10} and SD of Cr, Fe, Ni, Mn, Ti and Zn. Most of these elements (Cr, Ni, Fe, Ti) are tracers of the steel plant; as already showed, particles containing these elements are mainly characterized by coarse dimensions. Mn is also well correlated to SD; this element is also known as a source tracer for steel producing processes [51-52] but it is also used as tracer of non-combustive emissions from vehicular traffic [18, 53]. This source produces particles scarcely soluble and belonging to the coarse dimensional fraction of PM as well [54]. It is then reasonable to hypothesize that coarse and insoluble particles are deposited on leaf surface and easily washed out during the leaf washing step. For this kind of PM contribution, the determination of SD may constitute a reliable biomonitoring procedure. In the case of Mo, as already pointed out, a good correlation was found between washed leaves and soluble fraction of PM_{10}. Mo is present in PM_{10} mainly as soluble species belonging to the fine fraction; these characteristics promote a stronger interaction with leaf structure and washing procedure is not able to detach Mo-containing particles.

Table 2. Pearson's correlation coefficients calculated between SD and washed leaves element concentrations and their concentrations in the water-soluble and insoluble fractions of PM_{10}. Mean monthly concentrations at each site were included in the elaboration (N=30). Positive linear correlations (Pearson's coefficient > 0.8) between the two variables are reported in red.

Pearson's Coefficients	Ba	Cd	Cr	Cs	Cu	Fe	Li	Mn	Mo	Ni	Pb	Rb	Sb	Sn	Sr	Ti
SD/Water soluble PM_{10}	-0,06	0,31	0,74	0,31	-0,39	0,49	0,62	0,77	0,78	0,77	0,21	0,00	-0,65	0,34	-0,56	0,79
SD/Insoluble PM_{10}	-0,12	0,22	0,87	0,38	-0,08	0,93	0,25	0,92	0,16	0,95	-0,79	0,12	-0,74	0,53	-0,62	0,93
Washed leaves/Water soluble PM_{10}	0,01	0,18	0,49	0,10	0,08	0,31	0,67	0,73	0,90	0,63	0,02	0,51	0,45	-0,43	0,19	0,17
Washed leaves/Insoluble PM_{10}	-0,59	0,24	0,59	-0,14	0,18	0,02	-0,03	0,75	0,35	0,82	0,55	-0,08	0,43	-0,66	0,21	0,01

A positive correlation was found also between washed leaves and insoluble Ni. In this regard, it is worth noting that fine particles containing Ni were also individuated through SEM analysis (supplementary material S3; Fig. S3.1). These particles are probably released by the same high temperature process but contain Ni as insoluble species. The correlation between washed leaves and Ni may indicate that the uptake into leaf tissues is mainly driven by physical interaction of small particles with waxes layer and stomata pores. In particular, dimensions of *A. donax* stomata pores are reported to be 23.2 ± 1.7 µm for length and 9.7 ± 1.2 µm for width [55]. Even if particles

encapsulation in leaves structures, is reported to be a relevant mechanism for particles ≤ 10.6 μm, this process results to be dominant especially for fine particles ≤ 2.6 μm [28-29]. Correlations between SD results and PM_{10} element concentrations were much lower for all the other analyzed elements, tracers of other PM sources, whose strength was lower than the steel plant. For example, correlations were poor for water-soluble Cd, Cs, Rb and Tl, which have been identified as reliable tracers for biomass burning in the Terni basin [56-57] and weak for insoluble Cu and Sn, which are well-known as rail network and vehicular traffic tracers [11, 31, 58-59]. Then, SD of atmospheric elements can be then considered reliable only for the evaluation of the impact of strong PM sources (steel plant and vehicular traffic).

3.3. Comparison Between River Water Samples and A. donax Leaves Elemental Content

To evaluate the potential influence of river water pollutants on the elemental composition of leaves, where heavy metals adsorbed by roots can be stored and transferred [60-61], we analyzed the element concentrations of water samples (Fig. 1). Since metals adsorbed by roots are expected to be included in leaf tissues, element concentrations in river water were compared with the element concentrations in washed leaves (Fig. 5). It is worth underlining that some of the analyzed elements are known to be micro-nutrients for this riparian species. In this context, low concentrations of Cu are known to be relevant for plant growth and development, while Mn and Zn are connected to enzymatic processes, playing essential metabolic roles [8, 62-63].

The steel plant tracers (Cr, Fe, Mo, Ni and Ti), previously individuated for PM_{10}, showed their maximum concentrations in the river water samples collected at TE5 (Fig. 5). On the contrary, high concentrations were not found at TE6, where high concentrations in *A. donax* washed leaves were instead found. Indeed, wastewater systems for the treatment of the effluents from cold and hot rolling sections of the steel plant are located in the southern part of the steel industry plant, at the close proximity to TE5 [64]. We can thus hypothesize that the higher concentrations of Cr, Fe, Mo, Ni and Ti at TE5 water samples are related to local disposal of steel plant wastewater in the Nera river. Due to the heavy metal hyper-accumulate ability of this riparian species [65-66], high concentrations of these steel plant tracers in washed leaves, may be then due to the influence of river water contamination. The very relevant differences at TE6 (still strongly affected by emissions from the steel plant,) underlined the lower reliability of leaves for the evaluation of the river heavy-metal contamination.

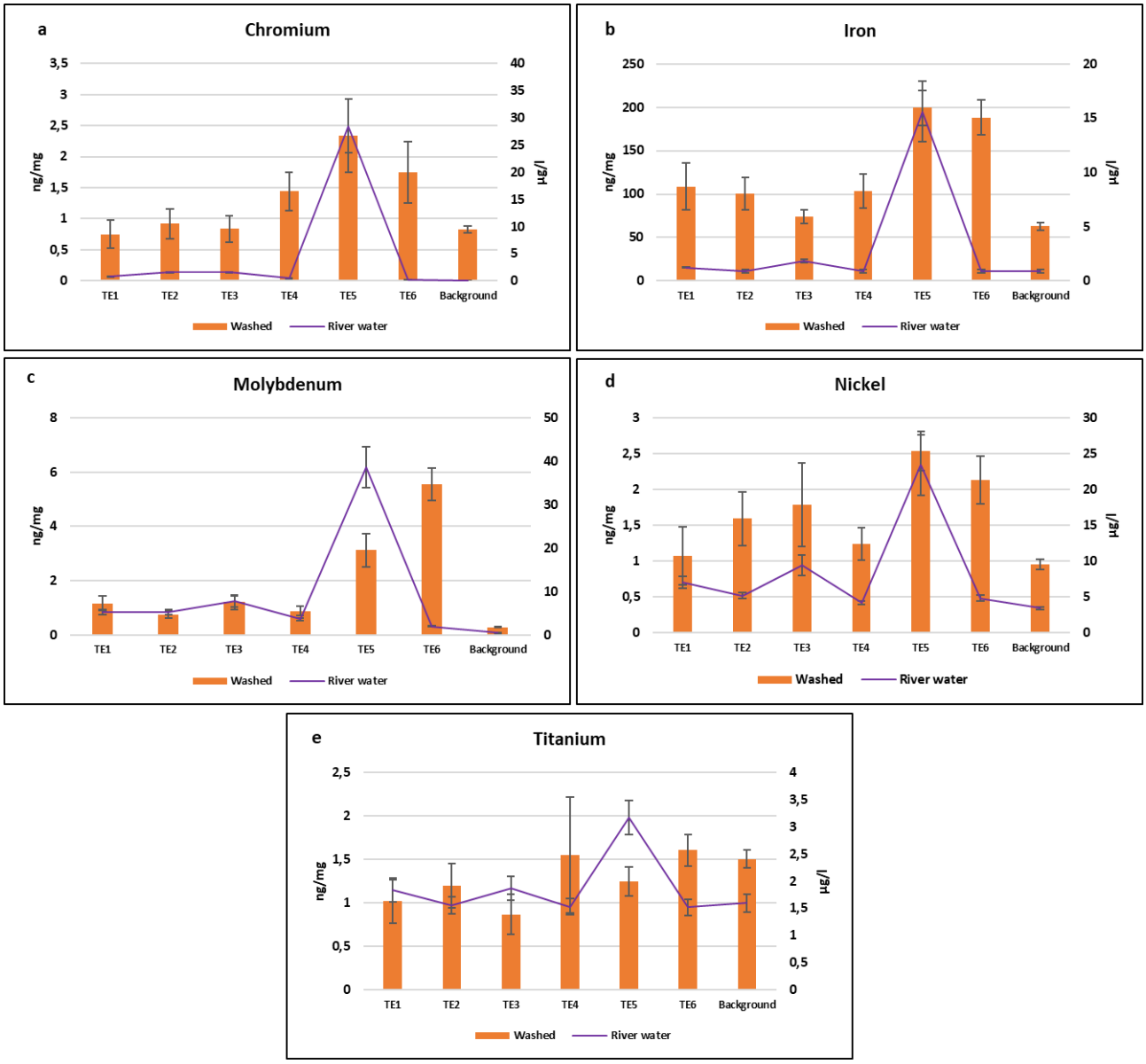

Fig. 5. Comparison between averaged concentrations of Cr, Mo, Ni detected in river water samples (µg L^{-1}) and *A. donax* washed leaves (ng mg^{-1}). Standard deviations calculated between monthly concentrations are reported.

We also calculated Pearson's correlation coefficients between element concentrations detected in river water samples and washed leaves (Table 3). Correlations were in general much lower than those related to PM_{10} concentrations. The highest correlation between these two datasets was found for Cd; this result could be explained by considering the hyper-accumulate and translocation ability of *A. donax* toward Cd [67]. However, in this set of measurements, Cd showed a low variability in both river water and washed leaves (supplementary material S2; Table S2.2, S2.3) and this is reasonably

the main reason of the significant correlation found. Then, the use of this riparian species seems to have a low reliability for the evaluation of the concentration in the river water.

Table 3. Pearson's correlation coefficients calculated between river water and washed leaves element concentrations. Mean monthly concentrations at each site were included in the elaboration (N=30). Positive linear correlations (Pearson's coefficient > 0.8) between the two variables are reported in red.

Pearson's Coefficients	Ba	Cd	Cr	Cs	Cu	Fe	Li	Mn	Mo	Ni	Pb	Rb	Sb	Sn	Sr	Ti
Washed leaves/ River Water	0,38	0,81	0,76	0,18	0,34	0,53	-0,20	-0,55	0,17	0,71	-0,10	-0,35	0,06	-0,20	-0,44	-0,23

4. Conclusions

For the first time in this study, we were able to compare the different influence of PM_{10} atmospheric pollution and river contamination, acting in parallel in the study area of Terni, on the elemental content of *A. donax* leaves.

Thanks to the availability of newly developed PM_{10} samplers (HSRS), spatially-resolved element concentrations were detected in PM_{10} samples and compared to SD results. This was helpful to evaluate the reliability of this biomonitoring approach, based on the utilization of leaves and the chemical characterization of leaf deposed PM, for the evaluation of atmospheric element concentrations. The good correlations between SD results and atmospheric PM_{10} concentrations of Cr, Fe, Ni, Mn, Zn and Ti, confirmed the reliability of these results for the evaluation of the impact related to intense local emission sources..

On the othe hand, in our study washed leaves and river water element concentrations were poorly correlated, underlying a lower efficiency of this biological approach for the evaluation of the river contamination.

These preliminary results encourage further investigations on the utilization of this riparian species, largely distributed in urban areas of Italy, for future studies on PM leaf deposition. It also encorauges its application as a low-cost alternative for the monitoring of atmospheric PM and its elemental components.

Acknowledgments

This work was funded by the project 2017 RG11715C7C8801CF (Principal Investigator Dr. S. Canepari) and the project 2018 AR1181641E22B570 (Principal Investigator Dr. L. Massimi) financed by Sapienza University of Rome.

The authors gratefully thank FAI Instruments (Fonte Nuova, Rome, Italy), the citizens of Terni and the Terni district of ARPA Umbria (regional agency for environmental protection), with special regard to Giancarlo Caiello, Caterina Austeri and Marco Pompei, for the support in the installation and management of the sampling equipment as well as for the help in the choice of the sampling sites and Iqra Javed for providing language help.

Author Contributions

S. Canepari and L. Massimi conceived and planned the monitoring and the experiments; M. Ristorini and L. Massimi performed the samplings; M. L. Astolfi and L. Massimi performed the chemical analyses; M. Ristorini and L. Massimi elaborated the data; M. Ristorini wrote the manuscript; S. Canepari and L. Massimi coordinated the group and supervised the manuscript.

Conflicts of Interest

The authors declare no conflicts of interest.

References

1. Perdue: R. E. Arundo donax—Source of musical reeds and industrial cellulose 1958, Econ Bot, 12: 368. https://doi.org/10.1007/BF02860024
2. Bell, G. P. Ecology and management of Arundo donax, and approaches to riparian habitat restoration in Southern California 1997, Plant Invasions: studies from North America and Europe, pp. 103-113.
3. Papazoglou, E. G.; Karantounias, G. A.; Vemmos S. N.; Bouranis, D. L. Photosynthesis and growth responses of giant reed (Arundo donax L.) to the heavy metals Cd and Ni 2005, Environ. Int. 31(2), 243-249. https://doi.org/10.1016/j.envint.2004.09.022
4. Nsanganwimana, F.; Marchand, L.; Douay, F.; Mench, M. Arundo donax L., a candidate for phytomanaging water and soils contaminated by trace elements and producing plant-based

feedstock. A review 2014, Int J Phytoremediation 16, 982–1017. DOI: 10.1080/15226514.2013.810580

5. Bonanno, G. Comparative performance of trace element bioaccumulation and biomonitoring in the plant species Typha domingensis, Phragmites australis and Arundo donax 2013, Ecotoxicol. Environ. Saf. 97, 124-130. https://doi.org/10.1016/j.ecoenv.2013.07.017
6. Bonanno, G.; Borg, J. A.; Di Martino, V. Levels of heavy metals in wetland and marine vascular plants and their biomonitoring potential: A comparative assessment 2017, Sci. Total Environ. 576, 796-806. https://doi.org/10.1016/j.scitotenv.2016.10.171
7. Fiorentino, N.; Ventorino, V.; Rocco, C.; Cenvinzo, V.; Agrelli, D.; Gioia, L.; Di Mola, L.; Adamo, P.; Pepe, O.; Fagnano, M. Giant reed growth and effects on soil biological fertility in assisted phytoremediation of an industrial polluted soil 2017, Sci. Total Environ. 575, 1375-1383. https://doi.org/10.1016/j.scitotenv.2016.09.220
8. Bonanno, G. Arundo donax as a potential biomonitor of trace element contamination in water and sediment 2012, Ecotoxicol. Environ. Saf. 80, 20–27. doi:10.1016/j.ecoenv.2012.02.005
9. Szczepaniak, K.; Biziuk, M. Review: Ecotoxicology, Aspects of the biomonitoring studies using mosses and lichens as indicators of metal pollution 2003, Environ. Res 93, 221–230. doi:10.1016/S0013-9351(03)00141-5
10. Abril, G. A.; Wannaz, E. D.; Mateos, A. C.; Pignata, M. L. Biomonitoring of airborne particulate matter emitted from a cement plant and comparison with dispersion modelling results 2014 Atmos. Environ. 8, 154-163, https://doi.org/10.1016/j.atmosenv.2013.10.020
11. Massimi, L.; Conti, M. E.; Mele, G.; Ristorini, M.; Astolfi, M. L.; Canepari, S. Lichen Transplants as Indicators of Atmospheric Element Concentrations: a High Spatial Resolution Comparison with PM10 Samples in a Polluted Area (Central Italy) 2019, Ecol. Indic. 101, 759-769. DOI: 10.1016/j.ecolind.2018.12.051
12. Urbat, M.; Lehndorff, E.; Schwark, L., Biomonitoring of air quality in the Cologne conurbation using pine needles as a passive sampler—Part I: magnetic properties 2004, Atmos. Environ. 38 (23), 3781-3792 https://doi.org/10.1016/j.atmosenv.2004.03.061
13. Lin, V. S. Research highlights: natural passive samplers – plants as biomonitors 2015. Environ. Sci.: Processes Impacts 17, 1137-1140. DOI: 10.1039/C5EM90016F

14. Sgrigna, G.; Baldacchini, C.; Esposito, R.; Calandrelli, R.; Tiwary, A.; Calfapietra, C. Characterization of leaf-level particulate matter for an industrial city using electron microscopy and X-ray microanalysis 2016, Sci Total Environ 548–549, 91–99. http://dx.doi.org/10.1016/j.scitotenv.2016.01.057

15. Janhall, S. Review on urban vegetation and particle air pollution e Deposition and dispersion 2015, Atmos. Environ. 105, 130-137. http://dx.doi.org/10.1016/j.atmosenv.2015.01.052

16. Gratani, L.; Crescente, M. F.; Varone L. Long-term monitoring of metal pollution by urban trees 2008, Atmos. Environ. 42, 8273–8277, doi:10.1016/j.atmosenv.2008.07.032.

17. Baldacchini, C.; Sgrigna, G.; Clarke, W.; Tallis, M.; Calfapietra, C. An ultra-spatially resolved method to quali-quantitative monitor particulate matter in urban environment 2019, Environ Sci Pollut Res Int. 26 (18), 18719-18729. doi: 10.1007/s11356-019-05160-8.

18. Thorpe, A.; Harrison, R. M., Sources and properties of non-exhaust particulate matter from road traffic: A review 2008, Sci. Total Environ. 400 270-282. doi:10.1016/j.scitotenv.2008.06.007

19. Slezakova, K.; Pires, J. C. M.; Pereira, M. C.; Martins, F. G.; Alvim-Ferraz, M. C. Influence of traffic emissions on the composition of atmospheric particles of different sizes—Part 2: SEM–EDS characterization 2008, J. Atmos. Chem. 60 (3), 221–236. https://doi.org/10.1007/s10874-008-9117-y

20. Pope III, C. A.; Burnett, R. T.; Thun, M. J.; Calle, E. E.; Krewski, D.; Ito, K.; Thurston, G. D. Lung cancer, cardiopulmonary mortality, and long-term exposure to fine particulate air pollution 2002, Jama, 287(9), 1132-1141.

21. Ebelt, S.T.; Petkau, A.J.; Vedal, S.; Fisher, T.V.; Brauer, M. Exposure of chronic obstructive pulmonary disease patients to particulate matter: relationships between personal and ambient air concentrations 2000, Journal of the Air and Waste Management Association 50 (7), 1081–1094.

22. Chen, L. C.; Lippmann, M. Effects of Metals within Ambient Air Particulate Matter (PM) on Human Health 2009, Inhal. Toxicol. 21(1), 1-31, DOI: 10.1080/08958370802105405

23. Anderson, J. O.; Thundiyil, J. G.; Stolbach, A. Clearing the Air: A Review of the Effects of Particulate Matter Air Pollution on Human Health 2012, J. Med. Toxicol. 8, 166–175 DOI 10.1007/s13181-011-0203-1

24. Pope III, C. A.; Dockery, D. W. Acute Health Effects of PM10 Pollution on Symptomatic and Asymptomatic Children 1992, AJRCCM Issues 145 (5). https://doi.org/10.1164/ajrccm/145.5.1123

25. Donaldson, K.; MacNee, W. Potential mechanisms of adverse pulmonary and cardiovascular effects of particulate air pollution (PM10) 2010, Int. J. Hyg. Environ. Health 203 (5-6), 411-415. https://doi.org/10.1078/1438-4639-00059

26. Sæbø, A.; Popek, R.; Nawrot, B.; Hanslin, H.M.; Gawronska, H.; Gawronski, S.W.; Plant species differences in particulate matter accumulation on leaf surfaces 2012, Sci Total Environ 427–428, 347–354. doi:10.1016/j.scitotenv.2012.03.084

27. Petroff, A.; Mailliat, A.; Amielh, M.; Anselmet, F.; Aerosol dry deposition on vegetative canopies. Part I: Review of present knowledge 2008, Atmos. Environ. 42, 3625–3653. doi:10.1016/j.atmosenv.2007.09.043

28. Terzaghi, E.; Wild, E.; Zacchello, G.; Cerabolini, B. E. L.; Jones, K. C.; Di Guardo, A. Forest Filter Effect: Role of leaves in capturing/releasing air particulate matter and its associated PAHs 2013, Atmos. Environ. 74, 378-384. https://doi.org/10.1016/j.atmosenv.2013.04.013

29. Hofman, J.; Wuyts, K.; Van Wittenberghe, S.; Brackx, M.; Samson, R. On the link between biomagnetic monitoring and leaf-deposited dust load of urban trees: Relationships and spatial variability of different particle size fractions 2014, Environ. Poll. 189, 63-72. https://doi.org/10.1016/j.envpol.2014.02.020

30. Sgrigna, G.; Sæbø, A.; Gawronski, S.; Popek, R.; Calfapietra, C. Particulate matter deposition on Quercus ilex leaves in an industrial city of central Italy 2015, Environ. Pollut. 197, 187–194. http://dx.doi.org/10.1016/j.envpol.2014.11.030

31. Massimi, L.; Ristorini, M.; Eusebio, M.; Florendo, D.; Adeyemo, A.; Brugnoli, D.; Canepari, S. Monitoring and evaluation of Terni (Central Italy) air quality through spatially resolved analyses 2017, Atmosphere 8(10), 200. doi:10.3390/atmos8100200

32. Moroni, B.; Ferrero, L.; Crocchianti, S.; Perrone, M. G.; Sangiorgi, G.; Bolzacchini, E.; Cappelletti, D. Aerosol dynamics upon Terni basin (Central Italy): results of integrated vertical profile measurements and electron microscopy analyses 2013, Rendiconti Lincei 24 (4) 319–328. doi: 10.1007/s12210-013-0230-8

33. Manigrasso, M.; Protano, C.; Astolfi, M. L.; Massimi, L.; Avino, P.; Vitali, M.; Canepari, S. Evidences of copper nanoparticle exposure in indoor environments: Long-term assessment, high-resolution field emission scanning electron microscopy evaluation, in silico respiratory dosimetry study and possible health implications 2017, Sci Total Environ 653, 1192-1203. https://doi.org/10.1016/j.scitotenv.2018.11.044

34. Zona. A.; Pasetto, R.; Fazzo, L.; Iavarone, I.; Bruno, C.; Pirastu, R.; Comba, P. Fifth report S.E.N.T.I.E.R.I 2019, Epidemiologia & Prevenzione, Rivista dell'Associazione italiana di epidemiologia 2-3, 43, Supplement 1, http://www.epiprev.it/materiali/2019/EP2-3_Suppl1/SENTIERI_FullText.pdf

35. https://www.arpa.umbria.it/monitoraggi/aria/Default.aspx

36. APHA, (1998) Standard methods for examination of water and waste water (20th. Ed.). Washington DC: American Public Health Association

37. Canepari, S.; Cardarelli, E.; Giuliano, A.; Pietrodangelo, A. Determination of metals, metalloids and non-volatile ions in airborne particulate matter by a new two-step sequential leaching procedure Part A: Experimental design and optimization 2006, Talanta 69, 581–587. doi:10.1016/j.talanta.2005.10.023

38. Canepari, S.; Cardarelli, E.; Pietrodangelo, A.; Strincone, M. Determination of metals, metalloids and non-volatile ions in airborne particulate matter by a new two-step sequential leaching procedure Part B: Validation on equivalent real samples 2006, Talanta 69, 588–595. doi:10.1016/j.talanta.2005.10.024

39. Canepari, S.; Pietrodangelo, A.; Perrino, C.; Astolfi, M. L.; Marzo, M. L. Enhancement of source traceability of atmospheric PM by elemental chemical fractionation 2009, Atmos. Environ. 43 (31), 4754-4765. https://doi.org/10.1016/j.atmosenv.2008.09.059

40. Piacentini, D.; Falasca, G.; Canepari, S.; Massimi, L. Potential of PM-selected components to induce oxidative stress and root system alteration in a plant model organism 2019, Environ. Int. 132, 105094. https://doi.org/10.1016/j.envint.2019.105094

41. Astolfi, M. L.; Marconi, E.; Protano, C.; Vitali, M.; Schiavi, E.; Mastromarino, P.; Canepari, S. Optimization and validation of a fast digestion method for the determination of major and trace elements in breast milk by ICP-MS 2018, Anal. Chim. Acta 1040, 49-62. https://doi.org/10.1016/j.aca.2018.07.037

42. Cressie, N. Spatial Prediction and Ordinary Kriging 1988, Math. Geol. 20 (4), 405–421. https://doi.org/10.1007/BF00892986

43. Cressie, N. The origins of kriging 1990, Math. Geol. 22 (3),239–252. https://doi.org/10.1007/BF00889887

44. Blair, M.; Stevens, T.L. Steel Castings Handbook, 6th ed.; Steel Founders' Society and ASM International: Novelty, OH, USA, 1995; pp. 2–34.

45. Adachi, K.; Tainosho, Y. Characterization of heavy metal particles embedded in tire dust 2004, Environ. Int. 30 (8), 1009-1017. https://doi.org/10.1016/j.envint.2004.04.004

46. Birmili, W.; Allen, A. G.; Bary, F.; Harrison, R. M. Trace Metal Concentrations and Water Solubility in Size-Fractionated Atmospheric Particles and Influence of Road Traffic 2006, Environ. Sci. Technol. 40, 1144-1153. DOI: 10.1021/es0486925

47. Litschke, T.; Kuttler, W. On the reduction of urban particle concentration by vegetation – a review 2008, Meteorol. Z. 17, (3), 229-240. DOI: 10.1127/0941-2948/2008/0284

48. Morakinyo, T. E.; Lam, Y. F. Simulation study of dispersion and removal of particulate matter from traffic by road-side vegetation barrier 2016, Environ Sci Pollut Res 23, 6709–6722. DOI 10.1007/s11356-015-5839-y.

49. Umbrìa, A.; Galan, M.; Munoz, M.J.; Martìn, R. Characterization of atmospheric particles: analysis of particles in the Campo de Gibraltar 2004, Atmosfera 17 (4), 191-206. ISSN 0187-6236.

50. Bouhsina, S.; Cazier, F.; Noual, H.; Dewaele, D.; Delbende A.; Courcot, D.; Aboukais, A. Characteristics of suspended particulate matter emitted from an iron and steel company – A multi technique approach for search of tracers 2008, Chem. Eng. Trans. 16:79.

51. Tunno, B. J.; Dalton, R.; Michanowicz, D. R.; Shmool, J. L. C.; Kinnee, E.; Tripathy, S.; Cambal, L.; Clougherty, J. E. Spatial patterning in PM2.5 constituents under an inversion-focused sampling design across an urban area of complex terrain 2016, J Expo Sci Environ Epidemiol 26, 385–396. doi:10.1038/jes.2015.59

52. Thurston, G. D.; Ito, K.; Lall, R. A source apportionment of U.S. fine particulate matter air pollution 2011, Atmos. Environ. 45 (24) 3924-3936. https://doi.org/10.1016/j.atmosenv.2011.04.070

53. Song, F.; Gao, Y. Size distributions of trace elements associated with ambient particular matter in the affinity of a major highway in the New Jersey–New York metropolitan area 2011, Atmospheric Environ. 45 (37), 6714-6723. https://doi.org/10.1016/j.atmosenv.2011.08.031

54. Canepari, S.; Perrino, C.; Olivieri, F.; Astolfi, M. L. Characterisation of the traffic sources of PM through size-segregated sampling, sequential leaching and ICP analysis 2008, Atmospheric Environ. 42(35), 8161-8175. https://doi.org/10.1016/j.atmosenv.2008.07.052

55. Shakoor, S. A.; Soodan, A. M.; Kumar, K. Morphological Diversity and Frequency of Phytolith Types in Gaint Reed Arundo donax (L.) 2014, World Appl. Sci. J. 29 (7) 926-932. DOI: 10.5829/idosi.wasj.2014.29.07.14

56. Simonetti, G.; Buiarelli, F.; Di Filippo, P.; Pomata, D.; Riccardi, C.; Ristorini, M.; Astolfi, M. L.; Canepari, S. Spatial Distribution of Levoglucosan and Alternative Biomass Burning Tracers in an Urban and Industrial Hot-spot of Central Italy, ATMOSRES- paper under review

57. Minguillón, M. C.; Querol, X.; Baltensperger, U.; Prévôt, A. S. H. Fine and coarse PM composition and sources in rural and urban sites in Switzerland: Local or regional pollution? 2012, Sci Total Environ 427–428, 191-202. https://doi.org/10.1016/j.scitotenv.2012.04.030

58. Gietl, J. K.; Lawrence, L.; Thorpe, A., J.; Harrison, R. M. Identification of brake wear particles and derivation of a quantitative tracer for brake dust at a major road 2010, Atmos. Environ. 44 (2), 141-146. https://doi.org/10.1016/j.atmosenv.2009.10.016

59. Dongarrà, G.; Manno, E.; Varrica, D. Possible markers of traffic-related emissions 2008, Environ. Monit. Assess. 154:117. https://doi.org/10.1007/s10661-008-0382-7

60. Mirza, N.; Pervez, A.; Mahmood, Q.; Shah, M. M.; Shafqat, M. N. Ecological restoration of arsenic contaminated soil by Arundo donax L 2011, Ecol. Eng. 37, 1949– 1956. doi:10.1016/j.ecoleng.2011.07.006

61. Barbosa, B.; Boléo, S.; Sidella, S.; Costa, J.; Duarte, M.; Mendes, B.; Cosentino, S. L.; Fernando A. L. Phytoremediation of Heavy Metal-Contaminated Soils Using the Perennial Energy Crops Miscanthus spp. and Arundo donax L. 2015, Bioenerg. Res. 8, 1500–1511. DOI 10.1007/s12155-015-9688-9

62. Carranza-Álvarez, C.; Alonso-Castro, A. J.; Alfaro-De La Torre, M. C; García-De La Cruz, R. F. Accumulation and Distribution of Heavy Metals in Scirpus americanus and Typha latifolia

from an Artificial Lagoon in San Luis Potosí, México 2007, Water Air Soil Pollut. 188, 297–309. DOI 10.1007/s11270-007-9545-3

63. Kabata-Pendias, A.; Mukherjee, A. B. Trace Elements from Soil to Human 2007, Springer. ISBN 978-3-540-32714-1

64. Capelli, L.; Sironi, S.; Del Rosso, R.; Céntola, P.; Rossi, A.; Austeri, C. Olfactometric approach for the evaluation of citizens' exposure to industrial emissions in the city of Terni, Italy 2011, Sci. Total Environ. 409 (3), 595-603. https://doi.org/10.1016/j.scitotenv.2010.10.054

65. Sabeen, M.; Mahmood, Q.; Irshad, M.; Fareed, I.; Khan, A.; Ullah, F.; Hussain, J.; Hayat, Y.; Tabassum S. Cadmium Phytoremediation by Arundo donax L. from Contaminated Soil and Water 2013, BioMed Research International, 9 pages http://dx.doi.org/10.1155/2013/324830

66. Atma, W.; Larouci, M.; Meddah, B.; Benabdeli, K.; Sonnet, P. Evaluation of the phytoremediation potential of Arundo donax L. for nickel-contaminated soil 2017, Int J Phytoremediat 19 (4), 377-386, DOI:10.1080/15226514.2016.1225291

67. Fiorentino, N.; Fagnano, M.; Adamo, P.; Impagliazzo, A.; Mori, M.; Pepe, O.; Ventorino, V.; Zoina, A. Assisted phytoextraction of heavy metals: compost and Trichoderma effects on giant reed (Arundo donax L.) uptake and soil N-cycle microflora 2013, Italian J. Agronomy 8, 244-254. doi:10.4081/ija.2013.e29

Supplementary Material S1.

Table S1.1. Limits of detection (LODs) of the concentrations (µg/L) detected in water samples of the analyzed elements, set at 3 times the standard deviation (SD) of 10 replicate blank determinations.

	UoM	LODs
Ba	µg/L	1.6
Cd	µg/L	0.0088
Cr	µg/L	0.24
Cs	µg/L	0.0095
Cu	µg/L	0.15
Fe	µg/L	1.8
Li	µg/L	0.011
Mn	µg/L	0.11
Mo	µg/L	0.99
Ni	µg/L	0.14
Pb	µg/L	0.02
Rb	µg/L	0.026
Sb	µg/L	0.0094
Sn	µg/L	0.043
Sr	µg/L	0.7
Ti	µg/L	0.079
Zn	µg/L	4.3

Table S1.2. Limits of detection (LODs) of the concentrations (µg/L) detected in PM_{10} samples, of the water-soluble and insoluble fraction of the analyzed elements, set at 3 times the standard deviation (SD) of 10 replicate blank determinations.

	UoM	LODs Water-soluble Fraction	LODs Insoluble Fraction
Ba	µg/L	3.7	0.44
Cd	µg/L	0.0038	0.0031
Cr	µg/L	0.081	0.86
Cs	µg/L	0.0033	0.0017
Cu	µg/L	0.2	0.24
Fe	µg/L	3	9.6
Li	µg/L	0.0063	0.004
Mn	µg/L	0.17	0.17
Mo	µg/L	0.049	0.012
Ni	µg/L	0.35	0.17
Pb	µg/L	0.1	0.15
Rb	µg/L	0.031	0.023
Sb	µg/L	0.0094	0.0094
Sn	µg/L	0.013	0.027
Sr	µg/L	0.2	0.57
Ti	µg/L	0.15	0.4
Zn	µg/L	15	47

Table S1.3. Limits of detection (LODs) of the concentrations (µg/L) detected in washed and unwashed *A. donax* leaves, of the water-soluble and insoluble fraction of the analyzed elements, set at 3 times the standard deviation (SD) of 10 replicate blank determinations.

	UoM	LODs *A. donax* leaves
Ba	µg/L	6.7
Cd	µg/L	0.33
Cr	µg/L	0.22
Cs	µg/L	0.0021
Cu	µg/L	0.12
Fe	µg/L	30
Li	µg/L	0.014
Mn	µg/L	1.1
Mo	µg/L	0.13
Ni	µg/L	0.18
Pb	µg/L	0.059
Rb	µg/L	0.028
Sb	µg/L	0.011
Sn	µg/L	0.019
Sr	µg/L	0.63
Ti	µg/L	0.47
Zn	µg/L	4.2

Supplementary Material S2.

Table S2.1. Average mean (AM) values and standard deviations of element concentrations detected in unwashed *A. donax* leaves at the six monitoring sites.

***A. donax* Unwashed Leaves Element Concentrations**												
		TE1		**TE2**		**TE3**		**TE4**		**TE5**		**TE6**	
	UoM	**AM**	**SD**	**AM**	**SD**	**AM**	**SD**	**AM**	**SD**	**AM**	**SD**	**AM**	**SD**
Ba	ng/mg	13	1.1	5	0.2	16	1.7	16	1.8	32	3.5	47	5.2
Cd	ng/mg	0.26	0.047	1.6	0.28	3.4	0.61	1.6	0.29	3.9	0.7	0.26	0.047
Cr	ng/mg	1.2	0.053	1.6	0.092	1.6	0.2	2.2	0.17	6.2	0.98	6.6	1.2
Cs	ng/mg	0.18	0.032	0.23	0.034	0.2	0.022	0.078	0.0097	0.071	0.008	0.031	0.0015
Cu	ng/mg	5.7	0.59	6.6	0.79	5.2	0.49	5.1	0.47	8.9	1.4	11	2.3
Fe	ng/mg	125	14	117	12	133	15	110	11	271	47	269	48
Li	ng/mg	0.037	0.0043	0.047	0.0067	0.053	0.0086	0.036	0.0041	0.055	0.009	0.086	0.014
Mn	ng/mg	36	3.4	26	1.9	15	0.63	51	7.1	31	2.6	128	18
Mo	ng/mg	1.2	0.15	0.87	0.073	1.3	0.15	0.94	0.085	3.9	0.77	5.7	0.97
Ni	ng/mg	1.1	0.08	1.8	0.19	1.9	0.23	1.3	0.098	3.4	0.51	4.1	0.45
Pb	ng/mg	0.2	0.033	0.15	0.012	0.18	0.027	0.35	0.063	0.3	0.042	0.33	0.053
Rb	ng/mg	30	5.6	36	4.7	33	4.2	31	6.2	25	4.1	26	4.2
Sb	ng/mg	0.021	0.0033	0.009	0.0007	0.039	0.0078	0.01	0.0007	0.009	0.0007	0.024	0.0044
Sn	ng/mg	0.053	0.0062	0.055	0.0066	0.051	0.0058	0.06	0.008	0.055	0.0066	0.058	0.0075
Sr	ng/mg	17	1.1	22	1.8	23	2	32	3.8	28	2.9	53	10
Ti	ng/mg	1.8	0.16	1.6	0.13	1.5	0.12	1.7	0.15	2.7	0.39	3.8	0.42
Zn	ng/mg	26	4	36	7.5	34	6.9	27	4.2	36	4	51	10

Table S2.2. Average mean (AM) values and standard deviations (SD) of element concentrations detected in washed *A. donax* leaves at the six monitoring sites.

***A. donax* Washed Leaves Element Concentrations**												
		TE1		**TE2**		**TE3**		**TE4**		**TE5**		**TE6**	
	UoM	**AM**	**SD**	**AM**	**SD**	**AM**	**SD**	**AM**	**SD**	**AM**	**SD**	**AM**	**SD**
Ba	ng/mg	5.3	0.22	5.4	0.22	5.3	0.21	16	2	31	4.3	46	6.9
Cd	ng/mg	0.26	0.047	1.1	0.21	3.3	0.59	1.6	0.29	3.8	0.68	0.26	0.046
Cr	ng/mg	0.75	0.051	0.92	0.077	0.84	0.063	1.4	0.19	2.3	0.49	1.7	0.19
Cs	ng/mg	0.16	0.029	0.21	0.036	0.16	0.027	0.078	0.04	0.069	0.0084	0.022	0.0008
Cu	ng/mg	5.2	0.55	6.5	0.85	5.1	0.53	4.5	0.4	7.4	1.1	8.7	1.5
Fe	ng/mg	109	14	100	12	74	6.4	103	12	199	20	188	42
Li	ng/mg	0.026	0.0028	0.029	0.0035	0.03	0.0038	0.033	0.0046	0.045	0.0088	0.062	0.01
Mn	ng/mg	35	3.4	24	1.7	14	0.53	48	6.7	27	2	121	17
Mo	ng/mg	1.2	0.14	0.74	0.058	1.2	0.15	0.88	0.081	3.1	0.56	5.6	0.72
Ni	ng/mg	1.1	0.093	1.6	0.2	1.8	0.26	1.2	0.12	2.5	0.25	2.1	0.36
Pb	ng/mg	0.14	0.022	0.047	0.0025	0.18	0.036	0.13	0.021	0.29	0.038	0.25	0.045
Rb	ng/mg	29	5.4	36	4.6	34	4.1	30	6	25	4	25	4.2
Sb	ng/mg	0.02	0.003	0.009	0.001	0.0089	0.001	0.0093	0.0011	0.0092	0.0011	0.0089	0.001
Sn	ng/mg	0.016	0.0013	0.015	0.0013	0.017	0.0012	0.048	0.0076	0.017	0.0013	0.016	0.0012
Sr	ng/mg	16	0.99	18	1.3	15	0.93	31	3.9	27	3	52	5.2
Ti	ng/mg	1	0.089	1.2	0.12	0.87	0.065	1.5	0.21	1.2	0.13	1.6	0.22
Zn	ng/mg	26	4.1	35	3.8	22	2.9	26	4.3	35	4.3	51	6.1

Table S2.3. OK (ordinary kriging) interpolated concentrations of water-soluble fraction of atmospheric elements at the six monitoring sites.

Water-soluble Interpolated Atmospheric Element Concentrations							
	UoM	**TE1**	**TE2**	**TE3**	**TE4**	**TE5**	**TE6**
Ba	ng/m^3	6.1	4.7	4.1	4.7	5.3	4.8
Cd	ng/m^3	0.03	0.047	0.052	0.032	0.039	0.05
Cr	ng/m^3	0.88	1.3	2	1.1	1.9	1.9
Cs	ng/m^3	0.012	0.017	0.017	0.015	0.015	0.016
Cu	ng/m^3	2.5	2.6	2.7	1.5	2.5	1.9
Fe	ng/m^3	9.8	11	10	7.5	9.9	12
Li	ng/m^3	0.059	0.088	0.12	0.085	0.11	0.12
Mn	ng/m^3	4.2	4.3	2.6	3.8	4.8	5.6
Mo	ng/m^3	2.3	3.0	2.4	4.8	14	11
Ni	ng/m^3	0.92	0.81	1.2	0.68	1.1	1.7
Pb	ng/m^3	0.32	0.41	0.42	0.4	0.29	0.36
Rb	ng/m^3	0.34	0.43	0.4	0.3	0.36	0.37
Sb	ng/m^3	0.45	0.35	0.26	0.51	0.31	0.29
Sn	ng/m^3	0.25	0.16	0.18	0.15	0.16	0.17
Sr	ng/m^3	1.7	2.1	1.4	1.7	1.9	1.8
Ti	ng/m^3	0.08	0.091	0.12	0.089	0.1	0.13
Zn	ng/m^3	13	14	21	13	16	18

Table S2.4. OK (ordinary kriging) interpolated concentrations of insoluble fraction of atmospheric elements at the six monitoring sites.

Insoluble Interpolated Atmospheric Element Concentrations							
	UoM	**TE1**	**TE2**	**TE3**	**TE4**	**TE5**	**TE6**
Ba	ng/m^3	7.3	6.9	4.9	6.2	6.5	4
Cd	ng/m^3	0.006	0.022	0.016	0.021	0.025	0.026
Cr	ng/m^3	13	14	30	12	45	48
Cs	ng/m^3	0.021	0.03	0.035	0.025	0.031	0.032
Cu	ng/m^3	8.9	7.3	9.3	4.7	11	6.6
Fe	ng/m^3	351	344	577	218	332	504
Li	ng/m^3	0.12	0.1	0.15	0.087	0.15	0.1
Mn	ng/m^3	6.3	7.1	3.5	5.3	11	14
Mo	ng/m^3	0.8	1.3	1.4	0.96	2.1	4.1
Ni	ng/m^3	4.8	6.3	4.3	3.4	19	23
Pb	ng/m^3	3	3.3	4.6	3	4.5	3.4
Rb	ng/m^3	0.45	0.32	0.43	0.16	0.44	0.3
Sb	ng/m^3	0.66	0.4	0.3	0.64	0.73	0.25
Sn	ng/m^3	2	1.7	2.1	0.85	2.3	1
Sr	ng/m^3	1.2	1.4	1	2.4	2.3	1.3
Ti	ng/m^3	4.5	4.3	7.1	3.6	7.1	8
Zn	ng/m^3	30	32	57	26	40	34

Table S2.5. Average mean (AM) values and standard deviations of element concentrations detected in river water samples at the six monitoring sites.

River Water Element Concentrations												
		TE1		TE2		TE3		TE4		TE5		TE6	
	UoM	AM	SD	AM	SD	AM	SD	AM	SD	AM	SD	AM	SD
Ba	µg/l	96	11.2	66	5.3	71	6.0	60	4.3	95	11	86	9.0
Cd	µg/l	0.012	0.00057	0.013	0.00065	0.019	0.0014	0.033	0.0042	0.036	0.0050	0.034	0.0044
Cr	µg/l	0.84	0.022	1.56	0.077	1.61	0.082	0.53	0.0089	28	5.4	0.30	0.0028
Cs	µg/l	0.15	0.016	0.14	0.014	0.20	0.028	0.10	0.0068	0.24	0.038	0.11	0.0077
Cu	µg/l	1.4	0.19	0.84	0.065	1.4	0.18	0.93	0.079	2.15	0.42	1.28	0.15
Fe	µg/l	1.2	0.068	1.9	0.16	1.9	0.16	1.9	0.17	16	2.8	1.9	0.17
Li	µg/l	6.3	1.1	4.9	0.65	7.2	1.4	5.4	0.79	7.9	0.87	4.7	0.6
Mn	µg/l	0.12	0.014	0.13	0.014	0.13	0.014	0.057	0.0028	0.14	0.016	0.12	0.013
Mo	µg/l	5.2	0.59	5.2	0.59	7.8	1.3	3.6	0.28	39	4.6	2.0	0.087
Ni	µg/l	7.1	0.83	5.2	0.45	9.4	1.5	4.2	0.29	23	4.2	4.9	0.39
Pb	µg/l	0.14	0.017	0.035	0.0029	0.053	0.0066	0.037	0.0032	0.029	0.0019	0.037	0.0032
Rb	µg/l	3.3	0.56	1.7	0.15	2.3	0.27	1.8	0.16	2.6	0.35	2.0	0.20
Sb	µg/l	0.094	0.016	0.055	0.0054	0.091	0.015	0.051	0.0047	0.19	0.026	0.055	0.0055
Sn	µg/l	0.20	0.028	0.23	0.030	0.0094	0.00020	0.012	0.00035	0.024	0.0013	0.053	0.0064
Sr	µg/l	978	172	859	133	1084	211	904	147	986	175	900	146
Ti	µg/l	1.8	0.22	1.6	0.15	1.9	0.22	1.5	0.15	3.2	0.32	1.5	0.15
Zn	µg/l	4.4	0.18	4.4	0.017	5.4	0.26	4.5	0.18	5.3	0.26	4.3	0.17

2.4. (D) Evaluation of Rapid Analytical Methods for Human Exposure Assessment to Toxic Elements

Determination of toxic element concentrations in biological matrices is useful for monitoring environmental and occupational exposure, for evaluating relationships between health effects and PM chemical composition and sources, and for assessing the related human health risks.

For these reasons, we evaluated the suitability of different biological matrixes for human biomonitoring exposure to environmental pollution and we developed and validated rapid analytical methods for routine elemental analysis of a significant number of biological samples. We evaluated human exposure to toxic elements, such as arsenic, lead, mercury and cadmium, which rank 1st, 2nd, 3rd, and 7th, respectively, on the U.S.A. National Priorities List (NPL) of the Agency for Toxic Substances and Disease Registry (ATSDR, 2015). Generally, humans uptake Hg As, Pb and Cd through the respiratory or digestive systems, as well as via dermal absorption.

To estimate an individual exposure to Hg, analytical methods for blood, urine, or tissues, such as nail or hair, have been investigated. Among the several suitable biological matrices for biomonitoring studies, human hair presents numerous advantages because it is a stable, non-invasive matrix that is easy to collect, storage and transport and has a high Hg concentration. Human hair has been used in few studies for the determination of toxic element concentrations by cold vapor generation atomic fluorescence spectrometry (CV-AFS). However, because of the lack of standardized hair analysis procedures it is difficult to compare and interpret the results from different studies and reach significant conclusions; furthermore, analytical performances of methods used for biomonitoring are infrequently documented. Therefore, we developed and validated a rapid and very sensitive analytical method, using CV-AFS, for total Hg determination in human hair that can be used in biomonitoring studies involving a large number of samples.

In addition, we compared the performance of some hair sample treatments and we optimized and validated a new rapid treatment of human hair for screening analysis and biomonitoring studies. We evaluated the accuracy, precision and detection/quantification limits of a fast, sensible and reliable analytical method for multi-elemental (40 elements) analysis of biological samples by ICP-MS and ICP-OES. The analytical performance and quality control of the optimized procedure were evaluated by application of certified material of hair, spiked samples and in-field samples of Eritrean hair.

Breast milk is a another suitable matrix for biomonitoring exposure to environmental pollution. Assessing the levels of Hg As, Pb and Cd in breast milk may provide valuable information on the maternal toxic load and serves as an indicator for prenatal and post-natal exposure of infants to these

chemicals. Moreover, recent studies have shown that some strains of probiotic lactobacilli can reduce elemental toxicity in humans. For these reasons, we examined the exposure to As, Cd, Hg and Pb in newborn children and in mothers and then we evaluated the capacity of a multi-strain probiotic to protect the infants from exposure to these toxic elements.

2.4.1. (D1) Simple and Rapid Method for the Determination of Mercury in Human Hair by Cold Vapour Generation Atomic Fluorescence Spectrometry

Microchemical Journal (2019), *150*, 104186

Maria Luisa Astolfi [a,*], Carmela Protano [b], Elisabetta Marconi [b], Daniel Piamonti [c], Lorenzo Massimi [a], Marco Brunori [c], Matteo Vitali [b], Silvia Canepari [a]

[a] Department of Chemistry, Sapienza University, Piazzale Aldo Moro 5, 00185 Rome, Italy;
[b] Department of Public Health and Infectious Diseases, Sapienza University, Piazzale Aldo Moro 5, 00185 Rome, Italy;
[c] Department of Cardiovascular, Respiratory, Nephrology, Anaesthesiology and Geriatric Science, Sapienza University, Viale del Policlinico 155, 00161 Rome, Italy.

Abstract: The aim of the study was to develop and validate a rapid method for the analysis of the total Hg concentration in human hair, specifically, Eritrean hair. For total Hg determination, the cold vapour generation atomic fluorescence spectrometry (CV-AFS) technique was used, and the results were compared with those of the more frequently used advanced mercury analyser (AMA). Samples were prepared by washing the hair and collecting two samples; the first was used for the direct analysis of Hg by AMA and the second was digested for Hg determination by CV-AFS. The results of field hair sample analysis indicate that the two data sets were fully comparable (median: AMA, 0.11 mg kg^{-1}; CV-AFS, 0.12 mg kg^{-1}) and were not statistically different (Mann–Whitney test, *p*-value = 0.944). The two techniques showed results with good coefficients of determination (R^2 = 0.98) despite the different operating ranges. The AMA and CV-AFS methods were validated using a certified reference hair sample, yielding, respectively, trueness biases of 7.4% and 7.2%, intra-day repeatability (relative standard deviation (RSD), %) of 3.2% and 6.0%, inter-day reproducibility (RSD, %) of 5.3% and 8.2%, and expanded standard measurement uncertainties of 8.9% and 17%, respectively. Analyses of blank measurements by AMA and CV-AFS yielded a detection limit of 0.0004 and 0.004 mg kg^{-1} of Hg for 5 and 20 mg samples of human hair, respectively. Both techniques are simple, easy to use, and relatively inexpensive, and the method validation parameters indicate sensitivity, precision, and reliability. In conclusion, the use of AMA should be considered over CV-AFS in hair analysis to reduce sample handling and, consequently, lower the risk of contamination,

use fewer samples, and allow more economical analyses. In contrast, CV-AFS using optimised fast digestion in an open vessel heated in a water bath instead of AMA allows short analysis times and automation, thus allowing high sample throughput for routine analysis and human biomonitoring studies.

Keywords: validation; inter-technique comparison; toxic element; AMA; CV-AFS; biomonitoring.

1. Introduction

Mercury is a naturally occurring hazardous and extremely toxic heavy metal that has several adverse ecological and health effects [1,2]. Hg has many different chemical forms (elemental, inorganic, and organic) and all are toxic [3-8].

Generally, humans uptake Hg through the respiratory or digestive systems, as well as via dermal absorption [9]. Exposure to methylmercury from fish consumption or vaporous mercury (Hg^0), which is emitted from various sources such as metallic Hg, dental amalgams, and the air as a result of industry, pharmacology, gold mining, and agriculture, via inhalation [1,6,10-12].

To estimate an individual's exposure to Hg, analytical methods for blood, urine, or tissues, such as nail or hair, have been investigated [13-19]. Mercury levels in hair have been found to be a suitable indicator of dietary, environmental, and occupational human exposure [18,20]. In particular, methylmercury is the dominant species in hair (more than 80%), so total hair Hg analysis is often used as a measure of methylmercury exposure [8,18,19]. Based on impact studies of Hg on human health, the World Health Organisation (WHO) established a normal hair Hg concentration of 2 $\propto$g g^{-1} and a tolerance threshold value of 10 $\propto$g g^{-1} [8]. Among the several suitable biological matrices for biomonitoring studies [18,21-25], human hair presents numerous advantages because it is a stable, non-invasive matrix that is easy to collect (sampling can be performed on-site by the subject), storage (refrigeration and preservatives are not needed), and transport and has a high Hg concentration [18,20,26]. This is very important when considering biomonitoring in developing countries and remote areas where immediate sample cooling to 4 °C or even freezing below -18 °C to prevent degradation and to reduce bacterial growth is not available.

For Hg determination in biological samples, the most common instrumental techniques are atomic absorption spectroscopy (AAS) [27-32] and inductively coupled plasma–mass or optical emission spectrometry (ICP-MS or ICP-OES, respectively) [15,33-37], typically coupled to cold vapour generation (CV) for matrix separation. However, memory effects can occur during the determination of total Hg by ICP-MS [38]. The use of CV atomic fluorescence spectrometry (AFS) is a good

alternative for total Hg determination, and it has been used for the analysis of several food matrices [39]. Despite this, its use for hair analysis is documented only in very few works [3,19,40] for Sb [41] and other elements [20,42-45]. In all these techniques, the sample must be introduced as a homogeneous liquid sample, and, thus, the digestion of the sample is necessary. Sample pre-treatment comprises the addition of aggressive or oxidising chemicals before Hg determination. Generally, HNO_3 or a mixture of HNO_3 and H_2O_2 in various proportions is employed [20]. The afforded digest is stable and characterised by a low residual acidity, residual carbon content, and dissolved solid concentration [20,46]. In particular, the ICP signal of Hg with an ionisation potential similar to that of C (10.4 and 11.4 eV, respectively) may increase because of charge transfer reactions with C [47]. On the other hand, the residual acidity can severely suppress the analytical signal [20,48,49]. Recently, direct Hg analysis by means of automated commercial instruments, such as the Advanced Mercury Analyser (AMA), Trace Mercury Analyser (TMA), or Direct Mercury Analyser (DMA) has become increasingly popular, especially given their advantages of not requiring sample pre-treatment or extraction and the possibility of analysing both liquid and solid matrices and carrying out economic analysis [50-56].

Because of the lack of standardised hair analysis procedures (including sample treatment methods), it is difficult to compare and interpret the results (intervals and reference values) from different studies and reach significant conclusions [18]. In particular, recent reviews have revealed that the analytical performances (detection/quantification limits and accuracy) of methods used for biomonitoring are infrequently documented [20,57].

Thus, the aim of this study was to develop and validate a rapid and very sensitive analytical method using CV-AFS for total Hg determination in hair that can be used in biomonitoring studies involving a large number of samples. The performance of the proposed method is compared with that of the most frequently used oxygen combustion–gold amalgamation procedure.

2. Experimental

2.1. Instrumentation

Total Hg determination was carried out using an AMA (AMA-254, Altec Ltd., Prague, Czech Republic) and CV-AFS (AFS 8220, Beijing Titan Instrumental Co., Ltd., Beijing, China) with oxygen (99.995% purity; SOL Spa, Monza, Italy) and argon (99.999% purity; SOL Spa, Monza, Italy) as carrier gases, respectively.

An ICP–OES (Vista MPX CCD Simultaneous; Varian, Victoria, Mulgrave, Australia) using axial-view mode and equipped with a cyclonic spray chamber was used for the determination of the C

content in the final digests and some other transition metals in the hair samples. A radiofrequency power of 1.4 kW, plasma gas flow rate of 15.0 L min^{-1}, auxiliary gas flow rate of 1.5 L min^{-1}, nebuliser gas flow rate of 0.80 L min^{-1}, and wavelength of 193.091 nm were used as operational conditions, as reported previously [22].

An analytical balance (sensitivity 0.01 mg; Gibertini E50S Gibertini Elettronica, Milan, Italy) was used to weigh both real and certified samples of human hair samples and solid reagents. A water bath instrument (WB12; Argo Lab, Modena, Italy) with electronic temperature control was used for open vessel digestion.

2.2. Reagents, Standards and Materials

Calibration standard solutions were obtained using suitable multi-standard stock solutions of Hg (1002 ± 7 mg L^{-1}; SCP Science, Baie D'Urfé, Canada). Deionised H_2O (resistivity ≤18.3 MΩ cm) was generated by an Arioso Power I RO-UP Scholar UV deioniser (Human Corporation, Songpa-Ku, Seoul, Korea). HNO_3 (assay >67%; residue < 1 mg L^{-1}; Promochem, LGC Standards GmbH, Wesel, Germany) and H_2O_2 (assay > 30%; Promochem, LGC Standards GmbH, Wesel, Germany) were high-purity solvents used for trace analysis.

Five percent HCl (assay >36%; residue <3 mg L^{-1}; Promochem, LGC Standards GmbH, Wesel, Germany) was used as a carrier, and 0.05% $NaBH_4$ (Sigma–Aldrich, St. Louis, USA) in 0.05% NaOH (assay >98%, anhydrous pellets, RPE for analysis, ACS – ISO; Carlo Erba Reagents, Milan, Italy) was used as a reducing agent for CV-AFS analysis.

Calibration solutions for residual C determination by ICP-OES and synthetic matrices for the enhancement or suppression of the CV-AFS analytical signal were prepared in the range from 20 to 200 mg L^{-1} by sequential dilution of a stock solution (1000 mg L^{-1} of C). This solution was prepared by the dissolution of anhydrous citric acid (assay ≥99.5%, ACS reagent; Sigma–Aldrich Chemie GmbH, Steinheim, Germany) in boiled deionised water following a previously published method [46]. Y was chosen as an internal standard for C determination to control the nebuliser efficiency, as reported in our previous works [58-60]. The concentration of Y in the samples introduced to the ICP-OES was 100 ∝g L^{-1} and was prepared freshly before every run from the standard stock solution (1000 ± 2 mg L^{-1}; Panreac Química, Barcelona, Spain).

A single standard solution of several transition metals, Co, Cu, Mn, Ni, Fe, and Zn, ranging from 0.01 mg L^{-1} to 50 mg L^{-1} was prepared in 3% HNO_3 from single standard stock solution (1000 ± 5 mg L^{-1}; Merck KGaA, Darmstadt, Germany) and used for the evaluation of possible interference in the atomic fluorescence emission signal and for the preparation of the ICP-OES calibration curve.

European reference material (ERM) DB001 trace elements in human hair (sample no. 0196; Joint Research Centre, Geel, Belgium) was used for analytical method validation and quality control. Syringe filters with cellulose nitrate (GVS Filter Technology, Indianapolis, USA) membranes (0.45-μm pore size) were used to filter the digests obtained by acid digestion. Graduated tubes (2.5, 5, and 10 mL in polypropylene) were purchased from Artiglass S.R.L. (Due Carrare, PD, Italy).

2.3. Samples

Adult (18–50 years) hair of both sexes (18 males and 22 females) living in a small rural agricultural area of Asmara (Eritrea, Africa) was selected from a larger population participating in the 'Medeber project', a research project carried out in collaboration with the Italian non-profit organisation 'ASS.ITER Onlus' (https://www.assiter.org/Progetto-Medeber.htm). The population was uniform when considering the hair colour (black), type of hair (curly), ethnic and geographical origin, and living habits. Stainless-steel scissors were used to cut the hair samples (about 0.1 g) after washing with shampoo and drying, as reported by other authors [61,62]. The samples were stored in plastic bags with identification tags and shipped to the laboratory for further treatment and analysis. In the laboratory, the hair strands were further cut into smaller pieces (3–5 mm).

2.4. Total Hg Determination by AMA

The certified and field hair sample were weighed (ranging from 5 to 10 mg) into the analysing shuttle (in Ni) and introduced into the instrument without any pre-treatment. Then, the sample was dried at 120 °C and thermally and chemically decomposed at 750 °C. After sample combustion, Hg is selectively trapped and pre-concentrated by gold amalgamation and quantified by atomic absorption spectrometry. A low-pressure Hg vapour lamp was then used as the light source at the working wavelength of 253.7 nm. The operating conditions were: one repeat; drying time, 30 s; decomposition time, 100 s; and waiting time, 40 s. The total analysis time was about 5 min for each sample. A calibration curve was plotted using two calibration ranges: 0.2–20 and 50–500 ng. The instrument automatically switched to the highest calibration range if an absorption of more than 0.8 was measured. The calibration of the AMA-254 analyser is very high and remains valid for a period of at least 6 months. Control of the goodness of the calibration was carried out before each analytical run by analysing a concentration standard equal to 1 ng of Hg. A blank (i.e., an empty sample Ni boat) was analysed periodically to verify that Hg was not carried over between samples. Blank readings were typically < 0.0012 absorbance units, corresponding to values of < 0.004 ng of Hg. Roughly every 100 samples, a new boat was used after heating it twice to remove potential traces of Hg.

Certified and field hair samples were analysed in six and two replicates, respectively. Blanks were deducted from all measurements.

2.5. Total Hg Determination by CV-AFS

Certified and field hair samples were weighed (ranging from 15 to 30 mg) in polypropylene tubes, mixed with 0.5 mL of 67% HNO_3 and 0.25 mL of 30% H_2O_2, and heated in a water bath for 20 min to a temperature of 95 °C. Up to 120 samples can be digested together. All digests were diluted to a volume of 10 mL with deionised water and then filtered through a pre-cleaned syringe filter, taking care to discard the first 2.5 mL of the solution necessary for the pre-washing of the filter.

Table 1. Optimized experimental parameters of the cold vapor generation atomic fluorescence spectrometry.

Parameter	**Setting**
High voltage of PMT (V)	275
Atomizer height (mm)	10
Current of lamp (mA)	60
Measurement mode	Standard curve
Read mode	Peak area
Lamp	Mercury hollow cathode lamp, 253.7 nm
Read time (s)	15
Delay time (s)	0.5
Repetition time	1
Flow rate of shield gas (Ar) (mL min^{-1})	1000
Flow rate of carrier gas (Ar) (mL min^{-1})	300
$NaBH_4$ solution concentration (v/v)	0.05%, stabilized with 0.5% NaOH
$NaBH_4$ flow rate (mL min^{-1})	3.6
HCl solution concentration (v/v)	5%
HCl flow rate (mL min^{-1})	2.5
Sample volume (mL)	1.0

All the filters were previously washed with 30 mL of 2% HNO_3 to reduce the blank values. All digests were further diluted in a 1:2 ratio with 6% HCl for Hg determination by CV-AFS and analysed

without dilution for C determination by ICP-OES. The operational parameters of CV-AFS (Table 1) were in accordance with the manufacturer's recommendations.

The flow injection system used for CV generation (Fig. S1) consisted of a peristaltic pump, reaction mixer and two sequential gas liquid separators (GLS). Ar was used as carrier gas to transport the analytes to AFS and as shielding gas for the atomizer. The Ar/H_2 flame was maintained by the H_2 generated parallel to the cold vapor reaction of HCl with $NaBH_4$. A high performance hollow cathode lamp (General Research Institute for Nonferrous Metals, Beijing, China) was used as the radiation source.

Standard solutions for CV-AFS external calibration (nine points) ranging from 0.01 to 1.5 $\propto$g L^{-1} were matrix–matched and freshly prepared before every run. The analysis time for Hg determination by CV-AFS was about 1 min for each sample. Certified and field hair samples were analysed in six and two replicates, respectively. Ten blank solutions, consisting of deionised water and reagents, were analysed together with each digested sample set in order to subtract the background signal arising from reagents, and to trace and control the contributions from possible sample contamination. Blanks were deducted from all measurements.

2.6. Validation

After method optimisation, validation was carried out according to previously reported methods [63,64] based on the linearity, limits of detection (LODs) and quantification (LOQs), accuracy (trueness and precision as repeatability and intermediate precision), robustness (minor changes), selectivity, and standard measurement of uncertainty. Furthermore, the developed methods were applied to the field hair samples.

The quality of the results was checked with control charts (Fig. S2 and S3). In particular, both the evaluation of the blank level before and during the measurements and the instrumental drift were checked. The drift was controlled by measuring a standard solution (0.4 $\propto$g L^{-1} and 1 ng for Hg by CV-AFS and by AMA, respectively) immediately after the calibration curve, after every 10 samples, and at the end of the analytical sequence. The percentage drift (d%) was calculated based on the formula reported in a previous work [22]. Further details are given in section S1.

All possible sources of uncertainty must be carefully identified [64,65]. When the major contributions to uncertainty have been determined, a good estimate of the measurement uncertainty can be made by concentrating effort on the largest and most significant contributions. Subsequently, the uncertainty components are quantified, and the combined uncertainty is calculated [64,65]. In this study, the following contributions to the combined measurement uncertainty were selected: weight

of the hair sample (u_{mass}), instrumental calibration (u_{cal}), repeatability of the measurements (u_{rip}), and trueness bias (u_{bias}). Then, the combined uncertainty (u_C) was calculated as the square root of the sum of the squares of all contributes. In contrast, the expanded measurement uncertainty (U_e) was:

$$U_e = u_C \times k,$$

where k is the coverage factor of 2, which considers a normal distribution of measurements with a 95% confidence level.

2.7. Statistical elaboration

Data analyses were performed using IBM-SPSS Statistics for Windows (version 25.0, released 2017; IBM Corp., Armonk, NY, USA). Values below the LOD were designated as half the LOD value, as recommended for small datasets [66,67]. A descriptive statistical elaboration of field hair samples was carried out by calculating the most important descriptors, such as arithmetic mean, median, and 25^{th}–75^{th} percentiles. In addition, the Mann–Whitney test was used to compare the differences in the Hg levels obtained by AMA and CV-AFS and to evaluate the effect of age, and gender on the Hg concentrations.

3. Results and Discussion

3.1. Method Optimisation

Two analytical techniques were compared to evaluate the total Hg concentration in hair samples: AMA and CV-AFS. These techniques were selected for their good performance and because they differ significantly in their general principles and their associated sample preparation methods (Table 2). AMA is based on atomic absorption detection and does not require any sample preparation, whereas CV-AFS is based on atomic fluorescence intensity detection following digestion of the samples.

The first tests involving AMA were performed to select the optimal instrumental parameters. Considering the recommendations of the instrument manual, tests were carried out by varying the drying and decomposition times, respectively, from 10 to 60 s and from 100 to 150 s for hair sample masses ranging from 5 to 10 mg. The recommended waiting time is 40 s. The concentration measured was within the uncertainty range of the certified value of ERM DB001 (Table 2) using the following conditions: one repeat and drying, decomposition and waiting times of 30, 100, and 40 s, respectively. To check the possible gain in sensitivity, attempts to increase the sample uptake from 10 to 50 mg were made. However, such a sample uptake led to a gradual memory effect on the instrumental signal

and, sometimes, excessive gas (CO_2) development during the sample decomposition process, which are not compatible with the high number of samples for analysis.

Table 2. Linearity, slope [b ± s(b)] and intercept [a ± s(a)] of calibration graphs (y = a + bx), detection (LODs) and quantification (LOQs) limits, trueness bias percentage (bias%), precision [repeatability as relative standard deviation percentage (RSD%), intra-day and inter-day reproducibility (RSD%)] and other information for the determination of Hg by using advanced mercury analyzer (AMA) and cold vapor atomic fluorescence spectrometry (CV-AFS).

Analytical characteristics	**AMA**	**CV-AFS**
Linear range	0.1–4 ng	0.01–1.5 ∝g L^{-1}
Slope	0.0255 ± 0.0002 ng^{-1}	13100 ± 32 L $\propto g^{-1}$
Intercept	0.00144 ± 0.00036	154 ± 15
LOD (mg kg^{-1})	0.0004	0.004
LOQ (mg kg^{-1})	0.01	0.01
Bias%	7.4	7.2
RSD% intra-day	3.2	6.0
RSD% inter-day	5.3	8.2
Other information		
Sample preparation	No (analysis of sample in both liquid and solid form)	Acid digestion (analysis of sample only in liquid form)
Calibration	Valid for thousands of samples and a period of months	Daily calibration is required
Time for sample	5 min	1 min
Daily sample analysis *based on 8 hour working day*	96	480
Time for sample preparation *1 or 120 samples*	0	About 45 min or 8.5 h (addition of reagents, 1 min; dilution, 1 min; filtration, 1 min; pre-cleaning of filter, 1 min; time of digestion, 20 min; and cooling, 20 min)
Element	Hg	As, Bi, Cd, Ge, Hg, Pb, Sb, Se, Sn, Te, and Zn
Carrier and/or reduction solution	No	Yes

Hair samples must undergo a process of digestion before analysis by CV-AFS. The selection of the sample mass and choice of the decomposition agent together with their volumes and temperature was made based on the literature [68]. Sample decomposition was carried out in an open vessel heated in a water bath (95 °C) for 20 min because the use of the polypropylene tubes that are subsequently used for the autosampler in the CV-AFS analysis allows for the significant reduction in sample and reagent amount, treatment time, and sample handling compared to microwave acid digestion [22]. Further, disadvantages arising from vessel assembly and analytical operations, i.e. sample weighing, addition of reagents, sample digestion, and digest dilution, are minimised by using a single tube without the need for sample and solution transfer.

As is well known, to obtain digested samples with good characteristics (i.e., low residual carbon content), it is necessary to use an oxidising mixture, such as HNO_3 and H_2O_2 [20]. However, an excess of HNO_3 in the final digested sample makes the reduction process inefficient because of the oxidation of the reducing agents [41,48]. Thus, the residual carbon content and residual acidity in final digests were determined. The concentrations of HCl and $NaBH_4$/NaOH to be added were evaluated in the digested sample to reduce Hg^{2+} to volatile Hg^0. The atomic fluorescence signal (at a wavelength of 253.7 nm) can only be measured for Hg^0 which, separated from the solution, reaches the torch. The preliminary experiments were performed by varying HCl from 1% to 5%, NaOH from 0.1% to 0.5%, and $NaBH_4$ from 0.05% to 1% in duplicate to evaluate the atomic fluorescence signal response. Considering both the intensity and stability of the signal, 5% HCl (v/v), 0.5% NaOH (m/v), and 0.05% $NaBH_4$ (m/v) were used in further studies of this work.

3.2. Method Validation

The optimised conditions for both total Hg determination by AMA and CV-AFS were used to validate the methods. The performance criteria of the methods, including linearity, selectivity (interference study), LODs and LOQs, repeatability, intermediate precision, and trueness were defined and reported in Table 2. In addition, a comparison between some characteristics of the two analytical techniques are illustrated in Table 2.

3.2.1. Linearity

The AMA has an internal calibration system that automatically selects the most appropriate concentration range. The hair samples were analysed with the AMA in the most sensitive range (0.2–20 ng). The slope and the intercept of the calibration curves were 0.0255 ± 0.0002 ng^{-1} and 0.00144 ± 0.00036, respectively (Table 2). The AMA linearity was verified by the use of one-way ANOVA

test from 21 calibration points with seven Hg concentration levels ranging from 0.1 to 4 ng, excluding the calibration blanks, on three different days [69]. The stability of the AMA internal calibration, instrumental drift, possible cross-contamination, and memory effects were daily checked using control charts (Fig. S2), and the control standard solution (1 ng) and the blanks (HNO_3 1%, v/v) were monitored.

The CV-AFS linearity was studied from 27 calibration points with 9 Hg concentration levels ranging from 0.01 to 1.5 ∝g L^{-1}, excluding the calibration blanks, on three different days. The calibration standards were sequentially analysed daily in order of peak concentrations, and a minimum R^2 value ≥0.999 was considered. The slope and the intercept of the calibration curves were 13100 ± 32 L g^{-1} and 154 ± 15, respectively (Table 2). The CV-AFS linearity range was verified by the use of one-way ANOVA test [69]. In addition, for CV-AFS, the control standard solution (0.4 ∝g L^{-1}) and the blanks [HNO_3 3.5% (v/v) : HCl 3% (v/v), 1:3], instrumental drift, cross-contamination, and memory effects were checked daily using control charts to monitor for possible systematic errors (Fig. S3). Further details on linearity and control charts used for both methods by AMA and CV-AFS are given in section S2.

3.2.2. Selectivity

The selectivity was evaluated to ensure that there were no significant matrix effects that would otherwise could generate bias. As reported by other authors [70], AMA can suffer from matrix effects. To check the selectivity of the AMA method, the recoveries of hair samples (5 mg) spiked with standard solutions at 1, 3, and 10 ng of Hg concentration (two replicates for each) were measured. A regression line (abscissa = concentration added; ordinate = concentration found) was plotted. According to Student's test (p = 0.62 with 10 degrees of freedom and at significance level α = 0.01), the slope (1.03) and the intercept (0.198) of the regression line (R^2 = 0.999) did not differ from 1 and 0, respectively; thus, the selectivity was acceptable.

Traditional CV systems may suffer from severe matrix interference from many coexisting transition metal ions [41,48,71-74] because transition metals can, depending on their concentration, cause interference in the CV via parallel reactions with the reducing reagent (KBH_4 or $NaBH_4$) and, consequently, could influence the Hg transport to the atomiser [41,71-74]. With the objective of studying the effect of potential interfering transition metals (Cd, Co, Cr, Cu, Fe, Mn, Ni, Ti, V, and Zn) and residual C in the final digests on the atomic fluorescence Hg signal, a 0.4 μg L^{-1} Hg solution was analysed by CV in the absence and presence of different concentrations (0.005, 0.05, 0.25, 0.5, 2.5, 5, and 25 mg L^{-1}; one replicate) of these metals and (50, 100, and 200 mg L^{-1}; two replicates) of

C, respectively. A signal was considered free of interference when generated by a Hg standard solution in the absence of potential interfering elements; a value of 100% was attributed to this signal, and the IFS obtained in the presence of transition metals proportional to this value were calculated. The elements interference was determined as the concentration that decreases or increased the atomic fluorescence emission signal by 10% in relation to the original signal. The results for C (105 ± 2 mg L^{-1}) and those shown in Fig. 1 indicate that C, Cr, Mn, and Zn do not cause interference, whereas Cd, Ni, Ti, and V cause a marked increase in the Hg signal from 25 mg L^{-1}, Cu and Fe from 5 mg L^{-1}, and Co from 0.5 mg L^{-1}. To evaluate the possibilities of interference in the hair samples, the ERM DB001 and field hair samples were analysed using ICP-OES for C determination, and the transition metal concentrations reported in the literature were considered [54,62,75-78]. The residual C content found in the final digests of ERM DB001 (<90 mg L^{-1}) and in the field samples (<60 mg L^{-1}) obtained by water bath digestion (WBD) treatment did not cause interference in the atomic fluorescence Hg signal. The maximum values for the various metals are Cd (6.8 mg kg^{-1}), Co (25.4 mg kg^{-1}), and Mn (15.0 mg kg^{-1}) as reported by Amartey et al. [77]; Cr (84.6 mg kg^{-1}), Cu (427 mg kg^{-1}), Fe (697 mg kg^{-1}), Ni (331 mg kg^{-1}), and Zn (10000 mg kg^{-1}) as reported by Kumakli et al. [75]; Ti (2.71 mg kg^{-1}) as reported by Rodushkin and Axelsson [78]; and V (0.21 mg kg^{-1}) as reported by Luo et al. [68]. In the proposed method, the hair sample mass was 20 mg and solution must be diluted to 10 mL, thus, the levels of the naturally occurring elements in this matrix will not interfere in the generation of volatile Hg.

3.2.3. LODs and LOQs

The LODs and LOQs were calculated for both methods by AMA and CV-AFS following the recommendations of the International Union of Pure and Applied Chemistry (IUPAC) [79]. These values were 0.002 and 0.07 ng for AMA and 0.01 ∝g L^{-1} and 0.02 ∝g L^{-1} for CV-AFS, which correspond to concentrations of 0.0004 and 0.01 mg kg^{-1} (sample hair mass of 5 mg) or 0.004 and 0.01 mg kg^{-1} (sample hair mass of 20 mg and volume of 10 mL), respectively. The obtained LODs and LOQs are comparable to previously reported AMA analysis of hair [55,56,80] and CV-AFS analysis [19,40]. Moreover, the limits obtained here for total Hg are similar or lower than those previously reported using CV-AAS [30], ICP-MS [36,81], and DMA [14].

3.2.4. Accuracy

The residual acidity in the final digest obtained by WBD, which ranged from 0.84 to 0.86 mol L^{-1}, did not influence the accuracy of the CV-AFS method. In fact, the concentration of the ERM-DB001

samples analysed by AMA (0.338 ± 0.011 mg kg^{-1}) or treated by WBD and analysed by CV-AFS (0.339 ± 0.020 mg kg^{-1}) with optimised operating conditions of both instruments was within the uncertainty range of the certified value (0.365 ± 0.028 mg kg^{-1}; Table 2). To determine if the differences between the certified values (C_{ERM}) and found values ($\bar{X}$) were statistically insignificant, the following condition was verified: *t* calculated (t_{calc}) ≤ *t* tabulated (t_{tab}), where

$$t_{calc} = |C_{ERM} - \bar{X}| / \sqrt{\frac{s_{rip}^2}{n} + u_{ERM}^2},$$

s_{rip} = standard deviation under repeatability conditions,

n = number of replicates (6), and

u_{ERM} = certified uncertainty.

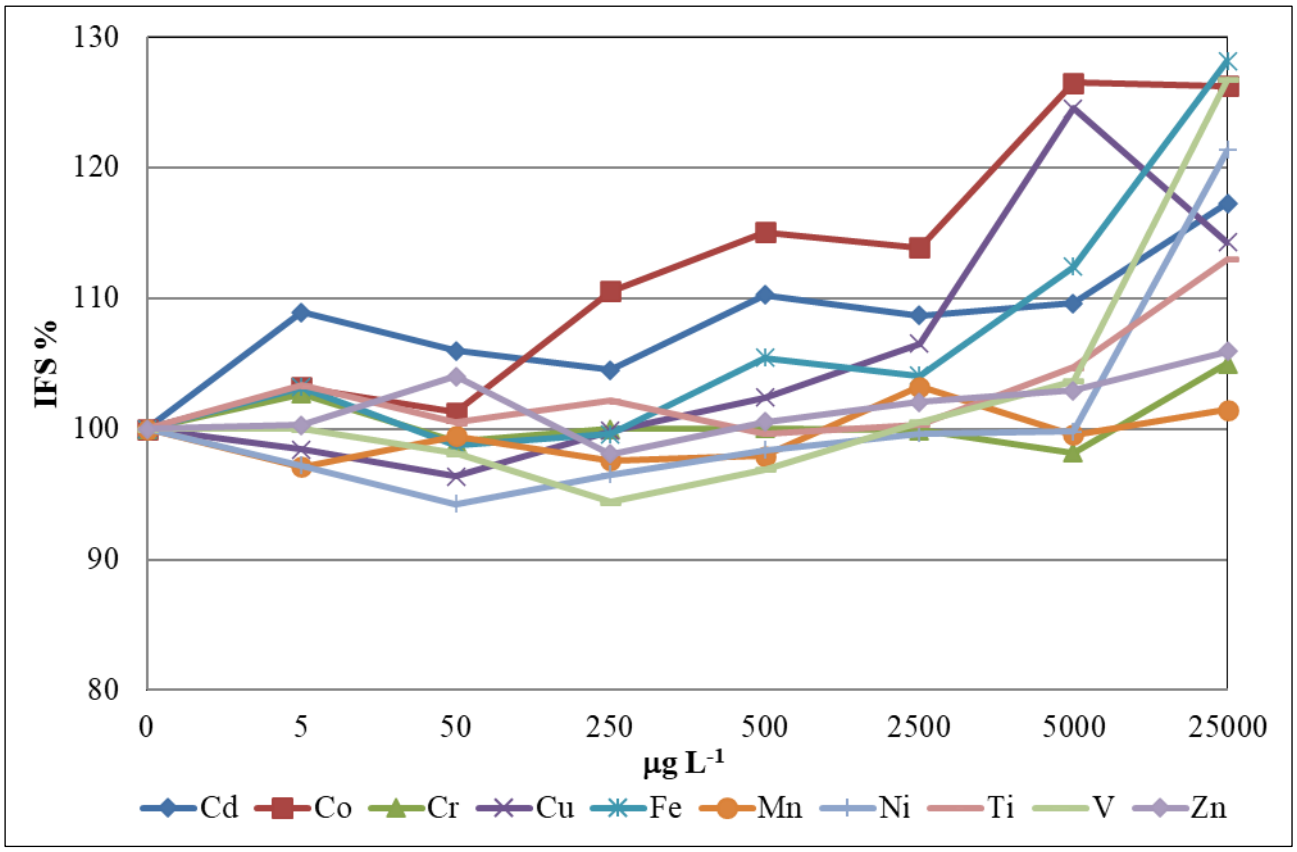

Fig. 1. Studies of the effect of potential interference of Cd, Co, Cr, Cu, Fe, Mn, Ni, Ti, V and Zn concentrations in the Hg atomic fluorescence signal (IFS).

Considering that the uncertainty of the certified reference material is contained in the previous formula, it is assumed that the number of degrees of freedom is infinite, from which it follows that the t_{tab} for comparison with the t_{calc} is equal to 2. The t_{calc} for AMA and CV-AFS (0.96 and 0.89,

respectively) are lower than t_{tab} (assumed equal to two), so we concluded that the methods are exact at the concentration level of the certified reference material.

The precision was determined from the repeatability (intra-day) and the in-laboratory reproducibility (inter-day). In both cases, the precision is expressed as the relative standard deviation in percent (RSD%), and six replicates of ERM DB001 (ca. 5 or 20 mg of mass for AMA and CV-AFS, respectively) in one run (repeatability intra-day) and over three different days (reproducibility inter-day) were considered. The results (all with RSD% <10%) are reported in Table 2.

The expanded standard measurement uncertainties, expressed as a percentage and with a coverage factor of 2, were estimated according to the adopted procedure to be 8.9% and 17% for AMA and CV-AFS, respectively. The percent contribution of each factor to the overall combined uncertainty is plotted in Fig. 2. It can be observed that, for both methods, the lowest contribution to the Hg uncertainty is given by u_{mass}, whereas the highest uncertainties appear to be u_{bias} in the case of AMA and u_{cal} for the CV-AFS method. The performances of two methods were considered satisfactory; thus, both the AMA and the CV-AFS can be considered accurate, reproducible, sensitive, reliable, and suitable techniques for Hg analysis.

3.3. Field Eritrean Hair Samples

The same number (n = 40) of random field hair samples from healthy adult Eritreans living in Asmara were analysed by the two selected methods, AMA and CV-AFS. The Hg concentrations in terms of mean and standard deviation (SD), median, and 25th and 75th percentiles obtained from the field hair samples are listed in Table 3. None of the Hg concentrations in the hair samples were below the LOD of either method.

The following three Hg concentrations in female hair obtained by AMA and CV-AFS were excluded because they exceeded the average by more than three standard deviations (1.50 mg kg^{-1}): 5.67 and 11.4 mg kg^{-1} (both 30 years old) and 8.24 mg kg^{-1} (42 years old). The results of the analysis of hair samples from Eritreans by the two methods were in very good agreement. High correlations (R^2 = 0.98) were observed by the linear regression between AMA and CV-AFS methods, as shown in Fig. 3. Moreover, statistically equivalent results (U-value = 2570, Z-score = 0.0719, and p-value = 0.944) were obtained from the Mann–Whitney two tailed test at a significance level of α = 0.01. The mean Hg concentrations were 0.25 ± 0.34 mg kg^{-1} for AMA and 0.24 ± 0.32 mg kg^{-1} for CV-AFS. The median values and range (minimum to maximum) for AMA and CV-AFS were 0.11 (0.01–1.63) mg kg^{-1} and 0.12 (0.03–1.51) mg kg^{-1}, respectively. According to previously work [58,59], the equivalence between the two methods can also be evaluated in terms of the relative differences (Δ_{rel})

of the data obtained by AMA or CV-AFS for each sample. Further details are given in section S3. The Δ_{rel} value is 15%, which is comparable to the expanded uncertainty of the two methods.

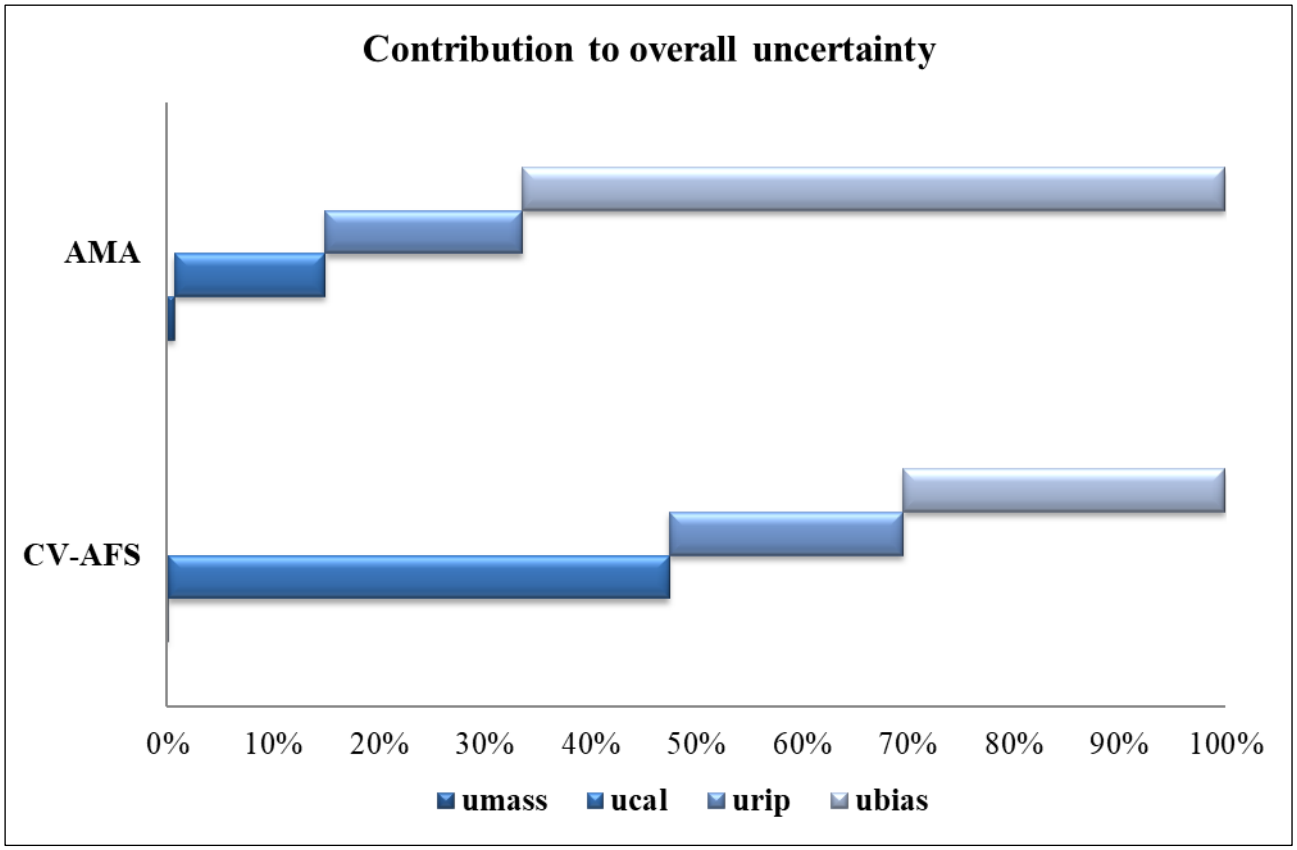

Fig. 2. Contribution of each factor to the overall combined uncertainty [the uncertainty associated with the weighing of hair sample (u_{mass}), the instrumental calibration (u_{cal}), the repeatability of the measurements (u_{rip}), and the trueness bias (u_{bias})] for Hg by using Advanced Mercury Analyzer (AMA) and cold vapor atomic fluorescence spectrometry (CV-AFS).

Many studies have shown that gender is unlikely to play a role in determining Hg accumulation [6,11, 82], but Hg concentrations in hair samples have been observed to vary with age [51, 83-85]. In this study, the participants were divided into two groups based on their age and on their gender: 18–29 years old (N = 19, 13 males and 6 females) and 30–50 years old (N = 18, 5 males and 13 females). No significant differences in the Hg concentrations, as reported in Table 3, were found using the Mann–Whitney tests (two tailed tests at significance level $\alpha = 0.05$) between the two age and gender groups in the whole study area. In addition, gender did not influence this parameter, as has also been observed for young Spanish subjects [86]. Other authors [51] have also observed comparable high Hg concentrations in the hair of the two sexes of the residents of a mining district in Colombia (the

geometric mean in the hair of males 15.98 mg kg^{-1}, whereas those of females was 8.55 mg kg^{-1}). No differences in Hg levels with age of individuals from a contaminated area in coastal Eastern Sicily in Italy [14], Lower Silesia, south-west Poland [87], and Upper Maroni, French Guiana [88] were observed. Furthermore, factors such as age, sex, and the number of dental amalgam fillings had no effect on mercury in the hair [27].

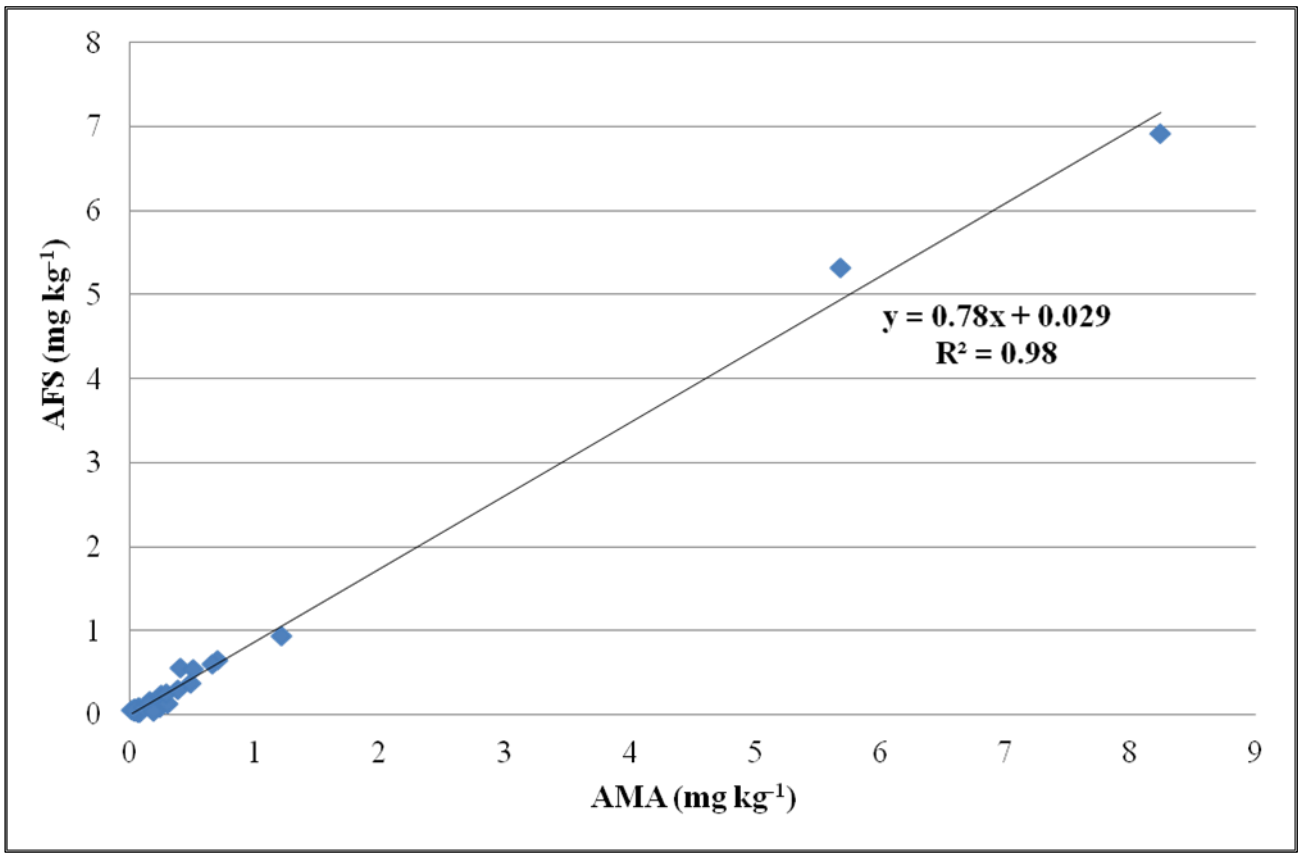

Fig. 3. Comparison between the AMA and the AFS measurements in in-field hair samples.

Because of the lack of data on Hg concentrations in African hair, the results of the analysis of an Eritrean population in the present study (Table 3) were compared with those of other studies conducted worldwide [27,34,36,62,78]. The average Hg level (0.21 ± 0.24 mg kg^{-1}) was found comparable only with that of a Swedish population (0.26 ± 0.14 mg kg^{-1}) obtained by Rodushkin and Axelsson [78] and lower than the mean levels reported in other studies: half that of Poland (0.50 ± 0.39 mg kg^{-1}) measured by Chojnacka et al. [62], one-third of that from Italy (0.66 ± 0.59 mg kg^{-1}) measured by Domanico et al. [34], one-tenth of that from Iran for non-fishing families (2.27 ± 2.10 mg kg^{-1}) obtained by Okati and Esmaili-sari [27], and one-twenty-fifth that from Spain (5.38 mg kg^{-1}) measured by Raposo et al. [36].

Table 3. Hg concentrations (mg kg^{-1}) in hair samples of Eritreans (Africa) according to gender and age (years). Mann–Whitney two tailed test at significance level $\alpha = 0.05$ was used for the effect of age (p_y) and gender (p_{m-f}) on Hg concentrations.

	18-29 years					30-50 years					All years								
	N	**m**	**SD**	**min**	**max**	**N**	**m**	**SD**	**min**	**max**	**N**	**m**	**SD**	**median**	**25p**	**75p**	**min**	**max**	**p_y**
Male	13	0.23	0.32	0.03	1.14	5	0.17	0.22	0.05	0.55	17	0.22	0.29	0.12	0.05	0.18	0.03	1.14	0.928
Female	6	0.27	0.20	0.06	0.60	13	0.27	0.41	0.04	1.50	20	0.26	0.34	0.11	0.05	0.28	0.04	1.50	0.865
All gender	19	0.24	0.28	0.03	1.14	18	0.24	0.36	0.04	1.50	37	0.24	0.32	0.12	0.05	0.26	0.03	1.50	0.984
p_{m-f}		0.638					0.779					0.802							

These differences can be attributed to environmental and occupational exposures, hair colour, ethnic and geographical origin, and seafood consumption [26,51,87,89,90]. Therefore, it is very important to establish reference ranges for each country and to obtain information on eating habits and lifestyle. Finally, in our study, only one participant showed a Hg level (11.4 mg kg^{-1}) above the safe limit of 10 mg kg^{-1} recommended by WHO [8].

4. Conclusion

The Hg contents of 40 hair samples were quantified using two very different techniques, AMA and CV-AFS. The analytical performances demonstrated that both techniques are sensitive, precise, and reliable. In addition, hair analysis indicated that the two techniques are consistent, giving similar results for Hg quantification. This means that either technique could be used for this kind of determination. On the other hand, the use of AMA may be preferable to CV-AFS for reduced sample handling and more economical analysis, whereas the use of CV-AFS compared to AMA could be considered preferable to reduce analysis time (1 min vs. 5 min for each sample, respectively) and for automation. Considering the time involved in all the operations necessary for a rapid optimised open-vessel digestion (120 samples; addition of reagents, dilution, filtration, pre-cleaning of filter, time of digestion and cooling), the time required using the CV-AFS method is approximately equal to that of the AMA method (10 h). The risk of sample contamination is always possible in each step of the analytical procedure. To trace and control the contributions from possible sample contaminations for CV-AFS method, the method blanks, consisting of reagents, should be considered together with each sample set treated by open-vessel digestion..

Finally, the Hg levels in the hair of this study population do not pose a health problem, and no significant differences were observed with gender or age.

Acknowledgements

This study did not receive any specific grants from funding agencies in the public, commercial, or not-for-profit sectors.

The authors would like to express their sincere gratitude to the participants in this study.

Author Contributions

M.L. Astolfi: Conceptualization, Methodology, Validation, Formal analysis, Writing - original draft, Writing - review & editing, Project administration. C. Protano: Software, Data curation, Writing -

review & editing. E. Marconi: Investigation, Visualization. D. Piamonti: Resources. L. Massimi: Investigation, Data curation. M. Brunori: Resources, Funding acquisition. M. Vitali: Writing - review & editing, Supervision. S. Canepari: Resources, Supervision, Funding acquisition.

Conflicts of Interest

The authors declare no conflicts of interest.

References

[1] Z.F. Anual, W. Maher, F. Krikowa, L. Hakim, N.I. Ahmad, S. Foster, Mercury and risk assessment from consumption of crustaceans, cephalopods and fish from West Peninsular Malaysia, Microchem. J. 140 (2018) 214–221. https://doi.org/10.1016/j.microc.2018.04.024.

[2] H. Hui-Wen, S.M. Ullrich, T.W. Tanton, Burdens of mercury in residents of Temirtau, Kazakhstan I: hair mercury concentrations and factors of elevated hair mercury levels, Sci. Total Environ. 409 (2011) 2272–2280. https://doi.org/10.1016/j.scitotenv.2009.12.040.

[3] Y. Gao, Z. Shi, Z. Long, P. Wu, C. Zheng, X. Hou, Determination and speciation of mercury in environmental and biological samples by analytical atomic spectrometry, Microchem. J. 103 (2012) 1–14. https://doi.org/10.1016/j.microc.2012.02.001.

[4] EFSA, Scientific opinion on the risk for public health related to the presence of mercury and methylmercury in food, EFSA J. 10 (2012) 2985.

[5] World Health Organization (WHO), UNEP DTIE Chemicals Branch and WHO Department of Food Safety, Zoonoses and Foodborne Diseases, Guidance for identifying populations at risk from mercury exposure. Geneva, Switzerland (2008).

[6] World Health Organization (WHO), Elemental Mercury and Inorganic Mercury Compounds: Human Health Aspects in: Concise international chemical assessment document 50, Geneva, Switzerland (2003).

[7] World Health Organization (WHO), Inorganic mercury in: Environmental Health Criteria 118, Geneva, Switzerland (1991).

[8] World Health Organization (WHO), Methylmercury in: Environmental Health Criteria 101, Geneva, Switzerland (1990).

[9] T. Morisset, A. Ramirez-Martinez, N. Wesolek, A.C. Roudot, Probabilistic mercury multimedia exposure assessment in small children and risk assessment, Environ. Int. 59 (2013) 431–441. https://doi.org/10.1016/j.envint.2013.07.003.

[10] T.D. Saint'Pierre, R.C.C. Rocha, C.B. Duyck, Determination of Hg in water associate to crude oil production by electrothermal vaporization inductively coupled plasma mass spectrometry, Microchem. J. 109 (2013) 41–45. https://doi.org/10.1016/j.microc.2012.05.005.

[11] H. Fakour, A. Esmaili-Sari, F. Zayeri, Scalp hair and saliva as biomarkers in determination of mercury levels in Iranian women: Amalgam as a determinant of exposure, J. Hazard Mater. 177 (2010) 109–113. https://doi.org/10.1016/j.jhazmat.2009.12.002.

[12] T.M. Clarkson, L. Magos, The toxicology of mercury and its chemical compounds, Crit. Rev. Toxicol. 36 (2006) 609–662. https://doi.org/10.1080/10408440600845619.

[13] M. Schlathauer, V. Reitsam, R. Schierl, K. Leopold, A new method for quasi-reagent-free biomonitoring of mercury in human urine, Anal. Chim. Acta 965 (2017) 63–71. https://doi.org/10.1016/j.aca.2017.02.036.

[14] M. Bonsignore, S. Tamburrino, E. Oliveri, A. Marchetti, C. Durante, A. Berni, E. Quinci, M. Sprovieri, Tracing mercury pathways in Augusta Bay (southern Italy) by total concentration and isotope determination, Environ. Pollut. 205 (2015) 178–85. https://doi.org/10.1016/j.envpol.2015.05.033.

[15] Y. Wu, Y.I. Lee, L. Wu, X. Hou, Simple mercury speciation analysis by CVG-ICP-MS following TMAH pre-treatment and microwave-assisted digestion, Microchem. J. 103 (2012) 105–109. https://doi.org/10.1016/j.microc.2012.01.011.

[16] P. Avino, G. Capannesi, M. Manigrasso, E. Sabbioni, A. Rosada, Element assessment in whole blood, serum and urine of three Italian healthy sub-populations by INAA, Microchem. J. 99 (2011) 548–555. https://doi.org/10.1016/j.microc.2011.07.008.

[17] J.J. Berzas Nevado, R.C. Rodríguez Martín-Doimeadios, M. Jiménez Moreno, J.L. Martins do Nascimento, A.M. Herculano, M.E. Crespo-López, Mercury speciation analysis on cell lines of the human central nervous system to explain genotoxic effects, Microchem. J. 93 (2009) 12–16. https://doi.org/10.1016/j.microc.2009.03.008.

[18] M. Esteban, A. Castaño, Non-invasive matrices in human biomonitoring: a review, Environ. Int. 35 (2009) 438–449. https://doi.org/10.1016/j.envint.2008.09.003.

[19] M. Berglund, B. Lind, K.A. Björnberg, B. Palm, Ö. Einarsson, M. Vahter, Inter- individual variations of human mercury exposure biomarkers: a cross-sectional assessment, Environ. Health 3 (2005) 4–20. https://doi.org/10.1186/1476-069X-4-20.

[20] D. Pozebon, G.L. Scheffler, V.L. Dressler, Elemental hair analysis: A review of procedures and applications, Anal. Chim. Acta 992 (2017) 1–23. https://doi.org/10.1016/j.aca.2017.09.017.

[21] M.L. Astolfi, C. Protano, E. Schiavi, E. Marconi, D. Capobianco, L. Massimi, M. Ristorini, M.E. Baldassarre, N. Laforgia, M. Vitali, S. Canepari, P. Mastromarino, A prophylactic multi-strain probiotic treatment to reduce the absorption of toxic elements: In-vitro study and biomonitoring of breast milk and infant stools, Environ. Int. 130:104818 (2019), https://doi.org/10.1016/j.envint.2019.05.012.

[22] M.L. Astolfi, E. Marconi, C. Protano, M. Vitali, E. Schiavi, P. Mastromarino, S. Canepari, Optimization and validation of a fast digestion method for the determination of major and trace elements in breast milk by ICP-MS, Anal. Chim. Acta 1040 (2018) 49–62. https://doi.org/10.1016/j.aca.2018.07.037.

[23] C. Protano, S. Canepari, M.L. Astolfi, S. D'Onorio De Meo, M. Vitali, Urinary reference ranges and exposure profile for lithium among an Italian paediatric population, Sci. Total Environ. 619 (2018) 58–64. https://doi.org/10.1016/j.scitotenv.2017.11.090.

[24] C. Protano, M.L. Astolfi, S. Canepari, R. Andreoli, A. Mutti, F. Valeriani, V. Romano Spica, A. Antonucci, V. Mattei, S. Martellucci, M.Vitali, Exposure to individual and multiple carcinogenic metals during paediatric age: an experience from an Italian urban scenario, Ann. Ig. 29 (2017) 494–503. https://doi.org/10.7416/ai.2017.2180.

[25] C. Di Dato, D. Gianfrilli, E. Greco, M.L. Astolfi, S. Canepari, A. Lenzi, A.M. Isidori, E. Giannetta, Profiling of selenium absorption and accumulation in healthy subjects after prolonged l-selenomethionine supplementation, J. Endocrinol. Invest. 40 (2017) 1183–1190. https://doi.org/10.1007/s40618-017-0663-5.

[26] P. Li, S. Guo, J. Zhao, Y. Gao, Y.F. Li, Human biological monitoring of mercury through hair samples in China, Bull. Environ. Contam. Tox. 102 (2019) 701–707. https://doi.org/10.1007/s00128-019-02563-8.

[27] N. Okati, A. Esmaili-sari, Determination of mercury daily intake and hair-to-blood mercury concentration ratio in people resident of the coast of the Persian Gulf, Iran, Arch. Environ. Contam. Toxicol. 74 (2018) 140–153. https://doi: 10.1007/s00244-017-0456-z.

[28] P. Jeevanaraj, Z. Hashim, S.M., Elias, A.Z. Aris, Total mercury (THg), lead (Pb), cadmium (Cd) and arsenic (As) in hair samples: method validation and quantification among women at reproductive age in Selangor, Int. J. Sci. Basic Appl. Res. 24 (2015) 332–347.

[29] I. Molina-Villalba, M. Lacasaña, M. Rodríguez-Barranco, A.F. Hernández, B. Gonzalez-Alzaga, C. Aguilar-Garduño, F. Gil, Biomonitoring of arsenic, cadmium, lead, manganese and mercury in urine and hair of children living near mining and industrial areas, Chemosphere 124 (2015) 83–91. https://doi.org/10.1016/j.chemosphere.2014.11.016.

[30] S.M. Vieira, R. de Almeida, I.B. Holanda, M.H. Mussy, R.C. Galvão, P.T.B. Crispim, J.G. Dorea, W.R. Bastos, Total and methyl-mercury in hair and milk of mothers living in the city of Porto Velho and in villages along the Rio Madeira, Amazon, Brazil, Int. J. Hyg. Environ. Health 216 (2013) 682–689. https://doi.org/10.1016/j.ijheh.2012.12.011.

[31] D.P. Torres, V.L.A. Frescura, A.J. Curtius, Simple mercury fractionation in biological samples by CV AAS following microwave-assisted acid digestion or TMAH pre-treatment, Microchem. J. 93 (2009) 206–210. https://doi.org/10.1016/j.microc.2009.07.003.

[32] P. Montuori, E. Jover, A. Pagano, J.M. Bayona, M. Triassi, Improvements on a total mercury determination method in human hair using graphite-furnace atomic absorption spectrophotometry detection, J. Prev. Med. Hyg. 48 (2007) 43–46. https://doi.org/10.15167/2421-4248/jpmh2007.48.2.89.

[33] A.R. Grabeklis, A.V. Skalny, A.A. Skalnaya, I.V. Zhegalova, S.V. Notova, A.L. Mazaletskaya, M.G. Skalnaya, A.A. Tinkov, Hair mineral and trace element content in children with down's syndrome, Biol. Trace Elem. Res. 188 (2019) 230–238. https://doi.org/10.1007/s12011-018-1506-8.

[34] F. Domanico, G. Forte, C. Majorani, O. Senofonte, F. Petrucci, V. Pezzi, A. Alimonti, Determination of mercury in hair: comparison between gold amalgamation absorption spectrometry and mass spectrometry, J. Trace Elem. Med. Biol. 43 (2017) 3–8. https://doi.org/10.1016/j.jtemb.2016.09.008

[35] E.J. Drobyshev, N.D. Solovyev, N.B. Ivanenko, M.Y. Kombarova, A.A. Ganeev, Trace element biomonitoring in hair of school children from a polluted area by sector field inductively coupled plasma mass spectrometry, J. Trace Elem. Med. Biol. 39 (2017) 14–20. https://doi.org/10.1016/j.jtemb.2016.07.004.

[36] J.C. Raposo, P. Navarro, A. Sarmiento, E. Arribas, M. Irazola, R.M. Alonso, Analytical proposal for trace element determination in human hair, Application to the Biscay province population, northern Spain, Microchem. J. 116 (2014) 125–134. https://doi.org/10.1016/j.microc.2014.04.012.

[37] A.N. Anthemidis, G.A. Zachariadis, C.E. Michos, J.A. Stratis, Time-based on-line preconcentration cold vapour generation procedure for ultra-trace mercury determination with inductively coupled plasma atomic emission spectrometry, Anal. Bioanal. Chem. 379 (2004) 764–769. https://doi.org/10.1007/s00216-004-2593-2.

[38] C.F. Harrington, S.A. Merson, T.M. D' Silva, Method to reduce the memory effect of mercury in the analysis of fish tissue using inductively coupled plasma mass spectrometry, Anal. Chim. Acta 505 (2004) 247–254. https://doi.org/10.1016/j.aca.2003.10.046.

[39] S.L.C. Ferreira,W.N.L. dos Santos, I.F. dos Santos, M.M.S. Junior, L.O.B. Silva, U.A. Barbosa, F.A. de Santana A.F. de S. Queiroz, Strategies of sample preparation for speciation analysis of inorganic antimony using hydride generation atomic spectrometry, Microchem. J. 114 (2014) 22–31. https://doi.org/10.1016/j.microc.2013.11.019.

[40] K.A. Bjornberg, M. Vahter, K. Petersson-Grawe, A. Glynn, S. Cnattingius, P.O. Darnerud, S. Atuma, M. Aune, W. Becker, M. Berglund, Methylmercury and inorganic mercury in Swedish

pregnant women and incord blood: influence of fish consumption, Environ. Health Perspect. 111 (2003) 637–641. https://doi.org/10.1289/ehp.111-1241457.

[41] M.C. Cardozo, D.D. Cavalcante, D.L. Silva, W.N.D Santos, M.A. Bezerra, Multivariate optimization of a method for antimony determination by hydride generation atomic fluorescence spectrometry in hair samples of patients undergoing chemotherapy against Leishmaniasis, An. Acad. Bras. Ciênc. 88 (2016), 1179–1190. https://doi.org/10.1590/0001-3765201620150250.

[42] Z. Wang, X. Wang, Q. Wang, X. Xiong, H. Luo, K. Huang, Recent developments in chemical vapor generation atomic spectrometry for zinc detection, Microchem. J. (2019) 104052. https://doi.org/10.1016/j.microc.2019.104052.

[43] Y. Chen, M. Li, L. Fu, X. Hou, X. Jiang, Simultaneous determination of trace cadmium and lead in single human hair by tungsten electrothermal vaporization-flame atomic fluorescence spectrometry, Microchem. J. 114 (2014) 182–186. https://doi.org/10.1016/j.microc.2014.01.002.

[44] B. Liu, F. Wu, X. Li, Z. Fu, Q. Deng, C. Mo, J. Zhu, Y. Zhu, H. Liao, Arsenic, antimony and bismuth in human hair from potentially exposed individuals in the vicinity of antimony mines in Southwest China, Microchem. J. 97 (2011) 20–24. https://doi.org/10.1016/j.microc.2010.07.008.

[45] S. Ni, R. Li, A. Wang, Heavy metal content in scalp hair of the inhabitants near Dexing Copper Mine, Jiangxi Province, China, Sci. China Earth Sci. 54 (2011) 780–788. https://doi.org/10.1007/s11430-011-4194-1.

[46] E.I. Muller, J.P. Souza, C.C. Muller, A.L.H. Muller, P.A. Mello, C.A. Bizzi, Microwave-assisted wet digestion with H_2O_2 at high temperature and pressure using single reaction chamber for elemental determination in milk powder by ICP-OES and ICP-MS, Talanta 156–157 (2016) 232–238. https://doi.org/10.1016/j.talanta.2016.05.019.

[47] Z. Hu, S. Hu, S. Gao, Y. Liu, S. Lin, Volatile organic solvent-induced signal enhancements in inductively coupled plasma-mass spectrometry: a case of studyof methanol and acetone, Spectrochim. Acta Part B 59 (2004) 1463–1470. https://doi.org/10.1016/j.sab.2004.07.007.

[48] R. Irizarry, J. Moore, Y. Cai, Atomic fluorescence determination of selenium using hydride generation technique, Int. J. Environ. Anal. Chem. 79 (2001) 97–109. https://doi.org/10.1080/03067310108035902.

[49] L. Jian, W. Goessler, K.J. Irgolic, Mercury determination with ICP-MS: signal suppression by acids, Fresenius J. Anal. Chem. 366 (2000) 48–53. https://doi.org/10.1007/s002160050010.

[50] R. Pérez, T. Suelves, Y. Molina, F. Corpas-Burgos, V. Yusà, Biomonitoring of mercury in hair of children living in the Valencian Region (Spain). Exposure and risk assessment, Chemosphere 217 (2019) 558–566. https://doi.org/10.1016/j.chemosphere.2018.11.017.

[51] H. Gutiérrez-Mosquera, S.B. Sujitha, M.P. Jonathan, S.K. Sarkar, F. Medina-Mosquera, H. Ayala-Mosquera, G. Morales-Mira, L. Arreola-Mendoza, Mercury levels in human population from a mining district in Western Colombia, J. Environ. Sci. 68 (2018) 83–90. https://doi.org/10.1016/j.jes.2017.12.007.

[52] A.C. Alves, M.S. Monteiro, A L. Machado, M. Oliveira, A. Boia, A. Correia, N. Oliveira, A.M.V.M. Soares, S. Loureiro, Mercury levels in parturient and newborns from Aveiroo region Portugal, J. Toxicol. Environ. Health Part A 80 (2017) 697–709. https://doi.org/10.1080/15287394.2017.1286926.

[53] M. Esteban, B.K. Schindler, J.A. Jiménez, H.M. Koch, J. Angerer, M. Rosado, S. Gómez, L. Casteleyn, M. Kolossa-Gehring, K. Becker, L. Bloemen, G. Schoeters, E. Den Hond, O. Sepai, K. Exley, M. Horvat, L.E. Knudsen, A. Joas, R. Joas, D. Aerts, P. Biot, D. Borošová, F. Davidson, I. Dumitrascu, M.E. Fischer, M. Grander, B. Janasik, K. Jones, L. Kasparova, T. Larssen, M. Naray, F. Nielsen, P. Hohenblum, R. Pinto, C. Pirard, G. Plateel, J.S. Tratnik, J. Wittsiepe, A. Castaño, Equas Reference Laboratories, Mercury analysis in hair: Comparability and quality assessment within the transnational COPHES/DEMOCOPHES project, Environ. Res. 141 (2014) 24–30. https://doi.org/10.1016/j.envres.2014.11.014.

[54] K. Chojnacka, A. Zielinska, I. Michalak, H. Gorecki, The effect of dietary habits on mineral composition of human scalp hair, Environ. Toxicol. Pharmacol. 30 (2010) 188–194. https://doi.org/10.1016/j.etap.2010.06.002.

[55] S. Díez, S. Delgado, I. Aguilera, B. Pérez-Gómez, M. Torrent, J. Sunyer, J.M. Bayona, Prenatal and early childhood exposure to mercury and methylmercury in Spain, a high-fish-consumer country, Arch. Environ. Contam. Toxicol. 56 (2009) 615–622. https://doi.org/10.1007/s00244-008-9213-7.

[56] S. Díez, P. Montuori, X. Querol, J.M. Bayona, Total mercury in the hair of children by combustion atomic absorption spectrometry (Comb-AAS), J. Anal. Toxicol. 31 (2007) 144–149. https://doi.org/10.1093/jat/31.3.144.

[57] P. Wołowiec, I. Michalak, K. Chojnacka, M. Mikulewicz, Hair analysis in health assessment, Clin. Chim. Acta 419 (2013) 139–171. https://doi.org/ 10.1016/j.cca.2013.02.001.

[58] M.E. Conti, S. Canepari, M.G. Finoia, G. Mele, M.L. Astolfi, Characterization of Italian multifloral honeys on the basis of their mineral content and some typical quality parameters, J. Food Compost. Anal. 74 (2018) 102–113. https://doi.org/10.1016/j.jfca.2018.09.002.

[59] M.L. Astolfi, P. Di Filippo, A. Gentili, S. Canepari, Semiautomatic sequential extraction of polycyclic aromatic hydrocarbons and elemental bio-accessible fraction by accelerated solvent extraction on a single particulate matter sample, Talanta 174 (2017) 838–844. https://doi.org/10.1016/j.talanta.2017.06.072.

[60] A. Campopiano, A. Cannizzaro, F. Angelosanto, M.L. Astolfi, D. Ramires, A. Olori, S. Canepari, S. Iavicoli, Dissolution of glass wool, rock wool and alkaline earth silicate wool: morphological and chemical changes in fibers, Regul. Toxicol. Pharm. 70 (2014) 393–406. https://doi.org/10.1016/j.yrtph.2014.05.023.

[61] M.I. Szynkowska, M. Marcinek, A. Pawlaczyk, J. Albińska, Human hair analysis in relation to similar environmental and occupational exposure, Environ. Toxicol. Pharmacol. 40 (2015) 402–408. https://doi.org/10.1016/j.etap.2015.07.005.

[62] K. Chojnacka, H. Górecka, A. Chojnacki, H. Górecki, Inter-element interactions in human hair, Environ. Toxicol. Pharmacol. 20 (2005) 368–374. https://doi.org/10.1016/j.etap.2005.03.004.

[63] M. Thompson, S.L.R. Ellison, R. Wood, Harmonized guidelines for single-laboratory validation of methods of analysis (IUPAC technical report), Pure Appl. Chem. 74 (2002) 835–855. https://doi.org/10.1351/pac200274050835.

[64] Eurachem/Citac Guide, Quantifying uncertainty in analytical measurement, 2nd Edition, (2000). https://www.eurachem.org/images/stories/Guides/pdf/QUAM2012_P1.pdf. Accessed 24 September 2018.

[65] Sinal, ACCREDIA, Esempi applicativi di valutazione dell'incertezza nelle misurazioni chimiche, 2000 (in Italian) http://gpa.sinal.it/UploadDocs/319_DT0002_4rev0.PDF. Accessed 24 September 2018.

[66] P. Hewett, G.H. Ganser, A comparison of several methods for analyzing censored data, Ann. Occup. Hyg. 51 (2007) 611–632. https://doi.org/10.1093/annhyg/mem045.

[67] J.U. Clarke, Evaluation of censored data methods to allow statistical comparisons among very small samples with below detection limit observations, Environ. Sci. Technol. 32 (1998) 177–183. https://doi.org/10.1021/es970521v.

[68] R. Luo, X. Zhuo, D. Ma, Determination of 33 elements in scalp hair samples from inhabitants of a mountain village of Tonglu city, China, Ecotoxicol. Environ. Saf. 104 (2014) 215–219. https://doi.org/10.1016/j.ecoenv.2014.03.006.

[69] L. Brüggemann, W. Quapp, R. Wennrich, Test for non-linearity concerning linear calibrated chemical measurements, Accred. Qual. Assur. 11 (2006) 625–631. https://doi.org/10.1007/s00769-006-0205-x.

[70] V. Vacchina, F. Séby, R. Chekri, J. Verdeil, J. Dumont, M. Hulin, V. Sirot, J.L. Volatier, R. Serreau, A. Rousseau, T. Simon, T. Guérin, Optimization and validation of the methods for the total mercury and methylmercury determination in breast milk, Talanta 167 (2017) 404–410. https://doi.org/10.1016/j.talanta.2017.02.046.

[71] P.Y. Hu, X. Wang, L. Yang, H.Y. Yang, Y.Y. Tang, H. Luo, X.L. Xiong, X. Jiang, K. Huang, Speciation of mercury by hydride generation ultraviolet atomization-atomic fluorescence spectrometry without chromatographic separation, Microchem. J. 143 (2018) 228–233. https://doi.org/10.1016/j.microc.2018.08.013.

[72] L. Wu, Z. Long, L. Liu, Q. Zhou, Y.I. Lee, C. Zheng, Microwave-enhanced cold vapor generation for speciation analysis of mercury by atomic fluorescence spectrometry, Talanta 94 (2012) 146–151. https://doi.org/10.1016/j.talanta.2012.03.009.

[73] P. Wu, L. He, C.B. Zheng, X.D. Hou, R.E. Sturgeon, Applications of chemical vapor generation in non-tetrahydroborate media to analytical atomic spectrometry, J. Anal. At. Spectrom. 25 (2010) 1217–1246. https://doi.org/10.1039/c003483e.

[74] L.J. Shao, W.E. Gan, Q.D. Su, Determination of total and inorganic mercury in fish samples with on-line oxidation coupled to atomic fluorescence spectrometry, Anal. Chim. Acta 562 (2006) 128–133. https://doi.org/10.1016/j.aca.2006.01.039.

[75] H. Kumakli, A.V. Duncan, K. McDaniel, T.F. Mehari, J. Stephenson, L. Maple, Z. Crawford, C.L. Macemore, C.M. Babyak, S.O. Fakayode, Environmental biomonitoring of essential and toxic elements in human scalp hair using accelerated microwave-assisted sample digestion and inductively coupled plasma optical emission spectroscopy, Chemosphere 174 (2017) 708–715. https://doi.org/10.1016/j.chemosphere.2017.02.032.

[76] S.K. Sahoo, S. Mishra, Z.S. Žunić, H. Arae, F. Gjergj, P. Stegnar, L. Benedik, U. Repinc, R. Kritsananuwat, Distribution of uranium and selected trace metals in Balkan human scalp hair using inductively coupled plasma mass spectrometry, Int. J. Mass Spectrom. 373 (2014) 15–21. https://doi.org/10.1016/j.ijms.2014.08.020.

[77] E. O. Amartey, A. B. Asumadu-Sakyi, C. A. Adjei, F. K. Quashie, G. O. Duodu, N. O. Bentil, Determination of heavy metals concentration in hair pomades on the Ghanaian market using atomic absorption spectrometry technique, Br. J. Pharmacol. Toxicol. 2 (2011) 192–198.

[78] I. Rodushkin, M. D. Axelsson, Application of double focusing sector field ICP-MS for multielemental characterization of human hair and nails. Part II. A study of the inhabitants of northern Sweden, Sci. Total Environ. 262 (2000) 21–36. https://doi.org/10.1016/S0048-9697(00)00531-3.

[79] IUPAC. Compendium of Chemical Terminology, 2nd ed. (the "Gold Book"). Compiled by A. D. McNaught and A. Wilkinson. Blackwell Scientific Publications, Oxford (1997). Online version (2019) created by S. J. Chalk. ISBN 0-9678550-9-8. https://doi.org/10.1351/goldbook. Accessed 3 August 2019.

[80] D. Borošová, K., Slotová, E. Fabiánová, Mercury content in hairs of mother-child pairs in Slovakia as a biomarker of environmental exposure, Acta Chim. Slov. 7 (2014) 119–122. https://doi.org/10.2478/acs-2014-0020.

[81] N. Ferré-Huguet, M. Nadal, M. Schuhmacher, J.L. Domingo, Monitoring metals in blood and hair of the population living near a hazardous waste incinerator: temporal trend, Biol. Trace Elem. Res.128 (2008) 191–199. https://doi.org/10.1007/s12011-008-8274-9.

[82] M. Janicka, Ł.J. Binkowski, M. Błaszczyk, J. Paluch, W. Wojtaś, P. Massanyi, R. Stawarz, Cadmium, lead and mercury concentrations and their influence on morphological parameters in blood donors from different age groups from southern Poland, J. Trace Elem. Med. Biol. 29 (2015) 342–346. https://doi.org/10.1016/j.jtemb.2014.10.002.

[83] Y. Li, X. Zhang, L. Yang, H. Li, Levels of Cd, Pb, As, Hg, and Se in hair of residents living in villages around Fenghuang polymetallic mine, southwestern China, Bull. Environ. Contam. Toxicol. 89 (2012) 125–128. https://doi.org/10.1007/s00128-012-0650-7.

[84] F.L. Barbieri, J. Gardon, Hair mercury levels in Amazonian populations: Spatial distribution and trends, Int. J. Health Geogr. 8:71 (2009) 1–20. https://doi.org/10.1186/1476-072X-8-71.

[85] A.F. Amaral, M. Arruda, S. Cabral, A.S. Rodrigues, Essential and non-essential trace metals in scalp hair of men chronically exposed to volcanogenic metals in the Azores, Portugal, Environ. Int. 34 (2008) 1104–1108. https://doi.org/10.1016/j.envint.2008.03.013.

[86] M.J. González-Muñoz, A. Peña, I. Meseguer, Monitoring heavy metal contents in food and hair in a sample of young Spanish subjects, Food Chem. Toxicol. 46 (2008) 3048–3052. https://doi.org/10.1016/j.fct.2008.06.004

[87] K. Chojnacka, H. Górecka, H. Górecki, The effect of age, sex, smoking habit and hair color on the composition of hair, Environ. Toxicol. Pharmacol. 22 (2006) 52–57. https://doi.org/10.1016/j.etap.2005.11.006.

[88] M. Fujimura, A. Matsuyama, J.P. Harvard, J.P. Bourdineaud, K. Nakamura, Mercury contamination in humans in Upper Maroni, French Guiana between 2004 and 2009, Bull. Environ. Contam. Tox. 88 (2012) 135–139. https://doi.org/10.1007/s00128-011-0497-3.

[89] I. Kvestad, S. Vabø, M. Kjellevold, O.J. Nøstbakken, L.K. Midtbø, M. Hysing, M.W. Markhus, L. Madsen, K. Handeland, I.E. Graff, Ø. Lie, L. Frøyland, K.M. Stormark, L. Dahl, J. Øyen, Fatty fish, hair mercury and cognitive function in Norwegian preschool children: Results from the randomized controlled trial FINS-KIDS, Environ. Int. 121 (2018) 1098–1105. https://doi.org/10.1016/j.envint.2018.10.022.

[90] A. Castaño, F. Cutanda, M. Esteban, P. Pärt, C. Navarro, S. Gómez, M. Rosado, A. López, E. López, K. Exley, B.K. Schindler, E. Govarts, L. Casteleyn, M. Kolossa-Gehring, U. Fiddicke, H. Koch, J. Angerer, E. Den Hond, G. Schoeters, O. Sepai, M. Horvat, L.E. Knudsen, D. Aerts, A. Joas, P. Biot, R. Joas, J.A. Jiménez-Guerrero, G. Diaz, C. Pirard, A. Katsonouri, M. Cerna, A.C. Gutleb, D. Ligocka, F.M. Reis, M. Berglund, I.R. Lupsa, K. Halzlová, C. Charlier, E. Cullen, A. Hadjipanayis, A. Krsková, J.F. Jensen, J.K. Nielsen, G. Schwedler, M. Wilhelm, P. Rudnai, S. Középesy, F. Davidson, M.E. Fischer, B. Janasik, S. Namorado, A.E. Gurzau, M. Jajcaj, D. Mazej, J.S. Tratnik, K. Larsson, A. Lehmann, P. Crettaz, G. Lavranos, M. Posada, Fish consumption patterns and hair mercury levels in children and their mothers in 17 EU Countries, Environ. Res. 141 (2015) 58–68. https://doi.org/10.1016/j.envres.2014.10.029.

Supplementary Material S1.

The percentage drift (d%) was calculated based on the following formula:

$d\% = (Cn - Ci)/Ci \times 100$,

where C_i is the initial concentration (in nanograms or micrograms per litre for AMA or CV-AFS, respectively) measured in the control standard solution immediately after the calibration curve and rinsing the blanks up to an absorbance signal <0.0012 units for AMA or instrumental atomic fluorescence signals (IFS) <90 units, and C_n is the standard control concentration measured during the analytical sequence. A maximum *d*% of ± 10% was considered acceptable, whereas for values of *d*% >10%, new instrument calibrations were performed, and the last 10 samples were analysed before exceeding *d*%.

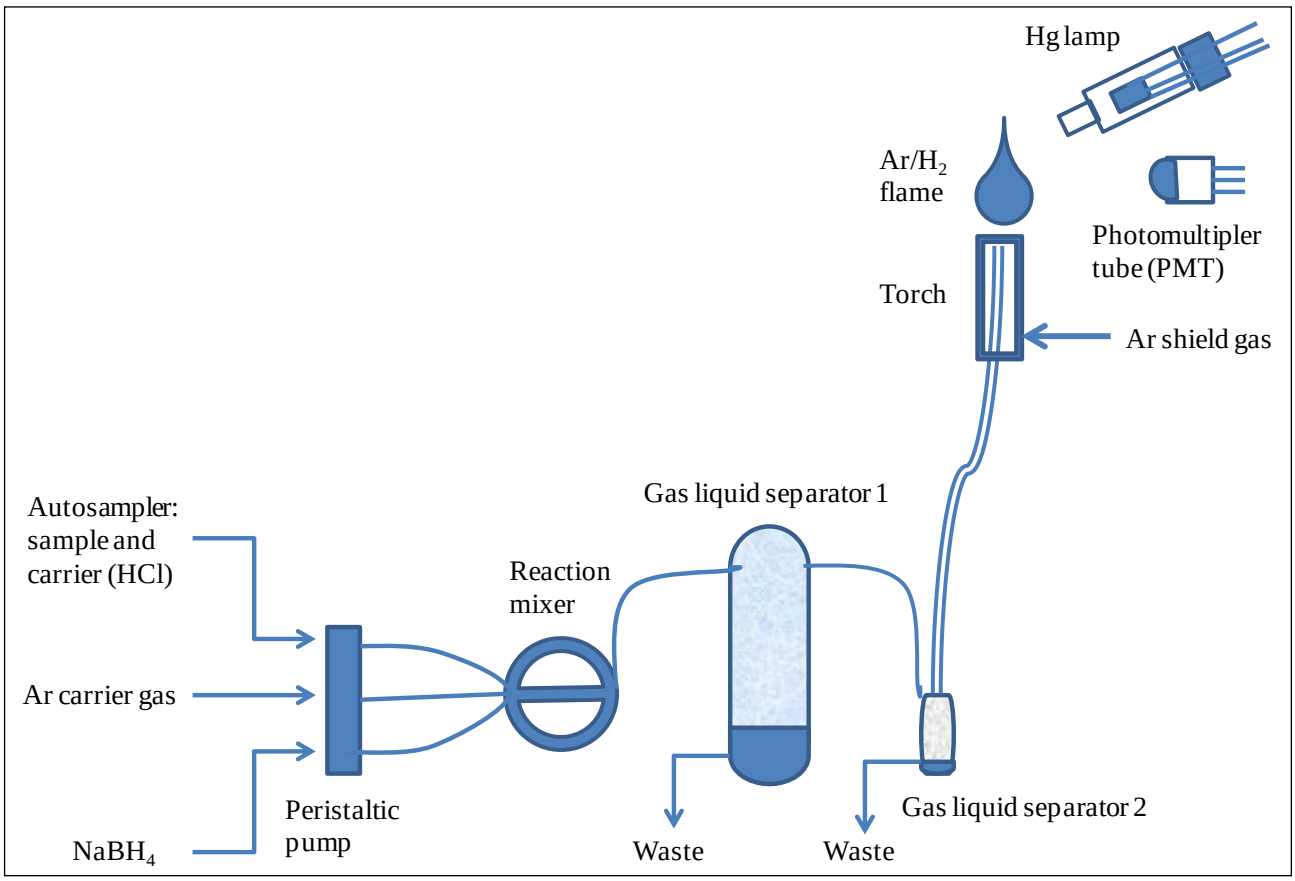

Fig. S1. Schematic diagram of cold vapor generation atomic fluorescence spectrometry (CV-AFS).

Supplementary Material S2.

The results obtained for the statistical F-test based on the means of the deviation squares (one-way ANOVA test) indicate that the linear regression model of AMA is acceptable. The value from this test (F_{test}) was lower than the corresponding value of the F-distribution with $I - 2$ ($I = 7$; number of concentration levels) and $N - I$ ($N = 21$; number of calibration points) degrees of freedom at significance level $\alpha = 0.01$.

As reported in Fig. S2, the mean values achieved for a standard solution of Hg at 1 ng and blanks were 1.00 ± 0.08 ng (12 replicates) and 0.0007 ± 0.0003 (100 replicates) absorbance units, respectively. The confidence interval was empirically set at mean ± 2SD. The control charts indicate that the concentrations found were usually well within the confidence interval and that the points were randomly distributed above and below the mean value.

For CV-AFS, the value from one-way ANOVA test (F_{test}) was compared with the corresponding value of the F-distribution with $I - 2$ ($I = 9$; number of concentration levels) and $N - I$ ($N = 27$; number of calibration points) degrees of freedom and at significance level $\alpha = 0.01$. The hypothesis of linearity was acceptable.

As reported in Fig. S3, the mean values achieved for a control standard solution and blanks were 0.40 ± 0.01 µg L-1 (20 replicates) and 38 ± 26 (64 replicates) IFS units, respectively. In particular, in the case of the measurements reported in Fig. S3 (panel b) on the third day, d <10%, but the values are outside the confidence interval (± 2SD); therefore, corrective actions were taken. These included the preparation of new reagents and new optimisation and calibration of the instrument, as well as re-reading the analysed samples.

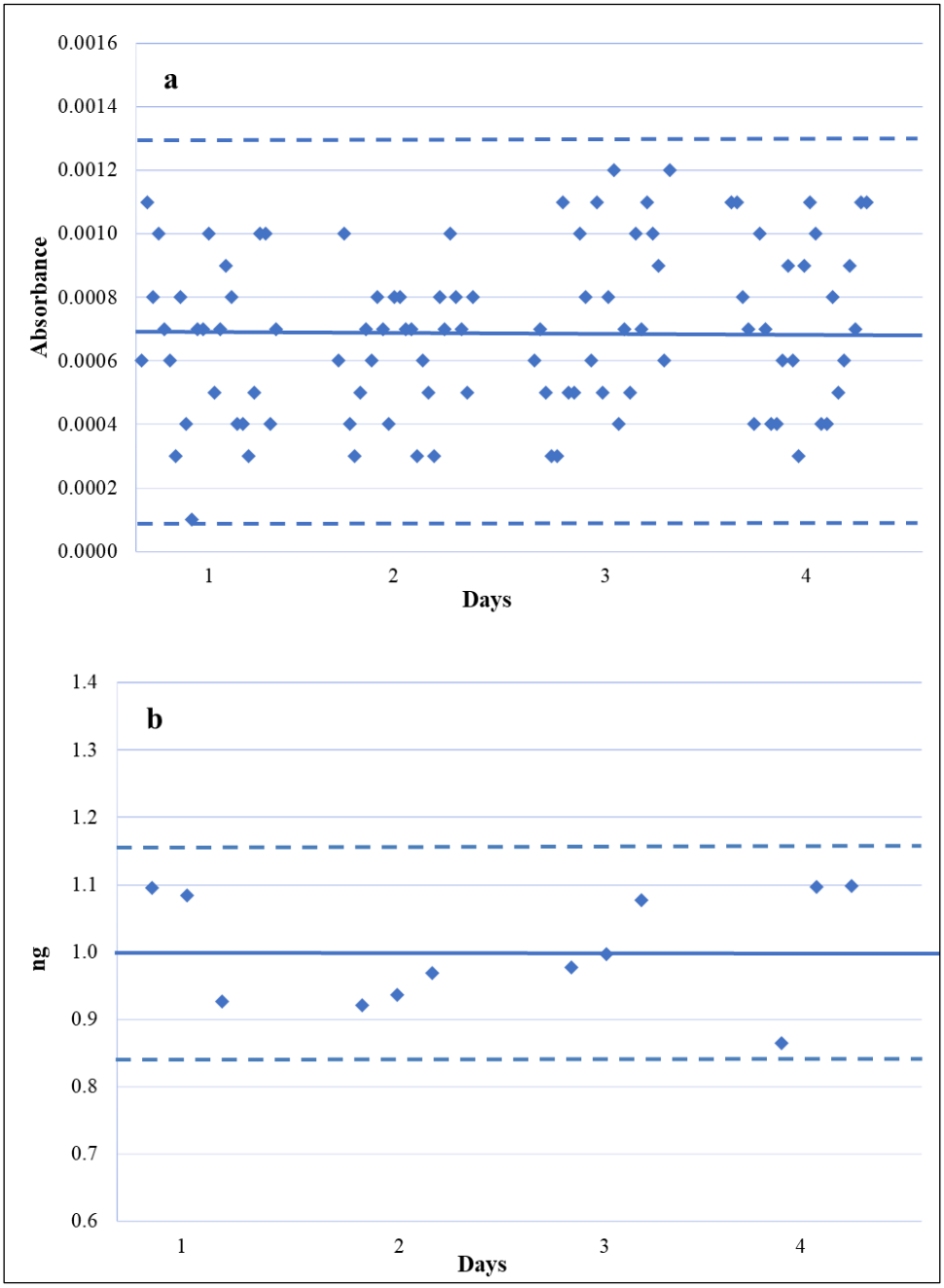

Fig. S2. Advanced mercury analyzer control charts for (a) absorbance signal of blank values and (b) control standard solution at 1 ng. The interval of confidence (—) was set to mean ± 2 SD, on four days.

Supplementary Material S3.

The equivalence between the two methods can also be evaluated in terms of the relative differences (Δ_{rel}) of the data obtained by AMA or CV-AFS for each sample, which were calculated as follows:

$$\Delta_{rel} = \frac{\Delta}{\overline{C}} * 100,$$

$$\Delta = \sqrt{\frac{\sum_{i=1}^{N} (C_{iAMA} - C_{iAFS})^2}{2N}},$$

$$\overline{C} = \frac{\sum_{i=1}^{N} (C_{iAMA} + C_{iAFS})}{2N},$$

where C_{iAMA} and C_{iAFS} are the concentration (mg kg^{-1}) of the field hair samples obtained by AMA and CV-AFS, respectively; $\overline{C}$ is the mean concentration over all samples, and N is the total number of the samples.

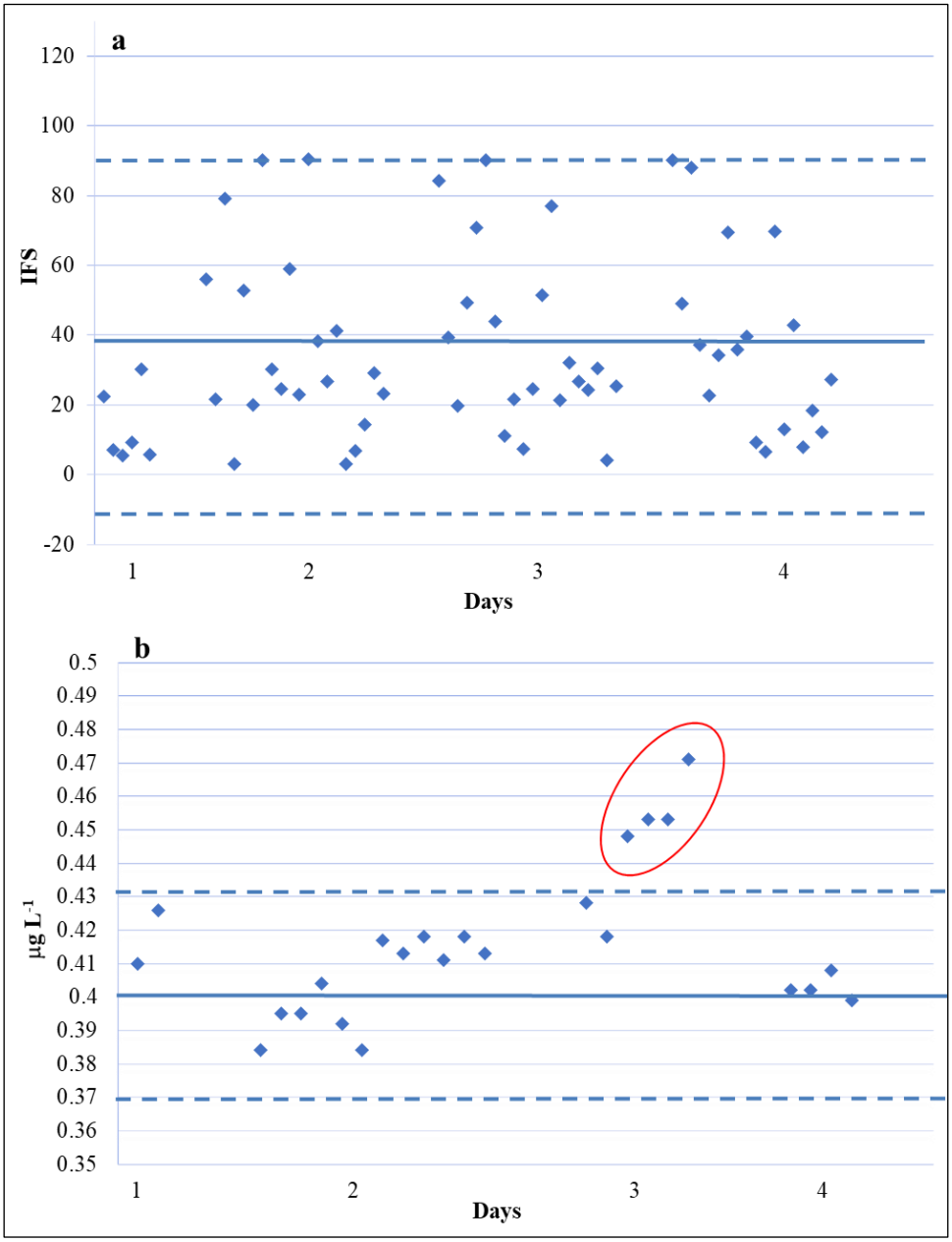

Fig. S3. Cold vapor generation atomic fluorescence spectrometry control charts for (a) instrumental fluorescence signals (IFS) of blank values and (b) control standard solution at 0.4 µg L^{-1}. The interval of confidence (—) was set to mean ± 2 SD, on four days.

2.4.2. (D2) A New Rapid Treatment of Human Hair for Elemental Determination by Inductively Coupled Mass Spectrometry

Analytical Methods (2019), *Reviewed*

Maria Luisa Astolfi [a,*], Carmela Protano [b], Elisabetta Marconi [b], Lorenzo Massimi [a], Marco Brunori [c], Daniel Piamonti [c], Matteo Vitali [b], Silvia Canepari [a]

[a] Department of Chemistry, Sapienza University, Piazzale Aldo Moro 5, 00185 Rome, Italy;
[b] Department of Public Health and Infectious Diseases, Sapienza University, Piazzale Aldo Moro 5, 00185 Rome, Italy;
[c] Department of Cardiovascular, Respiratory, Nephrology, Anaesthesiology and Geriatric Science, Sapienza University, Viale del Policlinico 155, 00161 Rome, Italy.

Abstract: Advancements in sample preparation for performing elemental analysis are coming from the dissemination of microwave-assisted procedures, but there is still room for improvements by looking for fast and easily applicable procedures. In the present study, the open-vessel digestion sample treatment (19–21 °C or 95 °C) was compared with closed-vessel microwave-assisted digestion (180 °C). Detection and quantification limits, accuracy, precision, residual carbon content, and residual acidity were quantified with certified and in-field hair samples. Human hair samples (0.02 g) were digested with HNO_3/H_2O_2 (2:1) in an open vessel heated to 95 °C. The residual carbon content $<87 \pm 6$ mg L^{-1} and a residual acidity $<0.86 \pm 0.10$ mol L^{-1} in the final digested samples. The elements (Al, As, B, Ba, Be, Bi, Ca, Cd, Ce, Co, Cr, Cs, Cu, Fe, Ga, K, La, Li, Mg, Mn, Mo, Na, Nb, Ni, P, Pb, Rb, Sb, Se, Si, Sn, Sr, Te, Ti, Tl, U, V, W, Zn, and Zr) were determined with quadrupole inductively coupled plasma mass spectrometry equipped with a collision-reaction interface. A detection limit (0.00002–30 mg kg^{-1}), precision (repeatability <11% and intermediate precision <13%), trueness bias (-4–9%), and recovery (90–110% for all the elements except for Cr = 65% and Fe = 79%) were observed. The results indicate that the proposed method is suitable for routine multi-elemental analysis in human hair studies.

Keywords: optimization; validation; multi-elemental analysis; ICP-MS; human hair; biomonitoring.

1. Introduction

Elements are naturally present in the environment at various concentration levels that increase by anthropogenic activities (industrial, domestic, agricultural, and medical) and technological applications.[1–8] Determination of the elemental concentration in biological matrices is useful for monitoring environmental and occupational exposure and for assessing the related human health risks and effectiveness of preventive measures.[9,10] In fact, even small levels of toxic elements can cause adverse effects.[11–13] Element toxicity depends on several factors including the dose, route of exposure, and chemical species, as well as the age, gender, genetics, and nutritional status of exposed individuals.[14] This is especially true for infants who are more sensitive to toxic effects than adults owing to their rapid growth, organ immaturity, and nervous system susceptibility during their first year.[15,16] Suitable biological matrices for biomonitoring studies are human hair, urine, meconium, breast milk, nails, and saliva.[10,17–21] Hair has the advantage that it is a stable matrix with easy collection, transport, and storage.[10,22–25] In addition, while the urine and blood levels of a monitored substance are representative of very recent exposure, hair retains a substance for long periods, therefore provide information on short- and long-term exposure as well as temporal exposure patterns by segmental analysis.[10,26–28] In fact, hair is a peripheral tissue of slow metabolism and it excrete the elements into its structure during the growth process.[29–32] The main disadvantages of this matrix are the difficulty in differentiating between endogenous from exogenous contaminants and the variations in hair colour and care, age, gender, and ethnical and geographical origin.[10,22–24,33–35] Moreover, the lack of a standardised methodology (mainly with respect to sample washing and treatment) and different human lifestyles may reflect on the hair elemental content.[11,33,34,36–37] Many washing procedures for removing exogenous trace elements from hair and nail samples have been proposed.[9,38–39] Standardized washing procedures become a fundamental requirement to compare different experimental data from inter-laboratory studies.[40] An ideal washing procedure would remove only external contaminants and leave endogenous elements intact.[40] The International Atomic Energy Agency (IAEA) guidelines recommended the only use of the acetone–water–water–water–acetone sequence as washing procedure.[39] However, even a non-ionic detergent such as Triton X-100 seems to be able to remove just the external contamination.[41] Thus, there is a pressing need for the development and optimisation of standard methods to perform the appropriate elemental analysis of hair samples.[9,33,36]

The main analytical techniques employed for the elemental analysis of hair samples are inductively coupled plasma-mass or -optical emission spectrometry (ICP-MS or ICP-OES, respectively), particle-induced X-ray emission (PIXE) spectrometry, instrumental neutron activation analysis (INAA), electrothermal atomic absorption spectrometry (ET-AAS), flame atomic absorption spectrometry (FAAS), hydride generation atomic absorption spectrometry (HG-AAS), total reflection X-ray fluorescence (TXRF), cold vapour atomic fluorescence spectrometry (CV-AFS), and cold vapour atomic absorption spectrometry (CV-AAS).[9,33,42–44] ICP-OES has been applied towards the determination of elements present in higher concentrations in hair, while ICP-MS has mostly been used for the analysis of trace and ultra-trace elements.[33] However, the use of ICP-MS for the determination of the major elements in hair has also been reported.[45–47] Inductively coupled plasma-sector field mass spectrometry (ICP-SFMS) is able to resolve many spectral interferences and provides greater sensitivity and resolving power than the conventional quadrupole ICP-MS.[43,48–50] Methods for the ICP-SFMS quantification of major elements in biological matrices have also been reported.[43,51–52] Laser ablation ICP-MS can provide spatial resolution and temporal tracking of the monitoring of elements in hair strands.[33,53]

ICP-MS is one of the best techniques for the characterisation of the elemental composition of samples in terms of accuracy, specificity, dynamic range, multi-element capability, and precision.[54,55] However, this technique displays unwanted spectral and non-spectral interferences that might change with the elemental composition of the analysed samples.[54,56–58] Most of these interferences can be reduced by using a collision-reaction interface (CRI) or dynamic reaction cells.[27,34,40,47,56,57,59–62] Additionally, to avoid errors due to matrix effects, the samples should be previously digested to completely dissolve the matrix.[33,63] Many methods to oxidise hair samples have been reported, the most common being microwave-assisted digestion.[9,33,64,65] Generally, HNO_3 or a mixture of HNO_3 and H_2O_2 in various proportions has been employed.[9,33] The digest should be stable before being introduced, by pneumatic nebulisation, into the ICP-based system.[63,66] The digested solution should be characterised by a low residual acidity, residual carbon content (RCC), and dissolved solid concentration. Incomplete hair decomposition can cause RCC in the sample solution. The ICP signal of elements with a similar ionisation potential to that of C may increase due to C charge transfer reactions.[33,67] On the other hand, the acidity of the digests can severely suppress the analytical signal during ICP-MS analysis.[33,67]

Detection/quantification limits and analysis of certified reference material of hair or analyte recovery tests are not cited in a large number of publications.[9,33] The objective of this study was to evaluate the effect of hair sample treatments on elemental hair composition. A fast, sensible, and reliable analytical method for screening analysis and biomonitoring studies was optimised and validated.

2. Experimental

2.1. Instrumentation

In this work, two systems were used for hair sample preparation. A microwave system (Ethos1 Touch Control; Milestone, Sorisole, Bergamo, Italy) equipped with six polytetrafluoroethylene (PTFE) or 20 quartz vessels was used for closed-vessel microwave digestion (CD). The vessels were irradiated with a maximum power of 1000 W and all the experiments were carried out at maximum temperature (180 °C) and pressures ≤40 bar. The other system was a water bath (WB12; Argo Lab, Modena, Italy) with an electronic temperature control using up to 120 polypropylene vessel (Artiglass s.r.l., Due Carrare, PD, Italy) for open-vessel digestion (OD). Maximum temperature and pressure up to 95 °C (± 0.2 °C) and ~1 bar, respectively, were used for this system.

The determination on elemental contents was performed using an ICP-mass spectrometer (820-MS; Bruker, Bremen, Germany) equipped with a CRI and glass nebuliser (0.4 mL min-1; MicroMistTM; Analytik Jena AG, Jena, Germany). Standard mode was used to quantify all the elements except for As, Cr, Fe, Mn, Se, and V, which were determined by CRI with He and H2 (99.9995% purity; SOL Spa, Monza, Italy) as cell gases. An ICP–optical emission spectrometer (Vista MPX CCD Simultaneous; Varian, Victoria, Mulgrave, Australia), in axial view mode and equipped with a cyclonic spray chamber, was used to determine the C content and S levels of the final digests and to check the quality of the data through inter-technique comparison. For the analysis of the certified material samples obtained after acid digestion with HF, inert components (demountable torch with alumina injector, 1.8 mm, and PTFE injector holder; Sturman-Masters inert spray chamber, double pass, white Ertalyte; Agilent, Santa Clara, CA, United Stades) were employed in the ICP-OES set-up. The ICP-MS and ICP-OES optimised instrumental parameters are summarised in Table 1.

2.2. Chemicals and Samples

All reagents were analytical grade. Water was purified using a deioniser system (resistivity, ≤18.3 MΩ cm; Arioso Power I RO-UP Scholar UV; Human Corporation, Songpa-Ku, Seoul, Korea). HCl (assay >36%; residue <3 mg L^{-1}; Promochem, LGC Standards GmbH, Wesel, Germany), HF (assay >40%; residue <2 mg L^{-1}; ACS reagent; Sigma-Aldrich Chemie GmbH, Steinheim, Germany), HNO_3 (assay >67%; residue <1 mg L^{-1}; Promochem, LGC Standards GmbH, Wesel, Germany), and H_2O_2 (assay >30%; Promochem, LGC Standards GmbH, Wesel, Germany) were used for hair digestion.

A multi-element stock solutions (1.000 ± 0.005 mg L^{-1} As= Arsenic, Al = Aluminium, Ba = Barium, Be = Beryllium, Bi = Bismuth, Cd = Cadmium, Cr = Chromium, Cs = Caesium, Cu = Copper, Ga = Gallium, La = Lanthanum, Li = Lithium, Mn = Manganese, Mo = Molybdenum, Nb = Niobium, Ni = Nickel, Pb = Lead, Rb = Rubidium, Sb = Antimony, Se = Selenium, Sn = Tin, Te = Tellurium, Ti = Titanium, Tl = Thallium, U = Uranium, V = Vanadium, W = Tungsten, and Zr = Zirconium; 5.00 ± 0.03 mg L^{-1} Ce = Cerium and Co = Cobalt; 10.00 ± 0.05 mg L^{-1} Fe = Iron and Zn = Zinc; 50.00 ± 0.25 mg L^{-1} P = Phosphorus and Si = Silicon; 55.00 ± 0.25 mg L^{-1} B = Boron and Sr = Strontium; 500.0 ± 2.5 mg L^{-1} K = Potassium, Mg = Magnesium, and Na = Sodium; 1000 ± 5 mg L^{-1} Ca = Calcium and S = Sulfur; Ultra Scientific/Agilent Technologies, North Kingstown, RI, USA) were used for ICP-MS (seven-point) and ICP-OES (eight-point) determination. A standard solution of Yttrium (Y; 5 µg L^{-1} and 100 µg L^{-1} from 1000 ± 2 mg L^{-1}; Panreac Química, Barcelona, Spain) for both ICP-MS and ICP-OES, and Scandium (Sc), Rhodium (Rh), Indium (In), and Thorium (Th) (10 µg L^{-1} from 1000 ± 5 mg L^{-1}; Merck KGaA, Darmstadt, Germany) for ICP-MS only was used as an internal standard to control the nebuliser efficiency. [68–71] A standard solution containing 5 µg L^{-1} Ba, Be, Ce, Co, In, Pb, Mg, Tl, and Th was prepared daily in 1% HNO_3 from a multi-standard stock solution (10.00 ± 0.05 mg L^{-1}; Spectro Pure, Ricca Chemical Company, Arlington, TX, USA) to select the best operating parameters for the ICP-MS analysis. They were optimized to obtain the signal/background ratio for ^{9}Be >25000 cps, ^{115}In >250000 cps, ^{232}Th >100000 cps, CeO^{+}/Ce^{+} <1% or <2% with CRI, Ba^{++}/Ba^{+} <3%, and background <5 cps.

Table 1. Operational condition for inductively coupled plasma-mass spectrometry (ICP-MS) and -optical emission spectrometry (ICP-OES) measurements.

Flow Parameters (L min^{-1})	ICP-MS		ICP-OES
Plasma Flow	18.0		15.0
Auxiliary Flow	1.80		1.50
Sheath Gas	0.18		-
Nebuliser Flow	1.00		0.75
Other			
Sampling Dept or Observation View	6.5		axial
Radiofrequency Power (kW)	1.40		1.0
Pump Rate (rpm)	3		20
Stabilisation delay (s)	35		40
	Isotope (m/z) quantified in standard mode	Isotope (m/z) quantified with CRI[a]	Emission line (nm)
	^{7}Li, ^{9}Be, ^{11}B, ^{23}Na, ^{24}Mg, ^{27}Al, ^{28}Si, ^{31}P, ^{39}K, ^{49}Ti, ^{51}V, ^{59}Co, ^{60}Ni, ^{65}Cu, ^{66}Zn, ^{71}Ga, ^{85}Rb, ^{88}Sr, ^{90}Zr, ^{93}Nb, ^{98}Mo, ^{112}Cd, ^{118}Sn, ^{121}Sb, ^{125}Te, ^{133}Cs, ^{137}Ba, ^{139}La, ^{140}Ce, ^{182}W, ^{205}Tl, ^{208}Pb, ^{209}Bi, ^{238}U	^{44}Ca, ^{51}V, ^{52}Cr, ^{55}Mn, ^{56}Fe, ^{75}As, ^{76}Se	Al 396.152, As 188.980, B 249.772, Ba 455.403, Be 234.861, Bi 223.061, C 193.027, Ca 317.933, Cd 226.502, Ce 418.659, Co 228.615, Cr 267.716, Cs 697.327, Cu 324.754, Fe 259.940, Ga 294.363, K 769.897, La 379.477, Li 670.783, Mg 279.078, Mn 257.610, Mo 202.032, Na 589.592, Nb 295.088, Ni 231.604, P 213.618, Pb 182.143, Rb 420.179, S 180.669, Sb 206.834, Se 196.026, Si 251.611, Sn 189.927, Sr 407.771, Te 214.282, Ti 336.122, Tl 351.923, U 263.553, V 292.401, W 239.708, Zn 206.200, Zr 339.198
Internal standard	^{45}Sc, ^{71}Y, ^{103}Rh, ^{115}In, ^{232}Th	^{45}Sc, ^{71}Y	Y 371.029

The reference solutions used for RCC determination were prepared in the concentration range 20–200 mg L^{-1} by sequential dilution of a carbon stock solution (1000 mg L^{-1} C). This solution was prepared by dissolution of anhydrous citric acid (assay ≥99.5%, ACS reagent; Sigma-Aldrich Chemie GmbH, Steinheim, Germany) in boiled deionised water.[63,66,67]

Standardised sodium hydroxide solution (0.5 mol L^{-1}; assay >98%, anhydrous pellets, RPE – for analysis – ACS – ISO; Carlo Erba Reagents, Milan, Italy) was prepared to determine the residual acidity in the final digested samples by acid-base titration.[63]

European reference material (ERM) DB001 [trace elements (As, Cd, Cu, Hg, Pb, Se, and Zn) in human hair homogeneous powder; sample n. 0196; Joint Research Centre, Geel, Belgium] and in-field hair samples were used for the analytical method validation and quality control.

2.2.1. In-field Human Hair Samples

Scalp hair was collected from healthy adult male (13) and female (10) volunteers from a small rural agricultural area of Asmara (Eritrea, Africa). The subjects were selected from a larger population, participating in the "Medeber project", a research project carried out in collaboration with the Italian non-profit organization "ASS.ITER. Onlus" (https://www.assiter.org/Progetto-Medeber.htm). The population was uniform when considering the age (27 ± 8 yr), hair colour (black), type of hair (curly), ethnical and geographical origin, and lifestyle. Moreover, because the participants lived in the same environment, the differences in exogenous sources were minimised. After washing the scalp hair of each volunteer with shampoo and drying using a previously reported method,[23,72] ~0.05 g hair was cut from the nape of each individual close to the scalp (length, ~1 cm). Stainless steel scissors and disposable vinyl gloves were used to avoid contamination. The hair samples were placed into labelled polyethylene bags, transported to the laboratory, and stored at room temperature (19–21 °C).

2.3. Analytical Procedures

Some parameters are critical to attain the proper experimental conditions that promote oxidative processes in the digestion of samples containing organic compounds. These include the mixture and amounts of reagents, applied temperature and pressure, and heating time.[33,66] For this purpose, different sample treatments were compared using the HNO_3/H_2O_2 mixtures as the digestion reagents, in accordance with the other methods reported in the literature.[11,33,36,47,59,60,62,65,73–76]

Initially, 0.2 g certified material, chosen according to the certificate instructions, was submitted to all acid digestion treatments. In the OD, weighed amounts of ERM DB001 (six replicates) were transferred into the polypropylene tubes, mixed with 1 mL 67% HNO_3 and 0.5 mL 30% H_2O_2, and digested for 24 h under a fume hood at room temperature (19–21 °C; ODRT) or heated in a WB12 system for 20 min to 95 °C (OD95°C). In the CD, weighed amounts of the certified material (six replicates) were transferred into quartz vessels, mixed with 1 mL 67% HNO_3, 0.5 mL 30% H_2O_2, and 1.5 mL deionised water, and subsequently heated to 180 °C with microwave energy for 40 minutes (CD180°C). For the faster sample treatment (OD95°C) was to assess the influence of the sample mass testing a mass quantity

tenfold lower (0.02 g; OD*95°C) and half the reagents (0.5 mL 67% HNO_3 and 0.25 mL 30% H_2O_2).

Total acid dissolution of the certified hair sample (0.2 g; six replicates) was achieved with 1 mL 30% HCl and 3 mL 67% HNO_3 (CD*) and by 1 mL 40% HF, 1 mL 30% HCl, and 3 mL 67% HNO_3 (CD**) in a microwave oven equipped with a PTFE vessel. The heating program used was the same as that reported previously for CD180°C. For the analysis of the HF-comprising solution, the ICP-OES equipment was arranged with inert components (demountable torch with alumina injector, and PTFE injector holder; inert Sturman-Masters spray chamber).

All the solutions obtained by digestion were diluted with deionised water to a volume of 10 mL and subsequently filtered through a pre-cleaned syringe filter, taking care to discard the first ~ 2.5 mL of the solution, necessary for the pre-washing of the filter, and collect 5 mL of the remaining solution in a new tube. All the filters were previously washed with 30 mL 2% (v/v) HNO_3 to reduce the blank values. The solution obtained by all the different digestion procedures (except by ODRT) was clear and without visible solid residues. The digests obtained by OD*95°C and those obtained by CD* or CD** were analysed by ICP-MS and ICP-OES, respectively, without further dilution. All the other digests were further diluted (1:2) with deionised water prior to ICP-MS analysis to achieve <5% v/v acidity, according to the user manual. The summary of the characteristics of the hair sample treatments used in the present study is shown in Table S1.

Ten blank solutions, comprising deionised water and the reagents, were also tested together with each sample set digested to trace and control the contributions from possible sample contamination. The blanks were deducted from all the measurements. The method blank concentrations are reported in Tables S2 and S3.

2.3.1. Validation

The analytical performance and quality control of the optimised procedure were evaluated by application of hair certified material, spiked samples and in-field hair samples. The limits of detection (LODs), lower and upper limits of quantification (LLOQs and ULOQs), linearity, accuracy (trueness bias or recovery), precision (repeatability and intermediate precision), and uncertainty were determined for each element.[77–83]

Evaluation of the blank level prior to measurement and ICP-MS instrumental drift were checked in all analyses. Drift was checked by analysing the fourth calibration standard (5 µg L^{-1} Al, As, Ba, Be, Bi, Cd, Cr, Cs, Cu, Ga, La, Li, Mn, Mo, Nb, Ni, Pb, Rb, Sb, Se, Sn, Te, Ti, Tl, U, V, W, and Zr; 25 µg L^{-1} Ce and Co; 50 µg L^{-1} Fe and Zn; 250 µg L^{-1} P and Si; 275 µg L^{-1} B and Sr; 2500 µg L^{-1} K, Mg, and Na, and 5000 µg L^{-1} Ca) immediately after the calibration curve, after every 20 samples, and at the end of the analytical sequence. A maximum percent drift of ± 10% was considered acceptable for all elements.

The LOD was calculated according to the formula:[84]

$LOD = 3 \times RSD\% \times BEC/100$,

where RSD% is the relative standard concentration percentage of the method blank (n = 10) measured for each digestion procedure and BEC is the background equivalent concentration (mg kg^{-1}) measured during the analytical sequence. The ULOQ and LLOQ are the highest and lowest standard curve points that can still be used for quantification; they are the values below and above which, respectively, the highest/lowest concentration of an element that can be accurately measured. Together, the ULOQ and LLOQ define the range of quantification for the assay. The LODs, ULOQs and LLOQs are shown in Tables 2, S3, and S4. Although ICP-MS is well known for benefiting from a wide linear concentration range,[55] linearity (Table 2) was verified by the Mandel fitting test.[85,86]

Accuracy (recovery% or trueness bias%) was evaluated using the certified material. Other recovery studies were carried out by adding a known amount of the elements to ERM DB001 (six replicates, 0.02 g). The multi-standard solution comprised all the investigated elements except for the certified elements and not certified elements with informative values (As, Cd, Cu, Pb, Se, and Zn and Al, B, Ba, Be, Bi, Ca, Co, Cr, Cs, Fe, Li, Mg, Mn, Mo, Ni, P, Sb, Sn, Ti, Tl, U, V, W, and Zr, respectively), in concentrations 10 times higher than those of the third calibration standard (2 µg L^{-1} Ga, La, Rb, and Te; 10 µg L^{-1} Ce; 100 µg L^{-1} Si; 110 µg L^{-1} Sr; and 1000 µg L^{-1} K, and Na). The spiked samples were submitted to the overall procedure, the metals quantified by the established conditions, and the respective recoveries calculated. An acceptance limit R% in the range 90–110% was considered as valid according to the criteria described in Commission Decision 2002/657/EC.[77,82]

Table 2. Summary of results for the characteristic parameters of the analytical method using open-vessel digestion heated in a water bath to 95°C (sample amount 0.02 g).

Element	LOD[a]	BEC[a]	LLOQ[a]	ULOQ[a]	N[a]	Linearity range (log)	Characteristics of the ICP-MS calibration curve (n = 3, mean ± SD)			Bias% or R%[a]	RSD%[a] Intra-day	RSD%[a] Inter-day	U%[a]
							Slope	y-intercept	Correlation coefficient				
Al	0.07	0.6	0.3	10	6	1.6	34670 ± 16542	57499 ± 12676	0.9996 ± 0.0004	94[c]	2.4	6.7	5.9
As	0.02	0.01	0.3	10	6	1.6	93 ± 4	6 ± 5	0.9990 ± 0.0004	-0.4[b]	11	13	26
B	2	6	14	1400	7	2.0	8256 ± 3821	118926 ± 31140	0.9994 ± 0.0004	91[c]	6.0	11	15.2
Ba	0.5	3	0.3	25	7	2.0	6991 ± 3703	56532 ± 11099	0.9984 ± 0.0014	107[c]	10	11	26.3
Be	0.0002	0.0003	0.3	25	7	2.0	8936 ± 2240	8 ± 2	0.9996 ± 0.0002	98[c]	9.2	10	23.2
Bi	0.0002	0.0003	0.3	10	6	1.6	45073 ± 9326	35 ± 9	0.9994 ± 0.0003	109[c]	7.1	7.3	18.0
Ca	10	130	250	25000	7	2.0	473 ± 148	160587 ± 10311	0.9963 ± 0.0054	93[c]	0.3	5.1	0.3
Cd	0.0001	0.0002	0.3	10	6	1.6	7120 ± 1419	3 ± 1	0.9996 ± 0.0003	5.0[b]	2.1	2.9	5.4
Ce	0.0006	0.0010	1	130	7	2.0	63867 ± 16240	209 ± 77	0.9994 ± 0.0002	94[d]	5.3	3.4	13.4
Co	0.001	0.005	1	50	6	1.6	22760 ± 6952	197 ± 58	0.9991 ± 0.0001	95[c]	1.0	3.5	2.5
Cr	0.006	0.01	0.3	25	7	2.0	1130 ± 230	20 ± 7	0.9993 ± 0.0005	65[c]	3.1	4.6	7.8
Cs	0.0004	0.0003	0.3	25	7	2.0	57190 ± 9885	39 ± 2	0.9994 ± 0.0002	108[c]	8.5	4.4	21.4
Cu	0.01	0.03	0.3	25	7	2.0	4596 ± 887	356 ± 58	0.9991 ± 0.0004	-1.0[b]	3.0	4.1	7.6
Fe	0.07	0.2	3	250	7	2.0	2436 ± 484	1640 ± 358	0.9992 ± 0.0004	79[c]	5.0	7.1	12.7
Ga	0.0007	0.0003	0.3	25	7	2.0	14969 ± 5103	20 ± 12	0.9991 ± 0.0002	94[d]	6.8	2.7	17.1
K	30	60	130	13000	7	2.0	18820 ± 6839	3232276 ± 1249765	0.9979 ± 0.0017	93[d]	11	12	30.2
La	0.0002	0.0006	0.3	10	6	1.6	71927 ± 19592	132 ± 48	0.9992 ± 0.0002	102[d]	7.3	2.8	18.3
Li	0.004	0.006	0.3	25	7	2.0	42190 ± 14359	609 ± 61	0.9995 ± 0.0002	93[c]	5.6	4.8	14.1
Mg	3	10	130	13000	7	2.0	10857 ± 3213	33603 ± 15652	0.9992 ± 0.0003	102[c]	4.2	5.4	10.5
Mn	0.01	0.02	0.3	25	7	2.0	7226 ± 1400	372 ± 65	0.9987 ± 0.0008	101[c]	7.9	6.4	19.8
Mo	0.002	0.002	0.3	25	7	2.0	9642 ± 1549	52 ± 16	0.9995 ± 0.0001	94[c]	3.7	3.5	9.4
Na	4	7	130	13000	7	2.0	19317 ± 7423	388706 ± 21984	0.9965 ± 0.0030	102[d]	11	3.8	26.7
Nb	0.0001	0.0001	0.3	25	7	2.0	38390 ± 9011	8 ± 1	0.9992 ± 0.0000	92[c]	8.2	9.7	20.8
Ni	0.003	0.04	0.3	25	7	2.0	4706 ± 1502	479 ± 47	0.9990 ± 0.0004	105[c]	1.0	5.6	2.5
P	3	20	13	250	5	1.3	1350 ± 445	61864 ± 21578	0.9996 ± 0.0001	101[c]	4.2	5.3	10.5
Pb	0.005	0.02	0.3	25	7	2.0	27833 ± 6030	981 ± 394	0.9994 ± 0.0000	-4.0[b]	4.0	5.0	10
Rb	0.002	0.005	0.3	25	7	2.0	34907 ± 10185	435 ± 37	0.9991 ± 0.0002	92[d]	11	4.0	27.2
Sb	0.0008	0.002	0.3	25	7	2.0	13503 ± 986	37 ± 6	0.9992 ± 0.0003	90[c]	11	12	28.5
Se	0.05	0.05	0.3	5	5	1.3	45,3 ± 5,9	6 ± 2	0.9993 ± 0.0005	9.0[b]	4.4	3.7	11.1
Si	5	100	13	1300	7	2.0	8388 ± 4585	2492680 ± 120990	0.9987 ± 0.0012	95[d]	0.6	2.6	1.4
Sn	0.0003	0.002	0.3	25	7	2.0	12551 ± 2571	74 ± 33	0.9994 ± 0.0001	95[c]	9.8	10	24.8
Sr	0.03	0.2	14	1400	7	2.0	28263 ± 7564	13687 ± 1426	0.9988 ± 0.0005	100[d]	2.8	6.0	7.1
Te	0.002	0.002	0.3	10	6	1.6	677 ± 157	6 ± 3	0.9990 ± 0.0006	91[d]	3.6	4.2	4.2
Ti	0.02	0.06	0.3	25	7	2.0	1736 ± 472	171 ± 52	0.9997 ± 0.0002	92[c]	7.0	4.4	17.6
Tl	0.00005	0.0001	0.3	10	6	1.6	39273 ± 7889	11 ± 5	0.9991 ± 0.0003	92[c]	9.0	5.0	22.7
U	0.00002	0.0001	0.3	10	6	1.6	77110 ± 26626	19 ± 9	0.9995 ± 0.0001	107[c]	7.4	4.8	18.7
V	0.004	0.002	0.3	25	7	2.0	1321 ± 225	9 ± 2	0.9988 ± 0.0005	106[c]	7.1	6.0	17.9
W	0.0008	0.002	0.3	25	7	2.0	14440 ± 2998	41 ± 12	0.9991 ± 0.0005	90[c]	9.2	5.5	23.2
Zn	0.2	1	3	100	6	1.6	4161 ± 2546	6267 ± 3787	0.9984 ± 0.0006	5.0[b]	4.8	4.8	12
Zr	0.0007	0.001	0.3	10	6	1.6	25057 ± 5615	65 ± 7	0.9990 ± 0.0002	90[c]	9.1	6.0	22.9

[a] Abbreviations: LOD, limit of detection (n = 10; mg kg^{-1}); BEC, background equivalent concentration (mg kg^{-1}); LLOQ and ULOQ, lower and upper limit of quantification (mg kg^{-1}); N, number of the concentration levels; bias%, trueness bias percentage (n = 6); R%, recovery percentage (n = 6); RSD%, relative standard deviation percentage (n = 6 for precision intra-day or repeatability and n = 18 for precision inter-day or reproducibility); U%, uncertainty percentage.

[b,c,d] The trueness bias percentage was calculated for the certified elements indicated with the superscript letter b (n = 6); the recovery percentage was calculated for the non-certified elements with the superscript letter c (n = 6); and the spiked recovery percentage was used to determine the accuracy of the method for non-certified elements with the superscript letter d (n = 6).

The precision of the measurements was ascertained using repeatability and intermediate precision studies. Repeatability [relative standard deviation percentages (RSD%) intra-day] and intermediate precision (RSD%, inter-day) were evaluated using one set of certified material (six spiked and six unspiked) samples on the same day or analysed during three different days over a period of three weeks (seven-day intervals), respectively. The accuracy and precision results are shown in Tables 2, and 3. The selectivity of the proposed method was evaluated through the study of the interference in the ICP-MS analysis (section 2.3.2).[58,80,87] Finally, uncertainty of methods was estimated for each element (Table 2).[67,77,78,83] A criterion arbitrarily based on the repeatability of analytical signal for certified material samples (six replicates) was used, in agreement with other authors.[67] Then, an expanded uncertainty was estimated, which was calculated using the standard uncertainty (as RSD%) multiplied by the coverage factor (k = 2.52).[67,88]

2.3.2. Evaluation of the Interference on ICP-MS Analysis

Hair is mainly composed of protein and elements such as C, O, H, N, P, and S.[71] These elements, which are usually present in the sample matrix together with Ar plasma, nebulised water, and dissolved/entrained air produce polyatomic interferences.[58,67] The maximum RCC for accurate analysis by ICP-MS should be as low possible to minimise spectral interferences and C deposits in the interface. In particular, RCC increases the ICP signal of some elements by C charge transfer reactions.[33,67] This increase is more prominent in elements with an ionisation potential similar to that of C (11.26 eV), as As (9.82 eV), Be (9.32 eV), and Se (9.75 eV).[63,89] For better evaluation and control of ICP-MS interference, ICP-OES was used to determine the C and S levels. For the evaluation of the spectral interference (especially important for isotopes ≤100 amu), enhancement and suppression of the analytical signal was achieved from the evaluation of trueness bias for As, Cu, Se and Zn (Tables 2, and 3), the recovery of the other elements (Tables 2, S5 and S6) from 0.02 g and 0.2 g hair certified material (section 2.3.1), and by inter-technical comparison between ICP-MS and ICP-OES.

Correction of the matrix effect, caused by the different viscosity and acid concentrations between the calibration and sample solutions, was achieved using the internal standards 45Sc,

79Y, 103Rh, 115In, and 232Th. These were carefully selected by considering the closeness of the ionisation 28Si, 31P, 39K, 49Ti, 51V, 59Co, and 60Ni; 79Y for 65Cu, 66Zn, 71Ga, potential, m/z ratio, spectral interferences, and chemical properties. 45Sc was used for 7Li, 9Be, 11B, 23Na, 24Mg, 27Al, 85Rb, 88Sr, 90Zr, and the elements determined with CRI (44Ca, 51V, 52Cr, 55Mn, 56Fe, 75As, and 76Se); 103Rh for 93Nb and 98Mo; 115In for 112Cd, 118Sn, 121Sb, 125Te, 133Cs, 137Ba, 139La, and 140Ce; and 232Th for 182W, 205Tl, 208Pb, 209Bi, and 238U.

2.4. Statistical Analysis

Statistical analyses were carried out using IBM SPSS Statistics 25 software (IBM Corp., Armonk, NY, USA). For each element, values below the LOD were designated as half the LOD, as recommended for small datasets.[90] When the percentage of values <LOD was more than 20%, the element was excluded from the statistical elaboration.

Descriptive statistics were elaborated for each element level of the in-field hair sample (Table 4).

The normality of each element level in certified material was tested by use of the Kolmogorov-Smirnov test. Then, the differences in the concentration obtained with different sample treatments were tested by the one-way ANOVA test with Bonferroni post-hoc tests for the normally distributed elements and by Kruskal-Wallis test with pairwise post-hoc tests for the not normally distributed elements. The results (Tables 2, 3, S5 and S6) were considered statistically significant for p-values <0.05.

3. Results and Discussion

3.1. Comparison of the Hair Sample Treatments

HNO_3 and H_2O_2 were used as reagents because they allow the oxidation of almost all organic compounds and cause minor spectral interferences or problems in ICP-MS compared to other reagents (HCl, HClO, HF or H_2SO_4).[17,33,58,63] The reagent amount was selected considering the maximum volume of the digestion vessels and the minimum dilution of the sample to have a final acidity of the sample <5% as recommended by the ICP-MS manual. First, the RCC and residual acidity for all the hair sample treatments were evaluated (section 3.1.1). Then, the influence of acid digestion treatment on elemental analysis was studied (sections 3.1.2 and 3.1.3).

3.1.1. RCC and Residual Acidity

As shown in Fig. 1, lower RCC values were obtained when the digestion temperature was increased (CD180°C; 79 ± 2 mg L^{-1} C). The residual acidities decreased at higher digestion temperatures owing to the consumption of HNO_3 by the oxidative processes and its decomposition under heating. For the 0.2 g certified material digests, the residual acidities varied from 0.79 ± 0.01 mol L^{-1} for ODRT to 0.60 ± 0.02 mol L^{-1} for OD95°C; for the 0.02 g samples (OD*95°C) the acidity was 0.86 ± 0.01 mol L^{-1}. Furthermore, these data were found to be comparable with the values reported in the literature using other digestion methods.[63,66,67] Therefore, the results suggested that all the digests obtained using the three treatments were suitable for ICP-OES and ICP-MS analyses. Digests with C concentrations ≤8 g L^{-1} do not present any C related effects in the ICP-OES data of most elements.[63,67] As and Se are not affected by polyatomic ion interferences due to C up to concentrations of 348 ± 23 mg L^{-1} (ODRT) and for Be up to 256 ± 23 mg L^{-1} (OD95°C according to the trueness bias% (Tables 2, and 3) and R% (Table 2) values.

Table 3. Certified and measured concentration (mg kg^{-1}; mean ± standard deviation) of the certified material ERM DB001 (n = 6; 0.2 g) using different sample treatments [room temperature open-vessel digestion (ODRT), open-vessel digestion heated to 95°C (OD95°C), and closed-vessel microwave-assisted digestion (CD180°C)].

Element	Certified concentration	Measured concentration			Normal distribution of data[a]	P[b]
		OD_{RT}	$OD_{95°C}$	$CD_{180°C}$		
As	0.044 ± 0.006	0.0449 ± 0.0028	0.0431 ± 0.0026	0.0438 ± 0.0027	Yes	N.S.
Cd	0.125 ± 0.007	0.116 ± 0.009	0.118 ± 0.008	0.118 ± 0.003	Yes	N.S.
Cu	33 ± 4	34.6 ± 0.7	33.6 ± 1.1	34.0 ± 1.6	Yes	N.S.
Pb	2.14 ± 0.20	2.18 ± 0.13	2.07 ± 0.17	2.10 ± 0.02	Yes	N.S.
Se	3.24 ± 0.24	3.24 ± 0.06	3.22 ± 0.23	2.90 ± 0.04	Yes	N.S.
Zn	209 ± 12	217 ± 4	218 ± 8	225 ± 8	Yes	N.S.

[a] According to Kolmogorov-Smirnov test

[b] The results were considered statistically significant for p-values <0.05 (one-way ANOVA test for the normally distributed elements). N.S. = Not significant.

3.1.2. Analytical Characteristics

There are various methods (approaches) and their variations for estimation of LOD.[91] Background signal plays an important role in detection limits determination. All signals are measured in the presence of some degree of background, which can originate from a variety

of sources, including detector and electronic characteristics for ICP-OES, and interfering ions formed in the source or from the matrix for ICP-MS, or contamination.

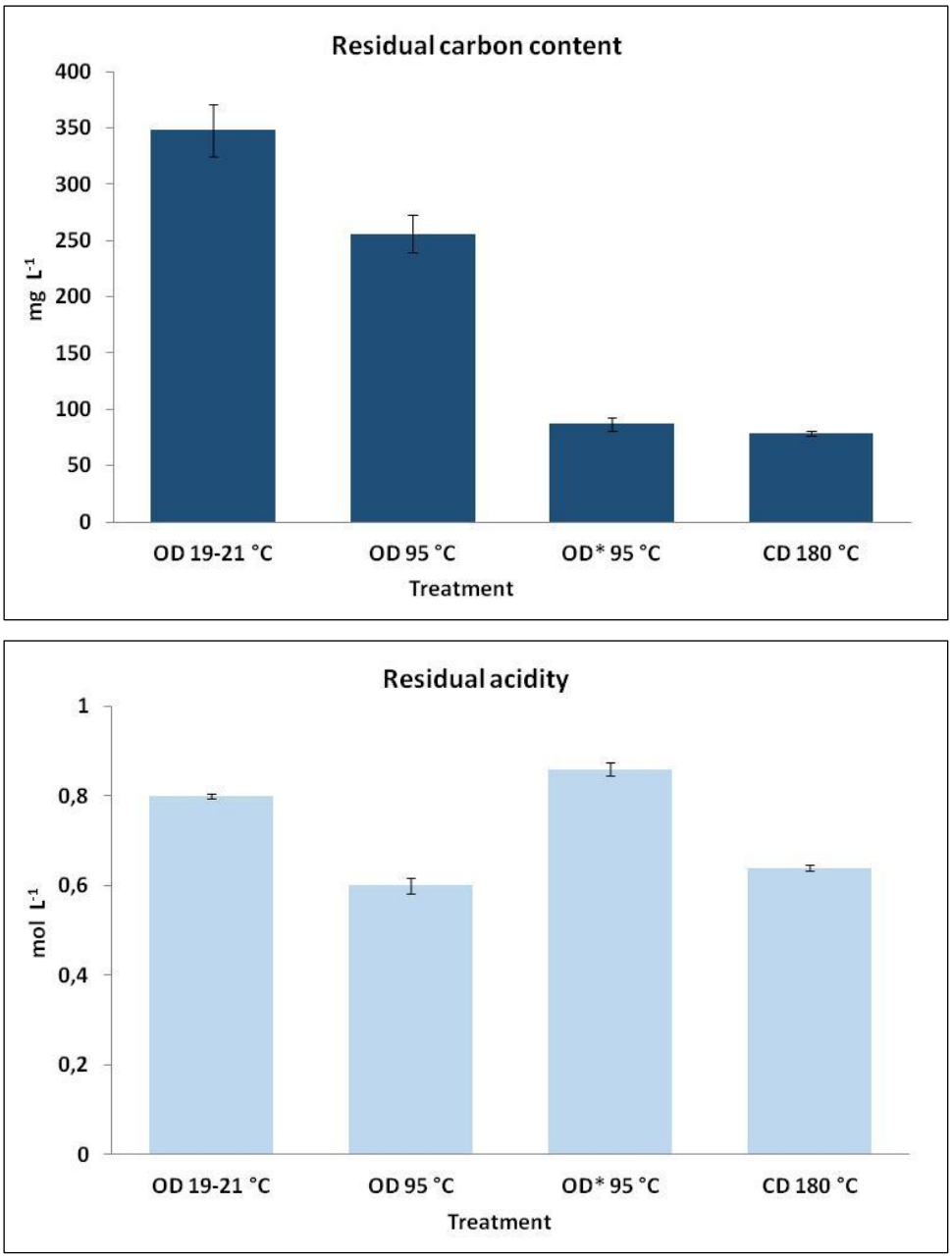

Fig. 1. Residual carbon contents (upper panel) and residual acidity (lower panel) using different acid digestion treatments [open-vessel digestion (OD19–21°C, OD95°C and OD*95°C), and closed-vessel microwave-assisted digestion (CD180°C)] of the certified material ERM DB001 [0.2 g samples except for OD*95°C treatment (0.02 g samples)].

The LODs were calculated considering both the BEC and the method blank. The data in Tables 2, and S4 show that OD95°C presents LOD values similar to or better than those obtained by ODRT and CD180°C, while the values obtained by OD*95°C were the highest. These results were attributed to the smaller sample amount compared to those of the other treatments. This is however acceptable if one considers that a method that allows the analysis of a small sample quantity (e.g., in newborns) is very useful. Comparison of the proposed method (OD95°C) with others published for trace element determination in hair by ICP-MS revealed that the LODs of certified element are similar than the literature values (Table S1).[40,60,73,74,92]

Generally, good agreement between the experimental results and the certified concentrations was observed, with trueness bias percentages in the range -5–10% for all the elements (Tables 2, and 3). The RSD% for the repeatability did not exceed the 10%-limit (Tables 2 and 3) for all the certified elements except for As by OD*95°C (RSD% = 11%). This was attributed to the smaller sample amount considered for OD*95°C.

The satisfactory analytical characteristics obtained indicated that for the determination of As, Cd, Cu, Pb, Se, and Zn it is possible to use all three digestion methods, even if the OD95°C treatment is the fastest procedure. With the OD95°C and ODRT treatments the samples can be digested and diluted directly in polypropylene tubes, which are directly used for the ICP-MS analysis. In addition, different from quartz or PTFE vessels, the flasks used in the OD95°C were single-use polypropylene autosampler tubes that do not require cleaning steps, thereby reducing contamination from residual impurities. The summary of performance characteristics and total sample digestion time for open- and closed-vessels preparation procedures were reported in Table S1.

3.1.3. Contents of the Non-certified Elements in ERM DB001

Tables S5 and S6 list the data of the contents of the non-certified elements in ERM DB001, which can be used as reference and/or comparison values in other studies.

The data obtained by ICP-MS analysis (Table S5) were higher than the LOD values for all the elements and different sample treatments used, except for K by ODRT and OD*95°C and Te by ODRT, OD96°C, and OD*95°C that were lower than the LOD. For B, Bi, Cs, Mg, Mn, Mo, Na, Ni, P, Sn, and V no statistical differences at the 95% confidence level were observed between ODRT, OD95°C, and CD180°C (Table S5). The levels of Cr, Fe, Ga, Li, Nb, Rb, Tl,

and Zr by OD95°C and ODRT were significantly lower than those obtained by CD180°C. Using the same reagent mixture HNO_3/H_2O_2 (2:1) but varying the temperature from 95 to 180 °C and the pressure from ~1 to ~40 bar, only Cr, Nb, Si, and Ti by OD*95°C were significantly (p-values <0.05; Table S5) than those obtained by CD180°C. This can be attributed to the influence of the sample mass and amounts of reagents used, since in OD*95°C the mass is tenfold smaller than that in OD95°C while the reagents are only halved.

The data obtained by ICP-OES analysis (Table S6) were higher than the LOD values for Al, Ba, Ca, Cr, Fe, Mg, Mn, Ni, P, Si, Sn, Sr, Ti, and Zr from CD*, and CD**; Co and La from CD*; and Mo from CD**. Cs could not be analysed because axial view ICP-OES is strongly affected by ionisation interference when elements with low ionisation potentials coexist in the sample.[93] At the same pressure and temperature, the reagent mixture displayed a strong influence on some of the elements (Table S6). In particular, the use of the HCl/HNO_3 (1:3) or $HF/HCl/HNO_3$ (1:1:3) mixture led to a significant increase in the Fe and Ti levels compared to those obtained by CD180°C (H_2O_2/HNO_3, 1:2). On the other hand, the use of an $HF/HCl/HNO_3$ mixture led to a significant decrease in the Ca level obtained by CD** compared to that obtained by CD180°C. It was not possible to evaluate the effect of the different mixtures used for B, Be, Bi, Ce, Co, Ga, K, La, Li, Mo, Na, Nb, Rb, Sb, Te, Tl, U, V and W because the results were lower than the LODs by CD* and/or CD**.

Finally, good agreement between the experimental results obtained by OD*95°C and the informative values of ERM DB001 was observed, with R% in the range 90–109% for all the elements except for Cr and Fe (Tables 2, and S5).

3.2. Validation Parameters of the Proposed Method

The composition of the digestion mixture for OD*95°C was optimized by comparing 200, 500 or 1000 μL 67% HNO_3 in the presence of 100, 250 or 500 μL of 30% H_2O_2. The mixture with 500 μL HNO_3 and 250 μL H_2O_2 yielded the most complete digestion (with the absence of visible residue of sample) and thus was used for the subsequent experiments.

Considering all the above results and applying the developed method to the field samples, the performance of the faster sample treatment (open-vessel digestion heated to 95 °C for 20 min, Table S1) was also evaluated for all the non-certified elements by analysis of ERM DB001 (0.02 g) spiked using multi-element standard solution, as described in section 2.3.1. Notably, although the addition of known amounts of analytes in aqueous solution does not allow to

evaluate the efficiency of the digestion procedure in decomposing the hair matrix, the study of recoveries can allow an evaluation of matrix effects and losses or increases in the concentration of the analytes compared to the added amounts.

For each element, the LLOQ, ULOQ, number of the concentration levels, and the calibration curve's slope, y-intercept and correlation coefficient are shown in Table 2. The calibration curve was selected to cover the range of concentrations obtained in human hair sample. In the whole validation, at least five levels (including zero) were used in the construction of each part of the calibration curve.[82] The dynamic range was different for each element (from 1.3- to 2.0-log), with LLOQ ranging from 0.3 to 250 mg kg^{-1}. The comparison of dynamic range with previously published methods is shown in Table S1.[43,74] The dynamic range is related to the variability of the elemental concentrations in the considered matrices and to the characteristics of the used instrument. In particular, the ICP-SFMS has greater sensitivity and resolving power than a quadrupole ICP-MS and therefore allows the determination of the elements over a wide range of concentrations.[43] The linear regression was verified by means of the Mandel fitting test for all elements. The correlation coefficient for calibration curves (analysed on three different days) ranged from 0.9963 to 0.9997.

The obtained LODs using OD*95°C (Tables 2) were similar or even better than those reported by other authors.[40,60,74,92] The comparison of the performance of the proposed method with respect to previous methods was shown in table S1. It was not possible to compare the LODs determined for Ce, La, Nb, and P because they were not reported in the considered literature. Generally, acceptable trueness bias percentages in the range -4–9% for all the certified elements and good recoveries in the range 90–110% were observed for all the non-certified elements except for Cr (65%) and Fe (79%) obtained by OD*95°C, as previously discussed (Tables 2, and S5). The precision was evaluated using repeatability and intermediate precision studies. As reported in Table 2, the RSD% values ranged from 0.3 to 11% for repeatability and from 2.6 to 13% for intermediate precision. This also confirmed that the minor changes applied in the experiments for the evaluation of inter-day precision did not affect the robustness of the method. Therefore, the results of the spiked ERM DB001 (Table 2) confirmed that under the selected conditions the interference was resolved, negligible, or adequately corrected. The spectral effects from the different polyatomic species observed during the analysis of the complex samples can seriously interfere with the determination of

many isotopes (mainly ≤100 amu).[67,94] These effects were negligible for C ≤50 g kg^{-1}, P ≤150 mg kg^{-1}, and S ≤50 g kg^{-1}.

3.3. In-field Application of the Proposed Method

The proposed method was carried out on hair sampled from 23 subjects (Table 4). The final digests presented carbon contents lower than 56 ± 2 mg L^{-1}, thereby allowing ICP-MS analysis without any significant C interference (section 3.1.1).

The relative repeatability (r_{rel}) of the in-field hair sample measurements was calculated as previously reported works.[68,69] The r_{rel} was <10%, resulting comparable to the repeatability, which was determined by repeated application of the to the spiked certified material (Table 3).

Table 4 lists the main descriptive statistical parameters of the elements in human scalp hair. In many cases, the standard deviation is larger than the mean, reflecting the distribution of the element contents due to the biological variability of each subject rather than the precision of a series of measurements repeated on the same quantity.[95] The differences in the element levels in hair are most likely caused by environmental exposure, ethnic and geographic origin, and dietary habits.[11,96] Considering the whole population of hair samples, the essential elements (Ca, Cu, Fe, K, Mg, Na, and Zn) presented the highest concentrations. Other studies from other parts of the world have reported comparable concentrations in human scalp hair.[96,97–99] Notably, the overall average levels of the macro- and essential elements observed in the hair samples met the recommended daily values of Ca, 1000 mg; K, 3500 mg; Mg, 400 mg; Na, 2400 mg; and Fe, 18 mg for humans.[96,100] On the other hand, the average concentrations of the some toxic elements (0.040 ± 0.030 mg kg^{-1} for As, 0.036 ± 0.032 mg kg^{-1} for Cd, 0.77 ± 0.58 mg kg^{-1} for Ni, 2.7 ± 2.7 mg kg^{-1} for Pb) were relatively low in agreement with other authors.[96]

The mean concentrations observed in this study for Al, Ba, Co, Mn, Si, Ti, Sr, V, and Zr were higher than the mean levels reported in the literature. [23,74,101] On the other hand, other element (Sn, Sb, La, Ce, Tl, Bi, Cs, U, V, Co, and Zr) levels were lower than those reported for hair in other geographical areas (Poland[23], China[74], and South Serbia[101]). These differences were attributed to environmental exposure, hair colour, ethnical and geographical origin, and dietary and smoking habits.[10,33,74,96] Therefore, it is very important to establish reference ranges for each country.

Table 4. Number of valid data (N) and concentrations (mg Kg^{-1}] of each element in the hair samples compared to the mean or range levels (mg Kg^{-1}) reported in other studies.

Element	Whole population						Mean ± SD or range levels from other studies		
	N	Mean	SD	Median	Minimum	Maximum	Chojnacka et al.[23]	Luo et al.[74]	Sahoo et al.[101]
Al	20	42	24	44	<0.07	72	8.30 ± 5.83	2.13 ± 2.20	-
As	21	0.041	0.030	0.031	<0.02	0.092	0.834 ± 0.325	0.18 ± 0.17	-
B	3	<2	-	<2	<2	<2	0.872 ± 2.32	0.45 ± 1.29	-
Ba	23	7.9	6.5	5.6	2.0	28.2	2.05 ± 1.56	0.37 ± 0.54	-
Be	0	<0.0002	-	<0.0002	<0.0002	<0.0002	-	<0.0050	-
Bi	21	0.016	0.024	0.009	<0.0002	0.083	0.209 ± 0.503	-	-
Ca	23	2024	810	1940	872	3810	2154 ± 1378	331.03 ± 1.71	-
Cd	23	0.036	0.032	0.021	0.007	0.142	0.0904 ± 0.0618	0.028 ± 0.070	0.012-3.63
Ce	23	0.061	0.045	0.047	0.005	0.176	0.164 ± 0.237	-	-
Co	23	0.13	0.13	0.08	0.03	0.54	0.848 ± 0.127	0.0077 ± 0.014	-
Cr	23	0.49	0.50	0.32	0.10	1.85	1.20 ± 0.81	0.41 ± 0.45	-
Cs	20	0.0023	0.0021	0.0019	<0.0004	0.0085	-	0.00062 ± 0.0014	0.001-0.013
Cu	23	12	5	11	8	31	21.5 ± 29.8	8.73 ± 3.55	-
Fe	23	128	103	99	31	386	23.0 ± 6.92	7.51 ± 31.12	7.4-32.9
Ga	23	0.019	0.013	0.016	0.006	0.053	-	0.019 ± 0.025	-
K	23	2300	1900	1580	130	5990	61.8 ± 50.8	-	-
La	23	0.028	0.021	0.022	0.0005	0.078	0.559 ± 0.389	-	-
Li	23	0.056	0.039	0.049	0.015	0.178	0.108 ± 0.075	<0.0050	-
Mg	23	259	130	209	110	662	83.9 ± 51.3	27.99 ± 18.62	-
Mn	23	7.5	5.8	6.5	1.1	26.1	0.730 ± 0.414	0.83 ± 1.16	0.5-5.2
Mo	23	0.06	0.08	0.04	0.03	0.37	0.538 ± 1.723	0.047 ± 0.029	-
Na	23	3090	2460	2500	411	9430	370 ± 285	-	-
Nb	6	0.0017	0.0037	<0.0001	<0.0001	0.0141	-	-	-
Ni	23	0.77	0.58	0.69	0.21	2.61	0.951 ± 0.809	0.20 ± 0.75	0.16-1.16
P	23	163	20	155	137	195	154 ± 44	-	-
Pb	23	3.4	4.2	2.5	0.1	17.5	3.08 ± 1.69	1.11 ± 1.98	-
Rb	23	1.4	1.2	1.0	0.1	4.2	2.29 ± 2.51	0.049 ± 0.13	-
Sb	23	0.084	0.076	0.062	0.024	0.300	-	1.17 ± 1.00	-
Se	23	0.6	0.1	0.6	0.4	0.7	-	0.64 ± 0.13	-
Si	23	165	48	159	91	252	59.7 ± 47.2	-	-
Sn	23	0.32	0.30	0.24	0.05	1.31	3.40 ± 3.33	-	-
Sr	23	8.0	4.7	6.4	2.3	17.6	4.66 ± 4.68	0.75 ± 1.39	0.18-4.5
Te	2	<0.002	-	<0.002	<0.002	0.0033	-	-	-
Ti	23	4.9	1.3	4.5	3.8	8.4	1.91 ± 2.95	0.70 ± 0.30	-
Tl	23	0.0023	0.0013	0.0023	0.0005	0.0057	-	0.012 ± 0.020	-
U	23	<0.00002	-	<0.00002	0.0006	0.0175	-	0.0018 ± 0.0028	0.00009-0.449
V	23	0.31	0.16	0.25	0.13	0.80	0.845 ± 0.335	0.021 ± 0.027	-
W	23	<0.0008	-	<0.0008	<0.0008	<0.0008	-	-	-
Zn	23	148	37	149	78	238	230 ± 142	168.21 ± 34.92	124-213
Zr	23	0.13	0.13	0.08	0.01	0.58	0.374 ± 0.645	0.0082 ± 0.020	-

4. Conclusions

The digestion of small-size hair samples (0.02 g) were established. The RCC values and residual acidity of the obtained digests indicate that the OD*95°C sample treatment is a promising alternative to conventional acid digestion in a microwave oven as a sample preparation method for subsequent elemental determination by ICP-based techniques. Only the results of the Cr, Nb, Si, and Ti concentration obtained by OD*95°C were significantly lower than those obtained by CD180°C. On the other hand, at the same pressure and temperature, the reagent mixture displayed a strong influence on some of the elements. In particular, the use of the HCl/HNO_3 (1:3) or $HF/HCl/HNO_3$ (1:1:3) mixture led to a significant increase in the Fe and Ti levels compared to those obtained by CD180°C (H_2O_2/HNO_3, 1:2). Additionally, the use of polypropylene tubes that are subsequently used for ICP-MS analysis allows a good reduction in sample and reagent amounts, treatment time, and sample handling compared to those of closed-vessel microwave-assisted digestion. Moreover, the disadvantages from vessel assembly are eliminated and all the analytical operations, i.e. sample weighing, addition of reagents, sample digestion, and digest dilution, are carried out in each autosampler tube without transferring the sample and solutions. This approach avoids contamination and provides satisfactory detection limits and good performance. OD95°C appears the fastest procedure compared to the investigated processes and can be easily applied to the screening routine analysis of large batches of hair samples.

The field data may be employed as baseline information for future environmental pollution abatement programs.

Conflicts of Interest

There are no conflicts to declare.

Acknowledgements

The authors are especially grateful to all the participants for their generous contribution.

References

1 M. Manigrasso, C. Protano, M.L. Astolfi, L. Massimi, P. Avino, Vitali and S. Canepari, *Sci. Total Environ.,* 2019, 653, 1192–1203.

2 L. Massimi, M.E. Conti, G. Mele, M. Ristorini, M.L. Astolfi and S. Canepari, *Ecol. Indic.*, 2019, 101, 759-769.

3 S. Canepari, P. Castellano, M.L. Astolfi, S. Materazzi, R. Ferrante, D. Fiorini and R. Curini, *Environ. Sci. Pollut. Res.*, 2018, 25, 1448-1459.

4 S. Canepari, E. Marconi, M.L. Astolfi, C. Perrino and C. Farao, *E3S Web of Conferences*, 2013, 1, 07004-p.1-07004-p.3. DOI: 10.1051/e3sconf/20130107004.

5 S. Canepari, M.L. Astolfi, F. Marcovecchio, M. Maretto and C. Perrino, *E3S Web of Conferences*, 2013, 1, 20002-p.1-20002-p.3. DOI: 10.1051/e3sconf/20130120002.

6 E. Marconi, S. Canepari, M.L. Astolfi and C. Perrino, *Procedia Environ. Sci.*, 2011, 4, 209-217.

7 M.L. Astolfi, S. Canepari, M. Catrambone, C. Perrino and A. Pietrodangelo, *Environ. Chem. Lett*., 2006, 3, 186-191.

8 M.L. Astolfi, S. Canepari, E. Cardarelli, S. Ghighi and M.L. Marzo, *Ann. Chim*., 2006, 96, 183-194.

9 P. Wołowiec, I. Michalak, K. Chojnacka and M. Mikulewicz, *Clin. Chim. Acta*, 2013, 419, 139-171.

10 M. Esteban and A. Castaño, Environ. Int., 2009, 35, 438-449.

11 E. Tamburo, D. Varrica, G. Dongarrà, *Sci. Total Environ.*, 2016, 573, 996-1002.

12 P. Aggett, G.F. Nordberg and M. Nordberg, in *Handbook on the Toxicology of Metals*, ed. G.F. Nordberg, B.A., Fowler, M. Nordberg, Elsevier, Academic Press, 4th edition, 2015, 281-297.

13 WHO, *Trace Elements in Human Nutrition and Health World Health Organization*, Geneva, 1996, https://www.who.int/nutrition/publications/micronutrients/9241561734/en, (accessed March 2019).

14 P.B. Tchounwou, C.G. Yedjou, A.K. Patlolla, and D.J. Sutton, in *Molecular, clinical and environmental toxicology*, Luch A. (eds), Springer, Basel, Experientia Supplementum 101, 2012, 133-164.

15 C.P.J. Isaac, A. Sivakumar and C.R.P. Kumar, *Bull. Environ. Contam. Toxicol*., 2012, 88, 145-149.

16 A. Oskarsson, I.P. Hallén, J. Sundberg and K.P. Grawé, *Analyst*, 1998, 123, 19-23.

17 M.L. Astolfi, E. Marconi, C. Protano, M. Vitali, E. Schiavi, P. Mastromarino and S. Canepari, *Anal. Chim. Acta*, 2018, 1040, 49-62.

18 C. Protano, S. Canepari, M.L. Astolfi, S. D'Onorio De Meo and M. Vitali, *Sci. Total Environ*., 2018, 619, 58-64.

19 C. Protano, M.L. Astolfi, S. Canepari, R. Andreoli, A. Mutti, F. Valeriani, V. Romano Spica, A. Antonucci, V. Mattei, S. Martellucci and M. Vitali, *Ann. Ig.*, 2017, 29, 494-503.

20 C. Di Dato, D. Gianfrilli, E. Greco, M.L. Astolfi, S. Canepari, A.Lenzi, A.M. Isidori and E. Giannetta, *J. Endocrinol. Invest.*, 2017, 40, 1183-1190.

21 C. Protano, M.L. Astolfi, S. Canepari and M. Vitali, *Sci. Total Environ.*, 2016, 557, 378-385.

22 K. Chojnacka, A. Zielińska, I. Michalak and H. Górecki, *Environ. Toxicol. Pharmacol.*, 2010, 30, 188-194.

23 K. Chojnacka, I. Michalak, A. Zielińska, H. Górecka and H. Górecki, *Ecotoxicol. Environ. Saf.*, 2010, 73, 2022-2028.

24 K. Chojnacka, H. Górecka and H. Górecki, *Environ. Toxicol. Pharmacol.*, 2006, 22, 52-57.

25 K. Chojnacka, H. Górecka and H. Górecki, *Sci. Total Environ.*, 2006, 366, 612-620.

26 E.J. Drobyshev, N.D. Solovyev, N.B. Ivanenko, M.Y. Kombarova and A.A. Ganeev, *J. Trace Elem. Med. Biol.*, 2017, 39, 14-20.

27 H. Skröder, M. Kippler, B. Nermell, F. Tofail, M. Levi, S.M. Rahman, R. Raquib and M. Vahter, *Environ. Health Perspect.*, 2017, 125, 067021-1-067021-9, DOI: 10.1289/EHP1239.

28 T.G. Kazi, N. Jalbani, N. Kazi, M.B. Arain, M K. Jamali, H.I. Afridi, G.A. Kandhro, R.A. Sarfraz, A.Q. Shah and R. Ansari, *Biol. Trace Elem. Res.*, 2009, 127, 16-27.

29 C.R. Robbins in *Chemical Composition of Different Hair Types*, Springer-Verlag, Berlin, Heidelberg, 2012, 105-176.

30 M.N. Rashed and F. Hossam, *Environ. Bioindic.*, 2007, 2, 131-145.

31 R. Pereira, R. Ribeiro and F. Goncalves, *Sci. Total Environ.*, 2004, 327, 81-92.

32 W.I. Mortada, M.A. Sobh, M.M. El-Defrawy and S.E. Farahat, *Environ. Res.*, 2002, 90, 104-110.

33 D. Pozebon, G.L. Scheffler and V.L. Dressler, *Anal. Chim. Acta*, 2017, 992, 1-23.

34 A.V. Skalny, M.G. Skalnaya, A.A. Tinkov, E.P. Serebryansky, V.A. Demidov, Y.N. Lobanova, A.R. Grabeklis, E.S. Berezkina, I.V. Gryazeva, A.A. Skalny, O.A. Skalnaya, N.G. Zhivaev and A.A. Nikonorov, *Environ. Monit. Assess.*, 2015, 187:677, 1-8.

35 A. Taylor, Ann. Clin. Biochem., 1986, 23, 364-378.

36 M. Mikulewicz, K. Chojnacka, T. Gedrange and H. Górecki, *Environ. Toxicol. Pharmacol.*, 2013, 36, 1077-1086.

37 M.I. Szynkowska, A. Pawlaczyk, E. Wojciechowska, S. Sypniewski and T. Paryjczak, *Pol. J. Environ. Stud.*, 2009, 18, 1151-1161.

38 R.R. Eastman, T.P. Jursa, C. Benedetti, R.G. Lucchini and D.R. Smith, *Environ. Sci. Technol*., 2013, 47, 1629-1637.

39 International Atomic Energy Agency, *IAEA tecdoc* 330, Vienna, 1985.

40 J.C. Raposo, P. Navarro, A. Sarmiento, E. Arribas, M. Irazola and R.M. Alonso, *Microchem. J.*, 2014, 116, 125-134.

41 P. Borella, S. Rovesti, E. Caselgrandi, and A. Bargellini, *Microchim. Acta*, 1996, 123, 271-280.

42 M.L. Astolfi, C. Protano, E. Marconi, D. Piamonti, L. Massimi, M. Brunori, M. Vitali and S. Canepari, *Microchem. J.*, 2019, 150, 104186.

43 S. Grassin-Delyle, M. Martin, O. Hamzaoui, E. Lamy, C. Jayle, E. Sage, I. Etting, P. Devillier and J. C. Alvarez, *Talanta*, 2019, 199, 228-237.

44 K. Gellein, S. Lierhagen, P.S. Brevik, M. Teigen, P. Kaur, T. Singh, T.P. Flaten and T. Syversen, *Biol. Trace Elem. Res.*, 2008, 123, 250-260.

45 M.U. Ali, G. Liu, B. Yousaf, H. Ullah, Q. Abbas, M.A.M. Munir and S. Irshad, *Environ. Pollut.*, 2019, 244, 809-817.

46 A.R. Grabeklis, A.V. Skalny, A.A. Skalnaya, I.V. Zhegalova, S.V. Notova, A.L. Mazaletskaya, M.G. Skalnaya and A.A. Tinkov, *Biol. Trace Elem. Res.*, 2019, 188, 230-238.

47 A.A. Tinkov, M. G. Skalnaya, N.V. Simashkova, T.P. Klyushnik, A.A. Skalnaya, G. Bjørklund, S.V. Notova, E.V. Kiyaeva and A.V. Skalny, *Biomed. Pharmacother.*, 2019, 109, 174-180.

48 I. Rodushkin, E. Engström, A. Stenberg and D.C. Baxter, *Anal. Bioanal. Chem*, 2004, 380, 247-257.

49 I. Rodushkin and M.D. Axelsson, Sci. Total Environ., 2000, 262, 21-36.

50 I. Rodushkin and M.D. Axelsson, Sci. Total Environ., 2000, 250, 83-100.

51 J.M. Harrington, D.J. Young, A.S. Essader, S.J. Sumner and K.E. Levine, *Biol. Trace Elem. Res.*, 2014, 160, 132–142.

52 B. Bocca, R. Madeddu, Y. Asara, P. Tolu, J.A. Marchal and G. Forte, *J. Trace Elem. Med. Biol.*, 2011, 25, 19–26.

53 I. Rodushkin and M.D. Axelsson, Sci. Total Environ., 2003, 305, 23-39.

54 A. Alimonti, B. Bocca and F. Ruggieri, *Rapporti ISTISAN 15/30* (in Italian), Istituto Superiore di Sanità, Rome, 2015, 1-47. http://old.iss.it/binary/publ/cont/15_30_web.pdf (accessed September 2018).

55 F. Laborda, J. Medrano and J.R. Castillo, *J. Anal. At. Spectrom.*, 2004, 19, 1434-1441.

56 R.F.S. Salazar, M.B.B. Guerra, E.R. Pereira-Filho and J.A. Nobrega, *Talanta*, 2011, 86, 241-247.

57 S.D. Tanner, V.I. Baranov and D.R. Bandura, *Spectrochim. Acta Part B*, 2002, 57, 1361-1452.

58 T.W. May and R.H. Wiedmeyer, *At. Spectrosc.*, 1998, 19, 150-155.

59 B. Campanella, M. Onor, A. D'Ulivo, R. Giannecchini, M. D'Orazio, R. Petrini and E. Bramanti, *Sci. Total Environ.*, 2016, 548, 33-42.

60 D. Varrica, E. Tamburo, N. Milia, E. Vallascas, V. Cortimiglia, G. De Giudici, G. Dongarrà, E. Sanna, F. Monna and R. Losno, *Environ. Res.*, 2014, 134, 366-374.

61 A. Miklavčič, A. Casetta, J.S. Tratnik, D. Mazej, M. Krsnik, M. Mariuz, K. Sofianou, Z. Spirić, F. Barbone and M. Horvat, *Environ. Res.*, 2013, 120, 7-17.

62 S. Ciardullo, G. Taviani, R. Mattei and S. Caroli, *J. Environ. Monit.*, 2005, 7, 1332-1334.

63 E.I. Muller, J.P. Souza, C.C. Muller, A.L.H. Muller, P.A. Mello and C.A. Bizzi, *Talanta*, 2016, 156-157, 232-238.

64 C.A. Bizzi, M.F. Pedrotti, J.S. Silva, J.S. Barin, J.A. Nóbrega and E.M.M. Flores, *J. Anal. At. Spectrom.*, 2017, 32, 1448-1466.

65 J. Moreda-Piñeiro, E. Alonso-Rodríguez, P. López-Mahía, S. Muniategui-Lorenzo, D. Prada-Rodríguez, A. Moreda-Piñeiro and P. Bermejo-Barrera, *Anal. Bioanal. Chem.*, 2007, 388, 441-449.

66 J.A. Nóbrega, C. Pirola, L.L. Fialho, G. Rota, C.E.K.M.A. de Campos Jordão and F. Pollo, *Talanta*, 2012, 98, 272-276.

67 A.L. Muller, J.S. Oliveira, P.A. Mello, E.I. Muller and E.M. Flores, *Talanta*, 2015, 136, 161-169.

68 M.E. Conti, S. Canepari, M.G. Finoia, G. Mele and M.L. Astolfi, *J. Food Compost. Anal.*, 2018, 74, 102-113.

69 M.L. Astolfi, P. Di Filippo, A. Gentili and S. Canepari, *Talanta*, 2017, 174, 838-844.

70 A. Campopiano, A. Cannizzaro, F. Angelosanto, M.L. Astolfi, D. Ramires, A. Olori, S. Canepari and S. Iavicoli, *Regul. Toxicol. Pharm.*, 2014, 70, 393-406.

71 S. Canepari, F. Padella, M.L. Astolfi, E. Marconi and C. Perrino, *Aerosol Air Qual. Res.*, 2013, 13, 1619-1629.

72 M.I. Szynkowska, M. Marcinek, A. Pawlaczyk and J. Albińska, *Environ. Toxicol. Pharmacol.*, 2015, 40, 402-408.

73 E. Varhan Oral, *J. Turk. Chem. Soc., Sect. A: Chem.*, 2016, 3.3, 367-380.

74 R. Luo, X. Zhuo and D. Ma, *Ecotoxicol. Environ. Saf.*, 2014, 104, 215-219.

75 Y. Li, X. Zhang, L. Yang and H. Li, *Bull. Environ. Contam. Toxicol.*, 2012, 89, 125-128.

76 F. Shah, T.G. Kazi, H.I. Afridi, N. Kazi, J.A. Baig, A.Q. Shah, S. Khan, N.F. Kolachi and S.K. Wadhwa, *Biol. Trace Elem. Res.*, 2011, 141, 131-149.

77 P. Olmedo, A. Pla, A. F. Hernández, O. López-Guarnido, L. Rodrigo and F. Gil, *Anal. Chim. Acta*, 2010, 659, 60-67.

78 S. D'Ilio, F. Petrucci, M. D'Armato, M. Di Gregorio, O. Senofonte and N. Violante, *Anal. Chim. Acta*, 2008, 624, 59-67.

79 UNI CEI EN ISO/IEC 17025, 2005. Milano (Italy): UNI Ente Nazionale Italiano di Unificazione.

80 I. Taverniers, M. De Loose and E. Van Bockstaele, *Trends Analyt. Chem.*, 2004, 23, 535-552.

81 M. Thompson, S.L.R Ellison and R. Wood, *Pure Appl. Chem.*, 2002, 74, 835-855.

82 Commission Decision 2002/657/EC of 12 August 2002 implementing Council Directive 96/23/EC concerning the performance of analytical methods and the interpretation of results, https://eur-lex.europa.eu/legal-content/EN/TXT/PDF/?uri=CELEX:32002D0657&from=EN, (accessed March 2019).

83 Eurachem/Citac Guide CG 4, Quantifying uncertainty in analytical measurement, ed. S.L.R. Ellison (LGC, UK), A. Williams (UK), Third Edition, 2000, https://www.eurachem.org/images/stories/Guides/pdf/QUAM2012_P1.pdf, (accessed September 2018).

84 Bruker, https://www.bruker.com/fileadmin/user_upload/8-PDF-Docs/Separations_MassSpectrometry/Literature/literature/ApplicationNotes/CA-270689_Typical%20Detection%20Limits%20for%20the%20aurora%20M90.pdf (accessed November 2019).

85 L. Brüggemann, W. Quapp and R. Wennrich, *Accred. Qual. Assur*., 2006, 11, 625-631.

86 J. Mandel, *The statistical analysis of experimental data*, John Wiley & Sons, New York, London, Sydney, 1964, 1-410.

87 M. Thompson, S.L.R. Ellison and R. Wood, *Pure Appl. Chem.*, 2006, 78, 145-196.

88 JCGM 100:2008. *Evaluation of measurement data - Guide to the expression of uncertainty in measurement, Joint Committee for Guides in Metrology*, 2008.

https://www.bipm.org/utils/common/documents/jcgm/JCGM_100_2008_E.pdf (accessed May 2019).

89 Z. Hu, S. Hu, S. Gao, Y. Liu and S. Lin, *Spectrochim. Acta B*, 2004, 59, 1463-1470.

90 R.W. Hornung and L D. Reed, Appl. Occup. Environ. Hyg., 1990, 5, 46-51.

91 L.V. Rajaković, D.D. Marković, V.N. Rajaković-Ognjanović and D.Z. Antanasijević, *Talanta*, 2012, 102, 79-87.

92 M.T. Llorente Ballesteros, I. Navarro Serrano and S. Izquierdo Alvarez, *J. Trace Elem. Med. Biol.*, 2016, 43, 113-120.

93 Y. Morishige and A. Kimura, *Industrial Materials, SEI technical review*, 2008, 66, 106-111.

94 E. McCurdy, G. Woods and D. Potter, *Application Metals Analysis*, Agilent Technologies, 2006, 1-8, https://www.agilent.com/cs/library/applications/5989-4905EN.pdf (accessed March 2019)

95 O. Senofonte, N. Violante and S. Caroli, *J. Trace Elem. Med. Biol.*, 2000, 14, 6-13.

96 H. Kumakli, A.V. Duncan, K. McDaniel, T.F. Mehari, J. Stephenson, L. Maple, Z. Crawford, C.L. Macemore, C.M. Babyak and S.O. Fakayode, *Chemosphere*, 2017, 174, 708-715.

97 Y. Li, L. Yang, W. Wang, H. Li, J. Lv and X. Zou, *Sci. Total Environ.*, 2011, 409, 1385-1390.

98 S. Zaichick and V. Zaichick, *Biol. Trace Elem. Res*., 2010, 134, 41-54.

99 M.J. Gonzalez-Muñoz, A. Peña and I. Meseguer, *Food Chem. Toxicol.*, 2008, 46, 3048-3052.

100 US-FDA, Food and Drug Administration. Guidance for industry: a food labelling guide (14. Appendix F: Calculate the percent daily value for the appropriate nutrients) 2013,

http://www.fda.gov/Food/GuidanceRegulation/GuidanceDocumentsRegulatoryInformation/LabelingNutrition/ucm064928.html (accessed January 2019).

101 S.K. Sahoo, S. Mishra, Z.S. Žunić, H. Arae, F. Gjergj, P. Stegnar, L. Benedik, U. Repinc and R. Kritsananuwat, *Int. J. Mass Spectrom.*, 2014, 373, 15-21.

Supplementary Material S1

Table S1. Summary of the characteristics of the hair analytical methods used in the present study and comparison with previous methods.

Reference	Decomposition procedure	Total sample digestion time	Analyte and remarks	LOD[a]	ULOQ or LOQ[b]	Linearity range (log)
This study	20 mg of hair + 0.5 mL HNO3 and 0.25 mL H_2O_2 in open-vessel heated in a water bath to 95 °C (OD*95°C) for 20 min -> volume completed to 10 mL with deionized water	About 40 min for 120 samples (time of digestion, 20 min; and cooling, 20 min)	40 elements; the ICP-MS instrument was operated in CRI mode for As, Ca, Cr, Fe, Mn, Se and V; In, Sc, Rh, Th and Y as internal standards; method validation using hair certified material and in-field hair samples and analyte recovery tests were carried out	0.02 ∝g kg^{-1} (U) to 30 mg kg^{-1} (K)	0.3 mg kg^{-1} (Al, As, Ba, Be, Bi, Cd, Cr, Cs, Cu, Ga, La, Li, Mn, Mo, Nb, Ni, Pb, Rb, Sb, Se, Sn, Te, Ti, Tl, U, V, W and Zr) to 250 mg kg^{-1} (Ca)	1.3 to 2
	200 mg of hair certified material + 1 mL HNO_3 and 0.5 mL H_2O_2 in open-vessel heated in a water bath to 95 °C (OD95°C) for 20 min -> volume completed to 20 mL with deionised water	About 40 min for 120 samples (time of digestion, 20 min; and cooling, 20 min)		0.01 ∝g kg^{-1} (Tl) to 10 mg kg^{-1} (Ca)		
	200 mg of hair certified material + 1 mL HNO_3 and 0.5 mL H_2O_2 in open-vessel at room temperature (ODRT) for 24 h -> volume completed to 20 mL with deionised water	About 24 h for >120 samples (time of digestion, 24 h)		0.02 ∝g kg^{-1} (Be, Tl and U) to 10 mg kg^{-1} (Ca)	0.05 mg kg^{-1} (Al, As, Ba, Be, Bi, Cd, Cr, Cs, Cu, Ga, La, Li, Mn, Mo, Nb, Ni, Pb, Rb, Sb, Se, Sn, Te, Ti, Tl, U, V, W and Zr) to 50 mg kg^{-1} (Ca)	1.2 to 2
	200 mg of hair certified material + 1 mL HNO_3 and 0.5 mL H_2O_2 + 1.5 mL deionised water in closed-vessel heated to 180 °C with microwave energy (CD180°C) for 40 min -> volume completed to 10 mL with deionised water	About 100 min for 20 samples (closing and opening of the 20 quartz vessels, 10 min; time of digestion, 40 min; cooling, 20 min; washing vessels 20 min; and transfer of digests into the polypropylene tubes, 10 min)		0.01 ∝g kg^{-1} (U) to 4 mg kg^{-1} (K)		
	200 mg of hair certified material + 1 mL HCl and 3 mL HNO_3 in closed-vessel	About 75 min for six samples	41 elements using ICP-OES; Y as internal standard	0.01 mg kg^{-1} (Be and Pb) to 300 mg kg^{-1} (S)	0.1 mg kg^{-1} (Be, Cd, La, Mn) to 1000 mg kg^{-1} (C)	0.5 to 2

	heated to 180 °C with microwave energy (CD*180°C) for 40 min -> volume completed to 10 mL with deionised water	(closing and opening of the six PTFE vessels, 5 min; time of digestion, 40 min; cooling, 20 min; washing vessels 5 min; and transfer of digests into the polypropylene tubes, 5 min)				
	200 mg of hair certified material + 1 mL HF, 1 mL HCl and 3 mL HNO_3 in closed-vessel heated to 180 °C with microwave energy (CD**180°C) for 40 min -> volume completed to 10 mL with deionised water	About 75 min for six samples (closing and opening of the six PTFE vessels, 5 min; time of digestion, 40 min; cooling, 20 min; washing vessels 5 min; and transfer of digests into the polypropylene tubes, 5 min)	41 elements using ICP-OES; Y as internal standard	0.02 mg kg^{-1} (Pb) to 300 mg kg^{-1} (S)		
Ballesteros et al.[1]	10 - 20 mg hair + 1 mL Triton X-100 + 1 mL HNO_3 left in contact for 16 h at 80 °C	-	Al, As, Ag, Ba, Bi, Cd, Cr, Co, Cu, Fe, Mn, Mo, Ni, Pb, Se, Sr, Tl and Zn; Ge and Rh as internal standards	0.001 ∝g kg^{-1} (Tl) to 0.9 mg kg^{-1} (Fe)	-	-
Grassin-Delile et al.[2]	10 mg hair + 10 µL internal standard solution (10 µg mL^{-1} gallium and iridium, and 100 µg mL^{-1} In and Sc) + 200 ∝L HNO_3 and 200 µL H_2O_2 in microwave reaction chamber at 1500 W (220 °C) and 110 bar for 25 min -> volume completed to 6 mL with deionised water	-	38 elements; the ICP-SFMS instrument was operated in low-, medium- or high resolution mode, depending on interferences and sensitivity; method validation using commercial reference standards and in-house quality control samples	-	0.0001nM (Hf) to 10 ∝M (Al)	1.3 to 7
Luo et al.[3]	20 mg of hair + 0.8 mL HNO_3 and 0.2 mL H_2O_2 in an electric heating block at 90 °C for 3h -> volume completed to 10 mL with deionised water	-	33 elements; Ge, In, Li, Tb and Y as internal standards; method validation analyzing a certified reference material	0.1 ∝g kg^{-1} (Cs and Th) to 10.9 mg kg^{-1} (Ca)	0.5 ∝g kg^{-1} (Cs, Mo,Th, Tl and U) to 25 mg kg^{-1} (Ca)	2 to 5.3
Raposo et al.[4]	200 mg of hair + 10 mL 5% (v/v) HNO_3 in microwave oven -> volume completed to 50 mL	-	22 elements; Sc, Y, Rh and Ho as internal standards; the spray chamber was cooled (2 °C) to reduce MO^+ formation in the ICP; Ca, K, Mg and Sr determined by ICP OES	0.007 mg kg^{-1} (As) to 1.5 mg kg^{-1} (Ca, Na and K)	-	-
Varrica et al.[5]	150 mg of hair + 3 mL HNO_3 in contact for 24 h at room temperature -> addition	-	21 elements; Re, Sc and Y as internal standards; the ICP-MS instrument was operated in DRC	0.6 ∝g kg^{-1} (Sb) to 0.063 mg kg^{-1} (Fe)	-	-

of 0.5 mL H_2O_2 -> standing for more 24 h -> volume elevated to 25 mL with water	mode for As, Cr, Fe, Se and V; standard addition calibration and analyte recovery tests were carried out

[a] LOD, limit of detection (mg kg^{-1}).
[b] LLOQ or LOQ, lower limit of quantification or limit of quantification (mg kg^{-1}).

Supplementary Material S2

Table S2. Method blanks [n = 10; mean (µg kg^{-1}) and relative standard deviation percent (RSD%)] for each element obtained by inductively coupled plasma mass spectroscopy.

	ODRT[a]		OD95°C[a]		OD*95°C[a]		CD180°C[a]	
Element	mean	RSD%	mean	RSD%	mean	RSD%	mean	RSD%
Al	78	3.8	105	17	852	4.1	145	15
As	3.8	76	3.9	50	15	38	2.0	17
B	72	27	46	38	527	8.0	63	30
Ba	93	29	313	5.8	2049	5.9	239	63
Be	0.11	10	0.14	30	0.68	21	0.13	11
Bi	0.18	39	0.30	31	2.4	31	0.41	31
Ca	44000	36	81000	11	270000	2.8	76000	1.5
Cd	0.20	34	0.27	109	1.8	24	0.35	34
Ce	0.43	26	4.4	30	2.8	18	0.6	16
Co	0.27	18	3.0	74	2.5	10	0.5	42
Cr	10	16	20	46	67	22	13	29
Cs	0.073	42	0.10	42	0.50	46	0.14	28
Cu	42	22	45	26	229	7.9	30	33
Fe	142	32	134	42	884	10	226	28
Ga	0.020	50	0.060	71	0.13	78	0.023	66
K	2600	11	3300	5.4	15000	14	2400	14
La	0.25	23	0.19	60	1.4	15	0.30	29
Li	0.38	25	0.28	39	2.2	20	0.77	29
Mg	1100	23	1000	49	5300	9.1	3500	26
Mn	12	29	10	23	63	23	25	28
Mo	9.1	5.1	4.3	7.0	28	27	3.9	6.4
Na	6200	29	7600	13	43000	20	12000	1.1
Nb	0.42	44	0.15	63	0.90	40	0.14	28
Ni	29	17	35	4.9	150	2.2	30	5.7
P	4600	3.3	4000	4.2	20000	5.8	4500	7.5
Pb	10	15	9.3	3.0	57	9.4	10	24
Rb	1.8	46	1.0	33	8.2	11	1.6	16
Sb	0.53	36	0.35	51	1.8	18	0.69	22
Se	3.1	63	0.29	88	30	33	1.1	73
Si	5800	6.5	5200	4.8	27000	1.6	9500	2.5
Sn	0.45	11	0.48	28	3.6	6.4	0.94	7.5
Sr	71	27	53	28	300	5.6	200	32
Te	0.27	43	0.31	60	1.9	44	0.26	45
Ti	9.1	2.8	12	4.5	70	10	13	7.9
Tl	0.040	50	0.65	21	0.15	33	0.023	65
U	0.037	57	0.21	61	0.23	12	0.057	37
V	0.54	66	0.31	18	10	61	0.48	88
W	2.5	38	1.1	15	9.4	20	1.1	19
Zn	230	20	390	65	2500	5.1	460	9.3
Zr	1.0	14	0.63	3.4	3.9	21	1.0	16

[a] The method blanks were obtained using different acid digestion treatments [room temperature open-vessel digestion (OD_{RT}), open-vessel digestion heated to 95°C ($OD_{95°C}$ or $OD^*_{95°C}$), and closed-vessel microwave-assisted digestion ($CD_{180°C}$)]. Mass of certified material = 0.2 g for all treatments except for OD*95°C (0.02 g).

Supplementary Material S3

Table S3. Method blanks [n = 10; mean and relative standard deviation percentage (RSD%); mg kg^{-1}], background equivalent concentration (BEC; mg kg^{-1}), limit of detection (LOD; mg kg^{-1}), lower and upper limit of quantification (LLOQ and ULOQ; mg kg^{-1}) for each element obtained by inductively coupled plasma-optical emission spectroscopy.

Element	CD*[a]				CD**[a]				CD* and CD**		
	Mean	RSD%	BEC	LOD	Mean	RSD%	BEC	LOD	LLOQ	ULOQ	Linearity range (log)
Al	0.11	12	1	0.4	0.093	6	1	0.2	1	5	0.7
As	1.8	5.4	0.5	0.1	1.8	2.2	0.6	0.04	3	10	0.5
B	4.5	22	14	9	4.1	39	6	7	20	300	1.2
Ba	0.98	21	0.5	0.3	0.95	22	0.5	0.3	1	5	0.7
Be	0.0019	11	0.04	0.01	0.0025	51	0.04	0.07	0.1	5	1.7
Bi	0.15	10	0.5	0.1	0.16	61	0.3	0.5	1	5	0.7
C	760	2.5	500	40	740	3.6	500	50	1000	10000	1.0
Ca	7.8	73	100	200	3.0	108	60	200	250	5000	1.3
Cd	0.0056	28	0.05	0.04	0.0031	18	0.05	0.03	0.1	5	1.7
Ce	0.036	13	0.4	0.2	0.098	22	0.5	0.3	1	25	1.4
Co	0.036	31	0.1	0.1	0.037	38	0.1	0.1	0.3	25	1.9
Cr	0.040	16	0.2	0.1	0.042	27	0.2	0.1	0.3	5	1.2
Cs[b]	-	-	-	-	-	-	-	-	-	-	-
Cu	0.15	16	0.4	0.2	0.18	25	0.5	0.4	1	5	0.7
Fe	0.20	8	0.5	0.1	0.21	22	0.5	0.3	1	50	1.7
Ga	0.19	10	0.9	0.3	0.11	15	1.0	0.4	1	5	0.7
K	0.19	70	100	200	0.23	80	100	200	250	2500	1.0
La	0.020	40	0.05	0.06	0.018	37	0.04	0.04	0.1	5	1.7
Li	0.15	12	0.1	0.05	0.15	15	0.1	0.06	0.5	5	1.0
Mg	1.1	27	7	6	0.95	40	6	8	25	2500	2.0
Mn	0.0037	33	0.05	0.05	0.0075	43	0.05	0.06	0.1	5	1.7
Mo	0.019	62	0.05	0.09	0.018	48	0.09	0.1	0.5	5	1.0
Na	8.1	31	10	10	8.2	35	10	11	25	2500	2.0
Nb	0.15	30	0.6	0.6	0.11	36	0.6	0.7	1	5	0.7
Ni	0.012	40	0.4	0.4	0.014	44	0.3	0.4	0.5	5	1.0
P	0.43	39	13	16	0.20	60	11	20	25	250	1.0
Pb	2.1	1.8	0.2	0.01	2.1	1.1	0.5	0.02	3	10	0.5
Rb	0.85	5.5	3	0.6	1.0	13	4	2	3	10	0.5
S	7.4	56	200	300	7.4	54	200	300	500	10000	1.3
Sb	0.17	34	0.6	0.6	0.29	36	0.7	0.8	1	5	0.7
Se	1.3	4.1	4	1	1.4	9.4	2	1	3	10	0.5
Si	1.9	78	6	20	4.0	76	8	20	25	250	1.0
Sn	0.12	62	0.1	0.2	0.068	42	0.05	0.06	1	5	0.7
Sr	0.036	27	0.2	0.2	0.022	32	0.2	0.2	1	300	2.5
Te	0.46	47	1	1	0.42	44	2	2	3	10	0.5
Ti	0.020	40	0.2	0.2	0.051	30	0.3	0.2	0.3	5	1.2
Tl	0.26	52.8	1	2	0.29	52	2	2	3	10	0.5
U	0.83	8.5	2	1	0.77	6.4	1	0.2	3	10	0.5
V	0.028	29	0.2	0.2	0.012	28	0.1	0.1	0.3	5	1.2
W	0.19	29	2	2	0.19	27	2	2	3	10	0.5
Zn	0.37	20	2	1	0.20	45	2	2	3	50	1.2
Zr	0.12	10	0.2	0.05	0.12	5	0.2	0.03	0.5	5	1.0

[a] The method blanks were obtained using closed-vessel microwave-assisted digestion (CD) with different reagents (CD*: HNO3/HCl; CD**: HNO3/HCl/HF; sample mass 0.2 g).

[b] Cs could not be analysed because axial view ICP-OES is strongly affected by ionisation interference when elements with low ionisation potentials coexist in the sample.

Supplementary Material S4

Table S4. Background equivalent concentration (BEC; mg kg^{-1}), limit of detection (LOD; mg kg^{-1}), lower and upper limit of quantification (LLOQ and ULOQ; mg kg^{-1}) for each element obtained by inductively coupled plasma mass spectroscopy.

Element	BEC	ODRT	OD95°C	CD180°C	All		
		LOD	LOD	LOD	LLOQ	ULOQ	Linearity range (log)
Al	0.1	0.01	0.1	0.1	0.05	2	1.6
As	0.003	0.007	0.004	0.001	0.05	2	1.6
B	1	1	1	1	3	300	2.0
Ba	0.5	0.4	0.1	0.9	0.05	5	2.0
Be	0.0001	0.00002	0.00005	0.00002	0.05	5	2.0
Bi	0.0001	0.0001	0.00005	0.00005	0.05	2	1.6
Ca	30	30	10	1	50	5000	2.0
Cd	0.0000	0.00003	0.0001	0.00003	0.05	2	1.6
Ce	0.0002	0.0002	0.0002	0.0001	0.3	30	2.0
Co	0.001	0.001	0.002	0.001	0.3	10	1.5
Cr	0.002	0.001	0.003	0.002	0.05	5	2.0
Cs	0.0001	0.0001	0.0001	0.0001	0.05	5	2.0
Cu	0.01	0.004	0.01	0.01	0.05	5	2.0
Fe	0.05	0.05	0.06	0.04	0.5	50	2.0
Ga	0.0001	0.0001	0.0001	0.0001	0.05	5	2.0
K	10	3	2	4	30	2500	1.9
La	0.0001	0.0001	0.0002	0.0001	0.05	2	1.6
Li	0.001	0.001	0.001	0.001	0.05	5	2.0
Mg	2	2	4	2	30	2500	1.9
Mn	0.004	0.003	0.003	0.003	0.05	5	2.0
Mo	0.0004	0.0001	0.0001	0.0001	0.05	5	2.0
Na	1	1	1	0.05	30	2500	1.9
Nb	0.00002	0.00003	0.00004	0.00002	0.05	5	2.0
Ni	0.009	0.005	0.001	0.001	0.05	5	2.0
P	4	0.4	1	1	3	50	1.2
Pb	0.004	0.002	0.0003	0.003	0.05	5	2.0
Rb	0.001	0.001	0.001	0.0005	0.05	5	2.0
Sb	0.0003	0.0003	0.0004	0.0002	0.05	5	2.0
Se	0.01	0.02	0.03	0.02	0.05	1	1.3
Si	20	4	3	2	3	250	1.9
Sn	0.0003	0.0001	0.0003	0.0001	0.05	5	2.0
Sr	0.04	0.03	0.03	0.04	3	300	2.0
Te	0.0004	0.0005	0.0006	0.0006	0.05	2	1.6
Ti	0.01	0.001	0.001	0.003	0.05	5	2.0
Tl	0.00001	0.00002	0.00001	0.00002	0.05	2	1.6
U	0.00001	0.00002	0.00002	0.00001	0.05	2	1.6
V	0.0005	0.001	0.0003	0.001	0.05	5	2.0
W	0.0003	0.0003	0.0001	0.0002	0.05	5	2.0
Zn	0.3	0.2	0.5	0.1	0.5	20	1.6
Zr	0.0002	0.0001	0.00002	0.0001	0.05	2	1.6

[a] The method blanks were obtained using different sample treatments [room temperature open-vessel digestion (OD_{RT}), open-vessel digestion heated to 95°C ($OD_{95°C}$), and closed-vessel microwave-assisted digestion ($CD_{180°C}$); sample amount 0.2 g].

Supplementary Material S5

Table S5. Concentrations of the certified material [ERM DB001; n=6; median ± inter quartile range (IQR); mean (m) ± standard deviation (SD)] obtained for each element by inductively coupled plasma-mass spectrometry.

Element	Unit	Informative concentration	Sample treatment[a]								Normal distribution of data[b]	P[c]
			OD_{RT}		$OD_{95°C}$		$OD^*_{95°C}$		$CD_{180°C}$			
			median ± IQR	mean ± SD	median ± IQR	m ± SD	median ± IQR	m ± SD	median ± IQR	m ± SD		
Al	mg kg^{-1}	18.1	14.6 ± 1.1	**14.9 ± 1.1**^{f}	16.9 ± 0.7	16.9 ± 0.7	17.0 ± 0.3	17.0 ± 0.4	18.0 ± 1.0	**18.0 ± 1.0**^{f}	Yes	**0.014**^{f}
B	mg kg^{-1}	3.1	2.87 ± 0.49	3.13 ± 0.54	3.26 ± 0.22	3.26 ± 0.22	2.82 ± 0.12	2.82 ± 0.12	3.33 ± 0.22	3.33 ± 0.22	Yes	N.S.
Ba	mg kg^{-1}	0.90	**0.485 ± 0.019**^{e}	0.498 ± 0.022	0.524 ± 0.001	0.524 ± 0.001	**1.01 ± 0.10**^{e}	1.00 ± 0.10	0.883 ± 0.074	0.929 ± 0.084	No	**0.028**^{e}
Be	∝g kg^{-1}	2.9	2.21 ± 0.04	**2.21 ± 0.04**^{e,f}	2.35 ± 0.01	**2.35 ± 0.01**^{g}	2.77 ± 0.32	**2.84 ± 0.32**^{e,g}	2.71 ± 0.08	**2.70 ± 0.08**^{f}	Yes	**0.010**^{e}, **0.040**^{f}, **0.041**^{g}
Bi	∝g kg^{-1}	9.0	10.1 ± 1.1	10.1 ± 1.1	9.7 ± 1.0	9.7 ± 1.0	10.4 ± 0.5	10.4 ± 0.5	9.78 ± 0.29	9.94 ± 0.32	Yes	N.S.
Ca	mg kg^{-1}	1028	**1039 ± 17**^{d}	1039 ± 17	**946 ± 12**^{d}	946 ± 12	956 ± 4	956 ± 4	973 ± 14	973 ± 14	No	**0.028**^{d}
Ce	∝g kg^{-1}	-	174 ± 6	**178 ± 7**^{e}	180 ± 6	**180 ± 6**^{g}	225 ± 9	**225 ± 9**^{e,g,i}	190 ± 4	**190 ± 4**^{i}	Yes, after ln-trasformation	**<0.001**^{e,,g}, **0.002**^{i}
Co	∝g kg^{-1}	106	94.7 ± 2.4	**94.7 ± 2.4**^{e}	94.1 ± 1.6	**94.1 ± 1.6**^{g}	101 ± 1	**101 ± 1**^{e,g}	96.9 ± 1.2	96.9 ± 1.2	Yes	**0.008**^{e}, **0.005**^{g}
Cr	∝g kg^{-1}	500	191 ± 20	**201 ± 22**^{e,f}	207 ± 18	**215 ± 20**^{g,h}	325 ± 10	**325 ± 10**^{e,g,i}	519 ± 11	**515 ± 12**^{f,h,i}	Yes	**<0.001**^{e,f,g,h,i}
Cs	∝g kg^{-1}	1.2	0.42 ± 0.10	0.48 ± 0.11	0.57 ± 0.02	0.56 ± 0.02	1.23 ± 0.08	1.23 ± 0.08	1.12 ± 0.07	1.17 ± 0.08	No	N.S.
Fe	mg kg^{-1}	22.6	10.6 ± 0.8	**10.5 ± 0.8**^{d,e,f}	12.9 ± 0.2	**12.9 ± 0.2**^{d,g,h}	17.5 ± 0.6	**17.5 ± 0.6**^{e,g}	18.6 ± 0.3	**18.6 ± 0.3**^{f,h}	Yes	**0.005**^{d}, **<0.001**^{e,f,g,h}
Ga	∝g kg^{-1}	-	4.80 ± 0.21	**4.86 ± 0.21**^{e,f}	5.11 ± 0.02	**5.11 ± 0.02**^{g,h}	5.87 ± 0.40	**5.90 ± 0.40**^{e,g}	6.20 ± 0.22	**6.25 ± 0.22**^{f,h}	Yes	**0.006**^{e}, **0.001**^{f}, **0.029**^{g}, **0.003**^{h}
K	mg kg^{-1}	-	<3	<3	3.0 ± 1.2	3.3 ± 1.2	<30	<30	5.53 ± 0.24	5.50 ± 0.24	-	-
La	∝g kg^{-1}	-	94.3 ± 4.0	**95.8 ± 4.2**^{e}	89.9 ± 1.3	**89.9 ± 1.3**^{g}	110 ± 6	**110 ± 6**^{e,g}	101 ± 2	101 ± 2	Yes	**0.010**^{e}, **0.001**^{g}
Li	∝g kg^{-1}	48	12.5 ± 2.0	**13.7 ± 2.2**^{d,e,f}	21.6 ± 1.1	**21.1 ± 1.1**^{d,g,h}	44.9 ± 2.5	**44.8 ± 2.5**^{e,g,i}	34.3 ± 0.9	**34.7 ± 1.0**^{f,h,i}	Yes	**0.007**^{d}, **<0.001**^{e,f,g,h,i}
Mg	mg kg^{-1}	63.5	56.0 ± 3.0	57.4 ± 3.2	55.8 ± 0.3	55.8 ± 0.3	65.0 ± 1.9	64.9 ± 1.9	65.0 ± 1.6	64.1 ± 1.8	No	N.S.
Mn	∝g kg^{-1}	442	452 ± 4	452 ± 4	436 ± 8	436 ± 8	445 ± 25	445 ± 25	479 ± 39	479 ± 39	Yes	N.S.
Mo	∝g kg^{-1}	200	164 ± 40	164 ± 40	180 ± 27	165 ± 30	191 ± 7	188 ± 7	216 ± 6	217 ± 6	Yes	N.S
Na	mg kg^{-1}	-	12.2 ± 1.2	11.9 ± 1.2	10.7 ± 2.6	10.2 ± 2.6	13.2 ± 1.0	13.2 ± 1.0	14.0 ± 2.0	14.7 ± 2.1	Yes	N.S.

Nb	∝g kg^{-1}	-	2.01 ± 0.17	**2.01 ± 0.17^{e,f}**	1.61 ± 0.04	**1.61 ± 0.04^{g,h}**	2.55 ± 0.15	**2.55 ± 0.15^{e,g,i}**	3.22 ± 0.18	**3.19 ± 0.18^{f,h,i}**	Yes	**0.012^{e}, <0.001^{f,g,h}, 0.004^{i}**
Ni	∝g kg^{-1}	780	640 ± 9	640 ± 9	670 ± 6	670 ± 6	821 ± 6	821 ± 6	825 ± 29	828 ± 29	No	N.S.
P	mg kg^{-1}	142.2	127 ± 9	131 ± 9	129 ± 1	129 ± 1	143 ± 6	144 ± 6	141 ± 4	140 ± 4	Yes	N.S.
Rb	∝g kg^{-1}	-	4.17 ± 0.53	**4.44 ± 0.57^{d,e,f}**	6.67 ± 0.12	**6.67 ± 0.13^{d,g,h}**	16.4 ± 2.2	**16.7 ± 2.2^{e,g}**	18.7 ± 0.2	**18.7 ± 0.2^{f,h}**	Yes, after ln-trasformation	**0.003^{d}, <0.001^{e,f,h}**
Sb	∝g kg^{-1}	128	87.7 ± 1.3	**87.7 ± 1.3^{e}**	83.4 ± 6.1	**87.2 ± 6.9^{g}**	112 ± 13	**113 ± 13^{e,g}**	92.0 ± 1.9	91.8 ± 1.9	Yes, after ln-trasformation	**0.017^{e}, 0.014^{g}**
Si	mg kg^{-1}	-	93.6 ± 3.1	93.6 ± 3.1	91.5 ± 0.9	91.5 ± 0.9	**89.8 ± 0.4^{i}**	89.8 ± 0.4	**110 ± 1^{i}**	110 ± 1	No	**0.013^{i}**
Sn	∝g kg^{-1}	440	429 ± 51	430 ± 51	424 ± 11	424 ± 11	410 ± 40	417 ± 41	409 ± 23	423 ± 26	Yes	N.S.
Sr	mg kg^{-1}	-	1.48 ± 0.14	**1.56 ± 0.16^{d,e}**	2.18 ± 0.22	**2.22 ± 0.22^{d}**	2.23 ± 0.06	**2.23 ± 0.06^{e}**	1.88 ± 0.11	1.95 ± 0.12	Yes	**0.004^{d,e}**
Te	∝g kg^{-1}	-	<0.5 -	<0.5 -	<0.6 -	<0.6 -	<2 -	<2 -	<0.6 -	<0.6 -	-	-
Ti	mg kg^{-1}	109	75.4 ± 5.3	**78.3 ± 5.9^{d,e}**	45.3 ± 3.5	**45.3 ± 3.5^{d,g,h}**	160 ± 5	**160 ± 5^{e,g,i}**	87.1 ± 1.9	**86.0 ± 2.2^{h,i}**	Yes, after ln-trasformation	**<0.001^{d,e,g,h,i}**
Tl	∝g kg^{-1}	0.48	0.340 ± 0.035	**0.343 ± 0.035^{e,f}**	0.370 ± 0.025	**0.373 ± 0.025^{h}**	0.450 ± 0.040	**0.443 ± 0.040^{e}**	0.500 ± 0.020	**0.500 ± 0.020^{f,h}**	Yes	**0.026^{e}, 0.002^{f}, 0.007^{h}**
U	∝g kg^{-1}	10.1	8.37 ± 0.40	**8.61 ± 0.46^{e}**	8.72 ± 0.20	**8.72 ± 0.20^{g}**	11.2 ± 0.7	**10.8 ± 0.8^{e,g}**	9.95 ± 0.23	9.83 ± 0.25	Yes	**0.003^{e}, 0.005^{g}**
V	∝g kg^{-1}	49.3	57.0 ± 8.8	57.3 ± 8.8	50.0 ± 2.3	50.0 ± 2.3	49.0 ± 2.5	49.1 ± 2.5	54.6 ± 2.1	54.2 ± 2.1	Yes	N.S.
W	∝g kg^{-1}	15.2	10.6 ± 0.1	10.6 ± 0.1	**10.1 ± 0.2^{g}**	10.0 ± 0.2	**12.2 ± 2.7^{g}**	13.0 ± 2.8	10.4 ± 0.7	10.1 ± 0.7	No	**0.039^{g}**
Zr	∝g kg^{-1}	64	34.1 ± 3.1	**34.5 ± 3.2^{e,f}**	36.7 ± 4.1	**35.8 ± 4.2^{g,h}**	56.8 ± 3.6	**56.8 ± 3.6^{e,g}**	61.8 ± 0.2	**61.9 ± 0.2^{f,h}**	Yes	**<0.001^{e,f,g,h}**

[a] Mass of certified material = 0.2 g for all treatments [room temperature open-vessel digestion (ODRT), open-vessel digestion heated to 95°C (OD95°C), and closed-vessel microwave-assisted digestion (CD180°C)] except for OD*95°C (0.02 g).

[b] According to Kolmogorov-Smirnov test.

[c] The results marked in bold were considered statistically significant for p-values <0.05 (one-way ANOVA test with Bonferroni post-hoc tests for the normally distributed elements and by Kruskal-Wallis test with pairwise post-hoc tests for the not normally distributed elements). Same superscript letters within rows are significantly different: "d" for OD_{RT}-$OD_{95°C}$, "e" for OD_{RT}-$OD^*_{95°C}$, "f" for OD_{RT}-$CD_{180°C}$, "g" for $OD_{95°C}$-$OD^*_{95°C}$, "h" for $OD_{95°C}$-$CD_{180°C}$, "i" for $OD^*_{95°C}$-$CD_{180°C}$. N.S. = not significant.

Supplementary Material S6

Table S6. Concentrations of the certified material [ERM DB001; n=6; mean (m) ± standard deviation (SD)] obtained for each element by inductively coupled plasma-optical emission spectrometry.

Element	Unit	Sample treatment[a]		Normal distribution of data[b]	p[c]
		CD*	CD**		
		m ± SD	m ± SD		
Al	mg kg^{-1}	16.6 ± 0.9	17.6 ± 1.0	Yes	N.S.
B	mg kg^{-1}	<9	<7	-	-
Ba	mg kg^{-1}	1.07 ± 0.12	1.06 ± 0.15	Yes	N.S.
Be	∝g kg^{-1}	<10	<70	-	-
Bi	∝g kg^{-1}	<100	<500	-	-
Ca	mg kg^{-1}	**976 ± 9**[f]	**910 ± 14**[e,f]	Yes	**0.019**[e], **0.022**[f]
Ce	∝g kg^{-1}	<200	<300	-	-
Co	∝g kg^{-1}	116 ± 27	<100	-	-
Cr	∝g kg^{-1}	512 ± 15	519 ± 3	Yes	N.S.
Cs	∝g kg^{-1}	nd	nd	-	-
Fe	mg kg^{-1}	**22.5 ± 0.7**[d]	**21.5 ± 0.7**[e]	Yes	**0.004**[d], **0.013**[e]
Ga	∝g kg^{-1}	<300	<400	-	-
K	mg kg^{-1}	<200	<200	-	-
La	∝g kg^{-1}	102 ± 19	<40	-	-
Li	∝g kg^{-1}	<50	<60	-	-
Mg	mg kg^{-1}	59.3 ± 1.0	56.6 ± 3.0	Yes	N.S.
Mn	∝g kg^{-1}	446 ± 33	450 ± 42	Yes	N.S.
Mo	∝g kg^{-1}	<90	112 ± 42	-	-
Na	mg kg^{-1}	<10	<11	-	-
Nb	∝g kg^{-1}	<600	<700	-	-
Ni	∝g kg^{-1}	839 ± 72	779 ± 40	Yes	N.S.
P	mg kg^{-1}	139 ± 7	136 ± 6	Yes	N.S.
Rb	∝g kg^{-1}	<600	<2000	-	-
Sb	∝g kg^{-1}	<600	<800	-	-
Si	mg kg^{-1}	95.9 ± 5.8	106 ± 13	Yes	N.S.
Sn	∝g kg^{-1}	476 ± 84	373 ± 100	Yes	N.S.
Sr	mg kg^{-1}	2.07 ± 0.01	2.03 ± 0.07	Yes	N.S.
Te	∝g kg^{-1}	<1000	<2000	-	-
Ti	mg kg^{-1}	**110 ± 4**[d]	**107 ± 7**[e]	Yes	**0.010**[d], **0.016**[e]
Tl	∝g kg^{-1}	<2000	<2000	-	-
U	∝g kg^{-1}	<1000	<200	-	-
V	∝g kg^{-1}	<200	<100	-	-
W	∝g kg^{-1}	<2000	<2000	-	-
Zr	∝g kg^{-1}	62.5 ± 7.8	63 ± 20	Yes	N.S.

[a] Mass of certified material = 0.2 g for all the treatments [closed-vessel microwave-assisted digestion (CD180°C) for ICP-MS, and CD* or CD** for ICP-OES].

[b] According to Kolmogorov-Smirnov test

[c] The results marked in bold were considered statistically significant for p-values <0.05 (one-way ANOVA test for the normally distributed elements). Same superscript letters within rows are significantly different: "d" for $CD_{180°C}$-CD*, "e" for $CD_{180°C}$-CD**, and "f" for CD*-CD**. N.S. = Not significant.

[i] Not determined (nd) = Cs could not be analysed because axial view ICP-OES is strongly affected by ionisation interference when elements with low ionisation potentials coexist in the sample.

References

102 M.T. Llorente Ballesteros, I. Navarro Serrano and S. Izquierdo Alvarez, *J. Trace Elem. Med. Biol.*, 2016, 43, 113-120.

103 S. Grassin-Delyle, M. Martin, O. Hamzaoui, E. Lamy, C. Jayle, E. Sage, I. Etting, P. Devillier and J. C. Alvarez, *Talanta*, 2019, 199, 228-237.

104 R. Luo, X. Zhuo and D. Ma, *Ecotoxicol. Environ. Saf.*, 2014, 104, 215-219.

105 J.C. Raposo, P. Navarro, A. Sarmiento, E. Arribas, M. Irazola and R.M. Alonso, *Microchem. J.*, 2014, 116, 125-134.

106 D. Varrica, E. Tamburo, N. Milia, E. Vallascas, V. Cortimiglia, G. De Giudici, G. Dongarrà, E. Sanna, F. Monna and R. Losno, *Environ. Res.*, 2014, 134, 366-374.

2.4.3. (D3) A Prophylactic Multi-Strain Probiotic Treatment to Reduce the Absorption of Toxic Elements: In-Vitro Study and Biomonitoring of Breast Milk and Infant Stools

Environment international (2019), *130*, 104818

Maria Luisa Astolfi [a,*], Carmela Protano [b], Elisa Schiavi [b], Elisabetta Marconi [b], Daniela Capobianco [b], Lorenzo Massimi [a], Martina Ristorini [a], Maria Elisabetta Baldassarre [c], Nicola Laforgia [c], Matteo Vitali [b], Silvia Canepari [a], Paola Mastromarino [b]

[a] Department of Chemistry, Sapienza University, Piazzale Aldo Moro 5, 00185 Rome, Italy;
[b] Department of Public Health and Infectious Diseases, Sapienza University, Piazzale Aldo Moro 5, 00185 Rome, Italy;
[c] Department of Biomedical Science and Human Oncology, Section of Neonatology and Neonatal Intensive Care Unit, University "Aldo Moro" of Bari, Piazza Giulio Cesare 11, 70124 Bari, Italy.

Abstract: Potential exposure to toxic elements initially occurs during gestation and after birth via breast milk, which is the principal source of nutrients for infants during the first months of life. In this study, we evaluated whether maternal oral supplementation with a multi-strain probiotic product can protect infants from exposure to arsenic (As), cadmium (Cd), mercury (Hg), and lead (Pb) via breast milk. *In-vitro* studies of the bacterial strains present in this probiotic product showed a high bacterial tolerance for As, Cd, Hg, and Pb, and good binding capacity for Cd, Hg, and Pb (72%, 81%, and 64%, respectively) within 1 hour of contact. We evaluated concentrations (5 mg L^{-1} for Cd and Pb, and 2 mg L^{-1} for Hg) that largely exceeded the provisional tolerable weekly intake of these toxic elements via food or water applicable for human consumption. Changes in the levels of these elements in breast milk and newborn stools were evaluated in the control (orally supplemented with placebo) and experimental (orally supplemented with probiotic) groups at birth (t0), 15 days (t15), and 30 days after delivery (t30). Elemental analysis of breast milk did not show significant differences between the control and experimental groups at different stages of lactation; however, stool samples obtained from newborns of mothers supplemented with the probiotic product showed that Cd levels were significantly reduced (by 26%) at t15 compared with the levels of the controls. Our data did not show an association between concentration of toxic elements in breast milk and that in newborn stools.

Indeed, the concentration of Cd, Hg, and Pb in breast milk decreased during the lactation period, whereas the levels of these elements in newborn stools were stable over time. Although our *in-vitro* data indicate that the consortium of these probiotic strains can absorb toxic compounds, this study was limited by its small sample size and potential uncontrolled confounding effects, such as maternal diet and lifestyle. Therefore, we could not confirm whether prophylactic use of this probiotic product can reduce the absorption of toxic elements. The risk assessment in the studied population evidenced a margin of exposure (MOE) of 1, or between 1 and 10 for Pb, and lower than 50 for As. This poses a potential risk for breastfed infants, indicating that interventions aimed to avoid breastfeeding-related health risks remain a major challenge in public health.

Keywords: breast milk; meconium; probiotic; biomonitoring; toxic element; risk assessment.

1. Introduction

Chemical elements are naturally present in the environment, where their distribution is determined by biogeochemical cycles. Industrial, domestic, agricultural, medical, and technological applications increase the levels of these elements above those occurring naturally, resulting in contaminated water, air, soil, crops, and animals (WHO, 2004; Astolfi et al., 2006a, 2006b; ATSDR, 2007a, 2007b; EFSA, 2009a; Marconi et al., 2011; Kim et al., 2016; Astolfi et al., 2017; Ha et al., 2017; Canepari et al., 2018; Manigrasso et al., 2019). Indeed, toxic elements are present in foods such as vegetables (Noli and Tsamos, 2016; Shaheen et al., 2016; Li et al., 2017), fish (Miklavčič et al., 2013; Saha et al., 2016; Gu et al., 2017; Makedonski et al., 2017), dairy products (Suturović et al., 2014; Shahbazi et al., 2016), cereals (Cuadrado et al., 2000; Akinyele and Shokunbi, 2015), and water (Chowdhury et al., 2016). Therefore, the food chain is a major source of exposure to toxic elements for the general population (Morel et al., 1998; Kachenko and Singh, 2006; Sharma et al., 2007; Bensefa-Colas et al., 2011; JECFA, 2011; Arnich et al., 2012; Miklavčič et al., 2013).

Toxic elements can cross the mammary glands and enter breast milk (Gundacker et al., 2010; Al-Saleh et al., 2011; Vacchina et al., 2017), which is the most important source of nutrients during the first months of life (Solomon et al., 2002; LaKind et al., 2004; Kunter et al., 2017; Lehmann et al., 2018). Breast milk can be a pathway for maternal excretion of toxic elements and a potential source of exposure for infants (LaKind et al., 2004; EPA, 2011; Ljung Björklund et al., 2012; Ettinger et al., 2014; Rebelo and Caldas 2016). This is concerning, because infants are particularly sensitive to toxic effects due to their rapid growth, organ immaturity, and vulnerability of the nervous system during the first year of life (Isaac et al., 2012). In addition, newborns absorb metals more readily than do

adults, and have a lower capacity to excrete compounds in bile, thereby decreasing body clearance (Oskarsson et al., 1998; Rebelo and Caldas, 2016). Thus, even relatively low levels of toxic elements in breast milk can represent a risk for infant health (Rebelo and Caldas, 2016). Arsenic (As), lead (Pb), mercury (Hg), and cadmium (Cd) rank 1st, 2nd, 3rd, and 7th, respectively, on the U.S.A. National Priorities List (NPL) of the Agency for Toxic Substances and Disease Registry (ATSDR, 2015). Compounds containing inorganic As (IAs) and Cd, and inorganic Pb, are classified as carcinogens (Group I) and as probable carcinogens (Group IIA) in humans, respectively, by the International Agency for Research in Cancer (IARC, 2016). Mercury, in the form of methylmercury (MeHg) or inorganic (IHg) mercury, is classified by IARC (2016) as probable carcinogen in humans (Group IIB) or not classifiable as to its carcinogenicity (Group III), respectively. MeHg and IHg are teratogenic and neurotoxic, especially in the developing brain (WHO, 1991, 2010; NRC, 2000; JECFA, 2004; Clarkson and Magos, 2006; Ceccatelli et al., 2010). All these elements can exert serious effects on the health of children, affecting numerous systems and organs (Al-Saleh et al., 2011, 2016; Shrader-Frechette et al., 2012; Valent et al., 2013; Yurdakök, 2015; Rebelo and Caldas, 2016; Kunter et al., 2017). However, the health effects related to the intake of these elements via human milk have not been extensively studied.

Assessing the levels of toxic chemicals in breast milk provides information on the maternal toxic load, and serves as an indicator for prenatal and post-natal exposure of infants to these chemicals (Solomon et al., 2002; Almeida et al., 2008; Al-Saleh et al., 2011; Ettinger et al., 2014; De Felip et al., 2014; Yurdakök, 2015; Dursun et al., 2016). The composition of breast milk varies over time (Emmett and Rogers, 1997; Ballard and Morrow, 2013). Consequently, the concentrations of essential or toxic elements may change during lactation (Krachler et al., 1998; Almeida et al., 2008). The transport of toxic elements into breast milk occurs via the same pathways as those used for other milk components and essential trace elements (Oskarsson et al.,1998; Rebelo and Caldas, 2016). However, differences in the metabolism of essential trace elements and toxic pollutants can cause specific changes in the level of each element. Moreover, the composition of human milk is not constant and depends on the nutritional status and diet of the mother, as well as her stage of lactation, socio-demographic status, and lifestyle (García-Esquinas et al., 2011; Ballard and Morrow, 2013; Vieira et al., 2013; Grzunov Letinić et al., 2016). Breast milk, which can be obtained non-invasively, is a suitable biological matrix for biomonitoring exposure to environmental pollution and related risks to human health (Esteban and Castaño, 2009; Björklund et al., 2012, Yurdakök, 2015; Grzunov Letinić et al., 2016). Breast milk is also suitable for evaluating the effectiveness of preventive measures (Fürst et al., 1994; Norén et al., 2000). Urine, stool, saliva, nails, and hair can also be

obtained non-invasively and are used for biomonitoring exposure to toxic elements (Claeys-Thoreau et al., 1987; Kikuchi et al., 2003; Esteban and Castaño, 2009; Protano et al., 2016; Protano et al., 2017; Protano et al., 2018). Risk management is meant to reduce life-long exposure because toxic elements are accumulated long before pregnancy, and are released during gestation and lactation, posing a health risk to the offspring (Yurdakök, 2015).

The use of beneficial bacteria represents a potential preventive strategy. Recent studies have shown that some strains present in human microbiota, and some strains of probiotic lactobacilli, can reduce pesticide absorption in humans and wildlife (Trinder et al., 2015), and elemental toxicity in humans (Bisanz et al., 2014) and animals (Salim et al., 2011; Breton et al., 2013). Indeed, different species of lactic acid bacteria can adsorb heavy metals on their cell-wall surfaces (biosorption) or accumulate them inside the cell (bioaccumulation) (Bhakta et al., 2012; Daisley et al., 2018; Kinoshita, 2019). This has prompted the use of these organisms in biotechnology (Halttunen et al. 2007; Mrvčić et al., 2012), novel detoxification therapies (Brudnak, 2002; Urban and Kuthan, 2004; Zhai et al. 2013), and dietary strategies (Gerbino et al., 2014).

In this study, we evaluated the effects of prophylactic treatment with a multi-strain probiotic product on the concentrations of toxic elements in breast milk and newborn stools at different time points during lactation. For this, we used a sensitive analytical method to determine the total levels of As, Cd, Hg (estimated as MeHg), and Pb. *In-vitro* studies were conducted to verify tolerance and binding ability of these bacterial strains for As, Cd, Hg, and Pb. Additionally, we assessed the risk of toxic element intake via breastfeeding.

2. Materials and Methods

2.1. In-vitro Study: Design, Participants and Specimen Collection

This study included 29 women who were recruited in a previous study (Mastromarino et al., 2015; ClinicalTrials.gov Identifier: NCT01367470). The present study was randomized, double blind, placebo-controlled, and designed to examine the health-promoting effects of supplementation with a probiotic product during pregnancy and first month of breast-feeding. The probiotic mixture used for supplementation contained *Lactobacillus* (*L.) paracasei* DSM 24733, *L. plantarum* DSM 24730, *L. acidophilus* DSM 24735, *L. delbrueckii* subsp. *bulgaricus* DSM 24734, three strains of bifidobacteria (*B. longum* DSM 24736, *B. breve* DSM 24732, and *B. infantis* DSM 24737), and one strain of *Streptococcus thermophilus* DSM 24731. This product is produced by Danisco-Dupont, WI, USA and is currently sold in Continental Europe and USA under the brand Vivomixx® and Visbiome®, respectively. In Korea, this product is commercialized under the brand name De Simone Formulation.

This probiotic product was packaged in bags containing 9×10^{11} viable lyophilized bacteria. Mothers were recruited between April 2011 and December 2013 from the Department of Medical Science and Oncology, Section of Gynaecology and Obstetrics, Policlinico Hospital, University of Bari. One bag of probiotic or placebo (corn starch) was consumed daily before a meal starting at the 36th week of pregnancy and stopping at 4 weeks after delivery. A nutritionist provided dietary guidelines to each mother according to the anthropometric values collected, and in accordance with the current recommendations for diet during pregnancy set by the Italian Ministry of Health (2011).

The control group included 13 mothers and 13 infants, and the treated group included 16 mothers and 18 infants. Infants received nutrition by breastfeeding exclusively during the study period. Breast milk (87 samples) and newborn stools (90 samples) were collected into sterile polypropylene tubes on day 1, 15, and 30. Samples of colostrum and meconium were collected on day 1. Milk was collected using a manual breast-pump after the nipple and areola were cleaned by wiping with a swab soaked in sterile water. During transport to the hospital, the collected samples were maintained at a temperature of ~4°C in a portable thermal refrigerator. The samples were then stored at −80°C until further analyses.

2.2. In-vitro Study

2.2.1. Bacterial Strains

For each assay, the lyophilized probiotic was resuspended in distilled sterile water (EuroClone S.p.A., MI, Italy), or in de Man, Rogosa and Sharpe (MRS) broth (CM0359; Oxoid S.p.A., MI, Italy) containing 0.05% w/v L-cysteine hydrochloride (≥ 98%; Sigma-Aldrich, St. Louis, MO, USA) and allowed to equilibrate under anaerobic conditions for 5 h at 37°C. The cell suspension was centrifuged (ALC International, Cologno Monzese, MI, Italy) at 2500 *g* for 10 min, and the pellet was resuspended in MRS broth to achieve a final concentration of 5×10^8 or 5×10^{10} bacterial cells mL^{-1}. The bacteria were incubated at 37°C using a thermostatic shaking incubator for 1 h in distilled sterile water, or for 1 and 24 h in MRS broth supplemented with 0.05% w/v L-cysteine hydrochloride under anaerobic conditions. This was performed to evaluate bacterial tolerance and capacity for element binding, as described in section 2.2.2.

2.2.2. Tolerance and Element-binding Assays

Bacterial tolerance was assessed to determine the maximal concentration of each metal not affecting bacterial viability, and to evaluate the capacity of the probiotic strains to bind nontoxic concentrations of As, Cd, Hg, and Pb. For this, a 600-L inoculum of probiotic strains (10^{11} bacteria mL^{-1}) was

resuspended in culture medium, placed into 24-well polystyrene microplates (Corning Life Sciences, Tewksbury, MA, USA), and treated with an equal volume of: 0 to 2 mg L^{-1} Hg, or 0 to 5 mg L^{-1} As, Cd, or Pb, for 1 h; or with 0 to 10 mg L^{-1} Hg, or 0 to 50 mg L^{-1} As, Cd, or Pb, for 24 h.. High elemental concentrations, exceeding those outlined in regulatory guidelines [Commission Regulation (EC) No 1881/2006; Council Directive 98/83/EC], were used to assess the effects of these bacterial strains under severe conditions. In our single-element bacterial tolerance assays, we used a range of concentrations to examine the resistance and maintenance of binding capacity in these bacterial strains under unfavourable conditions; similar assessments have been conducted in several previous studies (Halttunen et al., 2007; Kinoshita 2019; Kinoshita et al., 2013; Mrvčić et al., 2012; Rial et al., 2011).

Dilutions of standard stock solutions of 1002 ± 7 mg L^{-1} Hg (SCP Science, Baie D'Urfeé, Canada) and 1.000 ± 0.005 mg L^{-1} As, Cd, or Pb (Ultra Scientific/Agilent Technologies, North Kingstown, RI, USA) were freshly prepared prior to use in culture using deionized water (resistivity ≤ 18.3 MΩ cm; generated by an Arioso Power I RO-UP Scholar UV deionizer, Human Corporation, Songpa-Ku, Seoul, South Korea). The initial culture pH was ~5 or 6 for water and MRS broth, respectively. After culturing, viable microorganisms were identified by plating serial 10-fold dilutions of each sample onto MRS-agar plates. All assays were performed in triplicate. Colony counts were conducted after a 48-h incubation at 37°C under anaerobic conditions. To evaluate element binding, culture samples were centrifuged at 9400 g for 15 min (Eppendorf s.r.l., MI, Italy), separated into supernatant and pellet, and stored -20°C until chemical analysis (described in section 2.3). The original standard solution containing C_0 mg L^{-1} of each element served as control concentration. Element uptake (U) was expressed as a percentage and calculated using the following equation:

$$U\% = (C_0 - C_1) / C_0 * 100$$

where C_0 and C_l (mg L^{-1}) are element concentrations prior to, and post, adsorption, respectively.

2.3. Analysis

2.3.1. Determination of Total As, Cd and Pb Levels

Samples of breast milk (500 L), stool (~100 mg), and pellets and supernatants (1 mL) of bacterial cells used in the binding experiments were transferred into 2.5-, 5-, and 10-mL graduated polypropylene tubes (Artiglass s.r.l., Due Carrare, PD, Italy) and subjected to acid digestion in an open vessel heated in a water bath at 80°C (WBD;) as described previously (Di Dato et al., 2017; Astolfi et al., 2018). We used 1 mL 67% HNO_3 and 0.5 mL 30% H_2O_2 high-purity solvents (Promochem, LGC Standards GmbH, Wesel, Germany) for trace analysis of breast milk and probiotic

culture samples; for analysis of stool samples, the volumes of these reagents were reduced by half. The solutions were diluted with deionized water to a final volume of 10 mL. Then, the solutions were filtered through a pre-cleaned syringe filter (cellulose nitrate membranes, 0.45-µm pore size; GVS Filter Technology, Indianapolis, IN, USA), ensuring to discard the first 2.5 mL of the solution needed to pre-flush the filter, and collecting ~7.5 mL of the remaining solution into a new tube. All the filters were pre-washed with 30 mL of 2% HNO_3 to reduce blank values. Breast milk samples were diluted at 1:2, and probiotic culture samples were diluted at 1:2, 1:10, 1:20, or 1:100, using deionized water; stool samples were analysed without any further dilution. Ten blank solutions, consisting of deionized water and reagents (H_2O_2 and HNO_3), were treated concurrently with each digestion of the sample set; this was done to subtract the background signal due to unreacted reagents, and to control for contributions from possible sample contaminants. A quadrupole inductively coupled plasma mass spectrometer (ICP-MS, model 820-MS; Bruker, Bremen, Germany), equipped with a collision-reaction interface (CRI) and glass nebulizer (0.4 mL min^{-1}; Analytik Jena AG, Jena, Germany), was used to determine total levels of ^{75}As-, ^{112}Cd-, and ^{208}Pb. The typical spectral interferences in ^{75}As were reduced by using a CRI with 30 mL min^{-1} He and 70 mL min^{-1} H_2 (99.9995% purity; SOL Spa, Monza, Italy) as cell gases to the sampler and skimmer cones, respectively. Further details on instrumental conditions and method parameters can be found in Astolfi et al. (2018) and Conti et al. (2019). Six-point matrix-matched external standard calibration was performed in the 0.5–50 g L^{-1} range for all elements by serially diluting a multi-standard stock solution of 1.000 ± 0.005 mg L^{-1} of As, Cd, and Pb. To control for nebulizer efficiency, 5 g L^{-1} yttrium (Y) was prepared using a standard stock solution (1000 ± 2 mg L^{-1}; Panreac Química, Barcelona, Spain) and used as internal standard for all the measurements. Y was successfully used as internal standard in our previous works (Campopiano et al., 2014; Astolfi et al., 2018; Conti et al., 2019). ICP-MS was tuned daily using 1% HNO_3 and 5 g L^{-1} Ba, Be, Ce, Co, In, Pb, Mg, Tl, and Th prepared from a multi-standard stock solution (10.00 ± 0.05 mg L^{-1}; SpectroPure, Ricca Chemical Company, Arlington, TX, USA) to ensure optimal instrument performance.

The limits of detection (LODs) and limits of quantification (LOQs) were set at 3 and 10 times the standard deviation (SD) of 10 replicate blank determinations, respectively. The values of blanks, subjected to similar sample preparation and analytical procedures, were deducted from all measurements. For breast milk and infant stools, the LOD and LOQ values, respectively, were as follows: 1 and 2 g kg^{-1} for As, 0.1 and 0.2 g kg^{-1} for Cd, and 2 and 4 g kg^{-1} for Pb in breast milk (Astolfi et al., 2018); 10 and 40 g kg^{-1} for As, 0.2 and 0.8 g kg^{-1} for Cd, and 10 and 30 g kg^{-1} for Pb in infant stools. The values for supernatants and pellets of bacterial cells were as follows: 0.1–152 g

L^{-1} and 0.3–507 g L^{-1} for As, 0.1–9 g L^{-1} and 0.3–28 g L^{-1} for Cd, and 1–17 g L^{-1} and 3–58 g L^{-1} for Pb in supernatants; 0.003–0.04 g $(5 \times 10^{10}$ bacterial cells$)^{-1}$ and 0.009–0.1 g $(5 \times 10^{10}$ bacterial cells$)^{-1}$ for As, 0.0004–0.006 g $(5 \times 10^{10}$ bacterial cells$)^{-1}$ and 0.001–0.02 g $(5 \times 10^{10}$ bacterial cells$)^{-1}$ for Cd, and 0.0004–0.005 g $(5 \times 10^{10}$ bacterial cells$)^{-1}$ and 0.001–0.02 g $(5 \times 10^{10}$ bacterial cells$)^{-1}$ for Pb in pellets.

Standard reference materials [SRM 1954 Organic Contaminants in Fortified Human Milk, National Institute of Standards and Technology (NIST), Gaithersburg, MD, USA) were used to validate our method for breast milk analysis, which was used as reported previously (Astolfi et al., 2018). This method provides satisfactory detection limits and good performance (recovery percentages 89–96%, coefficient of variation <6%, and relative repeatability <14%) for determination of As, Cd, and Pb levels in breast milk. Due to the lack of certified reference materials for trace elements, the accuracy of the results obtained for stool, supernatant, and pellet samples was assessed by evaluating percent recovery (R%) using samples of the same matrix fortified with multi-standard solution. These fortified samples contained all the elements at concentrations 20 times higher than those in the third calibration standard (2 g L^{-1} As, Cd, and Pb). These fortified samples were also subjected to the same WBD treatment as the unfortified samples. R% was calculated using the same equation as that used for determination of U (section 2.2.2.), but in this case, C_0 denotes the concentration of elements in the spiked samples, and C_1 denotes the concentration of elements in native samples. The resultant values were in good agreement with the spiked values (As: 100 ± 3%, Cd: 105 ± 7%, and Pb: 98 ± 4% in infant stool; As: 104 ± 5% and 107 ± 6%, Cd: 102 ± 4% and 100 ± 3%, and Pb: 105 ± 7% and 102 ± 6% in supernatants and pellets, respectively).

2.3.2. Determination of Total Hg Levels

Total Hg determination was carried out via Advanced Mercury Analyzer (AMA-254, Altec Ltd., Prague, Czech Republic), which can be used to analyse a liquid or solid sample directly, without any sample preparation. Moreover, analysis by AMA-254 is rapid and less prone to contamination than that using other similar instruments. Briefly, each sample was dried and then thermally decomposed. The generated gaseous decomposition products were carried in an oxygen stream (99.995% purity; SOL Spa) through the catalytic section of the furnace filled with a catalyst and maintained at constant temperature of approximately 750°C. The vapours of Hg(0) were then selectively trapped on a gold-based amalgamator that was rapidly heated to release the mercury vapours. Mercury was detected using a single-wavelength atomic absorption spectrophotometer at 253.65 nm. The seven-point matrix-matched external standard calibration was performed by serially diluting a standard stock

solution in 1% HNO_3 v/v to obtain solutions in the concentration range of 0.1–2 g L^{-1} or 1–40 g L^{-1}; these solutions were then used for the analysis of breast milk or stool samples, and supernatant or pellet samples obtained from *in-vitro* cultures, respectively. Deionized water was used for serial dilutions.

Breast milk and stool samples were thawed at 19 to 21°C and immediately analyzed using AMA-254. The supernatants and pellets from the binding experiments were thawed at 19 to 21°C, digested using WBD (described in section 2.3.1), filtered (cellulose nitrate membranes, 0.45-µm pore size; GVS Filter Technology, Indianapolis, IN, USA), and diluted with deionized water at 1:2 or 1:10, respectively. The drying and decomposition temperatures were set at 120 and 750°C, respectively. Drying, decomposition, and waiting times were set for 100 L (two repeats) of breast milk and 30 mg (one repeat) of stools at 70 s, 120 s, and 45 s; 100-L (one repeat) of each supernatant or pellet was digested at 30 s, 100 s, and 30 s. Under these conditions, the Hg recovery level for all the spiked samples ranged from 96 to 109%, the coefficient of variation was <10%, and relative repeatability was <13%. These values are considered acceptable by other studies (Vacchina et al., 2017). R% was calculated using the same equation as that used to determine U% (section 2.2.1.), but in this case, C_0 denotes the concentration of elements in the spiked samples, and C_1 denotes the concentration of elements in native samples. Internal quality controls (e.g., reagent blanks to monitor possible cross-contamination or memory effects) were included in the analysis of total Hg content as described previously (Vacchina et al., 2017). The LODs and LOQs, calculated as 3 and 10 times the SD of blank determination (10 replicates), respectively, were 0.02 µg L^{-1} and 0.1 µg L^{-1} in breast milk, 0.7 µg kg^{-1} and 2 µg kg^{-1} in infant stools, 4 µg L^{-1} and 15 µg L^{-1} in supernatants, and 0.02 µg $(5 \times 10^{10}$ bacterial cells$)^{-1}$ and 0.06 µg $(5 \times 10^{10}$ bacterial cells$)^{-1}$ in pellets, respectively. The LOQs, obtained for total Hg in breast milk, were in the same range as previously found in studies using AMA (Ursinyova and Masanova, 2005; Vacchina et al., 2017).

2.4. Assessment of Risk Posed to Infants by Breast Milk

The health-based guidance values for Cd, Hg, and MeHg are provided as provisional tolerable weekly intake (PTWI) at 2.5g kg^{-1} body weight (BW)/week (EFSA, 2012a), 4g kg^{-1} BW/week (JECFA, 2011a), and 1.6 g kg^{-1} BW/week (JECFA, 2004). The values for As and Pb are provided as benchmark dose lower bound (BMDL), which uses a lower confidence level at 3.0 g kg^{-1} BW/day and 21.0 g kg^{-1} BW/week (JECFA, 2011a), and at 0.5 g kg^{-1} BW/day and 3.5 g kg^{-1} BW/week (developmental toxicity in children; EFSA, 2010), respectively. In our study, the risks of exposure to Cd, Hg, and MeHg through breast milk were assessed by comparing element intake with PTWI and expressing it

as a percentage, as shown in equation 1. Risk may exist when the percentage is higher than 100. For As and Pb, risk is assessed by estimating the margin of exposure (MOE). MOE is defined as a reference point derived from the dose-response relationship, and can be calculated by dividing BMDL by estimated element intake, as shown in equation 2 (Rebelo and Caldas, 2016). In order to not to represent a public health concern, an MOE should be as high as possible (≥ 50 for As, based on $BMDL_{0.5}$, and ≥ 10 for Pb, based on $BMDL_1$) (EFSA, 2005, 2010, 2014). It is important to emphasize, however, that MOE is not a quantification of risk for exposure to a chemical; MOE is only an indication of the level of concern (Benford, 2016; Rebelo and Caldas, 2016). For exposure assessment, the daily or weekly intakes (μg kg^{-1} BW/day or μg kg^{-1} BW/week) of As, Cd, Hg, MeHg, and Pb were calculated for each breast-milk sample, obtained at different stages of lactation, and for each child, according to equation 3. MeHg was not measured, but was considered to represent 50% of the total Hg (THg) present in accordance with Rebelo and Caldas (2016). The following equations were used:

$$\%PTWI = \text{weekly intake} \times 100/PTWI \quad (1)$$

$$MOE = \text{weekly BMDL/weekly intake} \quad (2)$$

$$\text{Intake} = \text{milk consumption} \times [\text{toxic element}]/\text{BW of infant} \quad (3)$$

where “milk consumption” is the average amount of breast milk (L) consumed per infant per day or week; toxic element is the mean concentration of As, Cd, Hg (MeHg), and Pb (g L^{-1}) detected in the collected breast milk samples; and “BW” is the body weight (kg) of the infant. The average daily consumption of breast milk by nursing infants was 143 mL/kg-day (1.00 L/kg-week) at 0 to 7 days after birth (t0), 156 mL/kg-day (1.90 L/kg-week) at 2 weeks after birth (t15), and 150 mL/kg-day (1.05 L/kg-week) at 4 weeks after birth (t30) as reported in Tables 15-16 of the U.S. Environmental Protection Agency (EPA, 2011). The body weight at t0 lactation stage corresponds to the body weight at birth (3.10 ± 0.71 kg for the control groups and 3.34 ± 0.49 kg for the group treated with probiotic). For the other lactation stages (t15 and t30), body weight was calculated separately for boys and girls (9 boys and 9 girls in the control group, and 10 boys and 3 girls in the experimental group) using Tables 38 and 49 provided by the World Health Organization (WHO, 2006).

2.5. Statistical Analysis

Statistical analyses of element concentrations recovered from breast milk and infant stools were performed using IBM-SPSS Statistics for Windows (version 25.0, released 2017; IBM Corp., Armonk, NY, USA). Values below the LOD were designated as half the LOD value, as recommended for small datasets (Clarke, 1998; Hewett and Ganser, 2007). First, we calculated the percentage of values under the LOD for each monitored element. When the percentage under the LOD was ≥ 30%, the element was excluded from statistical analysis. For the other elements, a descriptive statistical evaluation was carried out by calculating the most important descriptors such as arithmetic mean, median, minimum and maximum level, and 25–75th percentile. Prior to other analyses, the normality of distribution of each elemental concentration was evaluated via Kolmogorov-Smirnov test. In all cases, the distribution was normal after natural logarithmic data transformation. Thus, univariate analyses were conducted using parametric techniques on ln-transformed values (*t*-test for independent samples or ANOVA with Bonferroni post-hoc tests). The results were considered statistically significant at p-values <0.05. A *t*-test was used to compare differences in the level of each element between control and experimental groups, while ANOVA was used to evaluate differences in the concentrations of each element recovered at each stage of lactation (t0, t15, t30). Kendall's tau coefficients, at a significance level of 0.05, were used for correlation analysis of elemental levels per each stage of lactation.

3. Results and Discussion

3.1. In-vitro Study

3.1.1. Tolerance Assessment

Because of the composition of microbial cell walls, microbial cells are natural adsorbents of metal ions (Blackwell et al., 1995). Various studies have shown that certain microorganisms can adsorb, tolerate, and/or bioaccumulate toxic elements, thereby preventing adverse effects on human health (Mrvčić et al., 2012; Gerbino et al., 2014). The bacterial strains evaluated in our study were able to tolerate and survive at up to 5 mg L^{-1} As, Cd, and Pb, and at up to 2 mg L^{-1} Hg, for 24 h in MRS broth (C_1 concentration, Fig. 1). Dose-dependent toxic activity was observed at higher concentrations of metal ions. At a concentration of 10 mg L^{-1} (C_2 concentration, Fig. 1), Cd reduced bacterial viability by 55%. However, at the highest concentration of 50 mg L^{-1} (C_3 concentration, Fig. 1), the other elements exhibited low toxicity; bacterial viability was inhibited by 29, 25, and 20% by As, Hg, and Pb, respectively. Bacteria exposed to 5 mg L^{-1} As, Cd, and Pb, and 2 mg L^{-1} Hg, in water and broth showed no inhibition of tolerance at 1 h post-exposure. These results agree with those obtained in a

study examining 53 different lactic-acid bacteria, in which 11 strains showed high tolerance and ability to bind Cd and Pb from water and MRS (De Boever et al., 2000).

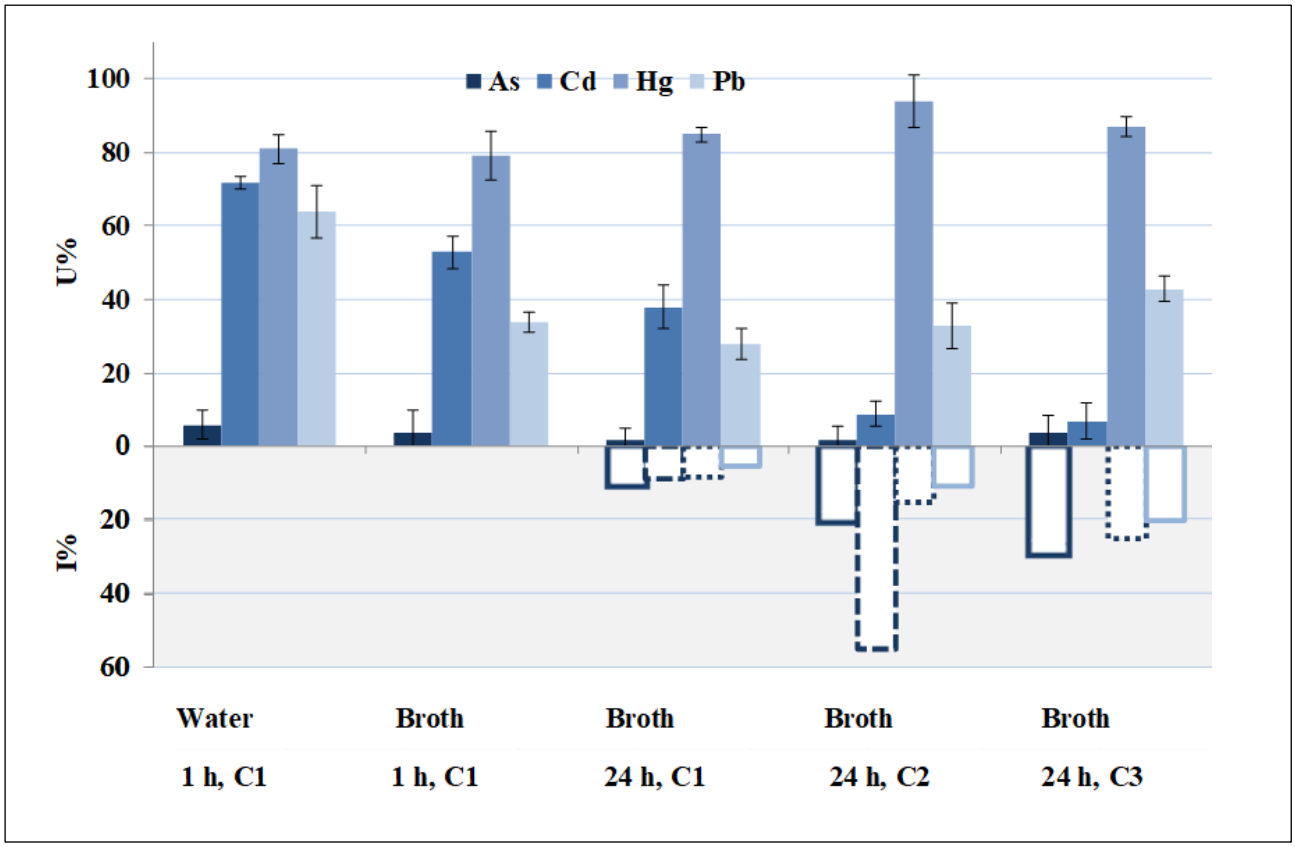

Fig. 1. Bacterial capacity to bind toxic elements [uptake percentage (U%); mean ± standard deviation] in Man, Rogosa and Sharpe (MRS) broth supplemented with 0.05% w/v L-cysteine hydrochloride (cys) or in deionized water. Inhibition of bacterial viability (I%), assessed using tolerance assays in broth (MRS/cys), is shown below. The concentrations used were: C1: As, Cd, Pb at 5 mg L^{-1} and Hg at 2 mg L^{-1}; C2: As, Cd, Hg and Pb at 10 mg L^{-1}; C3: As, Cd, Hg, and Pb at 50 mg L^{-1} (I% of Cd was not measured at this concentration).

3.1.2. Element-binding Assays

The binding of elements by bacteria is a complex process that depends on characteristics of the elements, physiological properties of the bacterial strain, and physico-chemical characteristics of the environment such as pH, temperature, contact time, and element concentration (Mrvčić et al., 2012). pH is one of the key parameters that can influence the biosorption of elements. As pH value changes in aqueous solutions, the chemical characteristics of metal ions, and competition between metal cations and protons for cell-wall binding sites, can also change. At pH <3, the binding of metal ions

is negligible and increases with increase of the initial pH value to 6 (Mrvčić et al., 2012). With increases in pH, the solubility of metal ions decreases, and precipitation of metal ions can occur (Mrvčić et al., 2012). For these reasons, we opted to perform *in-vitro* assessments at the two most common pH levels of 5 (in water) and 6 (in MRS broth)] at 37°C. Binding assays were performed using a constant number of bacteria, similar to that found in the human intestine (5×10^{10} bacteria mL^{-1}), because variation in microbial biomass concentration alters the contact area and number of possible bonding sites for metal ions. In particular, increasing the concentration of microbial biomass increases the amount of bound metal ions (Mrvčić et al., 2012). In our study, the best values of U% for Cd (72%) and Pb (64%) were obtained in water at 1 h, and for Hg in broth at 24 h (85%); U% for As under all conditions was very low. The binding of elements to probiotic bacteria is a rapid process. In water, the binding process requires only 1 h. Previous studies (Halttunen et al., 2007; Teemu et al., 2008) show that the genera *Lactobacillus* and *Bifidobacterium* can bind Pb and Cd in solution in 5 min to 1 h, and that the elements are strongly sequestered by the cell even at 48 hours after the initial binding takes place. Ibrahim et al. (2006) compared the abilities of *Lactobacillus rhamnosus* LC-705 and *Propionibacterium freudenreichii* to bind and absorb Pb and Cd in solution, and found that these bacteria can rapidly bind maximal amounts of metal after only 1 h of exposure. Daisley et al. (2018) showed that several strains of lactobacilli can significantly reduce the amount of Pb and Cd in solution. In that study, the relative binding capacity of LGR-1 strain decreased at higher concentrations of Pb and Cd (Daisley et al., 2018). Conversely, our results indicate that the binding efficiency of probiotic strains grown in consortia increases with increasing Pb concentration but decreases with increasing concentration of Cd. These differences are likely due to variations in experimental conditions used in these studies.

Due to competition among metal ions, the presence of other ions increases the ionic strength of solutions and negatively affects the process of biosorption (Mrvčić et al., 2012). Consequently, the best values for U% were obtained at pH 5 in water. Indeed, the MRS broth is rich in other elements such as K (from dipotassium hydrogen phosphate, 2.0 g L^{-1}), Na (from sodium acetate $3H_2O$, 5.0 g L^{-1}), Mg (from magnesium sulphate 7 H_2O, 0.2 g L^{-1}), and Mn (from manganese sulphate $4H_2O$, 0.05 g L^{-1}) (Sharpe at al., 1966). In a previous study, the best values for binding were achieved with Cd and Pb ions, but not with those of As (Mrvčić et al., 2012). Unlike Pb and Cd, As is a negatively charged species, which may be why probiotic bacteria cannot readily bind As (U% equal to approximately 4%).

Indeed, the bacterial binding of metal ions results from electrostatic interactions between the net negative surface charge of the bacterial cell and the positively charged metal ion (Monachese et al.,

2012). To the best of our knowledge, few studies have reported on the ability of lactobacilli or gut bacteria to bind and absorb Hg (Kinoshita 2019; Kinoshita et al., 2013; Monachese et al., 2012). Our *in-vitro* procedures show that more than 79% of Hg is sequestered by bacteria in both water and broth at concentrations ranging from 2 mg L^{-1} to 50 mg L^{-1}. During this process, the bacteria showed a high tolerance for Hg at all the assessed concentrations and time points (1 and 24 h), and less than 25% reduction in bacterial viability was observed at higher ionic concentrations. It is possible that the bacteria can also bind and sequester cationic Hg in the human gastrointestinal tract. Organic mercury, the main source of which is fish, is fat soluble, readily absorbed across the intestinal epithelium, and can be bioaccumulated. Bacterial detoxification of organic Hg involves the conversion of methylated Hg to inorganic Hg^{2+} that is not as readily absorbed by the gastrointestinal tract, and then to Hg^{0}, which is poorly absorbed (Monachese et al., 2012).

3.2. In vivo Study

3.2.1. Levels of Toxic Elements in Breast Milk

The levels of As, Cd, Hg, and Pb in breast milk samples from women supplemented with placebo and the probiotic product were analysed, and the differences in the concentration of toxic elements in colostrum (t0), transitional (t15), and mature milk samples (t30) were compared between the two groups (Table S1, Supplementary Material). As was excluded from statistical analysis because the LOD was ≥ 30%. No significant differences in the mean levels of Cd, Hg, or Pb were observed between the two groups at any of the time points. Therefore, for all the time points, milk samples from the control group and the experimental group were considered a single population.

Table 1 shows the statistical data for As, Cd, Hg, and Pb in breast milk samples, and summarizes the literature findings related to the contamination of human milk with these elements.

3.2.1.1. Arsenic

As was detected in 45% of colostrum and transitional milk samples, and in 62% of mature breast milk samples, with a mean level of 1.4 ± 2.3 g L^{-1}, 1.7 ± 2.9g L^{-1}, and 1.3 ± 1.3g L^{-1}, respectively. When present, As concentrations exceeded the limit of 0.6 g L^{-1} reported by the World Health Organization (WHO, 1989). The observed levels were higher than those reported in Germany for all lactation stages (Sternowsky et al., 2002), and in Italy and Sweden for mature milk (Miklavčič et al., 2013; Björklund et al., 2012). As concentrations were lower than those reported in Portugal for colostrum and mature milk (Almeida et al., 2008) and in Poland for mature milk (Klein et al., 2017); however, the ranges detected in our study (<1–12.1 g L^{-1} and <1–5.7g L^{-1}) were comparable to those reported. These

differences in the range of, and mean, concentration levels of As in breast milk among the various countries are likely due to multiple factors such as exposure of lactating mothers to As through contaminated drinking water and diet. Indeed, drinking water can be naturally high in As, typically present in its inorganic form (EFSA, 2009a; JECFA, 2011a). Furthermore, As in breast milk is associated with frequent consumption of fish and seafood (Miklavčič et al., 2013). We observed no statistically significant difference in As levels at the stages examined in our study; these results are in agreement with those of Sternowsky et al. (2002).

3.2.1.2. Cadmium

Cd was detected in 93, 90, and 79% of colostrum, transitional, and mature breast-milk samples, respectively. The mean Cd concentrations (0.9 ± 1.1 g L^{-1}, 0.37 ± 0.28g L^{-1}, and 0.36 ± 0.51 g L^{-1} in colostrum, transitional, and mature breast-milk, respectively) were below the limit of 1 g L^{-1} set by the WHO (1989) and the Italian reference range (Alimonti et al., 2010). The content of Cd in colostrum was comparable to that observed in the breast milk of nursing mothers in Austria and Croatia (Krachler et al., 1998; Grzunov Letinić et al., 2016), but higher than those reported in Greece, Poland, and Slovakia (Leotsinidis et al., 2005; Poniedziałek et al., 2018; Ursinyova and Masanova, 2005). In transitional milk samples, Cd levels were comparable to those reported in Austria (Krachler et al., 1998), lower than those reported in Croatia (Grzunov Letinić et al., 2016), and higher than those reported in Greece (Leotsinidis et al., 2005). In mature milk samples, Cd levels were comparable or lower than those reported in other studies from Italy and Europe, except for those by De Felipe et al. (2014) and Björklund et al. (2012). These regional differences in Cd concentrations may stem from various levels of exposure to Cd via diet [legumes, cereals, and potatoes (0.02–0.13 mg kg^{-1}); EFSA, 2009b] and cigarette smoke (CDC, 2009; ATSDR, 2012).

Table 1. Percentage of data points below the limit of detection (%N <LODs), concentration (g L^{-1}) of toxic elements in breast milk samples obtained at different stages of lactation [colostrum (t0), transitional (t15), and mature milk samples (t30)], and comparison with other studies and reference ranges (g kg^{-1} or g L^{-1})[a].

Element	This work						Italian reference range[b]	Levels in Italy		Levels in Europe		WHO[c] reference range
	Stage of lactation	%N <LOD	Mean ± SD	Median	Range (min–max)	Range (percentile 25°–75°)		Mean ± SD or median (range)	References	Mean ± SD or median (range)	Country; references	
As	t0	55	1.4 ± 2.3	<1	<1–12.1	<1–1.28	-	-	-	0.15 (0.15–1.1) <1.2 7.8 ± 2.2 (3.6–14.0)	Germany; Sternowsky et al., 2002 Poland; Poniedziałek et al., 2018 Portugal; Almeida et al., 2008	0.2–0.6
	t15	55	1.7 ± 2.9	<1	<1–12.2	<1–1.1		-	-	0.15 (0.15–0.8)	Germany; Sternowsky et al., 2002	
	t30	38	1.3 ± 1.3	<1	<1–5.7	<1–1.3		<1 (<1–12) <3 0.3 (0.04–12)	Astolfi et al., 2018 De Felip et al., 2014 Miklavčič et al., 2013	0.15 (0.15–2.8) 3.86 ± 1 (3.03–7.9) 5.8 ± 1.1 (4.2–7.8) 0.55 ± 0.70 (0.041–4.6)	Germany; Sternowsky et al., 2002 Poland; Klein et al., 2017 Portugal; Almeida et al., 2008 Sweden; Björklund et al., 2012	
Cd	t0	7	0.9 ± 1.1	0.6	<0.1–5.4	0.2–1.0	1–5	-	-	1.1 (<0.18–5.0) 0.88 (0.60–1.2)[e] 0.19 ± 0.15 (nd–0.70) <0.26 0.43 (nd–1.7)	Austria; Krachler et al., 1998 Croatia; Grzunov Letinić et al., 2016 Greece; Leotsinidis et al., 2005 Poland; Poniedziałek et al., 2018 Slovakia; Ursinyova and Masanova, 2005	<1
	t15	10	0.37 ± 0.28	0.29	<0.1–1.17	0.16–0.47		-	-	0.3 (<0.18–0.8) 0.76 (0.58–1.2)[d] 0.14 ± 0.12 (nd–0.49)	Austria; Krachler et al., 1998 Croatia; Grzunov Letinić et al., 2016 Greece; Leotsinidis et al., 2005	
	t30	21	0.36 ± 0.51	0.18	<0.1–2.0	0.11–0.30		<0.5[e] 0.4 ± 0.6 (0.1–2.2) 0.8 ± 0.2 <0.1	Abballe et al., 2008 Astolfi et al., 2018 Coni et al., 2000 De Felip et al., 2014	<0.18 (<0.18–0.6) 0.96 (0.68–1.3)[d] 2.1 ± 2.1 (0.21–7.35) 1.31 (1.15–1.41)[f] 0.086 ± 0.045 (0.028–0.27)	Austria; Krachler et al., 1998 Croatia; Grzunov Letinić et al., 2016 Poland; Winiarska-Mieczan et al., 2014 Spain; García-Esquinas et al., 2011 Sweden; Björklund et al., 2012	
Hg	t0	0	1.5 ± 1.3	0.9	0.3–5.6	0.6–1.9	-	-	-	1.59 ± 1.2 7.7 ± 11 3.9 (2.9–7.6)[d] 0.94 (nd–4.74) 0.29 (0.06–2.1)	Austria; Gundacker et al., 2002 Austria; Rossipal and Krachler, 1998 Croatia; Grzunov Letinić et al., 2016 Slovakia; Ursinyova and Masanova, 2005 Sweden; Björnberg et al., 2005	1.4–1.7
	t15	3	0.52 ± 0.44	0.36	<0.02–1.59	0.20–0.56		-				

										3.6 (3.2–4.5)[d]	Croatia; Grzunov Letinić et al., 2016	
	t30	3	0.57 ± 0.42	0.43	<0.02–1.36	0.25–0.92		2.63–3.53[e] <0.3 0.2 (<0.045–28) 0.3 ± 1.3 (0–28.3)	Abballe et al., 2008 De Felip et al., 2014 Miklavčič et al., 2013 Valent et al., 2013	0.2 (0.1–2) 0.8 ± 1.2 1.8 (0.98–3.4)[d] 0.2 (<0.045–2.4 or 2.9)[g] 0.6 (<0.045–12) 0.53 (0.45–0.62)[f] 0.14 (0.07–0.37)	Austria; Gundacker et al., 2010 Austria; Rossipal and Krachler, 1998 Croatia; Grzunov Letinić et al., 2016 Croatia or Slovenia; Miklavčič et al., 2013 Greece; Miklavčič et al., 2013 Spain; García-Esquinas et al., 2011 Sweden; Björnberg et al., 2005	
Pb	t0	17	7.5 ± 7.0	5.2	<2–22.4	2.1–10.0	6–25	-	-	1.63 ± 1.7 1.0 (0.2–5.6) 5.0 (2.6–10)[d] 0.48 ± 0.60 (nd–2.36) 1.3 ± 1.8 (1.0–15.1) 1.55 ± 1.4 (0.06–5.43) 4.7 (nd–24.4)	Austria; Gundacker et al., 2002 Austria; Krachler et al., 1998 Croatia; Grzunov Letinić et al., 2016 Greece; Leotsinidis et al., 2005 Poland; Poniedziałek et al., 2018 Portugal; Almeida et al., 2008 Slovakia; Ursinyova and Masanova, 2005	2–5
	t15	31	6.1 ± 8.4	2.5	<2–35.3	<2–6.4		-	-	2.0 (<0.12–8.7) 3.4 (1.9–5.6)[d] 0.15 ± 0.25 (nd–0.94)	Austria; Krachler et al., 1998 Croatia; Grzunov Letinić et al., 2016 Greece; Leotsinidis et al., 2005	
	t30	31	2.4 ± 1.3	2.5	<2–6.2	<2–3.0		0.85–1.07[e] 2 ± 2 (<2–7) 13 ± 6 2.59–5.99	Abballe et al., 2008 Astolfi et al., 2018 Coni et al., 2000 De Felip t al., 2015	1.5 (<0.12–9.9) 2.6 (1.7–4.7)[d] 1.02 ± 0.26 (0.52–1.44) 6.3 ± 4.6 (0.49–12) 0.94 ± 1.0 (0.07–4.03) 15.6 (12.9–18.7)[f] 1.5 ± 0.90 (0.74–6.4)	Austria; Rossipal and Krachler, 1998 Croatia; Grzunov Letinić et al., 2016 Poland; Klein et al., 2017 Poland; Winiarska-Mieczan et al., 2014 Portugal; Almeida et al., 2008 Spain; García-Esquinas et al., 2011 Sweden; Björklund et al., 2012	

nd: not detected.

[a] Differences in concentrations of trace elements in human milk examined using mass-basis (g kg^{-1}), and compared with concentrations examined using volume-basis (g L^{-1}), are negligibly small because the density of human milk is approximately 1.03 g mL^{-1} (EPA, 2011). Therefore, concentrations of trace elements in human milk, expressed in g kg^{-1} or g L^{-1}, have the same numerical values.

[b] Italian reference range by Alimonti et al. (2010). The data refer to the 25^{th}–75^{th} percentiles and 36 mothers.

[c] Joint FAO/WHO Expert Committee on Food Additives (JECFA, 1989). This was a study on composition of human milk acquired at approximately 3 months after the birth of the child.

[d] Results are presented as median (interquartile range). The data for Cd and Pb are reported for non-smokers; the data reported for Hg assume 1–2 instances of seafood consumption per week.

[e] The values for Cd were <LOQ for all areas of Venice with low, medium, and high consumption (LC, MC, and HC) of local fish and fishery products, and in Rome.

[f] Results are reported as geometric mean (at 95% confidence interval).

[g] Median (range) levels in breast milk acquired from Slovenian, Croatian, and Greek women were 0.2 (<0.045–2.9), 0.2 (<0.045–2.4), and 0.6 (<0.045–12), respectively.

3.2.1.3. Mercury

Mercury was detected in all the colostrum samples and in 97% of transitional and mature milk samples. The mean values of Hg (1.5 ± 1.3 g L^{-1}, 0.52 ± 0.44g L^{-1}, and 0.57 ± 0.42 g L^{-1}), assessed at each time point, were below the limits of 1 g L^{-1} set by the WHO (1989). Hg concentrations were comparable to those reported by other studies from Italy and Europe, except for those reported in Croatia, for all the lactation stages (Grzunov Letinić et al., 2016). Specifically, the Hg concentrations reported in Austria for colostrum (Rossipal and Krachler, 1998), and in Italy for mature milk (Abballe et al., 2008), are higher than the values obtained in our present study. The high levels measured in Croatia were associated with seafood intake, a typical dietary habit observed in coastal areas (Grzunov Letinić et al., 2016).

3.2.1.4. Lead

In 83% of colostrum samples and in 69% of transitional and mature breast-milk samples, the levels of Pb were above the LOD, with a mean concentration of 7.5 ± 7.0g L^{-1}, 6.1 ± 8.4g L^{-1}, and 2.4 ± 1.3g L^{-1}, respectively. The mean levels at t0 and t15 exceeded the limit of 5 g L^{-1} set by the WHO (1989), but were within the Italian reference range (Alimonti et al., 2010). The concentration of Pb in our samples was greater than those reported in other European countries. Only studies from Italy, Poland, and Spain reported higher Pb levels in mature breast milk than those detected in our samples (Coni et al., 2000; Winiarska-Mieczan et al., 2014; García-Esquinas et al., 2011). Air pollution is a major source of Pb exposure (Yurdakök, 2015). Urban pollution and industrial activities also influence Pb content in food (Yurdakök, 2015). The content of Pb in breast milk is related to diet (consumption of fish and potatoes) and lifestyle (smoking tobacco) (Gundacker et al., 2002; García-Esquinas et al., 2011; Yurdakök, 2015). Furthermore, inadequate intake of calcium during lactation can determine the release of Pb from the mother's bony deposits (Ettinger et al., 2009).

3.2.1.5. Differences in Concentration Levels During Lactation Period

Table 2 shows the differences in the levels of Cd, Pb, and Hg in breast milk during the time of lactation. The concentrations of Cd, Hg, and Pb decreased during the first month of lactation; those of Hg and Pb in breast milk samples were significantly different ($p < 0.05$) at different sampling times. Hg levels were significantly higher ($p^* < 0.05$) at t0 compared with those sampled at t15 and at t30, while the level of Pb was significantly higher ($p^* < 0.05$) at t0 compared with that at t30. Although the concentration of Cd was reduced by approximately two-thirds in samples of transitional and mature milk compared with that in colostrum samples, the difference was not significant, perhaps due

to the high variability of values. In general, higher elemental concentrations are found in the colostrum fraction than in transitional or mature milk (Krachler et al., 1998; Rossipal and Krachler, 1998; Björnberg et al., 2005; Almeida et al., 2008; Grzunov Letinić et al., 2016). This occurs because colostrum, transitional, and mature milk contain different levels of protein, fat, and other ligands that can bind trace elements. Elements principally bind to proteins; thus, a physiological decrease in the levels of proteins and other ligands during the course of lactation determines a reduction in the content of these elements in breast milk (Ballard and Morrow, 2013; EPA, 2011). Our results show that the levels of Hg and Cd were reduced by approximately two thirds after 15 days of lactation, while Pb was reduced by two thirds only after 1 month.

Table 2. Comparison of toxic-element concentrations in samples of colostrum (t0), transitional milk (t15), and mature milk (t30).

Element	$t_{\text{lactation stages}}$	ANOVA[a]			Bonferroni correction[b]				
		N; N*	F	p	Mean difference	p*	Standard error	95% confidence interval on the difference between the means	
								Lower	Lower
Cd	t0–15	2; 78	2.40	0.097	0.444	0.472	0.311	-0.317	1.20
	t0–30				0.654	0.101	0.303	-0.0867	1.40
	t15–30				0.210	1.00	0.303	-0.531	0.952
Hg	t0–15	2; 81	8.67	0.0004	0.916*	0.001	0.249	0.307	1.52
	t0–30				0.880*	0.002	0.249	0.271	1.49
	t15–30				-0.0359	1.00	0.249	-0.645	0.573
Pb	t0–15	2; 83	6.11	0.003	0.406	0.305	0.245	-0.193	1.00
	t0–30				0.864*	0.002	0.247	0.260	1.47
	t15–30				0.458	0.202	0.248	-0.146	1.07

[a] ANOVA was used to compare variability in element concentration within the groups. Values (F) were obtained using N-1 (N = number of lactation stages) and N*-3 degrees of freedom (N* = number of valid data points) at significance level $\alpha = 0.05$.

[b] Bonferroni post-hoc test was used to compare differences in mean elemental levels in breast-milk samples at different stages of lactation.

As shown in Table 3, examining the different breastfeeding stages separately enabled us to highlight a significant positive correlation ($p < 0.01$) between the levels of Cd and Pb for all three stages of lactation. This is likely because Cd and Pb are equally distributed among the low-molecular-weight components present in breast milk, while Hg can interact with a broader range of milk proteins

(Gundacker and Zödl, 2005; Rebelo and Caldas, 2016). The significant correlation between Pb and Cd is likely due to their common source and equal distribution among the low-molecular-weight components present in human milk. Much of Pb and Cd in breast milk is not due to mother's exposure during lactation (Yurdakök, 2015). In fact, during the mobilization of calcium for foetal skeletal development, which occurs in maternal bones during pregnancy, Pb and Cd can enter maternal blood circulation (Yurdakök, 2015), resulting in the transfer of some Pb and Cd into breast milk (Yurdakök, 2015).

Table 3. Kendall's tau-b correlation (K) of toxic-element concentrations in samples of colostrum (t0), transitional milk (t15), and mature milk (t30).

Parameters		t0		t15		t30	
		Cd	Hg	Cd	Hg	Cd	Hg
Hg	K	0.067	1.00	0.131	1.00	0.196	1.00
	p	0.640	-	0.362	-	0.148	-
	N	26	28	26	28	28	28
Pb	K	0.542[a]	0.115	0.496[a]	0.072	0.355[a]	0.029
	p	0.0001	0.395	0.0004	0.593	0.009	0.834
	N	26	28	26	28	28	28

[a] Values (K) were obtained using N (N = number of cases) at significance level $\alpha = 0.01$ (two-tailed).

3.2.2. Levels of Toxic Elements in Newborn Stools

We compared the concentrations of toxic elements in stools of newborns from experimental and control groups; the stools were obtained concurrently with the sampling of breast milk at t0, t15, and t30 (Table S2, Supplementary Material). As and Pb were excluded from statistical analysis because their levels were below the LOD (Table 4). Hg faecal levels were similar between the two groups, while that of Cd was significantly different (p=0.006) between the two populations at t15. In particular, the mean Cd concentration was significantly lower in the stools of newborns whose mothers were administered the probiotic product. Table 4 shows the levels of As, Cd, Hg, and Pb in infant stool samples, and summarizes the literature data related to the presence of these toxic elements in newborn stools. Measuring the concentration of toxic elements in the meconium of newborns allows for evaluation of intrauterine exposure (Ramirez et al., 2000; Ostrea et al., 2002; Turker et al., 2006; Unuvar et al., 2007; Esteban and Castaño, 2009); however, few studies have evaluated this matrix.

Table 4. Percentage of data points below the limits of detection (%N <LODs), concentration (g kg^{-1}) of toxic elements in infant stools sampled at different times (t0, t15, and t30), and comparison of our results with those obtained in other studies.

Element	Values obtained in the present study							Levels of toxic elements in samples of newborn stools examined in previous studies	
	Stage of lactation		%N <LODs (over time)	Mean ± SD	Median	Range (min–max)	Range (percentile 25°–75°)	Mean ± SD or median (range)	Country; references[a]
As	t0		68	<10	<10	<10–41.7	<10–10.7	37.3 (28.6)** 60 (<5–110) or 70 (<5–102)*	Taiwan; Jiang et al., 2014 Turkey; Hamzaoglu et al., 2014
	t15		96	<10	<10	<10–11.5	<10		
	t30		93	<10	<10	<10–15	<10		
	Overall		86	<10	<10	<10–41.7	<10		
Cd[b]	t0	C	0	9.7 ± 2.6	9.5	5.3–14.8	7.9–10.6	<4 (<4–130) 7.27 (10.9)** 30 (<5–135) or 35.5 (<5–69)* 2.3 (55.6)**	Canada; Arbuckle et al., 2016 Taiwan; Jiang et al., 2014 Turkey; Hamzaoglu et al., 2014 Turkey; Türker et al., 2006
		E	0	8.5 ± 1.0	8.3	6.9–9.9	7.8–9.4		
	t15	C	0	12.3 ± 3.4	11.2	8.4–20.9	10.1–14.4		
		E	0	9.1 ± 2.7	8.4	6.2–14.5	7.1–10.1		
	t30	C	0	12.2 ± 4.8	11.1	6.1–22.7	8.6–15.3		
		E	0	10.4 ± 2.7	10.3	4.8–14.0	9.5–11.3		
	Overall	C	0	11.4 ± 3.9	10.5	5.3–22.7	8.9–13.8		
		E	0	9.3 ± 2.3	9.3	4.8–14.5	7.6–10.2		
Hg	t0		0	38 ± 30	36	8–86	21–41	4.0 (0.4–128) <10 (<10–140) 82.6 (43.9)** <5 (<5–160) or <5 (<5–44)*	Austria; Gundacker et al., 2002 Canada; Arbuckle et al., 2016 Taiwan; Jiang et al., 2014 Turkey; Hamzaoglu et al., 2014
	t15		0	28 ± 28	18	1–72	11–37		
	t30		0	34 ± 37	27	4–81	6–55		
	Overall		0	33 ± 29	29	1–86	8–45		
Pb	t0		35	17 ± 14	13	<10–57	<10–27	15.5 (1.9–103) <4 (<4–480) 19.4 (24.0)** 84 (<5–429) or 41 (<5–330)* 46.5 (1400)**	Austria; Gundacker et al., 2002 Canada; Arbuckle et al., 2016 Taiwan; Jiang et al., 2014 Turkey; Hamzaoglu et al., 2014 Turkey; Türker et al., 2006
	t15		39	24 ± 20	26	<10–89	<10–34		
	t30		37	22 ± 19	20	<10–72	<10–36		
	Overall		37	21 ± 18	18	<10–89	<10–32		

[a] The data by Hamzaoglu et al. (2014) refer to industrial and not industrial districts (*). Jiang et al. (2014) and Türker et al. (2006) show the inter-quartile range in brackets (**). The data by Türker et al. (2006) are reported in mg kg^{-1}.

[b] The data for Cd are reported separately for two populations [Control (C) and Experimental (E)], because there was a significant difference between the two groups.

Currently, there are no available data on the content of toxic elements in faecal samples obtained in Italy, and few studies have reported on the content of toxic elements in faecal samples obtained in other European countries. Therefore, we compared the results generated in this study with those reported outside of the European continent. We detected As in only 14% of our samples (10% in meconium, 2% at t15, and 2% at t30) with a mean level <10g kg^{-1} for all the sampling time points. This value is lower than those reported in Taiwan and Turkey (Jiang et al., 2014; Hamzaoglu et al., 2014).

Table 5. Cd and Hg concentrations in infant stools sampled at different time points (T).

Element[a]	T	ANOVA[b]			Bonferroni correction[c]				
		N; N*	F	p	Mean difference	p*	Standard error	95% confidence interval on the difference between the means	
								Lower	Lower
Control									
	t0–15				-0.248	0.108	0.080	-0.516	0.0211
Cd	**t0–30**	2; 49	2.95	0.062	-0.200	0.107	0.203	-0.464	0.0653
	t15–30				0.0479	0.107	1.00	-0.217	0.313
Experimental									
	t0–15				-0.0376	0.104	1.00	-0.304	0.228
Cd	**t0–30**	2; 31	1.27	0.297	-0.169	0.110	0.408	-0.449	0.111
	t15–30				-0.131	0.110	0.727	-0.412	0.149
Overall									
	t0–15				0.789	0.740	0.928	-1.30	2.88
Hg	**t0–30**	2; 83	0.783	0.481	0.849	0.785	0.908	-1.36	3.06
	t15–30				0.0601	0.785	1.000	-2.15	2.28

[a] Cd data are reported separately for two newborn populations [Control (C) and Experimental (E)], because at t15, the means were significantly different (p* <0.05). Conversely, all data on Hg were combined without distinguishing the two groups, because there were no significant differences between the groups.

[b] ANOVA was used to compare variability in element concentration within the groups with that among the groups. Values (F) were obtained using N-1 (N = number of lactation stages) and N*-3 degrees of freedom (N* = number of valid data points) at significance level $\alpha = 0.05$.

[c] The Bonferroni post-hoc test was used to compare mean differences in elemental levels in infant stools sampled at different stages of lactation. Elemental concentrations were not significantly different (p* >0.05) at any of the lactation stages.

Cd was detected in all our samples, with a mean level of 8.5 ± 1.0g kg^{-1} and 9.7 ± 2.6g kg^{-1} in the meconium of control newborns of placebo-treated and probiotic-treated mothers, respectively. These

values are higher than those reported in the literature, with the exception of those obtained in Turkey (Hamzaoglu et al., 2014). Hg was also detected in all the samples, with an overall mean level of 33 ± 29 g kg^{-1}. This value was higher than those reported in other countries, but lower than that obtained in Taiwan, where the frequency of fish intake may influence Hg concentrations (Jiang et al., 2014). Finally, Pb was detected in 61% of all samples (18% in meconium, 21% at t15, and 22% at t30) with an overall mean level of 21 ± 18g kg^{-1}. The mean level of Pb in meconium (17 ± 14g kg^{-1}) was higher than those reported in Austria and Canada (Gundacker et al., 2002; Arbuckle et al., 2016), but lower than those reported in Taiwan and Turkey (Jiang et al., 2014; Türker et al., 2006; Hamzaoglu et al., 2014).

3.2.2.1. Differences in Concentration Levels Over Time

No significant differences in faecal Hg and Cd over time were observed (Table 5).

In contrast with results obtained for breast milk, elemental levels did not decrease in stools sampled from birth to 1 month of age; therefore, the samples were combined for correlation analysis (Table 6).

No significant correlation (p >0.05) was found between faecal Cd and Hg concentrations, and between those in infant stools and breast milk, sampled at all the stages of lactation (Table 6).

Table 6. Kendall's tau-b correlation (K) of Cd and Hg concentrations between infant stools and breast milk sampled at all the stages of lactation.

Parameters[a]			Control				Probiotic-treated			
			Breast milk		Infant stools		Breast milk		Infant stools	
			Cd	Hg	Cd	Hg	Cd	Hg	Cd	Hg
Cd	Infant stools	K	-0.153	-0.022	1.00	-0.067	-0.138	0.063	1.00	0.071
		p	0.112	0.819	-	0.851	0.277	0.622	-	0.805
Hg		K	0.067	0.200	-0.067	1.00	-0.143	-0.074	0.071	1.00
		p	0.851	0.573	0.851	-	0.621	0.802	0.805	-

[a] As and Pb were excluded from statistical analysis because their levels were below the LOD. Values (K) were obtained at significance level α = 0.05 (two-tailed), using the N (N = number of cases) of 52 and 34 control and treated individuals, respectively.. The Cd and Hg concentrations were not significantly correlated (p >0.05) as assessed at different times.

3.3. Characterization of Intake of, and Exposure to, Toxic Elements in Infants

For each lactation time, the mean levels of As, Cd, Hg, and Pb, detected in breast-milk samples (Table 1), were used to estimate the average daily or weekly intake of each toxic element in infants at different time points (Table S3 and Table 7). When milk supply is abundant, the infant's milk intake is positively associated with infant weight. Because the mean weight of boys is greater than that of girls of the same age, intake is also associated with the sex of the infant (Institute of Medicine (US) Committee on Nutritional Status During Pregnancy and Lactation 1991; U.S. EPA, 2011). Initially, we compared weekly toxic element intake between boys and girls at different lactation stages (Table S3). There were no significant differences between the means of the two groups at different lactation stages. Therefore, these data were combined for further analyses.

3.3.1. Arsenic

In breast milk, As is present essentially as inorganic arsenic (IAs) (Fängström et al., 2008). Therefore, for purposes of risk assessment, the levels shown in Table 1 for total As were assumed to correspond to those of IAs. As shown in Table 7, the average weekly intake of As by infants at each time point (1st, 3rd and 5th week) was 1.5, 1.9, and 1.3 g kg^{-1} BW/week, all of which are less than the PTWI previously set by the WHO (15 g kg^{-1} BW/week; JECFA, 1989). However, in 2010, the Joint FAO/WHO (JECFA, 2010, 2011a) concluded that the PTWI previously adopted for As was no longer safe for humans, and established a benchmark dose and lower confidence level ($BMDL_{0.5}$) of 3 g kg^{-1} BW/day (or 21 g kg^{-1} BW/week) as the new reference point for risk assessment. Using the approach currently employed to characterize the risk of exposure to toxic elements, we obtained mean MOEs of 14, 11, and 16 at 1st, 3rd and 5th week, respectively, which are higher than 10 but lower than 50. An MOE of 50 or higher for As, based on $BMDL_{0.5}$ obtained in a human study, would pose low concern from a public-health standpoint (Rebelo and Caldas, 2016). However, our results were limited by the percentage of data points that fell below the limit of detection (55% of both colostrum and transitional milk samples and 38% of mature breast milk samples). The intake shown by our data is greater than the weekly intake of As reported by the European Food Safety Authority (EFSA et al., 2014) for 3-month-old European infants (0.28 g/kg BW/week, 6.1 kg BW, 800 mL of breast milk) and by Sternowsky et al. (2002) for 3-month-old German infants (0.14–0.42 g/kg BW/week, 6 kg BW, 790 mL of breast milk).

Table 7. Intake and risk characterization for toxic element levels in breast milk sampled at different lactation stages by comparison with health-based guidance values for Cd and Hg as provisional tolerable weekly intake (PTWI), and for As and Pb as estimated margin of exposure (MOE). As, Cd, Hg, MeHg, and Pb intake values, reported by other studies conducted in Italy and other European geographical areas, are also shown.

Element	Age (weeks)	This work				Other studies in Europe			Maximum tolerable daily intake FAO/WHO[d]
		Daily intake[a] (μg kg^{-1} BW/day)	Weekly intake[a] (μg kg^{-1} BW/week)	%PTWI[b]	MOE[c]	Weekly intake mean or median*	Country; reference	Observation: age, body weight and consumption of breast milk	
As	1	0.21 ± 0.33 (<0.1–1.72)	1.5 ± 2.3 (<1–12.1)	9.7	14	-	-	-	12∝g/day (or 14 ∝g/kg BW/week)
	3	0.27 ± 0.44 (<0.2–1.90)	1.9 ± 3.1 (<1–13.3)	12	11	-	-	-	
	5	0.19 ± 0.19 (<0.2–0.86)	1.3 ± 1.3 (<1–6.0)	8.9	16	0.28 0.14–0.42	Europe; EFSA[e], 2014; Germany; Sternowsky et al., 2002	3 months, 6.1 kg, 800 mL; 3 months, 6 kg, 790 mL;	
Cd	1	0.12 ± 0.15 (<0.01–0.78)	0.9 ± 1.0 (<0.1–5.4)	34	-	0.098*	Greece; Leotsinidis et al., 2005	3 days, 3.4 kg, 100 mL/kg-day	6.4∝g/day (or 7.5 ∝g/kg BW/week)
	3	0.058 ± 0.043 (<0.02–0.18)	0.41 ± 0.30 (<0.1–1.28)	16	-	0.182*	Greece; Leotsinidis et al., 2005	14 days, 150 mL/kg-day	
	5	0.051 ± 0.069 (<0.02–0.29)	0.36 ± 0.48 (<0.1–2.05)	14	-	1.80	Poland; Winiarska-Mieczan et al., 2014	1 month, 4.5 kg, 700 mL/day	
Hg	1	0.22 ± 0.19 (0.05–0.80)	1.6 ± 1.4 (0.3–5.6)	39	-	-	-	-	4 ∝g/day (or 4.7 ∝g/kg BW/week)
	3	0.084 ± 0.077 (<0.003–0.25)	0.59 ± 0.54 (<0.02–1.74)	15	-	-	-	-	
	5	0.089 ± 0.068 (<0.003–0.20)	0.62 ± 0.48 (<0.02–1.43)	15	-	-	-	-	
MeHg[f]	1	0.11 ± 0.10 (0.02–0.40)	0.78 ± 0.68 (0.17–2.80)	49	-	-	-	-	-
	3	0.042 ± 0.039 (<0.003–0.12)	0.29 ± 0.27 (<0.02–0.87)	18	-	-	-	-	
	5	0.044 ± 0.034 (<0.003–0.10)	0.31 ± 0.24 (<0.02–0.72)	19	-	0.09–0.62	Europe; EFSA[f], 2012b	under 6 months, 6.1 kg, 800 mL/day	
Pb	1	1.1 ± 1.0 (<0.3–3.2)	7.8 ± 7.3 (<2–22.4)	31	0.45	0.28* 5.4	Greece; Leotsinidis et al., 2005; Slovakia; Ursinyova and Masanova, 2005	3 days, 3.4 kg, 100 mL/kg-day; daily milk consumption is 1/6 of BW	21 ∝g/day (or 24.5 ∝g/kg BW/week)
	3	1.0 ± 1.4 (<0.3–5.5)	6.8 ± 9.8 (<2–38.5)	27	0.51	0.49*	Greece; Leotsinidis et al., 2005	14 days, 150 mL/kg-day	
	5	0.35 ± 0.18 (<0.3–0.93)	2.5 ± 1.3 (<2–6.5)	9.9	1.4	2.94	Poland; Winiarska-Mieczan et al., 2014	1 month, 4.5 kg, 700 mL	

[a] Mean ± SD and (minimum–maximum) range. BW: body weight. Daily or weekly intake of toxic elements at different age of the newborn (1st, 3rd, and 5th week) was estimated using the mean level of toxic elements reported in Table 1 and daily milk consumption as follows: 474 mL per 3.3 kg at 0-7 days after birth; 590 mL per 3.8 kg at 2 weeks after birth; and 651 mL per 4.3 kg at 4 weeks after birth (U.S. EPA, 2011).

[b] Health-based guidance values for Cd, Hg, and MeHg as PTWI were set at 2.5g kg^{-1} BW/week (EFSA, 2012a), 4g kg^{-1} BW/week (JECFA, 2011a), and 1.6 g kg^{-1} BW/week (JECFA, 2004), respectively. Percentages of PTWI were also calculated for As and Pb with respect to the previously established PTWI of 15 μg kg^{-1} BW/week (JECFA, 1989) and 25 μg kg^{-1} BW/week (JECFA, 1999), respectively. Risk may exist when percent PTWI is higher than 100.

[c] Health-based guidance values for As and Pb, with BMDL at a lower confidence level, were set at 3.0 g kg^{-1} BW/day or 21.0 g kg^{-1} BW/week (JECFA, 2011a), and at 0.5 g kg^{-1} BW/day or 3.5 g kg^{-1} BW/week, respectively (EFSA, 2010). An MOE should be as high as possible (≥50 for As based on $BMDL_{0.5}$ and ≥10 for Pb based on $BMDL_1$) in order to not represent a public health concern (EFSA, 2005, 2010, 2014).

[d] The values (μg/day) set by the Joint FAO/WHO Expert Committee on Food Additives can be found in Table 32 of JECFA, 1989, and refer to the body weight of 6 kg.

[e] Mean intake of As was estimated using EFSA guidelines for 3-month-old European infants.

[f] MeHg was not measured because it was considered to represent 50% of the THg present (Rebelo and Caldas, 2016). EFSA (2012b) assessed MeHg levels in European infants less than 6 months of age (6.1 kg BW) using contamination data from Miklavčič et al. (2013) and Valent et al. (2013).

3.3.2. Cadmium

As shown in Table 7, the average weekly intake of Cd in infants decreased during the course of lactation from 0.9 to 0.41 and 0.36 g kg^{-1} BW/week. These values are lower than the PTWI of 2.5 mg kg^{-1} BW/week set by the EFSA (EFSA et al., 2014). Our calculated values are greater than the intakes of 0.098 (3 days, 100 mL kg^{-1} day) and 0.182g kg^{-1} BW/week (14 days, 150 mL kg^{-1} day) reported for Greece by Leotsinidis et al. (2005), but lower than those reported for Poland (1.80 g kg^{-1} BW/week, 1 month, 4.5 kg, 700 mL/day of breast milk) by Winiarska-Mieczan et al. (2014).

3.3.3. Mercury

Only THg was analysed in breast milk samples. Currently, the PTWIs for Hg are those for IHg (4 g kg^{-1} BW/week) and MeHg (1.6 g kg^{-1} BW), which is relevant for pregnant women and infants (JECFA, 2011b). The mean ratio of MeHg to THg in breast milk varies widely from 0 to 0.6, but is mostly at ~0.5 (EFSA, 2012; Rebelo and Caldas, 2016; Vacchina et al., 2017). MeHg represents 50% of the THg present (Rebelo and Caldas., 2016). We estimated a THg mean intake of 1.6 ± 1.4 g kg^{-1} BW/week for the first week with respect to the third (0.59 ± 0.54 g/ kg^{-1} BW/week) and fifth (0.62 ± 0.48 g kg^{-1} BW/week) week. These values are lower than the PTWI of 4g kg^{-1} BW/week (JECFA, 2011a) and maximum tolerable intake value of 4.7 g kg^{-1} BW/week set by FAO/WHO (JECFA, 1989). Based on our previous assumption, the MeHg mean intake in this study corresponded to 0.11 g kg^{-1} BW/day, or 0.78 g kg^{-1} BW/week in colostrum, representing 49% of PTWI. The mean MeHg weekly intake in mature milk (0.31 g kg^{-1} BW/week) was within the average range reported by EFSA (2012b).

3.3.4. Lead

In this study, the average weekly intake of Pb in infants was 7.8, 6.8, and 2.5 g kg^{-1} BW/week for the first, third, and fifth week, respectively (Table 7). These values, also observed for Cd, show a decreasing trend during the course of lactation, and all are lower than the PTWI of 25 g kg^{-1} BW/week previously set by the Joint FAO/WHO (1999). Our calculated values for Pb intake are higher than those reported in several European countries including Greece (0.28 and 0.49 g kg^{-1} BW/week median weekly intake in colostrum and transitional milk, respectively) (Leotsinidis et al., 2005) and Slovakia (5.40 g kg^{-1} BW/week mean weekly intake for transitional milk) (Ursinyova and Masanova, 2005), but lower than those reported in Poland for mature milk (2.94 g kg^{-1} BW/week) (Winiarska-Mieczan, 2014). Using the approach currently employed to characterize the risk of exposure to Pb, and a $BMDL_1$ of 0.5 g kg^{-1} BW/day (EFSA, 2010; 3.5 g kg^{-1} BW/week), we calculated the mean MOEs of

0.45, 0.51, and 1.4 for the first, third, and fifth week, respectively. The MOEs calculated in the present study were below 1, or between 1 and 10, indicating a potential risk to breastfed infants in accordance with the guidelines of EFSA (2010).

4. Conclusions

Toxic elements, found in breast milk, show particularly high concentrations in colostrum; thus, during breastfeeding, substantial amounts of elements are transferred to the intestine of the newborn. In this study, we assessed a novel application of a specific probiotic formulation to promote detoxification in humans, and protect the health of nursing mothers and their infants. Preliminary *in-vitro* experiments with the bacterial strains present in this probiotic product showed a high bacterial tolerance for As, Cd, Hg, and Pb, and good binding capacity for Cd, Hg, and Pb within 1 hour of contact. Toxic element levels in the breast milk of women treated orally with this probiotic product from 36th week of pregnancy to 4 weeks postpartum did not differ significantly from the levels in women treated with placebo over the same time period. Our data did not show any association between toxic element concentration in breast milk and newborn stools. Indeed, the concentration of Cd, Hg, and Pb in breast milk decreased over time, whereas elemental levels in newborn stools were stable from birth to 1 month of age. However, we found a significantly lower concentration of Cd at t15 in the stools of newborns whose mothers consumed the probiotic product.

Our *in-vitro* data indicate that probiotic strains grown in consortia can absorb toxic elements. However, the present study was limited by its small sample size and potential uncontrolled confounding effects, such as details of maternal diet and lifestyle. For these reasons, we were unable to draw definitive conclusions on the potential prophylactic use of this probiotic product for the reduction of absorption of toxic elements.

Future studies should focus on the ability of probiotic products to block toxic element absorption in humans. This can be evaluated by analysing blood, hair, urine, and faecal samples to obtain a total measurement of element absorption and elimination, and to characterize optimal bacterial strains for bioprotection and detoxification of the human body from heavy metals and other contaminants.

The risk assessment, performed in the present study, evidenced that exposure to toxic elements may occur immediately after birth through breast milk, the sole food source for infants for the first months of life. It is, therefore, necessary to improve our understanding of the possible health consequences of chemical exposure from human milk in order to minimize the risk of potentially harmful effects in infants and children.

Acknowledgements

This work was partially supported by the Sapienza University of Rome [grant number RP11715C819E4A20].

The authors would like to express their sincere gratitude to the women and their infants participating in this study. The authors would like to thank Iqra Javed for her assistance with the English language in the final version of the manuscript.

Conflicts of Interest

There are no conflicts to declare.

References

Abballe, A., Ballard, T.J., Delatte, E., di Domenico, A., Ferri, F., Fulgenzi, A.R., Grisanti, G., Iacovella, N., Ingelido, A.M., Malish, M., Miniero, R., Porpora, M.G., Risica, S., Ziemacki, G., de Felip, E., 2008. Persistent environmental contaminants in human milk: concentrations and time trends in Italy. Chemosphere 73, S220–S227. https://doi.org/10.1016/j.chemosphere.2007.12.036.

Akinyele, I.O., Shokunbi, O. S., 2015. Concentrations of Mn, Fe, Cu, Zn, Cr, Cd, Pb, Ni in selected Nigerian tubers, legumes and cereals and estimates of the adult daily intakes. Food Chem. 173, 702–708. https://doi.org/10.1016/j.foodchem.2014.10.098.

Alimonti, A., Bocca, B., Mattei. D., Pino, A., 2010. Biomonitoring of the Italian population to metals: reference values 1990–2009, Rapporti ISTISAN 10/22 (in Italian), Istituto Superiore di Sanità, Rome.

Almeida, A.A., Lopes, C.M., Silva, A.M., Barrado, E., 2008. Trace elements in human milk: correlation with blood levels, inter-element correlations and changes in concentration during the first month of lactation. J. Trace Elem. Med. Biol. 22, 196–205. https://doi.org/10.1016/j.jtemb.2008.03.007.

Al-Saleh, I., Shinwari, N., Mashhour, A., Mohamed, G.E.D., Rabah, A., 2011. Heavy metals (lead, cadmium and mercury) in maternal, cord blood and placenta of healthy women. Int. J. Hyg. Environ. Health 214, 79–101. https://doi.org/10.1016/j.ijheh.2010.

Al-Saleh, I., Nester, M., Abduljabbar, M., Al-Rouqui, R., Eltabache, C., Al-Rajudi, T., Elkhatib, R., 2016. Mercury exposure and its effects on Saudi breastfed infant's neurodevelopment. Int. J. Hyg. Environ. Health 219, 129–141. https://doi.org/10.1016/j.ijheh.2015.10.002.

Arbuckle, T.E., Liang, C.L., Morisset, A.S., Fisher, M., Weiler, H., Cirtiu, C.M., Legrand, M., Davis, K., Ettinger, A.S., Fraser, W.D., 2016. Maternal and fetal exposure to cadmium, lead, manganese and mercury: the MIREC study. Chemosphere 163, 270–282. https://doi.org/10.1016/j.chemosphere.2016.08.023.

Arnich, N., Sirot, V., Rivière, G., Jean, J., Noël, L., Guérin, T., Leblanc, J.C., 2012. Dietary exposure to trace elements and health risk assessment in the 2nd French total diet study. Food Chem. Toxicol. 50, 2432–2449. https://doi.org/10.1016/j.fct.2012.04.016.

Astolfi, M.L., Canepari, S., Catrambone, M., Perrino, C., Pietrodangelo, A., 2006a. Improved characterisation of inorganic components in airborne particulate matter. Environ. Chem. Lett. 3, 186–191. https://doi.org/10.1007/s10311-005-0029-7.

Astolfi, M.L., Canepari, S., Cardarelli, E., Ghighi, S., Marzo, M.L., 2006b. Chemical fractionation of elements in airborne particulate matter: Primary results on PM10 and PM2.5 samples in the Lazio region (Central Italy). Ann Chim. 96, 183–194. https://doi.org/10.1002/adic.200690018.

Astolfi, M.L., Di Filippo, P., Gentili, A., Canepari, S., 2017. Semiautomatic sequential extraction of polycyclic aromatic hydrocarbons and elemental bio-accessible fraction by accelerated solvent extraction on a single particulate matter sample. Talanta 174, 838–844. https://doi.org/10.1016/j.talanta.2017.06.072.

Astolfi, M.L., Marconi, E., Protano, C., Vitali, M., Schiavi, E., Mastromarino, P., Canepari, S., 2018. Optimization and validation of a fast digestion method for the determination of major and trace elements in breast milk by ICP-MS. Anal. Chim. Acta 1040, 49–62. https://doi.org/10.1016/j.aca.2018.07.037.

ATSDR, 2007a. Toxicological profile for lead. Agency for Toxic Substances and Disease Registry. U.S. Department of Health and Human Services.

ATSDR, 2007b. Toxicological profile for arsenic. Agency for Toxic Substances and Disease Registry. U.S. Department of Health and Human Services.

ATSDR, 2012. Toxicological profile for cadmium. Agency for Toxic Substances and Disease Registry, U.S. Department of Health and Human Services.

ATSDR, 2015. The priority list of hazardous substances that will be the candidates for toxicological profiles. Agency for Toxic Substances and Disease Registry.

Ballard, O., Morrow, A.L., 2013. Human milk composition: nutrients and bioactive factors. Pediatr. Clin. 60, 49–74. https://doi.org/10.1016/j.pcl.2012.10.002.

Benford, D.J., 2016. The use of dose-response data in a margin of exposure approach to carcinogenic risk assessment for genotoxic chemicals in food. Mutagenesis 31, 329–331. https://doi.org/10.1093/mutage/gev064.

Bensefa-Colas, L., Andujar, P., Descatha, A., 2011. Mercury poisoning. Rev. Med. Interne 32, 416–424. https://doi.org /10.1016/j.revmed.2009.08.024.

Bhakta, J.N., Ohnishi, K., Munekage, Y., Iwasaki, K., Wei, M.Q., 2012. Characterization of lactic acid bacteria-based probiotics as potential heavy metal sorbents. J. Appl. Microbiol. 112, 1193–1206. https://doi.org/10.1111/j.1365-2672.2012.05284.x.

Bisanz, J.E., Enos, M.K., Mwanga, J.R., Changalucha, J., Burton, J.P., Gloor, G.B., Reid, G., 2014. Randomized open-label pilot study of the influence of probiotics and the gut microbiome on toxic metal levels in Tanzanian pregnant women and schoolchildren. mBio 5, e01580-14. https://doi.org/10.1128/mBio.01580-14.

Björklund, K.L., Vahter, M., Palm, B., Grandér, M., Lignell, S., Berglund, M., 2012. Metals and trace element concentrations in breast milk of first time healthy mothers: a biological monitoring study. Environ. Health 11, 92. https://doi.org/10.1186/1476-069X-11-92.

Björnberg, K.A., Vahter, M., Berglund, B., Niklasson, B., Blennow, M., Sandborgh-Englund, G., 2005. Transport of methylmercury and inorganic mercury to the fetus and breast-fed infant. Environ. Health Perspect. 113, 1381–1385. https://doi.org/10.1289/ehp.7856.

Blackwell, K.J., Singleton, I., Tobin, J.M., 1995. Metal cation uptake by yeast: a review. Appl. Microbiol. Biotechnol. 43, 579–584. https://doi.org/10.1007/BF00164757.

Breton, J., Daniel, C., Dewulf, J., Pothion, S., Froux, N., Sauty, M., Thomas, P., Pot, B., Foligné, B., 2013. Gut microbiota limits heavy metals burden caused by chronic oral exposure. Toxicol. Lett. 222, 132–138. https://doi.org/10.1016/j.toxlet.2013.07.021.

Brudnak, M.A., 2002. Probiotics as an adjuvant to detoxification protocols. Med. Hypotheses 58, 382−385. https://doi.org/10.1054/mehy.2001.1442.

Campopiano, A., Cannizzaro, A., Angelosanto, F., Astolfi, M.L., Ramires, D., Olori, A., Canepari, S., Iavicoli, S., 2014. Dissolution of glass wool, rock wool and alkaline earth silicate wool: morphological and chemical changes in fibers. Regul. Toxicol. Pharm. 70, 393–406. https://doi.org/10.1016/j.yrtph.2014.05.023.

Canepari, S., Castellano, P., Astolfi, M.L., Materazzi, S., Ferrante, R., Fiorini, D., Curini, R., 2018. Release of particles, organic compounds, and metals from crumb rubber used in synthetic turf under chemical and physical stress. Environ. Sci. Pollut. Res. 25, 1448–1459. https://doi.org/10.1007/s11356-017-0377-4.

CDC, 2009. Fourth Report on Human Exposure to Environmental Chemicals. Centers for Disease Control and Prevention. US Department of Health and Human Services, Atlanta, GA.

Ceccatelli, S., Daré, S., Moors, M., 2010. Methylmercury-induced neurotoxicity and apoptosis. Chem. Biol. Interact. 188, 301–308. https://doi.org/10.1016/j.cbi.2010.04.007.

Chowdhury, S., Mazumder, M.J., Al-Attas, O., Husain, T., 2016. Heavy metals in drinking water: occurrences, implications, and future needs in developing countries. Sci. Total Environ. 569, 476–488. https://doi.org/10.1016/j.scitotenv.2016.06.166.

Claeys-Thoreau, F., Thiessen, L., Bruaux, P., Ducoffre, G., Veruyn, G., 1987. Assessment and comparison of human exposure to lead between Belgium, Malta, Mexico and Sweden. Int. Arch. Occup. Environ. Health 59, 31–41. https://doi.org/10.1007/BF00377676.

Clarke, J.U., 1998. Evaluation of censored data methods to allow statistical comparisons among very small samples with below detection limit observations. Environ. Sci. Technol. 32, 177–183. https://doi.org/10.1021/es970521v.

Clarkson, T.W., Magos, L., 2006. The toxicology of mercury and its chemical compounds. Crit. Rev. Toxicol. 8, 609–662. https://doi.org/10.1016/j.jtemb.2012.02.004.

Commission Regulation (EC) No. 1881/2006 of 19 December 2006 setting maximum levels for certain contaminants in foodstuffs.

Council Directive 98/83/EC of 3 November 1998 on the quality of water intended for human consumption.

Coni, E., Bocca, B., Galoppi, B., Alimonti, A., Caroli, S., 2000. Identification of chemical species of some trace and minor elements in mature breast milk. Microchem. J. 67, 187–194. https://doi.org/10.1016/S0026-265X(00)00116-8.

Conti, M.E., Canepari, S., Finoia, M.G., Mele, G., Astolfi, M.L., 2018. Characterization of Italian multifloral honeys on the basis of their mineral content and some typical quality parameters. J. Food Compos. Anal. 74, 102–113. https://doi.org/10.1016/j.jfca.2018.09.002.

Cuadrado, C., Kumpulainen, J., Carbajal, A., Moreiras, O., 2000. Cereals contribution to the total dietary intake of heavy metals in Madrid, Spain. J. Food Compos. Anal. 13, 495–503. https://doi.org/10.1006/jfca.2000.0937.

Daisley, B.A., Monachese, M., Trinder, M., Bisanz, J.E., Chmiel, J.A., Burton, J.P., Reid, G., 2018. Immobilization of cadmium and lead by Lactobacillus rhamnosus GR-1 mitigates apical-to-basolateral heavy metal translocation in a Caco-2 model of the intestinal epithelium. Gut Microbes 14, 1–13. https://doi.org/10.1080/19490976.2018.1526581.

De Boever, P.D., Deplancke, B., Verstraete, W., 2000. Fermentation by gut microbiota cultured in a simulator of the human intestinal microbial ecosystem is improved by supplementing a soygerm powder. J. Nutr. 130, 2599–2606. https://doi.org/10.1093/jn/130.10.2599.

De Felip, E., Bianchi, F., Bove, C., Cori, L., D'Argenzio, A., D' Orsi, G., Fusco, M., Miniero, R., Ortolani, R., Palombino, R., Parlato, A., Pelliccia, M.G., Peluso, F., Piscopo, G., Pizzuti, R., Porpora, M.G., Protano, D., Senofonte, O., Spena, S.R., Simonetti, A., di Domenico, A., 2014. Priority persistent contaminants in peopledwelling in critical areas of Campania Region, Italy (SEBIOREC biomonitoring study). Sci. Total Environ. 487, 420–435. https://doi.org/10.1016/j.scitotenv.2014.04.016.

Di Dato, C., Gianfrilli, D., Greco, E., Astolfi, M.L., Canepari, S., Lenzi, A., Isidori, A. M., Giannetta E., 2017. Profiling of selenium absorption and accumulation in healthy subjects after prolonged l-

selenomethionine supplementation. J. Endocrinol. Invest. 40, 1183–1190. https://doi.org/10.1007/s40618-017-0663-5.

Dursun, A., Yurdakok, K., Yalcin, S.S., Tekinalp, G., Aykut, O., Orhan, G., Morgil, G.K., 2016. Maternal risk factors associated with lead, mercury and cadmium levels in umbilical cord blood, breast milk and newborn hair. J. Matern. Fetal Neonatal Med. 29, 954–961. https://doi.org/10.3109/14767058.2015.1026255.

EFSA, 2005. Opinion of the Scientific Committee on are quest from EFSA related to a harmonized approach for risk assessment of substances which are both genotoxic and carcinogenic. EFSA J. 282, 1–31. https://doi.org/10.2903/j.efsa.2005.282.

EFSA, 2009a. Panel on Contaminants in the Food Chain (CONTAM), Scientific opinion on arsenic in food. EFSA J. 7, 1351. https://doi.org/10.2903/j.efsa.2009.1351.

EFSA, 2009b. Cadmium in food: scientific opinion of the Panel on Contaminants in Food Chain. European Food Safety Authority. EFSA J. 980, 1–139. https://doi.org/10.2903/j.efsa.2009.980.

EFSA, 2010. Scientific Opinion on lead in food. European Food Safety Authority. EFSA Panelon Contaminants in the Food Chain (CONTAM). EFSA J. 8, 1570. https://doi.org/10.2903/j.efsa.2010.1570.

EFSA, 2012a. Cadmium dietary exposure in the European Population. European Food Safety Authority. EFSA J. 10, 2551. https://doi.org/10.2903/j.efsa.2012.2551.

EFSA, 2012b. Scientific Opinion on the risk for public health related to the presence of mercury and methyl mercury in food. European Food Safety Authority EFSA Panel on Contaminants in the Food Chain (CONTAM). EFSA J. 10, 2985. https://doi.org/10.2903/j.efsa.2012.2985.

EFSA, 2014. Dietary exposure to inorganic arsenic in the European population. Scientific Report of EFSA. European Food Safety Authority. EFSA J.12, 3597. https://doi.org/10.2903/j.efsa.2014.3597.

Emmett, P.M., Rogers, I.S., 1997. Properties of human milk and their relationship with maternal nutrition. Early Hum. Dev. 49, S7–S28. https://doi.org/10.1016/S0378-3782(97)00051-0.

Esteban, M., Castaño, A., 2009. Non-invasive matrices in human biomonitoring: a review. Environ. Int. 35, 438-449. https://doi.org/10.1016/j.envint.2008.09.003.

Ettinger, A.S., Lamadrid-Figueroa, H., Tellez-Rojo, M.M., Mercado-Garcia, A., Peterson, K.E., Schwartz, J., Hu, H., Hernandez-Avila, M., 2009. Effect of calcium supplementation on blood lead levels in pregnancy: a randomized placebo controlled trial. Environ. Health Perspect. 117, 26–31. https://doi.org/10.1289/ehp.11868.

Ettinger, A.S., Roy, A., Amarasiriwardena, C.J., Smith, D., Lupoli, N., Mercado-García, A., Lamadrid-Figueroa, H., Tellez-Rojo, M. M., Hu, H., Hernández-Avila, M., 2014. Maternal blood, plasma, and breast milk lead: lactational transfer and contribution to infant exposure. Environ. Health Perspect. 122, 87–92. https://doi.org/10.1289/ehp.1307187.

Fängström, B., Moore, S., Nermell, B., Kuenstl, L., Goessler, W., Grandér, M., Kabir, I., Palm, B., El Arifeen, S., Vahter, M., 2008. Breast-feeding protects against arsenic exposure in Bangladeshi infants. Environ. Health Perspect. 116, 963–969. https://doi.org/10.1289/ehp.11094.

Fürst, P., Fürst, C., Wilmers, K., 1994. Human milk as a bioindicator for body burden of PCDDs, PCDFs, organochlorine pesticides, and PCBs. Environ. Health Perspect. 102, 187–193. https://doi.org/10.1289/ehp.102-1566908.

García-Esquina, E., Pérez-Gómez, B., Fernández, M.A., Pérez-Mexeira, A.M., Gil, E., de Paz, C., Iriso, A., Sanz, J.C., Astray, J., Cisneros, M., de Santos, A., Asensio, A., García-Sagredo, J.M., García, J.F., Vioque, J., Pollán, M., López-Abente, G., González, M.J., Martínez, M., Bohigas, P. A., Pastor, R., Aragonés, N., 2011. Mercury, lead and cadmium in human milk in relation to diet, lifestyle habits and sociodemographic variables in Madrid (Spain). Chemosphere 85, 268–275. https://doi.org/10.1016/j.chemosphere.2011.05.029.

Gerbino, E., Carasi, P., Tymczyszyn, E.E., Gómez-Zavaglia, A, 2014. Removal of cadmium by *Lactobacillus kefir* as a protective tool against toxicity. J. Dairy Res. 81, 280–287. https://doi.org/10.1017/S0022029914000314.

Greenfield, H., Southgate, D.A.T., 2003. Food composition data: Production, Management and Use. 2nd ed. Food and Agriculture Organization of the United Nations, Rome, Italy, Chapter 9 and Table 9.1. http://www.fao.org/docrep/008/y4705e/y4705e00.htm.

Grzunov Letinić, J., Matek Sarić, M., Piasekc, M., Jurasović, J., Varnaic, V.M., Grgec, A.S., Orct, T., 2016. Use of human milk in the assessment of toxic metal exposure and essential element status

in breastfeeding women and their infants in coastal Croatia. J. Trace Elem. Med. Biol. 38, 117–125. https://doi.org/10.1016/j.jtemb.2016.08.002.

Gu, Y.G., Lin, Q., Huang, H.H., Wang, L.G., Ning, J.J., Du, F.Y., 2017. Heavy metals in fish tissues/stomach contents in four marine wild commercially valuable fish species from the western continental shelf of South China Sea. Mar. Pollut. Bull. 114, 1125–1129. https://doi.org/10.1016/j.marpolbul.2016.10.040.

Gulson, B.L., Mizon, K.J., Palmer, J.M., Korsch, M.J., Taylor, A.J., Mahaffey, K.R., 2004. Blood lead changes during pregnancy and postpartum with calcium supplementation. Environ. Health Perspect. 112, 1499–1507. https://doi.org/10.1289/ehp.6548.

Gundacker, C., Pietschnig, B., Wittmann, K.J., Lischka, A., Salzer, H., Hohenauer, L., Schuster, E., 2002. Lead and mercury in breast milk. Pediatrics 110, 873–878. https://doi.org/10.1542/peds.110.5.873.

Gundacker C., Zödl B., 2005. Heavy metals in breast milk: implications for toxicity. In: Preedy, V.R., Watson, R.R. (Eds.), Reviews in Food and Nutrition Toxicity vol. 4. CRC Press, Boca Raton, Florida, pp. 1–28.

Gundacker, C., Fröhlich, S., Graf-Rohrmeister, K., Eibenberger, B., Jessenig, V., Gicic, D., Prinz, S., Wittmann, K. J., Zeisler, H., Vallant B., Pollak, A., Husslein P., 2010. Perinatal lead and mercury exposure in Austria. Sci. Total Environ. 408, 5744–5749. https://doi.org/10.1016/j.scitotenv.2010.07.079.

Ha, E., Basu, N., Bose-O'Reilly, S., Dórea, J. G., McSorley, E., Sakamoto, M., Chan, H.M., 2017. Current progress on understanding the impact of mercury on human health. Environ. Res. 152, 419–433. https://doi.org/10.1016/j.envres.2016.06.042.

Halttunen, T., Salminen, S., Tahvonen, R., 2007. Rapid removal of lead and cadmium from water by specific lactic acid bacteria. Int. J. Food Microbiol. 114, 30–35. https://doi.org/10.1016/j.ijfoodmicro.2006.10.040.

Hamzaoglu, O., Yavuz, M., Turker, G., Savli, H., 2014. Air pollution and heavy metal concentration in colostrum and meconium in two different districts of an industrial city: A preliminary report. Int. Med. J. 21, 77–82.

Hewett, P., Ganser, G.H., 2007. A comparison of several methods for analyzing censored data. Ann. Occup. Hyg. 51, 611–32. https://doi.org/10.1093/annhyg/mem045.

IARC, 2016. International Agency for Research on Cancer. Classified by the IARC Monographs.

Ibrahim, F., Halttunen, T., Tahvonen, R., Salminen, S., 2006. Probiotic bacteria as potential detoxification tools: assessing their heavy metal binding isotherms. Can. J. Microbiol. 52, 877–885. https://doi.org/10.1139/w06-043.

Institute of Medicine (US) Committee on Nutritional Status During Pregnancy and Lactation. Nutrition During Lactation. Washington (DC): National Academies Press (US); 1991. 5, Milk Volume. Available from: https://www.ncbi.nlm.nih.gov/books/NBK235589/ (accessed December 4, 2018).

Isaac, C.P.J., Sivakumar, A., Kumar, C.R.P., 2012. Lead levels in breast milk, blood plasma and intelligence quotient: a health hazard for women and infants. Bull. Environ. Contam. Toxicol. 88, 145–149. https://doi.org/10.1007/s00128-011-0475-9.

JECFA, 1989. Evaluation of certain food additives and contaminants: Thirty-third report of the Joint FAO/WHO Expert Committee on Food Additives. Geneva.

JECFA, 1999. Evaluation of certain food additives and contaminants: Fifty-third report of the Joint FAO/WHO Expert Committee on Food Additives. Rome.

JECFA, 2004. Evaluation of certain food additives and contaminants: Sixty-first report of the Joint FAO/WHO Expert Committee on Food Additives. WHO Technical Report Series, No. 922.

JECFA, 2010. Evaluation of certain contaminants in food: Seventy-second report of the Joint FAO/WHO Expert Committee on Food Additives. Rome.

JECFA, 2011a. Evaluation of certain contaminants in food: Seventy-second report of the Joint FAO/WHO Expert Committee on Food Additives. WHO Technical Report Series, No. 959.

JECFA, 2011b. Safety Evaluation of Certain Contaminants in Food: Seventy-third meeting of the Joint FAO/WHO Expert Committee on Food Additives. WHO Technical Report Series, No. 960.

Jiang, C.B., Hsi, H.C., Fan, C.H., Chien, L.C., 2014. Fetal exposure to environmental neurotoxins in Taiwan. PloS one 9, e109984. https://doi.org/10.1371/journal.pone.0109984.

Kachenko, A.G., Singh, B., 2006. Heavy metals contamination in vegetables grown in urban and metal smelter contaminated sites in Australia. Water Air Soil Pollut. 169, 101–123. https://doi.org/10.1007/s11270-006-2027-1.

Kikuchi, Y., Nomiyama, T., Kumagai, N., Dekio, F., Uemura, T., Takebayashi, T., Nishiwaki, Y., Matsumoto, Y., Sano, Y., Hosoda, K., Watanabe, S., Sakurai, H., Omae, K., 2003. Uptake of cadmium in meals from the digestive tract of young non-smoking Japanese female volunteers. J. Occup. Health 45, 43–52. https://doi.org/10.1539/joh.45.43.

Kim, K. H., Kabir, E., Jahan, S. A., 2016. A review on the distribution of Hg in the environment and its human health impacts. J. Hazard. Mater. 306, 376–385. https://doi.org/10.1016/j.jhazmat.2015.11.031.

Kinoshita, H., Sohma, Y., Ohtake, F., Ishida, M., Kawai, Y., Kitazawa, H., Saito, T., Kimura, K., 2013. Biosorption of heavy metals by lactic acid bacteria and identification of mercury binding protein. Res. Microbiol. 164, 701–709. https://dx.doi.org/10.1016/j.resmic.2013.04.004.

Kinoshita, H., 2019. Biosorption of heavy metals by lactic acid bacteria for detoxification. Methods Mol. Biol. 1887, 145–157. https://doi.org/10.1007/978-1-4939-8907-2_13.

Klein, L.D., Breakey, A.A., Scelza, B., Valeggia, C., Jasienska, G., Hinde, K., 2017. Concentrations of trace elements in human milk: Comparisons among women in Argentina, Namibia, Poland, and the United States. PloS one 12, 1–16. https://doi.org/10.1371/journal.pone.0183367.

Krachler, M., Li, F.S., Rossipal, E., Irgolic, K.J., 1998. Changes in the concentrations of trace elements in human milk during lactation. J. Trace Elements Med. Biol. 12, 159–176. https://doi.org/10.1016/S0946-672X(98)80005-9.

Kunter, İ., Hürer, N., Gülcan, H.O., Öztürk, B., Doğan, İ., Şahin, G., 2017. Assessment of aflatoxin M1 and heavy metal levels in mothers breast milk in Famagusta, Cyprus. Biol. Trace Elem. Res.175, 42–49. https://doi.org/10.1007/s12011-016-0750-z.

LaKind, J.S., Wilkins, A.A., Berlin Jr., C.M., 2004. Environmental chemicals in human milk: a review of levels, infant exposures and health, and guidance for future research. Toxicol. Appl. Pharmacol. 198, 184–208. https://doi.org/10.1016/j.taap.2003.08.021.

Lehmann, G.M., LaKind, J.S., Davis, M.H., Hines, E.P., Marchitti, S.A., Alcala, C., Lorber, M., 2018. Environmental Chemicals in Breast Milk and Formula: Exposure and Risk Assessment Implications. Environ. Health Perspect. 126, 096001-1-20. https://doi.org/10.1289/EHP1953.

Leotsinidis, M., Alexopoulos, A., Kostopoulou-Farri, E., 2005. Toxic and essential trace elements in human milk from Greek lactating women: association with dietary habits and other factors. Chemosphere, 61, 238–247. https://doi.org/10.1016/j.chemosphere.2005.01.084.

Li, F.L., Shi, W., Jin, Z.F., Wu, H.M., Sheng, G.D., 2017. Excessive uptake of heavy metals by greenhouse vegetables. J. Geochem. Explor. 173, 76–84. https://doi.org/10.1016/j.gexplo.2016.12.002.

Makedonski, L., Peycheva, K., Stancheva, M., 2017. Determination of heavy metals in selected black sea fish species. Food Control 72, 313–318. https://doi.org/10.1016/j.foodcont.2015.08.024.

Manigrasso, M., Protano, C., Astolfi, M.L., Massimi, L., Avino, P., Vitali, M., Canepari, C., 2019. Evidences of copper nanoparticle exposure in indoor environments: Long-term assessment, high-resolution field emission scanning electron microscopy evaluation, in silico respiratory dosimetry study and possible health implications. Sci. Total Environ. 653, 1192–1203. https://doi.org/10.1016/j.scitotenv.2018.11.044

Marconi, E., Canepari, S., Astolfi, M.L., Perrino, C., 2011. Determination of Sb(III), Sb(V) and identification of Sb-containing nanoparticles in airborne particulate matter. Procedia Environ. Sci. 4, 209–217. https:// doi:10.1016/j.proenv.2011.03.025.

Mastromarino, P., Capobianco, D., Miccheli, A., Praticò, G., Campagna, G., Laforgia, N., Capursi, T., Baldassarre, M. E., 2015. Administration of a multistrain probiotic product (VSL# 3) to women in the perinatal period differentially affects breast milk beneficial microbiota in relation to mode of delivery. Pharmacol. Res. 95, 63–70. https://doi.org/10.1016/j.phrs.2015.03.013.

Miklavčič, A., Casetta, A., Tratnik, J.S., Mazej, D., Krsnik, M., Mariuz, M., Sofianou, K., Spirić, Z., Barbone, F., Horvat, M., 2013. Mercury, arsenic and selenium exposure levels in relation to fish consumption in the Mediterranean area. Environ. Res. 120, 7–17. https://doi.org/10.1016/j.envres.2012.08.010.

Ministry of Health (2011), Istituto Superiore di Sanità, CeVEAS (Centro per la valutazione dell'efficacia dell'assistenza sanitaria). Linee Guida Gravidanza Fisiologica. https://www.salute.gov.it/imgs/C_17_pubblicazioni_1436_allegato.pdf (accessed 31 July 2018).

Monachese, M., Burton, J.P., Reid, G., 2012. Bioremediation and human tolerance to heavy metals through microbial processes: a potential role for probiotics? Appl. Environ. Microbiol. 78, 6397–6404. https://doi.org/10.1128/AEM.01665-12.

Morel, F.M.M., Kraepiel, A.M.L., Amyot, M., 1998. The chemical cycle and bioaccumulation of mercury. Annu. Rev. Ecol. Syst. 29, 543–566. https://doi.org/10.1146/annurev.ecolsys.29.1.543.

Mrvčić, J., Stanzer, D., Solić, E., Stehlik-Tomas, V., 2012. Interaction of lactic acid bacteria with metal ions: opportunities for improving food safety and quality. World J. Microbiol. Biotechnol. 28, 2771–2782. https://doi.org/10.1007/s11274-012-1094-2.

Noli, F., Tsamos, P., 2016. Concentration of heavy metals and trace elements in soils, waters and vegetables and assessment of health risk in the vicinity of a lignite-fired power plant. Sci. Total Environ. 563, 377–385. https://doi.org/10.1016/j.scitotenv.2016.04.098.

Norén, K., Meironyté, D., 2000. Certain organochlorine and organobromine contaminants in Swedish human milk in perspective of past 20–30 years. Chemosphere 40, 1111–1123. https://doi.org/10.1016/S0045-6535(99)00360-4.

NRC (National Research Council), 2000. Toxicological Effects of Methylmercury. Washington DC: National Academy Press.

Oskarsson, A., Hallén, I.P., Sundberg, J., Grawé, K.P., 1998. Risk assessment in relation to neonatal metal exposure. Analyst 123, 19-23. https://doi.org/10.1039/A705136K.

Ostrea Jr, E.M., Morales, V., Ngoumgna, E., Prescilla, R., Tan, E., Hernandez E., Baens Ramirez, G., Cifra, H.L., Manlapaz, M.L., 2002. Prevalence of fetal exposure to environmental toxins as determined by meconium analysis. Neurotoxicology 23, 329–339. https://doi.org/10.1016/S0161-813X(02)00077-3.

Poniedziałek, B., Rzymski, P., Pięt, M., Gąsecka, M., Stroińska, A., Niedzielski, P., Mleczek, M., Rzymski, P., Wilczak, M., 2018. Relation between polyphenols, malondialdehyde, antioxidant

capacity, lactate dehydrogenase and toxic elements in human colostrum milk. Chemosphere 191, 548–554. https://doi.org/10.1016/j.chemosphere.2017.10.098.

Protano, C., Canepari, S., Astolfi, M.L., D'Onorio De Meo, S., Vitali, M., 2018. Urinary reference ranges and exposure profile for lithium among an Italian paediatric population. Sci. Total Environ. 619–620, 58–64. https://doi.org/10.1016/j.scitotenv.2017.11.090.

Protano, C., Astolfi, M.L., Canepari, S., Andreoli, R., Mutti, A., Valeriani, F., Romano Spica, V., Antonucci, A., Mattei, V., Martellucci, S., Vitali, M.., 2017. Exposure to individual and multiple carcinogenic metals during paediatric age: an experience from an Italian urban scenario. Ann. Ig. 29, 494–503. https://doi:10.7416/ai.2017.2180.

Protano, C., Astolfi, M.L., Canepari, S., Vitali, M., 2016. Urinary levels of trace elements among primary school-aged children from Italy: The contribution of smoking habits of family members. Sci. Total Environ. 557–558, 378–385. https://doi: 10.1016/j.scitotenv.2016.03.073.

Ramirez, G.B., Cruz, C.V., Pagulayan, O., Ostrea, E., Dalisay, C., 2000. The Tagum study I: analysis and clinical correlates of mercury in maternal and cord blood, breast milk, meconium and infants' hair. Pediatrics 106, 774–781. https://doi.org/10.1542/peds.106.4.774.

Rebelo, F. M., Caldas, E. D., 2016. Arsenic, lead, mercury and cadmium: Toxicity, levels in breast milk and the risks for breastfed infants. Environ. Res. 151, 671–688. https://doi.org/10.1016/j.envres.2016.08.027.

Rial, D., Vázquez, J.A., Murado, M.A., 2011. Effects of three heavy metals on the bacteria growth kinetics: a bivariate model for toxicological assessment. Appl. Microbiol. Biotechnol. 90, 1095–1109. https://doi.org/10.1007/s00253-011-3138-1.

Rossipal, E., Krachler, M., 1998. Pattern of trace elements in human milk during the course of lactation. Nutr. Res. 18, 11-24. https://doi.org/10.1016/S0271-5317(97)00196-6.

Saha, N., Mollah, M.Z.I., Alam, M.F., Rahman, M.S., 2016. Seasonal investigation of heavy metals in marine fishes captured from the Bay of Bengal and the implications for human health risk assessment. Food Control 70, 110–118. https://doi.org/10.1016/j.foodcont.2016.05.040.

Salim, A.B., Badawy, I.H., Kassem, S.S., 2011. Effect of lactic acid bacteria against heavy metals toxicity in rats. J. Am. Sci. 7, 264–274. https://doi.org/10.7537/marsjas070411.41.

Shahbazi, Y., Ahmadi, F., Fakhari, F., 2016. Voltammetric determination of Pb, Cd, Zn, Cu and Se in milk and dairy products collected from Iran: An emphasis on permissible limits and risk assessment of exposure to heavy metals. Food Chem. 192, 1060-1067. https://doi.org/10.1016/j.foodchem.2015.07.123.

Shaheen, N., Irfan, N.M., Khan, I.N., Islam, S., Islam, M.S., Ahmed, M.K., 2016. Presence of heavy metals in fruits and vegetables: Health risk implications in Bangladesh. Chemosphere 152, 431-438. https://doi.org/10.1016/j.chemosphere.2016.02.060.

Sharma, R.K., Agrawal. M., Marshall. F.M., 2007. Heavy metals contamination of soil and vegetables in suburban areas of Varanasi, India. Ecotoxicol. Environ. Saf. 66, 258–266. https://doi.org/10.1016/j.ecoenv.2005.11.007

Sharpe, M.E., Fryer, T.F., Smith, D.G., 1966. Identification of the Lactic Acid Bacteria. In: Gibbs, B.M., Skinner, F.A. (Eds.), Identification Method for Microbiologists Part A. Academic Press, London and New York, pp. 65–79.

Shrader-Frechette, K., 2012. Taking action on developmental toxicity: scientists' duties to protect children. Environ. Health 11, 61. https://doi.org/10.1186/1476-069X-11-61.

Solomon, G.M., Weiss, P.M., 2002. Chemical contaminants in breast milk: time trends and regional variability. Environ. Health Perspect. 110, A339–A347. https://doi.org/10.1289/ehp.021100339.

Sternowsky, H.J., Moser, B., Szadkowsky, D., 2002. Arsenic in breast milk during the first 3 months of lactation. Int. J. Hyg. Environ. Health 205, 405-409. https://doi.org/10.1078/1438-4639-00161.

Suturović, Z., Kravić, S., Milanović, S., Đurović, A., Brezo, T., 2014. Determination of heavy metals in milk and fermented milk products by potentiometric stripping analysis with constant inverse current in the analytical step. Food Chem. 155, 120–125. https://doi.org/10.1016/j.foodchem.2014.01.030.

Teemu, H., Seppo, S., Jussi, M., Raija, T., Kalle, L., 2008. Reversible surface binding of cadmium and lead by lactic acid and bifidobacteria. Int. J. Food Microbiol. 125, 170–175. https://doi.org/10.1016/j.ijfoodmicro.2008.03.041.

Trinder, M., Bisanz, J.E., Burton, J.P., Reid, G., 2015. Probiotic lactobacilli: a potential prophylactic treatment for reducing pesticide absorption in humans and wildlife. Benef. microbes 6, 841–847. https://doi.org/10.3920/BM2015.0022.

Turker, G., Ergen, K., Karakoc, Y., Arisoy, A.E., Barutcu, U.B., 2006. Concentrations of toxic metals and trace elements in the meconium of newborns from an industrial city. Biol. Neonate 89, 244–250. https://doi.org/10.1159/000089953.

Unuvar, E., Ahmadov, H., Kiziker, A.R., Aydemir, B., Toprak, S., Ulker ,V., Ark, C., 2007. Mercury levels in cord blood and meconium of healthy newborns and venous blood of their mothers: clinical, prospective cohort study. Sci. Total Environ. 374, 60–70. https://doi.org/10.1016/j.scitotenv.2006.11.043.

Urban, P., Kuthan, R., 2004. Application of probiotics in the xenobiotic detoxification therapy. Nukleonika 49, 43–45.

Ursinyova, M., Masanova, V., 2005. Cadmium, lead and mercury in human milk from Slovakia. Food Addit. Contam. 22, 579–589. https://doi.org/10.1080/02652030500135201.

U.S. EPA, 2011. Exposure Factors Handbook 2011 Edition (Final Report). U.S. Environmental Protection Agency, Washington, DC, EPA/600/R-09/052F.

Vacchina, V., Séby, F., Chekri, R., Verdeil, J., Dumont, J., Hulin, M., Sirot, V., Volatier, J.L., Serreau, R., Rousseau, A., Simon, T., Guérin T., 2017. Optimization and validation of the methods for the total mercury and methylmercury determination in breast milk. Talanta 167, 404–410. https://doi.org/10.1016/j.talanta.2017.02.046.

Valent, F., Mariuz, M., Bin, M., Little, D. A., Mazej, D., Tognin, V., Tratnik, J., McAfee A.J., Mulhern, M.S., Parpinel, M., Carrozzi, M., Horvat, M., Tamburlini, G., Barbone, F., 2013. Associations of prenatal mercury exposure from maternal fish consumption and polyunsaturated fatty acids with child neurodevelopment: a prospective cohort study in Italy. J. Epidemiol. 23, 360–370. https://doi.org/10.2188/jea.JE20120168.

Vieira, S., de Almeida, R., Holanda, I.B.B., Mussy, M.H., Galvao, R.C.F., Crispim, P.T.B., Dorea, J.G., Bastos, W.R., 2013. Total and methylmercury in hair and milk of mothers living in the city of

Porto Velho and in villages along the Rio Madeira, Amazon, Brazil. Int. J. Hyg. Environ. Health 216, 682–689. https://doi.org/10.1016/j.ijheh.2012.12.011.

WHO, 1991. Inorganic Mercury. Environmental Health Criteria 118. Geneva: International Programme on Chemical Safety, World Health Organization.

WHO, 2004. Guidelines for Drinking-Water Quality, 3rd ed. Recommendations vol. World Health Organization, Geneva.

WHO, 2006. WHO child growth standards based on length/height, weight and age. WHO multicentre growth reference study group, Acta Pædiatrica Suppl. 450, 76–85.

WHO, 2010. Children's exposure to mercury compounds. Geneva.

World Health Organization and International Atomic Energy Agency, 1989. Minor and trace elements in breast milk: report of a joint WHO/IAEA collaborative study, Geneva/Vienna. https://www.who.int/iris/handle/10665/39678.

Winiarska-Mieczan, A., 2014. Cadmium, lead, copper and zinc in breast milk in Poland. Biol. Trace Elem. Res. 157, 36–44. https://doi.org/10.1007/s12011-013-9870-x.

Yurdakök, K., 2015. Lead, mercury, and cadmium in breast milk. J. Pediatr. Neonat. Individual. Med. 4, e040223, 1–11. https://doi.org/10.7363/040223.

Zhai, Q., Wang, G., Zhao, J., Liu, X., Tian, F., Zhang, H., Chen, W., 2013. Protective effects of Lactobacillus plantarum CCFM8610 against acute cadmium toxicity in mice. Appl. Environ. Microbiol. 79, 1508–1515. https://doi.org/10.1128/AEM.03417-12.

Supplementary Material S1.

Table S1. Comparison of toxic element concentrations among colostrum (t0), transitional (t15), and mature milk samples (t30) for Control (t_C) and Experimental (t_E) groups.

t_C–t_E	Element[a]	Levene's test[b] for equality of variances		t-test[b] for equality of means						
		F (0.05; 1; N-2)	p[c]	t	df	p[d]	Mean difference	Standard error difference	95% confidence interval of the difference	
									Lower	Upper
t0–0	Cd	0.000	0.995	-0.763	25	0.452	-0.395	0.518	-1.46	0.667
	Hg	0.212	0.649	0.306	26	0.762	0.0940	0.308	-0.538	0.726
	Pb	3.00	0.095	0.041	27	0.967	0.0159	0.384	-0.772	0.804
t15–15	Cd	0.760	0.392	-1.80	24	0.085	-0.581	0.323	-1.25	0.0859
	Hg	3.271	0.082	-0.882	26	0.386	-0.299	0.339	-0.996	0.398
	Pb	0.014	0.908	-1.86	27	0.074	-0.738	0.397	-1.55	0.0778
t30–30	Cd	2.24	0.146	-0.762	26	0.453	-0.383	0.502	-1.41	0.648
	Hg	0.750	0.394	-0.670	26	0.509	-0.279	0.417	-1.14	0.577
	Pb	0.847	0.366	-0.787	26	0.438	-0.177	0.225	-0.640	0.285

[a] As was excluded from statistical analysis because the percentage of data points under the LOD was ≥ 30%.

[b] Results for the independent samples were related using assumed equal variances (p >0.05). The values from Levene's test (F) and t-test were obtained with k-1 (k = 2 designates the number of different groups containing the sampled cases) and N-k (N is the total sample size) degrees of freedom (df) at significance level $\alpha = 0.05$.

[c] p-value obtained using Levene's test.

[d] p-value obtained using t-test.

Supplementary Material S2.

Table S2. Comparison of Cd and Hg concentrations among infant stools obtained at three sampling time points from Control (t_C) and Experimental (t_E) groups.

t_C–t_E	Element[a]	Levene's test[a] for equality of variances		t-test[a] for equality of means						
		F (0.05; 1; N-2)	p[c]	t	df	p[d]	Mean difference	Standard error	95% confidence interval on the difference between the means	
									Lower	Upper
t0–0	Cd	4.97	0.035	1.28	25	0.215	0.0974	0.0764	-0.0604	0.255
	Hg	3.30	0.167	-0.549	27	0.621	-0.761	1.39	-5.18	3.66
t15–15	Cd	0.038	0.847	2.98	27	0.006	0.307	0.103	0.0953	0.519
	Hg	1.30	0.337	-1.29	27	0.287	-1.40	1.08	-4.83	2.04
t30–30	Cd	2.01	0.168	0.856	26	0.400	0.128	0.149	-0.180	0.436
	Hg	1.62	0.403	1.14	26	0.372	0.601	0.526	-1.66	2.86

[a] Results for the independent samples were related using assumed equal variances ($p > 0.05$) except for that obtained for Cd at t0. The values from Levene's test (F) and *t*-test were obtained with k-1 (k = 2 designates the number of different groups containing the sampled cases) and N-k (N is the total sample size) degrees of freedom (df) at significance level $\alpha = 0.05$.

[c] p-value obtained using Levene's test.

[d] p-value obtained using t-test.

Supplementary Material S3.

Table S3. Comparison of toxic element weekly intake between boys and girls at different different stages of lactation [colostrum (t0), transitional milk (t15), and mature milk (t30)].

t_{boys}–t_{girls}	Element	Weekly intake (µg/kg BW/week, mean ± SD)		t-test[a] for equality of means		
		Boys	Girls	t	df	p
t0–0	As	1.7 ± 2.9	0.99 ± 0.78	0.849	27	0.403
	Cd	1.1 ± 1.3	0.58 ± 0.54	1.17	25	0.252
	Hg[b]	1.2 ± 1.1	1.7 ± 2.9	1.98	26	0.0586
	Pb	8.2 ± 7.8	7.0 ± 7.6	0.435	27	0.667
t15–15	As	2.1 ± 3.5	1.5 ± 2.4	0.454	27	0.653
	Cd	0.42 ± 0.36	0.39 ± 0.20	0.198	24	0.844
	Hg[b]	0.46 ± 0.43	0.82 ± 0.66	1.73	26	0.0946
	Pb	6.8 ± 8.7	7 ± 12	0.0098	27	0.992
t30–30	As	1.3 ± 1.4	1.4 ± 1.3	0.0716	27	0.943
	Cd	0.45 ± 0.60	0.21 ± 0.12	1.31	26	0.201
	Hg[b]	0.58 ± 0.49	0.69 ± 0.45	0.580	26	0.567
	Pb	2.8 ± 1.3	2.0 ± 1.3	1.49	26	0.149

[a] Results obtained using a t-test (t) for independent samples were derived with k-1 (k = 2 designates the number of different groups containing the sampled cases) and N-k (N is the total sample size) degrees of freedom (df) at significance level α = 0.05.

[b] MeHg was not measured and was considered to represent 50% of the THg content present (Rebelo and Caldas, 2016).

There were no significant differences in mean weekly intake in boys and girls at different lactation stages ($p > 0.05$).

References S3.

Rebelo, F. M., Caldas, E. D., 2016. Arsenic, lead, mercury and cadmium: Toxicity, levels in breast milk and the risks for breastfed infants. Environ. Res. 151, 671–688. https://doi.org/10.1016/j.envres.2016.08.027.

3. Conclusions and Perspectives

The first part of this research concerned the study of the relationships between different PM-selected components and the generation of oxidative processes in biological organisms. Three different oxidative potential assays were used as an exposure metric in assessing long-term health effects. The reliability of the OP methods as proxies of the production of ROS and RNS was evaluated and relationships between the oxidative potential of PM and its capacity to induce oxidative stress in living organisms were individuated. In addition, to evaluate the potential of NO to restore the cellular balance between the ROS and the RNS, the knowledge on NO involvement in the rice root system development after exposure to Cd and/or As was deepened. In the second part of the study, human health and climate impact of airborne PM released by specific emission sources was assessed through size distribution analyses of particulate matter in urban and industrial areas, indoor environments and workplaces. The third part of the study regarded the application to field campaigns of innovative monitoring techniques, such as biomonitoring and high spatial resolution analyses of PM. A new experimental approach that allows to obtain spatially-resolved information about PM concentration and chemical composition was described. The last part of the study was focused on the evaluation of human exposure to toxic elements. The suitability of different biological matrixes for human biomonitoring exposure to environmental pollution was evaluated and rapid analytical methods for routine elemental analysis of a significant number of biological samples were developed and validated.

The application of the three OP methods showed that the DCFH and DTT assays are more sensitive to fine particles and organic substances, exhibiting higher levels of oxidative potential for PM-selected components in which organic carbon is the predominant species, while the AA method was found to be more sensitive towards coarse particles and metals. The analysis of $O_2^{\bullet-}$ and NO production and cell membrane oxidation in *A. thaliana* roots confirmed the different capacity of the examined PM components to induce oxidative stress and verified the reliability of the OP assays for the prediction of the oxidative stress induction in biological organisms. Brake dust, pellet ash and urban dust were identified as the PM-selected components with the highest potential inducing oxidative stress and root development alteration. Moreover, the ability of brake dust and pellet ash to induce a significant oxidative stress response in living organisms was confirmed by the tests performed on the animal model *Caenorhabditis elegans*, which revealed the severe impact of these dusts on the survival and life span of the nematodes. The OPs were found to be strongly linked to the chemical composition of the PM released by different emission sources and DCFH appeared to be

the method that better simulate the cellular ROS and RNS generation pathways. Overall, the application of the different OP methods to PM-selected components was found to be an efficient tool to simulate the *in vivo* generation of oxidative stress, although targeted studies would be needed to confirm its reliability for the prediction of the PM effects on human health.

The chemical/size fractionation approach appeared to be helpful in providing valuable information for PM source apportionment in urban and industrial areas. Furthermore, the study of the size distribution of PM was found to be effective for the assessment of the health impact of PM released in indoor environments and in workplaces. High PM concentrations were found in livestock farming activity, in municipal solid waste composting plant, and above all in waste electrical and electronic equipment treatment facility, thus showing an increase in probability of developing lung cancer for people working in these environments. Nanoparticles containing insoluble Cu were found to be released by brush electric motors in the indoor environments of private dwellings. Insoluble nanoparticles are deemed to be able to enter organisms and their dimensions are the same of those found in brain tissue samples by other authors who speculated their possible translocation to brain through olfactory bulb, thus being particularly harmful to human health.

The high spatial resolution analysis of PM in the wide and dense monitoring network across Terni allowed us to evaluate the reliability of the biomonitoring techniques for the assessment of atmospheric element concentrations and for the evaluation of the impact of PM anthropogenic emission sources. Lichen transplants appeared to be reliable for high spatial resolution measurements of PM_{10} elemental components released at high concentrations by intense local emission sources such as the steel plant (Co, Cr, Fe, Mn, Mo, Nb, Ni, Ti and W) and the rail network (Cu, Sb and Sn). Dry deposition on *A. donax* leaves was also found to be an efficient biomonitoring method for the assessment of atmospheric element concentrations released by the steel industry pole. The innovative monitoring techniques allowed us to overcome the limits connected to the study of PM dispersion through the use of mathematical models and the limits associated to the high cost of a monitoring network based on traditional PM samplers. The new experimental approach, based on the mapping of spatially-resolved PM chemical data, enabled us to trace the intensive urban and industrial PM sources in the whole area of the Terni basin. We identified reliable and selective source tracers for rail network and vehicular traffic (Ba_s, Bi_i, Cu_i, Sb_i, Sn_i, Zr_i), soil resuspension (Ce_i, Cs_i, La_i, Li_i, Rb_i, Sr_i, U_i), biomass burning (Cd_s, Cs_s, K_s, Rb_s, Tl_s, WSOC) and steel plant (As_s, Co_i, Cr_i, Cr_s, Ga_s, Li_s, Mo_s, Mn_i, Mn_s, Nb_i, Ni_i, Pb_i, W_s, Zn_s).

This kind of high spatial resolution chemical data also promises to be effective for the optimization and validation of dispersion models and is a powerful tool for a reliable geo-referenced assessment

of population exposure to PM air pollutants. In fact, the spatial mapping of PM chemical components, combined with on-site human biomonitoring, will allow further investigations on relationships between adverse outcomes for human health and PM chemical composition and sources, useful to plan the mitigation measures that are necessary to protect citizens health in the area of study. To this aim, in further researches, we will analyze the oxidative potential of PM samples collected in different urban and industrial areas, assess their ability to induce oxidative stress and harmful effects on living organisms and evaluate the related human health risks through on-site biomonitoring, using the methods developed and validated in this study.

AMA and CV-AFS techniques were found to be sensitive, precise and reliable for the quantification of Hg content in hair samples. The use of AMA may be preferable to CV-AFS for reduced sample handling and less expensive analysis, whereas the use of CV-AFS assures reduced times of analysis. The OD*95°C hair samples treatment for subsequent elemental determination by ICP-based techniques turned out to be a promising, faster and more affordable alternative to conventional acid digestion in a microwave oven. Therefore, it can be easily applied for the screening routine analysis of large batches of hair samples. The assessment of Hg As, Pb and Cd levels in breast milk provided valuable information on the maternal toxic load and can be used as an indicator for prenatal and post-natal exposure of infants to these chemicals. Toxic elements showed particularly high concentrations in colostrum; thus, during breastfeeding, substantial amounts of elements are transferred to the intestine of the newborn. A novel application of a specific probiotic formulation appeared to be useful for detoxification in humans and health protection of nursing mothers and their infants.

The examined rapid analytical methods for routine analysis of trace elements in body matrices will be used to identify indicators of exposure to environmental pollution. A human biomonitoring study, already approved by the Ethical Committee of Policlinico Umberto I, will be performed on healthy children (5-11 years old) living in Terni. PM exposure will be assessed by analyzing in urinary samples the same elements found in environmental PM and oxidative stress will be assessed by the measurement of known urinary markers, such as oxidized products of nucleic acids. The human biomonitoring study will provide new evidences about the relationship between PM exposure and oxidative stress, using a total-exposure assessment approach. Moreover, the spatially-resolved chemical and oxidative potential data achieved in Terni will be used in further source apportionment studies for the evaluation of the contribution of the local emission sources to the total PM_{10} and for the assessment of their health and environmental impact.

4. Appendix

4.1. (E) Efficiency Evaluation of Food Waste Materials for the Removal of Pollutants from Wastewater

During the PhD research, we evaluated the potential of food waste materials as low-cost adsorbents for the removal of toxic elements, heavy metals and volatile organic compounds (VOCs) from wastewater. Discharge of wastewater from industrial activities is a critical environmental problem worldwide since it releases effluents particularly rich in toxic and carcinogenic pollutants. In the last few years, low-cost biomaterials, with high specific surface areas, such as agricultural and food waste by-products, have been widely used for wastewater treatment. In different studies, removal efficiency of food waste materials has been assessed by performing adsorption experiments of various pollutants in heterogeneous operating conditions, consequently it is difficult to compare the efficiency of the individual adsorbents. Therefore, in this study, we evaluated the adsorption capacity of food waste materials by comparing the removal efficiency of elements and VOCs from complex solutions, maintaining homogeneous experimental conditions, which allowed us comparing the adsorption capacity of the individual sorbents.

4.1.1. (E1) Efficiency Evaluation of Food Waste Materials for the Removal of Metals and Metalloids from Complex Multi-Element Solutions

Materials (2018), *11*(3), 334

Lorenzo Massimi [a,*], Antonella Giuliano [a], Maria Luisa Astolfi [a], Rossana Congedo [b], Andrea Masotti [c], Silvia Canepari [a]

[a] Sapienza University of Rome, Department of Chemistry, Piazzale Aldo Moro, 5, 00185 Roma, Italy;
[b] Istituto di Istruzione Superiore "Quinto Ennio", Corso Roma, 100, 73014 Gallipoli, Italy;
[c] Children's Hospital Bambino Gesù - IRCCS, Research Laboratories, Viale San Paolo, 15, 00145 Rome, Italy.

Abstract: Recent studies have shown the potential of food waste materials as low cost adsorbents for the removal of heavy metals and toxic elements from wastewater. However, the adsorption experiments have been performed in heterogeneous conditions, consequently it is difficult to compare the efficiency of the individual adsorbents. In this study, the adsorption capacities of 12 food waste materials were evaluated by comparing the adsorbents' efficiency for the removal of 23 elements from complex multi-element solutions, maintaining homogeneous experimental conditions. The examined materials resulted to be extremely efficient for the adsorption of many elements from synthetic multi-element solutions as well as from a heavy metal wastewater. The 12 adsorbent surfaces were analyzed by Fourier transform infrared spectroscopy and showed different types and amounts of functional groups, which demonstrated to act as adsorption active sites for various elements. By multivariate statistical computations of the obtained data, the 12 food waste materials were grouped in five clusters characterized by different elements' removal efficiency which resulted to be in correlation with the specific adsorbents' chemical structures. Banana peel, watermelon peel and grape waste resulted the least selective and the most efficient food waste materials for the removal of most of the elements.

Keywords: low-cost materials; food waste adsorbents; biosorption; adsorption capacities; elements' removal efficiency; metals; heavy metal wastewater; environmental remediation; adsorbent surfaces; adsorbents' chemical structures.

1. Introduction

Today, excessive release of wastewater particularly rich in heavy metals from industrial activities is a critical environmental problem worldwide [1]. Many metals and metalloids, which are toxic and carcinogenic, can cause various dysfunctions to plants, animals and humans. Therefore, their removal from polluted solutions becomes one of the focuses of environmental remediation.

There are several physic-chemical methods to remove elements from wastewater such as adsorption, chemical precipitation, solvent extraction, reverse osmosis, ion exchange and chemical reduction [1–3]. Adsorption is recognized as an effective and economic method for the removal of metals and metalloids because it offers high efficiency and flexibility in operation [4].

Different materials with high specific surface areas such as activated carbons, resins and zeolites, have been widely used for wastewater treatment [2,5]. However, to minimize the cost of such materials and provide more efficiency for the removal of metals, alternative approaches have been developed using low cost materials such as agricultural waste by-products [2]. These include the use of modified clay [6,7], soil [8], seed powder [9], sugar cane bagasse [10], coffee and tea waste [11–15], neem bark [16] maize tassels [17], modified coconut fiber [18], coconut husk [19], rice husk [20], oil palm shell [21], fly ash, lime, agricultural ash and saw dust [22–24].

Among the low cost materials, food waste adsorbents compete favorably in terms of cost, efficiency and ease of operation [25]. Roughly one third of the food produced in the world for human consumption every year is wasted. Food waste amounts to roughly US $680 billion in industrialized countries and US $310 billion in developing countries. Fruits and vegetables, as well as roots and tubers have the highest wastage rates of any food [26]. Therefore, in the perspective of sustainable development, the identification of a possible alternative use of these food waste is important.

Recent studies have shown that banana peel [27], apple peel [28], eggplant peel [29], potato peel [30], orange peel [31], lemon peel [32,33], watermelon peel [34,35], tomato peel [36], coffee waste [11,15,37,38] decaf coffee waste, carob peel and grape waste [39,40] are efficient adsorbents for the removal of heavy metals and toxic elements from wastewater. However, the removal efficiency of food waste materials has been assessed by performing adsorption experiments in heterogeneous operating conditions. Consequently, it is difficult to compare the adsorption capacities of the individual food waste adsorbents. In fact, most existing studies are focused on the evaluation of the elements' removal efficiency from synthetic mono-element solutions to define the adsorption isotherms and to obtain the optimum removal values of single elements.

The aim of this study is to evaluate the adsorption capacities of 12 food waste materials (potato peel, lemon peel, orange peel, watermelon peel, tomato peel, coffee waste, apple peel, banana peel, decaf

coffee waste, eggplant peel, carob peel and grape waste), comparing their efficiency for the removal of 23 elements (for the most of whom the adsorption capacities have never been assessed) from multi-element solutions (at pH 2.0 and pH 5.5), in homogeneous experimental conditions.

The use of multi-element solutions does not allow the identification of the adsorption isotherms of the single elements and the determination of the interaction mechanism for the adsorption, which in part have already been defined in previous studies [11,15,27–40]. In fact, the competitiveness between the metals for the adsorbents' active sites precludes obtaining the optimum removal values of the single elements. However, the use of multi-element solutions enables to evaluate and compare the efficiency of the individual food waste materials for the removal of various elements from a more complex matrix, closer to a real one. In fact, another goal of the study is to verify the potential of the food waste adsorbents on a real complex polluted matrix such as a heavy metal wastewater.

The porous surface of the food waste materials is particularly suited to adsorb different elements. In addition, the adsorbent surfaces have various types and amounts of functional groups, which may act as selective adsorption active sites for metals and metalloids. Other objectives of the study are to cluster the food waste materials through multivariate statistical computations of their FTIR spectra and to highlight possible correlations between the elements' removal efficiency and the adsorbents' chemical structures.

2. Materials and Methods

2.1. Preparation of the Food Waste Adsorbents

Potato peel, lemon peel, orange peel, watermelon peel, tomato peel, coffee waste, apple peel, banana peel, decaf coffee waste, eggplant peel, carob peel and grape waste were sun-dried for a week, grinded with a mortar and then sieved to retain particles sized between 0.25 and 0.125 mm. The obtained powders were washed three times with deionized water produced by an integrate water purification system (Arioso UP 900; Industrial Scientific Corporation, Pittsburg, PA, USA) and dried at 55 °C for 48 h in a vacutherm oven (Heraeus VT 6025; Kendro Laboratory Products, Hanau, Germany). Finally, the powders were weighed on an analytical balance (Gibertini Europe 60; Gibertini Elettronica Srl, Milano, Italy) to obtain different amounts of each adsorbent: 25, 50, 100 and 200 mg.

2.2 Preparation of Aqueous Solutions and Synthetic Multi-Element Solutions

Aqueous solutions at pH 2.0 and pH 5.5 were prepared using deionized water, HNO_3 (LGC Promochem India Private Ltd, Bangalore, India) 1% and NaOH (Merck Millipore Ltd, Billerica, MA, USA) 5%. Synthetic multi-element solutions at pH 2.0 and pH 5.5, containing Ag, As, Ba, Cd, Ce,

Co, Cr, Cu, Fe, Ga, In, La, Mo, Ni, Pb, Sb, Sn, Th, Ti, U, V, W, and Zn at the concentration of 1 mg/Kg were prepared by mixing different aliquots of mono-element standard solutions (Exaxol Italia Chemical Manufacturers Srl, Genoa, Italy; Ultra Scientific, North Kingstown, RI, USA; Merck Millipore Ltd, Billerica, MA, USA) into 10 mL of aqueous solution. The pH of the solutions was controlled using a pH meter (Crison MicropH 2002, Crisonb Instruments, Barcelona, Spain) and adjusted using HNO_3 1% and NaOH 5%. After 24 h, the synthetic multi-element solutions were filtered using syringes with cryolite transparent membranes (diameter: 25 mm, pore size: 0.45 µm; Merck Millipore Ltd, Billerica, MA, USA) to remove possible formed precipitates and then analyzed by inductively coupled plasma mass spectrometry (ICP-MS; Bruker 820-MS; Bruker Instruments, Billerica, MA, USA) to identify the elemental fractions really dissolved in solution (C_i - initial concentration) before the adsorption processes.

2.3. Preparation of Wastewater

Wastewater produced in a hydro-metallurgical process for the recovery of valuable elements by electronic boards (WEEE - waste of electric and electronic equipment) was used to verify the efficiency of the 12 food waste adsorbents for the removal of heavy metals from a real polluted matrix. The wastewater was obtained after the acid leaching of electronic boards and the following removal of valuable elements through fractional precipitation of hydroxides. It is a very complex and variable matrix, and contains a high amount of salts as well as a high variable content of elements: Al < 100 µg/L; Ba = 318 µg/L; Cr = 146 µg/L; Cu = 377000 µg/L; Fe < 200 µg/L; Mn = 7730 µg/L; Ni = 233000 µg/L; Pb = 72100 µg/L; Sn < 20 µg/L; and Zn = 2650000 µg/L [41]. Before performing adsorption experiments, the wastewater was diluted 1:100 with deionized water to reduce the amount of the adsorbates and to avoid the saturation of the adsorption active sites by the more concentrated metals. The pH of the diluted wastewater was 5.5.

2.4. Characterization of the Food Waste Adsorbents

The powders of the 12 food waste materials were analyzed by scanning electron microscopy (SEM; LEO 1450 VP; Carl Zeiss, Oberkochen, Germany) to assess their superficial aspect and porosity and by Fourier transform infrared spectroscopy (FTIR; IR Affinity Miracle 10; Shimadzu Scientific Instruments, Columbia, MD, USA) to identify the types and the amounts of functional groups present on their adsorbent surfaces. The powders were fixed to a specific support and coated with a thin layer of platinum metal before SEM analysis to make them surfaces conductive. The IR spectra were recorded in the range of 5000–600 cm^{-1} with a resolution of 5.0 cm^{-1}.

2.5. Adsorption Experiments

Adsorption experiments were performed by treating each of the 12 food waste adsorbents with 10 mL of the synthetic multi-element solution (containing Ag, As, Ba, Cd, Ce, Co, Cr, Cu, Fe, Ga, In, La, Mo, Ni, Pb, Sb, Sn, Th, Ti, U, V, W, and Zn at the concentration of 1 ppm) under controlled pH conditions (at pH 2.0 and pH 5.5). Increasing amounts (25, 50, 100 and 200 mg) of each adsorbent were exposed, in different experiments, to the multi-element solutions (at pH 2.0 and pH 5.5). The pH of the solutions was controlled after the exposure of each adsorbent which may cause slight changes of pH. A final adsorption experiment was performed treating 200 mg of each of the 12 food waste adsorbents with 10 mL of the diluted wastewater (pH 5.5) produced in a hydro-metallurgical process. Before performing the adsorption experiments, solubility percentage of each element of the synthetic multi-element solution at different pH was verified (supplementary material S1).

At pH 2.0, elements' solubility percentages are very high (except for W), thus at these acidic conditions it is possible to quantify the adsorption of the elements obtaining good quality analytical data. At pH 5.5, As, Ce, Fe, Ga, La, Pb, Sn, Th, Tl and U form insoluble hydroxides; consequently, their initial concentration (C_i) is very low and it is not possible to accurately quantify their removal. Most of the considered elements completely precipitate at pH higher than 5.5; therefore, the adsorption experiments were not performed at basic conditions.

The aqueous solutions containing different food waste adsorbents (blanks) and the synthetic multi-element solutions with and without the adsorbents were magnetically stirred (New Variomag Electronicruhrer Telemodul; Thermo Fisher Scientific Inc., Waltham, MA, USA) at 25 ± 2 °C and 200 rpm for 24 h to ensure the achievement of the equilibrium between the adsorbates and the adsorbents. After 24 h, the samples were filtered using a glass filtering system with nitrocellulose membranes (diameter: 45 mm, pore size: 0.45 µm; Merck Millipore Ltd, Billerica, MA, USA), the pH of the solutions was controlled. All the adsorption experiments were performed in duplicate.

Finally, samples were analyzed by inductively coupled plasma mass spectrometry (ICP-MS; Bruker 820-MS; Bruker Instruments, Billerica, MA, USA). Blank values due to the elements' release from the adsorbent materials were also evaluated. Details about the used instrumental conditions are reported in Canepari et al. (2006) and Protano et al. (2016) [42,43].

2.6. Elements' Adsorption Percentages

The elements' adsorption percentages were calculated from the elemental fractions dissolved in the synthetic multi-element solution after 24 h from its preparation (after precipitation phenomena) and after its filtration (C_i - initial concentration). In this way, the precipitated fractions of the elements,

not available for the adsorption processes, were not considered as removed by the food waste materials.

For each food waste adsorbent, the elements' adsorption percentages were calculated by subtracting to the concentration of the elements dissolved in solution before the adsorption processes (C_i - initial concentration), the difference between the elemental fraction not removed by the food waste adsorbent (C_e - equilibrium concentration) and the elemental fraction released in solution by the adsorbent itself (b_v - blank value). This value was divided by the concentration of the element dissolved in the initial multi-element solution (C_i - initial concentration) and multiplied per 100:

$$\text{Adsorption \%} = [C_i - (C_e - b_v)] / C_i \times 100 \quad (1)$$

2.7. Statistical Analyses

Multivariate statistical computations were performed using the statistical software R (R-project for statistical computing, Ver. 3.0, 32-bit). A first principal component analysis (PCA) was calculated on the spectral data obtained by FTIR spectroscopy of the food waste adsorbents in order to group the 12 materials as a function of the type and amount of functional groups present on their surfaces. A standard normal variate (SNV) autoscaling was operated to the spectral data before performing the PCA to correct multiplicative variations between the spectra caused by variations in sample physical properties or in sample preparation and presentation. A second PCA was performed on the data obtained by the adsorption experiments to group the food waste materials according to the obtained elements' adsorption percentages.

3. Results and Discussion

3.1. SEM Micrographs

Different micrographs (Fig. 1), which show the aspect and the porosity of the 12 adsorbent surfaces, were obtained by scanning electron microscopy (SEM). From the micrographs obtained by SEM, we observed that potato peel's surface appeared composed by globular formations; tomato peel showed a layered and flat surface; banana peel and grape waste revealed fibrous and lamellar structures; and watermelon peel, coffee waste and decaf coffee waste possessed the most porous surfaces.

The 12 food waste materials showed various superficial structures characterized by peculiar conformations and different abundance, morphology and size of pores. Various grades of porosity correspond to different superficial specific areas available for adsorption processes. Therefore, from this first qualitative observation, we can suppose that the food waste materials with the most porous surfaces may be able to remove a higher amount of elements from polluted solutions.

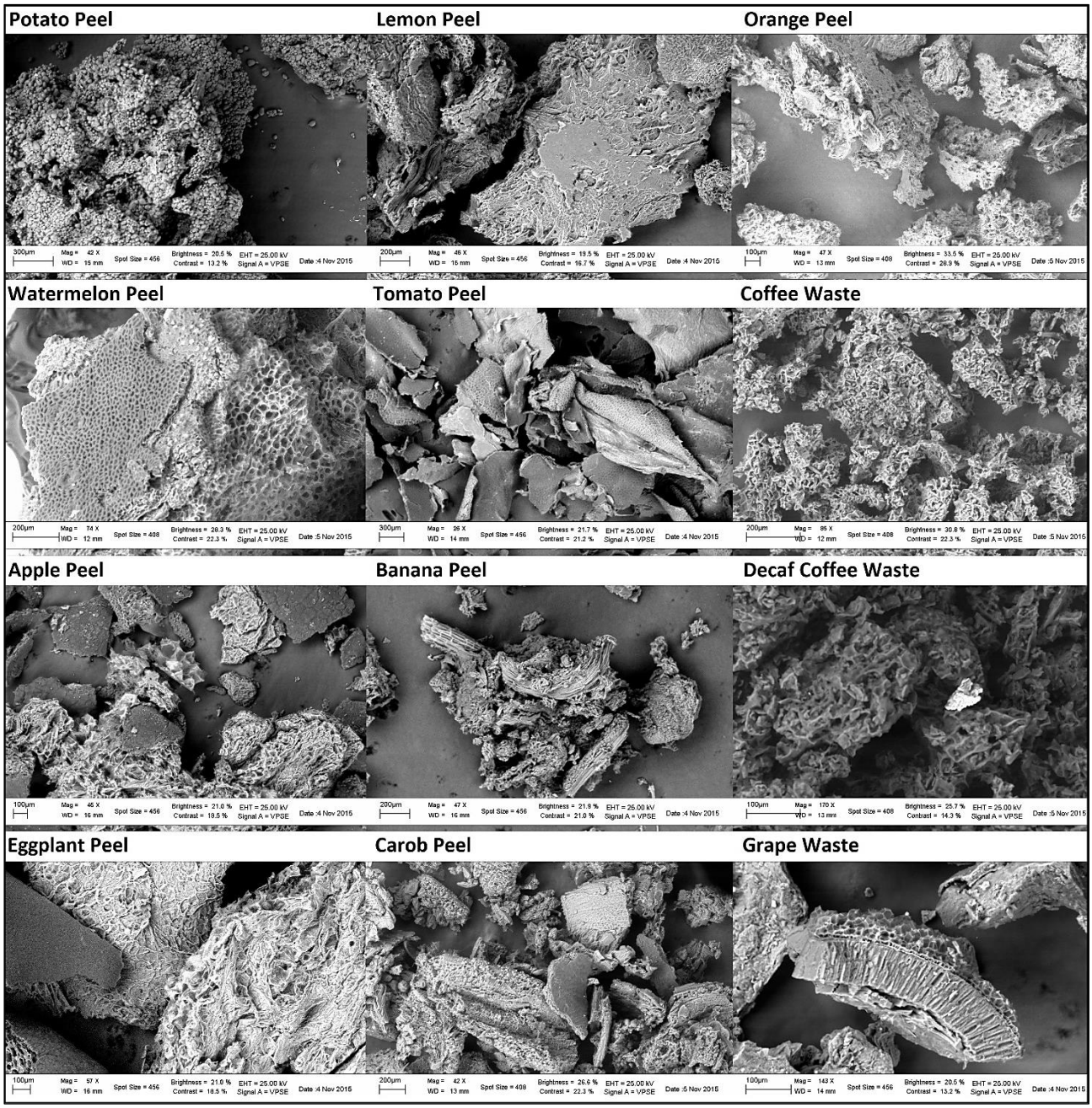

Fig. 1. Adsorbent surfaces′ micrographs (at 100, 200 and 300 μm) obtained by scanning electron microscopy (SEM).

3.2. FTIR Spectra

By Fourier transform infrared (FTIR) spectroscopy, functional groups present on the adsorbent surfaces were identified. The FTIR spectra of the 12 food waste materials in the range of 5000–600 cm^{-1} are shown in Fig. 2.

The broad band in the range of 3700 and 3000 cm^{-1} includes many vibrations modes corresponding to −OH of alcohols [44], phenols and carboxylic acids [36]. This region is greater in watermelon peel

and tomato peel spectra, whereas it appears reduced in eggplant peel and carob peel spectra. The two sharp bands at 2925 cm^{-1} and 2855 cm^{-1} belong to the C−H bonds of methyl and methylene groups of lipids [44]. These bands are more intense in banana peel, apple peel, coffee waste and decaf coffee waste spectra. The band at 1742 cm^{-1} corresponds to the C=O vibration in the carbonyl group of −COOH. The bands in the range of 1600−1400 cm^{-1} can be ascribed to C=C vibration of lipids, fatty acids and lignin moieties [36,44–47]. Fig. 2 shows that the bands from 1742 cm^{-1} to 1400 cm^{-1} are less intense in potato peel, carob peel and eggplant peel spectra. The region at 1400−900 cm^{-1} shows several types of vibrations including C−H, C−O−C, C−N and P−O of polysaccharides [44,48]. This region is greater in watermelon peel, tomato peel, lemon peel and orange peel spectra.

By the recorded FTIR spectra, similarities and differences of the chemical structures of the adsorbent surfaces were identified. Fig. 2 reveals that each food waste material has different functional groups which may act as selective active sites for metal and metalloid ions coordination.

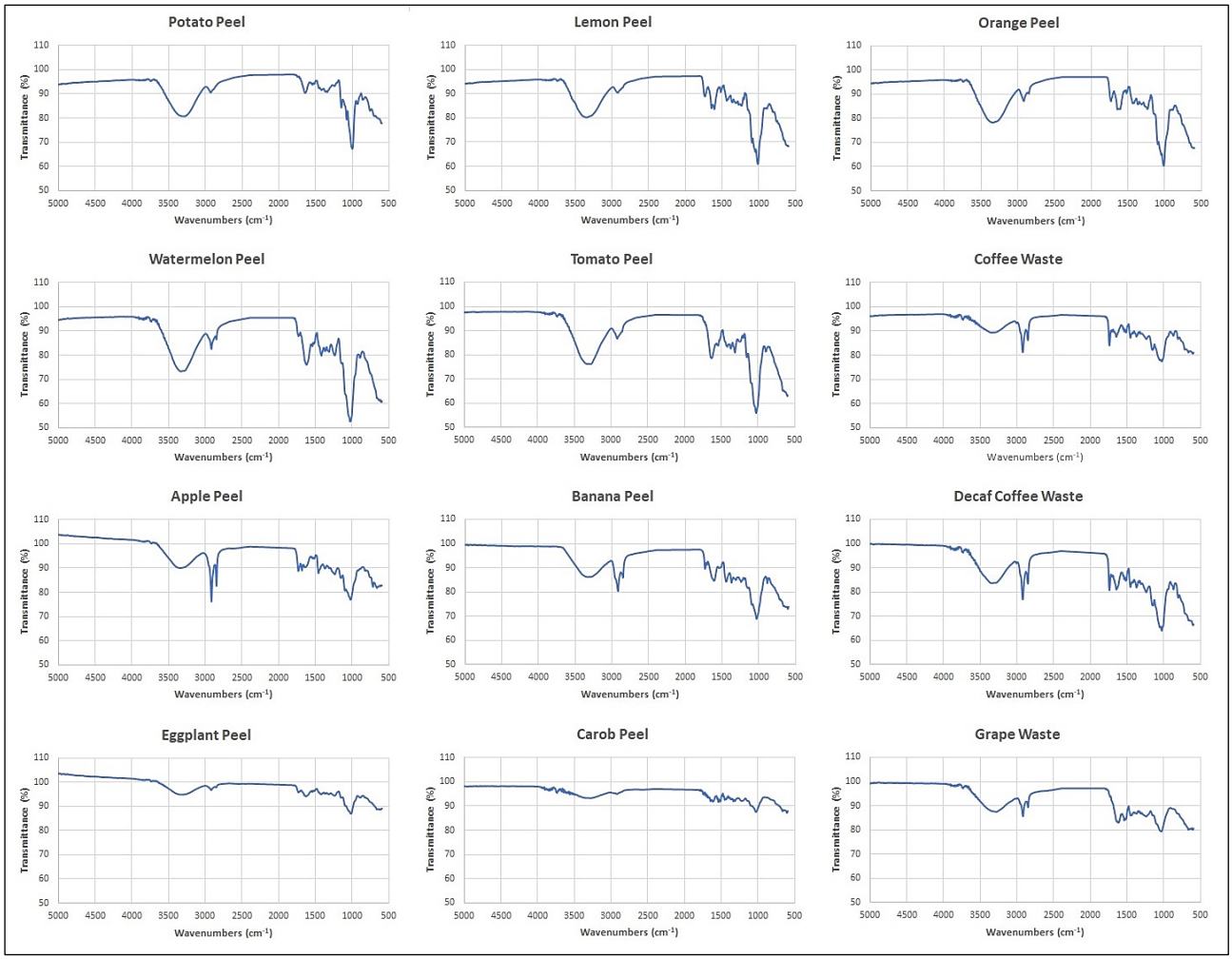

Fig. 2. Adsorbent′s FTIR spectra obtained by Fourier transform infrared spectroscopy (FTIR).

The spectral data obtained by FTIR spectroscopy were elaborated by performing multivariate statistical computations. Principal component analysis (PCA) of the spectral data allowed to group the food waste materials according to functional groups present on their adsorbent surfaces.

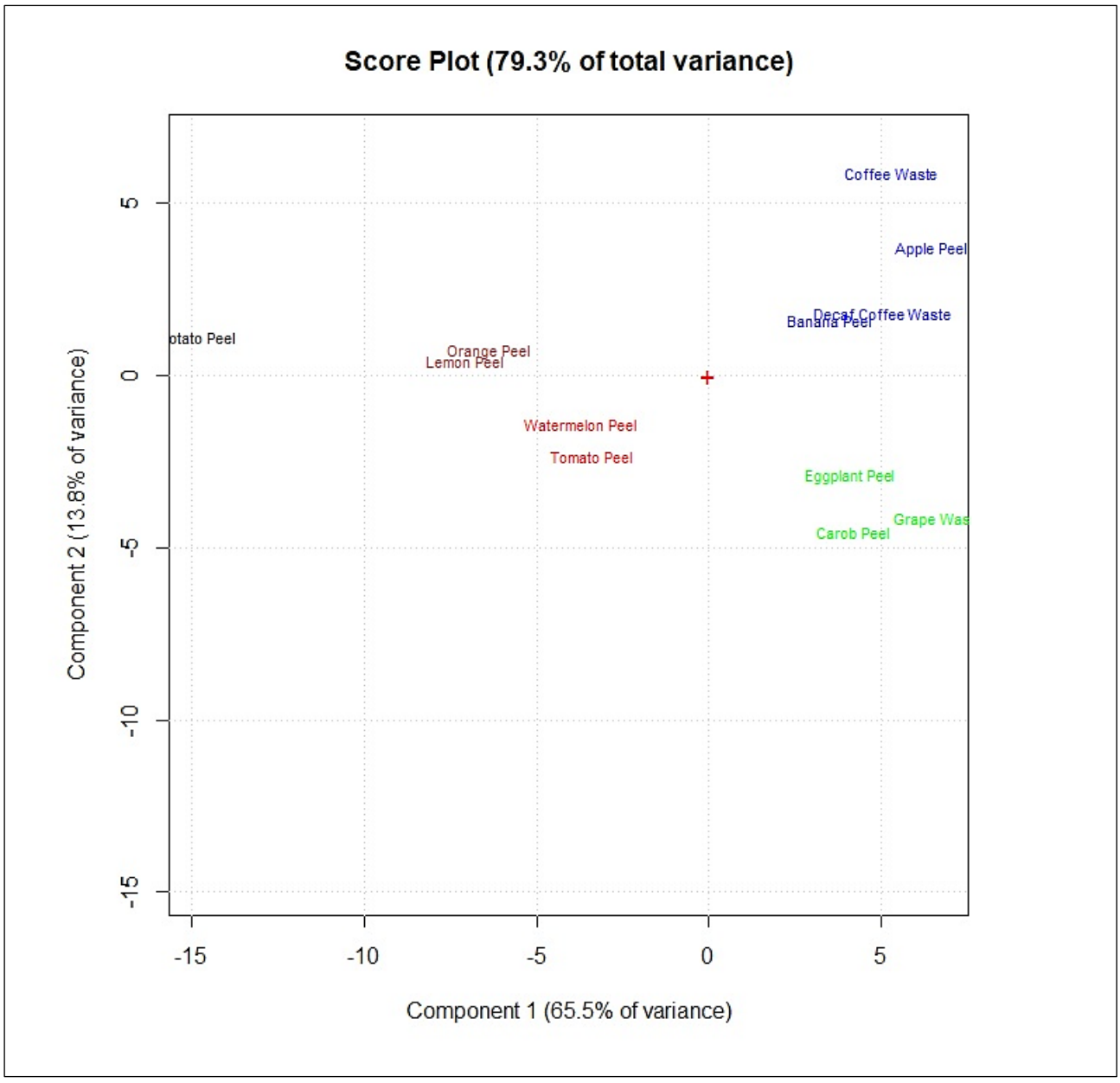

Fig. 3. Score plot of the principal component analysis performed on the obtained FTIR spectral data of the 12 food waste adsorbents.

3.3. Removal Efficiency of Food Waste Adsorbents from Synthetic Multi-element Solutions

Food waste materials are efficient adsorbents for the removal of many metals and metalloids from synthetic multi-element solutions at pH 2.0 and pH 5.5. Table 1 shows that the adsorption capacity

varies as a function of the pH and that each food waste adsorbent (200 mg) has a propensity to remove certain elements rather than others. At pH 5.5, As, Ce, Fe, Ga, La, Pb, Sn, Th, Tl, and U precipitate, thus it was not possible to quantify their removal.

At pH 2.0, some elements, such as Mo, Pb, Sb, Sn, Th, Ti and W, were adsorbed in high percentages by most of the food waste materials while others were removed in different percentages depending on the adsorbent exposed. For example, As was removed only by banana peel (adsorption percentages ~ 37%) and by carob peel, which was able to adsorb more than 75% of the As dissolved in solution. At pH 5.5, the food waste materials resulted less selective for the adsorption of Ag, Cd, Mo, V and Zn, which were removed in high percentages by most of the adsorbents. Decaf coffee waste, coffee waste, potato peel, apple peel, eggplant peel and carob peel resulted more efficient at pH 5.5 than at pH 2.0 for the removal of Ba, Cd, Ni, V and Zn, whereas orange peel appeared more efficient at pH 2.0. W was removed in higher percentages at pH 2.0 by all the adsorbents except watermelon peel. Orange peel and tomato peel removed in higher percentages Ag and Cu at pH 2.0, while coffee waste, decaf coffee waste, apple peel, eggplant peel and carob peel appeared more efficient for the removal of these elements at pH 5.5. Finally, orange peel adsorbed more than 85% of Zn at pH 2.0, whereas apple peel, carob peel, coffee waste and decaf coffee waste were able to remove more than 85% of Zn only at pH 5.5.

Banana peel, watermelon peel and grape waste resulted the most efficient adsorbents for the removal of most of the metals and metalloids from multi-element solutions at pH 2.0 as well as at pH 5.5. Elements' removal efficiency varies depending on the amount of adsorbent exposed in solution, as expected from the adsorption isotherms defined in previous studies [11,15,27–40].

Fig. 4 shows that, by increasing the amount of adsorbent (25, 50, 100 and 200 mg) in the multi-element solutions, the adsorption capacity of the food waste materials increases and the selectivity for the elements' removal decreases. In fact, metals and metalloids compete for certain active sites initially available in lower amounts on the adsorbent surfaces and completely occupied by the elements with the highest affinities. By doubling the amount of adsorbent, the removal percentages gradually increase because the higher availability of functional groups on the adsorbent surfaces progressively reduces the competitiveness between the elements.

In Fig. 4, we observe that the adsorption percentages of some elements (such as Ag, Ce, Mo, La and Pb for grape waste and Ag, La, Mo, U and W for coffee waste) are strictly correlated with the amount of adsorbent exposed. Mo, Sb, Sn and W were removed in high percentages just by 25 mg of grape waste and by 25 mg of coffee waste. These elements favorably competed in the adsorption processes, demonstrating higher affinities to certain functional groups of such food waste materials. Instead Ba,

Cd, Co, Ni and Zn were adsorbed in high percentages only by 200 mg of grape waste and watermelon peel which resulted the most efficient food waste adsorbents.

Table 1. Removal efficiency of the food waste adsorbents (200 mg) from multi-element synthetic solutions at pH 2.0 and pH 5.5.

	Potato Peel	Lemon Peel	Orange Peel	Watermel. Peel	Tomato Peel	Coffee Waste	Apple Peel	Banana Peel	Decaf C. Waste	Eggplant Peel	Carob Peel	Grape Waste
	Adsorption (%)						pH 2					
	m ± SD	m ± SD	m ± SD	m ± SD	m ± SD	m ± SD	m ± SD	m ± SD	m ± SD	m ± SD	m ± SD	m ± SD
Ag	71 ± 8	96 ± 2	99 ± 5	75 ± 6	100 ± 1	39 ± 9	34 ± 24	94 ± 2	47 ± 8	70 ± 3	55 ± 3	98 ± 1
As	< 10	< 10	< 10	< 10	< 10	< 10	< 10	37 ± 11	< 10	< 10	79 ± 2	< 10
Ba	18 ± 12	50 ± 6	92 ± 1	88 ± 2	71 ± 5	< 10	39 ± 17	80 ± 2	< 10	14 ± 4	20 ± 4	90 ± 3
Cd	17 ± 11	64 ± 4	92 ± 1	92 ± 1	66 ± 4	< 10	22 ± 5	88 ± 2	< 10	15 ± 5	14 ± 4	92 ± 2
Ce	24 ± 3	68 ± 1	100 ± 1	90 ± 1	38 ± 2	41 ± 6	59 ± 7	77 ± 1	15 ± 6	72 ± 2	42 ± 3	95 ± 1
Co	< 10	43 ± 6	43 ± 1	63 ± 5	32 ± 5	< 10	14 ± 2	46 ± 5	< 10	< 10	< 10	75 ± 7
Cr	< 10	15 ± 7	20 ± 2	28 ± 3	47 ± 3	< 10	34 ± 13	12 ± 2	14 ± 9	< 10	43 ± 10	66 ± 1
Cu	51 ± 8	75 ± 3	75 ± 1	< 10	62 ± 3	48 ± 6	49 ± 21	58 ± 1	43 ± 6	13 ± 1	60 ± 3	37 ± 1
Fe	42 ± 20	< 10	< 10	72 ± 11	38 ± 8	30 ± 19	13 ± 5	42 ± 2	11 ± 15	53 ± 13	40 ± 19	38 ± 1
Ga	31 ± 12	< 10	< 10	37 ± 3	29 ± 1	43 ± 5	40 ± 4	93 ± 1	41 ± 5	54 ± 4	36 ± 3	64 ± 2
In	73 ± 2	92 ± 1	76 ± 3	99 ± 1	55 ± 1	92 ± 2	92 ± 1	96 ± 1	87 ± 3	48 ± 1	89 ± 2	96 ± 1
La	15 ± 6	51 ± 1	75 ± 1	79 ± 1	37 ± 1	28 ± 7	40 ± 13	62 ± 1	33 ± 8	59 ± 1	22 ± 4	92 ± 1
Mo	94 ± 2	73 ± 2	87 ± 1	95 ± 5	88 ± 1	100 ± 1	99 ± 1	99 ± 1	100 ± 1	98 ± 1	99 ± 1	99 ± 1
Ni	< 10	49 ± 5	87 ± 1	82 ± 3	36 ± 5	< 10	< 10	71 ± 3	< 10	10 ± 3	10 ± 6	90 ± 3
Pb	77 ± 1	93 ± 1	< 10	99 ± 1	90 ± 1	29 ± 5	88 ± 1	97 ± 1	17 ± 3	95 ± 5	79 ± 1	95 ± 1
Sb	46 ± 5	25 ± 5	19 ± 5	43 ± 1	32 ± 8	81 ± 12	82 ± 11	88 ± 14	83 ± 12	72 ± 15	93 ± 14	70 ± 13
Sn	86 ± 13	66 ± 26	57 ± 27	91 ± 10	59 ± 14	99 ± 1	92 ± 8	97 ± 1	99 ± 1	92 ± 1	99 ± 1	97 ± 9
Th	96 ± 1	96 ± 1	< 10	96 ± 2	97 ± 1	98 ± 1	91 ± 5	98 ± 1	96 ± 1	97 ± 1	92 ± 1	95 ± 4
Ti	76 ± 6	61 ± 1	100 ± 1	77 ± 3	82 ± 1	99 ± 1	92 ± 4	99 ± 1	100 ± 1	98 ± 1	100 ± 1	99 ± 1
U	50 ± 7	45 ± 1	100 ± 1	72 ± 2	86 ± 1	44 ± 3	54 ± 7	88 ± 1	39 ± 3	82 ± 1	36 ± 4	91 ± 1
V	31 ± 12	13 ± 3	77 ± 1	64 ± 3	14 ± 9	15 ± 13	15 ± 1	75 ± 1	56 ± 9	26 ± 6	60 ± 3	85 ± 3
W	100 ± 5	67 ± 10	93 ± 14	67 ± 4	93 ± 3	100 ± 1	100 ± 2	100 ± 1	100 ± 1	100 ± 2	100 ± 1	99 ± 4
Zn	14 ± 12	55 ± 2	88 ± 2	86 ± 2	22 ± 5	< 10	13 ± 7	72 ± 3	< 10	< 10	< 10	85 ± 5
	Adsorption (%)						pH 5.5					
	m ± SD	m ± *SD*	m ± *SD*	m ± *SD*	m ± *SD*	m ± *SD*	m ± *SD*	m ± *SD*	m ± *SD*	m ± *SD*	m ± *SD*	m ± *SD*
Ag	94 ± 11	99 ± 3	< 10	99 ± 14	29 ± 1	98 ± 13	99 ± 34	96 ± 7	99 ± 11	99 ± 6	100 ± 4	75 ± 2
Ba	89 ± 12	93 ± 7	< 10	96 ± 2	97 ± 5	74 ± 13	99 ± 16	94 ± 10	78 ± 7	74 ± 8	92 ± 3	98 ± 2
Cd	90 ± 14	92 ± 12	12 ± 15	97 ± 11	79 ± 10	95 ± 7	95 ± 8	90 ± 8	95 ± 12	79 ± 8	94 ± 9	98 ± 9
Co	54 ± 10	45 ± 9	< 10	41 ± 9	41 ± 6	56 ± 9	44 ± 2	37 ± 4	51 ± 8	38 ± 3	78 ± 4	48 ± 8
Cr	< 10	15 ± 9	16 ± 10	23 ± 8	23 ± 5	< 10	18 ± 11	30 ± 2	< 10	29 ± 5	42 ± 9	11 ± 1
Cu	68 ± 18	78 ± 17	19 ± 5	92 ± 13	12 ± 8	95 ± 15	97 ± 28	77 ± 2	95 ± 9	85 ± 10	93 ± 8	86 ± 7
In	80 ± 4	72 ± 2	74 ± 5	86 ± 2	72 ± 1	66 ± 4	93 ± 2	98 ± 1	61 ± 4	52 ± 1	75 ± 5	96 ± 1
Mo	81 ± 5	80 ± 12	58 ± 7	94 ± 14	21 ± 2	93 ± 2	99 ± 10	95 ± 2	94 ± 1	97 ± 1	100 ± 2	74 ± 1
Ni	72 ± 11	85 ± 8	< 10	94 ± 7	57 ± 8	93 ± 9	94 ± 12	88 ± 3	92 ± 11	65 ± 2	89 ± 6	96 ± 6
Sb	26 ± 4	25 ± 6	< 10	32 ± 15	21 ± 8	52 ± 15	80 ± 16	86 ± 16	57 ± 14	52 ± 16	93 ± 15	< 10
V	82 ± 9	64 ± 3	11 ± 7	90 ± 14	55 ± 7	90 ± 12	99 ± 3	95 ± 11	91 ± 10	97 ± 9	100 ± 5	95 ± 5
W	25 ± 3	55 ± 26	71 ± 19	97 ± 15	< 10	20 ± 3	74 ± 2	< 10	35 ± 3	32 ± 4	99 ± 1	< 10
Zn	85 ± 9	90 ± 7	12 ± 19	95 ± 2	56 ± 10	90 ± 6	91 ± 8	79 ± 7	92 ± 15	37 ± 3	91 ± 9	96 ± 8

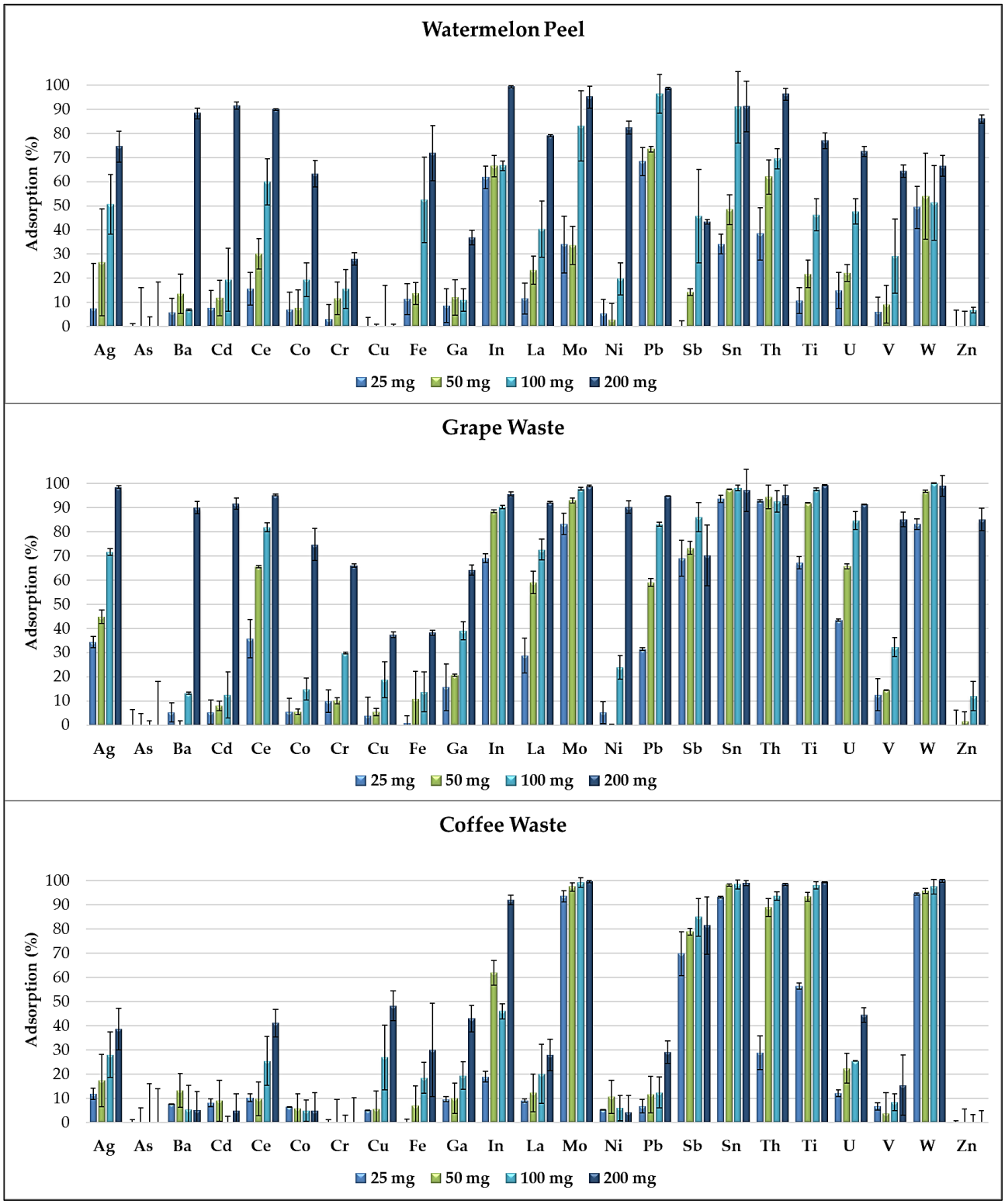

Fig. 4. Removal efficiency of watermelon peel, grape waste and coffee waste, exposed in increasing amounts (25, 50, 100 and 200 mg) to the multi-element solution at pH 2.0.

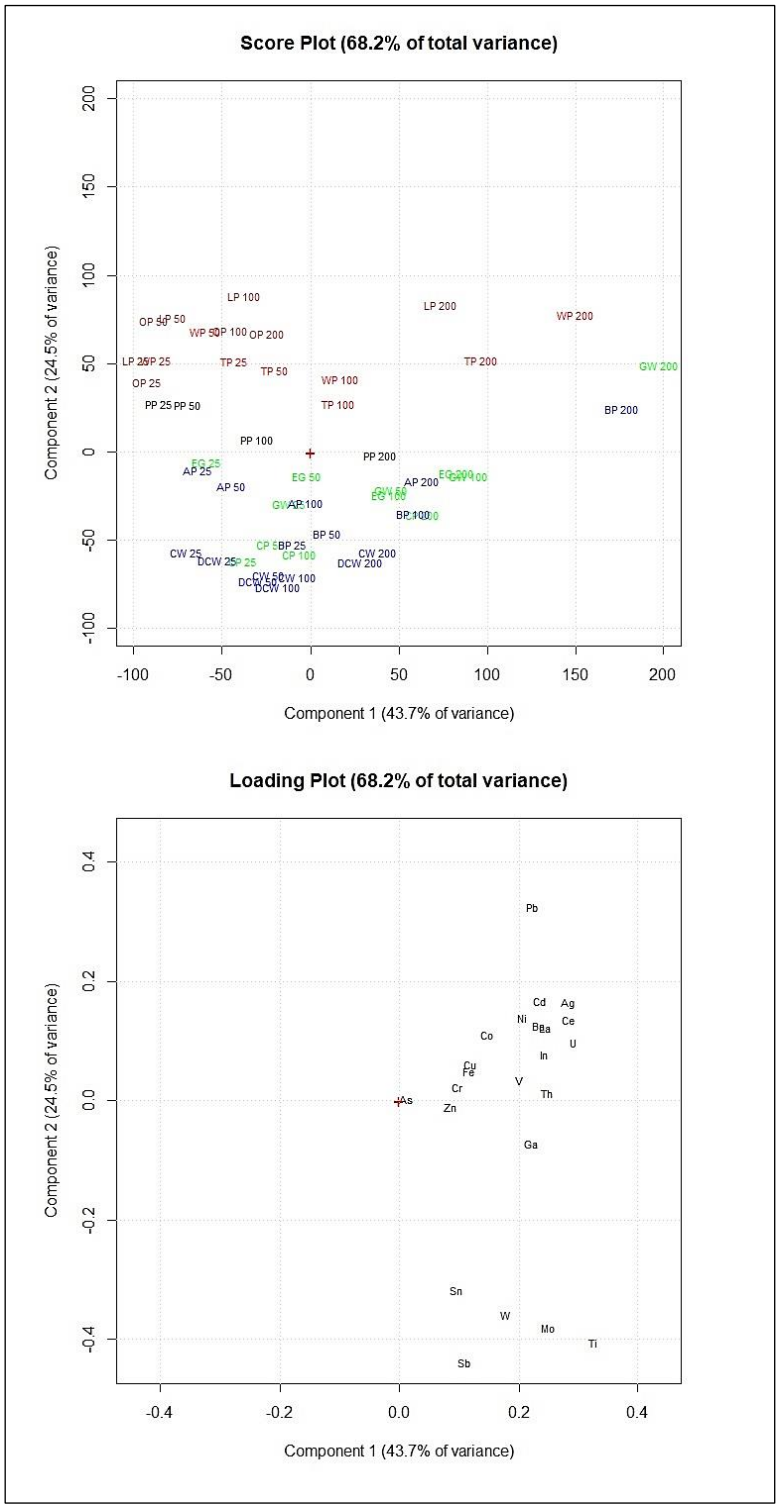

Fig. 5. Score plot and loading plot of the PCA performed on the data obtained by the adsorption experiments at pH 2.0. PP, potato peel; LP, lemon peel; OP, orange peel; WP, watermelon peel; TP, tomato peel; CW, coffee waste; AP, apple peel; BP, banana peel; DCW, decaf coffee waste; EG, eggplant peel; CP, carob peel; GW, grape waste; 25, 25 mg of adsorbent; 50, 50 mg of adsorbent; 100, 100 mg of adsorbent; 200, 200 mg of adsorbent.

Standard deviations of the results obtained by the adsorption experiments (performed in duplicate) are all under 25%.

Each food waste material showed a propensity to remove certain elements rather than others depending on the functional groups present on its adsorbent surface.

Principal component analysis of the data obtained by the adsorption experiments allowed clustering the food waste materials according to their elements' adsorption percentages. Fig. 5 shows the removal efficiency of the 12 food waste adsorbents, exposed in increasing amounts (25, 50, 100 and 200 mg) to the multi-element solution at pH 2.0.

Fig. 5 shows that coffee waste and decaf coffee waste have similar elements' removal efficiency as well as lemon peel and orange peel which are in the same part of the score plot. Sb, Sn, Mo, W and Ti (on the bottom part of the loading plot) were removed in high percentages by coffee waste and decaf coffee waste (on the bottom part of the score plot). Lemon peel, orange peel, watermelon peel and tomato peel (on the top of the score plot) showed lower adsorption percentages of these elements but appeared more efficient for the removal of the other metals and metalloids (Cr, Th, V, Fe, Cu, Co, In, U, Ba, La, Ni, Ce, Cd, Ag and Pb). Fig. 5 shows that increasing the amount of adsorbent exposed, the elements' removal efficiency considerably increased only for lemon peel, tomato peel, watermelon peel, grape waste and banana peel.

Comparing these results with the results obtained by the multivariate statistical analyses of the FTIR spectra allowed to highlight the potential correlations between the adsorbents' efficiency and their specific chemical structures. The adsorbents in Fig. 5 are marked in the same colors used in Fig. 3 to graphically correlate the removal efficiency of the food waste materials with the chemical structures of the adsorbent surfaces. The adsorbents of the red and brown clusters (watermelon peel, tomato peel, lemon peel and orange peel), which showed the highest amounts of −OH of alcohols, phenols and carboxylic acids, of C−H, C−O−C, C−N and P−O of polysaccharides and of C=C of lipids and lignin moieties, resulted more efficient for the removal of Cr, Th, V, Fe, Cu, Co, In, U, Ba, La, Ni, Ce, Cd, Ag and Pb. Instead, the adsorbents of the blue and green clusters (banana peel, apple peel, coffee waste, decaf coffee waste, grape waste, eggplant peel and carob peel), which appeared with lower amounts of these functional groups, showed higher adsorption capacities of As, Zn, Ga, Sb, Sn, Mo, W and Ti.

Therefore from the statistical elaboration of the obtained results we can suppose that the elements above the loading plot's center of Fig. 5 (Cr, Th, V, Fe, Cu, Co, In, U, Ba, La, Ni, Ce, Cd, Ag and Pb), which were removed in higher percentages by watermelon peel, tomato peel, orange peel and lemon peel, have higher affinities to −OH of alcohol groups and C−H, C−O−C, C−N and P−O of

polysaccharides than the elements below the loading plot's center (As, Zn, Ga, Sb, Sn, Mo, W and Ti).

3.4. Elements' Removal Efficiency of Food Waste Adsorbents in Wastewater

The removal efficiency of the food waste adsorbents was verified on a real polluted matrix assessing the adsorption of heavy metals from the heavy metal wastewater produced in a hydro-metallurgical process.

Fig. 6 shows that the 12 food waste materials can be efficiently used for the removal of heavy metals from real wastewater. Each adsorbent showed different removal efficiency. Coffee waste and decaf coffee waste resulted the most efficient for the removal of Cu, watermelon peel for Pb and grape waste for Ni and Zn. Standard deviations of the results obtained by the adsorption experiments from the heavy metal wastewater (performed in duplicate) are under 20%.

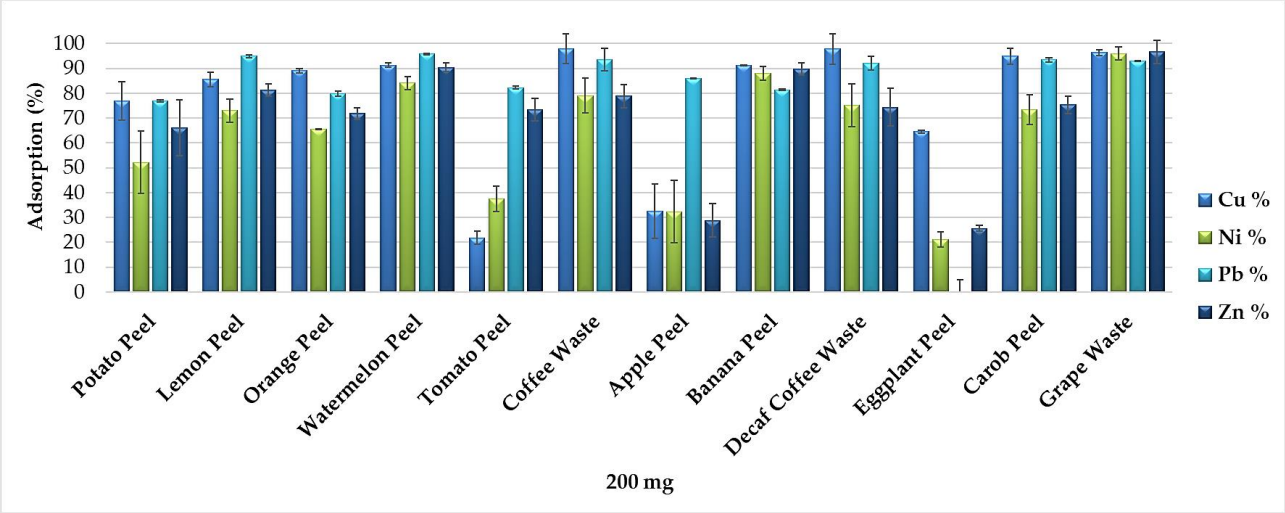

Fig. 6. Removal efficiency of the 12 food waste adsorbents (200 mg) from the heavy metal wastewater produced in a hydro-metallurgical process (pH 5.5).

These data confirm the results obtained by the adsorption experiments performed in synthetic multi-element solutions. However, food waste materials resulted less selective for the removal of metals and metalloids from the wastewater because of the lower competitiveness of the four heavy metals for the more available active sites of the adsorbent surfaces. On the other hand, banana peel, watermelon peel and grape waste resulted the most efficient and the least selective food waste adsorbents for the elements' removal from the heavy metal wastewater as well as from the synthetic multi-element solutions. Although the use of multi-element solutions does not allow the individuation

of the optimum elements' removal values, it enables evaluating and comparing the efficiency of the individual food waste adsorbents for the removal of various elements from a matrix close to a real one.

4. Conclusions

Many food waste materials used as low cost adsorbent for the treatment of wastewater were reported in the past. This work was aimed to evaluate the adsorption capacities of most of the studied food waste materials comparing their efficiency for the removal of more than 20 elements from complex multi-element solutions, in homogeneous experimental conditions.

The pH selected for adsorption experiments were pH 2.0 and pH 5.5. The latter pH value is just before the pH-zone of 5.5–8.0, where precipitation phenomena dominates. Elements' removal efficiency was evaluated from complex multi-element solutions to assess the potential of the food waste materials in industrial applications.

Maintaining homogeneous experimental conditions offered the possibility to evaluate and compare the adsorption capacities of 12 food waste materials.

Banana peel, watermelon peel and grape waste resulted the most efficient and the least selective adsorbents for the removal of most of the metals and metalloids from multi-element solutions (at pH 2.0 and pH 5.5) as well as from heavy metal wastewater.

The adsorbent surfaces were analyzed by FTIR spectroscopy and showed different types and amounts of functional groups, which demonstrated to act as adsorption active sites for various elements. The 12 food waste materials were grouped, through multivariate statistical computations of the FTIR spectra, into five different clusters, depending on the functional groups present on their adsorbent surfaces.

By comparing these results with those obtained by the multivariate statistical analyses of the elements' removal percentages, it was possible to highlight the potential correlations between the adsorbents' efficiency and their specific chemical structures.

Acknowledgements

The work was partially founded by Sapienza University of Rome. The authors gratefully thank Massimiliana Pietrantonio (ENEA Casaccia Research Centre) for her support in the FTIR spectroscopy analysis.

Author Contributions

L. Massimi is the principal investigator and wrote the paper; L. Massimi, A. Gargiulo, R. Congedo, A. Masotti and S. Canepari conceived and planned the experiments; R. Congedo prepared the food waste adsorbents; L. Massimi and A. Giuliano performed the experiments and analyzed the data; L. Massimi, A. Giuliano and M.L. Astolfi performed the chemical analysis; A. Masotti and S. Canepari revised a previous version of the manuscript; and S. Canepari coordinated the group.

Conflicts of Interest

The authors declare no conflicts of interest.

References

1. Fu, F.; Wang, Q. Removal of heavy metal ions from wastewaters: A review. *J. Environ. Manage.* 2011, *92*, 407–418, doi.org/10.1016/j.jenvman.2010.11.011.

2. Hegazi, H.A. Removal of heavy metals from wastewater using agricultural and industrial wastes as adsorbents. *HBRC J.* 2013, *9*, 276–282, doi:10.1016/j.hbrcj.2013.08.004.

3. Owlad, M.; Aroua, M.K.; Daud, W.A.W.; Baroutian, S. Removal of hexavalent chromium-contaminated water and wastewater: A review. *Water Air Soil Pollut.* 2009, *200*, 59–77, doi:10.1007/s11270-008.

4. Kamar, F.H.; Craciun, M.E.; Nechifor, A.C. Heavy metals: Sources, health effects, environmental effects, removal methods and natural adsorbent material as low-cost adsorbent: Short review. *Int. J. Sci. Technol. Res.* 2014, *3*, 2974–2979.

5. Aggarwal, D.; Goyal, M.; Bansal, R.C. Adsorption of chromium by activated carbon from aqueous solution. *Carbon* 1999, *37*, 1989–1997, doi:10.1016/S0008-6223(99)00072-X.

6. Singh, S.P.; Ma, L.Q.; Harris, W.G. Heavy metal interactions with phosphatic clay. *J. Environ. Qual.* 2001, *30*, 1961–1968, doi:10.2134/jeq2001.196.

7. Stathi, P.; Litina, K.; Gournis, D.; Giannopoulos, T.S.; Deligiannakis, Y. Physicochemical study of novel organoclays as heavy metal ion adsorbents for environmental remediation. *J. Colloid Interface Sci.* 2007, *316*, 298–309, doi:10.1016/j.jcis.2007.07.078.

8. Covelo, E.F.; Vega, F.A.; Andrade, M.L. Heavy metal adsorption and desorption by a Eutric Regosol and a District Regosol. *Geophys. Res. Abstr.* 2006, *8*, 04553.

9. Mataka, L.M.; Henry, E.M.T.; Masamba, W.R.L.; Sajidu, S.M. Lead remediation of contaminated water using *Moringa Stenopetala* and *Moringa oleifera* seed powder. *Int. J. Environ. Sci. Technol.* 2006, *3*, 131–139, doi:10.1007/BF03325916.

10. Mohan, D.; Singh, K.P. Single-and multi-component adsorption of cadmium and zinc using activated carbon derived from bagasse—an agricultural waste. *Water Res.* 2002, *36*, 2304–2318, doi:10.1016/S0043-1354(01)00447-X.

11. Tan, W.T. Copper (II) adsorption by waste tea leaves and coffee powder. *Pertanika* 1985, *8*, 223–230.

12. Tee, T.W.; Khan, A.R.M. Removal of lead, cadmium and zinc by waste tea leaves. *Environ. Technol.* 1988, *9*, 1223–1232, doi:10.1080/09593338809384685.

13. Minamisawa, M.; Minamisawa, H.; Yoshida, S.; Takai, N. Adsorption behavior of heavy metals on biomaterials. *J. Agric. Food. Chem.* 2004, *52*, 5606–5611, doi:10.1021/jf0496402.

14. Ahluwalia, S.S.; Goyal, D. Removal of heavy metals by waste tea leaves from aqueous solution. *Eng. Life Sci.* 2005, *5*, 158–162, doi:10.1002/elsc.200420066.

15. Agwaramgbo, L.; Lathan, N.; Edwards, S.; Nunez, S. Assessing lead removal from contaminated water using solid biomaterials: Charcoal, coffee, tea, fishbone, and caffeine. *J. Environ. Prot.* 2013, *4*, 741, doi:10.4236/jep.2013.47085.

16. Ayub, S.; Ali, S.I.; Khan, N.A. Efficiency evaluation of neem (*Azadirachta indica*) bark in treatment of industrial wastewater. *Environ. Pollut. Control J.* 2001, *4*, 34–38.

17. Zvinowanda, C.M.; Okonkwo, J.O.; Shabalala, P.N.; Agyei, N.M. A novel adsorbent for heavy metal remediation in aqueous environments. *Int. J. Environ. Sci. Technol.* 2009, *6*, 425–434, doi:10.1007/BF03326081.

18. Igwe, J.C.; Abia, A.A.; Ibeh, C.A. Adsorption kinetics and intraparticulate diffusivities of Hg, As and Pb ions on unmodified and thiolated coconut fiber. *Int. J. Environ. Sci. Technol* 2008, *5*, 83–92, doi:10.1007/BF03326000.

19. Tan, W.T.; Ooi, S.T.; Lee, C.K. Removal of chromium (VI) from solution by coconut husk and palm pressed fibres. *Environ. Technol.* 1993, *14*, 277–282, doi:10.1080/09593339309385290.

20. Srinivasan, K.; Balasubramanian, N.; Ramakrishna, T.V. Studies on chromium removal by rice husk carbon. *Indian J. Environ. Health* 1988, *30*, 376–387.

21. Khan, N.A.; Shaaban, M.G.; Hassan, M.A. Removal of heavy metal using an inexpensive adsorbent. In Proceedings of UM Research Seminar, University of Malaya, Kuala Lumpur, Malaysia, 11–12 March 1988; pp. 1–5.

22. Ajmal, M.; Rao, R.A.; K.; Siddiqui, B.A. Studies on removal and recovery of Cr (VI) from electroplating wastes. *Water Res.* 1996, *30*, 1478–1482, doi:10.1016/0043-1354(95)00301-0.

23. Xirokostas, N.; Korkolis, A.; Diamantopoulou, L.; Moutsatsou, A. Characterisation of metal retention agents and study of their application in liquid wastes. *Global Nest: Int. J.* 2003, *5*, 29–37.

24. Aliabadi, M.; Morshedzadeh, K.; Soheyli, H. Removal of hexavalent chromium from aqueous solution by lignocellulosic solid wastes. *Int. J. Environ. Sci. Technol.* 2006, *3*, 321–325, doi:10.1007/BF03325940.

25. Mohammed, M.A.; Shitu, A.; Tadda, M.A.; Ngabura, M. Utilization of various agricultural waste materials in the treatment of industrial wastewater containing heavy metals: A Review. *Int. Res. J. Environ. Sci.* 2014, *3*, 62–71.

26. Gustafsson, J.; Cederberg, C.; Sonesson, U.; Emanuelsson, A. The methodology of the FAO study: Global Food Losses and Food Waste-extent, causes and prevention" - FAO, 2011. Available online: http://www.diva-portal.org/smash/get/diva2:944159/FULLTEXT01.pdf (accessed on 23 February 2018).

27. Castro, R.S.; Caetano, L.; Ferreira, G.; Padilha, P.M.; Saeki, M.J.; Zara, L.F.; Martines, M.A.U.; Castro, G.R. Banana peel applied to the solid phase extraction of copper and lead from river water: preconcentration of metal ions with a fruit waste. *Ind. Eng. Chem. Res.* 2011, *50*, 3446–3451, doi:10.1021/ie101499e.

28. Mallampati, R.; Valiyaveettil, S. Apple peels - A versatile biomass for water purification? *ACS Appl. Mater. Interfaces* 2013, *5*, 4443–4449, doi:10.1021/am400901e.

29. Ibrahim, T. H.; Babar, Z. B.; Khamis, M. I. Removal of Lead (II) Ions from Aqueous Solution Using Eggplant Peels Activated Charcoal. *Sep. Sci. Technol.* 2015, *50*, 91–98, doi:10.1080/01496395.2014.948558.

30. Aman, T.; Kazi, A.A.; Sabri, M.U.; Bano, Q. Potato peels as solid waste for the removal of heavy metal copper (II) from waste water/industrial effluent. *Colloids Surf., B* 2008, *63*, 116–121, doi:10.1016/j.colsurfb.2007.11.013

31. Ugbe, F.A.; Pam, A.A.; Ikudayisi, A.V. Thermodynamic properties of chromium (III) ion adsorption by sweet orange (*Citrus sinensis*) peels. *Am. J. Anal. Chem.* 2014, *5*, 666, doi:10.4236/ajac.2014.510074.

32. Razafsha, A.; Ziarati, P. Removal of Heavy Metals from *Oryza sativa* Rice by Sour Lemon Peel as Bio-sorbent. *Biomed. Pharmacol. J.* 2016, *9*, 543–553, doi:10.13005/bpj/971

33. Arslanoglu, H.; Altundogan, H.S.; Tumen, F. Heavy metals binding properties of esterified lemon. *J. Hazard. Mater.* 2009, *164*, 1406–1413, doi:10.1016/j.jhazmat.2008.09.054

34. Lakshmipathy, R.; Sarada, N.C. Application of watermelon rind as sorbent for removal of nickel and cobalt from aqueous solution. *Int. J. Miner. Process.* 2013, *122*, 63–65, doi:10.1016/j.minpro.2013.03.002

35. Lakshmipathy, R.; Vinod, A.V.; Sarada, N.C. Watermelon rind as biosorbent for removal of Cd^{2+} from aqueous solution: FTIR, EDX, and Kinetic studies. *J. Indian Chem. Soc.* 2013, *90*, 1147–1154.

36. Mallampati, R.; Valiyaveettil, S. Application of tomato peel as an efficient adsorbent for water purification—alternative biotechnology? *RSC Adv.* 2012, *2*, 9914–9920, doi:10.1039/c2ra21108d.

37. Kyzas, G.Z. Commercial coffee wastes as materials for adsorption of heavy metals from aqueous solutions. *Materials* 2012, *5*, 1826–1840, doi:10.3390/ma5101826.

38. Kyzas, G.Z.; Bikiaris, D.N.; Kostoglou, M.; Lazaridis, N.K. Copper removal from aqueous systems with coffee wastes as low-cost materials. *E3S Web of Conferences* 2013, *1*, 25004, doi:10.1051/e3sconf/20130125004.

39. Polat, S.; Putun, E.; Kilic, M.; Putun, A.E. Biosorption of Cu (II) from aqueous solution by grape waste: Equilibrium, Kinetics and Thermodynamics. *J. Selcuk Univ. Nat. Appl. Sci.* 2013, 108–119.

40. Dwyer, K., Hosseinian, F.; Rod, M. The market potential of grape waste alternatives. *J. Food Res.* 2014, *3*, 91, doi:10.5539/jfr.v3n2p91.

41. Canepari, S.; Astolfi, M.L.; Marconi, E.; Farao, C. Caratterizzazione del refluo prodotto nel processo idrometallurgico per il recupero di elementi pregiati da schede elettroniche (RAEE) sviluppato da ENEA. Available online: http://www.enea.it/it/Ricerca_sviluppo/documenti/ricerca-di-sistema-elettrico/risparmio-energia-settore-civile/2014/rds-par2014-041.pdf (accessed on 23 February 2018)

42. Canepari, S.; Cardarelli, E.; Giuliano, A.; Pietrodangelo, A. Determination of metals, metalloids and non-volatile ions in airborne particulate matter by a new two-step sequential leaching procedure: Part A: Experimental design and optimisation. *Talanta* 2006, *69*, 581–587, doi:10.1016/j.talanta.2005.10.023.

43. Protano, C.; Astolfi, M.L.; Canepari, S.; Vitali, M. Urinary levels of trace elements among primary school-aged children from Italy: The contribution of smoking habits of family members. *Sci. Total Environ.* 2016, *557*, 378–385, doi:10.1016/j.scitotenv.2016.03.073.

44. Pujol, D.; Liu, C.; Gominho, J.; Olivella, M.À.; Fiol, N.; Villaescusa, I.; Pereira, H. The chemical composition of exhausted coffee waste. *Ind. Crops Prod.* 2013, *50*, 423–429, doi: 10.1016/j.indcrop.2013.07.056.

45. Lyman, D.J.; Benck, R.; Dell, S.; Merle, S.; Murray-Wijelath, J. FTIR-ATR analysis of brewed coffee: effect of roasting conditions. *J. Agric. Food. Chem.* 2003, *51*, 3268–3272, doi: 10.1021/jf0209793.

46. Kemsley, E.K.; Ruault, S.; Wilson, R.H. Discrimination between *Coffea arabica* and *Coffea canephora* variant robusta beans using infrared spectroscopy. *Food. Chem.* 1995, *54*, 321–326, doi:10.1016/0308-8146(95)00030-M.

47. Wang, N.; Lim, L.T. Fourier transform infrared and physicochemical analyses of roasted coffee. *J. Agric. Food. Chem.* 2012, *60*, 5446–5453, doi:10.1021/jf300348e.

48. Haussard, M.; Gaballah, I.; Kanari, N.; De Donato, P.; Barrès, O.; Villieras, F. Separation of hydrocarbons and lipid from water using treated bark. *Water Res.* 2003, *37*, 362–374, doi:10.1016/S0043-1354(02)00269-5.

Supplementary Material S1.

Before performing the adsorption experiments, solubility percentage of each element of the synthetic multi-element solution at different pH was verified. The solubility curves of all the elements were calculated at the experimental condition.

Synthetic multi-element solutions at different pH, containing Ag, As, Ba, Cd, Ce, Co, Cr, Cu, Fe, Ga, In, La, Mo, Ni, Pb, Sb, Sn, Th, Ti, U, V, W, Zn at the concentration of 1 mg/Kg were prepared by mixing different aliquots of mono-element standard solutions (Exaxol Italia Chemical Manufacturers Srl, Genoa, Italy; Ultra Scientific, North Kingstown, RI, USA; Merck Millipore Ltd, Billerica, MA, USA) into 10 mL of aqueous solution. The pH of the solutions was adjusted using HNO3 (LGC Promochem India Private Ltd, Bangalore, India) 1% and NaOH (Merck Millipore Ltd, Billerica, MA, USA) 5% and controlled using a pH meter (Crison MicropH 2002; Crison Instruments, Barcelona, Spain). After 24 hours, the synthetic multi-element solutions were filtered using syringes with cryolite transparent membranes (diameter: 25 mm, pore size: 0.45 µm; Merck Millipore Ltd, Billerica, MA, USA) to remove possible formed precipitates and then analyzed by inductively coupled plasma mass spectrometry (ICP-MS; Bruker 820-MS; Bruker Instruments, Billerica, MA, USA) to identify the elemental fractions really dissolved in solution (Ci – initial concentration) before the adsorption processes. From pH 2.1 to pH 4, elements' solubility percentages are very high (except for W), thus at these acidic conditions it is possible to quantify the adsorption of the elements obtaining good quality analytical data. From pH 5.7, As, Ce, Fe, Ga, La, Pb, Sn, Th, Tl and U form insoluble hydroxides; consequently, their initial concentration (Ci) is very low and it is not possible to accurately quantify their removal. Most of the considered elements completely precipitate at pH higher than 5.7; therefore the adsorption experiments were not performed at basic conditions.

The elements' adsorption percentages were calculated from the elemental fractions dissolved in the synthetic multi-element solution after 24 hours from its preparation (after precipitation phenomena) and after its filtration (Ci – initial concentration). In this way the precipitated fractions of the elements, not available for the adsorption processes, were not considered as removed by the food waste materials.

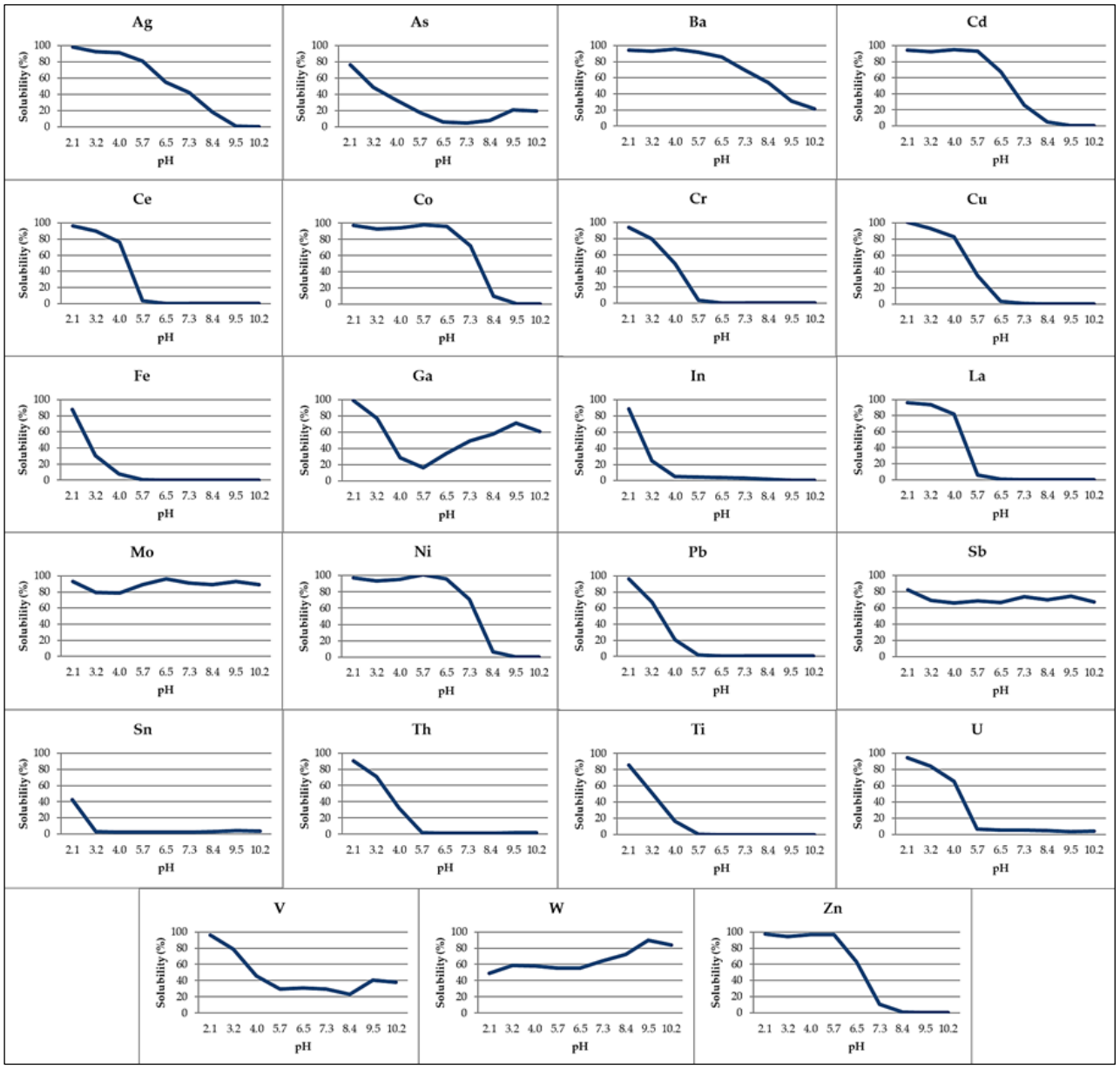

Fig. S1. Removal efficiency of the 12 food waste adsorbents (200 mg) from the heavy metal wastewater produced in a hydro-metallurgical process (pH 5.5).

4.1.2. (E2) Food Waste Materials Appear Efficient and Low-Cost Adsorbents for the Removal of Organic and Inorganic Pollutants from Wastewater

Research & Development in Material Science (2018), *5*(2), 1-3

Maria Agostina Frezzini [a], Antonella Giuliano [a], Joshua Treacy [b], Silvia Canepari [a], Lorenzo Massimi [a,*]

[a] Sapienza University of Rome, Department of Chemistry, Piazzale Aldo Moro, 5, 00185 Rome, Italy;
[b] DIT, Dublin Institute of Technology, School of Chemistry & Pharmaceutical Sciences, Kevin Street, Dublin 2, Dublin, Ireland.

1. Opinion

Excessive release of organic and inorganic pollutants, due to urbanization and industrialization is a critical environmental problem worldwide [1]. In fact, discharge of wastewater from industrial activities releases effluents particularly rich in toxic and carcinogenic pollutants. In the last few years, environmental remediation was focused on the use of low cost adsorbents for the removal of metals and metalloids from wastewater.

There are several physic-chemical methods to remove elements from wastewater (chemical precipitation, solvent extraction, reverse osmosis, adsorption, ion exchange and chemical reduction) [1–2]. Adsorption is recognized as an effective and economic method because it offers high efficiency and flexibility in operation [3]. The adsorption phenomenon, in which the transfer of matter is provided from a gas, liquid or dissolved solid phase (adsorbate) to a solid biological adsorbent surface (biosorbent) in contact with it, can be called: “biosorption”.

Different biomaterials with high specific surface areas like activated carbons, resins and zeolites have been widely used for heavy metal wastewater treatment. However, to minimize the cost, alternative approaches have been developed using low cost materials such as agricultural waste by-products [4]. These include the use of modified clay [5-6], soil [7], seed powder [8], sugar cane bagasse [9], coffee and tea waste [10–11], neem bark [12] maize tassels [13], modified coconut fiber [14], coconut husk [15], rice husk [16], oil palm shell [17], fly ash, lime, agricultural ash and saw dust [18–19].

Among these low-cost materials, food waste adsorbents compete favourably in terms of cost, efficiency and ease of operation [20]. Moreover, with the aim of sustainable development, recycling food waste, which amounts to US $680 billion in industrialized countries and US $310 billion in developing countries [21], is beneficial. Food waste adsorbents do not require modification reaction like other materials used in adsorption processes [22]; technical applicability and cost advantages are two key factors for the selection of food waste as low-cost adsorbents for treating wastewater.

In recent studies, the adsorption capacity of several food waste materials (banana peel [22], apple peel [23], eggplant peel [24], potato peel [25], orange peel [26], lemon peel [27-28], watermelon peel [29-30], tomato peel [31], coffee waste [10-11-32-33] decaf coffee waste, carob peel and grape waste [34-35]) has been assessed by performing adsorption experiments in heterogeneous operating conditions.

Fig. 1. Food waste materials' processing [36].

In a latest study [37], the efficiency of such food waste materials for the removal of metals and metalloids from complex multi-element solutions was evaluated in homogeneous experimental conditions, which allowed to compare the adsorption capacities of the individual adsorbents. The pH selected for the adsorption experiments were pH 2.0 and pH 5.5. The removal efficiency of the food waste adsorbents was also verified on a real polluted matrix; coffee waste and decaf coffee waste resulted the most efficient food waste adsorbents for the removal of Cu, watermelon peel for Pb and grape waste for Ni and Zn. This data confirmed the results obtained by the adsorption experiments performed in synthetic multi-element solutions. Banana peel, watermelon peel and grape waste resulted the most efficient and the least selective adsorbents for the removal of most of the metals and metalloids. Furthermore, the adsorbent surfaces of the food waste materials were analysed by FTIR spectroscopy and showed different types and amounts of functional groups, which demonstrated to act as adsorption active sites for various elements [37].

Considering the high efficiency of the examined low-cost adsorbents for the removal of inorganic pollutants, preliminary studies were conducted in our lab for assessing the potential of the

investigated food waste materials to adsorb volatile organic compounds from a real polluted matrix of leachate. Some recent studies have shown the efficiency of low cost materials for the removal of industrial organic dyes [38-33-39], polycyclic aromatic hydrocarbons [40] and phenolic compounds [41]. However, the food waste adsorbents' efficiency for the removal of volatile organic compounds was not investigated.

Our preliminary studies showed good adsorption capacities of the examined food waste materials for aliphatic and aromatic hydrocarbons. Therefore, it is worth to carry out further studies about volatile organic compounds' removal by food waste adsorbents.

References

1. Fu, F., & Wang, Q. (2011). Removal of heavy metal ions from wastewaters: a review. *Journal of environmental management*, *92*(3), 407-418.

2. Owlad, M., Aroua, M. K., Daud, W. A. W., & Baroutian, S. (2009). Removal of hexavalent chromium-contaminated water and wastewater: a review. *Water, Air, and Soil Pollution*, *200*(1-4), 59-77.

3. Kamar, F. H., Craciun, M. E., & Nechifor, A. C. (2014). Heavy metals: sources, health effects, environmental effects, removal methods and natura l adsorbent material as low-cost adsorbent: short review. Int JScientifi c Engineer Technol Res, 3, 2974-2979.

4. Hegazi, H. A. (2013). Removal of heavy metals from wastewater using agricultural and industrial wastes as adsorbents. *HBRC Journal*, *9*(3), 276-282.

5. Singh, S. P., Ma, L. Q., & Harris, W. G. (2001). Heavy metal interactions with phosphatic clay. *Journal of Environmental Quality*, *30*(6), 1961-1968.

6. Stathi, P., Litina, K., Gournis, D., Giannopoulos, T. S., & Deligiannakis, Y. (2007). Physicochemical study of novel organoclays as heavy metal ion adsorbents for environmental remediation. *Journal of colloid and interface science*, *316*(2), 298-309.

7. Covelo, E. F., Vega, F. A., & Andrade, M. L. (2006). Heavy metal adsorption and desorption by a Eutric Regosol and a District Regosol. In *Geophysical Research Abstracts* (Vol. 8, p. 04553).

8. Mataka, L. M., Henry, E. M. T., Masamba, W. R. L., & Sajidu, S. M. (2006). Lead remediation of contaminated water using Moringa Stenopetala and Moringa oleifera seed powder. *International Journal of Environmental Science & Technology*, *3*(2), 131-139.

9. Mohan, D., & Singh, K. P. (2002). Single-and multi-component adsorption of cadmium and zinc using activated carbon derived from bagasse—an agricultural waste. *Water research*, *36*(9), 2304-2318.

10. Tan, W. T. (1985). Copper (II) adsorption by waste tea leaves and coffee powder. Pertanika 1985, 8, 223–230.

11. Agwaramgbo, L., Lathan, N., Edwards, S., & Nunez, S. (2013). Assessing lead removal from contaminated water using solid biomaterials: Charcoal, coffee, tea, fishbone, and caffeine. *Journal of Environmental Protection*, *4*(07), 741.

12. Ayub, S.; Ali, S.I.; Khan, N.A. Efficiency evaluation of neem (Azadirachta indica) bark in treatment of industrial wastewater. Environ. Pollut. Control J. 2001, 4, 34–38.

13. Zvinowanda, C.M.; Okonkwo, J.O.; Shabalala, P.N.; Agyei, N.M. A novel adsorbent for heavy metal remediation in aqueous environments. Int. J. Environ. Sci. Technol. 2009, 6, 425–434.

14. Igwe, J.C.; Abia, A.A.; Ibeh, C.A. Adsorption kinetics and intraparticulate diffusivities of Hg, As and Pb ions on unmodified and thiolated coconut fiber. Int. J. Environ. Sci. Technol. 2008, 5, 83–92.

15. Tan, W.T.; Ooi, S.T.; Lee, C.K. Removal of chromium (VI) from solution by coconut husk and palm pressed fibres. Environ. Technol. 1993, 14, 277–282.

16. Srinivasan, K.; Balasubramanian, N.; Ramakrishna, T.V. Studies on chromium removal by rice husk carbon. Indian J. Environ. Health 1988, 30, 376–387.

17. Khan, N.A.; Shaaban, M.G.; Hassan, M.A. Removal of heavy metal using an inexpensive adsorbent. Proceedings of UM Research Seminar, University of Malaya, Kuala Lumpur, Malaysia, 11–12 March 1988; pp. 1–5.

18. Ajmal, M.; Rao, R.A.K.; Siddiqui, B.A. Studies on removal and recovery of Cr (VI) from electroplating wastes. Water Res. 1996, 30, 1478–1482.

19. Aliabadi, M., Morshedzadeh, K., & Soheyli, H. (2006). Removal of hexavalent chromium from aqueous solution by lignocellulosic solid wastes. *International Journal of Environmental Science & Technology*, *3*(3), 321-325.

20. Mohammed, M. A., Shitu, A., Tadda, M. A., & Ngabura, M. (2014). Utilization of various Agricultural waste materials in the treatment of Industrial wastewater containing Heavy metals: A Review. *International Research Journal of Environmental Science*, *3*(3), 62-71.

21. Gustafsson, J., Cederberg, C., Sonesson, U., & Emanuelsson, A. (2013). The methodology of the FAO study: Global Food Losses and Food Waste-extent, causes and prevention" -FAO, 2011.

22. Castro, R. S., Caetano, L., Ferreira, G., Padilha, P. M., Saeki, M. J., Zara, L. F., ... & Castro, G. R. (2011). Banana peel applied to the solid phase extraction of copper and lead from river water: preconcentration of metal ions with a fruit waste. *Industrial & Engineering Chemistry Research*, *50*(6), 3446-3451.

23. Mallampati, R., & Valiyaveettil, S. (2013). Apple Peels: A Versatile Biomass for Water Purification?. *ACS applied materials & interfaces*, *5*(10), 4443-4449.

24. Ibrahim, T. H., Babar, Z. B., & Khamis, M. I. (2015). Removal of Lead (II) Ions from Aqueous Solution Using Eggplant Peels Activated Charcoal. *Separation Science and Technology*, *50*(1), 91-98.

25. Aman, T., Kazi, A. A., Sabri, M. U., & Bano, Q. (2008). Potato peels as solid waste for the removal of heavy metal copper (II) from waste water/industrial effluent. Colloids and Surfaces B: Biointerfaces, 63(1), 116-121.

26. Ugbe, F. A., Pam, A. A., & Ikudayisi, A. V. (2014). Thermodynamic properties of chromium (III) ion adsorption by sweet orange (Citrus sinensis) peels. *American Journal of Analytical Chemistry*, *5*(10), 666.

27. Razafsha, A., & Ziarati, P. (2016). Removal of Heavy Metals from Oryza sativa Rice by Sour Lemon Peel as Bio-sorbent. *Biomedical and Pharmacology Journal*, *9*(2), 543-553.

28. Arslanoglu, H., Altundogan, H. S., & Tumen, F. (2009). Heavy metals binding properties of esterified lemon. *Journal of hazardous materials*, *164*(2-3), 1406-1413.

29. Lakshmipathy, R., & Sarada, N. C. (2013). Application of watermelon rind as sorbent for removal of nickel and cobalt from aqueous solution. *International Journal of Mineral Processing*, *122*, 63-65.

30. Lakshmipathy, R., Vinod, A. V., & Sarada, N. C. (2013). Watermelon rind as biosorbent for removal of Cd2+ from aqueous solution: FTIR, EDX, and Kinetic studies. *J Indian Chem Soc*, *90*, 1147-1154.

31. Mallampati, R., & Valiyaveettil, S. (2012). Application of tomato peel as an efficient adsorbent for water purification—alternative biotechnology?. *RSC Advances*, *2*(26), 9914-9920.

32. Kyzas, G. Z. (2012). Commercial coffee wastes as materials for adsorption of heavy metals from aqueous solutions. *Materials*, *5*(10), 1826-1840.

33. Kyzas, G. Z., Bikiaris, D. N., Kostoglou, M., & Lazaridis, N. K. (2013, January). Copper removal from aqueous systems with coffee wastes as low-cost materials. In *E3S Web of Conferences* (Vol. 1). EDP Sciences.

34. Polat, S., Putun, E., Kilic, M., & Putun, A. E. (2013). Biosorption of Cu (II) from aqueous solution by grape waste: Equilibrium, Kinetics and Thermodynamics. *Journal of Selcuk University Natural and Applied Science*, 108-119.

35. Dwyer, K., Hosseinian, F., & Rod, M. (2014). The market potential of grape waste alternatives. *Journal of Food Research*, *3*(2), 91.

36. Climate Change. North American Initiative on Food Waste Reduction and Recovery: http://www.cec.org/our-work/projects/north-american-initiative-food-waste-reduction-and-recovery.

37. Massimi, L., Giuliano, A., Astolfi, M. L., Congedo, R., Masotti, A., & Canepari, S. (2018). Efficiency Evaluation of Food Waste Materials for the Removal of Metals and Metalloids from Complex Multi-Element Solutions. *Materials*, *11*(3), 334.

38. Ali, I., Asim, M., & Khan, T. A. (2012). Low cost adsorbents for the removal of organic pollutants from wastewater. *Journal of environmental management*, *113*, 170-183.

39. Crini, G. (2006). Non-conventional low-cost adsorbents for dye removal: a review. *Bioresource technology*, *97*(9), 1061-1085.

40. Crisafully, R., Milhome, M. A. L., Cavalcante, R. M., Silveira, E. R., De Keukeleire, D., & Nascimento, R. F. (2008). Removal of some polycyclic aromatic hydrocarbons from petrochemical wastewater using low-cost adsorbents of natural origin. *Bioresource technology*, *99*(10), 4515-4519.

41. Ahmaruzzaman, M. (2008). Adsorption of phenolic compounds on low-cost adsorbents: a review. *Advances in colloid and interface science*, *143*(1-2), 48-67.

4.1.3. (E3) Food Waste Materials as Low-Cost Adsorbents for the Removal of Volatile Organic Compounds from Wastewater

Materials (2019), *12*(24), 4242

Maria Agostina Frezzini [a], Lorenzo Massimi [a], Maria Luisa Astolfi [a], Silvia Canepari [a], Antonella Giuliano [a,*]

[a] Department of Chemistry, Sapienza University of Rome, Piazzale Aldo Moro, 5, 00185 Rome, Italy.

Abstract: The aim of this work was to study the potential of food waste materials (banana peel, potato peel, apple peel, lemon peel, coffee waste, decaf coffee waste, grape waste, and carob peel) as low-cost adsorbents for the removal of aliphatic and aromatic volatile organic compounds (VOCs) from wastewater. The ability of examined food waste materials to adsorb VOCs from synthetic multi-component standard solutions was evaluated and the examined food waste materials showed high removal efficiency. Performances of coffee waste, grape waste, and lemon peel were detailed by using Trichloroethylene and p-Xylene in mono-component standard solutions. The adsorption capacity of the three selected food wastes was determined by using linear Langmuir and Freundlich isotherm models. Two errors functions, average percentage error (APE) and the chi-square test ($\chi 2$), were used for isotherm optimization prediction. Freundlich isotherm well described the adsorption of VOCs on the considered materials. According to the obtained results, a multilayer, physical, and cooperative adsorption process was hypothesized, particularly evident when the VOCs' concentrations are high. This was confirmed by the high adsorption efficiency percentages (E% > 80%) of VOCs from a real polluted matrix (urban solid waste leachate), containing high concentrations of total organic content.

Keywords: volatile organic compounds; adsorption; environmental remediation; food waste materials; wastewater treatment.

1. Introduction

Volatile organic compounds (VOCs), aliphatic and aromatic, are a wide class of organic pollutants extensively released in the environment from a variety of anthropogenic sources such as fuel storage and transport, industrial operations [1], manufacture and storage of paints, and combustion processes [2]. Most of the VOCs can cause direct and indirect harmful effects to humans as well as the environment. Moreover, they represent one of the main causes of chronic contamination, especially in industrialized countries, since their chemical and physical properties enable them to persist in the environment. Chlorinated volatile organic compounds (Cl-VOCs) and aromatic hydrocarbons (BTEXs; benzene, toluene, and xylenes) are ubiquitous contaminants frequently detected in the environment. Therefore, human exposure to Cl-VOCs and BTEX is very common; they enter the body through multiple routes, such as inhalation, ingestion, and dermal absorption [3–5]. The toxicity of these compounds is increased by the fact that VOCs are strongly lipophilic with a capacity to concentrate in fat deposits by determining a long-term exposure [6-7]. Since the beginning of the 20th century, Cl-VOCs were extensively used as solvents for processes such as dry cleaning, production of pesticides, paints, and refrigerants [8,9]. Among them, Trichloroethylene is one of the most prevalent and persistent contaminants detected in polluted environments [10] and has been classified as group 2A by IARC (International Agency for Research on Cancer), as probably carcinogenic to humans [11]. In fact, exposure to Trichloroethylene seems to cause harmful effects on central nervous system and on the immune and endocrine systems in adults [12], and may also contribute to certain types of cancers in adults and children [9].

BTEXs, which have been found mainly in sites contaminated by petrol, gasoline, and petrochemical products [13,14], are well known carcinogens [12,15] that can adversely affect various human organs [16] by causing, for example, irritation of the eyes and reduction of bone marrow function [17]. Hence, it appears indispensable to eliminate these hazardous and mutagenic chemicals from the environment [19].

Several methods for wastewater decontamination from organic pollutants are reported [19–22]. Among these, the adsorption process has been efficaciously used for the removal of organic as well as inorganic compounds from wastewater because of its safety and ease in operation [23–26]. One of the most used materials to adsorb organic pollutants is activated carbon [25,27–29]; however, it has some disadvantages, such as the high cost and the environmental problems related to the regeneration and disposal of its waste [30,31]. During the past years, several studies have been focused on the evaluation of low-cost and environmentally friendly technologies for the removal of pollutants from wastewater. Most of these studies regarded low-cost materials, mainly biosorbents, which were found

to be able to reduce availability and concentration of some organic compounds (mainly industrial organic dyes, polycyclic aromatic hydrocarbons, and phenolic compounds) [19,21,30–34].

Among the biosorbents, food waste materials appeared to be efficient for the removal of inorganic pollutants from wastewaters [35–41]. In a recent paper [42], food waste adsorbents were tested on a real polluted matrix and they showed high removal efficiency of various heavy metals. Biosorption by food waste materials has several benefits such as low production costs [43], free availability, and possible reuse of the biosorbents [44]. Moreover, it is essential to use waste as raw material for new products and new applications [45] as a renewable source of biomass [35]. The use of such residual materials might become a viable alternative for wastewater treatment with associated environmental and economic benefits [46].

Since the high danger of volatile organic compounds for humans and the environment along with the scarce amount of studies regarding the biosorption of VOCs by food waste materials, the evaluation of the performances of these materials as VOCs adsorbents constitutes an interesting issue that still should be investigated.

In this study, eight food waste materials (banana peel, potato peel, apple peel, lemon peel, coffee waste, decaf coffee waste, grape waste, and carob peel) were evaluated as potential low-cost biosorbents for the removal of VOCs from wastewater. With this aim, their adsorption efficiency and capacity of aliphatic/aromatic VOCs from multi-component and mono-component synthetic solutions and from a real polluted matrix were explored.

2. Materials and Methods

2.1. Preparation of the Biosorbents

Food waste powders (n = 8) were employed as low-cost adsorbents: banana peel, potato peel, apple peel, lemon peel, coffee waste, decaf coffee waste, grape waste and carob peel (Fig. A1, Appendix A). Preparation of the biosorbents followed the procedure detailed in a recent study [42]. Briefly, food waste materials were sun-dried for a week, grinded with a mortar and sieved to retain particles sized between 0.25 and 0.125 mm. The obtained powders were washed three times with deionized water (produced by an integrate water purification system; Arioso UP 900; Industrial Scientific Corporation, Pittsburg, PA, USA), dried at 55 °C for 48 h in a vacutherm oven (Heraeus VT 6025; Kendro Laboratory Products, Hanau, Germany), and then weighed on an analytical balance (Gibertini Europe 60; Gibertini Elettronica Srl, Milano, Italy).

2.2. Adsorption Experiments

First, removal efficiency of organic pollutants was explored by exposing each biosorbent to a synthetic multi-standard solution containing both aliphatic and aromatic VOCs (Trans-1,2-Dichloroethene, Dichloromethane, 1,1-Dichloroethene, 1,1-Dichloroethane, Chloroform, Carbon tetrachloride, Trichloroethylene, 1,2-Dichloropropane, 1,1,2-Trichloroethane, Tetrachloroethylene, Dibromochloromethane, 1,1,2-Tetrachloroethane, Bromoform, Methyl tert-butyl ether, Benzene, Toluene, Chlorobenzene, Ethylbenzene, m,p-Xylene, o-Xylene, 1,3-Dichlorobenzene, 1,4-Dichlorobenzene, 1,2-Dichlorobenzene). In these preliminary trials, 100 mg of each adsorbent was exposed to 10 mL multi-standard solutions at 20 µg/L by using 20 mL glass vials, hermetically sealed. Multi-standard solutions were obtained by diluting 2 mg/L multi-component solution, prepared by mixing proper aliquots of aliphatic and aromatic standard stock solutions (SPEX CertiPrep, Metuchen, New Jersey, USA) in methanol.

The adsorption kinetic was assessed by keeping both the mass of each waste material (100 mg) and the VOCs concentration (20 µg/L) constant, while increasing exposure time from 1 h to 24 h (1, 2, 3, 4, 5, 6, and 24 h).

All the samples were analysed to determine the equilibrium concentration (Ce), which is the amount of adsorbate remaining in solution after adsorption processes. Multi-component standard solutions without biosorbent were always treated together with each sample set, to trace and control possible VOCs' concentration variability due to loss by evaporation during treatment; VOCs' concentration of these solutions was used as initial concentration (C_0).

The performances of the food waste materials as biosorbents in a real polluted matrix were tested by exposing 100 mg of each food waste sorbent to 10 mL of an urban solid waste leachate. The same procedure described for the synthetic multi-standard solutions was applied to perform the exposure experiments and to determine C_0 and Ce. The total organic content (TOC) of this solution was measured by a TOC analyzer (TOC-VCSH; Shimadzu Corporation, Kyoto, Japan).

The pH of both multi-standard solutions and real polluted matrix, with and without biosorbents, was measured using a pH meter (Criston MicropH 2002, Crisonb Instruments, Barcelona, Spain).

According to results obtained from the just described preliminary trials, two selected target VOCs were chosen for deepening the study of adsorption behavior in synthetic mono-component solutions. Trichloroethylene and p-Xylene were representatives of aliphatic and aromatic classes, respectively. In these trials, adsorption capacity was calculated for three selected food wastes by varying VOCs' concentration in the range 25–2000 µg/L and by keeping constant at 100 mg the adsorbent amount. Coffee waste, grape waste, and lemon peel were chosen for this experimental procedure as

biosorbents, with reference to a recent paper in which all the considered food waste materials were characterized in detail by scanning electronic microscopy (SEM), Fourier transform infrared spectroscopy (FTIR), and principal component analysis (PCA) [40]. Specific surface areas were estimated by analyzing 1 g of each adsorbent by krypton gas physisorption (Porosimeter 3Flex 3500; Micromeritrics, GA, USA). Obtained values were included in the range 0.1–0.5 m2/g. These values were close to the detection limit of the technique and the high uncertainties (about 0.05 m2/g) did not allow a reliable comparison among materials.

Aromatic and aliphatic VOCs considered in this work were identified by comparison with the analytes registered in NIST Mass Spectral Library (1.6 NIST MS Software Version 2.3) of static headspace gas chromatography coupled to mass spectrometry (SHS-GC-MS) (probability of more than 70%) and quantified.

2.3. GC Analysis

Static headspace gas chromatography coupled to mass spectrometry (SHS-GC-MS; QHSS-40 Headspace sampler, QUMA Elektronik & Analitik GmbH, Wuppertal, Germany; Varian 431-GC and Varian 210-MS, Varian, California, CA, USA) was used for all the VOCs' analyses. After having chosen the exposure time, the glass vials containing the solutions (with or without the biosorbent) were maintained under stirring for 23 min at the constant temperature of 80 °C, then 1 µL of the vapor phase was injected in a capillary column (VF-624 30 m × 0.25 mm × 1 µm; stationary phase composition: equivalent of a 6% cyanopropyl-phenyl/94% dimethylpolysiloxane) with a Hamilton syringe (Hamilton Company, Bonaduz, Switzerland). Helium was used as carrier gas at the flow rate of 1 mL/min. The temperature was kept at 35 °C for 2 min, then it was increased to 50 °C at the rate of 6 °C per minute and, lastly, to 180 °C at the rate of 12 °C per minute. The total duration of the chromatographic run was 16 min.

Chromatograms were registered in selective ion monitoring mode (SIM) by selecting specific mass to charge ratios (m/z) for each analyte. The conditions employed to mass spectrometry and selected fragments and retention times of the considered VOCs and are summarized in Table A1 and Table A2 (Appendix A), respectively.

Final volume of each analysed sample was 10 mL and all the experiments were performed in triplicate. External standard solutions were used for quantification.

2.4. Calculation of Adsorption Efficiency and Adsorption Capacity

Adsorption efficiency (*E%*) was calculated by the following equation:

$$E\%= \left[\frac{(C_0 - C_e)}{C_0}\right]\cdot 100$$

where C_0 (mg/L) is the inlet VOCs and C_e (mg/L) is the equilibrium concentration after the adsorption process.

Regarding real polluted matrix, for identified species, the adsorption efficiency was roughly estimated by comparing the peak areas in the presence (A_e) and in the absence (A_0) of the biosorbent ($E\%= \left[\frac{(A_0 - A_e)}{A_0}\right]\cdot 100$) after adsorption processes.

Adsorption capacity Q_e (mg/g) was determined by following the procedure described in Wang and Qin [45], using a mass equilibrium equation:

$$Q_e= \frac{[(C_0 - C_e)\cdot V]}{m}$$

where V is the volume of solution (L) inside the vial and m is the amount (g) of food waste powder.

2.5. Adsorption Isotherms

The characterization of adsorption isotherms is considered one of the most appropriate methods for the assessment of the adsorbent capacity [47]. Adsorption isotherms play an important role in the predictive modelling procedures to understand what is going on during adsorption process and indicate how molecules, subjected to adsorption, distribute themselves between liquid and solid phases at equilibrium [48,49]. Linear regression analysis was used to obtain adjustable isotherm parameters. Table 1 summarizes the linear forms of Langmuir and Freundlich isotherm models used for this adsorption study. Although Langmuir isotherm model could be linearized into four different types, the reported Langmuir equation, defined Type I, is the most popular linear form used in available literature [50].

Table 1. Linear forms of Langmuir (Type I) and Freundlich isotherm models.

Isotherm models	Linear
Langmuir	$\frac{C_e}{Q_e}= \frac{1}{(K_L \cdot q_m)}+ \frac{C_e}{q_m}$
Freundlich	$\ln Q_e = \ln K_F + \left(\frac{1}{n} \cdot \ln C_e\right)$

For Langmuir isotherms, Ce (mg/L) is the equilibrium concentration after adsorption process, Qe (mg/g) is the adsorption capacity, qm (mg/g) and KL (in L/mg) are sorption equilibrium constants.

The constant KL is related to the free energy of adsorption and indicates affinity between the VOCs and the adsorbents [51].

In Freundlich isotherm, KF (mg/L) and n (dimensionless) are both constants indicative of sorption capacity and sorption intensity, respectively [52,53]. In particular, n indicates the favorability of the adsorption process [52]; a close to unit n value represents good adsorption capacity, meaning VOCs' adsorption is favorable [52]. The evaluation of the correlation coefficients (R2) is useful to predict which model best matches with the experimental data. In addition, the average percentage error (APE) and chi-square test ($\chi 2$) values were calculated in order to verify the validity of the isotherm models. APE and $\chi 2$, defined ad distribution functions, indicate the fit between the experimental and the predicted values of the adsorption capacity [54] and were used for isotherm optimization prediction [49]: if data from the model are similar to the obtained experimental data, the function values will be small number. APE and $\chi 2$ were calculated as follows:

$$APE\ (\%) = \left[\frac{\sum_{i=1}^{N}\left|\frac{\left(Q_{e,exp} - Q_{e,pre}\right)}{Q_{e,exp}}\right|}{N}\right] \cdot 100$$

$$\chi^2 = \sum_{i=1}^{N}\frac{\left(Q_{e,exp} - Q_{e,pre}\right)^2}{Q_{e,pre}}$$

where $Q_{e,exp}$, $Q_{e,pre}$ are experimental and predicted adsorption capacity, respectively; N is the number of observations in the experimental data.

3. Results and Discussion

3.1. Adsorption Efficiency from Multi-Component Solutions

Preliminary tests on synthetic multi-component solutions were performed in order to verify the general behavior of the considered food waste materials as VOCs' biosorbents. First, the rate of the adsorption process was evaluated by exposing the materials to a synthetic mixture of aromatic and aliphatic VOCs for increasing times (1, 2, 3, 4, 5, 6, and 24 h). As shown in Fig. A2 (Appendix A), preliminary tests confirmed that 1 h contact time was enough to reach a steady-state VOC concentration, regarding both the liquid/solid and the liquid/gas interfaces. Consequently, all the successive samples were analysed after one hour from preparation.

Adsorption efficiency of each examined food waste material (100 mg) from a mixture of aliphatic and aromatic VOCs at 20 µg/L is reported in Table 2. Data show that all the considered biosorbents exhibited some adsorption properties towards organic species; the efficiency of adsorption was very

low for some compounds and for some investigated adsorbents, with some exceptions. Coffee and decaf coffee waste appeared to be the most efficient for the removal of most of the organic compounds. For example, among the aromatic compounds, p-Xylene, o-Xylene, 1,2-Dichlorobenzene, 1,3-Dichlorobenzene, and 1,4-Dichlorobenzene were adsorbed in high percentages (E% > 50%); within the aliphatic compounds, Trichloroethylene, Tetrachloroethylene, and 1,1,2-Tetrachloroethane showed more than 40% of adsorption efficiency in presence of coffee and decaf coffee waste. Moreover, coffee waste was able to adsorb more than 90% of the Trans-1,2-Dichloroethene in multi-component solution. Apple peel seemed to be efficient for 1,1,2-Tetrachloroethane (E% > 50%) and for 1,2-Dichlorobenzene, 1,3-Dichlorobenzene and 1,4-Dichlorobenzene (E% > 30%). Lastly, it is worth noting that also grape waste adsorption efficiency is considerable for 1,2-Dichlorobenzene, 1,3-Dichlorobenzene and 1,4-Dichlorobenzene (E% > 40%) and 1,1,2-Tetrachloroethane (E% > 50%).

In general, looking at Table 2, aromatic compounds seem to be more retained than the aliphatic; moreover, coffee waste, decaf coffee waste, grape waste, and banana peel showed fairly good adsorption efficiency for both aliphatic and aromatic compounds.

Considering the efficiency of the examined low-cost adsorbents for the removal of VOCs from synthetic solutions, other experimental tests were conducted to confirm the potential of the investigated food waste materials to adsorb organic compounds from a real polluted matrix. The chosen real polluted matrix had a very high total organic content (TOC = 7500 mg/L), and a spontaneous pH of 6.5. In Table A3 (Appendix A), pH values both of multi-standard synthetic solutions and real polluted matrix are reported, with and without each adsorbent.

The real polluted matrix (a leachate of urban solid waste) contained a wide variety of VOCs; only some of them were identified by comparison with NIST library (>70% probability). The estimated adsorption efficiencies for these compounds are reported in Table 3. These data indicate that most of organic compounds is strongly retained by these adsorbents. In general, all the materials exhibited very good adsorption properties towards most of the VOCs and the results confirmed that coffee, decaf coffee, and grape waste were the most efficient biosorbents. Estimated efficiencies were much larger than those calculated in synthetic solutions. For example, coffee waste adsorption efficiency (E%) of Trichloroethylene was 43 ± 2 and 99 ± 12; lemon peel showed a Chlorobenzene E% of 10 ± 1 and 86 ± 12 and grape waste showed a m, p-Xylene E% of 34 ± 3 and 96 ± 5 in synthetic and real polluted matrix, respectively. This behavior may be due to the different VOCs' concentration range in real polluted sample compared to the synthetic one, and seems to indicate a cooperative mechanism of adsorption, meaning an increase in the amount of pollutants adsorbed when initial VOCs'

concentration was increased. Coffee waste, decaf coffee waste, and grape waste were confirmed to be the most efficient biosorbents for the removal of both aliphatic and aromatic VOCs.

3.2. Adsorption Capacity from Synthetic Mono-Component Solutions

Adsorption processes were further investigated by studying the adsorption isotherms of selected biosorbents and VOCs. Two selected target VOCs were chosen for deepening the study of adsorption behavior in synthetic mono-component solutions. Trichloroethylene and p-Xylene were chosen as representative of aliphatic and aromatic classes, respectively. In these trials, VOCs' concentration was varied in the range of 25–2000 µg/L, keeping constant at 100 mg the adsorbent amount. Adsorption capacity was calculated for three selected food waste biosorbents (coffee waste, grape waste, and lemon peel) according to the results obtained from a previous study, in which all the considered food waste materials were analysed by scanning electronic microscopy (SEM) and Fourier transform infrared spectroscopy (FTIR) [42]. In this study, FTIR spectra were elaborated by principal component analysis (PCA) to group the food waste materials in different clusters, according to functional groups present on the adsorbents' surfaces. First cluster included orange and lemon peel, and was characterized by OH of alcohols, phenols and carboxylic acids; CH, COC, CN, PO of polysaccharides and C=C of lipids and lignin moieties; lemon peel was chosen as representative of this cluster.

Second cluster included coffee and decaf coffee waste, apple, and banana peel, and was characterized by the highest amount of CH bonds of methyl and methylene groups of lipids; coffee waste was chosen as representative of this cluster. Third cluster included grape waste and carob peel and was characterized by the lowest amount of the identified functional groups; grape waste was chosen as representative of this cluster.

Adsorption capacity of coffee waste, grape waste and lemon peel towards Trichloroethylene and p-Xylene is graphically represented in Fig. 1. Plots a, b, and c show the adsorption curves of coffee waste, grape waste, and lemon peel for Trichloroethylene. As expected, the adsorption capacity of the three low-cost sorbents increases with increasing the pollutant exposure concentration. Trichloroethylene was adsorbed with the highest values of Qe (µg/g) in presence of coffee waste, while grape waste and lemon peel were found to be less efficient. Adsorption capacity curves show a quite complex trend and seem to indicate that the adsorbent saturation was reached at the tested conditions. Fig. 1 (plots d, e, f), shows the adsorption curves of coffee waste, grape waste, and lemon peel for p-Xylene. The trend of adsorption curves of p-Xylene with all the three biosorbents was in general quite similar to that seen for Trichloroethylene: an increase of adsorption capacity is observed

with the increase of pollutant's concentration. p-Xylene adsorption capacity appeared to be higher than that of Trichloroethylene for all the examined food waste materials. For example, coffee waste adsorption capacity can be recalled: the highest Qe value reached with Trichloroethylene and p-Xylene was 30 µg/g and 80 µg/g, respectively.

Table 2. Adsorption efficiency (100 mg of each biosorbent) of aliphatic and aromatic VOCs from multi-component synthetic solution (20 µg/L). Mean ± SD of three replicates is reported.

	Adsorption efficiency (*E%*) ± SD							
Aliphatic VOCs	**Banana peel**	**Potato peel**	**Apple peel**	**Lemon peel**	**Coffee waste**	**Decaf C. waste**	**Grape waste**	**Carob peel**
Trans-1,2-Dichloroethene	2.7 ± 0.4	0.6 ± 0.2	0.7 ± 0.4	1.6 ± 0.8	93 ± 18	7.6 ± 1.4	4.7 ± 1.6	2.3 ± 1.6
Dichloromethane	3.9 ± 0.2	5.7 ± 4.3	8.2 ± 3.2	7.1 ± 1.8	9.8 ± 0.7	13 ± 1	6.2 ± 1.9	3.7 ± 1.1
1,1-Dichloroethene	1.8 ± 0.3	1.1 ± 0.7	3.3 ± 0.8	3.1 ± 1.8	3.9 ± 0.5	12 ± 5	6.7 ± 1.2	1.7 ± 1.3
1,1-Dichloroethane	1.3 ± 0.8	5.6 ± 1.9	2.6 ± 0.2	13 ± 6	12 ± 2	16 ± 1	6.7 ± 1.7	3.1 ± 1.3
Chloroform	5.9 ± 5.4	7.2 ± 2.4	1.5 ± 0.5	5.1 ± 2.6	6.2 ± 2.3	13 ± 1	6.3 ± 1.1	7.7 ± 3.1
Carbon tetrachloride	39 ± 2	4.3 ± 1.9	11 ± 2	6.3 ± 0.3	17 ± 2	16 ± 5	37 ± 12	4.3 ± 1.7
Trichloroethylene	35 ± 1	16 ± 13	36 ± 1	44 ± 1	43 ± 2	51 ± 1	34 ± 2	36 ± 1
1,2-Dichloropropane	1.1 ± 0.2	0.9 ± 0.5	8.3 ± 6.4	4.7 ± 2.1	1.1 ± 0.2	16 ± 1	5.5 ± 3.2	3.8 ± 3.4
1,1,2-Trichloroethane	7.5 ± 6.5	5.4 ± 4.3	13 ± 5	14 ± 4	18 ± 4	25 ± 9	11 ± 1	2.5 ± 0.9
Tetrachloroethylene	17 ± 12	12 ± 4	11 ± 4	1.8 ± 0.9	35 ± 9	47 ± 10	42 ± 7	11 ± 2
Dibromochloromethane	43 ± 5	1.1 ± 0.8	2.5 ± 1.8	1.4 ± 0.8	13 ± 1	27 ± 3	11 ± 2	0.8 ± 0.3
1,1,2-Tetrachloroethane	39 ± 1	23 ± 2	57 ± 7	38 ± 1	73 ± 13	77 ± 1	51 ± 1	8.5 ± 1.8
Bromoform	57 ± 2	1.6 ± 0.9	17 ± 4	1.3 ± 0.6	19 ± 2	25 ± 2	25 ± 2	2.3 ± 0.7
Aromatic VOCs								
Methyl tert-butyl ether	1.8 ± 0.2	9.5 ± 1.9	1.8 ± 0.8	3.1 ± 2.3	10 ± 5	1.5 ± 1.4	1.5 ± 1.1	1.5 ± 1.1
Benzene	1.8 ± 0.8	2.8 ± 0.3	1.8 ± 0.2	1.3 ± 1.2	17 ± 1	19 ± 1	7.1 ± 0.5	5.9 ± 0.3
Toluene	12 ± 1	1.5 ± 1.1	8.5 ± 0.5	3.9 ± 0.3	31 ± 2	33 ± 2	19 ± 2	1.3 ± 0.8
Chlorobenzene	17 ± 1	5.5 ± 0.5	15 ± 1	10 ± 1	37 ± 1	42 ± 1	30 ± 1	2.5 ± 2.1
Ethylbenzene	7.1 ± 1.4	4.8 ± 1.8	9.5 ± 5.5	1.5 ± 0.7	28 ± 1	37 ± 3	24 ± 17	1.6 ± 0.4
m, p-Xylene	35 ± 1	12 ± 1	21 ± 1	15 ± 1	54 ± 1	56 ± 1	34 ± 3	3.3 ± 1.8
o-Xylene	28 ± 1	14 ± 3	24 ± 1	18 ± 4	57 ± 1	58 ± 1	33 ± 5	13 ± 2
1,3-Dichlorobenzene	35 ± 2	12 ± 1	34 ± 1	19 ± 2	67 ± 1	73 ± 2	48 ± 4	12 ± 1
1,4-Dichlorobenzene	43 ± 2	14 ± 1	36 ± 2	20 ± 1	68 ± 1	71 ± 1	47 ± 1	24 ± 1
1,2-Dichlorobenzene	36 ± 1	10 ± 2	37 ± 1	20 ± 2	67 ± 1	73 ± 2	47 ± 2	13 ± 2

These results agree with those obtained from the adsorption experiments in multi-component standard solutions. Coffee waste was found to be the most efficient biosorbent for the removal of both

Trichloroethylene and p-Xylene. The most plausible explanation comes from the chemical-physical properties of Trichloroethylene, p-Xylene, and coffee waste composition. FTIR spectra of coffee waste showed peaks of asymmetric and symmetric stretching of hydrophobic C-H bonds of methyl and methylene groups, attributed to the presence of lipids that are available in coffee samples in large amount [42,55]. Considering that Trichloroethylene and p-Xylene are both well-known lipophilic compound [56,57], a significant adsorption on lipid-rich coffee waste was expected. Moreover, according to the SEM micrographs, coffee waste has very porous surface [42] that allows it to adsorb a higher amount of pollutants from wastewater. Finally, lemon peel turned out to be the least efficient adsorbent for Trichloroethylene and p-Xylene with the highest Qe recorded value of 10 µg/g and 20 µg/g, respectively, probably because of its less porous surface and the presence of polar functional groups [42].

Table 3. Adsorption efficiency (100 mg of each biosorbent) of VOCs from real polluted matrix of urban solid waste leachate. Mean ± SD of three replicates is reported.

	Adsorption efficiency (*E%*) ± SD							
Aliphatic VOCs	**Banana peel**	**Potato peel**	**Apple peel**	**Lemon peel**	**Coffee waste**	**Decaf C. waste**	**Grape waste**	**Carob peel**
1,1-Dichloroethene	20 ± 5	38 ± 9	60 ± 10	79 ± 18	91 ± 16	89 ± 5	87 ± 6	71 ± 11
Dichloromethane	85 ± 11	85 ± 15	90 ± 18	96 ± 15	97 ± 9	97 ± 5	97 ± 10	93 ± 7
Chloroform	24 ± 9	13 ± 6	54 ± 12	83 ± 14	92 ± 10	93 ± 5	90 ± 9	69 ± 16
Trichloroethylene	44 ± 8	39 ± 6	56 ± 13	98 ± 16	99 ± 12	96 ± 6	97 ± 10	86 ± 9
Dibromochloromethane	8.6 ± 2.3	3.2 ± 1.4	47 ± 14	84 ± 10	95 ± 11	93 ± 2	89 ± 8	67 ± 6
Aromatic VOCs								
Toluene	31 ± 9	14 ± 7	59 ± 10	79 ± 18	93 ± 9	91 ± 9	89 ± 15	62 ± 8
Chlorobenzene	45 ± 8	15 ± 6	67 ± 18	86 ± 12	97 ± 9	93 ± 5	93 ± 7	71 ± 7
m, p-Xylene	64 ± 9	27 ± 11	78 ± 10	91 ± 14	99 ± 10	98 ± 2	96 ± 5	77 ± 10
o-Xylene	72 ± 11	26 ± 13	78 ± 12	92 ± 17	93 ± 9	95 ± 8	97 ± 9	78 ± 9
1,3-Dichlorobenzene	77 ± 13	37 ± 15	93 ± 18	98 ± 10	98 ± 7	98 ± 2	97 ± 11	87 ± 7

3.3. Adsorption Isotherms

Sorption equilibrium data for the two VOCs and the three food waste materials were fitted to the Langmuir and Freundlich isotherm models. Although many adsorption models were developed and applied in the literature [58,59], the Langmuir and Freundlich adsorption models are frequently used to describe adsorption mechanism.

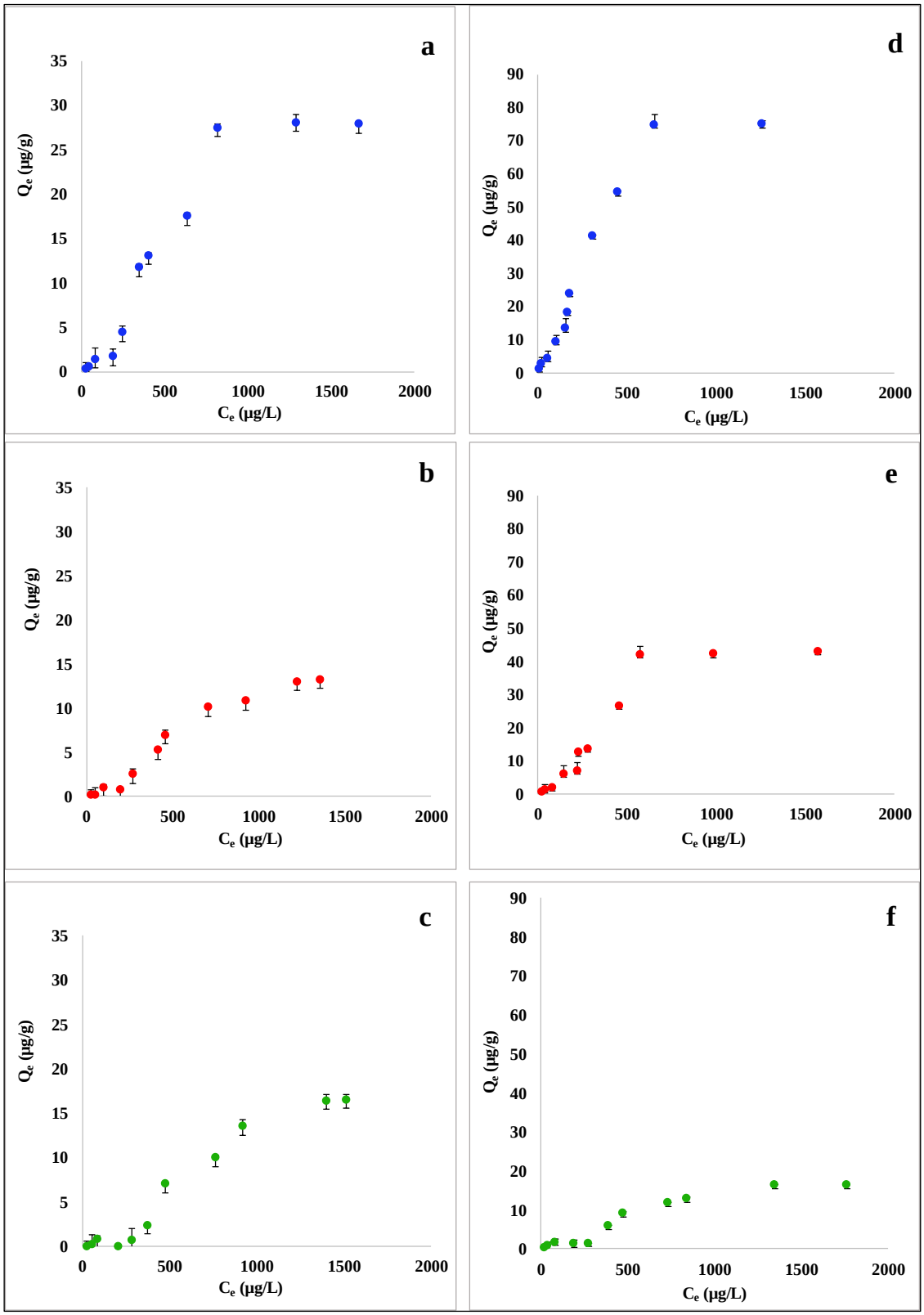

Fig. 1. Comparison of adsorption isotherms of coffee waste (a), grape waste (b) and lemon peel (c) with Trichloroethylene (from 25 to 2000 µg/L; 100 mg of each biosorbent) and coffee waste (d), grape waste (e) and lemon peel (f) with p-Xylene (from 25 to 2000 µg/L; 100 mg of each biosorbent). Mean ± SD of three replicates is reported.

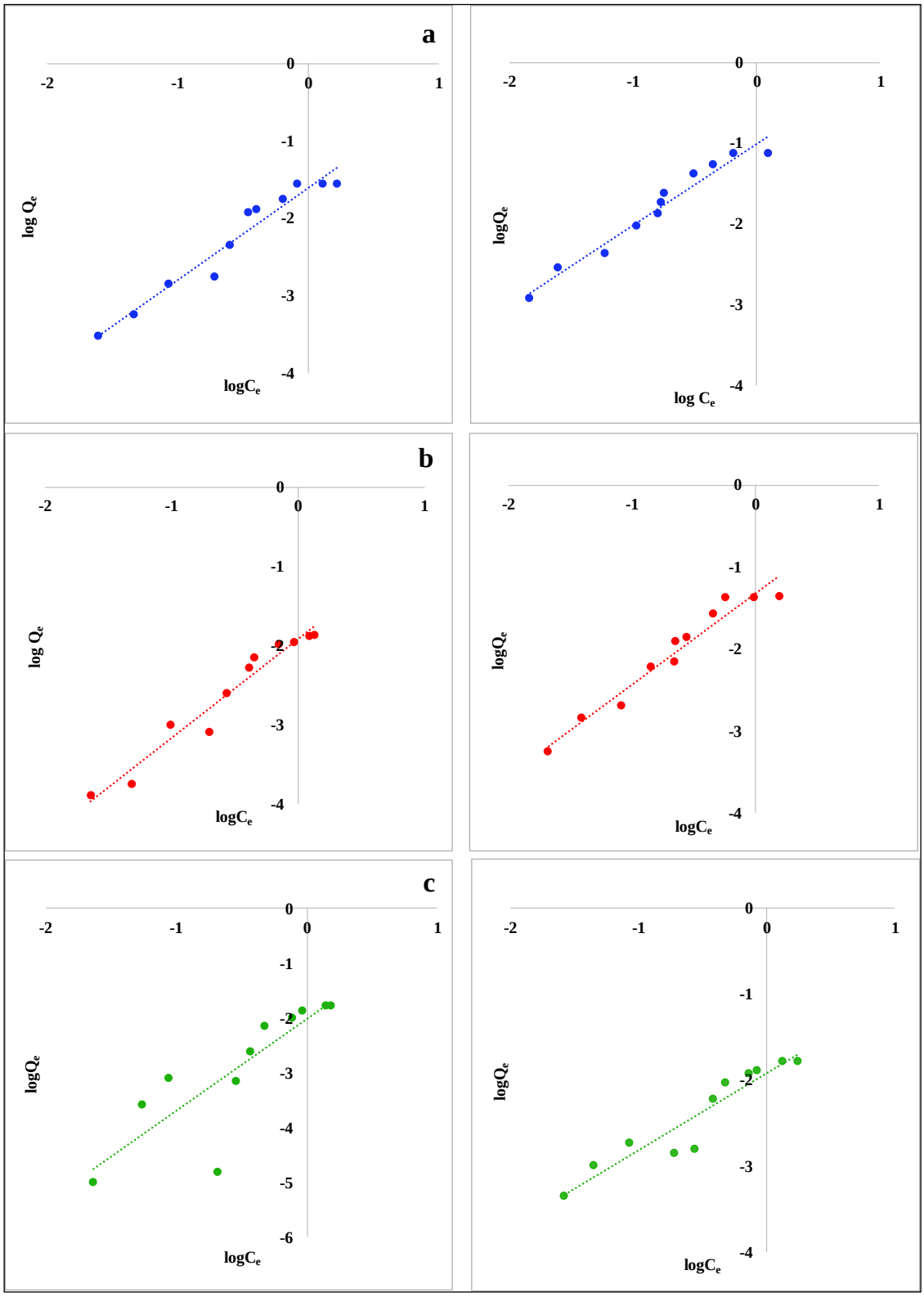

Fig. 2. Langmuir isotherms for Trichloroethylene with coffee waste (a), grape waste (b) and lemon peel (c); Freundlich isotherms for Trichloroethylene with coffee waste (d), grape waste (e) and lemon peel (f).

Although nonlinear isotherm forms are recommended in the field of batch adsorption research to avoid errors resulting from simple linear regression [49,60], in this study, linearized isotherm models were adopted due to the mathematical simplicity [51] and to immediately obtain semi-quantitative isotherm constants. Equilibrium data did not fit Langmuir model for both the studied VOCs and for the considered biosorbents. Since Langmuir isotherm cannot be applied in this work, the corresponding data are not reported. Linearized Freundlich adsorption isotherms for Trichloroethylene and p-Xylene are reported in Fig. 2.

The constants obtained by applying the Freundlich isotherm model are summarized in Table 4. The high correlation coefficients ($R2 \geq 0.9$) obtained by plotting logQe versus logCe for both Trichloroethylene and p-Xylene indicate that these adsorption processes are well represented by the Freundlich model. Lemon peel showed a lower correlation, but it's still significant.

Moreover, the values of n and KF of the Freundlich model indicate good adsorption intensity and capacity, respectively: n was close to unity for all the examined food waste adsorbents and for both Trichloroethylene and p-Xylene, indicating that VOCs adsorption is favorable [52]. Furthermore, the low values of APE and $\chi 2$ in association with higher R2 generate a satisfactory fit of Freundlich model to the experimental data, even if they are little higher for lemon peel. To explain these contrasting results, the adsorption processes simulated by the two models are to be considered. Langmuir model represents only monolayer adsorption processes [46] on the outer surface of the adsorbent, without considering any further adsorption [61]. Instead, Freundlich isotherm represents heterogeneous surfaces and sorbent systems [47,62] in aqueous systems [30], in which multilayer adsorption processes are included. According to the increase of the adsorption capacity with increasing of the VOCs' concentration, a multilayer adsorption process can be hypothesized. This is also confirmed by the n values reported in Table 4. In fact, when $n < 1$, the presence of an isotherm called "solvent-affinity isotherm" is suggested [62]; this kind of isotherm represents an increase of the adsorption energy with increasing concentration of pollutants on the adsorbents' surface. Thus, it can be assumed that aliphatic and aromatic VOCs are initially weakly detained by food waste materials through an adsorption on the active sites of the sorbents. At high concentrations, the active sites are completely occupied by the compounds and the adsorption of other pollutants is supported by Van der Waals forces with the molecules already adsorbed, making a physical adsorption within adsorbent layers. The result is an effective adsorption process within the adsorbent layers, caused by strong intermolecular attractions.

Table 4. Parameters of Langmuir and Freundlich isotherms for Trichloroethylene and p-Xylene.

	Langmuir					Freundlich				
	q_m (mg/g)	K_L (L/mg)	R^2	APE (%)	χ^2	K_F (mg/L)	n	R^2	APE (%)	χ^2
Trichloroethylene										
Coffee waste	-0.059	-0.26	0.11	3.4	$2.1 \cdot 10^{-5}$	0.026	0.83	0.99	2.9	$3.1 \cdot 10^{-5}$
Grape waste	-0.011	-0.51	0.31	0.81	$6.2 \cdot 10^{-7}$	0.012	0.79	0.99	5	$1.8 \cdot 10^{-5}$
Lemon peel	$-0.45 \cdot 10^{-3}$	-0.79	0.081	8	$6.7 \cdot 10^{-3}$	0.009	0.61	0.97	22	$1.3 \cdot 10^{-5}$
p-Xylene										
Coffee waste	0.44	0.23	0.091	2.9	$6.3 \cdot 10^{-5}$	0.11	0.98	0.99	0.91	$1.2 \cdot 10^{-5}$
Grape waste	-0.32	-0.11	0.032	4.1	$5.5 \cdot 10^{-5}$	0.051	0.89	0.98	0.86	$3.4 \cdot 10^{-6}$
Lemon peel	0.12	0.12	0.012	2.1	$1.9 \cdot 10^{-5}$	0.012	1.1	0.97	8	$1.1 \cdot 10^{-3}$

4. Conclusions

Food waste materials, that are available in large amount and at very low costs, appeared to be promising biosorbents for both aliphatic and aromatic VOCs in aqueous solutions. In general, the aromatic VOCs were better adsorbed than the aliphatic by most of the considered materials. This is confirmed by the high percentages of adsorption efficiency (E%).

Adsorption capacities (Qe) of three chosen food waste materials (coffee waste, grape waste, and lemon peel) with Trichloroethylene (chosen as representative of aromatic VOCs) and p-Xylene (chosen as representative of aliphatic Cl-VOCs) were investigated; coffee waste resulted the most efficient sorbent for the removal of both considered VOCs. This is probably due to the presence of lipids in coffee samples on which Trichloroethylene and p-Xylene compounds are efficiently adsorbed, due to their lipophilic nature.

Adsorption equilibrium isotherms showed that coffee waste is the most efficient material for both p-Xylene and Trichloroethylene adsorption. In all the examined systems, the sorption processes followed much more closely the Freundlich than the Langmuir isotherm model. This indicates a physical adsorption mechanism thanks to London-Van der Waals forces between solute and sorbent, through a cooperative adsorption mechanism, in which the already adsorbed molecules on the sorbent's surface facilitate the adsorption of other molecules. This kind of physical adsorption may be particularly beneficial in field applications, because it gives the adsorbents an opportunity to have great adsorption performance at high pollutant concentrations.

Evaluation of food waste performances as biosorbents in field still needs further deepening, such as the effects of pH on removal capacity, the assessment of the effects of sorbents' particle size, the

investigation of repetitive adsorption desorption cycles for material reusability investigation, or even the comparison between other food waste materials' adsorption capacity. Taking into account all the considerations, the results of this preliminary study suggest further investigations about the possible applicative use of these low-cost adsorbents for VOCs' removal from wastewater.
In this context, the efficient adsorption capacity of food waste materials at high VOCs' concentration was preliminarily confirmed by the excellent adsorption efficiencies obtained in a real polluted matrix.

Acknowledgements

This research did not receive any specific grant from funding agencies in the public, commercial, or not-for-profit sectors. The authors gratefully thank Rosanna Congedo (Higher Education Institution "Quinto Ennio") and Andrea Masotti (Children's Hospital Bambino Gesù – IRCCS Research Laboratories) for providing food waste materials, Isabella Masia for collaborating to the experimental tests and Iqra Javed for providing language help.

Author Contributions

M.A. Frezzini wrote the manuscript; A. Giuliano and M.A. Frezzini conceived the experiments and performed the chemical analyses; M.L. Astolfi supervised the analytical phase; L. Massimi and M.A. Frezzini analyzed the data; L. Massimi edited and supervised the manuscript; S. Canepari coordinated the group.

Conflicts of Interest: The authors declare no conflicts of interest.

References

1. Atkinson, R. Atmospheric chemistry of VOCs and NOx. *Atmospheric environment* 2000, *34*(12-14), 2063-2101.

2. Evuti, A. M. A synopsis on biogenic and anthropogenic volatile organic compounds emissions: hazards and control. *Int. J. Eng* 2013, *2*(5), 145.

3. Kim, J.; Lee, S. S.; Khim, J. Peat moss-derived biochars as effective sorbents for VOCs' removal in groundwater. *Environmental geochemistry and health* 2010, 1-10.

4. Masih, A.; Lall, A. S.; Taneja, A.; Singhvi, R. Inhalation exposure and related health risks of BTEX in ambient air at different microenvironments of a terai zone in north India. *Atmospheric environment* 2016, *147*, 55-66. https://doi.org/10.1016/j.atmosenv.2016.09.067.

5. Yang, J.; Wang, K.; Zhao, Q.; Huang, L.; Yuan, C. S.; Chen, W. H.; Yang, W. B. Underestimated public health risks caused by overestimated VOC removal in wastewater treatment processes. *Environmental Science: Processes & Impacts* 2014, *16*(2), 271-279.

6. Doherty, R. E. A history of the production and use of carbon tetrachloride, tetrachloroethylene, trichloroethylene and 1, 1, 1-trichloroethane in the United States: Part 1--historical background; carbon tetrachloride and tetrachloroethylene. *Environmental forensics* 2000, *1*(2), 69-81. https://doi.org/10.1006/enfo.2000.0010.

7. Huang, B.; Lei, C.; Wei, C.; Zeng, G. Chlorinated volatile organic compounds (Cl-VOCs) in environment—sources, potential human health impacts, and current remediation technologies. *Environment international* 2014, *71*, 118-138. https://doi.org/10.1016/j.envint.2014.06.013.

8. Beamer, P. I.; Luik, C. E.; Abrell, L.; Campos, S.; Martínez, M. E.; Sáez, A. E. Concentration of trichloroethylene in breast milk and household water from Nogales, Arizona. *Environmental science & technology* 2012, *46*(16), 9055-9061.

9. IARC. Summaries & evaluations. Trichloroethylene, 63; 1995a. p. 75.

10. U.S. EPA. Toxicity and exposure assessment for children's health. Trichloroethylene — TEACH chemical summary. Available online at: ttp://www.epa.gov/teach/chem_summ/TCE_summary.pdf, 2007.

11. Farhadian, M.; Vachelard, C.; Duchez, D.; Larroche, C. In situ bioremediation of monoaromatic pollutants in groundwater: a review. *Bioresource technology* 2008, *99*(13), 5296-5308. https://doi.org/10.1016/j.biortech.2007.10.025.

12. Kao, C. M.; Huang, W. Y.; Chang, L. J.; Chen, T. Y.; Chien, H. Y.; Hou, F. Application of monitored natural attenuation to remediate a petroleum-hydrocarbon spill site. *Water Science and Technology* 2006, *53*(2), 321-328. https://doi.org/10.2166/wst.2006.066.

13. ACGIH, T. BEIs based on the documentation of the threshold limit values for chemical substances and physical agents and biological exposure indices 2009 Cincinnati. In *OH American Conference of Governmental Industrial Hygienists* 2006.

14. Tunsaringkarn, T.; Siriwong, W.; Rungsiyothin, A.; Nopparatbundit, S. Occupational exposure of gasoline station workers to BTEX compounds in Bangkok, Thailand. *The international journal of occupational and environmental medicine* 2012, *3*(3 July).

15. Costa, A. S.; Romão, L. P. C.; Araújo, B. R.; Lucas, S. C. O.; Maciel, S. T. A.; Wisniewski Jr, A.; Alexandre, M. D. R. Environmental strategies to remove volatile aromatic fractions (BTEX) from petroleum industry wastewater using biomass. *Bioresource Technology* 2012, *105*, 31-39. https://doi.org/10.1016/j.biortech.2011.11.096.

16. Anjum, H.; Johari, K.; Gnanasundaram, N.; Ganesapillai, M.; Arunagiri, A.; Regupathi, I.; Thanabalan, M. A review on adsorptive removal of oil pollutants (BTEX) from wastewater using carbon nanotubes. *Journal of Molecular Liquids* 2018. https://doi.org/10.1016/j.molliq.2018.10.105.

17. Ali, I.; Asim, M.; Khan, T. A. Low cost adsorbents for the removal of organic pollutants from wastewater. *Journal of environmental management* 2012, *113*, 170-183. https://doi.org/10.1016/j.jenvman.2012.08.028.

18. Coin, R. J.; Niksa, M. J.; Elyanow, D. I. Wastewater treatment enhanced by electrochemistry. *Environmental Progress & Sustainable Energy* 1996, *15*(2), 122-127. https://doi.org/10.1016/j.biortech.2017.12.078.

19. Crisafully, R.; Milhome, M. A. L.; Cavalcante, R. M.; Silveira, E. R.; De Keukeleire, D.; Nascimento, R. F. Removal of some polycyclic aromatic hydrocarbons from petrochemical wastewater using low-cost adsorbents of natural origin. *Bioresource technology* 2008, *99*(10), 4515-4519. https://doi.org/10.1016/j.biortech.2007.08.041.

20. Zinkus, G. A.; Byers, W. D.; Doerr, W. W. Identify appropriate water reclamat'technologies. *Chemical Engineering Progress* 1998, 19.

21. Fierro, V.; Torné-Fernández, V.; Montané, D.; Celzard, A. Adsorption of phenol onto activated carbons having different textural and surface properties. *Microporous and mesoporous materials* 2008, *111*(1-3), 276-284. https://doi.org/10.1016/j.micromeso.2007.08.002.

22. Mohammed, M. A.; Shitu, A.; Tadda, M. A.; Ngabura, M. Utilization of various Agricultural waste materials in the treatment of Industrial wastewater containing Heavy metals: A Review. *International Research Journal of Environmental Science* 2014, *3*(3), 62-71.

23. Park, K. H.; Balathanigaimani, M. S.; Shim, W. G.; Lee, J. W.; Moon, H. Adsorption characteristics of phenol on novel corn grain-based activated carbons. *Microporous and Mesoporous Materials* 2010, *127*(1-2), 1-8. https://doi.org/10.1016/j.micromeso.2009.06.032.

24. Yu, L.; Wang, L.; Xu, W.; Chen, L.; Fu, M.; Wu, J.; Ye, D. Adsorption of VOCs on reduced graphene oxide. *Journal of Environmental Sciences* 2018, *67*, 171-178. https://doi.org/10.1016/j.jes.2017.08.022

25. Bansal, R. C.; Goyal, M. *Activated carbon adsorption*, 2005. CRC press.

26. Derbyshire, F.; Jagtoyen, M.; Andrews, R.; Rao, A.; Martin-Gullon, I.; Grulke, E. A. *Carbon materials in environmental applications*. Chemistry and physics of carbon, Marcel Dekker Inc.: New York, USA, 2001; pp. 1-66.

27. Zhang, X.; Gao, B.; Creamer, A. E.; Cao, C.; Li, Y. Adsorption of VOCs onto engineered carbon materials: A review. *Journal of hazardous materials* 2017, *338*, 102-123. https://doi.org/10.1016/j.jhazmat.2017.05.013.

28. Ahmaruzzaman, M. Adsorption of phenolic compounds on low-cost adsorbents: a review. *Advances in colloid and interface science* 2008, *143*(1-2), 48-67. https://doi.org/10.1016/j.cis.2008.07.002.

29. Baek, M. H.; Ijagbemi, C. O.; Se-Jin, O.; Kim, D. S. Removal of Malachite Green from aqueous solution using degreased coffee bean. *Journal of hazardous materials* 2010, *176*(1-3), 820-828. https://doi.org/10.1016/j.jhazmat.2009.11.110.

30. Crini, G. Non-conventional low-cost adsorbents for dye removal: a review. *Bioresource technology* 2006, *97*(9), 1061-1085. https://doi.org/10.1016/j.biortech.2005.05.001.

31. García-Sabido, D.; López-Mesas, M.; Carrillo-Navarrete, F. Chicken feather fibres waste as a low-cost biosorbent of acid Blue 80 dye. *Desalination and Water Treatment* 2016, *57*(8), 3732-3740. https://doi.org/10.1080/19443994.2014.986531.

32. Tan, X.; Liu, Y.; Zeng, G.; Wang, X.; Hu, X.; Gu, Y.; Yang, Z. Application of biochar for the removal of pollutants from aqueous solutions. *Chemosphere* 2015, *125*, 70-85. http://dx.doi.org/10.1016/j.chemosphere.2014.12.058.

33. Acharya, J.; Kumar, U.; Rafi, P. M. Removal of heavy metal ions from wastewater by chemically modified agricultural waste material as potential adsorbent-a review. *International Journal of Current Engineering and Technology* 2018, *8*(3), 526-530.

34. Agwaramgbo, L.; Lathan, N.; Edwards, S.; Nunez, S. Assessing lead removal from contaminated water using solid biomaterials: Charcoal, coffee, tea, fishbone, and caffeine. *Journal of Environmental Protection* 2013, *4*(07), 741. http://10.4236/jep.2013.47085.

35. Aman, T.; Kazi, A. A.; Sabri, M. U.; Bano, Q. Potato peels as solid waste for the removal of heavy metal copper (II) from waste water/industrial effluent. *Colloids and Surfaces B: Biointerfaces* 2008, *63*(1), 116-121. https://doi.org/10.1016/j.colsurfb.2007.11.013.

36. Fu, F.; Wang, Q. Removal of heavy metal ions from wastewaters: a review. *Journal of environmental management* 2011, *92*(3), 407-418. https://doi.org/10.1016/j.huajenvman.2010.11.011.

37. Lakshmipathy, R.; Sarada, N. C. Application of watermelon rind as sorbent for removal of nickel and cobalt from aqueous solution. *International Journal of Mineral Processing* 2013, *122*, 63-65. https://doi.org/10.1016/j.minpro.2013.03.002.

38. Mallampati, R.; Valiyaveettil, S. Application of tomato peel as an efficient adsorbent for water purification—alternative biotechnology?. *RSC Advances* 2012, *2*(26), 9914-9920.

39. Frezzini M.A.; Giuliano A.; Treacy J.; Canepari S.; Massimi L. Food Waste Materials Appear Efficient and Low-cost Adsorbents for the Removal of Organic and Inorganic Pollutants from Wastewater. *Interface science* 2018, *316*(2), 298-309. https://doi.org/10.31031/RDMS.2018.05.000608.

40. Massimi, L.; Giuliano, A.; Astolfi, M. L.; Congedo, R.; Masotti, A.; Canepari, S. Efficiency evaluation of food waste materials for the removal of metals and metalloids from complex multi-element solutions. *Materials* 2018, *11*(3), 334. https://doi.org/10.3390/ma11030334.

41. Vieira, R. H.; Volesky, B. Biosorption: a solution to pollution?. *International Microbiology* 2000, *3*(1), 17-24.

42. Kargi, F., & Cikla, S. (2006). Biosorption of zinc (II) ions onto powdered waste sludge (PWS): Kinetics and isotherms. *Enzyme and Microbial Technology*, 38(5), 705-710. https://doi.org/10.1016/j.enzmictec.2005.11.005.

43. Mirabella, N.; Castellani, V.; Sala, S. Current options for the valorization of food manufacturing waste: a review. *Journal of Cleaner Production* 2014, *65*, 28-41. https://doi.org/10.1016/j.jclepro.2013.10.051.

44. Scheufele, F. B., Módenes, A. N., Borba, C. E., Ribeiro, C., Espinoza-Quiñones, F. R., Bergamasco, R., & Pereira, N. C. Monolayer–multilayer adsorption phenomenological model: kinetics, equilibrium and thermodynamics. *Chemical Engineering Journal* 2016, *284*, 1328-1341. https://doi.org/10.1016/j.cej.2015.09.085.

45. Wang, X. S.; Qin, Y. Equilibrium sorption isotherms for of Cu2+ on rice bran. *Process Biochemistry* 2005, *40*(2), 677-680. https://doi.org/10.1016/j.procbio.2004.01.043.

46. Aly, Z.; Graulet, A.; Scales, N.; Hanley, T. Removal of aluminium from aqueous solutions using PAN-based adsorbents: characterisation, kinetics, equilibrium and thermodynamic studies. *Environmental Science and Pollution Research* 2014, *21*(5), 3972-3986.

47. Hamzaoui, M.; Bestani, B.; Benderdouche, N. The use of linear and nonlinear methods for adsorption isotherm optimization of basic green 4-dye onto sawdust-based activated carbon. *J. Mater. Environ. Sci* 2018, *9*(4), 1110-1118. https://doi.org/10.26872/jmes.2018.9.4.122.

48. Ho, Y. S. Isotherms for the sorption of lead onto peat: comparison of linear and non-linear methods. *Polish journal of environmental studies* 2006, 15(1).

49. Chen, X. Modeling of experimental adsorption isotherm data. *Information* 2015, *6*(1), 14-22. https://doi.org/10.3390/info6010014.

50. Aly, Z.; Luca, V. Uranium extraction from aqueous solution using dried and pyrolyzed tea and coffee wastes. *Journal of Radioanalytical and Nuclear Chemistry* 2013, *295*(2), 889-900.

51. Iqbal, M.; Saeed, A.; Zafar, S. I. FTIR spectrophotometry, kinetics and adsorption isotherms modeling, ion exchange, and EDX analysis for understanding the mechanism of Cd2+ and Pb2+ removal by mango peel waste. *Journal of hazardous materials* 2009, *164*(1), 161-171. https://doi.org/10.1016/j.jhazmat.2008.07.141.

52. Desta, M. B. Batch sorption experiments: Langmuir and Freundlich isotherm studies for the adsorption of textile metal ions onto teff straw (Eragrostis tef) agricultural waste. *Journal of thermodynamics* 2013, *2013*. http://dx.doi.org/10.1155/2013/375830.

53. Guechi, E. K.; Hamdaoui, O. Sorption of malachite green from aqueous solution by potato peel: kinetics and equilibrium modeling using non-linear analysis method. *Arabian journal of chemistry* 2016, *9*, S416-S424. https://doi.org/10.1016/j.arabjc.2011.05.011.

54. Largitte, L.; Pasquier, R. A review of the kinetics adsorption models and their application to the adsorption of lead by an activated carbon. *Chemical Engineering Research and Design* 2016, *109*, 495-504. https://doi.org/10.1016/j.cherd.2016.02.006.

55. Tan, K. L.; Hameed, B. H. Insight into the adsorption kinetics models for the removal of contaminants from aqueous solutions. *Journal of the Taiwan Institute of Chemical Engineers* 2017, *74*, 25-48. https://doi.org/10.1016/j.jtice.2017.01.024.

56. El-Khaiary, M. I.; Malash, G. F. Common data analysis errors in batch adsorption studies. *Hydrometallurgy* 2011, *105*(3-4), 314-320. https://doi.org/10.1016/j.hydromet.2010.11.005.

57. Dada, A. O.; Olalekan, A. P.; Olatunya, A. M.; Dada, O. Langmuir, Freundlich, Temkin and Dubinin–Radushkevich isotherms studies of equilibrium sorption of Zn2+ unto phosphoric acid modified rice husk. *IOSR Journal of Applied Chemistry* 2012, *3*(1), 38-45.

58. Febrianto, J.; Kosasih, A. N.; Sunarso, J.; Ju, Y. H.; Indraswati, N.; Ismadji, S. Equilibrium and kinetic studies in adsorption of heavy metals using biosorbent: a summary of recent studies. *Journal of hazardous materials* 2009, *162*(2-3), 616-645. https://doi.org/10.1016/j.jhazmat.2008.06.042.

Supplementary Materials S1.

Fig. S1. Food waste powders: a) Lemon peel, b) Grape waste, c) Coffee waste, d) Carob peel, e) Potato peel, f) Banana peel, g) Apple peel, h) Decaf coffee waste.

Table S1. GC-MS parameters for VOCs analyses.

	Retention time (min)	Fragments (m/z)	Acquisition (m/z range)
Aliphatic VOCs			
Trans-1,2-Dichloroethene	4.50 – 4.90	61 – 96 – 98	55 - 100
Dichloromethane	3.90 – 4.50	49 – 84 – 86	49 - 90
1,1-Dichloroethene	3.20 – 3.90	61 – 96 – 98	60 - 100
1,1-Dichloroethane	4.90 – 5.50	63 - 65 – 27	60 - 90
Chloroform	5.50 – 6.55	83 – 85 – 47	45 – 90
Carbon tetrachloride	6.70 – 6.90	117 – 121	75 – 125
Trichloroethylene	7.40 – 7.95	130 – 95 – 97	55 – 135
1,2-Dichloropropane	7.95 – 8.25	63 – 62 – 27	60 – 80
1,1,2-Trichloroethane	9.70 – 9.86	97 – 83 – 61	44 – 170
Tetrachloroethylene	9.86 – 10.10	166 – 164 – 129	160 - 175
Dibromochloromethane	10.10 – 10.75	129 – 127	80 – 132
1,1,2-Tetrachloroethane	11.78 - 11.87	81 - 82.8 - 83.8	80 – 85
Bromoform	11.73 – 12.02	173 – 171	75 – 180
Aromatic VOCs			
Methyl tert-butyl ether	1.11 – 2.10	44.8 – 45.8	40 - 48
Benzene	6.9 – 7.08	78 – 77	45 - 80
Toluene	9.15 – 9.45	91 - 92	60 - 100
Chlorobenzene	10.75 – 11.00	112 – 77 – 114	48 - 120
Ethylbenzene	11.00 – 11.13	91 - 106	85 - 110
m-Xylene	11.30 – 11.73	91 - 106	70 – 120
p-Xylene	11.30 – 11.73	91 - 106	70 - 120
o-Xylene	11.13 – 11.30	91 - 106	70 – 120
1,3-Dichlorobenzene	12.75 – 13.71	146 – 148 – 111	70 – 150
1,4-Dichlorobenzene	13.71 – 13.85	146 – 148 – 111	70 - 150
1,2-Dichlorobenzene	13.85 – 15.00	146 – 148 – 111	70 – 150

Supplementary Materials S2.

Table S2. Conditions employed to mass spectrometry (Varian 210-MS ion trap mass spectrometer with electron ionization).

Acquisition method	Ion trap temperature (°C)	Transfer line temperature (°C)	Vacuum manifold temperature (°C)
SIM (Single Ion Monitoring)	150 °C	180 °C	80 °C

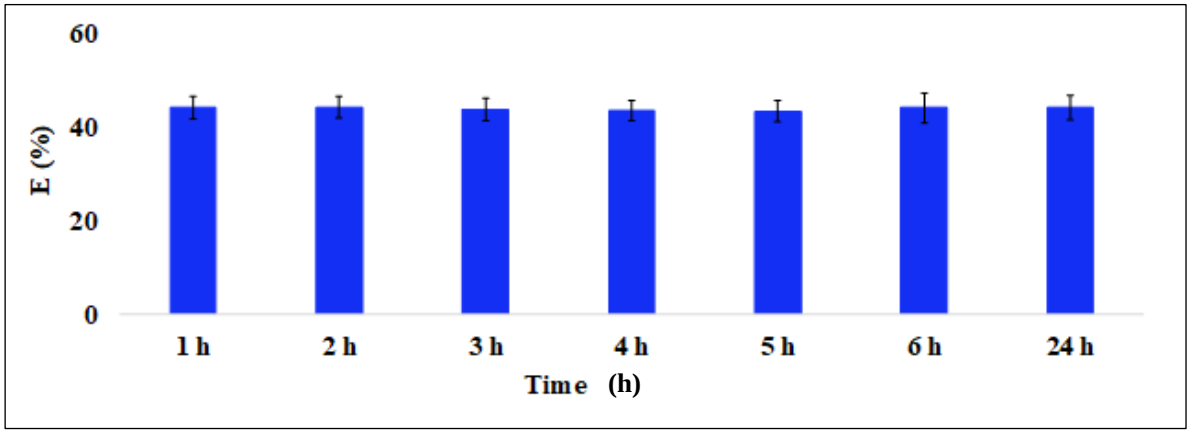

Fig. S2. Adsorption efficiency (E%; 100 mg of coffee waste) of Trichloroethylene after 1, 2, 3, 4, 5, 6 and 24 hours from preparation. Mean ± SD of three replicates is reported.

Table S1. pH of real polluted matrix and synthetic multi-component standard solution with and without the eight food waste materials.

Food Waste Materials	Real Polluted Matrix	Synthetic Multi-Component Standard Solution
Without adsorbents	6.5	7
Banana peel	5.5	5.8
Potato peel	6.4	7.5
Apple peel	5.9	4.7
Lemon peel	4.7	4.7
Coffee waste	6.2	5.9
Grape waste	6.1	7.1
Carob peel	5.9	5.3
Decaf Coffee waste	6.5	6.2

4.2. Conclusions and Perspectives

Food waste materials, which are available at very low costs and in large amount, were found to be efficient biosorbents for elements and for aliphatic and aromatic VOCs in aqueous solutions.

Maintaining homogeneous experimental conditions allowed us to evaluate and compare the adsorption capacities of 12 food waste materials. Banana peel, watermelon peel and grape waste were found to be the most efficient and the least selective adsorbents for the removal of most of the metals and metalloids from complex multi-element solutions, while coffee waste was found to be the most efficient sorbent for the removal of both examined VOCs. The surfaces of these biosorbents showed high porosity and different types of functional groups able to act as adsorption active sites for the considered pollutants. Moreover, in all the examined systems, the sorption processes followed much more closely the Freundlich than the Langmuir isotherm model, thus revealing a predominant physical adsorption mechanism thanks to London-Van der Waals forces between solute and sorbent. This kind of physical adsorption may be particularly beneficial in field applications, because it gives the adsorbents an opportunity to have great adsorption performance at high pollutant concentrations. The results of this preliminary study suggest further investigations about the possible applicative use of these food waste materials for the removal of toxic elements, heavy metals and VOCs from wastewater.